eman ta zabal zazu

Universidad del País Vasco
Euskal Herriko Unibertsitatea

CRM1/XPO1 nukleotiko esportazio hartzailearen fisiopatologia: funtzio zelularraren eta ituratze terapeutikoaren azterketa

---

Physiopathology of the nuclear export receptor CRM1/XPO1: studies on its cellular function and therapeutic targeting

Doktoretza-tesia

Maria Sendino Mouliet
(2022)

Zuzendariak:

José Antonio Rodríguez Pérez Doktorea

Miren Josu Omaetxebarria Ibarra Doktorea

Aurkibidea / Index

Laburdurak / Abbreviations

FARMAKOAK / *DRUGS*:

- **ActD:** Aktinomizina D / *Actinomycin D*
- **ALS:** Alisertib
- **CHX:** Zikloheximida / *Cycloheximide*
- **LMB:** Leptomizina B / *Leptomycin B*
- **SEL:** Selinexor
- **TAZ:** Tazemetostat
- **SINE:** Esportazio nuklearraren inhibitzaile hautakorra / *Selective inhibitor of nuclear export*

MINBIZI MOTAK / *CANCER TYPES*:

- **ALL:** Leuzemia linfozitiko akutua / *Acute lymphocytic leukaemia*
- **AML:** Leuzemia mieloide akutua / *Acute myeloid leukaemia*
- **CLL:** Leuzemia linfozitiko kronikoa / *Chronic lymphocytic leukaemia*
- **CML:** Leuzemia mieloide kronikoa / *Chronic myeloid leukaemia*
- **DLBCL:** B-zelula handien linfoma hedatsua / *Diffuse large B-cell lymphoma*
- **HCL:** Trikoleuzemia / *Hairy cell lymphoma*
- **HL:** Hodgkin linfoma / *Hodgkin lymphoma*
- **HNSCC:** Buru eta lepoko zelula eskatatsuen kartzinoma / *Head and neck squamous cell carcinoma*
- **MCL:** Mantuko zelulen linfoma / *Mantle cell lymphoma*
- **MM:** Mieloma anizkoitza / *Multiple myeloma*
- **MZL:** Area marginaleko linfoma / *Marginal zone lymphoma*
- **NHL:** Ez-Hodgkin linfoma / *Non-Hodgkin lymphoma*
- **NKTL:** Natural killer/T-zelulen linfoma / *Natural killer/T-cell lymphoma*
- **NSCLC:** Birikietako zelula ez-txikien minbizia / *Non-small-cell lung carcinoma*
- **PCNSL:** Nerbio-sistema zentraleko linfoma primarioa / *Primary central nervous system lymphoma*
- **PMBL:** B-zelulen linfoma mediastinal primarioa / *Primary mediastinal large B-cell lymphoma*
- **TCL:** T-zelulen linfoma / *T-cell lymphoma*

PROTEINA EDO GENEAK / *PROTEINS OR GENES*:

- **AP2B1:** *AP-2 complex subunit beta*
- **APX:** *Ascorbate peroxidase*
- **ATR:** *Serine/threonine-protein kinase ATR*
- **AURKA:** *Aurora Kinase A*
- **BCR-ABL:** *Breakpoint cluster region-proto-oncogene tyrosine-protein kinase*
- **BirA:** *Bifunctional ligase/repressor BirA*
- **BRCA1:** *Breast cancer type 1 susceptibility protein*

- **BRCA2:** *Breast cancer type 2 susceptibility protein*
- **c-ABL:** *Tyrosine-protein kinase ABL*
- **CBEP4:** *Cytoplasmic polyadenylation element-binding protein 4*
- **CD38:** *Cluster of differentiation 38*
- **CDC25C:** *M-phase inducer phosphatase 3*
- **CDC27:** *Cell division cycle protein 27 homolog*
- **CDC7:** *Cell division cycle 7-related protein kinase*
- **CHK1:** *Checkpoint kinase 1*
- **CK2α':** *Casein kinase II subunit alpha'*
- **cMyc:** *Myc proto-oncogene protein*
- **COMMD1:** *COMM domain-containing protein 1*
- **CRM1:** *Chromosome Region Mantenaince protein 1*
- **CRTC1:** *CREB-regulated transcription coactivator 1*
- **DEAF1:** *Deformed epidermal autoregulatory factor 1 homolog*
- **DMWD:** *Dystrophia myotonica WD repeat-containing protein*
- **DUB:** Deubikuitinasa / *Deubiquitinase*
- **EZH2:** *Enhancer of zeste homolog 2*
- **FGF1:** *Fibroblast growth factor 1*
- **FMRP:** *Fragile X mental retardation protein*
- **FR1OP:** *Centrosomal protein 43*
- **GFP:** Proteina fluoreszente berdea / *Green fluorescent protein*
- **HDAC1:** *Histone deacetylase 1*
- **HDAC5:** *Histone deacetylase 5*
- **hRio2:** *Serine/threonine-protein kinase RIO2*
- **HRP:** Errefau min peroxidasa / *Horseradish peroxidase*
- **Hxk2:** *Hexokinase 2*
- **IF2B:** *Translation initiation factor eIF-2B*
- **LIMD1:** *LIM domain containing protein 1*
- **MAP:** *Mitogen activated protein*
- **mDia2:** *Protein diaphanous homolog 3*
- **mRFP:** Proteina fluoreszente gorria / *Red fluorescent protein*
- **MSH2:** *DNA mismatch repair protein Msh2, MutS protein homolog 2*
- **MSH6:** *DNA mismatch repair protein Msh6, MutS protein homolog 6*
- **mTOR:** *Serine/threonine-protein kinase mTOR*
- **N:** nukleokapsida / *Nucleocapsid*
- **NF-κB:** *Nuclear factor kappa-light-chain-enhancer of activated B cells*
- **NPM1:** *Nucleophosmin*
- **NSD2:** Histone-lysine N-methyltransferase NSD2
- **NUP:** nukleoporina / *nucleoporin*
- **p53:** *Cellular tumor antigen p53*
- **PAX:** *Paired box protein Pax*
- **PER1:** *Period circadian protein homolog 1*
- **PKA:** *Protein kinase A*
- **PKI:** *Protein kinase inhibitor*
- **PLK1:** *Polo like kinase 1*
- **PRC2:** *Polycomb repressive complex 2*

- **pUL69:** *mRNA export factor ICP27 homolog*
- **Ran:** *GTP-binding nuclear protein Ran*
- **RanGAP1:** *Ran GTPase-activating protein 1*
- **RARA:** *Retinoic acid receptor alpha*
- **RCC1:** *Regulator of chromosome condensation*
- **RIP3:** *Receptor-interacting serine/threonine-protein kinase 3*
- **SBSN:** *Suprabasin*
- **SEPT6:** *Septin-6*
- **SHIP2:** *Phosphatidylinositol 3,4,5-trisphosphate 5-phosphatase 2*
- **SIR2:** *NAD-dependent protein deacetylase sirtuin-2*
- **SMAD4:** *Mothers against decapentaplegic homolog 4*
- **SNUPN:** *Snurportin 1*
- **SPN90:** *NCK-interacting protein with SH3 domain*
- **STK38:** *Serine/threonine-protein kinase 38*
- **TFE3:** *Transcrition factor E3*
- **TOP2A:** *Topoisomerase II*
- **TUBAL3:** *Tubulin alpha chain-like 3*
- **UAF1:** *USP1 associated factor 1*
- **UBR5:** *E3 ubiquitin-protein ligase UBR5*
- **USP12:** *Ubiquitin carboxyl-terminal hydrolase 12*
- **WDR20:** *WD repeat-containing protein 20*
- **WDR48**: *WD repeat-containing protein 48*
- **X11L2:** *Amyloid-beta A4 precursor protein-binding family A member 3*
- **XPO1:** *Exportin 1*
- **XPO2:** *Exportin 2*
- **YFP:** Proteina fluoreszente horia / *Yellow fluorescent protein*
- **ZO2:** *Tight junction protein ZO-2*

ERREAKTIBOAK / *REAGENTS*:

- **APS:** Amonio persulfatoa / *Ammonium Persulfate*
- **BP:** Biotin-fenola / *Biotin-phenol*
- **BSA:** Behi-albumina serikoa / *Bovine serum albumin*
- **DAPI:** 4',6-diamidino-2-fenilindoldun / *4',6-diamidino-2-phenylindole*
- **DMEM:** *Dulbecco's modified Eagle's medium*
- **DTT:** Ditiotreitol / *Dithiothreitol*
- **ECL:** Areagotutako kemiluminiszentzia / *Enchanced chemiluminescence*
- **EDTA:** Azido etilendiaminotetraazetikoa / *Ethylenediaminetetraacetic acid*
- **FBS:** Idi-umeki serum / *Fetal bovine serum*
- **GBP:** GFP lotzeko proteina / *GFP binding protein*
- **GI:** Garbiketa indargetzailea
- **NEM:** N-etilmaleimida / *N-ethylmaleimide*
- **NTP:** Nukleosido trifosfatoa / *Nucleoside triphosphate*
- **PBS:** Fosfatoarekin tanponatutako gatz soluzioa / *Phosphate buffered saline*
- **PIC:** Proteasa inhibitzaile nahastea / *Protease inhibitor complex*
- **PMSF:** Fenilmetilsulfonil fluoruroa / *Phenylmethylsulfonyl fluoride*

- **RPMI:** *Roswell Park Memorial Institute*
- **SDS:** Sodio dodezil sulfato / *Sodium dodecyl sulphate*
- **SDS-PAGE:** Sodio dodezil sulfato-poliakrilamida gel elektroforesia / *Sodium dodecyl sulphate–polyacrylamide gel electrophoresis*
- **TAE:** Tris-Azetiko-EDTA / *Tris-Acetate-EDTA*
- **TEMED:** Tetrametiletilenediamina / *Tetramethylethylenediamine*
- **TTBS:** Tween-Tris-arekin tanponatutako gatz-soluzioa / *Tween-Tris-buffered saline*
- **XTG9:** X-tremeGENE 9

BESTE BATZUK */ OTHERS*:

- **ϕ:** aminoazido hidrofobikoa / *Hydrophobic amino acid*
- **AGC:** *Automatic gain control*
- **ATP:** Adenosina trifosfatoa / *Adenosin triphosphate*
- **BioID:** *Biotin identification*
- **BM:** Hezur muin / *Bone marrow*
- **cDNA:** DNA kodetzailea / *coding DNA*
- **CI:** Konbinazio indizea / *Combination index*
- **C_{max}:** Kontzentrazio maximoa / *Maximum concentration*
- **cNES:** Nukleotiko esportazio seinale kandidatua / *Candidate nuclear export signal*
- **cNLS:** Nukleora lokalizatzeko seinale klasikoa / *Classic nuclear localization signal*
- **DDR:** *DNA damage response*
- **DNA:** Azido desoxirribonukleikoa / *Desoxirribonucleic acid*
- **EMA:** Sendagaien Europako agentzia / *European Medicines Agency*
- **FDA:** Elikagai eta sendagaien administrazioa / *Food and Drug Administration*
- **FDR:** *False discovery rate*
- **FG:** Fenilalanina-Glizina / *Phenilalanine-Glycine*
- **FI:** Fluoreszentzia intentsitatea / *Fluorescence intensity*
- **GDP:** Guanosina difosfatoa / *Guanosine diphosphate*
- **GIB/HIV:** Giza immunoeskasiaren birusa / *Human immunodeficiency virus*
- **GTP:** Guanosina trifosfatoa / *Guanosine triphosphate*
- **HBOC:** *Hereditary breast and ovarian cancer syndrome*
- **HCD**: *Higher-energy C-trap dissociation*
- **HGNC:** Geneen nomenklaturarako HUGO batzoredea / *HUGO Gene Nomenclature Committee*
- **HNPCC:** *Hereditary nonpolyposis colorectal cancer (Lynch syndrome)*
- **HPA:** Giza proteina atlasa / *Human protein atlas*
- **IGHV:** Immunoglobulinen kate astun aldakorra / *Immunoglobulin heavy-chain variable*
- **IP:** Immunoprezipitazioa / *Immunoprecipitation*
- **KF:** Kaltetutako frakzioa / *Affected fraction*
- **LC:** Kromatografia likidoa / *Liquid chromatography*
- **LFQ:** Etiketa gabeko kuantifikazioa / *Label free quantification*
- **m/z:** Masa/karga / *Mass/charge*
- **MCS:** *Multiple cloning site*
- **MMR:** *Mismatch repair*
- **mRNA:** RNA mezularia / *Messenger RNA*

- **MS/MS:** Tandem masa-espektrometria / *Tandem mass spectrometry*
- **MW:** Pisu molekularra / *Molecular weight*
- **N:** Nuklear / *Nuclear*
- **NES:** Nukleotiko esportazio seinalea / *Nuclear export signal*
- **NLS:** Nukleora lokalizatzeko seinalea / *Nuclear localization signal*
- **NPC:** Nukleoko poro-konplexua / *Nuclear pore complex*
- **NZ:** Nukleozitoplasmatikoa / *Nucleocytoplasmic*
- **PCR:** Polimerasaren kate-erreakzioa / *Polymerase chain reaction*
- **PEO/WPE:** Proteina erauzkin osoa / *Whole protein extract*
- **PGB/PPB:** Proteinen gertuko biotinilazioa / *Protein proximity biotinilation*
- **Q:** Kuartila / Quartile
- **Rev:** Alderantzizkoa / *Reverse*
- **RNA:** Azido erribonukleikoa / *Ribonucleic acid*
- **SV40:** Zimino birus 40 / *Simian virus 40*
- **TARGET:** Genenomikaz gidaturiko terapiarako garrantzitsuak diren tumore asaldurak / *Tumor alterations relevant for genomics-driven therapy*
- **T_m:** Urtze temperatura / *Melting temperature*
- **UA:** Ugaritze-arrazoia / *Proliferation ratio*
- **WN:** Wregex-NESmapper
- **Z:** Zitoplasmatikoa / *Cytoplasmatic*

Abstract

Cellular homeostasis crucially relies on the correct nucleocytoplasmic distribution of a vast number of proteins. Many of these proteins are dynamically shuttled between the nucleus and cytoplasm by specialized receptors, such as the nuclear export receptor CRM1/XPO1. By recognising and binding specific sequence motifs termed nuclear export signals (NESs), CRM1 mediates the translocation of hundreds of proteins to the cytoplasm, and thus regulates critical signalling pathways and cellular functions. Mutation and altered expression of CRM1 are common in human tumours, an observation that has recently brought CRM1 inhibition into the focus of anticancer therapy.

Several aspects of the physiopathology of CRM1 remain to be further investigated. On one hand, dozens of CRM1-dependent NESs have been reported, but the NES motifs of many potential cargos are still unknown. Furthermore, the CRM1/NES interaction has been characterized using structural and biochemical approaches *in vitro*, but mechanistic studies of CRM1-mediated export in a cellular context are still lacking. Moreover, a recurrent mutation in CRM1 (E571K) has been shown to possess oncogenic capacity, but the cellular effects of this mutation remain to be further characterized. On the other hand, although CRM1 inhibitors, such as selinexor, are already entering clinical use in cancer therapy, there is still limited knowledge about how these inhibitors can be combined with other targeted drugs, and what their global cellular effects can be.

The results presented in this PhD Thesis shed further light on these aspects of CRM1 physiopathology. On one hand, new functional NES motifs have been identified and characterized in several cellular and viral proteins, including (i) the cofactors of the USP12 deubiquitinase, (ii) potential CRM1 cargoes related to cancer, (iii) a recently-described set of small human proteins, termed micropeptides, and (iv) the nucleocapsid protein of human coronaviruses. These studies have been carried out using either a well-established nuclear export assay (termed Rev(1.4)-GFP assay) or a novel assay described here, termed $SRV_{B/A}$ assay. Furthermore, the $SRV_{B/A}$ assay has been used to gain mechanistic insight on CRM1-mediated NES export in a cellular context, by extensively analysing the effect of single amino acid mutations in the NES-binding region of CRM1, including the cancer hotspot mutation E571K. On the other hand, an *in silico* analysis of genes co-expressed with CRM1 has led to the selection of two potential candidates (EZH2 and AURKA) for selinexor-based combination treatments. Inhibitors of these proteins have been evaluated in combination with selinexor using a cellular model of acute myeloid leukaemia. The results suggest that combined

inhibition of CRM1 and AURKA warrants further investigation as a potential strategy for cancer therapy. Finally, a new proteomics approach based on compartment-specific proximity biotinylation of proteins using the APEX2 peroxidase has been developed and tested. This approach can be used to identify new CRM1 cargos, as well as to gain global insight into the cellular effect of CRM1 inhibition.

1. Sarrera

(Sendino et al., 2018 eta Sendino et al., 2020a-n oinarrituz berrikusi eta eguneratutako testua)

CRM1 (*Chromosome Region Mantenaince protein 1*) proteina legamietan kromosomen egituraren egonkortasunaz arduratzen den proteina gisa zen ezaguna. 1997. urtean, bestelako proteinak nukleotik zitoplasmara garraiatzeko, esportatzeko, gai dela aurkitu zen (Fornerod et al., 1997; Fukuda eta al., 1997; Stade et al., 1997; Ossareh-Nazari et al., 1997). Orduan, ez zen funtzio hori duen bestelako proteinarik ezagutzen, eta, hori dela eta, CRM1 proteinak XPO1 (*exportin 1*) izena ere hartu zuen. HUGO gene nomenklaturaren batzordearen (*HUGO Gene Nomenclature Committee;* HGNC) arabera sinbolo ofiziala XPO1 bada ere, tesi honetan CRM1 sinboloa erabiliko da, erabiliena baita literaturan.

CRM1ek esportatzen dituen proteinetan aminoazido sekuentzia laburrak ezagutzen eta lotzen dituela frogatu zuten garai hartan argitaratutako lanek. Sekuentzia labur horiei "nukleotiko esportazio seinale" (*nuclear export signal*, NES) izena eman zitzaien. CRM1ek 400 bat proteina zelular zein birikoren esportazioa bideratzeaz gain (Fung et al., 2021), hainbat RNA molekulen esportazioaren arduraduna ere bada (Hutten eta Kehlenbach, 2007; Okamura et al., 2015). Horrek, zelulen ongizaterako ezinbestekoak diren hainbat prozesutarako pieza gako egiten du CRM1. Esaterako, NF-κB (*nuclear factor kappa-light-chain-enhancer of activated B cells*) bidezidorrean edota zelula-zikloan CRM1en mendeko esportazioa gertatu gertatzen da (Turner eta Sullivan, 2008). Mitosian ere parte hartzen duela behatu izan da (Arnaoutov et al., 2005).

Guzti horrek CRM1 eta minbiziaren arteko erlazioa ikertzeko bide eman du, eta CRM1en mutatutako aldaerek zein CRM1en gainadierazpenak minbiziarekin lotura badutela baieztatu da. Hori horrela, CRM1 minbiziaren kontrako terapiarako itutzat hartu (Gravina et al., 2014a; Tan et al., 2014), eta hainbat ikuspuntu ezberdinetatik ikertu da (Koyama eta Matsuura, 2012; Fung eta Chook, 2014; Monecke et al., 2014). Ikerketa horiek klinikan erabilgarriak diren CRM1en inhibitzaileen gaineko ezagutza handitu dute. CRM1en deskribatutako lehen inhibitzailea leptomizina B (LMB) izenekoa izan zen (Kudo et al., 1998). Konposatu hori CRM1en inhibitzaile oso eraginkorra bada ere, gaixoetan kontrako efektu larriak sortzen ditu, eta beraz, ezin da klinikan erabili (Newlands et al., 1996). Badira baina SINE (*selective inhibitor of nuclear export*) familia osatzen duten beste inhibitzaile batzuk, zeinak eraginkorrak bezain seguruak diren (Senapedis et al., 2014). SINE horietako batzuek ikerketa preklinikoetan aurrera egin dute; inhibitzaile horietan aurreratuenak, selinexor izenekoak, entsegu klinikoetan ere aurrera egin du eta minbizi mota jakin batzuk tratatzeko oniritzia jaso du oraintsu bai AEBetan zein Europan (Food and Drug Administration, 2019, 2020a, 2020b; European Medicines Agency, 2021).

CRM1en gaineko ezagutza, bai bere funtzio fisiologikoei dagokienez baita minbiziarekin duen loturari dagokionez, zabala bada ere, zer argitu badago oraindik ere. Aipatzekoa da CRM1en mende esportatzen diren proteinen zerrenda osoa (CRM1en esportoma) osatzeke dagoela, eta horrekin lotuta, CRM1en mutazio ohikoenak edota CRM1en inhibitzaileek haren esportoman eragiten duten asaldura ere ikertzeke dago. CRM1 minbiziarekin zerikusia baduela ezaguna da eta bere inhibizioa eragiten duten farmakoak beste agente kimioterapiko batzuekin konbinatzeak minbiziari aurre egiteko baliagarria dela ikusi bada ere, beste konbinazio asko ikertzeke daude. Bestetik, CRM1ek NESak nola lotzen dituen deskribatu den arren, loturarako gakoak diren CRM1en aminoazidoek lotura horretan zenbateraino parte hartzen duten ez da sakon aztertu.

1.1. Nukleo eta zitoplasmaren arteko proteinen garraioa

Zelula eukariotoen berezitasun nabariena zelula barneko mintz-sistema bidezko konpartimentalizazioa da. Mintz-sistema horrek mugatutako bi konpartimentu nagusiak nukleoa eta zitoplasma dira. Konpartimentu horiek banatzen dituen mintzari gaineztadura nuklear izena ematen zaio, eta nukleoa eta zitoplasma fisikoki banatzen baditu ere, konpartimendu bien artean zelularen homeostasia mantentzeko beharrezkoa den etengabeko komunikazioa egikaritzea ahalbidetzen du. Komunikazio hori molekulen garraio nukleozitoplasmatikoaren bidez ematen da. Molekula gehienen garraioa gaineztadura nuklearraren zehar mihiztatuta dauden nukleoko poro-konplexu (*nuclear pore complexes*, NPC) izeneko kanal batzuetan zehar gertatzen da. Tamaina txikiko molekulek, horien artean 30 kDa baino txikiagoak diren proteinek ere, printzipioz, NPCak difusioz zeharkatu ditzakete; alabaina, NPCa zeharkatzen duten proteina gehientsuenak (baita oso handiak diren proteina-konplexuak ere) garraio-hartzaileei lotuko zaizkie energiaren mendeko prozesu baten bidez garraiatuak izateko (Knockenhauer eta Schwartz, 2016; Schmidt eta Görlich, 2016). Garraiatuak diren proteina horiei “kargo” izena eman zaie tesi honetan. Kargoen garraioa makineria espezializatu baten bidez ematen da. Makineria horrek hiru pieza nagusi ditu (1. irudia): (1) NPCak, (2) gaineztadura nuklearraren alde bien arteko Ran GTPasa txikiaren gradientea, zeinak garraioaren noranzkoa zehaztuko duen, eta (3) garraio-hartzaileak edo karioferinak, zeintzuek garraiatuko dituzten kargoetan seinale espezifikoak ezagutuko dituzten (Pemberton eta Paschal, 2005; Tran et al., 2014; Cautain et al., 2015).

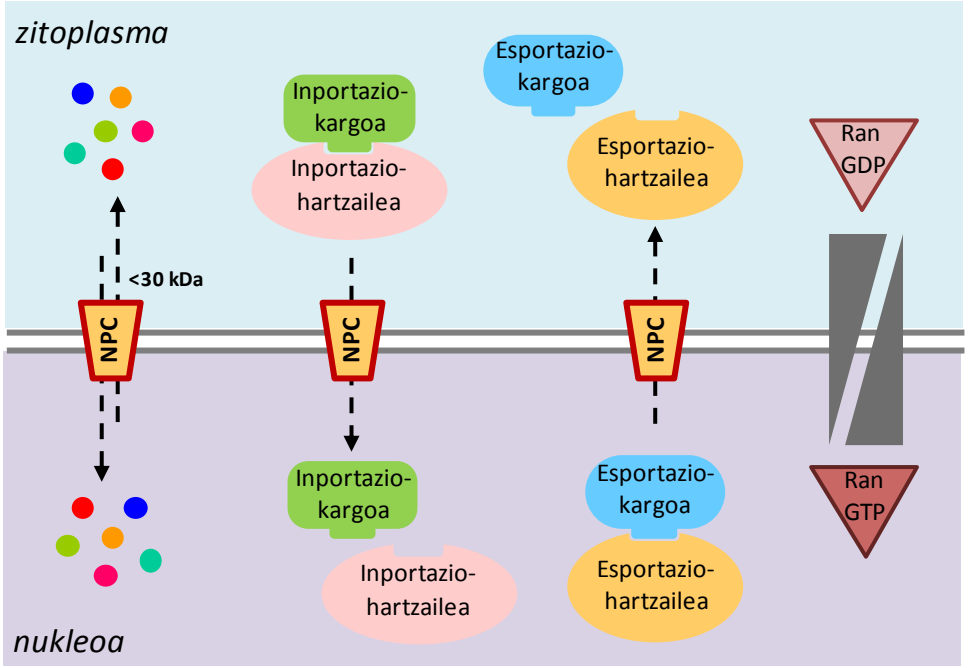

1. irudia: Nukleoko poro-konplexuetan (NPC) zeharreko proteina-garraio nukleozitoplasmatikoa. Proteina txikiak (<30 kDa), printzipioz, nukleoaren eta zitoplasmaren artean difusioz mugi daitezke NPCetan zehar. Proteina handiagoek, garraio- (inportazio- edo esportazio-) hartzaileen beharra dute konpartimentu batetik bestera mugitu ahal izateko. RanGTP/RanGDP gradienteak (RanGTP-kontzentrazio handia nukleoan, eta RanGDP-kontzentrazio handia zitoplasman) garraioaren noranzkoa finkatzen du.

NPCak, gaineztadura nuklearreko kanpo eta barne mintza fusionatzean agertzen diren poroetan txertatzen diren 30 bat nukleoporina (NUP) izeneko proteina ezberdinen hainbat kopiaz osaturik dauden konplexu proteiko handiak (∼ 120 MDa) dira (2. irudia). NPCek errotazio-simetria zortzikoitza (Gall, 1967) agertzen duten gainezarritako hiru eraztun itxurako egiturez eraturik daude; eraztun nuklearra, tarteko eraztuna eta eraztun zitoplasmatikoa. Neurri handi batean, NPCek gaineztadura nuklearraren planoarekiko simetria bikoitza ere erakusten dute. Simetria bikoitz gabeko zonaldeak bi dira; zitoplasmako aldean agertzen diren zitoplasmako filamentuak eta nukleoko aldean agertzen den saski nuklearra. Gainera, NPCaren erdialdean eratzen den kanalean egitura zehatzik ez duen fenilalanina-glizinatan (FG) aberatsak diren motiboez eratutako FG-motibo sarea eratzen da (Pemberton eta Paschal, 2005; Knockenhauer eta Schwartz, 2016; Lin et al., 2016; Lin eta Hoelz, 2019).

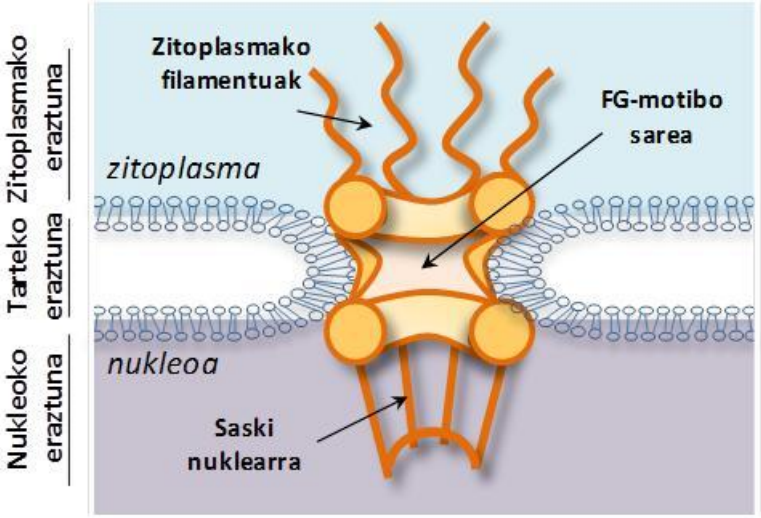

2. irudia: NPCaren eskema. Gaineztadura nuklearrarekiko NPCaren sekzio perpendikularra erakusten da. Bertan NPCaren atal ezberdinak adierazi dira.

FG-motibo sare horren propietate fisiko-kimikoei esker, tamaina jakin batetik gorako proteinak ezin dira nukleotik zitoplasmara edo zitoplasmatik nukleora era askean mugitu. Aurretik, tamaina muga hori 30 kDa-etan dagoela aipatu da, eta izan ere, denbora luzez NPCak muga hori duela kontsideratu da. Egun, tamaina-muga zehatz hori zalantzan jartzen da, eta FG-motibo difusio-sareak molekula txikienak handienak baino gutxiago atxikitzen dituela planteatu da (Timney et al., 2016).

Aipatutako garraio-makineria espezializatu horren bigarren pieza Ran GTPasa da. Ran GDPri (RanGDP) edo GTPri (RanGTP) lot dakioke garraio-hartzaile eta kargoen arteko elkarrekintza erregulatzeko (Pemberton eta Paschal, 2005; Tran et al., 2014; Cautain et al., 2015). RanGDParen kontzentrazioa zitoplasman da handia, RanGTParena, berriz, nukleoan (Ikusi 1. irudia). RanGDP/RanGTP gradientea mantentzen duten kofaktoreak bi dira: GTPasa aktibatzailea den RanGAP1 proteina zitoplasmatikoa, eta kromatinari lotutako nukleotidoak trukatzeko RCC1 proteina. Ran gradiente hori hain da determinantea garraioaren noranzkoa zehazteko, non, RanGTPren kontzentrazioa zitoplasman artifizialki emendatzeak garraioaren noranzkoa alderantzikatu dezakeen (Nachury eta Weis, 1999).

Azkenik, garraioa egikaritzeko kargoekin batera gaineztadura nuklearraren alde batetik bestera mugituko diren garraio-hartzaile edo karioferinak daude. Giza genomak 25 karioferina kodetzen ditu (Çağatay eta Chook, 2018); horietako zenbaitzuek kargoak gaineztadura nuklearrean zehar noranzko bietan garraia baditzakete ere, gehientsuenak nukleoranzko hartzaile gisa (inportinak) ala nukleotiko hartzaile gisa (esportinak) aritzen dira esklusiboki. Nukleora garraiatzen diren proteina gehienak α-inportina/β-inportina heterodimeroaren mende egiten dute, zitoplasmara garraiatzen direnak aldiz, CRM1en mende (3. irudia).

α-inportina/β-inportinaren zein CRM1en bidezko garraioan RanGTPak zuzeneko eragina du, hartzaile eta kargoen arteko elkarrekintzak modulatzen baititu (3. irudia). Izan ere, nukleoko RanGTPak, inportazio- zein esportazio- konplexuekin elkarrekiten du. Batetik, inportina/kargo konplexuen desmuntaketa bultzatzen du, horrela inportazio-kargoa nukleoan askatuz. Bestetik, CRM1 esportazio-hartzailearekin eta haren kargoekin bat eginez CRM1/kargo/RanGTP konplexu trimerikoa osatzen du, CRM1 eta kargoen arteko interakzioa egonkortzeko. Konplexu hori, zitoplasmara heldutakoan, RanGAP1ek GTParen hidrolisia eragingo du, eta esportazio-kargoa zitoplasman askatuko da (Dickmanns et al., 2015).

Garraio-hartzaile horiek behin kargoa dagokion konpartimentuan askatu dutela, birziklatuak izango dira. Inportazio hartzaileen kasuan, β-inportina RanGTPari lotuta igaroko du NPCa, α-inportinak ordea, RanGTPaz gain XPO2 esportinaren beharra izango du (Lu et al., 2021). CRM1ek berriz, bere kabuz igaroko du NPCa (Dickmanns et al., 2015).

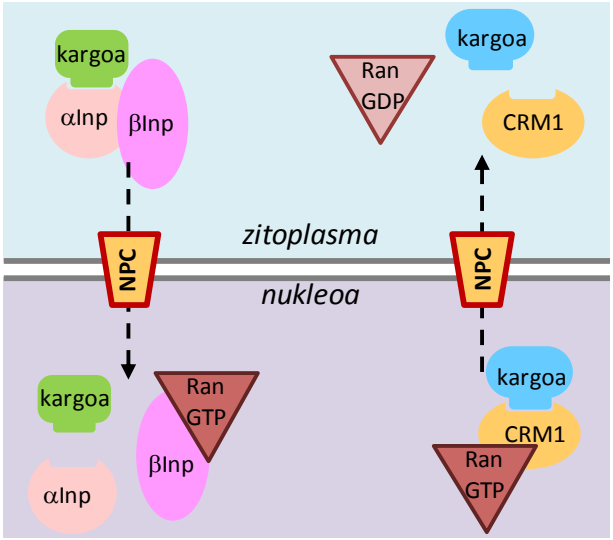

3. Irudia: Garraio nukleozitoplasmatikoaren mekanismo nagusiak. Ezkerraldean α-inportina/β-inportina (αInp/βInp) bidezko inportazioa ageri da. αInp/βInp heterodimeroak zitoplasman bere kargoak lotu eta NPCetan zehar nukleora garraiatzen ditu. Behin, konplexua nukleora heldu denean RanGTParekin elkarreragin eta inportazio-konplexua desmuntatzen da. Eskuinaldean CRM1en mendeko esportazioa ageri da. CRM1 hartzaileak nukleoan bere kargoak ezagutu, eta RanGTParekin batera, esportatua izango den konplexu trimerikoa eratzen du. Konplexu hori, zitoplasmara heltzean, GTParen hidrolisia medio dela desmuntatu, eta CRM1 hartzailea zein esportazio-kargoa askatuko dira.

Makineria horretaz gain, badira proteina jakin batzuen garraioa zorrozki erregulatzen duten bestelako mekanismo batzuk ere, hala nola, proteinen fosforilazioa (Nardozzi et al., 2010; Panayiotou et al., 2016), ubikuitinazioa (Rodríguez, 2014) edota garraio-kargoetan karioferinek ezagutuko dituzten seinaleak dimerizazioaren bidez estaltzea (Rodríguez et al., 2004; Engelsma et al., 2007).

1.1.1. Inportazio eta esportaziorako seinaleak

Karioferinek garraiatuko dituzten proteinetan dauden peptido-sekuentzia espezifikoak ezagutu eta lotzen dituzte. Peptido-sekuentzia horiek garraio nukleozitoplasmatikorako seinale moduan aritzen dira. Seinaleok bitarikoak izan daitezke: inportinek ezagutzen eta lotzen dituzten nukleora lokalizatzeko seinaleak, NLSak (*nuclear localization signals*), eta esportinek ezagutzen eta lotzen dituzten nukleotiko esportazio seinaleak, NESak (*nuclear export signals*).

1.1.1.1. Nukleora lokalizatzeko seinaleak (NLSak)

Inportaziorako ondoen karakterizatutako hartzaileak, α-inportina/β-inportina heterodimeroak alegia, NLS "klasikoa" ezagutzen du (*classic NLS,* cNLS). cNLSa aminoazido basikozko errenkada batez edo biz osatutako peptido-sekuentzia da. Errenkada bakarreko cNLSen adostasun-sekuentzia K-K/R-X-K/R da eta errenkada bikoena (K/R)(K/R)$X_{10-12}$$(K/R)_{3/5}$, non, X hizkiak edozein aminoazido adierazten duen eta $(K/R)_{3/5}$-k, bost aminoazidotik hiru lisina edo arginina direla (Soniat eta Chook, 2015). SV40 birusaren T-antigeno luzearen ^{126}PKKKRKV^{132} sekuentzia aminoazido basikozko errenkada bakarreko cNLSaren adibide da (Kalderon et al., 1984a, 1984b), nukleoplasminaren ^{155}KRPAATKKAGQAKKKK^{170} sekuentzia, aldiz, errenkada biko cNLSaren adibide (Dingwall et al., 1988).

NLS klasikoez gain, badaude beste inportinek ezagutzen dituzten NLS "ez-klasikoak". Horietan gehien ikertu direnak, inportina-β_2-ak ezagutzen dituen PY-NLSak dira. PY-NLSak egitura definitu gabeko 20-30 aminoazidozko peptido seinaleak dira. Sekuentzia horien C-muturrean R/K/H(X_{2-5})PY motiboa dago (X_{2-5} bi eta bost aminoazido arteko edozein sekuentzia izan daiteke). N-muturrean, aminoazido basiko edo hidrofobikozko errenkada egon daiteke, zeinak PY-NLSak bi azpitaldetan banatzen dituen, bPY-NLSak (basikoak) eta hPY-NLSak (hidrofobikoak) (Lu et al., 2021).

1.1.1.2. Nukleotiko esportazio seinaleak (NESak)

CRM1ek, "leuzinatan aberatsak" diren NES peptido-sekuentziak ezagutzen ditu. NES horietan 4-5 aminoazido hidrofobikok agertzen duten kokapenaren arabera adostasun-sekuentzia bat osatzen dute. Adostasun-sekuentzia klasikoa, $\phi^1X_{(2-3)}\phi^2X_{(2-3)}\phi^3X\phi^4$ sekuentzia da. ϕ sinboloak aminoazido hidrofobiko bat, normalean leuzina dena baina, isoleuzina, balina, fenilalanina edo metionina ere izan daitekeena adierazten du, eta X hizkiak edozein aminoazido (Kosugi et al., 2008). Adostasun-sekuentzia horrekin bat egiten duten NES motiboen adibide dira GIB birusaren Rev proteinaren ^{75}LPPLERLTL^{83} (Fischer et al., 1995) edo PKI proteinaren ^{37}LALKLAGLDI^{46} (Wen et al., 1995) sekuentziak. Adostasun-sekuentzia horri ϕ^0 posizioa ere gehi dakioke maiz, horrela gertatzen da adibidez SNUPN proteinaren NESaren kasuan

^{1}MEELSQALASSFSVSQ^{16}, non metionina ϕ^{0} posizioan aurkitzen den (Dong et al., 2009a). Aipaturiko adostasun-sekuentziaz gain, NESek konformazio jakina ere izan ohi dute: N-muturrean, α-helize egitura hartu ohi dute, eta C-muturrean, berriz, harizpi-erakoa (Dong et al., 2009b).

CRM1i lotzen zaizkion NES motiboentzako adostasun-sekuentzia eta egitura orokor bat definitu den arren, NES aktibo guztiek parametro horiek betetzen ez dituztela ikusi da. Adibidez, GIB birusaren Rev proteinaren NESak adostasun-sekuentzia betetzen badu ere, ez du α-helize/harizpi egitura erakusten. Horren ordez, CRM1i luzetara lotzen zaio (Güttler et al., 2010). NES aktibo guztiek adostasun-sekuentzia betetzen ez dutela, eta aurreikusitako egitura ere ez dutela agertzen ikusita, adostasun-NESen sailkapen zabalago bat proposatu da (1. taula) (Kosugi et al., 2008; Fung et al., 2015, 2017). Sailkapen zabalago hori NESek CRM1 lotzen duten noranzkoaren eta aminoazido hidrofobikoen kokapenaren araberakoa da. Horrela, CRM1en poltsiko hidrofobikoa klasikoki deskribatutakoaren noranzko berean lotzen duten NESak "*plus*" izendatu dira, eta oraintsu deskribatu diren eta CRM1 kontrako noranzkoan lotzen dutenak "*minus*" edo "*reverse*" (Fung et al., 2015). Gainera, aminoazido hidrofobikoen kokapenaren arabera mota ezberdineko *plus* zein *minus* NESak daude. *Plus* erakoak zazpi dira: 1a, 1b, 1c, 1d, 2, 3 eta 4, *minus* erakoak, ordea, lau: 1a-R, 1b-R, 1c-R eta 1d-R (Kosugi et al., 2008; Fung et al., 2015, 2017).

1. taula: Mota ezberdinetako NESen noranzkoa, sekuentzia eta egitura. Φ sinboloak leuzina, isoleuzina, balina, fenilalanina edo metionina aminoazidoa adierazten du, normalean leuzina, eta X hizkiak edozein aminoazido (Kosugi et al., 2008; Fung et al., 2015, 2017).

Noranzkoa	Mota	Sekuentzia	Egitura
Plus	1a	ΦXXXΦXXΦXΦ	Helize-harizpi egitura. α- (1a eta 1c motakoak) zein 3_{10}- (1b motakoak) helizeak motaren arabera
	1b	ΦXXΦXXΦXΦ	
	1c	ΦXXXΦXXXΦXΦ	
	1d	ΦXXΦXXXΦXΦ	
	2	ΦXΦXXΦXΦ	Begizta egitura
	3	ΦXXΦXXXΦXXΦ	α-helize egitura esklusiboki
	4	ΦXXΦXXXΦXXΦXXXΦ	3 motakoen bezalako α-helizea, gehi beste NES motetan agertzen ez den bosgarren aminoazido hidrofobikoa bere baitan hartzen duen harizpia
Minus	1a-R	ΦXΦXXΦXXXΦ	Harizpi-helize egitura (*Plus* 1 motakoen egitura bezalakoa alderantzikaturik)
	1b-R	ΦXΦXXΦXXΦ	
	1c-R	ΦXΦXXXΦXXXΦ	
	1d-R	ΦXΦXXXΦXXΦ	

NESen sekuentziak eta CRM1 lotzeko hartu behar duten egitura sakon aztertu bada ere, tesi proiektu honi hasiera eman zitzaionean ez zegoen NES mota ezberdinen eta CRM1en arteko elkarrekintza testuinguru zelular batean ikertzen zuen ikerketarik. Eta hori ezinbestekoa da NESen esportazioa nola ematen den osotasunean ulertzeko.

1.2. CRM1en egitura eta NESak lotzeko ezaugarri gakoak

CRM1 proteina helikoidal malgua da, non N- eta C-muturrak bata bestearengandik hurbil dauden (4A irudia). RanGTPa alde ahurrean lotzen da, NESak, ordea, alde ganbilean dagoen poltsiko hidrofobiko batera. NESak CRM1era lotu ahal izateko, CRM1en poltsikoa zabalik egon behar da, eta hori, C-helize eta H9 begizta izeneko egituren kokapen eta konformazioaren araberakoa da (Dong et al., 2009b; Monecke et al., 2009, 2014; Güttler et al., 2010; Koyama eta Matsuura, 2012; Fung eta Chook, 2014). NESak lotzeko poltsiko hidrofobikoa, alde zabal eta estuago bana ditu; zabalena *plus* erako NESen N-muturra kokatzen den aldea da, estua, aldiz, C-muturra kokatzen den aldea (4B irudia). Gainera, poltsikoan barna bost gune hidrofobiko daude, eta gune horiek dira, hain zuzen ere, NES bakoitzak hartzen duen egitura zehaztuko dutenak. Izan ere, NESen aminoazido hidrofobikoek poltsikoko aminoazido hidrofobikoekin (I521, L525, F561 eta F572) elkarreginez beteko dituzte gune horiek (4C irudia) (Kosugi et al., 2008; Dong et al., 2009b; Monecke et al., 2009; Güttler et al., 2010; Fung et al., 2017). Badira CRM1en aktibitate eta erregulazioarekin erlazionatuta dauden bestelako aminoazido ez hidrofobikoak ere (4C irudia), bereziki, C528, K568 eta E571 aminoazidoak. C528 aminoazidoa LMB zein SINE konposatuen itua da. CRM1en inhibitzaile horiek C528 aminoazidoa kobalenteki lotzen dute, poltsiko hidrofobikoa betez, eta beraz, kargoen esportazioa inhibituz (4D irudia). Bestalde, K568 aminoazidoak NESen kate nagusiarekin hidrogeno-loturak ezartzen ditu NESak CRM1i ondo lotu daitezen. Gainera, NESen antzekoak diren baina NES aktiboak ez diren peptidoetarako galbahe ere badela proposatu da (Fung et al., 2017). Horretaz gain, K568 aminoazidoak, CRM1en funtzionamendu fisiologikorako garrantzitsua den E571 aminoazidoarekin elkarrekintza elektrostatikoa ere ezartzen du. E571 aminoazidoa, geroago sakonago azalduko den bezala, zenbait minbizitan mutaturik agertzen da (Puente et al., 2011), eta mutazio horrek efektu onkogenikoa ere baduela behatu da (Taylor et al., 2019).

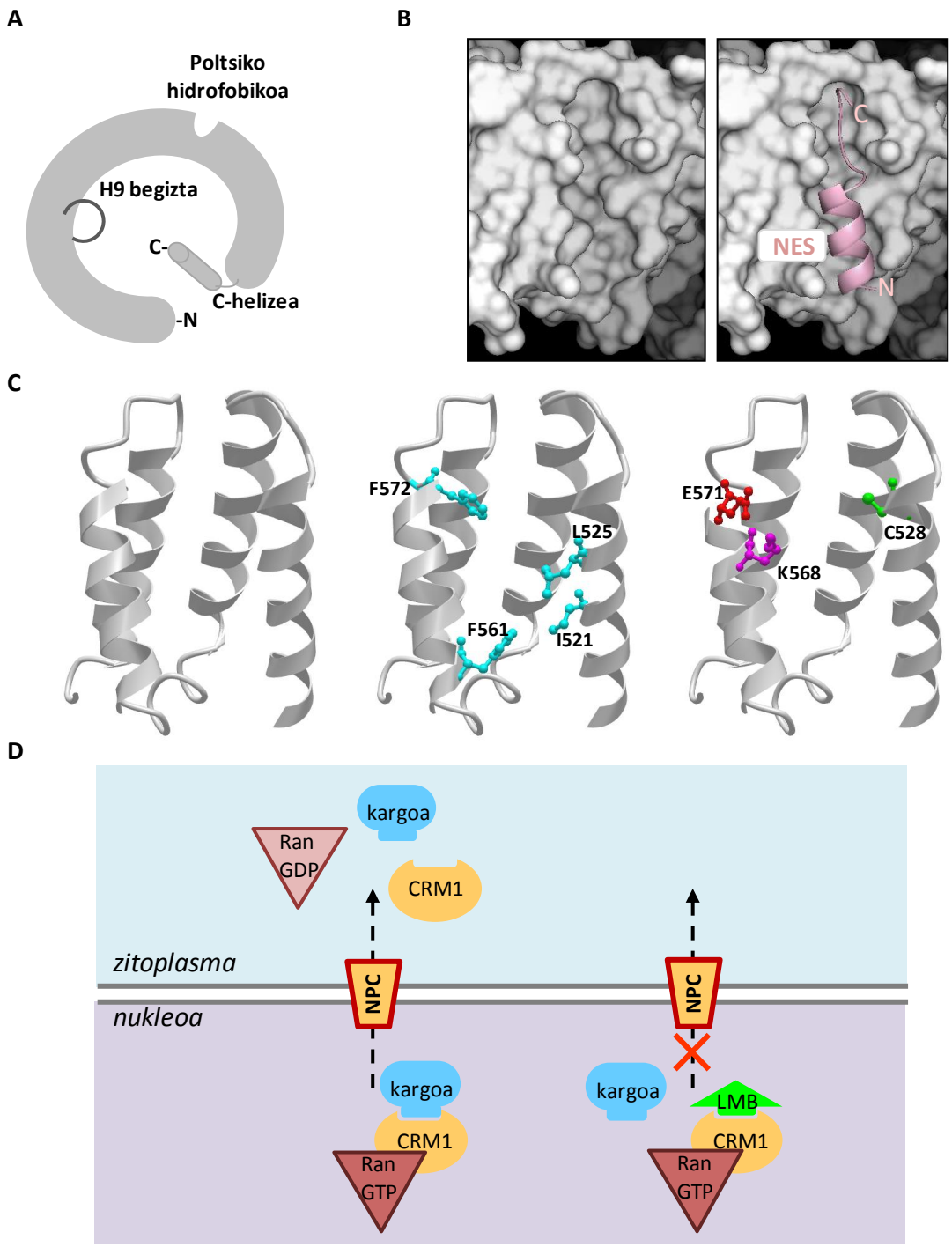

4. irudia: CRM1 proteina eta haren poltsiko hidrofobikoaren ezaugarri nagusiak eta CRM1en inhibizioa minbiziari aurre egiteko terapia bezala. A. CRM1 proteinaren egituraren irudi eskematikoa. NESak lotzen dituen poltsiko hidrofobikoa, eta poltsiko horren konformazioa erregulatzen duten C-helizea eta H9 begizta adierazten dira. B. UCSFko Chimera package (Pettersen et al., 2004) erabiliz eta CRM1en 3GJX estruktura (Monecke et al., 2009) erabiliz egindako poltsiko hidrofobiko hutsaren (ezkerrean) eta *plus* erako NESa (arrosa) loturik duen poltsikoaren (eskuman) irudiak. C. NCBIko iCn3D bisorearekin eta 3GJX estrukturarekin egindako poltsiko hidrofobiko hutsaren irudiak. Erdialdeko irudian, NESen loturarako gako diren aminoazido hidrofobikoak eta eskuinaldean, hidrofobikoak ez direnak baina NESen loturan edo CRM1en fisiopatologian garrantzitsuak diren aminoazidoak ageri dira. D. LMBk (edo SINE konposatuek) CRM1en poltsiko hidrofobikoa bete eta konplexu trimerikoaren eraketa oztopatzen dute. Ondorioz, kargoak ezin zaizkio CRM1i lotu eta horien esportazioa inhibiturik geratzen da.

1.3. CRM1en kargo eta NESen identifikaziorako hurbilketak

CRM1ek milatik gora kargo izan ditzakeela uste da, izan ere, egun, CRM1en 400 inguru kargo egiaztatu badira ere (http://prodata.swmed.edu/ LRNes/index.php; Xu et al., 2012; Fung et al., 2021), ikerketa proteomikoetan identifikatutako hainbat ustezko kargo konfirmatzeke daude oraindik ere (Thakar et al., 2013; Kirli et al., 2015). Guzti horietaz gain, kargo izateko inolako zantzurik ez dagoen beste horrenbeste proteina ere izan badirela uste da. Aipatu beharra dago, egiaztatu diren kargoen artean badirela NESa ezagutzen ez zaien hainbat proteina. Kargo eta motibo horien identifikazio eta karakterizazioan sakontzea ezinbestekoa da CRM1 fisiopatologia osotasunean ulertuko bada. Hori dela eta, tesi honetan CRM1en kargo berriak bilatu, eta kargo berri zein egiaztatutakoen NESak aztertu dira. Horretarako erabili diren hurbilketa esperimentalen (CRM1en inhibizioa, bioinformatika analisiak, esportazio-entseguak, ituratutako mutagenesia eta proteomika analisiak) funtsa deskribatuko da jarraian.

1.3.1. CRM1en inhibizioan oinarritutako esperimentuak

CRM1en kargoak identifikatzeko ohiko esperimentuetan zelulak LMBrekin tratatzen dira. Horrela, CRM1 inhibitu egiten da eta horren ondoriozko intereseko proteinen (endogenoak zein ektopikoki gainadierazitakoak) kokapen aldaketa azter daiteke.

Tipikoki, CRM1en kargo diren proteinek kokapen nuklearragoa agertuko dute CRM1 inhibitzean egoera basalean baino. Normalean, jokaera hori agertzen duten proteinak CRM1en kargo lez onartzen dira, eta agertzen ez dutenak baztertu. Hala ere, badira kasu jakin batzuk, zeintzuetan jokaera hori betetzeak ez duen proteina bat CRM1en kargo dela baieztatuko, eta ez betetzeak, ez duen ezeztatuko. Esaterako, CRM1en kargo den proteina batek kargo ez den beste proteina bat aldean eraman dezake (ingelesez *piggyback* mekanismoa bezala ezagutzen dena), eta ondorioz, kargo ez den proteinak kokapen nuklearragoa erakutsi zelulak LMBrekin tratatzean (Olazabal-Herrero et al., 2019). CRM1 inhibitzean kargo bat mekanismo ezberdinen bidez zitoplasman bahituta geratzea ere gerta daiteke, edota konstitutiboki nukleoan kokatzea. Lehenengoak aztertzeko zitoplasman bahituta geratzea eragiten duen mekanismo jakin hori zein den argitu eta inhibitu beharko da. Bigarrenak aztertzeko berriz, CRM1 gainadieraz daiteke, horrek konstitutiboki nukleoan kokatzen diren kargoen esportazioa nabarmenduko baitu kasu askotan (García-Santisteban et al., 2016, Taylor et al., 2019; Sendino et al., 2020a).

1.3.2. Analisi-bioinformatikoa: NES-iragarleak

NES-iragarleak proteinen aminoazido sekuentziak arakatu eta NESak izan daitezkeen sekuentziak, hau da, NES kandidatuak (*candidate NES*, cNES) bilatzeko gai diren tresna informatikoak dira. Badira cNESak bilatzeko NES-iragarle ezberdinak, esaterako, NetNES (la Cour et al., 2004), ELM (Gould et al., 2010), NESsential (Fu et al., 2011), NESmapper (Kosugi et al., 2014) edota Wregex (Prieto et al., 2014). NES-iragarle batek peptido-sekuentzia bat cNES gisara identifikatzeak ez du sekuentzia hori funtzionala izango denaren inolako ziurtasunik ematen. Izan ere, NES adostasun-sekuentzia betetzen duten aminoazido errenkadak asko badira ere, gehiengoa, ez da NES aktiboa. Beraz, NES-iragarleen bidez aurkitutako cNESak esperimentalki frogatu behar dira. Aktiboak direnetz jakiteko nahikoa izango da esportazio-entsegu baten bidez sekuentzia horien esportazio-aktibitatea aztertzea. cNESa proteina osoaren nukleotiko esportazioaren eragile dela baieztatzeko, aldiz, ituratutako mutagenesi esperimentuak egin beharko dira.

1.3.3. Esportazio-entseguak

Esportazio-entsegu gehienak cNESak bertan klonatzea ahalbidetuko duten plasmido erreportarietan oinarritzen dira. Erreportari mota ezberdinak daude, esaterako, $EYFP_2$-$SV40^{NLS}$ erreportaria (Fu et al., 2018), tesi honetan maiz erabili den Rev(1.4)-GFP erreportaria (Henderson eta Eleftheriou, 2000) edota tesi honetan SRV100 erreportarian (García-Santisteban et al., 2016) oinarrituz garatutako $SRV_{B/A}$ erreportaria (Taylor et al., 2019; Sendino et al., 2020a).

Erreportari horien kokapena era erraz batean aztertu ahal izateko, erreportariek, eskuarki, proteina fluoreszente bat edo antigorputzen bidez detektagarria den etiketa bat izango dute. Aipatutako erreportarien kasuan proteina fluoreszente edo etiketak, YFP, GFP eta Flag epitopoak dira hurrenez hurren. Etiketa horretaz gain, NES aktiborik izan ezean erreportaria nukleoan kokarazten duen seinaleren bat, NLSren bat (edo hainbat), ere izango dute. Horrela, erreportari batean cNES ez-aktibo bat klonatuz gero erreportaria nukleoan bahituta geratuko da (5. irudia). Kontrara, klonatutako cNESa aktiboa baldin bada, erreportariak zitoplasmaranzko kokapen aldaketa jasango du. Kontuan izan behar da, NES aktibo guztiek ez dutela aktibitate maila bera erakusten (Henderson eta Eleftheriou, 2000), eta beraz, zitoplasmaranzko lekualdaketa klonatutako cNES bakoitzaren aktibitatearen araberakoa izango da: cNESa zenbat eta aktiboagoa izan, erreportariak orduan eta kokapen zitoplasmatikoagoa agertuko du.

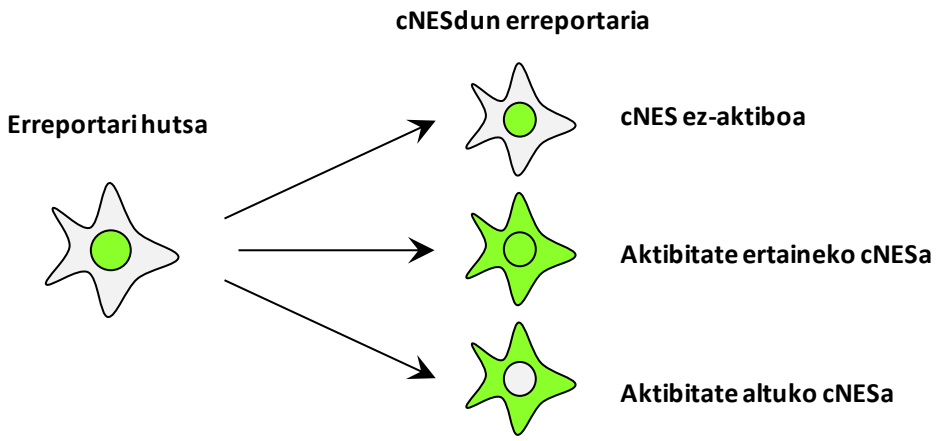

5. irudia: Esportazio-entseguetako emaitza posibleen adibidea. Esportazio-entseguetan erabili ohi diren erreportari hutsak nukleoan kokatzen dira NLSak direla eta. cNES bat erreportari horietako batean klonatzean, kodetutako proteinak kokapen zelular ezberdina agertuko du klonatutako cNESaren aktibitatearen arabera. Horrela, klonatutako cNESa aktiboa ez baldin bada, erreportaria nukleoan geratuko da, cNESa aktiboa bada ordea, erreportariak cNESaren aktibitatearen araberako zitoplasmaranzko lekualdaketa jasango du.

1.3.4. Ituratutako mutagenesia

NES sekuentzia batek proteina osoaren esportazioa eragiten duela baieztatu nahi baldin bada, proteinaren NESaren aminoazido hidrofobikoak (normalean Φ^3 eta Φ^4) mutatu eta horrek proteina osoaren testuinguruan duen eragina aztertu behar da (6. irudia) (Olazabal-Herrero et al., 2019; Sendino et al., 2020b). Proteina mutanteak proteina basatiaren kokapen bera mantentzen badu, identifikatutako NESak ez du proteina osoaren esportazioa bideratzen, aldiz, kokapen nuklearragoa erakusten badu, NES horrek badu zerikusia proteina osoaren esportazioan.

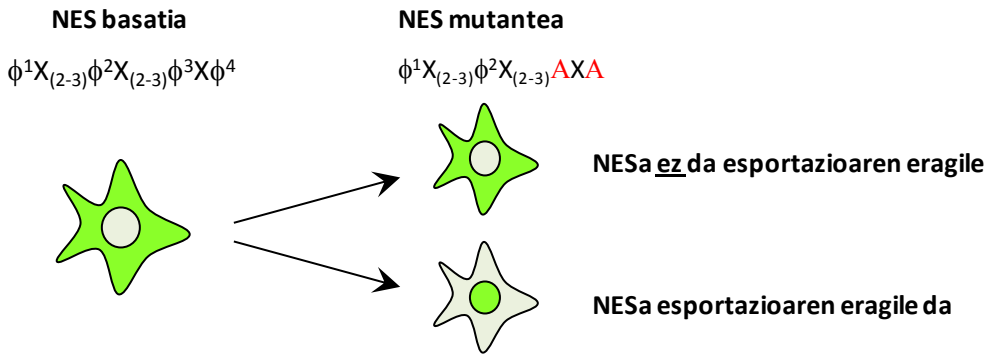

6. irudia: NES jakin batek proteina osoaren esportazioan duen eragina aztertzeko esperimentuaren adibidea. Identifikatutako NESaren aminoazido hidrofobikoak, normalean ϕ^3 eta ϕ^4, alaninaz ordezkatzen dira. Ikergai den NESak proteina osoaren esportazioan eragina badu, NES mutantedun proteinak proteina basatiak baino kokapen nuklearragoa erakutsiko du.

1.3.5. Analisi proteomikoak

Proteina jakin baten funtzioa osotasunean ulertzeko berarekin elkarri eragiten duen proteina multzoa, hots, bere interaktoma, ezagutu behar da. Hori, tandem masa-espektrometrian (MS/MS) oinarritutako proteomika erabiliz iker daiteke (Aebersold eta Mann, 2003).

Esan bezala, egun CRM1en kargo ugari ezagunak badira ere, ez da oraindik CRM1en esportazio-kargo bilduma osoa, CRM1en esportoma, ezagutzen. Era berean ez da ezagutzen CRM1en inhibizioak edota mutazioek CRM1en esportoman duten eragina ere. Guzti horrek, CRM1 proteomikarako aztergai oso interesgarria bilakatzen du.

CRM1en esportoma karakterizatzeko proteomikan oinarritutako hiru lan baino ez dira argitaratu. Horietako bik, Thakar eta Kirliren taldeek argitaratutakoek, CRM1 basatiaren esportoma dute ikergai (Thakar et al., 2013; Kirli et al., 2015), hirugarrenak berriz, Taylorren taldeak argitaratutakoak, minbizian maiz agertzen den CRM1en E571K mutazioak esportoman duen eragina (Taylor et al., 2019). Aipaturiko hiru ikerketetan, proteomika-laginak prestatzerako orduan oso ohikoak diren bi prozedura erabili dira: frakzionamendu zelularra eta afinitate-purifikazioa. Azken aldian garatu diren beste prozedura batzuk ere badira, esaterako proteinen gertuko markaketa. Prozedura berriok ez dira oraindik CRM1en esportoma ikertzeko erabili, hala ere, proteinen gertuko markaketa helburu horretarako prozedura interesgarria izan daitekeelakoan tesi honetan aukera hori ikertu da.

1.3.5.1. Frakzionamendu zelularra

CRM1en esportoma aztertzen duten ikerketetatik bik (Thakar et al., 2013; Taylor et al., 2019) frakzionamendu zelularra erabiltzen dute. Prozedura hori zelula edo ehunak bere barne konpartimenduak (esaterako, nukleoa eta zitoplasma) bere baitan mantenduz hautsi eta osagai horiek banatzean datza. Zelula edo ehunen hausturarako metodoak mekanikoak edo kimikoak izan daitezke, esaterako lagina sonikatzea edo medio hipotonikoan inkubatzea hurrenez hurren. Osagaien banaketarako metodo klasiko eta sinpleenak lagina hainbat zentrifugazio urratsetan banatzean edo lagina dentsitate gradiente batean zehar pasaraztean daude oinarrituta (7. irudia) (Lee et al., 2010-n berrikusia).

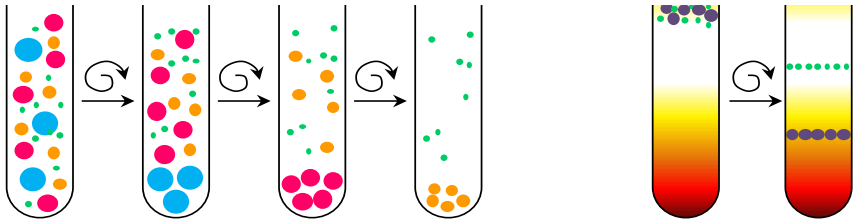

7. irudia: Frakzionamendu zelularrerako metodo klasikoak. Ezkerreko irudian laginean dauden osagaiak zentrifugazio diferentziala erabilita, hau da, ondoz ondoko zentrifugazio urratsetan nola banatzen diren irudikatzen da. Zentrifugazio bakoitzaren ostean gainjalkina jaso eta bertan geratu diren osagaiak banatzeko berriz ere zentrifugatu egiten da. Eskumako irudian dentsitate gradientearen arabera lagineko osagaiak nola banatzen diren ageri da. Tutuan dentsitate gradiente bat prestatzen da, eta lagina dentsitate gradiente horretan zehar pasarazten da. Horrela, osagai bakoitza bere dentsitate bera duen gradientearen zonaldean geratuko da.

Frakzionamendu zelularrak duen mugarik nabariena, konpartimentuen arteko kutsatzeak ekiditeko laginak prestatzerako orduan trebezia handia behar izaten dela da (Bosch et al., 2021-n berrikusia).

1.3.5.2. Afinitate-purifikazioa

CRM1en esportoma afinitate-purifikazioan oinarrituz ere ikertu izan da (Kirli eta al., 2015). Afinitate-purifikazio terminoak, orokorrean euskarri fisiko batean immobilizaturik dagoen estekatzaile espezifiko bat erabiliz laginetako intereseko materiala isolatzeari egiten dio erreferentzia (8. irudia). Euskarri fisikoak agarosazko bihitxoak edo bihitxo magnetikoak izaten dira gehienetan. Estekatzaileak askotarikoak izan daitezke, erabilienak baina, antigorputzak dira. Proteina endogenoen kontrako antigorputzak erabiltzea egoera fisiologikoaren azterketa ahalbidetuko du, askotan, ordea, ez da posible izaten intereseko proteinaren aurkako antigorputz espezifikorik aurkitzea. Beraz, nahiz eta proteina ektopikoen bidez berezkoa ez den egoera bat sortu, askotan probetxugarriago izaten da intereseko proteinari GFP edo Flag bezalako epitopo bat gehitzea eta epitopo horren kontrako antigorputz espezifikoak erabiltzea (Dunham et al., 2012-en berrikusia).

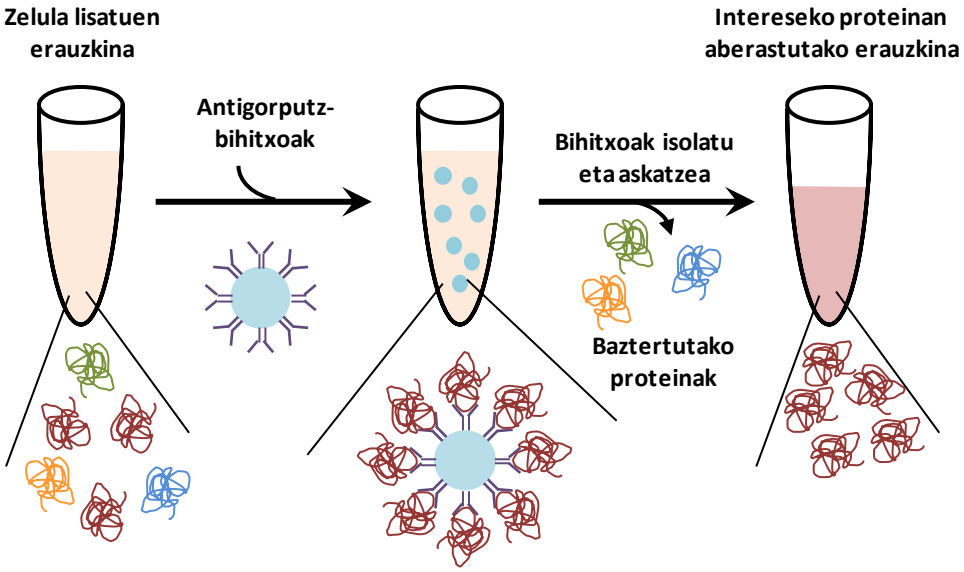

8. irudia: Afinitate-purifikazio metodoaren adibide eskematikoa. Zelula lisatuen erauzkinera interesezko proteinaren aurkako antigorputz-bihitxoak gehitzen dira. Nahasketa hori inkubatu egiten da bihitxoetako antigorputzek intereseko proteina lotu dezaten. Behin antigorputz-proteina elkarrekintza eman dela, bestelako proteinak laginetik baztertzen dira hainbat garbiketa urrats eginez. Garbiketa urrats horien baldintzak erabakigarriak dira intereseko proteina purutasun altuaz isolatu ahal izateko. Bukatzeko, bihitxoetako antigorputzen eta intereseko proteinaren elkarrekintza hautsi egingo da, adibidez, lagina irakinez. Horrela, bihitxoak baztertu eta intereseko proteina isolatu ahal izango da.

CRM1en esportoma ikertzeko, Kirli eta lankideek (2015) CRM1 bera immobilizaturik zuten agarosazko bihitxoak erabili zituzten. Bihitxo horiek erabilita, eta mediora RanGTP gehituta edo gehitu gabe, CRM1ekin elkarrekiten zuten proteinak aztertu zituzten. Behin garraio nukleozitoplasmatikoaren makineriaren osagaiak baztertuta, CRM1en esportoma RanGTPa gehitutako laginean aberastuta ageri ziren CRM1en interaktoreen bilduma bezala definitu zuten.

Tesi honetan, afinitate-purifikazioa bi hurbilketa ezberdinetan erabili da. Lehenengo hurbilketan, CRM1 basatia eta minbizi mutantea den E571K mutantea YFPrekin fusionatu eta epitopo hori ezagutzen duten GFParen aurkako antigorputz-bihitxoak erabili dira CRM1en aldaeron interaktomak isolatzeko helburuz. Interaktoma horien erkaketaz E571K mutazioak esportoman eragindako aldaketak azter daitezke. GFParen aurkako antigorputz-bihitxoak erabiliz emaitza onik ez da jaso eta bestelako hurbilketa bat erabiltzea erabaki da. Bigarren hurbilketa horretan, neutrabidina estekatzailea duen afinitate-purifikazioa CRM1en inhibizioarekin eta APEX2 peroxidasan oinarritutako proteinen gertuko biotinilazioarekin uztartu da. Horrela, CRM1 aktibo edo inhibiturik dagoela nukleo eta zitoplasmako proteomak era bereizian markatu eta isolatu dira (Sendino et al., 2021).

Agerikoa da beraz, afinitate-purifikazioak proteomikaren bidez aztertuko diren laginen prestaketarako aukera zabala eskaintzen duela. Hala ere, kontuan izan behar da ohikoa dela ahulak diren interakzioak galtzea (Bosch et al., 2021). Arazo horrek CRM1en esportoma aztertzerako orduan zuzeneko eragina du, izan ere, CRM1 eta bere kargoen arteko lotura oso ahula izaten da (Kutay eta Güttinger, 2005), eta beraz, prozesuan zehar CRM1en interaktoreen galera gerta daiteke.

1.3.5.3. Proteinen gertuko markaketa

Proteinen gertuko markaketa entzima-markatzaileen erabileran oinarritzen da. Substratu egokiaren presentzian, entzima horiek, inguruko proteinak kobalenteki markatzeko gai izango diren erradikal askeak eratuko dituzte. Erradikal askeak ugariagoak dira entzima markatzailetik gertu, eta ondorioz, entzimaren gertuko proteinek urrunekoek baino marka kobalente gehiago jasoko dute (Gingras et al., 2019). Markatutako proteinak gainontzeko proteinetatik afinitate-purifikazioz isolatuko dira. Jarraian, isolatutako proteina bilduma MS/MS bidez analizatuko da lagineko proteinak identifikatu ahal izateko (9. irudia).

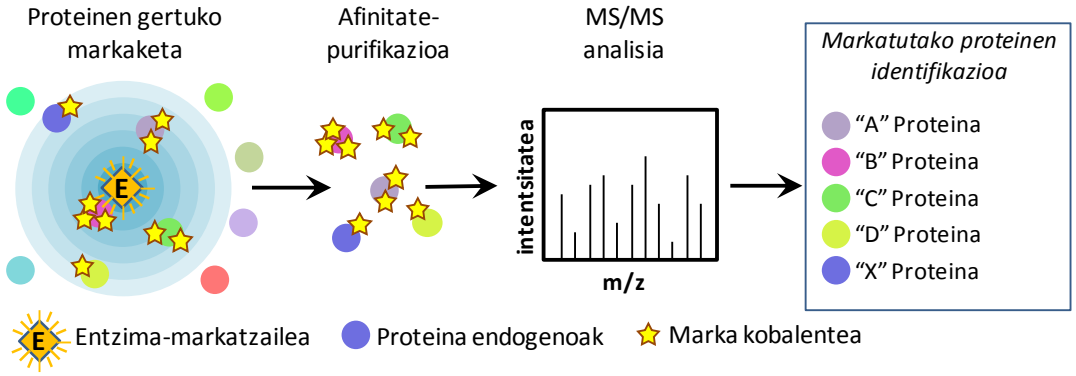

9. irudia: Proteinen gertuko markaketa bidezko proteinen identifikazioa. Entzima-markatzaileak, beharrezko substratuaren presentzian, inguruko proteinetan marka kobalenteak ezarriko ditu. Marka horiei esker, entzimatik gertu zeuden proteinak afinitate-purifikazioaren bidez isolatu ahal izango dira. Azkenik, purifikatutako proteinak MS/MS bidez identifikatuko dira.

Egun, gertuko markaketa egiteko gehien erabiltzen diren entzima-markatzaileak proteinen biotinilazioa eragiten dutenak dira, bereziki BirA motatako biotina-ligasak eta APX familiako peroxidasak (Bosch et al., 2021-en, eta Zhou eta Zou, 2021-en berrikusia).

1.3.5.3.1. BirA motako biotina-ligasak

Biotina-ligasek biotina eta ATPren presentzian lisinak erasoko dituen biotinil-5'-AMP erradikal-askea eratzen dute. Biotina-ligasetan oinarritutako proteinen gertuko markaketa metodologia 2012. urtean hasi zen garatzen, Roux eta lankideek BioID (*Biotin identification*) izena eman zioten markaketa sistema erabiliz lamina nuklearraren proteoma aztertu zutenean. BioID sisteman *Escherichia coli* bakterioaren BirA* izenaz ezaguna den BirA entzimaren R118G mutante promiskuoa (Kwon eta Beckett, 2000; Choi-Rhee et al., 2004; Cronan, 2005) interesezko kokapenera ituratzen da. Behin BirA* intereseko kokapenean dagoela, medioan biotina gehitzen da 15-24 orduko epean proteinen gertuko biotinilazioa (PGB) eman dadin (10. irudia) (Bosch et al., 2021-en berrikusia).

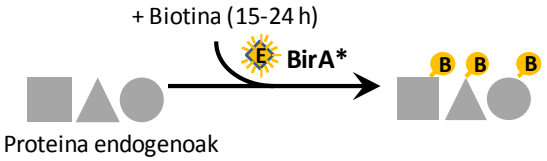

10. irudia: BirA* biotina-ligasak eragindako proteinen gertuko biotinilazioa. BirA* ligasa biotina mediora gehitu bezain pronto gertuko proteinak biotinilatuko dituzten erradikal askeak sortzen hasten da. Lagineko nahikoa proteinek biotina marka jasotzeko biotinilazio prozesua 15-24 orduz luzatu ohi da.

BioID sistema erabiliz lamina nuklearraren proteomaz gain, beste proteoma eta interaktoma asko ikertu dira, adibidez, nukleoko poro konplexuaren (Kim et al., 2014) edo mRNArekin erlazionatutako granuluen proteomak (Youn et al., 2018), eta, ugaztunon erribosomen kalitate kontroleko konplexuaren (Zuzow et al., 2018) edota NSD2 histona metiltransferasaren

interaktomak (Huang et al., 2019). Oso hedaturik dagoen arren, BioID sistemak baditu hainbat muga. Alde batetik, BirA* proteina oso handia ez bada ere, 35 kDa, proteina jakin batzuen interaktoma aztertzean elkarrekintza jakinak oztopa ditzakeela ikusi da (Kim et al., 2016a). Bestetik, BioID bidezko biotinilazioa prozesu nahiko geldoa da, eta beraz, nukleotiko esportazioa bezalako prozesu oso dinamiko edo momentu iragankorrak metodologia horren bitartez aztertzea ez da posible izaten.

Oztopo horiei aurre egiteko biotina-ligasetan oinarritutako beste metodologia batzuk garatu dira. BioID2 sisteman, adibidez, BirA* baino nabari txikiagoa den (27 kDa), *Aquifex aeolicus* bakterioaren BirA entzimaren R40G mutante promiskuoa erabiltzen da (Kim et al., 2016a). BioID2 bidez, kardiomiozito primarioen N-kaderinaren (Li et al., 2019), mitokondrio barneko PKAren (Ould-Amer eta Hebert-Chatelain, 2020) edota p38α MAP kinasaren (Prikas et al., 2020) interaktomak aztertu dira. Erreakzio denbora murrizten duten irtenbideak ere topatu dira. 2018an 10 minutuko epean inguruko proteinak biotinila ditzaketen bi sistema garatu ziren, TurboID eta MiniTurbo (Branon et al., 2018). Biotina-ligasetan oinarrituta proteinen gertuko markaketarako garatutako azken metodoa AirID sistema da (Kido et al., 2020), zeinetan markaketa-erradioa murriztuz analisi proteomikoetan faltsu positibo gutxiago gertatzea lortu den.

1.3.5.3.2. APX motako peroxidasak

Peroxidasei dagokienez, egun gehien erabiltzen direnak ilar edo sojaren APX askorbato peroxidasan dute oinarria. APXn oinarritutako lehen entzima-markatzailea APEX peroxidasa izan zen. APEX 28 kDa-etako entzima monomerikoa da, eta APX entzima homodimerikoan K14D/W41F/E112K mutazioak eraginez sortu zen (Martell et al., 2012). Hasiera batean, APEX mikroskopio elektronikorako laginen prestaketarako zitoplasma bezalako inguru erreduzitzaileetan aktibitatea mantentzen duen entzima baten beharra asetzeko sortu zen, gerora ordea, mikroskopio elektronikorako laginak prestatzeko aproposa izateaz gain, MS/MSrako laginak prestatzeko ere aproposa dela ikusi zen (Rhee et al., 2013). Izan ere, APEX entzimak biotin-fenola substratutzat hartuta, eta H_2O_2-rekin aktibatzen bada, biotin-fenoxil erradikalak sortzen ditu (Rhee et al., 2013). Erradikal aske horiek gertuko proteinen tirosina, triptofano, histidina eta zisteina aminoazidoak eraso ditzakete. Horrela, minutu bateko epean entzimatik gertu dauden proteinak biotinaz kobalenteki markatuta geratuko dira (11. irudia). APEX entzima erabiliz, giza mitokondrioen matrizeko (Rhee et al, 2013), mintz mitokondrialen arteko espazioa (Hung et al., 2014) edo zilio primarioen proteomak (Mick et al., 2015) ikertu dira adibidez.

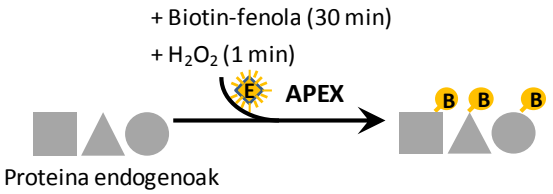

11. irudia: APEX peroxidasak eragindako proteinen gertuko biotinilazioa. APEX (edo APEX2) gainadierazten duten zelulak biotin-fenolarekin (substratuarekin) inkubatu behar dira ordu erdiz zelulek substratua barnera dezaten. Jarraian, H_2O_2-a gehituz APEX peroxidasa aktibatu egiten da eta minutu bateko epean inguruko proteinen biotinilazioa ematen da.

APEX peroxidasa proteoma zein interaktomak aztertzeko oso erabilia izan bada ere, aktibitate biotinilatzailea hobetu zitekeenaren usteaz Lam eta lankideek, APEX peroxidasatik abiatuz hainbat mutazio frogatu zituzten. Azkenik, A134P mutaziodun APEX entzimak, APEX2 izenaz ezagutzen dena, jatorrizko APEX entzimak baino aktibitate nabarmen altuagoa duela ikusi zuten (Lam et al., 2015). APEX2 peroxidasak gertuko proteinak markatzeko beharrezko prozedura, APEX peroxidasarena berdina da (ikusi 11. Irudia). APEX2 peroxidasa erabiliz, esaterako, lamina nuklearrareko lamin-B1 proteinaren (Tran et al., 2021), FGF1en (Zhen et al., 2018), ugaztunon erribosomen kalitate konplexuaren (Zuzow et al., 2018) eta STK38 kinasaren (Martin et al., 2019) interaktomak edota tantaka lipidikoen (Bersuker eta Olzmann, 2019) proteomak aztertu dira.

Proteinen gertuko markaketa proteoma eta interaktoma aunitz aztertzeko erabili bada ere, gaur egun arte ez da CRM1en esportoma aztertzeko erabili, ezta, jakina, CRM1en inhibizioak eragindako kargoen kokapen aldaketak aztertzeko ere. Hori dela eta, tesi honetan, metodologia horretan oinarriturik hurbilketa berri bat sortu da azterketa horiek aurrera eraman ahal izateko (Sendino et al., 2021).

1.4. CRM1en inhibizioa minbiziaren aurkako hurbilketa terapeutiko bezala

Atal honetan CRM1ek minbiziarekin duen erlazioa eta haren inhibizioa minbizia tratatzeko estrategia bezala erabiltzen duten ikerketetan jasotako emaitzak deskribatuko dira. Lehenik eta behin, tumore ezberdinak aztertzean CRM1 kodetzen duen genean (*XPO1*) aurkitu diren mutazio eta gainadierazpen erako asaldurak azalduko dira. Jarraian, CRM1en inhibitzaile diren SINEak, bereziki selinexor, minbiziari aurre egiteko erabiltzen duten ikerketa prekliniko eta klinikoetan jasotako emaitzak berrikusi eta azalduko dira.

Aipatu beharra dago, SINEak gehien bat minbizia tratatzeko terapia bezala ikertu badira ere, mielinaren degradazioa eragiten duten gaixotasunak (Haines et al., 2015) edo infekzio birikoak (Pickens eta Tripp, 2018; Kashyap et al., 2021) tratatzeko ere erabilgarriak izan daitezkeela. Ildo horretan, selinexor farmakoa COVID-19 tratatzeko erabiltzen duten bi entsegu kliniko (NCT04349098 eta NCT04534725) daude ClinicalTrials webgunean (https://clinicaltrials.gov/). Lehenengo entseguan selinexor COVID-19 akutua duten gaixoak tratatzeko erabiltzen da. Bigarrenean aldiz, COVID-19 arina duten baina paziente onkologikoak direnak tratatzeko.

1.4.1. Proteinen kokapen nukleozitoplasmatikoaren asaldura minbizian

Proteina zelular jakinen kokapen egokia mantendu ezean, gaixotasun larriak sor daitezke. Hain da horrela, non, minbiziarekin erlazionatutako proteinen kokapen nukleozitoplasmatikoaren asaldura ohiko gertakaria den tumore zeluletan. Esaterako, egoera fisiologikoetan nukleoan kokatzen diren p53 edo BRCA2 bezalako tumore ezabatzaileak zitoplasman kokatzen badira, euren aktibitatea galdu eta tumoregenesia bultza dezakete (Hung eta Link, 2011; Hill et al., 2014; Wang eta Li, 2014; Dickmanns et al., 2015).

Minbizi zeluletan proteinen kokapen nukleozitoplasmatikoa asalda dezaketen mekanismoak hainbat dira. Batetik, proteina jakin baten garraio normala eragozten duten mutazioak gerta daitezke, mutazio horiek proteina basatiak duen NES edo NLS baten aktibitatea murritz dezakete, edota seinale berri bat sortu. Adibidez, BRCA2 tumore ezabatzailearen mutazio jakinak normalean eskuragarri ez dagoen NES seinale bat eskuragarri egin eta proteina horren kokapen zitoplasmatiko aberrantea eragin dezake (Jeyasekharan et al., 2013). Modu bertsuan, NPM1 onkoproteinan irakurtarauaren aldaketa eragiten duten mutazioak deskribatu dira. Mutazio horien ondorioz, NES seinale berri bat sortu, eta NPM1ek kokapen zitoplasmatiko aberrantea erakusten du (Mariano et al., 2006). Bestetik, akatsa garraio makinerian bertan egon daiteke (Mor et al., 2014), bai makineria horren pieza bat mutaturik dagoelako,

esaterako, minbizi hematologikoetan maiz gertatzen diren eta CRM1en mendeko esportazioa asaldatzen duten NUP98 eta NUP214 nukleoporinei eragiten dieten translokazio kromosomikoak (Takeda et al., 2010; Takeda eta Yaseen, 2014; Saito et al., 2016), bai piezaren baten adierazpena asaldatuta dagoelako, adibidez, β-inportina hartzailearen gainadierazpena (Wang eta Li, 2014). Garraio makineriaren akatsek proteina askoren, eta maiz RNAren, kokapenean aldaketak eragingo dituzte.

CRM1en kasuan, hartzailearen funtzio normalari eragin diezaioketen mutazioak zein adierazpen aberrantea behatu izan dira minbizi mota ezberdinetan. Asaldura horiek CRM1en kargo diren proteina askoren kokapen nukleozitoplasmatiko ezohikoa eragin dezakete.

1.4.1.1. CRM1en mutazioak minbizian: E571 aminoazidoaren mutazio errepikakorra tumore hematologikoetan

Tumore hematologiko ezberdinetan CRM1en E571 azido glutamikoari eragiten dioten ordezkapen mutazioak (gehienbat E571K) aurkitu dira maiz (2. taula). Azpimarratzekoa da, orain dela gutxi, mutazio horrek onkogenesi prozesua bultzatzen duela frogatu dela (Taylor et al., 2019).

2. taula: Tumore hematologiko ezberdinetan aurkitutako CRM1 E571 mutazioaren maiztasuna. Taula honen bertsio luzatua 1. taula gehigarrian ikus daiteke.

Minbizi mota	Mutazioaren maiztasuna	Erreferentziak
Leuzemia linfozitiko kronikoa (CLL)	317/6126 (% 5,17)	Puente et al., 2011; Quesada et al., 2011; Balatti et al., 2012; Landau et al., 2013, 2015; Damm et al., 2014; Jeromin et al., 2014; Lawrence et al., 2014; Messina et al., 2014; Guièze et al., 2015; Hernández et al., 2015; Ojha et al., 2015; Sutton et al., 2015; Vollbrecht et al., 2015; Amin et al., 2016; Jain et al., 2016; Cosson et al., 2017; Quijada-Álamo et al., 2017; Takahashi et al., 2018; Hu et al., 2019; Taylor et al., 2019; Gángó et al., 2020; Machnicki et al., 2020
B-zelulen linfoma mediastinal primarioa (PMBL)	36/138 (% 26,09)	Dubois et al., 2016; Jardin et al., 2016; Taylor et al., 2019
Hodgkin linfoma (HL)	69/374 (% 18,45)	Camus et al., 2016, 2021; Jardin et al., 2016; Tiacci et al., 2018; Liang et al., 2019; Wienand et al., 2019; Taylor et al., 2019; Van Slambrouck et al., 2020
B-zelula handien linfoma hedatsua (DLBCL)	25/1187 (% 2,11)	Dubois et al., 2016; Jardin et al., 2016; Taylor et al., 2019
Trikoleuzemia (HCL)	1/24 (% 4,2)	Maitre et al., 2018
B-zelula helduen neoplasma	1/12 (% 8,3)	Taylor et al., 2019
Area marginaleko linfoma (MZL)	1/4 (% 25)	Taylor et al., 2019

CRM1en E571K mutazio errepikakorra orain 10 urte deskribatu zen lehendabizi leuzemia linfozitiko kronikoko (CLL) pazienteetan (Puente et al., 2011). Mutazio hori CLL gaixoen % 5ak agertzen du (ikusi 2. taula) eta IGHV (*immunoglobulin heavy-chain variable*) ez-mutatuarekin erlazionatu izan da maiz (Puente et al., 2011; Jeromin et al., 2014; Jain et al., 2016). IGHV ez-mutatua CLL pazientetan prognosi okerrarekin erlazionatzen bada ere, CRM1en mutazioa ez da pronostiko okerrarekin erlazionatu (Jain et al., 2016). CRM1en E571K mutazioa ohiko gertakaria da Hodgkin linfoma (HL, % 18) eta B-zelulen linfoma mediastinal primario (PMBL, % 26) gaixoen artean ere. CLL gaixoekin gertatzen den bezala, HL gaixoetan ere ez da mutazioaren eta pronostiko okerraren arteko erlaziorik topatu (Camus et al., 2016); PMBL gaixoetan aldiz, mutazioa progresio gabeko biziraupen laburragoarekin korrelazioan dago (Jardin et al., 2016). Gainera, CRM1en E571K mutazioa hondar-gaixotasun minimoaren biomarkatzaile moduan erabiltzea planteatu da HL zein PMBL pazienteetan (Camus et al., 2017). CRM1en E571 mutazioa zenbait tumore solidotan topatu izan bada ere, tumore hematologikoetan baino maiztasun askoz ere baxuagoan aurkitzen da horrelakoetan (Lin et al., 2014, Pitt et al., 2016; Taylor et al., 2019).

E571 aminoazidoa CRM1ek NESak lotzeko duen poltsiko hidrofobikotik hurbil kokatzen da (ikusi 4C irudia). Kokapen horrek, lotura zuzena izan dezake CRM1en E571K mutazioak C-muturra negatiboki kargaturik duten NES batzuen esportazioa emendatzearekin (García-Santisteban et al., 2016).

1.4.1.2. CRM1en adierazpen aberrantea giza minbizietan

CRM1en adierazpen maila, bai mRNA bai proteina mailan, zenbait minbizitan ikertu da, eta salbuespenak badiren arren (Xie et al., 2016), orokorrean minbizi ehunetan gainadierazita dagoela aurkitu da (Noske et al., 2008; Huang et al., 2009; Shen et al., 2009; Yao et al., 2009; Pathria et al., 2012; Akagi et al., 2013; Inoue et al., 2013; Kojima et al., 2013; Schmidt et al., 2013; Zhang et al., 2013; Zhou et al., 2013; Tai et al., 2014; van der Watt et al., 2014; Yang et al., 2014a; Liu et al., 2016; Sun et al., 2016, 2017; Conforti et al., 2017; Saulino et al., 2018; Xia et al., 2018; Yue et al., 2018; Birnbaum et al., 2019; Chen et al., 2019; Cruz-Ramos et al., 2019; Duijvesz et al., 2019; Fan et al., 2020; Jiang et al., 2020; Wu et al., 2020; Zhu et al., 2020). Gainadierazpen hori gainera, pronostiko txarrarekin erlazionatu da hainbat minbizitan, hala nola, leuzemia mieloide akutuan (AML; Kojima et al., 2013), B-zelula handien linfoma hedatsuan (DLBCL; Fan et al., 2020), mieloma anizkoitzean (MM; Tai et al., 2014), glioman (Shen et al., 2009; Liu et al., 2016; Wu et al., 2020), biriketako zelula ez-txikien minbizian (NSCLC; Akagi et al., 2013), timo epitelioko tumoreetan (Conforti et al., 2017), obulutegiko minbizian (Noske et al., 2018), hestegorriko zelula eskatatsuen kartzinoman (van der Watt et

al., 2014; Yang et al., 2014a), pankrea minbizian (Huang et al., 2009; Birnbaum et al., 2019; Zhu et al., 2020), bularreko minbizian (Yue et al., 2018) edota kartzinoma hepatozelularrean (Chen et al., 2019). Badira CRM1en gainadierazpenaren eta pronostiko okerraren artean ezarritako korrelazioa betetzen ez duten salbuespen batzuk. Esaterako, urdaileko minbizian (Zhou et al., 2013; Sun et al., 2017) eta osteosarkoman (Yao et al, 2009; Jiang et al., 2020), zeintzuetan ez dagoen argi gainadierazpenaren eta pronostikoaren artean korrelaziorik ote dagoen. Guzti hori 2. taula gehigarrian dago zehatzago deskribatuta.

CRM1en adierazpen maila altuagoak haren kargo askoren banaketa nukleozitoplasmatikoa asalda lezakeela pentsa badaiteke ere, oraindik ez dira gainadierazpen horren ondorio molekularrak guztiz argitu. CRM1en gainadierazpena eragiten duten mekanismo molekularrak ere ez dira oraindik guztiz argitu. Zenbait linfoma (Jardin et al., 2016) eta leuzemia linfozitiko kronikoan (CLL; Cosson et al., 2017) CRM1en mRNAren gainadierazpena eta *XPO1* genea dagoen 2p eskualde kromosomikoaren anplifikazioarekin korrelazioan dagoela topatu da. Bestalde, CRM1en transkripzioa minbizian maiz asaldaturik aurkitzen diren cMyc eta p53 (van der Watt eta Leaner, 2011; Golomb et al., 2012) proteinek erregulatzen dutela ikusi da ere. Beraz, baliteke, cMyc edo p53 proteinek tumore jakin batzuetan agertzen duten asaldurak CRM1en gainadierazpen aberrantearen erantzuleak izatea.

1.4.1.3. CRM1en inhibizioa minbiziaren aurkako terapian

1.4.1.3.1. Esportazio nuklearraren inhibitzaile hautakorren (SINEen) garapen eta azterketa preklinikoa

CRM1 minbiziaren kontrako itu bezala identifikatu aurretik, LMBk tumoreen aurkako aktibitatea duela aurkitu zen. Horrek, LMB entsegu kliniko batean erabiltzea eragin zuen, lortutako emaitza, ordea, ez zen esperotakoa izan. Izan ere, LMBk toxikotasun altua erakutsi zuen pazienteetan (Newlands et al., 1996), eta beraz, minbiziaren aurkako farmako gisa baztertu zuten.

Pazienteetan erabiltzeko alboratu bazen ere, LMBrekin egindako *in vitro* esperimentuak CRM1en inhibizioa minbiziaren tratamendurako baliagarria izan zitekeenaren kontzeptu-froga izan ziren. Esperimentu horietako adibide bezala, leuzemia mieloide kronikoko (CML) zelulatan egindakoak aipa daitezke.

CRM1 nukleotiko esportazio hartzaile bezala deskribatu eta gutxira, c-ABL kinasa CRM1en kargo zela aurkitu zen. c-ABL kinasaren NESa haren C-muturrean dago, eta BCR-ABL fusio proteinan kontserbaturik dago (Taagepera et al., 1998). Garai hartan, BCR-ABL fusio proteina adierazten zuten pazienteen tratamenduak izugarri egin zuen hobera imatinib kinasa

inhibitzaileari esker (Druker et al., 1996; le Coutre et al., 1999). Guzti hori kontuan izanik, CML zelulak imatinib eta LMB konbinazioarekin tratatu ziren eta BCR-ABL onkoproteina nukleoan bahituta geratzen zela, eta CML zelulen apoptosia eragiten zela frogatu zen (Vigneri eta Wang, 2001). Beranduago egindako esperimentuetan, LMBk imatinibarekiko erresistentzia gainditzea eragin dezakeela ikusi zen (Kancha et al., 2008).

CRM1en inhibizioa minbiziari aurre egiteko estrategia eraginkorra izan daitekeela iradoki zuten *in vitro* egindako zenbait ikerketen emaitzek (Turner eta Sullivan, 2008-en berrikusia). Horrek, klinikan erabilgarriak izan daitezkeen CRM1en inhibitzaileak lortzeko premia sortu zuen. Gerora CRM1 inhibitzeko gai diren hainbat konposatu natural zein sintetiko aurkitu dira (Senapedis et al., 2014-n, eta Tan et al., 2014-n berrikusia). LMBren antzera, konposatu horiek, CRM1en C528 aminoazidora kobalenteki lotzen dira, CRM1en poltsiko hidrofobikoa betez, eta hortaz, bertara NESak lotzea ekidinez. Inhibitzaile horietako batzuk, esaterako CBS9106 edo S109, LMB ez bezala, CRM1 era itzulgarrian inhibitzen dute, eta *in vivo* eginiko ikerketa preklinikoetan LMBk duena baino toxikotasun baxuagoa erakutsi dute (Sakakibara et al., 2011; Liu et al., 2016). Inhibitzaile berriekin eginiko ikerketek CRM1 inhibitzeak minbiziari aurre egiteko izan dezakeen onura are nabariagoa egin dute (Turner et al., 2009).

CRM1en inhibitzaile gehienak *in vitro* edo sagu heteroinjertoetan baino ez dira entseatu. SINE familiako konposatu batzuk ordea, entsegu kliniko aurreratuetan frogatzen ari dira jada (3. taula), eta bada, selinexor delakoa minbizi paziente jakin batzuetan erabiltzeko ere onartua da (Food and Drug Administration, 2019, 2020a, 2020b; European Medicines Agency, 2021).

SINE lehen belaunaldia 2012. urtean garatu zen CRM1/NES elkarrekintzaren egituran oinarrituz (Kalid et al., 2012; Lapalombella et al., 2012). Lehen belaunaldi hori CRM1en inhibizio itzulgarri geldoa eragiten duten hainbat konposatuk (KPT-127, KPT-185, KPT-205, KPT-227, KPT-249, KPT-251, KPT-276, KPT-330 (selinexor)) osatzen dute. 3. taulan beha daitekeenez, SINEak minbizi hematologiko zein minbizi solidoen hainbat modelo preklinikotan erabili dira. Ikerketa horietan, SINEek minbizi zelulen aurkako aktibitate sendoa erakutsi dute, bai *in vitro* zein *in vivo,* zelula hazkuntza inhibituz, apoptosia eraginez eta zelula-zikloa bahituz. Zelula osasuntsuetan, ordea, efektu toxiko minimoa dute. Gainera, hainbat SINEk, bereziki selinexorrek, minbizi zelulek beste farmakoekiko duten sentikortasuna emendatzen dute eta iturratutako terapian erabiltzen diren beste farmako batzuekin sinergia erakusten dute (ikusi 3. eta 4. taula gehigarriak).

SINE horiekin lortutako emaitza itxaropentsuak ikusirik, bigarren belaunaldiko SINE bat ere garatu da: KPT-8602 (eltanexor), zeina ikerketa preklinikoetan erabiltzen hasi diren (3. Taula).

3. taula: SINEekin egindako ikerketa preklinikoen laburpena. ALL: leuzemia linfozitiko akutua; AML: leuzemia mieloide akutua; CLL: leuzemia linfozitiko kronikoa; CML: leuzemia mieloide kronikoa; DLBCL: B-zelula handien linfoma hedatsua; HNSCC: buru eta lepoko zelula eskatatsuen kartzinoma; MCL: mantuko zelulen linfoma; MM: mieloma anizkoitza; NHL: ez-Hodgkin linfoma; NSCLC: Biriketako zelula ez-txikien minbizia; PCNSL: nerbio-sistema zentraleko linfoma primarioa; PMBL: B-zelulen linfoma mediastinal primarioa; TCL: T-zelulen linfoma.

SINEa	Minbizi motak	Erreferentziak
KPT-127	Pankreakoa	Azmi et al., 2013a
KPT-185	ALL, AML, bularrekoa, CLL, giltzurrunekoa, MCL, melanoma, MM, NHL, NSCLC, obulutegikoa, pankreakoa, PMBL, prostatakoa, urdailekoa	Lapalombella et al., 2012; Ranganathan et al., 2012; Azmi et al., 2013a, 2013b; Inoue et al., 2013; Kojima et al., 2013; Salas Fragomeni et al., 2013; Turner et al., 2013; Zhang et al., 2013; Cheng et al., 2014; Gao et al., 2014; Mendonca et al., 2014; Tai et al., 2014; Wang et al., 2014; Han et al., 2015; Miyake et al., 2015; Jardin et al., 2016; Kim et al., 2016b; Chen et al., 2017; Sekihara et al., 2017; Subhash et al., 2018; Sexton et al., 2019; Mendes et al., 2020; Wei et al., 2020
KPT-205	Pankreakoa	Azmi et al., 2013a
KPT-227	Pankreakoa	Azmi et al., 2013a
KPT-249	MM	Turner et al., 2013
KPT-251	AML, bularrekoa, CLL, giltzurrunekoa, glioblastoma, melanoma, mesotelioma, NHL, prostatakoa	Lapalombella et al., 2012; Azmi et al., 2013b; Etchin et al., 2013a; Inoue et al., 2013; Salas Fragomeni et al., 2013; Cheng et al., 2014; Mendonca et al., 2014; Gravina et al., 2014b, 2017; De Cesare et al., 2015; Green et al., 2015; Muqbil et al., 2016
KPT-276	AML, bularrekoa, glioblastoma, MCL, melanoma, mesotelioma, MM, NHL, NSCLC, urdailekoa	Ranganathan et al., 2012; Azmi et al., 2013b; Salas Fragomeni et al., 2013; Schmidt et al., 2013; Turner et al., 2013; Zhang et al., 2013; Cheng et al., 2014; Wang et al., 2014; Yang et al., 2014b; De Cesare et al., 2015; Green et al., 2015; Han et al., 2015; Muqbil et al., 2016
KPT-330 selinexor	AML, ALL, bularrekoa, CLL, DLBCL, fibrosarcoma, gibelekoa, giltzurrunekoa, glioblastoma, glioma pediatrikoa, heste meharreko tumore neuroendokrinoak, HNSCC, kolon eta ondestekoa, liposarkoma, maskurikoa, MCL, melanoma, mesotelioma, mielofibrosia, MM, NHL, NSCLC, obulutegikoa, osteosarkoma, pakreakoa, PCNSL, PMBL, prostatakoa, sarkoma, timo epiteliokoa, tiroidekoa, urdailekoa, heldu zein umeen hainbat minbizia	Etchin et al., 2013b; Salas Fragomeni et al., 2013; Turner et al., 2013, 2016a, 2016b, 2020; Walker et al., 2013; Cheng et al., 2014; Gravina et al., 2014b, 2017; Mendonca et al., 2014; Sun et al., 2014; Tai et al., 2014; Wettersten et al., 2014; Yang et al., 2014b; Zheng et al., 2014; Zhong et al., 2014; De Cesare et al., 2015; Green et al., 2015; Hing et al., 2015; Kazim et al., 2015; Miyake et al., 2015; Ranganathan et al., 2015; Attiyeh et al., 2016; Ferreiro-Neira et al., 2016; Jardin et al., 2016; Kashyap et al., 2016, 2018; Kim et al., 2016b; Muqbil et al., 2016; Nakayama et al., 2016; Rosebeck et al., 2016; Sun et al., 2016; Wrobel et al., 2016; Arango et al., 2017; Azmi et al., 2017, 2020; Burke et al., 2017; Chen et al., 2017; Conforti et al., 2017; Cosson et al., 2017; Garg et al., 2017a, 2017b; Muz et al., 2017; Nair et al., 2017; Aboukameel et al., 2018; Argueta et al., 2018; Baek et al., 2018; Barazeghi et al. 2018; Brunetti et al., 2018; Corno et al., 2018; Luedtke et al., 2018; Marcus et al., 2018; Ming et al., 2018; Saenz-Ponce et al., 2018; Schaffer et al., 2018; Shang et al., 2018; Subhash et al., 2018; Wahba et al., 2018; Zhang et al., 2018; Abeykoon et al., 2019; Aladhraei et al., 2019; Currier et al., 2019; Kapoor et al., 2019; Khan et al., 2019; Kulkoyluoglu-Cotul et al., 2019; Lim et al., 2019; Liu et al., 2019; Sexton et al., 2019; Tarantelli et al., 2019; Yan et al., 2019; Zhu et al., 2019a; Bonolo de Campos et al., 2020; Brinton et al., 2020; DeSisto et al., 2020; Fischer et al., 2020; Jiménez et al., 2020; Martini et al., 2020; Jeitany et al., 2021
KPT-8602 eltanexor	AML, ALL, CLL, DLBCL, gibelekoa, NHL, mielofibrosia, MM, prostatakoa, tiroidekoa, urdailekoa	Aboukameel et al., 2018; Gruffaz et al., 2019; Khan et al., 2019; Liu et al., 2019; Lucas et al., 2019; Sexton et al., 2019; Yan et al., 2019; Fischer et al., 2020; Turner et al., 2020; Verbeke et al., 2020

CRM1en inhibitzaileen mekanismoari dagokionez, efektua kokapen egokia galdu duten tumore ezabatzaile eta hazkuntzaren-erregulatzaile aktibitatea duten proteinak, adibidez, p53, nukleoan birkokatzean oinarritzen dela uste da. Horrela, proteina horiek euren ohiko funtzioa berreskuratuko bailukete. Aipatutakoa hipotesia onargarritzat hartu ohi bada ere, errealitatea haratago doala uste da gaur egun. Batetik, CRM1ek minbizian zerikusia duten kargo asko dituelako. Bestetik, CRM1ek esportazioan aritzeaz gain, zeluletan beste zeregin batzuk ere badituelako. Eta azkenik, tumoregenesia prozesu oso konplexua delako, eta beraz, tumore mota batetik bestera SINEen eraginaren mekanismo molekular eta zelularrak zeharo ezberdinak izan daitezkeelako. 3. eta 4. taula gehigarrietan minbizi jakin batzuen testuinguruan SINEek duten eragin ezberdinaren erantzule izan daitezkeen proteina edo bidezidor espezifikoak daude zerrendatuta; esaterako, aurretik aipatutako BCR-ABL onkoproteina CMLan (Vigneri eta Wang, 2001) edota NF-κB bidezidorra biriketako minbizian (Kim et al., 2016b).

1.4.1.3.2. Selinexor minbizi pazienteetan: entsegu klinikoak eta klinikan erabiltzeko oniritzia

Eraginkortasun zein tolerantziari dagokionez, selinexor farmakoak beste lehen belaunaldiko SINEak baino emaitza hobeak eman ditu ikerketa preklinikoetan. Hori dela eta, selinexor fase klinikoan minbizi pazienteen tratamendu bezala ikertzeko onartu da. 4. taulan 2021eko urtarrilera arte ClinicalTrials.gov webgunean (https://clinicaltrials.gov) aurki zitezkeen selinexorrekin egindako entsegu klinikoak zerrendatu dira. Entsegu kliniko bakoitzean jasotako emaitzen laburpena 5. taula gehigarrian laburbiltzen dira.

4. taula: Selinexor erabiltzen duten ikerketa klinikoak.

Minbizi mota	Erreferentzia eta IDa
Tumore solido aurreratuak	Abdul Razak et al., 2016 (ID: NCT01607905)
Sarkoma	Gounder et al., 2016 (ID: NCT01896505)
Leuzemia pediatriko akutu errefraktarioa	Alexander et al., 2016 (ID: NCT02212561)
NHL	Kuruvilla et al., 2017 (ID: NCT01607892)
AML	Garzon et al., 2017 (ID: NCT01607892); Wang et al., 2018 (ID: NCT02573363); Bhatnagar et al., 2019 (ID: NCT02093403); Fiedler et al., 2020 (ID: NCT02249091); Sweet et al., 2020 (ID: NCT02403310); Taylor et al., 2020 (ID: NCT02228525)
MM	Chen et al., 2018 (ID: NCT01607892); Bahlis et al., 2018 (ID: NCT02343042); Vogl et al., 2018 (NCT02336815); Chari et al., 2019 (ID: NCT02336815); Jakubowiak et al., 2019 (ID: NCT02199665); Grosicki et al., 2020 (ID: NCT03110562)
DLBCL	Kalakonda et al., 2020 (ID: NCT02227251)
Kastrazioarekiko erresistentea den prostata minbizia	Wei et al., 2018 (ID: NCT02215161)
Bular minbizia triple negatibo metastasikoa	Shafique et al., 2019 (ID: NCT02402764)

Minbizi ginekologikoak	Vergote et al., 2020 (ID: NCT02269293)
Obulutegi eta endometrioko minbiziak	Rubinstein et al., 2021 (ID: NCT01607905)
Hodi pankreatikoko adenokartzinoma	Azmi et al., 2020 (ID: NCT02178436)
Ondesteko minbizi metastasikoa	Nilsson et al., 2020 (ID: NCT02384850)
T-zelulen linfoma (TCL) edo natural killer/T-zelulen linfoma (NKTL) errefraktorio edo gaixoberrituak	Tang et al., 2021 (ID: NCT03212937)

Aipatutakoaz gain, bigarren belaunaldikoa den eltanexor farmakoarekin egindako entsegu kliniko bat ere badago jada (NCT02649790). Kasu horretan, eltanexor, dexametasonarekin eta DNA metiltransferasaren inhibitzailea den ASTX727rekin konbinatzen da.

Selinexorren erabilerak emaitza oso positiboak izan ditu aipaturiko entsegu kliniko horietako askotan. Hain da horrela, non, Estatu Batuetako Elikagai eta Sendagaien Administrazioak (FDA; *Food and Drug Administration)* zein Europako Sendagaien Agentziak (EMA; *European Medicines Agency)* selinexor farmakoa, XPOVIO™ merkataritza-izenaz AEBetan eta Nexpovio® izenaz Europan, minbizi paziente jakinak tratatzeko oniritzia eman duten. 2019ko uztailean, MM paziente jakinak selinexor dexametasonarekin batera erabiltzeari onespena eman zitzaion AEBetan (Food and Drug Administration, 2019). Horretarako, MM pazienteek helduak izan behar dute, eta gaixoberritze edo minbizi errefraktarioa pairatu behar dute. Gainera, aurretik beste lau terapia jaso behar izan dituzte eta bi proteasoma inhibitzaile, bi immunomodulatzaile eta anti-CD38 antigorputz monoklonal batekiko gaixotasun errefraktarioa izan behar dute. 2021ko martxoan, EMAk ere, baldintza horiek betetzen dituzten pazienteak selinexor eta dexametasona konbinazioarekin tratatzeko onespena eman zuen. 2020ko abenduan FDAk, gutxienez aurretik beste tratamendu bat jaso duten MM pazienteetan selinexor dexametasona eta proteasomaren inhibitzaile den bortezomibekin batera erabiltzeko oniritzia eman zuen ere (Food and Drug Administration, 2020a). AEBetan gainera, FDAk 2020ko ekainean, selinexor bakarka erabiltzeko onartu zuen aurretik bi terapia sistemikok porrot egin duten eta gaixoberritze edo minbizi errefraktarioa duten DLBCL paziente helduetan (Food and Drug Administration, 2020b).

2. Hipotesi eta helburuak

CRM1 garraio-hartzaileak zelularen homeostasia mantentzeko ezinbestekoa den ehunka kargoren nukleotiko esportazioa egikaritzen du kargo horien NESak ezagutuz eta horiekin elkarreginez. NESen identifikazioa gako da CRM1en kargoen esportazioa nola erregulatzen den ulertu nahi baldin bada. Egun, CRM1ek esportatzen dituen kargo askoren NESak ezagunak dira, beste kargo askoren NESak, ordea, ezezagunak dira. Horretaz gain, CRM1ek NESak non eta nola lotzen dituen estrukturalki eta biokimikoki ikertu bada ere, orain arte ez da mekanismo hori zelularen testuinguruan aztertu. Guzti hori kontuan izanda tesi proiektu honetan ondorengo **hipotesia** planteatu da: nukleotiko esportazio-aktibitatea ikergai duten entsegu zelularrak erabilita, NESek proteina zelular zein birikoen erregulazio eta funtzioan duten papera ezagutu eta CRM1en mendeko NESen esportazioaren inguruko ezagutzan sakon daiteke.

Beste alde batetik, CRM1 minbiziari aurre egiteko itu bezala duen papera gero eta nabariagoa da. Tesi hau aribidean zela, AEBetan zein Europan minbizi paziente jakinak tratatzeko CRM1en inhibitzailea den selinexor farmakoaren erabilera onartu zen. CRM1en inhibizioa klinikan erabiltzen hasi bada ere, selinexor eta beste farmako batzuen konbinazio potentzialen gaineko ezagutza, edota CRM1en inhibizioak haren esportoman eragiten duen asalduraren gainekoa oso mugatua da egun. Hori dela eta, tesi honetan bigarren **hipotesi** bat planteatzen da: CRM1en inhibizioa bestelako itu terapeutiko batzuen inhibizioarekin konbinatzea minbizia tratatzeko estrategia interesgarria izan daiteke; halaber, CRM1en inhibizioak zelula mailan duen eragina aztertzeko, azken aldian garatutako gertuko markaketan oinarritutako hurbilketa proteomikoak aproposak izan daitezke.

Aipatutako bi hipotesiak argitzeko ondorengo helburuak planteatzen dira:

- 1. helburua: NESen ikerketan askotan erabilitako, zein, berriki garatutako nukleotiko esportazio-entseguak erabiliz giza eta birus NES berriak bilatzea eta deskribatzea.
- 2. helburua: Entsegu zelular horiek erabilita CRM1en mendeko NESen esportazioa sakontasunean aztertzea eta minbizi-mutazioek prozesu horretan izan dezaketen eragina ikertzea.
- 3. helburua: Selinexor eta bestelako iturratutako farmakoen konbinazio berriak bilatzea eta *in vitro* ebaluatzea.
- 4. helburua: CRM1en inhibizioa aztergai duen hurbilketa proteomiko berri bat garatu eta ebaluatzea.

3. Material eta metodoak

3.1. Tresna bioinformatikoak

3.1.1. NES-iragarleak

CRM1en mende esportatzen diren kargoetan NES motiboak aurresateko Wregex (Prieto et al., 2014) eta NESmapper (Kosugi et al., 2014) NES-iragarleak erabili dira. NES-iragarle horiek proteina sekuentziak arakatzen dituzte NES seinaleak izan daitezkeen sekuentzien bila. Aurkitutako NES kandidatuek (cNES), NESen adostasun sekuentzietako aminoazido gakoek duten posizioaren arabera puntuazio bat jasotzen dute.

3.1.2. Aminoazido sekuentziak lerrokatzeko tresnak

Sekuentzien antzekotasuna ikertzeko sekuentziak lerrokatzen dituen Clustal Omega (https://www.ebi.ac.uk/Tools/msa/clustalo/; Sievers eta Higgins, 2014) erabili da.

3.1.3. Proteinen 3D irudiak sortzeko tresnak

CRM1 proteinaren poltsiko hidrofobikoaren irudiak sortzeko NCBIko iCn3D (https://www.ncbi.nlm.nih.gov/Structure/icn3d/full.html) eta UCSFko Chimera package (Pettersen et al., 2004) tresnak erabili dira. Erabilitako estruktura PDBko (*Protein Data Bank*) 3GJX (Monecke et al., 2009) izan da.

3.1.4. Gene ezberdinen adierazpena *XPO1* genearen adierazpenarekin korrelazioan dagoen aztertzeko tresnak

CRM1 gainadierazita agertzen den tumoreetan gainadierazita azaltzen diren bestelako itu terapeutikoak aztertzeko, Broad institutuko CGA TARGET (*tumor alterations relevant for genomics-driven therapy)* datu basetik (https://software.broadinstitute.org/cancer/cga/target; v3) TARGET zerrenda lortu da. TARGET zerrendan, minbiziaren diagnostikoarekin, terapiaren erantzunarekin eta pronostikoarekin zuzenean erlazionaturik dauden 135 gene ageri dira.

TARGET zerrendako 135 geneen adierazpena *XPO1*en (CRM1 kodetzen duen genearen) adierazpenarekin erkatzeko CANCERTOOL (Cortazar et al., 2018) eta cBioPortal (Cerami et al., 2012; Gao et al., 2013) tresna bioinformatikoak erabili dira. CANCERTOOL bular, birika, prostata, eta kolon eta ondesteko minbizietako azterketa egiteko erabili da, eta cBioPortal berriz, azterketa leuzemia mieloide akutuan (AML) egiteko. Gene ezberdinak korrelazioan dauden aztertzeko erabilitako CANCERTOOL zein cBioPortal tresnak ezagunak diren ikerketetan oinarritzen dira; 5. taulan azterketa honetarako erabilitako ikerketen zerrenda ikus daiteke.

5. taula: *XPO1* eta TARGET zerrendako geneen arteko korrelaziorik dagoen aztertzeko erabili diren ikerketak. Ikerketa horietako datuak CANCERTOOL (Cortazar et al., 2018) eta cBioPortal (Cerami et al., 2012; Gao eta al., 2013) erabiliz atzitu dira. TCGA eta colonomic ikerketako datuak hurrengo webgunean topa daitezke hurrenez hurren: https://cancergenome.nih.gov/; https://www.colonomics.org/.

Bular minbizia	Birika adenokartzinoma	Prostata minbizia	Kolon eta ondeste minbizia	AML
Pawitan et al., 2005 Wang et al., 2005 Ivshina et al., 2006 Lu et al., 2008 TCGA (RNA-seq)	Chitale et al., 2009 Shedden et al., 2008 Wilkerson et al., 2012 TCGA (RNA-seq)	Lapointe et al., 2004 Glinsky et al., 2004 Varambally et al., 2005 Taylor et al., 2010 Grasso et al., 2012 TCGA (RNA-seq)	Jorissen et al., 2009 Kemper et al., 2012 Laibe et al., 2012 Marisa et al., 2013 Roepman et al., 2014 TCGA (RNA-seq) Colonomics	Tyner et al., 2018 Liu et al., 2018

CANCERTOOL eta cBioPortal erabiliz, 5. taulako ikerketa guztietan *XPO1* eta TARGET zerrendako gene bakoitzaren adierazpena korrelazioan dagoen aztertu da. Korrelazioa adierazten duten -1etik 1era doazen balioak lortu dira; balio negatiboek alderantzizko korrelazioa adierazten dute, positiboek, korrelazio zuzena eta 0 balioak korrelazio eza. Lortutako $> 0,2$ edo $< -0,2$ balio esanguratsuak ($p < 0,05$) hautatu eta tumore mota ezberdinetan, eta orokorrean, *XPO1* eta TARGET zerrendako gene bakoitzarentzako korrelazioaren batez bestekoa kalkulatu da. Adibidez, *XPO1* eta *BRCA1* geneek AMLn korrelazioa agertzen duten ikertzeko, gene bien adierazpenak erkatzean Tyner eta lankideen (2018) ikerketan lortutako balioarekin (0,489) eta Liu eta lankideen (2018) ikerketan lortukoarekin (0,583) batez bestekoa kalkulatu da (0,536). TARGET zerrendako 135 geneek tumore mota ezberdinetan *XPO1*ekin duten korrelazioa kalkulatu eta balio horiekin gene bakoitzerako batez besteko orokor bat kalkulatu da. Adibidez, *BRCA1*en adibidearekin jarraituz, bular, birika, prostata, kolon eta ondeste, eta AML minbizietan *XPO1*ek eta *BRCA1*ek duten korrelazio balioen batez bestekoekin (0,152, 0,403, 0,088, 0,371 eta 0,536 hurrenez hurren) batez besteko orokor bat kalkulatu da (0,310). Korrelazio datu guztiak 6., 7., 8., 9. eta 10. taula gehigarrietan ageri dira tumore motaren arabera xehatuta, eta 11. taula gehigarrian aztertutako tumore guztiak batera hartuz.

3.2. Klonazioak eta mutagenesia

Klonazio eta mutagenesia plasmidoak eratzeko teknikak dira. Klonazioa, metodo ezberdinen bidez eratuko diren intsertoak intereseko bektorean txertatzea da; mutagenesia, ordea, jada erabilgarria den plasmido batean mutazioak eratzea da. Tesi honetan erabili diren, baina espresuki tesi honetarako sortu ez diren plasmidoak 12. taula gehigarrian ageri dira.

3.2.1. Murrizte-entzimetan oinarritutako klonazio metodoak

3.2.1.1. Bektoreen prestaketa

Bektore moduan erabiliko den 1,5-2 μg DNA zirkular (plasmidoa) intereseko murrizte-entzimatan inkubatu da 3 orduz 37 °C-tan. Indargetzaile ezberdina behar duten entzimak erabili diren kasuetan, digestio-sekuentziala egin da, hau da, lehenik eta behin plasmidoa entzima batekin digeritu da, ostean, moztutako DNA QIAquick PCR purifikazio-kita (Qiagen) erabilita purifikatu da, eta bukatzeko, bigarren entzimarekin digeritu da.

QIAquick PCR purifikazio-kitarekin DNA purifikatzeko, lehenik eta behin DNA bolumen bakoitza PB indargetzailearen 5 bolumenekin nahastu da. Jarraian, nahasketa QIAquick zutabe batera transferitu eta minutu batez 13000 bira minututan (rpm-tan) zentrifugatu da. Zutabean zehar iragazitako fluxua baztertu eta zutabea 700 μl PE indargetzailearekin garbitu da 2 x 1 minutuz, 13000 rpm-tan zentrifugatuz. DNA atxikita duen zutabea mikrozentrifuga-tutu garbi batera transferitu, 50 μl H_2O gehitu, 5 minutuz giro tenperaturan inkubatu eta 13000 rpm-tan minutu batez zentrifugatu da DNA eluitzeko. Zentrifugazio guztiak giro tenperaturan egin dira.

Bektoreen berligazioa ekiditeko, digeritutako bektoreak ordu bateko hiru ziklotan desfosforilatu dira DNA kate bakun edo bikoitzetako 5’ muturretako fosfatoak kentzen dituen fosfatasa alkalinoa (Roche) erabiliz. Bukatzeko, desfosforilazio erreakziora 2 μl 0,5 M azido etilendiaminotetraazetikoa (EDTA) gehitu eta 65 °C-tan inkubatu da 10 minutuz fosfatasa alkalinoaren erreakzioa geldiarazteko.

Digeritu eta desfosforilaturiko bektoreak QIAquick PCR purifikazio-kita erabiliz purifikatu dira, eta DNA 30 μl H_2O-tan eluitu da.

3.2.1.2. Intsertoen prestaketa

Intsertoak lau metodo ezberdinen bidez lortu dira: azpiklonazioz, hibridazioz, PCR bidez eta gBlock bidez.

3.2.1.2.1. Azpiklonazioa

Azpiklonazioa, intereseko intsertoa aurretik plasmido batean klonaturik dagoenean eta beste bektore batean txertatu nahi denean erabiltzen da (12. irudia). Azpiklonazioa egiteko ezinbestekoa da intsertoa jatorrizko plasmidotik ateratzeko erabiliko diren murrizte-entzimak eta bektore hartzailea mozteko erabiliko direnak berdinak izatea. Gainera, irakurtaraua ere mantendu beharra dago. Metodo honen bidez eratutako plasmidoak 13. taula gehigarrian ageri dira.

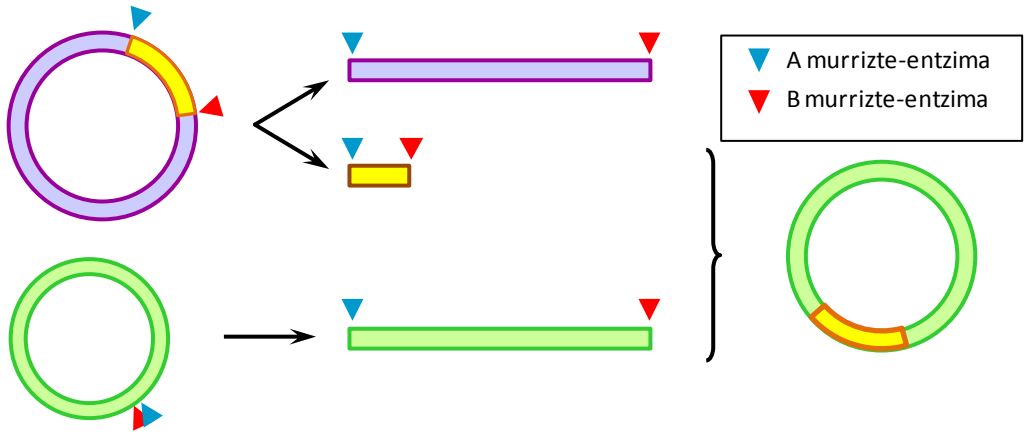

12. irudia: Azpiklonazio prozedura. Jatorrizko plasmidoa (bektore morea eta intserto horia) A eta B murrizte-entzimekin moztean bektorea linearizatu eta intsertoa askatu egiten da. Entzima berdinekin bektore hartzailea (berdea) digerituz gero, bektore hori ere linearizatu egingo da. Horrela, bektore hartzaile linearizatuaren eta intsertoaren muturrak bateragarriak izango dira, eta beraz, plasmido berria (berde eta horia) sortzeko aukera egongo da.

Prozedura zehatza ondorengoa da: jatorrizko plasmidoa murrizte-entzima egokiekin 3 orduz eta 37 °C-tan digeritu da aurretik azaldu bezala. Ostean, digeritutako DNA, bektore eta intsertoa ondo bereizi arte, % 1,5 agarosa (1X TAE etidio bromuroarekin) gel batean banatu da 100 V-tan. Pisu molekularraren markatzailetzat, GeneRuler 1 kb DNA ladder plus (ThermoFisher Scientific) erabili da. Gelean, UV-transiluminazioz, DNA ikusi eta intsertoaren DNA banda geletik moztu da. Banda horretako DNA QIAquick gel-erauzketa kita (Qiagen) erabiliz purifikatu da. Gel-bandako DNA QIAquick gel-erauzketa kitarekin erauzi eta purifikatzeko, lehenik eta behin gel zatia QG indargetzailearen 3 bolumenetan disolbatu da 50 °C-tan 10 minutuz noizbehinka gogor astinduz. Erabili beharreko QG indargetzaile bolumena kalkulatzeko gel zatiaren mg-ak eta indargetzailearen µl-ak pareko hartu dira, horrela, gel zatiak 50 mg pisatzen baditu, 150 µl QG indargetzailetan disolbatu da. Ostean, isopropanol bolumen bat gehitu, nahastura osoa QIAquick zutabe batera transferitu eta 13000 rpm-tan minutu batez zentrifugatu da. Zutabean zehar iragazitako fluxua baztertu, zutabera PE indargetzailearen 750 µl gehitu eta zutabea 13000 rpm-tan minutu batez zentrifugatu da. DNA atxikita duen zutabea mikrozentrifuga-tutu garbi batera transferitu, 50 µl H_2O gehitu, 5 minutuz giro tenperaturan inkubatu eta 13000 rpm-tan minutu batez zentrifugatu da DNA eluitzeko. Zentrifugazio guztiak giro tenperaturan egin dira.

3.2.1.2.2. Hibridazio bidezko intsertoaren prestaketa

Hibridazio bidezko intsertoaren preskaketa partzialki gainjar daitezkeen bi oligonukleotido hibridatzean eta kate bakuneko DNA luzatzean datza (13. irudia). Prozedura honen bidez eratutako plasmidoak 14. taula gehigarrian ageri dira eta prozedurarako erabilitako hasleak 15. taula gehigarrian.

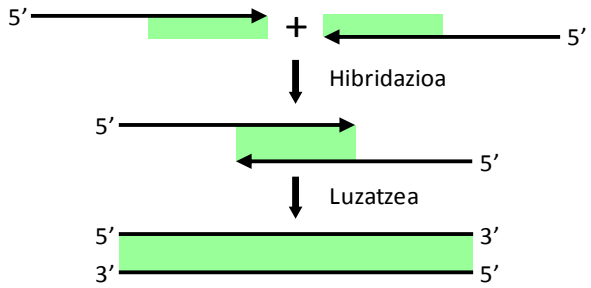

13. irudia: Hibridazio prozedura. Gezi beltzek hibridazioan erabiliko diren hasleak adierazten dituzte eta hasle bakoitzaren laukizuzen berdeak beste haslearekin hibridatuko duen fragmentua. Hasle horiek hibridatu eta luzatzean kate bikoitzeko DNA lortuko da.

Partzialki gainjartzen diren aurreranzko eta atzeranzko hasleak hibridatzeko, hasleok lehenik eta behin indargabetutako soluzioan 100 °C-tan inkubatu dira 5 minutuz eta ostean giro tenperaturan hozten utzi dira ordubetez. Hibridatutako hasleak DNA polimerasaren Klenow zatia erabiliz (Fermentas) luzatu dira 37 °C-tan 2 orduz inkubatuta. Erreakzio entzimatikoa geldiarazteko lagina 75 °C-tan inkubatu da 20 minutuz.

Kate bikoitzeko DNA zatiak murrizte-entzima egokiekin 37 °C-tan eta hiru orduz digeritu dira. Digestioaren produktuetako DNA QIAquick gel-erauzketa kitarekin purifikatu da 3.2.1.2.1. atalean azaldutako prozedura jarraituz.

3.2.1.2.3. PCR bidezko intsertoaren prestaketa

Intsertoak PCR bidez prestatzeko, jatorrizko DNA moldeari ezaugarri jakinak erantsiko dizkioten hasle espezifikoak erabili dira (14. irudia). Ezaugarri jakin horiek, murrizte-entzimek ezagutuko duten sekuentzia, epitopo etiketak edota proteinak zelula eukariotoetan behar bezala adieraztea ahalbidetuko duten sekuentziak, hala nola, Kozak sekuentzia, 5' muturreko hasiera kodona edota 3' muturreko stop kodona izango dira. Metodo honen bidez eratutako plasmidoak 16. taula gehigarrian ageri dira, eta prozedura aurrera eraman ahal izateko hasleen zerrenda 17. taula gehigarrian.

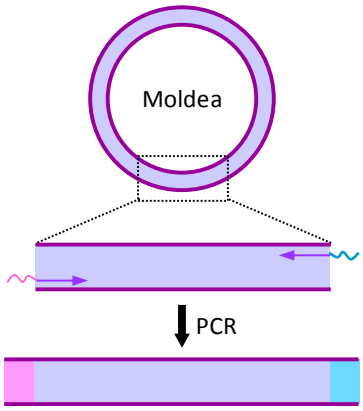

14. irudia: PCR bidezko intsertoen prestaketaren prozedura. Aurreranzko zein atzeranzko hasleak gezi bidez adierazten dira, gezien parte moreak moldearekiko osagarria den sekuentzia adierazten du, parte arrosak eta urdinak ordea, aurreranzko eta atzeranzko hasleetan barneratutako murrizteguneak eta bestelako ezaugarridun sekuentziak.

PCRa gauzatu ahal izateko ondorengo erreakzio eta PCR programa erabili da:

Erreaktiboa	Bolumena
H_2O	40,5 µl
10X Pfu ultra indargetzailea	5 µl
10 mM dNTP	1 µl
10 µM aureranzko haslea	1 µl
10 µM atzeranzko haslea	1 µl
DNA moldea (80 ng/µl)	1 µl
Pfu Ultra	0,5 µl
	Bolumen totala 50 µl

Tenperatura	Denbora	Zikloak
92 °C	2 min	1
92 °C	20 s	30
55 °C	40 s	
68 °C	40 s	
68 °C	3 min	1
4 °C	∞	

Sortutako PCR produktuek agarosa gelen bidez tamaina egokia dutela egiaztatu ondoren, QIAquick PCR purifikazio-kitarekin purifikatu dira. Ostean, intereseko murrizte-entzimekin digeritu, eta digestioaren produktua QIAquick PCR purifikazio-kitarekin purifikatu da. Digestio- eta purifikazio-prozedurak 3.2.1.1. atalean adierazitako prozedura berari jarraituz egin dira.

3.2.1.2.4. gBlock bidezko intsertoen prestaketa

gBlock-ak (Integrated DNA Technologies) neurrira egindako kate bikoitzeko DNA fragmentuak dira. Erabilitako gBlock sekuentziak 1. zerrenda gehigarrian ageri dira. Fragmentuok uretan disolbatu dira 50 °C-tan 20 minutuz inkubatuta. Behin disolbatuta, intereseko murrizte-entzimak erabilita digeritu dira 37 °C-tan 3 orduz. Jarraian, QIAquick PCR purifikazio-kita erabilita, 30 µl H_2O-tan eluituz purifikatu dira. Digestio- eta purifikazio-prozedurak 3.2.1.1. atalean erabilitako prozedura berari jarraituz egin dira. Metodo honen bidez eratutako plasmidoak 18. taula gehigarrian ageri dira.

3.2.1.3. Bektore eta intsertoen arteko ligazioa

Digeritutako bektore eta intsertoak agarosazko gelean banatu dira bakoitzaren tamaina egiaztatzeko eta kontzentrazio aldetik batak bestearekiko duen arrazoia ikuskatzeko. Ligazioak intserto:bektore arrazoia 3:1 dela prestatu dira. Ligaziorako disoluzioa 10X erreakzio-indargetzailea, 10 mM ATP, T4 DNA ligasa (hirurak ThermoFisher Scientific-ekoak), eta 10 µl-rarteko H_2O bolumenarekin prestatu da eta 4 °C-tan gau osoan mantendu da.

3.2.1.4. *E. coli* DH5α bakterioen transformazioa

Escherichia coli DH5α bakterio konpetenteak ligazio-produktuekin transformatu dira. Horretarako, izotzetan desizoztutako bakterioen 60 µl gehitu dira ligazio-tutura. Transformaziorako plasmidoa, aurretiaz sortu eta erabilitakoa bada, eta helburua plasmido gehiago ekoiztea denean, purifikatutako plasmidoaren 1 µl bakterioen 40 µl-rekin nahastu da. Bakterio/DNA nahasketa izotzetan inkubatu da ordubetez. Jarraian, nahasketari 37 °C-tan

30 segundoko txoke-termikoa eragin, eta berriz ere izotzetan mantendu da gutxienez 2 minutuz. Bakterio/DNA nahasketa aurretik berotutako 500 µl LB mediodun 15 ml-tako tutu batera transferitu da eta 37 °C-tan inkubatu da ordu batez eta 220 rpm-ko agitazioan. Inkubazioaren ostean, bakterio suspentsioaren 400 µl (ligazio berriaren kasuan), edo 40 µl (plasmido gehiago sortzeko denean), antibiotiko egokia duen LB plaka batean plakeatu da eta 37 °C-tan inkubatu da gau osoan.

Gau osoko inkubazioaren ostean, ondo bereiz daitezkeen koloniak esterilizatutako zotz batez ukitu dira. Kolonia ukitzeko erabilitako zotza antibiotiko egokia duen 10 ml LBtan sartu eta gau osoan zehar 37 °C-tan inkubatu da 220 rpm-ko agitazioaz.

3.2.2. Gunera zuzenduriko mutagenesia

Gunera zuzenduriko mutazioak eragiteko QuickChange Site-Directed Mutagenesis kita (Agilent Technnologies) erabili da. Oinarrian, gunera zuzenduriko mutagenesia PCR bidez intereseko mutazioa hasleen bidez sortzean datza (15. irudia). Metodo honen bidez eratutako plasmidoak 19. taula gehigarrian ageri dira.

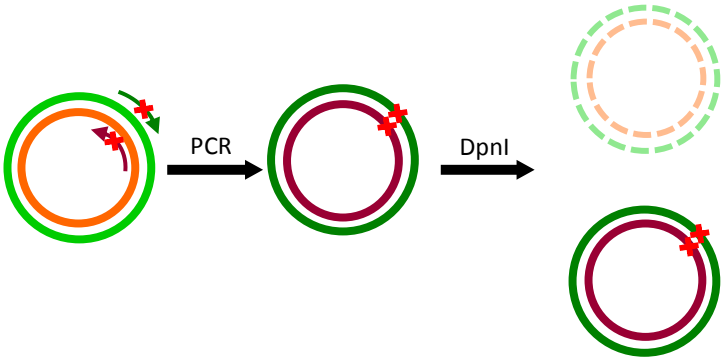

15. irudia: Gunera zuzenduriko mutagenesiaren bidezko plasmidoen eraketa. Gezi berde ilun eta granateak mutazioa (gurutze gorriaz adierazita) sortzeko erabiliko diren hasleak adierazten dituzte. Hasle horiek berde argiz eta laranjaz adierazita dagoen jatorrizko plasmidoa PCR bidez anplifikatzeko erabiliko dira. PCR prozesu horren ondorioz sortutako plasmidoak intereseko puntuan egongo dira mutatuta. Azkenik, PCR-produktua DpnI murrizte-entzimarekin digeritzen da jatorrizko plasmido degradatzeko.

Prozedura honen lehen urratsa, mutatu nahi den sekuentziarekiko osagarriak diren eta intereseko mutazioa eragingo duten hasleen diseinua da (hasleen zerrenda osoa 20. taula gehigarrian ikus daiteke). Hasle horiek diseinatzeko orduan PCRan zehar horien dimerizazioa gutxiagotzeko metodoa erabili da (Zheng et al., 2004). Hasleen urtze-tenperatura (Tm) optimoa 81 °C-tik gora dago eta ondorengo formularekin kalkulatu da:

$$Tm = 81{,}5 + 0{,}41 \times (\%\ GC) - \frac{675}{N} - \%\ base\ parekatze\ oker$$

Non *% GC*, haslearen zein ehuneko den guanina edo zitosina, eta *N*, base kopuru totala adierazten duten.

Diseinatutako hasleekin, eta mutatu nahi den plasmidoa moldetzat hartuta, intereseko mutazioa duen plasmidoa PCR bidez anplifikatu da. PCR erreakzio eta programa ondorengoak izan dira:

Erreaktiboa	Bolumena
H2O	38 µl
10x QuickChange Lightning indargetzailea	5 µl
QuickSolution	1,5 µl
dNTP mixa	1 µl
DNA moldea (≈ 50 ng/µl	1 µl
Aurreranzko haslea (100 ng/µl)	1,25 µl
Atzeranzko haslea (100 ng/µl)	1,25 µl
QuickChange Lightning entzima	1 µl
	Bolumen totala 50 µl

Tenperatura	Denbora	Zikloak
95 °C	2 min	1
95 °C	20 s	18
60 °C	10 s	
68 °C	5 min	
68 °C	5 min	1
4 °C	∞	

Ostean, PCR-produktuari 2 µl DpnI murrizte-entzima gehitu eta 37 °C-tan inkubatu da 5 minutuz. Entzima hori metilatutako DNArekiko espezifikoa den murrizte-endonukleasa bat da, eta beraz, moldetzat erabilitako mutatu gabeko plasmidoa baino ez du digerituko. Horrela PCR-produktuan mutaziodun plasmidoa besterik ez da egongo.

3.2.2.1. Gunera zuzenduriko mutagenesiko PCR produktuarekin XL10-Gold bakterioen transformazioa

Gunera zuzenduriko mutagenesiko PCR-produktuarekin XL10-Gold bakterio ultrakonpetenteak transformatu dira. Horretarako, bakterioak izotzetan desizoztu eta aurretik hotzetan mantendutako 15 ml-ko tutuetara 45 µl bakterio transferitu da. Bakterio tutura 2 µl β-merkaptoetanol gehitu eta suspentsioa izotzetan inkubatu da 2 minutuz. Jarraian, digeritutako PCR-produktuaren 2 µl bakterio suspentsiora gehitu eta nahasketa izotzetan inkubatu da 30 minutuz. Inkubazioa bukatutakoan bakterioei 42 °C-tako txoke-termikoa ezarri zaie 30 segundoz eta izotzetan mantendu dira gutxienez beste 2 minutuz. Bakterio/PCR produktu nahasketa, aurretik berotutako 500 µl LB mediodun 15 ml-tako tutu batera transferitu eta 37 °C-tan inkubatu da ordu betez eta 220 rpm-ko agitazioan. Azkenik, suspentsio horren 450 µl antibiotiko egokia duen LB plaka batean plakeatu da eta plaka gau osoan 37 °C-tan mantendu da. Hazitako bakterioen artean ondo isolatutako koloniak esterilizatutako zotz batekin ikutu eta LB medio likidotan hazi dira 3.2.1.4. atalean azaldu bezala.

3.2.3. Plasmidoen purifikazioa eta DNA sekuentziazioa

Plasmidoak purifikatzeko prozedura ohikoena QIAprep Spin Miniprep kita (Qiagen) erabilita burutu da. Plasmido kopuru handia lortzea beharrezkoa izan den kasuetan Gen Elute HP endotoxin-free plasmid Maxiprep (Sigma-Aldrich) kita erabili da. Ekoiztutako plasmidoen kontzentrazioa eta purutasuna Nanodrop Lite (ThermoFisher Scientific) erabilita neurtu da. Plasmidoen DNA sekuentzia egokia dela baieztatzeko StabVida enpresaren zerbitzuak kontratatu dira. Sekuentziazioan erabilitako hasleak 21. taula gehigarrian erakusten dira.

3.2.3.1. QIAprep Spin Miniprep bidezko plasmidoen purifikazioa

Bakterio-suspentsioak 3500 rpm-tan zentrifugatu dira 10 minutuz. Gainjalkina baztertu eta jalkina P1 indargetzaile hotzaren 250 µl-tan berreseki da. Lagin bakoitza tutu garbi batera transferitu eta P2 indargetzailearen 250 µl gehitu ostean, tutuak emeki irauli dira bakterioak lisatzeko. Jarraian, N3 indargetzailearen 350 µl gehitu eta tutuak berriz ere emeki irauli eta 10 minutuz zentrifugatu dira. Gainjalkina QIAprep spin zutabe batera transferitu eta minutu batez zentrifugatu da. Zutabean zehar iragazitako likidoa baztertu, eta zutabea PB indargetzailearen 500 µl gehituta eta minutu batez zentrifugatuta garbitu da. Zutabea bigarrenez garbitu da, kasu honetan, zutabera etanoldun PE indargetzailearen 750 µl gehituta eta zutabea birritan zentrifugatuz. Azkenik, zutabea tutu garbi batera transferitu da, 70 µl H_2O gehitu zaizkio eta 5 minutuz inkubatu ostean zutabea minutu batez zentrifugatu da DNA eluitzeko. Zentrifugazio guztiak, lehenengoa salbu, mahai gaineko mikrozentrifuga batean egin dira 13000 rpm-tan eta giro tenperaturan.

3.2.3.2. Gen Elute HP Endotoxin-free Plasmid Maxiprep bidezko plasmidoen purifikazioa

Plasmido kopuru handia ekoitzi nahi denean, koloniak medio likidotan hazterako orduan, 3.2.1.4. atalean azaldutako prozedura jarraitu beharrean, zotza antibiotikodun LB 5 ml-tan inkubatu da 6 orduz. Ostean, suspentsio horretatik 1 ml antibiotikodun LB 150 ml-tara transferitu da. Bakterioak 37 °C-tan eta 220 rpm-tan hazi dira gau osoan.

Bakterio-suspentsioa 50 ml-ko hiru tututan banatu eta 3220 g-tan zentrifugatu da 15 minutuz. Zentrifugazio tarte horretan, Gen Elute Maxiprep lotze-zutabeak prestatu dira; horretarako, zutabeak Sigma VM20 vacuum manifold-ean jarri dira, eta zutabeak prestatzeko soluzioaren 12 ml zutabeetan zehar igaroarazi da hutsa eraginez. Zentrifugazioaren osteko bakterio-suspentsioetako gainjalkinak baztertu, eta jalkinak RNAasa A berresekitze-soluzio hotzaren 12 ml-tan berreseki dira. Jarraian, 12 ml lisi-indargetzaile gehitu dira. Bakterioak lisatzeko, lehenik eta behin tutua emeki irauli da eta ostean 5 minutuz geldirik laga da. Tarte horretan, bakterio-lisatuen suspentsioa filtratzeko huts-sistema muntatu da. Horretarako, 50 ml-ko tutu

garbi bat VacCap tapoiaz tapatu da, eta bertara hutsa eragingo duen hodia eta GenElute HP endotoxinarik gabeko Maxiprep iragazkia lotu dira 16. irudian azaldu bezala. Lisatua neutralizazio-indargetzaile hotzaren 12 ml gehituta eta nahasketa iraulita neutralizatu da. Neutralizatuko soluzioa GenElute HP Maxiprep iragazkira transferitu eta hutsa eraginez iragazi da. Iragazitako soluziora lotze-indargetzailearen 9 ml gehitu dira, eta ondo nahastu ondoren, aurretiaz prestatutako lotze-zutabera transferitu da nahastea, hutsa eraginez zutabean zehar pasarazteko. Jarraian, lotze-zutabea 1 eta 2 garbiketa-indargetzaileen 12na ml hutsa eraginez zutabean zehar igaroarazita garbitu da. Bigarren garbiketaren ostean hutsa gutxienez 10 minutuz mantendu da zutabea sikatu dadin. Azkenik, lotze-zutabea 50 ml-ko tutu garbi batera transferitu da, 3 ml endotoxinarik gabeko H_2O gehitu, eta zutabea 3000 g-tan zentrifugatu da 10 minutuz.

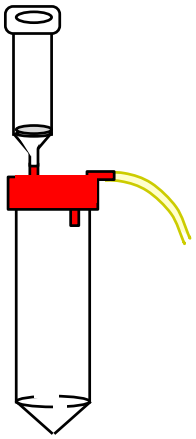

16. irudia: Bakterio-suspentsioa iragazteko muntaia. Tutu horiak hutsa eragingo du tapa gorriko tutuan eta horrek, bertara atxikitutako iragazkidun tutura isuritako bakterio-suspentsioa iragaztea eragingo du.

Nanodrop Lite-an purifikatutako DNAren kontzentrazioa neurtu da. Kontzentrazioa txikiegia izan denean, DNA kontzentratu egin da. Horretarako, eluitutako soluziora 300 µl sodio azetato 3 M eta 2,1 ml isopropanol gehitu dira, eta soluzioa 15 ml-ko tutu batera transferitu da. Tutua 15000 g-tan zentrifugatu da 30 minutuz eta 4 °C-tan. Jalkina 1,5 ml % 70 etanoletan berreseki da, eta beste 10 minutuz zentrifugatu da baldintza berdinetan. Jalkinaren gainean 100 µl endotoxinarik gabeko H_2O gehitu da eta gau osoan 4 °C-tan laga da DNA bertan disolbatzeko.

3.3. Zelula-hazkuntza

3.3.1. Zelula-lerroak eta hazkuntza baldintzak

Zelulak Dulbecco's modified Eagle's medioan (DMEM) edo Roswell Park Memorial Institute (RPMI) 1640 medioan hazi dira: giza zerbixeko adenokartzinomako HeLa zelulak eta giza enbrioien giltzurruneko 293T (HEK293T) zelulak idi-umeki serumaren (FBS) % 10 eta penizilina/estreptomizinaren % 1 duen DMEM mediotan hazi dira; mCherry etiketa duten giza hezur-muineko estromako HS5 zelulak % 10 FBS duen DMEM mediotan eta eGFP etiketadun

leuzemia mieloide akutuko MV4-11 zelulak berriz, % 10 FBS duen RPMI mediotan hazi dira. Guztiak 37 °C-an, % 5eko CO_2-dun atmosfera hezean. Hazkuntzan erabilitako medioak, FBS eta antibiotikoak Life-Technologieskoak dira.

Zelulak hazkuntzan mantendu ahal izateko, konfluentziara heldutakoan jaso eta diluituago erein dira berriro ere. Prozesu hori astean birritan egin da normalean. Zelula-lerroaren arabera prozesuak aldaketa txikiak izan ditu:

HeLa, HEK293T eta mCherry-HS5 zelulen kasuan, medio zaharra kendu, zelulak PBStan (fosfatoarekin indargabetutako gatz soluzioa) garbitu eta tripsinatan (Life-Technologies) 37 °C-an 2 minutu inguruz inkubatu ostean altxatu dira. HeLa eta HEK293T zelulen kasuan tripsinarekin inkubatzearen ondorioz altxatutako zelulak zuzenean medio berrian berreseki eta erein dira. mCherry-HS5 zelulen kasuan altxatutako zelulak 10 ml medio berritan berreseki eta 1500 rpm-tan zentrifugatu dira 5 minutuz. Jalkitako zelulak medio berritan berreseki eta erein dira.

eGFP-MV4-11 zelulak suspentsioan hazten den zelula-lerroa izanik, zelulak hazitako medioa jaso eta 1500 rpm-tan zentrifugatu da 5 minutuz. Jalkitako zelulak medio berritan berreseki eta erein dira.

3.3.2. Zelulen ereintza

Esperimentuetarako aurretik azaldu bezala jaso dira zelulak, eta esperimentu mota eta zelula-lerroaren arabera, zelula kopuru ezberdina erein da hazkuntza plaketan (6. taula).

6. taula: Esperimentu motaren arabera erabilitako zelula-lerroa eta hazkuntza baldintzak.

Esperimentu mota	Zelula-lerroa	Denbora	Hazkuntza plaka mota	Putzu edo plakako zelula kopurua
Immunofluoreszentzia	HEK293T eta HeLa	3 egun	12 putzutakoa estalkiarekin	% 60-80ko konfluentzian
Western plapaketa	HEK293T	3 egun	6 putzutakoa	% 60-80ko konfluentzian
GFP-Trap immunoprezipitazioa	HEK293T	3 egun	10 cm-ko plaka	$6,5 \times 10^6$
Neutrabidina afinitate-purifikazioa	HEK293T	3 egun	10 cm-ko plaka	$6,5 \times 10^6$
Ko-hazkuntzan eginiko farmako sinergia	mCherry-HS5	5 egun	96 putzutakoa	10^4
	eGFP-MV4-11	4 egun		4×10^4

Immunofluoreszentzia eta Western plapaketa esperimentuetarako zelulak % 60-80ko konfluentzian erein dira beirazko estalki esterildun (RS France) 12 putzutako hazkuntza plaketan (Sarstedt) edo 6 putzutako hazkuntza plaketan (Costar) hurrenez hurren.

Beste esperimentuetan, zelulak jasotakoan, suspentsioko zelula kopurua Neubauer ganbara erabiliz zehaztu da. Zelula-suspentsio bakoitza bi aldiz kargatu da Neubauer ganbaran eta aldi bakoitzean bi karratutan dauden zelulak zenbatu dira, guztira lau karraturen batez bestekoa kalkulatzeko. Zelulak zenbatzerakoan, karratuko goiko eta eskumako lerroak ukitzen dituzten zelulak ez dira zenbatu, zelulok birritan zenbatzea ekiditeko. Zenbatutako zelulen batez bestekoa 10^4-z biderkatu da jatorrizko suspentsioko ml-ko zelula kopurua ezagutzeko.

eGFP-MV4-11 zelulen kasuan izan ezik, beste zelula guztien kasuan zelulak esperimentuaren lehen egunean erein dira. eGFP-MV4-11 zelulak ordea, esperimentuaren bigarren egunean. eGFP-MV4-11 zelulak ko-hazkuntzan eginiko farmakoen sinergia esperimentuetan erabili dira mCherry-HS5 zelulekin batera. Esperimentu mota horietan, lehenengo egunean mCherry-HS5 zelulak erein dira, eta 24 ordura, mCherry-HS5 zelulak plakari ondo atxikita daudela, medio zaharra kendu eta eGFP-MV4-11 zelulak mCherry-HS5 zelulen gainean erein dira.

3.3.3. DNAren transfekzioa

Zelulak erein eta 24 ordura DNA transfekzioak egin dira X-tremeGENE 9 (XTG9) transfekzio-agentea (Roche Diagnostics) erabilita. Transfekzio-agentea antibiotiko eta FBS gabeko DMEMarekin nahastu, eta tantaka DNA plasmido jakina duen tutura gehitu da 1:2 DNA:XTG9 arrazoian. DMEM-XTG9-DNA tutua emeki nahastu eta 25 minutuz inkubatu da giro tenperaturan. Inkubazio denbora igaro bitartean zelulei medioa aldatu zaie, medio zaharra kenduz eta zuzenean berria gehituz. Jarraian, tutuko edukia zeluletara gehitu da tantaka eta plaka mugimendu zirkularretan emeki mugituz.

Erabilitako plakaren arabera DNA, DMEM/XTG9, eta hazkuntza medioaren bolumen ezberdinak erabili dira (7. taula).

7. taula: DNAren transfekziorako plaka motaren araberako DNA, XTG9 eta hazkuntza medio kopuruak.

Plaka mota	DNA ng	DMEM/XTG9 µl	Hazkuntza medio µl
12 putzutakoa	600	37,5	750
6 putzutakoa	1200	75	1500
10 cm	7200	450	9000

3.3.4. Tratamendu farmakologikoak

Zelulak tratatzeko, farmakoaren kontzentrazio handiagoa duen medioa zelulen ohiko hazkuntza mediora gehitu da (8. taula).

8. taula: Tesi honetan erabilitako farmakoen zehaztasunak. Farmakoaren izena, merkataritza-etxea eta bertan duen erreferentzia, biltegiratze kontzentrazioa, amaierako kontzentrazioa eta putzuan egiten den diluzioa adierazten dira.

Farmakoa	Merkataritza-etxea	Erreferentzia	Biltegiratze kontzentrazioa	Amaierako kontzentrazioa	Putzuko diluzioa
Zikloheximida (CHX)	Sigma-Aldrich	01810	10 mg/ml	10 μg/ml	1:4
Aktinomizina D (ActD)	Sigma-Aldrich	A9415	5 mg/ml	5 μg/ml	1:4
Leptomizina B (LMB)	Apollo-Scientific	BIL2101	6 μg/ml	6 ng/ml	1:4
Selinexor (SEL)	Selleckchem	S7252	100 μM	25 nM, 50 nM, 100 nM, 200 nM	1:2
Alisertib (ALS)	Selleckchem	S1133	100 μM	1 μM, 2 μM, 3 μM, 4,5 μM	1:2
Tazemetostat (TAZ)	Selleckchem	S7128	1 mM	250 nM, 1,25 μM, 2,5 μM 3,75 μM, 5 μM	1:2

8. taulako farmakoek ondorengo funtzioak dituzte:

- Zikloheximida (CHX), proteinen sintesia geldiarazteko erabili da pRev(1.4)-GFP bektorean oinarritutako esportazio entseguetan (3.6.1. atala). Proteinen sintesia geldiaraziz, esportazio-entseguan zitoplasman antzemandako GFP seinalea esportazio nuklearraren ondorioa baino ez dela ziurtatzen da.
- Aktinomizina D (ActD), Rev proteinaren NLSak gidatutako nukleoranzko inportazioa oztopatzeko erabili da. Inportazioa oztopatzeak, pRev(1.4)-GFP bektorean oinarritutako esportazio-entseguetan (3.6.1. atala) NES ahulen aktibitatea sumatzea ahalbidetzen du.
- Leptomizina B (LMB) CRM1 proteinaren poltsiko hidrofobikora lotzen da, poltsikoa betez eta bertara kargoak lotzea ekidinez. Beraz, LMB CRM1en mendeko esportazioaren inhibitzaile da. Tesi honetan, zitoplasman kokatzen diren proteinak edo NES aktibo bat duten proteinak CRM1en mende esportatzen diren baieztatzeko erabili da, baita, analisi proteomikoen bidez CRM1en inhibizioak proteina endogenoen banaketa azpizelularrean asaldurarik eragiten duen aztertzeko ere.
- Selinexor (SEL) ere, CRM1 proteinaren poltsiko hidrofobikora lotzen da eta LMBren moduan, CRM1en mendeko esportazioa inhibitzen du. Selinexor, klinikan erabiltzeko onartuta dago bai AEBetan bai Europan (Food and Drug Administration, 2019, 2020a, 2020b, European Medicines Agency, 2021). Tesi honetan farmakoen sinergia esperimentuetan erabili da.
- Alisertib (ALS), aurora kinasa Aren inhibitzailea da. Farmako honek pazienteetan erabiltzeko oniritzik jaso ez badu ere, entsegu klinikoen hirugarren fasera heldu da

(O'Connor et al., 2019). Alisertib, farmakoen sinergia esperimentuetan erabili da selinexor farmakoarekin batera.

– Tazemetostat (TAZ), S-adenosil metioninakin lehiatzen da EZH2 histona-metiltransferasara lotzeko. EZH2ra lotzean haren aktibitatea inhibitu egiten du. TAZ klinikan erabiltzeko onartua izan da AEBetan (Food and Drug Administration, 2020c, 2020d). Tesi honetan farmakoen sinergia esperimentuetan erabili da selinexor farmakoarekin batera.

3.4. Farmakoen sinergia ko-hazkuntzan neurtzeko entseguak

Farmakoen arteko sinergia Ramasamy eta lankideek (2012) garatutako modelo sistema batean neurtu da. Sistema horretan, minbizi hematologikoko zelulak hezur muineko estromako zelulen gainean hazten dira. Kasu honetan eGFP etiketa fluoreszentearekin markatutako MV4-11 leuzemia mieloide akutuko (AML) zelulak eta mCherry etiketa fluoreszenteaz markatutako HS5 hezur muineko estromako zelulak erabili dira. Etiketa ezberdinak izateak, batera hazten diren zelulak era bereizian eta erraz batean aztertzea ahalbidetuko du.

mCherry-HS5 zelulak 96 putzutako plaketako 48 putzutan (7. zutabetik 12. zutabera) erein dira 10^4 zelula/putzuko kontzentrazioan. Ereintzatik 24 ordura, zelulen medioa kendu eta plaketako putzu guztietan (A1-A3 eta A7-A9 putzuak salbu) 100 µl eGFP-MV4-11 zelula-suspentsio gehitu da $4x10^5$ zelula/ml-ko kontzentrazioan. Jarraian, intereseko farmakoaren amaierako kontzentrazioaren bikoitza duen 100 µl RPMI medio gehitu da. Baldintza bakoitza hiruna putzutan errepikatu da, bai eGFP-MV4-11 bakarrik ereindako putzuetan, zein mCherry-HS5 zelulekin batera ereindakoetan. Erabilitako farmakoak selinexor (SEL), alisertib (ALS) eta tazemetostat (TAZ) izan dira, bai banaka zein SEL/ALS edo SEL/TAZ konbinazioetan 8. taulan aipatutako kontzentrazioetan. Kontrol laginei 100 µl RPMI medio gehitu zaie eta eGFP-MV4-11 zelularik gehitu ez den putzuetan (A1-A3 eta A7-A9) RPMI medioaren 200 µl gehitu da.

3.4.1. Zelulen ugaritze analisia

Tratamendu farmakologikoa gehitu eta segituan zein 72 ordura, plakako putzu bakoitzeko fluoreszentzia-intentsitatea (FI) neurtu da. Neurketak, FLx800 plaka irakurlean (BioTek Instruments) egin dira. eGFP-MV4-11 zelulen ugaritzea neurtzeko, laginak 488 nm-tan kitzikatu dira eta emisioa 528 nm-tan jaso da, mCherry-HS5 zelulena neurtzeko ordea, laginak 584 nm-tan kitzikatu dira eta emisioa 607 nm-tan jaso da.

eGFP-MV4-11 zelulen ugaritze-arrazoia (UA) neurtzeko, lehenik eta behin, zelulak bakarrik edo ko-hazkuntzan hazitakoan esperimentuak duen atzeko-seinalea (*background*) kalkulatu da; bakarrik hazitako eGFP-MV4-11 zelulentzako atzeko-seinalea A1-A3 putzuetan jasotako

fluoreszentzia intentsitatearen batez bestekoa izango da, mCherry-HS5 zelulekin hazitako eGFP-MV4-11 zelulena ordea, A7-A9 putzuetakoa. Behin atzeko-seinalea kenduta, zelulak tratatu eta 72 ordura putzu bakoitzean jasotako fluoreszentzia seinalea, zelulak tratatu eta segituan jasotakoarekin zatitu da. Hau da:

$$UA = \frac{FI_{72\,h} - background_{72h}}{FI_0 - background_0}$$

Ugaritze-arrazoiak erabiliz kaltetutako-frakzioak (KF) kalkulatu dira:

$$KF = \frac{UA_{kontrol} - UA_{lagina}}{UA_{kontrol}}$$

KF balioekin, farmako eta farmako konbinazio bakoitzaren esperimentu guztien KF batez bestekoak eta desbiderapen estandarrak adierazten dituzten grafikoak egin dira. Gainera, batez besteko balio horietan oinarrituta eta Calcusyn softwarea erabilita (Biosoft), farmakoen konbinazioen sinergia-efektua kalkulatu da.

mCherry-HS5 zelulen kasuan, UA kalkulatzerakoan arazoak izan dira, t_0 denboretan neurketa zentzugabeak lortu baitira. Beraz, t_{72} denborak baino ez dira kontuan hartu. Kasu horietan KFak neurtzeko UA erabili beharrean t_{72} denborako FI datuak erabili dira atzeko-seinalea kenduta.

3.4.2. Apoptosi-analisia

eGFP-MV4-11 zelulak fixatzeko plakako putzu bakoitzera 60 µl % 4 paraformaldehido PBStan gehitu eta ondo berreseki da. Fixatutako zelulen plakak 4 °C-tan mantendu dira fluxu-zitometria analisiak burutu arte. Analisi horiek Accuri™ C6plus fluxu zitometroan (Becton Dickinson) egin dira eta lortutako datuak, BD CSampler softwarearekin (v.1.0.264.21) prozesatu dira.

Emaitzok, baldintza bakoitzean kontrolarekiko dagoen zelula apoptotiko kopurua kalkulatzeko erabili dira, horretarako, lagineko apoptosi balioari kontroleko apoptosi balioa kendu zaio. Balioen batez bestekoa eta desbiderapen estandarrak adierazi dira grafikoetan.

3.4.3. Efektu sinergistikoaren analisia

Zelulak farmako birekin tratatzean farmako horien elkarrekintzak zer nolako efektua duen aztertzeko Calcusyn softwarea (Biosoft) erabili da. Software hori Chou eta Talalayk 1984an konbinazio indizea (CI) zehazteko garatutako metodoan oinarritzen da. CIak bi farmakoren arteko elkarrekintza kuantitatiboki neurtzen du, horrela, CI ≥ 1,1 bada, efektua antagonikoa dela adierazten du, 0,9 < CI < 1,1 bada, efektu batukorra eta CI ≤ 0,9 bada, efektu sinergistikoa.

Efektu antagonikoak, bi farmakoren konbinazioaren efektua, farmako biek banaka duten efektuaren batuketaz espero zitekeen efektua baino baxuagoa dela adierazten du. Efektu batukorrak, bi farmakoen konbinazioaren efektua, farmako biek banaka dutenaren batuketaren baliokidea dela adierazten du. Eta efektu sinergistikoak, farmako bien konbinazioaren efektua, farmako biek banaka duten efektuaren batuketaz espero zitekeen efektua baino altuagoa dela adierazten du (Chou, 2006).

3.5. Fluoreszentziako mikroskopia teknikak

3.5.1. Mikroskopiarako laginen prestaketa

Fluoreszentziako mikroskopiaren bidez aztertutako lagin guztiak % 3,7 formaldehido (Sigma-Aldrich) PBStan fixatu dira ordu erdiz. Fixaketa bukatzean, laginak berezko fluoreszentzia badu (gainadierazitako proteinek YFP, GFP, sinGFP4a edo mRFP etiketa dutelako), lagina birritan PBStan garbitu eta portetan muntatu da DNA (nukleoak) ikustea ahalbidetzen duen 4',6-diamidino-2-fenilindoldun (DAPI) Vectashield muntaketa medio akuosoa (Vector Laboratories) erabilita.

Gainadierazitako proteinek berezko fluoreszentzia ez badute ordea, zelulen fixaketa eta laginaren muntaketa pausuen artean gainadierazitako proteinak antigorputzen bidez tindatu dira. Horretarako, zelulak fixatu ostean, PBStan garbitu eta % 0,2 Triton X-100 (Sigma-Aldrich) PBStan iragazkortu dira 10 minutuz. Iragazkortze-prozesuaren ostean lagina birritan PBStan garbitu da eta ordubetez blokeo-soluziotan (% 3 behi albumina seriko (BSA; Millipore) PBStan) inkubatu da. Jarraian, zelulak blokleo-soluziotan diluitutako antigorputz primarioan (anti-Myc edo anti-Flag) inkubatu dira ordubetez, eta inkubazio denbora igarotakoan, zelulak birritan PBSarekin garbitu eta minutu batez blokeo-soluziotan mantendu dira. Bukatzeko, zelulak blokeo-soluziotan diluitutako antigorputz sekundarioan inkubatu dira beste ordubetez eta ilunpetan. Azken inkubazio hori bukatzean lagina prest dago aurretik azaldu bezala mikroskopiarako portetan muntatzeko. Immunofluoreszentziarako erabilitako antigorputzak 9. taulan ageri dira.

9. taula: Immunofluoreszentziarako erabilitako antigorputzak.

Antigorputza	Merkataritza-etxea	Erreferentzia	Animalia	Diluzioa
Myc-Tag	Cell Signaling Technology	9B11	Sagua	1:300
Flag M2	Sigma-Aldrich	SLBK1346V	Sagua	1:400
Sagu AF488	ThermoFisher Scientific	A-10680	Ahuntza	1:400
Sagu AF633	ThermoFisher Scientific	A-21050	Ahuntza	1:400
Sagu AF594	ThermoFisher Scientific	A-11005	Ahuntza	1:400

3.5.2. Mikroskopia

Laginak Euskal Herriko Unibertsitateko (UPV/EHU) ikerkuntzarako zerbitzu orokorretako (SGIker) Mikroskopia Analitikoa eta Bereizmen Handikoa Biomedikuntzan Zerbitzuan (UPV/EHU) aztertu dira. Laginak modu orokorrean behatzeko eta zelulen kontaketetarako fluoreszentziako Zeiss Axioskop mikroskopioa erabili da, eta zenbait argazki mikroskopio hori, Nikon DS-Qi1Mc kamara eta NIS-Elements softwarea erabiliz hartu dira. Kasu gehienetan baina, argazkiak Zeiss Apotome2 fluoreszentziako mikroskopioan hartu dira Zen2.6 Blue edition softwarea erabiliz. Emaitzen atalean erakusten diren argazkiak Axioskop mikroskopioan egindakoak badira, argazkien oinetan adieraziko da, eta ezer ez adieraztekotan Apotome2 mikroskopioan hartu direla esan nahi du.

3.5.3. Irudi-analisia

Irudi-analisia, Fiji softwarerako (Schindelin et al., 2012) Ignacio Arganda-Carreras doktorearekin batera eta MorphoLibJ bilduma (Legland et al., 2016) erabilita garatutako script batekin (Olazabal-Herrero et al., 2019) egin da. Script horren bidez, proteina jakin batek nukleo eta zitoplasmaren artean duen banaketa era semi-kuantitatiboan aztertu da. Analisiarekin hasi aurretik irudi-konposatuak osatu dira. Irudi horietan kanal ezberdinak gainezartzen dira kanal bakoitzaren jatorrizko ezaugarriak galdu gabe. Irudi-konposatuak eratzeko, Zeiss Apotome2 mikroskopioan eremu berdinen sekzio optikoko eta ohiko fluoreszentziako argazkiak hartu dira. Argazki horiekin eta Fiji softwarea erabilita (i) ikertzeke dagoen kanaleko sekzio optikoko argazkia, (ii) maskara-zitoplasmatikoa (ikertuko den eremua) mugatuko duen kanalaren sekzio optikoko argazkia, eta (iii) nukleoen ohiko fluoreszentziazko argazkiak konbinatu dira. Ikertzeke dagoen kanala eta maskara-zitoplasmatikoa mugatuko duen kanala entseguaren arabera berdina izan daiteke: ezberdinak izango dira ikertu nahi den proteinaren kokapena gainadierazitako beste proteina baten mendekoa baldin bada, eta berdinak horrelako mendekotasunik agertzen ez baldin bada (17. irudia).

Mendekotasun eza:

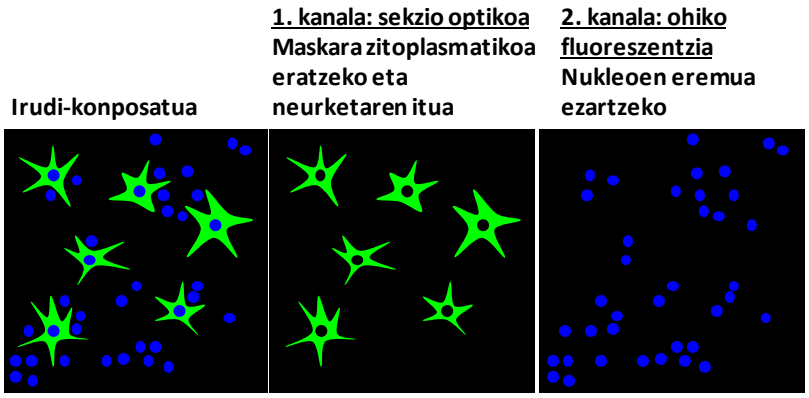

Mendekotasuna dago:

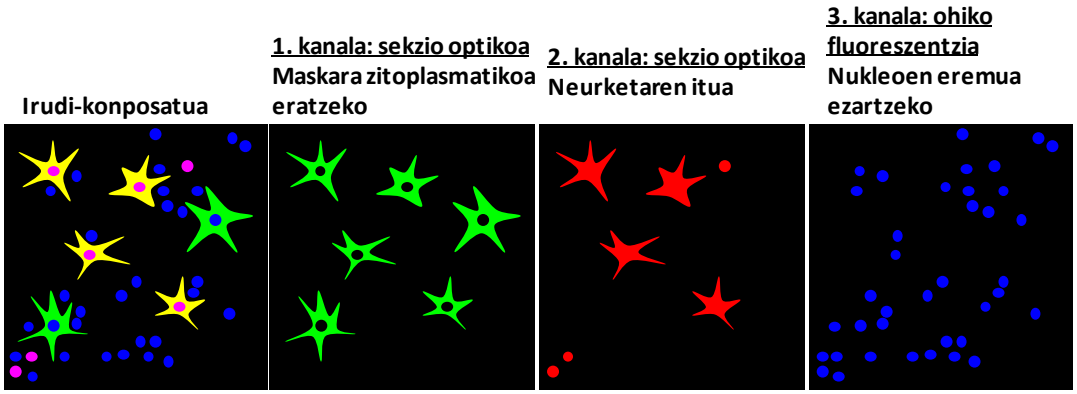

17. irudia: Irudi-analisirako erabili diren irudi-konposatuen kanal bakoitza nolakoa den eta zertarako erabili den adierazten duen irudi eskematikoa. Goiko panelean proteina baten kokapena beste baten mendekoa ez denean erabili diren irudi-konposatuen adibidea agertzen da. 1. kanala sekzio optikoan eginiko argazkia da eta maskara-zitoplasmatikoaren eremua mugatzeko eta fluoreszentziaren intentsitatea neurtzeko erabiltzen da. 2. kanala ohiko fluoreszentziako argazkia da eta 1. kanala erabiliz mugatutako eremuaren barruan nukleoak bilatzeko erabiltzen da. Beheko panelean proteina baten kokapena beste bat adieraztearen mendekoa denean erabili diren irudi-konposatuen adibidea agertzen da. 1. kanala sekzio optikoan eginiko argazkia da eta maskara-zitoplasmatikoaren eremua mugatzeko erabiltzen da. 2. kanala sekzio optikoan eginiko argazkia da eta fluoreszentziaren intentsitatea neurtzeko erabiltzen da. 3. kanala ohiko fluoreszentziako argazkia da eta 1. kanala erabiliz mugatutako eremuaren barruan nukleoak bilatzeko erabiltzen da.

Eratutako irudi-konposatu horiekin eta garatutako scripta erabiliz proteina jakinari dagokion fluoreszentzia intentsitatearen batez bestekoa nukleoan eta nukleoaren inguruan birtualki eratzen den eraztun zitoplasmatikoan neurtuko da. Horretarako, ezinbestekoa da scriptari kanal bakoitza zertarako erabili behar duen, nukleoak banatzeko tolerantzia zein den, eta non eta nolako eraztuna eratu behar duen adieraztea (10. taula).

10. taula: Irudi-analisiaren bidez proteina fluoreszenteen kokapena aztertzeko scripterako parametroak. Proteinen arteko mendekotasuna ez dagoenean eta mendekotasuna dagoenean erabili diren parametroak adierazten dira.

	Mendekotasunik gabe	Mendekotasunarekin
Nukleoen kanala	2	3
Neurketen eremua mugatzeko kanala	1	1
Neurketen kanala	1	2
Tolerantzia	1	1
Eraztun zitoplasmatikoaren lodiera	2	2
Nukleoaren ertzetik eraztun zitoplasmatikorako distantzia	4	4

Analisirako parametroak ezarri direla, scriptak irudi-konposatua hartu eta maskara-zitoplasmatikoa eratzen du, hau da, neurketetarako eremua zehazten du (18. irudia). Jarraian, maskara hori hartuta, nukleoen kanalera doa eta maskara-zitoplasmatikoa nukleoen kanalarekin gainezartzean maskara-zitoplasmatikoaz estalita geratzen diren nukleoak hautatzen ditu. Nukleoak hautatuta, irudi-konposatura bueltatu eta neurketak egingo diren kanalean nukleo horiei dagozkien eremuetan eta horien inguruan ezartzen diren eraztunetan fluoreszentzia intentsitatea neurtzen da. Bukatzeko, eremu bakoitzean neurtutako fluoreszentzia intentsitatearen batez bestekoak kalkulatzen ditu. Fluoreszentziaren intentsitatearen batez bestekoa neurtzeaz gain, scriptak nukleoen zirkulartasuna, perimetroa, eta proteina baten banaketa nukleozitoplasmatikoa nolakoa den zehazteko erabili daitezkeen beste hainbat parametro ere neur ditzake.

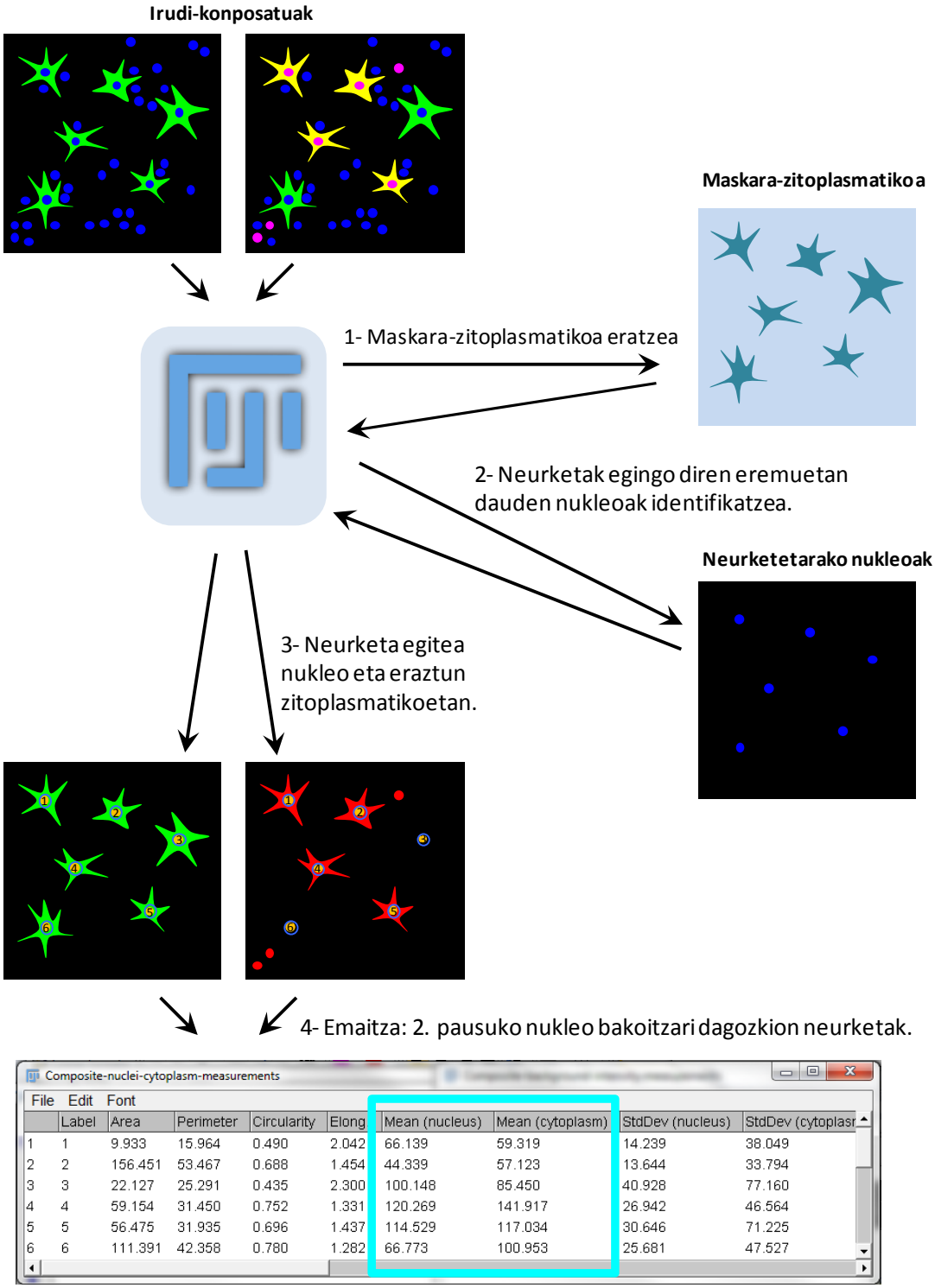

	Label	Area	Perimeter	Circularity	Elong	Mean (nucleus)	Mean (cytoplasm)	StdDev (nucleus)	StdDev (cytoplasr
1	1	9.933	15.964	0.490	2.042	66.139	59.319	14.239	38.049
2	2	156.451	53.467	0.688	1.454	44.339	57.123	13.644	33.794
3	3	22.127	25.291	0.435	2.300	100.148	85.450	40.928	77.160
4	4	59.154	31.450	0.752	1.331	120.269	141.917	26.942	46.564
5	5	56.475	31.935	0.696	1.437	114.529	117.034	30.646	71.225
6	6	111.391	42.358	0.780	1.282	66.773	100.953	25.681	47.527

18. irudia: Irudi-analisirako sortutako scriptak egiten dituen urratsen eskema. Irudi-konposatutik hasita eta 10. taulan aipatutako parametroak ezarri ostean, lehenengo pausua (1) maskara-zitoplasmatikoak eratzea da. Maskara horrek neurketa zein eremuren barruan egingo den mugatzen du. Jarraian, (2) maskara-zitoplasmatikoarekin irudi-konposatura bueltatu eta nukleoen kanalean maskara-zitoplasmatikoaren barne dauden nukleoak hautatzen dira. Bukatzeko, (3) irudi-konposatura bueltatu eta neurketak egingo diren kanalean hautatutako nukleoen (horiz) eta horien inguruan sortzen dituen eraztunetan (urdinez) egiten dira neurketak. Emaitza (4) zelula bakoitzari dagozkion hainbat neurketa dira, urdin argiz tesi honetan proteina jakinen banaketa nukleozitoplasmatikoa aztertzeko kontuan izan diren neurketak markatu dira.

Scripta erabiliz ikertzeko eremuak ondo ezarri direla ziurtatzeko, lortutako emaitzak zelulaz zelula berraztertu dira eskuz. Gainera, eskuz ere, zelularik gabeko eremua mugatu da atzealdeko fluoreszentzia neurtzeko. Zelula bakoitzaren nukleo eta zitoplasmaren fluoreszentzia balioari zelula hori agertu den argazkiko atzealdeko fluoreszentzia balioa kendu zaio.

Behin analizatuko diren zelula guztien nukleo eta zitoplasmako fluoreszentzia balioak zuzenduta (atzealdeko fluoreszentzia kenduta), zelula bakoitzean analizatzeke dagoen proteinak duen banaketa nukleozitoplasmatikoa kalkulatu da:

$$Banaketa\ nukleozitoplasmatikoa = log_2\left(\frac{nukleoko\ fluoreszentzia}{zitoplasmako\ fluoreszentzia}\right)$$

Formula horretatik erauzitako datuekin, eta GraphPad Prism softwarea erabiliz, zelula bakoitzaren banaketa nukleozitoplasmatikoaren balioa, laginaren batez bestekoa balioa eta desbiderapen estandarrak erakusten duten grafikoak irudikatu dira. Lagin ezberdinak Mann-Whitney U testaren bidez konparatu dira eta $p < 0,05$ balioak esanguratsu kontsideratu dira.

3.6. Esportazio-entseguak

Tesi lan honetan bi esportazio-entsegu mota erabili dira: Rev(1.4)-GFP erreportarian oinarritutakoa (Henderson eta Eleftheriou, 2000) eta $SRV_{B/A}$ erreportarian oinarritutakoa (Taylor et al., 2019; Sendino et al., 2020a). Lehen esportazio-entseguaren erabilera oso zabalduta dago, Scopus datu basearen arabera 345 aldiz aipatu da (2022ko urtarrilean kontsultatuta); bigarren entsegua ordea, lan honen garapenaren emaitza da. Atal honetan metodologiari dagozkion zehaztasunak baino ez dira azalduko, oinarrizko arrazoia emaitzekin batera azalduko da.

3.6.1. Rev(1.4)-GFP erreportarian oinarritutako entseguak

Rev(1.4)-GFP erreportarian oinarritutako esportazio-entsegua (Henderson eta Eleftheriou, 2000), NES kandidatuen (cNES) edo NES ezagunen baina esportazio-aktibitate ezezaguna duten motiboen esportazio-aktibitatea neurtzeko erabili da. Aztertzeke dauden sekuentziak pRev(1.4)-GFP bektorean klonatu dira BamHI eta AgeI murrizteguneen artean (19. irudia).

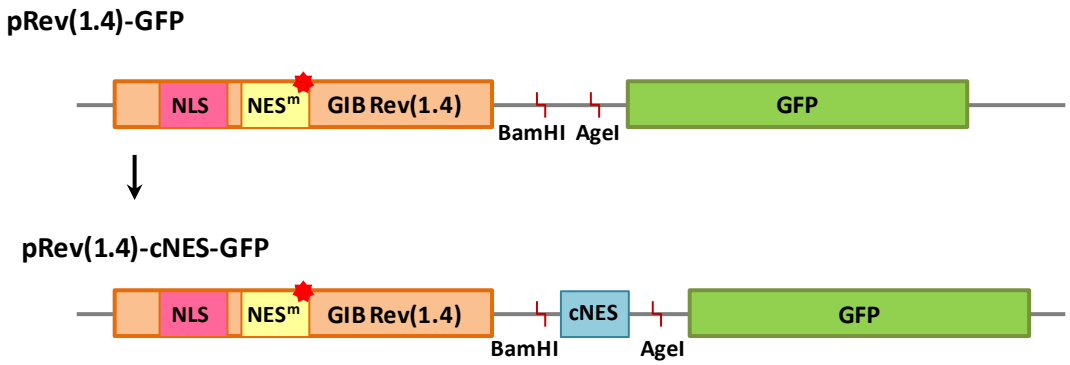

19. irudia: pRev(1.4)-GFP eta pRev(1.4)-cNES-GFP erreportarien irudi eskematikoa. pRev(1.4)-GFP erreportariak laranjaz adierazitako GIB birusaren Rev proteinaren bertsio mutante bat (1.4) eta berdez adierazitako GFP proteina fluoreszentea adierazten ditu. Rev(1.4) proteinak aktiboa den NLS bat (arrosaz adierazita) eta NES mutatu bat (horiz eta izar gorriaz adierazita) ditu. Rev(1.4) eta GFP proteinen sekuentzia-kodetzaileen artean BamHI eta AgeI murrizteguneak daude, zeintzuek cNESak pRev(1.4)-GFP erreportarian klonatzea ahalbidetuko duten pRev(1.4)-cNES-GFP erreportaria lortuz. cNESek erreportarian hartzen duten kokapena urdinez adierazi da.

Rev(1.4)-GFP erreportarian oinarritutako entseguak HeLa zelulatan egin dira 12 putzutako plaketan. pRev(1.4)-cNES-GFP bakoitza bi putzutan transfektatu da. Putzu bateko zelulak CHXrekin tratatu dira, bestekoak ordea, CHX eta ActDrekin. Kontrol bezala pRev(1.4)-GFP bektore hutsa transfektatu eta tratatu da.

Laginok mikroskopiarako prestatu dira eta Axioskop fluoreszentziako mikroskopioa erabilita gutxienez 200 zelula nuklear, nukleozitoplasmatiko edo zitoplasmatiko kategoriatan sailkatu dira. Sailkapen horrekin ehunekoak kalkulatu eta 11. taula erabiliz cNESen esportazio-aktibitatea neurtu da. Aktiboak diren motiboei 1 eta 9 arteko balioak eman zaizkie 1 aktiboetan ahulena delarik eta 9 aktiboena.

11. taula: Henderson eta Eleftheriouk (2000) deskribatutako NESen aktibitatea mailakatzeko sistema. Ikertutako NES aktibo bakoitzaren aktibitate mailari 1 eta 9 arteko balioa eman zaio fusio-proteinak erakutsitako kokapen nukleozitoplasmatikoaren arabera.

NESaren aktibitate maila	GFPa partzialki metatzen da zitoplasman (zelulen %)		GFPa guztiz metatzen da zitoplasman (zelulen %)	
	-ActD	+ActD (3 h)	-ActD	+ActD (3 h)
1	<20	20-50	0	0
2	<50	51-80	0	0
3	<50	>80	-	<20
4			<20	20-50
5			<20	51-80
6			<20	>80
7			20-50	>80
8			51-80	>80
9			>80	>80

3.6.2. $SRV_{B/A}$ erreportarian oinarritutako entseguak

$SRV_{B/A}$ entseguak HEK293T zelulatan egin dira 12 putzutako plaketan. Ikergaia den NESa bere baitan duen $SRV_{B/A}$ erreportaria (SRV-NES) bera bakarrik zein YFP-CRM1en aldaera ezberdinekin batera transfektatu da. Transfekzioa eta 24 ordura laginak mikroskopiarako prestatu dira anti-Flag eta AF594 antigorputzekin tindatuz.

Entsegu honen emaitzak hiru metodo ezberdin erabiliz analizatu dira:

Lehenengo metodoa: erreportariak hartzen duen kokapen nukleozitoplasmatiko orokorra begiz klasifikatu da bost kategoriatan: guztiz nuklearra (N), gehienbat nuklearra (N > Z), nuklear eta zitoplasmatikoa neurri berean (NZ), gehienbat zitoplasmatikoa (Z > N) eta guztiz zitoplasmatikoa (Z).

Bigarren metodoa: pRev(1.4)-GFP erreportarian oinarritutako esportazio-entseguan egin bezala erreportariaren kokapena nuklear (N), nukleozitoplasmatiko (NZ) edo zitoplasmatiko (Z) kategorietan sailkatu da gutxienez lagineko 200 zelulatan. Kategoria bakoitzean sailkatutako zelulen ehunekoak kalkulatu dira. Ehuneko horiekin NES/CRM1 aldaera konbinazio ezberdinen esportazioa konparatzea errazteko 0tik 100era doan SRV esportazio-aktibitate maila (SRV balio bezala izendatuko dena) kalkulatu da hurrengo formula erabiliz.

$$SRV\ balioa = 0 \times (\%\ N) + 0{,}5 \times (\%\ NZ) + 1 \times (\%\ Z)$$

Hirugarren metodoa: 3.5.3. atalean azaldutako Fiji softwarearen bidezko irudi-analisia erabili da. Funtsean, erreportariaren kontrako antigorputzek sortutako fluoreszentzia nukleoan eta zitoplasman semi-kuantitatiboki neurtzean eta konpartimendu bietan jasotako fluoreszentziaren arteko arrazoia kalkulatzean datza.

Hiru metodo horiek egoera ezberdinetan edo zehaztasun maila ezberdina duten emaitzak lortzeko helburuarekin aplikatu dira. Lehen metodoaren bidez lortutako emaitzek erreportariaren kokapen orokorraren informazioa ematen dute. Bigarren metodoak, lehenengo metodoa baino informazio zehatzagoa ematen du, eta nahiz eta erreportariak zelularen barne hartzen duen kokapena kategoria orokorretan sailkatu, emaitza kuantifikagarriak lortzeko bidea eman du. Bigarren metodologia hori García-Santisteban eta lankideek (2016) erabilitakoan oinarritu da. Hirugarren metodoari dakionez, erabilitako metodologien artean emaitza zehatzenak ematen dituena da. Metodo horrekin lortutako emaitzek, erreportariak zelula bakoitzean duen kokapena zein orokorrean lagin osoan duena islatzen dute.

3.7. Proteinen analisirako teknikak

3.7.1. Proteinen gertuko biotinilazioa

APEX2 peroxidasarekin fusionatutako proteina gainadierazten duten zelulak 500 µM biotin-fenoldun (BP) hazkuntza mediotan inkubatu dira 30 minutuz eta 37 °C-tan. Inkubazioa bukatzean, zelulen mediora APEX2 peroxidasa aktibatuko duen H_2O_2-a gehitu da 10 mM-eko amaierako kontzentrazioan. Zelulak minutu batez mantendu dira H_2O_2-dun mediotan eta jarraian *Quencher* soluziotan (10 mM sodio askorbato, 5 mM Trolox, 10 mM azida sodikoa PBStan) garbitu dira hiru aldiz. Hirugarren garbiketan *Quencher* soluzioa segituan kendu ordez, zelulak 5 minutuz inkubatu dira ilunpetan. Azkenik, zelulak PBStan garbitu dira (Hung et al., 2016-etik moldatutako protokoloa).

3.7.2. Proteina erauzketa

6 putzutako plaketako zelulak jasotzeko, zelulak PBStan garbitu eta putzu bakoitzean Laemmli lisi-indargetzailearen 100 µl gehitu da. Laginak putzuetatik mikrozentrifuga tutuetara transferitu dira. Lagin horiek 95 °C-tan irakin dira 5-10 minutuz.

Proteomika analisietarako proteina-erauzkinak lortzeko erabilitako metodoa proteomikarako laginak prestatzeko prozedura biak azaltzen diren atalean azalduko dira (3.7.6.2. eta 3.7.7.2. atalak).

3.7.3. Proteinen kuantifikazioa: Lowry metodoa

Proteinen erauzkinetako proteina-kontzentrazioa zehazteko, Bio-Rad Protein Assay kitaren bidezko Lowry metodo eraldatua erabili da. Behi-albumina serikoa (BSA) estandar gisa erabili da. Laburbilduz, A erreaktiboa eta S erreaktiboa 50:1 proportzioan nahastu dira. Nahasketa horretatik 25 µl gehitu zaizkie aztertzeko dauden lagin diluituei eta BSA estandarrei. Ondoren, B erreaktiboaren 200 µl gehitu dira eta nahasketa 15 minutuz inkubatu da giro-tenperaturan. Inkubazioa bukatzean, putzu bakoitzaren 750 nm-tako xurgapena neurtu da PowerWave340 (BioTek Instruments) mikroplaka-irakurgailua erabilita.

3.7.4. Proteinak gelean ikusarazteko teknikak

3.7.4.1. Sodio dodezil sulfato-poliakrilamida gel elektroforesia (SDS-PAGE)

Poliakrilamidazko gelak behetik eta aldeetatik hermetikoki itxita dauden bi kristalen artean polimerizatu dira. Goiko aldean, laginak kargatzea ahalbidetuko duten putzuak sortzeko orraziak jarri dira. Gel bakoitza bi ataletan dago banaturik; pilatze-gela eta banatze-gela. Pilatze-gela, gelaren goiko aldean kokatzen da eta poliakrilamida kontzentrazio txikia (% 5) dauka. Proteinak bertan kargatzen dira, eta pilatze-gelaren azpian dagoen banatze-gelera

proteina guztiak aldi berean heltzea eragiten du. Esan bezala, banatze-gela pilatze-gelaren azpian dago eta horrek duen poliakrilamida kontzentrazio handiagoari esker (% 12), proteinak euren pisu molekularraren arabera banatzen ditu (Laemmli, 1970).

Proteina laginak (20-40 µg proteina putzuko) Bio-Rad MiniPROTEAN Tetra Cell elektroforesi bertikal sisteman banatu dira, korronte elektrikoaren intentsitate konstantepean eta 1X proteina elektroforesi-indargetzailetan murgilduta. Geletan banatutako proteinen tamainak estimatzeko, PageRuler Plus Stained Protein Ladder (ThermoFisher Scientific) eta Precision Plus Protein™ Dual Color (Bio-Rad) proteina-estandarrak erabili dira.

3.7.4.2. Western plapaketa

Elektroforesiaren bidez banandutako proteinak nitrozelulosazko mintzetara (Bio-Rad) transferitu dira bi orduz, 4 °C eta 100 V-tan, Bio-Rad Mini Trans-Blot® transferentzia-sistema erabiliz. Transferentzia gertatzeko gela eta mintzak 1X transferentzia-indargetzailetan murgildu dira. Transferentzia bukatutakoan mintzak Ponceau S-tan (Sigma) tindatu dira transferentzia ondo eman dela ziurtatzeko. Jarraian, mintzak TTBStan garbitu eta blokeo-soluziotan (% 5 esne gaingabetua TTBStan) inkubatu dira ordubetez agitazio geldoan.

Behin mintzak blokeatuta, mintzak blokeo-soluziotan diluitutako antigorputz primarioarekin inkubatu dira ordubetez giro-tenperaturan edo gau osoan zehar 4 °C-tan agitazio geldoan. Jarraian, 5 minutuko hiru garbiketa egin dira TTBStan. Mintza garbi dagoela, blokeo-soluziotan diluitutako HRPdun (*Horseradish peroxidase;* errefau min peroxidasa) antigorputzak gehitu dira eta beste ordubetez inkubatu dira giro-tenperaturan eta agitazio geldoan. Erabilitako antigorputzak 12. taulan ageri dira. Bukatzeko, mintzak beste 3 aldiz garbitu dira TTBStan eta Pierce ECL Plus detekzio-agentea eta ChemiDoc (Bio-Rad) irudi softwarea erabiliz errebelatu dira.

12. taula: Western plapaketan erabilitako antigorputzak.

Antigorputza	Merkataritza-etxea	Erreferentzia	Animalia	Diluzioa	Inkubazio baldintzak
GFP monoklonala	Chromotek	3H9	Arratoia	1:1000	4 °C gau osoa /1 h giro-tenperatura
GFP poliklonala	Abcam	Ab290	Untxia	1:1000	4 °C gau osoa
Myc-Tag	Cell Signaling technologiy	9B11	Sagua	1:2000	4 °C gau osoa
Biotina-HRP	Cell Signaling technology	7075S	Ahuntza	1:1000	1 h giro-tenperatura
Arratoi-HRP	Santa Cruz	sc-3823	Ahuntza	1:3000	1 h giro-tenperatura
Untxi-HRP	Santa Cruz	sc-2030	Ahuntza	1:3000	1 h giro-tenperatura
Sagu-HRP	Santa Cruz	sc-3697	Ahuntza	1:3000	1 h giro-tenperatura

3.7.4.3. Zilar tindaketa

Proteomikaren bidez aztertuko diren laginetan proteina kopurua zenbatesteko, proteomika zerbitzura bidaliko den lagin bolumenaren % 10 zilar-tindaketaren bidez aztertu da. Tindaketak SilverQuest Kitaren (ThermoFisher Scientific) fabrikatzailearen argibideei jarraituz egin dira. Laburrean azalduta, lehenik eta behin, SDS-PAGE gelak MiliQ uretan garbitu eta % 40 etanol eta % 10 azido azetiko soluzioan fixatu dira ordubetez. Inkubazioa bukatzean, gelak 10 minutuko lau inkubaziotan, etanoletan garbitu (% 30 etanol), sentikortu (% 30 etanol, % 10 SilverQuest kit sensitizer), berriz ere etanoletan garbitu eta MiliQ uretan garbitu dira. Jarraian, tindaketa-soluziotan (% 1 SilverQuest kit stainer) inkubatu dira 15 minutuz, eta gehiegizko zilar ioiak kentzeko 30 segundoz MiliQ uretan garbitu dira. Gelak errebelatzeko, errebelatze-soluziotan (% 10 SilverQuest Kit developer eta 100 ml soluzioko Silverquest kit developer enhancerraren tanta bat) inkubatu dira bandek intentsitate nahikoa lortu arte. Momentu horretan, erreaktibo geldiarazlea gehitu eta 10 minutuz inkubatu da gela tindaketa-erreakzioa gelditzeko. Bukatzeko gelak MiliQ uretan garbitu dira.

3.7.4.4. *Coomassie* tindaketa

SDS-PAGE gelak GelCode Blue Stain (ThermoFisher Scientific) mediotan bi orduz murgilduta eta agitazio leunean mantenduz tindatu dira. Gehiegizko tindagaia kentzeko gelak MiliQ uretan inkubatu dira hiru orduz.

3.7.5. Masa-espektrometria analisiak

GFP-trap bihitxo magnetikoetatik, zein neutrabidina-agarosa bihitxoetatik eluitutako proteinen laginak Euskal Herriko Unibertsitateko (UPV/EHU) ikerkuntzarako zerbitzu orokorretako (SGIker) Proteomika zerbitzuan analizatu dira. Horretarako, eluitutako proteinen erauzkinak SDS-PAGE bidez banatu eta proteinen geleango digestio triptikoa egin da. Digestiotik erauzitako peptidoak 3.7.5.3. atalean adierazitakoaren arabera analizatu dira likido-kromatografia-tandem masa-espektrometria (LC-MS/MS) erabiliz. Lortutako masa-espektroak MaxQuant softwarea (Cox eta Mann, 2008) erabiliz analizatu dira.

3.7.5.1. Masa-espektrometriaren oinarriak

Masa-espektrometrian oinarritutako proteomikan, zelula edo ehunetatik erauzitako proteinak SDS-PAGE geletan bana daitezke eta gelean bertan digeritu proteasa espezifikoak, tripsina esaterako, erabiliz. Proteinetatik eratorritako peptidoak kromatografiaren bidez banatu eta masa-espektrometroan analizatzen dira, peptidook ioinizatu eta masa/karga arrazoiaren (m/z) arabera banatuz (Steen eta Mann, 2004). Behin peptidoak euren m/z-ren arabera banatu direla, analizatzailearen barneko kolisio-ganbaran fragmentatuko dira gas inerte baten aurkako

kolisioen ondorioz, horrela, peptido aitzindarien informazioaz gain, peptidoen fragmentuen informazioa ere lortuko da (Aebersold eta Mann, 2003; Steen eta Mann, 2004). Peptido aitzindarien gaineko informazioaz gain, peptidoak kolisio-ganbaran fragmentatu, eta eratorritako fragmentuon informazioa ere analizatzeari tandem MS edota MS/MS deritzo. Ioi aitzindariaren eta horri dagozkion fragmentuen MS/MS datu esperimentalak datu-base bateko proteinei dagozkien peptidoen masa teorikoekin alderatzen dituen softwarea erabiltzen da laginean egon daitezkeen proteinak identifikatzeko.

3.7.5.2. Geleango digestio triptikoa

SDS-PAGE geletako intereseko zatiak ebaki eta geleango proteinen digestio triptikoa egin da Shevchenko et al.,1996-etik moldatutako protokoloa erabiliz. Labur azaltzeko, digestioa hiru urratsetan egin da: lehenengo urratsean eta proteinen disulfuro zubiak apurtzeko, gel zatiak 45 minutuz inkubatu dira 10 mM DTT 50 mM NH_4CO_3-tan eta 56 °C-tan; bigarrenean, eta apurtutako disulfuro zubi horiek berriz ere sortzea ekiditeko, zatiok iluntasunean eta 30 minutuz, 25 mM iodoazetamida NH_4CO_3-tan inkubatu dira giro-tenperaturan, eta hirugarrenean, 50 mM NH_4CO_3-tan 12,5 ng/ml kontzentrazioan diluitutako tripsinatan (Roche Diagnostics) inkubatu dira zatiok 37 °C-tan gau osoan. Azken inkubazio horren gainjalkin likidoa jaso, eta jalkineko gel zatietatik peptidoak birritan erauzi dira: lehenik 25 mM NH_4CO_3 eta azetonitrilotan, eta ostean, % 0,1 azido trifluoroazetiko eta azetonitrilotan. Erauzitako peptidoak aurretik jasotako gainjalkinarekin batu eta SpeedVac (ThermoFisher Scientific) zentrifugan sikatu dira. Bukatzeko, sikatutako peptidoak % 1 azido trifluoroazetikotan berreseki eta etxeko C18 (3M Empore C18) zutabeetan zehar pasarazi dira gatzgabetu, garbitu eta kontzentratzeko. Ostean, laginak berriro ere SpeedVacean sikatu eta % 0,1eko azido formikoan berreseki dira masa espektrometroan kargatu aurretik.

3.7.5.3. Likido-kromatografia-tandem masa-espektrometria (LC-MS/MS) analisiak

MS analisiak nanospray flex ioi iturri baten bidez konektatuta dauden EASY-nLC 1200 likido-kromatografia sistema, eta Q Exactive HF-X masa-espektrometroan (ThermoFisher Scientific) egin dira. Peptido triptikoak Acclaim PepMap RSLC (75 µm x 25 cm, ThermoFisher Scientific) zutabe analitiko batera konektatutako Acclaim PepMap100 (75 µm x 2 cm, ThermoFisher Scientific) aurre-zutabe batean kargatu dira. Peptidoak 300 nl/min-ko fluxuan eluitu dira zutabetik ondorengo azetonitrilo-gradientea erabiliz: % 2,4tik % 24ra 45 minutu, % 24tik % 32ra 2 minutu, % 32tik % 80ra minutu bat eta 12 minutu % 80an; gradiente osoan zehar azido formikoaren kontzentrazioa % 0,1ean mantendu da. Masa-espektrometroa ioi positibo funtzioan erabili da, eta 375-1800 m/z tarteko MS *scan* osoak jaso dira 60000-ko

bereizmenarekin (200 m/z-tan). Intentsitate altueneko 10 ioiak HCD (*Higher-energy C-trap dissociation*) disoziazioz fragmentatu dira 28ko kolisio energia normalizatuarekin, eta MS/MS espektroak 15000-ko bereizmenarekin (200 m/z-tan) jaso dira. Ioien gehienezko injekzio-denbora 50 ms-koa izan da lehen zundaketarako, eta 100 ms-koa MS/MS *scan*-etarako neutrabidina-agarosa bihitxoetatik eluitutako peptidoen kasuan; GFP-trap bihitxoetatik jasotako laginentzako berriz, 100 ms-koa izan da lehen zundaketarako injekzio-denbora, eta 120 ms-koa MS/MS *scan*-etarako. *Automatic Gain Control* (AGC) itu-balioak 3e6 eta 5e5 izan dira lehen zundaketarako eta MS/MS *scan*-etarako hurrenez hurren. Isolatze-leihoa 1,4 m/z-n ezarri da, eta 45 segundoko esklusio-leiho dinamikoa erabili da. Karga bakarreko ioiak, kargarik esleitu gabeko ioiak eta baita >5 kargako ioiak ere baztertu egin dira MS/MS analisietatik. Datuak Xcalibur softwarea (ThermoFisher Scientific) erabiliz jaso dira.

3.7.5.4. Datuen prozesamendua eta analisi bioinformatikoa

Prozesatu gabeko artxiboak MaxQuant (v.1.6.0.16) (Cox eta Mann, 2008) erabiliz prozesatu dira UniProtKB SwissProt Human datu basea erabilita (GFP-trap immunoprezipitazioko laginekin 2017-02ko bertsioa erabili da, neutrabidina-agarosa afinitate-purifikazioko laginekin, ordea, 2017-11koa, zeinetara APEX2dun proteinen sekuentziak eskuz gehitu diren). Bilaketetarako hurrengo parametroak erabili dira: aitzindarien eta fragmentuen tolerantziak 8 ppm eta 20 ppm-koak hurrenez hurren, tripsinak gehien jota bi mozketa egin gabe uztea, oxidazioa eta azetilazioa (proteinen amino-muturra) eraldaketa aldakor gisa hartu dira, eta karbamidometilazioa eraldaketa finko gisa. Peptido eta proteinen *False Discovery Rate*-a (FDR) % 1ean ezarri da.

3.7.6. RanGTPasa aktibitaterik ez duen Ran mutante bat erabiliz CRM1/kargo/RanGTP konplexua egonkortzean oinarritutako hurbilketa esperimentala

3.7.6.1. Laginen prestaketa

Bi esperimentu egin dira (20. irudia), bietan 10 cm-ko 9 plaka erabili dira. Plaka guztietan HEK293T zelulak erein, eta 24 ordura transfekzioak egin dira. Bi esperimentuetako plaka guztietan Myc epitopoarekin fusionatutako RanGTPasa aktibitaterik ez duen Ran proteinaren Q69L mutantea gainadierazi da. Horretaz gain, lehen esperimentuan; hiru plakatan YFP-CRM1 basatia gainadierazi da, beste hiru plakatan YFP-CRM1en E571K minbizi mutantea eta azkeneko 3 plakatan kargoak lotzeko gai ez den eta kontrol gisa erabili den YFP-CRM1^{4x} (Dong et al., 2009a). Bigarren esperimentuan, hiru plakatan YFP-CRM1 basatia, beste hiru plakatan YFP-CRM1^{4x} (Dong et al., 2009a) eta azken hiru plaketan pEYFP-C1 bektore hutsa (Clontech) gainadierazi dira.

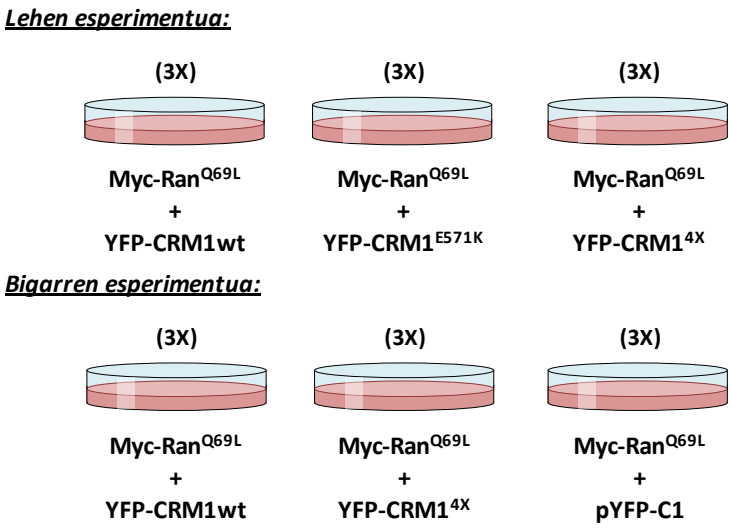

20. irudia: CRM1/kargoa/RanGTP konplexua egonkortzean oinarritutako hurbilketa esperimentalean eginiko esperimentuetan erabilitako laginak.

3.7.6.2. Zelulak jasotzea eta lisatzea

Lehenengo esperimentuaren kasuan, zelulak PBStan behin garbitu dira eta jarraian zelulen lisiari ekin zaio. Bigarren esperimentuaren kasuan, zelulak PBStan garbitu, tutuetan jaso eta bederatzi alikuotak -20 °C-tan gorde dira. Gordetako alikuota horietatik hiru (transfekzio egoera bakoitzeko alikuota bana) lisatu eta aztertu egin dira.

Lisia era berean eman da bi esperimentuetan, horretarako, zelulei, plakan (lehen esperimentua) edo tutuetan (bigarren esperimentua) egon, % 1 PMSF (ThermoFisher Scientific) eta % 1 proteasa inhibitzaile nahasketa (Roche) duen Pierce lisi-indargetzailearen (ThermoFisher Scientific) 1 ml gehitu zaie. Lehen esperimentuko plaketako zelulak mikrozentrifuga tutuera transferitu dira. Tutuak, bai lehen zein bigarren esperimentukoak, 30 minutuz eta 4 °C-tan errotazioan inkubatu dira. Inkubazioak iraun bitartean, laginak 5-10 minuturo pipetarekin ondo berreseki dira. Laginak 10 minutuz 13000 rpm-tan zentrifugatu dira 4 °C-tan. Gainjalkin bakoitza bi alikuotatan banatu da, bata 100 µl-ko alikuota txikia, zelula erauzkin osoan dauden proteinak Western plapaketa bidez aztertzeko erabiliko dena, eta bestea 950 µl-ko alikuota, zeina GFP-Trap®_M bihitxoekin nahastuko den. 100 µl-ko alikuotak 20 µl 6X proteina karga-indargetzailerekin nahastu eta 95 °C-tan irakin dira 5 minutuz, -20 °C-tan gorde aurretik.

3.7.6.3. GFP-Trap®_M bihitxo magnetikoak erabilita eginiko immunoprezipitazioa

Aurreko atalean aipatutako 950 µl-ko alikuotak, aurretiaz lisi-indargetzailetan orekatutako 30 µl GFP-Trap®_M bihitxorekin nahastu eta 4 °C eta errotazioan inkubatu dira 3 orduz. Inkubazioa bukatzean, lehen esperimentuko laginek bere baitan jarraitu dute hurrengo

urratsera arte, bigarren esperimentuko lagin bakoitza ordea, hirutan banatu da (A, B eta C azpilaginak). Lehen esperimentuko lagin eta bigarren esperimentuko azpilagin bakoitza birritan garbitu da 500 µl lisi-indargetzailetan; lehen esperimentuko laginen, eta bigarren esperimentuko A azpilaginen garbiketetarako, aurreko pausuetan erabilitako lisi-indargetzaile berbera erabili da, hau da, 150 mM NaCl-dun lisi-indargetzailea. B eta C azpilaginen garbiketetarako lisi-indargetzaileko gatz kontzentrazioa handiagotu egin da, horrela, B azpilaginen garbiketatarako 200 mM NaCl-dun lisi-indargetzailea eta C azpilaginen garbiketetarako 400 mM NaCl-dun lisi-indargetzaileak erabili dira (gainontzeko erreaktiboen kontzentrazioa mantendu egin da). Azkenik, bihitxoak 60 µl 1X proteina karga-indargetzailetan berreseki eta 95 °C-tan irakin dira 5 minutuz, -20 °C-tan gorde aurretik.

3.7.7. APEX2 peroxidasaren bidezko gertuko proteinen biotinilazioan oinarritutako hurbilketa esperimentala

3.7.7.1. Proteomikarako laginen prestaketa

HEK293T zelulak 10 cm-ko 6 plaketan erein eta 24 ordura, 3 plakatako zelulak zitoplasmako proteinen biotinilazioa eragingo duen APEX2zit markatzailearekin eta beste 3 plakatakoak nukleoko proteinena eragingo duen APEX2nuk markatzailearekin transfektatu dira (21. irudia). Transfektatu eta 24 ordura, hirukote bakoitzeko plaka bana LMBrekin tratatu da. Plaka horiekin 3.7.1. atalean azaldutako proteinen gertuko biotinilazio protokoloa jarraitu da. APEX2zit edo APEX2nuk gainadierazten duten, eta LMB tratamendurik ez duten zelulen plaka banatan ez da H_2O_2-rik gehitu; lagin horiek berezko biotinilazioaren kontrolak izango dira. Horrela, markatzaile bakoitzerako ondorengo egoerak lortuko dira: kontrol egoera (-LMB/-H_2O_2), egoera basala (-LMB/+H_2O_2) eta CRM1 inhibitutako egoera (+LMB/+H_2O_2).

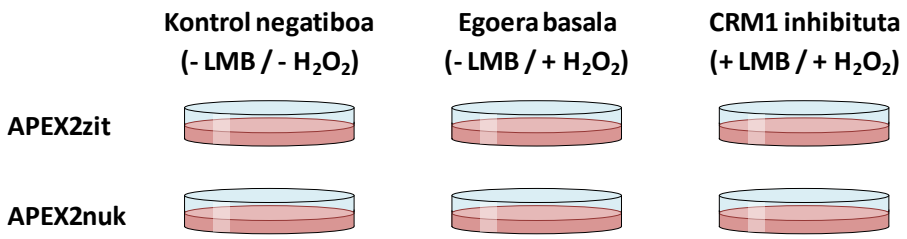

21. irudia: APEX2 peroxidasaren bidezko gertuko proteinen biotinilazioan oinarritutako hurbilketa esperimentalean eginiko esperimenturako prestatutako laginak.

3.7.7.2. Zelulak jasotzea eta lisatzea

Aurreko atalean azaldutako sei plaketako zelulak tripsina erabilita altxatu, eta plaka bakoitzeko zelulak 10 ml PBStan jaso dira. 10 ml horiek bi alikuotatan banatu dira: 1 ml-ko alikuota bat biotinilazioa Western plapaketaren bidez aztertzeko eta 9 ml-ko beste alikuota bat

neutrabidina-agarosa afinitate-purifikaziorako. Alikuota guztiak 13000 rpm-tan zentrifugatu dira 5 minutuz. Gainjalkinak baztertu egin dira.

Western plapaketarako gordetako alikuotetako zelulak Laemmli-lisi-indargetzailearen 200 µl gehituta eta 95 °C-tan 10 minutuz inkubatuta lisatu dira.

Proteomikarako gordetako alikuotetako zelulak neutrabidina afinitate-purifikaziorako lisi-indargetzaile eta proteasa inhibitzaile-nahasketaren (Roche) 2,9 ml-tan berreseki da. Lisia gertatzeko, laginak errotazioan inkubatu dira 30 minutuz eta 4 °C-tan. Inkubazioa bukatzean laginak 20 G xiringen zehar pasarazi dira. Bukatzeko, laginak 14000 rpm-tan zentrifugatu dira 5 minutuz eta 4 °C tan. Gainjalkinak hurrengo atalean azalduta dagoen afinitate-purifikaziorako gorde dira.

3.7.7.3. Neutrabidina-agarosa bihitxoak erabilita eginiko afinitate-purifikazioa

Laginak (2,5 ml) aurretik 25 ml lotze-indargetzailetan orekatutako PD10 (Healthcare) zutabeetan kargatu dira. Zutabe horietan lagineko molekula handi eta txikiak banatuko dira, eta beraz, laginean dauden gatzak eta bestelako pisu molekular txikiko molekulak baztertuko dira. Atxikitako proteinak PD10 zutabeetatik eluitzeko 3,5 ml lotze-indargetzaile gehitu dira zutabeetara, eta eluzioa, 250 µl 25X proteasa inhibitzaile-nahasketadun lotze-indargetzailedun tutuetan egin da. Eluitutako laginetik 50 µl Western plapaketaren bidezko azterketarako jaso dira. Gainontzeko 200 µl-tako bolumenera 150 µl Pierce High Capacity NeutrAvidin agarosa-bihitxo (ThermoFisher Scientific) gehitu dira. Laginok 3 orduz inkubatu dira errotazioan, lehen 40 minutuak giro-tenperaturan eta gainerako 120 minutuak 4 °C-tan. Hiru orduko inkubazioa bukatzean eta bihitxoetara lotu ez dena baztertzeko, laginak 1000 rpm-tan zentrifugatu dira 2 minutuz eta 10 °C-tan. Bihitxoetan biotinilatu gabeko ahalik eta proteina gutxien geratzeko, bihitxoak hainbat aldiz garbitu eta zentrifugatu dira: garbiketak PBStan prestatutako sei garbiketa-indargetzaile (GI) ezberdinen 10 ml-tan egin dira 2 minutuz eta giro-tenperaturan, eta zentrifugazioak, 11000 rpm-tan, 2 minutuz eta 10 °C-tan. Indargetzaile bakoitzarekin egindako garbiketa kopurua eta ordena ondorengoa da: GI1 (8 M urea, % 0,25 SDS) bi garbiketa, GI2 (6 M guanidina-HCl) hiru garbiketa, GI3 (6,4 M urea, 1 M NaCl, % 0,2 SDS) garbiketa bakarra, GI4 (4 M urea, 1 M NaCl, % 10 isopropanol, % 10 etanol, % 0,2 SDS) hiru garbiketa, GI1 garbiketa bakarra, GI5 (8 M urea, % 1 SDS) garbiketa bakarra eta GI6 (% 2 SDS) hiru garbiketa. Azken garbiketaren ostean, eta biotinilatutako proteinen eta bihitxoen artean ematen diren interakzioak hausteko, bihitxoak eluzio-indargetzailearen 80 µl-tan (250 mM Tris-HCl pH 7,5, 100 mM DTT, % 40 glizerol, % 4 SDS, % 0,2 bromofenol urdin) inkubatu dira 5 minutuz eta 95 °C-tan. Lotze-indargetzailea eta GI3 indargetzailearen kasuan

izan ezik, zeinak 32 °C-tan erabili diren, beste indargetzaile guztiak giro-tenperaturan erabili dira.

Azkenik, eluitutako materiala bihitxoetatik banatzeko, laginak Vivaclear Mini 0.8 μm PES filtrodun zutabeetan (Sartorious) zehar pasarazi dira 14000 rpm-tan zentrifugatuz minutu batez. Behin bihitxoak kenduta, lagineko proteinak SDS-PAGEz banatu dira eta gelak *Coomassie* erabilita tindatu dira. Gel horietatik APEX2dun proteinei, abidinari eta fronteari dagozkien pisu molekularreko bandak baztertu egin dira laginetan kontzentrazio txikiagoan dauden proteinen identifikazioa oztopatu ez dezaten. Hemendik aurrerako laginen prozesamendua UPV/EHUko SGIker Proteomika zerbitzuan egin da (3.7.5. atala).

3.7.7.4. Identifikatutako proteina-zerrenden kudeaketa

Proteomika zerbitzutik identifikatutako proteinen bi zerrenda multzo jaso dira: APEX2zit proteina erabilita biotinilatutako proteinena eta APEX2nuk proteina erabilita biotinilatutakoena. Zerrenda multzo bakoitzean kontrol laginean (-LMB/-H_2O_2), egoera basalari dagokion laginean (-LMB/+H_2O_2) eta CRM1 inhibitutako egoerari dagokion laginean (+LMB/+H_2O_2) identifikatutako proteinak ageri dira, beraz, aurretik aipatutako multzo bakoitzeko hiruna zerrenda jaso dira. Zerrenda horietan bi modutara identifikaturiko proteina-taldeak daude: MS/MS bidez identifikatutakoak eta *by matching* erara identifikatutakoak. MS/MS bidez identifikatuta egoteak laginean proteina horri dagokion peptido bat behintzat aurkitu dela esan nahi du, *by matching* identifikatuta egoteak aldiz, esperimentu bereko, zerrenda multzo bereko, beste laginetan aurkitu diren peptidoekin konparatuz lagin horretan ere proteina hori egon daitekeela esan nahi du. Laginen azterketarako MS/MS bidez identifikatutako proteinak baino ez dira erabili.

Identifikatutako proteina asko proteina taldeetan ageri dira. Proteina talde berean taldekatutako proteinek, maiz proteina beraren isoformak direnak, peptido berdinak partekatzen dituztelako ageri dira talde berean. Esperimentu batetik bestera, zerrenda multzo batetik bestera, proteina talde horiek ez dute zertan berdinak izan; gauzak horrela eta zerrendetako proteinen konparazioa errazte aldera, talde horietako proteinak banatu eta proteina horietan isoforma nagusia hautatu da.

Horretaz gain, kontrol laginean (-H_2O_2) identifikatutako proteinak, zeluletan berezko biotinilazioa jasaten duten proteinak alegia, gainontzeko laginetan identifikatuz gero ezabatu egin behar dira.

Aipaturiko iragazketa horien osteko zerrendatik fidagarritasun handiaz, hau da, 0 baino intentsitate altuagoarekin eta gutxienez bi peptidorekin, identifikatutako proteinak hautatu dira, eta horrela, identifikatutako proteinen behin betiko zerrenda osatu da.

3.7.7.5. Identifikatutako proteinen analisia

Proteina zerrendetako datuekin bi analisi mota egin dira: batetik laginen arteko erkaketak egin dira eta bestetik egoera basalean aurretiaz zein kokapenetan deskribatu diren aztertu da. Laginen arteko erkaketak egiteko Venn diagramak erabili dira (Bardou et al., 2014; http://jvenn.toulouse.inra.fr/app/index.html). Identifikatutako proteinak aurretiaz non deskribatu diren aztertzeko, UniProt datu-basera (UniProt Consortium, 2019; https://www.uniprot.org/ 2020-10-22an kontsultatuta) jo da eta identifikatutako proteinak *Gene Ontology*-ko *Subcellular location* sailkapenaren arabera aztertu dira.

3.8. Material eta metodo gehigarriak

1X PBS (pH 7,6)

137 mM NaCl
2,7 mM KCl
1,8 mM KH_2PO_4
8,1 mM Na_2HPO_4

TAE (50X)
2 M Tris base
0,05 M EDTA
% 0,05 azido azetiko (v/v)

Agarosa gela
% 1,5 agarosa (w/v)
% 0,01 etidio bromuro (v/v)
1X TAE

DNA karga-indargetzailea
% 0,2 Orange G (w/v)
% 40 sakarosa

Biltze gela (SDS-PAGE)
63 mM Tris-HCl pH 6,8
% 0,1 SDS (v/v)
% 5 akrilamida
% 0,1 TEMED
% 0,1 APS

Banatze gela (SDS-PAGE)
376 mM Tris HCl-pH 8.8
% 0,1 SDS (v/v)
% 12 Akrilamida
% 0,04 TEMED
% 0,1 APS

Proteina elektroforesi-indargetzailea
0,25 mM Tris base
1,92 mM glizina
% 1 SDS

Transferentzia-indargetzailea
120 mM Tris base
40 mM glizina
% 20 metanol

Proteina karga-indargetzailea (6X)
375 mM Tris-HCl pH 6,8
% 50 Glizerol (v/v)
% 12 SDS (w/v)
% 15 β-merkaptoetanol (v/v)
% 0,06 bromofenol urdina (w/v)

TTBS (pH 7,6)
20 mM Tris base
137 mM NaCl
% 0,1 Tween 20

Lisi-indargetzailea (GFP-traperako)
Pierce lisi-indargetzailea (ThermoFisher Scientific)
% 0,001 PMSF (v/v)
% 0,001 PIC (Roche) (v/v)

Laemmli lisi-indargetzailea
125 mM Tris-HCl pH 6,8
% 20 glizerol
% 4 SDS

Quencher soluzioa
10 mM sodio askorbato
5 mM Trolox
10 mM azida sodikoa
PBStan

Lisi-indargetzailea (Neutrabidina afinitate-purifikaziorako)
8 M urea
% 1 SDS
50 mM NEM

Lotze-indargetzailea
3 M urea
1 M NaCl
% 0,25 SDS
50 mM NEM

Garbiketa-indargetzailea 1 (GI1)
8 M urea
% 0,25 SDS
PBStan

Garbiketa-indargetzailea 2 (GI2)
6 M guanidina-HCl
PBStan

Garbiketa-indargetzailea 3 (GI3)
6,4 M urea
1M NaCl
% 0,2 SDS
PBStan

Garbiketa-indargetzailea 4 (GI4)
4 M urea
1 M NaCl
% 10 isopropanol
% 10 etanol
% 0,2 SDS
PBStan

Garbiketa-indargetzailea 5 (GI5)
8 M urea
% 1 SDS
PBStan

Garbiketa-indargetzailea 6 (GI6)
% 2 SDS
PBStan

Eluzio-indargetzailea
250 mM Tris-HCl pH 7,5
100 mM DTT
% 40 glizerol
% 4 SDS
% 0,2 bromofenol urdin

4. Emaitzak / Results

4.1. NES identifikazioa eta CRM1en mendeko NESen esportazioaren inguruko azterketa mekanistikoak

Sarreran aipatu bezala, CRM1ek kargoen NES izeneko aminoazido-sekuentzia espezifikoak ezagutu eta lotzen ditu kargook nukleotik zitoplasmara garraiatu ahal izateko. Ezagutzen diren CRM1i lotzen zaizkion NES aktiboen sekuentziak oinarritzat hartuta, ϕ_1-$X_{2\text{-}3}$-ϕ_2-$X_{2\text{-}3}$-ϕ_3-X-ϕ_4 NES adostasun-sekuentzia sortu da, non, aminoazido hidrofobikoak ϕ sinboloaz adierazten diren (Kosugi et al., 2008; Monecke et al., 2009). Adostasun-sekuentzia horrek, eta horretan oinarritutako bestelako ikerketek (Fung eta al., 2015, 2017; Güttler et al., 2010), NES kandidatuak bioinformatikoki bilatzea ahalbidetu dute. Bilaketa horietako emaitzak, ordea, zelularen testuinguruan frogatu behar dira, NES adostasun-sekuentziari doitzen zaion aminoazido segida oro ez baita CRM1i lotu eta esportatuko den NES aktiboa. NESen aktibitatea baliozkotzeko beraz, zelularen testuinguruan egindako esportazio-entseguen beharra dago. Entseguen artean aipatu beharrekoa da tesi honetan maiz erabilitako Rev(1.4)-GFP erreportarian oinarritutakoa (Henderson eta Eleftheriou, 2000), eta baita jarraian aurkeztuko den $SRV_{B/A}$ erreportarian oinarritutako esportazio-entsegu berria ere.

Egun, CRM1en mende esportatzen diren 400 inguru kargoren NESak identifikaturik dauden arren (http://prodata.swmed.edu/LRNes/index.php; Xu et al., 2012; Fung et al. 2021), beste horrenbeste balizko kargo badirela proposatu da (Kirli et al., 2015). Balizko kargo askoren NES sekuentziak ezezagunak dira eta horiek zehaztea ezinbestekoa da; izan ere, kargo jakin baten NESaren sekuentzia zehaztuz gero, sekuentzia hori mutatu daiteke, eta modu horretan, proteina horren funtzioetan CRM1en mende esportatua izateak zein eragin duen argitu daiteke (Castro-Piedras et al., 2021). NES sekuentzia beratik haratago, CRM1 eta NESen arteko elkarrekintza estrukturalki zein biokimikoki ere ikertu bada ere (Dong et al., 2009b; Monecke et al., 2009; Güttler et al., 2010; Fung et al., 2015, 2017; Fu et al., 2018), zelularen testuinguruan CRM1en mendeko NESen esportazioa mekanistikoki ez dago sakontasunean azterturik. Ezagutza hori gako izan daiteke adibidez, minbizian maiz agertzen den E571K mutazioak zelula mailan duen eragina ulertzeko. Izan ere, mutazio horrek NES jakinen esportazioa asaldatzen duela (García-Santisteban et al., 2016) eta efektu onkologikoa baduela (Taylor et al., 2019) ezaguna bada ere, ez da orokorrean esportazioan duen eragina ezagutzen.

Gauzak horrela, tesi-atal honetan arlo horiek aztertzerakoan lortutako emaitzak aurkezten dira. Alde batetik, hainbat NES berri identifikatu dira; beste alde batetik, CRM1en mendeko NESen esportazioa mekanistikoki ikertu da, eta azkenik, CRM1 basatiaren esportoma eta E571K mutantearen esportoma aztertu eta erkatzeko estrategia berri bat diseinatu da.

4.1.1. NES berrien peskizan Rev(1.4)-GFP esportazio-entsegua erabiliz

Rev(1.4)-GFP erreportarian oinarritutako nukleotiko esportazio-entsegua (Henderson eta Eleftheriou, 2000), hemendik aurrera Rev(1.4)-GFP esportazio-entsegu bezala izendatuko dena, ezezagunak diren NES motibo berriak bilatzeko edo ezagunak diren NESen aktibitate maila neurtzeko erabilgarria den entsegua da.

pRev(1.4)-GFP bektorea, NES ez-aktiboa duen giza immunoeskasiaren birusaren (GIB) mutatutako Rev proteinaz, Rev(1.4) izendatzen dena, eta GFP proteina fluoreszenteaz dago osaturik. Rev proteina basatiak, NLS eta NES seinale bana ditu, proteina basatiaren inportazio eta esportazioa bideratzen dutenak. 22. irudian adierazita dagoen bezala, Rev proteina basatiaren nukleoranzko inportazioa, zein nukleotiko esportazioa era erraz batean inhibitu daiteke zelulak aktinomizina D (ActD) edo leptomizina B-rekin (LMB) tratatuz, hurrenez hurren.

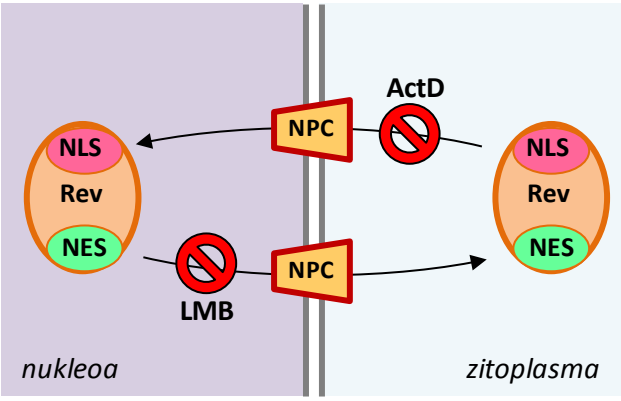

22. irudia: GIBaren Rev proteina basatiaren garraio nukleozitoplasmatikoa. Rev proteina basatiaren NLSak eragiten duen proteinaren inportazioa zelulak ActDrekin tratatuz inhibi daiteke, NESak eragindako esportazioa, aldiz, LMBrekin tratatuz (Henderson eta Eleftheriou, 2000-tik moldatutako irudia).

Rev(1.4) proteina mutanteak, ordea, jatorrizko NLSa bere baitan mantentzen duen arren, NES ez-aktiboa du. Hau da, nukleora inportatu daiteke, baina ez nukleotik esportatu (23. irudia). Ondorioz, Rev(1.4) proteina mutanteak kokapen nuklearra hartuko du zeluletan gainadieraztean. Esportazio ahalmen hori, pRev(1.4)-GFP bektorean aktiboa den NES bat barneratuz berreskura daiteke. Eta hori da, hain zuzen ere, esportazio-entsegu honen oinarria.

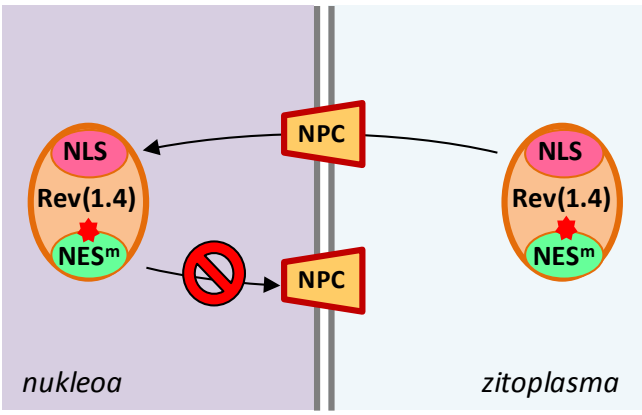

23. irudia: Rev(1.4) proteina mutantearen garraio nukleozitoplasmatikoa. Rev(1.4) proteina mutanteak Rev proteina basatiaren NLSa bere baitan mantentzen du, eta beraz, proteina aktiboa bezala zitoplasmatik nukleora garraiatzen da. NESa, ordea, mutaturik dauka (NES^m), eta horrek, proteina nukleotik zitoplasmara esportatzea ekiditen du.

NES aktibo guztiek ordea, ez dute Rev(1.4) proteinaren NLSak eragindako kokapen nuklearra gainditzeko behar besteko indarra, eta beraz, NES ahul bat duten Rev(1.4)-[NES]-GFP erreportariek nukleoan metatzeko joera izango dute. Joera hori ActD tratamenduaren bidez alderantzikatu daiteke. Izan ere, ActDk NLSak eragindako inportazioa inhibitzen du. Hortaz, ikergai den NESaren aktibitatea ahula bada ere, Rev(1.4)-GFP esportazio-entseguak NES hori detektatzeko aukera ematen du. ActD erabiltzeaz gain, entsegu mota honetan zikloheximida (CHX) farmakoa ere erabili ohi da. Zikloheximidak proteinen sintesia inhibitzen du, eta beraz, zitoplasman detektatutako seinale fluoreszentea esportatu diren proteinetatik, eta ez sintetizatu berri diren proteinetatik datorrela, ziurta daiteke (24. irudia).

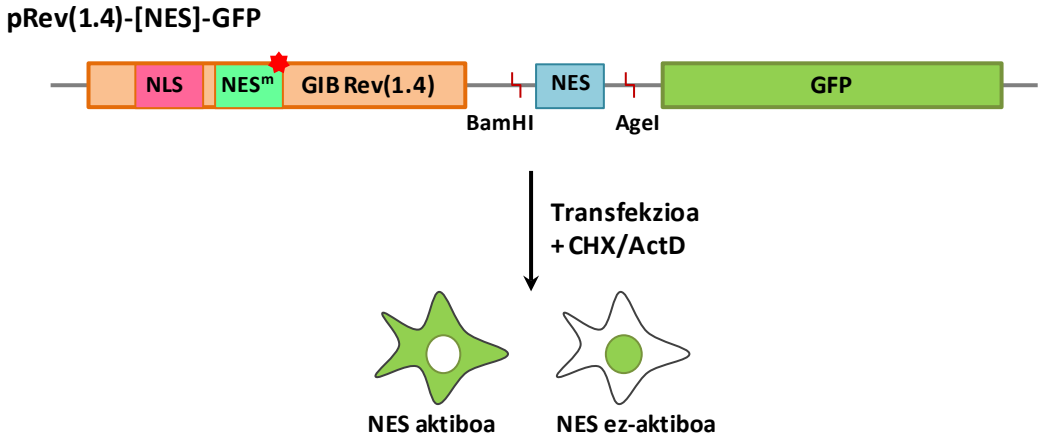

24. irudia: Rev(1.4)-GFP erreportarian oinarritutako esportazio-entsegua. pRev(1.4)-[NES]-GFP plasmidoak HeLa zelulen bi laginetan transfektatzen dira. 24 ordura, lagin biak CHXrekin tratatzen dira proteinen sintesia eteteko. Horretaz gain, lagin bietako bat ActDrekin tratatzen da Rev(1.4) proteinaren NLSak bultzatutako inportazioa inhibitzeko. Erreportariak HeLa zelulatan agertzen duen kokapen nukleozitoplasmatikoa aztertuz testatzen ari den NESa (urdinez) aktiboa den edo ez den jakin daiteke.

Esportazio-entsegu honek NESak detekta ditzake, baita oso ahulak direnak ere. Gainera, zelulak ActDrekin tratatu diren edo tratatu ez diren arabera, Rev(1.4)-[NES]-GFP erreportariek zelula-populazioan erakusten duten banaketa nukleozitoplasmatikoa aztertuta, ikergai den NES motiboaren esportazio-aktibitatea mailaka daiteke. NES ahulenek “1” aktibitate maila lortuko dute, eta sendoenek “9” (ikusi 11.taula).

Hurrengo ataletan ikusiko den bezala, Rev(1.4)-GFP esportazio-entsegua USP12/UAF1/WDR20 konplexuaren esportazioaren eragile den NESa aztertzeko, CRM1en mende esportatzen diren eta minbiziarekin erlazionatuta dauden balizko kargoen NESak bilatzeko, eta gizakiak infektatzeko gai diren koronabirusen nukleokapsida proteinetan aurreikusitako NESak aztertzeko erabili da.

4.1.1.1. WDR20 proteinan identifikatutako NES berriak USP12/UAF1/WDR20 konplexuaren kokapen nukleozitoplasmatikoa zehazten du

Atal honetan aurkeztutako emaitzak Olazabal-Herrero et al., 2019, 2021 eta Sendino et al., 2020b-n argitaratu dira.

CRM1ek proteina askoren garraio nukleozitoplasmatikoa bideratzen du, eta beraz, gako da zelulan gertatzen diren prozesu ugariren erregulazioan. Prozesu horien artean, ubikuitinazio-bidezidorrak daude. Ubikuitinazioa itzulgarria den itzulpen osteko eraldaketa da, eta zeluletako proteina gehientsuenen egonkortasuna, funtzioa edota kokapena zuzentzen ditu (van der Veen eta Ploegh, 2012). Deubikuitinasak (DUB) ubikuitina-unitateak proteinetatik kentzen dituzten entzimak dira, eta funtsezko eginkizuna dute prozesu fisiologiko ugaritan (Komander et al., 2009). Tesi proiektu hau garatu deneko taldeak garraio nukleozitoplasmatikoa ikertzeaz gain, deubikuitinazio prozesua bera, eta garraio nukleozitoplasmatikoarekin duen lotura ere ikertzen du (García-Santisteban et al., 2012; Rodríguez, 2014; Olazabal-Herrero et al., 2019, 2021; Sendino et al., 2020b). Ikerketa horien lerroan, tesi atal honetan, CRM1ek, USP12 deubikuitinasak, UAF1 (*USP1 associated factor 1*) eta WDR20 (*WD repeat-containing protein 20*) kofaktoreekin batera eratzen duen konplexuaren kokapenean duen eragina ikertu da.

USP12 DUBa, tumore-ezabatzaile gisa jarduten duten USP (*ubiquitin-specific protease*) entzimen familiako kide da (Gangula eta Maddika, 2013; Li et al., 2013). USP12k ez du erabateko berezko deubikuitinatze-aktibitaterik. Guztiz aktibatzeko, USP12k, UAF1 (WDR48 (*WD repeat-containing protein 48*) izena ere hartzen duena) eta WDR20 kofaktoreekin batera USP12/UAF1/WDR20 konplexu-trimerikoa osatu behar du. Kofaktore bi horiek sinergistikoki jardungo dute USP12ren aktibitate deubikuitinatzailea nabari emendatuz (Kee et al., 2010).

USP12k zelulen fisiologian duen garrantzia ezaguna bada ere, oraindik ez dago argi non, zein konpartimentutan, kokatzen den zelulan, ezta aipaturiko kofaktoreek zer-nolako eragina izan dezaketen kokapen horretan, eraginik izatekotan. Badira USP12 gehienbat zitoplasmatikoa dela dioten ikerketak (Sowa et al., 2009; Urbé et al., 2012; Burska et al, 2013; Lehoux et al., 2014; Olazabal-Herrero et al., 2015), eta baita batez ere nuklearra dela diotenak (Joo et al., 2011; Jahan et al., 2016). Argi dagoena da, USP12 nukleoaren eta zitoplasmaren artean atzera eta aurrera mugitzen dela eta mugimendu hori CRM1ek bideratzen duela (Kouranti et al., 2010; Jahan et al., 2016). USP12k NES bat duela (^{77}KESLLTCLADLFHSI^{91}) ere proposatu izan da (Sanyal, 2016). Proposatutako NES hori ordea, zalantzan jar daiteke, alde batetik ez duelako

egun ezagutzen diren NES sekuentziekin antzekotasunik, eta bestetik sekuentzia hori NES aktibo bat dela baieztatzeko ebidentzia nahikorik ez zelako aurkeztu (Rodríguez, 2016).

Bestalde, USP12 aktiboa izateko UAF1 eta WDR20 kofaktoreen beharra duela aipatu da (Kee et al., 2010), baina orain arte ez da kofaktore horiek USP12ren kokapen nukleozitoplasmatikoan izan dezaketen papera ikertu. Beraz, tesi honetan, lehenik eta behin konplexu-trimerikoaren proteina bakoitzaren kokapena ikertu da. Jarraian, USP12 proteinan deskribatutako NESa zalantzan jarri, eta batetik, NES horrek benetan USP12ren esportazioa eragiten duenetz aztertu da; bestetik, UAF1 eta WDR20 proteinak CRM1en bidez esportatuak izatekotan, esportazio hori bidera dezaketen motiboak bilatu dira. Eta bukatzeko, WDR20 proteinak USP12/UAF1/WDR20 konplexuaren kokapenean duen eginkizuna ere aztertu da. Horretaz gain, WDR20 proteinaren homologoa izanik, USP12 proteinaren interaktorea den DMWD proteinaren esportazioa bidera dezaketen NES motiboak ere bilatu dira.

4.1.1.1.1. USP12 eta WDR20 proteinen kokapena CRM1en mendekoa da, UAF1ena, ordea, ez

USP12ren kokapenaren inguruan dagoen eztabaida dela eta, gainadierazitako USP12 deubikuitinasaren eta haren kofaktore diren UAF1 eta WDR20 proteinen kokapena CRM1en mendekoa denetz aztertu da. Horretarako, CRM1en inhibitzaile den LMB erabili da. 25. irudian beha daitekeen moduan, USP12 eta WDR20 proteinek kokapen nuklearragoa erakusten dute LMBrekin tratatutako zeluletan tratatu gabeko zeluletan baino. UAF1 proteinaren kokapena, aldiz, ez da zelulak LMBrekin tratatzearen arabera aldatzen. Hau da, USP12 eta WDR20 proteinen kokapena CRM1en mendekoa dela baiezta daiteke, UAF1ena, ordea, ez.

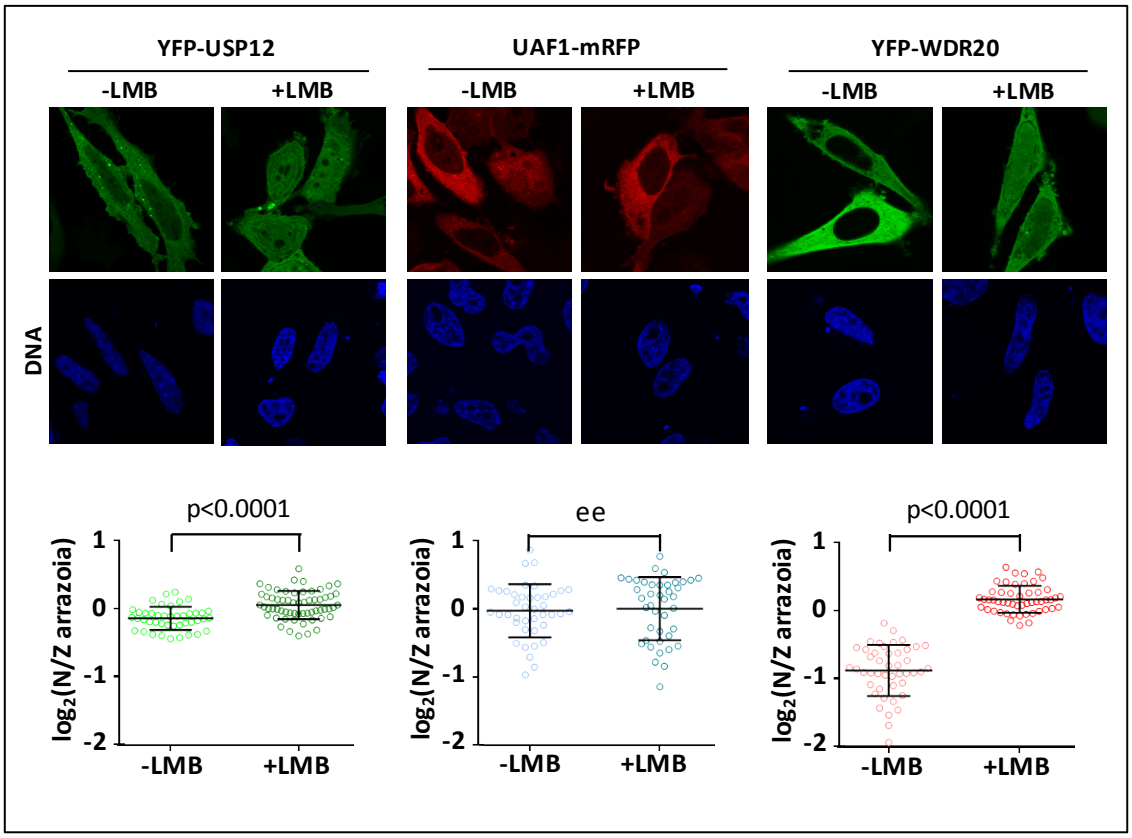

<u>25. irudia:</u> USP12 eta bere kofaktore den WDR20ren kokapena CRM1en mendekoa dela baiezta daiteke, UAF1 kofaktorearena, ordea, ez. Goiko aldean YFP-USP12, UAF1-mRFP eta YFP-WDR20 proteinek CRM1 aktibo dagoela (-LMB) edo CRM1 inhibiturik dagoela (+LMB) HeLa zelulatan hartzen duten kokapenaren fluoreszentziako irudi adierazgarriak ageri dira. Beheko aldean, proteina eta egoera bakoitzeko kokapenaren irudi-analisiaren emaitzak ageri dira. Zirkulu bakoitzak zelula bakar baten nukleoan antzematen den fluoreszentziaren eta zitoplasman antzematen denaren arrazoia 2 oinarriko logaritmoan, $\log_2$(N/Z arrazoia), adierazten du. Lagin bakoitzaren $\log_2$(N/Z arrazoia)-ren batez bestekoa eta desbiderapen estandarrak adierazten dira, baita Mann-Whitney U estatistikoa erabiltzean lortutako p balioa ere (ee: ez-esanguratsua).

Azpimarratzekoa da, CRM1 inhibitzean USP12 zein WDR20 proteinen banaketa nukleozitoplasmatikoa aldatzen den arren, ez direla nukleoan guztiz metatzen. Horrek, proteina horien nukleoranzko sarrera modu ez oso eraginkorrean ematen dela iradokitzen du. Eraginkortasun baxu hori, proteina horiek zitoplasman bahituta geratzearen edo NLS indartsurik ez izatearen ondorio izan daiteke. Aukera horiek USP12 proteinaren kasuan aztertzeko, YFP-USP12$^{[2NLS]}$ izeneko proteina sortu da, zeinak, SV40 birusaren T antigeno luzearen bi NLS (Kalderon et al., 1984a, 1984b) kopia dituen. YFP-USP12$^{[2NLS]}$ HEK293T zelulatan gainadierazitakoan nukleoan metatzen dela behatu da (26. irudia). Emaitza horrek, YFP-USP12 proteinaren nukleorantzako garraio ez eraginkorra NLS indartsurik ez duelako, eta ez proteina zitoplasman bahitzen duen mekanismoren bat dagoelako gertatzen dela adierazten du.

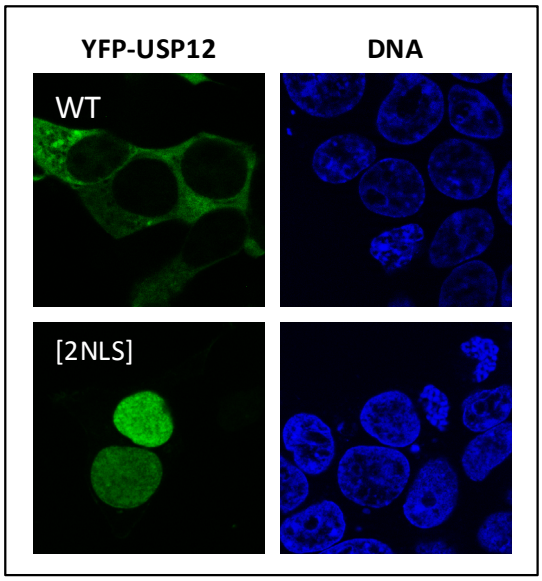

26. irudia: YFP-USP12[2NLS] proteinak HEK293T zelulatan kokapen gehienbat nuklearra agertzen du. YFP-USP12 proteina basatiak (WT) kokapen zitoplasmatikoa erakusten du; bi NLSdun bertsioak ([2NLS]), ordea, kokapen nuklearra. YFP-USP12[2NLS] gainadierazten duten zelula batzuek seinale fluoreszente ahula erakusten dute mintz plasmatikoan (ez erakutsia).

4.1.1.1.2. USP12 proteinarako aurretik proposatutako NESa ez da aktiboa

USP12 proteinaren ^{77}KESLLTCLADLFHSI^{91} aminoazido motiboa NEStzat proposatu da (Sanyal, 2016). Motibo horren sekuentzia, ordea, ez dator bat NESen gainean egun dagoen ezagutzarekin. Gainera, motibo horren esportazio-aktibitatea ez da esperimentalki frogatu, eta ondorioz, bere benetakotasuna zalantzan jarri da (Rodriguez, 2016). Gauzak horrela, ustezko NES horren sekuentzia (^{75}RKKESLLTCLADLFHSIAT^{93}) pRev(1.4)-GFP bektorean (Henderson eta Eleftheriou, 2000) klonatu eta esportazio-entsegu bat egin da. Entseguaren emaitza ezagutzeko, erreportariaren kokapena nuklear (N), nukleozitoplasmatiko (NZ) edo zitoplasmatiko (Z) kategorietan sailkatu da gutxienez 200 zelulatan, bai ActDrekin tratatutako zeluletan zein tratatu gabekoetan. 27. irudian beha daitekeenez, Rev(1.4)-[USP12^{NES}]-GFP erreportariak ez du Rev(1.4)-GFP kontrol negatiboak baino kokapen zitoplasmatikoagoa, ezta ActDren presentzian ere. Emaitza horrek, USP12 proteinarako NEStzat proposaturiko ^{77}KESLLTCLADLFHSI^{91} sekuentziak aktibitate esportatzailerik ez duela erakusten du.

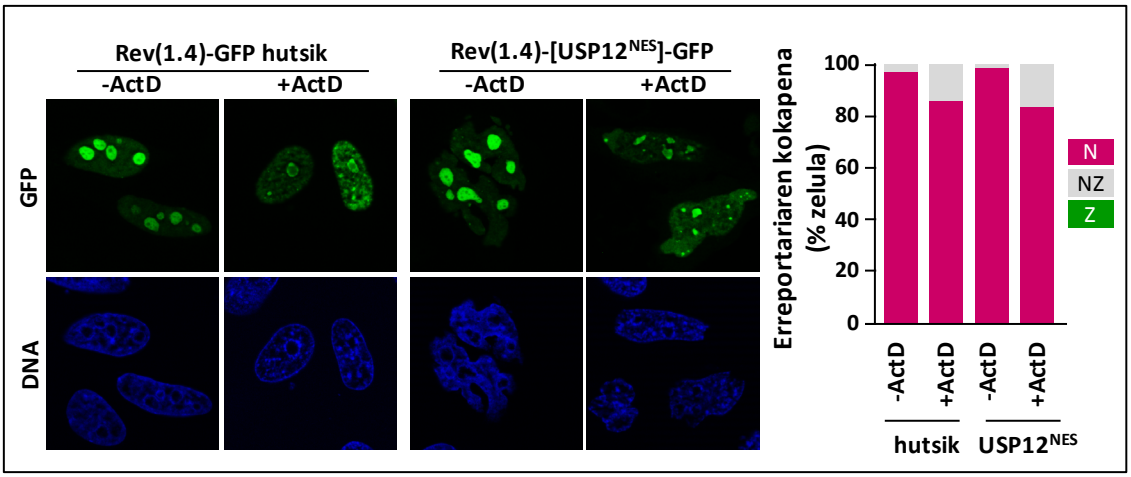

27. irudia: USP12 proteinarako proposaturiko NESak (^{77}KESLLTCLADLFHSI^{91}) ez-aktibo bezala jokatzen du esportazio-entseguan. Motibo hori aztertzeko erabilitako Rev(1.4)-GFP esportazio-entseguaren emaitzak. Ezkerraldean Rev(1.4)-GFP bektore hutsarekin edo proposaturiko NESa duen Rev(1.4)-[USP12^{NES}]-GFP bektorearekin transfektatutako HeLa zelulatan eginiko Rev(1.4)-GFP esportazio-entseguaren irudi adierazgarriak ageri dira, eskuinaldean, erreportariaren kokapena gutxienez 200 zelulatan nuklear (N), nukleozitoplasmatiko (NZ) edo zitoplasmatiko (Z) kategorietan sailkatuz lortutako emaitza semi-kuantitatiboa. Rev(1.4)-GFP kontrol negatiboak eta USP12 proteinarako proposatutako NESa adierazten duen erreportariak kokapen nuklearra agertzen dute bai ActDrekin tratatu gabeko zeluletan zein tratatutakoetan. Hau da, ikertutako motiboa ez da NES aktiboa.

Beste alde batetik, proposaturiko NESak proteina osoaren testuinguruan izan dezakeen funtzionaltasuna aztertu nahi izan da. Horretarako, YFP proteina fluoreszenteari fusionatutako USP12 proteinaren NEStzat hartutako ^{77}KESLLTCLADLFHSI^{91} sekuentziako aminoazido hidrofobikoak alaninara mutatu dira. Mutagenesi horren emaitza YFP-USP12^{NESmut} proteina da, zeinak 77 eta 91 aminoazidoen artean sekuentzia basatiaren ordez ondorengo sekuentzia duen: ^{77}KESAATCAADAAHSA^{91}.

YFP-USP12^{NESmut} proteina HeLa zelulatan gainadieraztean kokapen zitoplasmatikoa erakusten du; proteina basatiak erakusten zuenaren berdina (28. irudia). Horrek, Sanyal eta lankideek (Jahan et al., 2016; Sanyal, 2016) USP12 proteinarako proposaturiko NES sekuentziak haren esportazioa gidatzen ez duela iradokitzen du.

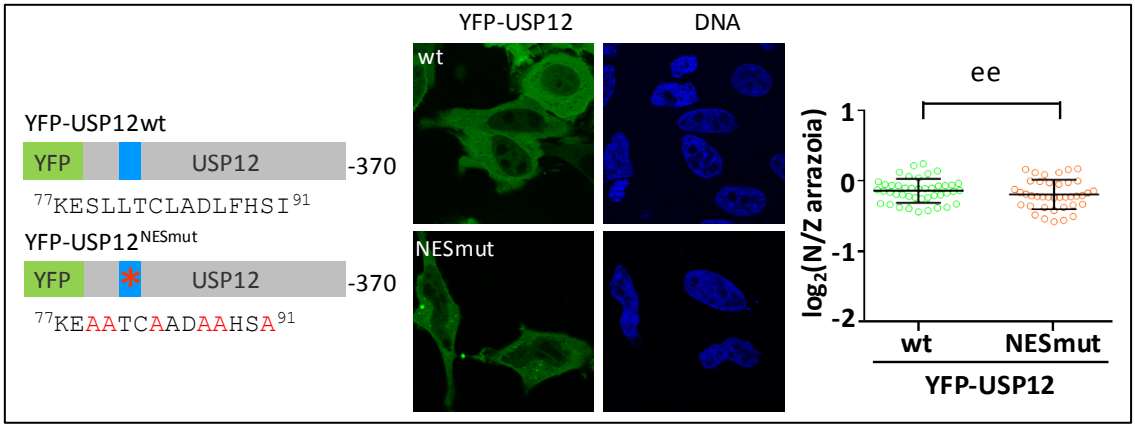

28. irudia: USP12 proteina osoaren testuinguruan USP12 proteinarako proposaturiko NESak ez du kokapen nukleozitoplasmatikoan eraginik. Ezkerraldean, YFP-USP12 basatirako (wt) proposaturiko NES sekuentziaren, eta aminoazido hidrofobikoak alaninaz mutaturik (gorriz) dituen sekuentziaren (^{NESmut}) adierazpen eskematikoak ageri dira. Erdialdean, YFP-USP12wt eta YFP-USP12^{NESmut} gainadierazten duten HeLa zelulen irudi adierazgarriak, eta eskuinaldean proteina horiek hartzen duten kokapenaren irudi-analisiaren emaitzak. Zirkulu bakoitzak zelula bakar baten nukleoan antzematen den fluoreszentziaren eta zitoplasman antzematen denaren arrazoia 2 oinarriko logaritmoan (log_2(N/Z arrazoia)) adierazten du. Lagin bakoitzaren log_2(N/Z arrazoia)-ren batez bestekoa eta desbiderapen estandarrak adierazten dira, ee: ez-esanguratsu (Mann-Whitney U estatistikoa). Fluoreszentziako irudien behaketaz, zein irudi-analisiaren bidez laginak aztertzean, YFP-USP12wt zein YFP-USP12^{NESmut} proteinek kokapen bera (gehienbat zitoplasmatikoa) agertzen dutela antzematen da.

4.1.1.1.3. WDR20 proteinak NES aktibo bat du

USP12 proteinarako proposaturiko NESa ezereztuta (ikusi 28. irudia), eta WDR20 proteinaren kokapena CRM1en mendekoa dela baieztatuta (ikusi 25. irudia), azken horrek NES aktibo bat ote duen ikertu da.

Horretarako, lehendabizi, 2016an Li eta lankideek USP12/UAF1/WDR20 konplexua X izpien difrakzioa erabiliz egindako modeloa erabilita, WDR20 proteinaren egitura aztertu da. WDR20k konplexuan duen egitura gehien bat β-harizpi erakoa da, egun dagoen NESen egituraren inguruko ezagutzarekin bat ez datorrena. Izan ere, NES seinale aktibo ohikoenek α-helize erako egitura izaten dute partzialki bada ere (Kosugi et al., 2008; Dong et al., 2009b; Fung et al., 2015, 2017). Alabaina, Li eta lankideen modeloan (2016), WDR20ren 394 eta 509 aminoazidoen arteko egitura ez dago deskribaturik, eta egun ere horrela jarraitzen du (Zhu et al., 2019b). Beraz, alde horretan NES sekuentziadun α-helizeren bat egotea gerta daiteke. Hori horrela, YFP-WDR20ren zati ezberdinen kokapena aztertzea erabaki da. Horretarako, hiru delezio-mutante egin dira; 1-390, 390-510 eta 510-569 aminoazidoen arteko zatiak hain zuzen ere (29A irudia). WDR20 proteina osoarekin egin bezala, zati horien kokapen zelularra CRM1 aktibo (-LMB) edo inhibiturik egon (+LMB) aztertu da (29B irudia). YFP-WDR20(1-390) eta YFP-WDR20(510-569) zatiek kokapen nukleozitoplasmatikoa hartzen dute CRM1 aktibo zein inhibiturik egon. YFP-WDR20(390-510) zatiak aldiz, proteina osoak duen kokapen berdina

erakusten du. Hau da, CRM1 aktibo dagoenean guztiz zitoplasmatikoa da, eta CRM1 inhibitzean, ordea, kokapen nukleozitoplasmatikoa hartzen du. Emaitza horrek WDR20 proteinaren 390 eta 510 aminoazidoen artean NES aktibo bat egon daitekeela iradokitzen du.

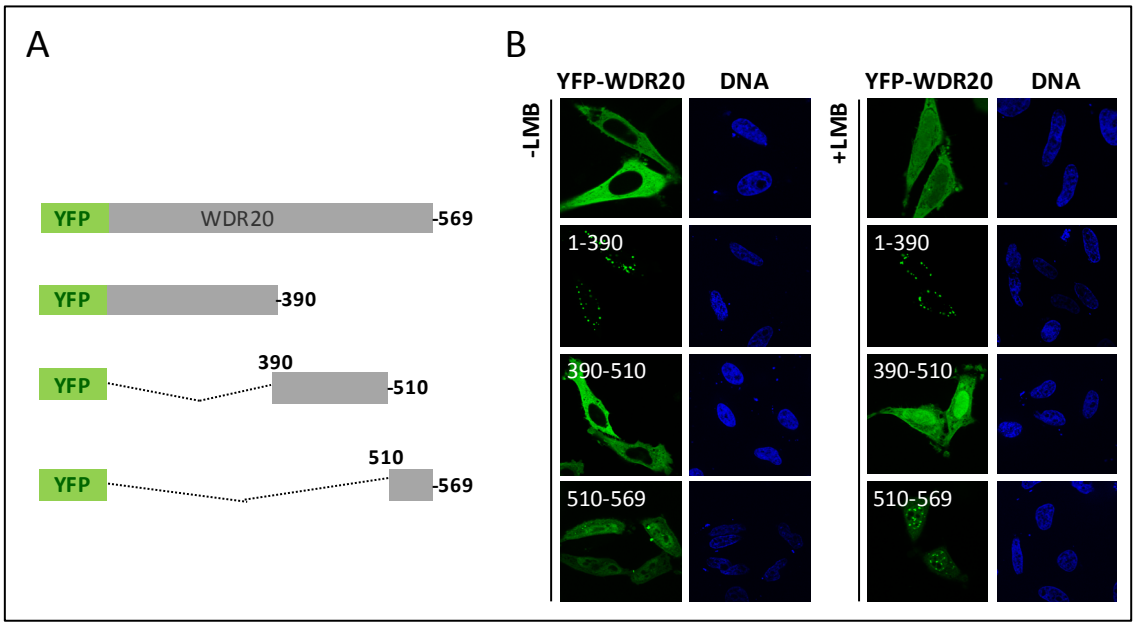

29. irudia: WDR20 proteinaren NESaren zonaldea mugatzeko esperimentua. A. YFP-WDR20 proteinaren delezio-mutanteen irudi eskematikoa. B. YFP-WDR20 osoa zein fragmentuak HeLa zelulatan erakusten duten kokapena, CRM1 aktibo (-LMB) edo inhibiturik dagoela (+LMB). WDR20 proteina osoak kokapen zitoplasmatikoa du CRM1 aktibo dagoenean, LMBrekin tratatzean aldiz, kokapen nukleozitoplasmatikoa hartzen du. Fragmentuei erreparatuz, proteina osoaren kokapen bera erakusten duen bakarra YFP-WDR20(390-510) fragmentua da.

Behin, WDR20 proteinak NESik izatekotan, zein zonaldetan izango duen zehaztuta, Wregex NES-iragarlea (Prieto et al., 2014) *relaxed* moduan erabili da proteina sekuentzia osoan NES sekuentzia kandidatuak bilatzeko (30. irudia) (hemendik aurrera, aktibitate-esportatzailerik dutela konfirmatu gabeko eta NES adostasun-sekuentziarekin bat egiten duten sekuentziak NES kandidatu edo cNES (*candidate* NES) bezala izendatuko dira; esperimentalki aktiboak direla konfirmatutakoak berriz, NES bezala). Iragarlearen arabera, motibo bakarra topatu da 390 eta 510 aminoazidoen artean, ^{454}IASGVSKFATL^{464} sekuentzia hain zuzen ere.

#	Entry	Start	End	Sequence	"!"	Score
1	sp|Q8TBZ3|WDR20_HUMAN	109	118	L-TAT-A-ES-V-S-L	4	63.1
2	sp|Q8TBZ3|WDR20_HUMAN	380	389	L-WD-L-TED-I-L-F	1	50.1
3	sp|Q8TBZ3|WDR20_HUMAN	454	464	I-ASG-V-SKF-A-T-L	3	43.3
4	sp|Q8TBZ3|WDR20_HUMAN	218	228	V-GEG-A-LNE-F-A-F	1	43.3
5	sp|Q8TBZ3|WDR20_HUMAN	246	254	V-FN-F-DS-V-E-L	1	35.9
6	sp|Q8TBZ3|WDR20_HUMAN	65	75	L-CFN-V-GRE-L-Y-F	4	35.1
7	sp|Q8TBZ3|WDR20_HUMAN	258	268	M-KSY-F-GGL-L-C-V	3	35.1
8	sp|Q8TBZ3|WDR20_HUMAN	532	542	A-HER-L-TVL-I-F-L	2	35.1
9	sp|Q8TBZ3|WDR20_HUMAN	288	298	V-WSF-V-DCR-V-I-A	2	23.1

30. irudia: Wregex NES-iragarleak *relaxed* moduan WDR20 proteinan aurkitutako cNESak. Aurkitutako bederatzi motiboetatik bakar bat (gorriz adierazita) dago 390-510 aminoazidoen artean.

WDR20 proteinaren 390 eta 510 aminoazidoen artean iragarleak aurkitutako cNESa eta haren alde banatako 4 aminoazido ere (hau da, ^{450}MDGAIASGVSKFATLSLHD^{468} sekuentzia) pRev(1.4)-GFP bektorean klonatu da (Rev(1.4)-[WDR20^{NES}]-GFP). Sekuentzia horren aktibitate esportatzailea Rev(1.4)-GFP esportazio-entsegua (Henderson eta Eleftheriou, 2000) erabiliz aztertzean aktiboa dela ikusi da (31. irudia). Rev(1.4)-[WDR20^{NES}]-GFP erreportariak tratatu gabeko (-ActD) zeluletan kokapen nukleozitoplasmatikoa hartzen du gehienbat. Zelulak ActDrekin tratatzean, ordea, kokapen askoz ere zitoplasmatikoagoa agertu du. Hori horrela, WDR20ren entseatutako motiboa NES aktiboa dela eta 6ko aktibitate esportatzailea duela zehaztu da.

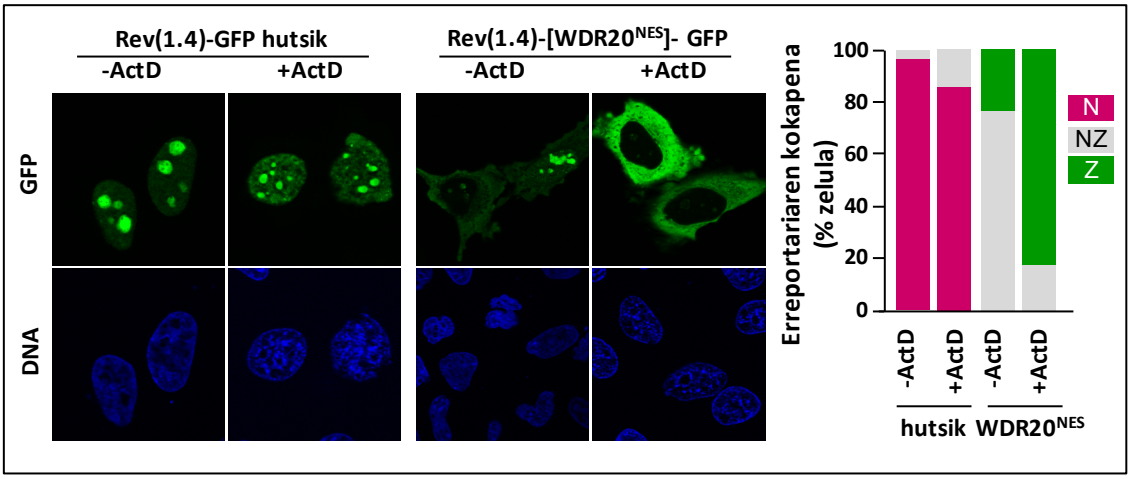

31. irudia: WDR20ren ^{450}MDGAIASGVSKFATLSLHD^{468} cNES motiboa aktiboa denetz aztertzeko eginiko esportazio-entseguaren emaitzak. Ezkerraldean, HeLa zelulatan eginiko Rev(1.4)-GFP esportazio-entseguaren irudi adierazgarriak ageri dira. Zelulak pRev(1.4)-GFP bektore hutsarekin eta aipatutako cNES motiboa duen erreportariaren bektorearekin transfektatu dira. Erreportarien kokapena zelulak ActDrekin tratatuta (+ActD), zein tratatu gabe (-ActD) aztertu da. WDR20ren NESak erreportariaren kokapen zitoplasmatikoa eragiten du. Eskuinaldean, entseguaren emaitza semi-kuantitatiboen grafikoa ageri da. Egoera bakoitzean gutxienez 200 zelula nuklear (N), nukleozitoplasmatiko (NZ) edo zitoplasmatiko (Z) kategorietan sailkatu dira. Lortutako emaitzaren arabera WDR20 proteinaren cNESaren aktibitate esportatzaileari 6ko balioa eman zaio (ikusi 11. taula).

4.1.1.1.4. Identifikatutako NES berriak WDR20 proteinaren CRM1en mendeko esportazioa gidatzen du

Identifikatutako NES berriak WDR20 proteina osoaren testuinguruan duen eragina aztertu da. Horretarako, NES motiboaren parte diren L464 eta L466 leuzina aminoazidoak mutatu eta alaninaz ordezkatu dira (32. irudia). Jarraian, WDR20^{NESmut} proteinaren kokapena aztertu da (32. irudia). ^{454}IASGVSKFATLSLHD^{468} motibo basatia proteina osoaren kokapenaren arduradun izatekotan, WDR20^{NESmut} proteinak WDR20 proteina basatiak (wt) LMBrekin tratatutako zeluletan agertzen duen antzeko kokapena agertu beharko luke, hau da, kokapen nukleozitoplasmatikoa. Eta hori da, hain zuzen ere, mutatutako proteinak agertu duen kokapena. Hortaz, WDR20 basatian deskribatu berri den NES motiboa haren nukleotiko esportazioaren eragilea dela baiezta daiteke.

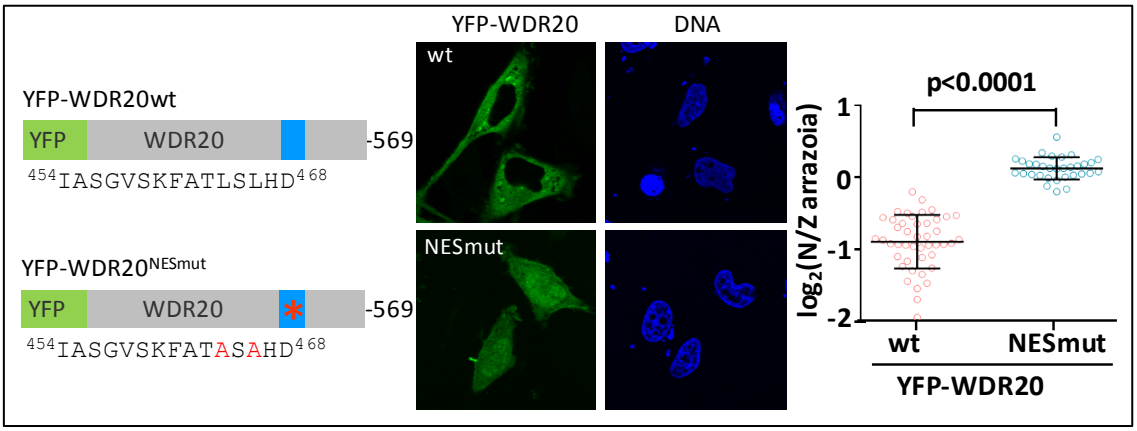

32. irudia: WDR20 proteinan deskribatutako NES berriak proteina osoaren CRM1en mendeko esportazioa gidatzen du. Ezkerraldean, WDR20 basati (wt) eta NES mutantedun (^{NESmut}) proteinen adierazpen eskematikoa ageri da. Jatorrizko 464 eta 466 leuzinak (L) alaninaz (A) ordezkatu dira mutantean (gorriz adierazita). Erdialdean, YFP-WDR20wt eta YFP-WDR20^{NESmut} gainadierazten duten HeLa zelulen irudi adierazgarriak, eta eskuinaldean proteinok hartzen duten kokapenaren irudi-analisiaren emaitza ageri da. Zirkulu bakoitzak zelula bakar baten nukleoan antzematen den fluoreszentziaren eta zitoplasman antzematen denaren arrazoia 2 oinarriko logaritmoan (log_2(N/Z arrazoia)) adierazten du. Lagin bakoitzaren log_2(N/Z arrazoia)-ren batez bestekoa eta desbiderapen estandarrak adierazten dira, baita Mann-Whitney U estatistikoa erabiltzean lortutako p balioa ere.

4.1.1.1.5. Identifikatutako NES berria WDR20ren homologoa den DMWD proteinan funtzionalki kontserbatuta dago

USP12 proteinak UAF1 eta WDR20 proteinekin elkarrekiteaz gain beste hainbat interaktore ere badituela deskribatu da, tartean oso gutxi ikertu den DMWD (*dystrophia myotonica WD repeat-containing protein*) (Sowa et al., 2009). DMWD proteinaren aminoazido sekuentziak WDR20 proteinarenarekiko antzekotasun handia agertzen du. Gainera, WDR20 proteinan deskribatutako NES motiboaren sekuentzia DMWD proteinan partzialki kontserbatuta dago, batez ere, sekuentziaren C-muturrean (33. irudia).

```
WDR20 MAT------EG---GGKEMNEIKTQFTTREGLYKLLPHSEYSRPNRV-----PFN----- 41
DMWD  MAAGGAEGGSGPGAAMGDCAEIKSQFRTREGFYKLLPGDGAARRSGPASAQTPVPPQPPQ 60
      **:      .*   .  :  ***:** ****:***** .  :* .       *.

WDR20 ---------------------------SQGSNPVRVSFVNLND---------------QS 59
DMWD  PPPGPASASGPGAAGPASSPPPAGPGPGPALPAVRLSLVRLGEPDSAGAGEPPATPAGLG 120
                                . .   **:*:*.*.:                .

WDR20 GNGDRLCFNVGRELYFYI---YKGVRKAADLSKPIDKRIYKGTQPTCHDFNHLTATAESV 116
DMWD  SGGDRVCFNLGRELYFYPGCCRRGSQRSIDLNKPIDKRIYKGTQPTCHDFNQFTAATETI 180
      ..***:***:*******     :* ::: **.*******************::**::*::

WDR20 SLLVGFSAGQVQLIDPIKKETSKLFNEERLIDKSRVTCVKWVPGSESLFLVAHSSGNMYL 176
DMWD  SLLVGFSAGQVQYLDLIKKDTSKLFNEERLIDKTKVTYLKWLPESESLFLASHASGHLYL 240
      ************ :* ***:*************::** :**:* ******.:*:**::**

WDR20 YNVEHTCGTTAPHYQLLKQGESFAVHTCKSKSTRNPLLKWTVGEGALNEFAFSPDGKFLA 236
DMWD  YNVSHPCASAPPQYSLLKQGEGFSVYAAKSKAPRNPLAKWAVGEGPLNEFAFSPDGRHLA 300
      ***.* *.:: *:*.******.*:*::.***: **** **:**** **********:.**

WDR20 CVSQDGFLRVFNFDSVELHGTMKSYFGGLLCVCWSPDGKYIVTGGEDDLVTVWSFVDCRV 296
DMWD  CVSQDGCLRVFHFDSMLLRGLMKSYFGGLLCVCWSPDGRYVVTGGEDDLVTVWSFTEGRV 360
      ****** ****:***: *:* *****************:*:**************.: **

WDR20 IARGHGHKSWVSVVAFDPYTTSVEEGDPMEFSGSDEDFQDLLHFGRDRANSTQSRLSKRN 356
DMWD  VARGHGHKSWVNAVAFDPYTTRAEEAATAAGADGE--RSGEEEEEEPEAAGTGSAGGAPL 418
      :**********..******** .**.     :..:   ..  .  . .* .* *  .

WDR20 STDSRPVSVTYRFGSVGQDTQLCLWDLTEDILFPHQPLSRARTHTNVMNATSPPAGSNGN 416
DMWD  SPLPKAGSITYRFGSAGQDTQFCLWDLTEDVLYPHPPLARTRTLPGTPGTTPPAASSSRG 478
      *   :  *:******.*****:********:*:** **:*:**  .. .:* * *.*. .

WDR20 SVTTPGNSVPPPLPRSNSLPHSAVSNA-GSKSSVMDGAIASGVSKFATLSLHDRKERHHE 475
DMWD  GE-PGPGPLPRSLSRSNSLPHPAGGGKAGGPGVAAEPGTPFSIGRFATLTLQERRDRGAE 537
      .     . :*  * ******* * ..  *. . . : .   .:.:****:*::*::*  *

WDR20 KDHKRNHSMGHISSKSSD--------KLNLVTKTKTDPAKTLGTPLCPRMEDVPLLEPLI 527
DMWD  KEHKRYHSLGNISRGGSGGSGSGGEKPSGPVPRSRLDPAKVLGTALCPRIHEVPLLEPLV 597
      *:*** **:*:**  .*.          . * ::: ****.*** ****:.:*******:

WDR20 CKKIAHERLTVLIFLEDCIVTACQEGFICTWGRPGKVVSFNP----------------- 569
DMWD  CKKIAQERLTVLLFLEDCIITACQEGLICTWARPGKAFTDEETEAQTGEGSWPRSPSKSV 657
      *****:******:******:******:****.****..: :

WDR20 -----------------    569
DMWD  VEGISSQPGNSPSGTVV    674
```

<u>33. irudia:</u> WDR20 (Q8TBZ3) eta DMWD (Q09019) proteinen aminoazidoen lerrokatzea CLUSTAL-OMEGA erabiliz. Letren kolorea aminoazidoen propietate fisikoen araberakoa da, eta beheko lerroko sinboloek posizio bakoitzeko aminoazidoa zenbateraino kontserbatzen den adierazten dute; "*" sinboloak sekuentzia bietan aminoazido berdina ageri dela adierazten du, ":" sinboloak sekuentzia bietako aminoazidoak berdinak izan ez arren oso antzeko ezaugarri fisikokimikoak dituztela, eta bukatzeko, "." sinboloak sekuentzia bietako aminoazidoek duten antzekotasuna baxua dela adierazten du. WDR20 proteinaren sekuentzian proteina horretan aurkitutako NESa karratu arrosa batez dago adierazirik. Sekuentzia hori, DMWD proteinan partzialki kontserbaturik dago, batez ere sekuentziaren C-muturrean.

WDR20 proteinan deskribatutako NESa, partzialki bada ere, DMWD proteinan kontserbatuta dagoenez, CRM1ek DMWDren kokapena ere gidatzen duenetz ikertu da. Horretarako lehen urratsa, Myc-DMWD gainadierazten duten zelulak LMBrekin tratatzea izan da. 34. irudian ikus daitekeen moduan, DMWD CRM1 aktibo dagoenean (-LMB), inhibiturik dagoenean (+LMB) baino kokapen zitoplasmatikoagoa hartzen du. Kokapen aldaketa hori WDR20 proteinarako baino nabarmen ahulagoa bada ere, agerikoa da DMWDren kokapena ere CRM1en mendekoa dela.

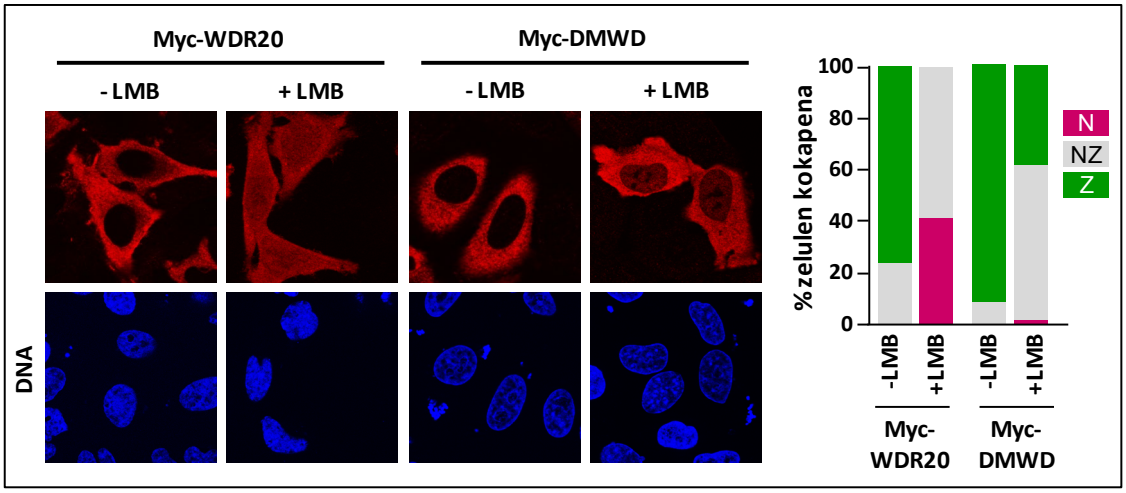

34. irudia: DMWDren kokapena CRM1en mendekoa da. Ezkerraldean, CRM1 aktibo (-LMB) edo inhibiturik egon (+LMB) gainadierazitako Myc-WDR20 eta Myc-DMWD proteinek hartzen duten kokapenaren irudi adierazgarriak erakusten dira. Eskuinaldean, proteina horiek zelula-populazioan hartzen duten kokapena adierazten duen grafikoa ageri da. Gutxienez 200 zelula nuklear (N), nukleozitoplasmatiko (NZ) edo zitoplasmatiko (Z) kategorietan sailkatu dira. CRM1 aktibo dagoenean Myc-WDR20 zein Myc-DMWD proteinek kokapen zitoplasmatikoa hartzen dute zelulen gehiengo handi batean. CRM1 inhibitzean, nukleoranzko lekualdaketa gertatzen da proteina bien kasuan, lekualdaketa WDR20 proteinaren kasuan nabariagoa da.

DMWDren kokapena CRM1en mendekoa dela ikusita, WDR20ren NESaren sekuentziaren homologoa den DMWDren sekuentzia ere NES aktiboa ote den ikertu da. Horretarako, ^{512}AEPGTPFSIGRFATLTLQE^{530} sekuentzia (ikusi 33. irudia) pRev(1.4)-GFP bektorean klonatu eta Rev(1.4)-GFP esportazio-entsegu bat egin da (35. irudia). ActDrekin tratatu gabeko (-ActD) zeluletan Rev(1.4)-[DMWD^{NES}]-GFP erreportariak kokapen gehienbat nuklearra erakusten du, zelulak ActDrekin tratatzean aldiz, kokapen ia erabat nukleozitoplasmatikoa. Kokapen horrek, WDR20ren NESaren homologoa den DMWDren sekuentzia NES aktiboa dela eta 3ko aktibitate esportatzailea duela erakusten du. Hau da, WDR20ren NESaren homologoa den DMWDren sekuentzia ere, ahulagoa bada ere, NES aktiboa da.

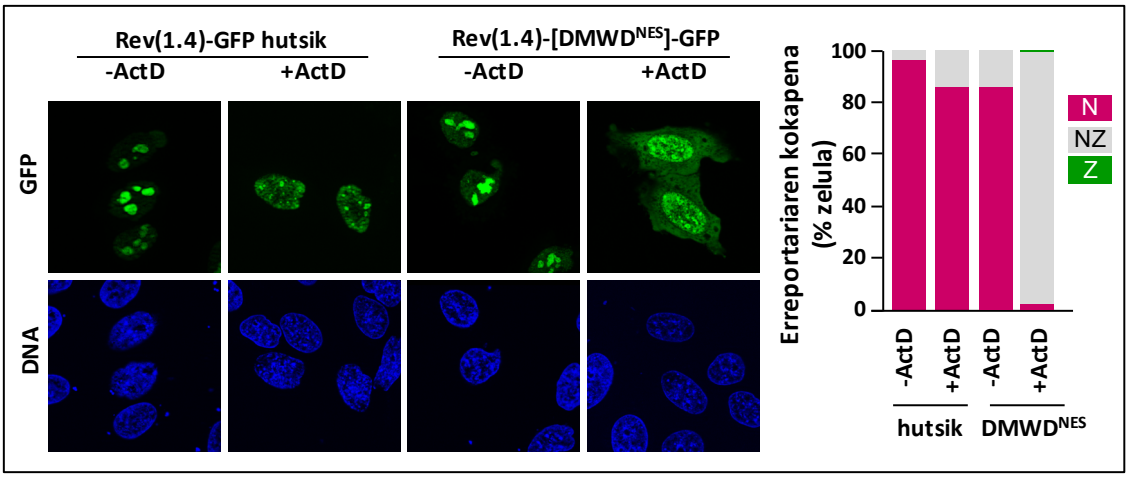

35. irudia: DMWD proteinaren (^{512}AEPGTPFSIGRFATLTLQE^{530}) NES kandidatua aktiboa da. Ezkerraldean Rev(1.4)-GFP bektore hutsarekin edo Rev(1.4)-[DMWD^{NES}]-GFP bektorearekin transfektatutako HeLa zeluletan eginiko Rev(1.4)-GFP esportazio-entseguaren irudi adierazgarriak ageri dira, eskuinaldean, erreportariaren kokapena gutxienez 200 zelulatan nuklear (N), nukleozitoplasmatiko (NZ) edo zitoplasmatiko (Z) kategorietan sailkatuz lortutako emaitza semi-kuantitatiboa. Zenbaketa horren arabera, eta Henderson eta Eleftheriouk (2000) argitaratutakoaren arabera, ikertutako NESak 3ko esportazio-aktibitatea du.

4.1.1.1.6. WDR20 proteinan identifikatutako NESak USP12/UAF1/WDR20 konplexuaren kokapena erregulatzen du

Tesi hau aurrera eramandako taldearen aurretiko esperimentuetan (Olazabal-Herrero et al., 2019) YFP-USP12 eta Myc-WDR20 proteinak bereizita gainadieraztean zitoplasmatikoak diren arren, proteina biak batera gainadieraztean (36A irudia), mintz plasmatikoranzko lekualdaketa jasaten dutela ikusi da. Lekualdaketa hori, nabariagoa da YFP-USP12 basatiaren ordez bi NLS seinaledun bertsioa erabiltzean (36B irudia).

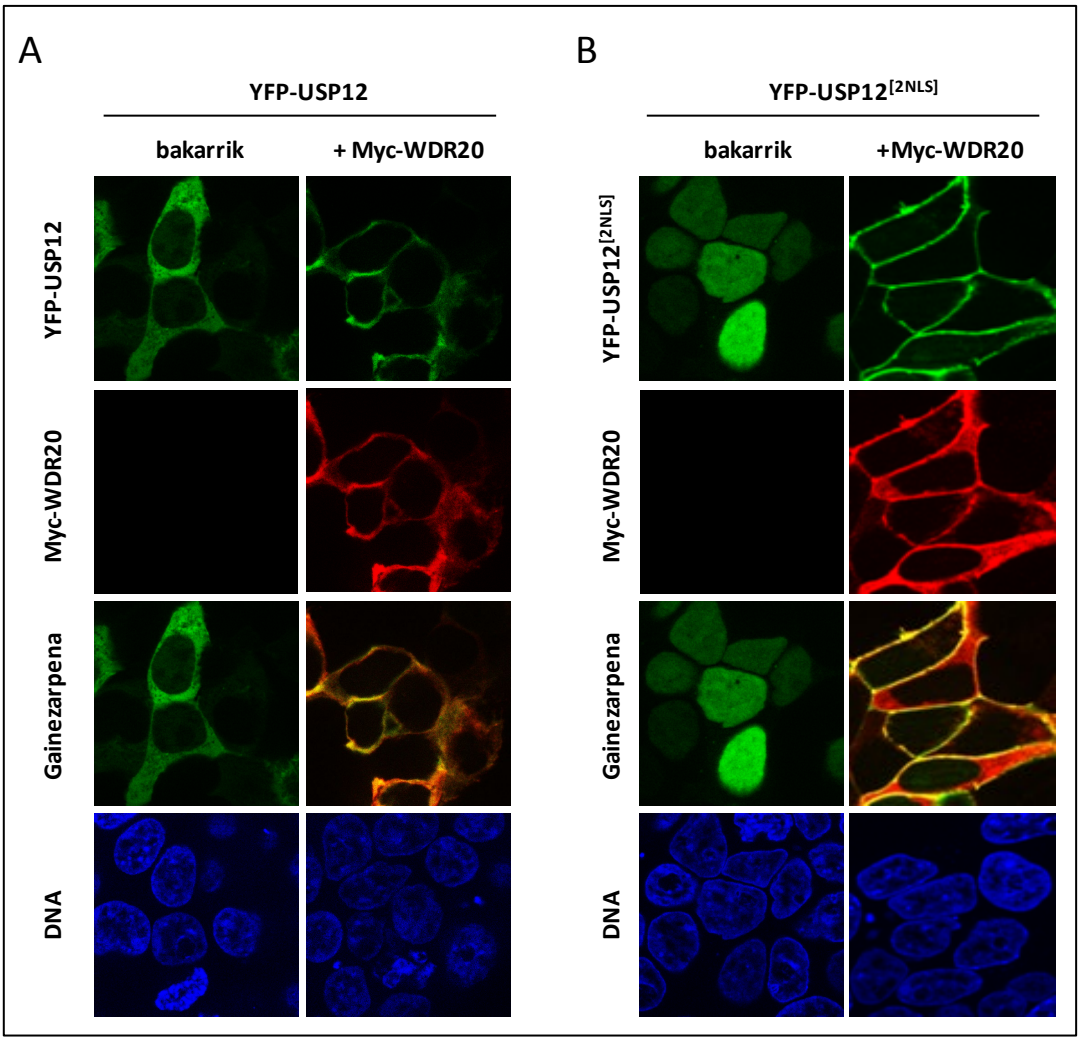

36. irudia: WDR20 proteinak USP12 proteina mintz plasmatikoan kokatzea eragiten du. YFP-USP12 basatia (A) edo YFP-USP12$^{[2NLS]}$ (B) HEK293T zelulatan bakarrik edo Myc-WDR20 proteinarekin batera gainadieraztean erakusten duten kokapenaren irudi adierazgarriak. Myc-WDR20 proteinak YFP-USP12 proteina mintz plasmatikoan kokatzea eragiten du (A panela). Kokapen aldaketa hori are nabariagoa da 2 NLSdun YFP-USP12 fusio proteina erabiltzean (B panela).

WDR20 proteinak USP12ren kokapena erabat aldatzen duela ikusita, WDR20 proteinan aurkitutako NES berriak USP12ren kokapenean eraginik duenetz ikertu da. Horretarako, berezko kokapen nuklearra duen YFP-USP12$^{[2NLS]}$, NESa mutaturik duen Myc-WDR20^{NESmut} proteinarekin batera gainadierazi da. 37. irudian beha daitekeenez, YFP-USP12$^{[2NLS]}$, Myc-WDR20 basatiarekin batera gainadieraztean gertatzen zenaren kontrara, YFP-USP12$^{[2NLS]}$, Myc-WDR20^{NESmut} proteinarekin batera gainadieraztean USP12 eta WDR20 proteinek kokapen gehienbat nuklearra erakusten dute. Emaitza horrek, USP12 proteina nukleotik at WDR20ri loturik, *piggyback* izenez ezaguna den mekanismoaren bidez, esportatzen dela iradokitzen du.

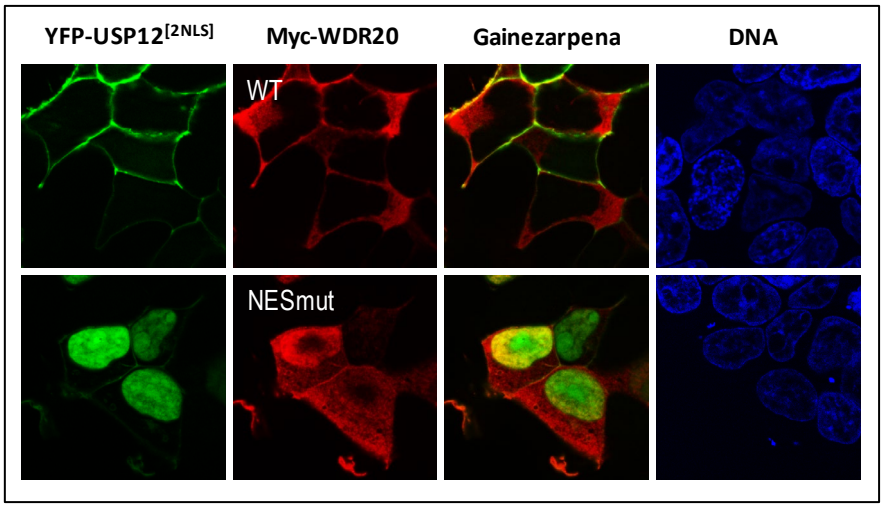

37. irudia: USP12ren nukleotiko esportazioa WDR20 proteinan deskribatutako NES berriaren mendekoa da. YFP-USP12[2NLS] eta Myc-WDR20 proteinaren aldaera basatia (WT) edo NES mutatua duena (NESmut) batera gainadierazten duten HEK293T zelulen fluoreszentziako irudi adierazgarriak. WDR20ren NES motiboaren mutazioak, gainadierazitako proteina biek kokapen nuklearragoa hartzea eragiten du.

Berriki identifikatutako WDR20ren NESak WDR20 proteina beraren zein USP12 proteinaren kokapena kontrolatzen duela ikusita, esportazio seinale horrek USP12/UAF1/WDR20 konplexuaren kokapenean duen eginkizuna ere ikertu da. Horretarako, Myc-WDR20 basatia edo Myc-WDR20^{NESmut}, YFP-USP12[2NLS] eta UAF1-mRFP proteinekin batera gainadierazi dira HEK293T zelulatan. 38. irudian ikus daitekeen bezala, Myc-WDR20 proteina basatia gainadierazten duten zeluletan, batera gainadierazitako hiru proteinak mintz plasmatikoan kokatzen dira. Myc-WDR20^{NESmut} gainadieraztean, ordea, konplexuko hiru proteinek kokapen nabari nuklearragoa erakusten dute.

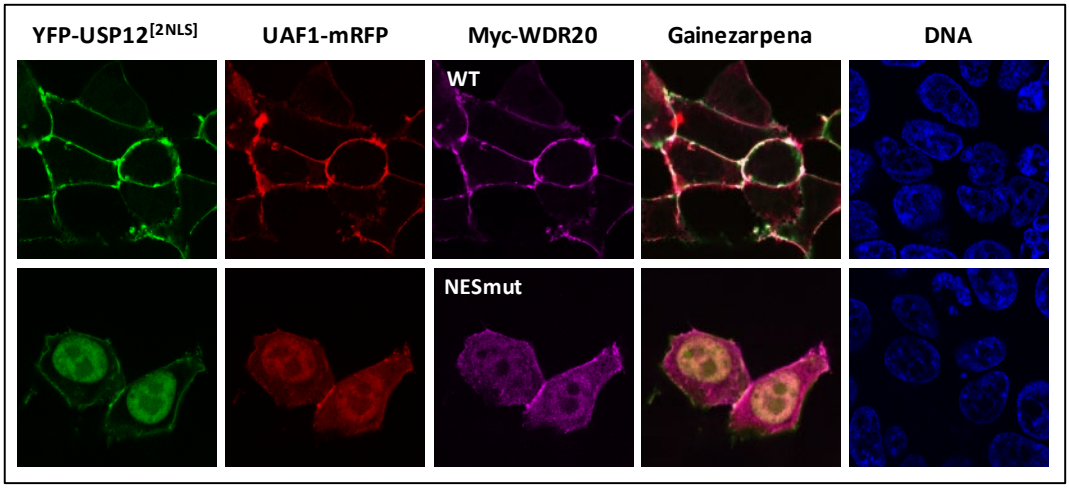

38. irudia: WDR20 proteinaren NESak USP12/UAF1/WDR20 konplexuaren CRM1en bidezko esportazioa bideratzen du. YFP-USP12[2NLS], UAF1-mRFP eta Myc-WDR20 proteina basatia (WT) edo NES motiboa mutaturik duena (NESmut) HEK293T zelulatan gainadierazi dira. Myc-WDR20 basatia gainadierazten den egoeran gainadierazitako hiru proteinak mintz-plasmatikoan kokatzen dira. Myc-WDR20^{NESmut} proteina erabiltzean, ordea, konplexuko proteinek kokapen nabarmen nuklearragoa erakusten dute.

Guzti horrek, WDR20 proteina USP12/UAF1/WDR20 konplexuaren esportazioaren arduraduna dela, eta hemen deskribatutako NES berriak esportazio horretan aparteko garrantzia duela iradokitzen du.

4.1.1.2. CRM1en minbizi-esportomako NESen peskizan

Atal honetan aurkeztutako emaitzak Sendino et al., 2020a-n argitaratu dira.

2015ean Kirli eta lankideek afinitate-purifikazioa eta masa-espektrometria uztartuz, HeLa zeluletako CRM1en balizko kargoen bilduma argitaratu zuten. CRM1en benetako kargo izateko probabilitatearen arabera identifikatutako proteinak 5 kategoriatan sailkatu zituzten: A kargoak, B kargoak, C (*low abundancy)* kargoak, *ambiguous* kargoak eta *non-binder* (kargoak ez diren proteinak). Balizko kargoen bilduma horri CRM1en mendeko esportoma izena eman zioten, eta 1000 balizko kargo (A, B, C, edo *ambiguous* kategorietakoak) baino gehiago biltzen ditu. Balizko kargo horien gehiengo zabala esperimentalki konfirmatzeke dago oraindik. Gainera, CRM1en kargotzat egiaztatuta dauden proteina askoren NESak ezezagunak dira.

CRM1ek minbiziaren garapen eta pronostikoarekin erlazio estua duela aurretik ere aipatu da. Hori horrela, CRM1en mendeko esportomako hainbat proteina minbiziarekin erlazionatuta egotea aurreikus daiteke. Aurreikuspen hori buruan, Kirli eta lankideek 2015ean zehaztutako esportomako proteinak, *The Human Protein Atlas*-ean (HPA; https://www.proteinatlas.org/; 18. bertsioa) minbiziarekin erlazionatutako proteina gisa sailkaturiko proteinekin erkatu dira. Erkaketa horretan komunak diren 136 proteina aurkitu dira eta "CRM1en minbizi-esportoma" delakoa osatzen dute (Sendino et al., 2018) (39. irudia). CRM1en minbizi-esportoma osatzen duten proteinen zerrenda xehatua 22. taula gehigarrian ageri da.

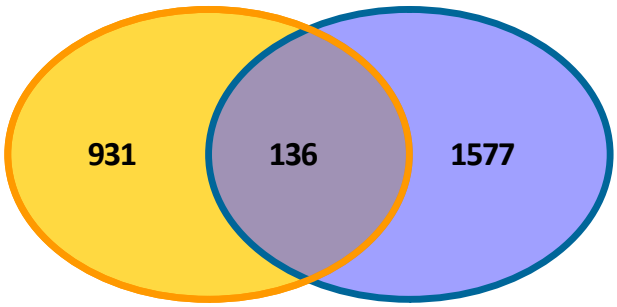

39. irudia: "CRM1en minbizi-esportoma". CRM1en mendeko esportoma (Kirli et al., 2015) eta *The Human Protein Atlas*-aren (18. bertsioa) arabera minbiziarekin erlazionaturik dauden proteinak erkatzen dira Venn diagraman. Erkaketa horretan talde bietarako komunak diren 136 proteina aurkitu dira. Proteinok "CRM1en minbizi-esportoma" osatzen dute (Sendino et al., 2018).

CRM1en minbizi-esportomako proteina asko ez dago oraindik CRM1en kargo bezala konfirmatuta, eta kargo baieztatuak direnen artean badira NES ezezagunak dituzten asko ere. Hori horrela, tesi honetan CRM1en minbizi-esportomako NESen bilaketari ekin zaio. Sekuentzia horiek ezagutzea, kargoak baieztatzeko bidea izateaz gain, analisi funtzionalak egiteko aukera ere zabaltzen dute.

4.1.1.2.1. NES-iragarleen bidezko cNESen bilaketa CRM1en minbizi-esportoman

CRM1en minbizi-esportomako NESak bilatzeko, 2015ean Kirli eta lankideek HeLa zeluletako CRM1en esportoma definitzean A eta B kargo bezala izendatu zituzten kargoak soilik hartu dira kontuan, hau da, 39. irudian aipatutako 136 proteinetatik 112 proteina (ikusi 22. taula gehigarria). 112 CRM1en balizko kargo horien sekuentzietan NES kandidatuak (cNESak) bilatzeko, Wregex (Prieto et al., 2014) eta NESmapper (Kosugi et al., 2014) NES-iragarleak erabili dira. Bilaketak ohiko noranzkoan (*plus*) zein orain gutxi Fung eta lankideek (2015) deskribatutako kontrako noranzkoan (*reverse* edo *minus*) (ikusi 1. taula) egin dira. Guztira 988 cNES iragarri dira; 507 *plus* erakoak eta 481 *minus* erakoak (23. eta 24. taula gehigarriak).

cNES guzti horiek Rev(1.4)-GFP esportazio-entseguaren bidez aztertzea ez da bideragarria. Beraz, noranzko bietako cNESak iragarle bakoitzarekin lortutako puntuazioaren araberako kuartiletan (Q) oinarrituta lau kategoriatan sailkatu dira. 13. taulan mailaketa sistema, eta maila bakoitzeko cNES kopurura laburbiltzen da.

13. taula: NES-iragarleetan oinarritutako cNESen sailkapena. Bi noranzkoetako cNESak Wregex (Prieto et al., 2014) eta NESmapper (Kosugi et al., 2014) iragarleek cNES bakoitza iragarritako kuartilaren (Q) arabera lau mailatan sailkatu dira. Maila bakoitzean aurkitutako cNES kopurua adierazten da.

Sailkapena	1 iragarlea	2 iragarlea	cNES kopurua
Lehen mailako *plus* cNES	Q1	Q1	7
Bigarren mailako *plus* cNES	Q2	Q1 edo Q2	19
Hirugarren mailako *plus* cNES	Q1	Q3, Q4 edo ez aurkitua	109
Laugarren mailako *plus* cNES	Q2, Q3 edo Q4	Q3, Q4 edo ez aurkitua	372
Lehen mailako *minus* cNES	Q1	Q1	10
Bigarren mailako *minus* cNES	Q2	Q1 edo Q2	12
Hirugarren mailako *minus* cNES	Q1	Q3, Q4 edo ez aurkitua	104
Laugarren mailako *minus* cNES	Q2, Q3 edo Q4	Q3, Q4 edo ez aurkitua	355

Sailkapen horretan oinarrituta, lehen eta bigarren mailako *plus* cNESak eta lehen mailako *minus* cNESak, hau da, 36 cNES hautatu eta Rev(1.4)-GFP esportazio-entseguaren bidez aztertu dira (14. taula).

14. taula: Rev(1.4)-GFP esportazio-entsegua erabiliz testatutako CRM1en minbizi-esportomako cNESak. Taulan cNES bakoitzaren identifikazio-kodea (ID), cNES bakoitzaren jatorrizko proteinak UniProtKB datu-basean duen sarrera, Kirli eta lankideen (2015) arabera A kargo edo B kargo kategoriakoa den, aztertutako cNES motiboak proteinan duen kokapena eta aminoazido sekuentzia, eta cNES bakoitza zein mailatan sailkatzen den adierazten da. WN (Wregex-NESmapper) IDa dutenak *plus* cNESak dira, Rev IDa (*reverse*) dutenak aldiz, *minus* cNESak.

cNES ID	UniProt sarrera	Kargo mota	cNES kokapena	cNES sekuentzia	Maila
WN1	sp|P36507|MP2K2_HUMAN	B	33-51	NLVDLQKKLEELELDEQQK	1
WN2	sp|Q9NZQ3|SPN90_HUMAN	A	282-300	SASDDLEALGTLSLGTTEE	1
WN3	sp|P19532|TFE3_HUMAN	A	418-436	QANRSLQLRIQELELQAQI	1
WN4	sp|Q8IXJ6|SIR2_HUMAN	A	37-55	DMDFLRNLFSQTLSLGSQK	1
WN5	sp|O15234|CASC3_HUMAN	B	457-475	SSTSGLEQDVAQLNIAEQN	1
WN6	sp|O15357|SHIP2_HUMAN	B	256-274	TGEQELESLVLKLSVLKDF	1
WN7	sp|O15534|PER1_HUMAN	B	483-501	DTDIQELSEQIHRLLLQPV	1
WN8	sp|O15357|SHIP2_HUMAN	B	625-643	RKEFEPLLRVDQLNLEREK	2
WN9	sp|O15534|PER1_HUMAN	B	1215-1233	PDDPLFSELDGLGLEPMEE	2
WN10	sp|Q14141-2|SEPT6_HUMAN	A	155-174	IAPTGHSLKSLDLVTMKKLD	2
WN11	sp|Q8IXJ6|SIR2_HUMAN	A	244-267	FSCMQSDFLKVDLLLVMGTSLQVQ	2
WN12	sp|O95071-2|UBR5_HUMAN	A	2206-2224	AEPGSILTELGGFEVKESK	2
WN13	sp|P42345|MTOR_HUMAN	A	1274-1292	RVSKDDWLEWLRRLSLELL	2
WN14	sp|P14635|CCNB1_HUMAN	A	138-156	AEEDLCQAFSDVILAVNDV	2
WN15	sp|O95684|FR1OP_HUMAN	A	352-370	EISIGEEIEEDLSVEIDDI	2
WN16	sp|P63010|AP2B1_HUMAN	A	256-274	VLSAVKVLMKFLELLPKDS	2
WN17	sp|P20042|IF2B_HUMAN	A	89-107	FDIDEAEEGVKDLKIESDV	2
WN18	sp|P42345|MTOR_HUMAN	A	649-668	VQVVADVLSKLLVVGITDPD	2
WN19	sp|P11274|BCR_HUMAN	A	1091-1111	VSGVATDIQALKAAFDVNNKD	2
WN20	sp|Q14145|KEAP1_HUMAN	A	272-290	RCHSLTPNFLQMQLQKCEI	2
WN21	sp|Q6UUV9-3|CRTC1_HUMAN	A	329-347	LSPLSPITQAVAMDALSLE	2
WN22	sp|P15923|TFE2_HUMAN	A	566-584	NEAFKELGRMCQLHLNSEK	2
WN23	sp|Q99081|HTF4_HUMAN	A	594-612	NEAFKELGRMCQLHLKSEK	2
WN24	sp|Q12778|FOXO1_HUMAN	B	62-80	SAAAVSADFMSNLSLLEES	2
WN25	sp|Q13492-2|PICAL_HUMAN	A	212-230	NEGIINLLEKYFDMKKNQC	2
WN26	sp|P35869|AHR_HUMAN	B	114-132	EGEFLLQALNGFVLVVTTD	2
Rev1	sp|P25963|IKBA_HUMAN	A	267-285	QQLGQLTLENLQMLPESED	1
Rev2	sp|Q16204|CCDC6_HUMAN	A	297-315	MREENLRLQRKLQREMERR	1
Rev3	sp|P19484|TFEB_HUMAN	A	431-449	KDLDLMLLDDSLLPLASDP	1
Rev4	sp|O95071-2|UBR5_HUMAN	A	209-227	LQRTNLDVNLAVNNLLSRD	1
Rev5	sp|O15357|SHIP2_HUMAN	B	261-279	LESLVLKLSVLKDFLSGIQ	1
Rev6	sp|P30260|CDC27_HUMAN	A	545-563	HLQKDVALSVLSKDLTDMD	1
Rev7	sp|O95071-2|UBR5_HUMAN	A	1607-1625	EDGSDMELDLLAAAETESD	1
Rev8	sp|Q9UDY2-3|ZO2_HUMAN	A	715-733	PIADIAMEKLANELPDWFQ	1
Rev9	sp|Q92997-2|DVL3_HUMAN	A	24-42	PAERVTLADFKGVLQRPSY	1
Rev10	sp|O95684|FR1OP_HUMAN	A	379-397	LTQDLTVSQLSDVADYLED	1

4.1.1.2.2. Iragarritako cNESen esportazio-aktibitatearen azterketa

14. taulako cNESak pRev(1.4)-GFP bektorean klonatu eta Rev(1.4)-GFP esportazio-entseguan erakusten duten esportazio aktibitatearen arabera 0 (ez aktibo) eta 9 arteko mailatan sailkatu dira. Guztira, 36 cNESetatik 25 dira aktiboak (40. irudia).

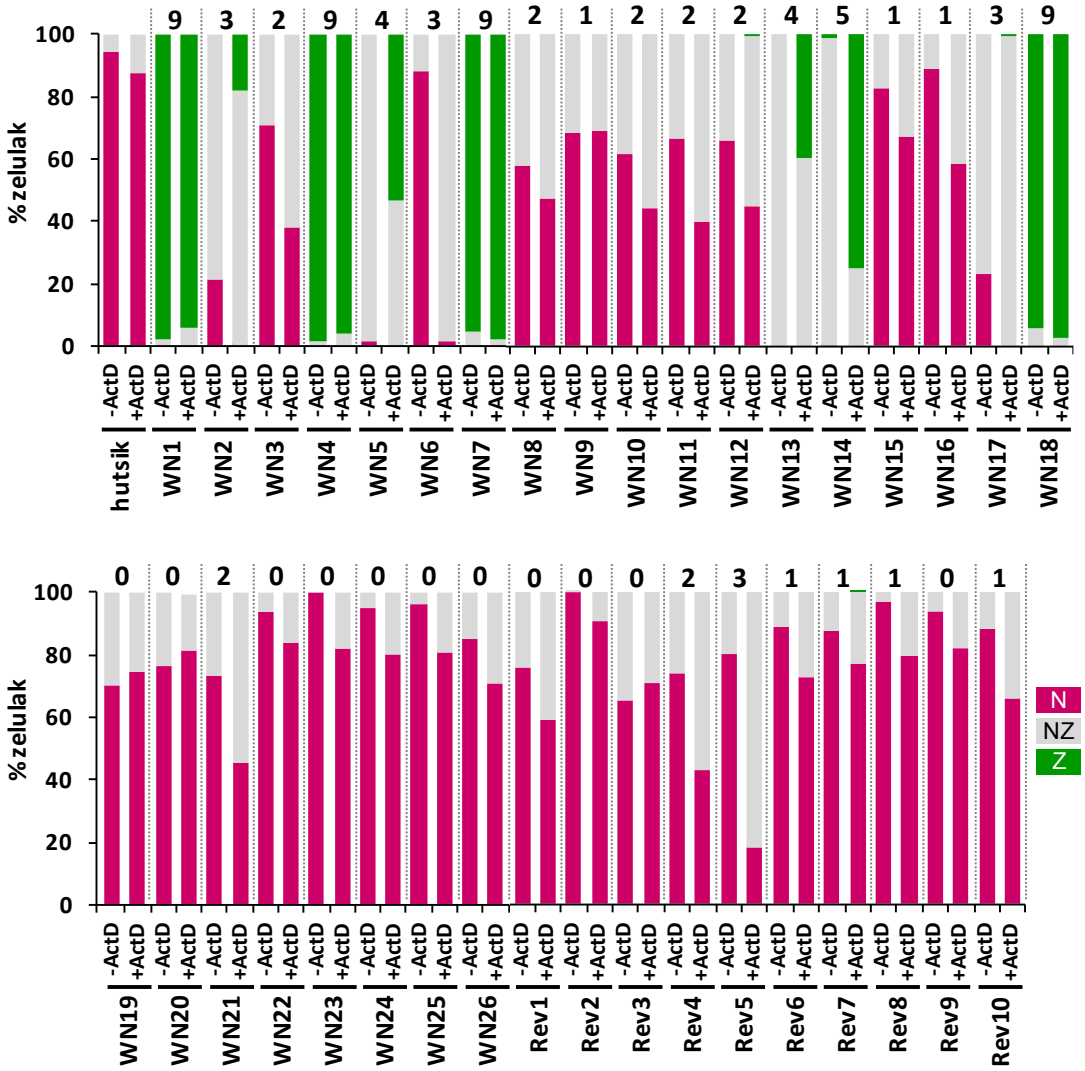

<u>40. irudia:</u> CRM1en minbizi-esportomako cNESekin egindako Rev(1.4)-GFP esportazio-entseguetako emaitzen grafikoak. 36 cNESetatik 25 dira aktiboak. Entseatutako motibo bakoitzak erakutsitako esportazio-aktibitatearen maila (0-9 artekoa) grafikoaren goialdean ageri da.

40. irudiari erreparatuz CRM1en minbizi-esportomako NES aktiboen artean aktibitate maila oso ezberdina duten NESak daudela beha daiteke. Orokorrean, *plus* eta *minus* NES aktiboak konparatuz gero, *plus* NESek esportazio-aktibitate altuagoa erakusten dute; *plus* NESek 3,84ko aktibitatea dute batez bestean, *minus*ek ordea, 1,5ekoa (41.irudia).

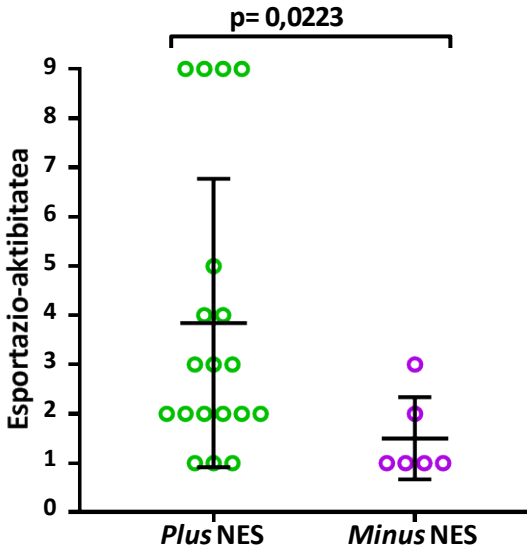

41. irudia: ***Plus* eta *minus* NESen aktibitatea konparatzen dituen grafikoa.** *Plus* NESek Rev(1.4)-GFP esportazio-entseguan lortutako batez besteko esportazio-aktibitatea 3,84koa da, *minus*ek lortutakoa ordea, 1,5ekoa. Grafikoko zirkulu bakoitzak Rev(1.4)-NES-GFP erreportari bat adierazten du. *Plus* eta *minus* NESen batez besteko balioak eta desbiderapen estandarrak adierazten dira. p balioa (Mann-Whitney U test) grafikoan adierazten da.

Iragarleen arabera lehen edo bigarren mailakoak diren *plus* NESak aztertzean ere ezberdintasun nabariak ageri dira. Aztertutako lehen mailako cNES guztiak aktiboak izan dira 5,57ko esportazio-aktibitate maila erakutsi dutelarik batez beste. Bigarren mailako *plus* cNESetan, ordea, 19 cNESetatik 7 ez dira aktiboak eta aktiboak diren gainontzekoen batez besteko aktibitate maila 3,09koa da, lehen mailako NESena baino baxuagoa (42. irudia).

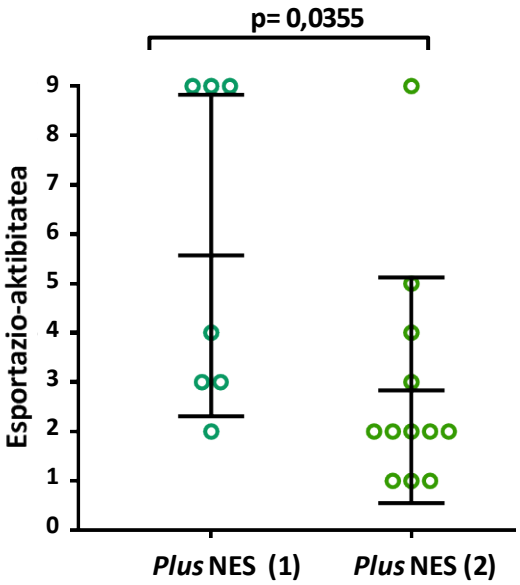

42. irudia: ***In silico* eginiko cNESen analisiaren arabera lehen (1) edo bigarren mailakoak (2) diren *plus* NESen aktibitatearen grafikoa.** Lehen mailako *plus* NESek Rev(1.4)-GFP esportazio-entseguan erakutsitako batez besteko esportazio-aktibitatea 5,57koa da, bigarren mailako *plus* NESek erakutsitakoa, ordea, 3,09koa. Grafikoko zirkulu bakoitzak Rev(1.4)-NES-GFP erreportari bat adierazten du. *Plus* NES talde bakoitzeko batez besteko balioak eta desbiderapen estandarrak adierazten dira. p balioa (Mann-Whitney U test) grafikoan adierazi da.

Rev(1.4)-GFP esportazio-entseguan aktibo diren 25 NES horietatik, WN1 (Fukuda et al., 1996), WN4 (North eta Verdin, 2007), WN5 (Macchi et al., 2003), WN7 (Vielhaber et al., 2001), WN13 (Bachmann et al., 2006) eta WN14 (Toyoshima et al., 1998) NES ezagunak dira. Gainontzeko 19ak, tesi honetan deskribatutako NES berriak dira. Deskribatutako NES berri horiek NESdb datu basearen (http://prodata.swmed.edu/LRNes/index.php; Xu et al., 2012; Fung et al., 2021) azken bertsioan erregistraturik daude jada.

4.1.2. Tresna berri baten sorrera: $SRV_{B/A}$ erreportarian oinarritutako esportazio-entsegua

Atal honetan aurkeztutako emaitzak Taylor et al., 2019 eta Sendino et al., 2020a-n argitaratu dira.

4.1.2.1. Rev(1.4)-GFP esportazio-entseguaren mugak eta $SRV_{B/A}$ erreportariaren sorrera

Rev(1.4)-GFP esportazio-entsegua NES berriak detektatzeko eta horien aktibitate maila neurtzeko baliabide oso aproposa bada ere, mugak ere baditu. Muga nagusia, CRM1en aldaera ezberdinek NESak esportatzeko duten gaitasuna era erraz batean neurtzeko aukerarik ematen ez duela da. Muga horri aurre egiteko, tesi proiektu honetan $SRV_{B/A}$ erreportaria sortu da.

$SRV_{B/A}$ erreportaria, García-Santisteban eta lankideek 2016an garatutako SRV100 biosentsoretik abiatuz sortu da. SRV100 biosentsoreak, surbibinaren lehen 100 aminoazidoak, NESa barne, SV40 birusaren T antigeno luzearen 2 NLS eta 3xFlag epitopoa adierazten ditu (43A irudia), eta CRM1en aldaera ezberdinek duten esportazio-ahalmena aztertzeko da aproposa. Horrela, SRV100 bera bakarrik HEK293T zelulatan gainadieraztean, NESaren eta NLSen arteko norgehiagokak biosentsorea nukleoan metatzea eragiten du (43B irudia). Biosentsorea, CRM1 basatiarekin (CRM1wt) edo kargoak esportatzeko gai den CRM1en mutante batekin gainadieraziz gero, zitoplasman metatuko da (García-Santisteban et al., 2016). Aldiz, kargoak esportatzeko ahalmenik ez duen CRM1en mutante batekin, esaterako, I521A/L525A/F561A/F572A mutantearekin (4X izenaz ezagunagoa; Dong et al., 2009a) batera gainadieraziz gero, biosentsorea nukleoan metatuko da.

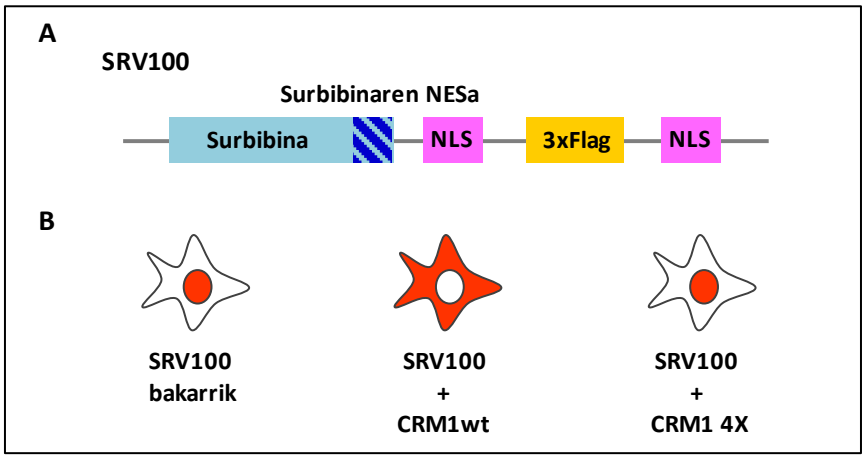

43. irudia: SRV100 biosentsorearen eskema eta HEK293T zelulatan erakusten duen kokapenaren irudi eskematikoa. A. SRV100 biosentsorearen eskema. Urdin argiaz surbibina proteinaren lehen 100 aminoazidoak, marra urdin ilun diagonalekin surbibinaren NESa, arrosaz SV40 birusaren T antigenoaren 2 NLS eta horiz 3xFlag epitopoa adierazten dira. B. SRV100 biosentsoreak HEK293T zelulatan gainadieraztean erakusten duen kokapena. Bakarrik gainadieraztean bi NLSek SRV100 nukleoan metatzea eragiten dute. CRM1 basatiarekin (wt) gainadieraztean surbibinaren NESak proteina zitoplasman metatzea eragiten du. Esportazio-ahalmenik ez duen CRM1en mutante batekin gainadieraztean, adibidez CRM1 4X mutantearekin (Dong et al., 2009a), bakarrik gainadieraztean gertatzen den era berean, SRV100 nukleoan metatzen da.

García-Santisteban eta lankideek (2016) SRV100 biosentsorea CRM1en aldaera ezberdinek zelulatan duten esportazio ahalmena aztertzeko baliagarria dela erakutsi zuten. SRV100 biosentsorea CRM1en aldaera ezberdinen esportazio ahalmena ebaluatzeko baliagarria bada ere, ez du NES ezberdinen aktibitate esportatzailea aztertzeko aukerarik ematen. Ezaugarri bi horiek esportazio-entsegu berean ebaluatzeko helburuarekin, tesi honetan, SRV100 biosentsoretik abiatuta $SRV_{B/A}$ erreportaria garatu da (Taylor et al., 2019; Sendino et al., 2020a). Gainera, sortutako erreportari berria, Rev(1.4)-GFP erreportariarekin bateragarria izatea bilatu da. Bateragarritasun horrek aztergai diren NESak erreportari baten plasmido kodetzailetik abiatuz bestean era errazean azpiklonatzea ahalbidetuko baitu. pRev(1.4)-GFP bektorean NESak BamHI eta AgeI murriztegunеak erabiliz klonatzen direnez, $SRV_{B/A}$ plasmidoan ere egoera hori sortu behar da. Horretaz gain, sortuko den bektore berriak ezin du surbibinaren NESa kodetu. Puntu bi horiek kontuan izanik, SRV100 plasmidoaren surbibinaren NES sekuentzia kodetzailearen alde banatan BamHI eta AgeI murriztegunеak eratu dira. Horrek, aldi berean surbibinaren NESa kanporatzea eta beste NES bat barneratzea ahalbidetuko du. Kontuan izan behar da, SRV100 plasmidoaren jatorrizko sekuentziak $SRV_{B/A}$ bertsiorako interesgarriak ez diren berezko BamHI eta AgeI murriztegunеak dituela (44. irudia), eta beraz, $SRV_{B/A}$ sortzeko NES sekuentziaren alde banatan BamHI eta AgeI guneak sortzeaz gain, bestelako BamHI eta AgeI guneak ezabatu behar dira.

Guzti hori kontuan izanik, $SRV_{B/A}$ erreportaria eratzeko modurik aproposena SRV100 plasmidotik SRV100 biosentsorearen sekuentzia kodetzaile osoa kanporatzea eta bertan $SRV_{B/A}$ erreportariaren sekuentzia kodetzailea barneratzea dela erabaki da. Hori egiteko, SRV100 erreportariaren sekuentzia kodetzailea BglII eta NotI murriztegunеak erabiliz kanporatu eta murriztegune berdinak erabiliz $SRV_{B/A}$ erreportariaren sekuentzia kodetzailea osoa barneratu da (44. irudia).

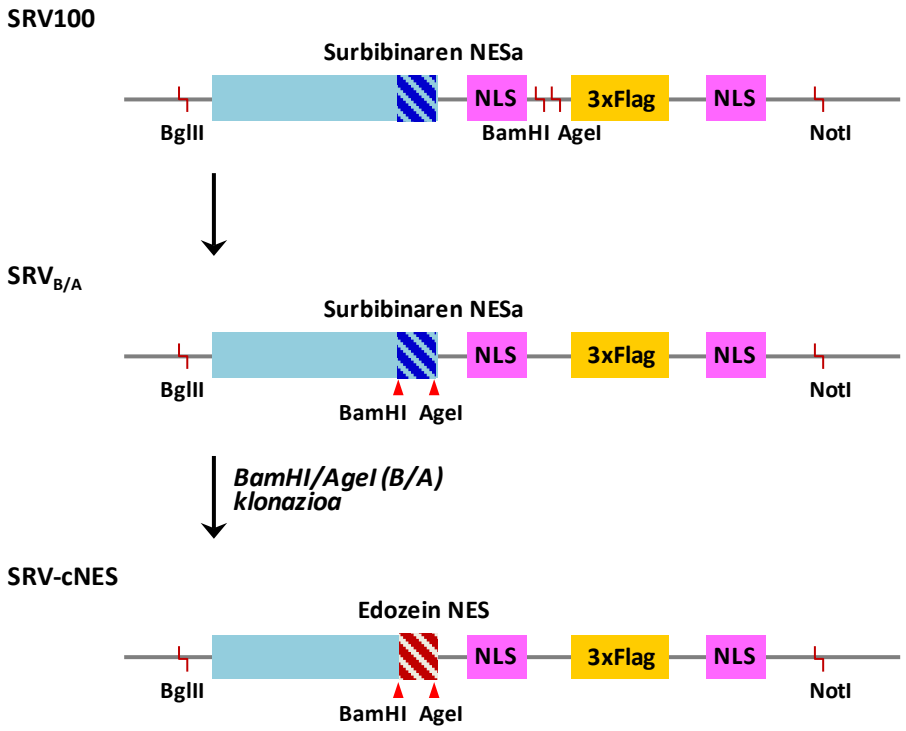

44. irudia: SRV$_{B/A}$ plasmidoaren sorrera SRV100 plasmidotik abiatuta. BglII eta NotI murrizteguneak erabilita SRV100 plasmidoaren sekuentzia kodetzailea kanporatu da. Bertan, proteina berdina kodetzen duen baina BamHI eta AgeI murrizteguneak kokapen ezberdinean dituen cDNA barneratu da. SRV$_{B/A}$ plasmidoan BamHI eta AgeI murrizteguneak surbibinaren NESaren alde banatan daude, surbibinaren NESaren ordez beste edozein cNES barneratzea ahalbidetuz.

SRV100 eta SRV$_{B/A}$ bektoreek proteina berdinerako kodetzen badute ere, bektoreko murrizteguneak aldatzeak, eta ondorioz, jatorrizko NESa beste edozein cNES motiborengatik ordezkatu ahal izateak, NES ezberdinen esportazio-aktibitatea eta CRM1en aldaera ezberdinen esportazio-ahalmena ikertzeko aukera asko zabaltzen du. Gainera, pRev(1.4)-GFP bektorearekin bateragarria denez, cNES berberak sistema bietan era errazean aztertzea ahalbidetzen du (45. irudia).

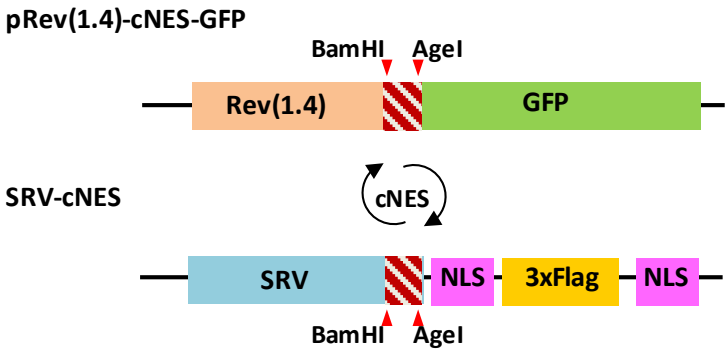

45. irudia: pRev(1.4)-GFP eta SRV$_{B/A}$ plasmidoak bateragarriak dira. pRev(1.4)-GFP zein SRV$_{B/A}$ plasmidoan ikertzeke dauden cNESak BamHI eta AgeI murrizteguneak erabilita klonatzen dira, beraz, cNES horiek plasmido batean klonaturik izanez gero, era errazean azpiklonatu daitezke bestean.

4.1.2.2. $SRV_{B/A}$ plasmidoan oinarritutako esportazio-entseguak

$SRV_{B/A}$ plasmidoan oinarritutako esportazio-entseguak, hemendik aurrera $SRV_{B/A}$ esportazio-entsegu bezala izendatuko direnak, NES kandidatu ezberdinen esportazio-aktibitatea eta CRM1en aldaera ezberdinen esportazio-ahalmena ikertzeko dira baliagarriak (46. irudia). $SRV_{B/A}$ erreportarian barneratutako cNESa aktiboa baldin bada, SRV100 erreportariarekin lortzen zen emaitza bera lortuko da, hau da, erreportaria bakarrik gainadieraztean nukleoan metatuko da, eta CRM1en mutante aktibo batekin batera gainadieraztean ordea, zitoplasman. Aldiz, barneratutako cNESa ez-aktiboa baldin bada, CRM1ek ez du ezagutuko, beraz, nahiz eta CRM1en aldaera aktibo batekin batera gainadierazi, nukleoan geratuko da.

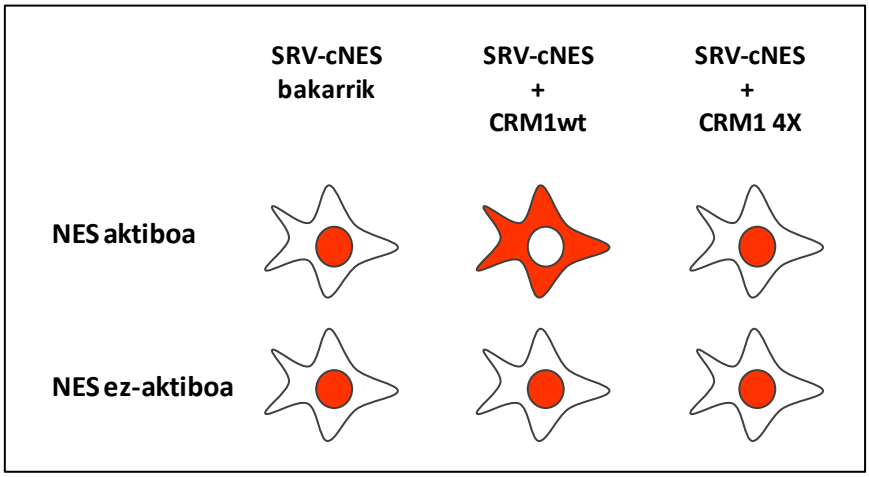

46. irudia: SRV-cNES erreportariaren barneratutako cNESaren aktibitatearen araberako, eta gainadierazitako CRM1 aldaeraren esportazio-ahalmenaren araberako $SRV_{B/A}$ esportazio-entseguaren emaitza azaltzen duen irudi eskematikoa. SRV-cNES erreportariaren cNESa aktiboa denean, erreportaria bakarrik gainadieraztean nukleoan metatuko da, CRM1en aldaera aktibo batekin batera gainadieraztean ordea, zitoplasman. Kontrara, barneratutako cNESa ez-aktiboa baldin bada, bakarrik zein edozein CRM1en aldaerarekin batera gainadieraztean erreportaria nukleoan metatuko da, CRM1ek ez baitu inolaz ere ezagutu eta esportatuko.

3.6.2. atalean azaldu den moduan, $SRV_{B/A}$ esportazio-entseguaren emaitza hiru metodo ezberdinekin aztertu da. Laburbilduz (47. irudia), lehenengo metodoan SRV-cNES proteinak laginean orokorrean hartzen duen kokapena guztiz nuklearretik guztiz zitoplasmatikora doazen bost kategoria ezberdinetan sailkatu da. Bigarren metodoan, SRV-cNES erreportariaren kokapenaren arabera, 200 zelula gutxienez zitoplasmatiko (Z), nukleozitoplasmatiko (NZ) edo nuklear (N) kategorietan sailkatu dira. Kontaketa horretan oinarrituta gainera, NES/CRM1 konbinazio ezberdinak konparatu ahal izateko esportazio-aktibitate mailari 0 eta 100 bitarteko balioa (SRV balioa bezala izendatu dena) eman zaio. Hirugarren metodoan berriz, FiJi softwarearen bidezko irudi-analisi semi-kuantitatiboa erabili da. Irudian aipaturiko hiru metodo horiekin aztertutako bi lagin ikus daitezke. Agerikoa den moduan, lagin berbera metodologia ezberdinekin aztertzean lortzen den funtsezko informazioa berdina da. Hala ere,

lortutako emaitzek zehaztasun maila ezberdina ematen dute, eta beraz, esperimentu bakoitzean lortu nahi den zehaztasun mailaren arabera metodo bat edo bestea aukeratuko da.

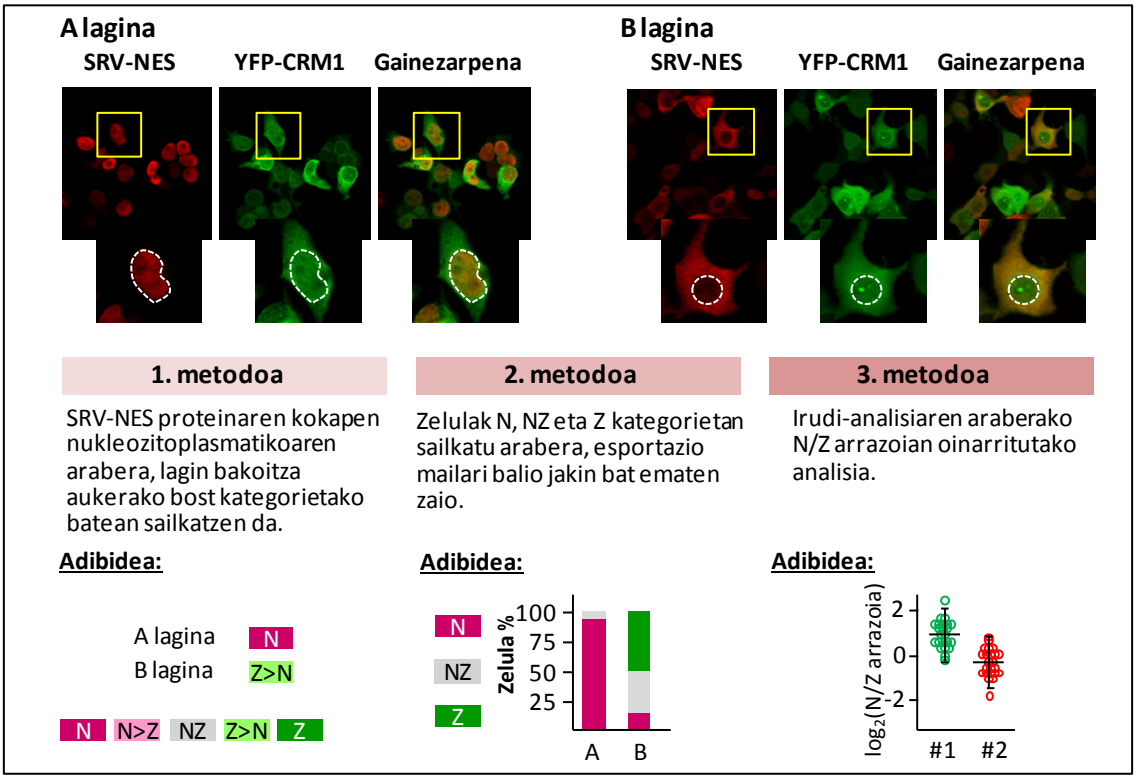

47. irudia: $SRV_{B/A}$ esportazio-entseguak analizatzeko hiru metodoak eta adibideak. Fluoreszentziako argazkiek bi SRV-cNES erreportari ezberdin erabiliz eginiko esportazio-entseguen adibideak erakusten dituzte. Laginaren argazki orokorra, zein argazki orokor horretako zelula bakar baten argazkiak daude erakusgai. Zelula bakarra erakusten den irudian, nukleoa marratxo zuriz inguratu da. Argazkien azpian $SRV_{B/A}$ esportazio-entseguak analizatzeko hiru metodoen nondik norako orokorrak eta lagin biak hiru metodoekin aztertzean lortutako emaitzak ageri dira. A lagina lehen metodoa erabiliz nuklear (N) bezala sailkatu da, bigarren metodoa erabiliz 4 balioko SRV balioa lortu du eta hirugarren metodoa erabiliz 0,9ko log_2(N/Z arrazoia) balioa. B laginari dagokionez, lehen metodoa erabilita gehienbat zitoplasmatiko (Z>N) bezala sailkatu da, bigarren metodoa erabilita 70eko SRV balioa lortu du eta hirugarren metodoa erabilita -0,3ko log_2(N/Z arrazoia) balioa.

4.1.2.2.1. $SRV_{B/A}$ esportazio-entsegua CRM1en minbizi-esportomako cNESen esportazio-aktibitatea aztertzeko

$SRV_{B/A}$ esportazio-entsegua balioztatzeko, eta baita $SRV_{B/A}$ eta Rev(1.4)-GFP esportazio-entseguetan lortzen diren emaitzak bateragarriak diren ikertzeko ere, aurretik Rev(1.4)-GFP esportazio-entseguan aztertutako (ikusi 40. irudia) eta aktibitate maila ezberdina erakutsi duten 22 cNES (15. taula) $SRV_{B/A}$ esportazio-entsegua erabiliz aztertu dira.

15. taula: $SRV_{B/A}$ erreportarian azpiklonatutako cNESak eta Rev(1.4)-GFP esportazio-entseguan lortu duten emaitza.

Azpiklonatutako cNESa	Rev(1.4)-GFP emaitza	Azpiklonatutako cNESa	Rev(1.4)-GFP emaitza
WN1	9	WN16	1
WN2	3	WN17	3
WN3	2	WN18	9
WN4	9	WN19	0
WN5	4	WN20	0
WN6	3	Rev1	0
WN7	9	Rev4	2
WN9	1	Rev5	3
WN13	4	Rev6	1
WN14	5	Rev7	0
WN15	1	Rev9	0

15. taulako cNESak $SRV_{B/A}$ plasmidoan azpiklonatu, eta eratorritako SRV-cNES erreportariak bakarrik zein YFP-CRM1 basatiarekin batera gainadierazi dira HEK293T zelulatan. Esportazio-entsegu horiek lehen azterketa metodoa erabiliz ebaluatu dira. Hau da, lagin bakoitza SRV-cNES erreportariak erakusten duen kokapen orokorraren arabera guztiz nuklear (N), gehienbat nuklear (N>Z), nukleozitoplasmatiko (NZ), gehienbat zitoplasmatiko (Z>N) edo guztiz zitoplasmatiko (Z) kategorietan sailkatu da (48. irudia).

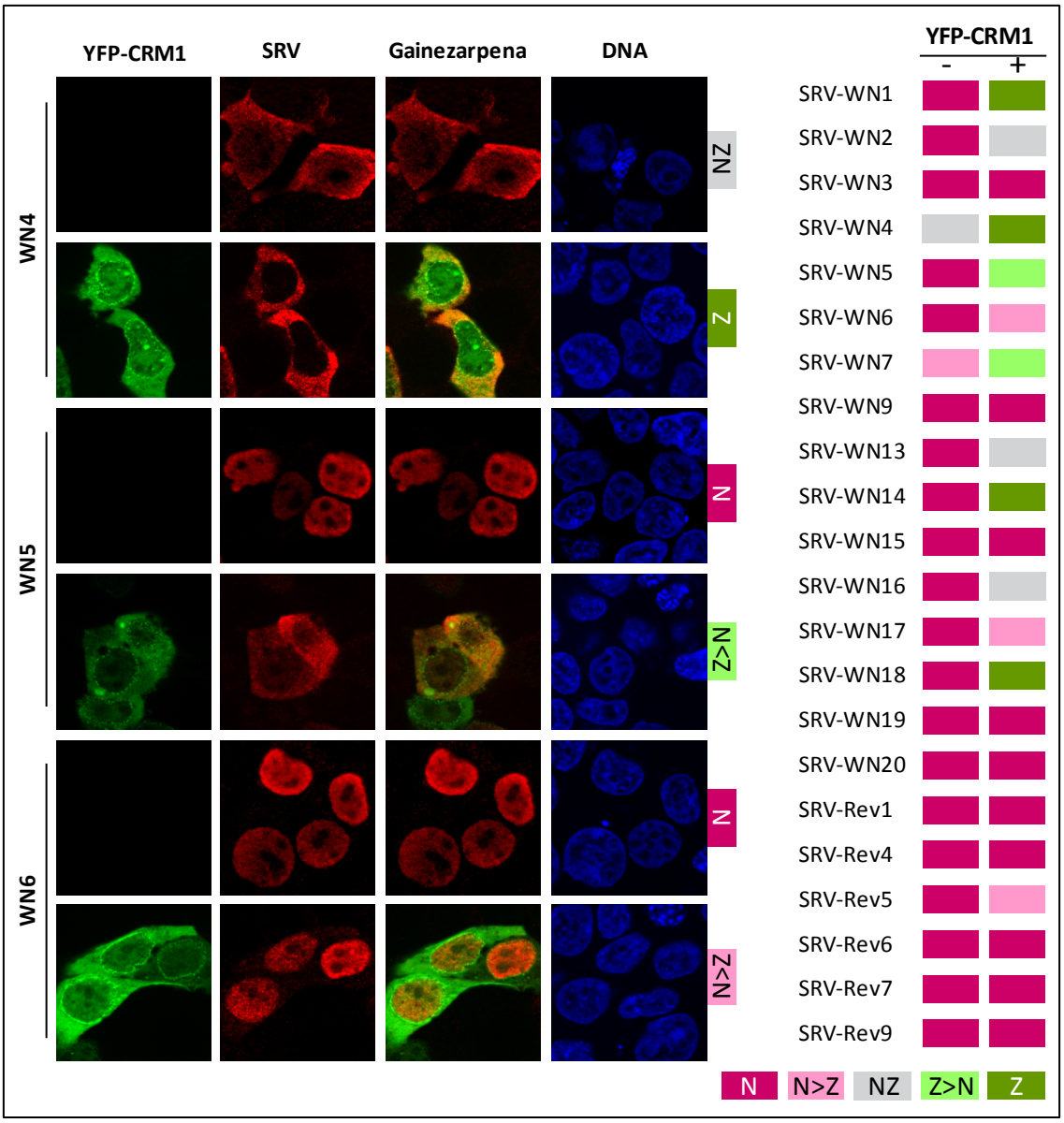

48. irudia: CRM1en minbizi-esportomako cNESak aztertzeko $SRV_{B/A}$ entsegua. Ezkerraldean hiru $SRV_{B/A}$ esportazio-entsegutan SRV-cNES erreportariek bakarrik zein YFP-CRM1 basatiarekin batera gainadieraztean erakutsitako kokapenaren fluoreszentziako argazki adierazgarriak ageri dira. Argazkiei eskuinaldean atxikitako etiketan, lagineko SRV-cNES erreportariaren kokapen orokorra zein den adierazten da. Eskuinaldeko panelean, $SRV_{B/A}$ esportazio-entseguan aztertutako cNES guztien emaitzak ageri dira bai bakarrik (-) zein YFP-CRM1 basatiarekin batera (+) gainadieraztean. Eskuinaldean azpian, etiketen koloreak eta kokapen zelularrak lotzen dituen legenda ageri da.

48. irudian beha daitekeenez, SRV-cNES erreportari gehienek bakarrik gainadieraztean kokapen guztiz nuklearra erakusten dute. Kokapen nuklearra erakutsi ez duten bakarrak WN4 eta WN7 izan dira, zeintzuek kokapen nukleozitoplasmatikoa eta kokapen gehienbat nuklearra erakutsi duten hurrenez hurren. YFP-CRM1 basatiarekin batera gainadieraztean *plus* erako cNESak (WN) dituzten erreportari gehienek zitoplasmaranzko lekualdaketa erakutsi dute, ez ordea *minus* (Rev) erakoek. *Minus* erako NESen kasuan zitoplasmaranzko aldaketa txiki bat jasan duen erreportari bakarra SRV-Rev5 izan da.

Emaitza horiek, Rev(1.4)-GFP entseguan lortutako emaitzekin konparatzean (49. irudia), hainbat antzekotasun behatu dira, baita ezberdintasun nabari batzuk ere. Alde batetik, entsegu bietan *plus* NESak (WN) *minus* (Rev) NESak baino nabari aktiboagoak dira. Gainera, Rev(1.4)-GFP esportazio-entseguan gutxienez 3ko esportazio-aktibitatea izan duen NES oro $SRV_{B/A}$ esportazio-entseguan YFP-CRM1 basatiarekin batera gainadieraztean, zitoplasmaranzko lekualdaketa partzial edo oso bat jasan du; lekualdaketa horiek ordea, ez dira berdinak izan Rev(1.4)-GFP entseguan emaitza berdina lortu duten NESen kasuan. Adibidez, WN5 eta WN13 NES motiboek 4ko esportazio-aktibitate maila erakutsi dute Rev(1.4)-GFP esportazio-entseguan, $SRV_{B/A}$ esportazio-entseguan aldiz, WN5 guztiz nuklear (N) izatetik gehienbat zitoplasmatikoa (Z>N) izatera igaro da CRM1ekin batera gainadieraztean, eta WN13, guztiz nuklear (N) izatetik nukleozitoplasmatiko (NZ) izatera. Bestalde, Rev(1.4)-GFP esportazio-entseguan 3 baino esportazio-aktibitate maila baxuagoa erakutsi duten cNESek, WN16 salbu, $SRV_{B/A}$ esportazio-entseguan aktibitate-esportatzailerik ez dutela nabarmendu beharra dago.

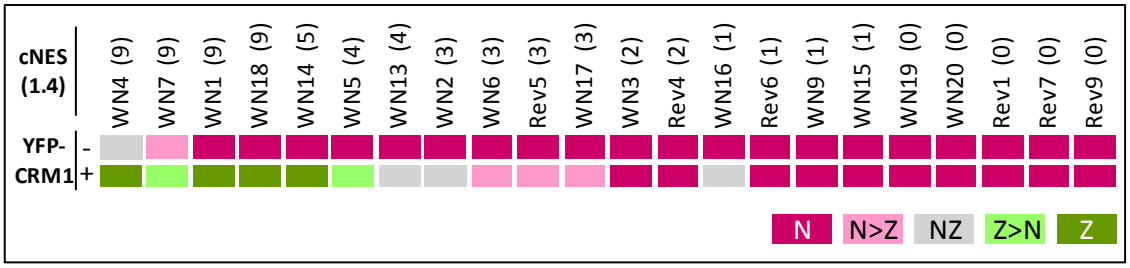

<u>49. irudia:</u> $SRV_{B/A}$ esportazio-entseguan aztertutako CRM1en minbizi-esportomako 22 cNESek lortutako emaitza Rev(1.4)-GFP esportazio-entseguan lortutako emaitzaren arabera antolatuta. Goiko partean eta parentesi artean cNES bakoitzak Rev(1.4)-GFP entseguan lortutako emaitza ageri da. Beheko partean, cNES bakoitzak $SRV_{B/A}$ entseguan bakarrik (-) zein YFP-CRM1 basatiarekin (+) batera gainadieraztean erakutsitako kokapen orokorra. Eskuinaldean azpian, etiketen koloreak eta kokapen zelularrak lotzen dituen legenda ageri da.

49. irudiko emaitzak ikusita Rev(1.4)-GFP eta $SRV_{B/A}$ esportazio-entseguetan lortutako emaitzak korrelazioan dauden aztertu nahi izan da. Helburu horrekin, 49. irudian erakutsitako 22 cNESek Rev(1.4)-GFP esportazio-entseguan eta $SRV_{B/A}$ esportazio-entseguan YFP-CRM1 basatiarekin batera gainadieraztean jasotako emaitzak kontrajarri dira (50. irudia). $SRV_{B/A}$ esportazio-entseguko emaitzak kualitatiboak direnez gero, kategoria bakoitzari balio bat eman zaio. Horrela, kokapen guztiz nuklearrak 0 balioa hartzen du (N = 0), gehienbat nuklearra den kokapenak 1 balioa (N>Z = 1), kokapen nukleozitoplasmatikoak 2 balioa (NZ = 2), gehienbat zitoplasmatikoa den kokapenak 3 balioa (Z>N = 3) eta kokapen guztiz zitoplasmatikoak 4 balioa (Z = 4).

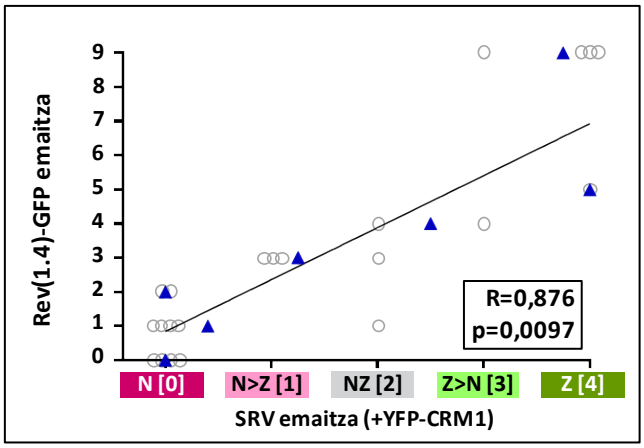

50. irudia: Rev(1.4)-GFP eta $SRV_{B/A}$ esportazio-entseguetan aztertutako 22 cNESen emaitzak kontrajartzen dituen grafikoa. Zirkulu bakoitzak aztertutako cNES bat irudikatzen du, eta hirukiek, Rev(1.4)-GFP esportazio-aktibitate maila bereko NESek batez bestean $SRV_{B/A}$ entseguan YFP-CRM1 basatiarekin batera gainadieraztean erakutsitako kokapena. Pearson korrelazioa (R) eta p balioak grafikoan adierazten dira.

50. irudiko grafikoan agerikoa da Rev(1.4)-GFP eta $SRV_{B/A}$ esportazio-entseguetako emaitzak korrelazioan daudela. Horrek, $SRV_{B/A}$ esportazio-entseguari bermea ematen dio. Gainera, entsegu biak erabilita osagarriak diren emaitzak lor daitezke. Izan ere, $SRV_{B/A}$ esportazio-entsegua NES motibo berriak bilatzeko erabilgarria dela esan badaiteke ere, baliteke, $SRV_{B/A}$ esportazio-entseguak aztertze lehen metodoaren bidez ebaluatzean Rev(1.4)-GFP esportazio-entseguaren bidez detekta daitezkeen esportazio-aktibitate baxua duten hainbat NES detektatzeko gai ez izatea. Aitzitik, Rev(1.4)-GFP entseguan aktibitate-maila ertain edo altua erakutsi duten NESen arteko ezberdintasunak aurkitzeko Rev(1.4)-GFP esportazio-entsegua baino aproposagoa izan daiteke $SRV_{B/A}$ esportazio-entsegua. Adibidez, aurretik aipatutako WN5 eta WN13 kasua, edota WN1, WN4, WN7 eta WN18 NESen aktibitatearen kasua da. Azken lau NES horiek Rev(1.4)-GFP esportazio-aktibitate maila gorena lortu dute, hau da, 9. SRV-WN1 eta SRV-WN18 erreportariak HEK293T zelulatan bakarrik gainadieraztean kokapen nuklearra erakusten dute, SRV-WN4 eta SRV-WN7 erreportariek, ordea, guztiz nuklearra ez den kokapena. Horrek, aipaturiko lau NESek Rev(1.4)-GFP esportazio-entseguan emaitza bera lortu arren, WN4 eta WN7 NESek WN1 eta WN18 NESek baino esportazio-aktibitate altuagoa dutela iradokitzen du.

4.1.2.2.2. $SRV_{B/A}$ esportazio-entsegua mikropeptidoetan NES berriak identifikatzeko

Azkenaldiko ikerketa proteogenomikoen hobekuntzek argi uzten dute, litekeena, zelulen proteomaren tamaina eta konplexutasuna gutxietsi izana dela. Bada, orain gutxi arte RNA ez-kodetzaile bezala sailkatutako hainbat RNA molekula 100 aminoazido baino laburragoak diren proteinetara, mikropeptidoetara, itzultzen direla ikusi da (Yeasmin et al., 2018). Mikropeptido horien funtzio biologikoen gaineko ezagutza nahiko murritza da oraindik ere (Hartford eta Lal, 2020). Esaterako, euren kokapen nukleozitoplasmatikoa ikertzeke dago. Mikropeptidoak hain dira txikiak, non posible den nukleoko poro konplexua difusio pasiboz zeharkatzea, eta nukleo eta zitoplasmaren artean aurrera eta atzera mugitzen egotea. Hala ere, izan ditzaketen funtzioek mikropeptido batzuek kokapen nukleozitoplasmatiko jakin bat behar izatea eragin dezakete, eta beraz, zitoplasma eta nukleoaren arteko garraio aktiboa jasatea. Horretarako, mikropeptidoek garraio nukleozitoplasmatikoaren makineriarekin elkarregiteko gai diren NLS edo NES seinaleak izango lituzkete.

Hori horrela eta $SRV_{B/A}$ esportazio-entsegua NESak bilatzeko tresna baliagarria dela berretsita, entsegu hori giza mikropeptidoetako NESak bilatzeko erabili da. Giza mikropeptidoak SmProt datu-basetik (Hao et al., 2018) lortu dira, eta CRM1en minbizi-esportomarekin egin bezala, Wregex (Prieto et al., 2014) eta NESmapper (Kosugi et al., 2014) NES-iragarleekin analizatu dira NES motibo kandidatuak bilatzeko asmoz. Mikropeptidoen kasuan, *plus* erako cNESak baino ez dira bilatu. Bilaketa horretan aurkitutako cNES guztiak 25. taula gehigarrian ageri dira.

Oraingoan ere, aurkitutako cNES kopurua oso altua izan da, eta beraz, bilatzaile bietan lehen kuartilean aurkitzen diren 10 cNES aukeratu dira mikropeptidoetan NES seinaleak bilatzeko lehen ahaleginerako (16. taula).

16. taula: Esperimentalki aztertzeko aukeratutako mikropeptidoen cNESak. Taulan mikropeptidoen cNESen identifikazio kodea (ID), SmProt datu-basean mikropeptidoek duten IDa, mikropeptidoaren aminoazido kopurua, cNESak mikropeptidoan hartzen duen kokapena eta cNESaren aminoazido sekuentziak adierazten dira.

cNES ID	SmProt ID	Aminoazido kopurua	cNES kokapena	cNES sekuentzia
MICROP-1	SPROHSA011142	96	13-31	KKEELLKQLDDLKVELSQL
	SPROHSA011145	47	13-31	
MICROP-2	SPROHSA018908	84	57-75	RDRLPVNVRELSLDDPEV
MICROP-3	SPROHSA012652	70	29-47	GLDDLDVALSNLEVKLEGS
MICROP-4	SPROHSA141226	78	40-58	DGTSDLPLKLEALSVKEDA
	SPROHSA141826	85	47-65	
MICROP-5	SPROHSA141543	68	5-23	ASASALQRLVEQLKLEAGV
MICROP-6	SPROHSA011811	57	30-48	SHYHETLGEALQGVELEFS
MICROP-7	SPROHSA010409	85	16-34	EESPENLFLELEKLVLEHS
MICROP-8	SPROHSA009911	99	78-96	RMSKEELRAKLSEFKLETR
MICROP-9	SPROHSA020870	100	46-64	LSKCGEELGRLKLVLLELN
MICROP-10	SPROHSA180177	93	49-67	AKIKLLTKELSVLKDLFLE
	SPROHSA180747	93	49-67	
	SPROHSA181614	93	49-67	

16. taulako hiru cNES, MICROP-3, MICROP-4 eta MICROP-8 izenekoak, ezin izan dira $SRV_{B/A}$ plasmidoan klonatu. Gainontzeko zazpiekin $SRV_{B/A}$ esportazio-entsegua egin da SRV-cNESak bakarrik zein YFP-CRM1 basatiarekin batera gainadieraziz (51. irudia). Esportazio-entsegu horren emaitza lehen analisi metodoarekin ikertu da (sailkapen orokorra). Bakarrik gainadieraztean, SRV-MICROP-2 erreportariak izan ezik, zeinak kokapen gehien bat nuklearra (N>Z) erakutsi duen, beste SRV-cNES guztiek kokapen guztiz nuklearra (N) erakutsi dute. YFP-CRM1 basatiarekin batera gainadieraztean, SRV-MICROP-1 eta SRV-MICROP-10 erreportariek zitoplasmaranzko lekualdaketa partziala erakutsi dute (N>Z), eta SRV-MICROP-5 eta SRV-MICROP-7 erabatekoa (Z). Esperotakoaren aurka, SRV-MICROP-2 erreportaria YFP-CRM1 basatiarekin batera gainadierazterakoan ez da erreportariaren zitoplasmaranzko lekualdaketarik behatu, eta horrek, MICROP-2 cNESaren esportazioa CRM1en mendekoa ez dela iradokitzen du. Oro har, ikertutako zazpi mikropeptidoen cNES motiboetatik lau aktiboak direla topatu da, eta horietako bi, MICROP-5 eta MICROP-7 alegia, esportazio-aktibitate altukoak.

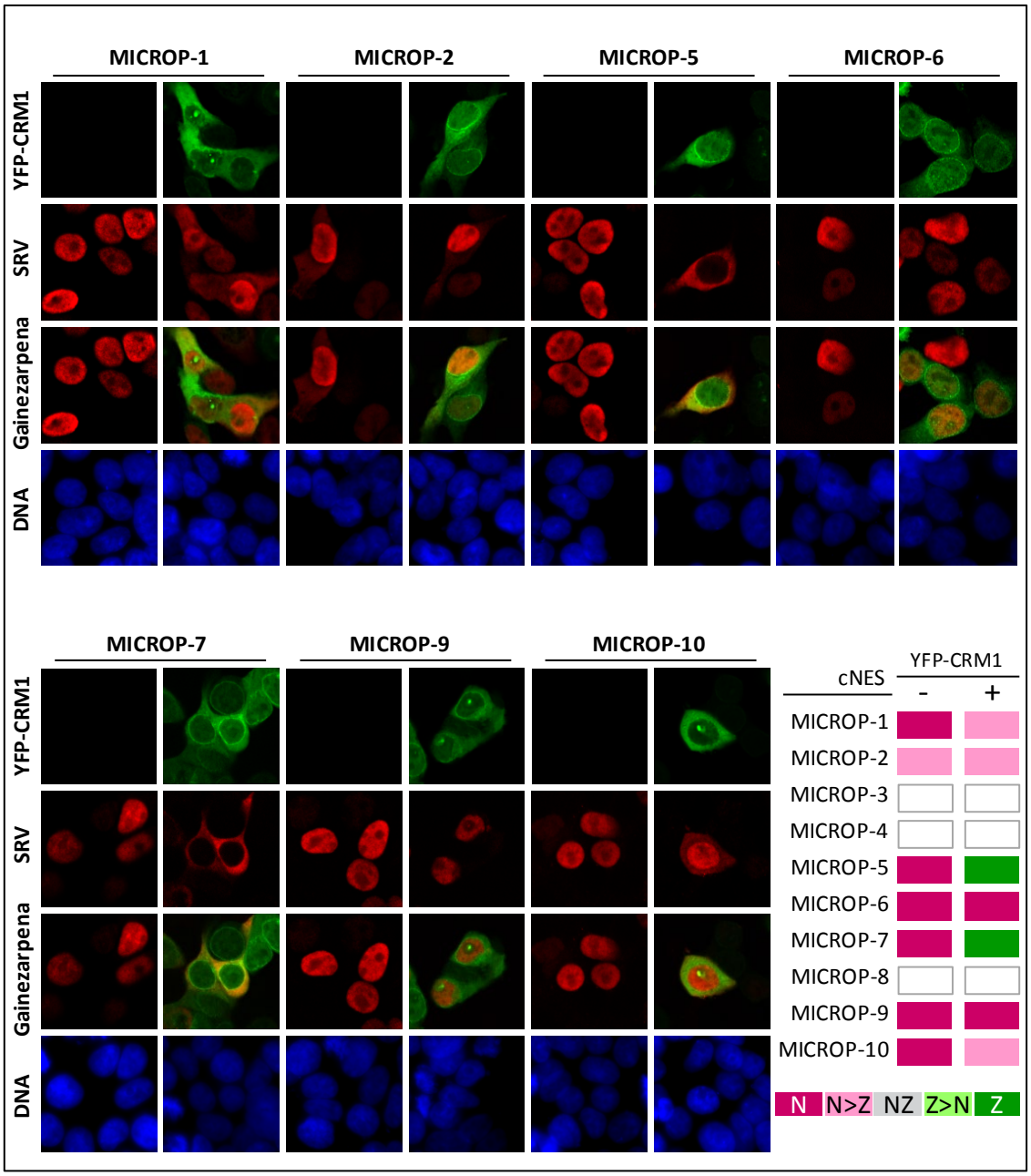

51. irudia: $SRV_{B/A}$ esportazio-entseguaren bidez giza mikropeptidoetan aurkitutako cNESen azterketa. Entseatutako SRV-cNES erreportari bakoitzaren argazki adierazgarriak erakusten dira, bai bakarrik (ezkerreko zutabea), zein YFP-CRM1 basatiarekin batera (eskumako zutabea) HEK293T zelulatan gainadieraztean. Eskumako beheko partean, $SRV_{B/A}$ esportazio-entsegua analisirako lehen metodoarekin aztertzean jasotako emaitzak ageri dira. SRV-MICROP-2 erreportariak izan ezik, zeina neurri txiki batean bada ere, partzialki zitoplasman kokatzen den (N>Z), beste guztiek kokapen erabat nuklearra erakusten dute HEK293T zelulatan bakarrik gainadieraztean. YFP-CRM1 basatiarekin batera gainadieraztean SRV-MICROP-2, SRV-MICROP-6 eta SRV-MICROP-9 erreportariek bakarrik gainadieraztean erakusten zuten kokapen berbera erakusten dute, SRV-MICROP-1 eta SRV-MICROP-10 erreportariek kokapen gehienbat nuklearra (N>Z) eta SRV-MICROP-5 eta SRV-MICROP-7 erreportariek kokapen erabat zitoplasmatikoa (Z). Karratu zuriek analisi bioinformatikoan aukeratutako baina $SRV_{B/A}$ plasmidoan klonatu ezin izan diren cNESak adierazten dituzte.

CRM1ek MICROP-5 eta MICROP-7 NESak esportatzen dituela ziurtasun handiagoz baieztatzeko, SRV-MICROP-5 edo SRV-MICROP-7 erreportariak YFP-CRM1ekin batera gainadierazten duten HEK293T zelulak LMBrekin tratatu dira. 52. irudian beha daitekeenez, erreportari biak YFP-CRM1 basatiarekin batera gainadieraztean erreportariok kokapen zitoplasmatikoa agertzen dute, CRM1 inhibitzean (+LMB) berriz, SRV-MICROP-5 erreportariak kokapen gehienbat nuklearra (N>Z) agertzen du, eta SRV-MICROP-7 erreportariak kokapen nuklearra (N). Emaitzok, MICROP-5 eta MICROP-7 NESak CRM1en bidez esportatzen direla berresten dute.

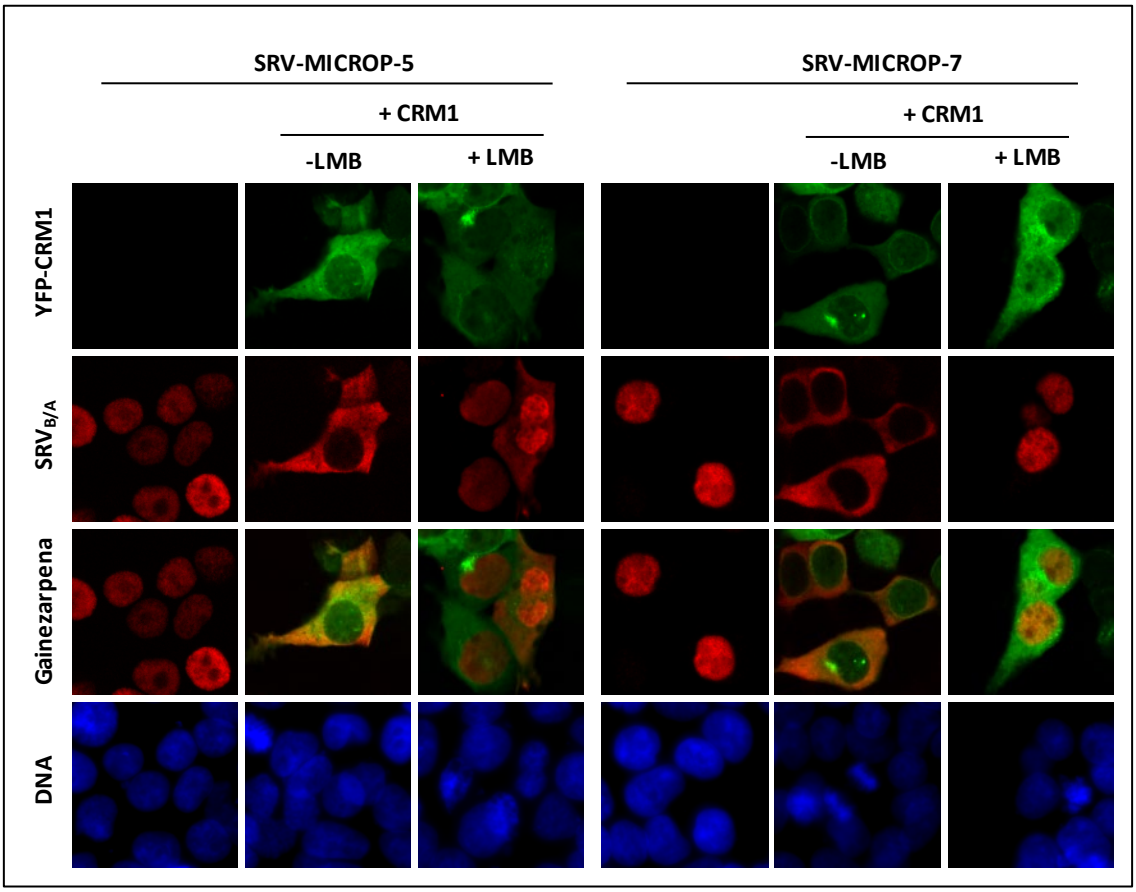

52. irudia: MICROP-5 eta MICROP-7 CRM1en mende esportatzen diren NESak dira. HEK293T zelulatan CRM1 inhibitzeak SRV-MICROP-5 eta SRV-MICROP-7 erreportarien kokapenean duen eraginaren argazki adierazgarriak erakusten dira. Erreportari biek kokapen nuklearra erakusten dute bakarrik gainadieraztean, eta kokapen zitoplasmatikoa YFP-CRM1 basatiarekin batera gainadieraztean. Zelulak LMBrekin tratatzean, SRV-MICROP-5 erreportariak kokapen gehienbat nuklearra erakusten du (N>Z), SRV-MICROP-7 erreportariak, ordea, kokapen erabat nuklearra (N).

MICROP-5 eta MICROP-7 NESak CRM1en mende esportatzen direla egiaztatuta, NES horiek dituzten mikropeptido osoak CRM1en mende esportatzen direnetz ikertu da. Horretarako, YFP proteinarekin fusionatutako SPROHSA141543 (MICROP-5 hartzen du barne) eta SPROHSA010409 (MICROP-7 hartzen du barne) mikropeptidoak (ikusi 16. taula) HEK293T zein HeLa zelulatan gainadierazi dira eta zelulotan LMB tratamenduak duen eragina ikertu da (53. irudia). Tratatu gabeko zeluletan fusio-proteina bien kokapen zitoplasmatikoa gailentzen

da. CRM1 inhibitzean, YFP-SPROHSA141543ren kokapena gehienbat zitoplasmatikoa izaten jarraitzen du, YFP-SPROHSA010409ren kokapena berriz, gehienbat nuklearra da. Hori horrela, SPROHSA010409 gaineztadura nuklearrean zehar aurrera eta atzera era aktiboan mugitzen den deskribatutako lehen mikropeptidoa da.

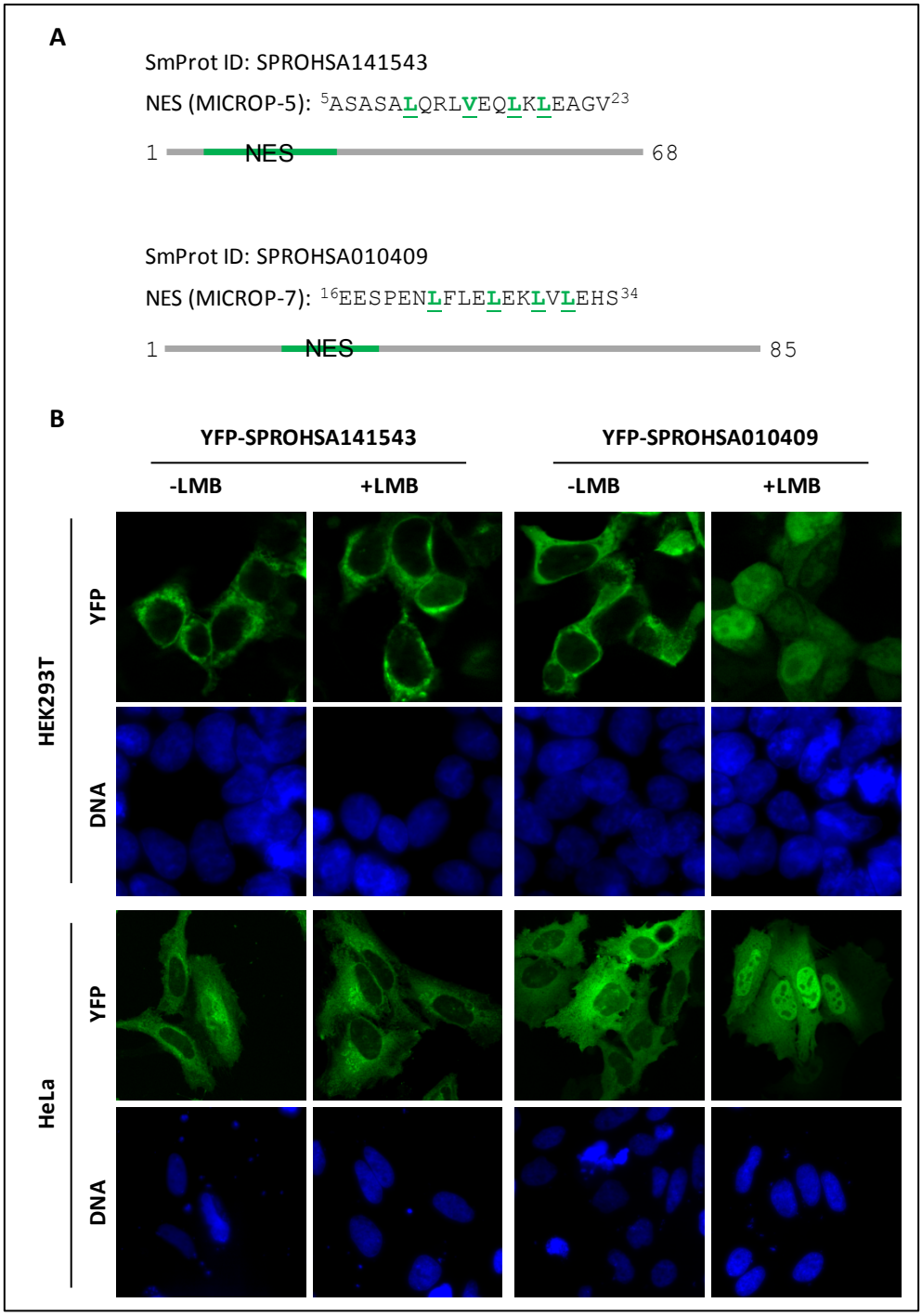

53. irudia: SPROHSA010409 kokapena CRM1en mendekoa da. A. MICROP-5 eta MICROP-7 NESek, hurrenez hurren, SPROHSA141543 eta SPROHSA010409 mikropeptidoetan duten kokapenaren irudi eskematikoak. NES bakoitzaren sekuentzia erakusten da, eta bertan, berdez eta azpimarratuta NESetan gako diren aminoazidoak. B. SPROHSA142543 eta SPROHSA010409 mikropeptidoak YFP proteinarekin fusionatu eta HEK293T zein HeLa zelulatan gainadieraztean eta CRM1 aktiboa (-LMB) edo ez aktiboa (+LMB) denean erakusten duten kokapenaren irudi adierazgarriak.

4.1.2.2.3. $SRV_{B/A}$ esportazio-entsegua CRM1en mendeko NESen esportazioa ikuspuntu mekanistiko batetik aztertzeko

CRM1en mendeko NESen esportazioaren hainbat aspektu biokimika eta biologia estrukturalaren alorretatik ikertu dira (Dong et al., 2009a; Monecke et al., 2009; Güttler et al., 2010; Fung et al., 2015, 2017; Fu et al., 2018). Analisi estrukturalek NESek CRM1en poltsiko hidrofobikoari heldu ahal izateko nolako egiturak dituzten erakutsi dute. Ezagutza hori, CRM1en poltsiko hidrofobikoko aminoazidoak mutatu, eta lortutako CRM1en aldaera horiekin *pull-down* entseguak eginez asko aberastu da. Adibidez, CRM1en poltsiko hidrofobikoko A541 alanina aminoazidoa, bera baino anitzez handiagoa den lisina batez ordezkatzean (A541K), CRM1 eta NESen arteko interakzioa neurri handi batean eragozten da (Güttler et al., 2010). Antzeko egoera ematen da CRM1en poltsiko hidrofobikoan dauden eta NESekin zuzenean elkarrekiten duten aminoazido hidrofobikoak (I521, L525, F561, F572) aldi berean alaninara mutatzean (I521A/L525A/F561A/F572A, 4X mutazioa; Dong et al., 2009a). Testuinguru zelular batean ere, SRV100 esportazio-entsegua erabilita, CRM1en A541K zein 4X mutazioek surbibinaren NESaren esportazioa eragozten dutela egiaztatu da (García-Santisteban et al., 2016).

NESekin elkarrekiten duten aminoazido ikertuenak aipaturiko aminoazido hidrofobikoak dira, baina badira, hidrofobikoak ez diren eta NESen loturan garrantzia handia dutenak ere, esaterako K568. Lisina horrek, NESen loturan parte hartzeaz gain, NESen antzekoak diren motibo ez-aktiboak CRM1era lotzea ekiditen du neurri handi batean, hau da, galbahe erara aritzen da (Fung et al., 2017). Gainera, K568 aminoazidoak minbizian maiz mutaturik ageri den E571 aminoazidoarekin ere elkarrekiten du (Fung et al., 2017). E571 aminoazidoa CRM1en poltsiko hidrofobikotik oso gertu dago, eta ez da harritzekoa aminoazido horren mutazioek NES batzuen esportazioan eragina izatea (García-Santisteban et al., 2016; Taylor et al., 2019; Baumhardt et al., 2020). Bada, aminoazido horren lisinaranzko mutazioak (E571K) efektu onkogenikoa duela ere behatu izan da (Taylor et al., 2019).

CRM1 eta NESen arteko loturan aipatutako aminoazido horiek duten funtzioa asko ikertu bada ere, testuinguru zelularrean NES ezberdinak lotzeko duten eginkizuna ez dago ondo zehazturik. Hori ikertzeko, ezagunak diren hainbat NES aukeratu dira eta CRM1 basatia zein CRM1en hainbat mutante erabiliz $SRV_{B/A}$ esportazio-entseguak egin dira. Horretaz gain, E571K eta K568A mutazioen efektua ere erkatu nahi izan da, bai NESen antzekoak diren motiboen esportazioan galbahe bezala aritzeko gaitasunean, zein CRM1en minbizi-esportomako NESak esportatzeko gaitasunean ere.

4.1.2.2.3.1. Poltsiko hidrofobikoko aminoazidoek CRM1en mendeko NESen esportazioan duten rolaren azterketa

CRM1en poltsiko hidrofobikoan kokatzen diren A541, I521, L525, F561, F572 eta K568 aipaturiko sei aminoazidoek (54. irudia), NES ezberdinen esportazioan duten papera aztertzeko, aminoazido horiek mutaturik dituzten YFP-CRM1en aldaerak eta SRV-NES erreportariak batera gainadierazi dira HEK293T zelulatan. Mutazioak ondorengoak izan dira: aminoazido hidrofobikoak alaninaz ordezkatu dira elkarrekintza hidrofobikoak apur daitezen (I521A, L525A, F561A eta F572A), alanina aminoazido txikia lisina aminoazido handiaz ordezkatu da (A541K) eragozpen esterikoa gerta dadin, eta NESekin elkarrekintza elektrostatikoak eratzen dituen karga positibodun lisina alaninaz ordezkatu da (K568A) elkarrekintza elektrostatiko horiek gertatzea eragozteko.

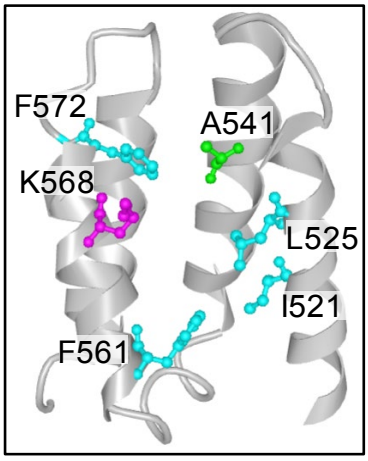

54. irudia: CRM1en poltsiko hidrofobikoan aztertuko diren aminoazidoen kokapena erakusten duen irudia. A541 aminoazidoa, berdez adierazita, aminoazido hidrofobikoak (I521, L525, F561, F572) urdinez eta NESekin elkarrekintza elektrostatikoa eratzen duen K568 arrosaz. Irudia NCBIko iCn3D tresna bioinformatikoa erabiliz eratu da PDBko 3GJX estruktura (Monecke et al., 2009) erabilita.

Sei mutante horien aktibitatea aztertzeko, jada ikerketa biokimiko eta estrukturaletan (Fung et al., 2017) zein esportazio-entseguetan (Fu et al., 2018) erabilitako 14 NES erabili dira: PKI, superPKI, PAX, HDAC5, FMRP, FMRP-1, SNUPN, Rev, SMAD4, mDia2, CDC7, X11L2, CBEP4 eta hRio2 (17. taula). Ikerketa horietan lortutako datuek bereziki interesgarri egiten dituzte aipatutako NESak hemen planteatutako $SRV_{B/A}$ esportazio-entsegurako. Izan ere, ikerketa horietan aukeratutako NESak CRM1en poltsikora nola lotzen diren, hau da, zein motakoak diren (1, 2, 3, 4 edo 1R) eta baita CRM1ekiko duten afinitatea ere (Fung et al., 2017) argitu da.

17. taula: CRM1en poltsiko hidrofobikoko aminoazidoek NESen esportazioan duten papera ikertzeko erabili diren NESen mota, sekuentzia eta CRM1 basatiarekiko afinitatea.

NES ID	Mota	Sekuentzia	Afinitatea (Kd)
superPKI	1	GNLNELALKLAGLDINKTE	4 nM
PKI	1	GNSNELALKLAGLDINKTE	34 nM
PAX	1	TRELDELMASLSDFKIQGL	700 nM
HDAC5	1	ETEEAETVSAMALLSVGAE	1600 nM
FMRP-1	1	LNYLKEVDQLRALERLQIDE	3000 nM
SNUPN	1	MEELSQALASSFSVSQDLNS	12500 nM
Rev	2	EPVPLQLPPLERLTLDCNE	1180 nM
FMRP	2	LNYLKEVDQLRLERLQIDE	2000 nM
SMAD4	2	HYERVVSPGIDLSGLTLQS	4600 nM
mDia2	3	SKNESVPEVEALLARLRAL	1600 nM
CDC7	3	AQDLRKLCERLRGMDSSTP	2000 nM
X11L2	4	ESSLQELVQQFEALPGDLV	1500 nM
CBEP4	1R	RPRTFDMHSLESSLIDIMR	800 nM
hRio2	1R	ARSFEMTEFNQALEEIKGQ	2800 nM

Aipaturiko 14 NESak, $SRV_{B/A}$ plasmidoan klonatu dira eta SRV-NES bakoitza bere aldetik edo YFP-CRM1en poltsiko hidrofobikoko 6 mutante ezberdinekin (I521A, L525A, F561A, F572A, A571K eta K568A), eta kontrol moduan erabili diren YFP-CRM1 basati eta YFP-$CRM1^{4X}$ mutante laukoitzarekin batera gainadierazi dira HEK293T zelulatan. Esportazio-entsegu horiek bigarren analisi metodoarekin analizatu dira. Hau da, prestatutako 126 egoerak lagin bakoitzean 200 zelula gutxienez zitoplasmatiko (Z), nukleozitoplasmatiko (NZ) edo nuklear (N) kategorietan sailkatuz analizatu dira (55. irudia).

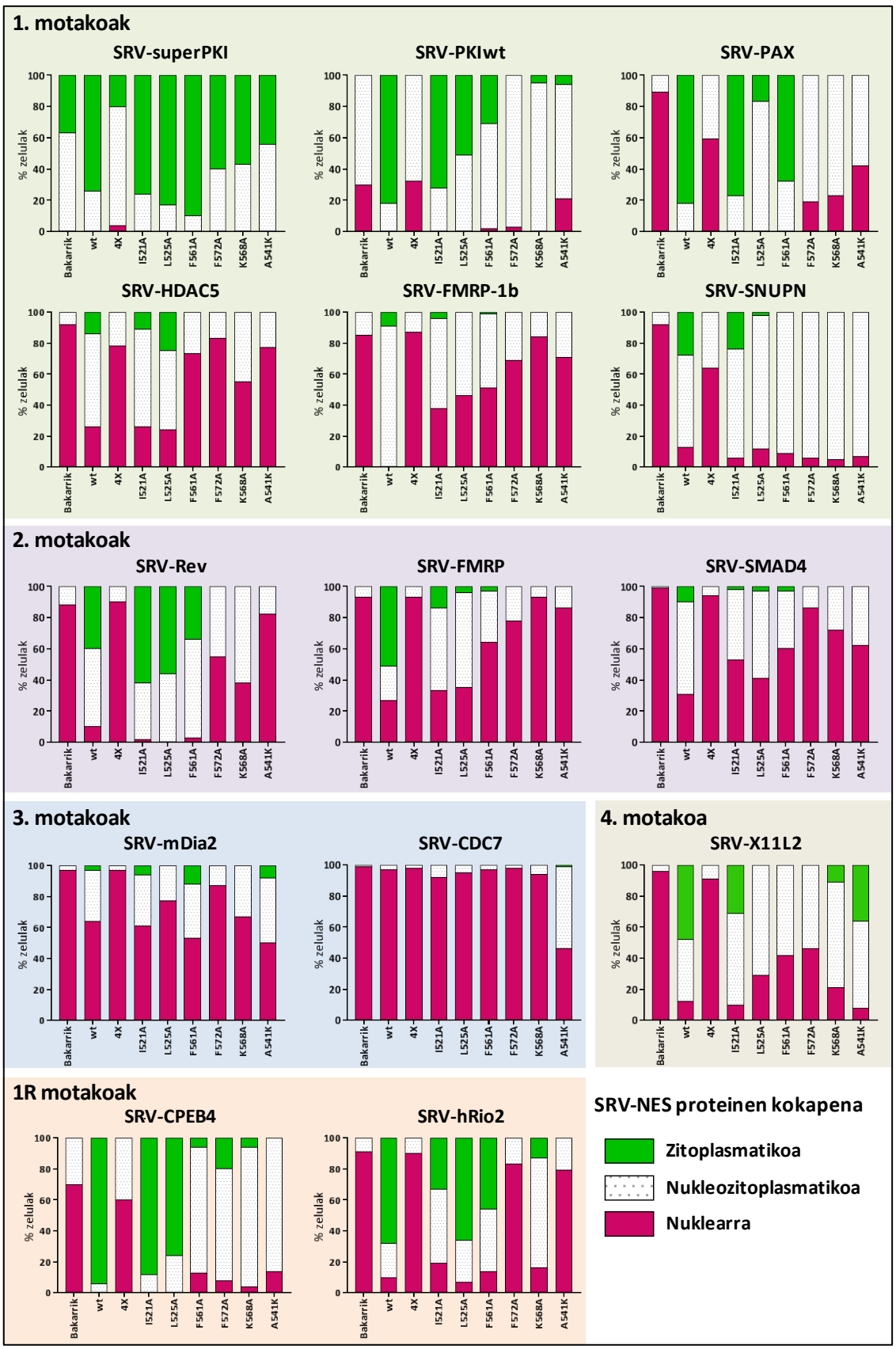

55. irudia: SRV-NES erreportariek bakarrik edo CRM1en aldaera ezberdinekin duten esportazio-aktibitatea erakusten duten grafikoak. SRV-NES erreportariak NES motaren arabera daude ordenaturik. Egoera bakoitzean 200 zelula gutxienez zitoplasmatiko (berdez), nukleozitoplasmatiko (zuriz eta puntu grisekin) edo nuklear (arrosaz) kategorietan sailkatu dira.

55. irudiko grafikoetan adierazitako ehunekoetatik abiatuz, egoera bakoitzaren esportazio-aktibitate maila konparatu ahal izateko SRV balio bat kalkulatu da. SRV balioak [0 x (% N) + 0,5 x (% NZ) + 1 x (% Z)] formulatik eratorri dira, beraz, 0tik 100ra doaz, non 0 balioak erreportariak kokapen erabat nuklearra erakusten duela adierazten duen, eta 100 balioak erreportariak kokapen guztiz zitoplasmatikoa erakusten duela. SRV balio horiek aipaturiko 126 egoerak erakusten dituen bero-mapa bat egiteko erabili dira (56. irudia).

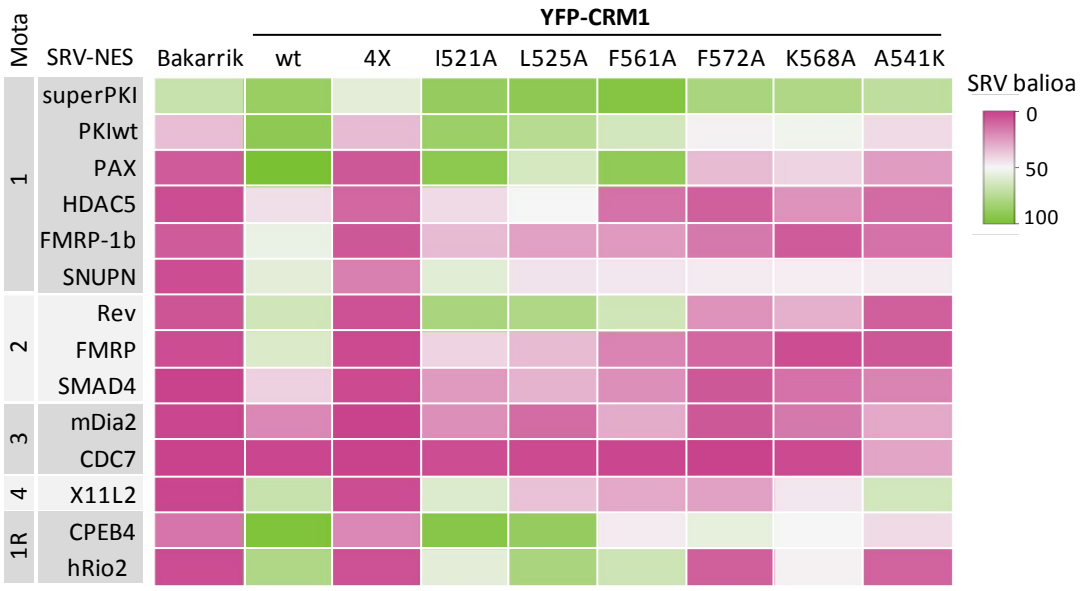

56. irudia: Entseatutako SRV-NES erreportari bakoitzak bere aldetik (bakarrik zutabea), zein CRM1en aldaera ezberdinekin batera gainadieraztean erakusten duen esportazio-aktibitate maila (SRV balioak) laburbiltzen duen bero-mapa. Balio altuak (berdez) esportazio eraginkorraren seinale dira, balio baxuak (arrosaz) esportazio efizientzia baxuaren seinale. Ezkerreko zutabean entseatutako NES bakoitza zein motakoa den adierazten da.

Bero-mapa horretan argi ikusten da SRV-NES erreportari gehienak bakarrik gainadieraziz gero kokapen oso nuklearra dutela: SRV-superPKI, SRV-PKIwt eta SRV-CPEB4 erreportariek izan ezik, beste guztiek 10 baino SRV balio baxuagoa lortu dute. YFP-CRM1 basatiarekin (wt) batera gainadieraztean, erreportari guztiek, SRV-CDC7 salbu, bakarrik gainadierazi direnean baino SRV balio nabari altuagoak lortu dituzte, hau da, efizienteki esportatuak dira. Espero zen moduan, kontrol bezala erabilitako 4X mutanteak erreportarien esportazioa kasik erabat ezabatzen du. Aminoazido hidrofobikoen mutazioen banakako eragina aldiz, 4X mutazioaren efektua baino nabari ahulagoa da. Banakako mutazio horiek eragin ezberdina dute: I521A eta L525A mutazioek eragin ahulena dutenak dira, hau da, esportazioa neurri txiki batean inhibitu dute kasu gehienetan, F572A mutazioak ordea, 4X mutazioaren eragin inhibitzailera heldu gabe, inhibizio maila altua erakutsi du. Aminoazido horiek SRV-NES erreportarien esportazioan duten eragina beraz, honela adieraz daiteke; L521 = L525 < F561 < F572. Gainera, ez da NES motaren araberako efekturik antzeman mutatutako aminoazido hidrofobikoaren arabera.

Hidrofobikoak ez diren ikertutako aminoazidoei dagokienez, K568 aminoazidoa alaninaz mutatzearen (K568A) eragina, F572A mutazioaren eraginaren oso antzekoa da, nahiz eta mutazioaren ondorioz hautsitako indarrak zeharo ezberdinak izan; elkarrekintza hidrofobikoa F572A mutazioaren kasuan eta elkarrekintza elektrostatikoa K568A mutazioaren kasuan. Azkenik, argi ikus daiteke A541K mutazioak erreportari guztien, SRV-X11L2 erreportaria salbu (4. motako NESa duen bakarra), esportazioa nabari murriztu duela.

4.1.2.2.3.2. E571K eta K568A mutazioen efektuaren erkaketa

Aipatu bezala, minbiziaren pronostiko eta garapenean gako den CRM1en E571 aminoazidoa CRM1en poltsiko hidrofobikotik gertu dago (57. irudia), eta bertan dagoen K568 aminoazidoarekin elkarrekintza elektrostatikoak sortzen ditu.

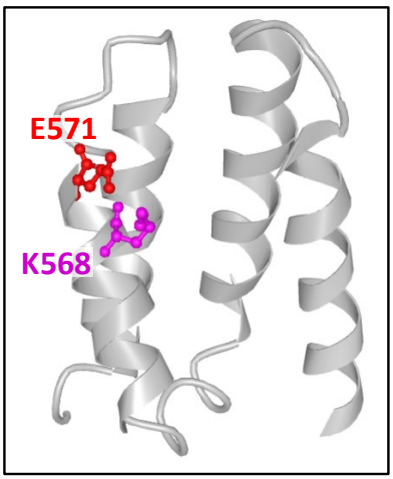

57. irudia: E571 eta K568 aminoazidoek CRM1 proteinan duten kokapena erakusten duen irudia. E571 aminoazidoa gorriz adierazita, K568 arrosaz. Irudia NCBIko iCn3D tresna bioinformatikoa erabiliz eratu da PDBko 3GJX estruktura (Monecke et al., 2009) erabilita.

E571 aminoazidoaren mutazioek NES jakin batzuen esportazioa asaldatu (García-Santisteban et al., 2016) eta CRM1 onkogeniko bilakatu dezakete (Taylor et al., 2019). Bestalde, K568 aminoazidoaren mutazioek (K568A edo K568M) NESen antzekoak diren motibo ez-aktiboak CRM1era lotzea ahalbidetzen dutela ikusi da *in vitro*. Izan ere, K568 aminoazidoa galbahe modura aritzen da egitura egokia ez duten NESen antzeko motiboak CRM1era lotu ez daitezen (Fung et al., 2017). Galbahe horrek NESen esportaziorako testuinguru zelular batean duen rola ez da aztertu oraindik, ezta minbiziarekin erlazionatutako E571 aminoazidoaren mutazioek galbahe horren eragina ezereztu dezaketen ere. Hori horrela, $SRV_{B/A}$ esportazio-entsegua E571K eta K568A mutazioen eragina konparatzeko erabili da: batetik, COMMD1, Hxk2 eta DEAF1 NESen antzeko motibo ez-aktiboen (Fung et al., 2017) nukleotiko esportazioan mutaziook duten eragina aztertu da, eta bestetik, CRM1en minbizi-esportomako lehen mailako *plus* NESen esportazioaren gaineko eragina aztertu da. Esportazio-entsegu guzti horiek hirugarren metodoaren bidez aztertu dira, hau da, Fiji softwareaz baliatuz irudi-analisiaren

bidez erreportari bakoitza gainadierazi den zelulen nukleoan agertzen duen fluoreszentzia intentsitatea eta zitoplasman agertzen duena neurtu da eta intentsitateon arteko arrazoia kalkulatu da.

Lehenik eta behin, E571K eta K568A mutazioek, COMMD1, Hxk2 eta DEAF1 NES antzeko motibo ez-aktiboen (Fung et al., 2017) esportazioan eraginik dutenetz aztertu da. Horretarako, motibo horiek $SRV_{B/A}$ plasmidoan klonatu dira, eta bakarrik zein YFP-CRM1 basati edo E571K eta K568A mutanteekin batera gainadierazi dira HEK293T zelulatan. Kontrol bezala, surbibinaren NESa mutaturik duen SRV100 ($SRV100^{NESm}$) erreportaria (García-Santisteban et al., 2016) erabili da. 58. irudian beha daitekeenez, entseatutako SRV erreportarien zein $SRV100^{NESm}$ kontrolaren kokapena gehienbat nuklearra da (log_2(N/Z arrazoia)> 0) egoera guztietan. YFP-CRM1 basatiarekin (wt) batera gainadieraztean SRV-COMMD1, SRV-Hxk2 eta SRV-DEAF1 erreportariek zitoplasmaranzko aldaketa ahul baina esanguratsua jasan dute, beraz, baliteke motibo horiek esportazio-aktibitate oso baxua duten NES aktiboak izatea. YFP-$CRM1^{K568A}$ mutantearen aktibitate esportatzailea YFP-CRM1 basatiak duenarekin alderatzean, SRV-COMMD1 erreportariaren esportazioa murriztu egiten dela behatzen da, SRV-DEAF1ena, ordea, handiagotu. SRV-Hxk2rena ere handiagotu dela beha daiteke, kasu horretan ordea, aldaketa ez da esanguratsua. Emaitza horiek aurretik *in vitro* lortutako emaitzekin bat datoz, izan ere, Fung eta lankideek (2017) ere Hxk2 eta DEAF1 motiboak, COMMD1 motiboa ez bezala, CRM1en K568A mutanteari basatiari baino gehiago lotzen zaizkiola topatu zuten. YFP-$CRM1^{E571K}$ mutanteak eragindako esportazioa YFP-CRM1 basatiak eragindakoarekin alderatzean, K568A mutantearekin gertatzen zen bezala, SRV-COMMD1 erreportariaren esportazioa murriztu egin dela ikusten da, SRV-Hxk2 eta SRV-DEAF1 erreportariei dagokienez, E571K mutazioak erreportarion esportazioa zerbait emendatu badu ere ez da emendapen esanguratsua izan. YFP-CRM1en K568A eta E571K mutazioen eragina zuzenean konparatzean, ezberdintasun esanguratsu bakarra SRV-COMMD1 erreportariaren kasuan agertzen da, izan ere, E571K mutazioak K568A mutazioak baino nabarmen gehiago murrizten baitu bere esportazioa.

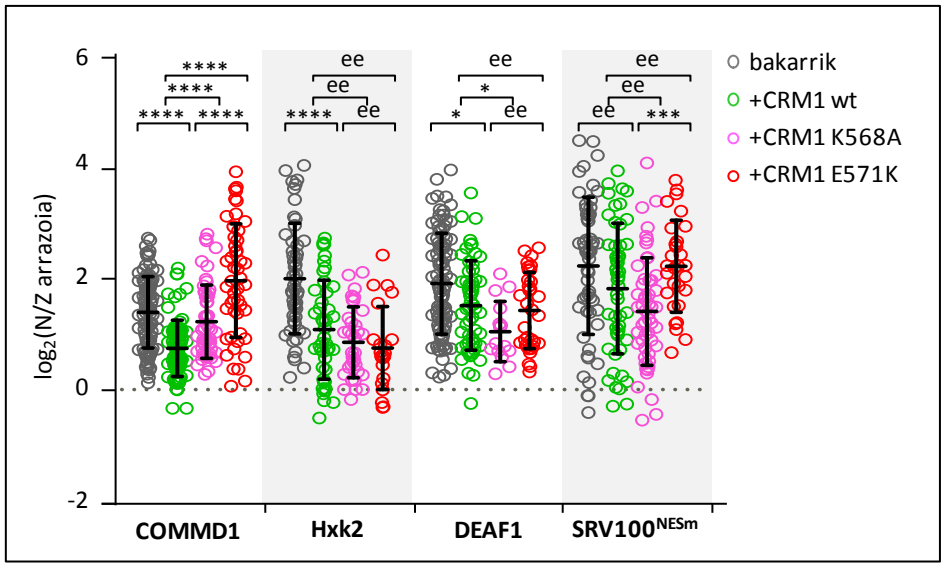

58. irudia: $SRV_{B/A}$ esportazio-entsegua YFP-CRM1en E571K eta K568A mutazioek NESen antzeko motibo ez-aktiboen esportazioan duten eragina konparatzeko. SRV-COMMD1, SRV-Hxk2 eta SRV-DEAF1 gehi kontrol bezala erabili den $SRV100^{NESm}$ erreportariak bakarrik, zein YFP-CRM1 basati (wt) edo K568A edo E571K mutanteekin batera gainadierazi dira HEK293T zelulatan. Irudi-analisiko zirkulu bakoitzak zelula bakar baten nukleoan antzematen den fluoreszentziaren eta zitoplasman antzematen denaren arrazoia 2 oinarriko logaritmoan (log_2(N/Z arrazoia)) adierazten du. Lagin bakoitzaren log_2(N/Z arrazoia)-ren batez bestekoa eta desbiderapen estandarrak adierazten dira. Mutante ezberdinen arteko esportazio gaitasunaren aldea p balioaren (Mann-Whitney U test) bidez adierazten dira grafikoan: (*) p<0,05; (***) p<0,001; (****) p<0,0001; ee, ez-esanguratsu.

Bestetik, NESen antzeko motibo ez-aktiboekin egindakoaren pareko analisia egin da CRM1en minbizi-esportomako lehen mailako *plus* NESak (WN1-WN7) erabiliz. 59. irudian beha daitekeen moduan, SRV-NES erreportari horiekin 4.1.2.2.1. atalean egindako analisian ikusitakoa konfirmatuz, erreportari guztiek, SRV-WN3 izan ezik, YFP-CRM1 basatiarekin batera gainadieraztean, bakarrik gainadieraztean baino kokapen nabari zitoplasmatikoagoa erakutsi dute. YFP-CRM1 basatiarekin alderatuta, K568A mutanteak aztertutako erreportari guztien esportazioa murrizten du, murrizketa hori, SRV-WN1, SRV-WN2, SRV-WN5 eta SRV-WN7 erreportarien kasuan da esanguratsua. YFP-CRM1 basatia E571K minbizi mutantearekin alderatzean, K568A mutantearekin alderatzean lortutakoaren antzeko emaitza lortzen da, E571K mutazioak ere era esanguratsuan murrizten baitu SRV-WN1, SRV-WN5 eta SRV-WN7 erreportarien esportazioa. Hau da, mutante biek SRV-WN1, SRV-WN5 eta SRV-WN7 erreportarien esportazioa nabarmen murrizten dute. Alabaina, E571K mutanteak erreportari horien esportazioa murrizteko duen ahalmena K568A mutanteak duena baino ahulagoa da.

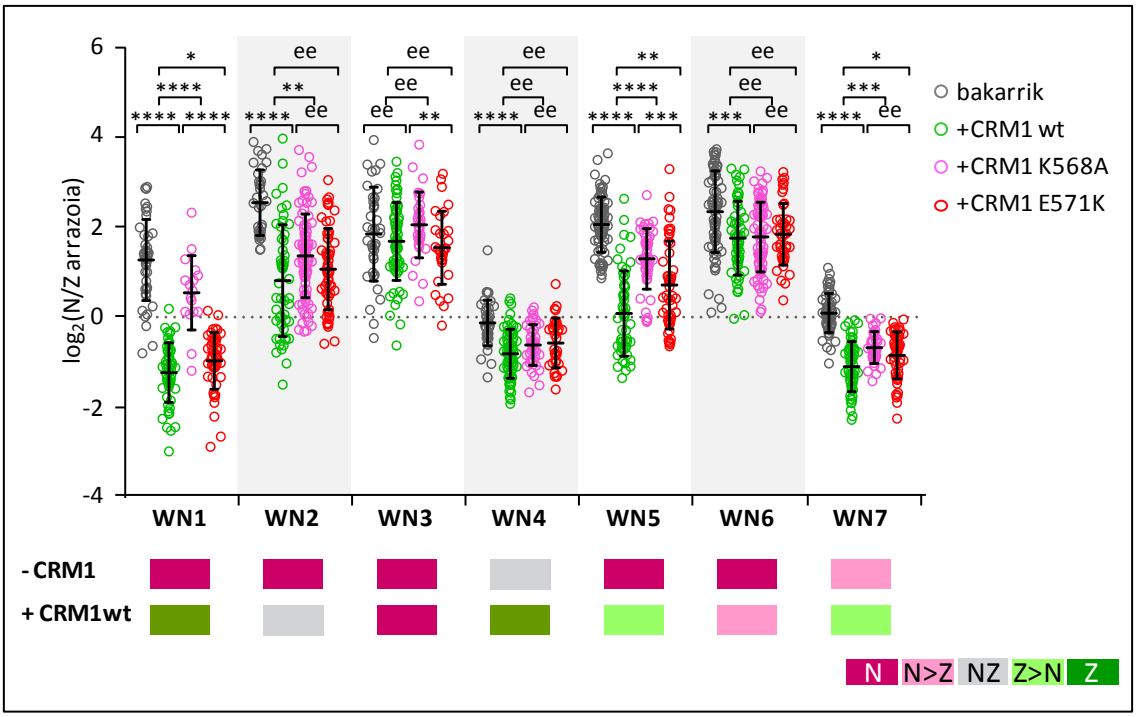

59. irudia: $SRV_{B/A}$ esportazio-entsegua YFP-CRM1en E571K eta K568A mutazioek CRM1en minbizi-esportomako lehen mailako *plus* NESen esportazioan duten eragina konparatzeko. CRM1en minbizi-esportomako lehen mailako *plus* NESak adierazten dituzten $SRV_{B/A}$ erreportariak bakarrik zein YFP-CRM1 basati (wt) edo K568A edo E571K mutanteekin batera gainadierazi dira HEK293T zelulatan. Irudi-analisiko zirkulu bakoitzak zelula bakar baten nukleoan antzematen den fluoreszentziaren eta zitoplasman antzematen denaren arrazoia 2 oinarriko logaritmoan (log_2(N/Z arrazoia) adierazten du. Lagin bakoitzaren log_2(N/Z arrazoia)-ren batez bestekoa eta desbiderapen estandarrak adierazten dira. Mutante ezberdinen arteko esportazio gaitasunaren aldea p balioaren (Mann-Whitney U test) bidez adierazten dira grafikoan: (*) p<0,05; (**); p<0,01; (***) p<0,001; (****) p<0,0001; ee, ez-esanguratsu. Grafikoaren behealdean 49. irudian erakutsitako emaitzen zati bat ageri da, analisirako hirugarren metodoarekin eta lehen metodoarekin lortutako emaitzen erkaketa modu errazagoan egitea ahalbidetzeko.

4.1.3. CRM1 basatiaren eta E571K minbizi mutantearen esportomak erkatzeko afinitate-purifikazioan oinarritutako estrategia berri baten diseinua eta balioztatzea

CRM1en E571K mutazioak efektu onkogenikoa duela behatu da (Taylor et al., 2019). Gainera, mutazio horrek CRM1ek zenbait NES ezagutu eta esportatzeko duen gaitasuna asaldatzen duela ere ikusi da SRV100 eta $SRV_{B/A}$ esportazio-entseguen bidez (García-Santisteban et al., 2016; Sendino et al., 2020a). Beraz, baliteke, kargo jakinen esportazioan eragiten duen asaldura horrek mutazioaren efektu onkogenikoan zerikusia izatea. Hala ere, esportazioa asaldatuta duen kargo bilduma zein den ez da oraindik ezagutzen. Tesi honetan, bilduma horretako kargoak bilatu nahian, CRM1 basatiaren eta mutantearen esportazioa erkatzeko afinitate-purifikazioan oinarritutako estrategia berri bat garatzeko saiakera egin da.

4.1.3.1. Estrategia berriaren oinarrizko arrazoia eta diseinua: CRM1/kargo/RanGTP konplexuaren egonkortzea RanGTPasa aktibitaterik ez duen Ran mutante bat erabiliz

CRM1 basatiaren eta E571K minbizi mutantearen esportomak erkatzeko estrategiaren oinarria, CRM1ek kargoen esportaziorako beharrezkoa duen konplexu-trimerikoa ezin banatzean datza. Sarreran aipatu den bezala, CRM1ek kargoak nukleotik zitoplasmara garraiatu ahal izateko CRM1/kargo/RanGTP konplexua eratu behar da nukleoan. Konplexua zitoplasmara heltzean RanGAP1 proteinak Ran proteinaren RanGTPasa aktibitatea estimulatu, eta RanGTPa RanGDPra hidrolizatuko da, eta ondorioz, CRM1ek kargoa askatuko du (60. irudia goiko panela) (Bischoff et al., 1994; Bischoff eta Görlich, 1997; Fornerod et al., 1997; Kutay et al., 1997). Hori horrela, hurbilketa honetan, konbertsio hori jasan ezin duen Ran proteinaren Q69L mutantea erabili da (Bischoff et al., 1994; Klebe et al., 1995). Horrela, Ran^{Q69L} mutantearekin eratutako konplexu-trimerikoak zitoplasmara heltzen ezin izango dira desmuntatu (60. irudia beheko panela) eta afinitate-purifikazioa erabiliz CRM1i lotutako proteinak, haren kargoak barne, isolatu ahal izango dira.

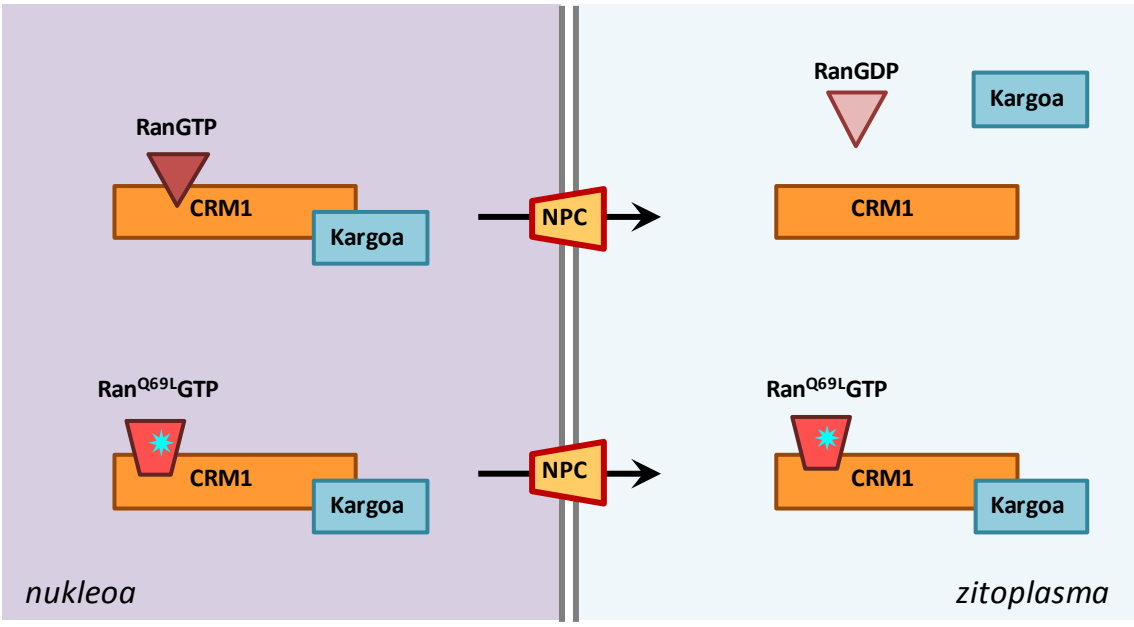

60. irudia: Esportazio konplexu-trimerikoen egonkortzean oinarritutako hurbilketa. Goialdean, CRM1ek kargoak zitoplasmara garraiatu ahal izateko ematen den egoera, ohiko egoera, ageri da. Nukleoan, CRM1ek kargoarekin eta RanGTParekin batera CRM1/kargo/RanGTP konplexuak eratzen ditu. Konplexu-trimeriko horiek zitoplasmara heltzean RanGAP1 proteinak Ran proteinaren GTPasa aktibitatea estimulatu eta RanGTPtik RanGDPrako hidrolisia ematen da. Hidrolisi horrek CRM1 eta kargoaren arteko lotura haustea, eta beraz, kargoa zitoplasman askatzea dakar. Behealdean, Ran^{Q69L} mutantea gainadieraztean emango den egoera. Ran^{Q69L} mutantea RanGAP1en estimulazioarekiko soraioa denez, konplexu-trimerikoa zitoplasmara heltzean ez da GTParen hidrolisirik emango eta CRM1ek ez ditu bere kargoak askatuko.

Konplexu-trimerikoak egonkortzea xede, Ran^{Q69L} mutanteaz baliatzen den sistema esperimental bat jarri da martxan. Sistema horretan, CRM1 (basati edo E571K mutantea) YFP proteinarekin fusionatu eta Myc-Ran^{Q69L}rekin batera gainadieraziko da zeluletan. Horrela, konplexu-trimeriko egonkorrak eratuko dira, eta YFParen kontrako afinitate-purifikazioaren bidez konplexu horiek erauzkinetatik isolatzeko aukera egongo da (61. irudia). Konplexuak erauzkinetatik isolatzeko GFP-Trap bihitxo magnetikoak erabili dira. Bihitxo horien gainazala GFPa zein horren hainbat eratorri, YFPa barne (Rothbauer et al., 2008), lotzeko gai den GBP proteinaz (*GFP binding protein*) estalita dago. Hortaz, CRM1ek fusionaturik duen YFP etiketari esker, YFP-CRM1/kargo/Myc-Ran^{Q69L}GTP konplexu-trimerikoak bihitxoetara lotuko dira eta iman batez era errazean isolatuko dira erauzkinetatik. Behin konplexu horiek isolatuta, CRM1 basatiaren zein mutantearen kargoak MS/MS bidez identifikatu ahal izango dira.

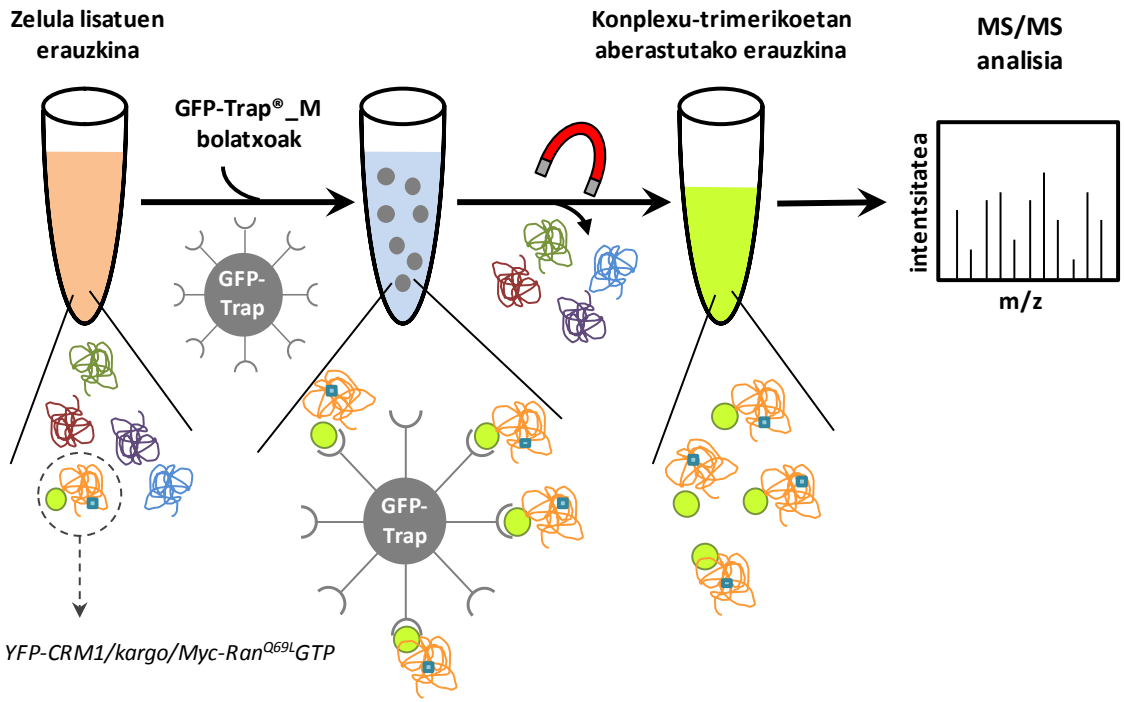

61. irudia: GFP-Trapean oinarritutako afinitate-purifikazioaren bidez CRM1en kargoak isolatzeko metodologiaren irudikapen eskematikoa. Zelulak jaso eta lisatu ostean erauzkinetara GFP-Trap®_M bihitxoak gehitzen dira. Bihitxo horiek gainazalean GBPak (*GFP binding protein*) dituzte barreiaturik GFPa edo horren eratorriak (YFPa adibidez) lotu ahal izateko. Hortaz, bihitxoak erauzkinetara gehitzean YFP-CRM1 horietara lotuko da. Bihitxoen izaera magnetikoari esker, eta iman batez baliatuz, YFP-CRM1 eta horrekin konplexua eratzen duten proteinak isolatu daitezke. Bukatzeko, isolatutako materiala MS/MS bidez aztertuko da CRM1en kargoak identifikatu ahal izateko.

CRM1 basatiaren esportoma eta minbizian maiz agertzen den E571K mutantearen esportomak erkatzeko 62. irudian adierazitako egoerak sortuko dira: zeluletan Myc-Ran^{Q69L} proteinarekin batera, YFP-CRM1 basatia, YFP-CRM1^{E571K}, eta kargoak lotzeko gai ez den eta kontrol bezala erabiliko den YFP-CRM1^{4X} mutantea (Dong et al., 2009a) gainadieraziko dira.

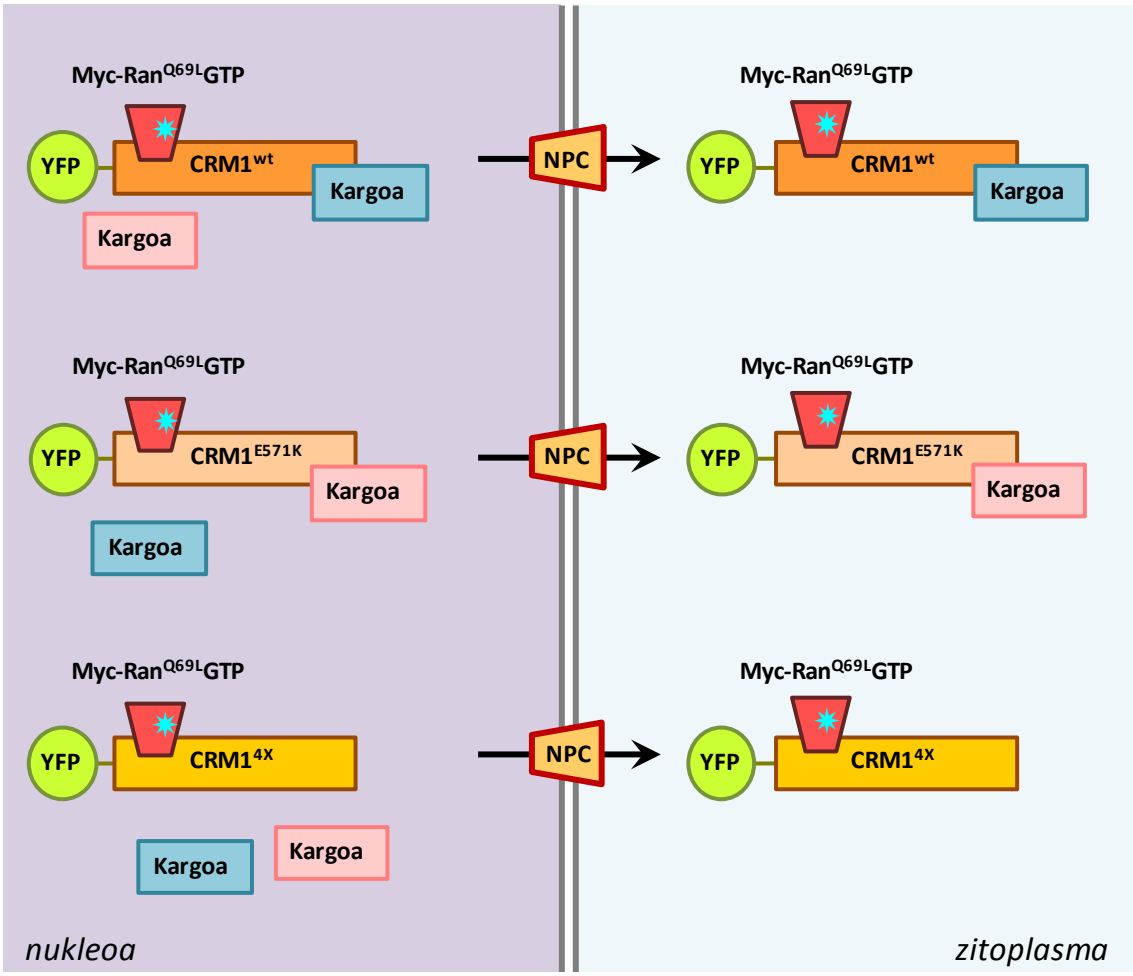

62. irudia: E571K mutazioak CRM1en esportoman eragindako aldaketak aztertzeko esperimentuaren diseinua. Egoera bakoitzean Myc-Ran^{Q69L} YFPari fusionatutako CRM1en aldaera ezberdin batekin batera gainadierazi da; aldaerak CRM1wt (basatia), CRM1^{E571K} minbizi mutantea, eta kargoak lotzeko gaitasun oso murriztua duen eta kontrol bezala erabiliko den CRM1^{4X} dira (Dong et al., 2009a).

4.1.3.2. Metodologiaren balioztatzea

Planteatutako estrategia baliagarria dela baieztatzeko lehen pausoa Myc-Ran^{Q69L} proteina YFP-CRM1 proteinaren aldaera ezberdinekin batera zeluletan gainadieraztean proteina biek agertzen duten kokapena aztertzea da (63. irudia). Ran^{Q69L} mutantea GTParen hidrolisirik eragiteko gai ez denez konplexu-trimerikoak ez askatzea espero da, eta beraz, Myc-Ran^{Q69L} eta YFP-CRM1ek kokapen bera agertzea. Kokapenaren azterketa HeLa zein HEK293T zelula-lerroetan egin da. 63. irudian beha daitekeenez, bai HeLa eta bai HEK293T zeluletan Myc-Ran^{Q69L} eta YFP-CRM1en aldaera ezberdinek kokapen bera agertzen badute ere, bategite hori nabariagoa da HEK293T zeluletan. Beraz, hurrengo analisietarako HEK293T zelula-lerroa hautatu da.

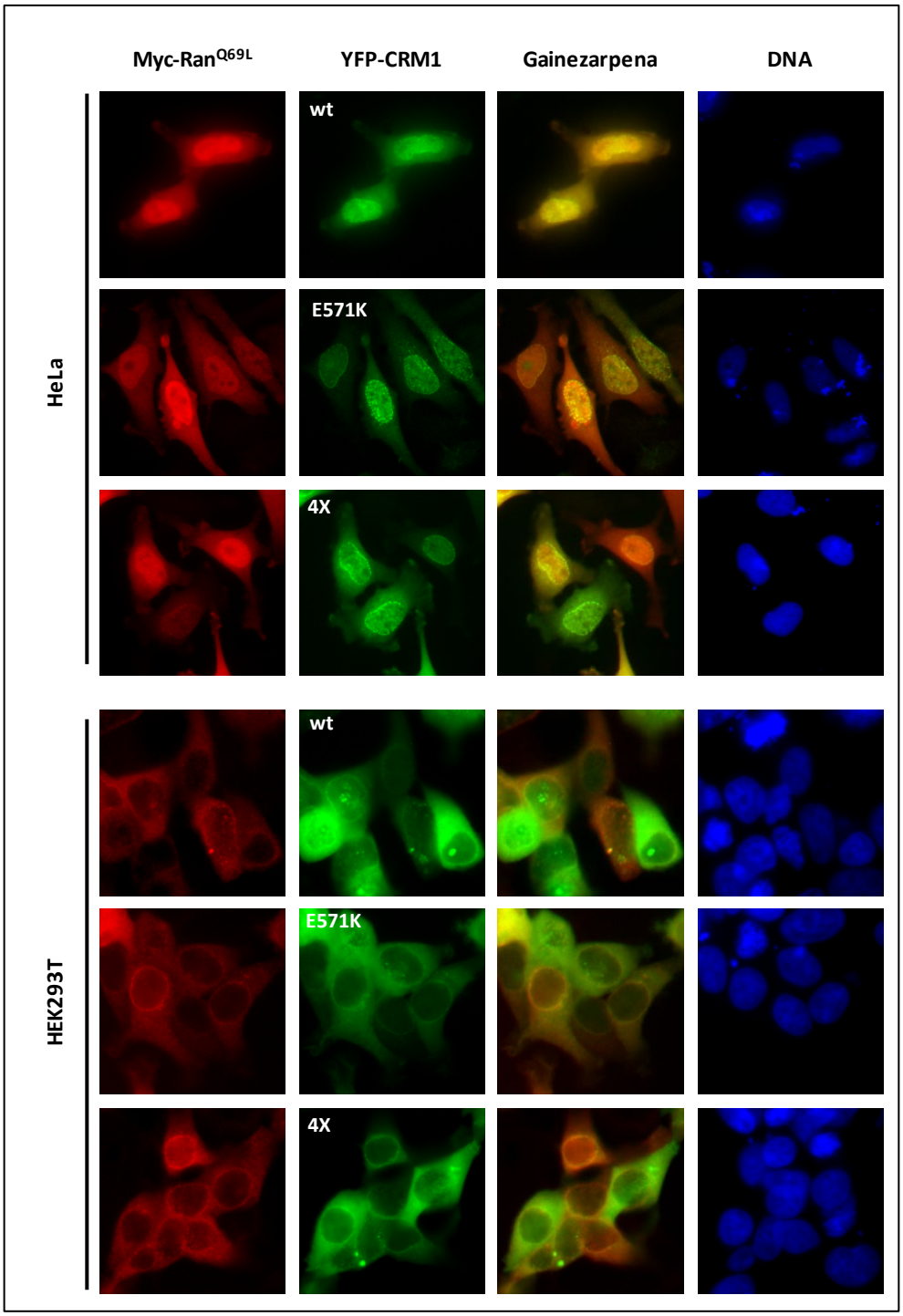

63. irudia: Myc-Ran^{Q69L} YFP proteinarekin fusionatutako CRM1en wt, E571K eta 4X aldaerek HeLa eta HEK293T zelula-lerroetan erakusten duten kokapenaren argazki adierazgarriak. Myc-Ran^{Q69L} proteinak eta YFP-CRM1en aldaerek kokapen bera agertu dute bi zelula-lerroetan, hala ere, kokapenean ematen den bategite hori nabariagoa da HEK293T zeluletan. Proteina bien kokapena HeLa zeluletan gehienbat nuklearra da, HEK293T zeluletan aldiz, kokapen zitoplasmatikoa gailentzen da. Argazkiak Axioskop fluoreszentzia mikroskopioarekin hartu dira.

Analisi proteomikorako bederatzi lagin prestatu dira: hiru laginetan Myc-Ran^{Q69L} eta YFP-CRM1 basatia (wt) gainadierazi dira, beste hiru laginetan Myc-Ran^{Q69L} eta YFP-CRM1^{E571K}, eta azken hiru laginetan Myc-Ran^{Q69L} eta YFP-CRM1^{4X}. Laginok UPV/EHUko SGIker Proteomika zerbitzura bidali aurretik, eta isolatzea lortu den proteina bilduma aurreikusteko, GFP-Trap

immunoprezipitazioan jasotako erauzkina SDS-PAGEz banatu eta gela zilarrez tindatu da. Gel horretan YFPri fusionaturiko CRM1en aldaera ezberdinen banda (150 kDa) oso nabaria da eta bestelako proteinen orbanak intentsitate baxuagoz ageri dira (64. irudia).

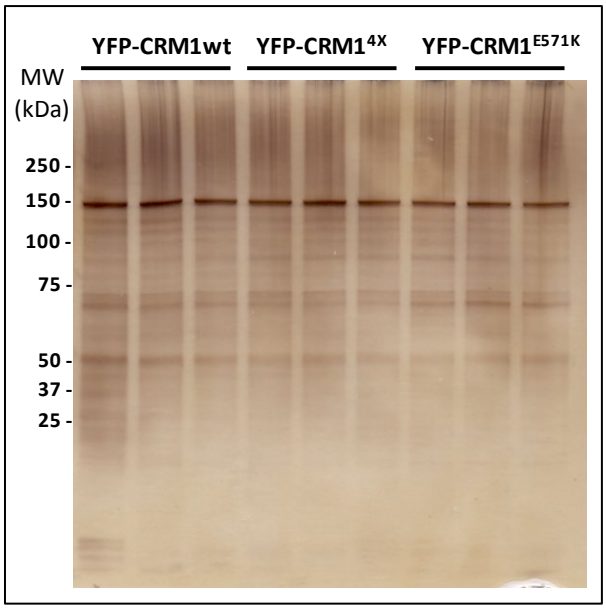

64. irudia: Konplexu-trimerikoak egonkortzean oinarritutako hurbilketa proteomikoan erabili diren proteina erauzkinen zilarrezko tindaketa. Lagin bakoitzaren hiru erreplikak SDS-PAGEz banatu dira. Ez da ez errepliken artean ez lagin batetik besterako ezberdintasun nabaririk ageri. Lagin guztietan YFP-CRM1en aldaera ezberdinei dagokion banda oso nabari bat, eta intentsitate baxuagoko hainbat banda ageri dira.

Laginak proteomika zerbitzuan aztertzean egondako arazo teknikoak direla eta, ezin izan ziren lagin guztiak aztertu. Egoera bakoitzeko lagin bateko emaitzak jasotzea lortu zen, hala ere, laginen artean esperotako alderik ez zen behatu, hiruretan identifikatutako proteina gehientsuenak berdinak dira eta. Horrek planteatutako estrategiak ez duela uste bezala funtzionatzen iradokitzen du.

Sistemak ondo funtzionatu ez duela ikusita, akatsa non egon daitekeen ikertu da. Horretarako, lehenik eta behin, Myc-Ran^{Q69L}, YFP bektore hutsarekin, YFP-CRM1 basatiarekin eta YFP-CRM1^{4X} mutantearekin HEK293T zelulatan transfektatu da (65. irudia). Espero bezala, Myc-Ran^{Q69L} YFP-CRM1 basatiarekin zein mutantearekin batera gainadieraztean, proteina biek kokapen bera agertu dute. YFP proteinarekin ordea, ez da horrelakorik gertatzen. Horrek, Myc-Ran^{Q69L} proteinaren eta YFP-CRM1en aldaera ezberdinen artean elkarrekintza gertatu gertatzen dela iradokitzen du.

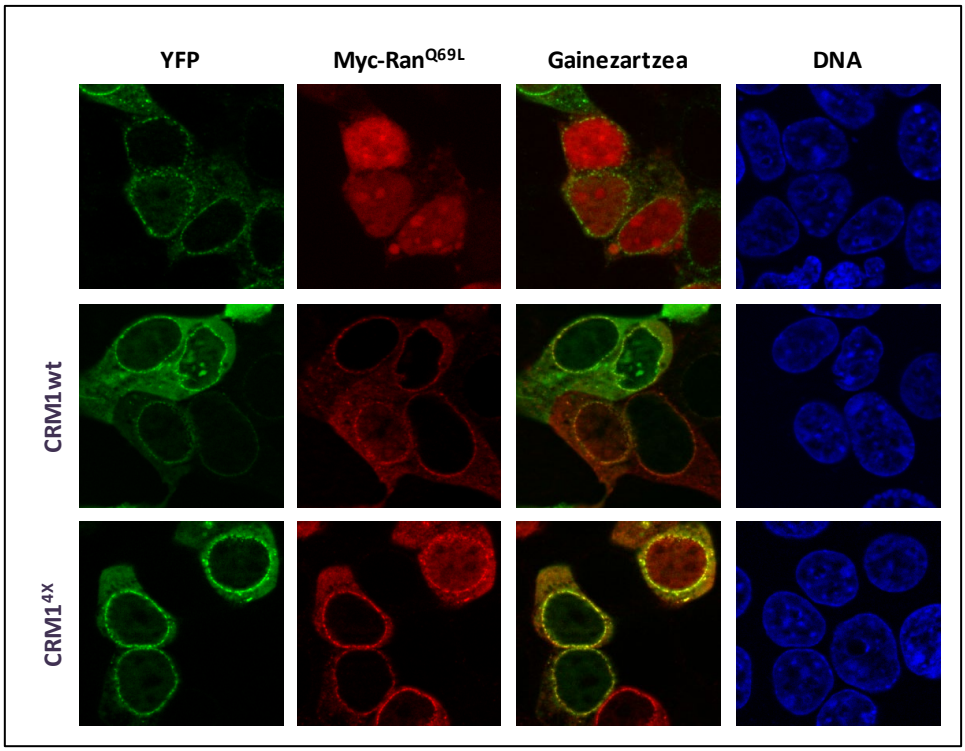

65. irudia: YFP, YFP-CRM1 basatia (wt) eta YFP-CRM1^{4X} Myc-Ran^{Q69L}rekin batera HEK293T zelulatan gainadieraztean hartzen duten kokapenaren argazki adierazgarriak. YFP-CRM1en aldaera biek eta Myc-Ran^{Q69L} proteinak kokapen bera agertzen dute, YFP eta Myc-Ran^{Q69L} proteinek, ordea, ez.

Behin gainadierazitako proteinek kokapen egokia agertzen dutela baieztatuta, GFP-Trap immunoprezipitazioa egin da. Kasu honetan, immunoprezipitazioan egiten den bihitxoen garbiketa gatz kontzentrazio ezberdina duten hiru indargetzaile ezberdinekin egin da. 66. irudian egoera eta garbiketa indargetzaile bakoitzarekin (A, B eta C) jasotako erauzkinak aztertzeko eginiko zilarrezko tindaketa, eta YFParen zein Myc epitopoaren aurkako Western plapaketak ageri dira. Egoera guztietan oso proteina gutxi detektatu dira zilarrezko tindaketaren bidez, nahiz eta teknika oso sentikorra izan. Gainera, Myc epitopoaren aurka egindako Western plapaketan ez da Myc-Ran^{Q60L} proteinari legokion banda ageri. Hortaz, Myc-Ran^{Q69L} eta YFP-CRM1 proteinek kokapen bera hartzen dutela immunofluoreszentziaz ikusi bada ere, Ran proteinaren Q69L mutanteak konplexu-trimerikoak afinitate-purifikazioz isolatzeko bezain beste egonkortzen ez dituela erakutsi dute zilarrezko tindaketak zein Western plapaketek. Emaitzok, konplexu-trimerikoa egonkortzean oinarritutako hurbilketa esperimentala baztertzea ekarri dute.

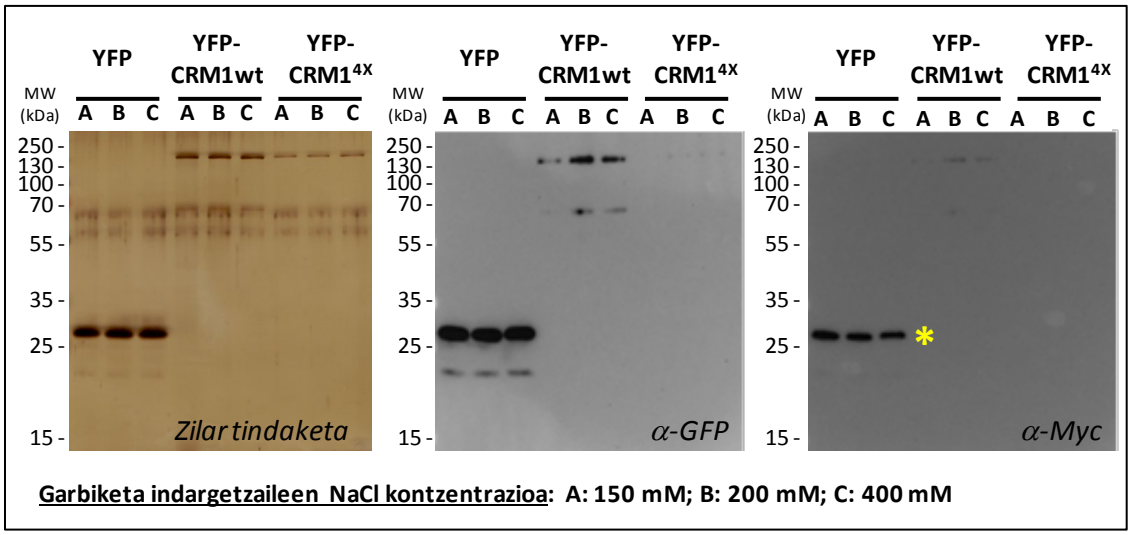

66. irudia: Zilarrezko tindaketa eta GFP eta Myc epitopoen aurkako Western plapaketak. Gainadierazitako proteinen masa molekularra: YFP: 26 kDa; YFP-CRM1: 150 kDa; Myc-Ran^{Q69L}: 25 kDa. Ezkerreko panelean GFP-Trap immunoprezipitazioan jasotako laginen zilarrezko tindaketa ageri da, bertan proteina kopuru baxua ageri da eta ez da bihitxoen garbiketetan erabilitako gatz-kontzentrazioaren mendeko alderik antzematen. Erdiko panelean YFParen aurkako Western plapaketa ageri da (GFParen aurkako antigorputza YFP proteina ere detektatzeko gai da). YFP-CRM1wt gainadierazi den laginen erauzkinetan ez da konplexu-trimerikoei legokiekeen banda multzo erako seinalerik antzeman. Eskumako panelean Myc epitopoaren aurkako Western plapaketa ageri da. Ez da Myc-Ran^{Q69L} proteinari legokiokeen bandarik antzeman. (Asterisko horiak YFParen aurkako plapaketaren ondoriozko kutsatzea adierazten du, izan ere, plapaketa horretarako TTBStan garbitatutako YFParen aurkako plapaketa egiteko erabilitako mintz bera erabili da.)

4.1.4. Giza koronabirusen nukleokapsida proteinetan proposaturiko NES motiboen azterketa

Atal honetan aurkeztutako emaitzak Sendino et al., 2020c-n argitaratu dira aurreargitalpen bezala.

2020ko martxoan COVID-19ari aurre egiteko gertatutako itxialdiaren ondorioz, tesi proiektu hau hainbat astez eten behar izan zen. Laborategian lanean berriz hasteko unea iritsi zenean, COVID-19 gaixotasuna eragiten duen SARS-CoV-2 koronabirusaren ezagutzan sakontzeko nork bere harri-koskorra ekarri nahi izan zuen, eta mundu osoko zientzialari askok koronabirusen ezaugarriak ikertzeari ekin genion. Kapitulu honetan, gizakiak infektatzeko gai diren koronabirus ezberdinen nukleokapsida (N) proteinan NESak karakterizatzeko tesi honetan egin diren ikerketak azaltzen dira. Izan ere, N proteinetan aurreikusitako garraio seinaleek koronabirusen patogenotasunarekin zerikusia badutela proposatu da (Gussow et al., 2020).

Gizakiak infektatzen dituzten koronabirusak zazpi dira, SARS-CoV, MERS-CoV, SARS-CoV-2, HCoV-NL63, HCoV-229E, HCoV-HKU1 eta HCoV-OC43, eta horietatik gaixotasun larria eragiteko gai, SARS-CoV, MERS-CoV eta SARS-CoV-2 baino ez. Patogenotasunean duten ezberdintasun horren eragile molekularrak ezagutzea garrantzitsua da gaixotasun larriei aurre egin ahal izateko. Ildo horretan, Gussow eta lankideek (2020) ikasketa automatikoko (*machine learning)* teknikak eta genomika konparatiboa erabiliz, patogenotasun altuko anduien eta patogenotasun baxuko anduien hainbat ezaugarri genomiko identifikatu dituzte.

In silico egindako analisi horretan, patogenotasun altuak lau proteinatan banatutako hamaika zonalde genomikorekin zerikusia duela proposatu da (Gussow et al., 2020). Lau proteina horietako bat, nukleokapsida (N) izenekoa, kodetzen duen genean patogenotasunarekin erlazionatu diren eta garraio nukleozitoplasmatikorako hainbat seinaletan (hiru NLS eta NES batean) aldaketak eragiten dituzten hainbat insertsio, delezio eta mutazio aurkitu dira. Patogenotasun altuko anduietan seinale horiek karga positibodun aminoazido gehiago dituzte, eta horrek seinale horien aktibitatea emendatzen duela proposatu da (Gussow et al., 2020). Karga positiboaren eta NLSen aktibitate inportatzailearen arteko erlazioa frogatu bada ere (Cokol et al., 2000), NESen kasuan ez da horrelakorik behatu. Are gehiago, NES adostasun-sekuentzia hain da malgua (Kosugi et al., 2008; Monecke et al., 2009; Güttler et al., 2010), non zail izaten den NESen aktibitatea aminoazido sekuentzian soilik oinarrituta iragartzea (Prieto et al., 2014).

Koronabirus anduien artean gertatzen den patogenotasun ezberdintasuna N proteinetan aurreikusitako NESen mendekoa denetz argitzeko, lehenik eta behin, NES motibo horiek CRM1en mende esportatzen direnetz aztertu beharko litzakete. Bigarrenik, NES horiek

aktiboak izatekotan, euren aktibitatea anduiaren patogenotasunarekin erlazioan dagoen aztertu beharko litzateke. Hirugarrenik, N proteina osoen kokapena NES horien mendekoa den aztertu beharko litzateke. Eta bukatzeko, koronabirus andui ezberdinen patogenotasuna N proteina osoen kokapen nukleozitoplasmatikoarekin korrelazioan dagoen aztertu beharko litzateke. Tesi honetan, lehen bi puntuak argitzeko, SARS-CoV-2, MERS-CoV, HCoV-NL63, HCoV-229E, HCoV-HKU1 eta HCoV-OC43 koronabirusen N proteinetan aurreikusitako NES motiboen aktibitatea esperimentalki ikertu da. Eta hirugarren puntua argitze aldera, YFP proteinarekin fusionatutako SARS-CoV-2 eta HCoV-NL63 birusen N proteina osoen kokapen nukleozitoplasmatikoa aztertu da.

4.1.4.1. Giza koronabirusen patogenotasuna ez dago N proteinen NES motiboen esportazio-aktibitatearekin korrelazioan

Gussow eta lankideek (2020) proposaturiko cNESen aktibitatea ikertzeko Rev(1.4)-GFP esportazio-entsegua (Henderson eta Eleftheriou, 2000) erabili da. Entsegu horretarako 18. taulan adierazten diren sekuentziak, SARS-CoV sekuentzia izan ezik, pRev(1.4)-GFP bektorean klonatu dira. SARS-CoV sekuentzia ez da aztertu SARS-CoV-2 sekuentziarekin duen antzekotasun altuarengatik.

18. taula: Giza koronabirusen N proteinetan aurreikusitako cNESen kokapen eta aminoazido sekuentzia. pRev(1.4)-GFP bektorean klonatutako sekuentzia osoa erakusten da, azpimarraturik dauden sekuentzien zatiak Gussow eta lankideek (2020) proposaturiko cNESak dira. e.e.: ez-entseatua.

Birusa	Iragarritako cNES motiboa
SARS-CoV-2	^{224}ALALLLLDRLNQLESKMSG^{230}
SARS-CoV (e.e.)	^{225}ALALLLLDRLNQLESKVSG^{231}
MERS-CoV	^{216}GGDLLYLDLLNRLQALESG^{222}
HCoV-HKU1	^{237}MADEIANLVLAKLGKDSKP^{243}
HCoV-OC43	^{238}MADQIASLVLAKLGKDATK^{244}
HCoV-NL63	^{187}SSSDLVAAVTLALKNLGFD^{193}
HCoV-229E	^{184}SQDDIMKAVAAALKSLGFD^{190}

67. irudian ikus daitekeenez, iragarritako cNES guztiak aktiboak dira. Aktibitate mailari dagokionez, ezberdintasun nabariak aurkitu dira. Esaterako, HCoV-HKU koronabirusaren N proteinaren NESak 1eko aktibitate maila du, HCoV-NL63renak, aldiz, 8koa.

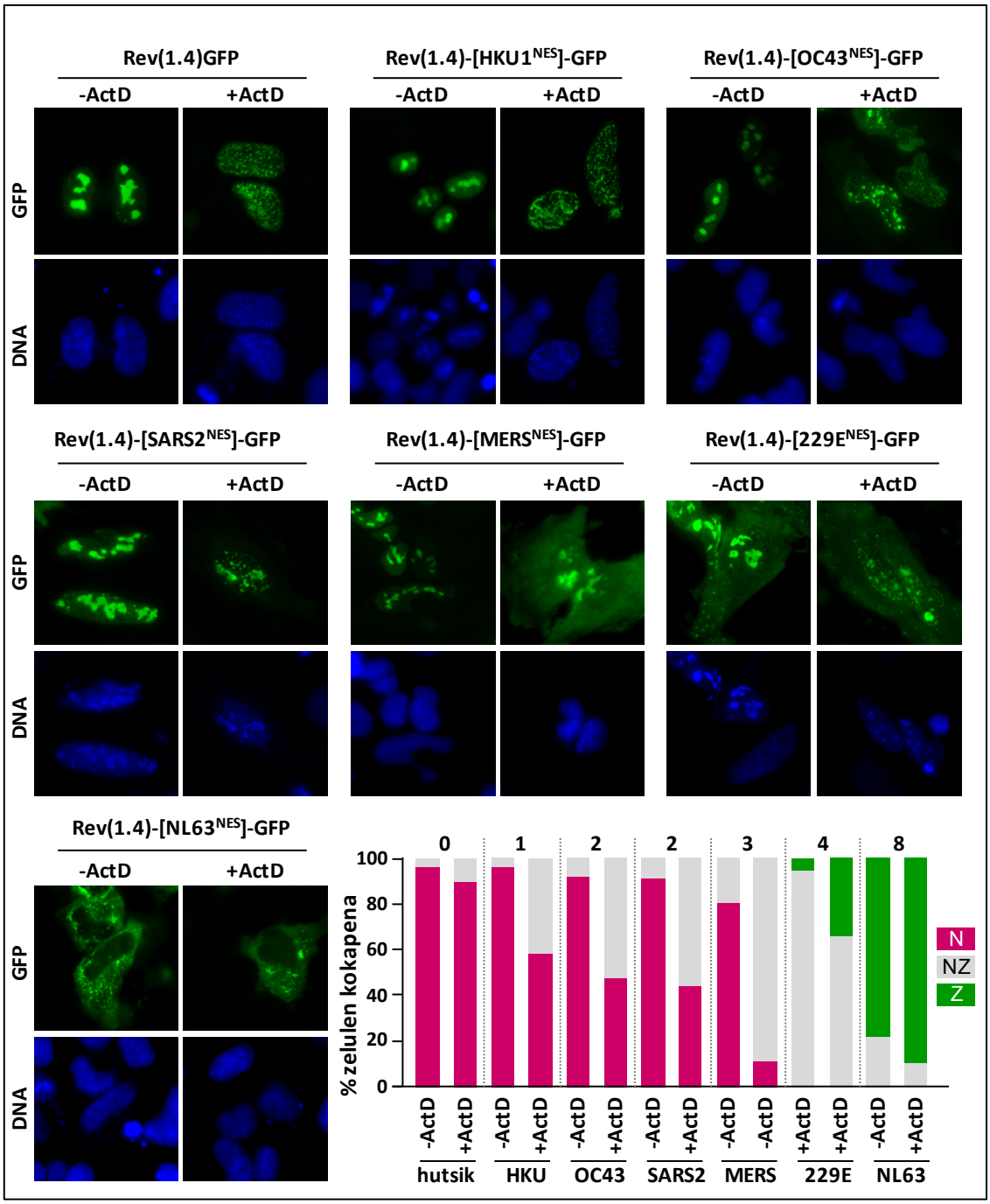

67. irudia: Giza koronabirusetan iragarritako cNESekin egindako Rev(1.4)-GFP esportazio-entsegua. Argazki paneletan giza koronabirusetan iragarritako cNESak txertaturik dituzten Rev(1.4)-GFP erreportariek HeLa zelulatan gainadierazita, eta ActDrekin tratatuta (+ActD) eta tratatu gabe (-ActD) erakusten duten kokapenaren irudi adierazgarriak ageri dira. Grafikoan proteina horiek erakusten duten kokapenaren kuantifikazioa eta Rev(1.4)-GFP esportazio-entseguan lortutako puntuazioa.

67. irudiari erreparatuta agerikoa da, koronabirus ezberdinen N proteinan aurreikusitako NESen aktibitatea jatorrizko birusaren patogenotasunarekin korrelazioan ez dagoela. Izan ere, gaixotasun arinak eragiten dituzten HCoV-HKU1, HCoV-OC43, HCoV-229E eta HCoV-NL63 koronabirusen NESek, 1, 2, 4 eta 8ko esportazio-aktibitate maila erakutsi dute, hurrenez hurren, esportazio-entseguan eta gaixotasun larriak eragiten dituzten SARS-CoV-2 eta MERS-CoV koronabirusenek, ordea, 2 eta 3koa.

4.1.4.2. CRM1en inhibizioak ez du SARS-CoV-2 ezta HCoV-NL63 koronabirusen nukleokapsida proteinen kokapen nukleozitoplasmatikoa aldatzen

Koronabirusetan aurreikusitako NESek esportazio-aktibitate maila oso ezberdinak dituztela ikusita, ezberdintasun horiek N proteina osoaren kokapenean eraginik dutenetz aztertu da. Horretarako, SARS-CoV-2 (2ko esportazio-aktibitate mailako NESa duena) eta HCoV-NL63 (8ko esportazio-aktibitate mailako NESa duena) koronabirusen N proteina osoak YFP proteinarekin fusionatu eta HEK293T zelulatan gainadierazi dira.

68. irudian antzeman daitekeenez, SARS-CoV-2 eta HCoV-NL63 koronabirusen N proteinek kokapen zitoplasmatikoa erakusten dute, bai CRM1 aktibo zein inhibiturik egon. Hau da, iragarritako NESen esportazio-aktibitate ezberdintasuna ez da proteina osoaren kokapenean islatzen. Beraz, badirudi CRM1ek ez duela eragin handirik SARS-CoV-2 eta HCoV-NL63 koronabirusen N proteinen kokapenean.

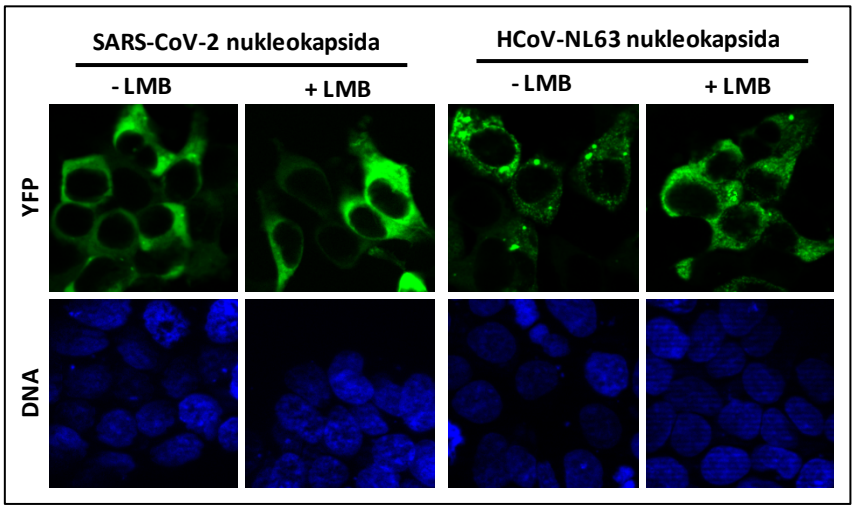

68. irudia: CRM1en mendeko esportazioak ez du paper erabakigarririk HCoV-NL63 eta SARS-CoV-2 koronabirusen N proteinen kokapen nukleozitoplasmatikoan. HCoV-NL63 eta SARS-CoV-2 koronabirusen nukleokapsida proteinek YFP proteinarekin fusionaturik HEK293T zelulatan gainadieraztean agertzen duten kokapenaren argazki adierazgarriak. Bai HCoV-NL63 bai SARS-CoV-2 birusaren N proteinek kokapen zitoplasmatikoa erakusten dute CRM1 aktibo (-LMB) zein inhibiturik (+LMB) egon.

4.2. CRM1 itu terapeutiko bezala erabiltzearen inguruko ikerketak

CRM1 minbiziaren garapen eta pronostikoarekin estuki erlazionaturik dago, eta bada, proteina hori inhibitzen duten farmakoak minbizia tratatzeko ere erabiltzen hasi dira. Gaur egunera arte, selinexor klinikan onartutako CRM1en inhibitzaile bakarra da. Farmako hori, bakarka edo beste farmakoekin konbinazioan, mieloma anizkoitza (MM, *multiple myeloma*) zein B-zelula handien linfoma hedatsua (DLBCL, *diffuse large B cell lymphoma*) pairatzen duten gaixo batzuen tratamenduan erabiltzeko onartua izan da (Food and Drug Administration, 2019, 2020a, 2020b, European Medicines Agency, 2021). Gainera, beste minbizi mota batzuetarako ere, fase kliniko aurreratuetan dago selinexor, etorkizun hurbil batean egun duen erabilera nabari hedatuko dela iradokiz. Klinikan etorkizun itxaropentsua ikusten bazaio ere, CRM1en inhibizioak zelula mailan duen eragin zehatza ez da oraindik ezagutzen. Inhibizioak CRM1en kargoen banaketa azpizelularra asaldatuko duela aurreikusten da. Kargo batzuen kasuan, asaldura hori jada baieztaturik dago (Brunetti et al., 2018), beste kasu askotan aldiz, asaldura hori nolakoa eta zenbatekoa den zehazteke dago.

Selinexor farmakoaren erabilera klinikoaren inguruko ezagutza zabaltze aldera, atal honetan bi ikerketa planteatzen dira. Batetik, minbizi ezberdinetan erabilgarriak izan daitezkeen selinexorren eta beste farmako batzuen konbinazio berriak aztertu dira. Bestetik, CRM1en inhibizioak zelula mailan duen eragina ikertzeko baliagarria den konpartimentu-espezifikoko proteinen markaketa eta proteomika uztartzen dituen sistema berri bat jarri da martxan. Hurbilketa berri horrek, selinexorrek eragindako kargoen banaketaren asaldurak aztertzeko aukera emango du.

4.2.1. Selection and *in vitro* evaluation of potential anticancer treatments combining selinexor with a second targeted drug

As described in the Introduction, the SINE compound selinexor has been recently approved for the treatment of specific subsets of cancer patients. Selinexor has been extensively tested *in vitro* in combination with other chemotherapy drugs, with encouraging results. For example, the combination of selinexor with daunorubicin or idarubicin, two inhibitors of topoisomerase II (TOP2A), shows synergistic effects on AML cells (Ranganathan et al., 2016). Importantly, *in vitro* studies suggest that selinexor, alone or in combination with other drugs, could also be useful in patients with solid tumours, and is currently undergoing clinical testing in this setting (www.clinicaltrials.gov).

Given that selinexor appears to be particularly effective when administered together with other therapeutic agents, potential new combinations of selinexor with other targeted drugs were explored in this thesis. In order to select drug candidates for testing, it was reasoned that co-(over)expression of CRM1 with the protein targeted by these agents could make tumour cells particularly susceptible to a combination therapy simultaneously inhibiting both targets. Thus, an *in silico* analysis was first carried out to evaluate how the mRNA expression of *XPO1* (the gene encoding CRM1) correlates with the expression of other relevant cancer genes in different tumour types. Afterwards, the combination of selinexor with drugs directed against two of these targets was tested *in vitro* using an experimental model of acute myeloid leukaemia (AML) cells co-cultured with cytoprotective bone marrow (BM) stromal cells (Ramasamy et al., 2012).

4.2.1.1. Correlation of *XPO1* gene expression with the expression of other cancer-target genes in different tumour types

The first step was to analyse the correlation of *XPO1* gene expression with the expression of a set of 135 cancer-related genes included in the CGA TARGET (tumour alterations relevant for genomics-driven therapy) database of the Broad Institute (v3). This database, available at (https://software.broadinstitute.org/cancer/cga/target, contains genes (hereafter referred to as TARGET genes) whose alteration in cancer is directly linked to a clinical action (i.e. genes with diagnostic, prognostic or predictive utility), and includes genes that encode the molecular targets of well-established and novel therapeutic agents. Correlation analyses were carried out using publicly available datasets from several cancer types, summarised in Table 19.

Table 19: Summary of studies used for the correlation analysis classified according to cancer type. Table shows each study reference, cohort size and ID number at GEO (ncbi.nlm.nih.gov/geo/) or dbGap (ncbi.nlm.nih.gov/gap/). Data for studies without this ID numbers are available at; TCGA: cancer.gov/about-nci/organisation/ccg/research/structural-genomics/tcga, Chitale et al.: cbio.mskcc.org/public/lung_array_data/, Colonomics: colonomics.org/ and Liu et al.: gdc-portal.nci.nih.gov/legacy-archive/. Data from the Glinsky et al. study were provided by MSKCC.

Cancer type	Study/Reference	Cohort size	ID
Breast cancer	Lu et al., 2008	131	GEO: GSE5460
	Ivshina et al., 2016	249	GEO: GSE4922
	TCGA	522	
	Pawitan et al., 2005	159	GEO: GSE1456
	Wang et al., 2005	286	GEO: GSE2034
Lung cancer	Chitale et al., 2009	128	
	Sheeden et al., 2008	442	GEO: GSE68465
	TCGA	514	
	Wilkerson et al., 2012	116	GEO: GSE26939
Prostate cancer	Glinsky et al., 2004	79	
	Grasso et al., 2012	88	GEO: GSE35988
	Lapointe et al., 2004	26	GEO: GSE3933
	Taylor et al., 2010	179	GEO: GSE21034
	TCGA	496	
	Varambally et al., 2005	19	GEO: GSE3325
Colorectal cancer	Colonomics	246	GEO: GSE44076
	Jorissen et al., 2009	290	GEO: GSE14333
	Kemper et al., 2012	90	GEO: GSE33113
	Laibe et al., 2012	130	GEO: GSE37892
	Marisa et al., 2013	585	GEO: GSE39582
	Roepman et al., 2014	188	GEO: GSE42284
	TCGA	374	
Acute myeloid leukaemia (AML)	Tyner et al., 2018	672	dbGaP: 30641
	Liu et al., 2018	200	

In the case of breast, lung, prostate, and colorectal cancer, correlation analysis was performed using CANCERTOOL (Cortazar et al., 2018), while the cBioPortal analysis suite (Cerami et al., 2012; Gao et al., 2013) was used to analyse AML data. An example of the results obtained using CANCERTOOL in the seven colorectal cancer datasets is shown in Figure 69. As illustrated in the figure, the expression of some TARGET genes was consistently correlated with the expression of *XPO1* across the different datasets, in either a positive (e.g. *EZH2*) or negative (e.g. *RARA*) manner.

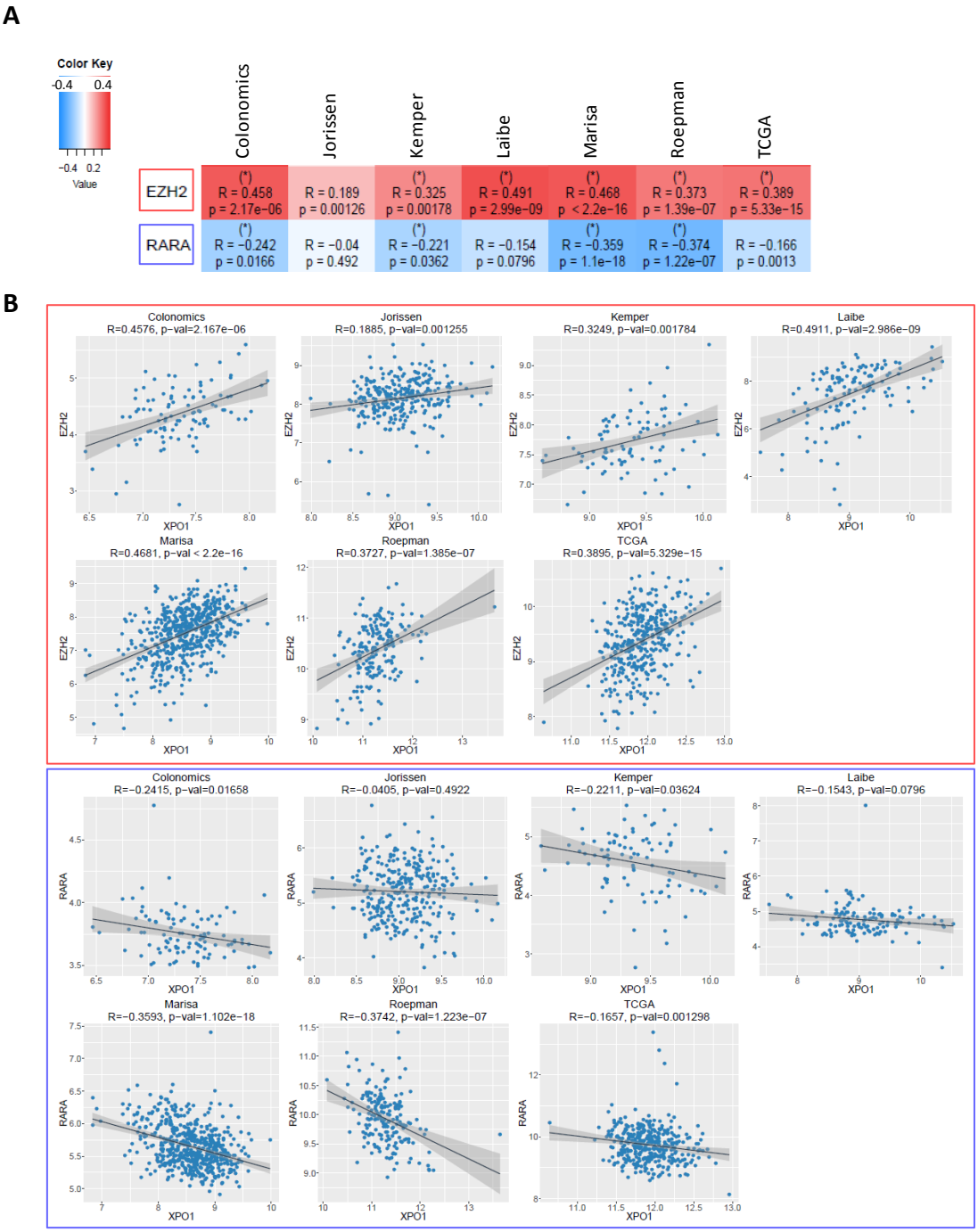

Figure 69: Example of the results of correlation analysis using CANCERTOOL. A. The heatmap shows how *XPO1* expression correlates with the expression of TARGET genes *EZH2* and *RARA* in seven datasets of colorectal cancer patients. Blue colour indicates inverse correlation, and red colour indicates direct correlation, with colour intensity representing the Pearson's correlation value (R), as indicated by the scale on the upper left corner. The R and p values are indicated inside each heatmap cell. B. The scatter plots show detailed correlation results between *XPO1* and *EZH2* or *RARA* genes across the seven colorectal cancer datasets. In every dataset analysed, the expression of *XPO1* was directly correlated with the expression of *EZH2*, and negatively correlated with the expression of *RARA*. Each dot in the graphs represents a tumour sample.

The pair wise correlation between the expression of *XPO1* and the expression of each of the 135 TARGET genes was determined in all datasets. Using only those statistically significant ($p \leq 0.05$) correlations with $R > 0.2$ or $R < -0.2$, the average correlation value of each *XPO1*-TARGET gene pair in every cancer type was calculated (Supplementary Tables 6-10). Finally, the average correlation (mean R value) across the five tumour types was calculated (Supplementary Table 11). As shown in Figure 70, the expression of 8 TARGET genes (*MSH2*, *ATR*, *MSH6*, *BRCA1*, *EZH2*, *BRCA2*, *AURKA* and *NPM1*) was positively correlated with *XPO1* expression with R > 0.2. These eight genes were therefore considered in order to select drugs that may be potentially combined with selinexor.

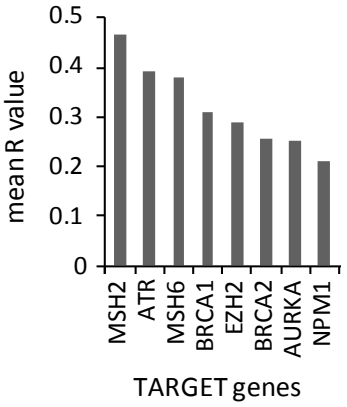

Figure 70: Graph showing the correlation between the expression of *XPO1* and TARGET genes mRNA. Only those correlations with a mean R value > 0.2 are shown.

4.2.1.2. Selection of potential targets and drugs for selinexor-based combination therapies

Table 20 shows the cytogenetic location of *XPO1* and the selected eight TARGET genes.

Table 20: Cytogenetic location of *XPO1* and eight TARGET genes whose mRNA expression is positively correlated (R > 0.2) with *XPO1* mRNA expression in human tumors.

Gene symbol	Gene name	Cytogenetic location
XPO1	Exportin 1	2p15
MSH2	MutS homolog 2	2p21-16.3
MSH6	MutS homolog 6	2p16.3
BRCA1	BRCA1 DNA repair associated	17q21.31
BRCA2	BRCA2 DNA repair associated	13q13.1
NPM1	Nucleophosmin 1	5q35.1
ATR	ATR serine/threonine kinase	3q23
AURKA	Aurora kinase A	20q13.2
EZH2	Enhancer of zeste homolog 2	7q36.1

A survey of the literature on the proteins encoded by these eight genes was carried out. Interestingly, seven of them (MSH2, MSH6, ATR, BRCA1, BRCA2, AURKA and NPM1) have roles in the DNA damage response (DDR), and some of them may be functionally related.

MSH2 and ***MSH6*** are tumour suppressor genes that code for the DNA mismatch repair (MMR) proteins MSH2 and MSH6. Loss-of-function mutations in *MSH2* and *MSH6* contribute to the development of various cancer types. In fact, germ line mutations affecting these genes cause hereditary nonpolyposis colorectal cancer (HNPCC) syndrome, also known as Lynch syndrome. HNPCC syndrome confers a nearly 80 % lifetime risk of developing cancer, especially colorectal and endometrial cancer (Gupta et al., 2019; Cerretelli et al., 2020). The MSH2 and MSH6 proteins show similar tissue-specific expression, and they usually heterodimerise to form the MutSα DNA MMR complex (Acharya et al., 1996). This complex is responsible for recognising single nucleotide mismatches, as well as insertion or deletion of one or two nucleotides (Stojic et al., 2004; Jiricny, 2006; Li, 2008). Importantly, *XPO1*, *MSH2* and *MSH6* are located in the same chromosome arm (2p), and relatively close one to each other (see Table 20). This physical proximity may, at least in part, explain why the expression of these genes is positively correlated in human tumours: their expression level may be commonly affected by the same structural chromosomal aberrations.

Germ line mutations in the tumour suppressor genes ***BRCA1*** and ***BRCA2*** cause a clinical condition known as hereditary breast and ovarian cancer syndrome (HBOC), which leads to the development of breast and ovarian cancer, and to a lesser extent of prostatic, pancreatic and colorectal cancer (Morris and Chan, 2015; McAlarnen et al., 2021; Yoshida, 2021). The best-characterised function of BRCA1 protein is in double strand break repair by homologous recombination, a process in which BRCA2 is also involved (Ciccia and Elledge, 2010; Roy et al., 2011; O'Kane et al., 2017; Wright et al., 2018). However, BRCA1 participates in several other DNA repair pathways, including MMR (Wang et al., 2001).

Nucleophosmin (NPM1), the protein encoded by the ***NPM1*** gene, is a multifunctional protein, mainly located in nucleoli, that plays a crucial role in ribosome biogenesis. It is also involved in centrosome duplication, DNA replication, recombination and repair, and may regulate the localisation and stability of several tumour suppressor proteins, including p53 (Lindström, 2011; Federici and Falini, 2013; López et al., 2020). NPM1 is frequently deregulated in cancer, and mutations in *NPM1* gene characterise a subset of AML patients (Falini et al., 2007).

The protein encoded by the ***ATR*** gene, is a serine/threonine kinase that becomes activated in response to single-strand DNA damage or replication stress (Zou et al., 2003). When activated, ATR protein phosphorylates and activates several downstream effectors in DNA repair, including BRCA1 (Tibbetts et al., 2000). The main ATR effector is the kinase CHK1 (Checkpoint kinase 1) (Yarden et al., 2002). CHK1 activation leads to repression of the phosphatase CDC25C, and ultimately provokes a G2/M cell cycle arrest (Karnitz and Zou, 2015; Liu et al.,

2020; Gorecki et al., 2021). Besides CDC25C, several other downstream targets can be regulated by CHK1, including Aurora kinase A (AURKA) (Krystyniak et al., 2006), the product of the *AURKA* gene.

AURKA plays an important role in the DDR process known as checkpoint recovery. DNA damage usually leads to cell cycle arrest due to activation of different checkpoints. If the damage is successfully repaired, the process of checkpoint recovery allows the cell cycle to resume. In the case of the G2/M checkpoint, this process depends crucially on the activation of PLK1 (Polo like kinase 1) (Gorecki et al., 2021), which is stimulated by AURKA (Macůrek et al., 2008). In addition to playing an essential role in the G2/M checkpoint, AURKA also functions in centrosome maturation and integrity, and bipolar spindle assembly (Magnaghi-Jaulin et al., 2019). *AURKA* is overexpressed in several tumour types, and its aberrant expression has been linked to drug resistance (Yan et al., 2016). Although overexpression of *AURKA* is linked to an adverse prognosis, and there are indeed studies indicating that it may have oncogenic effect (Wang et al., 2006), it has also been reported to function as a tumour suppressor protein (Damodaran et al., 2017).

Finally, ***EZH2*** encodes the protein enhancer of zeste homolog 2 (EZH2), a histone methyltransferase that plays an important role in global transcriptional regulation (Cao et al., 2002; Kuzmichev et al., 2002). EZH2 is the catalytic subunit of the polycomb repressive complex 2 (PRC2), which is able to silence gene expression by catalysing the trimethylation of histone H3 lysine 27, a repressive chromatin mark. Overexpression of *EZH2* or overactivation of EZH2, leading to increased transcriptional repression of tumour suppressor genes, is commonly found in solid tumours (Varambally et al., 2002; Kleer et al., 2003; Raaphorst et al., 2003; Sudo et al., 2005). In haematological cancers, however, both overexpression and loss-of-function mutation of *EZH2* have been found (Morin et al., 2010; Guglielmelli et al., 2011; Herrera-Merchan et al., 2012), suggesting that EZH2 could be functioning as either an oncoprotein or a tumour suppressor protein in a context-dependent manner (Kim and Roberts, 2016; Gan et al., 2018; Safaei et al., 2018; Eich et al., 2020).

Although the expression of these eight genes was found to correlate positively with the expression of *XPO1* in human tumours, it must be noted that not all of them encode suitable potential targets for selinexor-based combination therapies. Thus, *MSH2*, *MSH6*, *BRCA1* and *BRCA2* encode tumour suppressor proteins whose inhibition is not regarded as a valid therapeutic approach in cancer. On the other hand, while the protein products of *NPM1*, *ATR*, *EZH2* and *AURKA*, are considered druggable targets in cancer therapy, no reliable inhibitors of NPM1 are yet commercially available.

At the time when the drug selection was made in this thesis (in 2018), evidence was mounting on the importance of AURKA and EZH2 as targets for cancer therapy (Damodaran et al., 2017; Lee et al., 2017; Mohammad et al., 2017; Cheng and Xu, 2018; Dawei et al., 2018; Dimopoulos et al., 2018; Felgenhauer et al., 2018; Fioravanti et al., 2018; Herviou et al., 2018; Hou et al., 2018; Huang et al., 2018; Italiano et al., 2018; Kogiso et al., 2018; Li et al., 2018; Mochizuki et al., 2018; Payton et al., 2018; Serresi et al., 2018; Shaikh et al., 2018; Tremblay-LeMay et al., 2018; Tsai et al., 2018; Wen et al., 2018; Wu et al., 2018; Yang et al., 2018; Zheng et al., 2018), and specific inhibitors, such as alisertib (targeting AURKA) and tazemetostat (targeting EZH2) were commercially available.

Alisertib (MLN8237), the most clinically advanced AURKA inhibitor, is being tested in clinical trials, but is not yet approved for cancer treatment. Although alisertib did not perform well in the first phase 3 clinical trial in relapsed/refractory peripheral T-cell lymphoma patients (O'Connor et al., 2019; NCT01482962), it has obtained favourable results in several phase 1 and phase 2 trials in a number of cancers (Du et al., 2021).

Tazemetostat (Tazverik®, EPZ-6438, E-7438) has been the most successful EZH2 inhibitor in clinical trials, and it has recently received FDA approval for specific subsets of sarcoma and lymphoma patients (Food and Drug Administration, 2020c, 2020d).

Therefore, alisertib and tazemetostat were finally selected to be tested in combination with selinexor.

4.2.1.3. Description of the *in vitro* experimental setting: a cancer/stromal cell co-culture model

The effect of combining selinexor with alisertib or tazemetostat was experimentally tested in AML cells. These experiments were carried out between May and July 2019, during a 3 month research stage at the Department of Life Sciences of the University of Roehampton (London) under the supervision of Dr. Yolanda Calle. The group of Dr. Calle has previously developed, and extensively used, cancer/stromal cell co-culture models (Ramasamy et al., 2012) that allow evaluating the effect of drug treatments in a setting more closely resembling tumour conditions than cancer cell line monocultures.

Specifically, the analyses were carried out on MV4-11 AML cells seeded in co-culture with HS5 BM stromal cells (Figure 71). The two cell types stably express different fluorescent proteins: eGFP (green) in the case of MV4-11 cells, and mCherry (red) in the case of HS5 cells. This differential labelling allows independent, but concomitant, assessment of the effect of the

different drug treatments in both cancer and stromal cells. Importantly, by comparing the effect of treatments in co-cultured AML/stromal cells with their effect on AML cells growing alone, this experimental system allows to gauge how the presence of stromal cells influences drug response in cancer cells (Ramasamy et al., 2012).

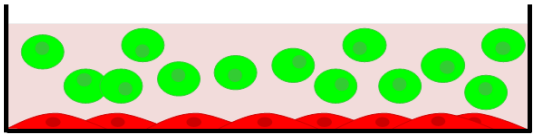

Figure 71: Scheme of the experimental AML setting. MV4-11 AML cells, expressing eGFP (green), grow in suspension in contact with BM HS5 cells expressing mCherry (red).

4.2.1.4. *In vitro* effect of selinexor/alisertib and selinexor/tazemetostat combination treatments on co-cultured AML/stromal cells

To evaluate the effect of the different drug combinations, cell proliferation and apoptosis were analysed in MV4-11 AML cells, either cultured alone or co-cultured with HS5 BM stromal cells. Additionally, the proliferation of the stromal cells in the co-culture setting was also assessed. Cell proliferation was determined by comparing the intensity of eGFP and mCherry fluorescent tags at time 0 and 72 h, while apoptosis of eGFP-MV4-11 cells was determined using flow cytometry.

The first step was to establish the range of drug concentrations to be used in these *in vitro* assays. As a general reference, the maximum concentration values (C_{max}) for each drug previously reported in the plasma of treated patients were initially considered: 1000 ng/ml (2.5 µM) for selinexor (Abdul Razak et al., 2016; Garzon et al., 2017), 4000 ng/ml (9 µM) for alisertib (Cervantes et al., 2012; Dees et al., 2012), and 3200 ng/ml (5 µM) for tazemetostat (Italiano et al., 2018). However, a series of preliminary experiments (not shown) revealed that in this *in vitro* experimental setting, the plasma C_{max} concentration of selinexor and alisertib caused extensive cell death as single agents and could, therefore, not be used for the combination studies. From these preliminary experiments, the following ranges of drug concentration were selected: 25 nM to 200 nM for selinexor, 1 µM to 4.5 µM for alisertib and 250 nM to 5 µM for tazemetostat. In all cases, the duration of the treatment was 72h.

4.2.1.4.1. Effect of selinexor, alisertib and tazemetostat as single agents

As single agents, selinexor and alisertib showed a dose-dependent antiproliferative effect on MV4-11 AML cells (Figure 72A). This decrease in AML cell proliferation, especially when treated with selinexor, was less pronounced when co-cultured with HS5 cells than when cultured alone, suggesting a partial protective effect of the stromal cells. Of note, an

antiproliferative effect of selinexor and alisertib on HS5 cells was also observed (Figure 72B), albeit less pronounced than the effect on AML cells. In contrast to selinexor and alisertib, tazemetostat did not decrease proliferation capacity in either condition or cell type (Figures 72A and 72B).

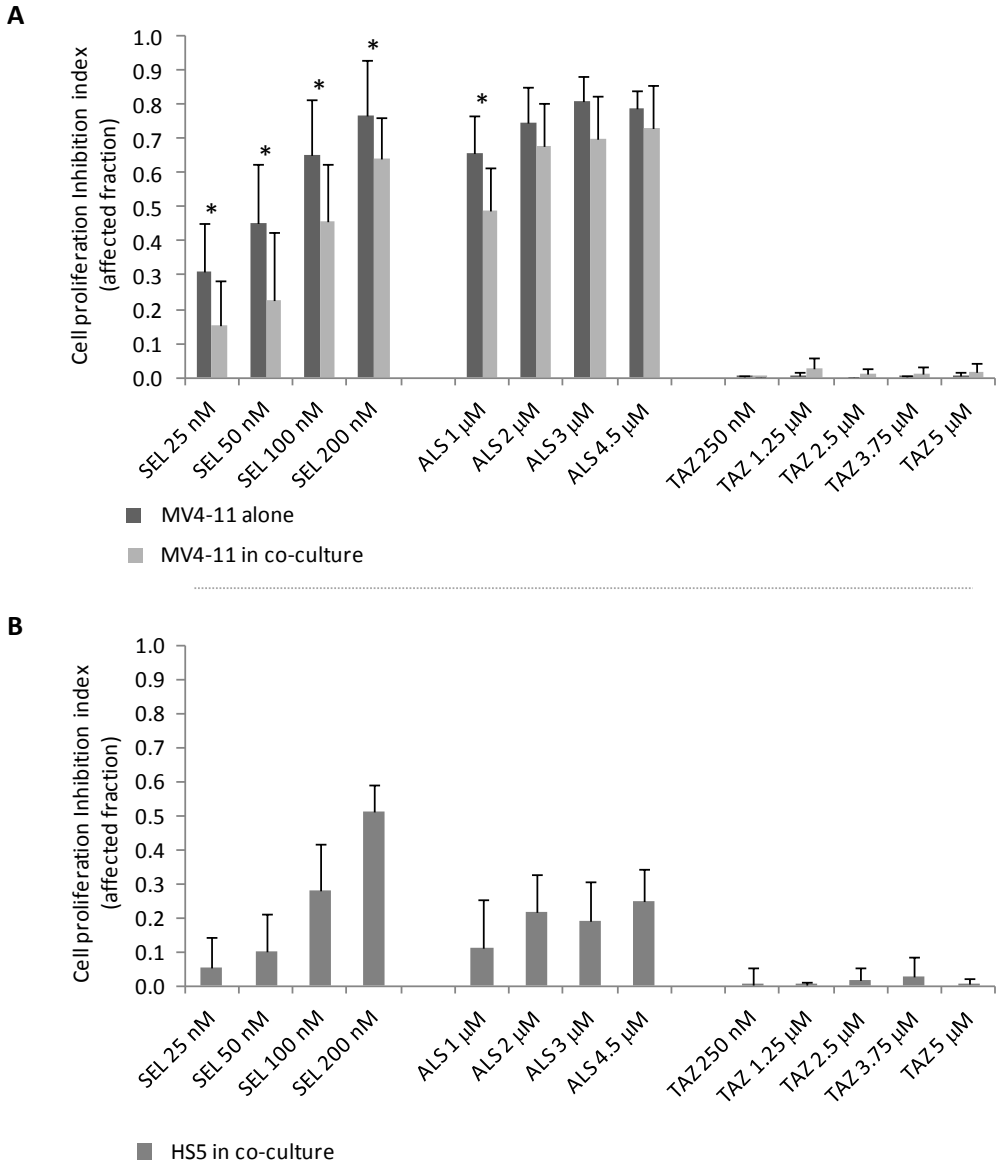

Figure 72: Antiproliferative effect of selinexor, alisertib and tazemetostat as single agents. Antiproliferative effect is shown in terms of cell proliferation inhibition of MV4-11 cells cultured alone or in co-culture with HS5 (panel A), and HS5 in co-culture with MV4-11 (panel B). Cells were treated with selinexor (SEL), alisertib (ALS) or tazemetostat (TAZ) for 72 h. Graphs shows the mean value and the standard deviation of eight experiments for selinexor and four experiments for both alisertib and tazemetostat. Three replicates of each condition were seeded per experiment. * represents $p < 0.05$ in ANOVA test for MV4-11 cells alone versus MV4-11 cells co-cultured with HS5 with the same treatment.

The pro-apoptotic effect of selinexor, alisertib and tazemetostat as single agents on AML cells was also evaluated (Figure 73). Selinexor showed a dose-dependent pro-apoptotic effect in AML cells grown alone or in co-culture. This increase in apoptosis was less pronounced in the co-culture setting, especially at the highest concentrations tested. In the case of alisertib, no

dose-dependent effect was observed neither in AML cells cultured alone nor in co-culture with BM stromal cells, suggesting that its maximum pro-apoptotic effect was reached at even the lowest dose used in these experiments. However, it cannot be ruled out that alisertib might have a dose-dependent pro-apoptotic effect when applied at lower concentrations. Of note, BM stromal cells do have a clear cytoprotective effect on AML cells when treated with alisertib in this cellular context. Finally, tazemetostat did not show any pro-apoptotic effect at the concentrations used.

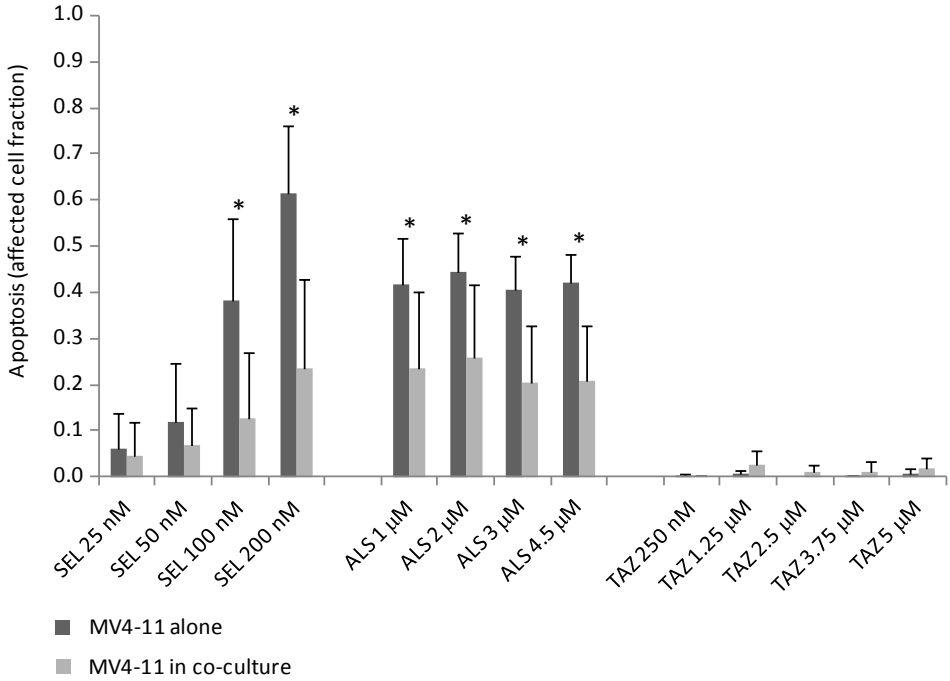

Figure 73: Pro-apoptotic effect of selinexor, alisertib and tazemetostat as single agents. Pro-apoptotic effect is shown in terms of affected fraction of MV4-11 alone or in co-culture with HS5 treated with selinexor (SEL), alisertib (ALS) or tazemetostat (TAZ) for 72 hours. Graph shows the mean value and the standard deviation of eight experiments for selinexor and four experiments both for alisertib and tazemetostat. Three replicates of each condition were seeded per experiment. * represents $p < 0.05$ in ANOVA test for MV4-11 cells alone versus MV4-11 cells co-cultured with HS5 with the same treatment.

4.2.1.4.2. Effect of the selinexor/alisertib combination treatment

The effect of selinexor/alisertib combination treatment was evaluated by calculating the combination index (CI), according to the method established by Chou and Talalay (1984). To this end, cells were treated with selinexor and alisertib as single agents or in combination at the indicated concentrations for 72 hours and both proliferation (Figure 74) and apoptosis (Figure 75) were measured.

The combination of selinexor and alisertib efficiently reduced MV4-11 AML and HS5 stromal cell proliferation (Figures 74A and 74B). As shown in Figure 74C, the effect of the combination was mostly additive ($1.1 > CI > 0.9$) when MV4-11 cells were cultured alone, and synergistic

(CI < 0.9) when they were co-cultured with HS5 stromal cells. Additionally, the proliferation of stromal cells was also inhibited in a synergistic manner by the selinexor/alisertib combination.

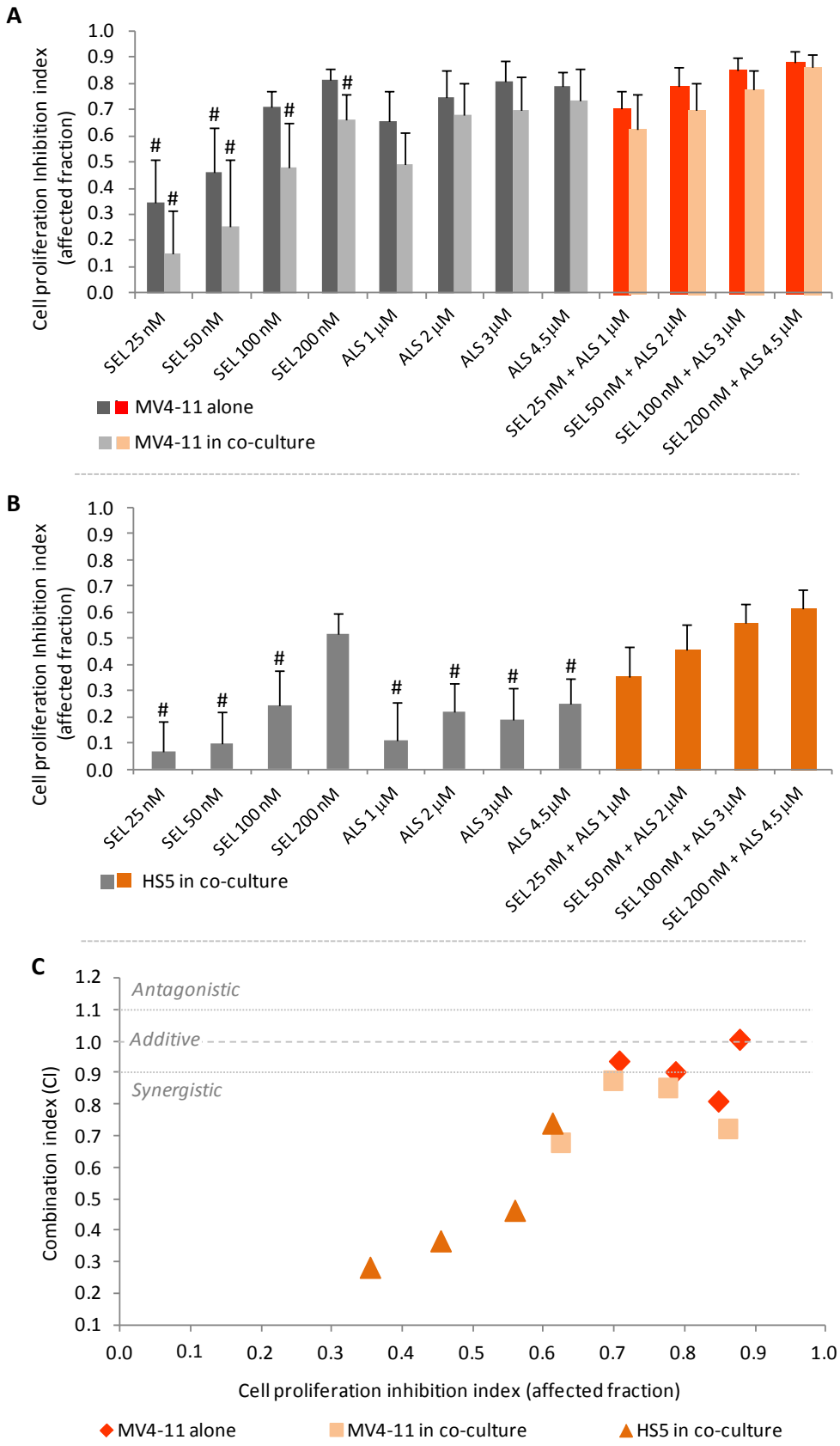

Figure 74: Antiproliferative effect of the selinexor/alisertib combination. A.B. Graphs showing the antiproliferative effect in terms of cell proliferation inhibition of MV4-11 cells cultured alone and in co-culture with HS5 cells (panel A) and of HS5 in co-culture (panel B) treated with selinexor (SEL) and alisertib (ALS) as

single agents (shaded in grey) or in combination (shaded in orange) for 72 h. The mean value and standard deviation of four independent combination experiments are shown. 3 replicates of each condition were seeded per experiment. * represents $p < 0.05$ in ANOVA test for MV4-11 cells alone versus MV4-11 cells co-cultured with HS5 with the same selinexor/alisertib combination, while # represents $p < 0.05$ in ANOVA test for single drug versus selinexor/alisertib combination. C. Graph showing the combination index (CI) for each selinexor and alisertib combination in the three cellular conditions tested. CI values below 0.9 indicate that the drug combination shows a synergistic effect. CI values between 0.9 and 1.1 indicate additive effect, and CI values above 1.1 indicate that the combination results in an antagonistic effect.

On the other hand, the selinexor/alisertib combination was also effective in promoting apoptosis both in MV4-11 AML cells cultured alone and co-cultured with HS5 BM cells (Figure 75A). It is noteworthy that the combination index (Figure 75B) revealed either antagonistic (CI > 1.1) or synergistic (CI < 0.9) effect of the combination at different affected fraction values (corresponding to the different drug doses used). The strongest synergistic effect was detected when MV4-11 cells were cultured alone. Similarly, a strong synergistic effect was determined in co-culture when the two highest doses of selinexor and alisertib were combined. However, the antagonist effect on the pro-apoptotic capacity of the two drugs when used in combination at the lowest concentrations on monocultures of MV4-11 cells suggests a complex interaction between these drugs in terms of pro-apoptotic effect in this experimental setting.

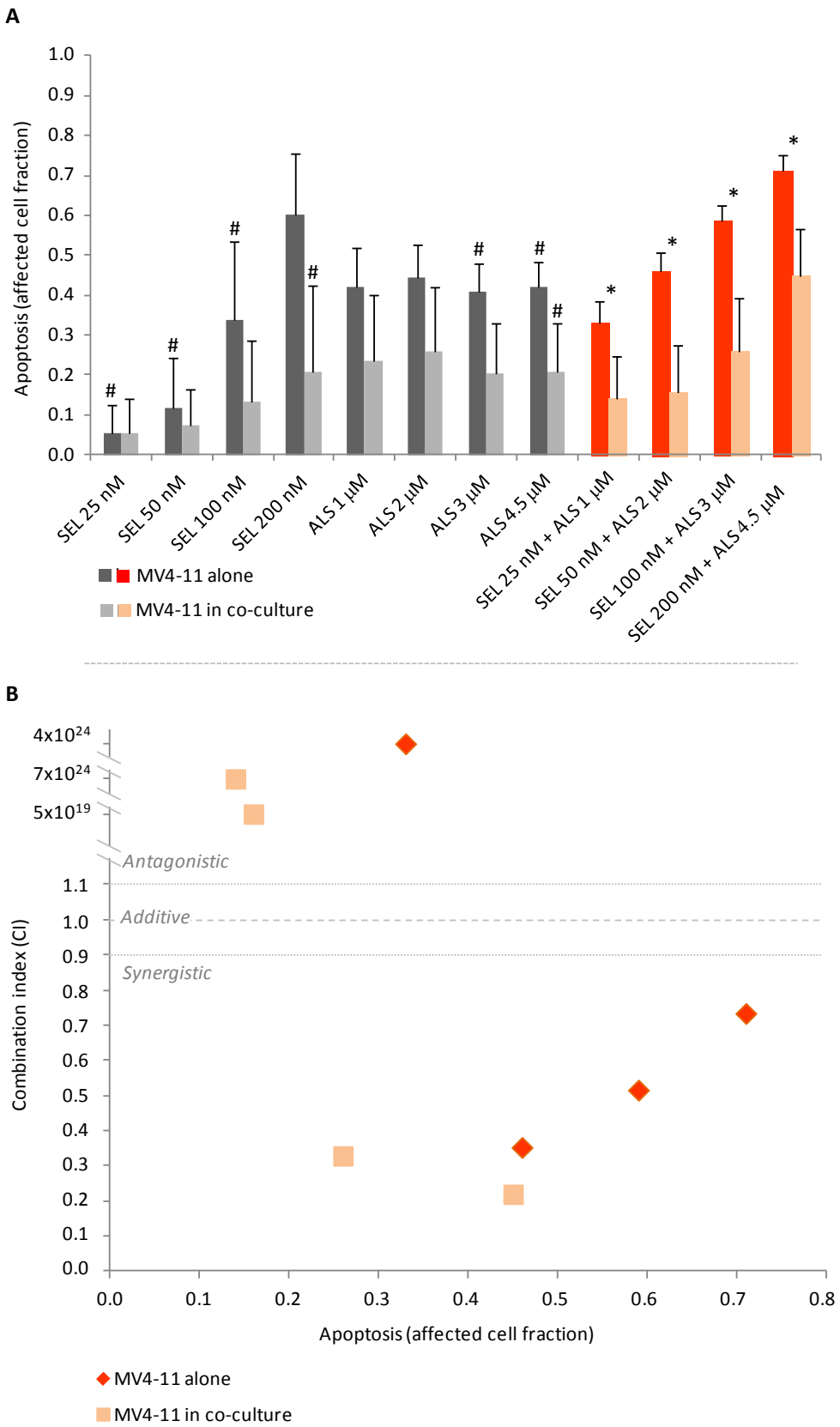

Figure 75: Pro-apoptotic effect of the selinexor/alisertib combination. A. Graph showing the pro-apoptotic effect in terms of affected fraction of MV4-11 AML cells alone and in co-culture treated with selinexor (SEL) and alisertib (ALS) as single agents (shaded in grey) or in combination (shaded in orange) for 72 h. The mean value and standard deviation of four independent combination experiments are shown. 3 replicates of each condition were seeded for experiment. * represents $p < 0.05$ in ANOVA test for MV4-11 cells alone versus MV4-11 cells co-cultured with HS5 with the same selinexor/alisertib combination, while # represents $p < 0.05$

in ANOVA test for single drug versus selinexor/alisertib combination. B. Graph showing the combination index (CI) for each selinexor and alisertib combination in the two cellular conditions tested. CI values below 0.9 indicate that the drug combination shows a synergistic effect. CI values between 0.9 and 1.1 indicate additive effect, and CI values above 1.1 indicate that the combination results in an antagonistic effect.

In summary, the combination of selinexor with alisertib shows synergistic antiproliferative effect on MV4-11 leukaemia cells, even in the presence of cytoprotective BM stromal cells by increasing the levels of apoptosis in AML cells. This is important, as the data show that the presence of BM stromal cells promotes otherwise a more cytostatic rather than cytotoxic effect of selinexor as a single agent. This increase in the pro-apoptotic effect of the combination on MV4-11 cells in co-culture correlates with the synergistic effect on the reduction of the proliferation of BM stromal cells. Inhibition of the proliferation and activity of the cytoprotective stroma by the drug combination may positively contribute to the enhanced efficacy to induce apoptosis in AML cells in the presence of stromal cells. However, at lower suboptimal concentrations of the two drugs, the effect of the combination on leukaemia cell apoptosis may be antagonistic, an effect that may be further supported by the presence of BM cytoprotective stroma. These *in vitro* results suggest that combination of selinexor with alisertib could result interesting, although it may be challenging to implement.

4.2.1.4.3. Effect of the selinexor/tazemetostat combination treatment

To evaluate the effect of the selinexor/tazemetostat combination treatment, cells were treated with both drugs, either alone or in combination, at the indicated concentrations for 72 hours and both proliferation (Figure 76) and apoptosis (Figure 77) were measured.

The antiproliferative effect of the selinexor/tazemetostat combination was not significantly different from the effect of selinexor as a single agent on MV4-11 AML cells (Figure 76A) or HS5 stromal cells (Figure 76B). The combination index (Figure 76C) revealed that the interaction between selinexor and tazemetostat was generally additive or antagonistic at the lowest affected fraction values, but some synergistic interactions were noted at higher affected fraction values (corresponding to higher drug doses). In particular, the proliferation of MV4-11 cells in co-culture was consistently reduced in a synergistic manner by the selinexor/tazemetostat combination at the highest affected fraction values.

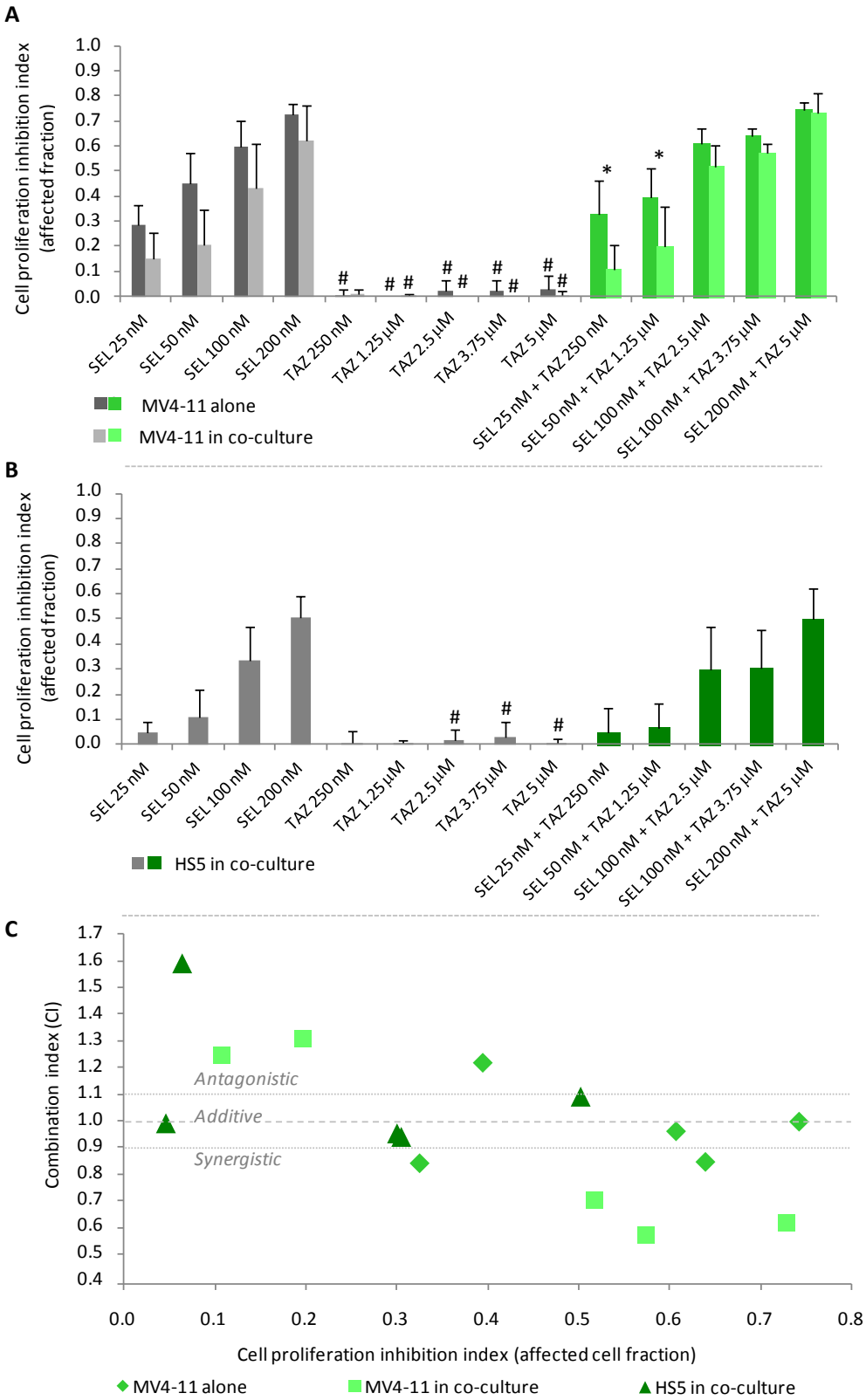

Figure 76: Antiproliferative effect of the selinexor/tazemetostat combination. A.B. Graphs showing the antiproliferative effect in terms of cell proliferation inhibition of MV4-11 alone and in co-culture (panel A) and of HS5 in co-culture (panel B) treated with selinexor (SEL) and tazemetostat (TAZ) as single agents (shaded in grey) or in combination (shaded in green) for 72 h. The mean value and standard deviation of four experiments are shown. 3 replicates of each condition were seeded per experiment. * represents $p < 0.05$ in ANOVA test for MV4-11 cells alone versus MV4-11 cells co-cultured with HS5 with the same selinexor/tazemetostat combination, while # represents $p < 0.05$ in ANOVA test for single drug versus selinexor/tazemetostat combination. C. Graph showing the combination index (CI) for each selinexor and

tazemetostat combination in the three cellular conditions tested. CI values below 0.9 indicate that the drug combination shows a synergistic effect. CI values between 0.9 and 1.1 indicate additive effect, and CI values above 1.1 indicate that the combination results in an antagonistic effect.

On the other hand, tazemetostat did not enhance the pro-apoptotic effect of selinexor on MV4-11 cells cultured alone or co-cultured with stromal cells (Figure 77A). In fact, the combination index (Figure 77B) reveals a mostly antagonistic effect of the combination.

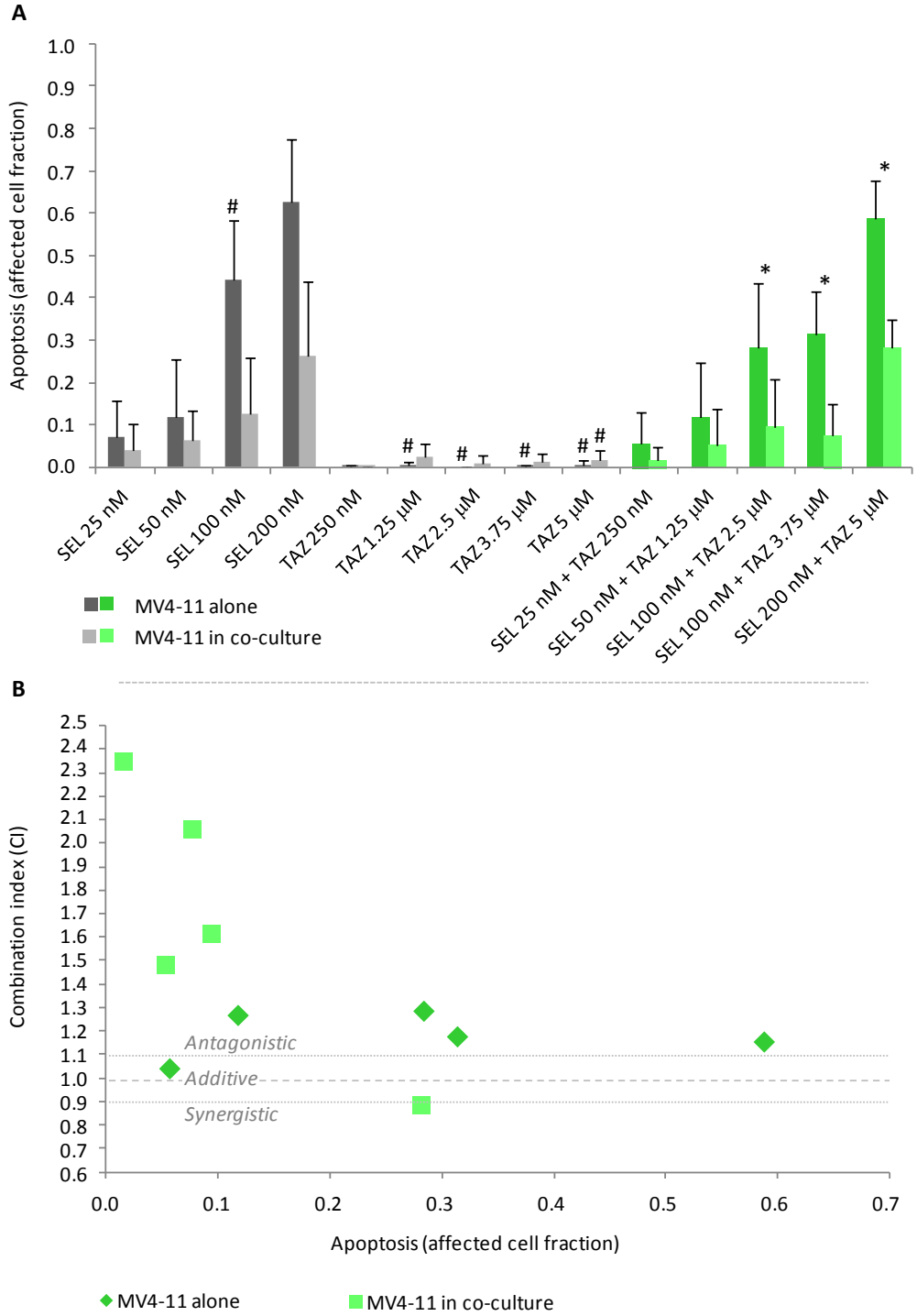

Figure 77: Pro-apoptotic effect of selinexor/tazemetostat combination. A. Graph showing the pro-apoptotic effect in terms of affected fraction of MV4-11 alone and in co-culture treated with selinexor (SEL) and tazemetostat (TAZ) as single agents (shaded in grey) or in combination (shaded in green) for 72 h. The mean

value and standard deviation of four experiments are shown. 3 replicates of each condition were seeded per experiment. * represents $p < 0.05$ in ANOVA test for MV4-11 cells alone versus MV4-11 cells co-cultured with HS5 with the same selinexor/tazemetostat combination, while # represents $p < 0.05$ in ANOVA test for single drug versus selinexor/tazemetostat combination. B. Graph showing the combination index (CI) for each selinexor and alisertib combination in the two tested cellular conditions. CI values below 0.9 indicate that the drug combination shows a synergistic effect. CI values between 0.9 and 1.1 indicate additive effect, and CI values above 1.1 indicate that the combination results in an antagonistic effect.

In summary, these *in vitro* results do not support the selinexor/tazemetostat combination as a promising treatment strategy. While some synergistic antiproliferative effects on AML cells were noted at the highest doses tested, antagonistic effects were observed at lower doses. More importantly, an antagonistic interaction between the two drugs in terms of pro-apoptotic effects was observed in most of the conditions tested. These results point to a cytostatic, rather than cytotoxic, effect of the drug combination.

4.2.2. Konpartimentu-espezifikoko gertuko biotinilazioa: CRM1en inhibizioaren eragina eta esportazio-kargoak identifikatzeko hurbilketa berria

Atal honetan aurkeztutako emaitzak Sendino et al., 2021-en argitaratu dira.

Selinexor eta beste SINE farmakoen erabilera klinikoaren testuinguruan, CRM1en inhibizioak zelula mailan duen eragina sakon ulertzea garrantzitsua da oso. CRM1 inhibitzean, haren kargo diren proteinen zitoplasmatik nukleoranzko lekualdaketa espero da. Aldaketa horiek ikertzeko ezinbestekoa da zitoplasma eta nukleoko proteomak era bereizian ikertu ahal izatea. Horretarako, frakzionamendu zelularra erabil daiteke. Metodologia hori, jada, CRM1en inhibizioarekin konbinatu izan da CRM1en kargo berriak bilatzeko (Thakar et al., 2013). Halere, frakzionamendu zelularraren bidez ez da erraza izaten purutasun handiko frakzioak lortzea, eta konpartimentu batetik besterako kutsatzeak ohikoak izaten dira (Bosch et al., 2021). Muga hori buruan, zitoplasma eta nukleoko proteomak era bereizian ikertzeko hurbilketa berri bat garatu da tesi honetan: konpartimentu-espezifikoko proteinen gertuko biotinilazioa, hemendik aurrera PGB moduan adieraziko dena.

PGBa (Roux et al., 2012) entzima-markatzaileen erabileran oinarritzen da. Entzima horiek, substratu egokiaren presentzian, inguruko proteinetan biotina marka kobalentea ezartzeko gai dira. Tesi honetan garatutako hurbilketaren kasuan, APEX2 peroxidasa erabili da (Lam et al., 2015). Entzima horrek, behin H_2O_2-rekin aktibatuta, minutu bat baino ez du behar markaketa eraginkorra gauzatzeko (Lam et al. 2015). Entzima hori, zitoplasma eta nukleora modu espezifikoan eta CRM1en mendekotasunik gabe ituratu da. Modu horretan, entzimaren ituraketa espezifikoak eragindako PGBa eta CRM1en inhibizioa konbinatu ahal izan da. Horrek, CRM1en inhibizioak eragindako aldaketak antzemateko, eta balizko kargo berriak identifikatzeko aukera ematen du. Atal honetan, guzti hori frogatzen duen kontzeptu-froga analisia aurkezten da.

4.2.2.1. Zitoplasmako eta nukleoko proteinen gertuko biotinilazioa eragingo duten APEX2an oinarritutako markatzaileen diseinu eta baliozkotzea

Zitoplasmako edo nukleoko proteinak era bereizian biotinaz markatu ahal izateko, lehen urratsa APEX2 peroxidasa (Lam et al., 2015) zitoplasman eta nukleoan espezifikoki kokatu araztea da (78. irudia). Gainera, APEX2 markatzaileen kokapena CRM1 aktibo edo inhibiturik dagoela egonkor mantendu behar da.

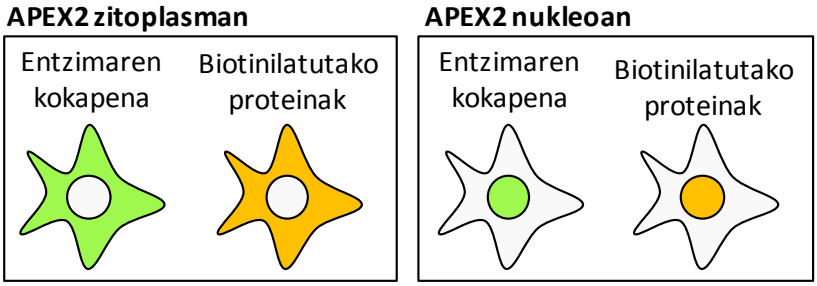

78. irudia: PGBaren bidez konpartimentu-espezifikoko proteinak identifikatzeko APEX2 peroxidasa zitoplasmara eta nukleora ituratuko da. APEX2 zitoplasmara ituratzean zitoplasman dauden proteinak biotinilatzea espero da, eta APEX2 nukleora ituratzean, aldiz, nukleoan daudenak.

APEX2 zitoplasmara edo nukleora ituratzeko helburuarekin, hainbat plasmido ezberdin sortu eta aztertu dira, betiere proteina fluoreszente bat (adibidez, YFP) eta APEX2 adierazten dutelarik.

4.2.2.1.1. APEX2 zitoplasmara ituratzeko plasmidoa: diseinua eta sortutako markatzaileen kokapena eta aktibitatearen baliozkotzea

APEX2 zitoplasmara ituratzeko, difusioz nukleora sartu ezingo den fusio-proteina handi bat eratzea izan da lehen saiakera. Horretarako, NPCaren difusio muga (~ 30 kDa) baino handiagoak diren bi proteina kodetzen dituzten bi plasmido eratu dira: pEYFP(2X)-APEX2 eta pEYFP(3X)-APEX2. Plasmido horiek APEX2rekin fusionatutako bi edo hiru YFP proteinaren kopia kodetzen dituzte, hurrenez hurren (79A irudia). HEK293T zelulatan gainadieraztean (79B irudia), fusio-proteina horiek kokapen gehien bat zitoplasmatikoa erakusten dute. CRM1 inhibitzean, YFP(3X)-APEX2 zitoplasman geratzen da, YFP(2x)-APEX2 proteinak, aldiz, nukleoranzko lekualdaketa nabaria jasaten du. Hori horrela, YFP(2X)-APEX2 proteina baztertu, eta YFP(3X)-APEX2 proteinarekin aurrera egitea erabaki da.

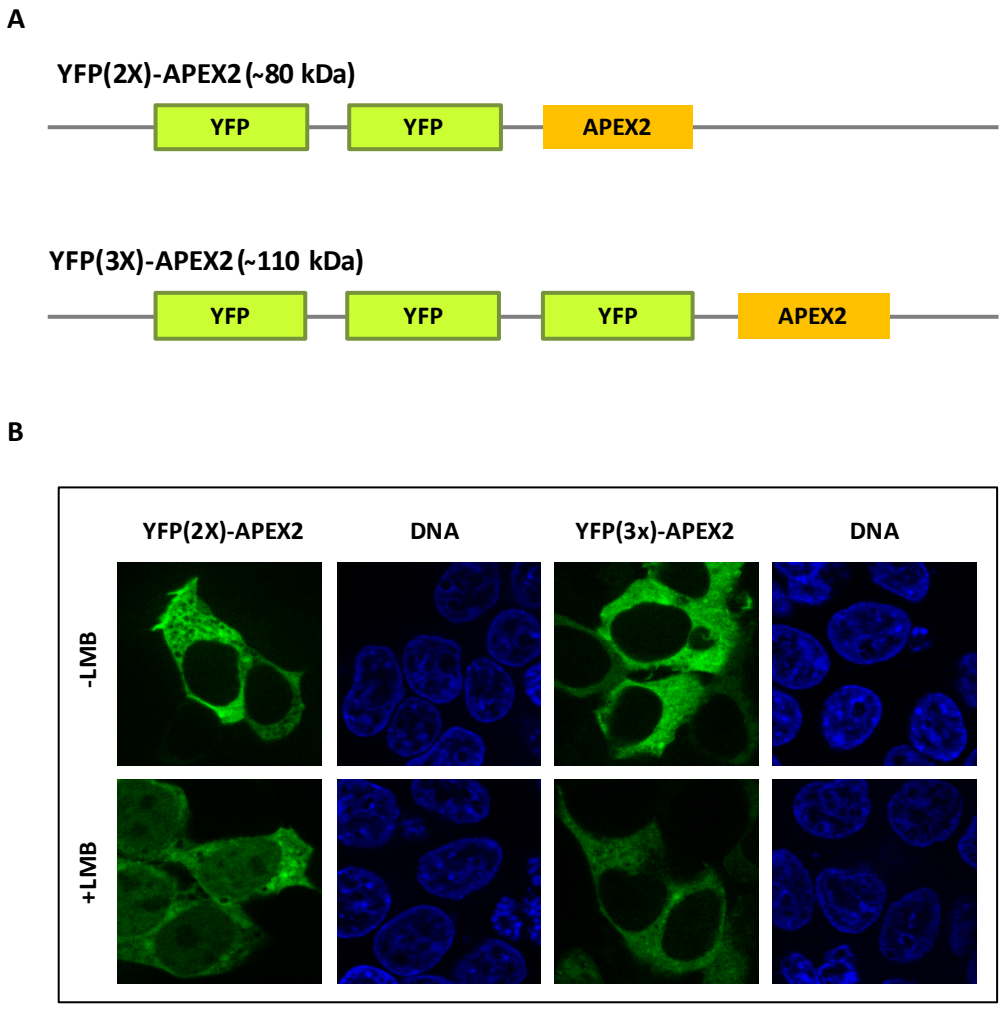

79. irudia: YFP(2X)-APEX2 eta YFP(3X)-APEX2 proteinen eskema eta kokapenaren azterketa. A. YFP(2X)-APEX2 eta YFP(3X)-APEX2 proteinen eskema. B. YFP(2X)-APEX2 eta YFP(3X)-APEX2 proteinak HEK293T zelulatan gainadieraztean hartzen duten kokapenaren irudi adierazgarriak. Egoera basalean (-LMB), proteina biek kokapen gehienbat zitoplasmatikoa erakusten dute. CRM1 inhibitzean (+LMB), YFP(3X)-APEX2 proteinak kokapen zitoplasmatikoa mantentzen du, YFP(2X)-APEX2 proteinak, ordea, nukleoranzko lekualdaketa nabaria jasaten du.

YFP(3X)-APEX2 proteina PGBa eragiteko gai den aztertzeko, biotinaren aurkako Western plapaketa egin da (80. irudia). APEX2 aktibatutako laginean (+H_2O_2), tamaina ezberdinetako banda ugari ageri dira, proteina bilduma zabala biotinilatu dela adieraziz. Emaitza horrek, YFP(3X)-APEX2 markatzailea PGBa eragiteko gai dela frogatzen du. Halere, YFParen aurkako plapaketan ere banda ugari antzematen dira, YFP(3X)-APEX2 proteina degradatu egin dela iradokiz. Beraz, pEYFP(3X)-APEX2 plasmidoa ere analisi proteomikoetarako baztertu egin da.

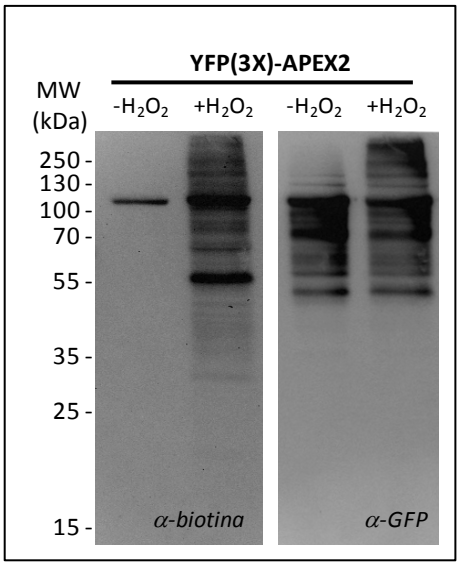

80. irudia: YFP(3X)-APEX2 markatzailearen aktibitatearen azterketa. YFP(3X)-APEX2 HEK293T zelulatan gainadierazi, PGBa eragiteko protokoloa jarraitu eta jasotako proteina erauzkinekin Western plapaketak egin dira. Biotinaren aurkako plapaketan, APEX2ren peroxidasa aktibitatea aktibatzean (+H_2O_2) tamaina ezberdineko banda ugari antzematen dira. Hau da, proteina bilduma zabala biotinaz markatu da. APEX2 peroxidasa aktibatu gabeko kontrol laginean (-H_2O_2) ordea, YFP(3X)-APEX2 proteinaren autobiotinilazioari dagokion banda (~ 110 kDa) baino ez da ageri. YFParen aurkako plapaketan (GFParen aurkako antigorputza erabili da, zeinak YFP proteina ere ezagutzen duen) banda multzo zabala ageri da egoera bietan. Kasu horretan, banda multzoak proteina markatzailea degradatu egin dela erakusten du.

Emaitza horiek ikusita, estrategiaz aldatzea erabaki da: APEX2dun proteina nukleora sartzea ekidin ordez, proteina hori era aktiboan zitoplasman kokatzea erabaki da. Hori, NES seinaleen bidez lortuko da. Gogoratu beharra dago ezinbestekoa dela CRM1 inhibitzean ere APEX2zit zitoplasman kokatzea. Beraz, erabiliko den NES seinalea ezin da CRM1en bidez esportatua izan. CRM1ekiko mendekotasunik ez duten bi NES seinale aukeratu dira zitoplasman kokatuko den plasmido bat sortzeko helburuaz, pUL69 (Lischka et al., 2001) eta RIP3 (Yang et al., 2004) proteinenak hain zuzen ere (81A irudia). Bi NES horiek CRM1ekiko mendekotasunik ez duen esportazioa eragiten dutela berresteko, YFP proteinarekin bakarka zein tandemean fusionatu dira (81B irudia) eta HEK293T zelulatan gainadierazi dira (81C irudia). YFP-pUL69^{NES} zein YFP-(2X)pUL69^{NES} proteinek kokapen nukleozitoplasmatikoa agertzen dute, YFP-RIP3^{NES} proteinak kokapen zitoplasmatikoa eta YFP-(2X)RIP3^{NES} proteinak agregatu ugariko kokapen zitoplasmatikoa. Lau proteina horien kokapena ez da CRM1 inhibitzean aldatu, eta beraz, NES seinale horiek CRM1ekiko mendekotasunik ez dutela berretsi da.

A

```
pUL69 NES: APPAQPPSQPQQHYSEGELEEDEDSDDA
RIP3 NES: GLLQSQCPRPWPLLCRLLKEVVLGMFYLHDQNPVLLHRD
```

B

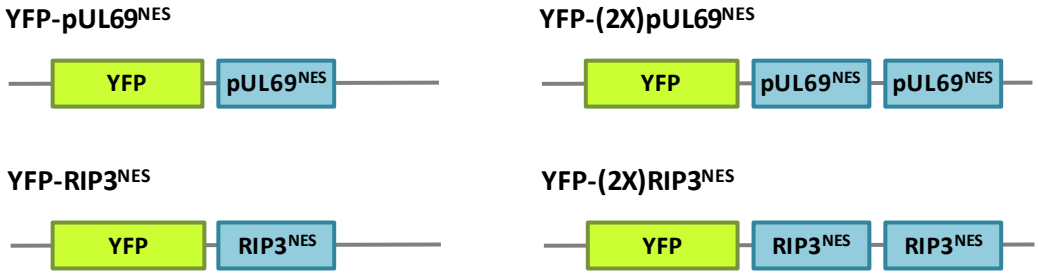

C

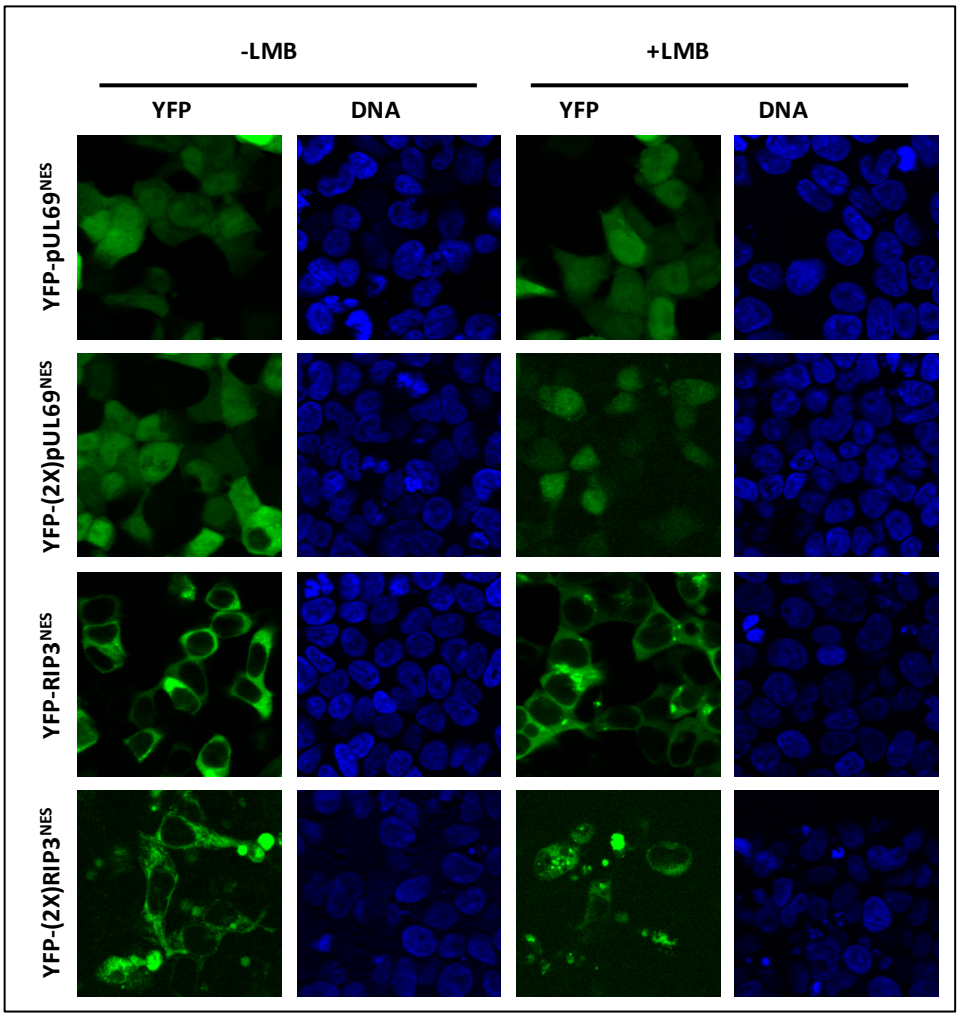

<u>81. irudia</u>: pUL69 eta RIP3 proteinen NESen azterketa. A. pUL69 eta RIP3 proteinen NES seinaleen sekuentziak. B. pUL69 eta RIP3 proteinen NESak bakarka zein tandemean YFP proteinarekin fusionatzean lortzen diren fusio-proteinen eskemak. C. B irudiko YFP-NES proteinek HEK293T zelulatan erakusten duten kokapenaren argazki adierazgarriak. Proteina guztiek CRM1en mendekoa ez den kokapena erakusten dute. pUL69 NESaren kopia bakarra edo bi dituzten proteinek kokapen nukleozitoplasmatikoa erakutsi dute, RIP3 proteinaren NES bakarra duen proteinak kokapen zitoplasmatikoa eta RIP3 proteinaren NES tandema duen proteinak agregatu ugariko kokapen zitoplasmatikoa.

81. irudian aztertutako proteinen kokapenari erreparatuz, hurrengo urratserako YFP-RIP3^{NES} proteina aproposena dela erabaki da. Izan ere, kokapen zitoplasmatiko esklusiboa erakusten du CRM1 aktibo edo inhibiturik egon, eta ez du inolako agregaturik eratzen. Beraz, YFP-RIP3^{NES} APEX2 entzimarekin fusionatu da YFP-RIP3^{NES}-APEX2 proteina sortzeko (82A irudia). Proteina hori HEK293T zelulatan gainadieraztean (82B irudia), proteinaren kokapen zitoplasmatiko argia antzematen da egoera basalean, LMBrekin tratatzean aldiz, nukleoranzko kokapen aldaketa nabaria gertatzen da.

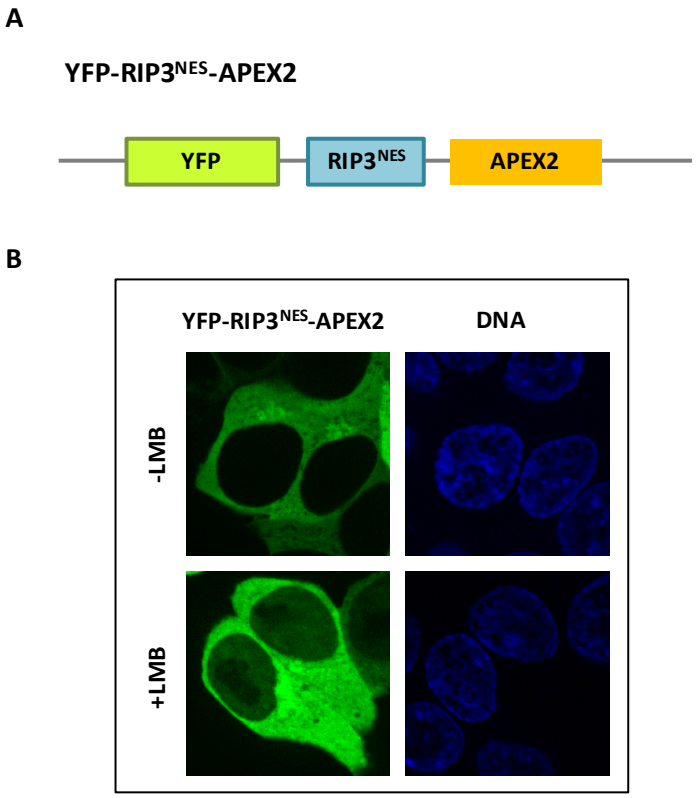

<u>82. irudia:</u> YFP-RIP3^{NES}-APEX2 proteinaren eskema eta kokapenaren azterketa. A. YFP-RIP3^{NES}-APEX2 proteinaren eskema. B. YFP-RIP3^{NES}-APEX2 HEK293T zelulatan gainadieraztean hartzen duen kokapen nukleozitoplasmatikoaren irudi adierazgarriak. Egoera basalean (-LMB) kokapen zitoplasmatiko argia erakusten du, zelulak LMBrekin tratatzean ordea, proteinaren nukleoranzko lekualdaketa nabaria dago.

Nukleoranzko lekualdaketa hori gutxitzeko asmoz, Frey eta lankideek (2018) deskribatutako sinGFP4a proteina fluoreszentea erabiltzea erabaki da. GFP proteinaren aldaera hori YFP proteina baino nabarmen astiroago translokatzen da NPCetan zehar (Frey et al., 2018). Horrela, YFP-RIP3^{NES}-APEX2 proteinatik abiatuz, sinGFP4a-RIP3^{NES}-APEX2 proteina sortu da (83A irudia). HEK293T zelulatan gainadieraztean (83B irudia), sinGFP4a-RIP3^{NES}-APEX2 proteinak kokapen guztiz zitoplasmatikoa agertzen du CRM1 aktibo zein inhibiturik egon.

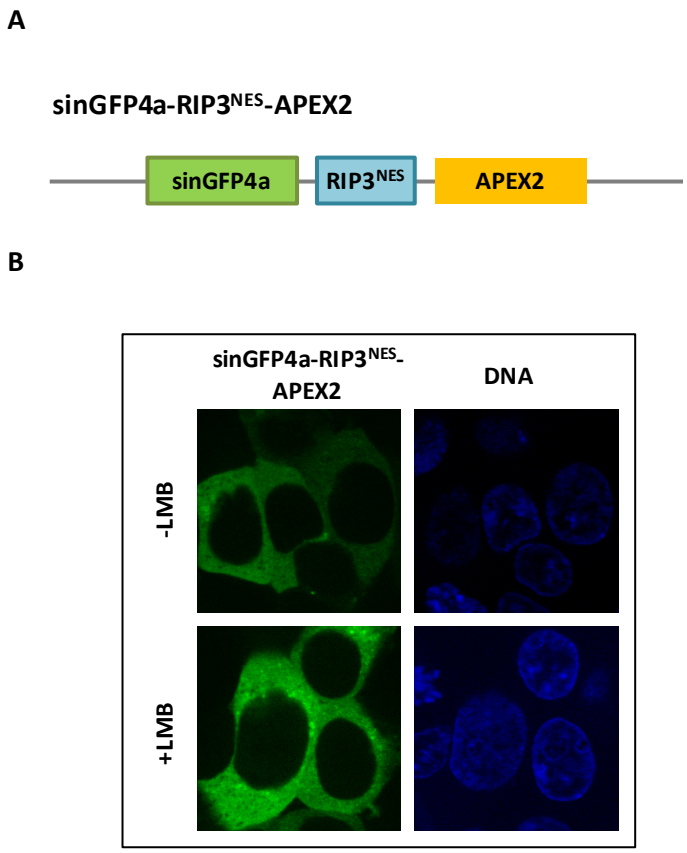

83. irudia: sinGFP4a-RIP3^{NES}-APEX2 proteinaren eskema eta kokapenaren azterketa. A. sinGFP4a-RIP3^{NES}-APEX2 proteinaren eskema. B. sinGFP4a-RIP3^{NES}-APEX2 HEK293T zelulatan gainadieraztean hartzen duen kokapen nukleozitoplasmatikoaren irudi adierazgarriak. Egoera basalean (-LMB) zein CRM1 inhibitutako egoeran (+LMB) kokapen zitoplasmatiko argia erakusten du.

Azken emaitza horrek, sinGFP4a-RIP3^{NES}-APEX2 proteinak zitoplasmako PGBa eragiteko kokapen egokia duela erakusten du. Beraz, hurrengo urratsa, proteina hori egonkorra dela eta PGBa eragiteko gai dela baieztatzea da. Horretarako, biotina eta GFParen aurkako Western plapaketak egin dira (84. irudia). Plapaketa horiek, sinGFP4a-RIP3^{NES}-APEX2 markatzailea biotinilazioa eragiteko gai dela, eta degradatzen ez dela frogatzen dute. Beraz, sinGFP4a-RIP3^{NES}-APEX2 markatzaile zitoplasmatiko moduan onartu da, eta hemendik aurrera, **APEX2zit** bezala izendatuko da.

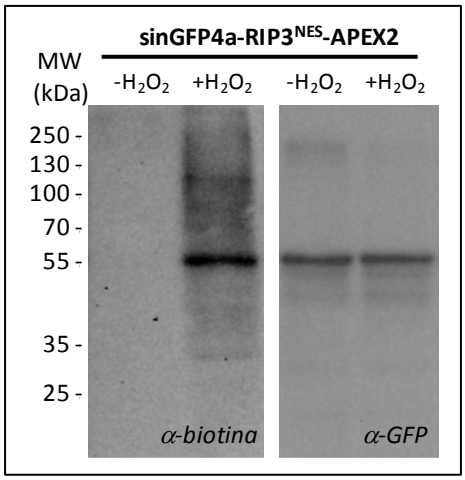

84. irudia: sinGFP4a-RIP3^{NES}-APEX2 proteinaren bidezko biotinilazioa. sinGFP4a-RIP3^{NES}-APEX2 HEK293T zelulatan gainadierazi, PGBa eragiteko protokoloa jarraitu, eta jasotako proteina erauzkinekin biotina zein GFParen aurkako Western plapaketak egin dira. Biotinaren aurkako plapaketan APEX2ren peroxidasa aktibitatea aktibatzean (+H_2O_2) tamaina ezberdinetako proteina bilduma zabala biotinilatu dela adierazten duen banda multzoa detektatu da. GFParen aurkako plapaketan aldiz, gainadierazitako proteinari dagokion banda nabarmena (~ 55 kDa) baino ez da agertu.

4.2.2.1.2. APEX2 nukleora ituratzeko plasmidoa: diseinua eta sortutako markatzaileen kokapena eta aktibitatearen baliozkotzea

APEX2 proteina nukleoan kokatzeko estrategia, APEX2 SV40 birusaren T antigeno luzearen NLSaren (Kalderon et al., 1984a, 1984b) zenbait kopiarekin fusionatzea izan da. Lehen saiakera batean, bi NLS, YFP eta APEX2 entzima dituen fusio-proteina eratu da (85A irudia). HEK293T zelulatan gainadieraztean (85B irudia), proteina horrek kokapen nukleozitoplasmatikoa erakutsi du.

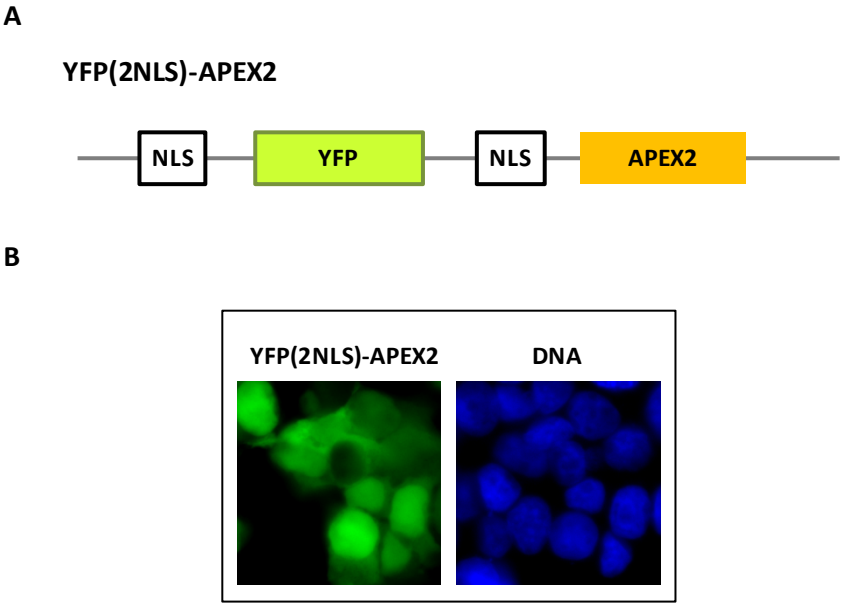

85. irudia: YFP(2NLS)-APEX2 proteinaren eskema eta kokapenaren azterketa. A. YFP(2NLS)-APEX2 proteinaren eskema. B. YFP(2NLS)-APEX2 HEK293T zelulatan gainadieraztean hartzen duen kokapen nukleozitoplasmatikoaren irudi adierazgarriak. Proteina horrek kokapen gehienbat nuklearra erakusten badu ere, gainadierazitako proteinaren frakzio handi bat zitoplasman geratzen da. Argazkiak Axioskop mikroskopioarekin egin dira.

Bigarren saiakera batean, lau NLS kopiadun YFP(4NLS)-APEX2 fusio-proteina sortu da (86A irudia). Proteina hori HEK293T zelulatan gainadieraztean (86B irudia), proteina guztiz nuklearra dela baieztatu da.

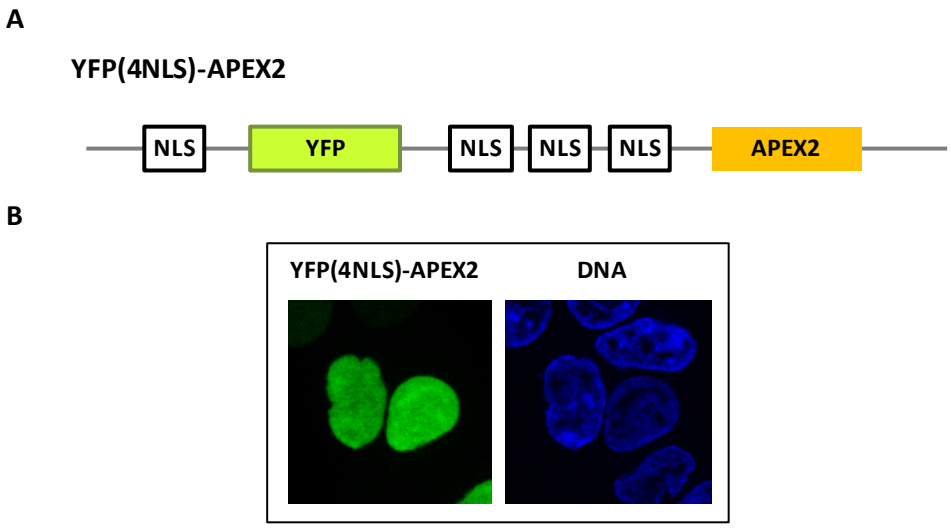

86. irudia: YFP(4NLS)-APEX2 proteinaren eskema eta kokapenaren azterketa. A. YFP(4NLS)-APEX2 proteinaren eskema. B. YFP(4NLS)-APEX2 HEK293T zelulatan gainadieraztean hartzen duen kokapen nukleozitoplasmatikoaren irudi adierazgarriak. YFP(4NLS)-APEX2 proteinak kokapen guztiz nuklearra erakusten du.

YFP(4NLS)-APEX2 proteinaren PGBa eragiteko gaitasuna biotinaren aurkako Western plapaketaren bidez aztertu da (87. irudia). APEX2 entzimaren peroxidasa aktibitatea aktibatutako laginean, proteina endogeno bilduma zabala biotinilatu dela behatzen da. Gainera, YFParen aurkako plapaketan YFP(4NLS)-APEX2 egonkorra dela ikusten da. Hori horrela, YFP(4NLS)-APEX2 markatzailea erabiltzea erabaki da, eta hemendik aurrera **APEX2nuk** bezala izendatuko da.

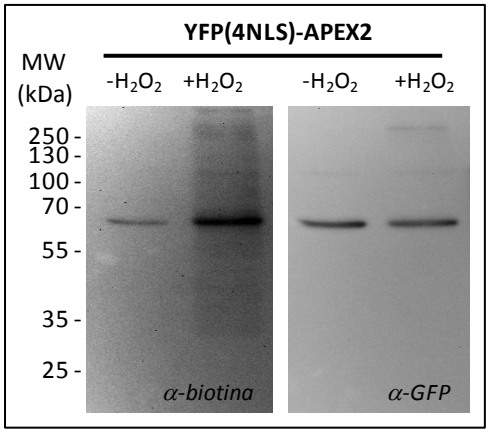

87. irudia: YFP(4NLS)-APEX2 proteinaren bidezko biotinilazioa. YFP(4NLS)-APEX2 HEK293T zelulatan gainadierazi, PGBa eragiteko protokoloa jarraitu eta jasotako proteina erauzkinekin Western plapaketak egin dira. Biotinaren aurkako plapaketan APEX2ren peroxidasa aktibitatea aktibatu ez denean ($-H_2O_2$), gainadierazitako proteinari dagokion banda bakarra ageri da (~ 65 kDa), aktibatutako egoeran ($+H_2O_2$) berriz, tamaina ezberdineko proteinei dagozkien hainbat banda ikus daitezke. Bestalde, YFParen aurkako plapaketan (GFParen aurkako antigorputza erabili da, zeinak YFPa ere ezagutzen duen), APEX2aren peroxidasa aktibitatea aktibatu edo ez, gainadierazitako proteinari dagokion banda nabarmena ageri da bakarrik.

4.2.2.2. Hurbilketa baliozkotzeko kontzeptu-froga erako esperimentua

CRM1en inhibizioak zitoplasma eta nukleoko proteometan eragiten dituen aldaketak ikertzeko, APEX2an oinarritutako konpartimentu-espezifikoko PGBa eta CRM1en inhibizioa konbinatu dira. Horretarako, HEK293T zelulak APEX2zit edo APEX2nuk plasmidoekin transfektatu dira. Markatzaile bakoitza hiru egoera ezberdinetan erabili da (88A irudia): (i) markaketaren kontrol negatibo bezala erabili den lagin bat, non, CRM1 aktiboa den eta APEX2 ez den aktibatu (-LMB/-H_2O_2), (ii) "egoera basala" izena eman zaion lagin bat, non, bai CRM1 eta bai APEX2 aktiboak diren (-LMB/+H_2O_2), eta (iii) "CRM1 inhibitutako egoera" izena eman zaion lagin bat, non, CRM1 inhibiturik dagoen eta APEX2 aktibo (+LMB/+H_2O_2).

Sei egoera esperimental horietako laginak prestatu dira, eta egoera bakoitzean biotinilatutako proteinak neutrabidina-agarosa bihitxoekin isolatu dira. Biotinaren kontrako Western plapaketa erabiliz (88B irudia), APEX2 aktibatutako laginetan proteinen biotinilazioa eman dela, eta biotinilatutako proteinak modu eraginkorrean isolatu direla egiaztatu da.

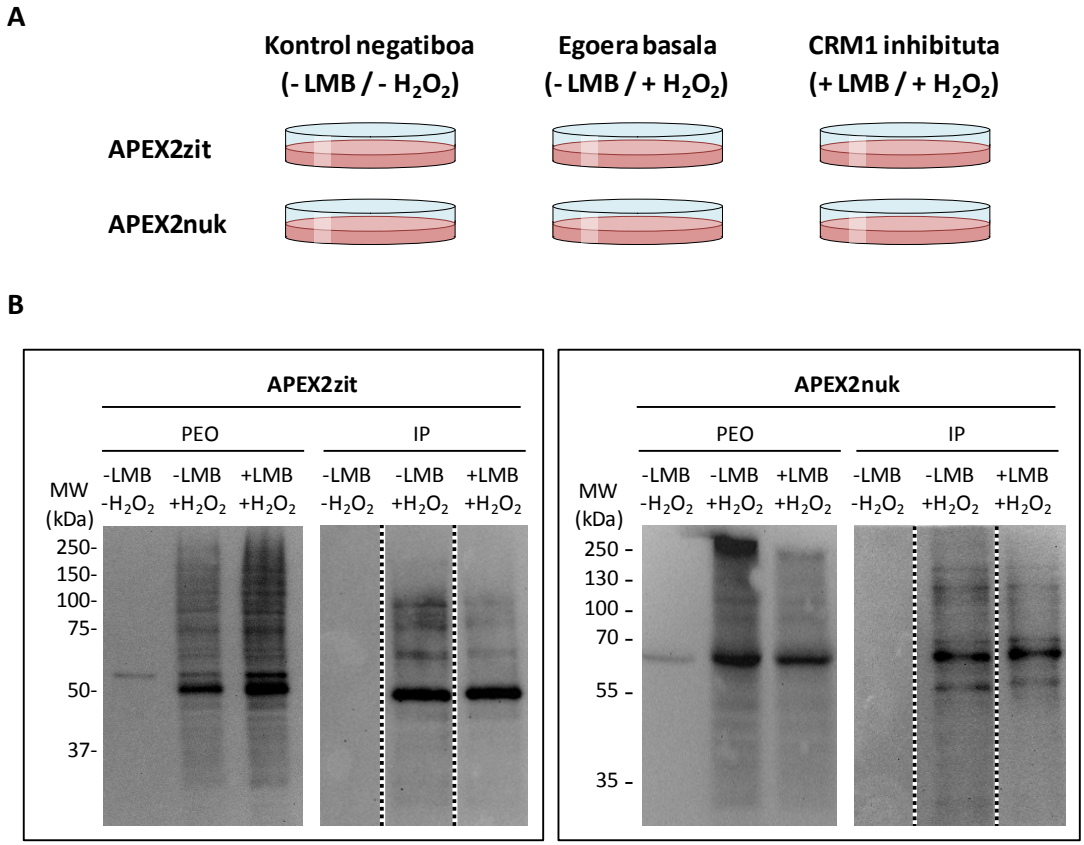

88. irudia: Proteomika analisirako erabiliko diren laginen egokitasuna berrestea. A. Proteomika analisirako erabiliko diren egoerak. Egoera bakoitza HEK293T zelulekin ereindako 10 cm-ko plaka banatan prestatu da. B. APEX2zit zein APEX2nuk adierazten duten proteina erauzkin osoekin (PEO) eta immunoprezipitazioan isolatutako proteinekin (IP) eginiko biotinaren aurkako Western plapaketak. PEO paneletan proteinen biotinilazio eraginkorra eman dela beha daiteke, IP paneletan aldiz, neutrabidina-agarosa bihitxoekin biotinaz markatutako proteinak isolatzeko prozesua eraginkorra izan dela. IP paneletan kaleak puntukako marraz banaturik daude, mintza moztu egin dela adierazteko.

Immunoprezipitazioan jasotako laginen egokitasuna berretsita, horiek kontzentratu eta SDS-PAGE bidez banatu dira. Gelak *Coomassie-z* tindatu, eta bestelako proteinen identifikazioa oztopa ez dezaten, APEX2dun fusio-proteinei, abidinari eta fronteari dagozkien bandak baztertu dira (89. irudia). Lagin bakoitzetik lortutako hiru zatiak UPV/EHU SGIker Proteomika zerbitzuan likido-kromatografia tandem masa-espektrometria (LC-MS/MS) erabiliz analizatu dira.

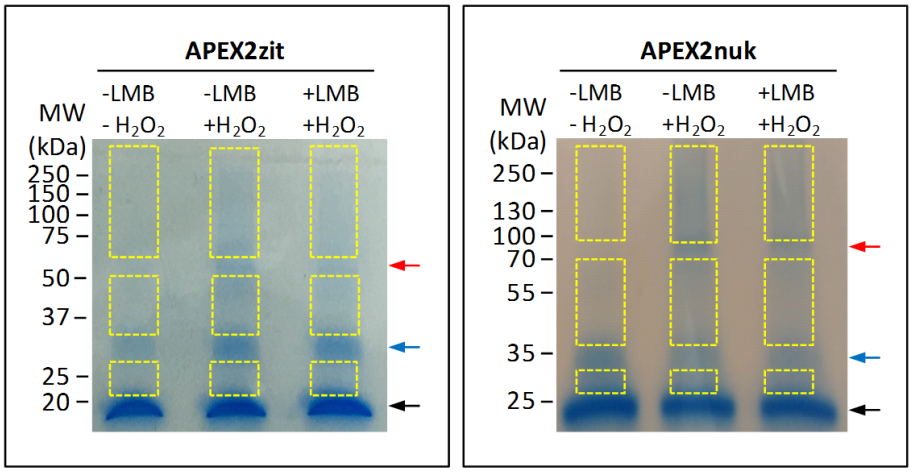

89. irudia: APEX2zit eta APEX2nuk laginen MS/MS analisirako prestaketa. Neutrabidinarekin afinitatez purifikatutako proteinak SDS-PAGE bidez banatu dira. Gelak *Coomassie* tindaketaren bidez tindatu, eta frontea (gezi beltza), abidinaren banda (gezi urdina), eta gainadierazitako APEX2dun markatzaileen bandak (gezi gorria) baztertu ostean, laukizuzen horiz adierazitako gel zatiak moztu dira. Laginok UPV/EHUko SGIker Proteomika zerbitzuan masa-espektrometriaz analizatu dira.

4.2.2.2.1. MS/MS analisien emaitzak (i): kontsiderazio orokorrak

MS/MS analisian guztira 2503 proteina ezberdin identifikatu dira. Horietatik, 1489 zorroztasun irizpideak kontuan hartuta identifikatu dira, hau da, gutxienez bi peptidorekin eta 0 baino intentsitate altuagoaz (21. taula). Markatzaile bakoitzarekin identifikatutako proteina kopurua antzekoa izan da: 1248 proteina APEX2zit markatzailearekin, eta 1318 APEX2nuk markatzailearekin. Identifikaziorako zorroztasun irizpideak aplikatuz gero, kopuru horiek 876 eta 952 izan dira hurrenez hurren. Era berean, egoera basalean (-LMB), zein CRM1 inhibitutako egoeran (+LMB), identifikatutako proteina kopurua ere antzekoa izan da: 1884 (zorroztasun irizpideak aplikatuz gero, 1451) egoera basalean, eta 1757 (zorroztasun irizpideak aplikatuta 1362) CRM1 inhibitutako egoeran.

21. taula: MS/MS analisiaren laburpena. Guztira identifikatutako proteinen kopurua, eta parentesi artean, zorroztasun irizpideak aplikatutakoan identifikatutakoena erakusten da. "Orotara" izeneko zutabe eta lerroan, identifikatutako proteinen batura ez erredundantea erakusten da.

	APEX2zit	APEX2nuk	Orotara
-LMB	1157 (842)	1195 (931)	1884 (1451)
+LMB	995 (767)	1156 (882)	1757 (1362)
Orotara	1248 (876)	1318 (952)	2503 (1489)

Egoera ezberdinetan identifikatutako proteina kopurua antzekoa izateak markatzaile bien aktibitate biotinilatzailea antzekoa dela, eta LMB tratamenduak ez duela aktibitate hori nabarmen eraldatzen iradokitzen du. Horrez gain, emaitza horiek lagin guztien prozesamendua antzekoa izan dela, eta arazo tekniko larririk egon ez dela bermatzen dute.

4.2.2.2.2. MS/MS analisien emaitzak (ii): konpartimentu-espezifikoko proteinen identifikazioa egoera basalean (-LMB)

APEX2zit markatzaileak biotinilatutako proteinak zitoplasmakoak direnetz, eta APEX2nuk markatzaileak biotinilatutakoak nukleokoak direnetz aztertu da. Lehenik eta behin, egoera basalean (-LMB) markatzaile bakoitzarekin eta zorroztasun irizpideak kontuan hartuta identifikatutako proteinak erkatu dira (90A irudia). Proteina gehienak, proteina erauzkin bakarrean identifikatu dira, 520 proteina APEX2zit erauzkinean eta 609 proteina APEX2nuk erauzkinean. Aurreikusi bezala, badaude markatzaile biekin identifikatu diren eta zelulan kokapen nukleozitoplasmatikoa izatea espero den hainbat proteina, 322 proteina hain zuzen ere. Emaitza horrek, APEX2zit eta APEX2nuk markatzaileek duten kokapen nukleozitoplasmatiko ezberdinari esker, proteina bilduma ezberdina biotinilatzeko gai direla erakusten du.

Jarraian, eta UniProtKB datu-basea erabilita, analisi honetan identifikatutako proteinak aurretik zein kokapenetan deskribatu diren aztertu da (90B irudia). APEX2zit erauzkinean identifikatutako proteinen % 65 zitoplasmatiko (edo zitoplasmatiko eta nuklear) gisara dago deskribatuta UniProtKBn; APEX2nuk erauzkinari dagokionez, identifikatutako proteinen % 71 nuklear (edo zitoplasmatiko eta nuklear) gisara.

Lortutako emaitzek beraz, agerian uzten dute APEX2zit eta APEX2nuk markatzaileak konpartimentu-espezifikoko proteinen biotinilaziorako markatzaile baliagarriak direla.

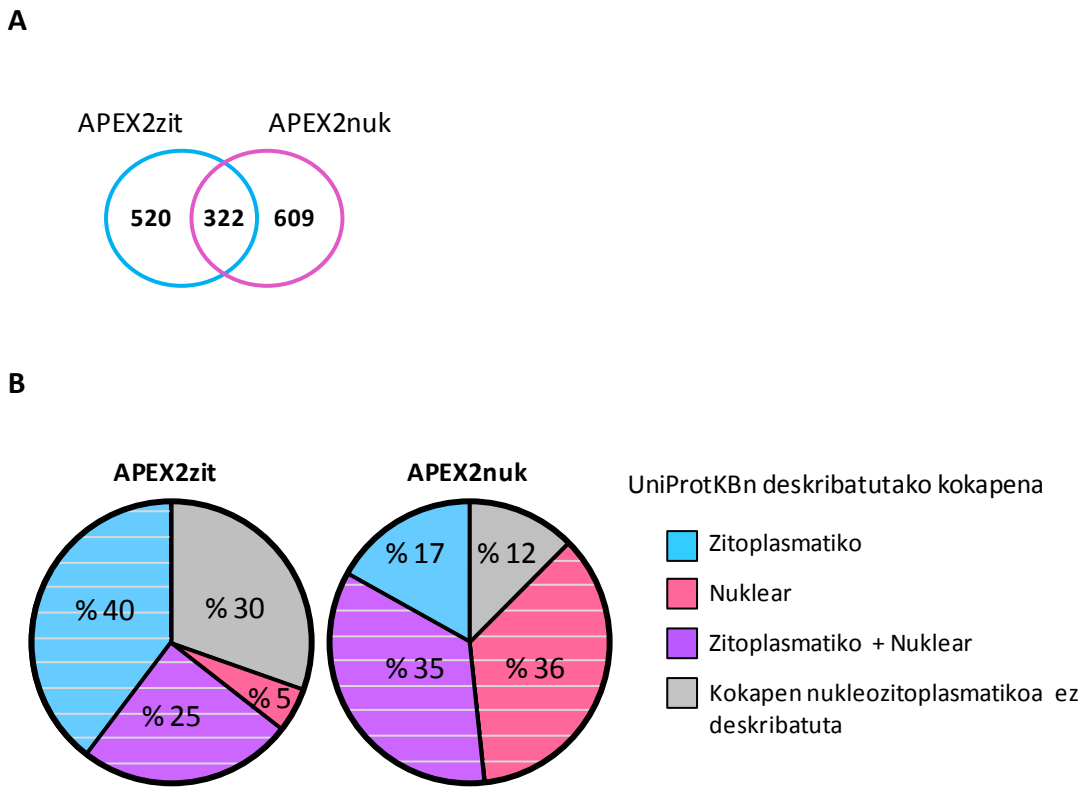

90. irudia: APEX2zit eta APEX2nuk markatzaileak konpartimentu-espezifikoko PGBrako baliagarriak dira. A. Egoera basalean APEX2zit eta APEX2nuk markatzaileak erabiliz identifikatutako proteinen Venn diagrama. B. Ikerketa honetan identifikatutako proteinek UniProtKB datu-basearen arabera duten kokapena erakusten duten sektore-diagramak. Lan honetan egindako analisiaren araberako kokapenek eta UniProtKBren araberakoek bat egiten dute ehuneko handi batean (marra horizontalek adierazita).

4.2.2.2.3. MS/MS analisien emaitzak (iii): CRM1en inhibizioak nukleo eta zitoplasmako proteometan duen eragina eta balizko kargoen identifikazioa

CRM1en inhibizioaren ondorioz, CRM1en kargoek zitoplasmatik nukleoranzko kokapen aldaketa oso edo partzial bat jasatea espero da. Jasaten duten lekualdaketaren arabera, eta analisia errazteko helburuz, tesi honetan kargoak hiru kategoriatan sailkatu dira (91. irudia). *Kargo prototipikoak* egoera basalean kokapen guztiz zitoplasmatikoa eta CRM1 inhibitzean kokapen guztiz nuklearra duten proteinak dira. *Muturreko kargo ez-prototipikoak*, egoera basalean kokapen guztiz zitoplasmatikoa eta CRM1 inhibitzean kokapen nukleozitoplasmatikoa, edo egoera basalean kokapen nukleozitoplasmatikoa eta CRM1 inhibitzean kokapen guztiz nuklearra dutenak dira. Azkenik, *tarteko kargo ez-prototipikoak* egoera basal zein CRM1 inhibitutako egoeran kokapen nukleozitoplasmatikoa duten proteinak dira, zeintzuetan CRM1en inhibizioak kokapen nuklearragoa eragiten duen.

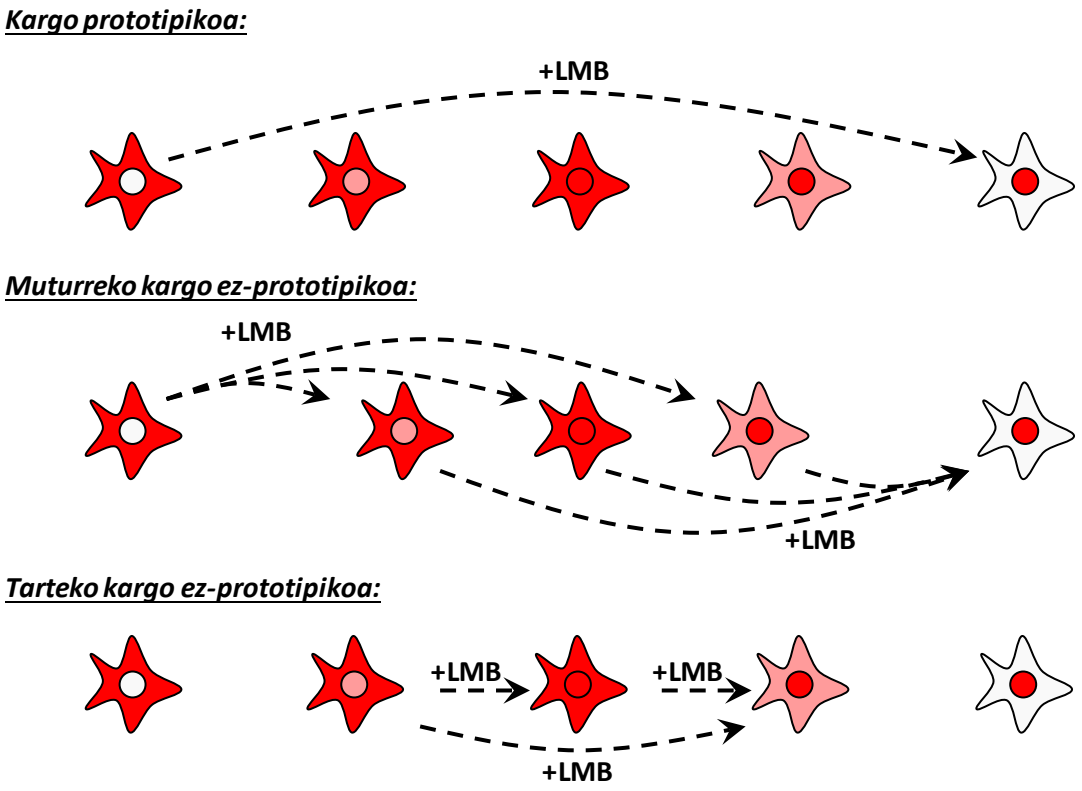

91. irudia: Tesi honetan analisi proteomikoen emaitzak aztertzeko definitutako CRM1en kargoen sailkapena. Egoera basalean erakusten duten kokapenaren eta LMB tratamenduak (geziez adierazita) eragindako nukleoranzko lekualdaketaren arabera CRM1en kargoak hiru kategoria ezberdinetan sailkatu dira. *Kargo prototipikoak,* egoera basalean guztiz zitoplasmatikoak eta CRM1 inhibitzean (+LMB) guztiz nuklearrak diren proteinak dira. *Muturreko kargo ez-prototipikoak,* egoera basalean kokapen guztiz zitoplasmatikoa agertzen duten eta CRM1 inhibitzean (+LMB) nukleo zein zitoplasman agertzen diren, edo egoera basalean nukleo zein zitoplasman agertzen diren eta CRM1 inhibitzean (+LMB) kokapen guztiz nuklearra agertzen duten proteinak dira. Eta azkenik, *tarteko kargo ez-prototipikoak* bai egoera basalean, bai CRM1 inhibitutako egoeran (+LMB), kokapen nukleozitoplasmatikoa agertzen dutenak dira, betiere, nukleoranzko lekualdaketa gertatzen bada.

Sailkapen hori bereziki da garrantzitsua hemen planteatutako lanean. Izan ere, aurkeztutako kontzeptu-froga erako esperimentuan egoera bakoitzeko lagin bana erabili da, eta beraz, ezin da proteomika kuantitatiboko analisirik egin. Ondorioz, atal honetan kargo prototipikoak eta muturreko kargo ez-prototipikoak baino ez dira bilatuko.

Kargo prototipikoak bilatzeko, 92. irudiko estrategia jarraitu da. Hau da, egoera basalean (-LMB) soilik APEX2zit markatzailea erabilita biotinilatzen diren proteinak, eta CRM1 inhibitzean (+LMB) soilik APEX2nuk markatzailea erabilita biotinilatzen diren proteinak bilatu dira.

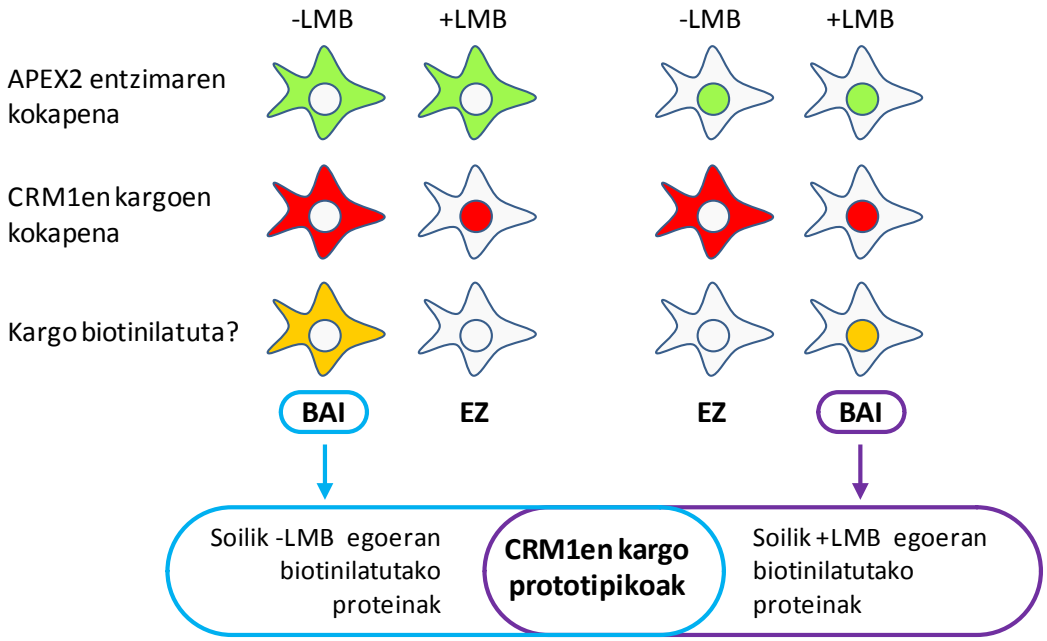

92. irudia: CRM1en kargo prototipikoak konpartimentu-espezifikoko PGBaren bidez identifikatzeko estrategia.

93. irudian ikus daitekeenez APEX2zit markatzailearekin egoera basalean esklusiboki 253 proteina identifikatu dira, eta APEX2nuk markatzailearekin CRM1 inhibitutako egoeran 123 dira esklusiboki identifikatutakoak. Proteina multzo horietan komunak diren proteinak lau dira: LIMD1 (*LIM domain containing protein 1*), TUBAL3 (*tubulin alpha chain-like 3*), SBSN (*suprabasin*) proteinaren bigarren isoforma eta CK2α' (*casein kinase II subunit alpha'*). Lau proteina horiek beraz, analisi honetan CRM1en balizko kargo prototipiko gisa identifikatu dira.

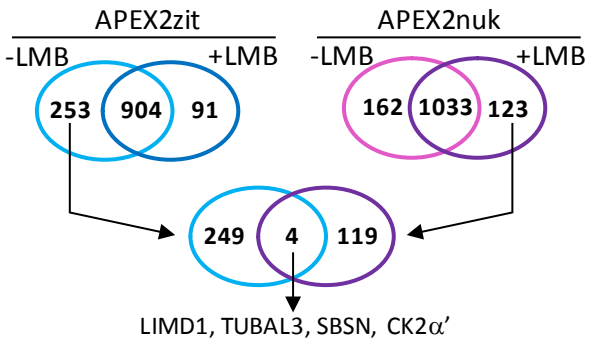

93. irudia: CRM1en balizko kargo prototipikoen identifikazioa. Egoera basalean (-LMB) eta CRM1 inhibitutako egoeran (+LMB) APEX2zit eta APEX2nuk markatzaileak erabiliz identifikatutako proteinak erkatzen dituzten Venn diagramak. Soilik APEX2zit markatzailearekin egoera basalean, eta soilik APEX2nuk markatzailearekin CRM1 inhibitutako egoeran identifikatutako proteinak erkatzean (beheko aldea) CRM1en lau balizko kargo aurkitzen dira: LIMD1, TUBAL3, SBSN eta CK2α'.

Kargo prototipikoez gain, balizko muturreko kargo ez-prototipikoak ere bilatu dira (94. irudia). Horretarako, batetik, egoera basalean soilik zitoplasman eta CRM1 inhibitutako egoeran nukleoan eta zitoplasman aurkitzen diren proteinak bilatu dira, eta bestetik, egoera basalean nukleoan eta zitoplasman, eta CRM1 inhibitutako egoeran soilik nukleoan agertzen direnak bilatu dira. Era horretan, 89 proteina identifikatu dira (26. taula gehigarria).

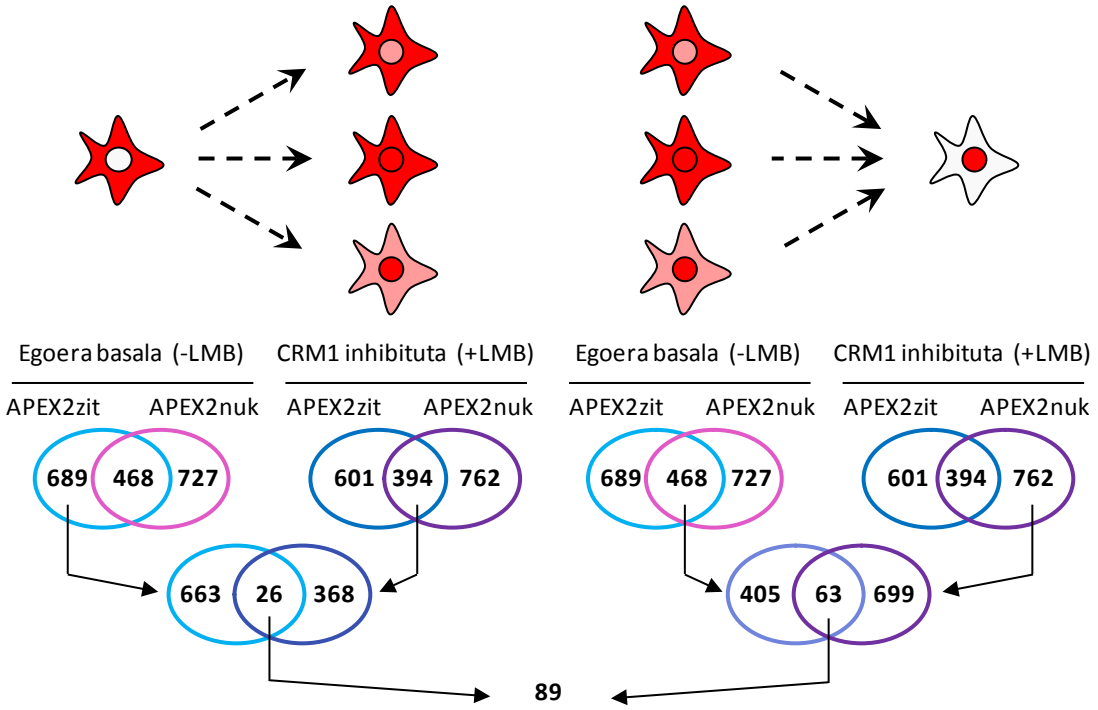

94. irudia: CRM1en balizko muturreko kargo ez-prototipikoen identifikazioa. Ezkerraldean, egoera basalean (-LMB) soilik APEX2zit markatzailearekin identifikatu diren proteinen bilduma, eta CRM1 inhibitzean (+LMB) APEX2zit zein APEX2nuk markatzaileekin identifikatu diren proteinen bilduma erkatu eta 26 proteina komun aurkitu dira. Eskuinaldean, egoera basalean (-LMB) APEX2zit zein APEX2nuk markatzaileekin identifikatu diren proteina bilduma, eta CRM1 inhibitzean (+LMB) APEX2nuk markatzailearekin bakarrik identifikatu diren proteinen bilduma erkatu eta 63 proteina identifikatu dira. Erkaketa bi horietan identifikatutako proteinak batuz analisi honetan identifikatutako kargo ez-prototipikoen bilduma lortzen da, 89 proteina alegia.

Guztira, kargo prototipikoak (ikusi 93. irudia) eta muturreko kargo ez-prototipikoak (ikusi 94. irudia) kontuan hartuta, 93 balizko kargo identifikatu dira. Kargo horietako zenbait CRM1en kargo gisa deskribatuta daude jada, esaterako, LIMD1 (Sharp et al., 2004;), TUBAL3 (Schwarzerová et al., 2019), SNUPN (*snurportin 1*) (Paraskeva et al., 1999), HDAC1 (*Histone deacetylase 1*) (Kim et al., 2010), edota RanGAP1 (*Ran GTPase-activating protein 1*) (Cha et al., 2015). Balizko kargoetako zenbait jada kargo lez identifikatuta egoteak, erabilitako prozedura eta estrategiaren baliozkotasuna bermatzen dute.

4.2.2.2.4. Balizko kargo berriak berresteko analisiak

Aurkeztutako analisi honetan balizko kargo prototipiko gisa identifikatutako SBSN eta CK2α' proteinak CRM1en kargoak direnik ez dago frogatuta. Hori ikertzeko SBSN eta CK2α' proteinak Myc epitopoarekin fusionatu, HEK293T zelulatan gainadierazi eta euren kokapena CRM1 aktibo edo inhibiturik dagoenean aztertu da. Myc-SBSN proteinaren kokapenak ez du CRM1en mendekotasunik agertzen (95. irudia); Myc-SBSN zitoplasman eta jariatze-besikulak izan daitezkeen egituretan metatzen da egoera basalean zein CRM1 inhibiturik dagoenean. Behatutako kokapen hori literaturan deskribatutakoarekin bat dator, SBSN jariatze-proteina legez deskribatuta baitago (Matsui et al., 2004; Moffatt et al., 2004).

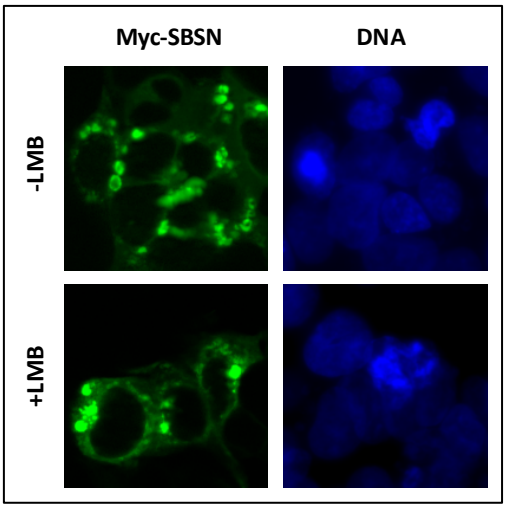

95. irudia: Myc-SBSN LMBrekin tratatu (+LMB) edo tratatu gabeko (-LMB) HEK293T zelulatan gainadieraztean hartzen duen kokapenaren irudi adierazgarriak.

Myc-CK2α'ri dagokionez, egoera basalean (-LMB) zein CRM1 inhibiturik dagoenean (+LMB) kokapen nukleozitoplasmatikoa agertzen du (96. irudia). Alabaina, laginak behatzean LMB tratamenduak nukleoranzko nolabaiteko lekualdaketa txikia eragin dezakeela antzematen da. Kokapen aldaketa hori irudi-analisi semi-kuantitatiboa eginez egiaztatu da. Gauzak horrela, CK2α' proteina CRM1en kargo berri lez proposatzen da hemen.

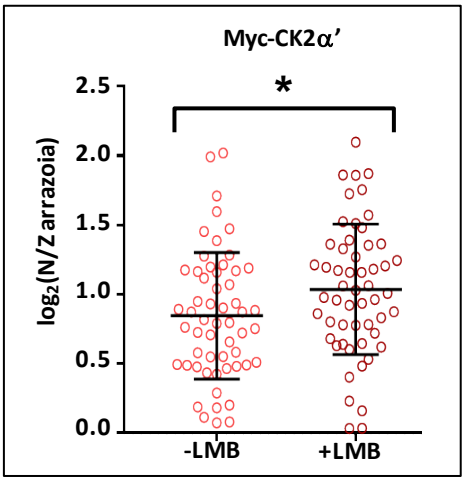

96. irudia: Gainadierazitako Myc-CK2α' proteinaren kokapen nukleozitoplasmatikoaren analisi semi-kuantitatiboaren emaitza erakusten duen grafikoa. Myc-CK2α' proteina HEK293T zelulatan gainadieraztean erakusten duen kokapen nukleozitoplasmatikoa irudi-analisiaren bidez aztertu da. Zirkulu bakoitzak zelula bakar baten nukleoan antzematen den fluoreszentziaren eta zitoplasman antzematen denaren arrazoia 2 oinarriko logaritmoan $\log_2$(N/Z arrazoia) adierazten du. Lagin bakoitzaren $\log_2$(N/Z arrazoia)-ren batez bestekoa eta desbiderapen estandarrak adierazten dira. Bi laginetako zeluletan Myc-CK2α' proteinak kokapen gehienbat nuklearra [$\log_2$(N/Z arrazoia)> 0] erakusten badu ere, CRM1en inhibizioak CK2α' nukleoan egoera basalean baino gehiago metatzea eragiten du (*p=0,0228; Mann-Whitney U test).

Laburbilduz, aurkeztutako kontzeptu-froga esperimentuan lortutako emaitzek, tesi honetan garatutako konpartimentu-espezifikoko PGB hurbilketa CRM1en inhibizioaren efektua eta haren kargoak bilatzeko erabilgarria dela iradokitzen dute.

5. Eztabaida

Eztabaida hau bi atal nagusitan banatu da. Lehen atalean, CRM1en funtzionamenduaren aspektu fisiologikoak jorratu dira, hala nola, CRM1en mendeko NES berriak bilatu eta karakterizatzean eginiko aurkikuntzak, zein CRM1en mendeko NESen esportazioaren ingurukoak. Bigarren atala, aldiz, patologian ardaztutako ikerketetan jasotako emaitzen inguruko eztabaidari dagokio. Kasu honetan, CRM1 minbiziari aurre egiteko itu gisa duen papera aztertu da, selinexor eta beste farmako batzuen konbinazio berriak ezbaian jarri dira, eta CRM1en inhibizioak haren esportoman eragiten duen efektua aztertzeko konpartimentu espezifikoko proteinen biotinilazioaren erabilgarritasuna ere eztabaidatu da.

5.1. CRM1en mendeko NES motiboen eta horiek CRM1ekin eratzen duten elkarrekintzaren inguruko ikerketak

5.1.1. NES berrien identifikazioa Rev(1.4)-GFP esportazio-entsegua erabiliz

Orain arte, USP12 deubikuitinasaren kokapen nukleozitoplasmatikoa ikergai duten hainbat lan argitaratu dira. Batzuetan USP12 gehienbat zitoplasmatikoa dela baieztatzen da (Sowa et al., 2009; Urbé et al., 2012; Burska et al, 2013; Lehoux et al., 2014; Olazabal-Herrero et al., 2015), beste batzuetan, ordea, gehienbat nuklearra dela (Joo et al., 2011). Kontrajarritako emaitza horiek bateragarriak direla ikusi izan da ikerketa berriagoetan. Izan ere, giza zein legami USP12 proteinak gaineztadura nuklearrean zehar aurrera eta atzera mugitzen diren CRM1en kargoak direla ikusi da (Kouranti et al., 2010; Jahan et al., 2016). Tesi honetan lortutako emaitzek, USP12ren kokapena, eta haren kofaktore diren WDR20 eta DMWD proteinen kokapena ere, CRM1en mendekoa dela egiaztatu dute. Aipatu beharra dago, CRM1en inhibizioak ez duela ez USP12 ez bere kofaktoreak esklusiboki nukleoan metatzea eragiten. Hori, proteina horiek nukleora eramango lituzkeen NLS indartsurik ez izateagatik gerta daiteke. USP12ren kasuan, NLS aktiborik ez ote duen egiaztatzeko, SV40 birusaren T antigeno luzearen bi NLS kopiarekin fusionatu da (YFP-USP12$^{[2NLS]}$), eta proteina hori nukleoan metatzen dela behatu da. DMWDren kasuan, NLS indartsuaren gabeziaz gain, zitoplasman bahiturik geratzen dela dirudi, izan ere, bere kasuan, CRM1 inhibitzean ematen den nukleoranzko lekualdaketa bereziki ahula da.

Emaitza horiek ikusita, USP12, eta harekin konplexua eratzen duten bestelako proteinak nukleora difusioz edo beste proteina baten NLSaz baliatuz, ingelesez *piggyback* izenez ezagutzen den mekanismoaren bidez, inportatzen direla planteatzen da hemen. Bada, aurretik ere, USP12ren inportazioa giza papilomabirusaren E1 proteinak bultza dezakeela deskribatu da (Lehoux et al., 2014). Argitaratutako informazio hori guztiz argitzeko, giza papilomabirusak

infektatu gabeko zeluletan USP12ren inportazioa bultza dezaketen proteinak bilatzeko esperimentu gehiago egin beharko lirateke.

Behin USP12 barne duten konplexuak nukleo eta zitoplasmaren artean garraiatzen direla baieztatuta, nukleotik zitoplasmaranzko esportazioa egikaritzen duten NES motiboak bilatu dira. Aipatu beharra dago, tesi honetan Rev(1.4)-GFP esportazio-entseguaren eta iturratutako mutagenesiaren bidez lortutako emaitzek, Sanyal eta lankideek proposaturiko NES motiboa (Jahan et al., 2016; Sanyal, 2016) aktiboa ez dela eta USP12/UAF1/WDR20 konplexuaren esportazioa WDR20 proteinan aurkitutako NES berriaren bidez ematen dela erakutsi dutela. NES berri horrek WDR20ren homologoa den DMWD proteinan aurkitu denarekin antzekotasun nabaria du, batez ere C-muturrean. Hala ere, WDR20 proteinaren NESa, CRM1 inhibitzean ikusitakoarekin bat eginez, DMWDrena baino nabarmen aktiboagoa da. WDR20 proteinak DMWDk baino NES aktiboagoa izatea, WDR20 zitoplasman bahituta ez geratzearen, eta beraz, zelulak berau esportatzeko behar altuagoa izatearen ondorio izan daiteke.

Tesi hau burututako taldean jasotako beste emaitza batzuek WDR20 proteinak USP12ren eta UAF1en mintz plasmatikoko kokapena erregulatzen duela erakutsi dute (Olazabal-Herrero et al., 2019). Emaitza hori eta tesi honetan aurkeztutako emaitzak konbinatuta, ondorengo eredua sortu da (97. irudia). Eredu horretan USP12/UAF1/WDR20 konplexua mintz plasmatiko, zitoplasma eta nukleoaren artean dinamikoki mugitzeko ahalmena duela erakusten da. Ahalmen hori ezinbestekoa izan daiteke konplexu deubikuitinatzaileak kokapen zelular ezberdina duten substratuetara hel daitezen.

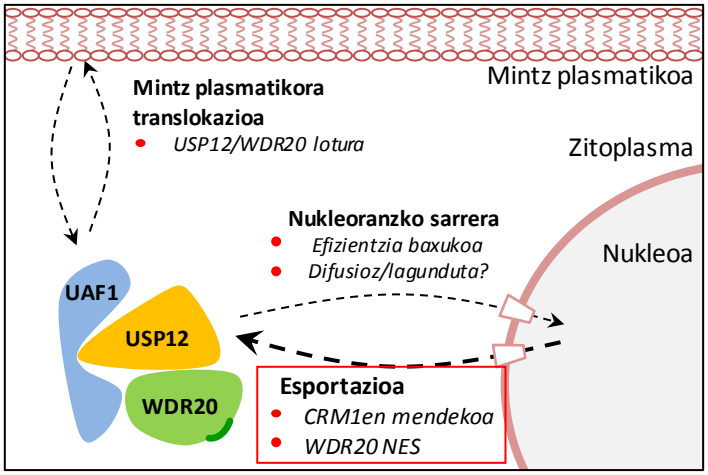

97. irudia: USP12/UAF1/WDR20 konplexuaren kokapen dinamikoa proposatzen duen eredua. USP12/UAF1/WDR20 konplexua mintz plasmatiko, zitoplasma eta nukleoaren artean lekualdatzen da. Nukleoranzko sarrera ez da prozesu oso efizientea, eta badirudi difusioz edo beste proteina baten NLSaz lagunduta gertatzen dela. Bestetik, esportazioa zein mintz plasmatikorako translokazioa, prozesu askoz ere efizienteagoak dira. Bi prozesu horiek WDR20 proteinak gidaturik daude. Tesi honetan esportazioa izan da sakontasunean ikertu den prozesua (karratu gorriaz adierazita), eta hori, WDR20 proteinan zehaztasunez karakterizatu den CRM1en mendeko NES batean (berde ilunaz adierazita) dago oinarriturik.

Rev(1.4)-GFP esportazio-entsegua USP12, WDR20 eta DMWD proteinen NES motibo kandidatuen esportazio-ahalmena aztertzeko erabiltzeaz gain, minbizi-esportomako NES kandidatuak (cNES) bilatzeko ere erabili da. Bilaketa horren lehen urratsa *in silico* egin da NES-iragarleen bidez. Aipatu beharra dago, modu honetan cNESak bilatzen direnean, ohikoena, *plus* erakoak bakarrik bilatzea izaten dela, kasu honetan, ordea, *plus* zein *minus* erakoak (Fung et al., 2015) bilatu dira. Noranzko bietako cNES kopuru antzekoa topatu da, 507 *plus* erakoak eta 481 *minus* erakoak. Iragarritako 988 cNES horietatik 36 hautatu dira (26 *plus* erakoak eta 10 *minus* erakoak) eta Rev(1.4)-GFP esportazio-entsegua erabiliz aktiboak direnetz ikertu da. Guztira, 25 dira NES aktiboak (19 *plus* erakoak eta 6 *minus* erakoak), eta horietatik 19 (13 *plus* eta 6 *minus* erakoak) NES berriak. 19 NES berri horiek, 14 proteina ezberdinetan (SPN90, TFE3, SHIP2, PER1, SEPT6, SIR2, UBR5, FR1OP, AP2B1, IF2B, mTOR, CRTC1, CDC27 eta ZO2) kokatzen dira (98. irudia), eta jada, NESdb datu basearen azken bertsiora (Xu et al., 2012; Fu et al., 2021; http://prodata.swmed.edu/LRNes/index.php) gehitu dira.

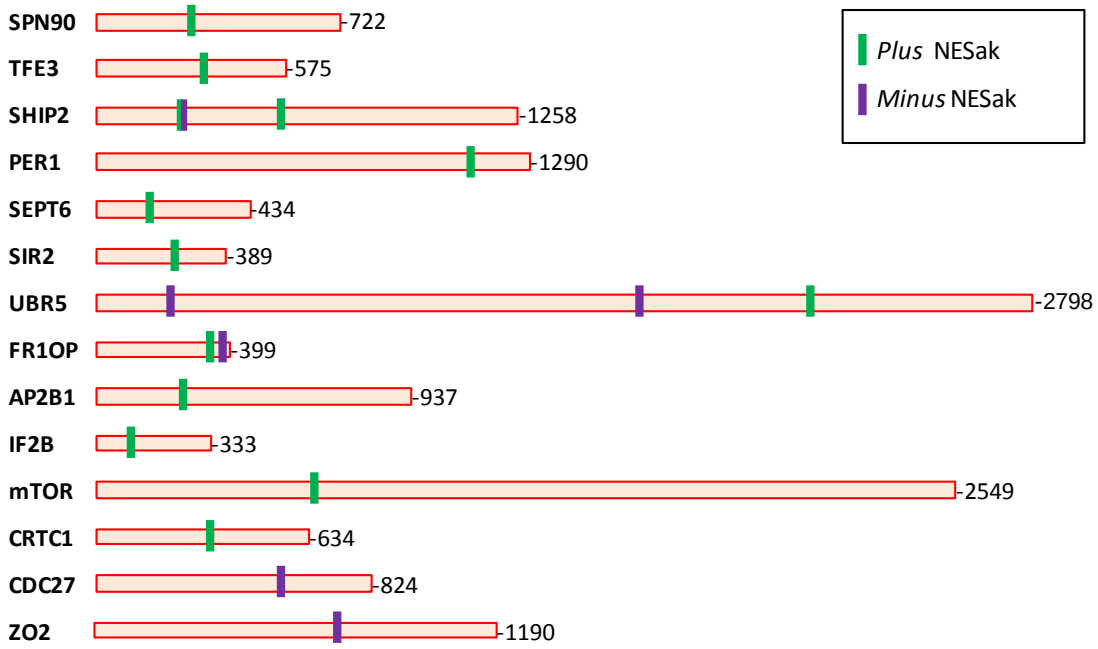

98. irudia: CRM1en minbizi-esportomako proteinetan aurkitutako NES berrien kokapenaren irudi eskematikoa. Guztira 19 NES berri aurkitu dira 14 proteina ezberdinetan; 13 *plus* motakoak, berdez adierazita, eta 6 *minus* motakoak, morez adierazita.

Kirli eta lankideek (2015) eginiko analisi proteomikoan, 14 proteina horiek CRM1en kargo gisara proposatu ziren. Proteina horiek NES aktiboak edukitzeak, CRM1en kargo direlako aukera indartzen du. Halere, aurkitutako NES berriek proteina osoaren testuinguruan duten eginkizuna sakonago ikertu beharko litzateke. Izan ere, baliteke aurkitutako NES horietako batzuek proteina osoren esportaziorik ez eragitea NESa CRM1ekiko eskuragarri ez egoteagatik. CRM1en minbizi-esportomaren azterketan lortutako emaitzen artean, SHIP2 proteinarena da

deigarria oso. Proteina horrek hiru NES motibo aktibo ditu, eta horietatik bi gainjarri egiten dira. Gainjartzen diren motiboak, bata *plus* erakoa (WN6: ^{256}TGEQELESLVLKLSVLKDF^{274}) da, eta bestea, *minus* erakoa (REV5: ^{261}LESLVLKLSVLKDFLSGIQ^{279}). Hori ikusirik, interesgarria izan liteke SHIP2 proteinak CRM1 lotzeko zein egitura hartzen duen aztertzea, eta CRM1ekin duen elkarrekintza 256-279 aminoazido errenkadaren bidez ematen bada, elkarrekintza hori zein noranzkotan ematen den jakitea.

Azpimarratzekoa da, *plus* zein *minus* NESak bilatu izanak, mota bietako NESen aktibitatea lehen aldiz erkatzeko aukera eman duela. Lortutako emaitzen arabera, *plus* NESek esportazio aktibitate altuagoa dute oro har, *minus* erakoak ahulagoak izateko joera dutela iradokiz.

5.1.2. $SRV_{B/A}$ erreportaria: NESak identifikatzeko eta CRM1en mendeko NESen esportazioari buruzko informazio mekanistikoa lortzeko tresna berria

NES berriak identifikatzeko edota CRM1en inhibitzaileen efektua aztertzeko erreportarien kokapenean oinarritutako entsegu zelularrak erabili dira maiz (Henderson eta Eleftheriou, 2000; Fetz et al., 2009; Kehlenbach eta Port, 2016). Bestalde, CRM1en mendeko NESen esportazioaren gainean dagoen ezagutza mekanistiko gehiena *in vitro* eginiko analisi biokimikoetatik eta estrukturaletatik eratorri da (Dong et al., 2009a, 2009b; Monecke et al., 2009, 2013; Güttler et al., 2010; Fox et al., 2011; Dian et al., 2013; Saito et Matsuura, 2013; Fung et al., 2015; 2017). Tesi honetan, NES berriak bilatzeko zein CRM1en mendeko esportazioaren inguruko ezagutza zabaltzeko aukera ematen duen tresna berri bat garatu da, $SRV_{B/A}$ erreportaria alegia (Taylor et al., 2019; Sendino et al., 2020a).

$SRV_{B/A}$ erreportaria, SRV100 erreportarian (García-Santisteban et al., 2016) oinarrituta garatu da. Erreportari berriak, edozein NES kandidatu (cNES) bertan klonatu eta edozein CRM1en aldaerak cNES hori esportatzeko duen gaitasuna ikertzea ahalbidetzen du.

Tesi honetan zehar, CRM1en aldaera/NES konbinazio asko ikertu izan dira, 234 hain zuzen ere. Konbinazio guzti horietan $SRV_{B/A}$ erreportariak erakusten duen kokapen nukleozitoplasmatikoa ebaluatzea lan ikaragarri handia da, are gehiago, kasu honetan bezala, prozesua automatizaturik ez baldin badago. Beraz, eskuz egin beharreko ebaluazio-lan hori errazteko hiru metodo ezberdin erabili dira (ikusi 47.irudia), eta nahiz eta metodook zailtasun maila gero eta handiagoa duten, eta gero eta denbora gehiago eskatzen duten, laginaren deskripzio zehatzagoa eskaintzen dute. Funtsean, metodo guztiekin emaitza bera lortzen da, ezberdintasuna, ordea, metodo bakoitzarekin lortzen den zehaztasun mailan eta emaitza lortzeko behar den denboran dago. $SRV_{B/A}$ esportazio-entsegu bakoitza aztertzeko metodoa

aukeratzeko irizpidea, erreportari bakoitzaren kokapen nukleozitoplasmatikoaren inguruko beharrezko zehaztasun maila izan da.

$SRV_{B/A}$ esportazio-entsegua balioztatzeko lehen urratsa, Rev(1.4)-GFP eta $SRV_{B/A}$ esportazio-entseguetan jasotako emaitzak konparagarriak direnetz aztertzea izan da. Horretarako, Rev(1.4)-GFP esportazio-entseguan ikertutako minbizi-esportomako zenbait NES kandidatu $SRV_{B/A}$ esportazio-entseguan ikertu dira. $SRV_{B/A}$ esportazio-entsegu horiek analisi lehen metodoarekin ebaluatu dira, hau da, erreportariak zelula-populazioan duen kokapena guztiz nuklearretik, guztiz zitoplasmatikora doazen bost kategoriatan sailkatuz. Jasotako emaitzek Rev(1.4)-GFP esportazio-entseguan lortutakoekin emaitzekin korrelazio argia agertzen dute. Hala ere, bategitea ez da erabatekoa, eta badirudi, $SRV_{B/A}$ esportazio-entsegua aproposagoa dela aktibitate altuagoa duten NESak aztertzeko. Batetik, Rev(1.4)-GFP esportazio-entseguak erakusten ez dituen NES indartsuenen arteko ezberdintasunak ikusgarri egiten dituelako, eta bestetik, $SRV_{B/A}$ esportazio-entsegua erabiltzean Rev(1.4)-GFP esportazio-entseguarekin detektagarriak diren NES ahul batzuk ez detektatzea gerta daitekeelako.

Bestalde, CRM1en funtzio fisiologikoak osotasunean ulertzeko, analisi estruktural eta biokimikoetako emaitzen esanahi zelularra aztertzea ezinbestekoa da. Tesi hau aribidean zela, Fu eta lankideek (2018) analisi biokimikoen bidez hainbat NESek CRM1ekiko duten afinitatea (K_d) aztertu, entsegu zelularren bidez NES horien esportazio-aktibitatea ikertu, eta balio biak korrelazio linealean daudela topatu zuten. Ikerketa hartan erabilitako NESak tesi honetan $SRV_{B/A}$ esportazio-entsegua erabilita ikertu dira, eta lortutako SRV balioak eta NES horiek CRM1ekiko duten afinitatea (K_d) ere korrelazio linealean daudela topatu da (99. irudia). Emaitza horrek garatutako esportazio-entsegu berriari bermea ematen dio.

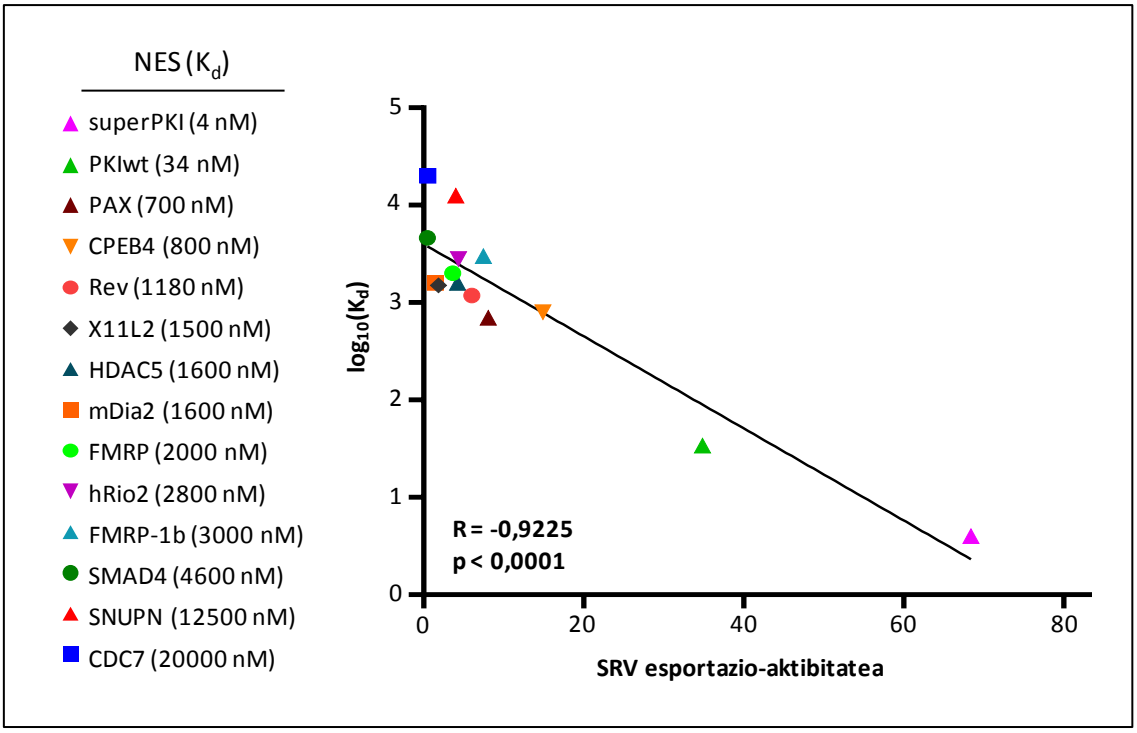

99. irudia: $SRV_{B/A}$ esportazio-entseguan ebaluatutako NESek CRM1ekiko duten afinitatea ($\log_{10}(K_d)$ bezala adierazita) eta erreportari bakoitza bakarrik gainadieraztean lortutako SRV balioak kontrajartzen dituen grafikoa. Aztertutako NESek CRM1ekiko duten afinitatea eta $SRV_{B/A}$ esportazio-entseguan erakutsi duten esportazio-aktibitatea korrelazioan dago. Pearson korrelazioa (R) eta p balioak grafikoan adierazten dira.

Fu eta lankideek (2018) lortutako emaitzekin bat eginez, afinitatearen eta esportazio-aktibitatearen arteko korrelazio nabaria aurkitu da. Hala ere, ikerketa bietan lortutako emaitzak alderatuz gero, euren artean ezberdintasunak badaudela nabaria da. Esaterako, Fu eta lankideek (2018) HeLa zelulatan egindako esportazio-entseguan, CRM1ekiko afinitate oso altua duen superPKI NES artifizialak ez zuen esportazio-aktibitaterik erakutsi. $SRV_{B/A}$ entsegua erabiliz aztertzerakoan, ordea, SRV-superPKI erreportariak HEK293T zelulatan kokapen zitoplasmatikoa erakusten du. Ezberdintasun hori bi arrazoi nagusi direla eta izan daiteke: batetik, erreportari bakoitzaren ezaugarri propioak, eta bestetik, zelula-lerro ezberdinak erabili izana. Azken arrazoi posible horrek, zelula-lerroen artean garraio nukleozitoplasmatikoa egikaritzen duen mekanismoan ezberdintasunak egon daitezkeela azpimarratzen du. Beraz, esportazio-aktibitatea entsegu zelularretan neurtzerakoan, ikerketa zein zelula-lerrotan egin den kontuan hartu beharreko aldagaia da.

$SRV_{B/A}$ esportazio-entsegua, azkenaldian deskribatutako mikropeptidomako (Yeasmin et al., 2018; Hartford et al., 2020) NES aktiboak bilatzeko ere erabili da. Mikropeptidoma 100 aminoazido baino laburragoak diren proteinen bilduma da. Mikropeptidoen gaineko lanak asko ez badira ere, jada mikropeptido batzuek nukleoan funtzioak dituztela topatu da, esaterako, DNAren konponketan (Slavoff et al., 2014) eta RNAren moztu-itsastean (Huang et al., 2017). Funtzio horiek izateak, mikropeptidoen banaketa azpizelularra zorrozki erregulaturik egon

daitekeela iradokitzen du. Ideia hori buruan, mikropeptido batzuk CRM1en kargo izan litezkeela planteatu da lan honetan. Hipotesi hori baieztatzeko, lehendabiziko urratsa SmProt datu basean (Hao et al., 2018), NES-iragarleak erabiliz, NES kandidatuak bilatzea izan da. Aurkitutako cNESetatik 7 $SRV_{B/A}$ esportazio-entseguan testatu dira, eta horietako bik esportazio-aktibitate altua dutela topatu da. Bi NES aktibo horiek SPROHSA010409 eta SPROHSA141543 mikropeptidoetan daude. SPROHSA010409 mikropeptidoak CRM1en mendeko esportazioa jasaten duela ere baieztatu da. Hori horrela, SPROHSA010409 gaineztadura nuklearrean zehar era aktiboan garraiatzen den deskribaturiko lehen mikropeptidoa da.

SPROHSA010409 mikropeptidoaren funtzio biologikoa, mikropeptido gehienen kasuan bezala, ezezaguna da. Edonola ere, SPROHSA010409 mikropeptidoarekin lortutako emaitzak mikropeptidoman CRM1en hainbat kargo egon daitekeenaren aukera zabaltzen du. Azpimarratzekoa da ere, NES motiboak aminoazido errenkada laburrak direnez, mikropeptido txikienetan ere (15-25 aminoazido) NESak egoteko aukerak egon badaudela. Mikropeptido txikienetan NESik egotekotan, horiek, “amu NESak” izan litezke CRM1entzako, eta beraz, CRM1en mendeko esportazioaren erregulaziorako gako izan litezke. Aukera hori zabalik badago ere, hori frogatzeko esperimentu gehiago egin beharko lirateke.

Azkenik, $SRV_{B/A}$ esportazio-entsegua aurretik eginiko ikerketa estruktural eta biokimikoetan (Dong et al., 2009a, 2009b; Monecke et al., 2009, 2013; Güttler et al., 2010; Fox et al., 2011; Dian et al., 2013; Saito eta Matsuura, 2013; Fung et al., 2015; 2017) jasotako informazioa osatzeko beharrezkoa den CRM1en mendeko NESen esportazioaren inguruko informazio mekanistikoa lortzeko ere erabili da. Helburu horrekin, CRM1en poltsiko hidrofobikoko mutazio bakun bat duten CRM1en hainbat aldaerek zenbait NES esportatzeko duten gaitasuna aztertu da. NES horiek, mota ezberdinetakoak dira, eta beraz, aminoazido hidrofobikoen kokapena ez da guztietan berdina. Gainera, analisi estrukturalen bidez aztertu dira, eta egitura oso ezberdinak agertu dituzte (Dong et al., 2009a; Monecke et al., 2009; Güttler et al., 2010; Fung et al., 2015, 2017). $SRV_{B/A}$ entseguetan lortutako emaitzak aztertzean, ez da NES motaren eta CRM1en aldaera ezberdinek NES horiek esportatzeko gaitasunaren arteko erlazio argirik aurkitu. Behatu dena baina zera izan da: edozein motako NESen esportaziorako CRM1en poltsiko hidrofobikoaren parterik estuenean dauden aminoazidoek (A541, K568 eta F572) parte zabalenean (I521, L525, F61) daudenak baino ekarpen handiagoa dutela. Nabarmentzekoa da gainera, K568 eta F572 aminoazidoen mutazioek antzeko eragina dutela NESen esportazioa murriztean nahiz eta bi aminoazido horiek NESekin elkarrekintza erabat ezberdinak ezarri (NESaren kate nagusiarekin hidrogeno zubia K568 aminoazidoaren kasuan,

eta interakzio hidrofobikoa NESaren albokatearekin F572 aminoazidoaren kasuan) (Dong et al., 2009a; Fung et al., 2017). Emaitza horiek, NESek CRM1en poltsiko hidrofobikoaren parte estuarekin duten elkarrekintza motibo horien esportaziorako bereziki garrantzitsua dela iradokitzen dute.

Aparteko garrantzia duten CRM1en E571 eta K568 aminoazidoen mutazioen eragina ere aztertu da tesi honetan. E571 minbizi hematologikoetan maiz mutaturik ageri den aminoazidoa da (Puente et al., 2011), eta K568 aminoazidoa NESen antzeko motibo ez-aktiboak CRM1i lot ez daitezen galbahe lanak egiten dituela deskribatu da (Fung et al., 2017). Bi aminoazido horiek elkarrengandik oso hurbil daude eta elkarrekintza elektrostatikoa eratzen dute (Fung et al., 2017). Beraz, baliteke minbizi mutazioak elkarrekintza hori apurtzea. Bi aminoazido horien elkarrekintza ikusirik, E571 eta K568 aminoazidoei eragiten dieten mutazioen eragina erkatu da. Lehenik eta behin, E571K eta K568A mutazioak dituzten CRM1en aldaerek, ez-aktibo gisa deskribatutako hiru NES-antzeko motibo (Hxk2, DEAF1 eta COMMD1 proteinetakoak) esportatzeko duten gaitasuna ikertu da. *In vitro* lortutako emaitzekin (Fung et al. 2017) bat eginez, K568A mutaziodun CRM1en aldaerak CRM1 basatiak baino pixka bat hobeto esportatzen ditu Hxk2 eta DEAF1 NES-antzeko motiboak dituzten $SRV_{B/A}$ erreportariak. Hau da, K568 aminoazidoa galbahe gisara funtzionatzen du testuinguru zelularrean ere. E571K mutazioari dagokionez, ez du CRM1ek NES-antzeko motibo horiek esportatzeko duen gaitasuna hobetu, eta horrek, minbizi-mutazioak galbahe hori indargabetzeko gai ez dela iradokitzen du. Azpimarratzekoa da, K568A mutazioak CRM1ek SRV-Hxk2 eta SRV-DEAF1 erreportariak esportatzeko duen gaitasuna emendatzen badu ere, emendapen hori nahiko txikia dela, eta inolaz ere *in vitro* ikusitakoaren (Fung et al., 2017) parekoa. Gainera, K568A mutazioak CRM1ek benetako NESak lotu (Fung et al., 2017) eta esportatzeko gaitasuna murrizten duela ere izan behar da kontuan (ikusi 56. irudia). Hori dela eta, nahiz eta tesi honetan egindako entsegu zelularrek, neurri batean behintzat, aurretik eginiko *in vitro* ikerketekin bat egin, entsegu zelularretan K568 aminoazidoak NESak benetakoak diren, hau da, aktibitate esportatzailerik duten ezartzeko galbahe gisa aritzeko duen gaitasuna sakonago aztertu beharko litzatekeela kontsideratzen da.

Halaber, K568A eta E571K mutazioek minbizi-esportomako hainbat NESen esportazioa murrizten dutela ikusi da. Hala ere, K568A mutazioak E571K minbizi mutanteak baino eragin sendoagoa agertu du. K568A eta E571K mutaziodun CRM1en aldaerak NES-antzeko motiboekin zein minbizi-esportomako NESekin konbinatzean jasotako emaitzek mutazio bi horiek ondorio biologiko ezberdina dutela iradokitzen dute. Aminoazido bien mutazioek ondorio biologiko ezberdina izatea naturalki gertatzen denarekin bat egiten du. Izan ere, E571

aminoazidoaren mutazioak ohikoak dira hainbat minbizi motatan. K568 aminoazidoaren mutazio naturalak, ordea, ez dira inoiz deskribatu. Gainera, baliteke, E571K mutazioak esportazioa inhibitzean duen eragin arinago hori, haren eragin onkogenikoarekin zuzenki erlazionatuta egotea, izan ere, esportazioa modu bortitzagoan inhibitzeak zelularen biziraupena konprometitzea ekar lezake.

5.1.3. CRM1 basatiaren eta minbizi mutantearen esportomak erkatzeko hurbilketa berri baten saiakera

$SRV_{B/A}$ esportazio-entsegua erabiliz, E571K mutazioak NES batzuen esportaziorako CRM1en gaitasuna aldatzen duela berretsi da tesi honetan. Eragin hori CRM1en esportoman zenbateraino islatzen den jakiteak CRM1en mutazio onkogenikoaren eraginaren informazio mekanistiko berria lortzeko interesgarri izan daitekeenez, tesi honetan, CRM1 basatiaren eta minbizi mutantearen esportomak konparatzeko erabilgarria izan daitekeen CRM1/kargo/Ran konplexu egonkorrak isolatzean oinarritzen den hurbilketa proteomiko berri bat planteatu da.

Ran proteinak gauzatu ohi duen GTParen hidrolisia ezinbesteko urratsa da CRM1ek bere kargoak zitoplasman aska ditzan. Lan honetan planteatutako hurbilketa berria GTPa hidrolizatzeko gai ez den Ran proteinaren mutazio batean (Q69L; Bischoff et al., 1994) dago oinarriturik. Ran^{Q69L} mutanteak GTPa hidrolizatu ezin duenez, CRM1/kargo/Ran^{Q69L}GTP konplexu-trimerikoa egonkorra izatea espero da, eta beraz, konplexu osoa YFP-CRM1en aurkako immunoprezipitazioz islotu ahal izatea espero da. Sistema martxan jarri, eta emaitzak jaso eta aztertzean, ordea, konplexu-trimerikoen haustura eman dela ikusi da. Gainadierazitako proteinak (YFP-CRM1 eta Myc-Ran^{Q69L}) zeluletan kokapen berbera izateak (ikusi 65. irudia), CRM1/kargo/Ran^{Q69L} konplexuak eratu eratzen direla iradokitzen du, eta beraz, konplexuen haustura immunoprezipitazio prozeduran zehar ematen dela ondoriozta daiteke.

5.1.4. Giza koronabirusen nukleokapsida (N) proteinaren NESen esportazio-aktibitatea generoarekin dago erlazionaturik, ez patogenotasunarekin

Egungo COVID-19 pandemiaren testuinguruan, koronabirusen patogenotasunean gako diren ezaugarri molekularrak ezagutzea ezinbesteko bilakatu da. Gussow eta lankideek (2020), ikasketa automatikoko teknikak (*machine learning*) eta genomika konparatiboa erabiliz, patogenotasun altuko (MERS-CoV, SARS-CoV eta SARS-CoV-2) eta patogenotasun baxuko (HCoV-NL63, HCoV-229E, HCoV-HKU1 eta HCoV-OC43) koronabirus anduien patogenotasun ezberdintasunaren eragile izan daitezkeen hainbat ezaugarri identifikatu zituzten. *In silico* eginiko lan hartan, nukleokapsida (N) proteinaren hiru NLStan eta NES batean hainbat delezio,

intsertzio eta ordezkapen mutazio gertatzen direla behatu zuten, eta mutazio horiek eragindako karga positibotasun altuagoa proteinaren garraio aktibitate emendatuarekin eta koronabirusen patogenotasun altuagoarekin erlazionatzen dela proposatu zuten. NLSen karga positiboa eta inportazio-aktibitatea korrelazioan daudela ezarri bada ere (Cokol et al., 2000), NESen kasuan ez da horrelakorik deskribatu. Gainera, karga positiboagoa duten NESak aktiboagoak balira ere, NES horiek proteina osoaren eta birusaren testuinguruan duten eragina esperimentalki aztertu beharko litzateke.

Aspektu horietako batzuk argitzeko, lehenik eta behin Rev(1.4)-GFP esportazio-entseguen bidez, aurreikusitako SARS-CoV-2, MERS-CoV, HCoV-NL63, HCoV-229E, HCoV-HKU1 eta HCoV-OC43 koronabirusen NESak aktiboak ote diren, eta aktiboak izatekotan, zenbateko aktibitate maila duten aztertu da. Esportazio-entseguan, proposatutako NES guztiak aktiboak direla eta aktibitate maila oso ezberdina (1 eta 8 arteko esportazio maila) dutela behatu bada ere, ezin izan da aktibitate mailaren eta patogenotasunaren arteko erlaziorik ezarri (100. irudia). Aitzitik, NES aktibitatearen eta koronabirusen generoaren arteko korrelazioa aurkitu da. Giza koronabirusak bi generotan banatzen dira, alfakoronabirusak eta betakoronabirusak. Alfakoronabirusek (HCoV-229E eta HCoV-NL63) 6ko esportazio-aktibitatea erakutsi dute batez bestean, betakoronabirusek (HCoV-HKU1, HCoV-OC43, SARS-CoV-2 eta MERS-CoV), aldiz, 2ko esportazio-aktibitatea.

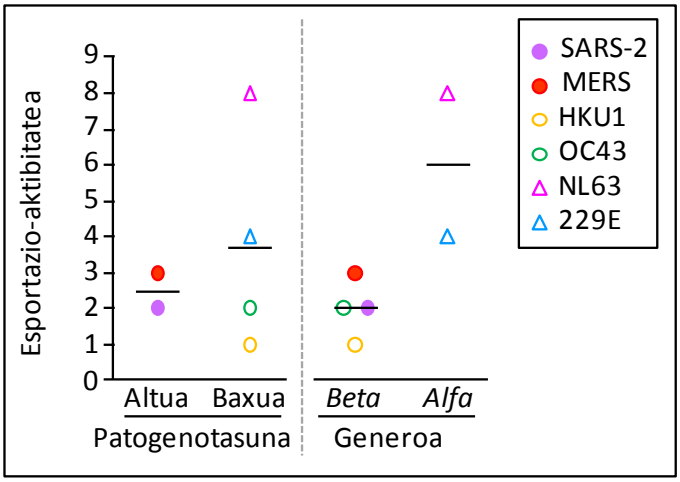

100. irudia: Giza koronabirusen N proteinan iragarritako NESen aktibitatea eta patogenotasuna edo generoa erlazionatzen dituen grafikoa. Ezkerraldean, aztertutako NES bakoitzaren esportazio-aktibitatea (Rev(1.4)-GFP esportazio-entseguaren arabera) koronabirusen patogenotasunarekin erlazionatzen da. Eskuinaldean, ordea, koronabirusen generoarekin. Marra horizontalek talde bakoitzeko batez bestekoa adierazten dute.

Gainera, YFPrekin fusionatutako HCoV-NL63 (patogenotasun baxua) eta SARS-CoV-2 (patogenotasun altua) birusen N proteinek kokapen erabat zitoplasmatikoa erakutsi dute bai CRM1 aktibo (-LMB) izan, bai inhibiturik (+LMB) egon. Hau da, aztertutako testuinguru

zelularrean, N proteinen kokapena ez da CRM1en mendekoa. Horrek, Gussow eta lankideek (2020) proposatutakoarekin kontrajarriz, aztertutako NES motiboak koronabirusen patogenotasunean gako ez direla iradokitzen du. Aipatu beharra dago, SARS-CoV birusaren N proteinan CRM1en mendekoa ez den NES bat deskribatuta dagoela (You et al., 2007), eta haren sekuentzia SARS-CoV-2 birusaren N proteinan mantendu egiten dela. Edonola ere, NES horren eta patogenotasunaren arteko erlaziorik ez da deskribatu.

5.2. Minbiziari aurre egiteko hurbilketa terapeutiko gisa CRM1en inhibizioak duen paperaren ikerketa

5.2.1. Selinexor eta beste ituratutako farmakoen konbinazio berrien aukeraketa eta analisia

CRM1en inhibitzaile den selinexor, bakarrik edo beste farmako batzuekin konbinazioan, tumore solido zein hematologikoen zelulekin egindako *in vitro* ikerketetan maiz erabili da (Turner et al., 2013, 2016a, 2016b, 2020; Salas Fragomeni et al., 2013; Mendonca et al., 2014; De Cesare et al., 2015; Hing et al., 2015; Kazim et al., 2015; Miyake et al., 2015; Ranganathan et al., 2015; Kashyap et al., 2016, 2018; Muqbil et al., 2016; Rosebeck et al., 2016; Sun et al., 2016; Wrobel et al., 2016; Arango et al., 2017; Burke et al., 2017; Chen et al., 2017; Garg et al., 2017a; Gravina et al., 2017; Muz et al., 2017; Nair et al., 2017; Aboukameel et al., 2018; Corno et al., 2018; Luedtke et al., 2018; Nie et al., 2018; Saenz-Ponce et al., 2018; Schaffer et al., 2018; Shang et al., 2018; Subhash et al., 2018; Zhang et al., 2018; Azmi et al., 2019; Currier et al., 2019; DeSisto et al., 2019; Khan et al., 2019; Kapoor et al., 2019; Kulkoyluoglu-Cotul et al., 2019; Lim et al., 2019; Sexton et al., 2019; Tarantelli et al., 2019; Yan et al., 2019; Zhu et al., 2019a; Brinton et al., 2020; Fischer et al., 2020; Martini et al., 2020; Jeitany et al., 2021). Ikerketa prekliniko askotan, selinexor dexametasona edota proteasomaren inhibitzaile diren bortezomib eta karfilzomib farmakoekin konbinatu da. Konbinazio horiek, ikerketa preklinikoetan erabiltzeaz gain, entsegu klinikoetan ere erabilgarriak direla ikusi da. Ondorioz, selinexor/dexametasona eta selinexor/dexametasona/bortezomib konbinazioak MM eta DLBCL paziente jakinak tratatzeko onartu dira (Food and Drug Administration, 2019, 2020a, 2020b, European Medicines Agency, 2021).

Aukera terapeutikoak zabaltzeko asmoz, tesi honetan selinexor eta beste ituratutako farmakoen konbinazio berriak bilatu eta *in vitro* ebaluatu dira. Balizko konbinazioak bilatzeko, *XPO1en* eta minbizian zerikusia duten beste 135 generen (TARGET zerrenda; https://software.broadinstitute.org/cancer/cga/target) artean korrelazio positiborik dagoenetz bilatu da AML, eta bular, prostata, birika, eta kolon eta ondeste minbizietan. Bilaketa hori,

hainbat datu basetan (ikusi 19. taula) egin da CANCERTOOL (Cortazar et al., 2018) eta cBioPortal (Cerami et al., 2012; Gao et al., 2013) tresna bioinformatikoak erabilita. *XPO1* gainadierazita topatu da maiz aipatutako minbizietan (Akagi et al., 2013; Kojima et al., 2013; Marisa et al., 2013; Yue et al., 2018; Cruz-Ramos et al., 2019; Duijvesz et al., 2019), beraz, *XPO1*ekin korrelazio positiboa agertzen duten bestelako geneak ere minbizi horietan gainadierazita egongo direla kontsideratu da.

XPO1 beste gene batekin batera gainadierazita bilatzearen arrazoia, batera gainadierazitako proteinak inhibituz gero, farmakoen arteko sinergia gerta daitekeela da. Izan ere, aurretik eginiko beste behaketa batzuek hipotesi hori bermatzen dute. Adibidez, AML zeluletan, non *XPO1* eta *TOP2A* geneak batera gainadierazten diren (101. irudia), CRM1 eta TOP2A inhibitzaileek sinergia erakusten dute *in vitro* eginiko ikerketetan (Ranganathan et al., 2016). Gainera, 101. irudian beha daitekeenez, AML zeluletan ez ezik, aipatutako tumore solidoetan ere *XPO1* eta *TOP2A* geneak korrelazioan daude.

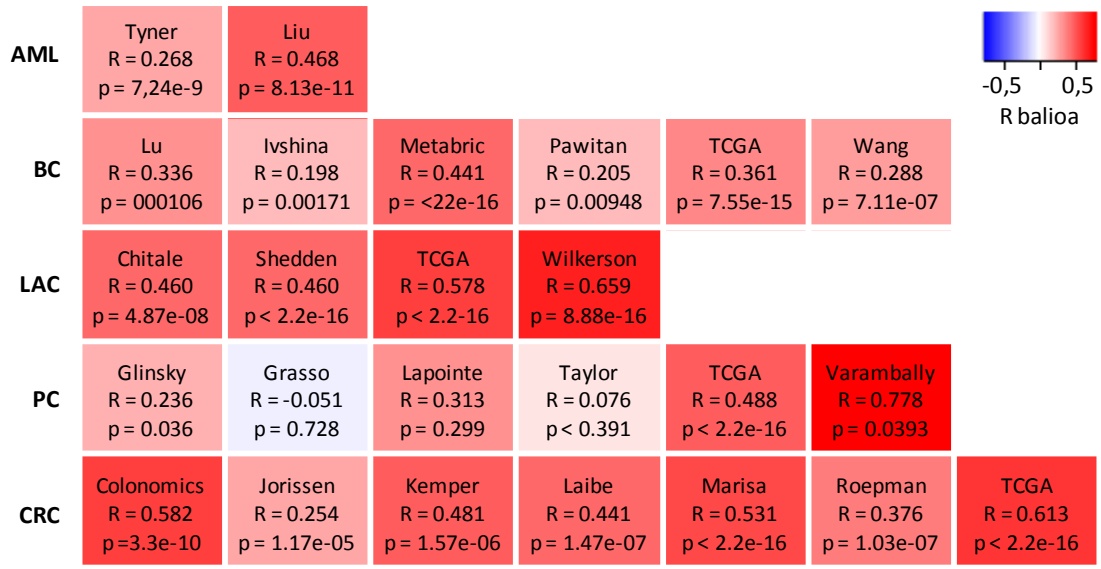

<u>101. irudia:</u> *XPO1* eta *TOP2A* geneen adierazpenaren arteko korrelazioa minbizia mota ezberdinetan. Irudiko bero-mapan leuzemia mieloide akutu (AML), bularreko minbizi (BC), birika adenokartzinoma (LAC), prostata minbizi (PC) eta ondesteko minbizia (CRC) pairatzen duten pazienteen laginekin eginiko ikerketa ezberdinetan *XPO1* eta *TOP2A* geneen adierazpenaren arteko korrelazioa ageri da. Kolore urdinak alderantzizko korrelazioa adierazten du eta gorriak korrelazio zuzena. Koloreen intentsitateak Pearsonen korrelazioaren balioa (R) adierazten du. Ikerketa bakoitzaren izena, R, eta p balioak bero-mapan adierazten dira.

*XPO1*en adierazpena TARGET zerrendako 135 geneen adierazpenarekin bost minbizi mota eta 21 ikerketa ezberdinetan konparatu da. R balioen batez bestekoak kalkulatu ostean, *XPO1*en gainadierazpena eta TARGET zerrendako zortzi generen, *MSH2*, *ATR*, *MSH6*, *BRCA1*, *EZH2*, *BRCA2, AURKA* eta *NPM1*, gainadierazpenen artean korrelazio positiboa dagoela topatu da. Zortzi gene horietatik lauk, *MSH2*, *MSH6*, *BRCA1* eta *BRCA2,* egun, minbiziari aurre egiteko itu

terapeutikotzat jotzen ez diren proteinak kodetzen dituzte, eta beraz, baztertu egin dira. *NPM1* ere alde batera utzi da, NPM1 proteinaren aurkako inhibitzaile fidagarririk ez dagoelako. Beraz, lan honetarako *ATR*, *EZH2* eta *AURKA* geneek kodetutako izen beeko proteinak inhibitzea baino ez da kontsideratu.

Hiru proteina horien artean bi aukeratu dira lehen analisietan inhibitzeko, EZH2 eta AURKA alegia. Horiek inhibitzeko, tazemetostat eta alisertib farmakoak erabili dira hurrenez hurren. Tazemetostat AEBtan minbizi paziente jakinak tratatzeko onartu den EZH2ren inhibitzailea da, eta alisertib, fase klinikora heldu den AURKAren inhibitzailea (Damodaran et al., 2017; Lee et al., 2017; Mohammad et al., 2017; Cheng and Xu, 2018; Dawei et al., 2018; Dimopoulos et al., 2018; Felgenhauer et al., 2018; Fioravanti et al., 2018; Herviou et al., 2018; Hou et al., 2018; Huang et al., 2018; Italiano et al., 2018; Kogiso et al., 2018; Li et al., 2018; Mochizuki et al., 2018; Payton et al., 2018; Serresi et al., 2018; Shaikh et al., 2018; Tremblay-LeMay et al., 2018; Tsai et al., 2018; Wen et al., 2018; Wu et al., 2018; Yang et al., 2018; Zheng et al., 2018; O'Connor et al., 2019; Food and Drug Administration, 2020c, 2020d). Aipatu beharra dago, lehen analisietarako ATR-ren inhibitzailerik aukeratu ez den arren, aukera hori ez dela inoiz baztertu. Izan ere, tesi hau idazten hasi orduko ATR-ren inhibitzaile den AZD-6738 farmakoa selinexorrekin konbinazioan LoVo eta HCT-116 ondesteko minbizi zelulen ugaritzean duen eragina neurtzeko hainbat esperimentu egin ziren. Esperimentu horietan hainbat arazo esperimental gertatu ziren eta ezin izan zen datu nahikorik lortu. Ildo horretan, Inouek eta lankideek (2021) ere ondesteko minbizi zeluletan selinexor/AZD-6738 konbinazioa frogatu dute, eta orain gutxi argitaratutako emaitzen arabera, selinexor eta AZD-6738 farmakoek efektu sinergistikoa dute ondesteko minbizi zeluletan. Aurkikuntza horrek, tesi honetan egindako analisi bioinformatikoaren oinarria sendoa dela erakusten du.

Aukeratutako farmakoak, tazemetostat eta alisertib, selinexorrekin konbinatu dira AML *in vitro* eredu-sistema batean (Ramasamy et al., 2012). Eredu-sistema horretan AML eta estromako zelulak elkarrekin hazten dira, eta farmakoek, bakarrik zein konbinazioan, zelula mota bien ugaritzea geldiarazten, eta AML zelulen apoptosia emendatzen duten eragina neurtu da.

Selinexor eta tazemetostat konbinatzean lortutako emaitzek konbinazio hori minbiziari aurre egiteko terapia gisa baliagarria ez dela iradokitzen dute. Izan ere, nahiz eta konbinazio dosi altuenetan zelulen ugaritzea geldiarazten eragin sinergistikoa erakutsi, eragin hori ez da apoptosia aztertzean ikusten. Beraz, ugaritzea geldiarazi arren, ez da minbizi zelulak akabatzea lortu. Gainera, kontuan izan behar da, tazemetostat farmakoaren kasuan erabilitako dosi altuenak pazienteen plasman neurtutako maximoak izan direla (Italiano et al., 2018), eta litekeena dela, pazienteak tratatzean zeluletara benetan heltzen den farmako kontzentrazioa

plasman agertzen dena baino txikiagoa izatea. Emaitza hauek bat datoz odoleko minbizi zelula ezberdinak tratatzean lortutakoarekin (Eich et al., 2020).

Selinexor eta alisertib farmakoen konbinazioari dagokionez, erabilitako dosi altuenek sinergistikoki eragiten dute apoptosia. Hala ere, kontuan izan behar da, dosi baxuagoetan konbinazioak efektu antagonikoa duela. CRM1 eta AURKA proteinak aldi berean inhibitzeak duen eragin molekularra ezezaguna bada ere, lan honetan p53ren mendeko eragina izan daitekeela planteatzen da, bi itu horiek p53 proteinarekin funtzionalki erlazionatuta baitaude. Batetik, AURKA proteinak p53 fosforilatzen du, tumore ezabatzaile horren aktibitatea eta egonkortasuna negatiboki erregulatuz (Katayama et al., 2004). Bestetik, p53 CRM1en esportazio kargoa da (Stommel et al., 1999). Beraz, AURKA eta CRM1 batera inhibitzeak, p53 proteinaren metatze nuklearra eta tumore ezabatzaile aktibitatea bultza dezakeela proposatzen da tesi honetan.

Laburbilduz, lortutako emaitzek selinexor eta alisertib farmakoen konbinazioa pazienteak tratatzeko aukera interesgarria izan daitekeela iradokitzen dute. Hala ere, aipatutako efektu antagonikoak saiheste aldera, farmako bien kontzentrazio ezberdinak frogatu beharko lirateke.

5.2.2. CRM1en inhibitzaileek zelula mailan duten eragina ezagutzeko hurbilketa berria: esportomaren azterketa APEX2an oinarritutako proteinen gertuko biotinilazioa

Tesi honetan CRM1en esportoma ikertzeko hurbilketa berri bat garatu da, zeinak konpartimentu-espezifikoko proteinen gertuko biotinilazioa (PGB), CRM1en inhibizioa, afinitate-purifikazioa eta MS/MS analisiak uztartzen dituen.

Hurbilketa berri horren erronkarik handiena PGBa eragingo duten markatzaileen diseinua izan da. APEX2 peroxidasan oinarritutako bi proteina markatzaile berri sortu dira: APEX2zit zitoplasmako proteinen markaketa eragingo duena, eta APEX2nuk nukleoko proteinena eragingo duena. Emaitzen atalean azaldu den bezala, markatzaile aproposak lortzea ez da lan erraza izan, eta hainbat fusio-poteina diseinatu, frogatu eta baztertu dira behin betikoak lortu arte.

Markatzaile aproposak lortuta, diseinatutako hurbilketa berria proteomikako kontzeptu-froga erako esperimentu baten bidez balioetsi da. Esperimentuaren diseinua sinplifikatze aldera, aztertutako egoeren erreplika bana, eta ez ohikoak diren hiru erreplikak, analizatu dira. Horrek, bi oztopo nagusi dakartza. Batetik, proteina-identifikazioaren ziurgabetasuna emenda daiteke. Hala ere, egoera basalean egindako esperimentuen emaitzek ziurgabetasun horrek ez duela hurbilketa bera baliogabetzen erakusten dute. Izan ere, espero bezala, APEX2zit

markatzailea erabiltzean identifikatutako proteina gehienak zitoplasmatiko (edo zitoplasmatiko eta nuklear) lez daude deskribaturik UniProtKB datu-basean, APEX2nuk erabiltzean ordea, nuklear (edo nuklear eta zitoplasmatiko) lez. Bestetik, egoera bakoitzeko lagin bakarra izateak, proteomika kuantitatiboa egitea eragozten du. Ondorioz, kargo prototipikoak eta muturreko kargo ez-prototipikoak (ikusi 91. irudia) baino ez dira bilatu. Bilaketa horietan, 4 balizko kargo prototipiko eta 89 balizko muturreko kargo ez-prototipiko identifikatu dira. Kargo horien artean badaude CRM1en kargo ezagunak diren hainbat proteina, esaterako, LIMD1 (Sharp et al., 2004), TUBAL3 (Schwarzerová et al., 2019), SNUPN (Paraskeva et al., 1999), HDAC1 (Kim et al., 2010), edota RanGAP1 (Cha et al., 2015) proteinak. Aurkitutako kargo horiek CRM1en kargo ezagunak izatea, garatutako estrategia berri honen oinarri sendoaren erakusle da.

CRM1en kargo gisa ezagunak ez diren balizko kargoetariko bi, SBSN eta CK2α', CRM1en kargo direnetz aztertu da. CK2α' aurretik ere kargotzat proposatu zen analisi proteomiko batean (Kirli et al., 2015). Hortik abiatuta, eta proposamen horretatik haratago, lan honetan CK2α'ren kokapen nukleozitoplasmatikoan ematen diren aldaketak aztertu dira LMB erabiliz. Lortutako emaitzek, CK2α' CRM1en kargo badela iradokitzen dute.

Kontzeptu-froga honetan LMB erabili da CRM1 inhibitzeko, baina eskuragarri dagoen beste edozein CRM1en inhibitzaile ere erabil zitekeen. Hortaz, tesi honetan garatutako hurbilketa berria CRM1en esportomaren ezagutzan sakontzeko, eta klinikan erabili ohi diren eta CRM1en inhibizioa helburu duten agente terapeutikoek, selinexor edo eltanexor kasu, zelula mailan duten eragina ikertzeko erabilgarria izan daiteke. Gainera, hurbilketa berri hau, CRISPR/CAS9 metodologiarekin uztartuz gero, CRM1 basati eta $CRM1^{E571K}$ minbizi mutantearen esportomak konparatzeko aukera dagoela aurreikusten da. Modu horretan, E571K mutazioak onkogenesian duen eragin mekanistikoaren inguruko informazioa lortuko litzateke.

6. Ondorioak/ Conclusions

1.- USP12/UAF1/WDR20 deubikuitinasa konplexuaren CRM1en mendeko nukleotiko esportazioa WDR20 proteinan deskribatutako NES berriaren bidez gertatzen da, eta ez, aurretik proposatutako USP12ren NESaren bidez.

2.- Tesi honetan garatutako $SRV_{B/A}$ esportazio-entsegua NES motiboak bilatu eta karakterizatzeko erabilgarria da.

2a) Minbiziarekin erlazionatuta dauden, eta aurreko analisi proteomiko batean CRM1en balizko kargo gisa identifikatutako hainbat proteinen NES motibo berriak identifikatzeak, proteina horiek CRM1en benetako kargoak direlako ideia sostengatzen du.

2b) Oraindik orain aurkitutako eta gutxi ikertutako mikropeptido izeneko proteina txikien banaketa azpizelularra CRM1en mendeko nukleotiko esportazioak erregula dezake. Tesi honetan, lehenengoz, giza mikropeptidoen NES aktiboak eta gaineztadura nuklearraren zehar era aktiboan mugitzen den lehen mikropeptidoa deskribatu dira.

2c) Orokorrean, orain gutxi deskribatutako *minus* NESek, ohiko *plus* erakoek baino esportazio-aktibitate maila baxuagoa dute.

2d) Giza koronabirusen nukleokapsida (N) proteinen aurreikusitako NESaren esportazio-aktibitate maila generoarekin dago erlazionaturik, ez patogenotasunarekin.

3.- $SRV_{B/A}$ esportazio-entseguak CRM1en mendeko NESen esportazioa egikaritzen duten aspektu mekanistikoen gaineko ezagutza zabaltzeko aukera ematen du.

3a) NES mota edozein dela ere, CRM1en poltsiko hidrofobikoko alde estuan dauden aminoazidoek alde zabalean daudenek baino eginkizun garrantzitsuagoa dute NESen esportazioan.

3b) Minbiziarekin erlazionaturiko CRM1en E571K mutazioaren eragina arina da NESen esportazioari dagokionez. Gertuko K568 aminoazidoaren mutazioak berriz, CRM1en aktibitate esportatzailea nabarmen murrizten du.

4.- Ran proteinaren GTPasa aktibitatea ezerezten duen Q69L mutazioak ez du CRM1/kargo/RanGTP konplexu-trimerikoa afinitate purifikazioz isolatzeko bezain beste egonkortzen. Beraz, CRM1i lotutako kargoak modu horretan isolatzea ezinezkoa da.

5.- CRM1 eta AURKA proteinen aldi bereko inhibizioa (selinexor/alisertib farmako konbinazioa erabiliz) minbiziari aurre egiteko balizko terapia gisa ikertzea arrazoituta dago.

6.- APEX2 peroxidasak eragindako konpartimendu-espezifikoko biotinilazioan oinarritutako hurbilketa proteomiko berria CRM1en inhibizioak zelula mailan duen eragina aztertzeko, zein CRM1en kargo berriak bilatzeko erabil daiteke.

1.- CRM1-dependent nuclear export of the USP12/UAF1/WDR20 deubiquitinase complex is mediated by a new NES motif in WDR20, and not by the previously reported NES in USP12.

2.- The novel $SRV_{B/A}$ nuclear export assay developed here is useful to identify and characterise NES motifs.

- **2a)** Identification of new functional NES in several cancer related proteins, previously reported as putative CRM1 cargos, further supports the view that these proteins are, indeed, cargos of CRM1.
- **2b)** Subcellular localisation of micropeptides, a recently discovered and largely unexplored class of small proteins, can be regulated by active CRM1-mediated nuclear export. The first functional NESs in the human micropeptidome and the first shuttling micropeptide have been identified here.
- **2c)** In general, the recently described *minus* NES motifs show a lower nuclear export-activity than classical *plus* NES motifs.
- **2d)** The strength of NES motifs in the nucleocapsid (N) protein of human coronaviruses is related to genus, but not to pathogenic capacity.

3.- The $SRV_{B/A}$ assay allows to gain insight into mechanistic aspects of CRM1-mediated NES export.

- **3a)** Irrespective of NES class, residues in the narrower section of CRM1 hydrophobic groove play a more important role in NES export than residues in the wider section of the groove.
- **3b)** A cancer-related mutation in CRM1 residue E571 has a subtle effect on NES export. In contrast, mutation of the nearby residue K568 more dramatically reduces CRM1 export activity.

4.- The Q69L mutation, which abrogates Ran GTPase activity, does not appear to sufficiently stabilise CRM1/cargo/RanGTP complexes to allow successful affinity purification of CRM1-bound cargos.

5.- Combined inhibition of CRM1 and AURKA (i.e. selinexor/alisertib drug combination) warrants further investigation as a potential strategy for cancer therapy.

6.- A new proteomics approach based on compartment-specific proximity biotinylation of proteins using the APEX2 peroxidase can be used to gain insight into the global cellular effect of CRM1 inhibition, as well as to identify CRM1 cargos.

7. Bibliografia / References

Abdul Razak, A. R., Mau-Soerensen, M., Gabrail, N. Y., Gerecitano, J. F., Shields, A. F., Unger, T. J., Saint-Martin, J. R., Carlson, R., Landesman, Y., McCauley, D., Rashal, T., Lassen, U., Kim, R., Stayner, L. A., Mirza, M. R., Kauffman, M., Shacham, S., & Mahipal, A. (2016). First-in-Class, First-in-Human Phase I Study of Selinexor, a Selective Inhibitor of Nuclear Export, in Patients With Advanced Solid Tumors. *Journal of clinical oncology: official journal of the American Society of Clinical Oncology*, *34*(34), 4142–4150. https://doi.org/10.1200/JCO.2015.65.3949

Abeykoon, J. P., Paludo, J., Nowakowski, K. E., Stenson, M. J., King, R. L., Wellik, L. E., Wu, X., & Witzig, T. E. (2019). The effect of CRM1 inhibition on human non-Hodgkin lymphoma cells. *Blood cancer journal*, *9*(3), 24. https://doi.org/10.1038/s41408-019-0188-6

Aboukameel, A., Muqbil, I., Baloglu, E., Senapedis, W., Landesman, Y., Argueta, C., Kauffman, M., Chang, H., Kashyap, T., Shacham, S., Neggers, J. E., Daelemans, D., Heath, E. I., & Azmi, A. S. (2018). Down-regulation of AR splice variants through XPO1 suppression contributes to the inhibition of prostate cancer progression. *Oncotarget*, *9*(82), 35327–35342. https://doi.org/10.18632/oncotarget.26239

Acharya, S., Wilson, T., Gradia, S., Kane, M. F., Guerrette, S., Marsischky, G. T., Kolodner, R., & Fishel, R. (1996). hMSH2 forms specific mispair-binding complexes with hMSH3 and hMSH6. *Proceedings of the National Academy of Sciences of the United States of America*, *93*(24), 13629–13634. https://doi.org/10.1073/pnas.93.24.13629

Aebersold, R., & Mann, M. (2003). Mass spectrometry-based proteomics. *Nature*, *422*(6928), 198–207. https://doi.org/10.1038/nature01511

Akagi, I., Okayama, H., Schetter, A. J., Robles, A. I., Kohno, T., Bowman, E. D., Kazandjian, D., Welsh, J. A., Oue, N., Saito, M., Miyashita, M., Uchida, E., Takizawa, T., Takenoshita, S., Skaug, V., Mollerup, S., Haugen, A., Yokota, J., & Harris, C. C. (2013). Combination of protein coding and noncoding gene expression as a robust prognostic classifier in stage I lung adenocarcinoma. *Cancer research*, *73*(13), 3821–3832. https://doi.org/10.1158/0008-5472.CAN-13-0031

Aladhraei, M., Al-Salami, E., Poungvarin, N., & Suwannalert, P. (2019). The roles of p53 and XPO1 on colorectal cancer progression in Yemeni patients. *Journal of gastrointestinal oncology*, *10*(3), 437–444. https://doi.org/10.21037/jgo.2019.01.17

Alexander, T. B., Lacayo, N. J., Choi, J. K., Ribeiro, R. C., Pui, C. H., & Rubnitz, J. E. (2016). Phase I Study of Selinexor, a Selective Inhibitor of Nuclear Export, in Combination With Fludarabine and Cytarabine, in Pediatric Relapsed or Refractory Acute Leukemia. *Journal of clinical oncology: official journal of the American Society of Clinical Oncology*, *34*(34), 4094–4101. https://doi.org/10.1200/JCO.2016.67.5066

Amin, N. A., Seymour, E., Saiya-Cork, K., Parkin, B., Shedden, K., & Malek, S. N. (2016). A Quantitative Analysis of Subclonal and Clonal Gene Mutations before and after Therapy in Chronic Lymphocytic Leukemia. *Clinical cancer research : an official journal of the American Association for Cancer Research*, *22*(17), 4525–4535. https://doi.org/10.1158/1078-0432.CCR-15-3103

Arango, N. P., Yuca, E., Zhao, M., Evans, K. W., Scott, S., Kim, C., Gonzalez-Angulo, A. M., Janku, F., Ueno, N. T., Tripathy, D., Akcakanat, A., Naing, A., & Meric-Bernstam, F. (2017). Selinexor (KPT-330) demonstrates anti-tumor efficacy in preclinical models of triple-negative breast cancer. *Breast cancer research : BCR*, *19*(1), 93. https://doi.org/10.1186/s13058-017-0878-6

Argueta, C., Kashyap, T., Klebanov, B., Unger, T. J., Guo, C., Harrington, S., Baloglu, E., Lee, M., Senapedis, W., Shacham, S., & Landesman, Y. (2018). Selinexor synergizes with dexamethasone to repress mTORC1 signaling and induce multiple myeloma cell death. *Oncotarget*, *9*(39), 25529–25544. https://doi.org/10.18632/oncotarget.25368

Arnaoutov, A., Azuma, Y., Ribbeck, K., Joseph, J., Boyarchuk, Y., Karpova, T., McNally, J., & Dasso, M. (2005). Crm1 is a mitotic effector of Ran-GTP in somatic cells. Nature cell biology, 7(6), 626–632. https://doi.org/10.1038/ncb1263

Attiyeh, E. F., Maris, J. M., Lock, R., Reynolds, C. P., Kang, M. H., Carol, H., Gorlick, R., Kolb, E. A., Keir, S. T., Wu, J., Landesman, Y., Shacham, S., Lyalin, D., Kurmasheva, R. T., Houghton, P. J., & Smith, M. A. (2016). Pharmacodynamic and genomic markers associated with response to the XPO1/CRM1 inhibitor selinexor (KPT-330): A report from the pediatric preclinical testing program. *Pediatric blood & cancer*, *63*(2), 276–286. https://doi.org/10.1002/pbc.25727

Azmi, A. S., Aboukameel, A., Bao, B., Sarkar, F. H., Philip, P. A., Kauffman, M., Shacham, S., & Mohammad, R. M. (2013a). Selective inhibitors of nuclear export block pancreatic cancer cell proliferation and reduce tumor growth in mice. *Gastroenterology*, *144*(2), 447–456. https://doi.org/10.1053/j.gastro.2012.10.036

Azmi, A. S., Al-Katib, A., Aboukameel, A., McCauley, D., Kauffman, M., Shacham, S., & Mohammad, R. M. (2013b). Selective inhibitors of nuclear export for the treatment of non-Hodgkin's lymphomas. *Haematologica*, *98*(7), 1098–1106. https://doi.org/10.3324/haematol.2012.074781

Azmi, A. S., Khan, H. Y., Muqbil, I., Aboukameel, A., Neggers, J. E., Daelemans, D., Mahipal, A., Dyson, G., Kamgar, M., Al-Hallak, M. N., Tesfaye, A., Kim, S., Shidham, V., M Mohammad, R., & Philip, P. A. (2020). Preclinical Assessment with Clinical Validation of Selinexor with Gemcitabine and Nab-Paclitaxel for the Treatment of Pancreatic Ductal Adenocarcinoma. *Clinical cancer research : an official journal of the American Association for Cancer Research*, *26*(6), 1338–1348. https://doi.org/10.1158/1078-0432.CCR-19-1728

Azmi, A. S., Li, Y., Muqbil, I., Aboukameel, A., Senapedis, W., Baloglu, E., Landesman, Y., Shacham, S., Kauffman, M. G., Philip, P. A., & Mohammad, R. M. (2017). Exportin 1 (XPO1) inhibition leads to restoration of tumor suppressor miR-145 and consequent suppression of pancreatic cancer cell proliferation and migration. *Oncotarget*, *8*(47), 82144–82155. https://doi.org/10.18632/oncotarget.19285

Bachmann, R. A., Kim, J. H., Wu, A. L., Park, I. H., & Chen, J. (2006). A nuclear transport signal in mammalian target of rapamycin is critical for its cytoplasmic signaling to S6 kinase 1. *The Journal of biological chemistry*, *281*(11), 7357–7363. https://doi.org/10.1074/jbc.M512218200

Baek, H. B., Lombard, A. P., Libertini, S. J., Fernandez-Rubio, A., Vinall, R., Gandour-Edwards, R., Nakagawa, R., Vidallo, K., Nishida, K., Siddiqui, S., Wettersten, H., Landesman, Y., Weiss, R. H., Ghosh, P. M., & Mudryj, M. (2018). XPO1 inhibition by selinexor induces potent cytotoxicity against high grade bladder malignancies. *Oncotarget*, *9*(77), 34567–34581. https://doi.org/10.18632/oncotarget.26179

Bahlis, N. J., Sutherland, H., White, D., Sebag, M., Lentzsch, S., Kotb, R., Venner, C. P., Gasparetto, C., Del Col, A., Neri, P., Reece, D., Kauffman, M., Shacham, S., Unger, T. J., Jeha, J., Saint-Martin, J. R., Shah, J., & Chen, C. (2018). Selinexor plus low-dose bortezomib and dexamethasone for patients with relapsed or refractory multiple myeloma. *Blood*, *132*(24), 2546–2554. https://doi.org/10.1182/blood-2018-06-858852

Balatti, V., Bottoni, A., Palamarchuk, A., Alder, H., Rassenti, L. Z., Kipps, T. J., Pekarsky, Y., & Croce, C. M. (2012). NOTCH1 mutations in CLL associated with trisomy 12. *Blood*, *119*(2), 329–331. https://doi.org/10.1182/blood-2011-10-386144

Barazeghi, E., Prabhawa, S., Norlén, O., Hellman, P., Stålberg, P., & Westin, G. (2018). Decrease of 5-hydroxymethylcytosine and TET1 with nuclear exclusion of TET2 in small intestinal neuroendocrine tumors. *BMC cancer*, *18*(1), 764. https://doi.org/10.1186/s12885-018-4579-z

Bardou, P., Mariette, J., Escudié, F., Djemiel, C., & Klopp, C. (2014). jvenn: an interactive Venn diagram viewer. *BMC Bioinformatics*, *15*(1), 293–300. https://doi.org/10.1186/1471-2105-15-293

Baumhardt, J. M., Walker, J. S., Lee, Y., Shakya, B., Brautigam, C. A., Lapalombella, R., Grishin, N., & Chook, Y. M. (2020). Recognition of nuclear export signals by CRM1 carrying the oncogenic E571K mutation. *Molecular biology of the cell*, *31*(17), 1879–1891. https://doi.org/10.1091/mbc.E20-04-0233

Bersuker, K., & Olzmann, J. A. (2019). Identification of Lipid Droplet Proteomes by Proximity Labeling Proteomics Using APEX2. *Methods in molecular biology*, *2008*, 57–72. https://doi.org/10.1007/978-1-4939-9537-0_5

Bhatnagar, B., Zhao, Q., Mims, A. S., Vasu, S., Behbehani, G. K., Larkin, K., Blachly, J. S., Blum, W., Klisovic, R. B., Ruppert, A. S., Orwick, S., Oakes, C., Ranganathan, P., Byrd, J. C., Walker, A. R., & Garzon, R. (2020). Selinexor in combination with decitabine in patients with acute myeloid leukemia: results from a phase 1 study. *Leukemia & lymphoma*, *61*(2), 387–396. https://doi.org/10.1080/10428194.2019.1665664

Birnbaum, D. J., Finetti, P., Birnbaum, D., Mamessier, E., & Bertucci, F. (2019). *XPO1* Expression Is a Poor-Prognosis Marker in Pancreatic Adenocarcinoma. *Journal of clinical medicine*, *8*(5), 596. https://doi.org/10.3390/jcm8050596

Bischoff, F. R., & Görlich, D. (1997). RanBP1 is crucial for the release of RanGTP from importin β-related nuclear transport factors. *FEBS Letters*, *419*(2–3), 249–254. https://doi.org/10.1016/S0014-5793(97)01467-1

Bischoff, F. R., Klebe, C., Kretschmer, J., Wittinghofer, A., & Ponstingl, H. (1994). RanGAP1 induces GTPase activity of nuclear Ras-related Ran. *Proceedings of the National Academy of Sciences of the United States of America*, *91*(7), 2587–2591. https://doi.org/10.1073/pnas.91.7.2587

Bonolo de Campos, C., Meurice, N., Petit, J. L., Polito, A. N., Zhu, Y. X., Wang, P., Bruins, L. A., Wang, X., Lopez Armenta, I. D., Darvish, S. A., Ahmann, G. J., Henderson, K. J., Tian, S., Kruse, J. J., Stewart, W. M., Larsen, J. T., Reeder, C. B., Dingli, D., Kapoor, P., Kumar, S. K., … Stewart, A. K. (2020). "Direct to Drug" screening as a precision medicine tool in multiple myeloma. *Blood cancer journal*, *10*(5), 54. https://doi.org/10.1038/s41408-020-0320-7

Bosch, J. A., Chen, C. L., & Perrimon, N. (2021). Proximity-dependent labeling methods for proteomic profiling in living cells: An update. *Wiley Interdisciplinary Reviews: Developmental Biology*, *10*(1), e392. https://doi.org/10.1002/wdev.392

Branon, T. C., Bosch, J. A., Sanchez, A. D., Udeshi, N. D., Svinkina, T., Carr, S. A., Feldman, J. L., Perrimon, N., & Ting, A. Y. (2018). Efficient proximity labeling in living cells and organisms with TurboID. *Nature biotechnology*, *36*(9), 880–887. https://doi.org/10.1038/nbt.4201

Brinton, L. T., Sher, S., Williams, K., Canfield, D., Orwick, S., Wasmuth, R., Cempre, C., Skinner, J., Lehman, A., Blachly, J. S., Byrd, J. C., & Lapalombella, R. (2020). Cotargeting of XPO1 Enhances the Antileukemic Activity of Midostaurin and Gilteritinib in Acute Myeloid Leukemia. *Cancers*, *12*(6), 1574. https://doi.org/10.3390/cancers12061574

Brunetti, L., Gundry, M. C., Sorcini, D., Guzman, A. G., Huang, Y. H., Ramabadran, R., Gionfriddo, I., Mezzasoma, F., Milano, F., Nabet, B., Buckley, D. L., Kornblau, S. M., Lin, C. Y., Sportoletti, P., Martelli, M. P., Falini, B., & Goodell, M. A. (2018). Mutant NPM1 Maintains the Leukemic State through HOX Expression. *Cancer cell*, *34*(3), 499–512.e9. https://doi.org/10.1016/j.ccell.2018.08.005

Burke, R. T., Marcus, J. M., & Orth, J. D. (2017). Inhibition of exportin-1 function results in rapid cell cycle-associated DNA damage in cancer cells. *Oncotarget*, *8*(24), 39460–39475. https://doi.org/10.18632/oncotarget.17063

Burska, U. L., Harle, V. J., Coffey, K., Darby, S., Ramsey, H., O'Neill, D., Logan, I. R., Gaughan, L., & Robson, C. N. (2013). Deubiquitinating enzyme Usp12 is a novel co-activator of the androgen receptor. *The Journal of biological chemistry*, *288*(45), 32641–32650. https://doi.org/10.1074/jbc.M113.485912

Çağatay, T., & Chook, Y. M. (2018). Karyopherins in cancer. *Current opinion in cell biology*, *52*, 30–42. https://doi.org/10.1016/j.ceb.2018.01.006

Camus, V., Miloudi, H., Taly, A., Sola, B., & Jardin, F. (2017). XPO1 in B cell hematological malignancies: from recurrent somatic mutations to targeted therapy. *Journal of hematology & oncology*, *10*(1), 47. https://doi.org/10.1186/s13045-017-0412-4

Camus, V., Stamatoullas, A., Mareschal, S., Viailly, P. J., Sarafan-Vasseur, N., Bohers, E., Dubois, S., Picquenot, J. M., Ruminy, P., Maingonnat, C., Bertrand, P., Cornic, M., Tallon-Simon, V., Becker, S., Veresezan, L., Frebourg, T., Vera, P., Bastard, C., Tilly, H., & Jardin, F. (2016). Detection and prognostic value of recurrent exportin 1 mutations in tumor and cell-free circulating DNA of patients with classical Hodgkin lymphoma. *Haematologica*, *101*(9), 1094–1101. https://doi.org/10.3324/haematol.2016.145102

Camus, V., Viennot, M., Lequesne, J., Viailly, P. J., Bohers, E., Bessi, L., Marcq, B., Etancelin, P., Dubois, S., Picquenot, J. M., Veresezan, E. L., Cornic, M., Burel, L., Loret, J., Becker, S., Decazes, P., Lenain, P., Lepretre, S., Lemasle, E., Lanic, H., … Jardin, F. (2021). Targeted genotyping of circulating tumor DNA for classical Hodgkin lymphoma monitoring: a prospective study. *Haematologica*, *106*(1), 154–162. https://doi.org/10.3324/haematol.2019.237719

Cao, R., Wang, L., Wang, H., Xia, L., Erdjument-Bromage, H., Tempst, P., Jones, R. S., & Zhang, Y. (2002). Role of histone H3 lysine 27 methylation in Polycomb-group silencing. *Science*, *298*(5595), 1039–1043. https://doi.org/10.1126/science.1076997

Castro-Piedras, I., Sharma, M., Brelsfoard, J., Vartak, D., Martinez, E. G., Rivera, C., Molehin, D., Bright, R. K., Fokar, M., Guindon, J., & Pruitt, K. (2021). Nuclear Dishevelled targets gene regulatory regions and promotes tumor growth. *EMBO reports*, *22*(6), e50600. https://doi.org/10.15252/embr.202050600

Cautain, B., Hill, R., de Pedro, N., & Link, W. (2015). Components and regulation of nuclear transport processes. *The FEBS journal*, *282*(3), 445–462. https://doi.org/10.1111/febs.13163

Cerami, E., Gao, J., Dogrusoz, U., Gross, B. E., Sumer, S. O., Aksoy, B. A., Jacobsen, A., Byrne, C. J., Heuer, M. L., Larsson, E., Antipin, Y., Reva, B., Goldberg, A. P., Sander, C., & Schultz, N. (2012). The cBio cancer genomics portal: an open platform for exploring multidimensional cancer genomics data. *Cancer discovery*, *2*(5), 401–404. https://doi.org/10.1158/2159-8290.CD-12-0095

Cerretelli, G., Ager, A., Arends, M. J., & Frayling, I. M. (2020). Molecular pathology of Lynch syndrome. *The Journal of pathology*, *250*(5), 518–531. https://doi.org/10.1002/path.5422

Cervantes, A., Elez, E., Roda, D., Ecsedy, J., Macarulla, T., Venkatakrishnan, K., Roselló, S., Andreu, J., Jung, J., Sanchis-Garcia, J. M., Piera, A., Blasco, I., Maños, L., Pérez-Fidalgo, J. A., Fingert, H., Baselga, J., & Tabernero, J. (2012). Phase I pharmacokinetic/pharmacodynamic study of MLN8237, an investigational, oral, selective aurora a kinase inhibitor, in patients with advanced solid tumors. *Clinical cancer research : an official journal of the American Association for Cancer Research*, *18*(17), 4764–4774. https://doi.org/10.1158/1078-0432.CCR-12-0571

Cha, K., Sen, P., Raghunayakula, S., & Zhang, X. D. (2015). The cellular distribution of RanGAP1 is regulated by CRM1-mediated nuclear export in mammalian cells. *PLoS ONE*, *10*(10), e0141309. https://doi.org/10.1371/journal.pone.0141309

Chari, A., Vogl, D. T., Gavriatopoulou, M., Nooka, A. K., Yee, A. J., Huff, C. A., Moreau, P., Dingli, D., Cole, C., Lonial, S., Dimopoulos, M., Stewart, A. K., Richter, J., Vij, R., Tuchman, S., Raab, M. S., Weisel, K. C., Delforge, M., Cornell, R. F., Kaminetzky, D., … Jagannath, S. (2019). Oral Selinexor-Dexamethasone for Triple-Class Refractory Multiple Myeloma. *The New England journal of medicine*, *381*(8), 727–738. https://doi.org/10.1056/NEJMoa1903455

Chen, C., Siegel, D., Gutierrez, M., Jacoby, M., Hofmeister, C. C., Gabrail, N., Baz, R., Mau-Sorensen, M., Berdeja, J. G., Savona, M., Savoie, L., Trudel, S., Areethamsirikul, N., Unger, T. J., Rashal, T., Hanke, T., Kauffman, M., Shacham, S., & Reece, D. (2018). Safety and efficacy of selinexor in relapsed or refractory multiple myeloma and Waldenstrom macroglobulinemia. *Blood*, *131*(8), 855–863. https://doi.org/10.1182/blood-2017-08-797886

Chen, L., Huang, Y., Zhou, L., Lian, Y., Wang, J., Chen, D., Wei, H., Huang, M., & Huang, Y. (2019). Prognostic roles of the transcriptional expression of exportins in hepatocellular carcinoma. *Bioscience reports*, *39*(8), BSR20190827. https://doi.org/10.1042/BSR20190827

Chen, Y., Camacho, S. C., Silvers, T. R., Razak, A. R., Gabrail, N. Y., Gerecitano, J. F., Kalir, E., Pereira, E., Evans, B. R., Ramus, S. J., Huang, F., Priedigkeit, N., Rodriguez, E., Donovan, M., Khan, F., Kalir, T., Sebra, R., Uzilov, A., Chen, R., Sinha, R., … Martignetti, J. A. (2017). Inhibition of the Nuclear Export Receptor XPO1 as a Therapeutic Target for Platinum-Resistant Ovarian Cancer. *Clinical cancer research : an official journal of the American Association for Cancer Research*, *23*(6), 1552–1563. https://doi.org/10.1158/1078-0432.CCR-16-1333

Cheng, T., & Xu, Y. (2018). Effects of Enhancer of Zeste Homolog 2 (EZH2) Expression on Brain Glioma Cell Proliferation and Tumorigenesis. *Medical science monitor : international medical journal of experimental and clinical research*, *24*, 7249–7255. https://doi.org/10.12659/MSM.909814

Cheng, Y., Holloway, M. P., Nguyen, K., McCauley, D., Landesman, Y., Kauffman, M. G., Shacham, S., & Altura, R. A. (2014). XPO1 (CRM1) inhibition represses STAT3 activation to drive a survivin-dependent oncogenic switch in triple-negative breast cancer. *Molecular cancer therapeutics*, *13*(3), 675–686. https://doi.org/10.1158/1535-7163.MCT-13-0416

Chitale, D., Gong, Y., Taylor, B. S., Broderick, S., Brennan, C., Somwar, R., Golas, B., Wang, L., Motoi, N., Szoke, J., Reinersman, J. M., Major, J., Sander, C., Seshan, V. E., Zakowski, M. F., Rusch, V., Pao, W., Gerald, W., & Ladanyi, M. (2009). An integrated genomic analysis of lung cancer reveals loss of DUSP4 in EGFR-mutant tumors. *Oncogene*, *28*(31), 2773–2783. https://doi.org/10.1038/onc.2009.135

Choi-Rhee, E., Schulman, H., & Cronan, J. E. (2004). Promiscuous protein biotinylation by Escherichia coli biotin protein ligase. *Protein Science*, *13*(11), 3043–3050. https://doi.org/10.1110/ps.04911804

Chou, T. C. (2006). Theoretical basis, experimental design, and computerized simulation of synergism and antagonism in drug combination studies. *Pharmacological Reviews*, *58*(3), 621–681. https://doi.org/10.1124/pr.58.3.10

Chou, T. C., & Talalay, P. (1984). Quantitative analysis of dose-effect relationships: the combined effects of multiple drugs or enzyme inhibitors. *Advances in Enzyme Regulation*, *22*, 27–55. https://doi.org/10.1016/0065-2571(84)90007-4

Ciccia, A., & Elledge, S. J. (2010). The DNA damage response: making it safe to play with knives. *Molecular cell*, *40*(2), 179–204. https://doi.org/10.1016/j.molcel.2010.09.019

Cokol, M., Nair, R., & Rost, B. (2000). Finding nuclear localization signals. *EMBO reports*, *1*(5), 411–415. https://doi.org/10.1093/embo-reports/kvd092

Conforti, F., Zhang, X., Rao, G., De Pas, T., Yonemori, Y., Rodriguez, J. A., McCutcheon, J. N., Rahhal, R., Alberobello, A. T., Wang, Y., Zhang, Y. W., Guha, U., & Giaccone, G. (2017). Therapeutic Effects of XPO1 Inhibition in Thymic Epithelial Tumors. *Cancer research*, *77*(20), 5614–5627. https://doi.org/10.1158/0008-5472.CAN-17-1323

Corno, C., Stucchi, S., De Cesare, M., Carenini, N., Stamatakos, S., Ciusani, E., Minoli, L., Scanziani, E., Argueta, C., Landesman, Y., Zaffaroni, N., Gatti, L., & Perego, P. (2018). FoxO-1 contributes to the efficacy of the combination of the XPO1 inhibitor selinexor and cisplatin in ovarian carcinoma preclinical models. *Biochemical pharmacology*, *147*, 93–103. https://doi.org/10.1016/j.bcp.2017.11.009

Cortazar, A. R., Torrano, V., Martín-Martín, N., Caro-Maldonado, A., Camacho, L., Hermanova, I., Guruceaga, E., Lorenzo-Martín, L. F., Caloto, R., Gomis, R. R., Apaolaza, I., Quesada, V., Trka, J., Gomez-Muñoz, A., Vincent, S., Bustelo, X. R., Planes, F. J., Aransay, A. M., & Carracedo, A. (2018). CANCERTOOL: A Visualization and Representation Interface to Exploit Cancer Datasets. *Cancer research*, *78*(21), 6320–6328. https://doi.org/10.1158/0008-5472.CAN-18-1669

Cosson, A., Chapiro, E., Bougacha, N., Lambert, J., Herbi, L., Cung, H. A., Algrin, C., Keren, B., Damm, F., Gabillaud, C., Brunelle-Navas, M. N., Davi, F., Merle-Béral, H., Le Garff-Tavernier, M., Roos-Weil, D., Choquet, S., Uzunov, M., Morel, V., Leblond, V., Maloum, K., … Nguyen-Khac, F. (2017). Gain in the short arm of chromosome 2 (2p+) induces gene overexpression and drug resistance in chronic lymphocytic leukemia: analysis of the central role of XPO1. *Leukemia*, *31*(7), 1625–1629. https://doi.org/10.1038/leu.2017.100

Cox, J., & Mann, M. (2008). MaxQuant enables high peptide identification rates, individualized p.p.b.-range mass accuracies and proteome-wide protein quantification. *Nature Biotechnology*, *26*(12), 1367–1372. https://doi.org/10.1038/nbt.1511

Cronan, J. E. (2005). Targeted and proximity-dependent promiscuous protein biotinylation by a mutant Escherichia coli biotin protein ligase. *The Journal of nutritional biochemistry*, *16*(7), 416–418. https://doi.org/10.1016/j.jnutbio.2005.03.017

Cruz-Ramos, E., Sandoval-Hernández, A., & Tecalco-Cruz, A. C. (2019). Differential expression and molecular interactions of chromosome region maintenance 1 and calreticulin exportins in breast cancer cells. *The Journal of steroid biochemistry and molecular biology*, *185*, 7–16. https://doi.org/10.1016/j.jsbmb.2018.07.003

Currier, A. W., Kolb, E. A., Gorlick, R. G., Roth, M. E., Gopalakrishnan, V., & Sampson, V. B. (2019). p27/Kip1 functions as a tumor suppressor and oncoprotein in osteosarcoma. *Scientific reports*, *9*(1), 6161. https://doi.org/10.1038/s41598-019-42450-0

Damm, F., Mylonas, E., Cosson, A., Yoshida, K., Della Valle, V., Mouly, E., Diop, M., Scourzic, L., Shiraishi, Y., Chiba, K., Tanaka, H., Miyano, S., Kikushige, Y., Davi, F., Lambert, J., Gautheret, D., Merle-Béral, H., Sutton, L., Dessen, P., Solary, E., … Bernard, O. A. (2014). Acquired initiating mutations in early hematopoietic cells of CLL patients. *Cancer discovery*, *4*(9), 1088–1101. https://doi.org/10.1158/2159-8290.CD-14-0104

Damodaran, A. P., Vaufrey, L., Gavard, O., & Prigent, C. (2017). Aurora A Kinase Is a Priority Pharmaceutical Target for the Treatment of Cancers. *Trends in pharmacological sciences*, *38*(8), 687–700. https://doi.org/10.1016/j.tips.2017.05.003

Dawei, H., Honggang, D., & Qian, W. (2018). AURKA contributes to the progression of oral squamous cell carcinoma (OSCC) through modulating epithelial-to-mesenchymal transition (EMT) and apoptosis via the regulation of ROS. *Biochemical and biophysical research communications*, *507*(1-4), 83–90. https://doi.org/10.1016/j.bbrc.2018.10.170

De Cesare, M., Cominetti, D., Doldi, V., Lopergolo, A., Deraco, M., Gandellini, P., Friedlander, S., Landesman, Y., Kauffman, M. G., Shacham, S., Pennati, M., & Zaffaroni, N. (2015). Anti-tumor activity of selective inhibitors of XPO1/CRM1-mediated nuclear export in diffuse malignant peritoneal mesothelioma: the role of survivin. *Oncotarget*, *6*(15), 13119–13132. https://doi.org/10.18632/oncotarget.3761

Dees, E. C., Cohen, R. B., von Mehren, M., Stinchcombe, T. E., Liu, H., Venkatakrishnan, K., Manfredi, M., Fingert, H., Burris, H. A., 3rd, & Infante, J. R. (2012). Phase I study of aurora A kinase inhibitor MLN8237 in advanced solid tumors: safety, pharmacokinetics, pharmacodynamics, and bioavailability of two oral formulations. *Clinical cancer research : an official journal of the American Association for Cancer Research*, *18*(17), 4775–4784. https://doi.org/10.1158/1078-0432.CCR-12-0589

DeSisto, J. A., Flannery, P., Lemma, R., Pathak, A., Mestnik, S., Philips, N., Bales, N. J., Kashyap, T., Moroze, E., Venkataraman, S., Kung, A. L., Carter, B. D., Landesman, Y., Vibhakar, R., & Green, A. L. (2020). Exportin 1 Inhibition Induces Nerve Growth Factor Receptor Expression to Inhibit the NF-κB Pathway in Preclinical Models of Pediatric High-Grade Glioma. *Molecular cancer therapeutics*, *19*(2), 540–551. https://doi.org/10.1158/1535-7163.MCT-18-1319

Dian, C., Bernaudat, F., Langer, K., Oliva, M. F., Fornerod, M., Schoehn, G., Müller, C. W., & Petosa, C. (2013). Structure of a truncation mutant of the nuclear export factor CRM1 provides insights into the auto-inhibitory role of its C-terminal helix. *Structure, 1993)*, *21*(8), 1338–1349. https://doi.org/10.1016/j.str.2013.06.003

Dickmanns, A., Monecke, T., & Ficner, R. (2015). Structural Basis of Targeting the Exportin CRM1 in Cancer. *Cells*, *4*(3), 538–568. https://doi.org/10.3390/cells4030538

Dimopoulos, K., Søgaard Helbo, A., Fibiger Munch-Petersen, H., Sjö, L., Christensen, J., Sommer Kristensen, L., Asmar, F., Hermansen, N., O'Connel, C., Gimsing, P., Liang, G., & Grønbaek, K. (2018). Dual inhibition of DNMTs and EZH2 can overcome both intrinsic and acquired resistance of myeloma cells to IMiDs in a cereblon-independent manner. *Molecular oncology*, *12*(2), 180–195. https://doi.org/10.1002/1878-0261.12157

Dingwall, C., Robbins, J., Dilworth, S. M., Roberts, B., & Richardson, W. D. (1988). The nucleoplasmin nuclear location sequence is larger and more complex than that of SV-40 large T antigen. *The Journal of cell biology*, *107*(3), 841–849. https://doi.org/10.1083/jcb.107.3.841

Dong, X., Biswas, A., & Chook, Y. M. (2009b). Structural basis for assembly and disassembly of the CRM1 nuclear export complex. *Nature structural & molecular biology*, *16*(5), 558–560. https://doi.org/10.1038/nsmb.1586

Dong, X., Biswas, A., Süel, K. E., Jackson, L. K., Martinez, R., Gu, H., & Chook, Y. M. (2009a). Structural basis for leucine-rich nuclear export signal recognition by CRM1. *Nature*, *458*(7242), 1136–1141. https://doi.org/10.1038/nature07975

Druker, B. J., Tamura, S., Buchdunger, E., Ohno, S., Segal, G. M., Fanning, S., Zimmermann, J., & Lydon, N. B. (1996). Effects of a selective inhibitor of the Abl tyrosine kinase on the growth of Bcr-Abl positive cells. *Nature medicine*, *2*(5), 561–566. https://doi.org/10.1038/nm0596-561

Du, R., Huang, C., Liu, K., Li, X., & Dong, Z. (2021). Targeting AURKA in Cancer: molecular mechanisms and opportunities for Cancer therapy. *Molecular cancer*, *20*(1), 15. https://doi.org/10.1186/s12943-020-01305-3

Dubois, S., Viailly, P. J., Mareschal, S., Bohers, E., Bertrand, P., Ruminy, P., Maingonnat, C., Jais, J. P., Peyrouze, P., Figeac, M., Molina, T. J., Desmots, F., Fest, T., Haioun, C., Lamy, T., Copie-Bergman, C., Brière, J., Petrella, T., Canioni, D., Fabiani, B., … Jardin, F. (2016). Next-Generation Sequencing in Diffuse Large B-Cell Lymphoma Highlights Molecular Divergence and Therapeutic Opportunities: a LYSA Study. *Clinical cancer research : an official journal of the American Association for Cancer Research*, *22*(12), 2919–2928. https://doi.org/10.1158/1078-0432.CCR-15-2305

Duijvesz, D., Rodriguez-Blanco, G., Hoogland, A. M., Verhoef, E. I., Dekker, L. J., Roobol, M. J., van Leenders, G., Luider, T. M., & Jenster, G. (2019). Differential tissue expression of extracellular vesicle-derived proteins in prostate cancer. *The Prostate*, *79*(9), 1032–1042. https://doi.org/10.1002/pros.23813

Dunham, W. H., Mullin, M., & Gingras, A. C. (2012). Affinity-purification coupled to mass spectrometry: Basic principles and strategies. *Proteomics*, *12*(10), 1576–1590. https://doi.org/10.1002/pmic.201100523

Eich, M. L., Athar, M., Ferguson, J. E., & Varambally, S. (2020). EZH2-targeted therapies in cancer: Hype or a reality. *Cancer Research*, *80*(24), 5449–5458. https://doi.org/10.1158/0008-5472.CAN-20-2147

Engelsma, D., Rodriguez, J. A., Fish, A., Giaccone, G., & Fornerod, M. (2007). Homodimerization antagonizes nuclear export of survivin. *Traffic*, *8*(11), 1495–1502. https://doi.org/10.1111/j.1600-0854.2007.00629.x

Etchin, J., Sanda, T., Mansour, M. R., Kentsis, A., Montero, J., Le, B. T., Christie, A. L., McCauley, D., Rodig, S. J., Kauffman, M., Shacham, S., Stone, R., Letai, A., Kung, A. L., & Thomas Look, A. (2013b). KPT-330 inhibitor of CRM1 (XPO1)-mediated nuclear export has selective anti-leukaemic activity in preclinical models of T-cell acute lymphoblastic leukaemia and acute myeloid leukaemia. *British journal of haematology*, *161*(1), 117–127. https://doi.org/10.1111/bjh.12231

Etchin, J., Sun, Q., Kentsis, A., Farmer, A., Zhang, Z. C., Sanda, T., Mansour, M. R., Barcelo, C., McCauley, D., Kauffman, M., Shacham, S., Christie, A. L., Kung, A. L., Rodig, S. J., Chook, Y. M., & Look, A. T. (2013a). Antileukemic activity of nuclear export inhibitors that spare normal hematopoietic cells. *Leukemia*, *27*(1), 66–74. https://doi.org/10.1038/leu.2012.219

European Medicines Agency. 2021. Nexpovio (selinexor). *(Report No. EMA/71773/2021*). Retrieved from https://www.ema.europa.eu/en/documents/overview/nexpovio-epar-medicine-overview_en-1.pdf

Falini, B., Nicoletti, I., Martelli, M. F., & Mecucci, C. (2007). Acute myeloid leukemia carrying cytoplasmic/mutated nucleophosmin (NPMc+ AML): biologic and clinical features. *Blood*, *109*(3), 874–885. https://doi.org/10.1182/blood-2006-07-012252

Fan, Z., Pei, R., Sha, K., Chen, L., Wang, T., & Lu, Y. (2020). Comprehensive characterization of driver genes in diffuse large B cell lymphoma. *Oncology letters*, *20*(1), 382–390. https://doi.org/10.3892/ol.2020.11552

Federici, L., & Falini, B. (2013). Nucleophosmin mutations in acute myeloid leukemia: a tale of protein unfolding and mislocalization. *Protein science: a publication of the Protein Society*, *22*(5), 545–556. https://doi.org/10.1002/pro.2240

Felgenhauer, J., Tomino, L., Selich-Anderson, J., Bopp, E., & Shah, N. (2018). Dual BRD4 and AURKA Inhibition Is Synergistic against MYCN-Amplified and Nonamplified Neuroblastoma. *Neoplasia*, *20*(10), 965–974. https://doi.org/10.1016/j.neo.2018.08.002

Ferreiro-Neira, I., Torres, N. E., Liesenfeld, L. F., Chan, C. H., Penson, T., Landesman, Y., Senapedis, W., Shacham, S., Hong, T. S., & Cusack, J. C. (2016). XPO1 Inhibition Enhances Radiation Response in Preclinical Models of Rectal Cancer. *Clinical cancer research: an official journal of the American Association for Cancer Research*, *22*(7), 1663–1673. https://doi.org/10.1158/1078-0432.CCR-15-0978

Fetz, V., Knauer, S. K., Bier, C., von Kries, J. P., & Stauber, R. H. (2009). Translocation Biosensors - Cellular System Integrators to Dissect CRM1-Dependent Nuclear Export by Chemicogenomics. *Sensors*, *9*(7), 5423–5445. https://doi.org/10.3390/s90705423

Fiedler, W., Chromik, J., Amberg, S., Kebenko, M., Thol, F., Schlipfenbacher, V., Christine Wilke, A., Modemann, F., Janning, M., Serve, H., Ganser, A., Bokemeyer, C., Theile, S., Deppermann, U., Kranich, A. L., & Heuser, M. (2020). A Phase II study of selinexor plus cytarabine and idarubicin in patients with relapsed/refractory acute myeloid leukaemia. *British journal of haematology*, *190*(3), e169–e173. https://doi.org/10.1111/bjh.16804

Fioravanti, R., Stazi, G., Zwergel, C., Valente, S., & Mai, A. (2018). Six Years (2012-2018) of Researches on Catalytic EZH2 Inhibitors: The Boom of the 2-Pyridone Compounds. *Chemical record*, *18*(12), 1818–1832. https://doi.org/10.1002/tcr.201800091

Fischer, M. A., Friedlander, S. Y., Arrate, M. P., Chang, H., Gorska, A. E., Fuller, L. D., Ramsey, H. E., Kashyap, T., Argueta, C., Debler, S., Byrne, M., Villaume, M. T., Shaver, A. C., Senapedis, W., Landesman, Y., Baloglu, E., Shacham, S., & Savona, M. R. (2020). Venetoclax response is enhanced by selective inhibitor of nuclear export compounds in hematologic malignancies. *Blood advances*, *4*(3), 586–598. https://doi.org/10.1182/bloodadvances.2019000359

Fischer, U., Huber, J., Boelens, W. C., Mattajt, L. W., & Lührmann, R. (1995). The HIV-1 Rev Activation Domain is a nuclear export signal that accesses an export pathway used by specific cellular RNAs. *Cell*, *82*(3), 475–483. https://doi.org/10.1016/0092-8674(95)90436-0

Food and Drug Administration. (2019). FDA grants accelerated approval to selinexor for multiple myeloma. Retrieved from https://www.fda.gov/drugs/resources-information-approved-drugs/fda-grants-accelerated-approval-selinexor-multiple-myeloma

Food and Drug Administration. (2020a). FDA approves selinexor for refractory or relapsed multiple myeloma. Retrieved from https://www.fda.gov/drugs/drug-approvals-and-databases/fda-approves-selinexor-refractory-or-relapsed-multiple-myeloma

Food and Drug Administration. (2020b). FDA approves selinexor for relapsed/refractory diffuse large B-cell lymphoma. Retrieved from https://www.fda.gov/drugs/resources-information-approved-drugs/fda-approves-selinexor-relapsedrefractory-diffuse-large-b-cell-lymphoma

Food and Drug Administration. (2020c). FDA approves first treatment option specifically for patients with epithelioid sarcoma, a rare soft tissue cancer. Retrieved from https://www.fda.gov/news-events/press-announcements/fda-approves-first-treatment-option-specifically-patients-epithelioid-sarcoma-rare-soft-tissue

Food and Drug Administration. (2020d). FDA granted accelerated approval to tazemetostat for follicular lymphoma. Retrieved from https://www.fda.gov/drugs/fda-granted-accelerated-approval-tazemetostat-follicular-lymphoma

Fornerod, M., Ohno, M., Yoshida, M., & Mattaj, I. W. (1997). CRM1 Is an Export Receptor for Leucine-Rich Nuclear Export Signals. *Cell*, *90*(6), 1051–1060. https://doi.org/10.1016/s0092-8674(00)80371-2

Fox, A. M., Ciziene, D., McLaughlin, S. H., & Stewart, M. (2011). Electrostatic interactions involving the extreme C terminus of nuclear export factor CRM1 modulate its affinity for cargo. *The Journal of biological chemistry*, *286*(33), 29325–29335. https://doi.org/10.1074/jbc.M111.245092

Frey, S., Rees, R., Schünemann, J., Ng, S. C., Fünfgeld, K., Huyton, T., & Görlich, D. (2018). Surface properties determining passage rates of proteins through nuclear pores. *Cell*, *174*, 202–217. https://doi.org/10.1016/j.cell.2018.05.045

Fu, S. C., Fung, H., Cağatay, T., Baumhardt, J., & Chook, Y. M. (2018). Correlation of CRM1-NES affinity with nuclear export activity. *Molecular biology of the cell*, *29*(17), 2037–2044. https://doi.org/10.1091/mbc.E18-02-0096

Fu, S. C., Imai, K., & Horton, P. (2011). Prediction of leucine-rich nuclear export signal containing proteins with NESsential. *Nucleic acids research*, *39*(16), e111. https://doi.org/10.1093/nar/gkr493

Fukuda, M., Asano, S., Nakamura, T., Adachi, M., Yoshida, M., Yanagida, M., & Nishida, E. (1997). CRM1 is responsible for intracellular transport mediated by the nuclear export signal. *Nature*, *390*(6657), 308–311. https://doi.org/10.1038/36894

Fukuda, M., Gotoh, I., Gotoh, Y., & Nishida, E. (1996). Cytoplasmic localization of mitogen-activated protein kinase kinase directed by its NH2-terminal, leucine-rich short amino acid sequence, which acts as a nuclear export signal. *The Journal of biological chemistry*, *271*(33), 20024–20028. https://doi.org/10.1074/jbc.271.33.20024

Fung, H. Y., & Chook, Y. M. (2014). Atomic basis of CRM1-cargo recognition, release and inhibition. *Seminars in cancer biology*, *27*, 52–61. https://doi.org/10.1016/j.semcancer.2014.03.002

Fung, H. Y., Fu, S. C., & Chook, Y. M. (2017). Nuclear export receptor CRM1 recognizes diverse conformations in nuclear export signals. *eLife*, *6*, e23961. https://doi.org/10.7554/eLife.23961

Fung, H. Y., Fu, S. C., Brautigam, C. A., & Chook, Y. M. (2015). Structural determinants of nuclear export signal orientation in binding to exportin CRM1. *eLife*, *4*, e10034. https://doi.org/10.7554/eLife.10034

Fung, H., Niesman, A., & Chook, Y. M. (2021). An update to the CRM1 cargo/NES database NESdb. *Molecular biology of the cell*, *32*(6), 467–469. https://doi.org/10.1091/mbc.E20-11-0694

Gall, J. G. (1967). Octagonal nuclear pores. *The Journal of cell biology*, *32*(2), 391–399. https://doi.org/10.1083/jcb.32.2.391

Gan, L., Yang, Y., Li, Q., Feng, Y., Liu, T., & Guo, W. (2018). Epigenetic regulation of cancer progression by EZH2: from biological insights to therapeutic potential. *Biomarker research*, *6*, 10. https://doi.org/10.1186/s40364-018-0122-2

Gángó, A., Alpár, D., Galik, B., Marosvári, D., Kiss, R., Fésüs, V., Aczél, D., Eyüpoglu, E., Nagy, N., Nagy, Á., Krizsán, S., Reiniger, L., Farkas, P., Kozma, A., Ádám, E., Tasnády, S., Réti, M., Matolcsy, A., Gyenesei, A., Mátrai, Z., … Bödör, C. (2020). Dissection of subclonal evolution by temporal mutation profiling in chronic lymphocytic leukemia patients treated with ibrutinib. *International journal of cancer*, *146*(1), 85–93. https://doi.org/10.1002/ijc.32502

Gangula, N. R., & Maddika, S. (2013). WD repeat protein WDR48 in complex with deubiquitinase USP12 suppresses Akt-dependent cell survival signaling by stabilizing PH domain leucine-rich repeat protein phosphatase 1 (PHLPP1). *The Journal of biological chemistry*, *288*(48), 34545–34554. https://doi.org/10.1074/jbc.M113.503383

Gao, J., Aksoy, B. A., Dogrusoz, U., Dresdner, G., Gross, B., Sumer, S. O., Sun, Y., Jacobsen, A., Sinha, R., Larsson, E., Cerami, E., Sander, C., & Schultz, N. (2013). Integrative analysis of complex cancer genomics and clinical profiles using the cBioPortal. *Science signaling*, *6*(269), pl1. https://doi.org/10.1126/scisignal.2004088

Gao, J., Azmi, A. S., Aboukameel, A., Kauffman, M., Shacham, S., Abou-Samra, A. B., & Mohammad, R. M. (2014). Nuclear retention of Fbw7 by specific inhibitors of nuclear export leads to Notch1 degradation in pancreatic cancer. *Oncotarget*, *5*(11), 3444–3454. https://doi.org/10.18632/oncotarget.1813

García-Santisteban, I., Arregi, I., Alonso-Mariño, M., Urbaneja, M. A., Garcia-Vallejo, J. J., Bañuelos, S., & Rodríguez, J. A. (2016). A cellular reporter to evaluate CRM1 nuclear export activity: functional analysis of the cancer-related mutant E571K. *Cellular and Molecular Life Sciences*, *73*(24), 4685–4699. https://doi.org/10.1007/s00018-016-2292-0

García-Santisteban, I., Bañuelos, S., & Rodríguez, J. A. (2012). A global survey of CRM1-dependent nuclear export sequences in the human deubiquitinase family. *The Biochemical journal*, *441*(1), 209–217. https://doi.org/10.1042/BJ20111300

Garg, M., Kanojia, D., Mayakonda, A., Ganesan, T. S., Sadhanandhan, B., Suresh, S., S, S., Nagare, R. P., Said, J. W., Doan, N. B., Ding, L. W., Baloglu, E., Shacham, S., Kauffman, M., & Koeffler, H. P. (2017a). Selinexor (KPT-330) has antitumor activity against anaplastic thyroid carcinoma in vitro and in vivo and enhances sensitivity to doxorubicin. *Scientific reports*, *7*(1), 9749. https://doi.org/10.1038/s41598-017-10325-x

Garg, M., Kanojia, D., Mayakonda, A., Said, J. W., Doan, N. B., Chien, W., Ganesan, T. S., Chuang, L. S., Venkatachalam, N., Baloglu, E., Shacham, S., Kauffman, M., & Koeffler, H. P. (2017b). Molecular mechanism and therapeutic implications of selinexor (KPT-330) in liposarcoma. *Oncotarget*, *8*(5), 7521–7532. https://doi.org/10.18632/oncotarget.13485

Garzon, R., Savona, M., Baz, R., Andreeff, M., Gabrail, N., Gutierrez, M., Savoie, L., Mau-Sorensen, P. M., Wagner-Johnston, N., Yee, K., Unger, T. J., Saint-Martin, J. R., Carlson, R., Rashal, T., Kashyap, T., Klebanov, B., Shacham, S., Kauffman, M., & Stone, R. (2017). A phase 1 clinical trial of single-agent selinexor in acute myeloid leukemia. *Blood*, *129*(24), 3165–3174. https://doi.org/10.1182/blood-2016-11-750158

Gingras, A. C., Abe, K. T., & Raught, B. (2019). Getting to know the neighborhood: using proximity-dependent biotinylation to characterize protein complexes and map organelles. *Current Opinion in Chemical Biology*, *48*, 44–54. https://doi.org/10.1016/j.cbpa.2018.10.017

Glinsky, G. V., Glinskii, A. B., Stephenson, A. J., Hoffman, R. M., & Gerald, W. L. (2004). Gene expression profiling predicts clinical outcome of prostate cancer. *The Journal of clinical investigation*, *113*(6), 913–923. https://doi.org/10.1172/JCI20032

Golomb, L., Bublik, D. R., Wilder, S., Nevo, R., Kiss, V., Grabusic, K., Volarevic, S., & Oren, M. (2012). Importin 7 and exportin 1 link c-Myc and p53 to regulation of ribosomal biogenesis. *Molecular cell*, *45*(2), 222–232. https://doi.org/10.1016/j.molcel.2011.11.022

Gorecki, L., Andrs, M., & Korabecny, J. (2021). Clinical Candidates Targeting the ATR-CHK1-WEE1 Axis in Cancer. *Cancers*, *13*(4), 795. https://doi.org/10.3390/cancers13040795

Gould, C. M., Diella, F., Via, A., Puntervoll, P., Gemünd, C., Chabanis-Davidson, S., Michael, S., Sayadi, A., Bryne, J. C., Chica, C., Seiler, M., Davey, N. E., Haslam, N., Weatheritt, R. J., Budd, A., Hughes, T., Pas, J., Rychlewski, L., Travé, G., Aasland, R., … Gibson, T. J. (2010). ELM: the status of the 2010 eukaryotic linear motif resource. *Nucleic acids research*, *38*(Database issue), D167–D180. https://doi.org/10.1093/nar/gkp1016

Gounder, M. M., Zer, A., Tap, W. D., Salah, S., Dickson, M. A., Gupta, A. A., Keohan, M. L., Loong, H. H., D'Angelo, S. P., Baker, S., Condy, M., Nyquist-Schultz, K., Tanner, L., Erinjeri, J. P., Jasmine, F. H., Friedlander, S., Carlson, R., Unger, T. J., Saint-Martin, J. R., Rashal, T., … Abdul Razak, A. R. (2016). Phase IB Study of Selinexor, a First-in-Class Inhibitor of Nuclear Export, in Patients With Advanced Refractory Bone or Soft Tissue Sarcoma. *Journal of clinical oncology : official journal of the American Society of Clinical Oncology*, *34*(26), 3166–3174. https://doi.org/10.1200/JCO.2016.67.6346

Grasso, C. S., Wu, Y. M., Robinson, D. R., Cao, X., Dhanasekaran, S. M., Khan, A. P., Quist, M. J., Jing, X., Lonigro, R. J., Brenner, J. C., Asangani, I. A., Ateeq, B., Chun, S. Y., Siddiqui, J., Sam, L., Anstett, M., Mehra, R., Prensner, J. R., Palanisamy, N., Ryslik, G. A., … Tomlins, S. A. (2012). The mutational landscape of lethal castration-resistant prostate cancer. *Nature*, *487*(7406), 239–243. https://doi.org/10.1038/nature11125

Gravina, G. L., Mancini, A., Colapietro, A., Marampon, F., Sferra, R., Pompili, S., Biordi, L. A., Iorio, R., Flati, V., Argueta, C., Landesman, Y., Kauffman, M., Shacham, S., & Festuccia, C. (2017). Pharmacological treatment with inhibitors of nuclear export enhances the antitumor activity of docetaxel in human prostate cancer. *Oncotarget*, *8*(67), 111225–111245. https://doi.org/10.18632/oncotarget.22760

Gravina, G. L., Senapedis, W., McCauley, D., Baloglu, E., Shacham, S., & Festuccia, C. (2014a). Nucleo-cytoplasmic transport as a therapeutic target of cancer. *Journal of hematology & oncology*, *7*, 85. https://doi.org/10.1186/s13045-014-0085-1

Gravina, G. L., Tortoreto, M., Mancini, A., Addis, A., Di Cesare, E., Lenzi, A., Landesman, Y., McCauley, D., Kauffman, M., Shacham, S., Zaffaroni, N., & Festuccia, C. (2014b). XPO1/CRM1-selective inhibitors of nuclear export (SINE) reduce tumor spreading and improve overall survival in preclinical models of prostate cancer (PCa). *Journal of hematology & oncology*, *7*, 46. https://doi.org/10.1186/1756-8722-7-46

Green, A. L., Ramkissoon, S. H., McCauley, D., Jones, K., Perry, J. A., Hsu, J. H., Ramkissoon, L. A., Maire, C. L., Hubbell-Engler, B., Knoff, D. S., Shacham, S., Ligon, K. L., & Kung, A. L. (2015). Preclinical antitumor efficacy of selective exportin 1 inhibitors in glioblastoma. *Neuro-oncology*, *17*(5), 697–707. https://doi.org/10.1093/neuonc/nou303

Grosicki, S., Simonova, M., Spicka, I., Pour, L., Kriachok, I., Gavriatopoulou, M., Pylypenko, H., Auner, H. W., Leleu, X., Doronin, V., Usenko, G., Bahlis, N. J., Hajek, R., Benjamin, R., Dolai, T. K., Sinha, D. K., Venner, C. P., Garg, M., Gironella, M., Jurczyszyn, A., … Delimpasi, S. (2020). Once-per-week selinexor, bortezomib, and dexamethasone versus twice-per-week bortezomib and dexamethasone in patients with multiple myeloma (BOSTON): a randomised, open-label, phase 3 trial. *Lancet*, *396*(10262), 1563–1573. https://doi.org/10.1016/S0140-6736(20)32292-3

Gruffaz, M., Yuan, H., Meng, W., Liu, H., Bae, S., Kim, J. S., Lu, C., Huang, Y., & Gao, S. J. (2019). CRISPR-Cas9 Screening of Kaposi's Sarcoma-Associated Herpesvirus-Transformed Cells Identifies XPO1 as a Vulnerable Target of Cancer Cells. *mBio*, *10*(3), e00866-19. https://doi.org/10.1128/mBio.00866-19

Guglielmelli, P., Biamonte, F., Score, J., Hidalgo-Curtis, C., Cervantes, F., Maffioli, M., Fanelli, T., Ernst, T., Winkelman, N., Jones, A. V., Zoi, K., Reiter, A., Duncombe, A., Villani, L., Bosi, A., Barosi, G., Cross, N. C., & Vannucchi, A. M. (2011). EZH2 mutational status predicts poor survival in myelofibrosis. *Blood*, *118*(19), 5227–5234. https://doi.org/10.1182/blood-2011-06-363424

Guièze, R., Robbe, P., Clifford, R., de Guibert, S., Pereira, B., Timbs, A., Dilhuydy, M. S., Cabes, M., Ysebaert, L., Burns, A., Nguyen-Khac, F., Davi, F., Véronèse, L., Combes, P., Le Garff-Tavernier, M., Leblond, V., Merle-Béral, H., Alsolami, R., Hamblin, A., Mason, J., … Schuh, A. (2015). Presence of multiple recurrent mutations confers poor trial outcome of relapsed/refractory CLL. *Blood*, *126*(18), 2110–2117. https://doi.org/10.1182/blood-2015-05-647578

Gupta, D., & Heinen, C. D. (2019). The mismatch repair-dependent DNA damage response: Mechanisms and implications. *DNA Repair*, *78*, 60–69. https://doi.org/10.1016/j.dnarep.2019.03.009

Gussow, A. B., Auslander, N., Faure, G., Wolf, Y. I., Zhang, F., & Koonin, E. V. (2020). Genomic determinants of pathogenicity in SARS-CoV-2 and other human coronaviruses. *Proceedings of the National Academy of Sciences of the United States of America*, *117*(26), 15193–15199. https://doi.org/10.1073/pnas.2008176117

Güttler, T., Madl, T., Neumann, P., Deichsel, D., Corsini, L., Monecke, T., Ficner, R., Sattler, M., & Görlich, D. (2010). NES consensus redefined by structures of PKI-type and Rev-type nuclear export signals bound to CRM1. *Nature structural & molecular biology*, *17*(11), 1367–1376. https://doi.org/10.1038/nsmb.1931

Haines, J. D., Herbin, O., de la Hera, B., Vidaurre, O. G., Moy, G. A., Sun, Q., Fung, H. Y., Albrecht, S., Alexandropoulos, K., McCauley, D., Chook, Y. M., Kuhlmann, T., Kidd, G. J., Shacham, S., & Casaccia, P. (2015). Nuclear export inhibitors avert progression in preclinical models of inflammatory demyelination. *Nature neuroscience*, *18*(4), 511–520. https://doi.org/10.1038/nn.3953

Han, X., Wang, J., Shen, Y., Zhang, N., Wang, S., Yao, J., & Shi, Y. (2015). CRM1 as a new therapeutic target for non-Hodgkin lymphoma. *Leukemia research*, *39*(1), 38–46. https://doi.org/10.1016/j.leukres.2014.10.003

Hao, Y., Zhang, L., Niu, Y., Cai, T., Luo, J., He, S., Zhang, B., Zhang, D., Qin, Y., Yang, F., & Chen, R. (2018). SmProt: a database of small proteins encoded by annotated coding and non-coding RNA loci. *Briefings in bioinformatics*, *19*(4), 636–643. https://doi.org/10.1093/bib/bbx005

Hartford, C., & Lal, A. (2020). When Long Noncoding Becomes Protein Coding. *Molecular and cellular biology*, *40*(6), e00528-19. https://doi.org/10.1128/MCB.00528-19

Henderson, B. R., & Eleftheriou, A. (2000). A comparison of the activity, sequence specificity, and CRM1-dependence of different nuclear export signals. *Experimental Cell Research*, *256*(1), 213–224. https://doi.org/10.1006/excr.2000.4825

Hernández, J. Á., Hernández-Sánchez, M., Rodríguez-Vicente, A. E., Grossmann, V., Collado, R., Heras, C., Puiggros, A., Martín, A. Á., Puig, N., Benito, R., Robledo, C., Delgado, J., González, T., Queizán, J. A., Galende, J., de la Fuente, I., Martín-Núñez, G., Alonso, J. M., Abrisqueta, P., Luño, E., … Grupo Cooperativo Español de Citogenética Hematológica (GCECGH) and Grupo Español de Leucemia Linfática Crónica (GELLC) (2015). A Low Frequency of Losses in 11q Chromosome Is Associated with Better Outcome and Lower Rate of Genomic Mutations in Patients with

Chronic Lymphocytic Leukemia. *PloS one*, *10*(11), e0143073. https://doi.org/10.1371/journal.pone.0143073

Herrera-Merchan, A., Arranz, L., Ligos, J. M., de Molina, A., Dominguez, O., & Gonzalez, S. (2012). Ectopic expression of the histone methyltransferase Ezh2 in haematopoietic stem cells causes myeloproliferative disease. *Nature communications*, *3*, 623. https://doi.org/10.1038/ncomms1623

Herviou, L., Kassambara, A., Boireau, S., Robert, N., Requirand, G., Müller-Tidow, C., Vincent, L., Seckinger, A., Goldschmidt, H., Cartron, G., Hose, D., Cavalli, G., & Moreaux, J. (2018). PRC2 targeting is a therapeutic strategy for EZ score defined high-risk multiple myeloma patients and overcome resistance to IMiDs. *Clinical epigenetics*, *10*(1), 121. https://doi.org/10.1186/s13148-018-0554-4

Hill, R., Cautain, B., de Pedro, N., & Link, W. (2014). Targeting nucleocytoplasmic transport in cancer therapy. *Oncotarget*, *5*(1), 11–28. https://doi.org/10.18632/oncotarget.1457

Hing, Z. A., Mantel, R., Beckwith, K. A., Guinn, D., Williams, E., Smith, L. L., Williams, K., Johnson, A. J., Lehman, A. M., Byrd, J. C., Woyach, J. A., & Lapalombella, R. (2015). Selinexor is effective in acquired resistance to ibrutinib and synergizes with ibrutinib in chronic lymphocytic leukemia. *Blood*, *125*(20), 3128–3132. https://doi.org/10.1182/blood-2015-01-621391

Hou, D., Che, Z., Chen, P., Zhang, W., Chu, Y., Yang, D., & Liu, J. (2018). Suppression of AURKA alleviates p27 inhibition on Bax cleavage and induces more intensive apoptosis in gastric cancer. *Cell death & disease*, *9*(8), 781. https://doi.org/10.1038/s41419-018-0823-3

Hu, B., Patel, K. P., Chen, H. C., Wang, X., Wang, F., Luthra, R., Routbort, M. J., Kanagal-Shamanna, R., Medeiros, L. J., Yin, C. C., Zuo, Z., Ok, C. Y., Loghavi, S., Tang, G., Tambaro, F. P., Thompson, P., Burger, J., Jain, N., Ferrajoli, A., Bose, P., … Wierda, W. G. (2019). Routine sequencing in CLL has prognostic implications and provides new insight into pathogenesis and targeted treatments. *British journal of haematology*, *185*(5), 852–864. https://doi.org/10.1111/bjh.15877

Huang, J. Z., Chen, M., Chen, D., Gao, X. C., Zhu, S., Huang, H., Hu, M., Zhu, H., & Yan, G. R. (2017). A Peptide Encoded by a Putative lncRNA HOXB-AS3 Suppresses Colon Cancer Growth. *Molecular cell*, *68*(1), 171–184.e6. https://doi.org/10.1016/j.molcel.2017.09.015

Huang, W. Y., Yue, L., Qiu, W. S., Wang, L. W., Zhou, X. H., & Sun, Y. J. (2009). Prognostic value of CRM1 in pancreas cancer. *Clinical and investigative medicine. Medecine clinique et experimentale*, *32*(6), E315.

Huang, X., LeDuc, R. D., Fornelli, L., Schunter, A. J., Bennett, R. L., Kelleher, N. L., & Licht, J. D. (2019). Defining the NSD2 interactome: PARP1 PARylation reduces NSD2 histone methyltransferase activity and impedes chromatin binding. *Journal of Biological Chemistry*, *294*(33), 12459–12471. https://doi.org/10.1074/jbc.RA118.006159

Huang, X., Yan, J., Zhang, M., Wang, Y., Chen, Y., Fu, X., Wei, R., Zheng, X. L., Liu, Z., Zhang, X., Yang, H., Hao, B., Shen, Y. Y., Su, Y., Cong, X., Huang, M., Tan, M., Ding, J., & Geng, M. (2018). Targeting Epigenetic Crosstalk as a Therapeutic Strategy for EZH2-Aberrant Solid Tumors. *Cell*, *175*(1), 186–199.e19. https://doi.org/10.1016/j.cell.2018.08.058

Hung, M. C., & Link, W. (2011). Protein localization in disease and therapy. *Journal of cell science*, *124*(Pt 20), 3381–3392. https://doi.org/10.1242/jcs.089110

Hung, V., Udeshi, N. D., Lam, S. S., Loh, K. H., Cox, K. J., Pedram, K., Carr, S. A., & Ting, A. Y. (2016). Spatially resolved proteomic mapping in living cells with the engineered peroxidase APEX2. *Nature protocols*, *11*(3), 456–475. https://doi.org/10.1038/nprot.2016.018

Hung, V., Zou, P., Rhee, H. W., Udeshi, N. D., Cracan, V., Svinkina, T., Carr, S. A., Mootha, V. K., & Ting, A. Y. (2014). Proteomic mapping of the human mitochondrial intermembrane space in live cells via ratiometric APEX tagging. *Molecular cell*, *55*(2), 332–341. https://doi.org/10.1016/j.molcel.2014.06.003

Hutten, S., & Kehlenbach, R. H. (2007). CRM1-mediated nuclear export: to the pore and beyond. Trends in cell biology, 17(4), 193–201. https://doi.org/10.1016/j.tcb.2007.02.003

Inoue, A., Robinson, F. S., Minelli, R., Tomihara, H., Rizi, B. S., Rose, J. L., Kodama, T., Srinivasan, S., Harris, A. L., Zuniga, A. M., Mullinax, R. A., Ma, X., Seth, S., Daniele, J. R., Peoples, M. D., Loponte, S., Akdemir, K. C., Khor, T. O., Feng, N., Roszik, J., … Carugo, A. (2021). Sequential administration of XPO1 and ATR inhibitors enhances therapeutic response in TP53-mutated colorectal cancer. *Gastroenterology*, *161(1),196–210*. https://doi.org/10.1053/j.gastro.2021.03.022

Inoue, H., Kauffman, M., Shacham, S., Landesman, Y., Yang, J., Evans, C. P., & Weiss, R. H. (2013). CRM1 blockade by selective inhibitors of nuclear export attenuates kidney cancer growth. *The Journal of urology*, *189*(6), 2317–2326. https://doi.org/10.1016/j.juro.2012.10.018

Italiano, A., Soria, J. C., Toulmonde, M., Michot, J. M., Lucchesi, C., Varga, A., Coindre, J. M., Blakemore, S. J., Clawson, A., Suttle, B., McDonald, A. A., Woodruff, M., Ribich, S., Hedrick, E., Keilhack, H., Thomson, B., Owa, T., Copeland, R. A., Ho, P., & Ribrag, V. (2018). Tazemetostat, an EZH2 inhibitor, in relapsed or refractory B-cell non-Hodgkin lymphoma and advanced solid tumours: a first-in-human, open-label, phase 1 study. *The Lancet. Oncology*, *19*(5), 649–659. https://doi.org/10.1016/S1470-2045(18)30145-1

Ivshina, A. V., George, J., Senko, O., Mow, B., Putti, T. C., Smeds, J., Lindahl, T., Pawitan, Y., Hall, P., Nordgren, H., Wong, J. E., Liu, E. T., Bergh, J., Kuznetsov, V. A., & Miller, L. D. (2006). Genetic reclassification of histologic grade delineates new clinical subtypes of breast cancer. *Cancer research*, *66*(21), 10292–10301. https://doi.org/10.1158/0008-5472.CAN-05-4414

Jahan, A. S., Lestra, M., Swee, L. K., Fan, Y., Lamers, M. M., Tafesse, F. G., Theile, C. S., Spooner, E., Bruzzone, R., Ploegh, H. L., & Sanyal, S. (2016). Usp12 stabilizes the T-cell receptor complex at the cell surface during signaling. *Proceedings of the National Academy of Sciences of the United States of America*, *113*(6), E705–E714. https://doi.org/10.1073/pnas.1521763113

Jain, P., Kanagal-Shamanna, R., Wierda, W., Keating, M., Sarwari, N., Rozovski, U., Thompson, P., Burger, J., Kantarjian, H., Patel, K. P., Medeiros, L. J., Luthra, R., & Estrov, Z. (2016). Clinical and molecular characteristics of XPO1 mutations in patients with chronic lymphocytic leukemia. *American journal of hematology*, *91*(11), E478–E479. https://doi.org/10.1002/ajh.24496

Jakubowiak, A. J., Jasielec, J. K., Rosenbaum, C. A., Cole, C. E., Chari, A., Mikhael, J., Nam, J., McIver, A., Severson, E., Stephens, L. A., Tinari, K., Rosebeck, S., Zimmerman, T. M., Hycner, T., Turowski, A., Karrison, T., & Zonder, J. A. (2019). Phase 1 study of selinexor plus carfilzomib and dexamethasone for the treatment of relapsed/refractory multiple myeloma. *British journal of haematology*, *186*(4), 549–560. https://doi.org/10.1111/bjh.15969

Jardin, F., Pujals, A., Pelletier, L., Bohers, E., Camus, V., Mareschal, S., Dubois, S., Sola, B., Ochmann, M., Lemonnier, F., Viailly, P. J., Bertrand, P., Maingonnat, C., Traverse-Glehen, A., Gaulard, P., Damotte, D., Delarue, R., Haioun, C., Argueta, C., Landesman, Y., … Leroy, K. (2016). Recurrent mutations of the exportin 1 gene (XPO1) and their impact on selective inhibitor of nuclear export compounds sensitivity in primary mediastinal B-cell lymphoma. *American journal of hematology*, *91*(9), 923–930. https://doi.org/10.1002/ajh.24451

Jeitany, M., Prabhu, A., Dakle, P., Pathak, E., Madan, V., Kanojia, D., Mukundan, V., Jiang, Y. Y., Landesman, Y., Tam, W. L., Kappei, D., & Koeffler, H. P. (2021). Novel carfilzomib-based combinations as potential therapeutic strategies for liposarcomas. *Cellular and molecular life sciences : CMLS*, *78*(4), 1837–1851. https://doi.org/10.1007/s00018-020-03620-w

Jeromin, S., Weissmann, S., Haferlach, C., Dicker, F., Bayer, K., Grossmann, V., Alpermann, T., Roller, A., Kohlmann, A., Haferlach, T., Kern, W., & Schnittger, S. (2014). SF3B1 mutations correlated to cytogenetics and mutations in NOTCH1, FBXW7, MYD88, XPO1 and TP53 in 1160 untreated CLL patients. *Leukemia*, *28*(1), 108–117. https://doi.org/10.1038/leu.2013.263

Jeyasekharan, A. D., Liu, Y., Hattori, H., Pisupati, V., Jonsdottir, A. B., Rajendra, E., Lee, M., Sundaramoorthy, E., Schlachter, S., Kaminski, C. F., Ofir-Rosenfeld, Y., Sato, K., Savill, J., Ayoub, N., & Venkitaraman, A. R. (2013). A cancer-associated BRCA2 mutation reveals masked nuclear export signals controlling localization. *Nature structural & molecular biology*, *20*(10), 1191–1198. https://doi.org/10.1038/nsmb.2666

Jiang, Y., Hou, J., Zhang, X., Xu, G., Wang, Y., Shen, L., Wu, Y., Li, Y., & Yao, L. (2020). Circ-XPO1 upregulates XPO1 expression by sponging multiple miRNAs to facilitate osteosarcoma cell progression. *Experimental and molecular pathology*, *117*, 104553. https://doi.org/10.1016/j.yexmp.2020.104553

Jiménez, I., Carabia, J., Bobillo, S., Palacio, C., Abrisqueta, P., Pagès, C., Nieto, J. C., Castellví, J., Martínez-Ricarte, F., Escoda, L., Perla, C., Céspedes Torrez, D. H., Boix, J., Purroy, N., Puigdefàbregas, L., Seoane, J., Bosch, F., & Crespo, M. (2020). Repolarization of tumor infiltrating macrophages and increased survival in mouse primary CNS lymphomas after XPO1 and BTK inhibition. *Journal of neuro-oncology*, *149*(1), 13–25. https://doi.org/10.1007/s11060-020-03580-y

Jiricny, J. (2006). The multifaceted mismatch-repair system. *Nature Reviews Molecular Cell Biology*, *7*(5), 335–346. https://doi.org/10.1038/nrm1907

Joo, H. Y., Jones, A., Yang, C., Zhai, L., Smith, A. D., 4th, Zhang, Z., Chandrasekharan, M. B., Sun, Z. W., Renfrow, M. B., Wang, Y., Chang, C., & Wang, H. (2011). Regulation of histone H2A and H2B deubiquitination and Xenopus development by USP12 and USP46. *The Journal of biological chemistry*, *286*(9), 7190–7201. https://doi.org/10.1074/jbc.M110.158311

Jorissen, R. N., Gibbs, P., Christie, M., Prakash, S., Lipton, L., Desai, J., Kerr, D., Aaltonen, L. A., Arango, D., Kruhøffer, M., Orntoft, T. F., Andersen, C. L., Gruidl, M., Kamath, V. P., Eschrich, S., Yeatman, T. J., & Sieber, O. M. (2009). Metastasis-Associated Gene Expression Changes Predict Poor Outcomes in Patients with Dukes Stage B and C Colorectal Cancer. *Clinical cancer research : an official journal of the American Association for Cancer Research*, *15*(24), 7642–7651. https://doi.org/10.1158/1078-0432.CCR-09-1431

Kalakonda, N., Maerevoet, M., Cavallo, F., Follows, G., Goy, A., Vermaat, J., Casasnovas, O., Hamad, N., Zijlstra, J. M., Bakhshi, S., Bouabdallah, R., Choquet, S., Gurion, R., Hill, B., Jaeger, U., Sancho, J. M., Schuster, M., Thieblemont, C., De la Cruz, F., Egyed, M., … Canales, M. A. (2020). Selinexor in patients with relapsed or refractory diffuse large B-cell lymphoma (SADAL): a single-arm, multinational, multicentre, open-label, phase 2 trial. *The Lancet. Haematology*, *7*(7), e511–e522. https://doi.org/10.1016/S2352-3026(20)30120-4

Kalderon, D., Richardson, W. D., Markham, A. F., & Smith, A. E. (1984a). Sequence requirements for nuclear location of simian virus 40 large-T antigen. *Nature*, *311*(5981), 33–38. https://doi.org/10.1038/311033a0

Kalderon, D., Roberts, B. L., Richardson, W. D., & Smith, A. E. (1984b). A short amino acid sequence able to specify nuclear location. *Cell*, *39*(3 Pt 2), 499–509. https://doi.org/10.1016/0092-8674(84)90457-4

Kalid, O., Toledo Warshaviak, D., Shechter, S., Sherman, W., & Shacham, S. (2012). Consensus Induced Fit Docking (cIFD): methodology, validation, and application to the discovery of novel Crm1 inhibitors. *Journal of computer-aided molecular design*, *26*(11), 1217–1228. https://doi.org/10.1007/s10822-012-9611-9

Kancha, R. K., von Bubnoff, N., Miething, C., Peschel, C., Götze, K. S., & Duyster, J. (2008). Imatinib and leptomycin B are effective in overcoming imatinib-resistance due to Bcr-Abl amplification and clonal evolution but not due to Bcr-Abl kinase domain mutation. *Haematologica*, *93*(11), 1718–1722. https://doi.org/10.3324/haematol.13207

Kapoor, I., Li, Y., Sharma, A., Zhu, H., Bodo, J., Xu, W., Hsi, E. D., Hill, B. T., & Almasan, A. (2019). Resistance to BTK inhibition by ibrutinib can be overcome by preventing FOXO3a nuclear export and PI3K/AKT activation in B-cell lymphoid malignancies. *Cell death & disease*, *10*(12), 924. https://doi.org/10.1038/s41419-019-2158-0

Karnitz, L. M., & Zou, L. (2015). Molecular Pathways: Targeting ATR in Cancer Therapy. *Clinical cancer research: an official journal of the American Association for Cancer Research*, *21*(21), 4780–4785. https://doi.org/10.1158/1078-0432.CCR-15-0479

Kashyap, T., Argueta, C., Aboukameel, A., Unger, T. J., Klebanov, B., Mohammad, R. M., Muqbil, I., Azmi, A. S., Drolen, C., Senapedis, W., Lee, M., Kauffman, M., Shacham, S., & Landesman, Y. (2016). Selinexor, a Selective Inhibitor of Nuclear Export (SINE) compound, acts through NF-κB deactivation and combines with proteasome inhibitors to synergistically induce tumor cell death. *Oncotarget*, *7*(48), 78883–78895. https://doi.org/10.18632/oncotarget.12428

Kashyap, T., Argueta, C., Unger, T., Klebanov, B., Debler, S., Senapedis, W., Crochiere, M. L., Lee, M. S., Kauffman, M., Shacham, S., & Landesman, Y. (2018). Selinexor reduces the expression of DNA damage repair proteins and sensitizes cancer cells to DNA damaging agents. *Oncotarget*, *9*(56), 30773–30786. https://doi.org/10.18632/oncotarget.25637

Kashyap, T., Murray, J., Walker, C. J., Chang, H., Tamir, S., Hou, B., Shacham, S., Kauffman, M. G., Tripp, R. A., & Landesman, Y. (2021). Selinexor, a novel selective inhibitor of nuclear export, reduces SARS-CoV-2 infection and protects the respiratory system in vivo. *Antiviral research*, *192*, 105115. https://doi.org/10.1016/j.antiviral.2021.105115

Katayama, H., Sasai, K., Kawai, H., Yuan, Z. M., Bondaruk, J., Suzuki, F., Fujii, S., Arlinghaus, R. B., Czerniak, B. A., & Sen, S. (2004). Phosphorylation by aurora kinase A induces Mdm2-mediated destabilization and inhibition of p53. *Nature genetics*, *36*(1), 55–62. https://doi.org/10.1038/ng1279

Kazim, S., Malafa, M. P., Coppola, D., Husain, K., Zibadi, S., Kashyap, T., Crochiere, M., Landesman, Y., Rashal, T., Sullivan, D. M., & Mahipal, A. (2015). Selective Nuclear Export Inhibitor KPT-330 Enhances the Antitumor Activity of Gemcitabine in Human Pancreatic Cancer. *Molecular cancer therapeutics*, *14*(7), 1570–1581. https://doi.org/10.1158/1535-7163.MCT-15-0104

Kee, Y., Yang, K., Cohn, M. A., Haas, W., Gygi, S. P., & D'Andrea, A. D. (2010). WDR20 regulates activity of the USP12 x UAF1 deubiquitinating enzyme complex. *The Journal of biological chemistry*, *285*(15), 11252–11257. https://doi.org/10.1074/jbc.M109.095141

Kehlenbach, R. H., & Port, S. A. (2016). Analysis of CRM1-Dependent Nuclear Export in Permeabilized Cells. *Methods in molecular biology (Clifton, N.J.)*, *1411*, 489–501. https://doi.org/10.1007/978-1-4939-3530-7_30

Kemper, K., Versloot, M., Cameron, K., Colak, S., de Sousa e Melo, F., de Jong, J. H., Bleackley, J., Vermeulen, L., Versteeg, R., Koster, J., & Medema, J. P. (2012). Mutations in the Ras-Raf Axis underlie the prognostic value of CD133 in colorectal cancer. *Clinical cancer research : an official journal of the American Association for Cancer Research*, *18*(11), 3132–3141. https://doi.org/10.1158/1078-0432.CCR-11-3066

Khan, H. Y., Ge, J., Nagasaka, M., Aboukameel, A., Mpilla, G., Muqbil, I., Szlaczky, M., Chaker, M., Baloglu, E., Landesman, Y., Mohammad, R. M., Azmi, A. S., & Sukari, A. (2019). Targeting XPO1 and PAK4 in 8505C Anaplastic Thyroid Cancer Cells: Putative Implications for Overcoming Lenvatinib Therapy Resistance. *International journal of molecular sciences*, *21*(1), 237. https://doi.org/10.3390/ijms21010237

Kido, K., Yamanaka, S., Nakano, S., Motani, K., Shinohara, S., Nozawa, A., Kosako, H., Ito, S., & Sawasaki, T. (2020). AirID, a novel proximity biotinylation enzyme, for analysis of protein-protein interactions. *eLife*, *9*, e54983. https://doi.org/10.7554/eLife.54983

Kim, D. I., Birendra, K. C., Zhu, W., Motamedchaboki, K., Doye, V., & Roux, K. J. (2014). Probing nuclear pore complex architecture with proximity-dependent biotinylation. *Proceedings of the National Academy of Sciences of the United States of America*, *111*(24), 2453–2461. https://doi.org/10.1073/pnas.1406459111

Kim, D. I., Jensen, S. C., Noble, K. A., Kc, B., Roux, K. H., Motamedchaboki, K., & Roux, K. J. (2016a). An improved smaller biotin ligase for BioID proximity labeling. *Molecular Biology of the Cell*, *27*(8), 1188–1196. https://doi.org/10.1091/mbc.E15-12-0844

Kim, J. Y., Shen, S., Dietz, K., He, Y., Howell, O., Reynolds, R., & Casaccia, P. (2010). HDAC1 nuclear export induced by pathological conditions is essential for the onset of axonal damage. *Nature Neuroscience*, *13*(2), 180–189. https://doi.org/10.1038/nn.2471

Kim, J., McMillan, E., Kim, H. S., Venkateswaran, N., Makkar, G., Rodriguez-Canales, J., Villalobos, P., Neggers, J. E., Mendiratta, S., Wei, S., Landesman, Y., Senapedis, W., Baloglu, E., Chow, C. B., Frink, R. E., Gao, B., Roth, M., Minna, J. D., Daelemans, D., Wistuba, I. I., … White, M. A. (2016b). XPO1-dependent nuclear export is a druggable vulnerability in KRAS-mutant lung cancer. *Nature*, *538*(7623), 114–117. https://doi.org/10.1038/nature19771

Kim, K. H., & Roberts, C. W. M. (2016). Targeting EZH2 in cancer. *Nature Medicine*, *22*(2), 128–134. https://doi.org/10.1038/nm.4036

Kirli, K., Karaca, S., Dehne, H. J., Samwer, M., Pan, K. T., Lenz, C., Urlaub, H., & Görlich, D. (2015). A deep proteomics perspective on CRM1-mediated nuclear export and nucleocytoplasmic partitioning. *eLife*, *4*, e11466. https://doi.org/10.7554/eLife.11466

Klebe, C., Bischoff, F. R., Ponstingl, H., & Wittinghofer, A. (1995). Interaction of the nuclear GTP-binding protein Ran with its regulatory proteins RCC1 and RanGAP1. *Biochemistry*, *34*(2), 639–647. https://doi.org/10.1021/bi00002a031

Kleer, C. G., Cao, Q., Varambally, S., Shen, R., Ota, I., Tomlins, S. A., Ghosh, D., Sewalt, R. G., Otte, A. P., Hayes, D. F., Sabel, M. S., Livant, D., Weiss, S. J., Rubin, M. A., & Chinnaiyan, A. M. (2003). EZH2 is a marker of aggressive breast cancer and promotes neoplastic transformation of breast epithelial cells. *Proceedings of the National Academy of Sciences of the United States of America*, *100*(20), 11606–11611. https://doi.org/10.1073/pnas.1933744100

Knockenhauer, K. E., & Schwartz, T. U. (2016). The Nuclear Pore Complex as a Flexible and Dynamic Gate. *Cell*, *164*(6), 1162–1171. https://doi.org/10.1016/j.cell.2016.01.034

Kogiso, M., Qi, L., Braun, F. K., Injac, S. G., Zhang, L., Du, Y., Zhang, H., Lin, F. Y., Zhao, S., Lindsay, H., Su, J. M., Baxter, P. A., Adesina, A. M., Liao, D., Qian, M. G., Berg, S., Muscal, J. A., & Li, X. N. (2018). Concurrent Inhibition of Neurosphere and Monolayer Cells of Pediatric Glioblastoma by Aurora A Inhibitor MLN8237 Predicted Survival Extension in PDOX Models. *Clinical cancer research : an official journal of the American Association for Cancer Research*, *24*(9), 2159–2170. https://doi.org/10.1158/1078-0432.CCR-17-2256

Kojima, K., Kornblau, S. M., Ruvolo, V., Dilip, A., Duvvuri, S., Davis, R. E., Zhang, M., Wang, Z., Coombes, K. R., Zhang, N., Qiu, Y. H., Burks, J. K., Kantarjian, H., Shacham, S., Kauffman, M., & Andreeff, M. (2013). Prognostic impact and targeting of CRM1 in acute myeloid leukemia. *Blood*, *121*(20), 4166–4174. https://doi.org/10.1182/blood-2012-08-447581

Komander, D., Clague, M. J., & Urbé, S. (2009). Breaking the chains: structure and function of the deubiquitinases. *Nature reviews. Molecular cell biology*, *10*(8), 550–563. https://doi.org/10.1038/nrm2731

Kosugi, S., Hasebe, M., Tomita, M., & Yanagawa, H. (2008). Nuclear export signal consensus sequences defined using a localization-based yeast selection system. *Traffic (Copenhagen, Denmark)*, *9*(12), 2053–2062. https://doi.org/10.1111/j.1600-0854.2008.00825.x

Kosugi, S., Yanagawa, H., Terauchi, R., & Tabata, S. (2014). NESmapper: Accurate Prediction of Leucine-Rich Nuclear Export Signals Using Activity-Based Profiles. *PLoS Computational Biology*, *10*(9), e1003841. https://doi.org/10.1371/journal.pcbi.1003841

Kouranti, I., McLean, J. R., Feoktistova, A., Liang, P., Johnson, A. E., Roberts-Galbraith, R. H., & Gould, K. L. (2010). A global census of fission yeast deubiquitinating enzyme localization and interaction networks reveals distinct compartmentalization profiles and overlapping functions in endocytosis and polarity. *PLoS biology*, *8*(9), e1000471. https://doi.org/10.1371/journal.pbio.1000471

Koyama, M., & Matsuura, Y. (2012). Mechanistic insights from the recent structures of the CRM1 nuclear export complex and its disassembly intermediate. *Biophysics*, *8*, 145–150. https://doi.org/10.2142/biophysics.8.145

Krystyniak, A., Garcia-Echeverria, C., Prigent, C., & Ferrari, S. (2006). Inhibition of Aurora A in response to DNA damage. *Oncogene*, *25*(3), 338–348. https://doi.org/10.1038/sj.onc.1209056

Kudo, N., Wolff, B., Sekimoto, T., Schreiner, E. P., Yoneda, Y., Yanagida, M., Horinouchi, S., & Yoshida, M. (1998). Leptomycin B inhibition of signal-mediated nuclear export by direct binding to CRM1. *Experimental cell research*, *242*(2), 540–547. https://doi.org/10.1006/excr.1998.4136

Kulkoyluoglu-Cotul, E., Smith, B. P., Wrobel, K., Zhao, Y. C., Chen, K., Hieronymi, K., Imir, O. B., Duong, K., O'Callaghan, C., Mehta, A., Sahoo, S., Haley, B., Chang, H., Landesman, Y., & Madak-Erdogan, Z. (2019). Combined Targeting of Estrogen Receptor Alpha and XPO1 Prevent Akt Activation, Remodel Metabolic Pathways and Induce Autophagy to Overcome Tamoxifen Resistance. *Cancers*, *11*(4), 479. https://doi.org/10.3390/cancers11040479

Kuruvilla, J., Savona, M., Baz, R., Mau-Sorensen, P. M., Gabrail, N., Garzon, R., Stone, R., Wang, M., Savoie, L., Martin, P., Flinn, I., Jacoby, M., Unger, T. J., Saint-Martin, J. R., Rashal, T., Friedlander, S., Carlson, R., Kauffman, M., Shacham, S., & Gutierrez, M. (2017). Selective inhibition of nuclear export with selinexor in patients with non-Hodgkin lymphoma. *Blood*, *129*(24), 3175–3183. https://doi.org/10.1182/blood-2016-11-750174

Kutay, U., & Güttinger, S. (2005). Leucine-rich nuclear export signals: born to be weak. *Trends in Cell Biology*, *15*(3), 121–124. https://doi.org/10.1016/j.tcb.2005.01.005

Kutay, U., Bischoff, F. R., Kostka, S., Kraft, R., & Görlich, D. (1997). Export of importin alpha from the nucleus is mediated by a specific nuclear transport factor. *Cell*, *90*(6), 1061–1071. https://doi.org/10.1016/s0092-8674(00)80372-4

Kuzmichev, A., Nishioka, K., Erdjument-Bromage, H., Tempst, P., & Reinberg, D. (2002). Histone methyltransferase activity associated with a human multiprotein complex containing the Enhancer of Zeste protein. *Genes & development*, *16*(22), 2893–2905. https://doi.org/10.1101/gad.1035902

Kwon, K., & Beckett, D. (2000). Function of a conserved sequence motif in biotin holoenzyme synthetases. *Protein Science*, *9*(8), 1530–1539. https://doi.org/10.1110/ps.9.8.1530

la Cour, T., Kiemer, L., Mølgaard, A., Gupta, R., Skriver, K., & Brunak, S. (2004). Analysis and prediction of leucine-rich nuclear export signals. *Protein engineering, design & selection : PEDS*, *17*(6), 527–536. https://doi.org/10.1093/protein/gzh062

Laemmli, U. K. (1970). Cleavage of structural proteins during the assembly of the head of bacteriophage T4. *Nature*, *227*(5259), 680–685. https://doi.org/https://doi.org/10.1038/227680a0

Laibe, S., Lagarde, A., Ferrari, A., Monges, G., Birnbaum, D., Olschwang, S., & COL2 Project (2012). A seven-gene signature aggregates a subgroup of stage II colon cancers with stage III. *Omics: a journal of integrative biology*, *16*(10), 560–565. https://doi.org/10.1089/omi.2012.0039

Lam, S. S., Martell, J. D., Kamer, K. J., Deerinck, T. J., Ellisman, M. H., Mootha, V. K., & Ting, A. Y. (2015). Directed evolution of APEX2 for electron microscopy and proteomics. *Nature Methods*, *12*(1), 51–54. https://doi.org/10.1038/nmeth.3179

Landau, D. A., Carter, S. L., Stojanov, P., McKenna, A., Stevenson, K., Lawrence, M. S., Sougnez, C., Stewart, C., Sivachenko, A., Wang, L., Wan, Y., Zhang, W., Shukla, S. A., Vartanov, A., Fernandes, S. M., Saksena, G., Cibulskis, K., Tesar, B., Gabriel, S., Hacohen, N., … Wu, C. J. (2013). Evolution and impact of subclonal mutations in chronic lymphocytic leukemia. *Cell*, *152*(4), 714–726. https://doi.org/10.1016/j.cell.2013.01.019

Landau, D. A., Tausch, E., Taylor-Weiner, A. N., Stewart, C., Reiter, J. G., Bahlo, J., Kluth, S., Bozic, I., Lawrence, M., Böttcher, S., Carter, S. L., Cibulskis, K., Mertens, D., Sougnez, C. L., Rosenberg, M., Hess, J. M., Edelmann, J., Kless, S., Kneba, M., Ritgen, M., … Wu, C. J. (2015). Mutations driving CLL and their evolution in progression and relapse. *Nature*, *526*(7574), 525–530. https://doi.org/10.1038/nature15395

Lapalombella, R., Sun, Q., Williams, K., Tangeman, L., Jha, S., Zhong, Y., Goettl, V., Mahoney, E., Berglund, C., Gupta, S., Farmer, A., Mani, R., Johnson, A. J., Lucas, D., Mo, X., Daelemans, D., Sandanayaka, V., Shechter, S., McCauley, D., Shacham, S., … Byrd, J. C. (2012). Selective inhibitors of nuclear export show that CRM1/XPO1 is a target in chronic lymphocytic leukemia. *Blood*, *120*(23), 4621–4634. https://doi.org/10.1182/blood-2012-05-429506

Lapointe, J., Li, C., Higgins, J. P., van de Rijn, M., Bair, E., Montgomery, K., Ferrari, M., Egevad, L., Rayford, W., Bergerheim, U., Ekman, P., DeMarzo, A. M., Tibshirani, R., Botstein, D., Brown, P. O., Brooks, J. D., & Pollack, J. R. (2004). Gene expression profiling identifies clinically relevant subtypes of prostate cancer. *Proceedings of the National Academy of Sciences of the United States of America*, *101*(3), 811–816. https://doi.org/10.1073/pnas.0304146101

Lawrence, M. S., Stojanov, P., Mermel, C. H., Robinson, J. T., Garraway, L. A., Golub, T. R., Meyerson, M., Gabriel, S. B., Lander, E. S., & Getz, G. (2014). Discovery and saturation analysis of cancer genes across 21 tumour types. *Nature*, *505*(7484), 495–501. https://doi.org/10.1038/nature12912

le Coutre, P., Mologni, L., Cleris, L., Marchesi, E., Buchdunger, E., Giardini, R., Formelli, F., & Gambacorti-Passerini, C. (1999). In vivo eradication of human BCR/ABL-positive leukemia cells with an ABL kinase inhibitor. *Journal of the National Cancer Institute*, *91*(2), 163–168. https://doi.org/10.1093/jnci/91.2.163

Lee, D. H., Kim, C. G., Lim, Y., & Shin, S. Y. (2017). Aurora kinase A inhibitor TCS7010 demonstrates pro-apoptotic effect through the unfolded protein response pathway in HCT116 colon cancer cells. *Oncology letters*, *14*(6), 6571–6577. https://doi.org/10.3892/ol.2017.7023

Lee, Y. H., Tan, H. T., & Chung, M. C. M. (2010). Subcellular fractionation methods and strategies for proteomics. *Proteomics*, *10*(22), 3935–3956. https://doi.org/10.1002/pmic.201000289

Legland, D., Arganda-Carreras, I., & Andrey, P. (2016). MorphoLibJ: Integrated library and plugins for mathematical morphology with ImageJ. *Bioinformatics*, *32*(22), 3532–3534. https://doi.org/10.1093/bioinformatics/btw413

Lehoux, M., Gagnon, D., & Archambault, J. (2014). E1-mediated recruitment of a UAF1-USP deubiquitinase complex facilitates human papillomavirus DNA replication. *Journal of virology*, *88*(15), 8545–8555. https://doi.org/10.1128/JVI.00379-14

Li, G. M. (2008). Mechanisms and functions of DNA mismatch repair. *Cell Research*, *18*(1), 85–98. https://doi.org/10.1038/cr.2007.115

Li, H., Lim, K. S., Kim, H., Hinds, T. R., Jo, U., Mao, H., Weller, C. E., Sun, J., Chatterjee, C., D'Andrea, A. D., & Zheng, N. (2016). Allosteric Activation of Ubiquitin-Specific Proteases by β-Propeller Proteins UAF1 and WDR20. *Molecular cell*, *63*(2), 249–260. https://doi.org/10.1016/j.molcel.2016.05.031

Li, X., Stevens, P. D., Yang, H., Gulhati, P., Wang, W., Evers, B. M., & Gao, T. (2013). The deubiquitination enzyme USP46 functions as a tumor suppressor by controlling PHLPP-dependent attenuation of Akt signaling in colon cancer. *Oncogene*, *32*(4), 471–478. https://doi.org/10.1038/onc.2012.66

Li, Y., Li, X., Pu, J., Yang, Q., Guan, H., Ji, M., Shi, B., Chen, M., & Hou, P. (2018). c-Myc Is a Major Determinant for Antitumor Activity of Aurora A Kinase Inhibitor MLN8237 in Thyroid Cancer. *Thyroid : official journal of the American Thyroid Association*, *28*(12), 1642–1654. https://doi.org/10.1089/thy.2018.0183

Li, Y., Merkel, C. D., Zeng, X., Heier, J. A., Cantrell, P. S., Sun, M., Stolz, D. B., Watkins, S. C., Yates, N. A., & Kwiatkowski, A. V. (2019). The N-cadherin interactome in primary cardiomyocytes as defined using quantitative proximity proteomics. *Journal of cell science*, *132*(3), jcs221606. https://doi.org/10.1242/jcs.221606

Liang, W. S., Vergilio, J. A., Salhia, B., Huang, H. J., Oki, Y., Garrido-Laguna, I., Park, H., Westin, J. R., Meric-Bernstam, F., Fabrizio, D., Miller, V. A., Stephens, P. J., Fanale, M. A., Ross, J. S., & Janku, F. (2019). Comprehensive Genomic Profiling of Hodgkin Lymphoma Reveals Recurrently Mutated Genes and Increased Mutation Burden. *The oncologist*, *24*(2), 219–228. https://doi.org/10.1634/theoncologist.2018-0058

Lim, S. L., Damnernsawad, A., Shyamsunder, P., Chng, W. J., Han, B. C., Xu, L., Pan, J., Pravin, D. P., Alkan, S., Tyner, J. W., & Koeffler, H. P. (2019). Proteolysis targeting chimeric molecules as therapy for multiple myeloma: efficacy, biomarker and drug combinations. *Haematologica*, *104*(6), 1209–1220. https://doi.org/10.3324/haematol.2018.201483

Lin, D. C., Hao, J. J., Nagata, Y., Xu, L., Shang, L., Meng, X., Sato, Y., Okuno, Y., Varela, A. M., Ding, L. W., Garg, M., Liu, L. Z., Yang, H., Yin, D., Shi, Z. Z., Jiang, Y. Y., Gu, W. Y., Gong, T., Zhang, Y., Xu, X., … Koeffler, H. P. (2014). Genomic and molecular characterization of esophageal squamous cell carcinoma. *Nature genetics*, *46*(5), 467–473. https://doi.org/10.1038/ng.2935

Lin, D. H., & Hoelz, A. (2019). The structure of the nuclear pore complex (An Update). *Annual Review of Biochemistry*, *88*, 725–783. https://doi.org/10.1146/annurev-biochem-062917-011901

Lin, D. H., Stuwe, T., Schilbach, S., Rundlet, E. J., Perriches, T., Mobbs, G., Fan, Y., Thierbach, K., Huber, F. M., Collins, L. N., Davenport, A. M., Jeon, Y. E., & Hoelz, A. (2016). Architecture of the symmetric core of the nuclear pore. *Science*, *352*(6283), aaf1015. https://doi.org/10.1126/science.aaf1015

Lindström M. S. (2011). NPM1/B23: A Multifunctional Chaperone in Ribosome Biogenesis and Chromatin Remodeling. *Biochemistry research international*, *2011*, 195209. https://doi.org/10.1155/2011/195209

Lischka, P., Rosorius, O., Trommer, E., & Stamminger, T. (2001). A novel transferable nuclear export signal mediates CRM1-independent nucleocytoplasmic shuttling of the human cytomegalovirus transactivator protein pUL69. *EMBO Journal*, *20*(24), 7271–7283. https://doi.org/10.1093/emboj/20.24.7271

Liu, J., Lichtenberg, T., Hoadley, K. A., Poisson, L. M., Lazar, A. J., Cherniack, A. D., Kovatich, A. J., Benz, C. C., Levine, D. A., Lee, A. V., Omberg, L., Wolf, D. M., Shriver, C. D., Thorsson, V., Cancer Genome Atlas Research Network, & Hu, H. (2018). An Integrated TCGA Pan-Cancer Clinical Data Resource to Drive High-Quality Survival Outcome Analytics. *Cell*, *173*(2), 400–416.e11. https://doi.org/10.1016/j.cell.2018.02.052

Liu, K., Zheng, M., Lu, R., Du, J., Zhao, Q., Li, Z., Li, Y., & Zhang, S. (2020). The role of CDC25C in cell cycle regulation and clinical cancer therapy: a systematic review. *Cancer cell international*, *20*, 213. https://doi.org/10.1186/s12935-020-01304-w

Liu, X., Chong, Y., Tu, Y., Liu, N., Yue, C., Qi, Z., Liu, H., Yao, Y., Liu, H., Gao, S., Niu, M., & Yu, R. (2016). CRM1/XPO1 is associated with clinical outcome in glioma and represents a therapeutic target by perturbing multiple core pathways. *Journal of hematology & oncology*, *9*(1), 108. https://doi.org/10.1186/s13045-016-0338-2

Liu, Y., Azizian, N. G., Dou, Y., Pham, L. V., & Li, Y. (2019). Simultaneous targeting of XPO1 and BCL2 as an effective treatment strategy for double-hit lymphoma. *Journal of hematology & oncology*, *12*(1), 119. https://doi.org/10.1186/s13045-019-0803-9

López, D. J., Rodríguez, J. A., & Bañuelos, S. (2020). Nucleophosmin, a multifunctional nucleolar organizer with a role in DNA repair. *Biochimica et biophysica acta. Proteins and proteomics*, *1868*(12), 140532. https://doi.org/10.1016/j.bbapap.2020.140532

Lu, J., Wu, T., Zhang, B., Liu, S., Song, W., Qiao, J., & Ruan, H. (2021). Types of nuclear localization signals and mechanisms of protein import into the nucleus. *Cell communication and signaling: CCS*, *19*(1), 60. https://doi.org/10.1186/s12964-021-00741-y

Lu, X., Lu, X., Wang, Z. C., Iglehart, J. D., Zhang, X., & Richardson, A. L. (2008). Predicting features of breast cancer with gene expression patterns. *Breast cancer research and treatment*, *108*(2), 191–201. https://doi.org/10.1007/s10549-007-9596-6

Lucas, F., Rogers, K. A., Harrington, B. K., Pan, A., Yu, L., Breitbach, J., Bundschuh, R., Goettl, V. M., Hing, Z. A., Kanga, P., Mantel, R., Sampath, D., Smith, L. L., Wasmuth, R., White, D. K., Yan, P., Byrd, J. C., Lapalombella, R., & Woyach, J. A. (2019). Eμ-TCL1xMyc: A Novel Mouse Model for Concurrent CLL and B-Cell Lymphoma. *Clinical cancer research : an official journal of the American Association for Cancer Research*, *25*(20), 6260–6273. https://doi.org/10.1158/1078-0432.CCR-19-0273

Luedtke, D. A., Su, Y., Liu, S., Edwards, H., Wang, Y., Lin, H., Taub, J. W., & Ge, Y. (2018). Inhibition of XPO1 enhances cell death induced by ABT-199 in acute myeloid leukaemia via Mcl-1. *Journal of cellular and molecular medicine*, *22*(12), 6099–6111. https://doi.org/10.1111/jcmm.13886

Macchi, P., Kroening, S., Palacios, I. M., Baldassa, S., Grunewald, B., Ambrosino, C., Goetze, B., Lupas, A., St Johnston, D., & Kiebler, M. (2003). Barentsz, a new component of the Staufen-containing ribonucleoprotein particles in mammalian cells, interacts with Staufen in an RNA-dependent manner. *The Journal of neuroscience : the official journal of the Society for Neuroscience*, *23*(13), 5778–5788. https://doi.org/10.1523/JNEUROSCI.23-13-05778.2003

Machnicki, M. M., Górniak, P., Pępek, M., Szymczyk, A., Iskierka-Jażdżewska, E., Steckiewicz, P., Bluszcz, A., Rydzanicz, M., Hus, M., Płoski, R., Makuch-Łasica, H., Nowak, G., Juszczyński, P., Jamroziak, K., Stokłosa, T., & Puła, B. (2021). Predictive significance of selected gene mutations in relapsed and refractory chronic lymphocytic leukemia patients treated with ibrutinib. *European journal of haematology*, *106*(3), 320–326. https://doi.org/10.1111/ejh.13550

Macůrek, L., Lindqvist, A., Lim, D., Lampson, M. A., Klompmaker, R., Freire, R., Clouin, C., Taylor, S. S., Yaffe, M. B., & Medema, R. H. (2008). Polo-like kinase-1 is activated by aurora A to promote checkpoint recovery. *Nature*, *455*(7209), 119–123. https://doi.org/10.1038/nature07185

Magnaghi-Jaulin, L., Eot-Houllier, G., Gallaud, E., & Giet, R. (2019). Aurora A Protein Kinase: To the Centrosome and Beyond. *Biomolecules*, *9*(1), 28. https://doi.org/10.3390/biom9010028

Maitre, E., Bertrand, P., Maingonnat, C., Viailly, P. J., Wiber, M., Naguib, D., Salaün, V., Cornet, E., Damaj, G., Sola, B., Jardin, F., & Troussard, X. (2018). New generation sequencing of targeted genes in the classical and the variant form of hairy cell leukemia highlights mutations in epigenetic regulation genes. *Oncotarget*, *9*(48), 28866–28876. https://doi.org/10.18632/oncotarget.25601

Marcus, J. M., Burke, R. T., Doak, A. E., Park, S., & Orth, J. D. (2018). Loss of p53 expression in cancer cells alters cell cycle response after inhibition of exportin-1 but does not prevent cell death. *Cell cycle, 17*(11), 1329–1344. https://doi.org/10.1080/15384101.2018.1480224

Mariano, A. R., Colombo, E., Luzi, L., Martinelli, P., Volorio, S., Bernard, L., Meani, N., Bergomas, R., Alcalay, M., & Pelicci, P. G. (2006). Cytoplasmic localization of NPM in myeloid leukemias is dictated by gain-of-function mutations that create a functional nuclear export signal. *Oncogene*, *25*(31), 4376–4380. https://doi.org/10.1038/sj.onc.1209453

Marisa, L., de Reyniès, A., Duval, A., Selves, J., Gaub, M. P., Vescovo, L., Etienne-Grimaldi, M. C., Schiappa, R., Guenot, D., Ayadi, M., Kirzin, S., Chazal, M., Fléjou, J. F., Benchimol, D., Berger, A., Lagarde, A., Pencreach, E., Piard, F., Elias, D., Parc, Y., … Boige, V. (2013). Gene expression classification of colon cancer into molecular subtypes: characterization, validation, and prognostic value. *PLoS medicine*, *10*(5), e1001453. https://doi.org/10.1371/journal.pmed.1001453

Martell, J. D., Deerinck, T. J., Sancak, Y., Poulos, T. L., Mootha, V. K., Sosinsky, G. E., Ellisman, M. H., & Ting, A. Y. (2012). Engineered ascorbate peroxidase as a genetically encoded reporter for electron microscopy. *Nature biotechnology*, *30*(11), 1143–1148. https://doi.org/10.1038/nbt.2375

Martin, A. P., Jacquemyn, M., Lipecka, J., Chhuon, C., Aushev, V. N., Meunier, B., Singh, M. K., Carpi, N., Piel, M., Codogno, P., Hergovich, A., Parrini, M. C., Zalcman, G., Guerrera, I. C., Daelemans, D., & Camonis, J. H. (2019). STK38 kinase acts as XPO1 gatekeeper regulating the nuclear export of autophagy proteins and other cargoes. *EMBO reports*, *20*(11), e48150. https://doi.org/10.15252/embr.201948150

Martini, S., Figini, M., Croce, A., Frigerio, B., Pennati, M., Gianni, A. M., De Marco, C., Daidone, M. G., Argueta, C., Landesman, Y., Zaffaroni, N., & Satta, A. (2020). Selinexor Sensitizes TRAIL-R2-Positive TNBC Cells to the Activity of TRAIL-R2xCD3 Bispecific Antibody. *Cells*, *9*(10), 2231. https://doi.org/10.3390/cells9102231

Matsui, T., Hayashi-Kisumi, F., Kinoshita, Y., Katahira, S., Morita, K., Miyachi, Y., Ono, Y., Imai, T., Tanigawa, Y., Komiya, T., & Tsukita, S. (2004). Identification of novel keratinocyte-secreted peptides dermokine-alpha/-beta and a new stratified epithelium-secreted protein gene complex on human chromosome 19q13.1. *Genomics*, *84*(2), 384–397. https://doi.org/10.1016/j.ygeno.2004.03.010

McAlarnen, L., Stearns, K., & Uyar, D. (2021). Challenges of Genomic Testing for Hereditary Breast and Ovarian Cancers. *The application of clinical genetics*, *14*, 1–9. https://doi.org/10.2147/TACG.S245021

Mendes, A., Jühlen, R., Martinelli, V., & Fahrenkrog, B. (2020). Targeted CRM1-inhibition perturbs leukemogenic NUP214 fusion proteins and exerts anti-cancer effects in leukemia cell lines with *NUP214* rearrangements. *Oncotarget*, *11*(36), 3371–3386. https://doi.org/10.18632/oncotarget.27711

Mendonca, J., Sharma, A., Kim, H. S., Hammers, H., Meeker, A., De Marzo, A., Carducci, M., Kauffman, M., Shacham, S., & Kachhap, S. (2014). Selective inhibitors of nuclear export (SINE) as novel therapeutics for prostate cancer. *Oncotarget*, *5*(15), 6102–6112. https://doi.org/10.18632/oncotarget.2174

Messina, M., Del Giudice, I., Khiabanian, H., Rossi, D., Chiaretti, S., Rasi, S., Spina, V., Holmes, A. B., Marinelli, M., Fabbri, G., Piciocchi, A., Mauro, F. R., Guarini, A., Gaidano, G., Dalla-Favera, R., Pasqualucci, L., Rabadan, R., & Foà, R. (2014). Genetic lesions associated with chronic lymphocytic leukemia chemo-refractoriness. *Blood*, *123*(15), 2378–2388. https://doi.org/10.1182/blood-2013-10-534271

Mick, D. U., Rodrigues, R. B., Leib, R. D., Adams, C. M., Chien, A. S., Gygi, S. P., & Nachury, M. V. (2015). Proteomics of Primary Cilia by Proximity Labeling. *Developmental Cell*, *35*(4), 497–512. https://doi.org/10.1016/j.devcel.2015.10.015

Ming, M., Wu, W., Xie, B., Sukhanova, M., Wang, W., Kadri, S., Sharma, S., Lee, J., Shacham, S., Landesman, Y., Maltsev, N., Lu, P., & Wang, Y. L. (2018). XPO1 Inhibitor Selinexor Overcomes Intrinsic Ibrutinib Resistance in Mantle Cell Lymphoma via Nuclear Retention of IκB. *Molecular cancer therapeutics*, *17*(12), 2564–2574. https://doi.org/10.1158/1535-7163.MCT-17-0789-ATR

Miyake, T., Pradeep, S., Wu, S. Y., Rupaimoole, R., Zand, B., Wen, Y., Gharpure, K. M., Nagaraja, A. S., Hu, W., Cho, M. S., Dalton, H. J., Previs, R. A., Taylor, M. L., Hisamatsu, T., Kang, Y., Liu, T., Shacham, S., McCauley, D., Hawke, D. H., Wiktorowicz, J. E., … Sood, A. K. (2015). XPO1/CRM1 Inhibition Causes Antitumor Effects by Mitochondrial Accumulation of eIF5A. *Clinical cancer research : an official journal of the American Association for Cancer Research*, *21*(14), 3286–3297. https://doi.org/10.1158/1078-0432.CCR-14-1953

Mochizuki, D., Misawa, Y., Kawasaki, H., Imai, A., Endo, S., Mima, M., Yamada, S., Nakagawa, T., Kanazawa, T., & Misawa, K. (2018). Aberrant Epigenetic Regulation in Head and Neck Cancer Due to Distinct EZH2 Overexpression and DNA Hypermethylation. *International journal of molecular sciences*, *19*(12), 3707. https://doi.org/10.3390/ijms19123707

Moffatt, P., Salois, P., St-Amant, N., Gaumond, M. H., & Lanctôt, C. (2004). Identification of a conserved cluster of skin-specific genes encoding secreted proteins. Gene, 334, 123–131. https://doi.org/10.1016/j.gene.2004.03.010

Mohammad, F., Weissmann, S., Leblanc, B., Pandey, D. P., Højfeldt, J. W., Comet, I., Zheng, C., Johansen, J. V., Rapin, N., Porse, B. T., Tvardovskiy, A., Jensen, O. N., Olaciregui, N. G., Lavarino, C., Suñol, M., de Torres, C., Mora, J., Carcaboso, A. M., & Helin, K. (2017). EZH2 is a potential therapeutic target for H3K27M-mutant pediatric gliomas. *Nature medicine*, *23*(4), 483–492. https://doi.org/10.1038/nm.4293

Monecke, T., Dickmanns, A., & Ficner, R. (2014). Allosteric control of the exportin CRM1 unraveled by crystal structure analysis. The FEBS journal, 281(18), 4179–4194. https://doi.org/10.1111/febs.12842

Monecke, T., Güttler, T., Neumann, P., Dickmanns, A., Görlich, D., & Ficner, R. (2009). Crystal structure of the nuclear export receptor CRM1 in complex with Snurportin1 and RanGTP. *Science*, *324*(5930), 1087–1091. https://doi.org/10.1126/science.1173388

Monecke, T., Haselbach, D., Voß, B., Russek, A., Neumann, P., Thomson, E., Hurt, E., Zachariae, U., Stark, H., Grubmüller, H., Dickmanns, A., & Ficner, R. (2013). Structural basis for cooperativity of CRM1 export complex formation. *Proceedings of the National Academy of Sciences of the United States of America*, *110*(3), 960–965. https://doi.org/10.1073/pnas.1215214110

Mor, A., White, M. A., & Fontoura, B. M. (2014). Nuclear trafficking in health and disease. *Current opinion in cell biology*, *28*, 28–35. https://doi.org/10.1016/j.ceb.2014.01.007

Morin, R. D., Johnson, N. A., Severson, T. M., Mungall, A. J., An, J., Goya, R., Paul, J. E., Boyle, M., Woolcock, B. W., Kuchenbauer, F., Yap, D., Humphries, R. K., Griffith, O. L., Shah, S., Zhu, H., Kimbara, M., Shashkin, P., Charlot, J. F., Tcherpakov, M., Corbett, R., … Marra, M. A. (2010). Somatic mutations altering EZH2 (Tyr641) in follicular and diffuse large B-cell lymphomas of germinal-center origin. *Nature genetics*, *42*(2), 181–185. https://doi.org/10.1038/ng.518

Morris, L. G., & Chan, T. A. (2015). Therapeutic targeting of tumor suppressor genes. *Cancer*, *121*(9), 1357–1368. https://doi.org/10.1002/cncr.29140

Muqbil, I., Aboukameel, A., Elloul, S., Carlson, R., Senapedis, W., Baloglu, E., Kauffman, M., Shacham, S., Bhutani, D., Zonder, J., Azmi, A. S., & Mohammad, R. M. (2016). Anti-tumor activity of selective inhibitor of nuclear export (SINE) compounds, is enhanced in non-Hodgkin lymphoma through combination with mTOR inhibitor and dexamethasone. *Cancer letters*, *383*(2), 309–317. https://doi.org/10.1016/j.canlet.2016.09.016

Muz, B., Azab, F., de la Puente, P., Landesman, Y., & Azab, A. K. (2017). Selinexor Overcomes Hypoxia-Induced Drug Resistance in Multiple Myeloma. *Translational oncology*, *10*(4), 632–640. https://doi.org/10.1016/j.tranon.2017.04.010

Nachury, M. V., & Weis, K. (1999). The direction of transport through the nuclear pore can be inverted. *Proceedings of the National Academy of Sciences of the United States of America*, *96*(17), 9622–9627. https://doi.org/10.1073/pnas.96.17.9622

Nair, J. S., Musi, E., & Schwartz, G. K. (2017). Selinexor (KPT-330) Induces Tumor Suppression through Nuclear Sequestration of IκB and Downregulation of Survivin. *Clinical cancer research: an official journal of the American Association for Cancer Research*, *23*(15), 4301–4311. https://doi.org/10.1158/1078-0432.CCR-16-2632

Nakayama, R., Zhang, Y. X., Czaplinski, J. T., Anatone, A. J., Sicinska, E. T., Fletcher, J. A., Demetri, G. D., & Wagner, A. J. (2016). Preclinical activity of selinexor, an inhibitor of XPO1, in sarcoma. *Oncotarget*, *7*(13), 16581–16592. https://doi.org/10.18632/oncotarget.7667

Nardozzi, J. D., Lott, K., & Cingolani, G. (2010). Phosphorylation meets nuclear import: a review. *Cell communication and signaling : CCS*, *8*, 32. https://doi.org/10.1186/1478-811X-8-32

Newlands, E. S., Rustin, G. J., & Brampton, M. H. (1996). Phase I trial of elactocin. *British journal of cancer*, *74*(4), 648–649. https://doi.org/10.1038/bjc.1996.415

Nie, D., Huang, K., Yin, S., Li, Y., Xie, S., Ma, L., Wang, X., Wu, Y., Xiao, J., Wang, J., Yang, W., & Liu, H. (2018). KPT-330 inhibition of chromosome region maintenance 1 is cytotoxic and sensitizes chronic myeloid leukemia to Imatinib. *Cell death discovery*, *4*, 48. https://doi.org/10.1038/s41420-018-0049-2

Nilsson, S., Stein, A., Rolfo, C., Kranich, A. L., Mann, J., Papadimitriou, K., Theile, S., Amberg, S., & Bokemeyer, C. (2020). Selinexor (KPT-330), an Oral Selective Inhibitor of Nuclear Export (SINE) Compound, in Combination with FOLFOX in Patients with Metastatic Colorectal Cancer (mCRC) - Final Results of the Phase I Trial SENTINEL. *Current cancer drug targets*, *20*(10), 811–817. https://doi.org/10.2174/1568009620666200628105727

North, B. J., & Verdin, E. (2007). Interphase nucleo-cytoplasmic shuttling and localization of SIRT2 during mitosis. *PloS one*, *2*(8), e784. https://doi.org/10.1371/journal.pone.0000784

Noske, A., Weichert, W., Niesporek, S., Röske, A., Buckendahl, A. C., Koch, I., Sehouli, J., Dietel, M., & Denkert, C. (2008). Expression of the nuclear export protein chromosomal region maintenance/exportin 1/Xpo1 is a prognostic factor in human ovarian cancer. *Cancer*, *112*(8), 1733–1743. https://doi.org/10.1002/cncr.23354

O'Kane, G. M., Connor, A. A., & Gallinger, S. (2017). Characterization, Detection, and Treatment Approaches for Homologous Recombination Deficiency in Cancer. *Trends in Molecular Medicine*, *23*(12), 1121–1137. https://doi.org/10.1016/j.molmed.2017.10.007

O'Connor, O. A., Özcan, M., Jacobsen, E. D., Roncero, J. M., Trotman, J., Demeter, J., Masszi, T., Pereira, J., Ramchandren, R., Beaven, A., Caballero, D., Horwitz, S. M., Lennard, A., Turgut, M., Hamerschlak, N., d'Amore, F. A., Foss, F., Kim, W. S., Leonard, J. P., Zinzani, P. L., … Lumiere Study Investigators (2019). Randomized Phase III Study of Alisertib or Investigator's Choice (Selected Single Agent) in Patients With Relapsed or Refractory Peripheral T-Cell Lymphoma. *Journal of clinical oncology : official journal of the American Society of Clinical Oncology*, *37*(8), 613–623. https://doi.org/10.1200/JCO.18.00899

Ojha, J., Ayres, J., Secreto, C., Tschumper, R., Rabe, K., Van Dyke, D., Slager, S., Shanafelt, T., Fonseca, R., Kay, N. E., & Braggio, E. (2015). Deep sequencing identifies genetic heterogeneity and recurrent convergent evolution in chronic lymphocytic leukemia. *Blood*, *125*(3), 492–498. https://doi.org/10.1182/blood-2014-06-580563

Okamura, M., Inose, H., & Masuda, S. (2015). RNA Export through the NPC in Eukaryotes. *Genes*, *6*(1), 124–149. https://doi.org/10.3390/genes6010124

Olazabal-Herrero, A., Bilbao-Arribas, M., Carlevaris, O., Sendino, M., Varela-Martinez, E., Jugo, B. M., Berra, E., & Rodriguez, J. A. (2021). The dystrophia myotonica WD repeat-containing protein DMWD and WDR20 differentially regulate USP12 deubiquitinase. *The FEBS journal*, *288*(20), 5943-5963. https://doi.org/10.1111/febs.15875

Olazabal-Herrero, A., García-Santisteban, I., & Rodríguez, J. A. (2015). Structure-function analysis of USP1: insights into the role of Ser313 phosphorylation site and the effect of cancer-associated mutations on autocleavage. *Molecular cancer*, *14*(1), 33. https://doi.org/10.1186/s12943-015-0311-7

Olazabal-Herrero, A., Sendino, M., Arganda-carreras, I., & Rodríguez, J. A. (2019). WDR20 regulates shuttling of the USP12 deubiquitinase complex between the plasma membrane , cytoplasm and nucleus. *European Journal of Cell Biology*, *98*(1), 12–26. https://doi.org/10.1016/j.ejcb.2018.10.003

Ossareh-Nazari, B., Bachelerie, F., & Dargemont, C. (1997). Evidence for a role of CRM1 in signal-mediated nuclear protein export. *Science*, *278*(5335), 141–144. https://doi.org/10.1126/science.278.5335.141

Ould-Amer, Y., & Hebert-Chatelain, E. (2020). Insight into the Interactome of Intramitochondrial PKA Using Biotinylation-Proximity Labeling. *International journal of molecular sciences*, *21*(21), 8283. https://doi.org/10.3390/ijms21218283

Panayiotou, R., Miralles, F., Pawlowski, R., Diring, J., Flynn, H. R., Skehel, M., & Treisman, R. (2016). Phosphorylation acts positively and negatively to regulate MRTF-A subcellular localisation and activity. *eLife*, *5*, e15460. https://doi.org/10.7554/eLife.15460

Paraskeva, E., Izaurralde, E., Bischoff, F. R., Huber, J., Kutay, U., Hartmann, E., Lührmann, R., & Görlich, D. (1999). CRM1-mediated recycling of snurportin 1 to the cytoplasm. *The Journal of cell biology*, *145*(2), 255–264. https://doi.org/10.1083/jcb.145.2.255

Pathria, G., Wagner, C., & Wagner, S. N. (2012). Inhibition of CRM1-mediated nucleocytoplasmic transport: triggering human melanoma cell apoptosis by perturbing multiple cellular pathways. *The Journal of investigative dermatology*, *132*(12), 2780–2790. https://doi.org/10.1038/jid.2012.233

Pawitan, Y., Bjöhle, J., Amler, L., Borg, A. L., Egyhazi, S., Hall, P., Han, X., Holmberg, L., Huang, F., Klaar, S., Liu, E. T., Miller, L., Nordgren, H., Ploner, A., Sandelin, K., Shaw, P. M., Smeds, J., Skoog, L., Wedrén, S., & Bergh, J. (2005). Gene expression profiling spares early breast cancer patients from adjuvant therapy: derived and validated in two population-based cohorts. *Breast cancer research: BCR*, *7*(6), R953–R964. https://doi.org/10.1186/bcr1325

Payton, M., Cheung, H. K., Ninniri, M., Marinaccio, C., Wayne, W. C., Hanestad, K., Crispino, J. D., Juan, G., & Coxon, A. (2018). Dual Targeting of Aurora Kinases with AMG 900 Exhibits Potent Preclinical Activity Against Acute Myeloid Leukemia with Distinct Post-Mitotic Outcomes. *Molecular cancer therapeutics*, *17*(12), 2575–2585. https://doi.org/10.1158/1535-7163.MCT-18-0186

Pemberton, L. F., & Paschal, B. M. (2005). Mechanisms of receptor-mediated nuclear import and nuclear export. *Traffic*, *6*(3), 187–198. https://doi.org/10.1111/j.1600-0854.2005.00270.x

Pettersen, E. F., Goddard, T. D., Huang, C. C., Couch, G. S., Greenblatt, D. M., Meng, E. C., & Ferrin, T. E. (2004). UCSF Chimera--a visualization system for exploratory research and analysis. *Journal of computational chemistry*, *25*(13), 1605–1612. https://doi.org/10.1002/jcc.20084

Pickens, J. A., & Tripp, R. A. (2018). Verdinexor Targeting of CRM1 is a Promising Therapeutic Approach against RSV and Influenza Viruses. *Viruses*, *10*(1), 48. https://doi.org/10.3390/v10010048

Pitt, S. C., Hernandez, R. A., Nehs, M. A., Gawande, A. A., Moore, F. D., Jr, Ruan, D. T., & Cho, N. L. (2016). Identification of Novel Oncogenic Mutations in Thyroid Cancer. *Journal of the American College of Surgeons*, *222*(6), 1036–1043.e2. https://doi.org/10.1016/j.jamcollsurg.2015.12.047

Prieto, G., Fullaondo, A., & Rodriguez, J. A. (2014). Prediction of nuclear export signals using weighted regular expressions (Wregex). *Bioinformatics*, *30*(9), 1220–1227. https://doi.org/10.1093/bioinformatics/btu016

Prikas, E., Poljak, A., & Ittner, A. (2020). Mapping p38α mitogen-activated protein kinase signaling by proximity-dependent labeling. *Protein Science*, *29*(5), 1196–1210. https://doi.org/10.1002/pro.3854

Puente, X. S., Pinyol, M., Quesada, V., Conde, L., Ordóñez, G. R., Villamor, N., Escaramis, G., Jares, P., Beà, S., González-Díaz, M., Bassaganyas, L., Baumann, T., Juan, M., López-Guerra, M., Colomer, D., Tubío, J. M., López, C., Navarro, A., Tornador, C., Aymerich, M., … Campo, E. (2011). Whole-genome sequencing identifies recurrent mutations in chronic lymphocytic leukaemia. *Nature*, *475*(7354), 101–105. https://doi.org/10.1038/nature10113

Quesada, V., Conde, L., Villamor, N., Ordóñez, G. R., Jares, P., Bassaganyas, L., Ramsay, A. J., Beà, S., Pinyol, M., Martínez-Trillos, A., López-Guerra, M., Colomer, D., Navarro, A., Baumann, T., Aymerich, M., Rozman, M., Delgado, J., Giné, E., Hernández, J. M., González-Díaz, M., … López-Otín, C. (2011). Exome sequencing identifies recurrent mutations of the splicing factor SF3B1 gene in chronic lymphocytic leukemia. *Nature genetics*, *44*(1), 47–52. https://doi.org/10.1038/ng.1032

Quijada-Álamo, M., Hernández-Sánchez, M., Robledo, C., Hernández-Sánchez, J. M., Benito, R., Montaño, A., Rodríguez-Vicente, A. E., Quwaider, D., Martín, A. Á., García-Álvarez, M., Vidal-Manceñido, M. J., Ferrer-Garrido, G., Delgado-Beltrán, M. P., Galende, J., Rodríguez, J. N., Martín-Núñez, G., Alonso, J. M., García de Coca, A., Queizán, J. A., Sierra, M., … Hernández-Rivas, J. M. (2017). Next-generation sequencing and FISH studies reveal the appearance of gene mutations and chromosomal abnormalities in hematopoietic progenitors in chronic lymphocytic leukemia. *Journal of hematology & oncology*, *10*(1), 83. https://doi.org/10.1186/s13045-017-0450-y

Raaphorst, F. M., Meijer, C. J., Fieret, E., Blokzijl, T., Mommers, E., Buerger, H., Packeisen, J., Sewalt, R. A., Otte, A. P., & van Diest, P. J. (2003). Poorly differentiated breast carcinoma is associated with increased expression of the human polycomb group EZH2 gene. *Neoplasia*, *5*(6), 481–488. https://doi.org/10.1016/s1476-5586(03)80032-5

Ramasamy, K., Khatun, H., Macpherson, L., Caley, M. P., Sturge, J., Mufti, G. J., Schey, S. A., & Calle, Y. (2012). Fluorescence-based experimental model to evaluate the concomitant effect of drugs on the tumour microenvironment and cancer cells. *British journal of haematology*, *157*(5), 564–579. https://doi.org/10.1111/j.1365-2141.2012.09103.x

Ranganathan, P., Kashyap, T., Yu, X., Meng, X., Lai, T. H., McNeil, B., Bhatnagar, B., Shacham, S., Kauffman, M., Dorrance, A. M., Blum, W., Sampath, D., Landesman, Y., & Garzon, R. (2016). XPO1 Inhibition using Selinexor Synergizes with Chemotherapy in Acute Myeloid Leukemia by Targeting DNA Repair and Restoring Topoisomerase IIα to the Nucleus. *Clinical cancer research : an official journal of the American Association for Cancer Research*, *22*(24), 6142–6152. https://doi.org/10.1158/1078-0432.CCR-15-2885

Ranganathan, P., Yu, X., Na, C., Santhanam, R., Shacham, S., Kauffman, M., Walker, A., Klisovic, R., Blum, W., Caligiuri, M., Croce, C. M., Marcucci, G., & Garzon, R. (2012). Preclinical activity of a novel CRM1 inhibitor in acute myeloid leukemia. *Blood*, *120*(9), 1765–1773. https://doi.org/10.1182/blood-2012-04-423160

Ranganathan, P., Yu, X., Santhanam, R., Hofstetter, J., Walker, A., Walsh, K., Bhatnagar, B., Klisovic, R., Vasu, S., Phelps, M. A., Devine, S., Shacham, S., Kauffman, M., Marcucci, G., Blum, W., & Garzon, R. (2015). Decitabine priming enhances the antileukemic effects of exportin 1 (XPO1) selective inhibitor selinexor in acute myeloid leukemia. *Blood*, *125*(17), 2689–2692. https://doi.org/10.1182/blood-2014-10-607648

Rhee, H.-W., Zou, P., Udeshi, N. D., Martell, J. D., Mootha, V. K., Carr, S. A., & Ting, A. Y. (2013). Proteomic mapping of mitochondria in living cells via spatially-restricted enzymatic tagging. *Science*, *339*(6125), 1328–1331. https://doi.org/10.1126/science.1230593

Rodríguez, J. A. (2014). Interplay between nuclear transport and ubiquitin/SUMO modifications in the regulation of cancer-related proteins. *Seminars in cancer biology*, *27*, 11–19. https://doi.org/10.1016/j.semcancer.2014.03.005

Rodríguez, J. A. (2016). Description of USP12 nuclear export sequence. *Proceedings of the National Academy of Sciences of the United States of America*, *113*(24), E3315–E3316. https://doi.org/10.1073/pnas.1606081113

Rodriguez, J. A., Schüchner, S., Au, W. W., Fabbro, M., & Henderson, B. R. (2004). Nuclear-cytoplasmic shuttling of BARD1 contributes to its proapoptotic activity and is regulated by dimerization with BRCA1. *Oncogene*, *23*(10), 1809–1820. https://doi.org/10.1038/sj.onc.1207302

Roepman, P., Schlicker, A., Tabernero, J., Majewski, I., Tian, S., Moreno, V., Snel, M. H., Chresta, C. M., Rosenberg, R., Nitsche, U., Macarulla, T., Capella, G., Salazar, R., Orphanides, G., Wessels, L. F., Bernards, R., & Simon, I. M. (2014). Colorectal cancer intrinsic subtypes predict chemotherapy benefit, deficient mismatch repair and epithelial-to-mesenchymal transition. *International journal of cancer*, *134*(3), 552–562. https://doi.org/10.1002/ijc.28387

Rosebeck, S., Alonge, M. M., Kandarpa, M., Mayampurath, A., Volchenboum, S. L., Jasielec, J., Dytfeld, D., Maxwell, S. P., Kraftson, S. J., McCauley, D., Shacham, S., Kauffman, M., & Jakubowiak, A. J. (2016). Synergistic Myeloma Cell Death via Novel Intracellular Activation of Caspase-10-Dependent Apoptosis by Carfilzomib and Selinexor. *Molecular cancer therapeutics*, *15*(1), 60–71. https://doi.org/10.1158/1535-7163.MCT-15-0488

Rothbauer, U., Zolghadr, K., Muyldermans, S., Schepers, A., Cardoso, M. C., & Leonhardt, H. (2008). A versatile nanotrap for biochemical and functional studies with fluorescent fusion proteins. *Molecular and Cellular Proteomics*, *7*(2), 282–289. https://doi.org/10.1074/mcp.M700342-MCP200

Roux, K. J., Kim, D. I., Raida, M., & Burke, B. (2012). A promiscuous biotin ligase fusion protein identifies proximal and interacting proteins in mammalian cells. *Journal of Cell Biology*, *196*(6), 801–810. https://doi.org/10.1083/jcb.201112098

Roy, R., Chun, J., & Powell, S. N. (2011). BRCA1 and BRCA2: different roles in a common pathway of genome protection. *Nature Reviews Cancer*, *12*(1), 68–78. https://doi.org/10.1038/nrc3181

Rubinstein, M. M., Grisham, R. N., Cadoo, K., Kyi, C., Tew, W. P., Friedman, C. F., O'Cearbhaill, R. E., Zamarin, D., Zhou, Q., Iasonos, A., Nikolovski, I., Xu, H., Soldan, K. N., Caird, I., Martin, M., Guillen, J., Eid, K. T., Aghajanian, C., & Makker, V. (2021). A phase I open-label study of selinexor with paclitaxel and carboplatin in patients with advanced ovarian or endometrial cancers. *Gynecologic oncology*, *160*(1), 71–76. https://doi.org/10.1016/j.ygyno.2020.10.019

Saenz-Ponce, N., Pillay, R., de Long, L. M., Kashyap, T., Argueta, C., Landesman, Y., Hazar-Rethinam, M., Boros, S., Panizza, B., Jacquemyn, M., Daelemans, D., Gannon, O. M., & Saunders, N. A. (2018). Targeting the XPO1-dependent nuclear export of E2F7 reverses anthracycline resistance in head and neck squamous cell carcinomas. *Science translational medicine*, *10*(447), eaar7223. https://doi.org/10.1126/scitranslmed.aar7223

Safaei, S., Baradaran, B., Hagh, M. F., Alivand, M. R., Talebi, M., Gharibi, T., & Solali, S. (2018). Double sword role of EZH2 in leukemia. *Biomedicine & pharmacotherapy*, *98*, 626–635. https://doi.org/10.1016/j.biopha.2017.12.059

Saito, N., & Matsuura, Y. (2013). A 2.1-Å-resolution crystal structure of unliganded CRM1 reveals the mechanism of autoinhibition. *Journal of molecular biology*, *425*(2), 350–364. https://doi.org/10.1016/j.jmb.2012.11.014

Saito, S., Cigdem, S., Okuwaki, M., & Nagata, K. (2016). Leukemia-Associated Nup214 Fusion Proteins Disturb the XPO1-Mediated Nuclear-Cytoplasmic Transport Pathway and Thereby the NF-κB Signaling Pathway. *Molecular and cellular biology*, *36*(13), 1820–1835. https://doi.org/10.1128/MCB.00158-16

Sakakibara, K., Saito, N., Sato, T., Suzuki, A., Hasegawa, Y., Friedman, J. M., Kufe, D. W., Vonhoff, D. D., Iwami, T., & Kawabe, T. (2011). CBS9106 is a novel reversible oral CRM1 inhibitor with CRM1 degrading activity. *Blood*, *118*(14), 3922–3931. https://doi.org/10.1182/blood-2011-01-333138

Salas Fragomeni, R. A., Chung, H. W., Landesman, Y., Senapedis, W., Saint-Martin, J. R., Tsao, H., Flaherty, K. T., Shacham, S., Kauffman, M., & Cusack, J. C. (2013). CRM1 and BRAF inhibition synergize and induce tumor regression in BRAF-mutant melanoma. *Molecular cancer therapeutics*, *12*(7), 1171–1179. https://doi.org/10.1158/1535-7163.MCT-12-1171

Sanyal S. (2016). Reply to Rodriguez: Mechanism of nuclear-cytosol shuttling of Usp12. *Proceedings of the National Academy of Sciences of the United States of America*, *113*(24), E3317–E3318. https://doi.org/10.1073/pnas.1606225113

Saulino, D. M., Younes, P. S., Bailey, J. M., & Younes, M. (2018). CRM1/XPO1 expression in pancreatic adenocarcinoma correlates with survivin expression and the proliferative activity. *Oncotarget*, *9*(30), 21289–21295. https://doi.org/10.18632/oncotarget.25088

Schaffer, M., Chaturvedi, S., Davis, C., Aquino, R., Stepanchick, E., Versele, M., Liu, Y., Yang, J., Lu, R., & Balasubramanian, S. (2018). Identification of potential ibrutinib combinations in hematological malignancies using a combination high-throughput screen. *Leukemia & lymphoma*, *59*(4), 931–940. https://doi.org/10.1080/10428194.2017.1349899

Schindelin, J., Arganda-Carreras, I., Frise, E., Kaynig, V., Longair, M., Pietzsch, T., Preibisch, S., Rueden, C., Saalfeld, S., Schmid, B., Tinevez, J. Y., White, D. J., Hartenstein, V., Eliceiri, K., Tomancak, P., & Cardona, A. (2012). Fiji: an open-source platform for biological-image analysis. *Nature methods*, *9*(7), 676–682. https://doi.org/10.1038/nmeth.2019

Schmidt, H. B., & Görlich, D. (2016). Transport Selectivity of Nuclear Pores, Phase Separation, and Membraneless Organelles. *Trends in biochemical sciences*, *41*(1), 46–61. https://doi.org/10.1016/j.tibs.2015.11.001

Schmidt, J., Braggio, E., Kortuem, K. M., Egan, J. B., Zhu, Y. X., Xin, C. S., Tiedemann, R. E., Palmer, S. E., Garbitt, V. M., McCauley, D., Kauffman, M., Shacham, S., Chesi, M., Bergsagel, P. L., & Stewart, A. K. (2013). Genome-wide studies in multiple myeloma identify XPO1/CRM1 as a critical target validated using the selective nuclear export inhibitor KPT-276. *Leukemia*, *27*(12), 2357–2365. https://doi.org/10.1038/leu.2013.172

Schwarzerová, K., Bellinvia, E., Martinek, J., Sikorová, L., Dostál, V., Libusová, L., Bokvaj, P., Fischer, L., Schmit, A. C., & Nick, P. (2019). Tubulin is actively exported from the nucleus through the Exportin1/CRM1 pathway. *Scientific reports*, *9*(1), 5725. https://doi.org/10.1038/s41598-019-42056-6

Sekihara, K., Saitoh, K., Han, L., Ciurea, S., Yamamoto, S., Kikkawa, M., Kazuno, S., Taka, H., Kaga, N., Arai, H., Miida, T., Andreeff, M., Konopleva, M., & Tabe, Y. (2017). Targeting mantle cell lymphoma metabolism and survival through simultaneous blockade of mTOR and nuclear transporter exportin-1. *Oncotarget*, *8*(21), 34552–34564. https://doi.org/10.18632/oncotarget.16602

Senapedis, W. T., Baloglu, E., & Landesman, Y. (2014). Clinical translation of nuclear export inhibitors in cancer. *Seminars in cancer biology*, *27*, 74–86. https://doi.org/10.1016/j.semcancer.2014.04.005

Sendino, M., Olazabal-Herrero, A., Rodriguez, J. A., & Omaetxebarria, M. J. (2020b). XPO1en bidezko garraio nukleozitoplasmikoa: oinarrizko mekanismoak eta hurbilketa esperimentalak. *Ekaia*, *37*, 221–239. https://doi.org/https://doi.org/10.1387/ekaia.20861

Sendino, M., Omaetxebarria, M. J., & Rodríguez, J. A. (2018). Hitting a moving target: inhibition of the nuclear export receptor XPO1/CRM1 as a therapeutic approach in cancer. *Cancer Drug Resistance*, *1*, 138–163. https://doi.org/10.20517/cdr.2018.09

Sendino, M., Omaetxebarria, M. J., Prieto, G., & Rodriguez, J. A. (2020a). Using a simple cellular assay to map NES motifs in cancer-related proteins, gain insight into CRM1-mediated NES export, and search for NES-harboring micropeptides. *International Journal of Molecular Sciences*, *21*(17), 6341. https://doi.org/10.3390/ijms21176341

Sendino, M., Omaetxebarria, M.J., Rodríguez, J.A. (2020c). The strength of a NES motif in the nucleocapsid protein of human coronaviruses is related to genus, but not to pathogenic capacity. *bioRxiv.* https://doi.org/10.1101/2020.10.06.328138

Sendino, M., Ramírez, J., Ugo Mayor, Prieto, G., Omaetxebarria, M.J., Rodríguez, J.A. (2021). Konpartimentu-espezifikoko gertuko biotinilazioa: XPO1en esportazio-kargoak identifikatzeko hurbilketa berria. *Ekaia, 41,* 151-169. https://doi.org/10.1387/ekaia.22591

Serresi, M., Siteur, B., Hulsman, D., Company, C., Schmitt, M. J., Lieftink, C., Morris, B., Cesaroni, M., Proost, N., Beijersbergen, R. L., van Lohuizen, M., & Gargiulo, G. (2018). Ezh2 inhibition in Kras-driven lung cancer amplifies inflammation and associated vulnerabilities. *The Journal of experimental medicine*, *215*(12), 3115–3135. https://doi.org/10.1084/jem.20180801

Sexton, R., Mahdi, Z., Chaudhury, R., Beydoun, R., Aboukameel, A., Khan, H. Y., Baloglu, E., Senapedis, W., Landesman, Y., Tesfaye, A., Kim, S., Philip, P. A., & Azmi, A. S. (2019). Targeting Nuclear Exporter Protein XPO1/CRM1 in Gastric Cancer. *International journal of molecular sciences*, *20*(19), 4826. https://doi.org/10.3390/ijms20194826

Shafique, M., Ismail-Khan, R., Extermann, M., Sullivan, D., Goodridge, D., Boulware, D., Hogue, D., Soliman, H., Khong, H., & Han, H. S. (2019). A Phase II Trial of Selinexor (KPT-330) for Metastatic Triple-Negative Breast Cancer. *The oncologist*, *24*(7), 887–e416. https://doi.org/10.1634/theoncologist.2019-0231

Shaikh, M. H., Idris, A., Johnson, N. W., Fallaha, S., Clarke, D., Martin, D., Morgan, I. M., Gabrielli, B., & McMillan, N. (2018). Aurora kinases are a novel therapeutic target for HPV-positive head and neck cancers. *Oral oncology*, *86*, 105–112. https://doi.org/10.1016/j.oraloncology.2018.09.006

Shang, E., Zhang, Y., Shu, C., Ishida, C. T., Bianchetti, E., Westhoff, M. A., Karpel-Massler, G., & Siegelin, M. D. (2018). Dual Inhibition of Bcl-2/Bcl-xL and XPO1 is synthetically lethal in glioblastoma model systems. *Scientific reports*, *8*(1), 15383. https://doi.org/10.1038/s41598-018-33784-2

Sharp, T. V., Munoz, F., Bourboulia, D., Presneau, N., Darai, E., Wang, H. W., Cannon, M., Butcher, D. N., Nicholson, A. G., Klein, G., Imreh, S., & Boshoff, C. (2004). LIM domains-containing protein 1 (LIMD1), a tumor suppressor encoded at chromosome 3p21.3, binds pRB and represses E2F-driven transcription. *Proceedings of the National Academy of Sciences of the United States of America*, *101*(47), 16531–16536. https://doi.org/10.1073/pnas.0407123101

Shedden, K., Taylor, J. M., Enkemann, S. A., Tsao, M. S., Yeatman, T. J., Gerald, W. L., Eschrich, S., Jurisica, I., Giordano, T. J., Misek, D. E., Chang, A. C., Zhu, C. Q., Strumpf, D., Hanash, S., Shepherd, F. A., Ding, K., Seymour, L., Naoki, K., Pennell, N., … Beer, D. G. (2008). Gene expression-based survival prediction in lung adenocarcinoma: a multi-site, blinded validation study. *Nature medicine*, *14*(8), 822–827. https://doi.org/10.1038/nm.1790

Shen, A., Wang, Y., Zhao, Y., Zou, L., Sun, L., & Cheng, C. (2009). Expression of CRM1 in human gliomas and its significance in p27 expression and clinical prognosis. *Neurosurgery*, *65*(1), 153–160. https://doi.org/10.1227/01.NEU.0000348550.47441.4B

Shevchenko, A., Wilm, M., Vorm, O., & Mann, M. (1996). Mass spectrometric sequencing of proteins from silver-stained polyacrylamide gels. *Analytical Chemistry*, *68*(5), 850–858. https://doi.org/10.1021/ac950914h

Sievers, F., & Higgins, D. G. (2014). Clustal Omega, accurate alignment of very large numbers of sequences. *Methods in molecular biology*, *1079*, 105–116. https://doi.org/10.1007/978-1-62703-646-7_6

Slavoff, S. A., Heo, J., Budnik, B. A., Hanakahi, L. A., & Saghatelian, A. (2014). A human short open reading frame (sORF)-encoded polypeptide that stimulates DNA end joining. *The Journal of biological chemistry*, *289*(16), 10950–10957. https://doi.org/10.1074/jbc.C113.533968

Soniat, M., & Chook, Y. M. (2015). Nuclear localization signals for four distinct karyopherin-β nuclear import systems. *The Biochemical journal*, *468*(3), 353–362. https://doi.org/10.1042/BJ20150368

Sowa, M. E., Bennett, E. J., Gygi, S. P., & Harper, J. W. (2009). Defining the human deubiquitinating enzyme interaction landscape. *Cell*, *138*(2), 389–403. https://doi.org/10.1016/j.cell.2009.04.042

Stade, K., Ford, C. S., Guthrie, C., & Weis, K. (1997). Exportin 1 (Crm1p) is an essential nuclear export factor. *Cell*, *90*(6), 1041–1050. https://doi.org/10.1016/s0092-8674(00)80370-0

Stojic, L., Brun, R., & Jiricny, J. (2004). Mismatch repair and DNA damage signalling. *DNA Repair*, *3*(8–9), 1091–1101. https://doi.org/10.1016/j.dnarep.2004.06.006

Stommel, J. M., Marchenko, N. D., Jimenez, G. S., Moll, U. M., Hope, T. J., & Wahl, G. M. (1999). A leucine-rich nuclear export signal in the p53 tetramerization domain: regulation of subcellular localization and p53 activity by NES masking. The EMBO journal, 18(6), 1660–1672. https://doi.org/10.1093/emboj/18.6.1660

Subhash, V. V., Yeo, M. S., Wang, L., Tan, S. H., Wong, F. Y., Thuya, W. L., Tan, W. L., Peethala, P. C., Soe, M. Y., Tan, D., Padmanabhan, N., Baloglu, E., Shacham, S., Tan, P., Koeffler, H. P., & Yong, W. P. (2018). Anti-tumor efficacy of Selinexor (KPT-330) in gastric cancer is dependent on nuclear accumulation of p53 tumor suppressor. *Scientific reports*, *8*(1), 12248. https://doi.org/10.1038/s41598-018-30686-1

Sudo, T., Utsunomiya, T., Mimori, K., Nagahara, H., Ogawa, K., Inoue, H., Wakiyama, S., Fujita, H., Shirouzu, K., & Mori, M. (2005). Clinicopathological significance of EZH2 mRNA expression in patients with hepatocellular carcinoma. *British journal of cancer*, *92*(9), 1754–1758. https://doi.org/10.1038/sj.bjc.6602531

Sun, H., Hattori, N., Chien, W., Sun, Q., Sudo, M., E-Ling, G. L., Ding, L., Lim, S. L., Shacham, S., Kauffman, M., Nakamaki, T., & Koeffler, H. P. (2014). KPT-330 has antitumour activity against non-small cell lung cancer. *British journal of cancer*, *111*(2), 281–291. https://doi.org/10.1038/bjc.2014.260

Sun, H., Lin, D. C., Cao, Q., Guo, X., Marijon, H., Zhao, Z., Gery, S., Xu, L., Yang, H., Pang, B., Lee, V. K., Lim, H. J., Doan, N., Said, J. W., Chu, P., Mayakonda, A., Thomas, T., Forscher, C., Baloglu, E., Shacham, S., … Koeffler, H. P. (2016). CRM1 Inhibition Promotes Cytotoxicity in Ewing Sarcoma Cells by Repressing EWS-FLI1-Dependent IGF-1 Signaling. *Cancer research*, *76*(9), 2687–2697. https://doi.org/10.1158/0008-5472.CAN-15-1572

Sun, Y. Q., Xie, J. W., Xie, H. T., Chen, P. C., Zhang, X. L., Zheng, C. H., Li, P., Wang, J. B., Lin, J. X., Cao, L. L., Huang, C. M., & Lin, Y. (2017). Expression of CRM1 and CDK5 shows high prognostic accuracy for gastric cancer. *World journal of gastroenterology*, *23*(11), 2012–2022. https://doi.org/10.3748/wjg.v23.i11.2012

Sutton, L. A., Ljungström, V., Mansouri, L., Young, E., Cortese, D., Navrkalova, V., Malcikova, J., Muggen, A. F., Trbusek, M., Panagiotidis, P., Davi, F., Belessi, C., Langerak, A. W., Ghia, P., Pospisilova, S., Stamatopoulos, K., & Rosenquist, R. (2015). Targeted next-generation sequencing in chronic lymphocytic leukemia: a high-throughput yet tailored approach will facilitate implementation in a clinical setting. *Haematologica*, *100*(3), 370–376. https://doi.org/10.3324/haematol.2014.109777

Sweet, K., Komrokji, R., Padron, E., Cubitt, C. L., Turner, J. G., Zhou, J., List, A. F., Sallman, D. A., Dawson, J. L., Sullivan, D. M., Chavez, J., Shah, B. D., & Lancet, J. E. (2020). Phase I Clinical Trial of Selinexor in Combination with Daunorubicin and Cytarabine in Previously Untreated Poor-Risk Acute Myeloid Leukemia. *Clinical cancer research: an official journal of the American Association for Cancer Research*, *26*(1), 54–60. https://doi.org/10.1158/1078-0432.CCR-19-2169

Taagepera, S., McDonald, D., Loeb, J. E., Whitaker, L. L., McElroy, A. K., Wang, J. Y., & Hope, T. J. (1998). Nuclear-cytoplasmic shuttling of C-ABL tyrosine kinase. *Proceedings of the National Academy of Sciences of the United States of America*, *95*(13), 7457–7462. https://doi.org/10.1073/pnas.95.13.7457

Tai, Y. T., Landesman, Y., Acharya, C., Calle, Y., Zhong, M. Y., Cea, M., Tannenbaum, D., Cagnetta, A., Reagan, M., Munshi, A. A., Senapedis, W., Saint-Martin, J. R., Kashyap, T., Shacham, S., Kauffman, M., Gu, Y., Wu, L., Ghobrial, I., Zhan, F., Kung, A. L., … Anderson, K. C. (2014). CRM1 inhibition induces tumor cell cytotoxicity and impairs osteoclastogenesis in multiple myeloma: molecular mechanisms and therapeutic implications. *Leukemia*, *28*(1), 155–165. https://doi.org/10.1038/leu.2013.115

Takahashi, K., Hu, B., Wang, F., Yan, Y., Kim, E., Vitale, C., Patel, K. P., Strati, P., Gumbs, C., Little, L., Tippen, S., Song, X., Zhang, J., Jain, N., Thompson, P., Garcia-Manero, G., Kantarjian, H., Estrov, Z., Do, K. A., Keating, M., … Ferrajoli, A. (2018). Clinical implications of cancer gene mutations in patients with chronic lymphocytic leukemia treated with lenalidomide. *Blood*, *131*(16), 1820–1832. https://doi.org/10.1182/blood-2017-11-817296

Takeda, A., & Yaseen, N. R. (2014). Nucleoporins and nucleocytoplasmic transport in hematologic malignancies. *Seminars in cancer biology*, *27*, 3–10. https://doi.org/10.1016/j.semcancer.2014.02.009

Takeda, A., Sarma, N. J., Abdul-Nabi, A. M., & Yaseen, N. R. (2010). Inhibition of CRM1-mediated nuclear export of transcription factors by leukemogenic NUP98 fusion proteins. The Journal of biological chemistry, 285(21), 16248–16257. https://doi.org/10.1074/jbc.M109.048785

Tan, D. S., Bedard, P. L., Kuruvilla, J., Siu, L. L., & Razak, A. R. (2014). Promising SINEs for embargoing nuclear-cytoplasmic export as an anticancer strategy. *Cancer discovery*, *4*(5), 527–537. https://doi.org/10.1158/2159-8290.CD-13-1005

Tang, T., Martin, P., Somasundaram, N., Lim, C., Tao, M., Poon, E., Yunon, M. J., Toh, S. Q., Yan, S. X., Farid, M., Chan, J. Y., & Lim, S. T. (2021). Phase I study of selinexor in combination with dexamethasone, ifosfamide, carboplatin, etoposide chemotherapy in patients with relapsed or refractory peripheral T-cell or natural-killer/T-cell lymphoma. *Haematologica*, *106*(12), 3170–3175. https://doi.org/10.3324/haematol.2020.251454

Tarantelli, C., Zhang, L., Curti, E., Gaudio, E., Spriano, F., Priebe, V., Cascione, L., Arribas, A. J., Zucca, E., Rossi, D., Stathis, A., & Bertoni, F. (2019). The Bruton tyrosine kinase inhibitor zanubrutinib (BGB-3111) demonstrated synergies with other anti-lymphoma targeted agents. *Haematologica*, *104*(7), e307–e309. https://doi.org/10.3324/haematol.2018.214759

Taylor, B. S., Schultz, N., Hieronymus, H., Gopalan, A., Xiao, Y., Carver, B. S., Arora, V. K., Kaushik, P., Cerami, E., Reva, B., Antipin, Y., Mitsiades, N., Landers, T., Dolgalev, I., Major, J. E., Wilson, M., Socci, N. D., Lash, A. E., Heguy, A., Eastham, J. A., … Gerald, W. L. (2010). Integrative genomic profiling of human prostate cancer. *Cancer cell*, *18*(1), 11–22. https://doi.org/10.1016/j.ccr.2010.05.026

Taylor, J., Mi, X., Penson, A. V., Paffenholz, S. V., Alvarez, K., Sigler, A., Chung, S. S., Rampal, R. K., Park, J. H., Stein, E. M., Tallman, M. S., Sen, F., Gönen, M., Abdel-Wahab, O., & Klimek, V. M. (2020). Safety and activity of selinexor in patients with myelodysplastic syndromes or oligoblastic acute myeloid leukaemia refractory to hypomethylating agents: a single-centre, single-arm, phase 2 trial. *The Lancet. Haematology*, *7*(8), e566–e574. https://doi.org/10.1016/S2352-3026(20)30209-X

Taylor, J., Sendino, M., Gorelick, A. N., Pastore, A., Chang, M. T., Penson, A. V., Gavrila, E. I., Stewart, C., Melnik, E. M., Herrejon Chavez, F., Bitner, L., Yoshimi, A., Lee, S. C., Inoue, D., Liu, B., Zhang, X. J., Mato, A. R., Dogan, A., Kharas, M. G., Chen, Y., … Abdel-Wahab, O. (2019). Altered Nuclear Export Signal Recognition as a Driver of Oncogenesis. *Cancer discovery*, *9*(10), 1452–1467. https://doi.org/10.1158/2159-8290.CD-19-0298

Thakar, K., Karaca, S., Port, S. A., Urlaub, H., & Kehlenbach, R. H. (2013). Identification of CRM1-dependent nuclear export cargos using quantitative mass spectrometry. *Molecular and Cellular Proteomics*, *12*(3), 664–678. https://doi.org/10.1074/mcp.M112.024877

Tiacci, E., Ladewig, E., Schiavoni, G., Penson, A., Fortini, E., Pettirossi, V., Wang, Y., Rosseto, A., Venanzi, A., Vlasevska, S., Pacini, R., Piattoni, S., Tabarrini, A., Pucciarini, A., Bigerna, B., Santi, A., Gianni, A. M., Viviani, S., Cabras, A., Ascani, S., … Falini, B. (2018). Pervasive mutations of JAK-STAT pathway genes in classical Hodgkin lymphoma. *Blood*, *131*(22), 2454–2465. https://doi.org/10.1182/blood-2017-11-814913

Tibbetts, R. S., Cortez, D., Brumbaugh, K. M., Scully, R., Livingston, D., Elledge, S. J., & Abraham, R. T. (2000). Functional interactions between BRCA1 and the checkpoint kinase ATR during genotoxic stress. *Genes & development*, *14*(23), 2989–3002. https://doi.org/10.1101/gad.851000

Timney, B. L., Raveh, B., Mironska, R., Trivedi, J. M., Kim, S. J., Russel, D., Wente, S. R., Sali, A., & Rout, M. P. (2016). Simple rules for passive diffusion through the nuclear pore complex. *The Journal of cell biology*, *215*(1), 57–76. https://doi.org/10.1083/jcb.201601004

Toyoshima, F., Moriguchi, T., Wada, A., Fukuda, M., & Nishida, E. (1998). Nuclear export of cyclin B1 and its possible role in the DNA damage-induced G2 checkpoint. *The EMBO journal*, *17*(10), 2728–2735. https://doi.org/10.1093/emboj/17.10.2728

Tran, E. J., King, M. C., & Corbett, A. H. (2014). Macromolecular transport between the nucleus and the cytoplasm: Advances in mechanism and emerging links to disease. *Biochimica et biophysica acta*, *1843*(11), 2784–2795. https://doi.org/10.1016/j.bbamcr.2014.08.003

Tran, J. R., Paulson, D. I., Moresco, J. J., Adam, S. A., Yates, J. R., Goldman, R. D., & Zheng, Y. (2021). An APEX2 proximity ligation method for mapping interactions with the nuclear lamina. *The Journal of cell biology*, *220*(1), e202002129. https://doi.org/10.1083/jcb.202002129

Tremblay-LeMay, R., Rastgoo, N., Pourabdollah, M., & Chang, H. (2018). EZH2 as a therapeutic target for multiple myeloma and other haematological malignancies. *Biomarker research*, *6*, 34. https://doi.org/10.1186/s40364-018-0148-5

Tsai, H. J., Jiaang, W. T., Shih, N. Y., Fletcher, J. A., Lin, M. J., Yang, M. Y., Chen, C. T., Hsu, T. J., Wu, C. C., Lin, H. Y., & Chen, L. T. (2018). BPR1J373, a novel multitargeted kinase inhibitor, effectively suppresses the growth of gastrointestinal stromal tumor. *Cancer science*, *109*(11), 3591–3601. https://doi.org/10.1111/cas.13773

Turner, J. G., & Sullivan, D. M. (2008). CRM1-mediated nuclear export of proteins and drug resistance in cancer. *Current medicinal chemistry*, *15*(26), 2648–2655. https://doi.org/10.2174/092986708786242859

Turner, J. G., Cui, Y., Bauer, A. A., Dawson, J. L., Gomez, J. A., Kim, J., Cubitt, C. L., Nishihori, T., Dalton, W. S., & Sullivan, D. M. (2020). Melphalan and Exportin 1 Inhibitors Exert Synergistic Antitumor Effects in Preclinical Models of Human Multiple Myeloma. *Cancer research*, *80*(23), 5344–5354. https://doi.org/10.1158/0008-5472.CAN-19-0677

Turner, J. G., Dawson, J. L., Grant, S., Shain, K. H., Dalton, W. S., Dai, Y., Meads, M., Baz, R., Kauffman, M., Shacham, S., & Sullivan, D. M. (2016a). Treatment of acquired drug resistance in multiple myeloma by combination therapy with XPO1 and topoisomerase II inhibitors. *Journal of hematology & oncology*, *9*(1), 73. https://doi.org/10.1186/s13045-016-0304-z

Turner, J. G., Dawson, J., Emmons, M. F., Cubitt, C. L., Kauffman, M., Shacham, S., Hazlehurst, L. A., & Sullivan, D. M. (2013). CRM1 Inhibition Sensitizes Drug Resistant Human Myeloma Cells to Topoisomerase II and Proteasome Inhibitors both In Vitro and Ex Vivo. *Journal of Cancer*, *4*(8), 614–625. https://doi.org/10.7150/jca.7080

Turner, J. G., Kashyap, T., Dawson, J. L., Gomez, J., Bauer, A. A., Grant, S., Dai, Y., Shain, K. H., Meads, M., Landesman, Y., & Sullivan, D. M. (2016b). XPO1 inhibitor combination therapy with bortezomib or carfilzomib induces nuclear localization of IκBα and overcomes acquired proteasome inhibitor resistance in human multiple myeloma. *Oncotarget*, *7*(48), 78896–78909. https://doi.org/10.18632/oncotarget.12969

Turner, J. G., Marchion, D. C., Dawson, J. L., Emmons, M. F., Hazlehurst, L. A., Washausen, P., & Sullivan, D. M. (2009). Human multiple myeloma cells are sensitized to topoisomerase II inhibitors by CRM1 inhibition. *Cancer research*, *69*(17), 6899–6905. https://doi.org/10.1158/0008-5472.CAN-09-0484

Tyner, J. W., Tognon, C. E., Bottomly, D., Wilmot, B., Kurtz, S. E., Savage, S. L., Long, N., Schultz, A. R., Traer, E., Abel, M., Agarwal, A., Blucher, A., Borate, U., Bryant, J., Burke, R., Carlos, A., Carpenter, R., Carroll, J., Chang, B. H., Coblentz, C., … Druker, B. J. (2018). Functional genomic landscape of acute myeloid leukaemia. *Nature*, *562*(7728), 526–531. https://doi.org/10.1038/s41586-018-0623-z

UniProt Consortium. (2019). UniProt: A worldwide hub of protein knowledge. *Nucleic Acids Research*, *47*(D1), D506–D515. https://doi.org/10.1093/nar/gky1049

Urbé, S., Liu, H., Hayes, S. D., Heride, C., Rigden, D. J., & Clague, M. J. (2012). Systematic survey of deubiquitinase localization identifies USP21 as a regulator of centrosome- and microtubule-associated functions. *Molecular biology of the cell*, *23*(6), 1095–1103. https://doi.org/10.1091/mbc.E11-08-0668

van der Veen, A. G., & Ploegh, H. L. (2012). Ubiquitin-like proteins. *Annual review of biochemistry*, *81*, 323–357. https://doi.org/10.1146/annurev-biochem-093010-153308

van der Watt, P. J., & Leaner, V. D. (2011). The nuclear exporter, Crm1, is regulated by NFY and Sp1 in cancer cells and repressed by p53 in response to DNA damage. *Biochimica et biophysica acta*, *1809*(7), 316–326. https://doi.org/10.1016/j.bbagrm.2011.05.017

van der Watt, P. J., Zemanay, W., Govender, D., Hendricks, D. T., Parker, M. I., & Leaner, V. D. (2014). Elevated expression of the nuclear export protein, Crm1 (exportin 1), associates with human oesophageal squamous cell carcinoma. *Oncology reports*, *32*(2), 730–738. https://doi.org/10.3892/or.2014.3231

Van Slambrouck, C., Huh, J., Suh, C., Song, J. Y., Menon, M. P., Sohani, A. R., Duffield, A. S., Goldberg, R. C., Dama, P., Kiyotani, K., Godfrey, J., Fitzpatrick, C., Kline, J., Smith, S. M., Jaffe, E. S., Hartmann, S., & Venkataraman, G. (2020). Diagnostic utility of STAT6^{YE361} expression in classical Hodgkin lymphoma and related entities. *Modern pathology : an official journal of the United States and Canadian Academy of Pathology, Inc*, *33*(5), 834–845. https://doi.org/10.1038/s41379-019-0428-0

Varambally, S., Dhanasekaran, S. M., Zhou, M., Barrette, T. R., Kumar-Sinha, C., Sanda, M. G., Ghosh, D., Pienta, K. J., Sewalt, R. G., Otte, A. P., Rubin, M. A., & Chinnaiyan, A. M. (2002). The polycomb group protein EZH2 is involved in progression of prostate cancer. *Nature*, *419*(6907), 624–629. https://doi.org/10.1038/nature01075

Varambally, S., Yu, J., Laxman, B., Rhodes, D. R., Mehra, R., Tomlins, S. A., Shah, R. B., Chandran, U., Monzon, F. A., Becich, M. J., Wei, J. T., Pienta, K. J., Ghosh, D., Rubin, M. A., & Chinnaiyan, A. M. (2005). Integrative genomic and proteomic analysis of prostate cancer reveals signatures of metastatic progression. *Cancer cell*, *8*(5), 393–406. https://doi.org/10.1016/j.ccr.2005.10.001

Verbeke, D., Demeyer, S., Prieto, C., de Bock, C. E., De Bie, J., Gielen, O., Jacobs, K., Mentens, N., Verhoeven, B. M., Uyttebroeck, A., Boeckx, N., De Keersmaecker, K., Maertens, J., Segers, H., & Cools, J. (2020). The XPO1 Inhibitor KPT-8602 Synergizes with Dexamethasone in Acute Lymphoblastic Leukemia. *Clinical cancer research : an official journal of the American Association for Cancer Research*, *26*(21), 5747–5758. https://doi.org/10.1158/1078-0432.CCR-20-1315

Vergote, I. B., Lund, B., Peen, U., Umajuridze, Z., Mau-Sorensen, M., Kranich, A., Van Nieuwenhuysen, E., Haslund, C., Nottrup, T., Han, S. N., Concin, N., Unger, T. J., Chai, Y., Au, N., Rashal, T., Joshi, A., Crochiere, M., Landesman, Y., Shah, J., Shacham, S., … Mirza, M. R. (2020). Phase 2 study of the Exportin 1 inhibitor selinexor in patients with recurrent gynecological

malignancies. *Gynecologic oncology*, *156*(2), 308–314. https://doi.org/10.1016/j.ygyno.2019.11.012

Vielhaber, E. L., Duricka, D., Ullman, K. S., & Virshup, D. M. (2001). Nuclear export of mammalian PERIOD proteins. *The Journal of biological chemistry*, *276*(49), 45921–45927. https://doi.org/10.1074/jbc.M107726200

Vigneri, P., & Wang, J. Y. (2001). Induction of apoptosis in chronic myelogenous leukemia cells through nuclear entrapment of BCR-ABL tyrosine kinase. Nature medicine, 7(2), 228–234. https://doi.org/10.1038/84683

Vogl, D. T., Dingli, D., Cornell, R. F., Huff, C. A., Jagannath, S., Bhutani, D., Zonder, J., Baz, R., Nooka, A., Richter, J., Cole, C., Vij, R., Jakubowiak, A., Abonour, R., Schiller, G., Parker, T. L., Costa, L. J., Kaminetzky, D., Hoffman, J. E., Yee, A. J., … Stewart, A. K. (2018). Selective Inhibition of Nuclear Export With Oral Selinexor for Treatment of Relapsed or Refractory Multiple Myeloma. *Journal of clinical oncology : official journal of the American Society of Clinical Oncology*, *36*(9), 859–866. https://doi.org/10.1200/JCO.2017.75.5207

Vollbrecht, C., Mairinger, F. D., Koitzsch, U., Peifer, M., Koenig, K., Heukamp, L. C., Crispatzu, G., Wilden, L., Kreuzer, K. A., Hallek, M., Odenthal, M., Herling, C. D., & Buettner, R. (2015). Comprehensive Analysis of Disease-Related Genes in Chronic Lymphocytic Leukemia by Multiplex PCR-Based Next Generation Sequencing. *PloS one*, *10*(6), e0129544. https://doi.org/10.1371/journal.pone.0129544

Wahba, A., Rath, B. H., O'Neill, J. W., Camphausen, K., & Tofilon, P. J. (2018). The XPO1 Inhibitor Selinexor Inhibits Translation and Enhances the Radiosensitivity of Glioblastoma Cells Grown *In Vitro* and *In Vivo*. *Molecular cancer therapeutics*, *17*(8), 1717–1726. https://doi.org/10.1158/1535-7163.MCT-17-1303

Walker, C. J., Oaks, J. J., Santhanam, R., Neviani, P., Harb, J. G., Ferenchak, G., Ellis, J. J., Landesman, Y., Eisfeld, A. K., Gabrail, N. Y., Smith, C. L., Caligiuri, M. A., Hokland, P., Roy, D. C., Reid, A., Milojkovic, D., Goldman, J. M., Apperley, J., Garzon, R., Marcucci, G., … Perrotti, D. (2013). Preclinical and clinical efficacy of XPO1/CRM1 inhibition by the karyopherin inhibitor KPT-330 in Ph+ leukemias. *Blood*, *122*(17), 3034–3044. https://doi.org/10.1182/blood-2013-04-495374

Wang, A. Y., Weiner, H., Green, M., Chang, H., Fulton, N., Larson, R. A., Odenike, O., Artz, A. S., Bishop, M. R., Godley, L. A., Thirman, M. J., Kosuri, S., Churpek, J. E., Curran, E., Pettit, K., Stock, W., & Liu, H. (2018). A phase I study of selinexor in combination with high-dose cytarabine and mitoxantrone for remission induction in patients with acute myeloid leukemia. *Journal of hematology & oncology*, *11*(1), 4. https://doi.org/10.1186/s13045-017-0550-8

Wang, Q., Zhang, H., Guerrette, S., Chen, J., Mazurek, A., Wilson, T., Slupianek, A., Skorski, T., Fishel, R., & Greene, M. I. (2001). Adenosine nucleotide modulates the physical interaction between hMSH2 and BRCA1. *Oncogene*, *20*(34), 4640–4649. https://doi.org/10.1038/sj.onc.1204625

Wang, S., Han, X., Wang, J., Yao, J., & Shi, Y. (2014). Antitumor effects of a novel chromosome region maintenance 1 (CRM1) inhibitor on non-small cell lung cancer cells in vitro and in mouse tumor xenografts. *PloS one*, *9*(3), e89848. https://doi.org/10.1371/journal.pone.0089848

Wang, X., & Li, S. (2014). Protein mislocalization: mechanisms, functions and clinical applications in cancer. *Biochimica et biophysica acta*, *1846*(1), 13–25. https://doi.org/10.1016/j.bbcan.2014.03.006

Wang, X., Zhou, Y. X., Qiao, W., Tominaga, Y., Ouchi, M., Ouchi, T., & Deng, C. X. (2006). Overexpression of aurora kinase A in mouse mammary epithelium induces genetic instability preceding mammary tumor formation. *Oncogene*, *25*(54), 7148–7158. https://doi.org/10.1038/sj.onc.1209707

Wang, Y., Klijn, J. G., Zhang, Y., Sieuwerts, A. M., Look, M. P., Yang, F., Talantov, D., Timmermans, M., Meijer-van Gelder, M. E., Yu, J., Jatkoe, T., Berns, E. M., Atkins, D., & Foekens, J. A. (2005). Gene-expression profiles to predict distant metastasis of lymph-node-negative primary breast cancer. *Lancet (London, England)*, *365*(9460), 671–679. https://doi.org/10.1016/S0140-6736(05)17947-1

Wei, N., Song, Y., Zhang, F., Sun, Z., & Zhang, X. (2020). Transcriptome Profiling of Acquired Gefitinib Resistant Lung Cancer Cells Reveals Dramatically Changed Transcription Programs and New Treatment Targets. *Frontiers in oncology*, *10*, 1424. https://doi.org/10.3389/fonc.2020.01424

Wei, X. X., Siegel, A. P., Aggarwal, R., Lin, A. M., Friedlander, T. W., Fong, L., Kim, W., Louttit, M., Chang, E., Zhang, L., & Ryan, C. J. (2018). A Phase II Trial of Selinexor, an Oral Selective Inhibitor of Nuclear Export Compound, in Abiraterone- and/or Enzalutamide-Refractory Metastatic Castration-Resistant Prostate Cancer. *The oncologist*, *23*(6), 656–e64. https://doi.org/10.1634/theoncologist.2017-0624

Wen, S., Wang, J., Liu, P., Li, Y., Lu, W., Hu, Y., Liu, J., He, Z., & Huang, P. (2018). Novel combination of histone methylation modulators with therapeutic synergy against acute myeloid leukemia in vitro and in vivo. *Cancer letters*, *413*, 35–45. https://doi.org/10.1016/j.canlet.2017.10.015

Wen, W., Meinkotht, J. L., Tsien, R. Y., & Taylor, S. S. (1995). Identification of a signal for rapid export of proteins from the nucleus. *Cell*, *82*(3), 463–473. https://doi.org/10.1016/0092-8674(95)90435-2

Wettersten, H. I., Landesman, Y., Friedlander, S., Shacham, S., Kauffman, M., & Weiss, R. H. (2014). Specific inhibition of the nuclear exporter exportin-1 attenuates kidney cancer growth. *PloS one*, *9*(12), e113867. https://doi.org/10.1371/journal.pone.0113867

Wienand, K., Chapuy, B., Stewart, C., Dunford, A. J., Wu, D., Kim, J., Kamburov, A., Wood, T. R., Cader, F. Z., Ducar, M. D., Thorner, A. R., Nag, A., Heubeck, A. T., Buonopane, M. J., Redd, R. A., Bojarczuk, K., Lawton, L. N., Armand, P., Rodig, S. J., Fromm, J. R., … Shipp, M. A. (2019). Genomic analyses of flow-sorted Hodgkin Reed-Sternberg cells reveal complementary mechanisms of immune evasion. *Blood advances*, *3*(23), 4065–4080. https://doi.org/10.1182/bloodadvances.2019001012

Wilkerson, M. D., Yin, X., Walter, V., Zhao, N., Cabanski, C. R., Hayward, M. C., Miller, C. R., Socinski, M. A., Parsons, A. M., Thorne, L. B., Haithcock, B. E., Veeramachaneni, N. K., Funkhouser, W. K., Randell, S. H., Bernard, P. S., Perou, C. M., & Hayes, D. N. (2012). Differential pathogenesis of lung adenocarcinoma subtypes involving sequence mutations, copy number, chromosomal instability, and methylation. *PloS one*, *7*(5), e36530. https://doi.org/10.1371/journal.pone.0036530

Wright, W. D., Shah, S. S., & Heyer, W. D. (2018). Homologous recombination and the repair of DNA double-strand breaks. *The Journal of biological chemistry*, *293*(27), 10524–10535. https://doi.org/10.1074/jbc.TM118.000372

Wrobel, K., Zhao, Y. C., Kulkoyluoglu, E., Chen, K. L., Hieronymi, K., Holloway, J., Li, S., Ray, T., Ray, P. S., Landesman, Y., Lipka, A. E., Smith, R. L., & Madak-Erdogan, Z. (2016). ERα-XPO1 Cross Talk Controls Tamoxifen Sensitivity in Tumors by Altering ERK5 Cellular Localization. *Molecular endocrinology (Baltimore, Md.)*, *30*(10), 1029–1045. https://doi.org/10.1210/me.2016-1101

Wu, C., Lyu, J., Yang, E. J., Liu, Y., Zhang, B., & Shim, J. S. (2018). Targeting AURKA-CDC25C axis to induce synthetic lethality in ARID1A-deficient colorectal cancer cells. *Nature communications*, *9*(1), 3212. https://doi.org/10.1038/s41467-018-05694-4

Wu, S., Qiao, Q., & Li, G. (2020). A Radiosensitivity Gene Signature and XPO1 Predict Clinical Outcomes for Glioma Patients. *Frontiers in oncology*, *10*, 871. https://doi.org/10.3389/fonc.2020.00871

Xia, L., Wang, M., Li, H., Tang, X., Chen, F., & Cui, J. (2018). The effect of aberrant expression and genetic polymorphisms of Rad21 on cervical cancer biology. *Cancer medicine*, *7*(7), 3393–3405. https://doi.org/10.1002/cam4.1592

Xie, Q. L., Liu, Y., & Zhu, Y. (2016). Chromosome region maintenance 1 expression and its association with clinical pathological features in primary carcinoma of the liver. *Experimental and therapeutic medicine*, *12*(1), 59–68. https://doi.org/10.3892/etm.2016.3283

Xu, D., Grishin, N. V., & Chook, Y. M. (2012). NESdb: a database of NES-containing CRM1 cargoes. *Molecular biology of the cell*, *23*(18), 3673–3676. https://doi.org/10.1091/mbc.E12-01-0045

Yan, D., Pomicter, A. D., Tantravahi, S., Mason, C. C., Senina, A. V., Ahmann, J. M., Wang, Q., Than, H., Patel, A. B., Heaton, W. L., Eiring, A. M., Clair, P. M., Gantz, K. C., Redwine, H. M., Swierczek, S. I., Halverson, B. J., Baloglu, E., Shacham, S., Khorashad, J. S., Kelley, T. W., … Deininger, M. W. (2019). Nuclear-Cytoplasmic Transport Is a Therapeutic Target in Myelofibrosis. *Clinical cancer research : an official journal of the American Association for Cancer Research*, *25*(7), 2323–2335. https://doi.org/10.1158/1078-0432.CCR-18-0959

Yan, M., Wang, C., He, B., Yang, M., Tong, M., Long, Z., Liu, B., Peng, F., Xu, L., Zhang, Y., Liang, D., Lei, H., Subrata, S., Kelley, K. W., Lam, E. W., Jin, B., & Liu, Q. (2016). Aurora-A Kinase: A Potent Oncogene and Target for Cancer Therapy. *Medicinal research reviews*, *36*(6), 1036–1079. https://doi.org/10.1002/med.21399

Yang, J., Bill, M. A., Young, G. S., La Perle, K., Landesman, Y., Shacham, S., Kauffman, M., Senapedis, W., Kashyap, T., Saint-Martin, J. R., Kendra, K., & Lesinski, G. B. (2014b). Novel small molecule XPO1/CRM1 inhibitors induce nuclear accumulation of TP53, phosphorylated MAPK and apoptosis in human melanoma cells. *PloS one*, *9*(7), e102983. https://doi.org/10.1371/journal.pone.0102983

Yang, X., Cheng, L., Yao, L., Ren, H., Zhang, S., Min, X., Chen, X., Zhang, J., & Li, M. (2014a). Involvement of chromosome region maintenance 1 (CRM1) in the formation and progression of esophageal squamous cell carcinoma. *Medical oncology (Northwood, London, England)*, *31*(9), 155. https://doi.org/10.1007/s12032-014-0155-9

Yang, Y., Ma, J., Chen, Y., & Wu, M. (2004). Nucleocytoplasmic shuttling of receptor-interacting protein 3 (RIP3): Identification of novel nuclear export and import signals in RIP3. *Journal of Biological Chemistry*, *279*(37), 38820–38829. https://doi.org/10.1074/jbc.M401663200

Yang, Y., Zhu, F., Wang, Q., Ding, Y., Ying, R., & Zeng, L. (2018). Inhibition of EZH2 and EGFR produces a synergistic effect on cell apoptosis by increasing autophagy in gastric cancer cells. *OncoTargets and therapy*, *11*, 8455–8463. https://doi.org/10.2147/OTT.S186498

Yao, Y., Dong, Y., Lin, F., Zhao, H., Shen, Z., Chen, P., Sun, Y. J., Tang, L. N., & Zheng, S. E. (2009). The expression of CRM1 is associated with prognosis in human osteosarcoma. *Oncology reports*, *21*(1), 229–235. https://doi.org/10.3892/or_00000213

Yarden, R. I., Pardo-Reoyo, S., Sgagias, M., Cowan, K. H., & Brody, L. C. (2002). BRCA1 regulates the G2/M checkpoint by activating Chk1 kinase upon DNA damage. *Nature genetics*, *30*(3), 285–289. https://doi.org/10.1038/ng837

Yeasmin, F., Yada, T., & Akimitsu, N. (2018). Micropeptides Encoded in Transcripts Previously Identified as Long Noncoding RNAs: A New Chapter in Transcriptomics and Proteomics. *Frontiers in genetics*, *9*, 144. https://doi.org/10.3389/fgene.2018.00144

Yoshida R. (2021). Hereditary breast and ovarian cancer (HBOC): review of its molecular characteristics, screening, treatment, and prognosis. *Breast cancer*, *28*(6), 1167–1180. https://doi.org/10.1007/s12282-020-01148-2

You, J. H., Reed, M. L., & Hiscox, J. A. (2007). Trafficking motifs in the SARS-coronavirus nucleocapsid protein. *Biochemical and biophysical research communications*, *358*(4), 1015–1020. https://doi.org/10.1016/j.bbrc.2007.05.036

Youn, J. Y., Dunham, W. H., Hong, S. J., Knight, J., Bashkurov, M., Chen, G. I., Bagci, H., Rathod, B., MacLeod, G., Eng, S., Angers, S., Morris, Q., Fabian, M., Côté, J. F., & Gingras, A. C. (2018). High-Density Proximity Mapping Reveals the Subcellular Organization of mRNA-Associated Granules and Bodies. *Molecular cell*, *69*(3), 517–532.e11. https://doi.org/10.1016/j.molcel.2017.12.020

Yue, L., Sun, Z. N., Yao, Y. S., Shen, Z., Wang, H. B., Liu, X. P., Zhou, F., Xiang, J. Y., Yao, R. Y., & Niu, H. T. (2018). CRM1, a novel independent prognostic factor overexpressed in invasive breast carcinoma of poor prognosis. *Oncology letters*, *15*(5), 7515–7522. https://doi.org/10.3892/ol.2018.8316

Zhang, K., Wang, M., Tamayo, A. T., Shacham, S., Kauffman, M., Lee, J., Zhang, L., Ou, Z., Li, C., Sun, L., Ford, R. J., & Pham, L. V. (2013). Novel selective inhibitors of nuclear export CRM1 antagonists for therapy in mantle cell lymphoma. *Experimental hematology*, *41*(1), 67–78.e4. https://doi.org/10.1016/j.exphem.2012.09.002

Zhang, W., Ly, C., Ishizawa, J., Mu, H., Ruvolo, V., Shacham, S., Daver, N., & Andreeff, M. (2018). Combinatorial targeting of XPO1 and FLT3 exerts synergistic anti-leukemia effects through induction of differentiation and apoptosis in *FLT3*-mutated acute myeloid leukemias: from concept to clinical trial. *Haematologica*, *103*(10), 1642–1653. https://doi.org/10.3324/haematol.2017.185082

Zhen, Y., Haugsten, E. M., Singh, S. K., & Wesche, J. (2018). Proximity Labeling by a Recombinant APEX2-FGF1 Fusion Protein Reveals Interaction of FGF1 with the Proteoglycans CD44 and CSPG4. *Biochemistry*, *57*(26), 3807–3816. https://doi.org/10.1021/acs.biochem.8b00120

Zheng, L., Baumann, U., & Reymond, J. L. (2004). An efficient one-step site-directed and site-saturation mutagenesis protocol. *Nucleic Acids Research*, *32*(14), e115. https://doi.org/10.1093/nar/gnh110

Zheng, N., Wang, L., Hou, Y., Zhou, X., He, Y., & Wang, Z. (2018). Rottlerin inhibits cell growth and invasion via down-regulation of EZH2 in prostate cancer. *Cell cycle (Georgetown, Tex.)*, *17*(21-22), 2460–2473. https://doi.org/10.1080/15384101.2018.1542897

Zheng, Y., Gery, S., Sun, H., Shacham, S., Kauffman, M., & Koeffler, H. P. (2014). KPT-330 inhibitor of XPO1-mediated nuclear export has anti-proliferative activity in hepatocellular carcinoma. *Cancer chemotherapy and pharmacology*, *74*(3), 487–495. https://doi.org/10.1007/s00280-014-2495-8

Zhong, Y., El-Gamal, D., Dubovsky, J. A., Beckwith, K. A., Harrington, B. K., Williams, K. E., Goettl, V. M., Jha, S., Mo, X., Jones, J. A., Flynn, J. M., Maddocks, K. J., Andritsos, L. A., McCauley, D., Shacham, S., Kauffman, M., Byrd, J. C., & Lapalombella, R. (2014). Selinexor suppresses downstream effectors of B-cell activation, proliferation and migration in chronic lymphocytic leukemia cells. *Leukemia*, *28*(5), 1158–1163. https://doi.org/10.1038/leu.2014.9

Zhou, F., Qiu, W., Yao, R., Xiang, J., Sun, X., Liu, S., Lv, J., & Yue, L. (2013). CRM1 is a novel independent prognostic factor for the poor prognosis of gastric carcinomas. *Medical oncology (Northwood, London, England)*, *30*(4), 726. https://doi.org/10.1007/s12032-013-0726-1

Zhou, Y., & Zou, P. (2021). The evolving capabilities of enzyme-mediated proximity labeling. *Current Opinion in Chemical Biology*, *60*, 30–38. https://doi.org/10.1016/j.cbpa.2020.06.013

Zhu, H., Zhang, T., Wang, F., Yang, J., & Ding, J. (2019b). Structural insights into the activation of USP46 by WDR48 and WDR20. *Cell discovery*, *5*, 34. https://doi.org/10.1038/s41421-019-0102-1

Zhu, J. H., Yan, Q. L., Wang, J. W., Chen, Y., Ye, Q. H., Wang, Z. J., & Huang, T. (2020). The Key Genes for Perineural Invasion in Pancreatic Ductal Adenocarcinoma Identified With Monte-Carlo Feature Selection Method. *Frontiers in genetics*, *11*, 554502. https://doi.org/10.3389/fgene.2020.554502

Zhu, Z. C., Liu, J. W., Yang, C., Zhao, M., & Xiong, Z. Q. (2019a). XPO1 inhibitor KPT-330 synergizes with Bcl-xL inhibitor to induce cancer cell apoptosis by perturbing rRNA processing and Mcl-1 protein synthesis. *Cell death & disease*, *10*(6), 395. https://doi.org/10.1038/s41419-019-1627-9

Zou, L., Liu, D., & Elledge, S. J. (2003). Replication protein A-mediated recruitment and activation of Rad17 complexes. *Proceedings of the National Academy of Sciences of the United States of America*, *100*(24), 13827–13832. https://doi.org/10.1073/pnas.2336100100

Zuzow, N., Ghosh, A., Leonard, M., Liao, J., Yang, B., & Bennett, E. J. (2018). Mapping the mammalian ribosome quality control complex interactome using proximity labeling approaches. *Molecular Biology of the Cell*, *29*(10), 1258–1269. https://doi.org/10.1091/mbc.E17-12-0714

8. Taula eta zerrenda gehigarriak / Supplementary tables

1. taula gehigarria: **Minbizi hematologiko ezberdinetan aurkitutako CRM1 E571 mutazioaren maiztasuna.**

Minbizi mota	CRM1 E571 mutatuta duten laginak	Erreferentzia
Leuzemia linfozitiko kronikoa (CLL)	4/165 (% 2,4)	Puente et al., 2011
	2/105 (% 1,9)	Quesada et al., 2011
	6/192 (% 3,1)	Balatti et al., 2012
	7/160 (% 4,4)	Landau et al., 2013
	33/969 (% 3,4)	Jeromin et al., 2014
	1/10 (% 10)	Messina et al., 2014
	6/24 (% 25)	Damm et al., 2014
	4/159 (% 2,5)	Lawrence et al., 2014
	2/12 (% 16,7)	Ojha et al., 2015
	13/136 (% 9,5)	Vollbrecht et al., 2015
	25/538 (% 4,6)	Landau et al., 2015
	17/114 (% 14,9)	Guièze et al., 2015
	2/25 (% 8)	Hernández et al., 2015
	14/180 (% 7,8)	Sutton et al., 2015
	7/61 (% 11,5)	Amin et al., 2016
	38/486 (% 7,8)	Jain et al., 2016
	25/436 (% 5,7)	Cosson et al., 2017
	4/56 (% 7,1)	Quijada-Álamo et al., 2017
	28/288 (% 9,7)	Takahashi et al., 2018
	37/680 (% 5,4)	Hu et al., 2019
	36/1265 (% 2,8)	Taylor et al., 2019
	1/20 (% 5)	Gángó et al., 2020
	5/45 (% 11,1)	Machnicki et al., 2020
CLL batura	317/6126 (% 5,17)	
B-zelulen linfoma mediastinal primarioa (PMBL)	7/18 (% 38,9)	Dubois et al., 2016
	28/117 (% 24)	Jardin et al., 2016
	1/3 (% 33,3)	Taylor et al., 2019
PMBL batura	36/138 (% 26,09)	
Hodgkin linfoma (HL)	22/91 (% 24,2)	Camus et al., 2016
	5/19 (% 26)	Jardin et al., 2016
	6/34 (% 18)	Tiacci et al., 2018
	4/13 (% 30,8)	Liang et al., 2019
	6/23 (% 26)	Wienand et al., 2019
	19/132 (% 14,4)	Taylor et al., 2019
	6/60 (% 10)	Camus et al., 2020
	1/2 (% 50)	Van Slambrouck et al., 2020
HL batura	69/374 (% 18,45)	
B-zelula handien linfoma hedatsua (DLBCL)	10/215 (% 4,7)	Dubois et al., 2016
	3/197 (% 1,5)	Jardin et al., 2016
	12/775 (% 1,5)	Taylor et al., 2019
DLBCL batura	25/1187 (% 2,11)	
Trikoleuzemia (HCL)	1/24 (% 4,2)	Maitre et al., 2018
B-zelula helduen neoplasma	1/12 (% 8,3)	Taylor et al., 2019
Area marginaleko linfoma (MZL)	1/4 (% 25)	Taylor et al., 2019

<u>2. taula gehigarria:</u> CRM1 proteinaren edo horren mRNAren gainadierazpena giza minbizietan. Legenda: IB: immunoblot; IF: immunofluoreszentzia; IHC: immunohistokimika; MA: mikroarray; qRT-PCR: Denbora errealeko PCR kuantitatiboa. LC-MS/MS: likido kromatografia-tandem masa espektrometria; DE: daturik ez.

Minbizi mota	Lagin kopurua (teknika)	Pronostikoarekin zerikusia	Oharrak	Erreferentzia
Leuzemia mieloide akutua (AML)	511 paziente (Alderantzizko faseko proteina arraya)	CRM1 adierazpen altua pronostiko txarrarekin erlazionatuta		Kojima et al., 2013
B-zelula handien linfoma hedatsua (DLBCL)	48 paziente TCGA datu-basetik	CRM1 adierazpen altua pronostiko txarrarekin erlazionatuta		Fan et al., 2020
Mantuko zelulen linfoma (MCL)	Adierazpen-array bilduma publikoetako datuak, gehi 3 paziente eta 8 zelula lerro (qRT-PCR)	DE	CRM1en adierazpen altuagoa MCL zeluletan	Zhang et al., 2013
Mieloma anizkoitza (MM)	Adierazpen-array bilduma publikoetako datuak	DE	CRM1en adierazpena gaixotasunak aurrera egin ahala emendatzen da	Schmidt et al., 2013
	351 paziente (Adierazpen-array bilduma publikoetako datuak) gehi 8 paziente (IB)	CRM1 adierazpen altua pronostiko txarrarekin erlazionatuta		Tai et al., 2014
Glioma	70 paziente (IHC+IB)	CRM1 adierazpen altua pronostiko txarrarekin erlazionatuta	CRM1 eta p27ren adierazpen maila alderantzizko korrelazioan	Shen et al., 2009
	273 paziente (Adierazpen-array bilduma publikoetako datuak) gehi 12 paziente (IB)	CRM1 adierazpen altua pronostiko txarrarekin erlazionatuta		Liu et al., 2016
	1552 paziente (Chinese Glioma Atlas and The Cancer Genome Atlas datu-baseetako datuak)	CRM1 adierazpen altua pronostiko txarrarekin erlazionatuta		Wu et al., 2020
Birikietako zelula ez-txikien minbizia (NSCLC)	148 paziente (microarray) gehi 291 paziente (qRT-PCR)	CRM1 adierazpen altua pronostiko txarrarekin erlazionatuta	CRM1, BRCA1, HIF1A eta DLC1 lehen faseko biriki adenokartzinoma pazienteen pronostikoa aurreikusteko baliagarriak	Akagi et al., 2013

Urdaileko minbizia	120 paziente (IHC)	CRM1 adierazpen altua pronostiko txarrarekin erlazionatuta		Zhou et al., 2013
	240 paziente (IHC)	CRM1 adierazpen baxua pronostiko txarrarekin erlazionatuta		Sun et al., 2017
Timo epitelioko tumoreak	118 paziente (IHC)	CRM1 adierazpen altua pronostiko txarrarekin erlazionatuta		Conforti et al., 2017
Obulutegiko minbizia	88 paziente (IHC)	CRM1 obulutegiko minbizia erasokorra pairatzen duten paziente azpitaldean adierazten da eta biziraupen pronostiko txarrarekin erlazionatzen da	CRM1 adierazpena ziklooxigenasa-2 adierazpenarekin korrelazioan	Noske et al., 2008
Gibeleko minbizia	154 paziente (IHC)	DE	CRM1 adierazpena tumore eta inguruko ehun normaletan ikertu da, soilik ehun normalean ere adierazten den kasuetan. Ez da ezberdintasunik topatu	Xie et al., 2016
Hestegorriko zelula eskatatsuen kartzinoma	220 paziente (IHC+IB+IF)	CRM1 adierazpena biziraupen laburragoarekin erlazionatuta	CRM1 ezabatzeak hestegorri minbiziko zelula lerroetan apoptosia eragiten du	Yang et al., 2014a
	56 paziente (IHC+qRT-PCR)	CRM1 adierazpen altua biziraupen laburragoarekin erlazionatuta	CRM1 kokapen azpizelularra asaldatuta minbizi zeluletan	van der Watt et al., 2014
Pankrea minbizia	69 paziente (IB)	CRM1 adierazpen altua pronostiko txarrarekin erlazionatuta		Huang et al., 2009
	Ehun mikroarrayko 76 sekzio (IHC- irudi analisi digital kuantitatibo (OTMIAS))		CRM1 adierazpen maila altuak surbibina maila altuekin eta ugaritze aktibitate altuarekin korrelazioan	Saulino et al., 2018
	646 (73 metastasiko and 573 minbizi primario) Adierazpen-array bilduma publikoetako datuak	CRM1 adierazpen altua pronostiko txarrarekin erlazionatuta	CRM1 adierazpen altuagoa lagin metastasikoetan tumore primarioetan baino	Birnbaum et al., 2019
	50 paziente (Gene expression omnibus datu-baseko datuak)	CRM1 adierazpena inbasio perineuralarekin erlazionatuta		Zhu et al., 2020

Prostata minbizia	34 ehun lagin (nano-LC-MS/MS, MA, IHC)		CRM1 adierazpen altuagoa besikula extrazelularretan inguruko ehun osasuntsuan baino	Duijvesz et al., 2019
Giltzurruneko minbizia	(IHC)	DE	CRM1 adierazpen maila tumorearen mailarekin korrelazioan	Inoue et al., 2013
Bularreko minbizia	280 paziente (IHC+IB)	CRM1 adierazpen altua pronostiko txarrarekin erlazionatuta		Yue et al., 2018
	Adierazpen-array bilduma publikoetako datuak eta *In vitro* (IB)	DE	CRM1 adierazpen maila altuagoa alfa estrogeno hartzaile negatibo zeluletan	Cruz-Ramos et al., 2019
Ewing sarcoma	37 paziente (IHC) gehi Adierazpen-array bilduma publikoetako datuak	DE		Sun et al., 2016
Osteosarkoma	57 paziente (IHC)	CRM1 adierazpen altua pronostiko hobearekin erlazionatuta		Yao et al., 2009
	In vitro (MA eta qRT-PCR)	CRM1 adierazpen altua pronostiko txarrarekin erlazionatuta		Jiang et al., 2020
Melanoma	83 paziente (31 tumore primario, 52 metastasiko) (MA)	DE	CRM1 gainadierazita melanoma metastasikoan	Pathria et al., 2012
Zerbixeko minbizia	120 paziente (IB)	DE	CRM1 adierazpena Rad21 adierazpenarekin korrelazioan	Xia et al., 2018
Kartzinoma hepatozelularra	Adierazpen-array bilduma publikoetako datuak	CRM1 adierazpen altua pronostiko txarrarekin erlazionatuta		Chen et al., 2019

3. taula gehigarria: Minbizi hematologikoetan SINEekin egindako ikerketa preklinikoak. ALL: leuzemia linfozitiko akutua; AML: leuzemia mieloide akutua; CML: leuzemia mieloide kronikoa; CLL: leuzemia linfozitiko kronikoa; MCL: mantuko zelula linfoma; MM: mieloma anizkoitza; NHL: ez-Hodgkin linfoma; PMBL: B-zelulen linfoma mediastinal primarioa; DLBCL: B-zelula handien linfoma hedatsua; TCL: T-zelulen linfoma; PCNSL: nerbio-sistema zentraleko linfoma primarioa.

Minbizi mota	Modelo preklinikoa	SINEa(k)	Zelula mailako efektua	Oharrak	Erreferentziak
ALL	In vivo/ heteroinjertoa	Eltanexor	Apoptosia	Dexametasonarekin efektu sinergistikoa	Verbeke et al., 2020
AML	*In vitro*/ heteroinjertoa	KPT-185 KPT- 276	Ugaritze murriztua, apoptosia, zelula zikloaren bahitzea, diferentziazio mieloidea		Ranganathan et al., 2012
	In vitro/ heteroinjertoa	KPT-251	Apoptosia		Etchin et al., 2013a
	In vitro/ pazienteetatik eratorritako zelulak	KPT-185	Ugaritze murriztua, apoptosia	MDM2 inhibitzailearekin efektu sinergistikoa. p53-mendeko apoptosia	Kojima et al., 2013
	In vitro/ heteroinjertoa	Selinexor		Dezitabinak selinexorren aktibitatea emendatzen du	Ranganathan et al., 2015
	In vitro/ heteroinjertoa	Selinexor	Apoptosia, diferentziazio mieloidea.	Sorafenibekin efektu sinergistikoa FLT3-mutazioa duten heteroinjertoetan	Zhang et al., 2018
	In vitro/ pazienteetatik eratorritako zelulak	Selinexor	Apoptosia, kolonien agertzearen inhibizioa	ABT-199-rekin efektu sinergistikoa	Luedtke et al., 2018
	In vitro/ heteroinjertoa	Selinexor	Hazkuntzaren inhibizioa, saguen biziraupen luzapena	NPM1 mutantea nukleoan birlokatzen du	Brunetti et al., 2018
	Sagu modeloa	Selinexor	Biziraupen luzapena	Midostaurin eta gilteritinibrekin efektu sinergistikoa	Brinton et al., 2020
ALL eta AML	*In vitro*/ heteroinjertoa	Selinexor	Apoptosia	Zelula hemapoietiko normaletan toxikotasun baxua	Etchin et al., 2013b
	In vitro	KPT-185	Bizi-gaitasun murriztua		Mendes et al., 2020
CML	*In vitro*/ heteroinjertoa	Selinexor	Ugartzearen inhibizioa, zelula zikloaren bahitzea eta apoptosia	Zelulak imatinibekiko sentikortzen ditu	Nie et al., 2018
ALL eta CML	*In vitro*/ sagu modeloa	Selinexor	Apoptosia	Tirosina kinasa inhibitzaileekiko erresistentziadun CML paziente batean gaixotasuna murriztu zen. PP2A berraktibazioarekin erlazionatutako mekanismoa	Walker et al., 2013

MM	*In vitro*/ pazienteetatik eratorritako zelulak/ heteroinjertoa/ sagu modeloa	KPT-276	Hazkuntzaren inhibizioa, apoptosia		Schmidt et al., 2013
	In vitro/ pazienteetatik eratorritako zelulak	Selinexor KPT-185 KPT-249 KPT-276	Apoptosia	Zelulak doxorubizina, bortezomib eta karfilzomibekiko sentikortzen dituzte. Estromako zelulek eragindako erresistentzia gaindiarazten dute	Turner et al., 2013
	In vitro/ heteroinjertoa	Selinexor KPT-185	Hazkuntzaren inhibizioa, apoptosia	Hezurren lisiaren inhibizioa. NF-κB bidezidor eta NFATc1-rekin erlazionatutako mekanismoak	Tai et al., 2014
	In vitro/ pazienteetatik eratorritako zelulak/ heteroinjertoa	Selinexor	Apoptosia	Karfilzomibekin efektu sinergistikoa. Kaspasa 10 eragindako apoptosia.	Rosebeck et al., 2016
	In vitro/ heteroinjertoa/ pazienteetatik eratorritako zelulak	Selinexor	Apoptosia, DNA kaltea	Doxorubizinarekiko erresistentzia gaindiarazten du. Doxorubizinarekin efektu sinergistikoa	Turner et al., 2016a
	In vitro/ heteroinjertoa/ pazienteetatik eratorritako zelulak	Selinexor	Hazkuntzaren inhibizioa	Bortezomib eta karfilzomibekiko erresistentzia gaindiarazten du. NF-κB bidezidorrarekin erlazionatutako mekanismoa	Turner et al., 2016b
	In vitro/ heteroinjertoa	Selinexor	Tumore progresioaren geldotzea, apoptosia	Hipoxiak eragindako bortezomib erresistentzia gaindiarazten du	Muz et al., 2017
	In vitro/ heteroinjertoa	Selinexor	Hazkuntzaren inhibizioa, apoptosia	Dexametasonarekin efektu sinergistikoa. Glukokortikoide hartzaile eta mTOR bidezidorrarekin erlazionaturiko mekanismoak	Argueta et al., 2018
	In vitro	Selinexor	Hazkuntzaren inhibizioa	ARV 825-rekin efektu sinergistikoa	Lim et al., 2019
	In vitro/ pazienteetatik eratorritako zelulak	Selinexor		Selinexorrarekiko erantzun altua pronostiko txarrarekin erlazionatuta	Bonolo de Campos et al., 2020
	In vitro/ heteroinjertoa	Selinexor Eltanexor	Apoptosia	Melfalanekiko erresistentzia gaindiarazten dute eta farmako horrekin sinergia erakusten dute ere. Selinexor - Melfalan konbinazioa I/II faseko entsegu klinikoetan dago NCT02780609	Turner et al., 2020
DLBCL	*In vitro*	Selinexor	Ugaritze murriztua	Ibrutinibekin efektu sinergistikoa	Schaffer et al., 2018

AML eta DLBCL	*In vitro*/ heteroinjertoa	Selinexor Eltanexor	Apoptosia, tumore hazkuntzaren murriztea	Benetoklaxekin efektu sinergistikoa	Fischer et al., 2020
CLL	*In vitro*/ heteroinjertoa	KPT-185 KPT-251	Apoptosia	Estromako zelulek eragindako erresistentzia gaindiarazten dute	Lapalombella et al., 2012
	In vitro/ sagu modeloa	Selinexor	Ugaritze murriztua		Zhong et al., 2014
	Pazienteetatik eratorritako zelulak/ sagu modeloa	Selinexor		Ibrutinibekin efektu sinergistikoa	Hing et al., 2015
	In vitro/ pazienteetatik eratorritako zelulak	Selinexor	Apoptosia	CRM1en mutazioak edo 2p kromosomaren gehiegizko kopiek selinexorrarekiko sentsibilitatea murrizten dute	Cosson et al., 2017
MCL	*In vitro*/ heteroinjertoa	KPT-185 KPT- 276	Hazkuntzaren inhibizioa, apoptosia		Zhang et al., 2013
	In vitro	KPT-185	Hazkuntzaren inhibizioa, ribosomen biogenesiaren errepresioa, minbizi zelulen metabolismoan asaldurak		Sekihara et al., 2017
	In vitro	Selinexor	Zelula zikloaren bahitzea, apoptosia	Ibrutinib baino eragin altuagoa tumoreetan	Ming et al., 2018
NHL	*In vitro*/ heteroinjertoa	KPT-185 KPT-251 KPT-276	Hazkuntzaren inhibizioa, apoptosia, zelula zikloaren bahitzea	p53 eta p73 mendeko efektu zelularra	Azmi et al., 2013a
	In vitro/ heteroinjertoa	KPT-185 KPT -276	Hazkuntzaren inhibizioa, apoptosia, zelula zikloaren bahitzea		Han et al., 2015
	In vitro/ sagu modeloa	Selinexor KPT-251 KPT-276	Apoptosia	Dexametasonak eta eberolimusek selenixorren aktibitatea emendatzen dute	Muqbil et al., 2016
	In vitro/ sagu modeloa	Selinexor Eltanexor	Apoptosia, hazkuntzaren inhibizioa	Eltanexor BCL2ren inhibitzaile den ABT199rekin efektu sinergistikoa	Liu et al., 2019
	In vitro	Selinexor	Ugaritze murriztua		Abeykoon et al., 2019
DLBCL	*In vitro*	Selinexor	Ugaritze murriztua	Ibrutinibekin efektu sinergistikoa	Schaffer et al., 2018
PMBL	*In vitro*	Selinexor KPT-185	Ugaritze murriztua, apoptosia	E571K mutazioak ez dio SINEen aktibitateari eragiten	Jardin et al., 2016

DLBCL eta CLL	*In vitro*	Selinexor	Apoptosia	Ibrutinibekin efektu sinergistikoa	Kapoor et al., 2019
CLL eta NHL	Sagu modeloa	Eltanexor	Biziraupen luzapena		Lucas et al., 2019
DLBCL eta MCL	*In vitro*	Selinexor	Tumore hazkuntzaren inhibizioa	Zanubrutinibekin efektu sinergistikoa entseatutako bost lerroetako hirutan	Tarantelli et al., 2019
PCNSL	Heteroinjertoa	Selinexor	Tumore hazkuntzaren inhibizioa, biziraupen luzatua		Jiménez et al., 2020
DLBCL eta AML	*In vitro*/ heteroinjertoa	Selinexor Eltanexor	Apoptosia, tumore hazkuntzaren murriztea	Benetoklaxekin efektu sinergistikoa	Fischer et al., 2020

4. taula gehigarria: **Tumore solidoetan SINEekin egindako ikerketa preklinikoak.**

Minbizi mota	Modelo preklinikoa	SINEa(k)	Zelula mailako efektua	Oharrak	Erreferentziak
Giltzurruneko minbizia	*In vitro*/ heteroinjertoa	KPT-185 KPT-251	Hazkuntzaren inhibizioa, apoptosia, ziklo zelularraren bahitzea	Sorafenib baino eragikorragoa	Inoue et al., 2013
	In vitro/ heteroinjertoa	Selinexor	Hazkuntzaren inhibizioa, apoptosia		Wettersten et al., 2014
Maskuriko minbizia	*In vitro*/ heteroinjertoa	Selinexor	Bizi gaitasun murriztua, ziklo zelularraren bahitzea, apoptosia	CRM1 adierazpen murriztua	Baek et al., 2018
Prostata minbizia	*In vitro*/ heteroinjertoa	Selinexor KPT-185 KPT-251	Ugaritze murriztua, apoptosia	Doxorubizinarekin efektu sinergistikoa	Mendonca et al., 2014
	In vitro/ heteroinjertoa	Selinexor KPT-251		Metastasiaren murriztea	Gravina et al., 2014b
	In vitro/ heteroinjertoa	Selinexor KPT-251	Hazkuntzaren inhibizioa, apoptosia, DNA kaltearen emendapena	Zelulak dozetaxelekiko sentikortzea	Gravina et al., 2017
	In vitro/ heteroinjertoa	Selinexor Eltanexor	Hazkuntzaren inhibizioa, biziraute luzatua	Selinexorek enzalutamida eta abirateronarekin efektu sinergistikoa	Aboukameel et al., 2018
Kolon eta ondesteko minbizia	*In vitro*/ heteroinjertoa	Selinexor	Ugaritze murriztua, apoptosia	Erradioterapiarekin efektu sinergistikoa	Ferreiro-Neira et al., 2016
	In vitro	Selinexor	Ugaritze murriztua		Aladhraei et al., 2019
Gibeleko minbizia	*In vitro*/ heteroinjertoa	Selinexor	Hazkuntzaren inhibizioa, apoptosia, ziklo zelularraren bahitzea		Zheng et al., 2014
Urdail eta gibeleko minbizia	*In vitro*	Eltanexor	Ugaritze murriztua, ziklo zelularraren bahitzea	p53 bidezidorraren aktibazioa	Gruffaz et al., 2019

Urdaileko minbizia	*In vitro*/ heteroinjertoa	Selinexor KPT-185 KPT-276	Hazkuntzaren inhibizioa, ziklo zelularraren bahitzea eta apoptosia	Selinexorrek irinotekanekin konbinazioan efektu sinergistikoa	Subhash et al., 2018
	In vitro/ heteroinjertoa	Selinexor Eltanexor KPT-185	Hazkuntzaren inhibizioa, apoptosia, ziklo zelularraren bahitzea	Nab-paklitaxelekiko eraginkortasuna emendatzen dute	Sexton et al., 2019
Pankrea minbizia	*In vitro*/ heteroinjertoa	KPT-185 KPT-127 KPT-205 KPT-227	Ugaritze murriztua, apoptosia	PAR-4rekin erlazionatutako mekanismoa	Azmi et al., 2013b
	In vitro/ heteroinjertoa	KPT-185	Ugaritzea eta migrazio murriztua, apoptosia	Fbw7 eta Notch-1ekin erlazionatutako mekanismoa.	Gao et al., 2014
	In vitro/ heteroinjertoa	Selinexor	Hazkuntzaren inhibizioa, apoptosia	Gemzitabinarekin efektu sinergistikoa.	Kazim et al., 2015
	In vitro	Selinexor	Ugaritze eta migrazio murriztua	miR-145 mikro RNArekin erlazionatutako mekanismoa	Azmi et al., 2017
	In vitro/ heteroinjertoa	Selinexor	Hazkuntzaren inhibizioa, apoptosia	Gemzitabina eta nab-paklitaxelekin efektu sinergistikoa	Azmi et al., 2020
Heste meharreko tumore neuroendokrinoak (SI-NET)	*In vitro*	Selinexor	Ugaritze murriztua, apoptosia		Barazeghi et al. 2018
Bular adeno-kartzinoma eta fibrosarkoma	*In vitro*	Selinexor	Ziklo zelularraren asaldurak		Marcus et al., 2018
Obulutegiko minbizia	*In vitro*	Selinexor KPT-185	Apoptosia	Kimioterapiarekin efektu sinergistikoa. IGF2BP1rekin erlazionaturiko mekanismoa	Miyake et al., 2015
	In vitro/ heteroinjertoa	Selinexor KPT-185	Apoptosia (p53-mendeko zein ez-mendekoa)	Platino-farmakoekiko erresistentzia gaindiarazten dute	Chen et al., 2017
	In vitro	Selinexor	Ugaritze murriztua, apoptosia	Zisplatinoarekin efektu sinergistikoa. FoxO1ekin erlazionatutako mekanismoa	Corno et al., 2018

Bularreko minbizia	*In vitro*/ heteroinjertoa	Selinexor KPT-185 KPT-251 KPT-276	Hazkuntzaren inhibizioa, apoptosia	STAT3 eta surbibinarekin erlazionaturiko mekanismoa	Cheng et al., 2014
	In vitro/ heteroinjertoa	Selinexor		Tamoxifekiko sentikortasuna itzultzen du	Wrobel et al., 2016
	In vitro/ heteroinjertoa	Selinexor	Hazkuntzaren inhibizioa	Bakarka eraginkorra, bular minbizi triple-negatiboaren aurkako kimioterapiarekin efektu sinergistikoa	Arango et al., 2017
	In vitro/ heteroinjertoa	Selinexor	Bizi gaitasun murriztua, tumorearen erregresioa	4-Hidroxi-tamoxifenarekin efektu sinergistikoa	Kulkoyluoglu-Cotul et al., 2019
	In vitro	Selinexor	Hazkuntzaren inhibizioa, apoptosia	TRAIL-R2xCD3 antigorputzarekin efektu sinergistikoa	Martini et al., 2020
Melanoma	*In vitro*/ heteroinjertoa	Selinexor KPT-185 KPT-251 KPT-276	Hazkuntzaren inhibizioa, apoptosia, ziklo zelularraren bahitzea	BRAF inhibitzaileekin efektu sinergistikoa BRAF mutaturik egon edo ez	Salas Fragomeni et al., 2013
	In vitro/ heteroinjertoa	Selinexor KPT-276	Hazkuntzaren inhibizioa, apoptosia	BRAF mutaturik egon edo ez	Yang et al., 2014b
Birikietako zelula ez-txikien minbizia (NSCLC)	*In vitro*/ heteroinjertoa	Selinexor	Ugaritze murriztua, apoptosia, ziklo zelularraren bahitzea	Zisplatinoarekin efektu sinergistikoa	Sun et al., 2014
	In vitro/ heteroinjertoa	KPT-185 KPT-276	Bizi gaitasun murriztua, apoptosia, ziklo zelularraren bahitzea	KPT-185 EGFR-TKIekiko erresistenteak diren NSCLC zeluletan eraginkorra	Wang et al., 2014
	In vitro/ heteroinjertoa	Selinexor KPT-185		Hilgarritasun sintetikoa KRASekin. NF-kB bidezidorrarekin erlazionatutako mekanismoa	Kim et al., 2016b
	In vitro/ sagu modeloa	Selinexor	Apoptosia	A-1331852rekin efektu sinergistikoa. Mcl-1 proteina maila murrizten du	Zhu et al., 2019a
	In vitro	KPT-185	Hazkuntzaren inhibizioa, apoptosia, migrazioaren inhibizioa		Wei et al., 2020

Sarkoma	*In vitro*/ heteroinjertoa	Selinexor	Hazkuntzaren inhibizioa, apoptosia	Proteasoma inhibitzaileekin efektu sinergistikoa. NF-κB bidezidorrarekin erlazionaturiko mekanismoa	Kashyap et al., 2016
	In vitro/ heteroinjertoa	Selinexor	Ziklo zelularraren bahitzea	Hainbat sarkoma ezberdidien aurka eraginkorra, liposarkoma eta estromako tumore gastrointestinalak barne	Nakayama et al., 2016
	In vitro/ heteroinjertoa	Selinexor	Hazkuntzaren inhibizioa, apoptosia	Marfilzomibek selinexorrarekiko sentikortasuna emendatzen du. NF-κB bidezidorrarekin eta surbibinarekin erlazionatutako mekanismoa	Nair et al., 2017
	In vitro/ heteroinjertoa	Selinexor	Hazkuntzaren inhibizioa, apoptosia, ziklo zelularraren bahitzea	Ewing sarkoma. IGF-1R-ren inhibitzailea den linsitinibekin efektu sinergistikoa	Sun et al., 2016
Osteosarkoma	*In vitro*	Selinexor	Bizi gaitasunaren murrizpena	CRM1 adierazpen maila murriztua. AZD1775rekin konbinazioan eraginkorragoa	Currier et al., 2019
Liposarkoma	*In vitro*/ heteroinjertoa	Selinexor	Hazkuntzaren inhibizioa, apoptosia, ziklo zelularraren bahitzea.		Garg et al., 2017b
	In vitro	Selinexor	Bizi gaitasunaren murrizpena	Carfilzomib kontzentrazio altuetan efektu sinergistikoa	Jeitany et al., 2021
Tiroideko minbizia	*In vitro*/ heteroinjertoa	Selinexor	Hazkuntzaren inhibizioa, apoptosia, ziklo zelularraren bahitzea	Doxorubizinarekin efektu sinergistikoa	Garg et al., 2017a
	In vitro/ heteroinjertoa	Selinexor Eltanexor	Hazkuntzaren inhibizioa	Lenbatinibekin efektu sinergistikoa	Khan et al., 2019

Timo epitelioko tumoreak	*In vitro*/ heteroinjertoa	Selinexor	Ugaritze murriztua, apoptosia (p53-mendeko zein ez-mendekoa)		Conforti et al., 2017
Glioblastoma	Pazienteetatik eratorritako zelulak/ heteroinjertoa	Selinexor KPT-251 KPT-276	Hazkuntzaren inhibizioa, apoptosia		Green et al., 2015
	In vitro/ heteroinjertoa	Selinexor		Erradioterapiarekiko sentikortasuna emendatzen du	Wahba et al., 2018
	In vitro/ heteroinjertoa	Selinexor	Bizi gaitasunaren murrizpena, apoptosia, tumore txikiagoak	ABT263rekin efektu sinergistikoa	Shang et al., 2018
Mesotelioma	*In vitro*/ heteroinjertoa	Selinexor KPT-251 KPT-276	Hazkuntzaren inhibizioa, apoptosia, ziklo zelularraren bahitzea	Surbibinaren inhibitzaile den YM155rekin efektu sinergistikoa	De Cesare et al., 2015
Glioblastoma	Pazienteetatik eratorritako zelulak/ heteroinjertoa	Selinexor KPT-251 KPT-276	Hazkuntzaren inhibizioa, apoptosia		Green et al., 2015
	In vitro/ heteroinjertoa	Selinexor		Erradioterapiarekiko sentikortasuna emendatzen du	Wahba et al., 2018
	In vitro/ heteroinjertoa	Selinexor	Bizi gaitasunaren murrizpena, apoptosia, tumore txikiagoak	ABT263rekin efektu sinergistikoa	Shang et al., 2018
Glioma pediatrikoa	*In vitro*/ heteroinjertoa	Selinexor	Hazkuntzaren inhibizioa	Bortezomib, daktinomizina eta binorelbinarekin efektu sinergistikoa	DeSisto et al., 2020
Buru eta lepoko zelula eskatatsuen kartzinoma (HNSCC)	*In vitro*/ heteroinjertoa	Selinexor	Tumore txikiagoak, apoptosia	Doxorubizinarekiko sentikortasuna emendapena. E2F7 nukleoan metatzen da.	Saenz-Ponce et al., 2018
Mielofibrosia	*In vitro*/ sagu modeloa	Selinexor Eltanexor	Apoptosia	Ruxolitinibekin efektu sinergistikoa	Yan et al., 2019
Mota ezberdinetako solido eta hematologikoak	*In vitro*/ heteroinjertoa	Selinexor	Apoptosia, hazkuntzaren inhibizioa	Dozetaxel, gemzitabina eta zisplatinoarekin efektu sinergistikoa.	Kashyap et al., 2018

Mota ezberdinetako solidoak	*In vitro*	Selinexor	DNA kaltea	DNA-kaltea eragiten duen farmakoekin efektu sinergistikoa	Burke et al., 2017
Minbizi pediatriko solido eta hematologikoak	*In vitro*/ heteroinjertoa	Selinexor		Hainbat minbizi pediatrikotan eraginkorra. TP53 mutaturik egon edo ez	Attiyeh et al., 2016

5. taula gehigarria: Giza minbizietan selinexor erabiltzen den ikerketa klinikoetan lortutako emaitzen laburpena. ID: ClinicalTrials.gov-en identifikazioa; MTD: gehienezko toleratutako dosia; RP2D: Gomendatutako II faseko dosia. OR: helburu-erantzuna. CR: erabateko erantzuna; CRi: erabateko erantzuna zenbaketa guztiz suspertu gabe, MLFS: morfologikoki leuzemia gabeko egoera, ORR: erantzun tasa orokorra, PR: erantzun partziala; SD: gaixotasun egonkorra.

Minbizi mota	Fasea	Oharrak	Erreferentzia/IDa
Tumore solido aurreratuak	I fasea	Selinexor bakarka erabilita. 189 paziente izena emanda. ≥ 3 mailako kontrako efektu ohikoenak: tronbozitopenia, nekea eta hiponatremia. RP2D 35 mg/m^2 astean birritan. 157 paziente ebaluagarri: 1 CR eta 5 PR.	Abdul Razak et al., 2016 ID: NCT01607905
Sarkoma	I fasea	Selinexor bakarka erabilita. 54 paziente izena emanda. ≥ 3 mailako kontrako efektu ohikoenak: nekea, tronbozitopenia, anemia, linfopenia eta leukopenia. 52 paziente ebaluagarri; % 33 SD.	Gounder et al., 2016 ID: NCT01896505
Leuzemia pediatriko akutu errefraktarioa	I fasea	Selinexor fludarabina eta zitarabinarekin konbinazioan. 18 paziente izena emanda. Selinexor 55 mg/m^{2}dosirarte jasangarria. 15 paziente ebaluagarri: % 47 CR.	Alexander et al., 2016 ID: NCT02212561
NHL	I fasea	Selinexor bakarka erabilita. 79 paziente izena emanda. ≥ 3 mailako kontrako efektu ohikoenak: tronbozitopenia, neutropenia, anemia, leukopenia, nekea eta hiponatremia. RP2D 60 mg. 70 paziente ebaluagarri: % 31 OR (4 CR eta 18 PR).	Kuruvilla et al., 2017 ID: NCT01607892
DLBCL	II fasea	Selinexor bakarka erabilita. 267 paziente izena emanda. 3 ≥ mailako kontrako efektu ohikoenak: tronbozitopenia, neutropenia, anaemia, nekea, hiponatremia, nausea, pirexia, pneumonia eta sepsia. 127 paziente ebaluagarri: % 12 CR eta % 17 PR.	Kalakonda et al., 2020 ID: NCT02227251
Hodi pankreatikoko adenokartzinoma	Ib fasea	Selinexor gemzitabina eta nab-paklitaxelekin konbinazioan. 9 paziente izena emanda. 3 ≥ mailako kontrako efektu ohikoenak: anemia, tronbozitopenia, nekea, leukopenia eta linfopenia. 5 paziente ebaluagarri: % 40 PR eta % 40 SD.	Azmi et al., 2020 ID: NCT02178436
Ondesteko minbizi metastasikoa	I fasea	Selinexor 5-fluorourazil, leukoborin eta oxaliplatinoakin konbinazioan. 10 paziente izena emanda. Tratamendu denbora laburra dela eta ez da aktibitate kliniko adierazgarririk antzeman.	Nilsson et al., 2020 ID: NCT02384850
Kastrazioarekiko erresistentea den prostata minbizia	II fasea	Selinexor bakarka erabilita. 14 paziente izena emanda. % 25 PR, tolantzia baxua.	Wei et al., 2018 ID: NCT02215161

AML	I fasea	Selinexor bakarka erabilita. 95 paziente izena emanda. ≥ 3 mailako kontrako efektu ez-hematologikoak: nekea. Dosi-limite toxizitaterik ez. RP2D 60 mg. 81 paziente ebaluagarri: % 14 OR.	Garzon et al., 2017 ID: NCT01607892
	I fasea	Selinexor zitarabina eta mitoxantronekin konbinazioan. 20 paziente izena emanda. Kontrako efektu larriak % 30, hildako bat. RP2D: 80 mg. 20 paziente ebaluagarri. % 70 ORR (10 CR).	Wang et al., 2018 ID: NCT02573363
	I fasea	Selinexor dezitabinarekin konbinazioan. 25 paziente izena emanda. ≥ 3 mailako kontrako efektu ohikoenak: hiponatremia asintomatikoa, neutropenia sukartsua, sepsia, hipofosfatemia eta pneumonia. PR2D: 60 mg. 21 paziente ebaluagarri: % 24 CR, % 14 CRi, % 9 MLFS, % 48 SD eta % 5 PR.	Bhatnagar et al., 2019 ID: NCT02093403
	I fasea	Selinexor daunorubizina eta zitarabinarekin konbinazioan. 21 paziente izena emanda. ≥ 3 mailako kontrako efektu ohikoenak: neutropenia sukartsua, diarrea, hiponatremia eta sepsia. RP2D: 80 mg astean birritan. 19 paziente ebaluagarri: % 42 CR eta % 11 CRi.	Sweet et al., 2020 ID: NCT02403310
	II fasea	Selinexor zitarabina eta idarubizinarekin konbinazioan. 42 paziente izena emanda. ≥ 3 mailako kontrako efektu ohikoenak: diarrea, anemia eta neutropenia sukartsua. RP2D: 60 mg astean birritan. 38 paziente ebaluagarri: % 24 CR, % 29 CRi, % 3 MLFS, % 37 SD eta % 8 PD.	Fiedler et al., 2020 ID: NCT02249091
	II fasea	Selinexor bakarka erabilita. paziente izena emanda. ≥ 3 mailako kontrako efektu ohikoenak: tronbozitopenia eta hiponatremia. 23 paziente ebaluagarri: % 26 CR eta % 52 SD.	Taylor et al., 2020 ID: NCT02228525
T-zelula periferikoen linfoma (TCL) edo naturalkiller/ T-zelulen linfoma (NKTL) errefraktorio edo gaixoberrituak	I fasea	Selinexor dexametasona, ifosfamida, karboplatino eta etoposidoarekin konbinazioan. 11 paziente izena emanda. 3 ≥ mailako kontrako efektu ohikoenak: tronbozitopenia, anemia, neutropenia eta hiponatremia. 10 paziente ebaluagarri: % 82 CR eta % 10 PR.	Tang et al., 2021 ID: NCT03212937

MM	I fasea	Dosia igotzeko fasea: Selinexor bakarka erabilita. 25 paziente izena emanda. Dosi-hedatze fase: Selinexor bakarka edo dexametasonarekin konbinazioan. 59 paziente izena emanda. ≥ 3 mailako kontrako efektu ohikoena: tronbozitopenia. RP2D: 80 mg gehi 20 mg dexametasona astean birritan ORR: % 4 Selinexor bakarka, % 50 dexametasonarekin konbinazioan.	Chen et al., 2018 ID: NCT01607892
	II fasea	Selinexor dexametasonarekin konbinazioan. 79 paziente izena emanda (gaixotasun multi-errefraktarioa). ≥ 3 mailako kontrako efektu ohikoenak: tronbozitopenia, anemia, neutropenia, hiponatremia, leukopenia eta nekea. % 21 ORR.	Vogl et al., 2018 NCT02336815
	Ib/II fasea	Selinexor bortezomib (dosi baxuan) eta dexametasonarekin konbinazioan. 42 paziente (MM gaixoberritze edo errefraktarioa). ≥ 3 mailako kontrako efektu ohikoenak: nekea, tronbozitopenia, neutropenia eta anemia. 40 paziente ebaluagarri: % 8 CR, % 23 PR oso ona, % 33 PR.	Bahlis et al., 2018 ID: NCT02343042
	I fasea	Dosia igotzeko fasea: Selinexor karfilzomib edo dexametasonarekin konbinazioan. 21 paziente izena emanda (MM gaixoberritze edo errefraktarioa). RP2D: Selinexor 60 mg, karfilzomib 20/27 mg/m^2 eta dexametasona 20mg astean birritan. ≥ 3 mailako kontrako efektu ohikoenak: tronbozitopenia, anaemia, linfopenia, neutropenia eta infekzioak. 21 paziente ebaluagarri: % 48 PR eta % 14 PR oso ona.	Jakubowiak et al., 2019 ID: NCT02199665
	IIb fasea	Selinexor dexametasonarekin konbinazioan. 122 paziente izena emanda (MM errefraktarioa). ≥ 3 mailako kontrako efektu ohikoenak: tronbozitopenia, neutropenia, leukopenia, nekea, nausea, anemia eta hiponatremia. 122 paziente ebaluagarri: 2 CR, 30 PR, 48 SD.	Chari et al., 2019 ID: NCT02336815
	III fasea	Selinexor, bortezomib eta dexametasona (SBD) versus bortezomib eta dexametasona (BD). 402 paziente izena emanda, 195 (% 49) SBD taldean eta 207 (% 51) BD taldean. ≥ 3 mailako kontrako efektu ohikoenak: tronbozitopenia, nekea, anemia eta pneumonia (kontrako efektuak ohikoagoak SBD taldean). Gaixotasunaren hedatze gabeko biziraute batez besteko denbora luzeagoa SBD taldean. SBD: % 17 CR. % 68 PR eta % 13 SD / BD: % 10 CR, % 62 PR eta % 19 SD.	Grosicki et al., 2020 ID: NCT03110562

Bular minbizia triple negatibo metastasikoa	II fasea	Selinexor bakarka erabilita. 10 paziente izena emanda. 3 ≥ mailako kontrako efektu ohikoenak: nekea, plaketen gutxitzea, disnea eta entzefalopatia. % 30 SD.	Shafique et al., 2019 ID: NCT02402764
Minbizi ginekologikoak	II fasea	Selinexor bakarka erabilita. 114 paziente izena emanda: 66, 23 eta 25 paziente obulutegiko, endometrioko eta zerbixeko minbiziarekin hurrenez hurren. 3 ≥ mailako kontrako efektu ohikoenak: tronbozitopenia, nekea, anemia, goragalea eta hiponatremia. 98 paziente ebaluagarri: PR: % 8 (obarikoan), % 9 (endometriokoan), eta % 4 (zerbixekoan).	Vergote et al., 2019 ID: NCT02269293
Obulutegi eta endometrioko minbiziak	I fasea	Selinexor karboplatino eta paklitaxelekin konbinazioan. 23 paziente izena emanda. 3 ≥ mailako kontrako efektu ohikoenak: leukopenia, neutropenia, linfopenia, anemia eta alanina transaminasen igoera. 20 paziente ebaluagarri: % 60 PR eta % 5 CR.	Rubinstein et al., 2021 ID: NCT01607905

<u>6. taula gehigarria:</u> *XPO1 vs* TARGET zerrendako geneen gainadierazpenaren korrelazio datu esanguratsuak bularreko minbizian. $\bar{x}$ sinboloak batez bestekoa adierazten du. / **<u>Supplementary Table 6:</u> *XPO1 vs* TARGET list genes overexpression correlation significant values in breast cancer.** $\bar{x}$ symbol indicates the mean value.

	Bularreko minbizia / Breast cancer					
	Lu	**Ivshina**	**Pawitan**	**TCGA**	**Wang**	$\bar{x}$
EZH2	0,288	0,233	0,293	0,473	0,408	0,339
MSH6	0,393	0,222	0,358	0,389	0,283	0,329
AURKA	0,311		0,318	0,417	0,335	0,276
MSH2	0,394		0,275	0,42	0,207	0,259
ATR	0,297		0,257		0,387	0,188
BRCA2	0,308		0,217	0,316		0,168
CCNE1	0,245			0,313	0,249	0,161
BRCA1	0,396			0,366		0,152
RHEB				0,393	0,225	0,124
DNMT3A	0,395				0,205	0,120
NPM1				0,257	0,26	0,103
NRAS				0,225	0,256	0,096
CREBBP					0,313	0,063
BRAF				0,302		0,060
CDK4				0,28		0,056
KRAS					0,274	0,055
GNAS	0,256					0,051
ALK	0,255					0,051
ASXL1			0,248			0,050
SMAD4	0,228					0,046
FLCN			0,226			0,045
EGFR	0,224					0,045
ETV6				0,221		0,044
ROS1	0,221					0,044
PIK3CB					0,218	0,044
IDH2				0,208		0,042
ERRFI1				0,202		0,040
RAB35				0,2		0,040
ATM						0,000
BAP1						0,000
BCL2						0,000
BRD2						0,000
BRD3						0,000
BRD4						0,000
c15orf55						0,000
CCND2						0,000
CCND3						0,000
CDH1						0,000
CDK12						0,000
CDK6						0,000
CDKN1B						0,000

CDKN2A	0,000
CDKN2B	0,000
CRKL	0,000
CTNNB1	0,000
ERBB2	0,000
ERBB4	0,000
ERCC2	0,000
ESR1	0,000
ETV4	0,000
ETV5	0,000
EWSR1	0,000
FBXW7	0,000
FGFR2	0,000
FGFR3	0,000
FLT3	0,000
GNAQ	0,000
HRAS	0,000
IDH1	0,000
IGF1R	0,000
JAK2	0,000
JAK3	0,000
MAP2K1	0,000
MAP2K4	0,000
MAPK1	0,000
MCL1	0,000
MDM2	0,000
MDM4	0,000
MED12	0,000
MEN1	0,000
MET	0,000
MLH1	0,000
MLL	0,000
MPL	0,000
MTOR	0,000
MYC	0,000
MYD88	0,000
NF1	0,000
NFKBIA	0,000
NKX2-1	0,000
NOTCH1	0,000
NOTCH2	0,000
NTRK3	0,000
PIK3CA	0,000
PTCH1	0,000
RAF1	0,000
RARA	0,000
RB1	0,000

RET						0,000
RNF43						0,000
RSPO2						0,000
SMAD2						0,000
SMARCA4						0,000
SMARCB1						0,000
SMO						0,000
STK11						0,000
SYK						0,000
TET2						0,000
TMPRSS2						0,000
TP53						0,000
TSC1						0,000
WT1						0,000
ZNRF3						0,000
CEBPA					-0,202	-0,040
ABL1			-0,203			-0,041
ERBB3				-0,205		-0,041
PIK3R1		-0,21				-0,042
AKT2					-0,211	-0,042
NF2	-0,212					-0,042
TSC2					-0,212	-0,042
AR					-0,218	-0,044
KDR				-0,222		-0,044
VHL			-0,224			-0,045
PTEN		-0,23				-0,046
RUNX1				-0,23		-0,046
FGFR1				-0,241		-0,048
ETV1				-0,255		-0,051
MAPK3			-0,259			-0,052
KIT	-0,261					-0,052
EPHA3				-0,27		-0,054
APC				-0,275		-0,055
MAP2K2					-0,278	-0,056
PDGFRA				-0,287		-0,057
AKT3				-0,304		-0,061
MAP3K1			-0,31			-0,062
GNA11	-0,25			-0,247		-0,099
AKT1			-0,282		-0,233	-0,103
ERG	-0,229			-0,289		-0,104
ARAF				-0,228	-0,402	-0,126
CDKN1A	-0,282		-0,434			-0,143
DDR2	-0,271	-0,229		-0,269		-0,154
CCND1		-0,258	-0,233	-0,287		-0,156
MITF	-0,19	-0,214	-0,255		-0,203	-0,172
PDGFRB		-0,257	-0,287	-0,289	-0,245	-0,216

<u>7. taula gehigarria:</u> *XPO1 vs* TARGET zerrendako geneen gainadierazpenaren korrelazio datu esanguratsuak birika adenokartzinoman. $\bar{x}$ sinboloak batez bestekoa adierazten du. / **<u>Supplementary Table 7:</u> *XPO1 vs* TARGET list genes overexpression correlation significant values in lung adenocarcinoma.** $\bar{x}$ symbol indicates the mean value.

	Birika adenokartzinoma / Lung adenocarcinoma				
	Chitale	**Shedden**	**TCGA**	**Wilkerson**	$\bar{x}$
MSH2	0,559	0,715	0,648	0,565	0,622
MSH6	0,564	0,662	0,592	0,58	0,600
ATR	0,508	0,738	0,404	0,476	0,532
EZH2	0,488	0,509	0,516	0,577	0,523
BRCA2	0,484	0,358	0,553	0,555	0,488
AURKA	0,458	0,321	0,482	0,647	0,477
PIK3CA	0,284	0,696	0,33	0,527	0,459
NRAS	0,35	0,491	0,384	0,467	0,423
BRCA1	0,427		0,535	0,651	0,403
CCNE1	0,365		0,427	0,624	0,354
PIK3CB	0,294	0,456		0,384	0,284
BRAF	0,402		0,312	0,413	0,282
CDK12	0,37	0,363	0,361		0,274
IDH1	0,339	0,438		0,247	0,256
DNMT3A	0,328	-0,264	0,392	0,505	0,240
NPM1		0,586		0,215	0,200
RAF1	0,388	0,405			0,198
MAP2K4	0,222	0,514			0,184
ASXL1	0,265	0,202	0,23		0,174
KRAS		0,421	0,264		0,171
CDKN2A	0,415			0,238	0,163
NF1	0,356	0,253			0,152
SMAD4		0,608			0,152
MED12	0,218			0,329	0,137
MAPK1	0,237	0,301			0,135
CRKL				0,528	0,132
MLH1		0,504			0,126
RB1		0,494			0,124
PTEN		0,482			0,121
HRAS	0,225			0,253	0,120
ATM		0,467			0,117
MAP2K2		0,448			0,112
SMAD2		0,432			0,108
SMARCB1				0,398	0,100
CDKN1B		0,388			0,097
FLCN				0,383	0,096
CTNNB1		0,377			0,094
ERBB2	0,358				0,090
MEN1	0,349				0,087
AKT1	0,339				0,085

RHEB	0,333				0,083
BRD3	0,298				0,075
CDK4				0,297	0,074
VHL			0,294		0,074
EWSR1	0,29				0,073
IDH2				0,272	0,068
GNAS				0,271	0,068
MAP2K1		0,262			0,066
NOTCH2		0,245			0,061
BRD2	0,241				0,060
RNF43				0,239	0,060
CREBBP	0,234				0,059
CDK6	0,215	-0,516	0,209	0,322	0,058
APC		0,227			0,057
ETV6	0,218				0,055
NF2		-0,272		0,46	0,047
JAK2		0,325		-0,301	0,006
c15orf55					0,000
CDH1					0,000
ERBB3					0,000
ERRFI1					0,000
FGFR3					0,000
GNAQ					0,000
IGF1R					0,000
MAP3K1					0,000
MDM4					0,000
MET					0,000
MLL					0,000
MYC					0,000
NFKBIA					0,000
PTCH1					0,000
RET					0,000
SMARCA4					0,000
TET2					0,000
ZNRF3					0,000
TSC1		0,39		-0,403	-0,003
SMO		-0,396		0,318	-0,020
MTOR	0,212	-0,34			-0,032
CCND1	-0,203				-0,051
TP53				-0,218	-0,055
ETV5			-0,221		-0,055
AKT3	-0,222				-0,056
EPHA3			-0,222		-0,056
TSC2				-0,232	-0,058
NOTCH1		-0,235			-0,059
ETV4		-0,239			-0,060
MDM2		-0,249			-0,062

AKT2		-0,572		0,32	-0,063
BAP1		-0,257			-0,064
ROS1			-0,257		-0,064
FBXW7	-0,264				-0,066
MITF	-0,264				-0,066
EGFR		-0,265			-0,066
PIK3R1	-0,28				-0,070
SYK				-0,284	-0,071
KIT				-0,286	-0,072
FGFR1	-0,299				-0,075
ABL1				-0,322	-0,081
MYD88				-0,34	-0,085
ALK		-0,344			-0,086
MCL1				-0,353	-0,088
BRD4		-0,355			-0,089
WT1		-0,38			-0,095
AR		-0,263		-0,202	-0,116
NKX2-1				-0,473	-0,118
KDR				-0,481	-0,120
ERCC2		-0,489			-0,122
RAB35		-0,492			-0,123
ETV1	-0,28		-0,231		-0,128
ARAF		-0,235	-0,311		-0,137
FGFR2		-0,32	-0,24		-0,140
CDKN2B		-0,363		-0,211	-0,144
PDGFRA	-0,281			-0,301	-0,146
CCND3			-0,268	-0,315	-0,146
TMPRSS2				-0,653	-0,163
RSPO2			-0,279	-0,38	-0,165
DDR2	-0,401	-0,278			-0,170
MPL		-0,681			-0,170
CDKN1A			-0,261	-0,453	-0,179
BCL2	-0,322	-0,403			-0,181
STK11		-0,497	-0,233		-0,183
MAPK3		-0,533	-0,203		-0,184
CEBPA	-0,315		-0,206	-0,253	-0,194
ERBB4	-0,218	-0,3	-0,304		-0,206
ESR1	-0,313	-0,539			-0,213
RUNX1		-0,51		-0,36	-0,218
JAK3	-0,216	-0,672			-0,222
CCND2	-0,276	-0,286	-0,224	-0,211	-0,249
GNA11	-0,312	-0,429		-0,423	-0,291
FLT3	-0,325	-0,632		-0,248	-0,301
PDGFRB	-0,361	-0,319	-0,254	-0,424	-0,340
ERG	-0,398	-0,215	-0,324	-0,496	-0,358
RARA		-0,547	-0,397	-0,5	-0,361
NTRK3	-0,386	-0,614	-0,298	-0,436	-0,434

<u>8. taula gehigarria:</u> *XPO1 vs* TARGET zerrendako geneen gainadierazpenaren korrelazio datu esanguratsuak prostata minbizian. $\bar{x}$ sinboloak batez bestekoa adierazten du. / **<u>Supplementary Table 8:</u> *XPO1 vs* TARGET list genes overexpression correlation significant values in prostate cancer.** $\bar{x}$ symbol indicates the mean value.

	Prostata minbizia / Prostate cancer						
	Glinsky	**Grasso**	**Lapointe**	**Taylor**	**TCGA**	**Varambally**	$\bar{x}$
MSH2	0,284	0,414	0,679	0,758	0,623		0,460
RB1		0,474		0,747	0,495	0,824	0,423
FBXW7	0,229			0,635	0,426	0,922	0,369
ATM				0,796	0,571	0,795	0,360
CTNNB1			0,834	0,858	0,314		0,334
ATR		0,366		0,825	0,592		0,297
NOTCH2			0,573	0,572	0,49		0,273
DDR2				0,373	0,338	0,805	0,253
MDM4		-0,312	0,659	0,717	0,44		0,251
PIK3CA				0,837	0,569		0,234
NF1				0,782	0,546		0,221
BRAF				0,759	0,553		0,219
TET2				0,622	0,656		0,213
MLH1		0,499		0,766			0,211
MSH6				0,725	0,533		0,210
PDGFRA				0,279		0,973	0,209
KRAS				0,706	0,534		0,207
GNAQ				0,827	0,371		0,200
APC				0,779	0,403		0,197
CCND2				0,252	0,926		0,196
SMAD2				0,77	0,369		0,190
MAP3K1				0,604	0,527		0,189
NRAS				0,724	0,347		0,179
MAPK1				0,69	0,374		0,177
VHL				0,518	0,533		0,175
PIK3CB				0,742	0,287		0,172
CDKN1B	0,355			0,411	0,262		0,171
JAK2				0,62	0,374		0,166
RAF1				0,719	0,247		0,161
CDK12				0,47	0,487		0,160
PIK3R1				0,661	0,262		0,154
MDM2				0,562	0,335		0,150
MYC			0,66	0,225			0,148
BRD2				0,423	0,435		0,143
CREBBP				0,365	0,493		0,143
MCL1				0,598	0,216		0,136
PDGFRB						0,797	0,133
NPM1				0,735			0,123
RHEB				0,707			0,118
MAP2K4	-0,239	0,284		0,648			0,116
AKT3				0,682			0,114

SMAD4				0,682			0,114
CRKL				0,204	0,448		0,109
PTEN				0,62			0,103
IDH1				0,578			0,096
PTCH1					0,533		0,089
BRCA1					0,527		0,088
EZH2	0,243		0,658		0,288	-0,684	0,084
CDH1				0,497			0,083
MED12					0,415		0,069
IDH2					-0,397	0,806	0,068
ESR1				-0,411		0,809	0,066
EPHA3				0,394			0,066
EWSR1				0,394			0,066
MAP2K1				0,389			0,065
GNAS				0,378			0,063
ASXL1					0,365		0,061
KDR				0,323			0,054
BRCA2				-0,294	0,612		0,053
KIT				0,31			0,052
MET				0,31			0,052
GNA11					0,292		0,049
ERRFI1				0,291			0,049
ETV6				0,274			0,046
CDK4				0,267			0,045
TSC2	0,267						0,045
MYD88					0,249		0,042
SYK					0,237		0,040
DNMT3A	0,243			-0,426	0,418		0,039
MITF				0,211			0,035
NOTCH1					0,209		0,035
ABL1	-0,308			0,221	0,282		0,033
TSC1			-0,596	0,358	0,345		0,018
AR				0,309	0,521	-0,791	0,007
NF2		-0,301		0,306			0,001
BCL2							0,000
c15orf55							0,000
ETV1							0,000
ETV5							0,000
FGFR2							0,000
FLCN	0,273			-0,645	0,372		0,000
MLL							0,000
MPL							0,000
RAB35							0,000
SMARCA4							0,000
TP53							0,000
BRD4				-0,311	0,303		-0,001
AURKA	0,257			0,221	0,299	-0,872	-0,016

BRD3		-0,301		-0,335	0,505		-0,022
FLT3		0,299		-0,455			-0,026
NTRK3				-0,22			-0,037
NFKBIA	-0,231						-0,039
RSPO2					-0,239		-0,040
ERG				0,232	0,205	-0,689	-0,042
RET				-0,274			-0,046
MAPK3					-0,29		-0,048
RUNX1				-0,29			-0,048
EGFR				0,232	0,396	-0,925	-0,050
MTOR		-0,298					-0,050
AKT1	-0,301						-0,050
ROS1				-0,622	0,316		-0,051
ERBB4				-0,322			-0,054
CCND1		-0,335					-0,056
ZNRF3		-0,384					-0,064
RNF43		-0,405					-0,068
ARAF					-0,507		-0,085
IGF1R				0,282		-0,792	-0,085
NKX2-1				-0,759	0,214		-0,091
MEN1				-0,55			-0,092
ETV4				-0,332	-0,236		-0,095
WT1				-0,593			-0,099
CDKN2A				-0,599			-0,100
FGFR3				-0,626			-0,104
CCNE1				-0,631			-0,105
BAP1				-0,428	-0,211		-0,107
ALK				-0,667			-0,111
AKT2		-0,346		-0,369			-0,119
CDKN2B				-0,735			-0,123
TMPRSS2			-0,751				-0,125
STK11				-0,414	-0,349		-0,127
ERCC2				-0,563	-0,242		-0,134
CDK6		-0,474	-0,62	0,283			-0,135
ERBB2	-0,233		-0,601				-0,139
FGFR1	-0,244		-0,605				-0,142
RARA	-0,269			-0,641			-0,152
JAK3			-0,656	-0,418			-0,179
CEBPA	0,227	-0,373		-0,617	-0,408		-0,195
ERBB3		-0,325				-0,865	-0,198
CDKN1A	-0,373		-0,604		-0,264		-0,207
SMO	-0,278	-0,477		-0,622			-0,230
SMARCB1				-0,256	-0,378	-0,928	-0,260
HRAS		-0,406		-0,717	-0,497		-0,270
MAP2K2				-0,328	-0,627	-0,771	-0,288
CCND3				-0,603	-0,303	-0,843	-0,292

9. taula gehigarria: ***XPO1 vs*** **TARGET zerrendako geneen gainadierazpenaren korrelazio datu esanguratsuak kolon eta ondesteko tumore primarioetan.** $\bar{x}$ sinboloak batez bestekoa adierazten du. / **Supplementary Table 9:** ***XPO1 vs*** **TARGET list genes overexpression correlation significant values in colorectal primary tumour.** $\bar{x}$ symbol indicates the mean value.

	Kolon eta ondesteko tumore primarioa / Colorectal primary tumour							
	Colon-omics	Jorissen	Kemper	Laibe	Marisa	Roepman	TCGA	$\bar{x}$
ATR	0,387	0,201	0,404	0,369	0,572	0,354	0,389	0,382
BRCA1	0,554		0,275	0,405	0,452	0,388	0,521	0,371
EZH2	0,458		0,325	0,481	0,468	0,373	0,389	0,356
MSH2	0,573		0,276	0,211	0,433	0,466	0,509	0,353
BRCA2	0,599		0,261	0,445	0,528		0,5	0,333
NPM1	0,486		0,312	0,269	0,35	0,215	0,27	0,272
AURKA	0,448			0,373	0,349	0,296	0,433	0,271
MSH6	0,592				0,356	0,277	0,521	0,249
CDK12	0,429	0,286		0,289	0,385		0,331	0,246
BRAF		0,201		0,366	0,518		0,613	0,243
RAF1		0,301	0,427	0,501	0,405			0,233
ASXL1		0,337	0,352	0,507	0,429			0,232
CTNNB1	0,4	0,228		0,214	0,231	0,345		0,203
CCNE1	0,294	0,209		0,324		0,257	0,33	0,202
EWSR1	0,4			0,437	0,221	0,25		0,187
MYC	0,496			0,333			0,26	0,156
ATM			0,245	0,227	0,272		0,247	0,142
CDK4	0,292			0,278			0,278	0,121
CDKN1B	0,273			0,276	0,296			0,121
FBXW7				0,253	0,365	0,224		0,120
TSC1		0,252		0,283	0,306			0,120
NRAS	0,267				0,251	0,297		0,116
NF1	0,235			0,273			0,286	0,113
GNAS			0,234	0,272	0,273			0,111
PIK3CB	0,259				0,306	0,212		0,111
RHEB			0,298		0,226	0,242		0,109
SMARCA4	0,399			0,347				0,107
MDM4				0,361	0,341			0,100
RB1	0,329				0,305			0,091
VHL	0,288						0,312	0,086
RNF43	0,206			0,325				0,076
IDH1	0,261					0,211		0,067
BRD4	0,268			0,2				0,067
MTOR	0,216		0,238					0,065
HRAS	0,202					0,239		0,063
PIK3CA					0,368			0,053
MET	0,36							0,051
MLH1	0,346							0,049
NOTCH1				0,321				0,046
ETV4				0,281				0,040

CDK6					0,277			0,040
KRAS					0,271			0,039
MED12				0,251				0,036
PTCH1	-0,221			0,268	0,202			0,036
PTEN					0,247			0,035
AKT1						0,246		0,035
CDKN2A						0,238		0,034
ETV1						0,238		0,034
SYK				0,273	0,206	-0,241		0,034
CCND1	0,235							0,034
FLCN				0,226				0,032
BRD2							0,22	0,031
JAK2					0,207			0,030
SMAD4					0,206			0,029
BRD3		0,261		0,257		-0,341		0,025
MAP2K1			-0,216			0,374		0,023
MEN1	0,347					-0,236		0,016
AKT2								0,000
ARAF								0,000
BAP1								0,000
c15orf55								0,000
CCND2								0,000
CCND3								0,000
CDH1								0,000
CEBPA								0,000
CREBBP								0,000
DNMT3A								0,000
EGFR								0,000
ERBB3								0,000
ERRFI1								0,000
ETV5								0,000
FGFR3								0,000
IGF1R								0,000
PIK3R1								0,000
SMO								0,000
TMPRSS2								0,000
TP53								0,000
WT1								0,000
ZNRF3								0,000
ABL1		0,248	-0,329					-0,012
MAPK1	0,3		-0,264	-0,21				-0,025
MDM2			-0,219					-0,031
RET	-0,231							-0,033
NKX2-1					-0,236			-0,034
IDH2			-0,243					-0,035
ROS1					-0,243			-0,035
FLT3	-0,247							-0,035

ERBB2		-0,249						-0,036
ERCC2					-0,249			-0,036
NOTCH2			-0,249					-0,036
STK11					-0,249			-0,036
CRKL			-0,252					-0,036
NF2					-0,271			-0,039
APC				-0,277				-0,040
ERBB4					-0,292			-0,042
MLL						-0,319		-0,046
PDGFRB	-0,328							-0,047
SMAD2		-0,334		-0,236		0,241		-0,047
AKT3	-0,336							-0,048
KDR			-0,351					-0,050
ERG	-0,395							-0,056
SMARCB1					-0,424			-0,061
NFKBIA			-0,216		-0,216			-0,062
ETV6						-0,215	-0,236	-0,064
MAP3K1	-0,222			-0,234				-0,065
RUNX1	-0,222					-0,252		-0,068
TET2		-0,213		-0,262				-0,068
ALK	-0,212	-0,294						-0,072
MYD88				-0,248	-0,263			-0,073
PDGFRA	-0,261			-0,261				-0,075
KIT			-0,263	-0,266				-0,076
MAP2K4			-0,243	-0,292				-0,076
RAB35		-0,245			-0,296			-0,077
MCL1			-0,217	-0,345				-0,080
EPHA3	-0,314			-0,251				-0,081
FGFR1	-0,37					-0,238		-0,087
MITF	-0,357			-0,251				-0,087
RSPO2	-0,212			-0,2	-0,208			-0,089
MPL			-0,243		-0,403			-0,092
ESR1					-0,41	-0,279		-0,098
AR			-0,215	-0,263	-0,232			-0,101
GNA11			-0,219	-0,206	-0,291			-0,102
GNAQ			-0,424	-0,296				-0,103
JAK3	-0,221				-0,287	-0,308		-0,117
DDR2	-0,362			-0,212		-0,25		-0,118
TSC2	-0,234					-0,378	-0,272	-0,126
NTRK3	-0,2	-0,206			-0,389	-0,208		-0,143
CDKN2B	-0,436			-0,421			-0,222	-0,154
MAP2K2			-0,223	-0,269	-0,351		-0,29	-0,162
RARA	-0,242		-0,221		-0,359	-0,374		-0,171
CDKN1A			-0,384	-0,32	-0,273		-0,251	-0,175
BCL2	-0,221	-0,207	-0,297	-0,382	-0,209			-0,188
FGFR2	-0,466		-0,253	-0,31	-0,332	-0,29		-0,236
MAPK3	-0,413	-0,253		-0,252	-0,385		-0,421	-0,246

<u>10. taula gehigarria:</u> *XPO1 vs* TARGET zerrendako geneen gainadierazpenaren korrelazio datu esanguratsuak leuzemia mieloide akutuan (AML). $\bar{x}$ sinboloak batez bestekoa adierazten du. / **<u>Supplementary Table 10:</u> *XPO1 vs* TARGET list genes overexpression correlation significant values in acute myeloid leukaemia (AML).** $\bar{x}$ symbol indicates the mean value.

	AML		
	Liu	**Tyner**	$\bar{x}$
MSH2	0,624	0,661	0,642
ATR	0,557	0,552	0,554
BRCA1	0,583	0,489	0,536
CDK6	0,505	0,531	0,518
MSH6	0,581	0,429	0,505
MLH1	0,393	0,484	0,439
NF1	0,509	0,209	0,359
NPM1	0,403	0,304	0,354
TP53		0,693	0,347
RUNX1	0,286	0,387	0,337
MEN1		0,658	0,329
FLT3	0,226	0,431	0,328
BCL2	0,291	0,351	0,321
RB1	0,380	0,246	0,313
SMARCA4		0,595	0,297
IDH1		0,580	0,290
CDK4		0,572	0,286
SMAD4	0,570		0,285
ERCC2		0,566	0,283
MTOR		0,559	0,280
PTEN	0,350	0,206	0,278
BRD3		0,533	0,266
AURKA	0,221	0,298	0,259
GNAQ	0,509		0,255
KIT	0,279	0,230	0,254
BRCA2	0,484		0,242
MED12		0,451	0,226
MYC		0,439	0,219
SMAD2	0,416		0,208
IDH2		0,380	0,190
ERBB2		0,375	0,188
MAP2K4	0,339		0,170
ZNRF3		0,332	0,166
DNMT3A		0,311	0,155
EZH2	0,303		0,151
SMARCB1		0,297	0,148
PIK3CB	0,271		0,136
CRKL	0,271		0,135
PIK3R1	0,510	-0,271	0,119
FGFR3		0,234	0,117

MDM4	0,221		0,111
CEBPA		0,221	0,110
ETV6		0,209	0,104
ATM		0,202	0,101
EWSR1		0,201	0,100
NRAS	0,478	-0,339	0,070
CDK12	0,371	-0,286	0,043
GNAS	-0,240	0,250	0,005
APC	0,331	-0,328	0,001
ABL1			0,000
ALK			0,000
AR			0,000
ASXL1			0,000
c15orf55			0,000
CCND1			0,000
CCND2			0,000
CCNE1			0,000
CDH1			0,000
CDKN2A			0,000
CDKN2B			0,000
DDR2			0,000
EGFR			0,000
EPHA3			0,000
ERBB3			0,000
ERBB4			0,000
ERG			0,000
ESR1			0,000
ETV1			0,000
ETV4			0,000
ETV5			0,000
FGFR2			0,000
IGF1R			0,000
JAK2			0,000
KDR			0,000
MAP3K1			0,000
MAPK1			0,000
MET			0,000
MITF			0,000
MLL			0,000
MPL			0,000
NF2			0,000
NKX2-1			0,000
NOTCH2			0,000
NTRK3			0,000
PDGFRA			0,000
PDGFRB			0,000
RNF43			0,000

ROS1			0,000
RSPO2			0,000
SMO			0,000
SYK			0,000
TMPRSS2			0,000
TSC1			0,000
WT1			0,000
TSC2	-0,334	0,328	-0,003
STK11	-0,286	0,254	-0,016
MDM2	0,202	-0,242	-0,020
BRAF	0,392	-0,486	-0,047
AKT1	-0,448	0,325	-0,062
PIK3CA	0,396	-0,549	-0,077
KRAS	0,390	-0,568	-0,089
FGFR1		-0,204	-0,102
PTCH1	-0,206		-0,103
NOTCH1	-0,219		-0,110
RET	-0,231		-0,116
TET2		-0,237	-0,119
AKT3		-0,239	-0,120
CDKN1B		-0,263	-0,131
GNA11	-0,269		-0,135
RHEB		-0,270	-0,135
CTNNB1		-0,277	-0,139
JAK3	-0,302		-0,151
BRD4	-0,304		-0,152
BRD2	-0,331		-0,165
ERRFI1		-0,339	-0,170
FLCN	-0,359		-0,180
AKT2	-0,397		-0,198
VHL		-0,400	-0,200
CCND3	-0,418		-0,209
MCL1		-0,438	-0,219
HRAS	-0,479		-0,240
FBXW7		-0,572	-0,286
BAP1	-0,361	-0,259	-0,310
MAP2K1	-0,311	-0,334	-0,323
MYD88	-0,412	-0,236	-0,324
MAP2K2	-0,468	-0,216	-0,342
CDKN1A	-0,411	-0,346	-0,379
CREBBP	-0,221	-0,587	-0,404
RAB35	-0,471	-0,341	-0,406
ARAF	-0,556	-0,309	-0,432
NFKBIA	-0,419	-0,491	-0,455
RAF1	-0,512	-0,476	-0,494
MAPK3	-0,597	-0,461	-0,529
RARA	-0,663	-0,531	-0,597

<u>11. taula gehigarria:</u> *XPO1 vs* TARGET zerrendako geneen gainadierazpenaren korrelazio datuak aztertutako minbizi guztien batez bestekoak kontuan izanik. $\bar{x}$ sinboloak batez bestekoa adierazten du. / **<u>Supplementary Table 11:</u> *XPO1 vs* TARGET list genes overexpression correlation considering mean values of all the tumours analysed.** $\bar{x}$ symbol indicates the mean value.

	Minbizi guztiak / All tumours					
	Bular/Breast	**Birika/Lung**	**Prostata/Prostate**	**Kolon eta Ondeste/Colorectal**	**AML**	$\bar{x}$
MSH2	0,259	0,622	0,460	0,353	0,642	0,467
ATR	0,188	0,532	0,297	0,382	0,554	0,391
MSH6	0,329	0,600	0,210	0,249	0,505	0,379
BRCA1	0,152	0,403	0,088	0,371	0,536	0,310
EZH2	0,339	0,523	0,084	0,356	0,151	0,291
BRCA2	0,168	0,488	0,053	0,333	0,242	0,257
AURKA	0,276	0,477	-0,016	0,271	0,259	0,254
NPM1	0,103	0,200	0,123	0,272	0,354	0,210
RB1	0,000	0,124	0,423	0,091	0,313	0,190
NRAS	0,096	0,423	0,179	0,116	0,070	0,177
NF1	0,000	0,152	0,221	0,113	0,359	0,169
MLH1	0,000	0,126	0,211	0,049	0,439	0,165
BRAF	0,060	0,282	0,219	0,243	-0,047	0,151
PIK3CB	0,044	0,284	0,172	0,111	0,136	0,149
CDK12	0,000	0,274	0,160	0,246	0,043	0,144
ATM	0,000	0,117	0,360	0,142	0,101	0,144
IDH1	0,000	0,256	0,096	0,067	0,290	0,142
PIK3CA	0,000	0,459	0,234	0,053	-0,077	0,134
SMAD4	0,046	0,152	0,114	0,029	0,285	0,125
CCNE1	0,161	0,354	-0,105	0,202	0,000	0,122
CDK4	0,056	0,074	0,045	0,121	0,286	0,116
DNMT3A	0,120	0,240	0,039	0,000	0,155	0,111
MYC	0,000	0,000	0,148	0,156	0,219	0,104
ASXL1	0,050	0,174	0,061	0,232	0,000	0,103
CTNNB1	0,000	0,094	0,334	0,203	-0,139	0,098
PTEN	-0,046	0,121	0,103	0,035	0,278	0,098
CDK6	0,000	0,058	-0,135	0,040	0,518	0,096
MED12	0,000	0,137	0,069	0,036	0,226	0,093
MDM4	0,000	0,000	0,251	0,100	0,111	0,092
SMAD2	0,000	0,108	0,190	-0,047	0,208	0,092
EWSR1	0,000	0,073	0,066	0,187	0,100	0,085
SMARCA4	0,000	0,000	0,000	0,107	0,297	0,081
MAP2K4	0,000	0,184	0,116	-0,076	0,170	0,079
KRAS	0,055	0,171	0,207	0,039	-0,089	0,077
GNAQ	0,000	0,000	0,200	-0,103	0,255	0,070
BRD3	0,000	0,075	-0,022	0,025	0,266	0,069
MEN1	0,000	0,087	-0,092	0,016	0,329	0,068
CRKL	0,000	0,132	0,109	-0,036	0,135	0,068
IDH2	0,042	0,068	0,068	-0,035	0,190	0,067
RHEB	0,124	0,083	0,118	0,109	-0,135	0,060

NOTCH2	0,000	0,061	0,273	-0,036	0,000	0,060
GNAS	0,051	0,068	0,063	0,111	0,005	0,060
TP53	0,000	-0,055	0,000	0,000	0,347	0,058
MAPK1	0,000	0,135	0,177	-0,025	0,000	0,057
MTOR	0,000	-0,032	-0,050	0,065	0,280	0,053
CDKN1B	0,000	0,097	0,171	0,121	-0,131	0,052
JAK2	0,000	0,006	0,166	0,030	0,000	0,040
ETV6	0,044	0,055	0,046	-0,064	0,104	0,037
PIK3R1	-0,042	-0,070	0,154	0,000	0,119	0,032
APC	-0,055	0,057	0,197	-0,040	0,001	0,032
FBXW7	0,000	-0,066	0,369	0,120	-0,286	0,027
TSC1	0,000	-0,003	0,018	0,120	0,000	0,027
KIT	-0,052	-0,072	0,052	-0,076	0,254	0,021
MET	0,000	0,000	0,052	0,051	0,000	0,021
ERBB2	0,000	0,090	-0,139	-0,036	0,188	0,021
ZNRF3	0,000	0,000	-0,064	0,000	0,166	0,020
RAF1	0,000	0,198	0,161	0,233	-0,494	0,020
CDKN2A	0,000	0,163	-0,100	0,034	0,000	0,019
VHL	-0,045	0,074	0,175	0,086	-0,200	0,018
CDH1	0,000	0,000	0,083	0,000	0,000	0,017
BRD2	0,000	0,060	0,143	0,031	-0,165	0,014
RNF43	0,000	0,060	-0,068	0,076	0,000	0,014
MAP3K1	-0,062	0,000	0,189	-0,065	0,000	0,012
MDM2	0,000	-0,062	0,150	-0,031	-0,020	0,007
TET2	0,000	0,000	0,213	-0,068	-0,119	0,005
PTCH1	0,000	0,000	0,089	0,036	-0,103	0,004
FGFR3	0,000	0,000	-0,104	0,000	0,117	0,003
SYK	0,000	-0,071	0,040	0,034	0,000	0,001
c15orf55	0,000	0,000	0,000	0,000	0,000	0,000
FLCN	0,045	0,096	0,000	0,032	-0,180	-0,001
ERCC2	0,000	-0,122	-0,134	-0,036	0,283	-0,002
NF2	-0,042	0,047	0,001	-0,039	0,000	-0,007
FLT3	0,000	-0,301	-0,026	-0,035	0,328	-0,007
RUNX1	-0,046	-0,218	-0,048	-0,068	0,337	-0,009
MLL	0,000	0,000	0,000	-0,046	0,000	-0,009
BCL2	0,000	-0,181	0,000	-0,188	0,321	-0,010
CCND2	0,000	-0,249	0,196	0,000	0,000	-0,011
ETV5	0,000	-0,055	0,000	0,000	0,000	-0,011
PDGFRA	-0,057	-0,146	0,209	-0,075	0,000	-0,014
EGFR	0,045	-0,066	-0,050	0,000	0,000	-0,014
SMARCB1	0,000	0,100	-0,260	-0,061	0,148	-0,015
ERRFI1	0,040	0,000	0,049	0,000	-0,170	-0,016
IGF1R	0,000	0,000	-0,085	0,000	0,000	-0,017
NOTCH1	0,000	-0,059	0,035	0,046	-0,110	-0,018
AKT1	-0,103	0,085	-0,050	0,035	-0,062	-0,019
ABL1	-0,041	-0,081	0,033	-0,012	0,000	-0,020
ROS1	0,044	-0,064	-0,051	-0,035	0,000	-0,021

ETV4	0,000	-0,060	-0,095	0,040	0,000	-0,023
EPHA3	-0,054	-0,056	0,066	-0,081	0,000	-0,025
CREBBP	0,063	0,059	0,143	0,000	-0,404	-0,028
ETV1	-0,051	-0,128	0,000	0,034	0,000	-0,029
KDR	-0,044	-0,120	0,054	-0,050	0,000	-0,032
MAP2K1	0,000	0,066	0,065	0,023	-0,323	-0,034
AKT3	-0,061	-0,056	0,114	-0,048	-0,120	-0,034
BRD4	0,000	-0,089	-0,001	0,067	-0,152	-0,035
TSC2	-0,042	-0,058	0,045	-0,126	-0,003	-0,037
DDR2	-0,154	-0,170	0,253	-0,118	0,000	-0,038
WT1	0,000	-0,095	-0,099	0,000	0,000	-0,039
RET	0,000	0,000	-0,046	-0,033	-0,116	-0,039
ALK	0,051	-0,086	-0,111	-0,072	0,000	-0,044
CCND1	-0,156	-0,051	-0,056	0,034	0,000	-0,046
ERBB3	-0,041	0,000	-0,198	0,000	0,000	-0,048
NKX2-1	0,000	-0,118	-0,091	-0,034	0,000	-0,049
ESR1	0,000	-0,213	0,066	-0,098	0,000	-0,049
SMO	0,000	-0,020	-0,230	0,000	0,000	-0,050
MCL1	0,000	-0,088	0,136	-0,080	-0,219	-0,050
AR	-0,044	-0,116	0,007	-0,101	0,000	-0,051
MPL	0,000	-0,170	0,000	-0,092	0,000	-0,053
TMPRSS2	0,000	-0,163	-0,125	0,000	0,000	-0,058
MITF	-0,172	-0,066	0,035	-0,087	0,000	-0,058
RSPO2	0,000	-0,165	-0,040	-0,089	0,000	-0,059
ERBB4	0,000	-0,206	-0,054	-0,042	0,000	-0,060
CEBPA	-0,040	-0,194	-0,195	0,000	0,110	-0,064
HRAS	0,000	0,120	-0,270	0,063	-0,240	-0,065
STK11	0,000	-0,183	-0,127	-0,036	-0,016	-0,072
FGFR2	0,000	-0,140	0,000	-0,236	0,000	-0,075
CDKN2B	0,000	-0,144	-0,123	-0,154	0,000	-0,084
AKT2	-0,042	-0,063	-0,119	0,000	-0,198	-0,085
MYD88	0,000	-0,085	0,042	-0,073	-0,324	-0,088
FGFR1	-0,048	-0,075	-0,142	-0,087	-0,102	-0,091
PDGFRB	-0,216	-0,340	0,133	-0,047	0,000	-0,094
BAP1	0,000	-0,064	-0,107	0,000	-0,310	-0,096
NFKBIA	0,000	0,000	-0,039	-0,062	-0,455	-0,111
ERG	-0,104	-0,358	-0,042	-0,056	0,000	-0,112
RAB35	0,040	-0,123	0,000	-0,077	-0,406	-0,113
GNA11	-0,099	-0,291	0,049	-0,102	-0,135	-0,116
NTRK3	0,000	-0,434	-0,037	-0,143	0,000	-0,123
CCND3	0,000	-0,146	-0,292	0,000	-0,209	-0,129
JAK3	0,000	-0,222	-0,179	-0,117	-0,151	-0,134
MAP2K2	-0,056	0,112	-0,288	-0,162	-0,342	-0,147
ARAF	-0,126	-0,137	-0,085	0,000	-0,432	-0,156
MAPK3	-0,052	-0,184	-0,048	-0,246	-0,529	-0,212
CDKN1A	-0,143	-0,179	-0,207	-0,175	-0,379	-0,217
RARA	0,000	-0,361	-0,152	-0,171	-0,597	-0,256

12. taula gehigarria: Tesi honetan zehar erabili baina espresuki sortu ez diren plasmidoak. Plasmido bakoitza zein ikerlariren eskutik lortu den, plasmido horren sorrera-datako ikerlariaren afiliazioa eta plasmidoa lehen aldiz agertutako erreferentzia edo merkataritza etxea adierazten dira.

Plasmidoa	Ikerlaria	Unibertsitatea	Erreferentzia /merkataritza etxea
pEYFP-C1			Clontech
pcDNA3 APEX2-NES	Dr. Alice Ting	Stanford University, California, AEB	Addgene
Myc-MSC	Dr. Anne Olazabal-Herrero	Euskal Herriko Unibertsitatea	Olazabal-Herrero et al., 2019
UAF1-mRFP	Dr. Anne Olazabal-Herrero	Euskal Herriko Unibertsitatea	Olazabal-Herrero et al., 2015
YFP-USP12	Dr. Anne Olazabal-Herrero	Euskal Herriko Unibertsitatea	Olazabal-Herrero et al., 2019
YFP-USP12$^{[2NLS]}$	Dr. Anne Olazabal-Herrero	Euskal Herriko Unibertsitatea	Olazabal-Herrero et al., 2019
YFP-WDR20	Dr. Anne Olazabal-Herrero	Euskal Herriko Unibertsitatea	Olazabal-Herrero et al., 2019
Myc-WDR20	Dr. Anne Olazabal-Herrero	Euskal Herriko Unibertsitatea	Olazabal-Herrero et al., 2019
pRev(1.4)-GFP	Dr. Beric Henderson	University of Sydney, Australia	Henderson eta Eleftheriou, 2000
Myc-DMWD	Dr. Anne Olazabal-Herrero	Euskal Herriko Unibertsitatea	Olazabal-Herrero et al., 2021
SRV100	Dr. Iraia García-Santisteban	Euskal Herriko Unibertsitatea	García-Santisteban et al., 2016
YFP-CRM1wt	Dr. José Antonio Rodríguez	University of Sydney, Australia	Rodríguez and Henderson, 2000
YFP-CRM1 4X	Dr. Iraia García-Santisteban	Euskal Herriko Unibertsitatea	García-Santisteban et al., 2016
YFP-CRM1 E571K	Dr. Iraia García-Santisteban	Euskal Herriko Unibertsitatea	García-Santisteban et al., 2016
YFP-CRM F572A	Dr. Iraia García-Santisteban	Euskal Herriko Unibertsitatea	García-Santisteban et al., 2016
YFP-CRM1 A541K	Dr. Iraia García-Santisteban	Euskal Herriko Unibertsitatea	García-Santisteban et al., 2016
SRV100^{NESm}	Dr. Iraia García-Santisteban	Euskal Herriko Unibertsitatea	García-Santisteban et al., 2016

13. taula gehigarria: Azpiklonazioz sortutako plasmidoak. Plasmido berriaren izena, intsertoa zein plasmidotik azpiklonatu den, plasmido berria eratzeko bektorea eta intsertoa, eta klonaziorako erabilitako murrizte-entzimak adierazten dira.

Plasmido berria	Jatorrizko plasmidoa	Bektorea	Intsertoa	Murrizte-entzimak
Myc-WDR20^{NESmut}	YFP-WDR20^{NESmut}	Myc-MSC	WDR20^{NESmut}	HIndIII/BamHI
SRV-WN1	pRev(1.4)-WN1-GFP	$SRV_{B/A}$	WN1	BamHI/AgeI
SRV-WN2	pRev(1.4)-WN2-GFP	$SRV_{B/A}$	WN2	BamHI/AgeI
SRV-WN3	pRev(1.4)-WN3-GFP	$SRV_{B/A}$	WN3	BamHI/AgeI
SRV-WN4	pRev(1.4)-WN4-GFP	$SRV_{B/A}$	WN4	BamHI/AgeI
SRV-WN5	pRev(1.4)-WN5-GFP	$SRV_{B/A}$	WN5	BamHI/AgeI

SRV-WN6	pRev(1.4)-WN6-GFP	$SRV_{B/A}$	WN6	BamHI/AgeI
SRV-WN7	pRev(1.4)-WN7-GFP	$SRV_{B/A}$	WN7	BamHI/AgeI
SRV-WN9	pRev(1.4)-WN9-GFP	$SRV_{B/A}$	WN9	BamHI/AgeI
SRV-WN13	pRev(1.4)-WN13-GFP	$SRV_{B/A}$	WN13	BamHI/AgeI
SRV-WN14	pRev(1.4)-WN14-GFP	$SRV_{B/A}$	WN14	BamHI/AgeI
SRV-WN15	pRev(1.4)-WN15-GFP	$SRV_{B/A}$	WN15	BamHI/AgeI
SRV-WN16	pRev(1.4)-WN16-GFP	$SRV_{B/A}$	WN16	BamHI/AgeI
SRV-WN17	pRev(1.4)-WN17-GFP	$SRV_{B/A}$	WN17	BamHI/AgeI
SRV-WN18	pRev(1.4)-WN18-GFP	$SRV_{B/A}$	WN18	BamHI/AgeI
SRV-WN19	pRev(1.4)-WN19-GFP	$SRV_{B/A}$	WN19	BamHI/AgeI
SRV-WN20	pRev(1.4)-WN20-GFP	$SRV_{B/A}$	WN20	BamHI/AgeI
SRV-Rev1	pRev(1.4)-Rev1-GFP	$SRV_{B/A}$	Rev1	BamHI/AgeI
SRV-Rev4	pRev(1.4)-Rev4-GFP	$SRV_{B/A}$	Rev4	BamHI/AgeI
SRV-Rev5	pRev(1.4)-Rev5-GFP	$SRV_{B/A}$	Rev5	BamHI/AgeI
SRV-Rev6	pRev(1.4)-Rev6-GFP	$SRV_{B/A}$	Rev6	BamHI/AgeI
SRV-Rev7	pRev(1.4)-Rev7-GFP	$SRV_{B/A}$	Rev7	BamHI/AgeI
SRV-Rev9	pRev(1.4)-Rev9-GFP	$SRV_{B/A}$	Rev9	BamHI/AgeI

14. taula gehigarria: Hibridazioz sortutako plasmidoak. Taulan plasmido berriaren izena, bektorea eta intsertoa, zein murrizte-entzimekin klonatu den eta hibridazioan erabilitako aurreranzko eta atzeranzko hasleak adierazten dira.

Plasmido berria	Bektorea	Intsertoa	Murrizte-entzimak	Aurreranzko haslea	Atzeranzko haslea
pEYFP(NLS)	pEYFP-C1	SV-40NLS	BglII/HindIII	UJAR206	UJAR207
pEYFP(2NLS)	pEYFP(NLS)	SV-40NLS	NheI/AgeI	UJAR208	UJAR209

15. taula gehigarria: Hibridaziorako erabilitako hasleen sekuentziak.

Haslea	5’ - 3’ sekuentzia
UJAR206	CTGCGTAGATCTGGAGGTCCAAAGAAGAAGAGGAAGGTGGGAGGTCAAGCTTCGCAC
UJAR207	GTGCGAAGCTTGACCTCCCACCTTCCTCTTCTTCTTTGGACCTCCAGATCTACGCAG
UJAR208	CGATCCGCTAGCGGCCACCATGCCAAAGAAGAAGAGGAAGGTGCTACCGGTCGCCAC
UJAR209	GTGGCGACCGGTAGCACCTTCCTCTTCTTCTTTGGCATGGTGGCCGCTAGCGGATCG

16. taula gehigarria: PCR bidez sortutako plasmidoak. Taulan plasmido berriaren izena, bektorea eta intsertoa, zein murrizte-entzimekin klonatu den eta PCRan erabilitako aurreranzko eta atzeranzko hasleak eta DNA moldea adierazten dira.

Plasmido berria	Bektorea	Intsertoa	Murrizte-entzimak	Aurrerazko haslea	Atzeranzko haslea	DNA moldea
pEYFP(2X)	pEYFP-C1	YFP	BglII/HindIII	UJAR202	UJAR203	pEYFP-C1
pEYFP(2X)-APEX2	pEYFP(2X)	APEX2	KpnI/BamHI	UJAR204	UJAR205	pcDNA3 APEX2-NES
pEYFP(3X)-APEX2	pEYFP(2X)-APEX2	YFP	BglII/BglII	UJAR202	UJAR212	pEYFP-C1
pEYFP-RIP3^{NES}-APEX2	pEYFP-RIP3^{NES}	APEX2	KpnI/BamHI	UJAR204	UJAR205	pcDNA3 APEX2-NES
pEYFP(2NLS)-APEX2	pEYFP(2NLS)	APEX2	KpnI/BamHI	UJAR204	UJAR205	pcDNA3 APEX2-NES
YFP-WDR20 (1-390)	pEYFP-C1	WDR20 (1-390)	HindIII/BamHI	MSM1	MSM2	YFP-WDR20
YFP-WDR20 (390-510)	pEYFP-C1	WDR20 (390-510)	HindIII/BamHI	MSM3	MSM4	YFP-WDR20
YFP-WDR20 (510-569)	pEYFP-C1	WDR20 (510-569)	HindIII/BamHI	MSM5	MSM6	YFP-WDR20
pRev(1.4)-DMWD^{NES}-GFP	pRev(1.4)-GFP	DMWD^{NES}	BamHI/AgeI	MSM17	MSM18	Myc-DMWD

17. taula gehigarria: PCRrako erabilitako hasleen sekuentziak.

Haslea	5'-3' sekuentzia
UJAR202	CTGCGTAGATCTGTGAGCAAGGGCGAGGAG
UJAR203	GTGCGAAGCTTGCTTGTACAGCTCGTCCATG
UJAR204	TTGCTAGGTACCGGAAAGTCTTACCCAACTGTG
UJAR205	GACAACGGATCCTTAGTCCAGGGTCAGGCGCTC
UJAR212	GTGCGAAGATCTCTTGTACAGCTCGTCCATG
MSM1	TTCGTCAAGCTTCAATGGCGACGGAGGGAGG
MSM2	TATGCGGATCCTTAAGGGAAAAGGATATCTTCTG
MSM3	TTCGTCAAGCTTCACCTCACCAACCCCTCTCAAG
MSM4	TATGCGGATCCTTATCCCAGAGTTTTAGCAGGGTC
MSM5	TTCGTCAAGCTTCAGGAACGCCCCTGTGTCCTC
MSM6	TATGCGGATCCTTAAGGATTAAAACTTACCAC
MSM17	CTGACGGATCCAGAGCCTGGCACACCATTC
MSM18	GTAAGACCGGTGGCCGCTCCTGCAGTGTGAG

18. taula gehigarria: gBlock bidez sortutako plasmidoak. Taulan plasmido berriaren izena, bektorea eta intsertoa, zein murrizte-entzimekin klonatu den eta gblockaren izena adierazten dira. gBlocken sekuentziak 1. zerrenda gehigarrian agertzen dira

Plasmido berria	Bektorea	Intsertoa	Murrizte-entzimak	gBlocka
pEYFP-pUL69^{NES}	pEYFP-C1	pUL69^{NES}	HindIII/EcoRI	Apexcyt 1
pEYFP-RIP3^{NES}	pEYFP-C1	RIP3^{NES}	HindIII/EcoRI	Apexcyt 1
pEYFP-(2X)pUL69^{NES}	pEYFP-C1	pUL69^{NES}-pUL69^{NES}	HindIII/EcoRI	Apexcyt 2

pEYFP-(2X)RIP3^{NES}	pEYFP-C1	RIP3^{NES}-RIP3^{NES}	HindIII/EcoRI	Apexcyt 2
sinGFP4a-RIP3^{NES}-APEX2 / APEX2zit	pEYFP-RIP3^{NES}-APEX2	sinGFP4a	NheI/BglII	sinGFP4a
pEYFP(4NLS)-APEX2 / APEX2nuk	pEYFP(2NLS)-APEX2	2Flag-3NLS	BglII/EcoRI	2Flag-3NLS
YFP-SBSN	pEYFP-C1	SBSN	HindIII/BamHI	SBSN
Myc-CK2α'	Myc-MSC	CK2a'	HindIII/BamHI	CK2α'
pRev(1.4)-USP12^{NES}-GFP	pRev(1.4)-GFP	USP12^{NES}	BamHI/AgeI	MSM6
YFP-USP12^{NESmut}	pEYFP-C1	USP12^{NESmut}	HindIII/BamHI	USP12-NESmut
pRev(1.4)-WDR20^{NES}-GFP	pRev(1.4)-GFP	WDR20^{NES}	BamHI/AgeI	WDR20-NES
pRev(1.4)-HKU^{NES}-GFP	pRev(1.4)-GFP	HKU^{NES}	BamHI/AgeI	CoV
pRev(1.4)-OC43^{NES}-GFP	pRev(1.4)-GFP	OC43^{NES}	BamHI/AgeI	CoV
pRev(1.4)-SARS2^{NES}-GFP	pRev(1.4)-GFP	SARS^{NES}	BamHI/AgeI	CoV
pRev(1.4)-MERS^{NES}-GFP	pRev(1.4)-GFP	MERS^{NES}	BamHI/AgeI	CoV
pRev(1.4)-229E^{NES}-GFP	pRev(1.4)-GFP	229E^{NES}	BamHI/AgeI	CoV
pRev(1.4)-NL63^{NES}-GFP	pRev(1.4)-GFP	NL63^{NES}	BamHI/AgeI	CoV
YFP-NL63-N	pEYFP-C1	NL63-N	HindIII/BamHI	NL63-N
YFP-SarsCoV2-N	pEYFP-C1	SARS-CoV2-N	HindIII/BamHI	SC2-N
pRev(1.4)-WN1-GFP	pRev(1.4)-GFP	WN1	BamHI/AgeI	NES1
pRev(1.4)-WN2-GFP	pRev(1.4)-GFP	WN2	BamHI/AgeI	NES1
pRev(1.4)-WN3-GFP	pRev(1.4)-GFP	WN3	BamHI/AgeI	NES1
pRev(1.4)-WN4-GFP	pRev(1.4)-GFP	WN4	BamHI/AgeI	NES1
pRev(1.4)-WN5-GFP	pRev(1.4)-GFP	WN5	BamHI/AgeI	NES1
pRev(1.4)-WN6-GFP	pRev(1.4)-GFP	WN6	BamHI/AgeI	NES1
pRev(1.4)-WN7-GFP	pRev(1.4)-GFP	WN7	BamHI/AgeI	NES2
pRev(1.4)-WN8-GFP	pRev(1.4)-GFP	WN8	BamHI/AgeI	NES2, NES5
pRev(1.4)-WN9-GFP	pRev(1.4)-GFP	WN9	BamHI/AgeI	NES2
pRev(1.4)-WN10-GFP	pRev(1.4)-GFP	WN10	BamHI/AgeI	NES2, NES5
pRev(1.4)-WN11-GFP	pRev(1.4)-GFP	WN11	BamHI/AgeI	NES3
pRev(1.4)-WN12-GFP	pRev(1.4)-GFP	WN12	BamHI/AgeI	NES2
pRev(1.4)-WN13-GFP	pRev(1.4)-GFP	WN13	BamHI/AgeI	NES2, NES5
pRev(1.4)-WN14-GFP	pRev(1.4)-GFP	WN14	BamHI/AgeI	NES2
pRev(1.4)-WN15-GFP	pRev(1.4)-GFP	WN15	BamHI/AgeI	NES2
pRev(1.4)-WN16-GFP	pRev(1.4)-GFP	WN16	BamHI/AgeI	NES2, MSM4
pRev(1.4)-WN17-GFP	pRev(1.4)-GFP	WN17	BamHI/AgeI	NES2, NES5
pRev(1.4)-WN18-GFP	pRev(1.4)-GFP	WN18	BamHI/AgeI	NES2, NES5, MSM4
pRev(1.4)-WN19-GFP	pRev(1.4)-GFP	WN19	BamHI/AgeI	NES3
pRev(1.4)-WN20-GFP	pRev(1.4)-GFP	WN20	BamHI/AgeI	NES2, NES5
pRev(1.4)-WN21-GFP	pRev(1.4)-GFP	WN21	BamHI/AgeI	NES2
pRev(1.4)-WN22-GFP	pRev(1.4)-GFP	WN22	BamHI/AgeI	NES3, NES6
pRev(1.4)-WN23-GFP	pRev(1.4)-GFP	WN23	BamHI/AgeI	NES5, MSM6
pRev(1.4)-WN24-GFP	pRev(1.4)-GFP	WN24	BamHI/AgeI	NES3
pRev(1.4)-WN25-GFP	pRev(1.4)-GFP	WN25	BamHI/AgeI	NES3
pRev(1.4)-WN26-GFP	pRev(1.4)-GFP	WN26	BamHI/AgeI	NES3, NES6

pRev(1.4)-Rev1-GFP	pRev(1.4)-GFP	Rev1	BamHI/AgeI	NES4
pRev(1.4)-Rev2-GFP	pRev(1.4)-GFP	Rev2	BamHI/AgeI	NES4, NES6, MSM4, MSM6
pRev(1.4)-Rev3-GFP	pRev(1.4)-GFP	Rev3	BamHI/AgeI	NES4
pRev(1.4)-Rev4-GFP	pRev(1.4)-GFP	Rev4	BamHI/AgeI	NES4
pRev(1.4)-Rev5-GFP	pRev(1.4)-GFP	Rev5	BamHI/AgeI	NES4
pRev(1.4)-Rev6-GFP	pRev(1.4)-GFP	Rev6	BamHI/AgeI	NES4
pRev(1.4)-Rev7-GFP	pRev(1.4)-GFP	Rev7	BamHI/AgeI	NES4
pRev(1.4)-Rev8-GFP	pRev(1.4)-GFP	Rev8	BamHI/AgeI	NES4
pRev(1.4)-Rev9-GFP	pRev(1.4)-GFP	Rev9	BamHI/AgeI	NES4
pRev(1.4)-Rev10-GFP	pRev(1.4)-GFP	Rev10	BamHI/AgeI	NES4, NES6
$SRV_{B/A}$	SRV100	$SRV_{B/A}$	BglII/NotI	SRVB/A
SRV-MICROP-1	$SRV_{B/A}$	MICROP-1	BamHI/AgeI	MICROP-NES1
SRV-MICROP-2	$SRV_{B/A}$	MICROP-2	BamHI/AgeI	MICROP-NES1
SRV-MICROP-5	$SRV_{B/A}$	MICROP-5	BamHI/AgeI	MICROP-NES1
SRV-MICROP-6	$SRV_{B/A}$	MICROP-6	BamHI/AgeI	MICROP-NES2
SRV-MICROP-7	$SRV_{B/A}$	MICROP-7	BamHI/AgeI	MICROP-NES2
SRV-MICROP-9	$SRV_{B/A}$	MICROP-9	BamHI/AgeI	MICROP-NES2
SRV-MICROP-10	$SRV_{B/A}$	MICROP-10	BamHI/AgeI	MICROP-NES2
YFP-SPROHSA141543	pEYFP-C1	SPROHSA141543	HindIII/BamHI	MP osoak
YFP-SPROHSA010409	pEYFP-C1	SPROHSA010409	HindIII/BamHI	MP osoak/ SPROHSA010409
SRV-PKI	$SRV_{B/A}$	PKI	BamHI/AgeI	NES7
SRV-superPKI	$SRV_{B/A}$	superPKI	BamHI/AgeI	Fung1
SRV-PAX	$SRV_{B/A}$	PAX	BamHI/AgeI	Fung2
SRV-HDAC5	$SRV_{B/A}$	HDAC5	BamHI/AgeI	Fung2
SRV-FMRP	$SRV_{B/A}$	FMRP	BamHI/AgeI	Fung2,MSM4
SRV-FMRP-1b	$SRV_{B/A}$	FMRP-1b	BamHI/AgeI	NES7
SRV-SNUPN	$SRV_{B/A}$	SNUPN	BamHI/AgeI	SNUPN
SRV-Rev	$SRV_{B/A}$	Rev	BamHI/AgeI	Fung1
SRV-SMAD4	$SRV_{B/A}$	SMAD4	BamHI/AgeI	Fung2
SRV-mDia2	$SRV_{B/A}$	mDia2	BamHI/AgeI	Fung1
SRV-CDC7	$SRV_{B/A}$	CDC7	BamHI/AgeI	Fung1
SRV-X11L2	$SRV_{B/A}$	X11L2	BamHI/AgeI	Fung2
SRV-CPEB4	$SRV_{B/A}$	CPEB4	BamHI/AgeI	Fung1
SRV-hRio2	$SRV_{B/A}$	hRio2	BamHI/AgeI	NES7
SRV-COMMD1	$SRV_{B/A}$	COMMD1	BamHI/AgeI	inactives
SRV-Hxk2	$SRV_{B/A}$	Hxk2	BamHI/AgeI	inactives
SRV-DEAF1	$SRV_{B/A}$	DEAF1	BamHI/AgeI	inactives
Myc-RanQ69L	Myc-MSC	RanQ69L	HindIII/BamHI	RanQ69L

19. taula gehigarria: Gunera zuzenduriko mutagenesi bidez sortutako plasmidoak. Taulan plasmido berriaren izena, erabilitako DNA moldea, eta aurreranzko zein atzeranzko hasleak adierazten dira.

Plasmido berria	DNA moldea	Aurreranzko haslea	Atzeranzko haslea
YFP-WDR20^{NESmut}	YFP-WDR20	MSM9	MSM10
YFP-CRM1 K568A	YFP-CRM1	MSM7	MSM8
YFP-CRM1 I521	YFP-CRM1	UJAR221	UJAR222
YFP-CRM1 L525A	YFP-CRM1	UJAR142	UJAR143
YFP-CRM1 F561A	YFP-CRM1	UJAR144	UJAR145

20. taula gehigarria: Gunera zuzenduriko mutagenesian erabilitako hasleen sekuentziak.

Haslea	sekuentzia (5'-3')
MSM9	AGCAAATTTGCAACAGCTTCAGCACATGACCGGAAGGAGAGGCACCACGAG
MSM10	TCTCCTTCCGGTCATGTGCTGAAGCTGTTGCAAATTTGCTGACCCCAGAAG
MSM7	AGACTGTAGTTAACGCGCTGTTCGAATTCATGCATGAGACCC
MSM8	GCATGAATTCGAACAGCGCGTTAACTACAGTCTTCAGAAATTTCC
UJAR221	AAACGATTTCTTGTTACTGTTGCAAAGGATCTATTAGGATTATGTGAACAG
UJAR222	AATCCTAATAGATCCTTTGCAACAGTAACAAGAAATCGTTTTTCGTCCTC
UJAR142	GTTGCAAAGGATCTAGCAGGATTATGTGAACAGAAAAGAGGCAAAG
UJAR143	GCCTCTTTTCTGTTCACATAATCCTGCTAGATCCTTTATAACAGTAAC
UJAR144	GAGAGCTCACTGGAAA**GC**TCTGAAGACTGTAGTTAACAAGCTG
UJAR145	CTACAGTCTTCAGAGCTTTCCAGTGAGCTCTCAAAAAACGTGG

21. taula gehigarria: Sekuentziazioan erabilitako hasleen sekuentziak.

Haslea	sekuentzia (5'-3')	Noranzkoa	Hibridazio-itua
UJAR17	agtccgccctgagcaaag	Aurreranzkoa	pEYFP-C1
UJAR18bis	aaacaagttaacaacaac	Atzeranzkoa	pEYFP-C1
UJAR49	gacgcaaatgggcggtag	Aurreranzkoa	pEYFP-C1
CRM1 seq1	tggtacagagtggtcatgg	Aurreranzkoa	CRM1
CRM1 seq2	ggatctattaggattatgtg	Aurreranzkoa	CRM1
CRM1 seq3	tcacttctccaacctgaacc	Atzeranzkoa	CRM1
CRM1 seq4	tgaacctgttgaggctgaag	Atzeranzkoa	CRM1
CRM1 seq5	tggaaatccagttaacaacc	Aurreranzkoa	CRM1
CRM1 seq6	ggatatattttgagacc	Aurreranzkoa	CRM1
CRM1 seq7	aatgtatacaagtgcctc	Aurreranzkoa	CRM1
MSM2	tatgcggatccttaagggaaaaggatatcttctg	Atzeranzkoa	WDR20
MSM3	ttcgtcaagcttcacctcaccaacccctctcaag	Aurreranzkoa	WDR20
MSM4	tatgcggatccttatcccagagttttagcagggtc	Atzeranzkoa	WDR20
MSM18	gtaagaccggtggccgctcctgcagtgtgag	Atzeranzkoa	DMWD
MSM19	gggttgatgaaatcttacgctggcggcctgctgtgtgtg	Aurreranzkoa	DMWD
MSM32	atagactggggtttggctg	Aurreranzkoa	CK2a'
MSM33	atggctccttccgaaagatc	Atzeranzkoa	CK2a'

<u>22. taula gehigarria:</u> CRM1en minbizi esportomako proteinak Kirli et al., 2015-en definitutako kargo kategorien arabera ordenatuta. / <u>Supplementary Table 22:</u> CRM1 cancer-exportome proteins classified in the categories defined in Kirli et al., 2015

Uniprot ID	Kargo mota / Cargo classification (Kirli et al., 2015)
>sp|Q96IF1|AJUBA_HUMAN	Cargo A
>sp|P63010|AP2B1_HUMAN	Cargo A
>sp|O14965|AURKA_HUMAN	Cargo A
>sp|O95999|BCL10_HUMAN	Cargo A
>sp|P11274|BCR_HUMAN	Cargo A
>sp|O60566|BUB1B_HUMAN	Cargo A
>sp|P22681|CBL_HUMAN	Cargo A
>sp|Q16204|CCDC6_HUMAN	Cargo A
>sp|P14635|CCNB1_HUMAN	Cargo A
>sp|Q12834|CDC20_HUMAN	Cargo A
>sp|P30260|CDC27_HUMAN	Cargo A
>sp|Q6P1J9|CDC73_HUMAN	Cargo A
>sp|O75175|CNOT3_HUMAN	Cargo A
>sp|Q6UUV9|CRTC1_HUMAN	Cargo A
>sp|Q6UUV7|CRTC3_HUMAN	Cargo A
>sp|O75534|CSDE1_HUMAN	Cargo A
>sp|P49674|KC1E_HUMAN	Cargo A
>sp|P67870|CSK2B_HUMAN	Cargo A
>sp|O60716|CTND1_HUMAN	Cargo A
>sp|P17844|DDX5_HUMAN	Cargo A
>sp|P26196|DDX6_HUMAN	Cargo A
>sp|Q9NSV4|DIAP3_HUMAN	Cargo A
>sp|P11532|DMD_HUMAN	Cargo A
>sp|Q92997|DVL3_HUMAN	Cargo A
>sp|P20042|IF2B_HUMAN	Cargo A
>sp|P60228|EIF3E_HUMAN	Cargo A
>sp|O15372|EIF3H_HUMAN	Cargo A
>sp|P42566|EPS15_HUMAN	Cargo A
>sp|O95684|FR1OP_HUMAN / >sp|O95684|CEP43_HUMAN	Cargo A
>sp|P62873|GBB1_HUMAN	Cargo A
>sp|Q13322|GRB10_HUMAN	Cargo A
>sp|Q9Y4H2|IRS2_HUMAN	Cargo A
>sp|Q14145|KEAP1_HUMAN	Cargo A
>sp|Q9UNF1|MAGD2_HUMAN	Cargo A
>sp|Q9UDY8|MALT1_HUMAN	Cargo A
>sp|Q13164|MK07_HUMAN	Cargo A
>sp|P42345|MTOR_HUMAN	Cargo A
>sp|P01106|MYC_HUMAN	Cargo A
>sp|Q9NZQ3|SPN90_HUMAN	Cargo A
>sp|Q96PU5|NED4L_HUMAN	Cargo A
>sp|P25963|IKBA_HUMAN	Cargo A
>sp|O00221|IKBE_HUMAN	Cargo A
>sp|P49757|NUMB_HUMAN	Cargo A
>sp|Q13442|HAP28_HUMAN	Cargo A
>sp|Q9BRP1|PDD2L_HUMAN	Cargo A
>sp|Q13492|PICAL_HUMAN	Cargo A

>sp|O00743|PPP6_HUMAN	Cargo A
>sp|Q13162|PRDX4_HUMAN	Cargo A
>sp|P10644|KAP0_HUMAN	Cargo A
>sp|P04049|RAF1_HUMAN	Cargo A
>sp|Q01201|RELB_HUMAN	Cargo A
>sp|P15880|RS2_HUMAN	Cargo A
>sp|P23396|RS3_HUMAN	Cargo A
>sp|Q15019|SEPT2_HUMAN	Cargo A
>sp|Q14141|SEPT6_HUMAN	Cargo A
>sp|Q9UHD8|SEPT9_HUMAN	Cargo A
>sp|Q15047|SETB1_HUMAN	Cargo A
>sp|Q8IXJ6|SIR2_HUMAN	Cargo A
>sp|Q13485|SMAD4_HUMAN	Cargo A
>sp|Q01130|SRSF2_HUMAN	Cargo A
>sp|Q9BZK7|TBL1R_HUMAN	Cargo A
>sp|Q99081|HTF4_HUMAN	Cargo A
>sp|P15923|TFE2_HUMAN	Cargo A
>sp|P19532|TFE3_HUMAN	Cargo A
>sp|P19484|TFEB_HUMAN	Cargo A
>sp|Q9Y2W1|TR150_HUMAN	Cargo A
>sp|Q9UDY2|ZO2_HUMAN	Cargo A
>sp|O60784|TOM1_HUMAN	Cargo A
>sp|Q99816|TS101_HUMAN	Cargo A
>sp|O95071|UBR5_HUMAN	Cargo A
>sp|Q9H6R7|CB044_HUMAN / >sp|Q9H6R7|WDCP_HUMAN	Cargo A
>sp|P30291|WEE1_HUMAN	Cargo A
>sp|P23025|XPA_HUMAN	Cargo A
>sp|P67809|YBOX1_HUMAN	Cargo A
>sp|Q07352|TISB_HUMAN	Cargo A
>sp|P47974|TISD_HUMAN	Cargo A
>sp|P35869|AHR_HUMAN	Cargo B
>sp|P05090|APOD_HUMAN	Cargo B
>sp|Q9NYF8|BCLF1_HUMAN	Cargo B
>sp|O15234|CASC3_HUMAN	Cargo B
>sp|O95067|CCNB2_HUMAN	Cargo B
>sp|P19784|CSK22_HUMAN	Cargo B
>sp|O00571|DDX3X_HUMAN	Cargo B
>sp|P35659|DEK_HUMAN	Cargo B
>sp|P18074|ERCC2_HUMAN	Cargo B
>sp|Q12778|FOXO1_HUMAN	Cargo B
>sp|O43524|FOXO3_HUMAN	Cargo B
>sp|P63092|GNAS2_HUMAN	Cargo B
>sp|O15357|SHIP2_HUMAN	Cargo B
>sp|Q13887|KLF5_HUMAN	Cargo B
>sp|P31025|LCN1_HUMAN	Cargo B
>sp|Q93052|LPP_HUMAN	Cargo B
>sp|P36507|MP2K2_HUMAN	Cargo B
>sp|P49137|MAPK2_HUMAN	Cargo B
>sp|P61244|MAX_HUMAN	Cargo B
>sp|Q02078|MEF2A_HUMAN	Cargo B
>sp|O75030|MITF_HUMAN	Cargo B
>sp|Q969V6|MKL1_HUMAN MKL /	Cargo B

>sp|Q969V6|MRTFA_HUMAN	
>sp|Q9Y6Q9|NCOA3_HUMAN	Cargo B
>sp|P19838|NFKB1_HUMAN	Cargo B
>sp|Q00653|NFKB2_HUMAN	Cargo B
>sp|P11940|PABP1_HUMAN	Cargo B
>sp|O15534|PER1_HUMAN	Cargo B
>sp|P41743|KPCI_HUMAN	Cargo B
>sp|O95997|PTTG1_HUMAN	Cargo B
>sp|Q04864|REL_HUMAN	Cargo B
>sp|Q04206|TF65_HUMAN	Cargo B
>sp|P46777|RL5_HUMAN	Cargo B
>sp|P31151|S10A7_HUMAN	Cargo B
>sp|Q9Y3F4|STRAP_HUMAN	Cargo B
>sp|Q9UPN9|TRI33_HUMAN	Cargo B
>sp|Q6NZY4|ZCHC8_HUMAN	Cargo B
>sp|Q5JTC6|AMER1_HUMAN	Low abundant cargo
>sp|Q96GD4|AURKB_HUMAN	Low abundant cargo
>sp|O15169|AXIN1_HUMAN	Low abundant cargo
>sp|P30305|MPIP2_HUMAN	Low abundant cargo
>sp|P35222|CTNB1_HUMAN	Low abundant cargo
>sp|Q9NQC7|CYLD_HUMAN	Low abundant cargo
>sp|Q9NRR4|RNC_HUMAN	Low abundant cargo
>sp|O15287|FANCG_HUMAN	Low abundant cargo
>sp|Q6UN15|FIP1_HUMAN	Low abundant cargo
>sp|Q9UQL6|HDAC5_HUMAN	Low abundant cargo
>sp|Q13233|M3K1_HUMAN	Low abundant cargo
>sp|Q99759|M3K3_HUMAN	Low abundant cargo
>sp|Q93074|MED12_HUMAN	Low abundant cargo
>sp|P42568|AF9_HUMAN	Low abundant cargo
>sp|Q13772|NCOA4_HUMAN	Low abundant cargo
>sp|Q15233|NONO_HUMAN	Low abundant cargo
>sp|P60201|MYPR_HUMAN	Low abundant cargo
>sp|Q92733|PRCC_HUMAN	Low abundant cargo
>sp|Q9BYW2|SETD2_HUMAN	Low abundant cargo
>sp|Q15797|SMAD1_HUMAN	Low abundant cargo
>sp|Q969G3|SMCE1_HUMAN	Low abundant cargo
>sp|O60347|TBC12_HUMAN	Low abundant cargo
>sp|Q15650|TRIP4_HUMAN	Low abundant cargo
>sp|O43542|XRCC3_HUMAN	Low abundant cargo

<u>23. taula gehigarria:</u> Wregex (Prieto et al., 2014) eta NESmapper (Kosugi et al., 2014) NES iragarleak erabiliz CRM1en minbizi-esportomako A eta B kargoetan aurkitutako *plus* NES kandidatu zerrenda.

https://drive.google.com/file/d/1-ep1p8NHbGzKjxeNndd9hpL6QwmPdvsK/view?usp=sharing

<u>24. taula gehigarria:</u> Wregex (Prieto et al., 2014) eta NESmapper (Kosugi et al., 2014) NES iragarleak erabiliz CRM1en minbizi-esportomako A eta B kargoetan aurkitutako *minus* NES kandidatu zerrenda.

https://drive.google.com/file/d/1kDBMum9jv-ErvKBCNFQtGLrqgvOqz3zS/view?usp=sharing

<u>25. taula gehigarria:</u> Wregex (Prieto et al., 2014) eta NESmapper (Kosugi et al., 2014) NES iragarleak erabiliz SmProt datu-baseko mikropeptidoetan aurkitutako NES kandidatu zerrenda. / <u>Supplementary Table 25:</u> cNESs found in SmProt micropeptides database using Wregex (Prieto et al., 2014) and NESmapper (Kosugi et al., 2014) NES predictors.

https://drive.google.com/file/d/1hL6WVycPfv0elnVuXW_O5uiu1oseAUYA/view?usp=sharing

<u>26. taula gehigarria:</u> Muturreko kargo ez-prototipiko bezala identifikatutako proteinak. Taulan Uniproteko sarrera, genea eta proteinaren izena adierazten dira.

Uniprot sarrera	Genea	Proteina
HNRC2_HUMAN	*HNRNPCL2 HNRNPCP5*	Heterogeneous nuclear ribonucleoprotein C-like 2 (hnRNP C-like-2)
HNRC3_HUMAN	*HNRNPCL3*	Heterogeneous nuclear ribonucleoprotein C-like 3
DX39A_HUMAN	*DDX39A DDX39*	ATP-dependent RNA helicase DDX39A (EC 3.6.4.13) (DEAD box protein 39) (Nuclear RNA helicase URH49)
PSD12_HUMAN	*PSMD12*	26S proteasome non-ATPase regulatory subunit 12 (26S proteasome regulatory subunit RPN5) (26S proteasome regulatory subunit p55)
PGRC1_HUMAN	*PGRMC1 HPR6.6 PGRMC*	Membrane-associated progesterone receptor component 1 (mPR) (Dap1) (IZA)
DFFA_HUMAN	*DFFA DFF1 DFF45 H13*	DNA fragmentation factor subunit alpha (DNA fragmentation factor 45 kDa subunit) (DFF-45) (Inhibitor of CAD) (ICAD)
HNRC1_HUMAN	*HNRNPCL1 HNRPCL1*	Heterogeneous nuclear ribonucleoprotein C-like 1 (hnRNP C-like-1) (hnRNP core protein C-like 1)
NPM3_HUMAN	*NPM3*	Nucleoplasmin-3
SPN1_HUMAN	*SNUPN RNUT1 SPN1*	Snurportin-1 (RNA U transporter 1)
HNRPC_HUMAN	*HNRNPC HNRPC*	Heterogeneous nuclear ribonucleoproteins C1/C2 (hnRNP C1/C2)
HNRC4_HUMAN	*HNRNPCL4*	Heterogeneous nuclear ribonucleoprotein C-like 4
HARS1_HUMAN	*HARS1 HARS HRS*	Histidine--tRNA ligase, cytoplasmic (EC 6.1.1.21) (Histidyl-tRNA synthetase) (HisRS)
TPR_HUMAN	*TPR*	Nucleoprotein TPR (Megator) (NPC-associated intranuclear protein) (Translocated promoter region protein)
TCTP_HUMAN	*TPT1*	Translationally-controlled tumor protein (TCTP) (Fortilin) (Histamine-releasing factor) (HRF) (p23)
NDKA_HUMAN	*NME1 NDPKA NM23*	Nucleoside diphosphate kinase A (NDK A) (NDP kinase A) (EC 2.7.4.6) (Granzyme A-activated DNase) (GAAD) (Metastasis inhibition factor nm23) (NM23-H1) (Tumor metastatic process-associated protein)
NUCL_HUMAN	*NCL*	Nucleolin (Protein C23)
RAB6A_HUMAN	*RAB6A RAB6*	Ras-related protein Rab-6A (Rab-6)
IMDH1_HUMAN	*IMPDH1 IMPD1*	Inosine-5'-monophosphate dehydrogenase 1 (IMP dehydrogenase 1) (IMPD 1) (IMPDH 1) (EC 1.1.1.205) (IMPDH-I)
NDKB_HUMAN	*NME2 NM23B*	Nucleoside diphosphate kinase B (NDK B) (NDP kinase B) (EC 2.7.4.6) (C-myc purine-binding transcription factor PUF) (Histidine protein kinase NDKB) (EC 2.7.13.3) (nm23-H2)
PSA5_HUMAN	*PSMA5*	Proteasome subunit alpha type-5 (Macropain zeta chain) (Multicatalytic endopeptidase complex zeta chain) (Proteasome zeta chain)

PUR8_HUMAN	*ADSL AMPS*	Adenylosuccinate lyase (ADSL) (ASL) (EC 4.3.2.2) (Adenylosuccinase) (ASase)
PP1G_HUMAN	*PPP1CC*	Serine/threonine-protein phosphatase PP1-gamma catalytic subunit (PP-1G) (EC 3.1.3.16) (Protein phosphatase 1C catalytic subunit)
IMA1_HUMAN	*KPNA2 RCH1 SRP1*	Importin subunit alpha-1 (Karyopherin subunit alpha-2) (RAG cohort protein 1) (SRP1-alpha)
BID_HUMAN	*BID*	BH3-interacting domain death agonist (p22 BID) (BID) [Cleaved into: BH3-interacting domain death agonist p15 (p15 BID); BH3-interacting domain death agonist p13 (p13 BID); BH3-interacting domain death agonist p11 (p11 BID)]
PP4C_HUMAN	*PPP4C PPP4 PPX*	Serine/threonine-protein phosphatase 4 catalytic subunit (PP4C) (Pp4) (EC 3.1.3.16) (Protein phosphatase X) (PP-X)
RAN_HUMAN	*RAN ARA24 OK/SW-cl.81*	GTP-binding nuclear protein Ran (Androgen receptor-associated protein 24) (GTPase Ran) (Ras-like protein TC4) (Ras-related nuclear protein)
2ABA_HUMAN	*PPP2R2A*	Serine/threonine-protein phosphatase 2A 55 kDa regulatory subunit B alpha isoform (PP2A subunit B isoform B55-alpha) (PP2A subunit B isoform PR55-alpha) (PP2A subunit B isoform R2-alpha) (PP2A subunit B isoform alpha)
SKP1_HUMAN	*SKP1 EMC19 OCP2 SKP1A TCEB1L*	S-phase kinase-associated protein 1 (Cyclin-A/CDK2-associated protein p19) (p19A) (Organ of Corti protein 2) (OCP-2) (Organ of Corti protein II) (OCP-II) (RNA polymerase II elongation factor-like protein) (SIII) (Transcription elongation factor B polypeptide 1-like) (p19skp1)
TBB4B_HUMAN	*TUBB4B TUBB2C*	Tubulin beta-4B chain (Tubulin beta-2 chain) (Tubulin beta-2C chain)
GTF2I_HUMAN	*GTF2I BAP135 WBSCR6*	General transcription factor II-I (GTFII-I) (TFII-I) (Bruton tyrosine kinase-associated protein 135) (BAP-135) (BTK-associated protein 135) (SRF-Phox1-interacting protein) (SPIN) (Williams-Beuren syndrome chromosomal region 6 protein)
TCPB_HUMAN	*CCT2 99D8.1 CCTB*	T-complex protein 1 subunit beta (TCP-1-beta) (CCT-beta)
RBM10_HUMAN	*RBM10 DXS8237E GPATC9 GPATCH9 KIAA0122*	RNA-binding protein 10 (G patch domain-containing protein 9) (RNA-binding motif protein 10) (RNA-binding protein S1-1) (S1-1)
2ABB_HUMAN	*PPP2R2B*	Serine/threonine-protein phosphatase 2A 55 kDa regulatory subunit B beta isoform (PP2A subunit B isoform B55-beta) (PP2A subunit B isoform PR55-beta) (PP2A subunit B isoform R2-beta) (PP2A subunit B isoform beta)
LMNB2_HUMAN	*LMNB2 LMN2*	Lamin-B2
UBXN1_HUMAN	*UBXN1 SAKS1*	UBX domain-containing protein 1 (SAPK substrate protein 1) (UBA/UBX 33.3 kDa protein)
KHDR1_HUMAN	*KHDRBS1 SAM68*	KH domain-containing, RNA-binding, signal transduction-associated protein 1 (GAP-associated tyrosine phosphoprotein p62) (Src-associated in mitosis 68 kDa protein) (Sam68) (p21 Ras GTPase-activating protein-associated p62) (p68)
FHL1_HUMAN	*FHL1 SLIM1*	Four and a half LIM domains protein 1 (FHL-1) (Skeletal muscle LIM-protein 1) (SLIM) (SLIM-1)
DX39B_HUMAN	*DDX39B BAT1 UAP56*	Spliceosome RNA helicase DDX39B (EC 3.6.4.13) (56 kDa U2AF65-associated protein) (ATP-dependent RNA helicase p47) (DEAD box protein UAP56) (HLA-B-associated transcript 1 protein)

TBB2A_HUMAN	*TUBB2A TUBB2*	Tubulin beta-2A chain (Tubulin beta class IIa)
FA50A_HUMAN	*FAM50A DXS9928E HXC26 XAP5*	Protein FAM50A (Protein HXC-26) (Protein XAP-5)
MCM6_HUMAN	*MCM6*	DNA replication licensing factor MCM6 (EC 3.6.4.12) (p105MCM)
RB39A_HUMAN	*RAB39A RAB39*	Ras-related protein Rab-39A (Rab-39)
PSMD6_HUMAN	*PSMD6 KIAA0107 PFAAP4*	26S proteasome non-ATPase regulatory subunit 6 (26S proteasome regulatory subunit RPN7) (26S proteasome regulatory subunit S10) (Breast cancer-associated protein SGA-113M) (Phosphonoformate immuno-associated protein 4) (Proteasome regulatory particle subunit p44S10) (p42A)
TEBP_HUMAN	*PTGES3 P23 TEBP*	Prostaglandin E synthase 3 (EC 5.3.99.3) (Cytosolic prostaglandin E2 synthase) (cPGES) (Hsp90 co-chaperone) (Progesterone receptor complex p23) (Telomerase-binding protein p23)
TRXR1_HUMAN	*TXNRD1 GRIM12 KDRF*	Thioredoxin reductase 1, cytoplasmic (TR) (EC 1.8.1.9) (Gene associated with retinoic and interferon-induced mortality 12 protein) (GRIM-12) (Gene associated with retinoic and IFN-induced mortality 12 protein) (KM-102-derived reductase-like factor) (Thioredoxin reductase TR1)
TPT1L_HUMAN		TPT1-like protein
PHF6_HUMAN	*PHF6 CENP-31 KIAA1823*	PHD finger protein 6 (PHD-like zinc finger protein)
P20D2_HUMAN	*PM20D2 ACY1L2*	Peptidase M20 domain-containing protein 2 (Aminoacylase-1-like protein 2)
ZN655_HUMAN	*ZNF655 VIK*	Zinc finger protein 655 (Vav-interacting Krueppel-like protein)
DAZP1_HUMAN	*DAZAP1*	DAZ-associated protein 1 (Deleted in azoospermia-associated protein 1)
UBA5_HUMAN	*UBA5 UBE1DC1*	Ubiquitin-like modifier-activating enzyme 5 (Ubiquitin-activating enzyme 5) (ThiFP1) (UFM1-activating enzyme) (Ubiquitin-activating enzyme E1 domain-containing protein 1)
JUPI2_HUMAN	*JPT2 C16orf34 HN1L L11*	Jupiter microtubule associated homolog 2 (Hematological and neurological expressed 1-like protein) (HN1-like protein)
GLOD4_HUMAN	*GLOD4 C17orf25 CGI-150 My027*	Glyoxalase domain-containing protein 4
RAB6B_HUMAN	*RAB6B*	Ras-related protein Rab-6B
OLA1_HUMAN	*OLA1 GTPBP9 PRO2455 PTD004*	Obg-like ATPase 1 (DNA damage-regulated overexpressed in cancer 45) (DOC45) (GTP-binding protein 9)
RPC5_HUMAN	*POLR3E KIAA1452*	DNA-directed RNA polymerase III subunit RPC5 (RNA polymerase III subunit C5) (DNA-directed RNA polymerase III 80 kDa polypeptide)
SAE1_HUMAN	*SAE1 AOS1 SUA1 UBLE1A*	SUMO-activating enzyme subunit 1 (Ubiquitin-like 1-activating enzyme E1A) [Cleaved into: SUMO-activating enzyme subunit 1, N-terminally processed]

TES_HUMAN	*TES*	Testin (TESS)
CSN3_HUMAN	*COPS3 CSN3*	COP9 signalosome complex subunit 3 (SGN3) (Signalosome subunit 3) (JAB1-containing signalosome subunit 3)
2ABG_HUMAN	*PPP2R2C*	Serine/threonine-protein phosphatase 2A 55 kDa regulatory subunit B gamma isoform (IMYPNO1) (PP2A subunit B isoform B55-gamma) (PP2A subunit B isoform PR55-gamma) (PP2A subunit B isoform R2-gamma) (PP2A subunit B isoform gamma)
HBS1L_HUMAN	*HBS1L HBS1 KIAA1038*	HBS1-like protein (ERFS)
ATG4B_HUMAN	*ATG4B APG4B AUTL1 KIAA0943*	Cysteine protease ATG4B (EC 3.4.22.-) (AUT-like 1 cysteine endopeptidase) (Autophagin-1) (Autophagy-related cysteine endopeptidase 1) (Autophagy-related protein 4 homolog B) (hAPG4B)
TX264_HUMAN	*TEX264 ZSIG11 UNQ337/PRO536*	Testis-expressed protein 264 (Putative secreted protein Zsig11)
MYPT1_HUMAN	*PPP1R12A MBS MYPT1*	Protein phosphatase 1 regulatory subunit 12A (Myosin phosphatase-targeting subunit 1) (Myosin phosphatase target subunit 1) (Protein phosphatase myosin-binding subunit)
JIP4_HUMAN	*SPAG9 HSS KIAA0516 MAPK8IP4 SYD1 HLC6*	C-Jun-amino-terminal kinase-interacting protein 4 (JIP-4) (JNK-interacting protein 4) (Cancer/testis antigen 89) (CT89) (Human lung cancer oncogene 6 protein) (HLC-6) (JNK-associated leucine-zipper protein) (JLP) (Mitogen-activated protein kinase 8-interacting protein 4) (Proliferation-inducing protein 6) (Protein highly expressed in testis) (PHET) (Sperm surface protein) (Sperm-associated antigen 9) (Sperm-specific protein) (Sunday driver 1)
BAG3_HUMAN	*BAG3 BIS*	BAG family molecular chaperone regulator 3 (BAG-3) (Bcl-2-associated athanogene 3) (Bcl-2-binding protein Bis) (Docking protein CAIR-1)
DNJB1_HUMAN	*DNAJB1 DNAJ1 HDJ1 HSPF1*	DnaJ homolog subfamily B member 1 (DnaJ protein homolog 1) (Heat shock 40 kDa protein 1) (HSP40) (Heat shock protein 40) (Human DnaJ protein 1) (hDj-1)
DCTN2_HUMAN	*DCTN2 DCTN50*	Dynactin subunit 2 (50 kDa dynein-associated polypeptide) (Dynactin complex 50 kDa subunit) (DCTN-50) (p50 dynamitin)
EPN4_HUMAN	*CLINT1 ENTH EPN4 EPNR KIAA0171*	Clathrin interactor 1 (Clathrin-interacting protein localized in the trans-Golgi region) (Clint) (Enthoprotin) (Epsin-4) (Epsin-related protein) (EpsinR)
CDV3_HUMAN	*CDV3 H41*	Protein CDV3 homolog
ASNS_HUMAN	*ASNS TS11*	Asparagine synthetase [glutamine-hydrolyzing] (EC 6.3.5.4) (Cell cycle control protein TS11) (Glutamine-dependent asparagine synthetase)
RAGP1_HUMAN	*RANGAP1 KIAA1835 SD*	Ran GTPase-activating protein 1 (RanGAP1)
CRK_HUMAN	*CRK*	Adapter molecule crk (Proto-oncogene c-Crk) (p38)
ACTZ_HUMAN	*ACTR1A CTRN1*	Alpha-centractin (Centractin) (ARP1) (Actin-RPV) (Centrosome-associated actin homolog)
AMPD2_HUMAN	*AMPD2*	AMP deaminase 2 (EC 3.5.4.6) (AMP deaminase isoform L)

UBE3A_HUMAN	*UBE3A E6AP EPVE6AP HPVE6A*	Ubiquitin-protein ligase E3A (EC 2.3.2.26) (E6AP ubiquitin-protein ligase) (HECT-type ubiquitin transferase E3A) (Human papillomavirus E6-associated protein) (Oncogenic protein-associated protein E6-AP) (Renal carcinoma antigen NY-REN-54)
LMAN2_HUMAN	*LMAN2 C5orf8*	Vesicular integral-membrane protein VIP36 (Glycoprotein GP36b) (Lectin mannose-binding 2) (Vesicular integral-membrane protein 36) (VIP36)
RIPK1_HUMAN	*RIPK1 RIP RIP1*	Receptor-interacting serine/threonine-protein kinase 1 (EC 2.7.11.1) (Cell death protein RIP) (Receptor-interacting protein 1) (RIP-1)
UBAP2_HUMAN	*UBAP2 KIAA1491*	Ubiquitin-associated protein 2 (UBAP-2)
DDI2_HUMAN	*DDI2*	Protein DDI1 homolog 2 (EC 3.4.23.-)
KAT3_HUMAN	*KYAT3 CCBL2 KAT3*	Kynurenine--oxoglutarate transaminase 3 (EC 2.6.1.7) (Cysteine-S-conjugate beta-lyase 2) (EC 4.4.1.13) (Kynurenine aminotransferase 3) (Kynurenine aminotransferase III) (KATIII) (Kynurenine--glyoxylate transaminase) (EC 2.6.1.63) (Kynurenine--oxoglutarate transaminase III)
MISSL_HUMAN	*MAPK1IP1L C14orf32*	MAPK-interacting and spindle-stabilizing protein-like (Mitogen-activated protein kinase 1-interacting protein 1-like)
TCPH_HUMAN	*CCT7 CCTH NIP7-1*	T-complex protein 1 subunit eta (TCP-1-eta) (CCT-eta) (HIV-1 Nef-interacting protein) [Cleaved into: T-complex protein 1 subunit eta, N-terminally processed]
GCP60_HUMAN	*ACBD3 GCP60 GOCAP1 GOLPH1*	Golgi resident protein GCP60 (Acyl-CoA-binding domain-containing protein 3) (Golgi complex-associated protein 1) (GOCAP1) (Golgi phosphoprotein 1) (GOLPH1) (PBR- and PKA-associated protein 7) (Peripheral benzodiazepine receptor-associated protein PAP7) [Cleaved into: Golgi resident protein GCP60, N-terminally processed]
GOPC_HUMAN	*GOPC CAL FIG*	Golgi-associated PDZ and coiled-coil motif-containing protein (CFTR-associated ligand) (Fused in glioblastoma) (PDZ protein interacting specifically with TC10) (PIST)
VTA1_HUMAN	*VTA1 C6orf55 HSPC228 My012*	Vacuolar protein sorting-associated protein VTA1 homolog (Dopamine-responsive gene 1 protein) (DRG-1) (LYST-interacting protein 5) (LIP5) (SKD1-binding protein 1) (SBP1)
PANK4_HUMAN	*PANK4*	4'-phosphopantetheine phosphatase (EC 3.1.3.-) (Inactive pantothenic acid kinase 4) (hPanK4)
ABCF2_HUMAN	*ABCF2 HUSSY-18*	ATP-binding cassette sub-family F member 2 (Iron-inhibited ABC transporter 2)
HDAC1_HUMAN	*HDAC1 RPD3L1*	Histone deacetylase 1 (HD1) (EC 3.5.1.98)

1. zerrenda gehigarria: Klonazioetan erabilitako gBlock-en deskribapen eta sekuentziak.

Apexcyt 1: pUL69 eta RIP3 proteinen banakako NES motiboak eta pUL69-RIP3 proteinen NES motiboen tandema. Tandemeko bi NESen artean hiru glizina aminoazido kodetzen dira. Motibo bakoitzaren 5' eta 3' muturretan HindIII eta EcoRI murriztegunеak daude.

5'- ctgc**aagctt**cagcacctccggcccaacctcccagtcaacctcaacagcattactcagagggtgaactgg
aagaggatgaggatagtgatgacgcctc**gaattc**gtactgga**aagctt**ctgggctgctgcaatcccaatg
tcctcggccatggccactcttgtgcagactgttaaaagaggttgtgttgggaatgttctatctgcatgac
caaaacccagtgttactgcatcgggattc**gaattc**agcgttgc**aagctt**cagctccacccgcacagccgc
catcgcagccacagcaacactatagcgaaggagagttagaggaagacgaagactcagacgatgctggagg
tggcggattattacagagtcagtgcccaagaccctggccgctcctttgtcgcttactgaaggaagtcgta
cttgggatgttttacttacacgatcagaatccggtactcttacacagagactc**gaattc**acgg -3'

Apexcyt 2: pUL69 proteinaren NES motiboaren eta RIP3 proteinaren NES motiboaren tandemak kodetzen duten sekuentziak. Tandemeko bi NES-en artean hiru glizina aminoazido kodetzen dira. Motibo bakoitzaren 5' eta 3' muturretan HindIII eta EcoRI murriztegunеak daude.

5'- ctgc**aagctt**cagggctgctgcaatcccaatgtcctcggccatggccactcttgtgcagactgttaaaag
aggttgtgttgggaatgttctatctgcatgaccaaaacccagtgttactgcatcgggatggaggtggcgg
attattacagagtcagtgcccaagaccctggccgctcctttgtcgcttactgaaggaagtcgtacttggg
atgttttacttacacgatcagaatccggtactcttacacagagactc**gaattc**agcgttgc**aagctt**cag
cacctccggcccaacctcccagtcaacctcaacagcattactcagagggtgaactggaagaggatgagga
tagtgatgacgccggcggaggtgctccacccgcacagccgccatcgcagccacagcaacactatagcgaa
ggagagttagaggaagacgaagactcagacgatgcttc**gaattc**acgg -3'

sinGFP4a: sinGFP4a proteina fluoreszentearen sekuentzia kodetzailea. Sekuentzia kodetzailearen 5' eta 3' muturretan NheI eta BglII murriztegunеak daude.

5'- tcagatccgctagcgctaccggtcgccaccatgacgtcgaaaggtgaagagctgtttacc
ggcactgtcccgattaaagttgaattggatggcgacgtcaatggccacaaattttccgtcaaaggcgagg
gcgaaggggacgccactgaagggaaactgactctgaaattcatctgtaccactggcaagttaccggtgcc
gtggccgactctggttactaccttaacttacggtgtgcaatgcttcgccaaatacccggaccatatgaag
aaacacgatttttcaaatccgcgatgccggaaggctacacccaggagcgtaccattgagttcaaagacg
atggtacttataaaaccaaggctgaagtgaaattcgagggcgacaccctggttaacaaaattgagctgaa
gggcgatgacttcaaagaggatggcaacattctgggtcacaagctggaatataaccacaactcgcatgac
gtcaaaatcgaagccgacaaagagaagaacggtatcaaggcgaactttaaaatcaaacataacgttgagg
acggcagcgaacaagaggcagatcataaacaggagaacaccccgatcggtgacggtccggttaaactgcc
tgataaccatactctttcaacgcagacgactcttagcaaagatcctaacgaaaaaaaagatcatatggtt
ctgaaagagaccgtcaccgcggcaggtattactaagggcgaggatgagaaagataagtccggactcagat
ctcgagctcaa -3'

2Flag-3NLS: 2Flag-3NLS kodetzen duen sekuentzia kodetzailea. Sekuentzia kodetzailearen 5' eta 3' muturretan BglII eta EcoRI murriztegunеak daude.

5'- tgcttgcgggatccaaccgcccccgaggccatcaacttcggctgcttcaccatcaagagcgacgtgtgga
gcccaccggtctgcttgtcaaatcaagcttcgggctgcatcaagagcaagggcaaggacagcctgagcga
cgacggcgtggacctgaagacccagcccgtgaggaacaccgagaggaccatctacgtgagggaccccacc
agcaactgaggatccggaaggtctgcccaagcttcgcaggaggcccagatcatgaagaagctgaggcacg
acaagctggtgtgaggatccggaaggtctgcccaagcttcggaggaggcccagatcatgaagaagctgaa
gcacgacaagctggtgcagtgaggatccggaagggtgtcc**agatct**ggaggtccaaagaagaagaggaag
gtgggaggtgactacaaagaccatgacggtgattataaagatcatgatatcgattacaaggatgacgatg
acaagggaggtccaaagaagaagaggaaggtgggaggtgactacaaagaccatgacggtgattataaaga
tcatgatatcgattacaaggatgacgatgacaagggaggtccaaagaagaagaggaaggtgggaggttc**g**
aattctgtcact -3'

SBSN: Suprabasina proteinaren sekuentzia kodetzailea. Sekuentzia kodetzailearen 5’ eta 3’ muturretan HindIII eta BamHI murriztegunеak daude. Sekuentzia kodetzaile eta BamHI murriztegunearen artean Stop kodona gehitu da.

5’- ttcgtc**aagctt**caatgcacctggctcgattggtaggaagctgcagcctgctcctgctcctgggggccct
gagtgggtgggcagctagtgatgacccaatcgaaaaagtgattgaaggcattaatagggtctcagtaat
gctgagcgggaagtcggaaaggccctggatggcatcaattccgggataacacacgcaggaagagaggttg
aaaaggtcttcaatggcctcagcaatatggggtctcacaccggcaaggaactggacaaaggggtacaggg
ccttaatcacgggatggataaggtagcgcatgagattaaccacgggatagggcaagctggcaaggaagca
gaaaagctggggcacggtgttaacaatgcggctggccaagcggggaaggaagcagataaagctgttcaag
gcttccatacaggcgtacatcaggcaggcaaggaagctgaaaagctcggtcagggggtcaaccatgctgc
agaccaggctgggaaggaagtggagaaacttggccagggggcacatcacgctgcagggcaagcaggcaag
gaattgcagaatgcccataacggcgtcaaccaggccagcaaggaagccaaccagctcttgaatggaaatc
atcagtcaggaagcagtagccatcaaggtggggcaaccacgactccgctcgcgtcaggggcttctgtcaa
tacgccatttattaatctcccagcgctctggcggtctgttgctaacatcatgccataa**ggatcc**gatcca
-3’

CK2α’: CK2α’ proteinaren sekuentzia kodetzailea. Sekuentzia kodetzailearen 5’ eta 3’ muturretan HindIII eta BamHI murriztegunеak daude. Sekuentzia kodetzaile eta BamHI murriztegunearen artean Stop kodona gehitu da.

5’- agctc**aagctt**cgatgccaggtcctgcagctggaagtagagcacgtgtctacgccgaggtgaacagtctg
aggagccgcgagtactgggactacgaggctcacgtcccgagctggggtaatcaagatgattaccaactgg
ttcgaaaacttggtcggggaaaatatagtgaagtatttgaggccattaatatcaccaacaatgagagagt
ggttgtaaaaatcctgaagccagtgaagaaaaagaagataaaacgagaggttaagattctggagaacctt
cgtggtggaacaaatatcattaagctgattgacactgtaaaggaccccgtgtcaaagacaccagctttgg
tatttgaatatatcaataatacagattttaagcaactctaccagatcctgacagactttgatatccggtt
ttatatgtatgaactacttaaagctctggattactgccacagcaagggaatcatgcacagggatgtgaaa
cctcacaatgtcatgatagatcaccaacagaaaaagctgcgactgatagattggggtctggcagaattct
atcatcctgctcaggagtacaatgttcgtgtagcctcaaggtacttcaagggaccagagctcctcgtgga
ctatcagatgtatgattatagcttggacatgtggagtttgggctgtatgttagcaagcatgatctttcga
agggaaccattcttccatggacaggacaactatgaccagcttgttcgcattgccaaggttctgggtacag
aagaactgtatgggtatctgaagaagtatcacatagacctagatccacacttcaacgatatcctgggaca
acattcacggaaacgctgggaaaactttatccatagtgagaacagacaccttgtcagccctgaggcccta
gatcttctggacaaacttctgcgatacgaccatcaacagagactgactgccaaagaggccatggagcacc
catacttctaccctgtggtgaaggagcagtcccagccttgtgcagacaatgctgtgctttccagtggtct
cacggcagcacgatga**ggatcc**accgga -3’

MSM6: USP12^{NES}, WN23, Rev2 NES motiboak. Motibo bakoitzaren 5’ eta 3’ muturretan BamHI eta AgeI murriztegunеak daude.

5’- actgaactgac**ggatcc**aaggaaaaaggagagccttcttacatgcttagcagatctcttccatagcatag
ccactcc**accggt**cttcgccgatc**gggatcc**aaatgaagcattcaaagagcttggccgaatgtgtcagct
tcacttgaagagtgaaaaacc**accggt**cttacatcgtta**ggatcc**aatgagagaagagaacttgaggctc
cagaggaagctgcagagggagatggagagaagacc**accggt**ctagcgtttcgac -3’

USP12-NESmut: USP12 proteinan Sanyalen taldeak (Jahan et al., 2016; Sanyal et al., 2016) argitaratutako NESa mutaturik duen USP12 proteinaren sekuentzia kodetzailea. Sekuentzia kodetzailearen 5’ eta 3’ muturretan HindIII eta BamHI murriztegunеak daude. Sekuentzia kodetzailearen eta BamHI murriztegunеen artean Stop kodona gehitu da.

5’- cggtcac**aagctt**gcatggaaatcctaatgacagtctccaaattcgcctccatctgtaccatgggcgcca
atgcttcggcattagagaaagagattggtccagaacagtttccggtcaatgagcactattttggattagt
caattttgggaatacctgctactgcaattcagttcttcaagcactttatttttgtcgtccatttcgggaa
aaagttcttgcgtataagagtcaacctaggaaaaaggagagcgctgctacatgcgcagcagatgccgccc
atagcgcagccactcagaagaaaaaggttggagtaatacccccctaagaagttcatcacaagattacggaa
agaaaatgagctttttgacaactacatgcaacaagatgcccatgaattcttaaattacctactaaataca
attgctgatattttacaagaagagagaaagcaggaaaaacaaaatggtcgtttacctaatggtaatattg
ataatgaaaataataacagcacaccagacccaacgtgggttcatgagatttttcagggaacattaactaa
tgaaaccagatgtcttacttgtgaaactataagcagcaaagatgaagatttttagacctttctgttgac
gtggaacaaaatacatcaattactcactgcttaaggggtttcagcaacacagaaactctgtgcagtgaat
acaagtattactgtgaagagtgtcgcagcaaacaggaagcacacaaacggatgaaagttaaaaaactgcc

catgattctagctctacacctgaagagatttaaatatatggatcaacttcatcgatatacaaaactctct
taccgggtagtttttcctttagaacttcgtctgtttaacacttcaggtgatgccaccaatccagacagaa
tgtacgaccttgttgctgttgtggttcactgtggaagtggtcccaatcgaggccattatattgcaatagt
taagagtcatgatttttggttgttgtttgatgacgacattgtagaaaaaatagatgcacaagctattgaa
gaattctacgggttgacatcagatatctcaaagaactctgagtctggttacatccttttctatcagtctc
gggactga**ggatcc**atca -3'

WDR20-NES: WDR20 proteinaren NES motibo kandidatuaren sekuentzia kodetzailea. 5' eta 3' muturretan BamHI eta AgeI murrizteguneak daude.

5'- gaatcccaagcttcgtgtgcaaaactaatgaaacttaaagggcacacggataatgtgaag
gcattgctattaaacagagatggcacgcaatgcctgtcaggcagttctgatgggacaattcgcctttgg
tcccttggccagcagagatgtatagcaacataccgagtccatgatgaaggtgtttgggcgctgcaagtca
atgatgccttcacacatgtgtattctggtggaagggacaggaagatttattgtacagacggttcagcagg
tagtgcagcaggtagtggtgaatttgattacaaagatcatgacggcgactataaggatcatgatattgat
tataaggatgacgacgataaaggatcagctggaagtgctgctggaagtggagaattttgtgcaaagctaa
tgaaactaaagggacataccgacaacgtaaaggctttactgttgaatagggacggtactcagtgtctatc
tggaagctcagacggtacaatacgtctatggtctctagggcaacaaaggtgtattgctacttaccgtgtg
cacgatgagggagtgtgggccctacaggtcaacgatgcatttactcacgtttactctggtggcagggata
ggaaaatttactgcactgattgaggatccgaatccctgtt**ggatcc**aatggacggggccattgcttctgg
ggtcagcaaatttgcaacactttcactacatgaccc**accggt**acttgga -3'

CoV: SARS-CoV2, HCoV-OC43, MERS-CoV, HCoV-HKU1, HCoV-229E eta HCoV-NL63 koronabirusen NES motibo kandidatuen sekuentzia kodetzaileak. Motibo bakoitzaren sekuentziaren 5' eta 3' muturretan BamHI eta AgeI murrizteguneak daude.

5'- gttgg**ggatcc**agcactggcacttctgctactggacagactgaaccagcttgagagcaagatgagcggcc
c**accggt**ttgcaa**ggatcc**aatggcagaccagatcgccagcctagtgctggctaagctaggtaaagacgc
taccaagcc**accggt**cgacga**ggatcc**aggtggagacctactttacctggaccttctgaacagactacag
gctctagagagcggtcc**accggt**cctgtt**ggatcc**aatggctgacgagatcgccaacctagtgcttgcaa
agcttggtaaggacagcaagcccccaccggtaagcaa**ggatcc**aagtcaggacgacatcatgaaagcagt
agctgccgctctaaaaagccttggatttgaccc**accggt**tcgcaa**ggatcc**aagtagcagtgatcttgtg
gctgcagttaccctagcactgaaaaacctaggattcgatcc**accggt**attatt -3'

NL63-N: HCoV-NL63 koronabirusaren nukleokapsida (N) proteinaren sekuentzia kodetzailea. Sekuentziaren 5' eta 3' muturretan HindIII eta BamHI murrizteguneak daude. Hasiera eta amaiera kodonak gehitu dira.

5'- agctc**aagctt**cgatggctagtgtaaattgggccgatgacagagctgctaggaagaaatttcctcctcct
tcattttacatgcctcttttggttagttctgataaggcaccatatagggtcattcccaggaatcttgtcc
ctattggtaagggtaataaagatgagcagattggttattggaatgttcaagagcgttggcgtatgcgcag
ggggcaacgtgttgatttgcctcctaaagttcatttttattacctaggtactggacctcataaggacctt
aaattcagacaacgttctgatggtgttgtttgggttgctaaggaaggtgctaaaactgttaataccagtc
ttggtaatcgcaaacgtaatcagaaacctttggaaccaaagttctctattgctttgcctccagagctctc
tgttgttgagttcgaggatcgctctaataattcatctcgtgctagcagtcgttcttcaactcgtaacaac
tcacgagactcttctcgtagcacttcaagacaacagtctcgcactcgttctgattctaaccagtcttctt
cagatcttgttgctgctgttactttggctttaaagaacttaggttttgataaccagtcgaagtcacctag
ttcttctggtacttccactcctaagaaacctaataagcctctttctcaacccagggctgacaagccttct
cagttgaagaaacctcgttggaagcgtgttcctaccagagaggaaaatgttattcagtgctttggtcctc
gtgattttaatcacaatatgggagattcagatcttgttcagaatggtgttgatgccaaaggttttccaca
gcttgctgagttgattcctaatcaggctgcgttattctttgatagtgaggttagcactgatgaagtgggt
gataatgttcagattacctacacctacaaaatgcttgtagctaaggataataagaaccttcctaagttca
ttgagcagattagtgcttttactaaacccagttctatcaaagaaatgcagtcacaatcatctcatgttgc
tcagaacacagtacttaatgcttctattccagaatctaaaccattggctgatgatgattcagccattata
gaaattgtcaacgaggttttgcattaa**ggatcc**accgga -3'

SC2-N: SARS-CoV-2 koronabirusaren nukleokapsida (N) proteinaren sekuentzia kodetzailea. Sekuentziaren 5' eta 3' muturretan HindIII eta BamHI murrizteguneak daude. Hasiera eta amaiera kodonak gehitu dira.

5'- agctc**aagctt**cgatgagtgataacggacctcagaaccagcgaaacgcgccacgtattacctttggtgga
cctagcgatagcaccggtagcaaccagaacggtgaacgtagcggtgcgcgtagcaaacagcgacgtcctc
agggactgccaaacaacaccgcgagctggtttaccgcgctgacccagcatggtaaagaagatctgaaatt
tcctcgtggacagggagtgccaattaacaccaacagcagccctgatgatcagattggatattatcgacgt

gcgacccgacgtattcgtggaggtgatggtaaaatgaaagatctgagcccacgatggtatttttattatc
tgggtaccggtcctgaagcgggactgccatatggtgcgaacaaagatggtattatttgggtggcgaccga
aggagcgctgaacaccccgaaagatcatattggaacccgtaaccctgcgaacaacgcggcgattgtactt
caactaccacagggtaccaccctgcctaaaggattttatgcggaaggtagccgtggaggtagccaggcga
gcagccgaagcagcagccgtagccgtaacagtagccgtaatagtacaccaggtagcagccgtggtaccag
ccctgcgcgaatggcgggaaacggaggtgatgcggcgctggcgctacttctgctcgatcgtctgaaccag
ctggaaagcaaaatgagcggtaagggtcagcagcagcagggacagaccgtgaccaagaaaagcgcggcgg
aagcgagcaaaaagccacgtcagaaacgaaccgcgaccaaagcgtataacgtgacccaggcgtttggtcg
tcgaggacctgaacagacccagggaaactttggtgatcaggaactgattcgtcagggtaccgattataaa
cattggccacagattgcgcagtttgcgcctagcgcgagcgcgtttttggaatgagccgtattggtatgg
aagtgaccccaagcggtacctggctgacctataccggagcgattaaactggatgataaagatcctaactt
taaagatcaggtgattctgctgaacaagcatattgatgcgtataaaacctttccacctaccgaacctaag
aaagataagaagaaaaaggcggatgaaacccaggcgctgccacagcgacagaagaaacagcagaccgtga
ccctgctgcctgcggcggatctggatgattttagcaaacagctacaacaaagcatgagtagcgcggatag
cacccaggcgtaa**ggatcc**accgga

NES 1: WN1, WN2, WN3, WN4, WN5 eta WN6 cNES motiboen sekuentzia kodetzaileak. Motibo bakoitzaren 5' eta 3' muturretan BamHI eta AgeI murrizteguneak daude.

5'- cctta**ggatcc**aaacctggtggacctgcagaagaagctggaggagctggaacttgacgagcagcagaagc
c**accggt**ccat**ggatcc**atcagcctctgatgacctggaagccctgggtacactgagcctggggaccacag
aggagcc**accggt**gcta**ggatcc**acaggccaaccgcagcctgcagctccgaattcaggaactagaactgc
aggcccagatccc**accggt**atca**ggatcc**agacatggacttcctgcggaacttattctcccagacgctca
gcctgggcagccagaagcc**accggt**tcct**ggatcc**atctagtacaagtggacttgagcaagatgtggcac
aactaaatatagcagaacagaatcc**accggt**cgta**ggatcc**aacaggggagcaggaactagagagcctgg
tgctgaagctgtcagtgctaaaggacttccc**accggt**cgttc -3'

NES 2: WN7, WN8, WN9, WN10, WN12, WN13, WN14, WN15, WN16, WN17, WN18, WN20 eta WN21 NES motiboen sekuentzia kodetzaileak. Motibo bakoitzaren 5' eta 3' muturretan BamHI eta AgeI murrizteguneak daude. WN8, WN10, WN13, WN16, WN17, WN18 eta WN20 motiboak ezin izan dira klonatu. Motibook NES5 edo MSM4 gblocketan ere gehitu dira.

5'- cctta**ggatcc**agacactgatatccaggagctgtcagagcagatccaccggctgctgctgcagcccgtccc
accggtccat**ggatcc**aaggaaagagtttgagcccctcctcagggtggaccagctcaacctggagcggga
gaagcc**accggt**gcta**ggatcc**acctgatgacccactcttctcagagctggatggactggggctggagcc
catggaagagcc**accggt**atca**ggatcc**aattgcccccacgggtcattccctgaagtctctggacctagt
gactatgaagaagctggaccc**accggt**tcct**ggatcc**agcagaacctggatcaatcctaactgaattggg
tggttttgaggtaaaagaatcaaaacc**accggt**cgta**ggatcc**aagggtctccaaagatgactggctgga
atggctgagacggctgagcctggagctgctgcc**accggt**ctta**ggatcc**agcagaagaagacctgtgtca
ggctttctctgatgtaattcttgcagtaaatgatgtgcc**accggt**cgaa**ggatcc**agagataagtattgg
tgaagagatagaagaagacctttctgtggaaatagatgacatccc**accggt**cgga**ggatcc**agtgctttc
agcggtaaaagtcctaatgaagtttctagaattgttacctaaggattctcc**accggt**agta**ggatcc**att
tgatattgatgaagctgaagaaggtgtaaaggatcttaagattgaaagtgatgttcc**accggt**tgta**gga
tcc**agtgcaagtggtggcagatgtgcttagcaaactgctcgtagttgggataacagatcctgaccc**accg
gt**cgtt**ggatcc**acgctgccactcgttgacgccgaacttcctgcagatgcagctgcagaagtgcgagatc
cc**accggt**cgtg**ggatcc**actgtccccgctgtcacccatcactcaggctgtagccatggacgccctgtct
ctggagcc**accggt**cgttc -3'

NES 3: WN11, WN19, WN22,WN24, WN25 eta WN26 cNES motiboen sekuentzia kodetzaileak. Motibo bakoitzaren 5' eta 3' muturretan BamHI eta AgeI murrizteguneak daude. WN22 eta WN26 motiboak ezin izan dira klonatu. Motibook NES6 gblockean ere gehitu dira.

5'- cctta**ggatcc**attctcctgtatgcagtcagacttcctgaaggtggacctcctcctggtcatgggtacct
ccttgcaggtgcagcc**accggt**ccat**ggatcc**agtgtccggtgtggccacggacatccaggcactgaagg
cagccttcgacgtcaataacaaggaccc**accggt**gcta**ggatcc**aaacgaggcctttaaggagctggggc
gcatgtgccaactgcacctcaacagcgagaagcc**accggt**atca**ggatcc**atcggctgccgctgtcagcg
ccgacttcatgagcaacctgagcttgctggaggagagccc**accggt**tcct**ggatcc**aaatgaaggaatta
ttaatttgttggaaaaatattttgatatgaaaaagaaccaatgccc**accggt**cgta**ggatcc**agaaggag
aattcttattacaggctctgaatggctttgtattagttgtcactacagatcc**accggt**cttaggatccag
ccgaaaaagtggcggaaaagctagaagctctctcggtgaaggaggagaccaaggagccaccggtcgaagg
atccaggggaaggaacgctgtcagaggccctgctgcagctgcagtttgatgatgaagacctgccaccggt
cggaggatccacggaaccttgaacacctcgaaatggtgcgggtgccctttctgggtggaccaccggtagt

aggatccagggctgctgcagtcccagtgccctcggccctggccgctcctttgccgcctgctgaaagaagt
ggtgcttgggatgttttacctgcacgaccagaacccggtgctcctgcaccgggacccaccggttgtagga
tccagctcgtcagctgcttgtcagccaaaaactggatatcaacttattagataatgtggtgccaccggtc
gttc -3'

NES 4: Rev1, Rev2, Rev3, Rev4, Rev5, Rev6, Rev7, Rev8, Rev9 eta Rev10 cNES motiboen sekuentzia kodetzaileak. Motibo bakoitzaren 5' eta 3' muturretan BamHI eta AgeI murriztegunеak daude. Rev2 eta Rev10 motiboak ezin izan dira klonatu. Rev2 motiboa NES6, MSM4 eta MSM6 gblocketan ere gehitu da, Rev10 motiboa aldiz, NES6 gblockean.

5'- cctta**ggatcc**acagcagctgggccagctgacactagaaaaccttcagatgctgccagagagtgaggacc
c**accggt**ccat**ggatcc**aatgagagaagagaacttgaggctccagaggaagctgcagagggagatggaga
gaagacc**accggt**gcta**ggatcc**aaaggatctggacctcatgctcctggacgactcactgctaccgctgg
cctctgatccacc**accggt**atca**ggatcc**acttcagagaacaaatcttgatgtgaaccttgctgtaaata
atttacttagccgggaccc**accggt**tcct**ggatcc**actagagagcctggtgctgaagctgtcagtgctaa
aggacttcctgtcaggcatccagcc**accggt**cgta**ggatcc**acatcttcaaaaagatgttgctctttcag
ttctgtcaaaagacttaacagacatggaccc**accggt**ctta**ggatcc**agaagacgggagtgatatggagc
tggacttgttagcagcagctgaaacagaaagtgatcc**accggt**cgaa**ggatcc**acccatagctgatatag
caatggaaaaattggctaatgagttacctgactggtttcaacc**accggt**cgga**ggatcc**acccgccgagc
gcgtcaccttggcggactttaagggcgttttgcagcgacccagctatcc**accggt**tgta**ggatcc**actca
cacaagatctgactgtatcccagctcagtgatgttgcggattatctggaagatcc**accggt**cgttc -3'

NES 5: WN8, WN10, WN13, WN17, WN18 eta WN20 cNES motiboen sekuentzia kodetzaileak. Motibo bakoitzaren 5' eta 3' muturretan BamHI eta AgeI murriztegunеak daude. WN18 ez da klonatzea lortu eta MSM4 gblockean ere gehitu da.

5'_ cctta**ggatcc**aaggaaagagtttgagcccctcctcagggtggaccagctcaacctggagcgggagaagc
c**accggt**ccat**ggatcc**aattgcccccacgggtcattccctgaagtctctggacctagtgactatgaaga
agctggaccc**accggt**gcta**ggatcc**aagggtctccaaagatgactggctggaatggctgagacggctga
gcctggagctgctgcc**accggt**atca**ggatcc**atttgatattgatgaagctgaagaaggtgtaaaggatc
ttaagattgaaagtgatgttcc**accggt**tcct**ggatcc**agtgcaagtggtggcagatgtgcttagcaaac
tgctcgtagttgggataacagatcctgaccc**accggt**cgta**ggatcc**acgctgccactcgttgacgccga
acttcctgcagatgcagctgcagaagtgcgagatccc**accggt**cttaggt -3'

NES 6: WN22, WN26, Rev2 eta Rev10 cNES motiboen sekuentzia kodetzaileak. Motibo bakoitzaren 5' eta 3' muturretan BamHI eta AgeI murriztegunеak daude. Rev2 motiboa ez da klonatzea lortu eta MSM4 eta MSM6 gblocketan ere gehitu da.

5'- cctta**ggatcc**aaacgaggcctttaaggagctggggcgcatgtgccaactgcacctcaacagcgagaagc
c**accggt**cgga**ggatcc**agaaggagaattcttattacaggctctgaatggctttgtattagttgtcacta
cagatcc**accggt**ttga**ggatcc**aatgagagaagagaacttgaggctccagaggaagctgcagagggaga
tggagagaagacc**accggt**cgtt**ggatcc**actcacacaagatctgactgtatcccagctcagtgatgttg
cggattatctggaagatcc**accggt**cggaggatccacggaaccttgaacacctcgaaatggtgcgggtgc
cctttctgggtggaccaccggtcgaaggatccaggggaaggaacgctgtcagaggccctgctgcagctgc
agtttgatgatgaagacctgccaccggtcgtga -3'

MSM4: WN16, WN18, rev2 eta FMRP NES motiboen sekuentzia kodetzaileak. Motiboen 5' eta 3' muturretan BamHI eta AgeI murriztegunеak daude. Rev2 motiboa ez da klonatzea lortu eta MSM6 gblockean ere gehitu da.

5'- actgaactgac**ggatcc**agtgctttcagcggtaaaagtcctaatgaagtttctagaattgttacctaagg
attctcc**accggt**cttcgccgatcg**ggatcc**agtgcaagtggtggcagatgtgcttagcaaactgctcgt
agttgggataacagatcctgaccc**accggt**cttacatcgttaggatccaatgagagaagagaacttgagg
ctccagaggaagctgcagagggagatggagagaagacc**accggt**atccgacgaagt**ggatcc**actgaact
atttaaaggaagtagaccagttgcgtttggagagattacaaattgatgagcc**accggt**ctagcgtttcga
c -3'

SRVB/A: $SRV_{B/A}$ fusio proteinaren sekuentzia kodetzailea. Sekuentziaren 5’ eta 3’ muturretan BglII eta NotI murrizteguneak daude. Hasiera eta amaiera kodonak gehitu dira.

5’- ttgcctca**agatct**tgccaccatgggtgccccgacgttgccccctgcctggcagccctttctcaaggacc
accgcatctctacattcaagaactggcccttcttggagggctgcgcctgcaccccggagcggatggccga
ggctggcttcatccactgccccactgagaacgagccagacttggcccagtgtttcttctgcttcaaggag
ctggaaggctgggagccagatgacgaccccatagaggaacataaaaaggatccatccggttgcgctttcc
tttctgtcaagaagcagtttgaagaattaacccttggtgaaaaaccggtcaccatgccaaagaagaagag
gaaggtggaggacccaccagtcgactacaaagaccatgacggtgattataaagatcatgatatcgattac
aaggatgacgatgacaagtatcggccgatgccaaagaagaagaggaaggtgtag**cggccg**cgagttca -
3’

MICROP-NES 1: MICROP-1, MICROP-2, MICROP-3, MICROP-4 eta MICROP-5 NES motibo kandidatuen sekuentzia kodetzaileak. 5’ eta 3’ muturretan BamHI eta AgeI murrizteguneak daude. MICROP-3 eta MICROP-4 ezin izan dira klonatu.

5’- gttgg**ggatcc**aaagaaggaggagctgctgaaacagctggacgacctgaaggtggagctgtcccagctgc
c**accggt**ttgcat**ggatcc**aatcagagatcggctgcctgtgaatgtccgagaactgagcctggatgatcc
tgaggtgcc**accggt**cgacga**ggatcc**agggctggacgacctggatgtggccctgagcaacctggaggtg
aagctggaggggtcgcc**accggt**cctgtt**ggatcc**agacggaacctcagatttgcccctcaaactggagg
ctctctccgtgaaggaagatgcacc**accggt**aagcaa**ggatcc**agctagcgcgagcgccctgcagcgctt
ggtagagcagctcaagttggaggctggcgtgcc**accggt**attatt -3’

MICROP-NES 2: MICROP-6, MICROP-7, MICROP-8, MICROP-9 eta MICROP-10 motibo kandidatuen sekuentzia kodetzaileak. 5’ eta 3’ muturretan BamHI eta AgeI murrizteguneak daude. MICROP-8 ezin izan da klonatu.

5’- gttgg**ggatcc**aagtcattaccatgaaactctgggagaagcacttcaaggggttgaattggaatttagtc
c**accggt**ttgcat**ggatcc**agaagaaagtccagaaaatttgttccttgaactagagaagcttgttttgga
acattcacc**accggt**cgacga**ggatcc**aagaatgagtaaggaagaactcagagctaagctttcagaattc
aagcttgaaactagacc**accggt**cctgtt**ggatcc**acttagcaagtgcggggaagagctgggtcgactca
agctagttcttctggagctcaaccc**accggt**aagcaa**ggatcc**agcaaaaatcaaattgctgaccaagga
attaagtgtactcaaagatttgtttcttgagcc**accggt**attatt -3’

MP osoak: SPROHSA141543 eta SPROHSA010409 mikropeptidoen sekuentziak kodetzaileak. 5’ eta 3’ muturretan HindIII eta BamHI murrizteguneak daude. SPROHSA010409 mikropeptidoa ezin izan da klonatu eta SPROHSA010409 gblockean gehitu da.

5’- ttcgtc**aagctt**caatgtcctccggggctagcgcgagcgccctgcagcgcttggtagagcagctcaagtt
ggaggctggcgtggagaggatcaaggtctctcaggcagctgcagagcttcaacagtactgtatgcagaat
gcctgcaaggatgccctgctggtgggtgttccagctggaagtaacccctccgggagcctagatcctgtg
ctttactctga**ggatcc**gcgtaccaactg**aagctt**caatgagtattaatgctgcagagttaaaacagctt
ctacaaagcaaagaagaaagtccagaaaatttgttccttgaactagagaaacttgttttggaacattcaa
aagatgatgacaatctggattctttgttggacagtgtagttggacttaagcagatgctggagtcatcagg
tgacccttacctctcagtgaccaggatgtagaaccagtactttcagctccagaatctcttcagaatctg
tttaacaataggtaa**ggatcc**gatcca -3’

SPROHSA010409: SPROHSA010409 mikropeptidoaren sekuentzia kodetzailea. 5’ eta 3’ muturretan HindIII eta BamHI murrizteguneak daude.

5’- ttcgtc**aagctt**caatgagtattaatgctgcagagttaaaacagcttctacaaagcaaagaagaaagtcc
agaaaatttgttccttgaactagagaaacttgttttggaacattcaaaagatgatgacaatctggattct
ttgttggacagtgtagttggacttaagcagatgctggagtcatcaggtgacccttacctctcagtgacc
aggatgtagaaccagtactttcagctccagaatctcttcagaatctgtttaacaataggtaa**ggatcc**ga
tcca -3’

NES 7: FMRP-1b, PKIwt eta hRio2 NES motiboen sekuentzia kodetzaileak. 5’ eta 3’ muturretan BamHI eta AgeI murrizteguneak daude.

5’- cctta**ggatcca**ctgaactatttaaaggaagtagaccagttgcgtgcattggagagattacaaattgatg
ag**ccaccggt**ccat**ggatcca**ggcaactcaaatgaattagccttgaaattagcaggtcttgatatcaaca
agacagaa**ccaccgg**tgcta**ggatcca**gcacggagttttgaaatgactgaattcaatcaagctttagaag
aaataaaagggcag**ccaccgg**tcgttc -3’

Fung 1: superPKI, Rev, mDia2, CDC7 eta CPEB4 NES motiboen sekuentzia kodetzaileak. 5’ eta 3’ muturretan BamHI eta AgeI murrizteguneak daude.

5’- actgaactgac**ggatcc**aggcaacttaaatgaattagccttgaaattagcaggtcttgatatcaacaaga
cagaacc**accggt**cttcgccgatcg**ggatcc**agagcctgtgcctcttcagctaccaccgcttgagagact
tactcttgattgtaacgagcc**accggt**cttacatcgtta**ggatcc**acgccccaggacattcgacatgcac
tcactggagagttcactcattgacataatgagacc**accggt**atccgacgaagt**ggatcc**atctaaaaatg
aatcagttcccgaagttgaagccctgctggcaagattacgagctttacc**accggt**attcgacatcac**gga
tcc**agcacaagacttgagaaaactctgtgagagactcaggggtatggattctagcactcccc**accggt**c
tagcgtttcgac -3’

Fung 2: PAX, HDAC5, FMRP, SMAD4 eta X11L2 NES motiboen sekuentzia kodetzaileak. 5’ eta 3’ muturretan BamHI eta AgeI murrizteguneak daude. FMRP motiboa ezin izan da klonatu eta MSM4 gblockean ere gehitu da.

5’- actgaactgac**ggatcc**agagtcaagccttcaggagctggtgcagcagtttgaagctctgccaggcgatc
tggtgcc**accggt**cttcgccgatcg**ggatcc**acactacgaacgagttgtatcacctggaattgatctctc
aggattaacactgcagagtcc**accggt**cttacatcgtta**ggatcc**actgaactatttaaaggaagtagac
cagttgcgtttggagagattacaaattgatgagcc**accggt**atccgacgaagt**ggatcc**agagaccgagg
aggccgagactgtgagcgccatggccttgctgtcggtgggggccgagcc**accggt**attcgacatcac**gga
tcc**aaccagggagctggacgagctgatggcttcgctgtcggatttcaagatccagggcctgcc**accggt**c
tagcgtttcgac -3’

SNUPN: SNUPN proteinaren NES motiboaren sekuentzia kodetzailea. 5’ eta 3’ muturretan BamHI eta AgeI murrizteguneak daude.

5’- cattgctagctggatccagcctcgaagctccgggcggttttggagaagttgaagctcagccgcgatgata
tcccaccggtctcaacgatagtggatccaaccaacttggaggccttgcagaagaagctggaggagctaga
gcttgatgagcagcagccaccggtactagttctaac**ggatcc**aatggaagagttgagtcaggccctggct
agtagcttttctgtgtctcaagatctgaacagccc**accggt**tccagtcata -3’

Inactives: Hxk2, DEAF1 eta COMMD1 NES motibo ez-aktiboen sekuentzia kodetzaileak. 5’ eta 3’ muturretan BamHI eta AgeI murrizteguneak daude.

5’- atccgcttcgtggatccacgcttcgagatgttccgagagctgaatgaggccttggaactcaaggatgccc
agccaccggtactcaatcg**ggatcc**agatgtgccaaaggaattgatgcaacaaattgagaattttgaaaa
aattttcactgttcc**accggt**aaagcgatt**ggatcc**agatgtgccaaaggaattgatgcaacaaattgag
aattttgaaaaaattttcactgttcc**accggt**acctgtacg**ggatcc**aaagacgctgtcagaggtagaag
aaagtatcagcacactgatcagccagcctaaccc**accggt**actgaacacg -3’

RanQ69L: RanQ69L mutantearen sekuetzia kodetzailea. 5’ eta 3’ muturretan HindIII eta BamHI murrizteguneak daude. BamHI murriztegunearen 5’ aldean Stop kodona gehitu da.

5’- ggatcgc**aagctt**cgatggctgcgcagggagagccccaggtccagttcaaacttgtattggttggtgatg
gtggtactggaaaaacgaccttcgtgaaacgtcatttgactggtgaatttgagaagaagtatgtagccac
cttgggtgttgaggttcatcccctagtgttccacaccaacagaggacctattaagttcaatgtatgggac
acagccggcctggagaaattcggtggactgagagatggctattatatccaagcccagtgtgccatcataa
tgtttgatgtaacatcgagagttacttacaagaatgtgcctaactggcatagagatctggtacgagtgtg
tgaaaacatccccattgtgttgtgtggcaacaaagtggatattaaggacaggaaagtgaaggcgaaatcc
attgtcttccaccgaaagaagaatcttcagtactacgacatttctgccaaaagtaactacaactttgaaa
agcccttcctctggcttgctaggaagctcattggagaccctaacttggaatttgttgccatgcctgctct
cgccccaccagaagttgtcatggacccagctttggcagcacagtatgagcacgacttagaggttgctcag
acaactgctctcccggatgaggatgatgacctgtga**ggatcc**atcgtcaac -3’

9. Appendix I: English version

eman ta zabal zazu

Universidad del País Vasco
Euskal Herriko Unibertsitatea

Physiopathology of the nuclear export receptor CRM1/XPO1: studies on its cellular function and therapeutic targeting

---

PhD Thesis

Maria Sendino Mouliet
(2022)

Supervisors:

Dr. José Antonio Rodríguez Pérez

Dr. Miren Josu Omaetxebarria Ibarra

E1. Introduction

(Revised and updated text based on Sendino et al., 2018 and Sendino et al., 2020a)

In 1997, a 120 kDa protein called CRM1, known to function as a chromosome region maintenance factor in yeast, was identified as the first receptor for the nuclear export of proteins, and it was consequently renamed exportin 1 (XPO1) (Fornerod et al., 1997; Fukuda and al., 1997; Stade et al., 1997; Ossareh-Nazari et al., 1997). According to the HGNC gene nomenclature committee, the official symbol for this protein is XPO1. However, since CRM1 is more commonly used in the literature, this is the symbol that has been used throughout this thesis.

In the initial reports, CRM1 was found to bind short amino acid sequences (so-called nuclear export signals or NESs) in proteins that were actively exported from the nucleus. Over the last two decades, many aspects of CRM1 physiopathology have been elucidated. Thus, CRM1 has been shown to mediate the nuclear export of not only about 400 cellular and viral proteins (Fung et al., 2021), but also of different types of RNA molecules (Hutten and Kehlenbach, 2007; Okamura et al., 2015). In fact, crucial signalling pathways, such as the NF-κB pathway, and essential cellular processes, such as cell cycle progression, have been shown to involve CRM1-dependent nuclear export steps (Turner and Sullivan, 2008). In addition, export-independent functions of CRM1 in mitosis have also been identified (Arnaoutov et al., 2005).

CRM1 alterations (including mutations and overexpression) are often found in cancer cells. This close relationship with tumour development has led to CRM1 being postulated as a possible target for cancer therapy (Gravina et al., 2014a; Tan et al., 2014), and consequently, CRM1 has been studied from a number of different perspectives (Koyama and Matsuura, 2012; Fung and Chook, 2014; Monecke et al., 2014). The results obtained in these studies have paved the way for the development of clinically useful CRM1 inhibitors. The first CRM1 inhibitor identified was leptomycin B (LMB) (Kudo et al., 1998). This drug is a very effective inhibitor of CRM1, but it shows high toxicity in patients (Newlands et al., 1996), and therefore, other CRM1 inhibitors have been sought, for instance the compounds of the so-called SINE (*selective inhibitor of nuclear export*) family (Senapedis et al., 2014). After being extensively tested in preclinical and clinical studies, one of the SINE compounds, selinexor, has recently been approved for the treatment of certain haematological cancer patients (Food and Drug Administration, 2019, 2020a, 2020b; European Medicines Agency, 2021), and is also undergoing clinical trials, with promising results, in patients with other tumour types.

E1.1. An overview of the nucleocytoplasmic transport of proteins

In eukaryotic cells, the nuclear envelope establishes a physical separation between the two major cellular compartments: the nucleus and the cytoplasm. Cellular homeostasis requires a continuous communication between these compartments through the bidirectional trafficking of molecules. This trafficking usually occurs through proteinaceous channels embedded in the nuclear envelope, termed nuclear pore complexes (NPCs). Small proteins (<30 kDa) could, in principle, move across the NPCs by diffusion. However, for most proteins, nucleocytoplasmic transport is an active, energy-dependent process (Knockenhauer and Schwartz, 2016; Schmidt and Görlich, 2016) that requires a specialised transport machinery with three crucial components (Figure E1): (1) the NPCs, (2) a gradient of the small GTPase Ran (bound to either GTP or GDP) across the nuclear envelope, which confers directionality to the transport, and (3) a family of soluble transport receptors (karyopherins) that recognise and bind specific transport signals in the proteins to be transported (the so-called "cargo proteins") (Pemberton and Paschal, 2005; Tran et al., 2014; Cautain et al., 2015).

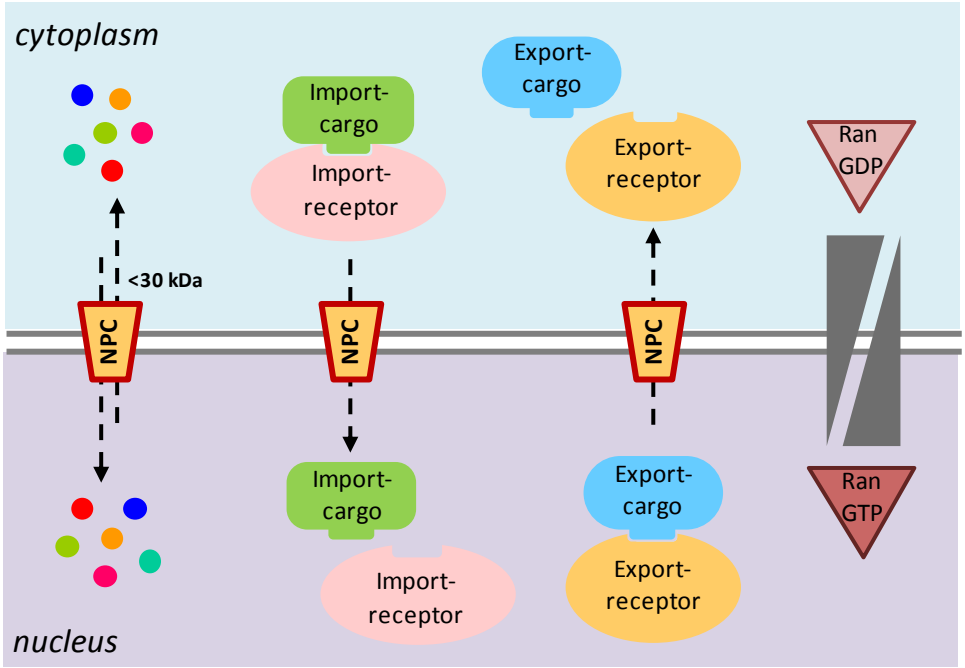

Figure E1: Protein transport through the NPCs. Small proteins (<30 kDa) could, in principle, enter and exit the nucleus by diffusion. However, transport of larger proteins needs to be mediated by import or export receptors. A RanGTP/RanGDP gradient across the nuclear envelope establishes transport direction.

NPCs are very large complexes (over 120 MDa in size) formed by the assembly of several copies of each of approximately 30 different proteins called nucleoporins (NUPs) (Figure E2). NPCs present a characteristic eight-fold rotational symmetry (Gall, 1967), and are composed by three stacked rings inserted into the nuclear envelope, with a series of filaments emanating to the cytoplasmic side of the NPC and a basket-like structure protruding to the nucleoplasmic

side. NUPs in the inner channel of the pore contain intrinsically disordered domains rich in phenyalanine-glycine (FG) repeats.

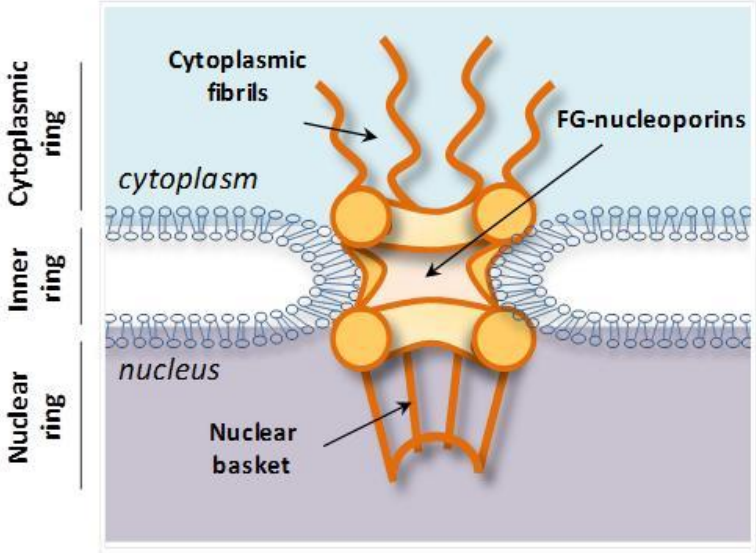

Figure E2: Schematic representation of the NPC. Cross-section of the NPC, with its different parts indicated.

These so-called FG-nucleoporins constitute a barrier that efficiently prevents proteins above a certain size from freely diffusing across the NPC. This threshold size for exclusion has long been believed to be relatively sharp (30 kDa), but a more recent study suggests that the NPC lacks such a firm size threshold (Timney et al., 2016).

The second piece of the nuclear transport machinery is the small GTPase Ran, which can be bound to either GDP (RanGDP) or GTP (RanGTP), and regulates the interaction between cargos and transport-receptors (Pemberton and Paschal, 2005; Tran et al., 2014; Cautain et al., 2015). There is a sharp gradient of RanGTP/RanGDP concentration across the nuclear envelope (see Figure E1). This gradient (a high concentration of RanGDP in the cytoplasm and a high concentration of RanGTP in the nucleus) is maintained by two Ran cofactors: RanGAP1 (a cytoplasmic GTPase activating protein) and RCC1 (a chromatin-bound nucleotide exchange factor). The RanGTP/RanGDP gradient determines the directionality of nucleocytoplasmic transport. In fact, it has been shown that, by artificially raising the concentration of RanGTP in the cytoplasm, the direction of the transport can be inverted (Nachury and Weis, 1999).

The last piece of the transport machinery are the transport-receptors or karyopherins. The human genome codes for approximately 25 different karyopherins (Çağatay and Chook, 2018). While some of these receptors can mediate bidirectional transport of cargos in and out of the nucleus, most of them function exclusively as either import receptors (importins) or export receptors (exportins). Most proteins that enter the nucleus are imported via the

importin-α/importin-β heterodimer, while most of the proteins that exit the nucleus do so by binding to the export receptor CRM1 (Figure E3).

Transport mediated by both importin-α/importin-β and CRM1 is modulated by RanGTP (Figure E3). RanGTP promotes disassembly of the importin/cargo complexes, leading to release of import cargos in the nucleus. Conversely, RanGTP stabilises the interaction between CRM1 and export cargos in the nucleus by forming a trimeric CRM1/cargo/RanGTP complex. This complex is disassembled upon GTP hydrolysis in the cytoplasmic side of the NPC, leading to release of the export cargo in the cytoplasm (Dickmanns et al., 2015).

Once the cargos have been released in the corresponding compartment, the receptors are recycled. To do so, importin-β binds RanGTP and importin-α binds both RanGTP and XPO2 (Lu et al., 2021), while CRM1 is recycled without binding any other protein (Dickmanns et al., 2015).

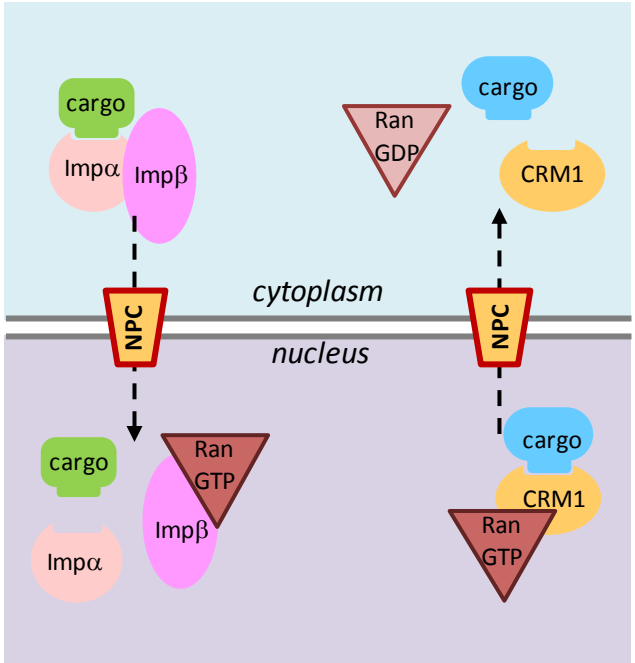

Figure E3: Main mechanisms that mediate nucleocytoplasmic transport. *Left*. Importin-α/importin-β (Impα/Impβ)-mediated nuclear import. The Impα/Impβ heterodimer binds its cargos in the cytoplasm, moves across the NPCs and, once in the nucleus, the cargo is released upon RanGTP interaction. *Right*. CRM1-mediated export. CRM1 forms a trimeric complex with its cargo and RanGTP in the nucleus. This complex is exported to the cytoplasm where GTP is hydrolysed and the cargo is released.

Beyond the basic transport machinery described above, multiple additional mechanisms may contribute to regulate the nucleocytoplasmic distribution of a given protein, in a dynamic and finely-tuned manner. These mechanisms include post-translational modifications, such as phosphorylation (Nardozzi et al., 2010; Panayiotou et al., 2016) or ubiquitination (Rodríguez,

2014), as well as masking/unmasking of the transport signals by homo/heterodimerisation (Rodríguez et al., 2004; Engelsma et al., 2007).

E1.1.1. Nuclear import and export signals

Karyopherins recognise and bind specific peptide sequences in the cargo protein, which function as nucleocytoplasmic transport signals, and can be broadly classified as nuclear localisation signals (NLSs, recognised by importins) or nuclear export signals (NESs, recognised by exportins).

E1.1.1.1. Nuclear localisation signals (NLSs)

The importin-α/importin-β heterodimer mediates nuclear import of cargos bearing a "classical" NLS or cNLS. cNLSs are peptide sequences characterised by the presence of one (monopartite) or two (bipartite) clusters of basic residues. Both types of NLSs have a consensus sequence, K-K/R-X-K/R for cNLSs with a single basic cluster and $(K/R)(K/R)X_{10\text{-}12}(K/R)_{3/5}$ for cNLSs with two clusters (X means any amino acid and $(K/R)_{3/5}$ indicates that three out of five amino acids are lysine or arginine (Soniat and Chook, 2015)). SV40 virus T-large antigen ^{126}PKKKRKV^{132} sequence is an example of monopartite cNLS (Kalderon et al., 1984a, 1984b), and nucleoplasmin ^{155}KRPAATKKAGQAKKKK^{170} sequence is an example of bipartite cNLS (Dingwall et al., 1988).

In addition to classical NLSs, there are "non-classical" NLSs recognised by other importins. Among them, the best-studied is the PY-NLS, which is recognised by importin-β_2. PY-NLSs are sequence motifs of 20 to 30 amino acids without a defined structure. At the C-terminal end of these sequences there is an $R/K/H(X_{2\text{-}5})PY$ motif, where $X_{2\text{-}5}$ means any sequence of between 2 and 5 amino acids. At the N-terminal end, there can be either a cluster of basic or hydrophobic amino acids, which leads to the classification of these sequences as bPY-NLSs (basic) or hPY-NLSs (hydrophobic) (Lu et al., 2021).

E1.1.1.2. Nuclear export signals (NESs)

CRM1 mediates nuclear export of proteins bearing the so-called "leucine-rich" NESs. NES motifs have a consensus sequence defined by the position of 4 or 5 hydrophobic amino acids. This consensus sequence can be represented as follows: $\phi^1X_{(2\text{-}3)}\phi^2X_{(2\text{-}3)}\phi^3X\phi^4$, where ϕ indicates hydrophobic residues (most commonly leucine, but can also be valine, isoleucine, phenylalanine or methionine) and X indicates any amino acid (Kosugi et al., 2008). Examples of NES motifs that match this sequence are the sequence ^{75}LPPLERLTL^{83} of the HIV virus Rev protein (Fischer et al., 1995) or the sequence ^{37}LALKLAGLDI^{46} of the PKI protein (Wen et al., 1995). A ϕ^0 position can also be present in some of these sequences, as it is the case of SNUPN

NES ^{1}MEELSQALASSFSVSQ^{16}, where methionine is found in the ϕ^0 position (Dong et al., 2009a). In addition to the above-mentioned consensus sequence, CRM1-binding NESs also tend to have a specific conformation: α-helix at their N-terminal end and loop at their C-terminal end (Dong et al., 2009b).

Although a general consensus sequence and structure have been defined for CRM1-dependent NES motifs, it has been observed that not all active NESs meet these parameters. For example, Rev NES meets the consensus sequence, but does not show the typical α-helix/loop conformation. Instead, it binds CRM1 in a completely extended conformation (Güttler et al., 2010). Given that not all active NESs meet the consensus sequence nor bind CRM1 in the same conformation, a broader NESs classification has been proposed (Table E1) (Kosugi et al., 2008; Fung et al., 2015, 2017). This classification takes into account both the position of the hydrophobic amino acids as well as the direction in which each NES binds CRM1. Thus, NESs that bind the hydrophobic groove of CRM1 in the originally-described direction have been termed "*plus*" NESs, and those (more recently reported) that bind it in the opposite direction have been termed "*minus*" or "reverse" NESs (Fung et al., 2015). According to the position of the hydrophobic amino acids, seven classes of *plus* NES (1a, 1b, 1c, 1d, 2, 3 and 4), and four classes of *minus* NES (1a-R, 1b-R, 1c -R and 1d-R) have been described (Kosugi et al., 2008; Fung et al., 2015, 2017).

Table E1: Direction, sequence and conformation of different NES classes. Φ represents leucine, isoleucine, valine, phenylalanine or methionine amino acids, and X represents any amino acid (Kosugi et al., 2008; Fung et al., 2015, 2017).

Direction	Class	Sequence	Conformation
Plus	1a	ΦXXXΦXXΦXΦ	Helix-loop peptides with either α-helices (class 1a, 1c) or 3_{10} helices (class 1b)
	1b	ΦXXΦXXΦXΦ	
	1c	ΦXXXΦXXXΦXΦ	
	1d	ΦXXΦXXXΦXΦ	
	2	ΦXΦXXΦXΦ	Loop-like
	3	ΦXXΦXXXΦXXΦ	All α-helix
	4	ΦXXΦXXXΦXXΦXXXΦ	α-helix β-turn. The first four Φ in helix and the fifth in loop
Minus	1a-R	ΦXΦXXΦXXXΦ	Helix-loop (as *plus* 1 classes but reversed)
	1b-R	ΦXΦXXΦXXΦ	
	1c-R	ΦXΦXXXΦXXXΦ	
	1d-R	ΦXΦXXXΦXXΦ	

E1.2. CRM1 structure and main characteristics for NES binding

As schematically illustrated in Figure E4A, CRM1 is a ring-shaped protein with a concave inner surface and a convex outer surface. RanGTP binds to the inner surface, and NESs dock into a hydrophobic groove in the outer surface of the receptor. The open/close state of the NES-binding groove is allosterically regulated by conformational rearrangements of two additional CRM1 elements, termed the H9 loop and the C-helix, which play a crucial role in the cycle of NES binding and release (Dong et al., 2009b; Monecke et al., 2009, 2014; Güttler et al., 2010; Koyama and Matsuura, 2012; Fung and Chook, 2014). The NES-binding groove is wider at one end (where the N-terminus of *plus* NESs binds), and then displays a constriction, becoming narrower at the other end (Figure E4B). A series of landmark studies a decade ago showed that NES peptides dock into five hydrophobic pockets of the CRM1 groove, and identified several key amino acids, including I521, L525, F561 and F572 that establish hydrophobic interactions with NES residues (Figure E4C) (Kosugi et al., 2008; Dong et al., 2009b; Monecke et al., 2009; Güttler et al., 2010). Subsequent analyses have also identified several non-hydrophobic amino acids that are important for the activity and regulation of CRM1 (Figure E4C), most prominently C528, K568, and E571. C528 is the crucial target of LMB and more clinically relevant CRM1 inhibitors, which covalently bind to this residue and block NES binding by physically occupying the groove (Figure E4D). On the other hand, K568 contributes to NES binding by hydrogen bonding with the NES backbone, and also appears to function as a “specificity filter” that physically blocks binding of those NES-like peptides whose structural features are not optimal for docking into the groove (Fung et al., 2017). Importantly, K568 establishes electrostatic interactions with E571, a CRM1 residue that is the target of recurrent mutations that act as oncogenic drivers in certain haematological malignancies (Puente et al., 2011; Taylor et al., 2019).

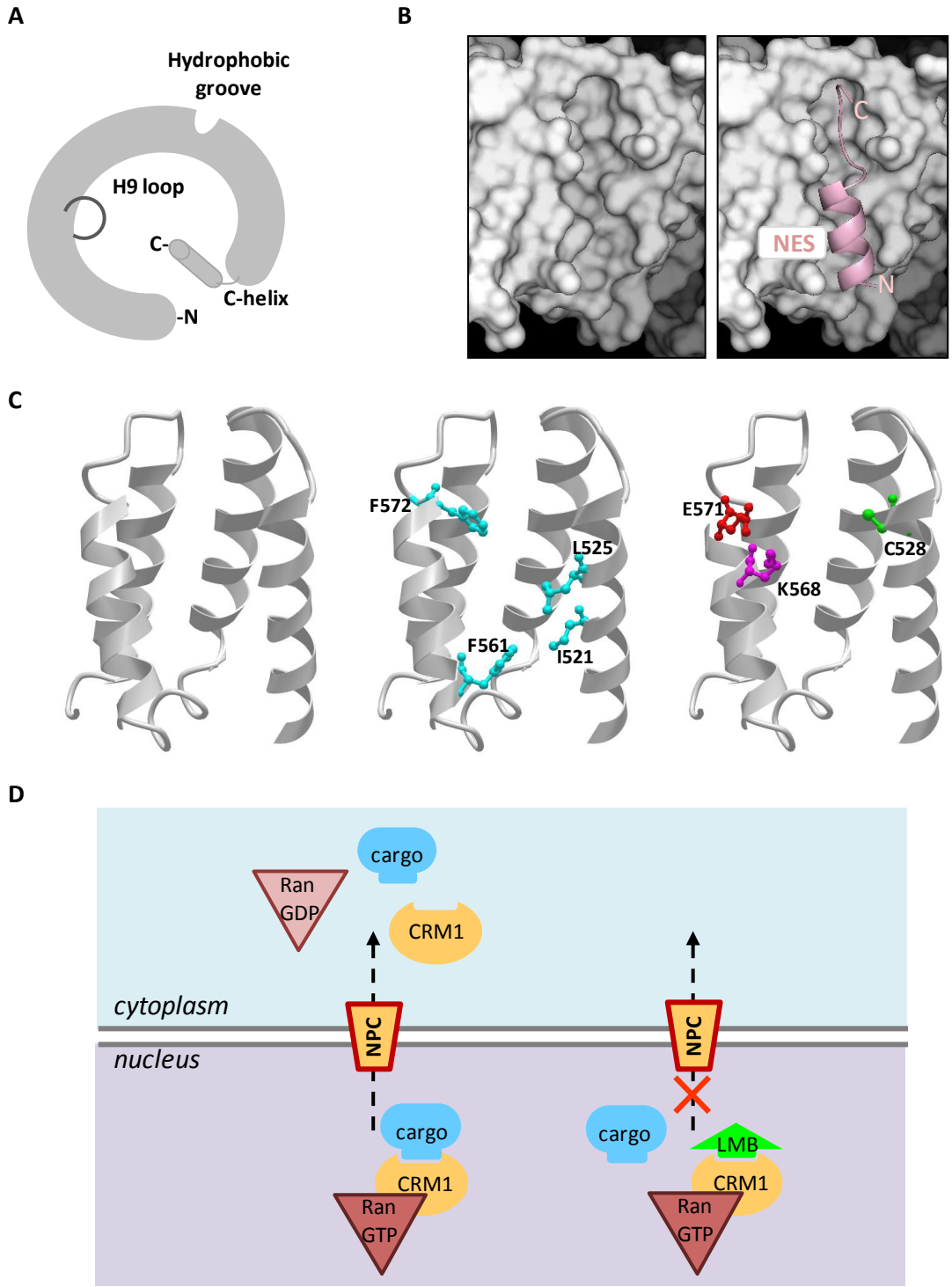

Figure E4: Structural features of CRM1 related to its nuclear export function, its role in cancer and its potential role as a therapeutic target. A. Schematic representation of CRM1 protein illustrating its general ring-shaped conformation, and showing the three structural motifs that are crucial for its function as a nuclear export receptor: the NES-binding groove, the H9 loop and the C-helix. B. Detailed views of the NES-binding groove on the molecular surface of CRM1. The UCSF Chimera package (Pettersen et al., 2004) and CRM1 structure 3GJX (Monecke et al., 2009) were used to generate the images. The left panel shows the empty groove and the right panel shows a *plus* NES peptide (pink) bound to the groove. C. View of the empty CRM1 NES-binding groove generated with NCBI iCn3D viewer from 3GJX. Middle panel shows hydrophobic residues key to NES binding, while right panel shows those non-hydrophobic amino acids related to CRM1 physiopathology. D. LMB (or SINE compounds) prevents formation of export complexes, and therefore cargo export, by covalently binding C528 residue and occupying the NES-binding groove of CRM1.

E1.3. Approaches to the identification of CRM1 cargos and NESs

The number of cellular proteins that may undergo CRM1-mediated nuclear export can be over 1000. Besides the approximately 400 CRM1 cargos that have been experimentally confirmed (Xu et al., 2012; Fung et al., 2021; http://prodata.swmed.edu/LRNes/index.php), proteomic studies have suggested many other possible cargos that remain to be validated (Thakar et al., 2013; Kirli et al., 2015). In addition, it is likely that there are many other cargos of CRM1 that are not yet suspected. Notably, even among the cargos that have been confirmed, many of them do not have a known NES. The identification and characterisation of these cargos and motifs is essential if the physiopathology of CRM1 is to be fully understood. For this reason, in this thesis new CRM1 cargos as well as the NES of known or new cargos have been searched for. To this end, several approaches described below, such as CRM1 inhibition, bioinformatics analyses, nuclear export assays, site-directed mutagenesis, and proteomics analyses, have been used.

E1.3.1. Experiments based on CRM1 inhibition

The most common type of experiment to identify CRM1 cargos involves the treatment of cells with LMB. In this way, CRM1 is inhibited, and a potential change in the localisation of the (endogenous or exogenous) proteins of interest can be assessed.

Typically, CRM1 cargos will show a more nuclear localisation when CRM1 is inhibited than in basal conditions. Usually, proteins that undergo this localisation change are considered CRM1 cargos. However, there are certain cases in which such behaviour does not imply that a protein is a direct CRM1 cargo, and conversely, certain proteins that do not show this behaviour cannot be discarded as cargos. For example, a protein that is not a direct CRM1 cargo but is exported by a piggyback mechanism may show a more nuclear localisation upon CRM1 inhibition (Olazabal-Herrero et al., 2019). Conversely, a cargo may not respond to CRM1 inhibition if it is retained in the cytoplasm unless the retention mechanism is identified and abrogated. Finally, some CRM1 cargos may be constitutively nuclear. Instead of CRM1 inhibition, CRM1 overexpression can be used to identify these cargos, as increasing the cellular concentration of the receptor may trigger their export (García-Santisteban et al., 2016, Taylor et al., 2019; Sendino et al., 2020a).

E1.3.2. Bioinformatics analyses: NES predictors

NES predictors are bioinformatics tools that allow *in silico* searching for NES motifs in proteins. These tools examine amino acid sequences searching for candidate NES (cNES). There are

different predictors available as webtools, such as NetNES (la Cour et al., 2004), ELM (Gould et al., 2010), NESsential (Fu et al., 2011), NESmapper (Kosugi et al., 2014) or Wregex (Prieto et al., 2014). It must be noted that NES prediction remains a challenging task and most of the amino acid motifs that meet the NES consensus are not active NESs. In fact, when a predictor finds a cNES, the predicted motif has to be experimentally analysed. Usually, the activity of the motif is first evaluated using a nuclear export assay. If the result of the assay is positive, it will be necessary to perform subsequent site-directed mutagenesis experiments to determine whether this motif is responsible for the nuclear export of the cargo protein.

E1.3.3. Nuclear export assays

Most export assays are based on cloning candidate NESs into a reporter plasmid. There are different types of reporter plasmids, such as the $EYFP_2$-$SV40^{NLS}$ (Fu et al., 2018), the Rev(1.4)-GFP that has been widely used in this thesis (Henderson and Eleftheriou, 2000) or the $SRV_{B/A}$ developed in this thesis (Taylor et al., 2019; Sendino et al., 2020a) from the original SRV100 reporter (García-Santisteban et al., 2016).

Usually, reporter proteins contain a fluorescent moiety or a tag (e.g., YFP, GFP or Flag), in order to easily analyse their localisation. In addition, reporter proteins bear one or more NLSs that lead to their nuclear localisation when no NES or a non-active NES is cloned into the plasmid (Figure E5). In contrast, if an active NES is cloned, the reporter protein will relocalise to the cytoplasm. The extent of the cytoplasmic relocation will depend on the level of activity of the cloned cNES, since not all active NESs have the same export activity (Henderson and Eleftheriou, 2000).

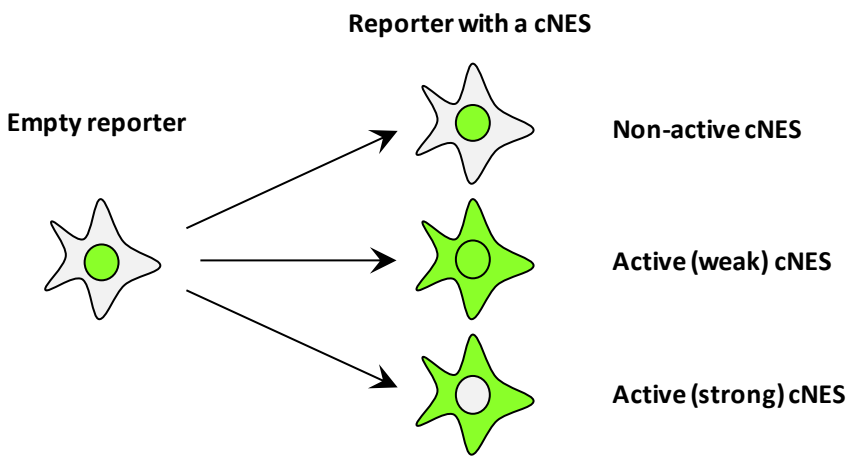

Figure E5: Example of the potential results of a nuclear export assay. Empty reporters (which contain one or more NLS motifs) are localised in the nucleus. When a cNES motif is cloned into these reporters, the resulting protein will present a different localisation depending on the export activity of the cloned motif. If a non-active cNES is cloned, the reporter will remain in the nucleus. However, if the cNES is active the reporter will relocalise to the cytoplasm. The level of export activity of the cloned cNES will determine to what extent the reporter relocalises to the cytoplasm.

E1.3.4. Site-directed mutagenesis

To verify that an NES motif is responsible for the export of its cognate protein, hydrophobic NES residues (often Φ^3 and Φ^4) are mutated, and the effect of these mutations is evaluated in the context of the full-length protein (Figure E6) (Olazabal-Herrero et al., 2019; Sendino et al., 2020b). If the identified NES is responsible for the export, a more nuclear localisation of the mutant protein would be expected.

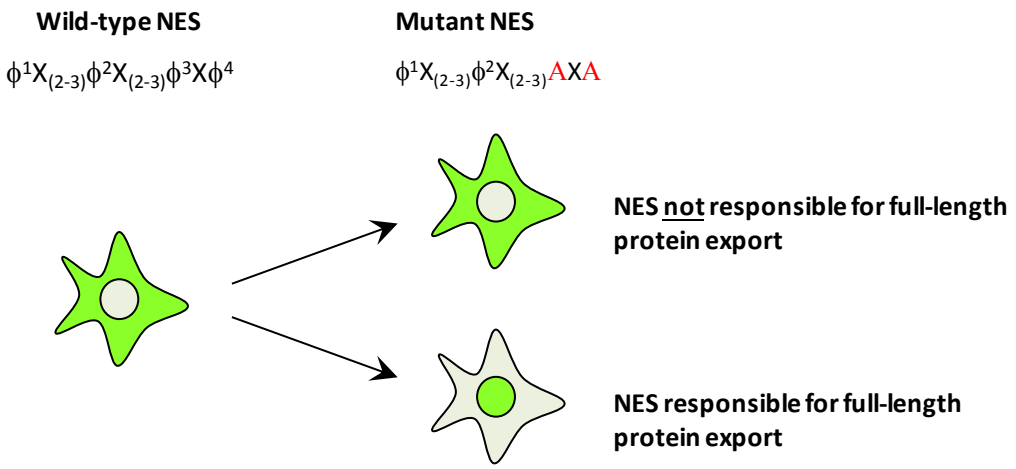

Figure E6: Example of a site-directed mutagenesis experiment analysing the effect of an NES in the export of the full-length protein. Hydrophobic NES amino acids (usually ϕ^3 and ϕ^4) are mutated to alanine. If the NES under analysis mediates the export of the full-length protein, the mutated protein will show a more nuclear localisation than the wild-type protein.

E1.3.5. Proteomics analyses

In order to wholly understand the function of a protein, it is necessary to characterise the full set of proteins that interact with it (i.e. its interactome). This global characterization is possible using tandem mass-spectrometry (MS/MS)-based proteomics approaches (Aebersold and Mann, 2003).

As previously mentioned, many CRM1 cargos are already known. However, the entire set of cargos exported by CRM1 (the so-called CRM1 "exportome") is not known yet. In addition, how inhibition or mutation of CRM1 can globally affect its exportome also remains largely to be determined. This makes CRM1 a very interesting candidate to be investigated using proteomics strategies.

Only three proteomics studies that aim to globally characterise CRM1 exportome have been published to date. Two of them (Thakar et al., 2013; Kirli et al., 2015) focused on the exportome of wild-type CRM1, while the last study (Taylor et al., 2019) reported putative exportome alterations caused by the recurrent CRM1 cancer-mutation E571K. These three studies used common procedures for sample preparation in proteomics: cell fractionation and affinity purification. More recently-developed procedures, such as proximity labelling of

proteins have not yet been used to investigate the CRM1 exportome, buy may represent an interesting alternative that has been explored on this thesis.

E1.3.5.1. Cell fractionation

Two of the CRM1 exportome studies (Thakar et al., 2013; Taylor et al., 2019) used cell fractionation, which consists in breaking cells and tissues without altering their inner compartments (e.g. nucleus and cytoplasm), so that the proteins from each compartment can be then isolated. Cells or tissues can be broken using mechanical (e.g. sonication) or chemical (e.g. incubation in hypotonic medium) methods. For the subsequent isolation of subcellular components, the most classical and simple methods are based on centrifugation, either subjecting the sample to several centrifugation steps under different conditions or using a density gradient (Figure E7) (reviewed in Lee et al., 2010).

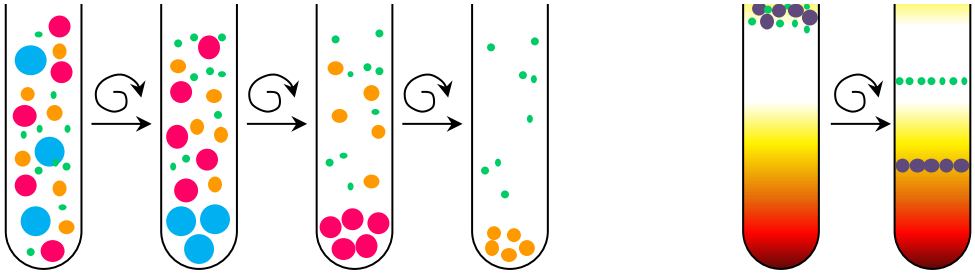

Figure E7: Classical methods for cell fractionation. The figure on the left shows how the components of the sample are isolated by successive centrifugation steps under different conditions. After each step, the supernatant is collected and centrifuged again to separate the remaining components. The figure on the right shows how the components of the sample are isolated using a density gradient. After centrifugation, the different components remain in the area of the gradient with their same density.

A potential caveat of cell fractionation approaches is that a great deal of skill is required when preparing samples to avoid cross-contamination between different compartments (reviewed in Bosch et al., 2021).

E1.3.5.2. Affinity purification

The CRM1 exportome has also been investigated using an affinity purification-based approach (Kirli et al., 2015). The term affinity purification refers to the isolation of a particular component from a sample using specific ligands immobilised on a physical support (usually agarose or magnetic beads) (Figure E8). Ligands can be of many types, but the most commonly used ones are antibodies. The use of antibodies against endogenous proteins allows the analysis to be carried in physiological conditions. However, it may be difficult to find specific antibodies against the protein of interest. Therefore, it is often more practical to ectopically express the protein of interest tagged with epitopes, such as GFP or Flag, and use tag-specific antibodies (reviewed by Dunham et al., 2012).

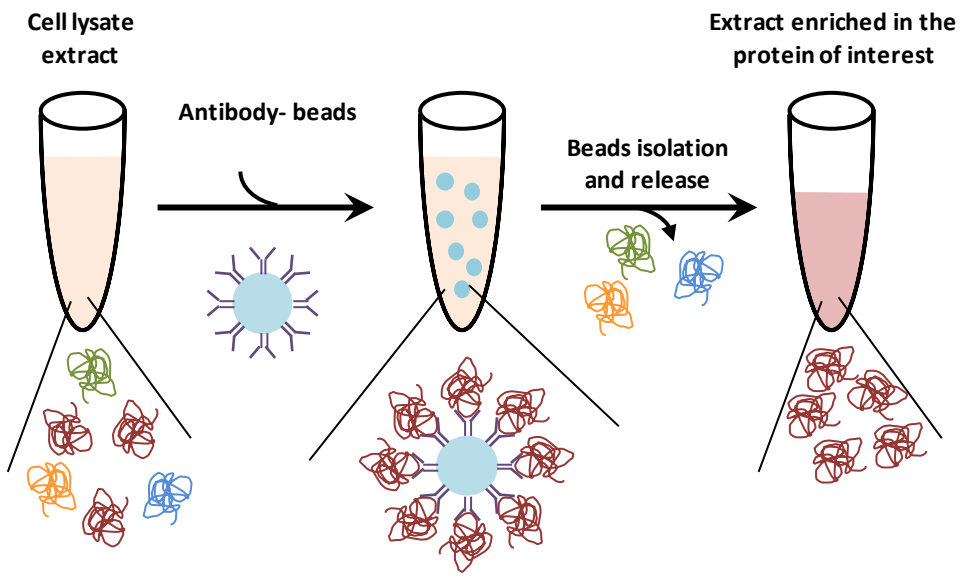

Figure E8: Schematic representation of the affinity purification method. Bead-conjugated antibodies against the protein of interest are added to the cell lysate. Following incubation, proteins not bound to the antibody beads are removed using washing steps. The conditions of these washing steps are crucial to allow efficient removal of contaminant proteins without removing the proteins that specifically interact with the protein of interest or breaking the antibody-protein interaction. After washing, the protein of interest and its interactors can be released (e.g. by boiling the sample) and purified.

To study the CRM1 exportome, Kirli and co-workers (2015) used CRM1 itself as the ligand immobilised on agarose beads to isolate proteins that differently interact with CRM1 in the presence or absence of RanGTP. After discarding other components of the nucleocytoplasmic transport machinery, they defined the CRM1 exportome as the set of proteins whose interaction with CRM1 increased in the presence of RanGTP.

E1.3.5.3. Protein proximity labelling

Protein proximity labelling is based on the use of specific enzymes that, in the presence of the right substrate, form free radicals that will be able to covalently label surrounding proteins. The closer to the labelling enzyme, the more free radicals will be available, so that the proteins near the enzyme will be labelled to a higher extent than those far away (Gingras et al., 2019). Labelled proteins can be subsequently isolated by affinity purification and identified using MS/MS (Figure E9).

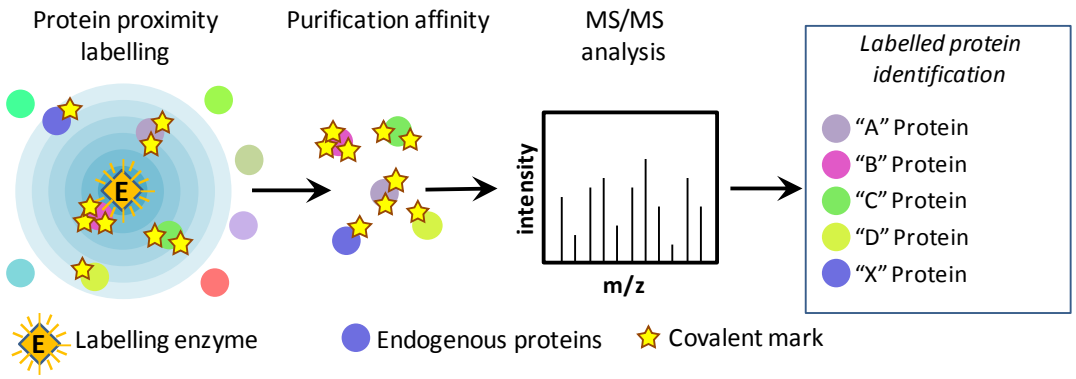

Figure E9: Protein identification by protein proximity labelling. In the presence of the appropriate substrate, the labelling enzyme will covalently label the surrounding proteins. This labelling will allow isolating the labelled proteins from the rest of cell components by affinity purification. Finally, the isolated proteins will be identified by MS/MS.

Nowadays, the most commonly used labelling enzymes are those that lead to protein biotinylation, in particular BirA biotin-ligases or APX family peroxidases (reviewed in Bosch et al., 2021; Zhou and Zou, 2021).

E1.3.5.3.1. BirA biotin-ligases

In the presence of biotin and ATP, biotin ligases will form biotinyl-5'-AMP free radicals, which are capable of attacking lysines. This methodology was first described in 2012, when Roux and co-workers analysed the nuclear lamina proteome using a labelling system they named BioID (*Biotin identification*). In this system, a promiscuous mutant of *Escherichia coli* BirA (R118G), known as BirA* (Kwon and Beckett, 2000; Choi-Rhee et al., 2004; Cronan, 2005) is fused to a certain protein, or targeted to the location of interest. Then, biotin is added to the cell media and protein proximity biotinylation (PPB) will occur over a 15-24 hour period (Figure E10) (reviewed in Bosch et al., 2021).

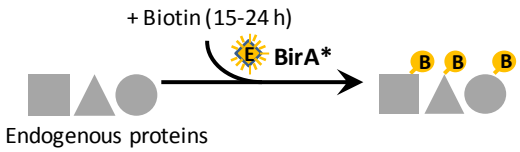

Figure E10: Protein proximity biotinylation mediated by the BirA* biotin-ligase. When biotin is added to cell media, BirA* will biotinylate its surrounding proteins. To ensure efficient labelling of proteins, this process usually takes between 15 and 24 hours.

In addition to the proteome of the nuclear lamina, BioID has been used to analyse many other proteomes and interactomes, including the proteomes of the nuclear pore complex (Kim et al., 2014) or mRNA-related granules (Youn et al., 2018), and the interactomes of the mammalian ribosome quality control complex (Zuzow et al., 2018) or the NSD2 histone methyltransferase (Huang et al., 2019). Although BioID is a commonly used system, it has several limitations. On one hand, although the BirA* protein is not very large (35 kDa), it may interfere in interactome

analyses (Kim et al., 2016a). On the other hand, BioID-mediated biotinylation is a relatively slow process, so this methodology is not well suited to study highly dynamic or transient processes, such as nuclear export.

To overcome these limitations, other labelling methodologies based on biotin-ligases have been developed. For example, in the BioID2 system, a smaller (27 kDa), BirA enzyme promiscuous mutant (R40G) from *Aquifex aeolicus* is used instead of *E. coli* BirA* (Kim et al., 2016a). BioID2 has been used to study for example, the interactomes of N-cadherin (Li et al., 2019), intramitochondrial PKA (Ould Amer and Hebert-Chatelain, 2020) or p38α MAP kinase (Prikas et al., 2020). On the other hand, to shorten the reaction time, enzymes like TurboID and MiniTurbo, which are capable of biotinylate proteins in 10 minutes (Branon et al., 2018), have been developed. Most recently, a novel system, termed AirID, has been reported (Kido et al., 2020). With this system, the labelling radius is smaller and thus, the number of false positives identified in proteome or interactome analyses is reduced.

E1.3.5.3.2. APX peroxidases

The most commonly used peroxidases for proximity biotinylation are those derived from pea or soy APX ascorbate peroxidases, such as APEX. The 28 kDa monomeric protein APEX was generated by introducing a series of mutations (K14D/W41F/E112K) into a homodimeric APX enzyme (Martell et al., 2012). APEX, which is capable of maintaining its activity in the reducing medium of the cytoplasm, was originally created as a tool for electronic microscopy analysis. Later, this enzyme was found to be also useful in sample preparation for MS/MS analyses (Rhee et al., 2013). When activated by H_2O_2, APEX uses biotin-phenol as substrate and forms biotin-phenoxyl free radicals (Rhee et al., 2013). These radicals attack tyrosine, tryptophan, histidine and cysteine residues from surrounding proteins, leading to the covalent biotinylation of these proteins (Figure E11). APEX has been used to analyse the proteomes of the human mitochondrial matrix and intermembrane space (Rhee et al., 2013; Hung et al., 2014), or the primary cilium (Mick et al., 2015).

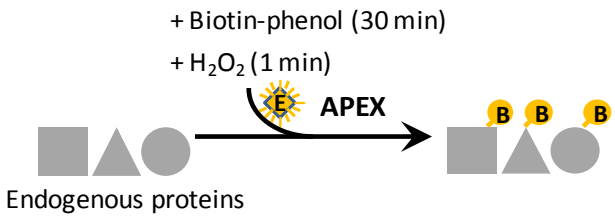

Figure E11: Protein proximity biotinylation mediated by the APEX peroxidase. Cells expressing APEX (or APEX2) are first incubated for half an hour in medium containing the substrate, biotin-phenol. The peroxidase is then activated by adding H_2O_2 to the medium, and the labelling reaction, causing the biotynilation of nearby proteins, is left to proceed for one minute.

In an attempt to increase labelling activity, Lam and co-workers (2015) tested the effect of different APEX mutations, and identified a more active variant (A134P), which they named APEX2. The procedure for APEX2-mediated proximity biotinylation is identical to the one used with APEX (see Figure E11). APEX2 has been used, for example, to analyse the proteome of lipid droplets (Bersuker and Olzmann, 2019) and the interactomes of the mammalian ribosome quality control complex (Zuzow et al., 2018), the nuclear lamina protein lamin-12 (Tran et al., 2021), FGF1 (Zhen et al., 2018), or STK38 kinase (Martin et al., 2019).

In summary, proximity protein labelling has been used in recent years to study several proteomes and interactomes. However, this methodology has not yet been applied to analyse the CRM1 exportome. Therefore, in this thesis, a new approach to investigate CRM1-mediated nuclear export, based on APEX2-mediated proximity labelling, has been designed and tested (Sendino et al., 2021).

E1.4. CRM1 inhibition as a therapeutic approach in cancer

In this section the relationship between CRM1 and cancer will be described, focusing on the alterations (mutations or overexpression) of the CRM1-coding gene (*XPO1*) that have been detected in different types of tumours. Furthermore, the results obtained in preclinical and clinical studies that use CRM1 inhibition as a therapy against cancer will be reviewed. Most of these studies have been carried out with the SINE compound selinexor.

It must be noted that, even if SINE-based therapy is principally focused to cancer treatment, there is emerging evidence that other conditions, such as demyelinating diseases (Haines et al., 2015) or viral infections (Pickens and Tripp, 2018; Kashyap et al., 2021) might be amenable to treatment with these compounds. In this regard, two clinical trials evaluating selinexor as a treatment for COVID-19 (NCT04349098 and NCT04534725) are registered in the ClinicalTrials website (https://clinicaltrials.gov/). In NCT04349098 selinexor is used to treat patients with acute COVID-19, while in NCT04534725 it is used to treat oncologic patients suffering from mild COVID-19.

E1.4.1. Altered nucleocytoplasmic localisation of proteins in cancer

Normal cell function relies on the correct subcellular distribution of hundreds of proteins. The presence of a critical protein in the wrong cellular compartment may have severe pathological consequences. For example, aberrant cytoplasmic localisation of a physiologically nuclear tumour suppressor protein may render this protein inactive, and thus contribute to tumourigenesis. In fact, mislocalisation of cancer-related proteins, including the products of prominent oncogenes and tumour suppressor genes, such as p53 or BRCA1, has been often demonstrated in human tumours (Hung and Link, 2011; Hill et al., 2014; Wang and Li, 2014; Dickmanns et al., 2015).

Nucleocytoplasmic localisation of proteins can be disrupted by different mechanisms in cancer cells. On one hand, the trafficking of a specific protein can be altered by a mutation that either interferes with the activity of its transport signals (NLSs or NESs) or that creates a novel signal in the mutant protein. For example, aberrant localisation of the tumour suppressor BRCA2 to the cytoplasm can result from mutations that unmask normally hidden NES sequences (Jeyasekharan et al., 2013), whereas cytoplasmic mislocalisation of certain NPM1 mutants is the result of a frameshift mutation that creates a novel strong NES, not present in the wild-type protein (Mariano et al., 2006). On the other hand, a general defect in the nucleocytoplasmic localisation of proteins may arise in tumour cells, if elements of the transport machinery themselves are genetically altered or aberrantly expressed (Mor et al.,

2014). Examples of genetic alterations targeting the nuclear transport machinery include chromosome rearrangements involving nucleoporin genes (e.g., NUP98 and NUP214) in haematological malignancies. The abnormal fusion proteins resulting from these translocations have been reported to disrupt CRM1-mediated export (Takeda et al., 2010; Takeda and Yaseen, 2014; Saito et al., 2016). Examples of nuclear transport factors abnormally expressed in tumours include the nuclear import receptor importin-β (Wang and Li, 2014)

In the case of CRM1, both aberrant expression and genetic alterations have been detected in different types of cancer, as detailed below. The abnormal CRM1 function that may result from these alterations would, in turn, disrupt the normal nucleocytoplasmic localisation of hundreds of CRM1 cargo proteins.

E1.4.1.1. CRM1 mutations in cancer: the recurrent E571 amino acid mutation in haematological tumours

Missense mutations affecting CRM1 glutamic acid residue E571 (mostly E571K) have been recurrently detected in haematological malignancies (Table E2). Of note, it has been recently described that this mutation is a driver event in the oncogenic process (Taylor et al., 2019).

Table E2: Recurrent CRM1 mutations in haematological malignancies. This table presents an updated and summarised version of the data shown in Table 2 in Sendino et al., 2018.

Type of malignancy	Mutation frequency	References
Chronic lymphocytic leukaemia (CLL)	317/6126 (5.17 %)	Puente et al., 2011; Quesada et al., 2011; Balatti et al., 2012; Landau et al., 2013, 2015; Damm et al., 2014; Jeromin et al., 2014; Lawrence et al., 2014; Messina et al., 2014; Guièze et al., 2015; Hernández et al., 2015; Ojha et al., 2015; Sutton et al., 2015; Vollbrecht et al., 2015; Amin et al., 2016; Jain et al., 2016; Cosson et al., 2017; Quijada-Álamo et al., 2017; Takahashi et al., 2018; Hu et al., 2019; Taylor et al., 2019; Gángó et al., 2020; Machnicki et al., 2020
Primary mediastinal B-cell lymphoma (PMBL)	36/138 (26.09 %)	Dubois et al., 2016; Jardin et al., 2016; Taylor et al., 2019
Hodgkin lymphoma (HL)	69/374 (18.45 %)	Camus et al., 2016, 2021; Jardin et al., 2016; Tiacci et al., 2018; Liang et al., 2019; Wienand et al., 2019; Taylor et al., 2019; Van Slambrouck et al., 2020
Diffuse large B-cell lymphoma (DLBCL)	25/1187 (2.11 %)	Dubois et al., 2016; Jardin et al., 2016; Taylor et al., 2019
Hairy cell lymphoma (HCL)	1/24 (4.2 %)	Maitre et al., 2018
Mature B-cell neoplasms	1/12 (8.3 %)	Taylor et al., 2019
Marginal zone lymphoma (MZL)	1/4 (25 %)	Taylor et al., 2019

The E571K mutation was first described 10 years ago in chronic lymphocytic leukaemia (CLL) (Puente et al., 2011). Around 5 % of CLL patients have this mutation (see Table E2), often associated with an unmutated IGHV status, an unfavourable prognostic marker (Puente et al., 2011; Jeromin et al., 2014; Jain et al., 2016). However, CRM1 mutation itself does not seem to predict poorer patient prognosis in CLL (Jain et al., 2016). Besides CLL, CRM1 E571K mutation is also a frequent event in Hodgkin's lymphoma (HL, 18 %) and in primary mediastinal B-cell lymphoma (PMBL, 26 %). While HL patients with CRM1 mutations do not appear to have a worse prognosis than patients with wild-type CRM1 (Camus et al., 2016), a shorter progression-free survival was reported for PMBL patients bearing CRM1 mutations (Jardin et al., 2016). Interestingly, it has been suggested that CRM1 mutations could represent useful biomarkers to evaluate minimal residual disease in both HL and PMBL (Camus et al., 2017). In contrast to haematological malignancies, CRM1 mutations have been very rarely found in solid tumours, although isolated instances have been reported (Lin et al., 2014, Pitt et al., 2016; Taylor et al., 2019).

Consistent with the position of the E571 residue proximal to the NES-binding site of CRM1 (see Figure E4C), it has been reported that the E571K mutation subtly increases the affinity of the receptor for some NESs with a negatively charged C-terminal end (García-Santisteban et al., 2016).

E1.4.1.2. Altered CRM1 expression in human tumours

The expression level of CRM1 at either the mRNA or protein level has been analysed in many different cancer types. CRM1 is frequently overexpressed in tumour samples with respect to the corresponding normal tissue (Noske et al., 2008; Huang et al., 2009; Shen et al., 2009; Yao et al., 2009; Pathria et al., 2012; Akagi et al., 2013; Inoue et al., 2013; Kojima et al., 2013; Schmidt et al., 2013; Zhang et al., 2013; Zhou et al., 2013; Tai et al., 2014; van der Watt et al., 2014; Yang et al., 2014a; Liu et al., 2016; Sun et al., 2016, 2017; Conforti et al., 2017; Saulino et al., 2018; Xia et al., 2018; Yue et al., 2018; Birnbaum et al., 2019; Chen et al., 2019; Cruz-Ramos et al., 2019; Duijvesz et al., 2019; Fan et al., 2020; Jiang et al., 2020; Wu et al., 2020; Zhu et al., 2020). In fact, CRM1 overexpression was observed in all solid tumour types and haematological malignancies examined, with the exception of liver cancer (Xie et al., 2016). In several of these studies, the potential prognostic significance of CRM1 expression has been evaluated. Higher CRM1 expression was associated with poorer prognosis in patients with acute myeloid leukaemia (AML; Kojima et al., 2013), diffuse large B-cell lymphoma (DLBCL; Fan et al., 2020), multiple myeloma (MM; Tai et al., 2014), glioma (Shen et al., 2009; Liu et al., 2016; Wu et al., 2020), non-small cell lung cancer (NSCLC; Akagi et al., 2013), thymic epithelial

tumours (Conforti et al., 2017), ovarian cancer (Noske et al., 2018), oesophageal squamous cell carcinoma (van der Watt et al., 2014; Yang et al., 2014a), pancreatic cancer (Huang et al., 2009; Birnbaum et al., 2019; Zhu et al., 2020), breast cancer (Yue et al., 2018) or hepatocellular carcinoma (Chen et al., 2019). However, contradictory findings on the prognostic value of CRM1 expression in gastric cancer (Zhou et al., 2013; Sun et al., 2017) and in osteosarcoma (Yao et al., 2009; Jiang et al., 2020) have been reporterd.

The molecular mechanisms responsible for CRM1 overexpression in cancer cells are still poorly characterised. Copy number gains at chromosomal region 2p, affecting the *XPO1* locus, have been found to correlate with high CRM1 mRNA expression in lymphomas (Jardin et al., 2016) and chronic lymphocytic leukaemia (CLL) (Cosson et al., 2017). In addition, *XPO1* transcription has been reported to be regulated by cMyc and p53 (van der Watt and Leaner, 2011; Golomb et al., 2012), two proteins that are frequently altered in cancer. Conceivably, disruption of this regulation may contribute to aberrant CRM1 expression in some tumours, although further studies are required to test this possibility.

E1.4.1.3. CRM1 inhibition in cancer therapy

E1.4.1.3.1. Development and preclinical evaluation of selective inhibitors of nuclear export (SINEs)

Even before CRM1 was identified as its cellular target, LMB had been found to possess antitumour activity, and it had been tested in a clinical trial (Newlands et al., 1996). LMB was found to have severe toxicities when administered to patients, precluding its development as a clinically useful drug.

Nevertheless, the availability of this potent and specific inhibitor made it possible to carry out proof-of-concept experiments testing the effect of CRM1 inhibition in different tumour settings. As an illustrative example, some early data regarding the effect of LMB treatment in chronic myelogenous leukaemia (CML) cells expressing the BCR-ABL oncoprotein will be briefly described. Shortly after the identification of CRM1 as a nuclear export receptor, the c-ABL kinase was identified as one of its cargos, bearing a C-terminal NES that is also present in the BCR-ABL fusion protein (Taagepera et al., 1998). At that time, treatment of BCR-ABL-positive CML patients was undergoing a dramatic improvement with the introduction of the kinase inhibitor imatinib (Druker et al., 1996; le Coutre et al., 1999). In this context, it was reported that the sequential combination of imatinib plus LMB led to the nuclear entrapment of BCR-ABL, which selectively induced apoptosis of CML cells (Vigneri and Wang, 2001).

Furthermore, subsequent experiments showed that the combination with LMB could overcome resistance to imatinib due to BCR-ABL amplification (Kancha et al., 2008).

These and other encouraging findings in different tumour types (reviewed in Turner and Sullivan, 2008) suggested that CRM1 inhibition might represent a valid strategy for cancer treatment, fostering the search for other, clinically useful, CRM1 inhibitors. Over the next years, several natural and synthetic inhibitors of CRM1 were reported (reviewed in Senapedis et al., 2014, and Tan et al., 2014). Similar to LMB, these compounds bind covalently to CRM1 residue C528, and occupy the NES-binding groove, blocking access to NESs. However, unlike LMB, some of these novel inhibitors, such as CBS9106, S109 or SINE compounds, bind to CRM1 in a reversible manner, which was associated to less severe toxicity in preclinical *in vivo* models (Sakakibara et al., 2011; Liu et al., 2016). Studies with these compounds further validated CRM1 inhibition as a relevant strategy for cancer treatment (Turner et al., 2009).

While most CRM1 inhibitors have only been tested *in vitro* or in mouse xenograft models, SINEs are undergoing development as potential anticancer drugs, and some of these compounds are already being evaluated in clinical trials (Table E3) or have been approved for the treatment of certain cancer patients (Food and Drug Administration, 2019, 2020a, 2020b; European Medicines Agency, 2021).

SINEs were developed in 2012 using structure-assisted relationship methodology combined with a novel computational approach termed consensus-induced fit docking (Kalid et al., 2012; Lapalombella et al., 2012), a strategy that relied crucially on the structures of NES-bound CRM1. The “first-generation” series of SINEs included a relative large number of slowly reversible CRM1 inhibitors, such as KPT-127, KPT-185, KPT-205, KPT-227, KPT-249, KPT-251, KPT-276 and KPT-330 (selinexor). As summarised in Table E3, SINE compounds have been extensively tested in preclinical models of many different haematological malignancies and solid tumours. In these models, SINEs have demonstrated potent *in vitro* and *in vivo* activity against cancer cells (including growth inhibition, induction of apoptosis, and cell cycle arrest), with only minor toxic effects on normal cells. Importantly, several SINEs (most prominently selinexor) have been shown to increase the sensitivity of cancer cells to currently used drugs and also to synergise with other targeted therapeutic agents.

In view of the favourable results obtained with the first generation, second generation SINEs, such as KPT-8602 (eltanexor) have been developed. Eltanexor is also currently been tested in preclinical studies (Table E3).

Table E3: Summary of preclinical studies with SINEs. ALL: acute lymphocytic leukaemia; AML: acute myeloid leukaemia; CLL: chronic lymphocytic leukaemia; CML: chronic myelogenous leukaemia; DLBCL: diffuse large B-cell lymphoma; HNSCC: head and neck squamous cell carcinoma; MCL: mantle cell lymphoma; MM: multiple myeloma; NHL: non-Hodgkin lymphoma; NSCLC: Non-small cell lung cancer; PCNSL: primary central nervous system lymphoma; PMBL: primary mediastinal B-cell lymphoma; TCL: T-cell lymphoma.

SINE	Type of malignancy	References
KPT-127	Pancreas cancer	Azmi et al., 2013a
KPT-185	ALL, AML, CLL, melanoma, MM, NHL, NSCLC, PMBL, breast, kidney, ovarian, pancreas, protate and gastric cancers	Lapalombella et al., 2012; Ranganathan et al., 2012; Azmi et al., 2013a, 2013b; Inoue et al., 2013; Kojima et al., 2013; Salas Fragomeni et al., 2013; Turner et al., 2013; Zhang et al., 2013; Cheng et al., 2014; Gao et al., 2014; Mendonca et al., 2014; Tai et al., 2014; Wang et al., 2014; Han et al., 2015; Miyake et al., 2015; Jardin et al., 2016; Kim et al., 2016b; Chen et al., 2017; Sekihara et al., 2017; Subhash et al., 2018; Sexton et al., 2019; Mendes et al., 2020; Wei et al., 2020
KPT-205	Pancreas cancer	Azmi et al., 2013a
KPT-227	Pancreas cancer	Azmi et al., 2013a
KPT-249	MM	Turner et al., 2013
KPT-251	AML, CLL, NHL, glioblastoma, melanoma, mesothelioma, breast, kidney and prostate cancers	Lapalombella et al., 2012; Azmi et al., 2013b; Etchin et al., 2013a; Inoue et al., 2013; Salas Fragomeni et al., 2013; Cheng et al., 2014; Mendonca et al., 2014; Gravina et al., 2014b, 2017; De Cesare et al., 2015; Green et al., 2015; Muqbil et al., 2016
KPT-276	AML, glioblastoma, MCL, melanoma, mesothelioma, MM, NHL, NSCLC, breast and gastric cancers	Ranganathan et al., 2012; Azmi et al., 2013b; Salas Fragomeni et al., 2013; Schmidt et al., 2013; Turner et al., 2013; Zhang et al., 2013; Cheng et al., 2014; Wang et al., 2014; Yang et al., 2014b; De Cesare et al., 2015; Green et al., 2015; Han et al., 2015; Muqbil et al., 2016
KPT-330 (selinexor)	AML, ALL, CLL, DLBCL, fibrosarcoma, glioblastoma, pediatric glioma, small bowel neuroendocrine tumours, HNSCC, liposarkoma, MCL, melanoma, mesothelioma, mielofibrosis, MM, NHL, NSCLC, osteosarcoma, sarcoma, PCNSL, PMBL, bladder, breast, liver, kidney colorectal, ovarian, pancreas prostate, thymic epithelial, thyroid, gastric, and other pediatric or adult cancers	Etchin et al., 2013b; Salas Fragomeni et al., 2013; Turner et al., 2013, 2016a, 2016b, 2020; Walker et al., 2013; Cheng et al., 2014; Gravina et al., 2014b, 2017; Mendonca et al., 2014; Sun et al., 2014; Tai et al., 2014; Wettersten et al., 2014; Yang et al., 2014b; Zheng et al., 2014; Zhong et al., 2014; De Cesare et al., 2015; Green et al., 2015; Hing et al., 2015; Kazim et al., 2015; Miyake et al., 2015; Ranganathan et al., 2015; Attiyeh et al., 2016; Ferreiro-Neira et al., 2016; Jardin et al., 2016; Kashyap et al., 2016, 2018; Kim et al., 2016b; Muqbil et al., 2016; Nakayama et al., 2016; Rosebeck et al., 2016; Sun et al., 2016; Wrobel et al., 2016; Arango et al., 2017; Azmi et al., 2017, 2020; Burke et al., 2017; Chen et al., 2017; Conforti et al., 2017; Cosson et al., 2017; Garg et al., 2017a, 2017b; Muz et al., 2017; Nair et al., 2017; Aboukameel et al., 2018; Argueta et al., 2018; Baek et al., 2018; Barazeghi et al.,2018; Brunetti et al., 2018; Corno et al., 2018; Luedtke et al., 2018; Marcus et al., 2018; Ming et al., 2018; Saenz-Ponce et al., 2018; Schaffer et al., 2018; Shang et al., 2018; Subhash et al., 2018; Wahba et al., 2018; Zhang et al., 2018; Abeykoon et al., 2019; Aladhraei et al., 2019; Currier et al., 2019; Kapoor et al., 2019; Khan et al., 2019; Kulkoyluoglu-Cotul et al., 2019; Lim et al., 2019; Liu et al., 2019; Sexton et al., 2019; Tarantelli et al., 2019; Yan et al., 2019; Zhu et al., 2019a; Bonolo de Campos et al., 2020; Brinton et al., 2020; DeSisto et al., 2020; Fischer et al., 2020; Jiménez et al., 2020; Martini et al., 2020; Jeitany et al., 2021
KPT-8602 (eltanexor)	AML, ALL, CLL, DLBCL, NHL, mielofibrosis, MM, prostate, gastric, thyroid and liver cancers	Aboukameel et al., 2018; Gruffaz et al., 2019; Khan et al., 2019; Liu et al., 2019; Lucas et al., 2019; Sexton et al., 2019; Yan et al., 2019; Fischer et al., 2020; Turner et al., 2020; Verbeke et al., 2020

In general terms, the anticancer effect of CRM1 inhibition is thought to rely on the relocation of mislocalised CRM1 cargos with tumour-suppressive and growth-regulatory functions (e.g., p53) to the nucleus, where they carry out their normal activity. However, this may be an overly simplistic view. Given the large number of potential CRM1 cargos with a role in cancer, the export-independent roles of CRM1, and the complex nature of the tumourigenesis process, the specific molecular and cellular mechanisms underlying the anticancer effect of SINEs may differ in different tumour settings. In this regard, preclinical studies are providing important information on tumour context-specific proteins and signalling pathways that may mediate SINE activity, such as the BCR-ABL oncoprotein in CML mentioned above (Vigneri and Wang, 2001), or the NF-κB pathway in lung cancer (Kim et al., 2016b).

E1.4.1.3.2. Selinexor in cancer patients: clinical trials and first approvals for clinical use

In preclinical studies, selinexor compared favourably to other first-generation SINEs in terms of the balance between potency and tolerability. Selinexor, an orally available drug, is the only compound of the series that has advanced into clinical development for human cancer. Table E4 shows the clinical trials involving selinexor published at ClinicalTrials.gov site (https://clinicaltrials.gov) until January 2021.

Table E4: Clinical trials in cancer using selinexor.

Type of Malignancy	Reference and ID
Advanced solid tumours	Abdul Razak et al., 2016 (ID: NCT01607905)
Sarcoma	Gounder et al., 2016 (ID: NCT01896505)
Refractory pediatric acute leukaemia	Alexander et al., 2016 (ID: NCT02212561)
NHL	Kuruvilla et al., 2017 (ID: NCT01607892)
AML	Garzon et al., 2017 (ID: NCT01607892); Wang et al., 2018 (ID: NCT02573363); Bhatnagar et al., 2019 (ID: NCT02093403); Fiedler et al., 2020 (ID: NCT02249091); Sweet et al., 2020 (ID: NCT02403310); Taylor et al., 2020 (ID: NCT02228525)
MM	Chen et al., 2018 (ID: NCT01607892); Bahlis et al., 2018 (ID: NCT02343042); Vogl et al., 2018 (NCT02336815); Chari et al., 2019 (ID: NCT02336815); Jakubowiak et al., 2019 (ID: NCT02199665); Grosicki et al., 2020 (ID: NCT03110562)
DLBCL	Kalakonda et al., 2020 (ID: NCT02227251)
Castration-resistant protstate cancer	Wei et al., 2018 (ID: NCT02215161)
Triple negative metastatic breast cancer	Shafique et al., 2019 (ID: NCT02402764)
Gynecological malignancies	Vergote et al., 2019 (ID: NCT02269293)

Ovarian and endometrial malignancies	Rubinstein et al., 2021 (ID: NCT01607905)
Pancreatic ductal adenocarcinoma	Azmi et al., 2020 (ID: NCT02178436)
Colorectal metastatic cancer	Nilsson et al., 2020 (ID: NCT02384850)
T-cell lymphoma (TCL) or relapsed or refractory natural killer/T-cell lymphoma (NKTL)	Tang et al., 2021 (ID: NCT03212937)

Moreover, there is also a clinical trial (NCT02649790) using the second-generation compound eltanexor in combination with dexamethasone and ASTX727, an inhibitor of DNA methyltransferase.

The positive results obtained in several clinical trials have led to selinexor approval by the FDA (Food and Drug Administration of the USA) and by the EMA (European Medicines Agency) under the trade names XPOVIO™ and Nexpovio®, respectively, for the treatment of certain cancer patients. On July 2019 it was approved by the FDA in combination with dexamethasone for adult patients with relapsed or refractory multiple myeloma (MM) who have received at least four prior therapies, and whose disease is refractory to at least two proteasome inhibitors, at least two immunomodulatory agents, and an anti-CD38 monoclonal antibody (Food and Drug Administration, 2019). The EMA approved selinexor in the same conditions as FDA did for relapsed or refractory MM patients on March 2021 (European Medicines Agency, 2021). On December 2020 the FDA authorised selinexor use in combination with bortezomib and dexamethasone for the treatment of adult patients with MM who have received at least one prior therapy (Food and Drug Administration, 2020a). On the other hand, on June 2020 selinexor use was approved for adult patients with relapsed or refractory diffuse large B-cell lymphoma (DLBCL) after at least two lines of systemic therapy (Food and Drug Administration, 2020b).

E2. Hypothesis and aims

By recognising and binding NES motifs, the nuclear export receptor CRM1 mediates the export of hundreds of cargos from the nucleus to the cytoplasm, thus contributing to maintain cellular homeostasis. Identification of NESs is a crucial step in understanding how export of CRM1 cargos is regulated. However, while the NES of many cargos have already been mapped, the NES motifs that mediate CRM1-mediated export of many other proteins are still unknown. Furthermore, although the details of CRM1-mediated NES export have been well studied from a structural and biochemical perspective, mechanistic studies on this important process in a cellular context are still largely lacking. With this in mind, the first **hypothesis** of this thesis is that, by applying cellular assays for nuclear export activity, it would be possible to identify and gain information on the role of NESs in the regulation and function of important cellular and viral proteins, and also to learn more about the mechanistic details of CRM1-mediated NES export.

On the other hand, CRM1 is emerging as a prominent target for anticancer therapy. While this thesis was in progress, the CRM1 inhibitor selinexor was granted approval both in the USA and in Europe for its use in the treatment of specific cancer patients. Although CRM1 inhibition is already in clinical use, there is still very limited knowledge about possible combinations of selinexor with other drugs, and about the cellular effect of CRM1 inhibition on its exportome. Therefore, the second **hypothesis** in this thesis is that, combining selinexor with other targeted therapeutic agents could be an interesting strategy for cancer treatment, and that novel proximity labelling-based proteomic approaches can be useful to characterise the cellular effect of CRM1 inhibition.

In order to test these hypotheses, the following aims were established:

- Aim 1: To identify and characterise new human and viral NESs using existing and newly-developed nuclear export assays.
- Aim 2: To apply these assays to further investigate the mechanism of CRM1-mediated NES export in a cellular context, and determine how this mechanism can be affected by cancer-related mutations.
- Aim 3: To select and evaluate *in vitro* novel combinations of selinexor with other targeted drugs.
- Aim 4: To design and evaluate a new proteomics approach to characterise the cellular effects of CRM1 inhibition.

E3. Results

E3.1. NES identification and mechanistic analysis of CRM1-mediated NES export

E3.1.1. Searching for new NESs using the Rev(1.4)-GFP nuclear export assay

The nuclear export assay based on the pRev(1.4)-GFP reporter (Henderson and Eleftheriou, 2000), hereafter referred to as the Rev(1.4)-GFP export assay, has been used in dozens of reported studies to search for new NESs, as well as to measure the export activity of known NESs.

The pRev(1.4)-GFP reporter encodes a mutant HIV Rev protein, named Rev(1.4), fused to GFP. Wild type Rev is a nucleocytoplasmic shuttling protein that bears both NLS and NES signals, which facilitate its nuclear import and export. As illustrated in Figure E12, the nuclear import and export of wild type Rev can be blocked by treating cells with actinomycin D (ActD) or leptomycin B (LMB), respectively.

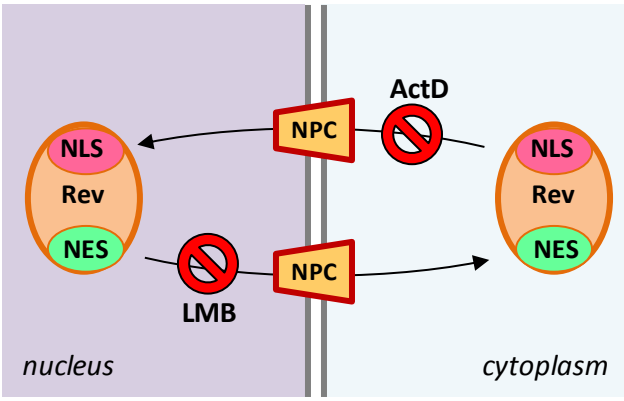

Figure E12: Nucleocytoplasmic transport of wild type HIV Rev protein. Rev NLS-mediated nuclear import can be blocked by ActD treatment, while NES-mediated nuclear export can be blocked by LMB treatment (adapted from Henderson and Eleftheriou (2000)).

The Rev(1.4) mutant protein, however, retains the NLS but bears a mutated, inactive NES. Thus, it can be imported, but not exported from the nucleus (Figure E13). As a result, the pRev(1.4)-GFP reporter protein accumulates in the nucleus when expressed in cells. Nuclear export of the reporter can be restored by cloning an active NES between the Rev(1.4) and the GFP moieties. This is precisely the basis of this export assay.

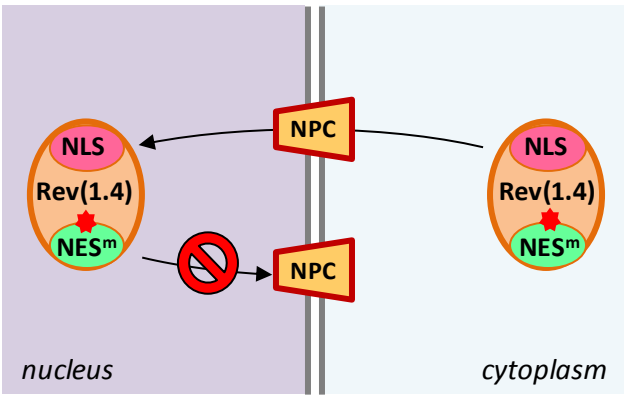

Figure E13: Nucleocytoplasmic transport of the Rev(1.4) mutant protein. Rev(1.4) bears the wild type NLS, but its NES has been mutationally inactivated (NES^{m}). Therefore, this mutant protein can be imported into the nucleus, but cannot be exported back to the cytoplasm.

Of note, not all active NESs are strong enough to overcome the nuclear import induced by Rev(1.4) NLS and, therefore, Rev(1.4)-[NES]-GFP reporters containing a weak NES will still tend to accumulate in the nucleus. This tendency can be prevented by treating cells with ActD, which blocks Rev NLS-mediated import, thus allowing detection of even weak NESs. A second drug, the protein synthesis inhibitor cycloheximide (CHX), is also used in this assay to ensure that the fluorescence detected in the cell cytoplasm is due to nuclear export and not to newly synthesised reporter proteins (Figure E14).

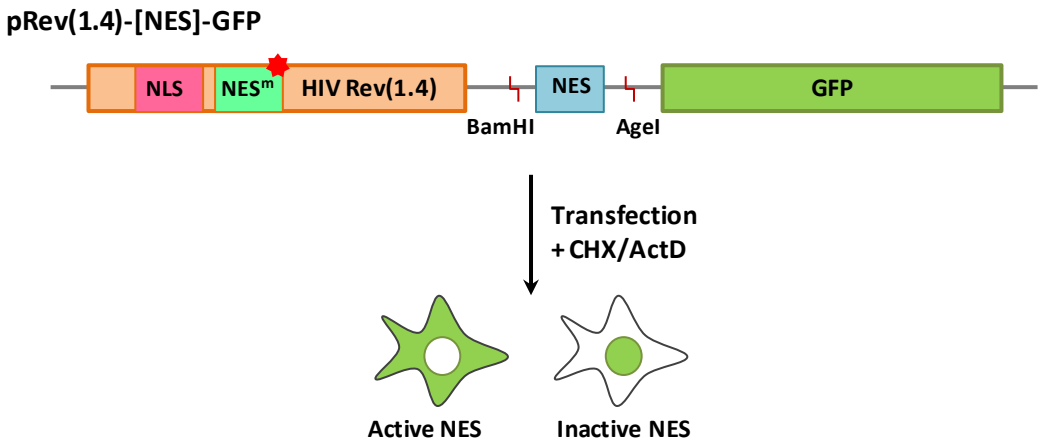

Figure E14: Nuclear export assay based on the Rev(1.4)-GFP reporter. pRev(1.4)-[NES]-GFP plasmids are transfected in two parallel samples of HeLa cells growing onto glass coverslips. 24 hours later, all cells are treated with CHX for 3 hours to block protein synthesis. One of the samples is also treated with ActD, to inhibit Rev(1.4) NLS-mediated import. Samples are then processed and the nucleocytoplasmic localisation of the reporter is analysed by fluorescence microscopy to determine whether the cloned NES (blue) is active or not.

Depending on the nucleocytoplasmic location of the reporter in the presence/absence of ActD, this cellular assay is able to rank NES activity at 9 different levels. The weakest NESs will obtain an export score of “1” and the strongest ones a score of “9” (Table E5).

Table E5: Scoring-system described by Henderson and Eleftheriou (2000) to rank NESs activity using the Rev(1.4)-GFP nuclear export assay. Depending on the location that each NES-containing reporter shows in the cell population (in the presence or absence of ActD), the NESs are classified in 9 activity levels from 1 (weakest) to 9 (strongest).

NES activity score	GFP partially accumulates in the cytoplasm (% cells)		GFP completely shifts to the cytoplasm (% cells)	
	-ActD	+ActD (3 h)	-ActD	+ActD (3 h)
1	<20	20-50	0	0
2	<50	51-80	0	0
3	<50	>80	-	<20
4			<20	20-50
5			<20	51-80
6			<20	>80
7			20-50	>80
8			51-80	>80
9			>80	>80

In this thesis, the Rev(1.4)-GFP assay was used to characterise the NES motif responsible for the nuclear export of the USP12/UAF1/WDR20 deubiquitinase complex, to search for novel NESs in cancer-related cargos of CRM1 and to test the export-activity of the predicted cNESs in the nucleocapsid protein of the human infecting coronaviruses.

E3.1.1.1. A newly identified NES in WDR20 mediates the nucleocytoplasmic localisation of the USP12/UAF1/WDR20 complex

The results described in this section have been published in Olazabal-Herrero et al., 2019, 2021, and Sendino et al., 2020b.

CRM1 mediates the nucleocytoplasmic transport of hundreds of proteins, and is therefore involved in the regulation of several cellular processes, such as the ubiquitination pathways. Ubiquitination is a reversible posttranslational modification that modulates stability, function and/or localisation of most cellular proteins (van der Veen and Ploegh, 2012). Deubiquitinases (DUBs) are the enzymes that catalyse the removal of ubiquitin moieties from substrate proteins and thus, play a crucial role in many physiological processes (Komander et al., 2009). In this regard, the group were this thesis has been carried out has a long-standing interest on how CRM1 modulates to the function of several human DUBs (García-Santisteban et al., 2012; Rodríguez, 2014; Olazabal-Herrero et al., 2019, 2021; Sendino et al., 2020b). In the context of these studies, the results presented in this section show how CRM1 and a previously undescribed NES regulate the localisation of the deubiquitinase complex formed by the DUB USP12 with its cofactors UAF1 (USP1 associated factor 1) and WDR20 (WD repeat-containing protein 20).

USP12 is a member of the USP (ubiquitin-specific protease) family of DUBs that has critical functions as a tumour suppressor (Gangula and Maddika, 2013; Li et al., 2013). The USP12 protein alone has very low intrinsic enzymatic activity. To become fully active, USP12 needs to bind its cofactors UAF1 (also known as WDR48 (WD repeat-containing protein 48) and WDR20, forming a trimeric complex USP12/UAF1/WDR20, which shows dramatically increased deubiquitinating activity (Kee et al., 2010).

It has been shown that USP12 is a nucleocytoplasmic shuttling protein whose nuclear export is mediated by CRM1 (Kouranti et al., 2010; Jahan et al., 2016). However, there are conflicting reports about the cellular compartment were USP12 is located, with several studies reporting either a mainly cytoplasmic (Sowa et al., 2009; Urbé et al., 2012; Burska et al., 2013; Lehoux et al., 2014; Olazabal-Herrero et al., 2015) or nuclear (Jahan et al., 2016; Joo et al., 2011) localisation. In addition, while Sanyal (2016) proposed a potential NES motif (^{77}KESLLTCLADLFHSI^{91}) in USP12, the experimental evidence presented to support this claim has been debated (Rodríguez, 2016). Thus, in this section an attempt was made to further clarify the factors that determine the transport and localisation of USP12, and to investigate what is the role, if any, of its cofactors in this process.

E3.1.1.1.1. The nucleocytoplasmic distribution of USP12 and WDR20, but not of UAF1, is CRM1-dependent

The effect of LMB on the nucleocytoplasmic distribution of epitope-tagged USP12, UAF1 and WDR20 was tested in HeLa cells. As shown in Figure E15, a three hour LMB treatment did not alter the distribution of UAF1-mRFP. In contrast, a statistically significant effect of LMB was observed on the distribution of YFP-USP12 and YFP-WDR20, indicating that both proteins are actively exported from the nucleus by the CRM1-mediated nuclear export pathway.

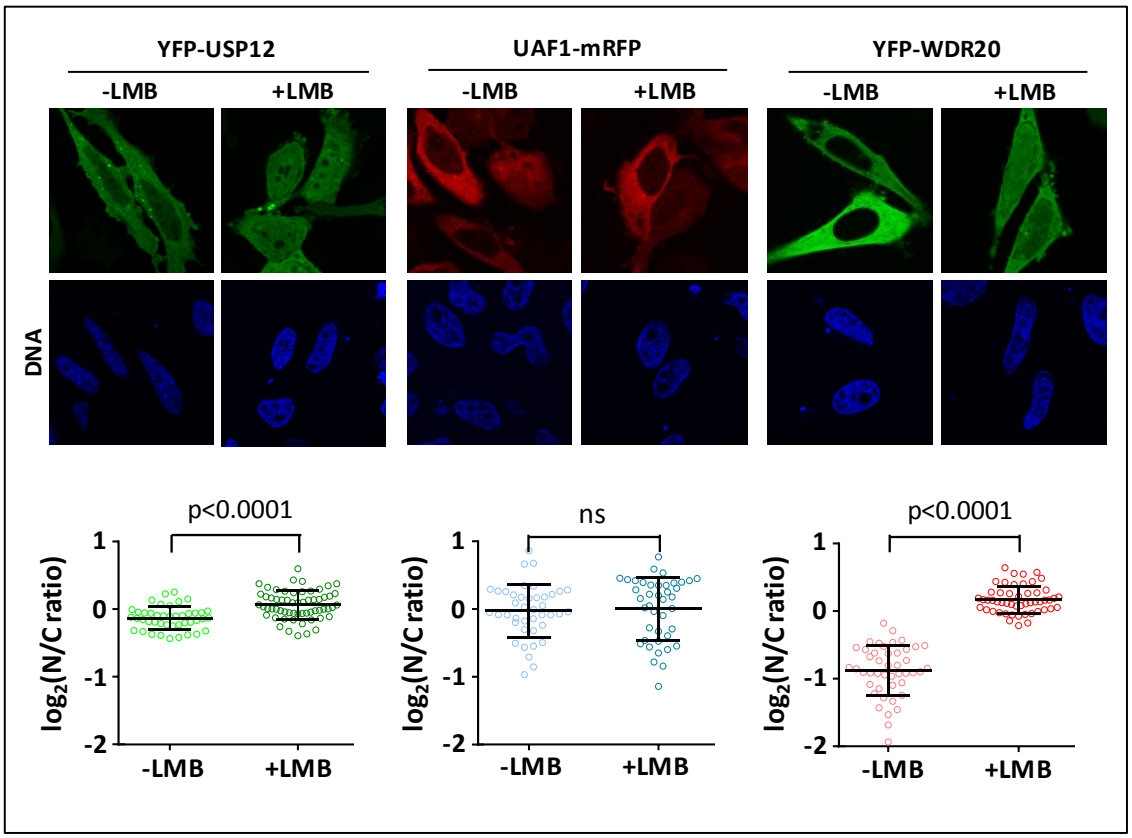

Figure E15: Nucleocytoplasmic localisation of USP12 and WDR20 is CRM1-dependent, whereas the localisation of UAF1 is not. Representative examples of the nucleocytoplasmic localisation of YFP-USP12, UAF1-mRFP and YFP-WDR20 in HeLa cells untreated (-LMB) or treated with LMB. The nucleocytoplasmic (N/C) ratio of each protein in untreated or LMB-treated cells was determined using image analysis and is shown in the graphs below. Each circle in the graph represents a single cell, and the mean (+/- SD) is also indicated. The data correspond to a single experiment where at least 40 transfected cells per condition were analysed. Comparable results were obtained in at least two independent experiments. p values (Mann-Whitney U test) are indicated (ns: non-significant).

Of note, YFP-USP12 and YFP-WDR20 were evenly distributed between nucleus and cytoplasm in LMB-treated cells, but they did not accumulate to a high level inside the nucleus. This observation suggests that the nuclear entry of these proteins is not a highly efficient process, which could be due to cytoplasmic retention or to the lack of strong NLSs. To gauge these possibilities, a version of YFP-USP12 bearing two copies of the strong SV40 large T antigen NLS (Kalderon et al., 1984a, 1984b) (YFP-USP12$^{[2NLS]}$) was generated. YFP-USP12$^{[2NLS]}$ readily

accumulated into the nucleus HEK293T cells (Figure E16), suggesting that the inefficient nuclear import of YFP-USP12 is most likely due to the lack of strong NLSs.

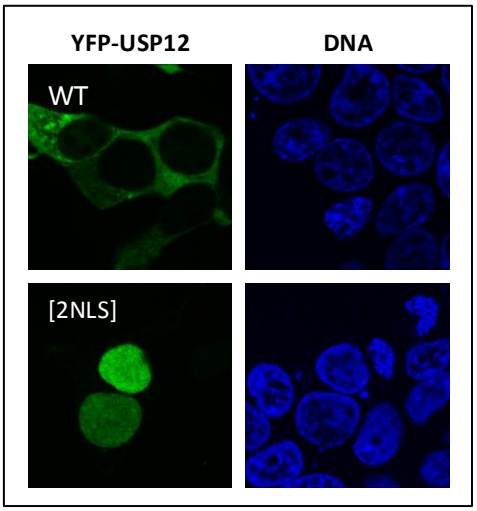

Figure E16: YFP-USP12[2NLS] protein expressed in HEK293T cells shows a predominantly nuclear localisation. YFP-USP12 wild type (WT) is localised at the cytoplasm. YFP-USP12[2NLS], however, is localised in the nucleus. Of note, a faint fluorescent signal at the plasma membrane was also noticeable in some cells expressing YFP-USP12[2NLS] (not shown).

E3.1.1.1.2. A previously reported NES in USP12 is not an active nuclear export determinant

The USP12 motif ^{77}KESLLTCLADLFHSI^{91} has been proposed to be a CRM1-dependent NES (Sanyal, 2016), but the experimental evidence supporting its putative export function was not conclusive. To test whether this motif is active or not, a USP12 fragment containing this sequence and flanking residues (^{75}RKKESLLTCLADLFHSIAT^{93}) was cloned into the pRev(1.4)-GFP plasmid and analysed using the Rev(1.4)-GFP nuclear export assay (Henderson and Eleftheriou, 2000). For this analysis a minimum of 200 cells per sample were classified in nuclear (N), nucleocytoplasmic (NC) or cytoplasmic (C) categories. As shown in Figure E17, the proposed USP12 NES was unable to increase the cytoplasmic localisation of the Rev(1.4)-GFP reporter, even in the presence of ActD. The USP12 motif ^{77}KESLLTCLADLFHSI^{91} was, therefore, classified as a non-functional NES-like motif.

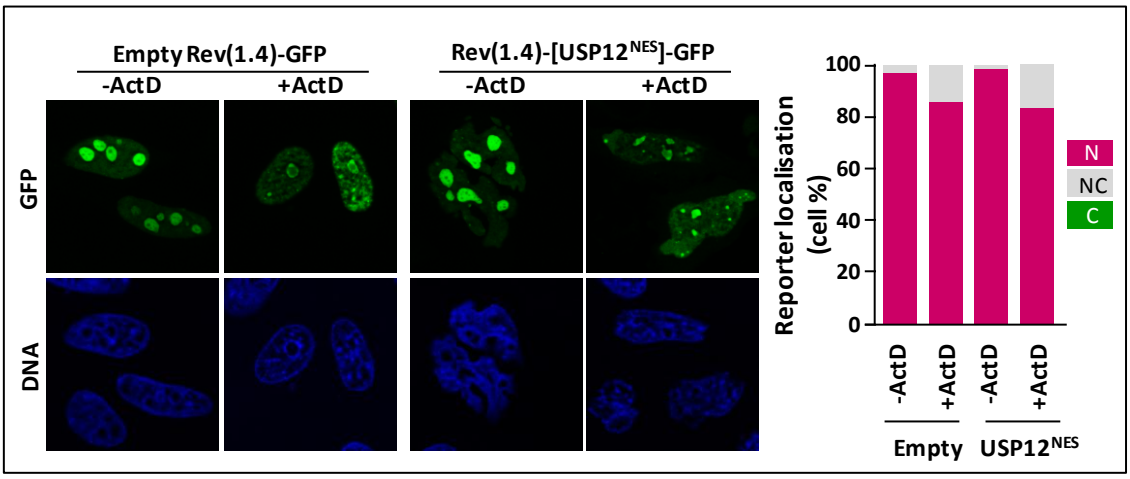

Figure E17: A previously reported NES motif in USP12 (^{77}KESLLTCLADLFHSI^{91}) is inactive in the Rev(1.4)-GFP nuclear export assay. *Left*. Fluorescence images showing representative examples of HeLa cells transfected with the empty Rev(1.4)-GFP reporter plasmid or with the plasmid Rev(1.4)-[USP12^{NES}]-GFP, containing the reported USP12 NES. *Right*. Graph showing the percentage of cells with mostly nuclear (N), nuclear and cytoplasmic (NC) or mostly cytoplasmic (C) localisation of the reporter. At least 200 transfected cells were scored per condition. Even in the presence of ActD, the reported USP12 NES motif was unable to promote nuclear export of Rev(1.4)-GFP.

Further supporting the view that the motif ^{77}KESLLTCLADLFHSI^{91} is not a direct determinant of USP12 nuclear export, the nucleocytoplasmic distribution of a full-length YFP-USP12^{NESmut} protein (bearing alanine mutations of the hydrophobic amino acids) was identical to that of wild type YFP-USP12 in HeLa cells (Figure E18).

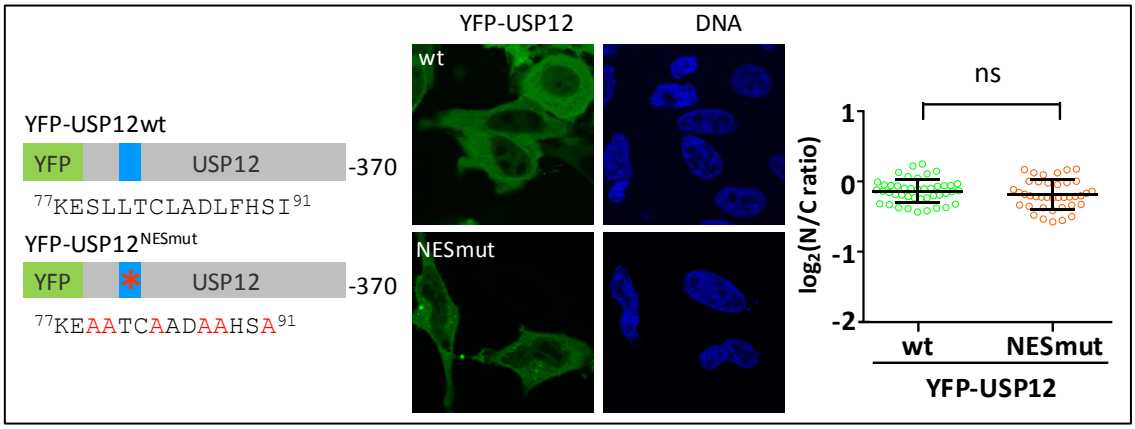

Figure E18: A previously reported NES motif is not a direct determinant of USP12 nuclear export. *Left*. Schematic representation of wild type YFP-USP12 and a NES mutant (YFP-USP12^{NESmut}) bearing six amino-acid substitutions indicated in red (Sanyal, 2016). *Centre*. Fluorescence images of HeLa cells expressing YFP-USP12wt and YFP-USP12^{NESmut}. *Right*. Graph showing the $\log_2$(N/C ratio) of both proteins determined using image analysis of at least 30 transfected cells per sample. Each circle in the graph represents a single cell, and the mean (+/- SD) is shown. ns: non-significant (Mann-Whitney U test).

E3.1.1.1.3. WDR20 bears a functional NES

The finding that the proposed USP12 NES is not functional led to the search for other NES motifs that may mediate export of the USP12/UAF1/WDR20 complex. As the nucleocytoplasmic localisation of WDR20 was clearly dependent on CRM1 (see Figure E15) the search was focused in this protein.

NESs usually adopt a characteristic secondary structure comprising an N-terminal α-helix followed by a C- terminal loop (Kosugi et al., 2008; Dong et al., 2009a; Fung et al., 2015, 2017). According to the reported structures (Li et al., 2016; Zhu et al., 2019b), WDR20 does not present any α-helical region. However, the region between residues 394–509 of WDR20 is not solved in these structures. Based on this structural information, a deletion analysis was carried out by generating three WDR20 fragments: 1–390, 390–510 and 510-569 (Figure E19A). YFP-tagged versions of these fragments were expressed in HeLa cells, and their localisation examined in the presence or absence of LMB (Figure E19B). Like full-length YFP-WDR20, YFP-WDR20(390–510) clearly relocated from the cytoplasm to the nucleus in LMB-treated cells, suggesting that a CRM1-dependent NES may be located within this fragment.

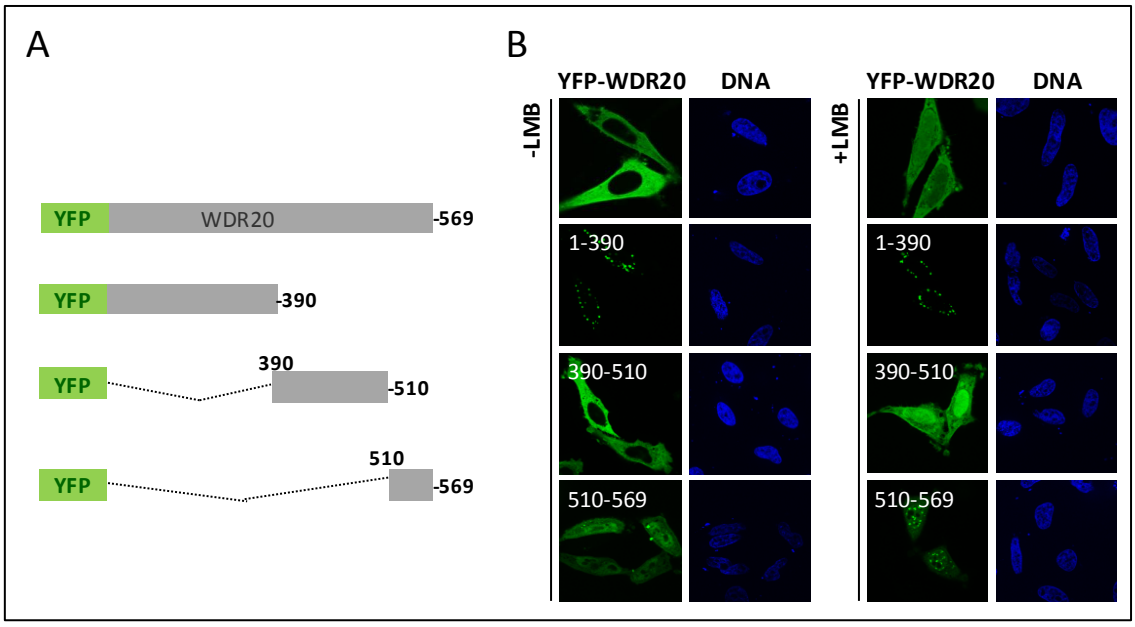

Figure E19: Mapping a potential NES-containing region in WDR20 protein. A. Schematic representation of YFP-tagged WDR20 deletion mutants. B. Fluorescence images of HeLa cells transfected with the different YFP-WDR20 deletion mutants and left untreated or treated with LMB. LMB treatment induced relocation of full-length YFP-WDR20 and YFP-WDR20 (390–510) from the cytoplasm to the nucleus.

Using the NES prediction tool Wregex (Prieto et al., 2014) in *relaxed* mode, several candidate NES (cNES) motifs were predicted in WDR20 amino acid sequence (Figure E20). Only one of these motifs (^{454}IASGVSKFATL^{464}) was located in the region 390-510.

#	Entry	Start	End	Sequence	"!"	Score
1	sp|Q8TBZ3|WDR20_HUMAN	109	118	L-TAT-A-ES-V-S-L	4	63.1
2	sp|Q8TBZ3|WDR20_HUMAN	380	389	L-WD-L-TED-I-L-F	1	50.1
3	sp|Q8TBZ3|WDR20_HUMAN	454	464	I-ASG-V-SKF-A-T-L	3	43.3
4	sp|Q8TBZ3|WDR20_HUMAN	218	228	V-GEG-A-LNE-F-A-F	1	43.3
5	sp|Q8TBZ3|WDR20_HUMAN	246	254	V-FN-F-DS-V-E-L	1	35.9
6	sp|Q8TBZ3|WDR20_HUMAN	65	75	L-CFN-V-GRE-L-Y-F	4	35.1
7	sp|Q8TBZ3|WDR20_HUMAN	258	268	M-KSY-F-GGL-L-C-V	3	35.1
8	sp|Q8TBZ3|WDR20_HUMAN	532	542	A-HER-L-TVL-I-F-L	2	35.1
9	sp|Q8TBZ3|WDR20_HUMAN	288	298	V-WSF-V-DCR-V-I-A	2	23.1

Figure E20: Candidate NES (cNES) motifs predicted by Wregex (*relaxed* mode) in WDR20 amino acid sequence. Only one of the predicted motifs (highlighted in red) was located within the region 390-510.

A WDR20 fragment (^{450}MDGAIASGVSKFATLSLHD^{468}), containing the predicted cNES plus eight flanking amino acids was cloned into the pRev(1.4)-GFP plasmid and tested using the Rev(1.4)-GFP nuclear export assay (Henderson and Eleftheriou, 2000). In marked contrast to the USP12 motif tested above (Sanyal, 2016), WDR20 cNES efficiently promoted the export of the Rev(1.4)-GFP reporter to the cytoplasm (Figure E21), indicating that this motif constitutes a functional NES. Using the assay scoring system (Henderson and Eleftheriou, 2000), a score of 6 was assigned to the WDR20 NES.

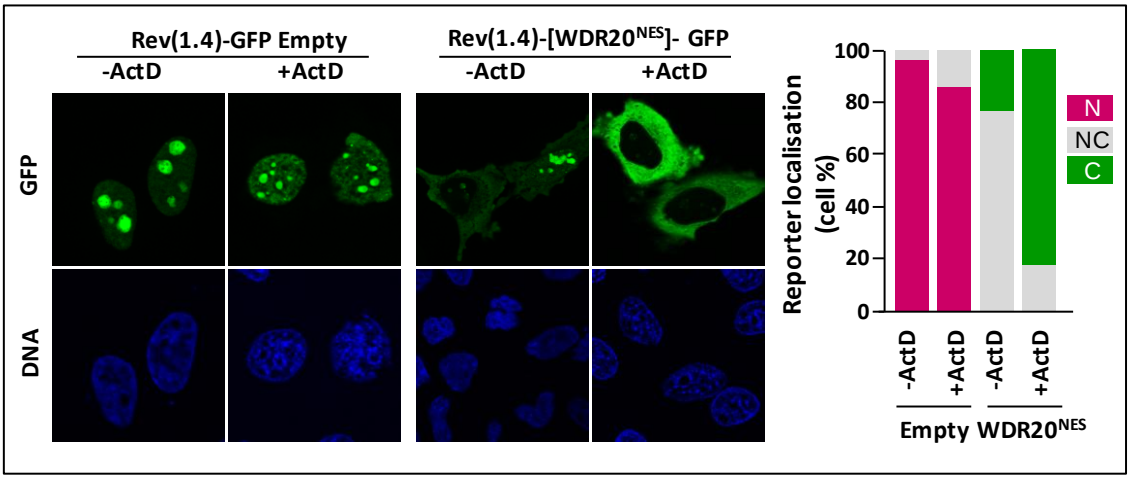

Figure E21: Results of a nuclear export assay to test the activity of the candidate WDR20 NES motif ^{450}MDGAIASGVSKFATLSLHD^{468}. *Left*. Fluorescence images showing representative examples of HeLa cells transfected with the empty Rev(1.4)-GFP plasmid or with the plasmid Rev(1.4)-[WDR20^{NES}]-GFP, containing the candidate WDR20 NES. *Right*. Graph showing the percentage of cells with mostly nuclear (N), nuclear and cytoplasmic (NC) or mostly cytoplasmic (C) localisation of the reporter. At least 200 transfected cells were scored per condition. The WDR20 candidate NES motif readily promoted nuclear export of the Rev(1.4)-GFP reporter, and was assigned a 6 nuclear export score (see Table E5).

E3.1.1.1.4. The identified NES motif mediates CRM1-dependent export of WDR20

To test whether the identified NES motif is an important determinant of the localisation of the full-length WDR20 protein, an NES-mutant version of YFP-WDR20 (YFP-WDR20^{NESmut}) bearing mutations in two leucine residues (L464A/L466A) was generated. As shown in Figure E22, these mutations fully mimicked the effect of LMB treatment, confirming that the ^{450}MDGAIASGVSKFATLSLHD^{468} motif is a novel NES that mediates CRM1-dependent nuclear export of WDR20.

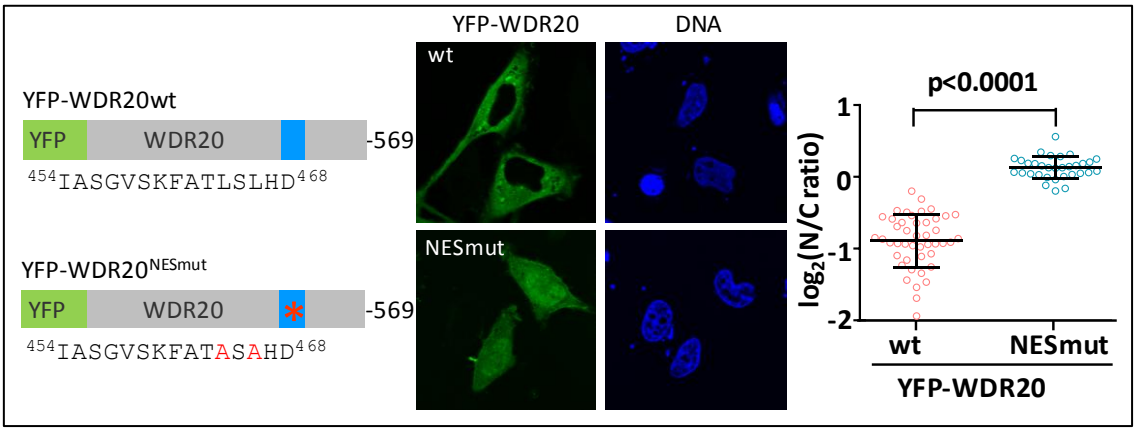

Figure E22: The identified NES motif mediates CRM1-dependent nuclear export of the full-length WDR20 protein. *Left*. Schematic representation of wild type (wt) YFP-WDR20 and YFP-WDR20^{NESmut}, a mutant bearing alanine substitutions of two NES residues (L464 and L466) (highlighted in red). *Centre*. Representative examples of HeLa cells expressing YFP-WDR20wt and YFP-WDR20^{NESmut}. *Right*. Graph showing the N/C ratio of both proteins determined using image analysis of at least 30 transfected cells per sample. Each circle in the graph represents a single cell, and the mean (+/- SD) is shown. p value (Mann-Whitney U test) is indicated.

E3.1.1.1.5. The newly identified NES in WDR20 is functionally conserved in its homolog DMWD

A poorly characterised homolog of WDR20, the dystrophia myotonica WD repeat-containing protein (DMWD) has been reported to also interact with USP12 (Sowa et al., 2009). DMWD shows a high degree of amino acid sequence similarity to WDR20, and the new WDR20 NES described above is partially conserved in DMWD sequence (Figure E23).

```
WDR20 MAT------EG---GGKEMNEIKTQFTTREGLYKLLPHSEYSRPNRV-----PFN----- 41
DMWD  MAAGGAEGGSGPGAAMGDCAEIKSQFRTREGFYKLLPGDGAARRSGPASAQTPVPPQPPQ 60
      **:      .*   .  :  ***:** ****:***** .  :* .       *.

WDR20 ---------------------------SQGSNPVRVSFVNLND---------------QS 59
DMWD  PPPGPASASGPGAAGPASSPPPAGPGPGPALPAVRLSLVRLGEPDSAGAGEPPATPAGLG 120
                                . .   **:*:*.*.:                .

WDR20 GNGDRLCFNVGRELYFYI---YKGVRKAADLSKPIDKRIYKGTQPTCHDFNHLTATAESV 116
DMWD  SGGDRVCFNLGRELYFYPGCCRRGSQRSIDLNKPIDKRIYKGTQPTCHDFNQFTAATETI 180
      ..***:***:*******     :* ::: **.*******************::**::*::

WDR20 SLLVGFSAGQVQLIDPIKKETSKLFNEERLIDKSRVTCVKWVPGSESLFLVAHSSGNMYL 176
DMWD  SLLVGFSAGQVQYLDLIKKDTSKLFNEERLIDKTKVTYLKWLPESESLFLASHASGHLYL 240
      ************ :* ***:*************::** :**:* ******.:*:**::**

WDR20 YNVEHTCGTTAPHYQLLKQGESFAVHTCKSKSTRNPLLKWTVGEGALNEFAFSPDGKFLA 236
DMWD  YNVSHPCASAPPQYSLLKQGEGFSVYAAKSKAPRNPLAKWAVGEGPLNEFAFSPDGRHLA 300
      ***.* *.:: *:*.******.*:*::.***: **** **:**** **********:.**

WDR20 CVSQDGFLRVFNFDSVELHGTMKSYFGGLLCVCWSPDGKYIVTGGEDDLVTVWSFVDCRV 296
DMWD  CVSQDGCLRVFHFDSMLLRGLMKSYFGGLLCVCWSPDGRYVVTGGEDDLVTVWSFTEGRV 360
      ****** ****:***: *:* *****************:*:**************.: **

WDR20 IARGHGHKSWVSVVAFDPYTTSVEEGDPMEFSGSDEDFQDLLHFGRDRANSTQSRLSKRN 356
DMWD  VARGHGHKSWVNAVAFDPYTTRAEEAATAAGADGE--RSGEEEEEEPEAAGTGSAGGAPL 418
      :**********..******** .**.     :..:   ..  .  . .* .* *  .

WDR20 STDSRPVSVTYRFGSVGQDTQLCLWDLTEDILFPHQPLSRARTHTNVMNATSPPAGSNGN 416
DMWD  SPLPKAGSITYRFGSAGQDTQFCLWDLTEDVLYPHPPLARTRTLPGTPGTTPPAASSSRG 478
      *   :  *:******.*****:********:*:** **:*:**  .. .:* * *.*. .

WDR20 SVTTPGNSVPPPLPRSNSLPHSAVSNA-GSKSSVMDGAIASGVSKFATLSLHDRKERHHE 475
DMWD  GE-PGPGPLPRSLSRSNSLPHPAGGGKAGGPGVAAEPGTPFSIGRFATLTLQERRDRGAE 537
      .     . :*  * ******* * ..  *. . . : .   .:.:****:*::*::*  *

WDR20 KDHKRNHSMGHISSKSSD--------KLNLVTKTKTDPAKTLGTPLCPRMEDVPLLEPLI 527
DMWD  KEHKRYHSLGNISRGGSGGSGSGGEKPSGPVPRSRLDPAKVLGTALCPRIHEVPLLEPLV 597
      *:*** **:*:**  .*.          . * ::: ****.*** ****:.:*******:

WDR20 CKKIAHERLTVLIFLEDCIVTACQEGFICTWGRPGKVVSFNP----------------- 569
DMWD  CKKIAQERLTVLLFLEDCIITACQEGLICTWARPGKAFTDEETEAQTGEGSWPRSPSKSV 657
      *****:******:******:******:****.****..: :

WDR20 -----------------    569
DMWD  VEGISSQPGNSPSGTVV    674
```

Figure E23: Alignment of WDR20 (Q8TBZ3) and DMWD (Q09019) amino acid sequences using CLUSTAL-OMEGA. Letters are coloured according to the physicochemical properties of the represented residue. An "*" (asterisk) indicates fully conserved residues. A ":" (colon) indicates residues with strongly similar properties. A "." (period) indicates residues with weakly similar properties as below. The NES identified in WDR20 protein is highlighted by a pink square. This sequence, especially on its C-terminal region, is partially conserved in DMWD.

The next step was to test whether DMWD was, like WDR20, exported by CRM1. As shown in Figure E24, both Myc-WDR20 and Myc-DMWD localised mainly to the cytoplasm of untreated cells. As expected, a clear relocation of Myc-WDR20 to the nucleus was observed upon LMB

treatment. In the case of Myc-DMWD, a less pronounced, but noticeable LMB-induced nuclear relocation was also observed. These findings show that DMWD, like WDR20, is a CRM1-dependent nucleocytoplasmic shuttling protein.

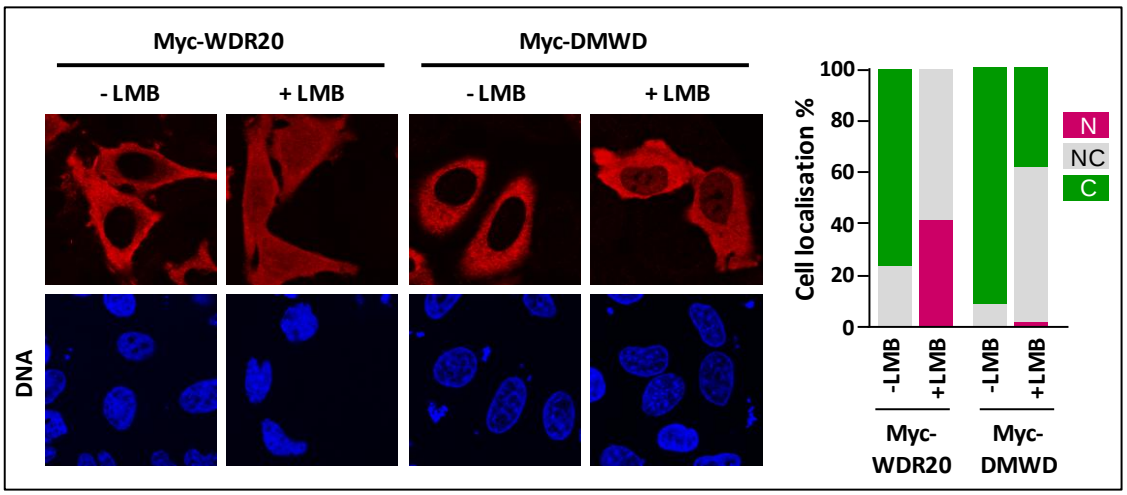

Figure E24: Effect of LMB on the nucleocytoplasmic localisation of Myc-WDR20 and Myc-DMWD. *Left*. Fluorescence microscopy images showing representative examples of the localisation of Myc-tagged WDR20 and DMWD in untreated (-LMB) cells or in cells treated with LMB. Cell nuclei were visualised by staining the DNA with DAPI. *Right*. Graphs representing the percentage of transfected cells where the Myc-tagged WDR20 and DMWD proteins is located mainly/exclusively in the nucleus (N), mainly/exclusively in the cytoplasm (C), or is similarly distributed between both compartments (NC). At least 200 transfected cells were analysed per sample.

Afterwards, the potential export activity of the DMWD sequence (^{512}AEPGTPFSIGRFATLTLQE^{530}) homolog to WDR20 NES was tested using the Rev(1.4)-GFP export assay. As shown in (Figure E25) DMWD NES was scored as 3. Thus, the NES motif is functionally conserved in WDR20 and DMWD, but the DMWD motif is markedly weaker than the corresponding sequence in WDR20.

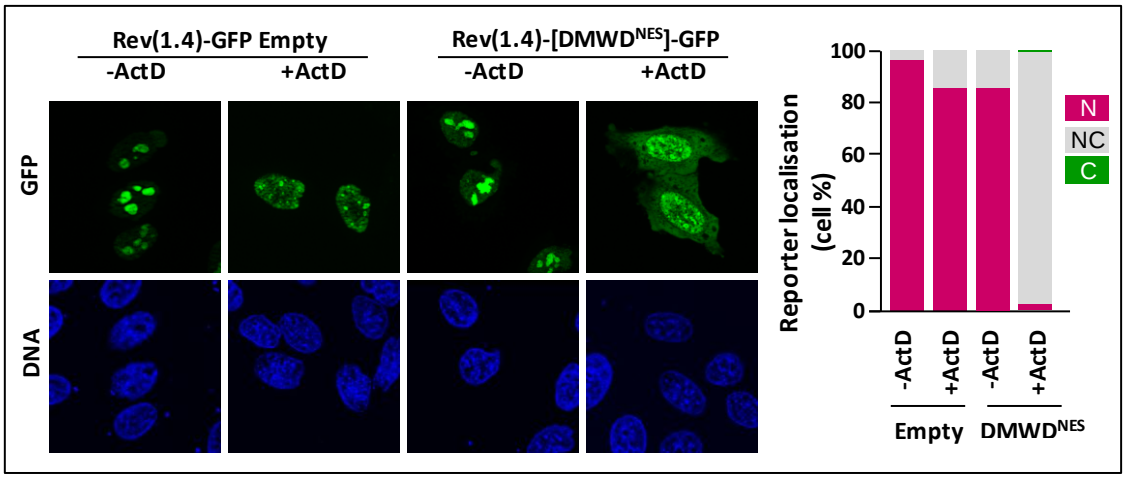

Figure E25: Results of a nuclear export assay to test the activity of the candidate DMWD NES motif (^{512}AEPGTPFSIGRFATLTLQE^{530}). *Left*. Fluorescence images showing representative examples of HeLa cells transfected with the empty Rev(1.4)-GFP plasmid or with the plasmid Rev(1.4)-[DMWD^{NES}]-GFP, containing the DMWD candidate NES. *Right*. Graph showing the percentage of cells with mostly nuclear (N), nuclear and cytoplasmic (NC) or mostly cytoplasmic (C) localisation of the reporter. At least 200 transfected cells were scored per condition. DMWD NES was scored as 3 in this assay.

E3.1.1.1.6. The newly identified NES in WDR20 protein regulates the nucleocytoplasmic localisation of the USP12/UAF1/WDR20 complex

Experiments by the group where this thesis was carried out (Olazabal-Herrero et al., 2019) showed that co-expression with Myc-WDR20 dramatically changes the localisation of YFP-USP12, promoting its relocation to the plasma membrane (Figure E26A). This relocation is even more noticeable using YFP-USP12[2NLS] (Figure E26B).

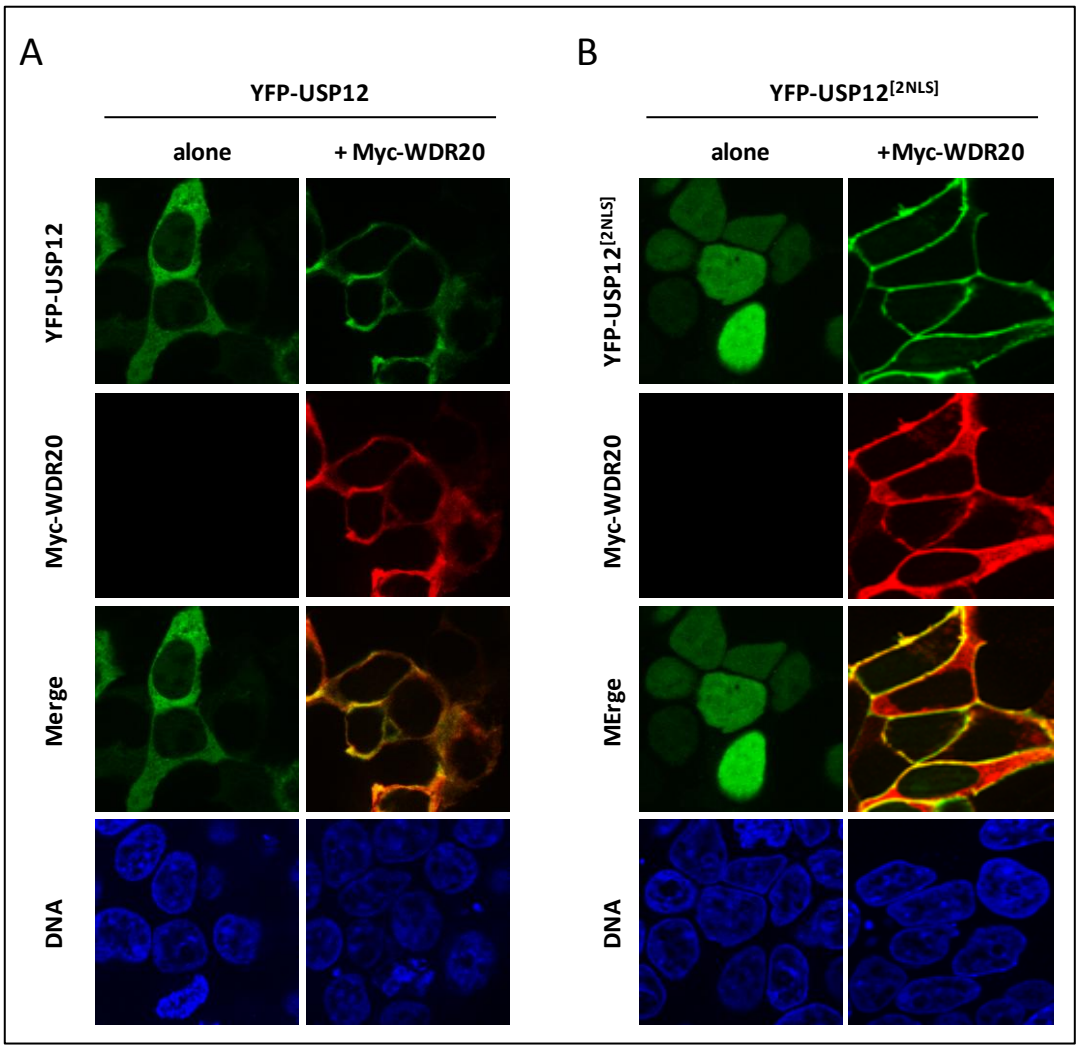

Figure E26: WDR20 protein relocates USP12 to the plasma membrane. Fluorescence images showing YFP-USP12 (A) or YFP-USP12[NLS] (B) alone or co-expressed with Myc-tagged WDR20 in HEK293T cells. Co-expression with Myc-WDR20 relocates YFP-USP12 to the plasma membrane (A). This relocation is even more noticeable using the YFP-USP12 construct bearing two NLSs (B).

Thus, the possibility that WDR20 NES mediates the nuclear export of USP12 was tested. In these experiments, the YFP-USP12[2NLS] variant, with increased nuclear import, was used to better visualise a potential effect of WDR20 NES mutations on USP12 nuclear export. HEK293T cells were co-transfected with YFP-USP12[2NLS] and either wild-type or NES-mutant Myc-WDR20. As shown in Figure E27, YFP-USP12[2NLS] located almost exclusively to the plasma membrane when co-expressed with wild-type Myc-WDR20. In striking contrast, YFP-USP12[2NLS]

located to both the nucleus and faintly to the plasma membrane when co-expressed with Myc-WDR20^{NESmut}. This result suggests that YFP-USP12 nuclear export is mediated by WDR20 through a so-called "piggyback" mechanism.

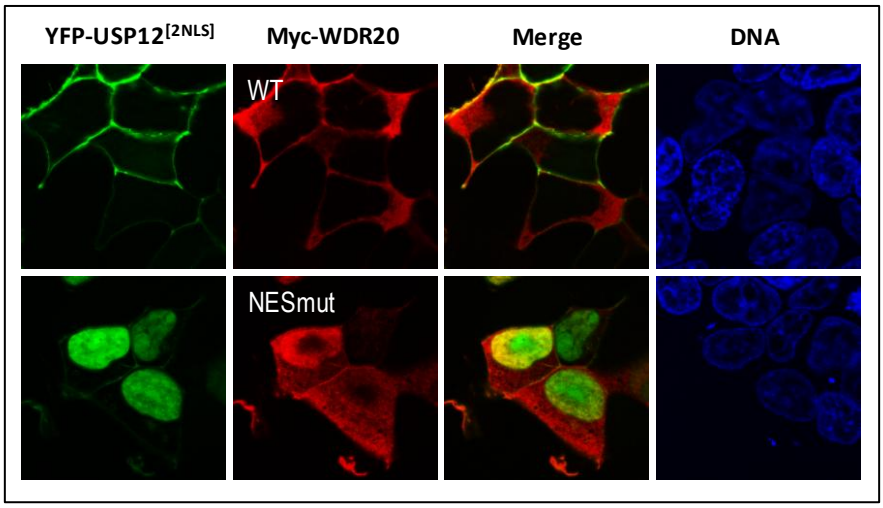

Figure E27: WDR20 NES mediates USP12 nuclear export. Fluorescence images of HEK293T cells co-expressing YFP-USP12$^{[2NLS]}$ with either wild-type (WT) Myc-WDR20 or Myc-WDR20^{NESmut}. WDR20 NES mutation leads to accumulation of co-expressed YFP-USP12$^{[2NLS]}$ and Myc-WDR20^{NESmut} in the nucleus.

Finally, triple co-transfection experiments were carried out to assess the role of WDR20 NES in the localisation of the ternary USP12/UAF1/WDR20 complex. HEK293T cells were co-transfected with YFP-USP12$^{[2NLS]}$, UAF1-mRFP, and wild-type or NES mutant Myc-WDR20. As shown in Figure E28 mutation of WDR20 NES resulted in a prominent relocation of the three co-expressed proteins to the nucleus.

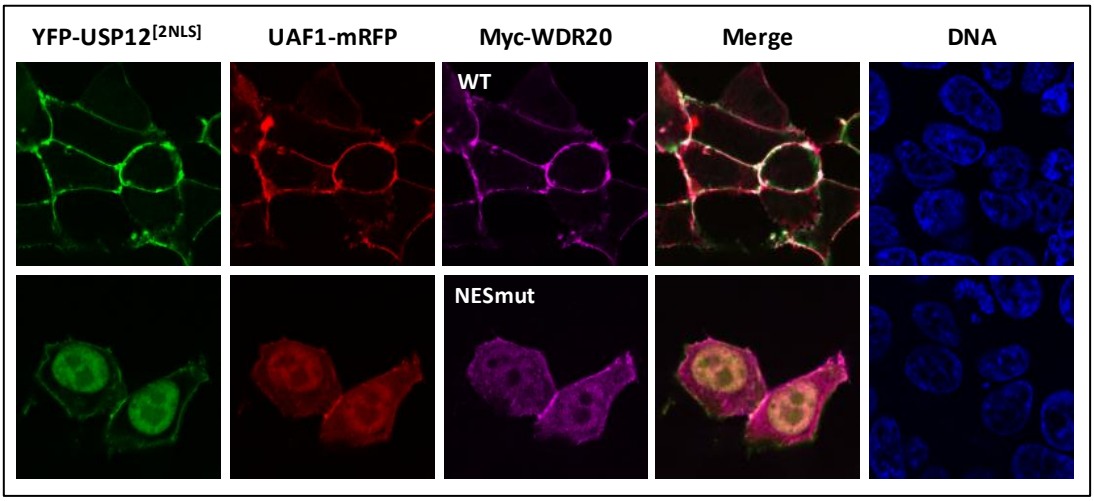

Figure E28: WDR20 NES mediates CRM1-dependent nuclear export of the USP12/UAF1/WDR20 deubiquitinase complex. Representative images of the results of a triple co-transfection experiment in HEK293T cells. Cells were co-transfected with YFP-USP12$^{[2NLS]}$, UAF1-mRFP and wild-type (WT) or NES mutant (NESmut) Myc-WDR20. When co-expressed, the three proteins localise almost exclusively to the plasma membrane. However, mutation of WDR20 NES leads to a significant accumulation of the three proteins in the nucleus.

Altogether, these findings strongly suggest that the novel NES in WDR20 identified here mediates CRM1-dependent nuclear export of the USP12/UAF1/WDR20 deubiquitinase complex.

E.3.1.1.2. Using the Rev(1.4)-GFP export assay to map NES motifs in cancer-related proteins

The results described in this section have been published in Sendino et al., 2020a.

The Rev(1.4)-GFP assay was also used in an wider effort to identify NESs in the proteins that conform the so-called "CRM1-cancer exportome". This term refers to a set of 136 proteins (Figure E29) that were identified as potential CRM1 cargos in the global exportome analysis performed by Kirli and co-workers (2015), and that are related to cancer, according to the Human Protein Atlas (v.18) (Sendino et al., 2018). A list of these proteins is available in supplementary Table 22.

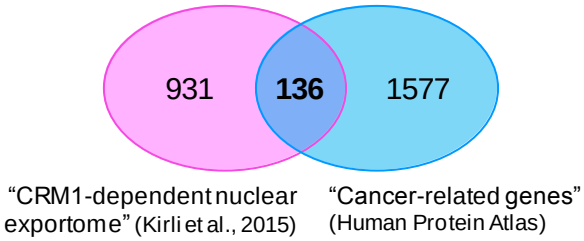

Figure E29: The "CRM1-cancer exportome". The Venn diagram shows the overlap between the list of potential CRM1 cargos identified in HeLa cells (Kirli et al., 2015) and the group of "cancer related genes" defined in the Human Protein Atlas (v.18). The 136 overlapping proteins represent what is referred to as the CRM1-cancer exportome (Sendino et al., 2018).

As a first step to search for NESs in the CRM1-cancer exportome, an *in-silico* prediction of putative NES motifs in 112 of these proteins (those classified as "CRM1 cargo A" or "CRM1 cargo B" by Kirli and co-workers (2015)) was carried out. Their amino acid sequence was analysed with two different programs: Wregex (Prieto et al., 2014) and NESmapper (Kosugi et al., 2014). In order to also predict potential reverse (*minus*) NES motifs, the amino acid sequence of each protein was inverted prior to being used as input for the analysis. A ranking approach, based on the score assigned by the programs to each predicted NES, was applied to select a reasonable number of candidate motifs to be experimentally tested. Thus, predicted NES motifs with scores within the first quartile for both programs were designed as Rank 1 candidates. Predicted motifs within the first quartile for one of the programs and within the second quartile for the other were designed as Rank 2. This *in silico* analysis identified 7 Rank 1 and 19 Rank 2 *plus* candidates and 10 Rank 1 *minus* candidates (Table E6).

Table E6: Candidate NESs (cNESs) from the CRM1-cancer exportome proteins tested here using the Rev(1.4)-GFP assay. cNES ID, UniProtKB entry, cargo type (A or B, according to Kirli and co-workers (2015)), cNES position in the full-length protein, cNES amino acid sequence, and Rank are shown in the Table. cNES IDs named as WN (Wregex-NESmapper) are *plus* cNESs, while cNES IDs named as Rev (Reverse) are *minus* cNESs.

cNES ID	UniProtKB entry	Cargo type	cNES position	cNES sequence	Rank
WN1	sp|P36507|MP2K2_HUMAN	B	33-51	NLVDLQKKLEELELDEQQK	1
WN2	sp|Q9NZQ3|SPN90_HUMAN	A	282-300	SASDDLEALGTLSLGTTEE	1
WN3	sp|P19532|TFE3_HUMAN	A	418-436	QANRSLQLRIQELELQAQI	1
WN4	sp|Q8IXJ6|SIR2_HUMAN	A	37-55	DMDFLRNLFSQTLSLGSQK	1
WN5	sp|O15234|CASC3_HUMAN	B	457-475	SSTSGLEQDVAQLNIAEQN	1
WN6	sp|O15357|SHIP2_HUMAN	B	256-274	TGEQELESLVLKLSVLKDF	1
WN7	sp|O15534|PER1_HUMAN	B	483-501	DTDIQELSEQIHRLLLQPV	1
WN8	sp|O15357|SHIP2_HUMAN	B	625-643	RKEFEPLLRVDQLNLEREK	2
WN9	sp|O15534|PER1_HUMAN	B	1215-1233	PDDPLFSELDGLGLEPMEE	2
WN10	sp|Q14141-2|SEPT6_HUMAN	A	155-174	IAPTGHSLKSLDLVTMKKLD	2
WN11	sp|Q8IXJ6|SIR2_HUMAN	A	244-267	FSCMQSDFLKVDLLLVMGTSLQVQ	2
WN12	sp|O95071-2|UBR5_HUMAN	A	2206-2224	AEPGSILTELGGFEVKESK	2
WN13	sp|P42345|MTOR_HUMAN	A	1274-1292	RVSKDDWLEWLRRLSLELL	2
WN14	sp|P14635|CCNB1_HUMAN	A	138-156	AEEDLCQAFSDVILAVNDV	2
WN15	sp|O95684|FR1OP_HUMAN	A	352-370	EISIGEEIEEDLSVEIDDI	2
WN16	sp|P63010|AP2B1_HUMAN	A	256-274	VLSAVKVLMKFLELLPKDS	2
WN17	sp|P20042|IF2B_HUMAN	A	89-107	FDIDEAEEGVKDLKIESDV	2
WN18	sp|P42345|MTOR_HUMAN	A	649-668	VQVVADVLSKLLVVGITDPD	2
WN19	sp|P11274|BCR_HUMAN	A	1091-1111	VSGVATDIQALKAAFDVNNKD	2
WN20	sp|Q14145|KEAP1_HUMAN	A	272-290	RCHSLTPNFLQMQLQKCEI	2
WN21	sp|Q6UUV9-3|CRTC1_HUMAN	A	329-347	LSPLSPITQAVAMDALSLE	2
WN22	sp|P15923|TFE2_HUMAN	A	566-584	NEAFKELGRMCQLHLNSEK	2
WN23	sp|Q99081|HTF4_HUMAN	A	594-612	NEAFKELGRMCQLHLKSEK	2
WN24	sp|Q12778|FOXO1_HUMAN	B	62-80	SAAAVSADFMSNLSLLEES	2
WN25	sp|Q13492-2|PICAL_HUMAN	A	212-230	NEGIINLLEKYFDMKKNQC	2
WN26	sp|P35869|AHR_HUMAN	B	114-132	EGEFLLQALNGFVLVVTTD	2
Rev1	sp|P25963|IKBA_HUMAN	A	267-285	QQLGQLTLENLQMLPESED	1
Rev2	sp|Q16204|CCDC6_HUMAN	A	297-315	MREENLRLQRKLQREMERR	1
Rev3	sp|P19484|TFEB_HUMAN	A	431-449	KDLDLMLLDDSLLPLASDP	1
Rev4	sp|O95071-2|UBR5_HUMAN	A	209-227	LQRTNLDVNLAVNNLLSRD	1
Rev5	sp|O15357|SHIP2_HUMAN	B	261-279	LESLVLKLSVLKDFLSGIQ	1
Rev6	sp|P30260|CDC27_HUMAN	A	545-563	HLQKDVALSVLSKDLTDMD	1
Rev7	sp|O95071-2|UBR5_HUMAN	A	1607-1625	EDGSDMELDLLAAAETESD	1
Rev8	sp|Q9UDY2-3|ZO2_HUMAN	A	715-733	PIADIAMEKLANELPDWFQ	1
Rev9	sp|Q92997-2|DVL3_HUMAN	A	24-42	PAERVTLADFKGVLQRPSY	1
Rev10	sp|O95684|FR1OP_HUMAN	A	379-397	LTQDLTVSQLSDVADYLED	1

The Rev(1.4)-GFP assay was used to evaluate export activity of all Rank 1 motifs and Rank 2 *plus* candidates. All in all, 36 candidates were tested and assigned an export score (hereafter referred to as "1.4 score") in a range between 0 (inactive motif) and 9 (Henderson and Eleftheriou, 2000). As shown in Figure E30, 25 of the 36 candidate sequences tested positive.

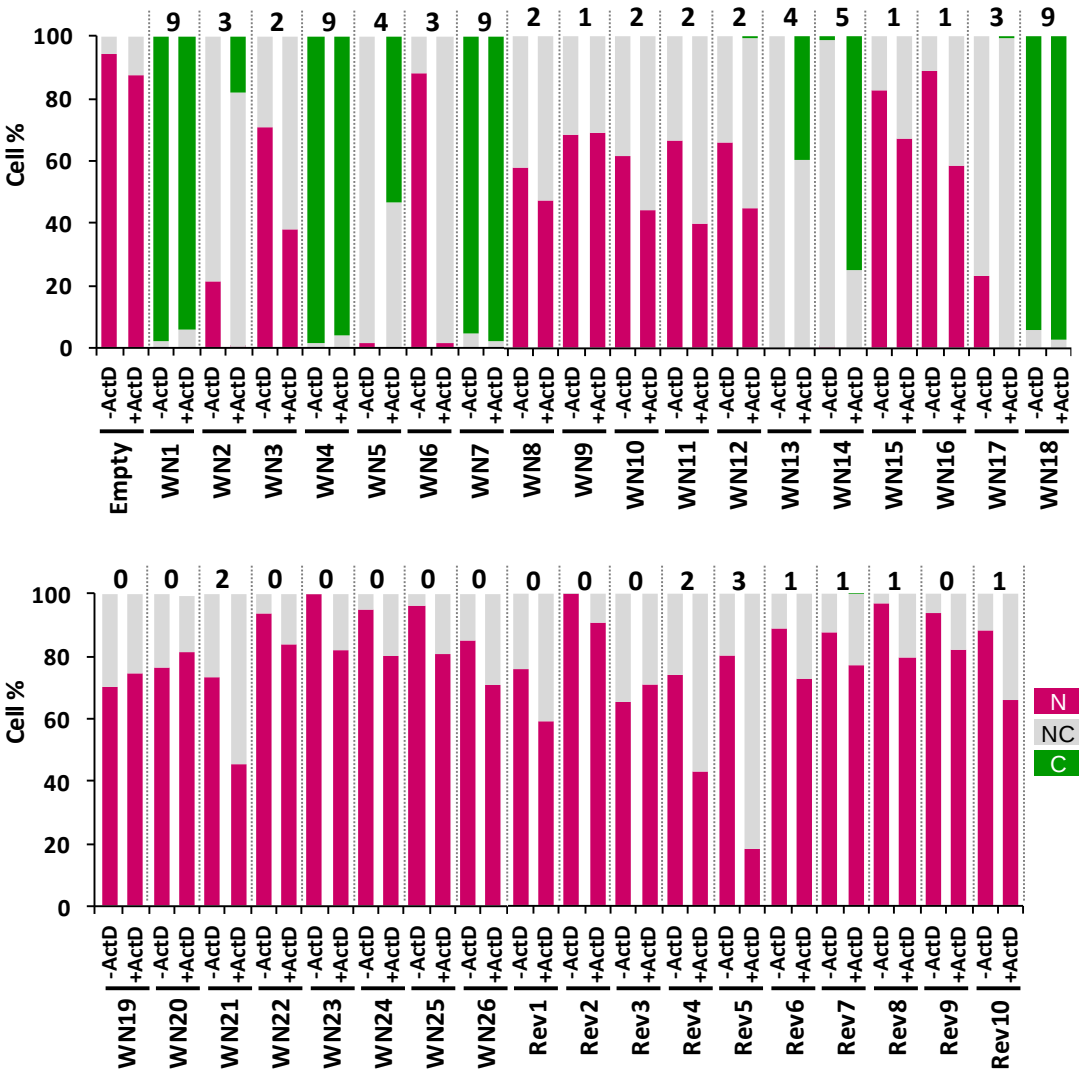

Figure E30: Graphs showing the results of Rev(1.4)-GFP export assays performed with candidate NESs predicted in the CRM1-cancer exportome protein set. 25 out of 36 cNES tested positive in the assay. The "1.4 score" of each motif is indicated above each bar.

As shown in Figure E30, 19 out of 25 *plus* (WN) candidate motifs tested positive, although 3 of them showed borderline activity (1.4 score= 1). On the other hand, 6 out of 10 *minus* (Rev) candidate motifs tested positive, 4 of them with borderline activity. The mean 1.4 score was 3.84 for *plus* motifs and 1.5 for *minus* motifs.

WN1 (Fukuda et al., 1996), WN4 (North and Verdin, 2007), WN5 (Macchi et al., 2003), WN7 (Vielhaber et al., 2001), WN13 (Bachmann et al., 2006) and WN14 (Toyoshima et al., 1998) motifs had been already described in the literature, while 19 motifs represent novel NES signals not previously reported, and have been included in a recently updated version of the NESdb database (http://prodata.swmed.edu/LRNes/index.php; Xu et al., 2012; Fung et al., 2021).

E3.1.2. Development of a novel tool: nuclear export assay based on the $SRV_{B/A}$ reporter

The results described in this section have been published in Taylor et al., 2019 and Sendino et al., 2020a

As detailed above, the Rev(1.4)-GFP nuclear export assay allows detecting and comparing the export activity of candidate NES motifs. In a previous work of the group another cellular assay, termed SRV100, was developed (García-Santisteban et al., 2016). This assay is based on a reporter that contains the NES of the human protein survivin, and can be used in co-transfection experiments to compare the export capacity of different CRM1 variants. To date, there is no single assay reported that allows both testing NES activity and CRM1 function. In an attempt to generate such a novel tool, the SRV100 reporter has been modified by removing two BamHI and AgeI restriction sites present in SRV100, and introducing them flanking the survivin NES. This change in BamHI/AgeI restriction sites allows replacing survivin NES by any other NES motif (Figure E31A) (Taylor et al., 2019; Sendino et al., 2020a). Importantly, this modified reporter, called $SRV_{B/A}$, was designed in such a manner that candidate NES motifs can be easily shuttled to and from the Rev(1.4)-GFP reporter (Figure E31B).

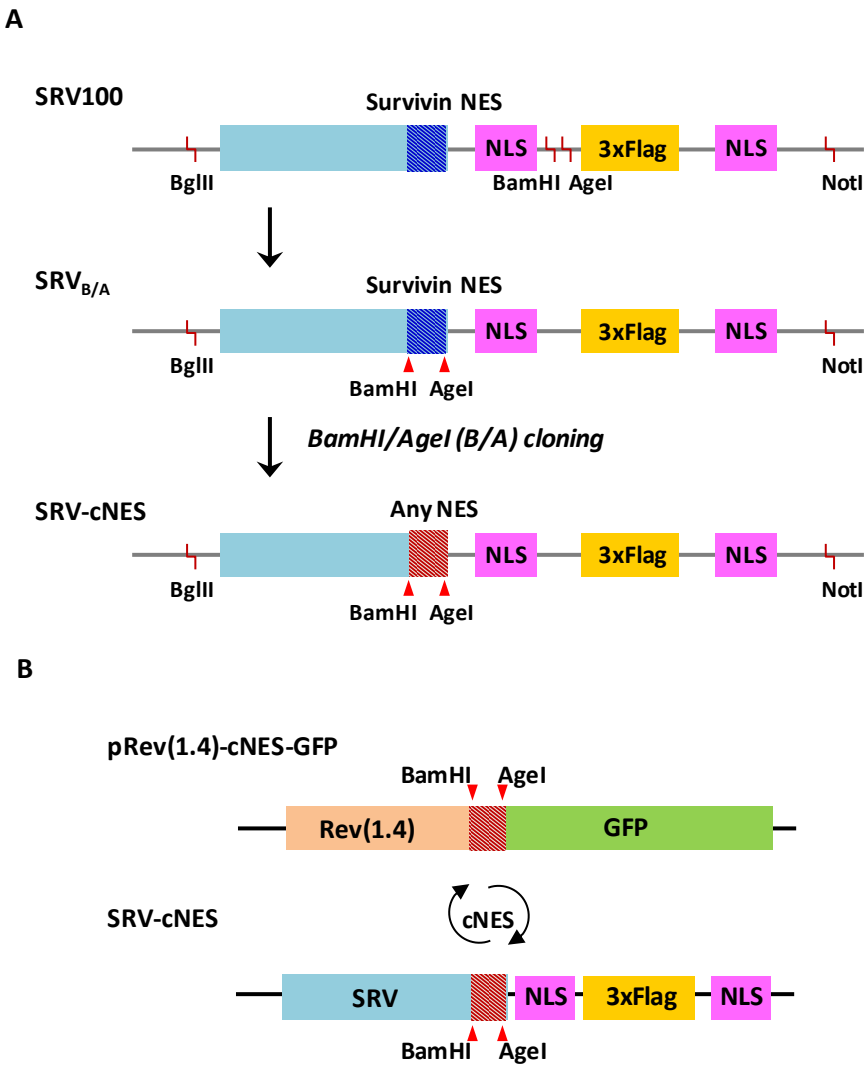

Figure E31: Description of the SRV$_{B/A}$ reporter. A. Schematic illustration showing the development and configuration of SRV$_{B/A}$. This reporter is derived from the previously described SRV100 reporter containing the NES of survivin (García-Santisteban et al., 2016). The original SRV100 plasmid bears BamHI and AgeI restriction sites, thus, to make it compatible with pRev(1.4)-GFP vector these sites were removed and reintroduced flanking the NES of survivin. In this manner, survivin NES can be replaced by any other NES. The SRV$_{B/A}$ reporter contains two copies of the SV40 NLS separated by three tandem copies of the Flag epitope. B. Schematic representation of the Rev(1.4)-GFP and SRV$_{B/A}$ reporters, illustrating how candidate NES motifs (cNES) can be easily shuttled between both reporters by BamHI/AgeI subcloning.

When SRV$_{B/A}$ reporters bearing candidate NES motifs are transfected alone or co-transfected with different CRM1 variants, their nucleocytoplasmic localisation depends on both the strength of the NES, and the export activity of the co-expressed CRM1 variant (Figure E32).

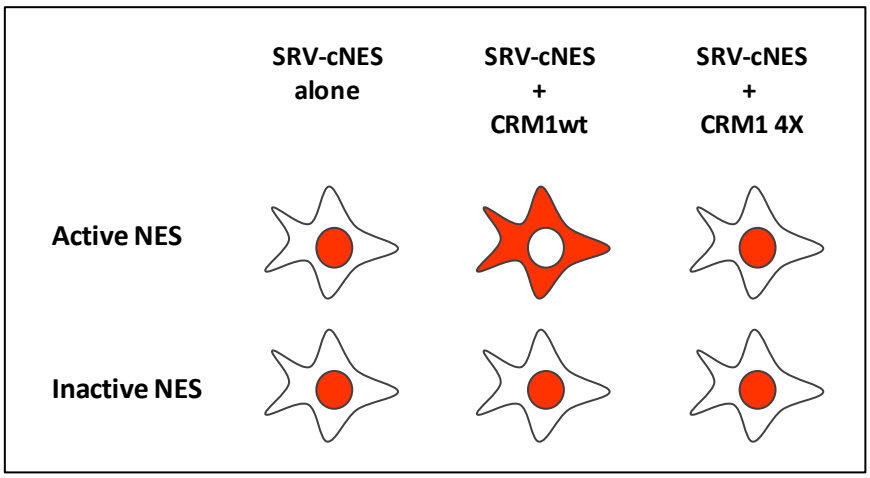

Figure E32: Schematic representation of the expected localisation of SRV-cNES reporters depending on the cNES strength and CRM1 activity. $SRV_{B/A}$ reporters containing a candidate NES (SRV-cNES) are transfected in HEK293T cells. When the NES is active, the localisation of the reporter transfected alone is mainly nuclear (due to efficient nuclear import mediated by the two SV40 NLSs), but becomes cytoplasmic when co-transfected with a functional version of CRM1 (e.g. CRM1 wt). If the co-transfected version of CRM1 is non-functional (e.g. CRM1 4X, bearing I521A/L525A/F561A/F572A mutations (Dong et al., 2009a)), the reporter remains in the nucleus. When the NES is inactive, the localisation of the reporter is nuclear, even if co-transfected with a functional CRM1.

The results of the $SRV_{B/A}$ nuclear export assays (i.e. the degree of nuclear or cytoplasmic localisation of the reporter) are assessed using anti-Flag immunostaining followed by fluorescence microscopy. Three assessment methods were used in this thesis, as described in Figure E33.

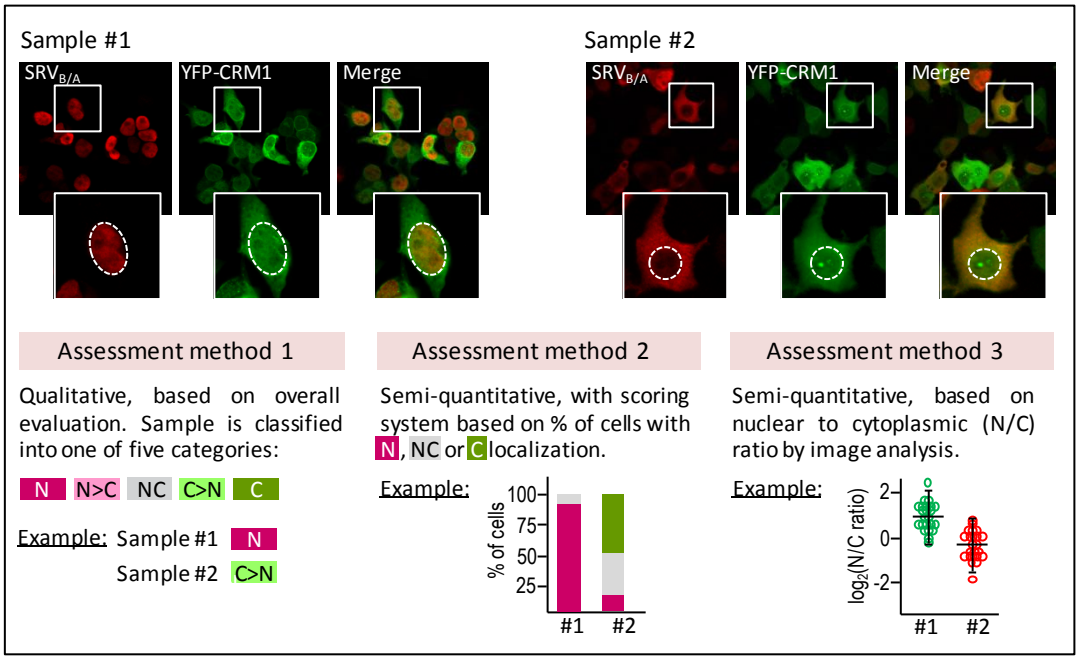

Figure E33: Assessment methods used in $SRV_{B/A}$ nuclear export assays. Microscopy images show examples of the results of the assay with two reporters that contain different NES motifs. Insets show the magnified image of a single cell of each sample, with the nucleus delimited by a dotted line. Under the images, the three different methods used to manually assess the localisation of the reporters in this thesis are described. Method 1 is a qualitative assessment, where the sample is ascribed, according to overall reporter localisation, to one of five categories: exclusively nuclear (N), mainly nuclear (N>C), nuclear and cytoplasmic (NC), mainly

cytoplasmic (C>N) or exclusively cytoplasmic (C). In the example, sample#1 is classified as N, and sample#2 as C>N. Method 2 is a more detailed, semi-quantitative assessment that was previously used with the SRV100 reporter (García-Santisteban et al., 2016). The localisation of the reporter in at least 200 individual cells per sample is evaluated, and classified as exclusively/mainly nuclear (N), nuclear and cytoplasmic (NC), or exclusively/mainly cytoplasmic (C). Based on the percentage of cells showing N, NC or C localisation of the reporter, a nuclear export score (termed "SRV export score") between 0 (no export) and 100 (complete export) was derived using the formula [0 x (% N) + 0.5 x (% NC) + 1 x (% C)]. Graphs show the results for sample#1 and sample#2, corresponding to "SRV export scores" of 4 and 70, respectively. Method 3, the most detailed and laborious assessment method, is based on image analysis to determine the nuclear to cytoplasmic (N/C) ratio of the anti-Flag (red) fluorescent signal corresponding to the $SRV_{B/A}$ reporter in an average of 50 cells per sample. Graphs illustrating the results for sample#1 and sample#2 are shown.

E3.1.2.1. Using the $SRV_{B/A}$ assay to identify novel NES motifs in cancer-related CRM1 cargos

In order to test how the $SRV_{B/A}$ assay compares to the Rev(1.4)-GFP assay for NES identification, a subset of 22 cNES motifs with different 1.4 scores (see Figure E30) was subcloned into the $SRV_{B/A}$ plasmid. These reporters were transfected into HEK293T cells either alone or with wild type YFP-CRM1 and, after anti-Flag immunostaining, their localisation was globally assessed by fluorescence microscopy (using assessment method 1) and classified as exclusively nuclear (N), mainly nuclear (N>C), nuclear and cytoplasmic (NC), mainly cytoplasmic (C>N) or exclusively cytoplasmic (C). The results obtained with the 22 reporters are summarised in Figure E34. When transfected alone, all but two reporters (those containing cNES motifs WN4 and WN7, both with a 1.4 score of 9) showed exclusively nuclear localisation. When co-transfected with wild type YFP-CRM1, all reporters containing cNES motifs with a 1.4 score above 2 showed partial or complete relocation to the cytoplasm. In contrast, all reporters containing cNES motifs with a 1.4 score equal or lower than 2, except SRV-WN16, were classified as exclusively nuclear, even when co-expressed with CRM1.

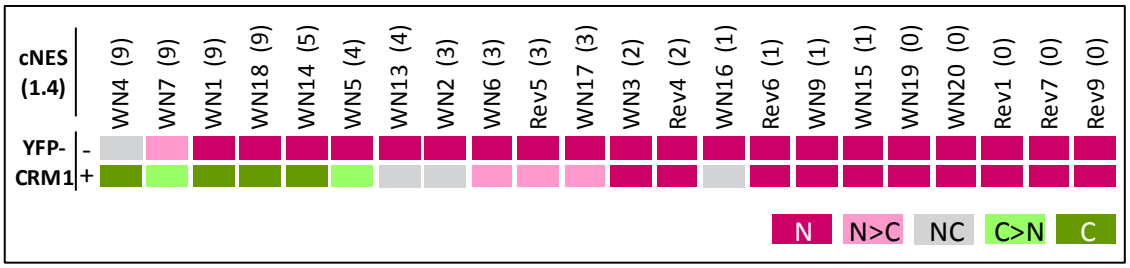

Figure E34: Summary of the localisation of 22 $SRV_{B/A}$ reporters containing cNES motifs predicted in cancer-related proteins. cNES ID and the 1.4 score for each motif are indicated. The localisation of each reporter expressed alone (-) or co-expressed with YFP-CRM1 wild type (+) was assessed using method 1. Ten motifs showed exclusively nuclear (N) localisation when co-expressed with YFP-CRM1, and were thus considered inactive in this assay.

In an attempt to evaluate the correlation between the results obtained with the two assays, 1.4 scores were plotted against the localisation of the $SRV_{B/A}$ reporters (when co-transfected with YFP-CRM1) (Figure E35). In order to be able to calculate the correlation coefficient, numerical values were assigned to the different $SRV_{B/A}$ localisations (N= 0; N>C= 1; NC= 2; C>N= 3; C= 4). As shown in the Figure, the results obtained with the Rev(1.4)-GFP and the $SRV_{B/A}$ assays were significantly correlated (R=0.876; p=0.0097). Of note, some sequence motifs with the lowest nuclear export activity (1.4 score equal or lower than 2) may be missed in the $SRV_{B/A}$ assay, when the localisation of reporters is qualitatively analysed. Conversely, the $SRV_{B/A}$ assay allowed detecting differences in activity between strong NES motifs. Thus, WN1, WN4, WN7 and WN18 were all assigned a 1.4 score of 9 (the highest possible in this assay), but

only SRV-WN4 and SRV-WN7 reporters showed partial cytoplasmic localisation when transfected alone, suggesting that WN4 and WN7 motifs are stronger NESs than WN1 and WN18.

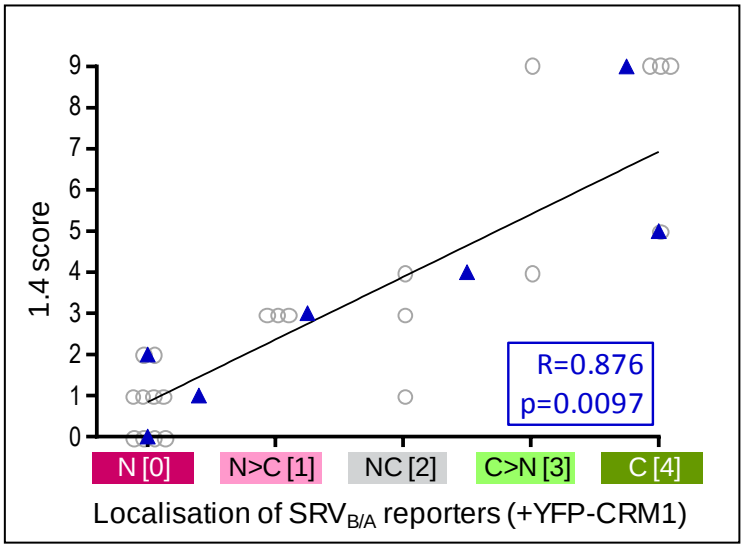

Figure E35: Graph showing the correlation between the results obtained with the Rev(1.4)-GFP and the SRV$_{B/A}$ assays for 22 cNES motifs that were tested using both systems. For each motif (represented as a grey circle), the score assigned using the Rev(1.4)-GFP assay (1.4 score, between 0 and 9) was plotted against the localisation (N, N>C, NC, C>N, or C) of the corresponding SRV$_{B/A}$ reporter when co-expressed with YFP-CRM1 wild type. In order to calculate the correlation coefficient between both sets of data, qualitative descriptions of SRV$_{B/A}$ localisations were assigned a numerical value (N= 0; N>C= 1; NC= 2; C>N= 3; C= 4). The mean of these values for cNES motifs with a given 1.4 score is represented as a blue triangle. Pearson correlation coefficient and p value are indicated.

E3.1.2.2. Using the $SRV_{B/A}$ assay to search for NES-harbouring micropeptides

Once the suitability of the $SRV_{B/A}$ assay as a tool to identify NESs was established, this assay was applied to search for new NES motifs in a poorly characterised section of the human proteome: the set of small proteins or micropeptides.

With the progressive improvements in proteogenomics analyses, it has become apparent that the size and complexity of the cellular proteome may have been previously underestimated. Thus, there is growing evidence that a subset of RNA molecules initially annotated as non-coding may, in fact, contain short open reading frames that are translated into micropeptides, small proteins shorter than 100 amino acids in length (Yeasmin et al., 2018). Thousands of different micropeptides may be expressed in a cell, but there is still very little information on their biological function (Hartford and Lal, 2020). An important aspect of micropeptide biology that remains to be investigated is their nucleocytoplasmic localisation. Given their small size, it is possible that many micropeptides can enter and exit the nucleus by passively diffusing through the nuclear pore. However, it is also possible that some micropeptides undergo active transport between the nucleus and the cytoplasm, and possess NLSs and/or NESs to interact with the nucleocytoplasmic transport machinery. To begin addressing this possibility, the $SRV_{B/A}$ assay was used to carry out a search for functional NESs in human micropeptides.

Human micropeptide sequences were retrieved from the SmProt database, a manually curated repository of small proteins detected or predicted in eight different species (Hao et al., 2018). *In silico* prediction of putative NES motifs in the amino acid sequences of micropeptides was carried out with Wregex (Prieto et al., 2014) and NESmapper (Kosugi et al., 2014) (no attempt to predict *minus* NES motifs was made in this case). All cNES found in micropeptides are shown in supplementary Table 25. Candidates were ranked as described in section E3.1.1.2. Ten of the highest-ranking candidates (Table E7) were selected for experimental testing, and seven were successfully cloned into the $SRV_{B/A}$ reporter.

Table E7: cNES found in micropeptides selected to be experimentally tested. Table shows cNES ID, the ID of the full length micropeptide in SmProt database, the length (number of amino acids) of each micropeptide, the cNES position in the micropeptide and its amino acid sequence.

cNES ID	SmProt ID	Number of amino acids	cNES position	Sequence
MICROP-1	SPROHSA011142	96	13-31	KKEELLKQLDDLKVELSQL
	SPROHSA011145	47	13-31	
MICROP-2	SPROHSA018908	84	57-75	RDRLPVNVRELSLDDPEV
MICROP-3	SPROHSA012652	70	29-47	GLDDLDVALSNLEVKLEGS
MICROP-4	SPROHSA141226	78	40-58	DGTSDLPLKLEALSVKEDA
	SPROHSA141826	85	47-65	
MICROP-5	SPROHSA141543	68	5-23	ASASALQRLVEQLKLEAGV
MICROP-6	SPROHSA011811	57	30-48	SHYHETLGEALQGVELEFS
MICROP-7	SPROHSA010409	85	16-34	EESPENLFLELEKLVLEHS
MICROP-8	SPROHSA009911	99	78-96	RMSKEELRAKLSEFKLETR
MICROP-9	SPROHSA020870	100	46-64	LSKCGEELGRLKLVLLELN
MICROP-10	SPROHSA180177	93	49-67	AKIKLLTKELSVLKDLFLE
	SPROHSA180747	93	49-67	
	SPROHSA181614	93	49-67	

When expressed alone into HEK293T cells, the localisation of all the reporters (determined using assessment method 1) was exclusively nuclear (N), except for SRV-MICROP-2 that showed also a faint cytoplasmic signal (N>C localisation) (Figure E36). When co-expressed with wild type YFP-CRM1, SRV-MICROP-5 and SRV-MICROP-7 reporters fully relocated to the cytoplasm (C localisation), SRV-MICROP-1 and SRV-MICROP-10 showed a minor relocation to the cytoplasm (N>C localisation) and SRV-MICROP-6 and SRV-MICROP-9 remained in the nucleus. Unexpectedly, the partial cytoplasmic localisation of SRV-MICROP-2 was not increased by co-expression with YFP-CRM1, suggesting that this motif may mediate CRM1-independent export or retention in the cytoplasm, rather than CRM1-mediated nuclear export. These findings identify at least two clearly active NES motifs (MICROP-5 in SPROHSA141543 micropeptide and MICROP-7 in SPROHSA010409 micropeptide).

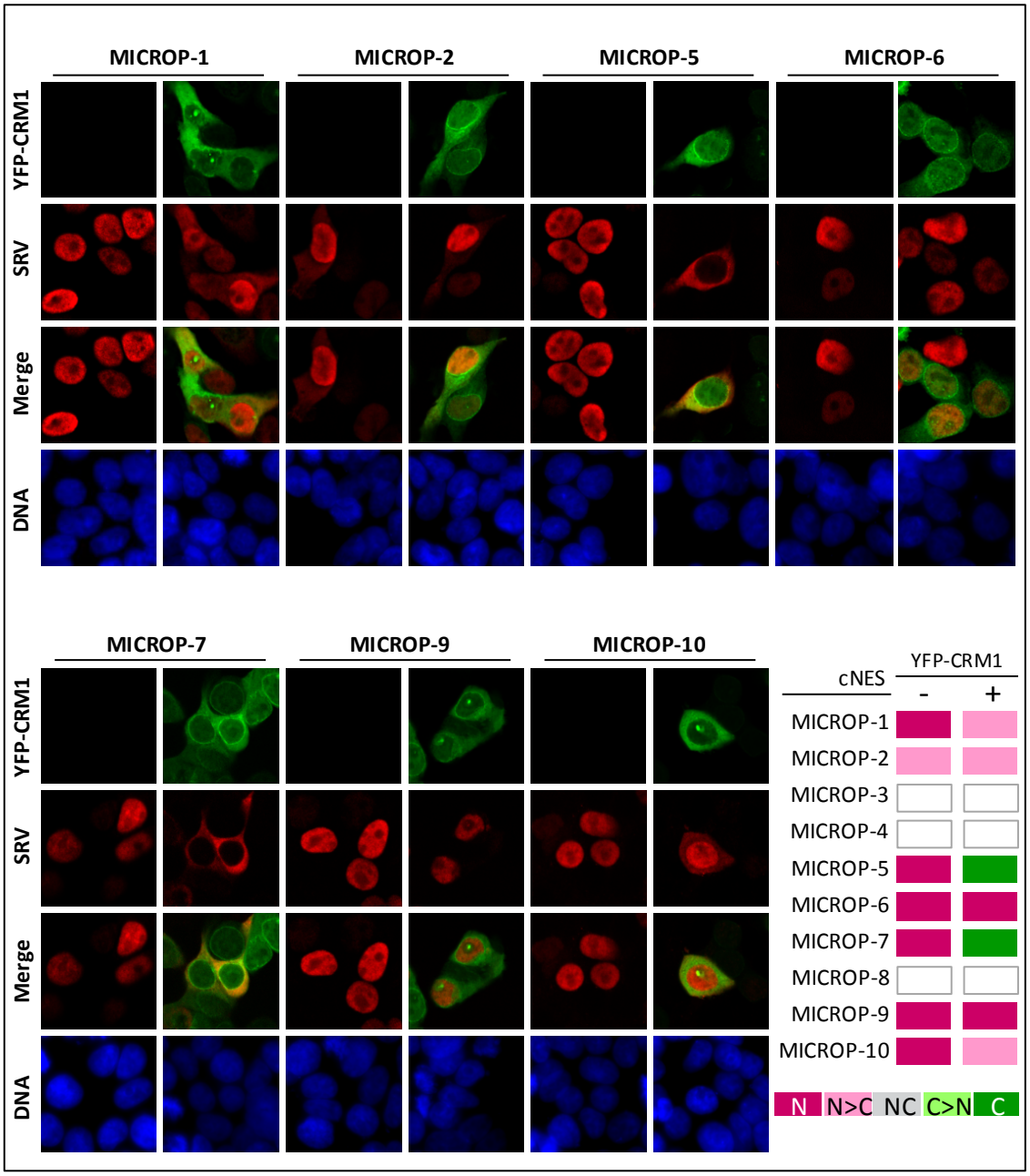

Figure E36: Using the $SRV_{B/A}$ assay to search for new NES motifs in human micropeptides. Fluorescence microscopy images showing representative examples of the localisation of $SRV_{B/A}$ reporters containing each of the seven micropeptide cNES motifs, when transfected alone or co-transfected with YFP-CRM1 wild type into HEK293T cells. The DNA-staining dye DAPI was used to visualise the nuclei. A summary of the localisation of $SRV_{B/A}$ reporters containing candidate NES motifs is shown in the bottom right side. The cNES ID for each motif are indicated to the left. The localisation of each reporter expressed alone (-) or co-expressed with YFP-CRM1 wild type (+) was assessed using method 1. Except SRV-MICROP-2, which showed a faint cytoplasmic signal (N>C localisation), all tested reporters showed exclusively nuclear (N) localisation when expressed alone. When co-expressed with YFP-CRM1, the localisation of SRV-MICROP-2, SRV-MICROP-6 and SRV-MICROP-9 reporters did not change, SRV-MICROP-1 and SRV-MICROP-10 partially relocated to the cytoplasm, and SRV-MICROP-5 and SRV-MICROP-7 fully relocated to the cytoplasm. White squares represent cNES that could not be successfully cloned into the $SRV_{B/A}$ plasmid.

To further confirm that MICROP-5 and MICROP-7 motifs are exported via CRM1, HEK293T cells co-expressing SRV-MICROP-5 or SRV-MICROP-7 with YFP-CRM1 wild type were treated with LMB (Figure E37). Blockade of CRM1-mediated export readily prevented cytoplasmic relocation of SRV-MICROP-7 and SRV-MICROP-5 reporters.

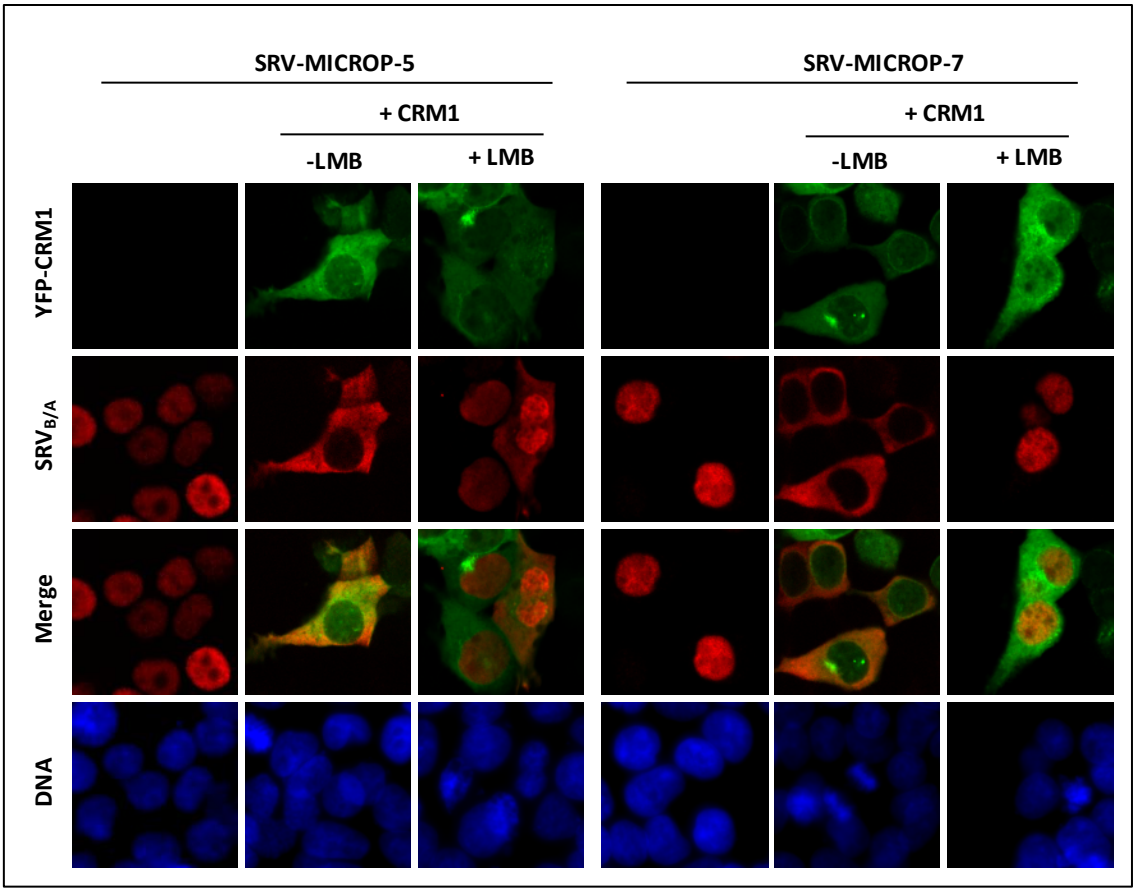

Figure E37: MICROP-5 and MICROP-7 are CRM1-dependent NESs. Representative images of HEK293T cells showing the effect of CRM1 inhibition on the localisation of SRV-MICROP-5 and SRV-MICROP-7 reporters. LMB treatment partially blocks the cytoplasmic relocation of SRV-MICROP-5 and completely blocks the cytoplasmic relocation of SRV-MICROP-7.

Having confirmed that MICROP-5 and MICROP-7 motifs are CRM1-dependent NESs, it was tested whether the export of the cognate full length micropeptides is also CRM1 dependent (Figure E38). YFP tagged full length micropeptides SPROHSA141543 (bearing MICROP-5) and SPROHSA010409 (bearing MICROP-7) were overexpressed in HeLa and HEK293T cells and their localisation in the absence or presence of LMB was analysed. Both YFP-SPROHSA141543 and YFP-SPROHSA010409 show a predominant cytoplasmic localisation in untreated cells. When CRM1 is blocked, the localisation of YFP-SPROHSA141543 remains predominantly cytoplasmic. However, the localisation of YFP-SPROHSA010409 becomes mostly nuclear, revealing its dependence on CRM1-mediated nuclear export.

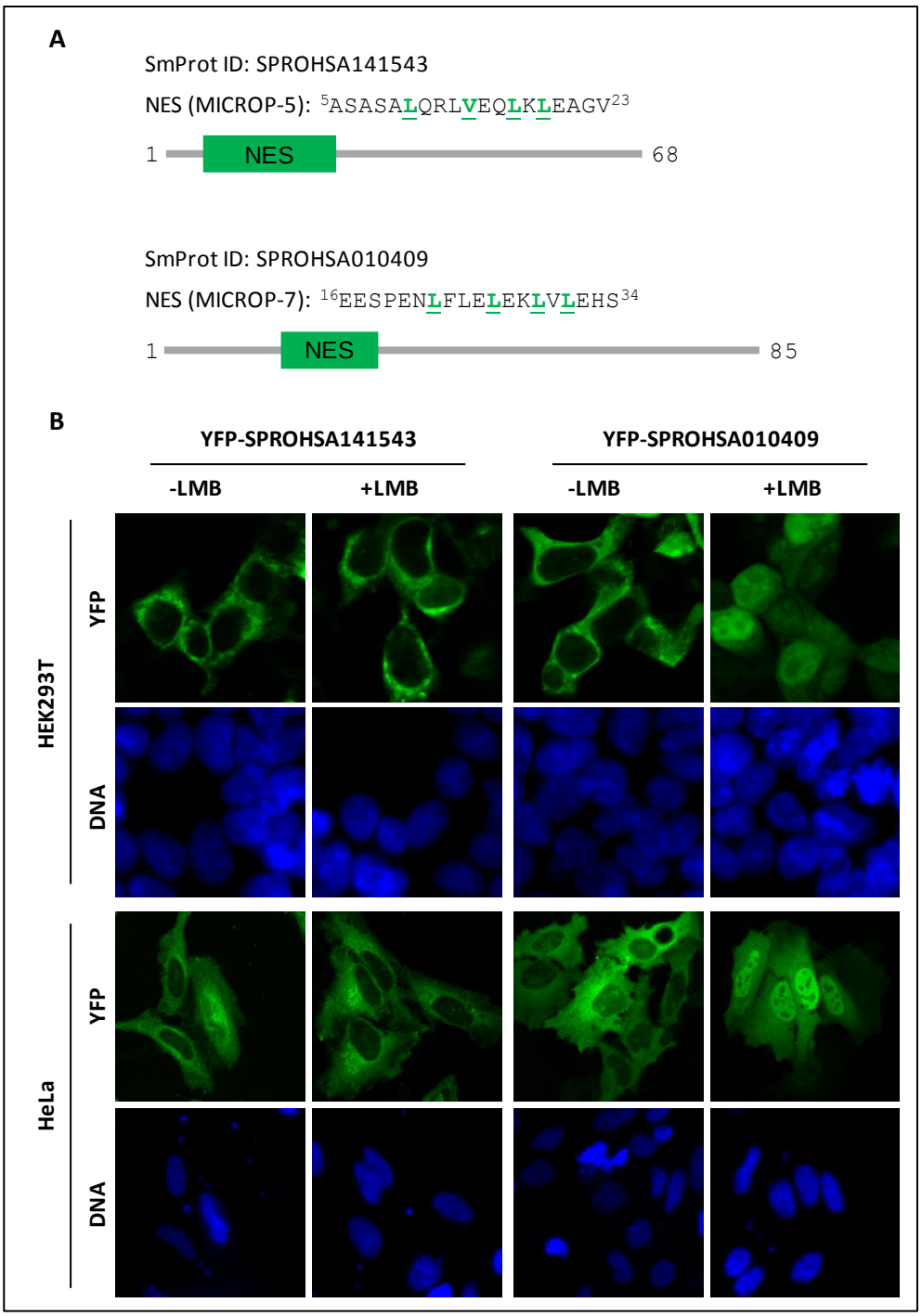

Figure E38: The localisation of SPROHSA010409 micropeptide is CRM1-dependent A. Schematic representation of human micropeptides SPROHSA141543 and SPROHSA010409 showing the position of the novel NESs identified (MICROP-5 and MICROP-7, respectively). The amino acid sequence of the NES motifs is indicated, with the hydrophobic residues that conform to the NES consensus highlighted in green. B. Fluorescence microscopy images of HEK293T and HeLa cells overexpressing YFP-tagged full length micropeptides SPROHSA141543 and SPROHSA010409. Cells were left untreated (-LMB) or treated with LMB for 3 h (+LMB).

E3.1.2.3. Using the $SRV_{B/A}$ assay to gain mechanistic insight into CRM1-mediated NES export. (i) Effect of single-residue mutations in the NES-binding groove

Previous structural and biochemical studies have revealed important mechanistic aspects of CRM1-mediated NES export (Dong et al., 2009a; Monecke et al., 2009; Güttler et al., 2010; Fung et al., 2015, 2017; Fu et al., 2018). Structural analyses revealed how NES peptides dock into the NES-binding groove of CRM1. These observations were supported by *in vitro* pull-down assays to evaluate how groove mutations affected NES interaction. Thus, it was shown that replacing groove residue A541 with a bulkier lysine (A451K) severely disrupted CRM1/NES interaction (Güttler et al., 2010). A similar disruption was observed when four groove residues that establish hydrophobic interactions with the NES (I521, L525, F561 and F572) were simultaneously mutated to alanine (I521A/L525A/F561A/F572A, referred to as the 4X mutation; Dong et al., 2009a). Using the SRV100 reporter-based cellular assay, García-Santisteban and co-workers (2016) previously confirmed that the A541K and 4X mutations prevent nuclear export of survivin NES.

To gain further mechanistic insight into CRM1-mediated NES export, the $SRV_{B/A}$ reporter was used in this thesis to investigate to what extent individual groove residues contribute to the export of different NES motifs in a cellular context. To this end, a panel of five YFP-CRM1 variants bearing single-residue mutations (I521A, L525A, F561A, F572A or A541K) in the hydrophobic groove amino acids whose position is illustrated in Figure E39 was generated. An alanine mutation of K568, the non-hydrophobic residue reported to contribute to NES binding (Fung et al., 2017), was also included in this analysis.

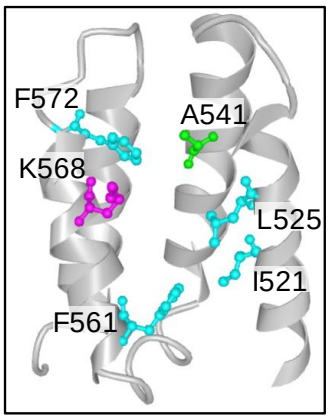

Figure E39: CRM1 NES-binding groove residues mutated in this study. View of the NES-binding groove of CRM1 generated with NCBI iCn3D viewer from PDB structure 3GJX (Monecke et al., 2009). The residues individually mutated in this study are highlighted using ball and stick representation in colours, while the remaining residues are represented using ribbon style.

The export activity of these mutants was interrogated using a panel of 14 extensively characterised NES motifs: PKI, superPKI, PAX, HDAC5, FMRP, FMRP-1b, SNUPN, Rev, SMAD4, mDia2, CDC7, X11L2, CPEB4 and hRio2 (Table E8). The binding of these NES peptides to CRM1 has been previously studied using structural and biochemical analyses (Fung et al., 2017), and their export activity has been analysed using a cellular assay (Fu et al., 2018). These well-studied NESs provide a unique resource to evaluate the export capacity of the different CRM1 mutants against a variety of motifs that belong to different NES classes (1, 2, 3, 4 and 1-R), and dock into the CRM1 groove using different backbone conformations (Fung et al., 2017).

Table E8: Class, sequence and afinity for CRM1 of the NESs used for analysing NES export mediated by different single-point CRM1 mutants.

NES ID	Class	Sequence	Affinity (K_d)
SuperPKI	1	GNLNELALKLAGLDINKTE	4 nM
PKI	1	GNSNELALKLAGLDINKTE	34 nM
PAX	1	TRELDELMASLSDFKIQGL	700 nM
HDAC5	1	ETEEAETVSAMALLSVGAE	1600 nM
FMRP-1	1	LNYLKEVDQLRALERLQIDE	3000 nM
SNUPN	1	MEELSQALASSFSVSQDLNS	12500 nM
Rev	2	EPVPLQLPPLERLTLDCNE	1180 nM
FMRP	2	LNYLKEVDQLRLERLQIDE	2000 nM
SMAD4	2	HYERVVSPGIDLSGLTLQS	4600 nM
mDia2	3	SKNESVPEVEALLARLRAL	1600 nM
CDC7	3	AQDLRKLCERLRGMDSSTP	2000 nM
X11L2	4	ESSLQELVQQFEALPGDLV	1500 nM
CBEP4	1R	RPRTFDMHSLESSLIDIMR	800 nM
hRio2	1R	ARSFEMTEFNQALEEIKGQ	2800 nM

$SRV_{B/A}$ reporters containing each of these 14 NES motifs were either transfected alone or co-transfected with YFP-CRM1-encoding plasmids into HEK293T cells. Besides the six mutants indicated above, wild-type YFP-CRM1 and the 4X mutant were included in the analysis as controls. All in all, 112 different combinations of CRM1 variant/SRV-NES reporter (plus each reporter alone) were tested in these experiments. The results of these assays were evaluated using assessment method 2. Thus, the percentage of cells where the reporter was located exclusively/mainly in the nucleus (N), the cytoplasm (C), or was similarly distributed between nucleus and cytoplasm (NC) was determined by counting at least 200 cells per sample (Figure E40).

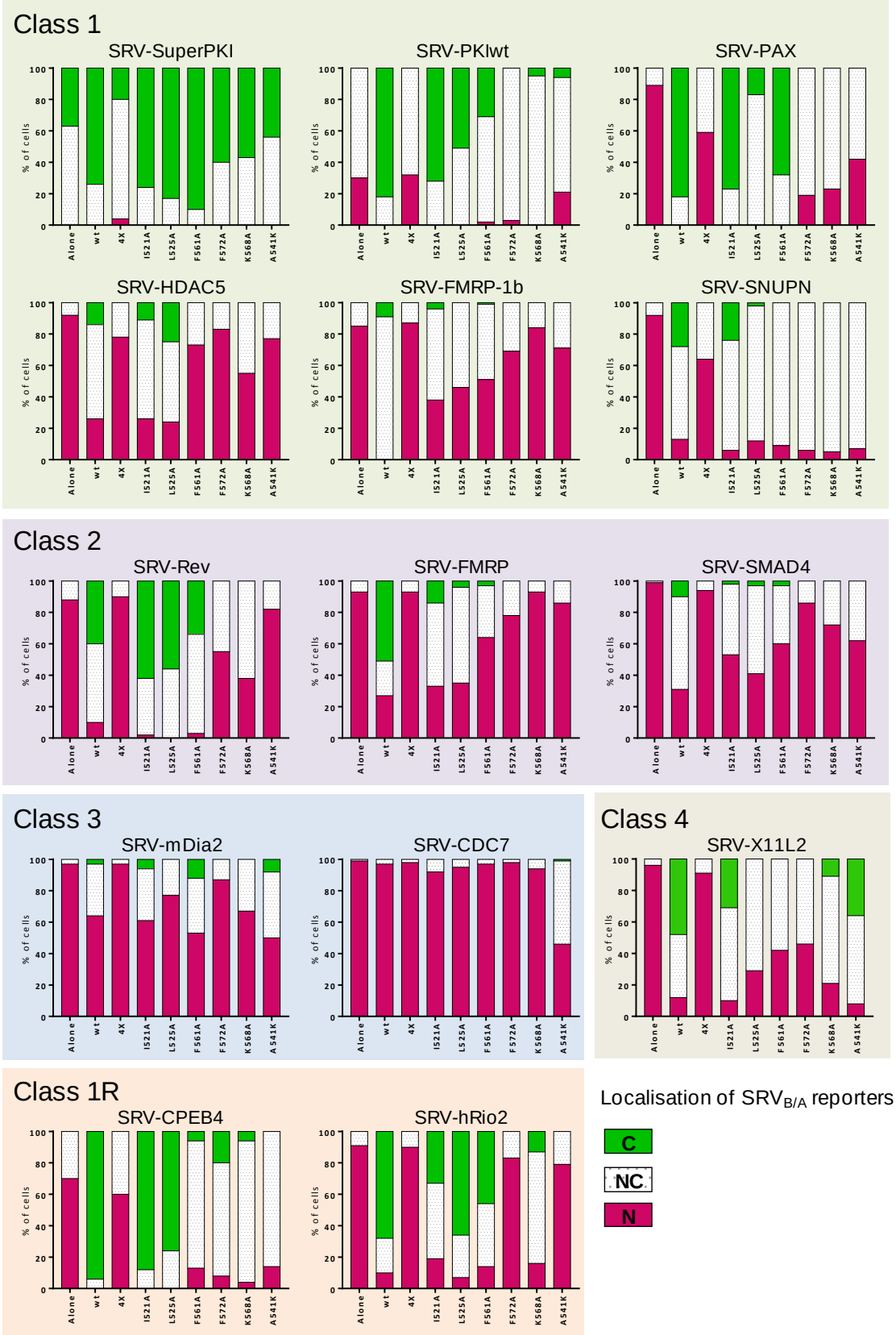

Figure E40: Graphs showing the results of SRV$_{B/A}$ export assays with 14 different NES reporters transfected alone or with different CRM1 variants. SRV-NES reporters are classified according to the class of the cloned NES. The localisation of the reporter was determined in at least 200 cells per sample. Bar colours represent the percentage of cells showing the indicated reporter localisation (N, NC or C).

From these semi-quantitative data, a nuclear export score (referred to as "SRV export score"), ranging between 0 (no export) and 100 (complete export) was derived using the formula [0 x (% N) + 0.5 x (% NC) + 1 x (% C). The SRV export scores for the full set of experiments are represented as a heat map in Figure E41. When expressed alone, the SRV export score was lower than 10 (corresponding to mainly nuclear localisation) for all the reporters except those containing PKI, superPKI and CPEB4 NES motifs. Co-expression with wild-type YFP-CRM1 readily induced nuclear export of all the reporters, with the exception of SRV-CDC7. As expected, simultaneous mutations in the four hydrophobic residues (4X) fully abrogated YFP-CRM1-induced export of all NESs, while individual mutations of these amino acids had less dramatic consequences. Interestingly, the different single-residue mutations decreased export to a different extent, with I521A and L525A having the mildest effect, and F572A being consistently the most detrimental. These findings suggest that the degree of contribution of these residues to NES export could be expressed as I521 = L525 < F561A < F572A, irrespective of NES class. Of note, the effect of the K568A mutation was remarkably similar to the effect of F572A, even if these CRM1 residues engage in different types of chemical interaction with the NES. Finally, the A541K mutation severely reduced export of most reporters, but had a minor effect on SRV-X11L2, the only reporter containing a class 4 motif.

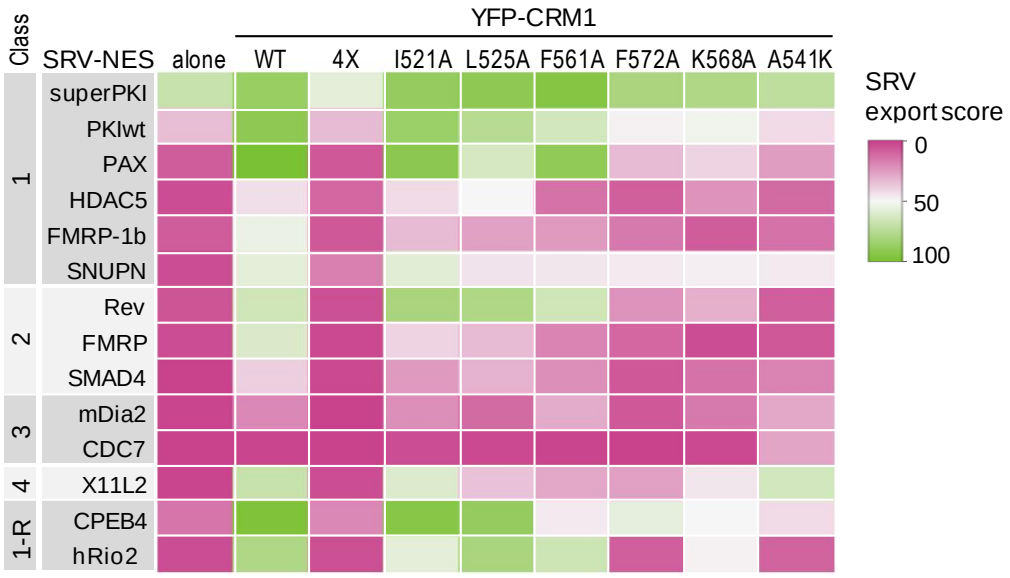

Figure E41: Heat map summarising the results obtained with the 14 reporters. The colour indicates the SRV export score for each CRM1 variant/NES combination, ranging from 0 (no export) to 100 (full export).

E3.1.2.4. Using the $SRV_{B/A}$ assay to gain mechanistic insight into CRM1-mediated NES export. (ii) Comparing the effect of E571K and K568A mutations

A particularly intriguing, and clinically relevant, aspect of CRM1-mediated NES export is the role of two adjacent, electrostatically-interacting residues, namely E571 and K568 (Figure E42).

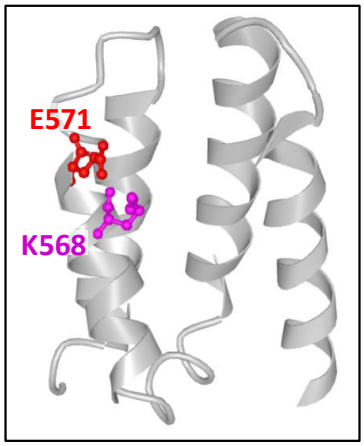

Figure 42: View of CRM1 NES-binding groove showing the position of E571 and K568 amino acids. The view was generated with NCBI iCn3D viewer using PDB structure 3GJX (Monecke et al., 2009). The E571 and K568 residues are highlighted using ball and stick representation, while the remaining residues are represented using ribbon style.

E571 residue mutations subtly alter nuclear export of certain NESs (García-Santisteban et al., 2016), and confer oncogenic potential to mutant CRM1 (Taylor et al., 2019). K568 mutations (K568A or K568M), on the other hand, have been shown to allow *in vitro* binding of some "inactive NES" motifs to CRM1, by disrupting a "selectivity filter" imposed by this residue that prevents docking of structurally inadequate NES-resembling peptides (Fung et al., 2017). The relevance of this "selectivity filter" for nuclear export in a cellular setting, and the possibility that it is abrogated by cancer-related mutations in E571 remained to be investigated. Thus, the $SRV_{B/A}$ assay was used to directly compare how the E571K and K568A mutations affect nuclear export of: (i) three "inactive NES" motifs previously characterised (COMMD1, Hxk2 and DEAF1) (Fung et al., 2017) and (ii) a subset of NES motifs from the CRM1-cancer exportome proteins described above. These $SRV_{B/A}$ export assays were evaluated using the assessment method 3. That is, after anti-Flag immunofluorescence, the intensity of the fluorescent signal of the reporters in the nucleus and the cytoplasm was quantified using image analysis, and the nuclear to cytoplasmic (N/C) ratio was calculated.

On one hand, SRV reporters containing COMMD1, Hxk2 and DEAF1 "NES-like" motifs (Fung et al., 2017) were either expressed alone or co-expressed with YFP-CRM1 (wild type, K568A or E571K) in HEK293T cells. A fourth reporter ($SRV100^{NESm}$), containing an export-deficient version of survivin NES mutated in two critical hydrophobic residues (García-Santisteban et al., 2016)

was also included for comparison in these assays. As shown in Figure E43, the localisation of the four reporters was mainly nuclear (log_2(N/C ratio)> 0) under all conditions. A minor, but statistically significant reduction in N/C ratio was noted for SRV-COMMD1, SRV-Hxk2 and SRV-DEAF1 upon co-expression with wild-type CRM1, suggesting that these motifs may be NESs with extremely low activity, rather than completely inactive NES-like motifs. In comparison to the wild-type receptor, co-expression with the K568A mutant reduced export of the SRV-COMMD1 reporter, but slightly increased nuclear export of SRV-Hxk2 and SRV-DEAF1, although only the results with the later reporter reached statistical significance. These results are generally consistent with those of previous *in vitro* analyses that found increased binding of Hxk2 and DEAF1, but not COMMD1 motifs, to K568A mutant CRM1 (Fung et al., 2017). In the case of the E571K mutant, the only statistically significant difference in comparison to wild type CRM1 was a reduction in the nuclear export of the SRV-COMMD1 reporter.

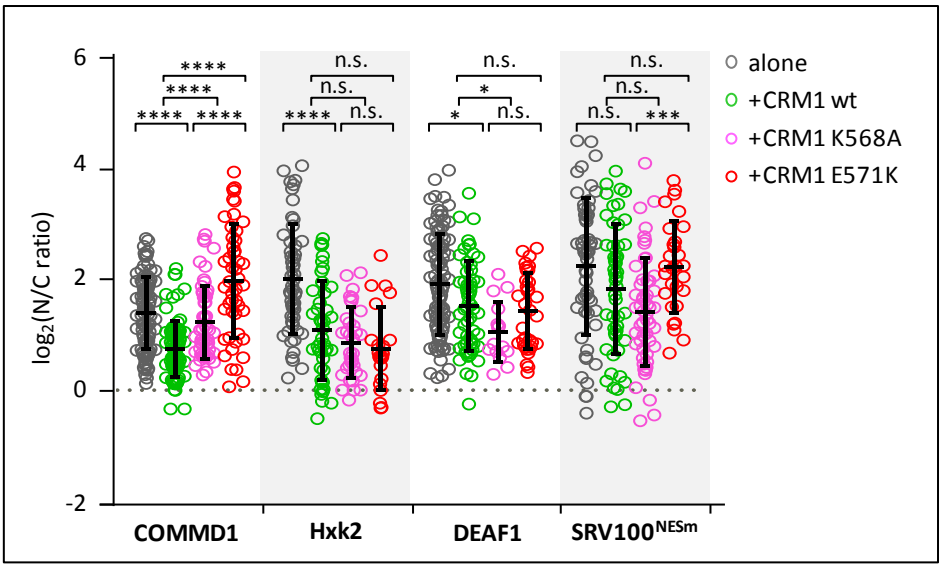

Figure E43: Using the $SRV_{B/A}$ assay to compare the effect of E571K and K568A mutations on the export of inactive "NES-like" motifs. Graph representing the nucleocytoplasmic localisation of three $SRV_{B/A}$ reporters containing NES-like motifs (COMMD1, Hxk2 and DEAF1; previously described as "inactive" (Fung et al., 2017)), plus an export defective mutant of survivin NES ($SRV100^{NESm}$), when expressed alone or when co-expressed with YFP-CRM1 (wild type, K568A or E571K). Each circle represents a single cell where the nuclear to cytoplasmic (N/C) ratio of the fluorescent signal corresponding to the reporter was determined by image analysis using Fiji. The mean (+/- SD) is also shown. The level of statistical significance of the differences between the compared samples (Mann-Whitney U test) is indicated by the asterisks as follows: (*) p<0.05; (***) p<0.001; (****) p<0.0001; ns, non-significant.

On the other hand, a similar analysis was carried out with a set of SRV reporters containing seven different NES motifs (WN1-WN7) identified in cancer-related proteins (Figure E44). Consistent with the results obtained using the assessment method 1, the localisation of all the reporters, except SRV-WN3, was significantly more cytoplasmic when co-expressed with wild-type YFP-CRM1 than when expressed alone. In comparison to the wild-type receptor, the K568A or E571K mutations significantly reduced the export of three reporters (SRV-WN1,

SRV-WN5 and SRV-WN7). Importantly, E571K mutation consistently led to a considerably less pronounced reduction in the nuclear export of these three reporters than K568A. Furthermore, K568A decreased nuclear export of a fourth reporter (SRV-WN2), which was efficiently exported by E571K. In summary, these results clearly indicate that the E571K mutation has a subtler effect on the nuclear export capacity of CRM1 than K568A.

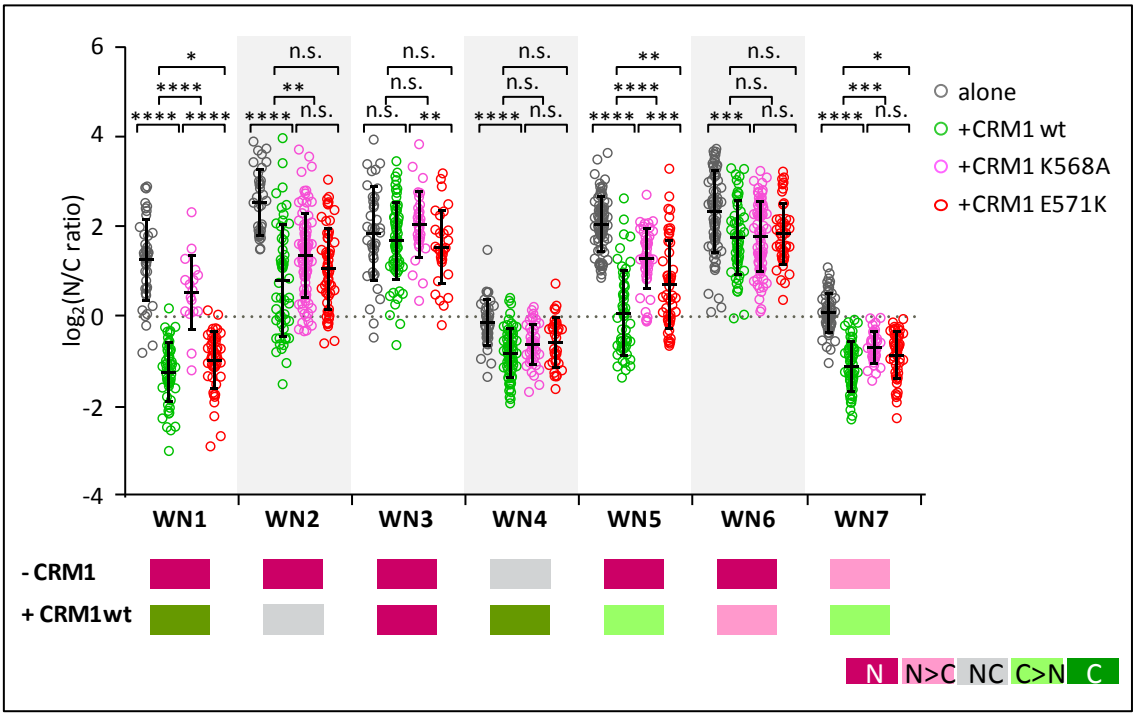

Figure E44: Using the $SRV_{B/A}$ assay to compare the effect of E571K and K568A mutations on the export of NES motifs from CRM1-cancer exportome proteins. Graph representing the nucleocytoplasmic localisation of seven $SRV_{B/A}$ reporters containing NES motifs identified in cancer-related proteins (WN1-7) when expressed alone or when co-expressed with YFP-CRM1 (wild type, K568A or E571K). Each circle represents a single cell where the nuclear to cytoplasmic (N/C) ratio of the fluorescent signal corresponding to the reporter was determined by image analysis using Fiji. The mean (+/- SD) is also shown. The level of statistical significance of the differences between the compared samples (Mann-Whitney U test) is indicated by the asterisks as follows: (*) p<0.05; (**) p<0.01; (***) p>0.001; (****) p<0.0001; ns, non-significant. In the bottom of the graph the results corresponding to these NESs that were previously shown in Figure E34 are shown again to make easier the comparison between the results obtained with assessment method 1 and 3.

E3.1.3. Design and evaluation of a new affinity purification strategy to compare the exportomes of wild-type and E571K mutant CRM1

The E571K mutation has been shown to confer oncogenic potential to CRM1 (Taylor et al., 2019). Since this change subtly alters recognition and export of certain NESs (García-Santisteban et al., 2016; Sendino et al., 2020a), its oncogenic nature may be due, at least in part, to altered export of crucial cargos. However, the question remains as to what these cargos may be. To begin addressing this issue, in this thesis a new affinity purification strategy was designed to compare the exportomes CRM1 wild-type (wt) and cancer mutant E571K.

E3.1.3.1. Rationale and design of the strategy: stabilisation of the trimeric complex CRM1/cargo/RanGTP by a non GTP-hydrolysing Ran mutant

The new strategy to compare CRM1 wild type and E571K mutant exportomes is based on the mechanism of CRM1-mediated export. As described in the Introduction, CRM1 binding to its cargos in the nucleus is stabilised by RanGTP. The CRM1/cargo/RanGTP trimeric complex moves across the NPC and, once in the cytoplasm, is destabilised by RanGAP1-stimulated conversion of RanGTP to RanGDP, the cargo is released, and the export process is completed (Bischoff et al., 1994; Bischoff and Görlich, 1997; Fornerod et al., 1997; Kutay et al., 1997) (Figure E45, upper panel). It seems reasonable to assume that, preventing RanGTP to RanGDP conversion by using a Ran mutant (Ran^{Q69L}) unable to hydrolyse GTP (Bischoff et al., 1994; Klebe et al., 1995) may render the CRM1/cargo/RanGTP interactions more stable (Figure E45, lower panel). This stabilisation would, in turn, allow a more efficient identification of cargos by affinity purification of the proteins bound to CRM1.

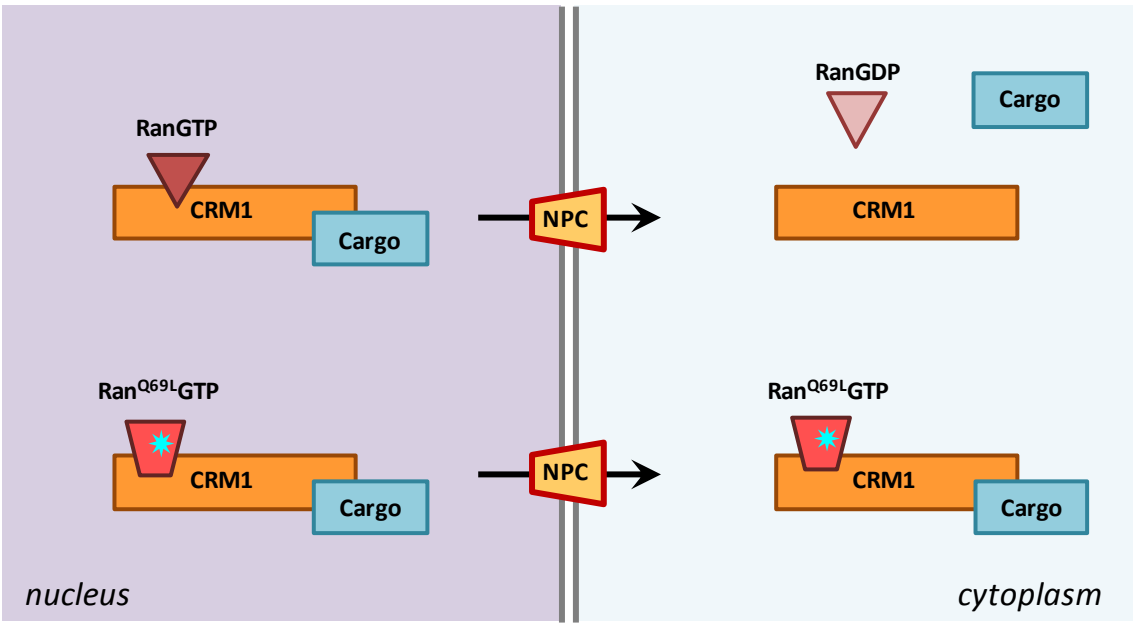

Figure E45: Rationale for an experimental strategy to identify CRM1 cargos based on the stabilisation of the trimeric CRM1/cargo/RanGTP complex. *Above*. In the nucleus, CRM1 forms a complex with the cargo and RanGTP. When this complex reaches the cytoplasm, RanGAP1 stimulates conversion of RanGTP to RanGDP, the complex is disassembled, and the cargo is released. *Bottom*. In cells overexpressing a Ran^{Q69L} mutant (unable to undergo RanGTP to RanGDP conversion) the trimeric complex would be stabilised, and consequently, CRM1 will not release its cargos.

Therefore, an experimental system was set up (Figure E46), where YFP tagged CRM1 (wt or E571K) was co-expressed in cells with Myc tagged Ran^{Q69L}. YFP-CRM1^{4x} mutant (unable to bind cargos (Dong et al., 2009a)) was also co-expressed with Myc-Ran^{Q69L} as a negative control.

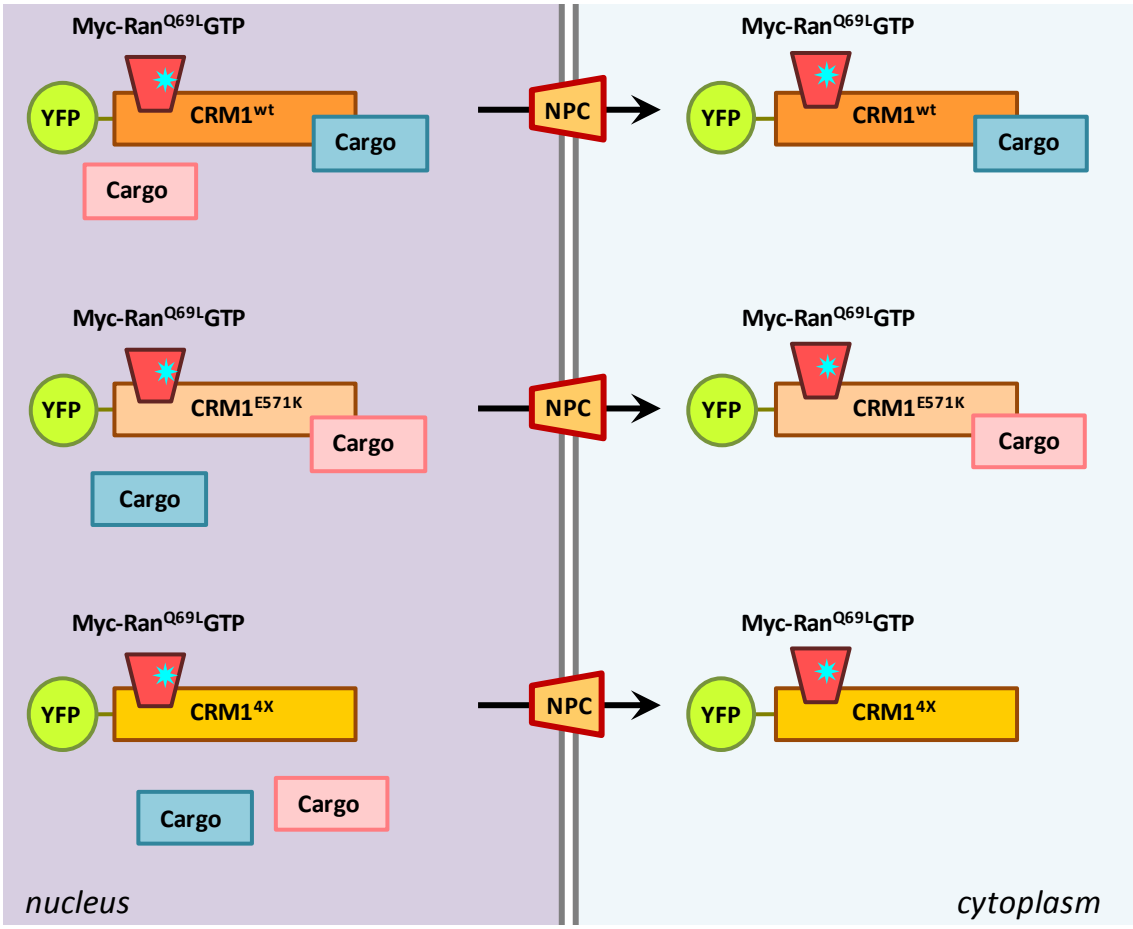

Figure E46: Experimental settings used to evaluate potential changes in the CRM1 exportome caused by the E571K mutation. In each setting, Myc tagged Ran^{Q69L} was co-expressed with one YFP tagged CRM1 variant: CRM1wt, the cancer mutant CRM1^{E571K} or the non functional CRM1^{4X}.

Afterwards, the trimeric complexes formed by the ectopic proteins and the endogenous cargos can be isolated using GFP-Trap magnetic beads (Rothbauer et al., 2008) (Figure E47), and the pulled down cargos identified by MS/MS-based proteomics.

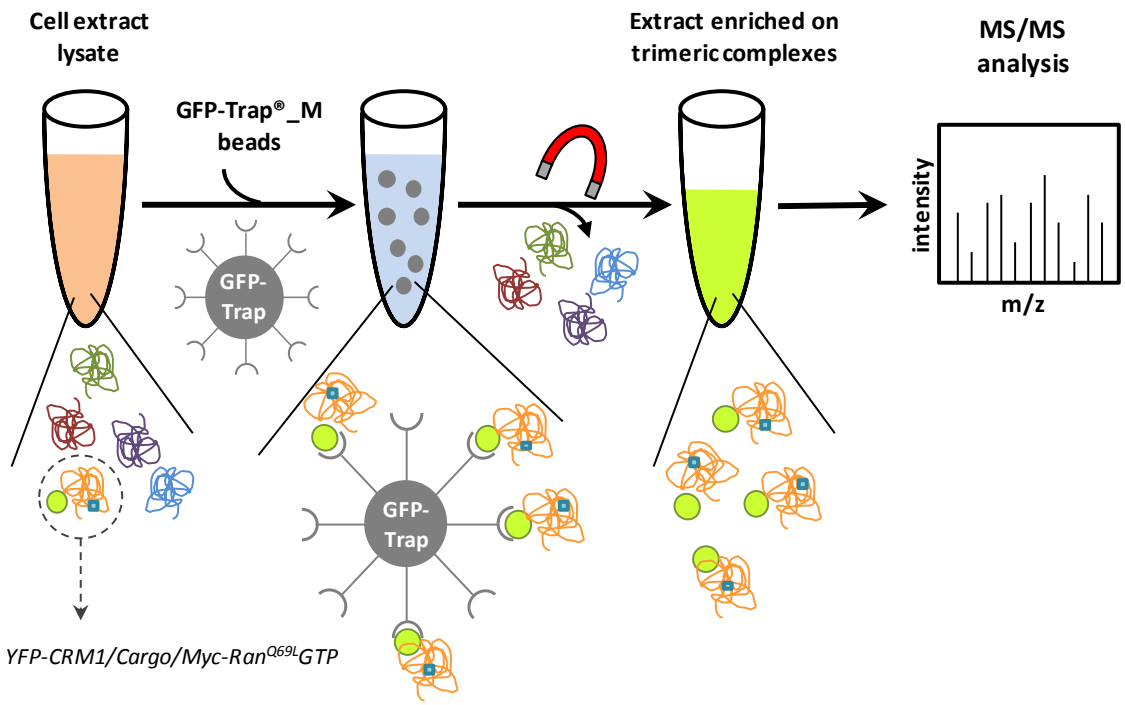

Figure E47: Schematic representation of GFP-Trap-based affinity purification of CRM1-bound cargos. After collecting and lysing cells, GFP-Trap®_M beads are added to the extract. The surface of these beads is covered by GBPs (GFP binding proteins) which will bind YFP. Using a magnet, the trimeric complexes can be isolated and subjected to MS/MS-based identification of the co-purified proteins (expectedly, CRM1 cargos).

E3.1.3.2. Evaluation of the strategy

The first step to evaluate the new strategy was to analyse the localisation of Myc-Ran^{Q69L} and the YFP-CRM1 variants in transfected HeLa and HEK293T cells (Figure E48). The two proteins show the same subcellular localisation, suggestive of interaction, in both cell lines, but was more noticeable in HEK293T cells and thus, this cell line was selected for subsequent analyses.

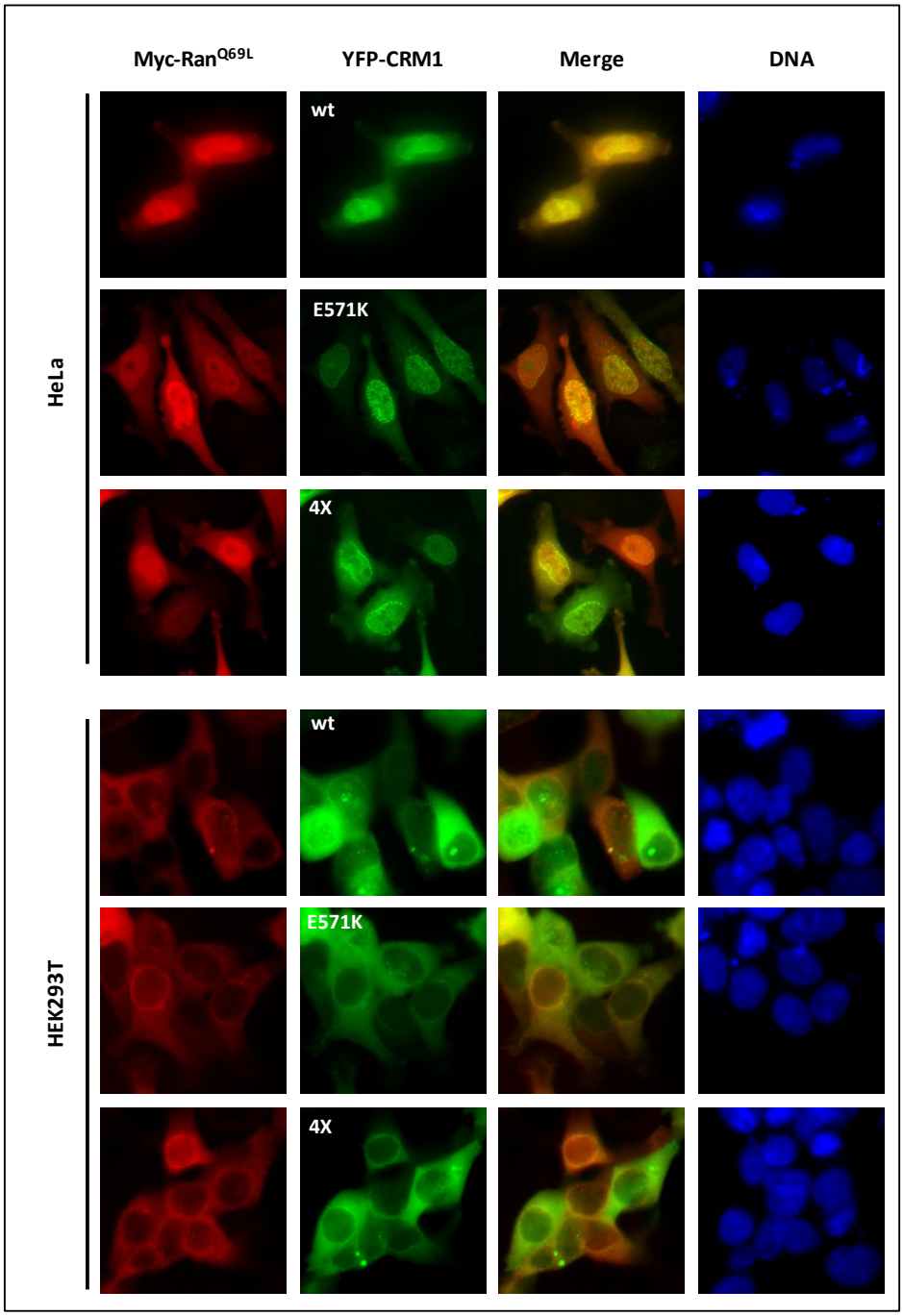

Figure E48: Representative images of HeLa and HEK293T cells overexpressing Myc tagged Ran^{Q69L} mutant and YFP tagged CRM1 variants wild type (wt), E571K and 4X. YFP-CRM1 variants and Myc-Ran^{Q69L} proteins show the same localisation in both cell lines, although it was clearer in HEK293T. In HeLa cells it is mostly nuclear, while in HEK293T it is cytoplasmic. Images were acquired using an Axioskop fluorescence microscope.

Nine samples (three biological replicates of each condition) were prepared for proteomics analysis: three samples co-expressing Myc-Ran^{Q69L} with YFP-CRM1wt, three samples co-expressing Myc-Ran^{Q69L} with YFP-CRM1^{E571K}, and three samples co-expressing Myc-Ran^{Q69L} with YFP-CRM1^{4X}. After GFP-trap pull down, isolated proteins were sent to the SGIker proteomics service of the UPV/EHU. Due to technical issues, only partial MS/MS data were obtained. Nevertheless, these data revealed that, unexpectedly, the same set of proteins was

identified in three experimental settings, suggesting that this new approach was not working as intended.

In an attempt to establish where the problem might be, two experiments were carried out. On one hand, Myc-Ran^{Q69L} was co-transfected with either the empty YFP vector, YFP-CRM1 wt or 4X mutant in HEK293T cells. As shown in Figure E49, Myc-Ran^{Q69L} show the same localisation as YFP-CRM1 variants, but not as YFP, suggesting that the interaction YFP-CRM1 (wt or 4X) and Myc-Ran^{Q69L} was taking place in cells.

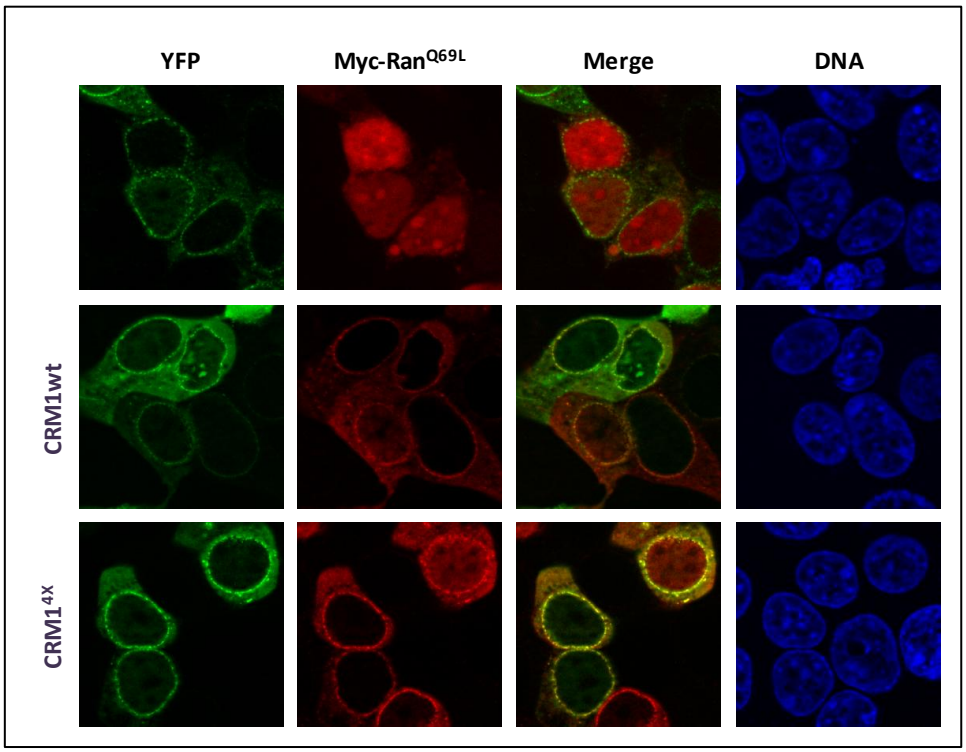

Figure E49: Representative images of YFP, YFP-CRM1wt and YFP-CRM1^{4X} co-expressed with Myc-Ran^{Q69L} in HEK293T cells. YFP-CRM1 variants show the same localisation as Myc-Ran^{Q69L}, while YFP does not.

On the other hand, a GFP-Trap pull down assay using washing buffers with different NaCl concentration was carried out, and the results were analysed by silver-staining and western-blot against YFP and Myc epitopes (Figure E50). Irrespective of the salt concentration used in the washing buffers, very few proteins were detected by silver staining. Importantly, no bands corresponding to Myc-Ran^{Q69L} were detected. These results indicate that, contrary to what was expected, the trimeric CRM1/cargo/RanGTP complexes were not sufficiently stabilised by the Ran^{Q69L} mutation, and were disrupted during the affinity purification. Thus, this strategy was not pursued further.

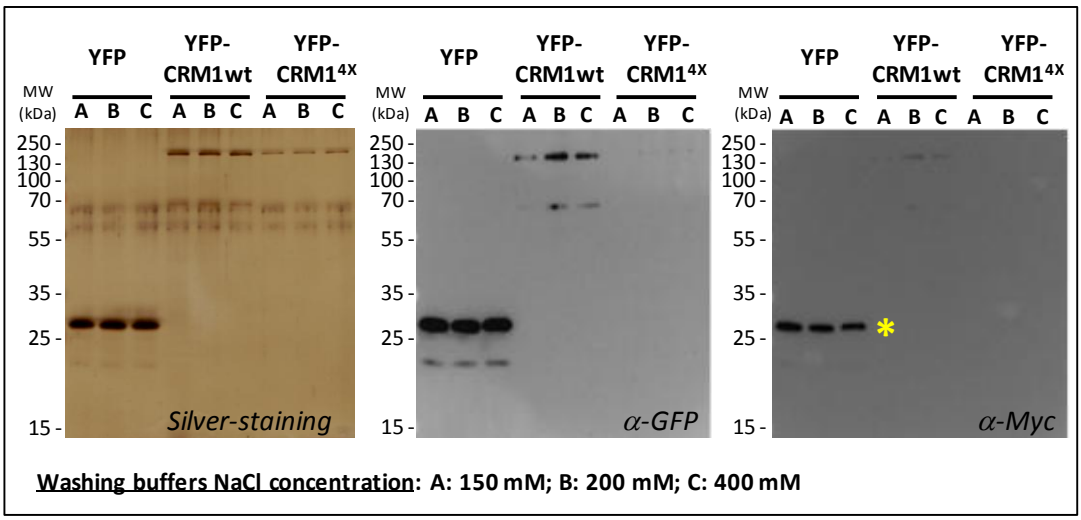

Figure E50: GFP-trap analysis of Myc-Ran^{Q69L}/YFP-CRM1 co-expressing HEK293T cells. The results were analysed using silver-staining and western-blotting against YFP and Myc epitopes. Expected approximate molecular weight of the overexpressed proteins: YFP: 26 KDa; YFP-CRM1: 150 KDa; Myc-Ran^{Q69L}: 25 KDa. *Left*. Silver-staining. Despite the high sensitivity of this method, few proteins were detected. *Middle*. Western-blot against YFP. No smears suggestive of YFP-CRM1 complexes containing cargos of different size were detected when was over-expressed. This suggests that the trimeric complexes get broken. *Right*. Western-blot against Myc epitope. No signal corresponding to Myc-Ran^{Q69L} was detected. The yellow asterisk indicates that these bands are not Myc-Ran^{Q69L}, but signal leaked from the anti-GFP blot.

E3.1.4. Evaluation of NES motifs predicted in the nucleocapsid protein of human coronaviruses

The results described in this section have been published as a preprint in Sendino et al., 2020c

In March 2020, this thesis project was suddenly interrupted when the population was confined for several weeks as a measure against the newly identified COVID-19 disease. When laboratory work could be resumed, an attempt was made to gain more knowledge on the biology of the COVID-19 causative agent, the SARS-CoV-2 coronavirus. This chapter describes the studies carried out to characterise NES motifs in the viral nucleocapsid (N) protein, which were reported to influence the pathogenic capacity of the different coronaviruses.

Seven members of the *Coronaviridae* family (SARS-CoV, SARS-CoV-2, MERS-CoV, HCoV-NL63, HCoV-229E, HCoV-HKU1 and HCoV-OC43) are known to infect humans, but only the first three cause severe disease. Identifying molecular determinants of coronaviruses pathogenicity is an important issue. In this regard, several genomic features that could differentiate highly pathogenic coronaviruses from less pathogenic strains were identified *in silico* using machine learning techniques and comparative genomics (Gussow et al., 2020).

Eleven genomic regions corresponding to four different viral proteins, including the nucleocapsid (N) protein, were found to predict a high pathogenic capacity, but the underlying biological mechanisms remain to be elucidated. Interestingly, pathogenicity-associated deletions, insertions and substitutions within the N protein mapped to four potential nucleocytoplasmic transport motifs: three nuclear localisation signals (NLSs) and one nuclear export signal (NES). In highly pathogenic strains, these four motifs showed an increased content of positively charged amino acids, and were proposed to have an enhanced transport activity (Gussow et al., 2020). However, while a direct correlation between positive charge and NLS activity has indeed been reported (Cokol et al., 2000), such a correlation cannot be extrapolated to the NES motif. The NES consensus pattern is remarkably loose (Kosugi et al., 2008; Monecke et al., 2009; Güttler et al., 2010), and thus, predicting NES activity solely from amino acid sequence is notoriously difficult (Prieto et al., 2014).

Four necessary steps towards elucidating the mechanism behind a potential relationship between coronaviruses pathogenicity and the proposed nucleocapsid NES motifs are (i) to establish if these sequence motifs are functional (i.e, capable of mediating CRM1-dependent nuclear export), (ii) to determine if their activity level (their strength) correlates with the

pathogenic capacity of the corresponding viral strain, (iii) to determine if NES-mediated CRM1-dependent export is a key determinant of full-length N protein localisation and (iv) to determine if the pathogenicity of the different coronavirus strains correlates with N protein localisation. To address the first two issues, candidate NES motifs predicted in the N protein of SARS-CoV-2, MERS-CoV, HCoV-NL63, HCoV-229E, HCoV-HKU1 and HCoV-OC43 were experimentally tested. The third issue was also addressed by analysing the nucleocytoplasmic localisation of YFP tagged N proteins from SARS-CoV-2 and HCoV-NL63.

E3.1.4.1. The pathogenic capacity of human coronavirus strains does not correlate with the export activity of their N protein NES motifs

To test the activity of the cNESs proposed by Gussow and co-workers (2020), the Rev(1.4)-GFP assay (Henderson and Eleftheriou, 2000) was used. The sequences indicated in Table E9, encompassing the predicted NES motifs were cloned into the pRev(1.4)-GFP vector. The SARS-CoV cNES motif, which is virtually identical to that of SARS-CoV-2, was not tested.

Table E9: Position and amino acid sequence of predicted NES motif in the nucleocapsid (N) protein of human coronaviruses. Amino acid sequence of a segment of the N protein from different coronavirus strains encompassing the proposed NES (Gussow et al., 2020) (underlined). These 19 amino acid-long sequences were tested using the Rev(1.4)-GFP nuclear export assay. n.a.: not assayed.

Virus	Predicted NES motifs
SARS-CoV-2	^{224}ALALLLLDRLNQLESKMSG^{230}
SARS-CoV (n.a.)	^{225}ALALLLLDRLNQLESKVSG^{231}
MERS-CoV	^{216}GGDLLYLDLLNRLQALESG^{222}
HCoV-HKU1	^{237}MADEIANLVLAKLGKDSKP^{243}
HCoV-OC43	^{238}MADQIASLVLAKLGKDATK^{244}
HCoV-NL63	^{187}SSSDLVAAVTLALKNLGFD^{193}
HCoV-229E	^{184}SQDDIMKAVAAALKSLGFD^{190}

As shown in Figure E51, the cNES tested were all functional in the export assay, but displayed a wide range of nuclear export activity (scores between 1 (HCoV-HKU) and 8 (HCoV-NL63)).

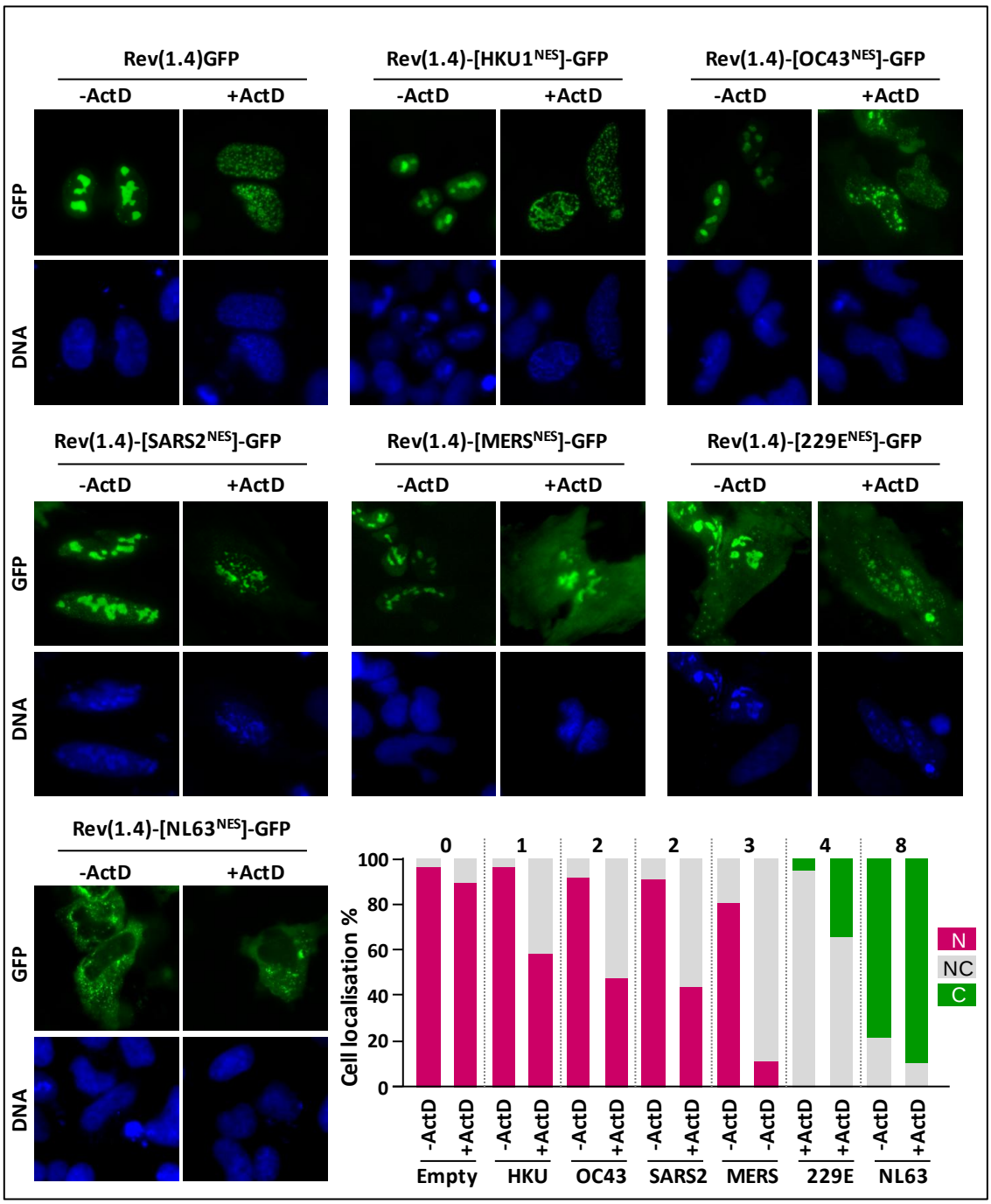

Figure E51: Experimental analysis of predicted NES motifs in human coronaviruses N protein. Images show representative examples of the results of the nuclear export assay in HeLa cells. Graphs represent the percentage of HeLa cells showing nuclear (N), nuclear and cytoplasmic (NC) or cytoplasmic (C) localisation of the reporter containing the indicated NES motif. At least 200 cells per sample were scored. From these percentages, each NES was assigned an export assay score as described in (Henderson and Eleftheriou, 2000), which is indicated in the graph by the numbers above the bars.

Importantly, and in contrast to what was proposed based on *in silico* analyses (Gussow et al., 2020), the differences in NES activity were not obviously related to pathogenicity. NESs of coronaviruses causing highly pathogenic diseases scored 2 (SARS-CoV-2) and 3 (MERS-CoV), while NESs of less pathogenic coronaviruses scored 1 (HCoV-HKU1), 2 (HCoV-OC43), 4 (HCoV-229E) and 8 (HCoV-NL63).

E3.1.4.2. CRM1 inhibition does not alter the nucleocytoplasmic localisation of neither HCoV-NL63 nor SARS-CoV-2 nucleocapsid proteins

Full-length N proteins of SARS-CoV-2 (NES scored 2) and a less pathogenic strain HCoV-NL63 (NES scored 8) were cloned as YFP fusion proteins and transiently expressed in HEK293T cells.

As shown in Figure E52, both SARS-CoV-2 and HCoV-NL63 N proteins are localised in the cytoplasm, even when CRM1 activity is blocked by LMB treatment. This finding suggests that CRM1 is not a key determinant for the localisation of these proteins.

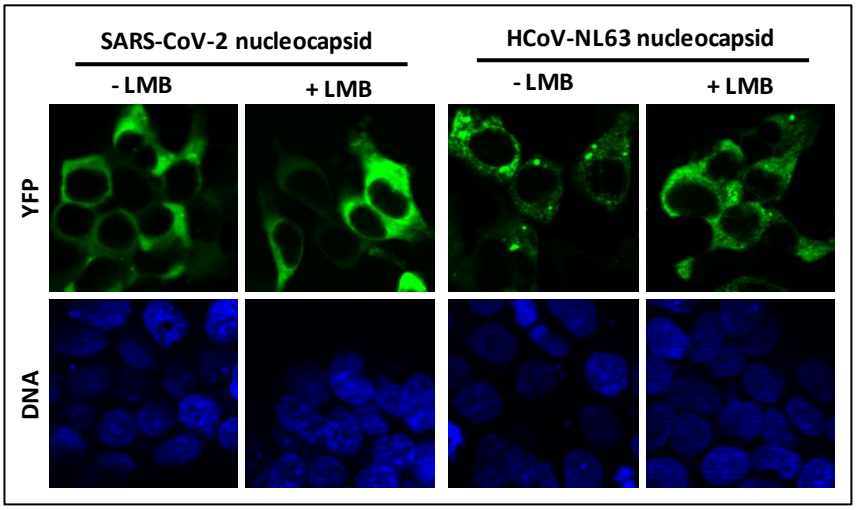

Figure E52: CRM1-dependent nuclear export is not a key determinant of the localisation of the N protein of SARS-CoV-2 and HCoV-NL63 coronaviruses. Fluorescence microscopy images of transfected HEK293T cells showing that YFP-tagged N proteins of SARS-CoV-2 and HCoV-NL63 coronaviruses locate in the cytoplasm both in untreated cells (-LMB) as well as in cells treated with the CRM1 inhibitor LMB for 3 h (+LMB).

E3.2. Studies on therapeutic targeting of CRM1

E3.2.1. Selection and *in vitro* evaluation of potential anticancer treatments combining selinexor with a second targeted drug

These results are presented in English in the main body of the Thesis (Section 4.2.1., page 147)

E3.2.2. Compartment-specific proximity biotinylation: a new approach to evaluate the effect of CRM1 inhibition and identify nuclear export cargos

The results described in this section have been published in Sendino et al., 2021

In order to support the clinical implementation of CRM1 inhibitors as therapeutic agents, it is necessary to develop methodologies to evaluate the effect that these inhibitors may have at the cellular level, in particular, a potential change in the localisation of CRM1 cargos. In this section, a new approach that combines CRM1 inhibition with proximity protein biotinylation (PPB), affinity purification and MS/MS to globally identify cellular proteins whose nucleocytoplasmic distribution is altered upon CRM1 inhibition will be presented, as well as a proof-of-concept experiment to validate this approach.

E3.2.2.1. Design and evaluation of APEX2-based markers for proximity biotinylation of cytoplasmic and nuclear proteins

This approach is based on the use of the APEX2 peroxidase (Lam et al., 2015) as a tool for proximity protein biotinylation. To specifically label the cytoplasmic or nuclear subproteomes and detect CRM1-dependent changes, APEX2 has to be exclusively and stably localised to the cytoplasm or nucleus, independently of CRM1 activity. Thus, two different fusion-proteins (termed APEX2zit and APEX2nuk) were generated here to be used as proximity biotinylation markers. In addition to APEX2 itself, these markers contain signals for cytoplasmic or nuclear targeting (i.e. NES or NLS), and a fluorescent protein that allows easy tracking of their localisation. As described below, several fusion protein configurations had to be tested before two suitable markers were obtained.

To create a **cytoplasmic marker for proximity biotinylation**, the first strategy was to fuse APEX2 to two or three copies of YFP. The aim was to create large proteins that could not passively enter the nucleus. However, using immunofluorescence and immunoblot analyses (not shown) it was found that YFP(2X)-APEX2 was not exclusively cytoplasmic when CRM1 was inhibited, and YFP(3X)-APEX2 was unstable, undergoing degradation when expressed in cells. This strategy was, therefore abandoned.

As an alternative strategy, APEX2 was actively localised to the cytoplasm using CRM1-independent NESs. Four YFP fusion proteins, containing one or two copies of the CRM1 independent NESs of pUL69 (Lischka et al., 2001) or RIP3 (Yang et al., 2004) proteins were created. After several preliminary tests (not shown), a fusion protein (YFP-RIP^{NES}-APEX2), containing a single copy of RIP3 NES, was selected (Figure E53). However, this protein was

found to partly relocate to the nucleus when CRM1 is inhibited. In an attempt to further reduce nuclear entry of the cytoplasmic marker, YFP was replaced by sinGFP4a (Figure E53), a GFP variant that translocates across the NPC much more slowly than YFP (Frey et al., 2018). When expressed in HEK293T cells sinGFP4a-RIP3^{NES}-APEX2 localised to the cytoplasm regardless of CRM1 activity.

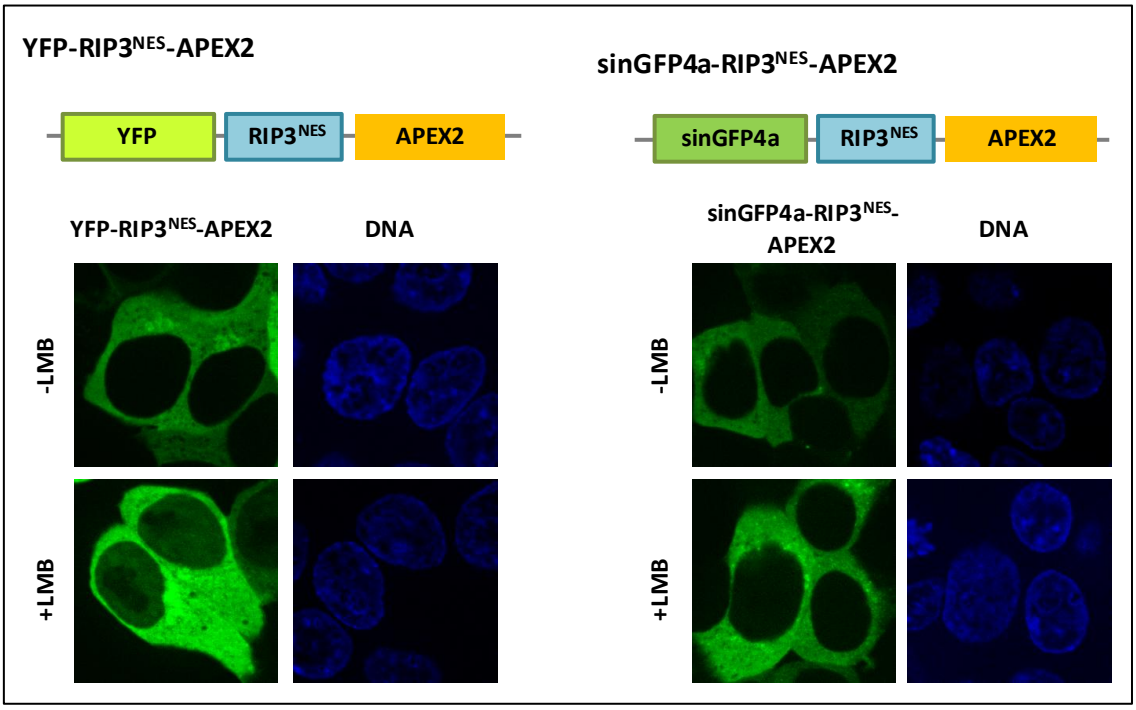

Figure E53: Configuration and nucleocytoplasmic localisation of the YFP-RIP3^{NES}-APEX2 and YFP-RIP3^{NES}-APEX2 fusion proteins. *Upper panels,* Schematic illustration of YFP-RIP3^{NES}-APEX2 (left) and sinGFP4a-RIP3^{NES}-APEX2 (right) proteins. *Bottom panels.* Representative images of YFP-RIP3^{NES}-APEX2 (left) and sinGFP4a-RIP3^{NES}-APEX2 (right) proteins localisation in HEK293T cells when CRM1 is active (-LMB) or inactive (+LMB). A faint YFP signal is visible in the nucleus of LMB-treated cells when YFP-RIP3^{NES}-APEX2 is expressed, but not when sinGFP4a-RIP3^{NES}-APEX2 is expressed.

Finally, using immunoblot analysis (Figure E54), sinGFP4a-RIP3^{NES}-APEX2 was found to be stable and capable of promoting protein biotinylation. Therefore, this fusion protein was accepted as cytoplasmic marker for proximity labelling and renamed **APEX2zit**.

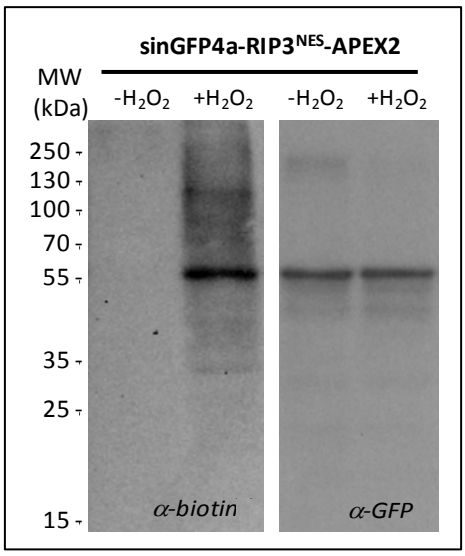

Figure E54: sinGFP4a-RIP3^{NES}-APEX2 is stable and capable of biotinylating surrounding proteins. Proximity protein biotinylation was induced in HEK293T cells overexpressing sinGFP4a-RIP3^{NES}-APEX2 using a described PPB protocol (Hung et al., 2016). The resulting protein extracts were analysed by western-blotting. The anti-biotin blot shows that, when activated (+H_2O_2), APEX2 is capable of biotinylating a collection of differently-sized proteins, while the anti- GFP blot shows that sinGFP4a-RIP3^{NES}-APEX2 is stable.

On the other hand, to create a **nuclear marker for proximity biotinylation**, two fusion proteins containing YFP, APEX2 and either two or four copies of the SV40 NLS (Kalderon et al., 1984a, 1984b) were created. The fusion-protein bearing four NLSs, YFP(4NLS)-APEX2, localises exclusively to the nucleus (Figure E55).

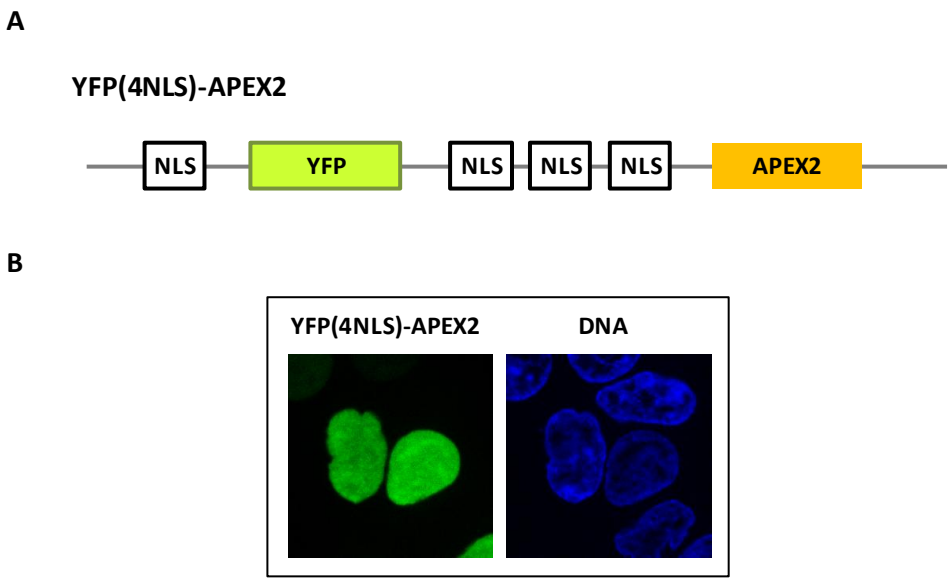

Figure E55: Configuration and nucleocytoplasmic localisation of the YFP(4NLS)-APEX2. A. Schematic illustration of YFP(4NLS)-APEX2 protein. B. Representative images of YFP(4NLS)-APEX2 localisation in HEK293T cells.

Immunoblot analysis (Figure E56) confirmed that YFP(4NLS)-APEX2 is stable and capable of promoting protein biotinylation. Therefore, this fusion protein was accepted as nuclear marker for proximity labelling and renamed **APEX2nuk**.

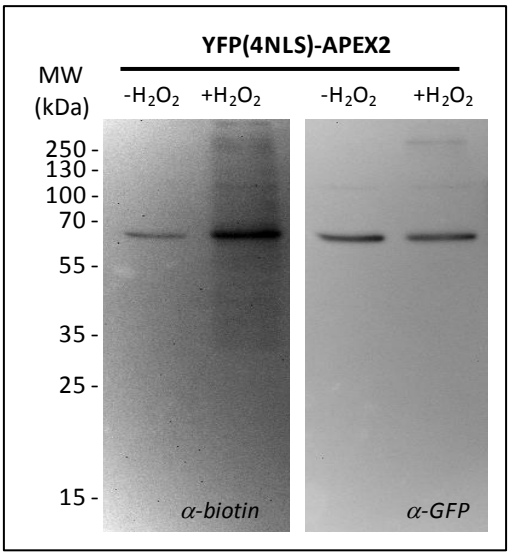

Figure E56: YFP(4NLS)-APEX2 is stable and capable of biotinylating surrounding proteins. Proximity protein biotinylation was induced in HEK293T cells overexpressing YFP(4NLS)-APEX2. The resulting protein extracts were analysed by western-blotting. Anti-biotin blot shows that, when activated (+H_2O_2), APEX2 is capable of biotinylating a collection of differently-sized proteins, while anti-GFP blot shows that YFP(4NLS)-APEX2 is stable.

E3.2.2.2. Proof-of-concept experiment to validate the proximity biotinylation approach

To determine if APEX2-based PPB represents a valid approach to analyse the effect of CRM1 inhibition on the nuclear and cytoplasmic subproteomes, HEK293T cells were transfected with either APEX2zit of APEX2nuk plasmids. For each marker, three experimental conditions were set up: (i) a negative control sample where CRM1 is functional but APEX2 is not activated (-LMB/-H_2O_2), (ii) a sample (named “basal condition”) where CRM1 is functional and APEX2 is activated (-LMB/+H_2O_2), and (iii) a sample (named “CRM1-inhibited condition”) where CRM1 function is blocked by LMB treatment and APEX2 is activated (+LMB/+H_2O_2).

24 hours after transfection, protein biotinylation was induced in these samples using a previously described protocol (Hung et al., 2016). Biotinylated proteins were isolated using a neutravidin-based affinity purification process, and analysed on an acrylamide gel (Figure E57). Gels were stained with Coomassie, and bands corresponding to the protein front, avidin and APEX2zit or APEX2nuk proteins were discarded, as they may interfere with the proteomics analysis. Finally, gel fragments, as indicated in Figure E57, were excised and sent to the SGIker proteomics facility of the UPV/EHU for MS/MS analysis.

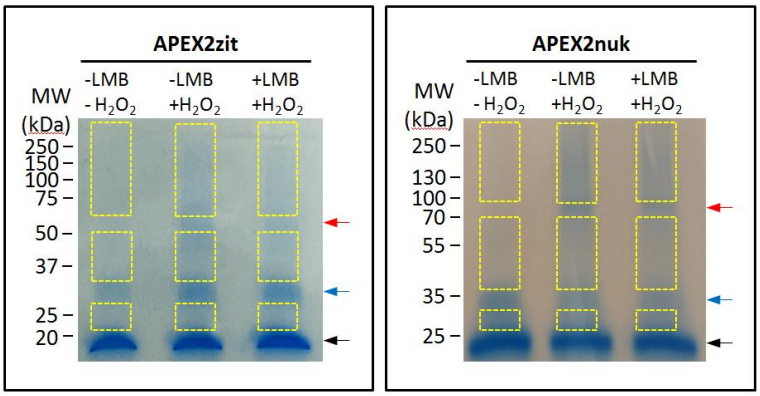

Figure E57: Preparation of samples for MS/MS analysis. Proteins isolated using neutravidin-based affinity purification were loaded into SDS-PAGE gels. Gels were stained using Coomassie, and the front line (black arrow), the avidin band (blue arrow) and the bands corresponding to APEX2 markers (red arrow) were discarded. Fragments surrounded by yellow squares were sent to the proteomics facility of the UPV/EHU.

E3.2.2.2.1. Results of MS/MS analysis (I): general considerations

All in all, MS/MS analysis led to the identification of a total of 2503 different proteins (Table E10). 1489 of these proteins were identified with at least 2 peptides and with an intensity higher than 0 (hereafter referred to as "stringent criteria"). As shown in Table E10, a similar amount of proteins were identified with APEX2zit (1248 proteins; 876 of them with stringent criteria) and APEX2nuk (1318 proteins; 952 of them with stringent criteria). Also similar was the number of proteins identified in both basal (-LMB) conditions (1884 proteins; 1451 of them with stringent criteria) and CRM1-inhibited (+LMB) conditions (1757 proteins; 1362 of them with stringent criteria).

Table E10: Summary of the results of MS/MS analysis. The total number of proteins identified is shown. Those identified using a more stringent criteria (at least 2 peptides and with an intensity higher than 0) are shown in brackets. The "Altogether" column and row show the non-redundant sum of the identified proteins.

	APEX2zit	APEX2nuk	Altogether
-LMB	1157 (842)	1195 (931)	1884 (1451)
+LMB	995 (767)	1156 (882)	1757 (1362)
Altogether	1248 (876)	1318 (952)	2503 (1489)

The comparable number of identified proteins suggests that both markers have similar biotinylating activity, which does not seem to be significantly altered by LMB treatment. Furthermore, these results indicate an absence of obvious technical problems with sample processing.

E3.2.2.2.2. Results of MS/MS analysis (ii): compartment-specific protein identification in basal conditions (-LMB)

In order to verify that APEX2zit and APEX2nuk allow compartment-specific protein labelling, it was investigated to what extent the proteins identified with each marker had the expected localisation in basal conditions (i.e. cytoplasmic proteins identified with APEX2zit and nuclear proteins identified with APEX2nuk). First, proteins identified with each marker in basal conditions were compared, focusing on those identified with stringent criteria. Reassuringly, as shown in Figure E58A, most proteins were identified only with APEX2zit (520 proteins) or with APEX2nuk (609 proteins). As expected, a subset of proteins (322 proteins, presumably locating to both the nucleus and the cytoplasm) were identified with both markers. These results show that, consistent with their different nucleocytoplasmic localisation, APEX2zit and APEX2nuk markers label a largely different set of cellular proteins.

Next, UniprotKB database was used to retrieve information on the previously reported nucleocytoplasmic localisation of the proteins identified in the MS/MS analysis. As shown in Figure E58B, UniProtKB contained information on the localisation of most of the proteins identified here. While 65 % of the proteins identified with APEX2zit are described in UniProtKB as cytoplasmic (or both cytoplasmic and nuclear) proteins, 71 % of the proteins identified with APEX2nuk are described as nuclear (or both nuclear and cytoplasmic) in UniProtKB.

Altogether, these findings indicate that APEX2zit and APEX2nuk are useful markers for compartment-specific protein biotinylation.

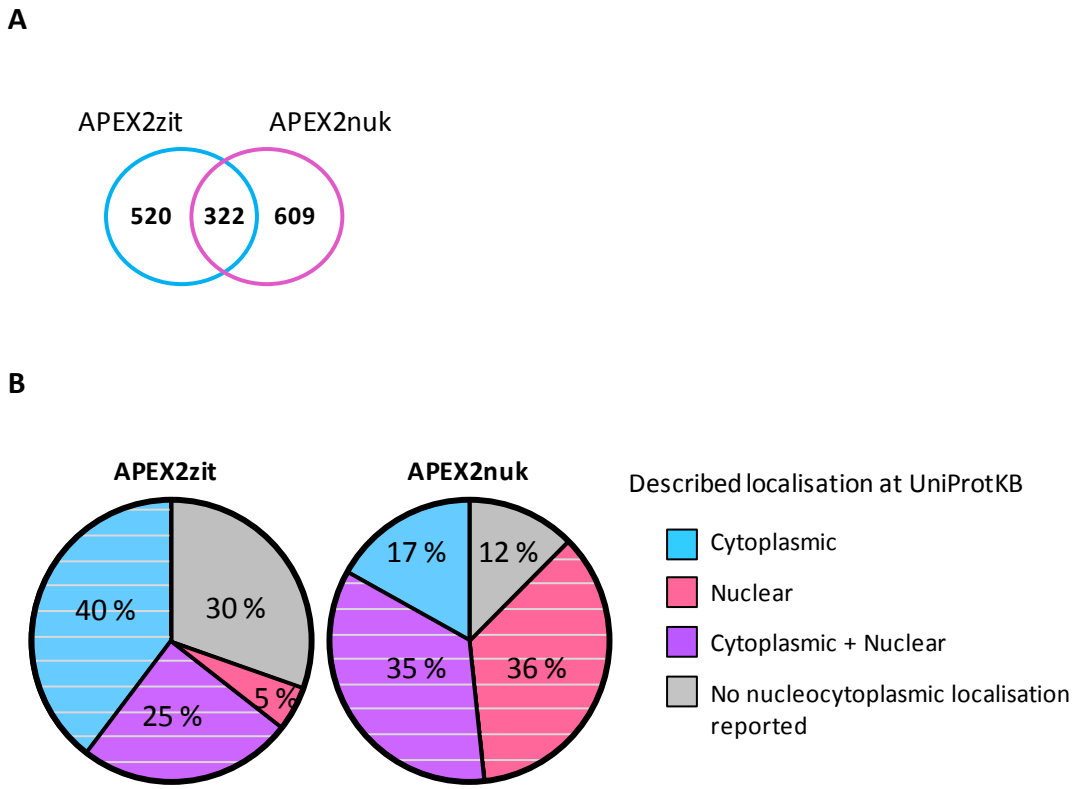

Figure E58: Validating APEX2zit and APEX2nuk as markers for compartment-specific biotinylation. A. Venn diagram comparing the proteins identified with APEX2zit and APEX2nuk in basal conditions. B. Sector graphs showing the previously described localisation (as reported in UniProtKB) of the proteins identified in the present analyses. For a high proportion of proteins (indicated by horizontal lines), these results are compatible with the previously reported nucleocytoplasmic localisation described in UniProtKB.

E3.2.2.2.3. Results of MS/MS analysis (iii): effect of CRM1 inhibition on nuclear and cytoplasmic proteomes, and identification of potential CRM1 cargos

In general, CRM1 inhibition is expected to increase nuclear accumulation of its cargos. For the purpose of the proteomics analyses carried out in this thesis, three cargo categories have been defined, depending on their nucleocytoplasmic localisation in basal (-LMB) or CRM1-inhibited (+LMB) conditions (Figure E59). *Prototypic cargos* are those proteins that show exclusively cytoplasmic localisation in basal conditions and exclusively nuclear localisation when CRM1 is inhibited. *Extreme non-prototypic cargos* are those proteins that are found exclusively in the cytoplasm in basal conditions and in the cytoplasm and the nucleus when CRM1 is inhibited or those that are found in the nucleus and cytoplasm in basal conditions and exclusively in the nucleus when CRM1 is inhibited. Finally, *intermediate non-prototypic cargos* are those proteins that are found in the cytoplasm and the nucleus both when CRM1 is active and inhibited, but whose localisation is more nuclear when CRM1 is inhibited.

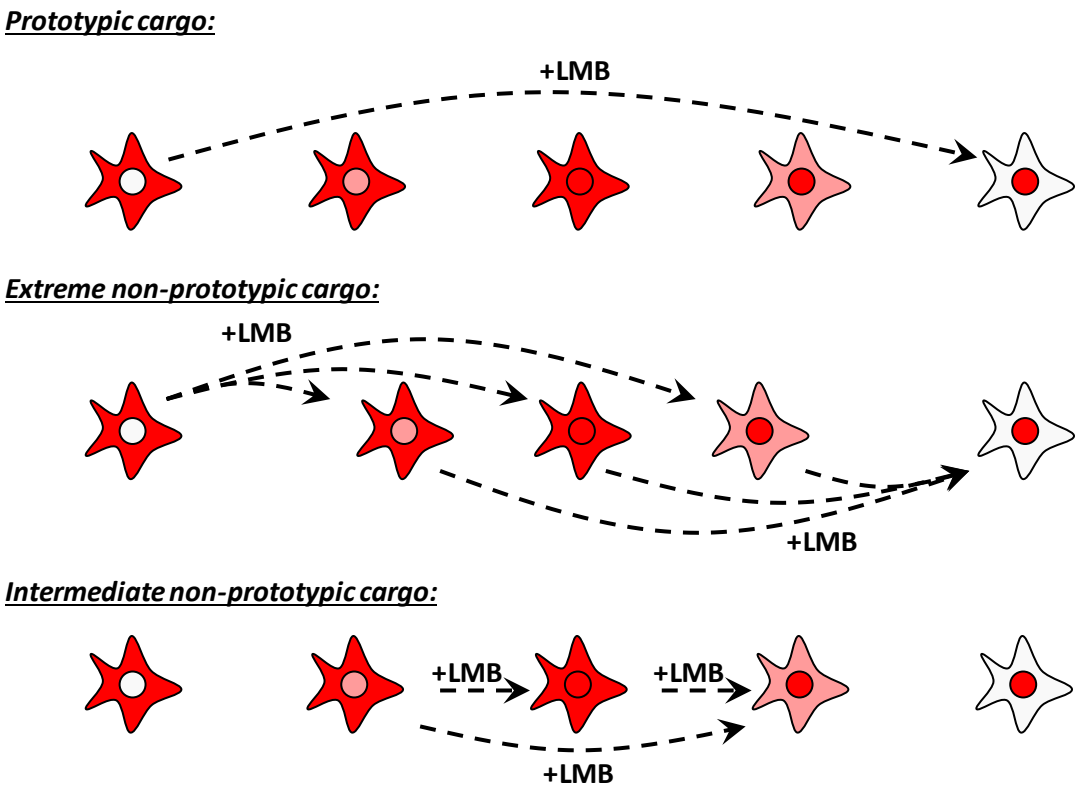

Figure E59: CRM1 cargo categories defined for the purpose of the proteomics analyses presented in this thesis. Cargo proteins are ascribed to three different categories according to their basal nucleocytoplasmic localisation and the extent of their relocation to the nucleus in response to CRM1 inhibition (+LMB, indicated by the arrows). *Prototypic cargos* are those that have an exclusively cytoplasmic localisation in basal conditions and an exclusively nuclear localisation when CRM1 is inhibited. Cargos that do not fulfil these conditions are termed non-prototypic, and are further divided into two subgroups: extreme and intermediate. *Extreme non-prototypic cargos* are those that are found exclusively in the cytoplasm in basal conditions and in the cytoplasm and the nucleus when CRM1 is inhibited or that are found in the nucleus and cytoplasm in basal conditions and exclusively in the nucleus when CRM1 is inhibited. *Intermediate non-prototypic* cargos are found in the cytoplasm and the nucleus both when CRM1 is active and inhibited, but their localisation is more nuclear when CRM1 is inhibited.

Of note, the proof-of-concept experiment described here has been carried out using a single sample for each condition, which precludes quantitative analysis. Therefore, only prototypic and extreme non-prototypic cargos could be identified in this experiment.

As illustrated in Figure E60, prototypic cargos were identified as those proteins biotinylated only by APEX2zit in basal (-LMB) condition, and biotinylated only by APEX2nuk in CRM1 inhibited condition (+LMB).

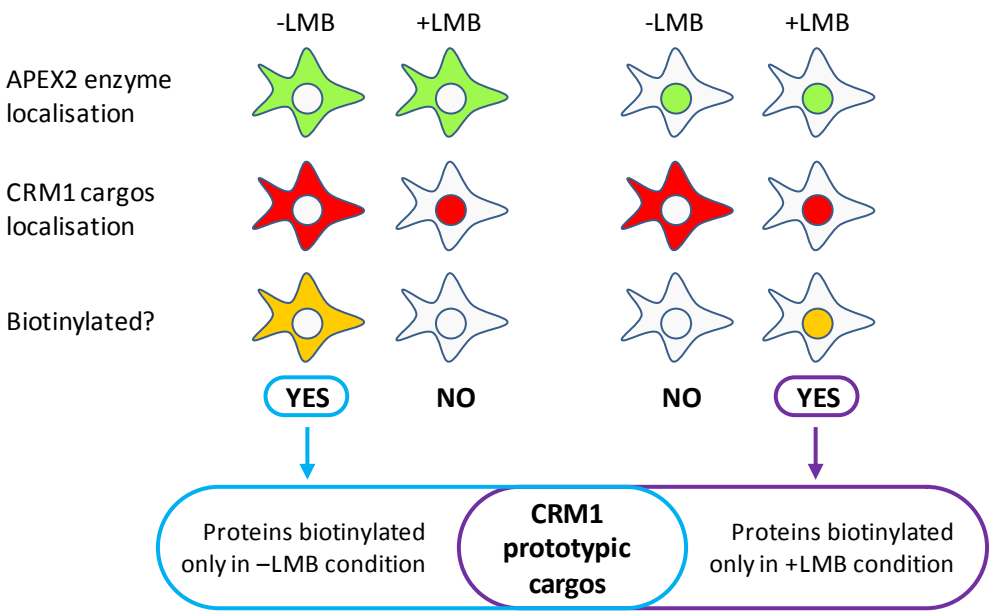

Figure E60: Strategy for identifying CRM1 prototypic cargos using compartment-specific PPB.

As shown in Figure E61, 253 proteins were exclusively labelled by APEX2zit in basal condition, while 123 were exclusively labelled by APEX2nuk in CRM1-inhibited condition. Four proteins common to both sets, representing putative prototypic CRM1 cargos, were identified: LIMD1 (LIM domain containing protein 1), TUBAL3 (tubulin alpha chain-like 3), the second isoform of SBSN (suprabasin) and CK2α' (casein kinase II subunit alpha').

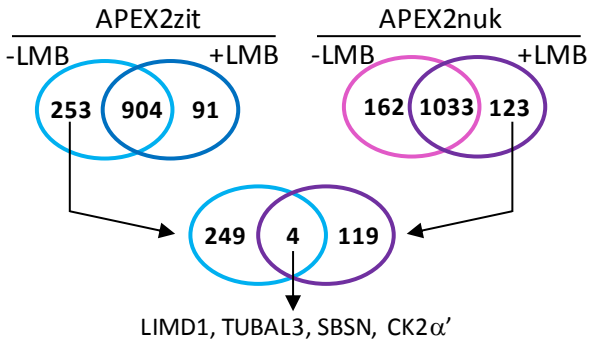

Figure E61: Identification of putative CRM1 prototypic cargos. Venn diagrams comparing the proteins exclusively labelled by APEX2zit in basal (-LMB) condition and those found exclusively labelled by APEX2nuk in CRM1-inhibited (+LMB) condition. Four proteins, LIMD1, TUBAL3, SBSN and CK2α', were identified as putative CRM1 prototypic cargos.

Putative extreme non-prototypic cargos were also searched for (Figure E62). For that purpose, on the one hand, proteins exclusively labelled by APEX2zit in basal condition, and labelled by both markers in CRM1-inhibited condition and, on the other hand, proteins labelled by both markers in basal condition and exclusively labelled by APEX2nuk in CRM1-inhibited condition were searched. These comparisons led to the identification of 89 proteins as putative extreme non-prototypic CRM1 cargos (Supplementary Table 26).

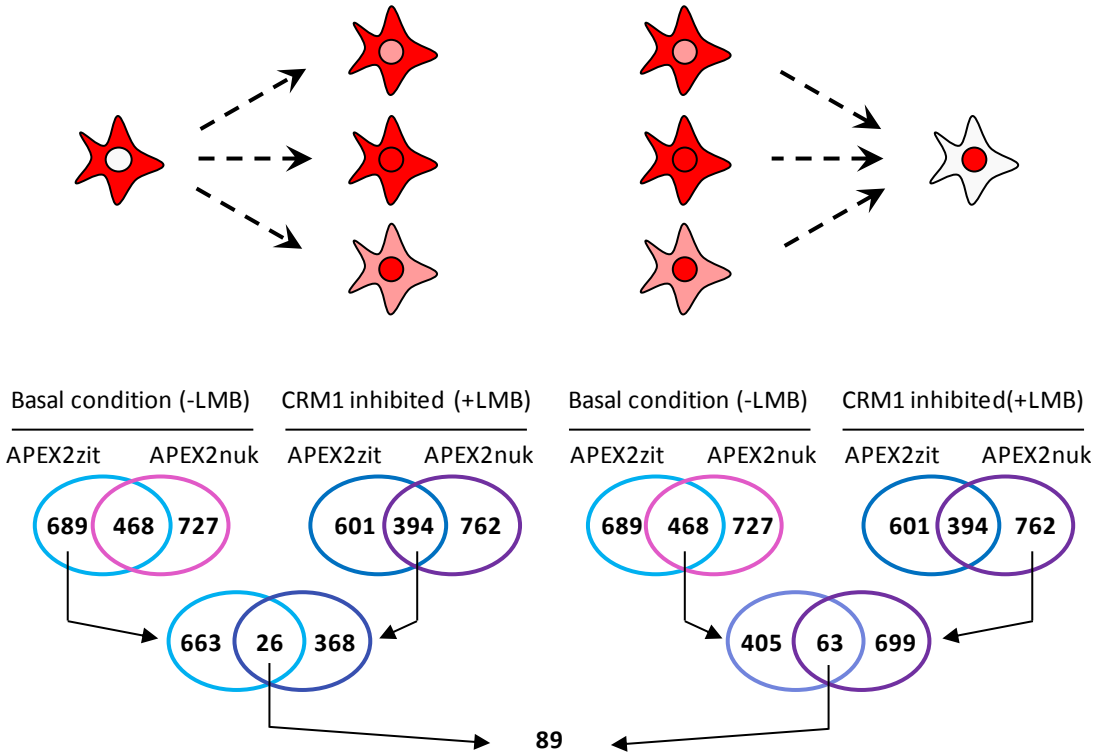

Figure E62: Identification of putative extreme non-prototypic CRM1 cargos. The different comparisons carried out are illustrated above, and the results of these comparisons are shown in the Venn diagrams below. Altogether, 89 proteins were identified as putative extreme non-prototypic CRM1 cargos.

All in all, 93 proteins were identified as potential CRM1 cargos in these analyses. Importantly, several previously reported CRM1 cargos, including LIMD1 (Sharp et al., 2004), TUBAL3 (Schwarzerová et al., 2019), SNUPN (snurportin 1) (Paraskeva et al., 1999), HDAC1 (Histone deacetylase 1) (Kim et al., 2010), and RanGAP1 (Ran GTPase-activating protein 1) (Cha et al., 2015), were identified in this analysis, suggesting that this strategy may be a valid approach to explore the CRM1 exportome and evaluate its changes in response to CRM1 inhibitors.

E3.2.2.2.4. Focused analysis to validate novel putative CRM1 cargos

Two proteins identified as putative prototypic cargos in these analyses, SBSN and CK2α', have not been previously reported to be exported by CRM1. Myc-tagged versions of these proteins were expressed in HEK293T cells, and their localisation assessed in the absence or presence of LMB. As shown in Figure E63, Myc-SBSN was found to localise to the cytoplasm and to accumulate in structures that might be secretory vesicles, as SBSN is described as a protein undergoing secretion (Matsui et al., 2004; Moffatt et al., 2004). The localisation of Myc-SBSN did not change in the presence of LMB, suggesting that it is not CRM1-dependent.

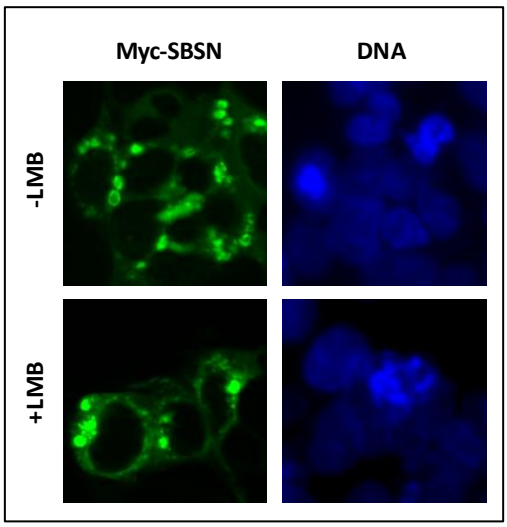

Figure E63: Representative images of Myc tagged SBSN localisation in HEK293T cells in the absence or presence of LMB.

On the other hand, Myc-CK2α' was found to localise to the nucleus and the cytoplasm both in basal conditions and when CRM1 is inhibited, but LMB treatment appeared to increase its nuclear accumulation. This subtle change in localisation was verified by semi-quantitative image analysis (Figure E64). Thus, based on these results CK2α' is proposed as a new CRM1 cargo.

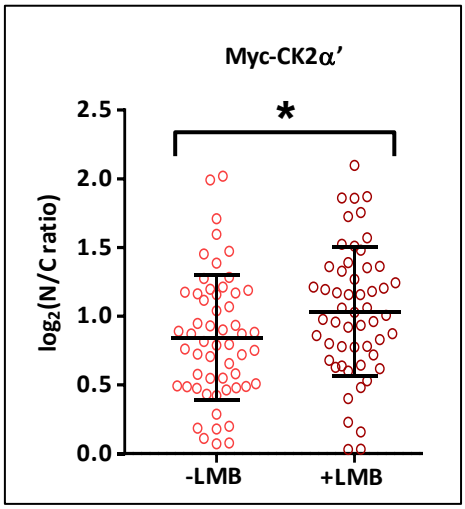

Figure E64: Graph representing the nucleocytoplasmic localisation of Myc tagged CK2α' in HEK293T cells. The N/C ratio of Myc-CK2α' in untreated or LMB-treated cells was determined using image analysis. Each circle in the graph represents a single cell, and the mean (+/- SD) is also indicated. CRM1 inhibition slightly increases the nuclear localisation of Myc-CK2α' (p=0.0228; Mann-Whitney U test).

Altogether, the results of the proof-of-concept experiment suggest that the compartment-specific PPB approach presented here may be useful to evaluate the effect of CRM1 inhibition and to identify nuclear export cargos.

E4. Discussion

The Discussion chapter has been divided in two main sections. In the first one, centred on basic physiological aspects of CRM1 function, the studies related to the identification and characterisation of CRM1-dependent NES motifs in human and viral proteins, as well as the observations on mechanistic aspects of CRM1-mediated NES export are discussed. The second part of the Discussion is focused on the emerging role of CRM1 as a therapeutic target in cancer, discussing the results on new potential combinations of the CRM1 inhibitor selinexor with other targeted drugs, and the use of compartment-specific protein biotinylation as a novel approach to evaluate the global effect of CRM1 inhibition on its exportome.

E4.1. Studies on CRM1-dependent NES motifs and CRM1-mediated NES export

E4.1.1. Identification of new NES motifs using the Rev(1.4)-GFP export assay

The subcellular localisation of the USP12 deubiquitinase has been a matter of controversy, with reports describing it as either a cytoplasmic (Sowa et al., 2009; Urbé et al., 2012; Burska et al., 2013; Lehoux et al., 2014; Olazabal-Herrero et al., 2015), or nuclear (Joo et al., 2011) protein. These seemingly contradictory observations can be reconciled by more recent publications, where yeast and human USP12 have been described as CRM1 cargos (Kouranti et al., 2010; Jahan et al., 2016) that might shuttle between both compartments. The results obtained in this thesis confirm that the localisation of USP12, as well as the localisation of its cofactors WDR20 and DMWD is, in fact, CRM1 dependent. Importantly, although these three proteins undergo nucleocytoplasmic shuttling, neither of them, especially DMWD accumulates to high levels in the nucleus when CRM1 is inhibited. This observation suggests that USP12 and its cofactors are not efficiently imported into the nucleus, probably due to the lack of active NLSs. Supporting this possibility, it was found that the fusion of two ectopic NLSs to USP12 (YFP-USP12$^{[2NLS]}$) readily induced its nuclear accumulation. In the case of DMWD, inefficient nuclear import seems to be combined with retention in the cytoplasm, as this protein enters the nucleus even less efficiently than WDR20.

Altogether, these results suggest that endogenous USP12 complexes may enter the nucleus by diffusion or by using a piggyback mechanism. In this regard, it has been described that the human papillomavirus (HPV) E1 protein can mediate nuclear import of USP12 (Lehoux et al., 2014). Further experiments are needed to identify other proteins that may facilitate USP12 import in cells not infected with HPV.

After confirming that USP12 complexes undergo dynamic transport between the nucleus and cytoplasm, NES motifs that may determine this shuttling were searched for. Importantly, using the Rev(1.4)-GFP export assay and site-directed mutagenesis, a previously reported NES in USP12 (Sanyal, 2016) was demonstrated to be non-functional. Moreover, it was seen that the nuclear export of the USP12/UAF1/WDR20 complex is mediated by a novel NES in WDR20. This NES is partially conserved in the WDR20 homolog DMWD. Of note, the DMWD NES is clearly weaker than WDR20 NES. This weaker export activity of DMWD NES may be related to the observation that DMWD seems to be more efficiently retained in the cytoplasm: if this is the case, the selective pressure to maintain a highly active NES would be reduced.

Additional data from the group were this thesis has been carried out have shown that WDR20 also regulates the localisation of USP12 and UAF1 to the plasma membrane (Olazabal-Herrero et al., 2019). Combined with these observations, the results presented in this thesis, support a model of dynamic localisation of USP12 complexes between the nucleus, the cytoplasm and the PM, as shown in (Figure E65). This dynamic localisation may be important to regulate access of these deubiquitinase complexes to substrates located in different cellular compartments.

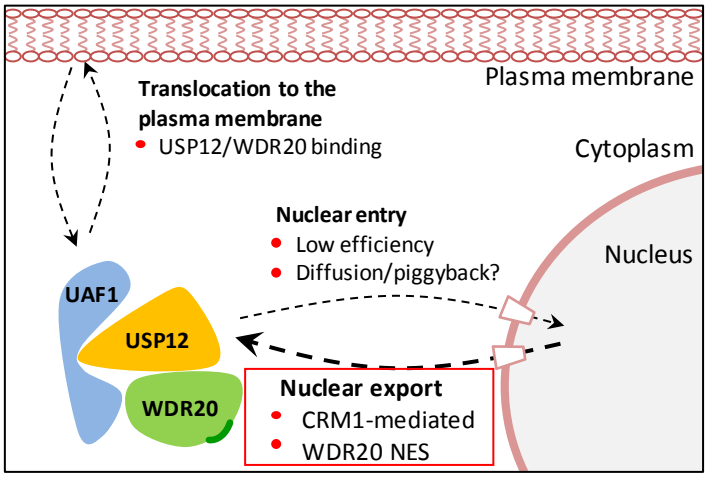

Figure E65: Proposed model illustrating the dynamic subcellular localisation of the USP12/UAF1/WDR20 complex. The USP12/UAF1/WDR20 complex shuttles between the plasma membrane, cytoplasm and nucleus. Nuclear import is not an efficient process and probably occurs by diffusion or piggyback mechanism. On the other hand, both the translocation to the plasma membrane and the nuclear export are efficient processes, and are dependent on WDR20. The work presented in this thesis (highlighted by a red rectangle) focused on the CRM1-related aspects of this model, in particular in the identification of a new NES in WDR20 (dark green).

Besides being instrumental to characterise the potential NES motifs in USP12, WDR20 and DMWD, the Rev(1.4)-GFP export assay was also used to search for novel NESs in the CRM1-cancer exportome. Candidate NES (cNES) motifs were identified *in silico* using NES predictors, and subsequently tested with the assay. Both classical *plus* NESs as well as for the

recently described reverse of *minus* NESs (Fung et al., 2015) were searched. The number of predicted cNESs was similar for both types of motifs (507 *plus* cNES and 481 *minus* cNES). 36 of the 988 cNES were selected (26 *plus* and 10 *minus*) and tested in the Rev(1.4)-GFP export assay. 25 motifs, (19 *plus* and 6 *minus*) tested positive in the assay. 19 of these motifs (13 *plus* and 6 *minus*) are new NES, not previously reported, that have now been added to NESdb NES database (Xu et al., 2012; Fu et al., 2021).

The NESs identified here are located in 14 different cancer-related proteins (SPN90, TFE3, SHIP2, PER1, SEPT6, SIR2, UBR5, FR1OP, AP2B1, IF2B, mTOR, CRTC1, CDC27 and ZO2) (Figure E66).

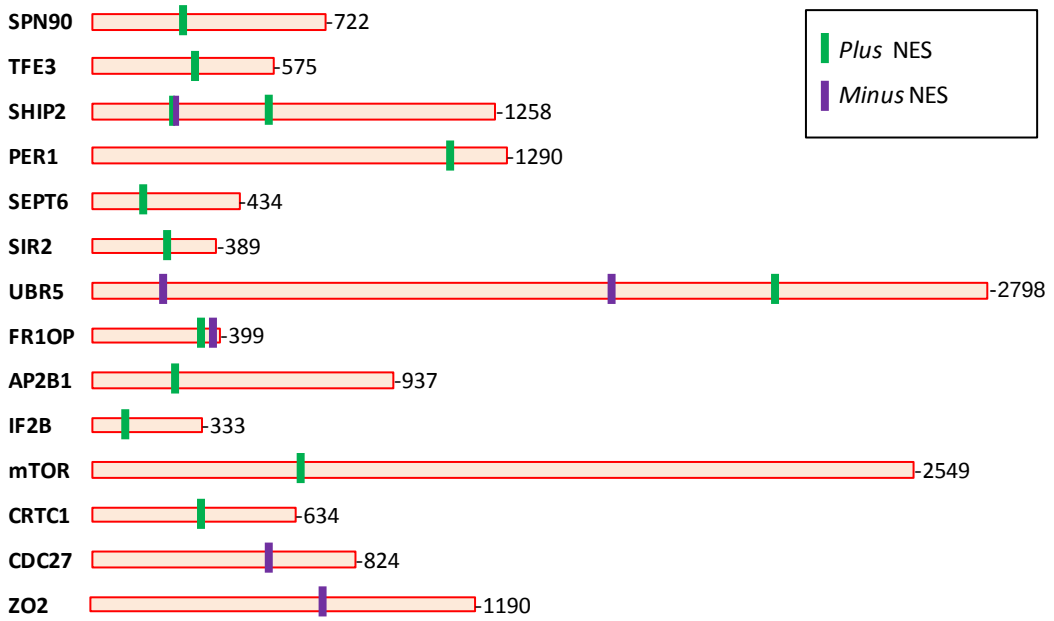

Figure E66: Schematic representation of the localisation of the new NESs found in CRM1-cancer exportome proteins. 19 new NESs have been found in 14 proteins. 13 of these motifs are *plus* NESs (indicated in green) and 6 of them are *minus* NESs (indicated in purple).

These proteins were previously proposed as potential cargos of CRM1 in the global exportome analysis carried out by Kirli and co-workers (2015). The finding that they contain functional NES motifs supports the view that these proteins are CRM1 cargos. However, the role of each of the identified motifs as *bona-fide* NESs needs to be validated, as some of these sequences might not be accessible for CRM1 binding in the context of their cognate full-length proteins. Among these results, a particularly noteworthy case is the SHIP2 protein, where three NESs were identified. Two of them are overlapping motifs, one *plus* (WN6: ^{256}TGEQELESLVLKLSVLKDF^{274}) and the other *minus* (REV5: ^{261}LESLVLKLSVLKDFLSGIQ^{279}). It would be interesting to apply structural analysis to establish whether the 256-279 segment of SHIP2 docks into CRM1 groove, and if so, in which direction it does.

Importantly, having extended the search to encompass both *plus* and *minus* NES motifs allowed to carry out for the first time a functional comparison between both types of motifs. The results presented in this thesis show that, on average, *plus* NESs show higher export activity than *minus* motifs, suggesting that *minus* motifs are, in general, weaker than *plus* motifs.

E4.1.2. The $SRV_{B/A}$ reporter: a new tool to identify new NESs and to obtain mechanistic information on CRM1-mediated NES export

Cellular assays, based on the localisation of reporter proteins, have been widely used to identify novel NESs and to test the effect of CRM1 inhibitors (Henderson and Eleftheriou, 2000; Fetz et al., 2009; Kehlenbach and Port, 2016). On the other hand, structural and *in vitro* biochemical analyses have been used to gain mechanistic insight into CRM1/NES interactions (Dong et al., 2009a, 2009b; Monecke et al., 2009, 2013; Güttler et al., 2010; Fox et al., 2011; Dian et al., 2013; Saito and Matsuura, 2013; Fung et al., 2017). In this thesis a new tool, the $SRV_{B/A}$ reporter (Taylor et al., 2019; Sendino et al., 2020a), is described. This tool can be used not only to identify novel NES motifs, but also to provide relevant information on mechanistic aspects of CRM1-mediated NES export (and thus, indirectly on CRM1/NES interaction).

The $SRV_{B/A}$ reporter is a modified, more versatile version of the SRV100 reporter (García-Santisteban et al., 2016) that allows cloning any candidate NES motifs, and testing their export by different CRM1 variants.

All in all, in this thesis, 234 CRM1 variant/NES combinations were studied using $SRV_{B/A}$-based nuclear export assays. In such an extensive study, the assessment of reporter localisation in a large number of samples represents a major bottleneck, unless an automated analysis platform (which was not available) is used. To facilitate manual sample analysis, three assessment methods (see Figure E33) that are increasingly time-consuming, but provide a correspondingly more detailed description of reporter localisation were used here. The criterion used to choose which method to apply in each case has been based on the need to obtain more or less detailed information about the nucleocytoplasmic localisation of the reporter.

The first step to validate the $SRV_{B/A}$ export assay was to directly compare its results with the results obtained using the widely used Rev(1.4)-GFP reporter (Henderson and Eleftheriou, 2000). For that purpose, a set of candidate NES motifs in CRM1-cancer exportome proteins were tested using both assays. When using a rapid qualitative method (assessment method 1) to assess the localisation of $SRV_{B/A}$ reporters, the results obtained with both assays are well

correlated. These results validate the use of the $SRV_{B/A}$ reporter as a tool to identify novel NESs. Remarkably, the $SRV_{B/A}$ assay may miss some of the weakest NES motifs detected by the Rev(1.4)-GFP assay, but it allows to better pinpoint differences in activity between some of the strongest NES motifs.

On the other hand, to better understand CRM1 function in a physiological context it is crucial to determine how the structural and biochemical information on CRM1/NES interaction translates into NES export activity in living cells. To do so, the $SRV_{B/A}$ assay has been applied here. While this thesis was in progress, the results of a similar analysis were reported (Fu et al., 2018). These authors evaluated a set of NESs comparing their affinity for CRM1 binding (measured *in vitro*) and their export-activity (evaluated using a cellular assay). In this thesis the same set of NESs was analysed using the $SRV_{B/A}$ assay. In line with the results of Fu and co-workers (2018), CRM1 binding affinity and the nuclear export activity results measured using the $SRV_{B/A}$ reporter are linearly correlated for NES motifs across a wide range of K_d values (Figure E67).

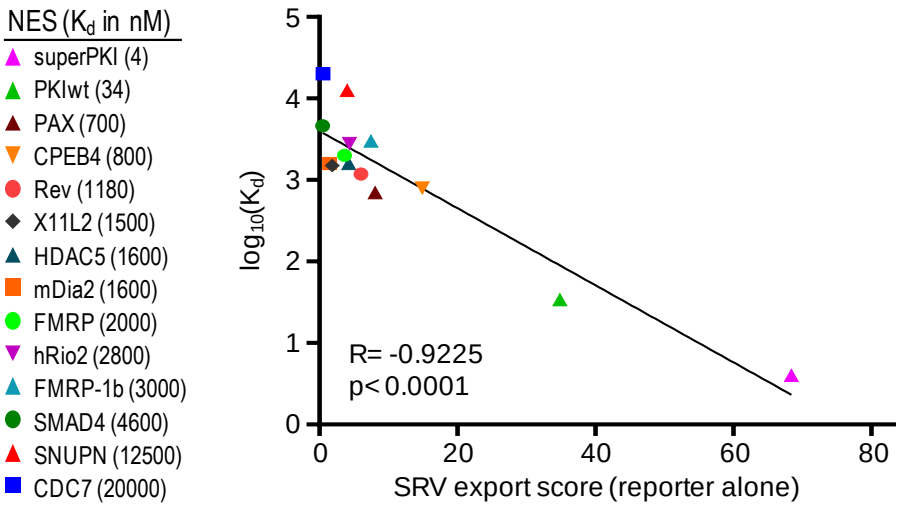

Figure E67: Correlation between CRM1 binding and export activity of a subset of NES motifs. The graph shows the correlation between the previously reported CRM1 binding affinity (expressed as $\log_{10}(K_d)$) of each NES peptide (Fu et al., 2018) and the nuclear export activity (SRV export score) of the corresponding reporter, when expressed alone. Pearson correlation coefficient (R) and p value are indicated.

Of note, there was a remarkable discrepancy between the results presented in this thesis and those of Fu and co-workers (2018), regarding the export activity of the so-called superPKI NES (an artificial NES motif with extremely high affinity for CRM1). The SRV-superPKI reporter displayed strong export activity, being located in the cytoplasm when expressed alone in HEK293T cells. In contrast, the superPKI NES motif did not promote nuclear export of the reporter used by Fu and co-workers (2018) in HeLa cells, and was classified as inactive. These conflicting observations can be due to the different configuration of the reporters, and to

potential differences in the endogenous nucleocytoplasmic transport machinery of the cell lines used (HEK293T *vs* HeLa). These results, therefore, highlight the importance of considering the influence of the experimental setting when using cellular assays to evaluate NES export activity.

Next, the $SRV_{B/A}$ assay was used to search for functional NES motifs within the recently uncovered micropeptidome, a potentially vast and still largely unexplored group of small proteins shorter than 100 amino acids in length (Yeasmin et al., 2018; Hartford and Lal, 2020). Although very few micropeptides have been characterised thus far, some of them have been shown to play a role in nuclear processes, such as DNA repair (Slavoff et al., 2014) and splicing (Huang et al., 2017), suggesting that the nucleocytoplasmic distribution of some of these small proteins needs to be actively regulated. To test the possibility that some micropeptides could represent novel CRM1 cargos, candidate NESs were predicted *in silico* in the human micropeptides reported in the SmProt database (Hao et al., 2018). 7 of the candidates were tested in the $SRV_{B/A}$ export assay. Two novel functional NES motifs in two separate micropeptides, SPROHSA141543 and SPROHSA010409, were identified. Moreover, subsequent results confirmed that the export of the full-length SPROHSA010409 micropeptide is mediated by CRM1. These findings reveal SPROHSA010409 as the first micropeptide able to shuttle in an active, CRM1-dependent manner across de nuclear envelope.

As it is the case for the vast majority of micropeptides, the potential role of SPROHSA010409 is still a mystery. It must be noted that the mere presence of these small proteins does not necessarily imply that all of them have a specific functional role. Nevertheless, these results provide the first evidence that the micropeptidome can be a yet unexplored source of novel CRM1 cargos. Intriguingly, CRM1-binding NES motifs could also be present in some of the smallest micropeptides (15-25 amino acids in length), which raises the interesting possibility that these micropeptides might act as “decoy NESs”, contributing to regulate CRM1-mediated nuclear export. Further experiments should test this possibility.

Finally, the $SRV_{B/A}$ export assay was used in an attempt to obtain mechanistic information on how CRM1 exports NESs, and thus extend and complement previous observations on CRM1/NES interaction from structural and biochemical studies (Dong et al., 2009a, 2009b; Monecke et al., 2009, 2013; Güttler et al., 2010; Fox et al., 2011; Dian et al., 2013; Saito and Matsuura, 2013; Fung et al., 2017). With that purpose, it was investigated how mutations in individual CRM1 groove residues affect export of a panel of well-characterised NESs motifs that belong to different NES classes. These NESs have variable patterns of hydrophobic residues, and structural studies have shown that they dock into the groove with different

backbone conformations, varying from all helix to an almost fully extended conformation (Dong et al., 2009a; Monecke et al., 2009; Güttler et al., 2010; Fung et al., 2015, 2017). No consistent relationship was observed between NES class and how export of these motifs is affected by the different groove mutations. However, it was found that, irrespective of NES class, mutation of CRM1 residues located in the narrower part of the groove (A541, K568 and F572) consistently had a more detrimental effect on NES export than mutation of residues located in the wider part (I521, L525 and F561). Remarkably, mutations in K568 and F572, two residues that engage in chemically different types of interactions with the NES (main chain hydrogen bonding in the case of K568, and side chain hydrophobic interactions in the case of F572) (Dong et al., 2009a; Fung et al., 2017) reduced NES export to a similar extent. These observations suggest that interaction of the NES motif with the narrower part of CRM1 groove may be particularly relevant for efficient NES export.

The effect of mutations in two particularly relevant CRM1 residues (E571 and K568) was also investigated in this thesis. E571 is recurrently mutated in human cancer (Puente et al., 2011), and K568 is reported to play a crucial role preventing docking of “NES-like” inactive NES motifs into the CRM1 groove (Fung et al., 2017). These residues are located in close proximity to each other, and establish an electrostatic interaction that might be abrogated by cancer-related mutations in E571. Given their close relationship, the effect of mutations affecting E571 and K568 residues was directly compared. First, CRM1 mutants K568A and E571K were tested against three $SRV_{B/A}$ reporters containing NES motifs previously characterised, and classified as inactive. In line with previous *in vitro* evidence showing that K568 functions as a “selectivity filter” for non-NES peptides (Fung et al., 2017), two reporters containing “inactive NESs” (SRV-Hxk2 and SRV-DEAF1) were slightly better exported by a CRM1 variant carrying a K568A mutation than by the wild type receptor. The cancer-related E571K mutation, on the other hand, does not appear to abrogate this filtering effect, as it did not lead to augmented export of any of the reporters. Importantly, the minor increment in nuclear export of the SRV-Hxk2 and SRV-DEAF1 reporters afforded by the K568A mutation in $SRV_{B/A}$ cellular assays does not reflect the markedly increased *in vitro* binding of this mutant to the Hxk2 and DEAF1 peptides reported previously (Fung et al., 2017). In this regard, it must be noted that besides abrogating the “selectivity filter”, the K568A mutation reduces binding of CRM1 to “true” NES peptides (Fung et al., 2017), and negatively impacts nuclear export activity (see Figure E44). These somewhat opposing effects represent a confounding factor that needs to be considered when interpreting the results of experiments with this particular CRM1 mutant. Thus, further studies are needed to better establish to what extent this residue contributes to select for “true” NES motifs.

On the other hand, the effect of E571K and K568A mutations against a set of $SRV_{B/A}$ reporters containing functional NES motifs identified in proteins belonging to the CRM1-cancer exportome was also compared. While both mutations significantly reduced the export of several of these reporters, the detrimental effect of the E571K mutation is consistently less pronounced than the effect of K568A. This subtler effect on nuclear export, and the finding that E571K does not abrogate the "selectivity filter" imposed by K568, indicates that, despite their close relationship, the biological consequences of E571 and K568 mutations are remarkably different. This is consistent with the fact that, while E571 mutations are highly prevalent in certain types of haematological malignancy, naturally-occurring K568 mutations have never been detected in human samples. Moreover, the subtle nature of the effects of E571K may be crucial for its oncogenic role, as mutations that more grossly disrupt CRM1-mediated export would probably be incompatible with cell survival.

E4.1.3. Testing a novel approach to compare the exportomes of wild-type and E571K mutant CRM1

It remains to be established to what extent the exportome of the E571K mutant differs from the exportome of the wild type receptor. This is an important issue that may be closely related to the pathogenic effect of this mutation. In an attempt to address this issue, and thus provide further mechanistic insight on the oncogenic role of mutant CRM1, a proteomic approach based on the isolation of "stabilised" CRM1/cargo/RanGTP complexes was developed and tested in this thesis.

This novel approach was based on using a Ran mutant (Q69L) incapable of hydrolysing GTP (Bischoff et al., 1994). Since GTP hydrolysis by Ran in the cytoplasm is a crucial step in the release of cargos, the trimeric CRM1/cargo/Ran^{Q69L} complexes are expected to be stable, and thus, this approach would allow isolating a collection of "trapped" cargos by pulling down YFP-CRM1. However, when this approach was tested, the analysis of MS/MS results indicated that it was unsuccessful. Further experiments revealed that, while CRM1/Ran^{Q69L} complexes appear to be present in cells (as suggested by CRM1/Ran^{Q69L} concordant localisation), these complexes are disrupted during the process of affinity purification.

E4.1.4. The strength of a NES motif in the nucleocapsid (N) protein of human coronaviruses is related to genus, but not to pathogenic capacity

In the context of the present COVID-19 pandemic, identifying molecular determinants of coronaviruses pathogenicity is an important issue. In this regard, several genomic features that could differentiate highly pathogenic coronaviruses (MERS-CoV, SARS-CoV and SARS-CoV-2)

from less pathogenic strains (HCoV-NL63, HCoV-229E, HCoV-HKU1 and HCoV-OC43) have been recently identified *in silico*, using machine learning techniques and comparative genomics (Gussow et al., 2020). Interestingly, pathogenicity-associated deletions, insertions and substitutions within the N protein mapped to four potential nucleocytoplasmic transport signals: three NLSs and one NES. Gussow and co-workers (2020) proposed that an enhanced transport activity of these sequences correlated with viral pathogenicity, but no experimental evidence (e.g. testing signal activity and localisation of the full-length proteins) supporting this view was presented.

To test the proposed correlation between pathogenicty and N protein NES activity, the NES motifs predicted by Gussow and co-workers (2020) in the N protein of SARS-CoV-2, MERS-CoV, HCoV-NL63, HCoV-229E, HCoV-HKU1 and HCoV-OC43 strains were experimentally tested using the Rev(1.4)-GFP export assay (Henderson and Eleftheriou, 2000). The six NES motifs tested were active, and displayed a wide range of nuclear export activity (scores between 1 and 8). However, in contrast to what has been proposed based on *in silico* analyses (Gussow et al., 2020), the differences in NES activity were not obviously related to pathogenicity (Figure E68). Rather, as shown in the Figure, the NESs of strains belonging to the genus *Alphacoronavirus* (HCoV-NL63 and HcoV-229E) were stronger (mean activity score= 6) than the NESs of the strains belonging to the genus *Betacoronavirus* (SARS-CoV-2, MERS-CoV, HCoV-HKU1 and HCoV-OC43; mean activity score= 2).

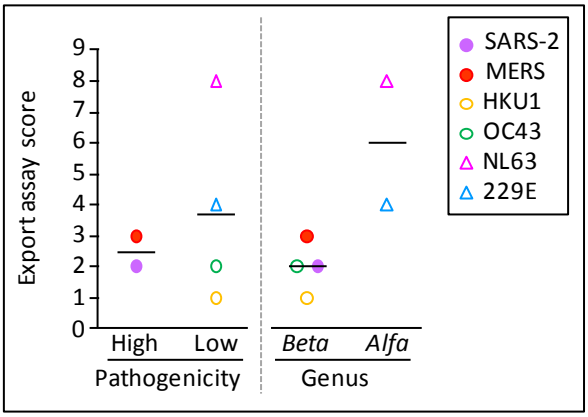

Figure E68: Relationship between the strength of the nucleocapsid NES and pathogenicity or genus of human coronaviruses. Graphs represent the strength (Rev(1.4)-GFP nuclear export assay score) of the nucleocapsid NESs in relation to the pathogenicity (left) or the genus (right) of the corresponding viral strain. Horizontal bars represent the mean activity of each group.

Furthermore, full-length, YFP tagged versions of the N proteins of HCoV-NL63 (low pathogenicity) and SARS-CoV-2 (high pathogenicity) were found to locate to the cytoplasm regardless of CRM1 activity. Altogether, these findings suggest that CRM1-mediated export does not play a prominent role in determining the localisation of these N proteins. Of note, the

N protein of SARS-CoV has been previously reported to bear a CRM1-independent NES sequence (You et al., 2007), conserved in SARS-CoV-2, whose potential link to pathogenicity remains to be tested. Nevertheless, contrary to previous suggestions (Gussow et al., 2020), the sequence motifs tested here are unlikely to be a crucial determinant of coronaviruses pathogenicity.

E4.2. Studies on CRM1 inhibition as a therapeutic approach in cancer treatment

E4.2.1. Selection and evaluation of new combinations of selinexor with other targeted drugs

Numerous *in vitro* studies have tested the CRM1 inhibitor selinexor alone or in combination with other drugs (Turner et al., 2013, 2016a, 2016b, 2020; Salas Fragomeni et al., 2013; Mendonca et al., 2014; De Cesare et al., 2015; Hing et al., 2015; Kazim et al., 2015; Miyake et al., 2015; Ranganathan et al., 2015; Kashyap et al., 2016, 2018; Muqbil et al., 2016; Rosebeck et al., 2016; Sun et al., 2016; Wrobel et al., 2016; Arango et al., 2017; Burke et al., 2017; Chen et al., 2017; Garg et al., 2017a; Gravina et al., 2017; Muz et al., 2017; Nair et al., 2017; Aboukameel et al., 2018; Corno et al., 2018; Luedtke et al., 2018; Nie et al., 2018; Saenz-Ponce et al., 2018; Schaffer et al., 2018; Shang et al., 2018; Subhash et al., 2018; Zhang et al., 2018; Azmi et al., 2019; Currier et al., 2019; DeSisto et al., 2019; Khan et al., 2019; Kapoor et al., 2019; Kulkoyluoglu-Cotul et al., 2019; Lim et al., 2019; Sexton et al., 2019; Tarantelli et al., 2019; Yan et al., 2019; Zhu et al., 2019a; Brinton et al., 2020; Fischer et al., 2020; Martini et al., 2020; Jeitany et al., 2021). Most of these preclinical combination studies have evaluated the effect of selinexor when administered with dexamethasone or the proteasome inhibitors bortezomib and carfilzomib. Some of these combinations were shown to be effective in clinical trials and, as a result, selinexor/dexamethasone and selinexor/dexamethasone/bortezomib combinations have been approved to treat certain subsets of MM and DLBCL patients (Food and Drug Administration, 2019, 2020a, 2020b; European Medicines Agency, 2021).

In an attempt to expand the repertoire of possible selinexor-based anticancer therapies, different combinations of selinexor with other targeted drugs were selected and evaluated here. To select candidate targets, the expression of *XPO1* was compared *in silico* with the expression of other 135 genes related to cancer (TARGET list; https://software.broadinstitute.org/cancer/cga/target) in AML and breast, prostate, colorectal and lung cancer using a number of databases (see Table 19) and tools such as CANCERTOOL (Cortazar et al., 2018) and cBioPortal (Cerami et al., 2012; Gao et al., 2013). *XPO1* is

overexpressed in the mentioned cancer types (Akagi et al., 2013; Kojima et al., 2013; Marisa et al., 2013; Yue et al., 2018; Cruz-Ramos et al., 2019; Duijvesz et al., 2019). Thus, those genes whose expression is directly correlated with *XPO1* expression, would also be overexpressed in these tumour types.

Supporting the idea that inhibition of two co-overexpressed proteins (i.e. CRM1 and a second target) could result in synergy, selinexor and a TOP2A inhibitor show a synergistic *in vitro* effect in cellular models of AML (Ranganathan et al., 2016), a cancer type where *XPO1* and *TOP2A* genes are co-overexpressed (Figure E69). Of note, the positive correlation between the expression of *XPO1* and *TOP2A* is maintained across different types of solid tumours, suggesting that this combination might be useful in other tumour types.

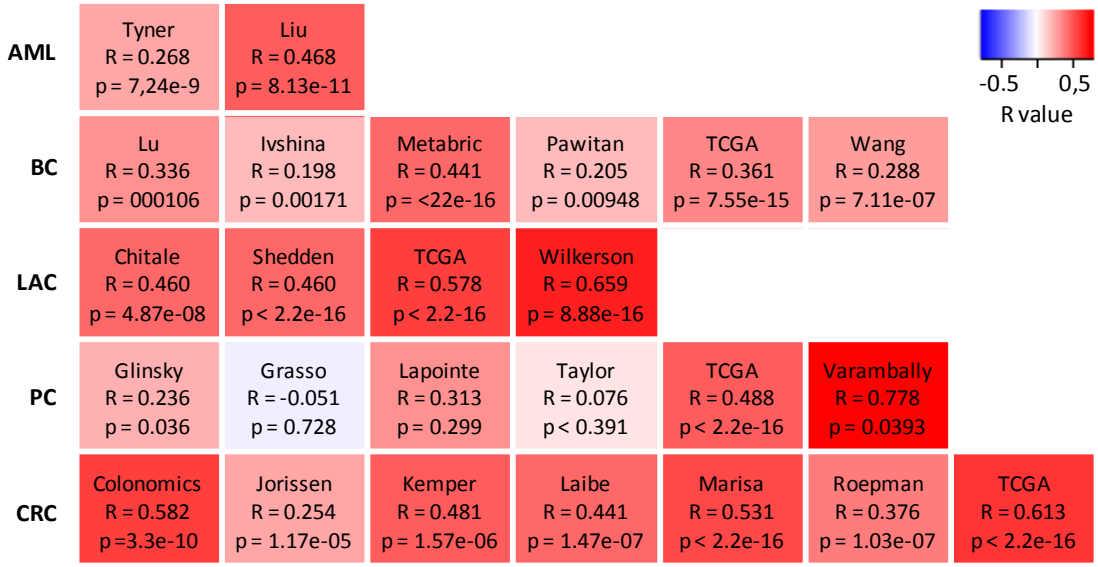

<u>Figure E69:</u> Correlation between the expression of *XPO1* and *TOP2A* genes across different tumour types. The heatmap shows how *XPO1* expression correlates with the expression of *TOP2A* in different datasets of acute myeloid leukaemia (AML), breast cancer (BC), lung adenocarcinoma (LAC), prostate cancer (PC), and colorectal cancer (CRC) patients. Blue colour indicates inverse correlation, and red colour indicates direct correlation, with colour intensity representing the Pearson's correlation value (R), as indicated by the scale on the top right corner. The dataset name, as well as the R and p values are indicated inside each heatmap cell.

The expression of *XPO1* and each of the other 135 TARGET genes was compared across five cancer types in 21 different studies. After calculating the mean R value, the eight genes (*MSH2*, *ATR*, *MSH6*, *BRCA1*, *EZH2*, *BRCA2*, *AURKA* and *NPM1*) whose expression shows the highest direct correlation with the expression of *XPO1* were initially selected. After a review of the literature, *MSH2*, *MSH6*, *BRCA1* and *BRCA2* were discarded, as they code for proteins that are not considered as druggable targets in cancer, and *NPM1* was also discarded since there is not a reliable inhibitor readily available. Therefore, only ATR, EZH2 and AURKA proteins were considered as potential targets to be inhibited in combination with CRM1.

For the initial experimental analyses presented in this thesis, EZH2 and AURKA inhibitors (tazemetostat and alisertib, respectively) were selected. Tazemetostat is an inhibitor of EZH2 approved in the USA to treat determined cancer patients, and alisertib is an AURKA inhibitor that has already been tested in clinical trials (Damodaran et al., 2017; Lee et al., 2017; Mohammad et al., 2017; Cheng and Xu, 2018; Dawei et al., 2018; Dimopoulos et al., 2018; Felgenhauer et al., 2018; Fioravanti et al., 2018; Herviou et al., 2018; Hou et al., 2018; Huang et al., 2018; Italiano et al., 2018; Kogiso et al., 2018; Li et al., 2018; Mochizuki et al., 2018; Payton et al., 2018; Serresi et al., 2018; Shaikh et al., 2018; Tremblay-LeMay et al., 2018; Tsai et al., 2018; Wen et al., 2018; Wu et al., 2018; Yang et al., 2018; Zheng et al., 2018; O'Connor et al., 2019; Food and Drug Administration, 2020c, 2020d). ATR inhibitors were not selected for these initial experiments, but were not definitively discarded. In fact, several preliminary experiments (not shown) with the combination of selinexor and the ATR inhibitor AZD-6738 were carried out in LoVo and HCT-116 colorectal cancer cell-lines, but insufficient data were obtained due to experimental problems. Interestingly, a synergistic effect of the selinexor/AZD-6738 combination in colorectal cells has recently been reported (Inoue et al., 2021), a finding that indirectly supports the criterion used here to choose potential targets for selinexor combinations.

The combinations of tazemetostat and alisertib with selinexor were evaluated in an *in vitro* model system where AML cells are seeded on top of stromal cells (Ramasamy et al., 2012). The effect of the drugs (individually and in combination) has been measured in terms of their ability to reduce the proliferation of both AML and stromal cells, as well as their capability to increase the apoptosis of AML cells.

The results presented here do not support the combination of selinexor with tazemetostat as a promising anticancer therapy. Although a synergistic antiproliferative effect was noted at the highest doses tested, no synergy in apoptosis induction was noted, suggesting that, even if the cancer cells do not continue to proliferate, they are not efficiently killed by the combination. Furthermore, the highest tazemetostat doses used in these experiments correspond to the highest doses measured in the plasma of patients (Italiano et al., 2018), and most likely a lower concentration of the drug is actually achieved in tumour cells. These results are consistent with data on the effect of EZH2 inhibition obtained in other types of haematological tumour cells (Eich et al., 2020).

More promising results were obtained with the combination of selinexor and alisertib, which showed synergistic apoptosis induction at the highest concentrations tested. However, an antagonistic effect of this combination was noted at lower doses. The molecular consequences

of simultaneously inhibiting CRM1 and AURKA are unknown. However, the observed effect may be partly mediated by p53, since both target proteins are functionally related to this important tumour suppressor. On the one hand, AURKA phosphorylates p53, negatively regulating its stability and tumour suppressor activity (Katayama et al., 2004). On the other hand, p53 is exported to the cytoplasm by CRM1 (Stommel et al., 1999). Therefore, concomitant inhibition of CRM1 and AURKA could result in higher levels of p53 in the nucleus, enhancing its tumour suppressor function.

In summary, these studies suggest that the selinexor/alisertib combination could be an interesting option for clinical use, and further preclinical tests are warranted. Nevertheless, the drug doses used have to be carefully studied to prevent potential antagonistic effects.

E4.2.2. A new approach to assess the cellular effect of CRM1 inhibitors: exploring the exportome using APEX2-based proximity labelling

In this thesis a new experimental approach to explore the CRM1 exportome has been designed and tested. This approach combines compartment-specific proximity protein biotinylation, CRM1 inhibition, affinity purification and MS/MS.

The major challenge in the development of this approach was the generation of APEX2-based markers, APEX2zit and APEX2nuk, needed for the specific labelling of cytoplasmic and nuclear subproteomes (compartment-specific biotinylation), respectively. As detailed in the Results section, a significant amount of testing and re-design was needed before properly functioning markers were obtained.

Next, a proof-of-concept experiment was performed to validate the new approach. For simplicity reasons, the experiment has been carried out using a single sample per condition, which potentially poses two main limitations. On one hand, it may increase the uncertainty of protein identification. However, this does not seem to be a reason for serious concern, as the collection of proteins identified with each marker was largely as expected. Thus, mostly cytoplasmic (or both cytoplasmic and nuclear) proteins were identified with APEX2zit while mostly nuclear (or both nuclear and cytoplasmic) proteins were identified with APEX2nuk. On the other hand, having a single sample per condition precludes quantitative proteomics analysis. As a result, only prototypic and extreme non-prototypic cargos (as defined in Figure E59) could be searched for. 4 prototypic and 89 extreme non-prototypic cargos were identified in this analysis. Supporting the validity of this approach, some of these proteins have been previously validated as CRM1 cargos, including LIMD1 (Sharp et al., 2004), TUBAL3

(Schwarzerová et al., 2019), SNUPN (Paraskeva et al., 1999), HDAC1 (Kim et al., 2010), or RanGAP1 (Cha et al., 2015). Most of the identified proteins, including SBSN and CK2α' have not been previously validated as CRM1 cargos, although CK2α' was proposed as a potential cargo in a global proteomics study (Kirli et al., 2015). The LMB-based experiments carried out with full-length CK2α' in this thesis provide additional evidence suggesting that CK2α' represents, in fact, a *bona fide* CRM1 cargo.

In summary, a new approach to assess the cellular effect of CRM1 inhibition as anticancer therapy and to identify CRM1 cargos was developed in this thesis. In the proof-of-concept experiment described here, LMB was used to inhibit CRM1. However, this approach can also be applied to clinically relevant inhibitors, such as selinexor or eltanexor, to better understand their cellular effects. Moreover, combining this strategy with CRISPR/CAS9-based genome editing would allow comparing the exportomes of wild-type and E571K mutant CRM1, providing mechanistic information on the oncogenic effect of this recurrent cancer mutation.

E5. Conclusions

This section is presented in English in the main body of the Thesis (Section 6 page 201)

II Eranskina: Argitalpenak/ Appendix II: Publications

Sendino *et al*. *Cancer Drug Resist* 2018;1:139-63
DOI: 10.20517/cdr.2018.09

Cancer
Drug Resistance

Review

Open Access

Hitting a moving target: inhibition of the nuclear export receptor XPO1/CRM1 as a therapeutic approach in cancer

Maria Sendino[1], Miren Josu Omaetxebarria[2], Jose Antonio Rodríguez[1]

[1]Department of Genetics, Physical Anthropology and Animal Physiology, University of the Basque Country (UPV/EHU), Leioa 48940, Spain.
[2]Department of Biochemistry and Molecular Biology, University of the Basque Country (UPV/EHU), Leioa 48940, Spain.

Correspondence to: Dr. Jose Antonio Rodríguez. Department of Genetics, Physical Anthropology and Animal Physiology, University of the Basque Country (UPV/EHU), Leioa 48940, Spain. E-mail: josean.rodriguez@ehu.es

How to cite this article: Sendino M, Omaetxebarria MJ, Rodríguez JA. Hitting a moving target: inhibition of the nuclear export receptor XPO1/CRM1 as a therapeutic approach in cancer. *Cancer Drug Resist* 2018;1:139-63. http://dx.doi.org/10.20517/cdr.2018.09

Received: 28 Jun 2018 **First Decision:** 24 Jul 2018 **Revised:** 3 Aug 2018 **Accepted:** 10 Aug 2018 **Published:** 19 Sep 2018

Science Editor: Godefridus J. Peters **Copy Editor:** Yuan-Li Wang **Production Editor:** Huan-Liang Wu

Abstract

Cellular homeostasis crucially relies on the correct nucleocytoplasmic distribution of a vast number of proteins and RNA molecules, which are shuttled in and out of the nucleus by specialized transport receptors. The nuclear export receptor XPO1, also called CRM1, mediates the translocation of hundreds of proteins and several classes of RNA to the cytoplasm, and thus regulates critical signaling pathways and cellular functions. The normal function of XPO1 appears to be often disrupted in malignant cells due to gene mutations or, most commonly, aberrant overexpression. Due to its important physiological roles and its frequent alteration in human tumors, XPO1 is a promising target for cancer therapy. XPO1 inhibitors have undergone extensive testing as therapeutic agents in preclinical models of cancer, with promising results. One of these inhibitors, Selinexor, is currently being evaluated in multiple clinical trials of different types of solid tumors and hematological malignancies. Here, we review several key aspects of XPO1 function, as well as the mechanisms that may lead to its alteration in cancer, and provide an update on the status of XPO1 inhibitors being developed as drugs for cancer therapy, including the definitive results of the first clinical trials with Selinexor that have been recently published.

Keywords: XPO1, CRM1, nucleocytoplasmic transport, Selinexor

INTRODUCTION

In 1997, a 120 kDa protein called CRM1, known to function as a chromosome region maintenance fac-

tor in yeast, was identified as the first receptor for the nuclear export of proteins, and it was consequently renamed exportin 1 (XPO1)[1-4]. In these initials reports, XPO1/CRM1 (hereafter referred to as XPO1) was found to be the cellular target for a potent inhibitor of nuclear export termed leptomycin B (LMB), and to bind short amino acid sequences (so-called nuclear export signals or NESs) in proteins that were actively exported from the nucleus. Over the last two decades, many aspects of XPO1 physiopathology have been elucidated. Thus, XPO1 has been shown to mediate the nuclear export of not only hundreds of cellular and viral proteins, but also of different types of RNA molecules[5,6]. In fact, crucial signaling pathways, such as the NF-κB pathway, and essential cellular processes, such as cell cycle progression, have been shown to involve XPO1-dependent nuclear export steps[7]. In addition, export-independent functions of XPO1 in mitosis have also been identified[8]. The normal function of XPO1 appears to be often disrupted in malignant cells. Thus, overexpression of the XPO1 mRNA or protein has been frequently reported in a variety of tumor types and recurrent XPO1 gene mutations have been detected in certain hematological malignancies, suggesting that XPO1 may represent a therapeutic target in cancer[9,10]. Importantly, the results of multiple cellular, biochemical and structural analyses have led to a detailed mechanistic understanding of XPO1 function[11-13], paving the way for the development of clinically useful inhibitors of XPO1. Several compounds targeting XPO1 have been extensively tested in preclinical studies, and one of them, Selinexor, is now undergoing clinical trials, with promising results in patients with different types of cancer.

THE PHYSIOLOGICAL ROLES OF XPO1

An overview of nucleocytoplasmic transport of proteins

In eukaryotic cells, the nuclear envelope establishes a physical separation between the two major cellular compartments: the nucleus and the cytoplasm. Cellular homeostasis requires continuous communication between these compartments through the bidirectional trafficking of molecules. This trafficking may occur by diffusion in the case of small molecules, or by budding of nuclear envelope-derived vesicles for a minority of specific proteins[14]. However, the vast majority of proteins can only enter and exit the nucleus through proteinaceous channels embedded in the nuclear envelope termed nuclear pore complexes (NPCs)[15,16]. For most proteins, nucleocytoplasmic transport is an active, energy-dependent process that requires a specialized transport machinery with three crucial components: (1) the NPCs; (2) a family of soluble transport receptors (karyopherins) that recognize and bind specific transport signals in the cargo proteins; (3) a gradient of the small GTPase Ran (bound to either GTP or GDP) across the nuclear envelope, which confers directionality to the transport [Figure 1A][17-19].

NPCs, recently reviewed by Knockenhauer and Schwartz[15] and Pemberton and Paschal[17], are very large complexes (over 120 MDa in size) formed by the assembly of several copies of each of approximately 30 different proteins called nucleoporins (NUPs). NPCs present a characteristic eight-fold rotational symmetry and are composed by three stacked rings inserted into the nuclear envelope, with a series of filaments emanating to the cytoplasmic side of the NPC and a basket-like structure protruding to the nucleoplasmic side [Figure 1B]. NUPs in the inner channel of the pore contain intrinsically disordered domains rich in phenyalanine-glycine (FG) repeats. These so-called FG-nucleoporins constitute a barrier that efficiently prevents proteins above a certain size from freely diffusing across the NPC. This threshold size for exclusion has long been believed to be relatively sharp (30-60 kDa), but a recent study suggests that the NPC lacks such a firm size threshold[20]. The selective barrier of the NPC can be overcome by large proteins (and even by very large nucleoprotein complexes, such as ribosomal subunits) through binding to karyopherins[21].

The human genome codes for approximately 20 different karyopherins[22]. While some of these receptors can mediate bidirectional transport of cargos in and out of the nucleus, most of them function exclusively as either import receptors (importins) or export receptors (exportins), such as XPO1. Karyopherins can recognize and bind specific peptide sequences in the cargo protein, which function as transport signals, and can be broadly classified as nuclear localization signals (NLSs, recognized by importins) or nuclear

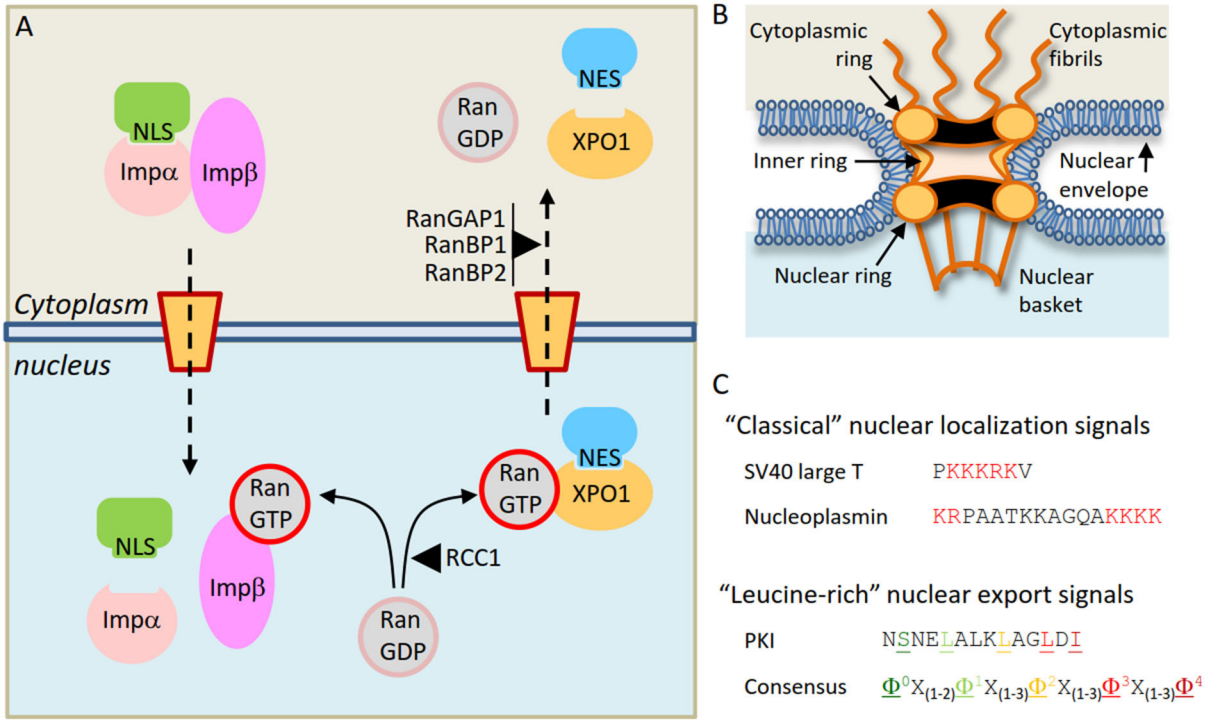

Figure 1. Receptor-mediated nucleocytoplasmic transport of proteins. A: Illustrative overview of the nuclear import of a cargo protein bearing a "classical" NLS mediated by the Importinα/Importinβ heterodimer (left) and the nuclear export of a cargo protein bearing a "leucine-rich" NES mediated by XPO1 (right); B: schematic depiction of the nuclear pore complex, illustrating its main structural features; C: examples of nucleocytoplasmic transport signals. The NLSs of SV40 large T antigen (monopartite) and nucleoplasmin (bipartite) are shown, with the basic residues that characterize "classical" NLSs highlighted in red. Below, the NES of PKI and a general consensus sequence of "leucine-rich" NESs are shown. The characteristic hydrophobic residues (represented by ϕ in the consensus) are highlighted in colors and underlined. NLS: nuclear localization signal; NES: nuclear export signal

export signals (NESs, recognized by exportins) [Figure 1C]. The best-characterized import receptor is the Importinα/Importinβ heterodimer, which mediates nuclear import of cargos bearing a "classical" NLS (a peptide sequence characterized by the presence of one or two clusters of basic residues)[23]. XPO1, the first nuclear export receptor to be identified, is also the best-characterized exportin. XPO1 mediates export of proteins bearing "leucine-rich" NESs, short peptides with a characteristic spacing of hydrophobic residues [Figure 1C]. Of note, some proteins possess both an NLS and an NES and can undergo cyclic shuttling between the nucleus and the cytoplasm[24]. Importinα/β and XPO1 mediate the nucleocytoplasmic transport of hundreds of different proteins. Other karyopherins, which are less well characterized, seem to have a more limited repertoire of cargos, and the transport signals that may mediate their binding remain, in most cases, yet to be identified.

Binding and release of a protein in the nucleus or the cytoplasm establishes the direction of its transport, and the key factor that regulates cargo binding and release by karyopherins is the small GTPase Ran, which can be bound to either GDP (RanGDP) or GTP (RanGTP)[17-19]. There is a RanGDP/RanGTP gradient across the nuclear envelope. This gradient (a high concentration of RanGDP in the cytoplasm and a high concentration of RanGTP in the nucleus) is maintained by the Ran cofactors RanGAP1 (a cytoplasmic GTPase activating protein) and RCC1 (a chromatin-bound nucleotide exchange factor). RanGTP promotes disassembly of the Importin/cargo complexes, leading to release of import cargos in the nucleus. Conversely, RanGTP stabilizes the interaction between XPO1 and export cargos in the nucleus by forming a trimeric XPO1/RanGTP/cargo complex. This complex is disassembled upon GTP hydrolysis in the cytoplasmic side of the NPC, leading to release of the export cargo in the cytoplasm. Thus, by regulating receptor/cargo interactions, the RanGTP/RanGDP gradient determines the directionality of nucleocytoplasmic transport.

In fact, it has been shown that, by artificially raising the concentration of RanGTP in the cytoplasm, the direction of the transport can be inverted[25].

Beyond the basic transport machinery described above, multiple additional mechanisms may contribute to regulate the nucleocytoplasmic distribution of a given protein in a dynamic and finely-tuned manner. These mechanisms include post-translational modifications, such as phosphorylation[26,27] or ubiquitination (reviewed by Rodríguez[28]), as well as masking/unmasking of the transport signals by homo/heterodimerization[29,30].

XPO1-mediated protein nuclear export: cargos, mechanisms and signals

XPO1 has a wide repertoire of cargos, including not only cellular proteins, but also viral proteins expressed in infected cells (reviewed by Ding *et al.*[31]).

Identification of XPO1 cargos has been greatly facilitated by the use of LMB as an inhibitor. In cellular experiments, cytoplasmic XPO1 cargos often relocate to the nucleus in the presence of LMB. This experimental approach cannot be used to demonstrate XPO1-mediated export of proteins that are constitutively located to the nucleus. An alternative approach in this case could be ectopic overexpression of the receptor, which promotes export of NES-containing nuclear cargos to the cytoplasm[32]. Besides LMB-based experiments, the identification, validation and characterization of XPO1 cargos often involve biochemical analyses to demonstrate RanGTP-dependent binding, as well as mutagenesis to map the NES. In over 15 years of research, hundreds of individual proteins were studied using these approaches and around 200 bona-fide XPO1-exported cargos were identified[33]. More recently, the introduction of tandem mass spectrometry (MS/MS)-based high throughput analyses has expanded the repertoire of potential XPO1 cargos (the so-called "XPO1 exportome") to above 1000 cellular proteins[34], although many of them still need to be further validated and their NESs identified.

The search for novel cargos is still on-going, and continues to provide further insight into the physiological relevance of XPO1. For example, it has been recently found that the NES-containing protein POST and the ubiquitin-binding protein UBIN form a complex that mediates XPO1-dependent nuclear export of polyubiquitinated proteins[35], a process that seems to be exacerbated in cancer cells treated with the proteasome inhibitor bortezomib[36]. These findings reveal a novel role for XPO1 in nuclear protein homeostasis that might also have important implications for cancer therapy.

From a mechanistic point of view, XPO1-mediated nuclear export consists essentially in the binding of an NES-containing protein in the nucleus and its release in the cytoplasm. The XPO1/NES interaction has low affinity, and needs to be stabilized by the cooperative binding of nuclear RanGTP, facilitated by the cofactor RanBP3[37-39]. Structural and biochemical studies carried out over the last decade have contributed to dissecting the series of molecular events that underlie the cycle of assembly and disassembly of the XPO1/RanGTP/NES complex (reviewed by Koyama and Matsuura[11], Fung and Chook[12] and Monecke *et al.*[13]). As schematically illustrated in Figure 2A, XPO1 is a ring-shaped protein with a concave inner surface and a convex outer surface. RanGTP binds to the inner surface, and NESs dock into a hydrophobic groove in the outer surface of the receptor. The open/close state of the NES binding groove is allosterically regulated by conformational rearrangements of two additional XPO1 structural elements, termed the H9 loop and the C-terminal extension, which play a crucial role in the cycle of NES binding and release.

As illustrated in Figure 1C, "leucine-rich" NESs conform to a loose consensus sequence with a characteristic spacing of hydrophobic residues[40,41]. Hundreds of different amino acid sequences have been experimentally validated as bona-fide NESs that bind the receptor with different affinity, and may be exported with different efficiency[33,42,43]. This high variability can be explained by the recent finding that NESs with differ-

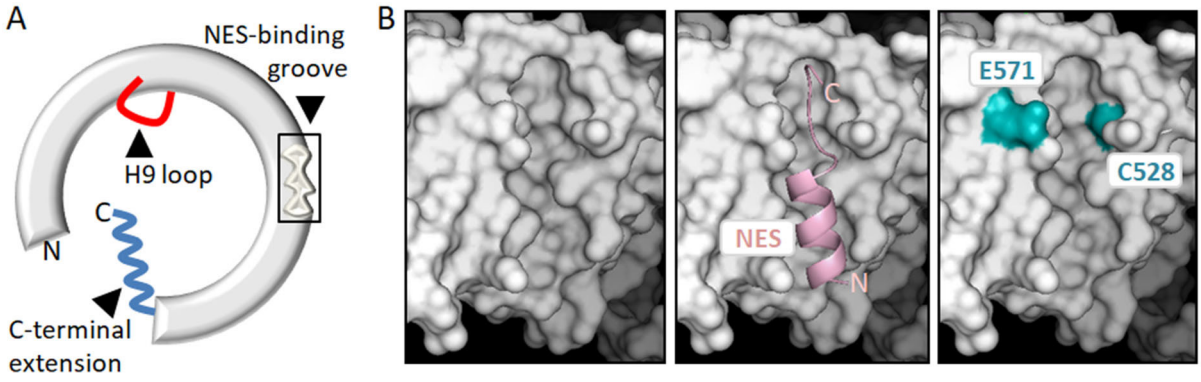

Figure 2. Structural features of XPO1 related to its nuclear export function, its role in cancer and its potential as a therapeutic target. A: Schematic representation of XPO1 protein illustrating its general ring-shaped conformation, and showing the three structural motifs that are crucial for its function as a nuclear export receptor: the NES-binding groove, the H9 loop and the C-terminal extension; B: detailed views of the NES-binding groove on the molecular surface of XPO1. The UCSF Chimera package[206] and XPO1 structure 3GJX[207] were used to generate the images. The left panel shows the empty groove, the middle panel shows a "leucine-rich" NES peptide (pink) bound to the groove. The right panel shows residues E571 and C528 highlighted in blue. E571 is a mutational hotspot in several hematological malignancies. C528 is the residue targeted by XPO1-inhibiting drugs, such as LMB or Selinexor. These compounds attach covalently to C528 and physically occupy the groove, blocking NES binding. NES: nuclear export signal; LMB: leptomycin B

ent backbone conformations can bind the receptor, and that not all export signals occupy the XPO1 NES-binding groove to the same extent[44].

"Leucine-rich" NESs dock into the groove and engage in predominantly hydrophobic interactions with several XPO1 residues. Two non-hydrophobic amino acids (C528 and E571) located in or near the NES-binding groove [Figure 2B] are of particular interest regarding the targeting of XPO1 and its potential role in cancer. On one hand, the amino acid E571 is recurrently mutated in certain hematological malignancies (see below), suggesting that mutation of this particular residue can be a driver event in some types of cancer. On the other hand, C528 is the crucial target for the effect of LMB and more clinically relevant XPO1 inhibitors, which covalently bind to this residue and block NES binding by physically occupying the groove. In fact, experimental mutation of C528 renders cells resistant to these inhibitors[45].

Role of XPO1 in RNA nuclear export

Following transcription in the nucleus, active export to the cytoplasm is an essential step during the biogenesis of many classes of RNA, and/or a critical requirement for their function (recently reviewed by Williams *et al.*[46]). Thus, messenger RNAs (mRNAs) need to be exported to undergo translation into proteins, while ribosomal RNAs (rRNAs), transfer RNAs (tRNAs), small nuclear RNAs (snRNAs), microRNAs (miRNAs) and long non-coding RNAs (lncRNAs) need to be transported to the cytoplasm in order to be processed or to carry out their cellular activities. Nuclear export of RNA is a tightly regulated process that involves the coordinated function of many different factors, including a large array of RNA-binding adaptor proteins as well as dedicated export receptors[6]. XPO1 plays a pervasive role in this process, mediating the nuclear export of several different classes of RNA.

XPO1 plays a prominent role in the export of 40S and 60S ribosomal subunits, containing rRNA, to the cytoplasm, which is a necessary step for their final maturation. The NES-containing protein Nmd3 functions as the adaptor for 60S subunit export, while the adaptor involved in the export of the 40S subunit remains to be identified[47].

In contrast to rRNAs, the vast majority of cellular mRNAs are exported to the cytoplasm by a receptor unrelated to karyopherins, called NXF1, but XPO1 mediates nuclear export of a subset of mRNAs[48]. Since

XPO1 does not bind mRNA directly, NES-containing RNA-binding proteins that act as adaptors to bridge the interaction between XPO1 and mRNA are essential in this process. These adaptors include NXF3[49], and the HuR/APRIL/pp32[50] or the eIF4E/LRPPRC[51] complexes. Interestingly, several mRNAs exported by XPO1 code for proteins that are involved in tumorigenesis-related processes, such as invasion and metastasis[46].

Finally, some RNA species with an important role in the regulation of gene expression (snRNA, lncRNA and miRNA) can also be exported by XPO1[52-54]. For example, although the major exporter of miRNAs is not XPO1 but another exportin called XPO5, XPO1 mediated-export plays a role in the export and biogenesis of specific subsets of miRNAs[55,56]. Intriguingly, XPO1 has also been reported to mediate the nuclear import of mature miRNAs[57].

Nuclear export-independent role of XPO1 as a key regulator of mitosis

Besides mediating the export of proteins and RNA to the cytoplasm, XPO1 also plays a role in processes that do not directly involve nuclear export, such as intranuclear trafficking of small nucleolar RNAs (snoRNAs) from Cajal bodies to the nucleolus[58]. A particularly relevant aspect of cell physiology where XPO1 carries out export-independent functions is mitosis[8]. This role of XPO1 has been reviewed by Forbes *et al.*[59].

In eukaryotic cells undergoing open mitosis, the breakdown of the nuclear envelope at the onset of prometaphase dramatically disrupts the nucleocytoplasmic compartmentalization. With no physical separation between nucleus and cytoplasm, the nuclear transport machinery, including certain transport receptors, NUPs and the Ran GTPase, is "repurposed" to carry out transport-independent mitotic functions, such as regulating the assembly of the mitotic spindle[59]. In this context, XPO1 has been shown to function as a "mitotic effector" of Ran, mediating RanGTP-dependent targeting of key mitotic proteins to specific spindle structures, such as the centrosomes or the kinetochore. Thus, the NES-containing protein pericentrin, a crucial scaffold for microtubule nucleation at the spindle poles, is recruited to the centrosomes by XPO1 in a RanGTP-containing trimeric complex that resembles the nuclear export complexes described above[60]. On the other hand, the stable microtubule-kinetochore interactions necessary for proper chromosome segregation appear to require XPO1-mediated recruitment of a protein complex containing RanGTP, RanGAP1 and the nucleoporin RanBP2 to the kinetochores[8].

The mitotic functions of XPO1, like its nuclear export activity, seem to be the subject of careful regulation through mechanisms that include phosphorylation[61] and competition with importins[62].

In summary, although its primary role may be in protein nuclear export, XPO1 is a multifaceted protein with roles in other processes. This functional complexity should be taken into account when interpreting the results of XPO1 inhibition studies.

PATHOLOGICAL ALTERATION OF XPO1 IN CANCER

Altered nucleocytoplasmic localization of proteins in cancer

Normal cell function relies on the correct subcellular distribution of thousands of proteins. The presence of a critical protein in the wrong cellular compartment may have severe pathological consequences. For example, aberrant cytoplasmic localization of a physiologically nuclear tumor suppressor protein may render this protein inactive, and thus contribute to tumorigenesis. In fact, mislocalization of cancer-related proteins, including the products of prominent oncogenes and tumor suppressor genes, has been often demonstrated in human tumors[63,64-66].

Nucleocytoplasmic localization of proteins can be disrupted by different mechanisms in cancer cells. On one hand, the trafficking of a specific protein can be altered by mutations that either interfere with the ac-

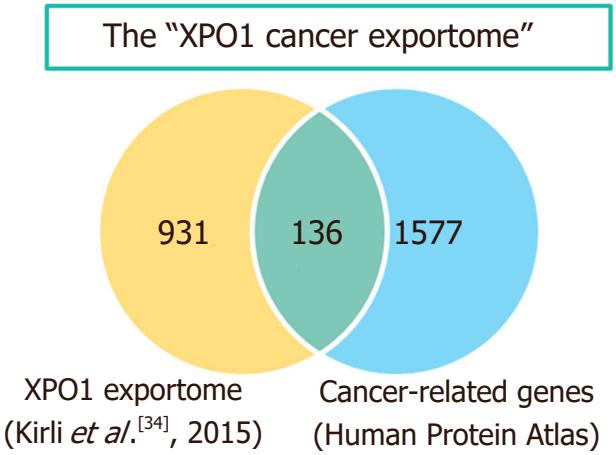

Figure 3. The "XPO1 cancer exportome". The Venn diagram shows the overlap between the list of potential XPO1 cargos identified in HeLa cells[34] and the group of "cancer related genes" defined in the Human Protein Atlas (v.18). The 136 overlapping proteins represent what could be referred to as the "XPO1 cancer exportome". The diagram was created using the jvenn web tool[208]

tivity of its transport signals (NLSs or NESs) or that create a novel signal in the mutant protein. For example, aberrant localization of tumor suppressors BRCA2[67] and PALB2[68] to the cytoplasm can result from mutations that unmask normally hidden NESs, whereas cytoplasmic mislocalization of certain NPM1 mutants is the result of a frameshift mutation that creates a novel strong NES, not present in the wild-type protein[69].

On the other hand, a general defect in the nucleocytoplasmic localization of proteins (and RNA) may arise in tumor cells, if elements of the transport machinery themselves are genetically altered or aberrantly expressed[70]. Examples of genetic alterations targeting the nuclear transport machinery include chromosome rearrangements involving nucleoporin genes (e.g., NUP98 and NUP214) in hematologic malignancies[71]. The abnormal fusion proteins resulting from these translocations have been reported to disrupt XPO1-mediated export[72,73]. Examples of nuclear transport factors abnormally expressed in tumors include the nuclear import receptors Importin β (see Dickmanns *et al.*[64] and references therein) and Importinα1 (see Christiansen and Dyrskjøt[74], and references therein).

In the case of XPO1, both aberrant expression and genetic alterations have been detected in different types of cancer, as detailed below. The abnormal XPO1 function that may result from these alterations would, in turn, hinder the normal nucleocytoplasmic localization of hundreds of XPO1 cargo proteins. In the context of the present review, those XPO1 cargos with a known role in the development of human tumors are of particular interest. In this regard, we note that the extended list of potential XPO1 cargos identified in HeLa cells by a recent high throughput analysis[34] includes 136 members of the protein class "cancer-related genes" registered in the Human Protein Atlas initiative (https://www.proteinatlas.org/) [Figure 3]. The set of cancer-related proteins exported by XPO1 (which could be referred to as the "XPO1 cancer exportome") includes prominent tumor suppressors, such as p53[75] and BRCA1[76], as well as protooncogenes, such as c-abl[77]. A more extensive account of cancer-related proteins that undergo XPO1-mediated nuclear export can be found in previous reviews[10,65,66,78,79].

Altered XPO1 expression in human tumors

The expression level of XPO1 at either the mRNA or protein level has been analyzed in many different cancer types. As summarized in Table 1, XPO1 is frequently overexpressed in tumor samples with respect to the corresponding normal tissue samples[80-99]. In fact, XPO1 overexpression was observed in all solid tumor types and hematologic malignances examined, with the exception of liver cancer[91].

Table 1. Expression of XPO1 in human cancer

Type of cancer	Number of samples (technique)	Relationship to prognosis	Remarks	Ref.
AML	511 patients (Reverse-phase protein array)	High XPO1 expression associated with poor prognosis		[80]
MCL	Data from public expression array data sets plus 3 patients and 8 cell lines (qRT-PCR)	NA	Higher expression in mantle cell lymphoma cells	[81]
MM	Data from public expression array data sets	NA	XPO1 expression increases with disease progression	[82]
	351 patients (data from public expression array data sets) plus 8 patients (IB)	High XPO1 expression associated with poor prognosis		[83]
Glioma	273 patients (data collected from public expression array data sets) plus 12 patients (IB)	High XPO1 expression associated with poor prognosis		[84]
	70 patients (IHC + IB)	High XPO1 expression associated with poor prognosis	XPO1 expression level inversely correlated with p27 level	[85]
Non-small cell lung cancer	148 patients (microarray) plus 291 patients (qRT-PCR)	High XPO1 expression associated with poor prognosis	XPO1, BRCA1, HIF1A and DLC1 constitute a robust prognostic classifier in stage I lung adenocarcinoma patients	[86]
Gastric cancer	240 patients (IHC)	Low XPO1 expression associated with poor prognosis		[87]
	120 patients (IHC)	High XPO1 expression associated with poor prognosis		[88]
Thymic epithelial tumors	118 patients (IHC)	High XPO1 expression associated with poor prognosis		[89]
Ovarian cancer	88 patients (IHC)	XPO1 is expressed in ovarian carcinomas with aggressive behavior and is related to poor patient survival	XPO1 expression correlated with cyclooxygenase-2 expression	[90]
Liver cancer	154 cases (IHC)	NA	XPO1 expression assessed in tumor and adjacent normal tissues	[91]
Esophageal squamous cell carcinoma	220 patients (IHC+IB+IF)	High XPO1 expression associated with shorter survival	XPO1 siRNA causes apoptosis in esophageal cancer cell lines	[92]
	56 patients (IHC+qRT-PCR)	Trend for shorter survival of patients with higher XPO1 expression	XPO1 localization also altered in cancer cells	[93]
Pancreas cancer	69 patients (IB)	High XPO1 expression associated with poor prognosis		[94]
Renal cancer	(IHC)	NA	Higher XPO1 expression in higher grade tumors	[95]
Breast carcinoma	280 patients (IHC + IB)	High XPO1 expression associated with poor prognosis		[96]
Ewing sarcoma	37 patients (IHC) plus data from public expression array data sets	NA	XPO1 is highly expressed in Ewing sarcoma	[97]
Osteosarcoma	57 patients (IHC)	High XPO1 expression associated with shorter survival		[98]
Melanoma	83 patients (31 primary, 52 metastatic) (MA)	NA	XPO1 overexpressed in metastatic melanoma	[99]

AML: Acute myeloid leukemia; MCL: mantle cell lymphoma; MM: multiple myeloma; IB: immunoblot; IF: immunofluorescence; IHC: immunohistochemistry; MA: microarray; qRT-PCR: quantitative real-time PCR; NA: not assessed

In several of these studies, the potential prognostic significance of XPO1 expression has been evaluated. Higher XPO1 expression was associated with poorer patient prognosis in patients with ovarian tumors[90], pancreatic tumors[94], esophageal tumors[92], gliomas[84,85], thymic epithelial tumors[89], and breast tumors[96]. In contrast, high XPO1 expression was related to better prognosis in osteosarcoma patients[98]. Finally, contradictory findings on the prognostic value of XPO1 expression in gastric cancer have been reported[87,88].

The molecular mechanisms responsible for XPO1 overexpression in cancer cells are still poorly characterized. Copy number gains at chromosomal region 2p, affecting the XPO1 locus, have been found to correlate with high XPO1 mRNA expression in lymphomas[100] and chronic lymphocytic leukemia (CLL)[101].

Table 2. Recurrent XPO1 mutations in hematological malignancies. More than 90% of the reported mutations are missense changes affecting XPO1 "hotspot" residue E571

Type of malignancy	Samples with XPO1 mutations	Ref.
Chronic lymphocytic leukemia	4/165 (2.4%)	[105]
	2/105 (1.9%)	[106]
	6/192 (3.1%)	[107]
	7/160 (4.4%)	[108]
	33/969 (3.4%)	[109]
	1/10 (10%)	[110]
	6/24 (25%)	[111]
	4/159 (2.5%)	[112]
	2/12 (16.7%)	[113]
	13/136 (9.5%)	[114]
	25/538 (4.6%)	[115]
	17/114 (14.9%)	[116]
	2/25 (8%)	[117]
	14/180 (7.8%)	[118]
	7/61 (11.5%)	[119]
	38/486 (7,8%)	[120]
	25/436 (5.7%)	[101]
	4/56 (7.1%)	[121]
	28/288 (9.7%)	[122]
Aggregate chronic lymphocytic leukemia	238/4116 (5.8%)	
Primary mediastinal B-cell lymphoma	28/117 (24%)	[100]
	7/18 (38.9%)	[123]
Aggregate primary mediastinal B-cell lymphoma	35/135 (25.9%)	
Hodgkin's lymphoma	22/91 (24.2%)	[104]
	5/19 (26%)	[100]
	6/34 (18%)	[124]
Aggregate Hodgkin's lymphoma	33/144 (22.9%)	
Other diffuse large B-cell lymphoma	1%-3%	[123]
	0%-1.5%	[100]

In addition, XPO1 transcription has been reported to be regulated by cMyc and p53[102,103], two proteins that are frequently altered in cancer. Conceivably, disruption of this regulation may contribute to aberrant XPO1 expression in some tumors, although further studies are required to test this possibility.

A recurrent *XPO1* gene mutation in hematological malignancies

Missense mutations of the glutamic residue E571 (mostly E571K) have been detected in around 25% of patients with two specific types of hematological malignancies: primary mediastinal B-cell lymphoma (PMBL)[100], and classical Hodgkin's lymphoma (HL)[104]. The E571 "hotspot" mutations in XPO1 were first detected by whole genome sequencing analysis of CLL samples[105]. A large number of targeted studies[100,101,104-124] [Table 2] have subsequently confirmed the presence of E571 missense mutations in around 5% of CLL patients.

In CLL, the presence of XPO1 mutations is often associated with unmutated IGHV status[105,109,120], but does not seem to be a marker of poor patient prognosis[120]. Similarly, HL patients with XPO1 mutations do not appear to have a worse prognosis than patients with wild type XPO1[104]. In contrast, a shorter progression-free survival was reported for PMBL patients bearing XPO1 mutations[100]. Interestingly, it has been suggested that XPO1 mutations could represent useful biomarkers to evaluate minimal residual disease in HL and PMBL[125].

Isolated instances of mutant XPO1 have been reported in esophageal[126] and thyroid cancer[127], but XPO1 genetic alterations seem to be a very rare event in solid tumors.

It is still unclear why XPO1 E571 mutations are particularly common in certain types of cancer, and why they may have different prognostic significance in different types of hematological malignancies. In fact, the molecular mechanisms that may be responsible for the pathogenic effect of XPO1 mutations remain to be established. Consistent with the location of the mutational "hotspot" proximal to the NES-binding site [Figure 2B], it has been reported that the E571K mutation subtly increases the affinity of the receptor for some NESs with a negatively charged carboxy-terminal end[32]. Conceivably, this could lead to altered export of one or more cargos, whose mislocalization might in turn contribute to tumorigenesis.

Given its frequent alteration in human tumors, and its crucial cellular roles described above, XPO1 has long been regarded as a potentially relevant target in cancer therapy.

XPO1 INHIBITION IN CANCER THERAPY

Development and preclinical evaluation of selective inhibitors of nuclear export

Even before XPO1 was identified as its cellular target, LMB (also called elactocin) had been found to possess antitumor activity, and it had been tested in a clinical trial[128].

LMB was found to have severe toxicities when administered to patients, precluding its development as a clinically useful drug[128]. Nevertheless, the availability of this potent and specific inhibitor made it possible to carry out proof-of-concept experiments testing the effect of XPO1 inhibition in different tumor settings. As an illustrative example, we will briefly describe some early data regarding the effect of LMB treatment in chronic myelogenous leukemia (CML) cells expressing the BCR-ABL oncoprotein. Shortly after the identification of XPO1 as a nuclear export receptor, the c-ABL kinase was identified as one of its cargos, bearing a C-terminal NES that is also present in the BCR-ABL fusion protein[77]. At that time, treatment of BCR-ABL-positive CML patients was undergoing a dramatic improvement with the introduction of the kinase inhibitor imatinib[129,130]. In this context, it was reported that the sequential combination of imatinib plus LMB led to the nuclear entrapment of BCR-ABL, which selectively induced apoptosis of CML cells[131]. Furthermore, subsequent experiments showed that the combination with LMB could overcome imatinib resistance due to BCR-ABL amplification[132].

These and other encouraging findings in different tumor types (reviewed by Turner and Sullivan[7]) suggested that XPO1 inhibition might represent a valid strategy for cancer treatment, fostering the search for other XPO1 inhibitors. Over the next years, several natural and synthetic inhibitors of XPO1 were reported (reviewed by Tan *et al.*[10] and Senapedis *et al.*[133]). Similar to LMB, these compounds bind covalently to XPO1 residue C528, and occupy the NES-binding groove, blocking access to NESs. However, unlike LMB, some of these novel inhibitors, such as CBS9106 or S109, bind to XPO1 in a reversible manner, which was associated to less severe toxicity in preclinical *in vivo* models[84,134]. Studies with these compounds further validated XPO1 inhibition as a relevant strategy for cancer treatment. For example, blocking nuclear export of topoisomerase II with the XPO1 inhibitor Ratjadone C was found to sensitize multiple myeloma (MM) cells to doxorubicin and etoposide[135].

While most XPO1 inhibitors have only been tested *in vitro* or in mouse xenograft, there is a series of compounds, termed selective inhibitors of nuclear export (SINEs) that are undergoing development as potential anticancer drugs, and some of these compounds are already being evaluated in clinical trials[133].

SINEs were developed in 2012 using structure-assisted relationship methodology combined with a novel computational approach termed consensus-induced fit docking[136,137], a strategy that relied crucially on the recently solved structures of NES-bound XPO1. The "first-generation" series of SINEs included a relative large number of slowly reversible XPO1 inhibitors, such as KPT-127, KPT-185, KPT-205, KPT-227, KPT-

249, KPT-251, KPT-276 and KPT-330 (Selinexor). As summarized in Tables 3 and 4, SINE compounds have been extensively tested in preclinical models of many different hematological malignancies[80,82,83,100,101,137-157] and solid tumors[89,95,97,158-188]. In these models, SINEs have demonstrated potent *in vitro* and *in vivo* activity against cancer cells (including growth inhibition, induction of apoptosis, and cell cycle arrest), with only minor toxic effects on normal cells. Importantly, several SINEs (most prominently Selinexor) have been shown to increase the sensitivity of cancer cells to currently used drugs, such as doxorubicin or the proteasome inhibitors bortezomib and carfilzomib, and also to synergize with other targeted therapeutic agents, such as ibrutinib (an inhibitor of Bruton tyrosine kinase) or linsitinib (an inhibitor of insulin-like growth factor receptor-1). A more extensive and detailed discussion of the preclinical results obtained with SINEs in specific tumor settings can be found in recent reviews[9,10,79,133,189].

In general terms, the anticancer effect of XPO1 inhibition is thought to rely on the relocation of mislocalized XPO1 cargos with tumor-suppressive and growth-regulatory functions (e.g., p53) to the nucleus, where they carry out their normal activity. In our opinion, this may be an overly simplistic view. Given the large number of potential XPO1 cargos with a role in cancer, the export-independent roles of XPO1, and the complex nature of the tumorigenesis process, the specific molecular and cellular mechanisms underlying the anticancer effect of SINEs may differ in different tumor settings. In this regard, as indicated in Tables 3 and 4, preclinical studies are providing important information on tumor context-specific proteins and signaling pathways that may mediate SINE activity, such as the BCR-ABL oncoprotein in CML mentioned above, or the NF-κB pathway in lung cancer[176].

Intriguingly, there is emerging evidence that, in addition to cancer, other conditions, such as demyelinating diseases[190] or viral infections[191] might be amenable to treatment with SINEs.

Evaluation of Selinexor in clinical trials

In preclinical studies, Selinexor compared favorably to other "first-generation" SINEs in terms of the balance between potency and tolerability. Selinexor, an orally available drug, is the only compound of the series that has advanced into clinical development for human cancer.

The ClinicalTrials.gov site (https://clinicaltrials.gov/, accessed on 11 Jun 2018) registers 60 clinical studies on different tumor types with Selinexor as single agent or in combination with other drugs. In addition, there are isolated clinical trials registered for other XPO1 inhibitors, such as the "second-generation" SINE compound KPT-8602 (Eltanexor) or the non-SINE compound SL-801.

Interim data from some clinical studies with Selinexor have been reported as meeting proceedings (some of these data are reviewed by Mahipal and Malafa[192]). Here, we will limit our discussion to the results of phase I and II trials that have undergone full peer-reviewed publication as PubMed-indexed articles (summarized in Table 5).

Abdul Razak *et al.*[193] evaluated the safety, pharmacokinetics, pharmacodynamics, and efficacy of Selinexor in 189 patients with advanced solid tumors, testing several doses and administration schedules. The most common grade 3 or 4 toxicities in this series were thrombocytopenia, fatigue, and hyponatremia. One hundred and fifty seven patients were evaluable for response. Seven patients achieved partial or complete response, and 27 patients achieved stable disease for ≥ 4 months. The authors concluded that Selinexor is a safe therapeutic with broad antitumor activity, and proposed a recommended phase II dose (RP2D) of 35 mg/m^2 with a twice-a-week dosing schedule.

Gounder *et al.*[194] carried out a phase I study on 54 patients with advanced soft tissue or bone sarcoma. Selinexor was administered twice per week at doses of 30 mg/m^2, 50 mg/m^2, or 60 mg flat dose. The most

Table 3. Summary of preclinical studies with "first-generation" SINEs in hematological malignancies

Malignancy type	Preclinical model(s)	SINE(s)	Cellular effects	Remarks	Ref.
MM	*In vitro*/patient-derived cells/xenograft/mouse model	KPT-276	Growth inhibition, apoptosis		[82]
	In vitro/patient-derived cells	Selinexor KPT-127 KPT-185 KPT-249 KPT-276	Reduced viability, apoptosis	SINEs sensitize MM cells to doxorubicin, bortezomib, and carfilzomib. Overcome stroma cell-promoted drug resistance	[138]
	In vitro/xenograft	Selinexor KPT-185	Growth inhibition, apoptosis	SINEs inhibit MM-induced bone lysis. Mechanism related to NF-κB pathway and NFATc1	[83]
	In vitro/patient-derived cells/xenograft	Selinexor	Apoptosis	Synergizes with carfilzomib. Apoptosis mediated by caspase 10	[139]
	In vitro/xenograft/patient biopsies	Selinexor	Apoptosis, DNA damage	Restores sensitivity to doxorubicin. Synergizes with doxorubicin	[140]
	In vitro/xenograft/patient biopsies	Selinexor	Growth inhibition	Restores sensitivity to bortezomib and carfilzomib. Mechanism related to NF-κB pathway	[141]
	In vitro/xenograft	Selinexor	Delay in tumor initiation and progression, apoptosis	Overcomes hypoxia-induced bortezomib resistance	[142]
	In vitro/xenograft	Selinexor	Growth inhibition, apoptosis	Synergizes with dexamethasone. Mechanism related to glucocorticoid receptor and mTOR pathway	[143]
AML	*In vitro*/xenograft	KPT-185 KPT-276	Reduced proliferation, apoptosis, cell cycle arrest, myeloid differentiation		[144]
	In vitro/xenograft	KPT-251	Apoptosis		[145]
	In vitro/patient-derived cells	KPT-185	Reduced proliferation, apoptosis	Synergizes with MDM2 inhibitor. p53-dependent apoptosis	[80]
	In vitro/xenograft	Selinexor		Priming with decitabine enhances Selinexor activity	[146]
	In vitro/xenograft		Apoptosis, myeloid differentiation	Synergizes with sorafenib in xenografts of FLT3-mutated AML	[147]
AML and ALL	*In vitro*/xenograft	Selinexor	Apoptosis	Little toxicity to normal haematopoietic cells	[148]
CLL	*In vitro*/xenograft	KPT-185 KPT-251	Apoptosis	SINEs counteract protective effects of the microenvironment	[137]
	In vitro/mouse model	Selinexor	Reduced proliferation		[149]
	Patient-derived cells/mouse models	Selinexor		Synergizes with ibrutinib	[150]
	In vitro/patient-derived cells	Selinexor	Apoptosis	XPO1 mutation or chromosome 2p gains decrease Selinexor sensitivity	[101]
CML and ALL	*In vitro*/mouse model	Selinexor	Apoptosis	Compassionate use in a patient with TKI-resistant CML reduced disease signs. Mechanism related to reactivation of PP2A	[151]
CML	*In vitro*/xenograft	Selinexor		Sensitizes CML cells to imatinib	[152]
MCL	*In vitro*/xenograft	KPT-185 KPT-276	Growth inhibition, apoptosis		[153]
	In vitro	KPT-185	Growth inhibition, repression of ribosomal biogenesis, alterations in cell metabolism		[154]
NHL	*In vitro*/xenograft	KPT-185 KPT-251 KPT-276	Growth inhibition, apoptosis, cell cycle arrest	Cellular effects dependent on p53 and p73	[155]
	In vitro/xenograft	KPT-185 KPT-276	Growth inhibition, apoptosis, cell cycle arrest		[156]
	In vitro/mouse model	Selinexor KPT-251 KPT-276	Apoptosis	Dexamethasone or everolimus enhance Selinexor activity	[157]
PMBL	*In vitro*	Selinexor KPT-185	Reduced proliferation, apoptosis	E571K mutation does not affect SINE activity	[100]

MM: multiple myeloma; AML: acute myeloid leukemia; ALL: acute lymphoblastic leukemia; CLL: chronic lymphocytic leukemia; CML: chronic myelogenous leukemia; MCL: mantle cell lymphoma; NHL: non-Hodgkin lymphoma; PMBL: primary mediastinal B-cell lymphoma

Table 4. Summary of preclinical studies with "first-generation" SINEs in human solid tumors

Tumor type	Preclinical model(s)	SINE(s)	Cellular effects	Remarks	Ref.
Renal cancer	*In vitro*/xenograft	KPT-185, KPT-251	Growth inhibition, apoptosis, cell cycle arrest	SINEs compare favorably to sorafenib	[95]
	In vitro/xenograft	Selinexor	Growth inhibition, apoptosis		[158]
Prostate cancer	*In vitro*/xenograft	Selinexor KPT-185, KPT-251	Reduced proliferation, apoptosis (no cell cycle arrest)	SINEs synergize with doxorubicin	[159]
	In vitro/xenograft	Selinexor, KPT-251		SINEs reduce bone metastasis	[160]
	In vitro/xenograft	Selinexor, KPT-251	Growth inhibition, apoptosis, increased DNA damage	SINEs sensitize cells to docetaxel	[161]
Breast cancer	*In vitro*/xenograft	Selinexor, KPT-185, KPT-251, KPT-276	Growth inhibition, apoptosis	Mechanism related to STAT3 and survivin	[162]
	In vitro/xenograft	Selinexor		Restores sensitivity to tamoxifen	[163]
	In vitro/xenograft	Selinexor	Growth inhibition	Effective as single agent and synergizes with chemotherapy in triple-negative BC	[164]
Ovarian cancer	*In vitro*	Selinexor, KPT-185	Apoptosis	SINEs synergize with chemotherapy. Mechanism related to IGF2BP1	[165]
	In vitro/xenograft	Selinexor, KPT-185	Apoptosis (p53-dependent and p53-independent)	Overcomes resistance to platinum compounds	[166]
	In vitro	Selinexor	Reduced proliferation, apoptosis	Synergizes with cisplatin. Mechanism related to FoxO1	[167]
Colorectal cancer	*In vitro*/xenograft	Selinexor	Reduced proliferation, apoptosis	Synergizes with radiotherapy	[168]
Liver cancer	*In vitro*/xenograft	Selinexor	Growth inhibition, apoptosis cell cycle arrest		[169]
Pancreatic cancer	*In vitro*/xenograft	KPT-185, KPT-127, KPT-205, KPT-227	Reduced proliferation, apoptosis	Mechanism related to PAR-4	[170]
	In vitro/xenograft	KPT-185	Reduced proliferation and migration, apoptosis	Mechanism related to Fbw7 and Notch-1	[171]
	In vitro/xenograft	Selinexor	Growth inhibition, apoptosis	Synergizes with gemcitabine	[172]
	In vitro	Selinexor	Reduced proliferation and migration	Mechanism related to miR-145 micro RNA	[173]
Non-small cell lung cancer	*In vitro*/xenograft	Selinexor	Reduced proliferation, apoptosis, cell cycle arrest	Synergizes with cisplatin. Effective against NSCLC cells with different molecular alterations	[174]
	In vitro/xenograft	KPT-185, KPT-276	Reduced viability, apoptosis, cell cycle arrest	KPT-185 active against NSCLC cell lines resistant to EGFR-TKIs	[175]
	In vitro/xenograft	Selinexor, KPT-185		Synthetic-lethal interaction with K-Ras. Mechanism related to NF-κB pathway	[176]
Thyroid cancer	*In vitro*/xenograft	Selinexor	Growth inhibition, apoptosis, cell cycle arrest	Synergizes with doxorubicin	[177]
Thymic epitelial tumors	*In vitro*/xenograft	Selinexor	Reduced proliferation, apoptosis	p53-dependent and independent effect	[89]
Sarcoma	*In vitro*/xenograft	Selinexor	Growth inhibition, apoptosis, cell cycle arrest	Study on liposarcoma	[178]
	In vitro/xenograft	Selinexor	Growth inhibition, apoptosis	Synergizes with proteasome inhibitors. Mechanism related to NF-κB pathway	[179]
	In vitro/xenograft	Selinexor	Cell cycle arrest	Activity against a wide variety of sarcoma models including liposarcoma and gastrointestinal stromal tumor	[180]
	In vitro/xenograft	Selinexor	Growth inhibition, apoptosis	Marfilzomib increases sensitivity to Selinexor. Mechanism related to NF-κB pathway and survivin	[181]
	In vitro/xenograft	Selinexor	Growth inhibition, apoptosis, cell-cycle arrest	Study on Ewing sarcoma. Synergizes with the IGF-1R inhibitor linsitinib	[97]
Mesothelioma	*In vitro*/xenograft	Selinexor, KPT-251, KPT-276	Growth inhibition, apoptosis, cell-cycle arrest	SINEs synergize with survivin inhibitor YM155	[182]
Glioma	Patient-derived cells/xenograft	Selinexor, KPT-251, KPT-276	Growth inhibition, apoptosis		[183]
	In vitro/xenograft	Selinexor		Enhances radiosensitivity of glioblastoma cells	[184]
Melanoma	*In vitro*/xenograft	Selinexor, KPT-185, KPT-251, KPT-276	Growth inhibition, apoptosis, cell cycle arrest	SINEs synergize with BRAF inhibitors. Independent of BRAF mutational status	[185]
	In vitro/xenograft	Selinexor, KPT-276	Growth inhibition, apoptosis	Independent of BRAF mutational status	[186]
Multiple types (solid)	*In vitro*	Selinexor	DNA damage (double-strand breaks)	Synergizes with DNA-damaging agents	[187]
Pediatric cancer (solid and hematological)	*In vitro*/xenograft	Selinexor		Activity against a broad range of pediatric cancer types. Independent of TP53 mutation status	[188]

Table 5. Summary of the results of published clinical studies of Selinexor in human malignancies

Tumor type	Phase	Remarks	Reference/ID
Advanced solid tumors	Phase I	Selinexor single agent. 189 patients enrolled. Most common grade ≥ 3 adverse events: thrombocytopenia, fatigue and hyponatremia. RP2D 35 mg/m^2 given twice weekly. 157 evaluable patients. 1 CR and 5 PR	[193] ID: NCT01607905
Sarcoma	Phase I	Selinexor single agent. 54 patients enrolled. Most common grade ≥ 3 adverse events: fatigue, thrombocytopenia, anemia, lymphopenia, and leucopenia. 52 evaluable patients. SD: 33%	[194] ID: NCT01896505
Pediatric refractory acute leukemia	Phase I	Selinexor combined with Fludarabine and Cytarabine. 18 patients enrolled. Selinexor tolerable at doses up to 55 mg/m^2 in pediatric patients. 15 evaluable patients. CR: 47%	[195] ID: NCT02212561
Non-Hodgkin lymphoma	Phase I	Selinexor single agent. 79 patients enrolled. Most common grade ≥ 3 adverse events: thrombocytopenia, neutropenia, anemia, leukopenia, fatigue, and hyponatremia. RP2D 60 mg. 70 evaluable patients. OR: 31% (including 4 CR and 18 PR)	[196] ID: NCT01607892
Acute myeloid leukemia	Phase I	Selinexor single agent. 95 patients enrolled. Most common grade ≥ 3 nonhematological adverse event: fatigue. No reported dose-limiting toxicities. RP2D 60 mg. 81 evaluable patients. OR: 14%	[197] ID: NCT01607892
	Phase I	Selinexor combined with cytarabine and mitoxantrone. 20 patients enrolled. Serious adverse events 30%, including one fatal adverse event. RP2D: 80 mg. 20 evaluable patients. Overall response rate 70% (including 10 CR)	[198] ID: NCT02573363
Multiple myeloma	Phase I	Dose-escalation phase: Selinexor as single agent in 25 patients enrolled. Dose-expansion phase: Selinexor as single agent or combined with dexamethasone. 59 patients enrolled. Most common grade ≥ 3 adverse event: thrombocytopenia. RP2D: 80 mg plus 20 mg dexamethasone given twice weekly. Objective response rate: 4% Selinexor as single agent, 50% when combined with dexamethasone	[199] ID: NCT01607892
	Phase II	Selinexor combined with dexamethasone. 79 patients (multi-refractory disease) enrolled. Most common grade ≥ 3 adverse events: thrombocytopenia, anemia, neutropenia, hyponatremia, leukopenia, and fatigue. Overall response rate 21%	[200]
Castration-resistant prostate cancer	Phase II	Selinexor as single agent. 14 patients (refractory to anti-androgenic therapy) enrolled. Some activity (PR 25%), but poor tolerability.	[201] ID: NCT02215161

ID: identifier at ClinicalTrials.gov; MTD: maximum-tolerated dose; RP2D: recommended Phase II dose; OR: objective response; CR: complete response; PR: partial response; SD: stable disease

common grade 3 or 4 toxicities in this series were fatigue, thrombocytopenia, anemia, lymphopenia, and leucopenia. In 52 evaluable patients, no objective responses were seen, but 17 patients achieved stable disease for ≥ 4 months. The authors concluded that Selinexor shows preliminary evidence of anticancer activity in sarcoma, and is well tolerated at a 60 mg flat dose.

Alexander *et al.*[195] evaluated the combination of Selinexor with fludarabine and cytarabine in 18 pediatric patients with relapsed or refractory leukemia. Selinexor was administered twice per week at several doses between 30 mg/m^2 and 70 mg/m^2. Dose-limiting reversible cerebellar toxicity was experienced by some patients treated with the 70 mg/m^2 dose. Seven of the 15 patients that were evaluable achieved complete response. The authors concluded that Selinexor combined with fludarabine and cytarabine shows promising response rates in pediatric patients with relapsed or refractory leukemia. A 55 mg/m^2 dose Selinexor is tolerable in this combination.

Kuruvilla *et al.*[196] evaluated Selinexor in 79 patients with different subtypes of non-Hodgkin lymphoma (NHL). In the dose-expansion phase of the study, Selinexor was administered at doses of 35 mg/m^2 or

60 mg/m^2. The most common grade 3 or 4 toxicities in this series were thrombocytopenia, neutropenia, anemia, leukopenia, fatigue, and hyponatremia. Twenty-two objective responses (4 of them complete responses) were observed in 70 evaluable patients. The authors concluded that Selinexor shows encouraging activity in NHL patients, and proposed 35 mg/m^2 Selinexor (60 mg flat dose) as the RP2D.

Garzon *et al.*[197] carried out a phase I dose-escalation study in 95 patients with relapsed or refractory acute myeloid leukemia (AML). Several doses and administration schedules were tested. The most common grade 3 or 4 toxicities were thrombocytopenia, anemia, fatigue, and neutropenia. Objective responses were observed in 11 of the 81 evaluable patients. The authors concluded that Selinexor is a safe therapy in AML patients, and established the RP2D at 35 mg/m^2 (60 mg flat dose) given twice weekly. Another phase I dose-escalation trial in AML evaluated the combination of Selinexor with high-dose cytarabine and mitoxantrone in 20 patients[198]. Selinexor doses of 60 mg or 80 mg were administered. Serious toxicities, including one fatal adverse event, occurred in 30% of the patients. The overall response rate was 70%, including 10 patients achieving complete remission. The authors concluded that Selinexor combined with high-dose cytarabine and mitoxantrone is a feasible and tolerable treatment in AML patients, and proposed 80 mg Selinexor twice weekly as the RP2D in this combination.

Chen *et al.*[199] evaluated Selinexor in 84 patients with heavily pretreated MM (81 patients) or Waldenstrom macroglobulinemia (3 patients). Single agent Selinexor was given to 25 patients in the dose-escalation phase. In the dose-expansion phase, Selinexor was administered in combination with dexamethasone to 59 patients. The most commonly reported grade 3 or 4 toxicity in this series was thrombocytopenia. Although the efficacy of Selinexor as single agent was modest, its combination with dexamethasone resulted in a significantly increased activity, with an objective response rate of 50%. The authors proposed a RP2D of 80 mg Selinexor plus 20 mg dexamethasone given twice weekly. This treatment regimen was administered to 79 patients with multi-refractory MM in a recently reported phase II study[200]. The overall response rate (the primary endpoint of the study) was 21% and the most frequent grade 3 or 4 toxicity was thrombocytopenia. In relation to these studies, a more extensive and detailed discussion on the clinical implementation of Selinexor in MM has been recently published[189].

The last clinical study on Selinexor published to date (May 2018) is a phase II trial that evaluated its efficacy and tolerability in 14 patients with metastatic, castration-resistant, prostate cancer[201]. Selinexor was administered twice weekly at a dose of 65 mg/m^2 that had to be subsequently reduced to a flat dose of 60 mg to improve tolerability. In fact, although Selinexor showed some evidence of clinical activity (reduction in prostate-specific antigen levels, and radiographic response), it was poorly tolerated in this patient population.

In summary, the results of these studies show that Selinexor, as single agent or in combination with other drugs, has broad clinical activity in multiple types of solid tumors and hematological malignancies and is generally well tolerated by patients. One of the most common high-grade toxicities experienced by patients treated with Selinexor is thrombocytopenia. The mechanism underlying this adverse event has been recently elucidated. Machlus *et al.*[202] have shown that thrombocytopenia results from reduced maturation of megakaryocyte progenitors due to Selinexor-mediated inhibition of thrombopoietin signaling. Importantly, the severity of thrombocytopenia could be reduced by temporary interruption of Selinexor treatment and administration of thrombopoietin mimetics to patients[202].

Altogether, these clinical data support the view that inhibition of XPO1 represents a valid therapeutic strategy in cancer.

CONCLUSION AND FUTURE DIRECTIONS

Twenty years after its identification as a receptor that mediates the nuclear export of proteins, there is compelling evidence that XPO1 represents a relevant target in cancer. Further basic, preclinical and clinical in-

vestigations are required to address several salient questions on the use of XPO1 inhibition as a therapeutic approach.

On one hand, novel XPO1 inhibitors with more favorable clinical properties are being developed. In this regard, a "second-generation" SINE (KPT-8602 or Eltanexor) has demonstrated improved tolerability in preclinical models[203-205] and is currently undergoing clinical evaluation.

On the other hand, it is necessary to further elucidate the mechanisms that mediate the oncogenic role of XPO1 alterations (overexpression or mutation) in different types of cancer and to better characterize the molecular and cellular mechanisms underlying the effect of XPO1 inhibitors. This basic mechanistic information, which is still rather limited, would be crucial to successfully implement XPO1-targeting drugs in the clinic, as it could help to design rational combinations with other agents, to identify subsets of patients that may benefit more from the treatment and to improve the clinical management of adverse effects.

DECLARATIONS

Acknowledgments

We thank our colleagues at the UPV/EHU Dr. Sonia Bañuelos (Dept. of Biochemistry and Molecular Biology), Dr. Gorka Prieto (Dept. of Communication Engineering) and Dr. Asier Fullaondo (Dept. of Genetics, Physical Anthropology and Animal Physiology) for their help in preparing Figures 2 and 3. Supported by grants from the Spanish Government MINECO-FEDER (SAF2014-57743-R), the Basque Country Government (IT634-13) and the University of the Basque Country (UFI11/20), as well as a fellowship from the Basque Country Government (to MS).

Authors' contributions

Conception of the work, draft and revision of the work: Sendino M, Omaetxebarria MJ, Rodríguez JA

Availability of data and materials

Not applicable.

Financial support and sponsorship

None.

Conflicts of interest

All authors declared that there are no conflicts of interest.

Ethical approval and consent to participate

Not applicable.

Consent for publication

Not applicable.

Copyright

REFERENCES

1. Fukuda M, Asano S, Nakamura T, Adachi M, Yoshida M, Yanagida M, Nishida E. CRM1 is responsible for intracellular transport mediated by the nuclear export signal. Nature 1997;390:308-11.
2. Fornerod M, Ohno M, Yoshida M, Mattaj IW. CRM1 is an export receptor for leucine-rich nuclear export signals. Cell 1997;90:1051-

60.
3. Stade K, Ford CS, Guthrie C, Weis K. Exportin 1 (Crm1p) is an essential nuclear export factor. Cell 1997;90:1041-50.
4. Ossareh-Nazari B, Bachelerie F, Dargemont C. Evidence for a role of CRM1 in signal-mediated nuclear protein export. Science 1997;278:141-4.
5. Hutten S, Kehlenbach RH. CRM1-mediated nuclear export: to the pore and beyond. Trends Cell Biol 2007;17:193-201.
6. Okamura M, Inose H, Masuda S. RNA export through the NPC in Eukaryotes. Genes (Basel) 2015;6:124-49.
7. Turner JG, Sullivan DM. CRM1-mediated nuclear export of proteins and drug resistance in cancer. Curr Med Chem 2008;15:2648-55.
8. Arnaoutov A, Azuma Y, Ribbeck K, Joseph J, Boyarchuk Y, Karpova T, McNally J, Dasso M. Crm1 is a mitotic effector of Ran-GTP in somatic cells. Nat Cell Biol 2005;7:626-32.
9. Gravina GL, Senapedis W, McCauley D, Baloglu E, Shacham S, Festuccia C. Nucleo-cytoplasmic transport as a therapeutic target of cancer. J Hematol Oncol 2014;7:85.
10. Tan DS, Bedard PL, Kuruvilla J, Siu LL, Razak AR. Promising SINEs for embargoing nuclear-cytoplasmic export as an anticancer strategy. Cancer Discov 2014;4:527-37.
11. Koyama M, Matsuura Y. Mechanistic insights from the recent structures of the CRM1 nuclear export complex and its disassembly intermediate. Biophysics (Nagoya-shi) 2012;8:145-50.
12. Fung HY, Chook YM. Atomic basis of CRM1-cargo recognition, release and inhibition. Semin Cancer Biol 2014;27:52-61.
13. Monecke T, Dickmanns A, Ficner R. Allosteric control of the exportin CRM1 unraveled by crystal structure analysis. FEBS J 2014;281:4179-94.
14. Speese SD, Ashley J, Jokhi V, Nunnari J, Barria R, Li Y, Ataman B, Koon A, Chang YT, Li Q, Moore MJ, Budnik V. Nuclear envelope budding enables large ribonucleoprotein particle export during synaptic Wnt signaling. Cell 2012;149:832-46.
15. Knockenhauer KE, Schwartz TU. The nuclear pore complex as a flexible and dynamic gate. Cell 2016;164:1162-71.
16. Schmidt HB, Görlich D. Transport selectivity of nuclear pores, phase separation, and membraneless organelles. Trends Biochem Sci 2016;41:46-61.
17. Pemberton LF, Paschal BM. Mechanisms of receptor-mediated nuclear import and nuclear export. Traffic 2005;6:187-98.
18. Tran EJ, King MC, Corbett AH. Macromolecular transport between the nucleus and the cytoplasm: advances in mechanism and emerging links to disease. Biochim Biophys Acta 2014;1843:2784-95.
19. Cautain B, Hill R, de Pedro N, Link W. Components and regulation of nuclear transport processes. FEBS J 2015;282:445-62.
20. Timney BL, Raveh B, Mironska R, Trivedi JM, Kim SJ, Russel D, Wente SR, Sali A, Rout MP. Simple rules for passive diffusion through the nuclear pore complex. J Cell Biol 2016;215:57-76.
21. Beck M, Hurt E. The nuclear pore complex: understanding its function through structural insight. Nat Rev Mol Cell Biol 2017;18:73-89.
22. Çağatay T, Chook YM. Karyopherins in cancer. Curr Opin Cell Biol 2018;52:30-42.
23. Soniat M, Chook YM. Nuclear localization signals for four distinct karyopherin-β nuclear import systems. Biochem J 2015;468:353-62.
24. Gama-Carvalho M, Carmo-Fonseca M. The rules and roles of nucleocytoplasmic shuttling proteins. FEBS Lett 2001;498:157-63.
25. Nachury MV, Weis K. The direction of transport through the nuclear pore can be inverted. Proc Natl Acad Sci U S A 1999;96:9622-7.
26. Nardozzi JD, Lott K, Cingolani G. Phosphorylation meets nuclear import: a review. Cell Commun Signal 2010;8:32.
27. Panayiotou R, Miralles F, Pawlowski R, Diring J, Flynn HR, Skehel M, Treisman R. Phosphorylation acts positively and negatively to regulate MRTF-A subcellular localisation and activity. Elife 2016;5:e15460.
28. Rodríguez JA. Interplay between nuclear transport and ubiquitin/SUMO modifications in the regulation of cancer-related proteins. Semin Cancer Biol 2014;27:11-9.
29. Rodriguez JA, Schüchner S, Au WW, Fabbro M, Henderson BR. Nuclear-cytoplasmic shuttling of BARD1 contributes to its proapoptotic activity and is regulated by dimerization with BRCA1. Oncogene 2004;23:1809-20.
30. Engelsma D, Rodriguez JA, Fish A, Giaccone G, Fornerod M. Homodimerization antagonizes nuclear export of survivin. Traffic 2007;8:1495-502.
31. Ding Q, Zhao L, Guo H, Zheng AC. The nucleocytoplasmic transport of viral proteins. Virol Sin 2010;25:79-85.
32. García-Santisteban I, Arregi I, Alonso-Mariño M, Urbaneja MA, Garcia-Vallejo JJ, Bañuelos S, Rodríguez JA. A cellular reporter to evaluate CRM1 nuclear export activity: functional analysis of the cancer-related mutant E571K. Cell Mol Life Sci 2016;73:4685-99.
33. Xu D, Farmer A, Collett G, Grishin NV, Chook YM. Sequence and structural analyses of nuclear export signals in the NESdb database. Mol Biol Cell 2012;23:3677-93.
34. Kirli K, Karaca S, Dehne HJ, Samwer M, Pan KT, Lenz C, Urlaub H, Görlich D. A deep proteomics perspective on CRM1-mediated nuclear export and nucleocytoplasmic partitioning. Elife 2015;4:e11466.
35. Hirayama S, Sugihara M, Morito D, Iemura SI, Natsume T, Murata S, Nagata K. Nuclear export of ubiquitinated proteins via the UBIN-POST system. Proc Natl Acad Sci U S A 2018;115:E4199-208.
36. Wu T, Chen W, Zhong Y, Hou X, Fang S, Liu CY, Wang G, Yu T, Huang YY, Ouyang X, Li HQ, Cui L, Yang Y. Nuclear export of ubiquitinated proteins determines the sensitivity of colorectal cancer to proteasome inhibitor. Mol Cancer Ther 2017;16:717-28.
37. Englmeier L, Fornerod M, Bischoff FR, Petosa C, Mattaj IW, Kutay U. RanBP3 influences interactions between CRM1 and its nuclear protein export substrates. EMBO Rep 2001;2:926-32.
38. Lindsay ME, Holaska JM, Welch K, Paschal BM, Macara IG. Ran-binding protein 3 is a cofactor for Crm1-mediated nuclear protein export. J Cell Biol 2001;153:1391-402.
39. Koyama M, Shirai N, Matsuura Y. Structural insights into how Yrb2p accelerates the assembly of the Xpo1p nuclear export complex.

Cell Rep 2014;9:983-95.
40. Kosugi S, Hasebe M, Tomita M, Yanagawa H. Nuclear export signal consensus sequences defined using a localization-based yeast selection system. Traffic 2008;9:2053-62.
41. Güttler T, Madl T, Neumann P, Deichsel D, Corsini L, Monecke T, Ficner R, Sattler M, Görlich D. NES consensus redefined by structures of PKI-type and Rev-type nuclear export signals bound to CRM1. Nat Struct Mol Biol 2010;17:1367-76.
42. Henderson BR, Eleftheriou A. A comparison of the activity, sequence specificity, and CRM1-dependence of different nuclear export signals. Exp Cell Res 2000;256:213-24.
43. Fu SC, Huang HC, Horton P, Juan HF. ValidNESs: a database of validated leucine-rich nuclear export signals. Nucleic Acids Res 2013;41:D338-43.
44. Fung HY, Fu SC, Chook YM. Nuclear export receptor CRM1 recognizes diverse conformations in nuclear export signals. Elife 2017;6:e23961.
45. Neggers JE, Vercruysse T, Jacquemyn M, Vanstreels E, Baloglu E, Shacham S, Crochiere M, Landesman Y, Daelemans D. Identifying drug-target selectivity of small-molecule CRM1/XPO1 inhibitors by CRISPR/Cas9 genome editing. Chem Biol 2015;22:107-16.
46. Williams T, Ngo LH, Wickramasinghe VO. Nuclear export of RNA: different sizes, shapes and functions. Semin Cell Dev Biol 2018;75:70-7.
47. Thomson E, Ferreira-Cerca S, Hurt E. Eukaryotic ribosome biogenesis at a glance. J Cell Sci 2013;126:4815-21.
48. Delaleau M, Borden KL. Multiple export mechanisms for mRNAs. Cells 2015;4:452-73.
49. Yang J, Bogerd HP, Wang PJ, Page DC, Cullen BR. Two closely related human nuclear export factors utilize entirely distinct export pathways. Mol Cell 2001;8:397-406.
50. Brennan CM, Gallouzi IE, Steitz JA. Protein ligands to HuR modulate its interaction with target mRNAs in vivo. J Cell Biol 2000;151:1-14.
51. Topisirovic I, Siddiqui N, Lapointe VL, Trost M, Thibault P, Bangeranye C, Piñol-Roma S, Borden KL. Molecular dissection of the eukaryotic initiation factor 4E (eIF4E) export-competent RNP. EMBO J 2009;28:1087-98.
52. Ohno M, Segref A, Bachi A, Wilm M, Mattaj IW. PHAX, a mediator of U snRNA nuclear export whose activity is regulated by phosphorylation. Cell 2000;101:187-98.
53. Xie M, Li M, Vilborg A, Lee N, Shu MD, Yartseva V, Šestan N, Steitz JA. Mammalian 5'-capped microRNA precursors that generate a single microRNA. Cell 2013;155:1568-80.
54. Noh JH, Kim KM, Abdelmohsen K, Yoon JH, Panda AC, Munk R, Kim J, Curtis J, Moad CA, Wohler CM, Indig FE, de Paula W, Dudekula DB, De S, Piao Y, Yang X, Martindale JL, de Cabo R, Gorospe M. HuR and GRSF1 modulate the nuclear export and mitochondrial localization of the lncRNA RMRP. Genes Dev 2016;30:1224-39.
55. Martinez I, Hayes KE, Barr JA, Harold AD, Xie M, Bukhari SIA, Vasudevan S, Steitz JA, DiMaio D. An Exportin-1-dependent microRNA biogenesis pathway during human cell quiescence. Proc Natl Acad Sci U S A 2017;114:E4961-70.
56. Sheng P, Fields C, Aadland K, Wei T, Kolaczkowski O, Gu T, Kolaczkowski B, Xie M. Dicer cleaves 5'-extended microRNA precursors originating from RNA polymerase II transcription start sites. Nucleic Acids Res 2018;46:5737-52.
57. Castanotto D, Lingeman R, Riggs AD, Rossi JJ. CRM1 mediates nuclear-cytoplasmic shuttling of mature microRNAs. Proc Natl Acad Sci U S A 2009;106:21655-9.
58. Pradet-Balade B, Girard C, Boulon S, Paul C, Azzag K, Bordonné R, Bertrand E, Verheggen C. CRM1 controls the composition of nucleoplasmic pre-snoRNA complexes to licence them for nucleolar transport. EMBO J 2011;30:2205-18.
59. Forbes DJ, Travesa A, Nord MS, Bernis C. Reprint of "Nuclear transport factors: global regulation of mitosis". Curr Opin Cell Biol 2015;34:122-34.
60. Liu Q, Jiang Q, Zhang C. A fraction of Crm1 locates at centrosomes by its CRIME domain and regulates the centrosomal localization of pericentrin. Biochem Biophys Res Commun 2009;384:383-8.
61. Wu Z, Jiang Q, Clarke PR, Zhang C. Phosphorylation of Crm1 by CDK1-cyclin-B promotes Ran-dependent mitotic spindle assembly. J Cell Sci 2013;126:3417-28.
62. Gilistro E, de Turris V, Damizia M, Verrico A, Moroni S, De Santis R, Rosa A, Lavia P. Importin-β and CRM1 control a RANBP2 spatiotemporal switch essential for mitotic kinetochore function. J Cell Sci 2017;130:2564-78.
63. Wang X, Li S. Protein mislocalization: mechanisms, functions and clinical applications in cancer. Biochim Biophys Acta 2014;1846:13-25.
64. Dickmanns A, Monecke T, Ficner R. Structural basis of targeting the exportin CRM1 in cancer. Cells 2015;4:538-68.
65. Hung MC, Link W. Protein localization in disease and therapy. J Cell Sci 2011;124:3381-92.
66. Hill R, Cautain B, de Pedro N, Link W. Targeting nucleocytoplasmic transport in cancer therapy. Oncotarget 2014;5:11-28.
67. Jeyasekharan AD, Liu Y, Hattori H, Pisupati V, Jonsdottir AB, Rajendra E, Lee M, Sundaramoorthy E, Schlachter S, Kaminski CF, Ofir-Rosenfeld Y, Sato K, Savill J, Ayoub N, Venkitaraman AR. A cancer-associated BRCA2 mutation reveals masked nuclear export signals controlling localization. Nat Struct Mol Biol 2013;20:1191-8.
68. Pauty J, Couturier AM, Rodrigue A, Caron MC, Coulombe Y, Dellaire G, Masson JY. Cancer-causing mutations in the tumor suppressor PALB2 reveal a novel cancer mechanism using a hidden nuclear export signal in the WD40 repeat motif. Nucleic Acids Res 2017;45:2644-57.
69. Mariano AR, Colombo E, Luzi L, Martinelli P, Volorio S, Bernard L, Meani N, Bergomas R, Alcalay M, Pelicci PG. Cytoplasmic localization of NPM in myeloid leukemias is dictated by gain-of-function mutations that create a functional nuclear export signal. Oncogene 2006;25:4376-80.

70. Mor A, White MA, Fontoura BM. Nuclear trafficking in health and disease. Curr Opin Cell Biol 2014;28:28-35.
71. Takeda A, Yaseen NR. Nucleoporins and nucleocytoplasmic transport in hematologic malignancies. Semin Cancer Biol 2014;27:3-10.
72. Takeda A, Sarma NJ, Abdul-Nabi AM, Yaseen NR. Inhibition of CRM1-mediated nuclear export of transcription factors by leukemogenic NUP98 fusion proteins. J Biol Chem 2010;285:16248-57.
73. Saito S, Cigdem S, Okuwaki M, Nagata K. Leukemia-associated Nup214 fusion proteins disturb the XPO1-mediated nuclear-cytoplasmic transport pathway and thereby the NF-κB signaling pathway. Mol Cell Biol 2016;36:1820-35.
74. Christiansen A, Dyrskjøt L. The functional role of the novel biomarker karyopherin α 2 (KPNA2) in cancer. Cancer Lett 2013;331:18-23.
75. Stommel JM, Marchenko ND, Jimenez GS, Moll UM, Hope TJ, Wahl GM. A leucine-rich nuclear export signal in the p53 tetramerization domain: regulation of subcellular localization and p53 activity by NES masking. EMBO J 1999;18:1660-72.
76. Rodríguez JA, Henderson BR. Identification of a functional nuclear export sequence in BRCA1. J Biol Chem 2000;275:38589-96.
77. Taagepera S, McDonald D, Loeb JE, Whitaker LL, McElroy AK, Wang JY, Hope TJ. Nuclear-cytoplasmic shuttling of C-ABL tyrosine kinase. Proc Natl Acad Sci U S A 1998;95:7457-62.
78. Fabbro M, Henderson BR. Regulation of tumor suppressors by nuclear-cytoplasmic shuttling. Exp Cell Res 2003;282:59-69.
79. Conforti F, Wang Y, Rodriguez JA, Alberobello AT, Zhang YW, Giaccone G. Molecular pathways: anticancer activity by inhibition of nucleocytoplasmic shuttling. Clin Cancer Res 2015;21:4508-13.
80. Kojima K, Kornblau SM, Ruvolo V, Dilip A, Duvvuri S, Davis RE, Zhang M, Wang Z, Coombes KR, Zhang N, Qiu YH, Burks JK, Kantarjian H, Shacham S, Kauffman M, Andreeff M. Prognostic impact and targeting of CRM1 in acute myeloid leukemia. Blood 2013;121:4166-74.
81. Zhang K, Wang M, Tamayo AT, Shacham S, Kauffman M, Lee J, Zhang L, Ou Z, Li C, Sun L, Ford RJ, Pham LV. Novel selective inhibitors of nuclear export CRM1 antagonists for therapy in mantle cell lymphoma. Exp Hematol 2013;41:67-78.
82. Schmidt J, Braggio E, Kortuem KM, Egan JB, Zhu YX, Xin CS, Tiedemann RE, Palmer SE, Garbitt VM, McCauley D, Kauffman M, Shacham S, Chesi M, Bergsagel PL, Stewart AK. Genome-wide studies in multiple myeloma identify XPO1/CRM1 as a critical target validated using the selective nuclear export inhibitor KPT-276. Leukemia 2013;27:2357-65.
83. Tai YT, Landesman Y, Acharya C, Calle Y, Zhong MY, Cea M, Tannenbaum D, Cagnetta A, Reagan M, Munshi AA, Senapedis W, Saint-Martin JR, Kashyap T, Shacham S, Kauffman M, Gu Y, Wu L, Ghobrial I, Zhan F, Kung AL, Schey SA, Richardson P, Munshi NC, Anderson KC. CRM1 inhibition induces tumor cell cytotoxicity and impairs osteoclastogenesis in multiple myeloma: molecular mechanisms and therapeutic implications. Leukemia 2014;28:155-65.
84. Liu X, Chong Y, Tu Y, Liu N, Yue C, Qi Z, Liu H, Yao Y, Liu H, Gao S, Niu M, Yu R. CRM1/XPO1 is associated with clinical outcome in glioma and represents a therapeutic target by perturbing multiple core pathways. J Hematol Oncol 2016;9:108.
85. Shen A, Wang Y, Zhao Y, Zou L, Sun L, Cheng C. Expression of CRM1 in human gliomas and its significance in p27 expression and clinical prognosis. Neurosurgery 2009;65:153-9.
86. Akagi I, Okayama H, Schetter AJ, Robles AI, Kohno T, Bowman ED, Kazandjian D, Welsh JA, Oue N, Saito M, Miyashita M, Uchida E, Takizawa T, Takenoshita S, Skaug V, Mollerup S, Haugen A, Yokota J, Harris CC. Combination of protein coding and noncoding gene expression as a robust prognostic classifier in stage I lung adenocarcinoma. Cancer Res 2013;73:3821-32.
87. Sun YQ, Xie JW, Xie HT, Chen PC, Zhang XL, Zheng CH, Li P, Wang JB, Lin JX, Cao LL, Huang CM, Lin Y. Expression of CRM1 and CDK5 shows high prognostic accuracy for gastric cancer. World J Gastroenterol 2017;23:2012-22.
88. Zhou F, Qiu W, Yao R, Xiang J, Sun X, Liu S, Lv J, Yue L. CRM1 is a novel independent prognostic factor for the poor prognosis of gastric carcinomas. Med Oncol 2013;30:726.
89. Conforti F, Zhang X, Rao G, De Pas T, Yonemori Y, Rodriguez JA, McCutcheon JN, Rahhal R, Alberobello AT, Wang Y, Zhang YW, Guha U, Giaccone G. Therapeutic effects of XPO1 inhibition in thymic epithelial tumors. Cancer Res 2017;77:5614-27.
90. Noske A, Weichert W, Niesporek S, Röske A, Buckendahl AC, Koch I, Sehouli J, Dietel M, Denkert C. Expression of the nuclear export protein chromosomal region maintenance/exportin 1/Xpo1 is a prognostic factor in human ovarian cancer. Cancer 2008;112:1733-43.
91. Xie QL, Liu Y, Zhu Y. Chromosome region maintenance 1 expression and its association with clinical pathological features in primary carcinoma of the liver. Exp Ther Med 2016;12:59-68.
92. Yang X, Cheng L, Yao L, Ren H, Zhang S, Min X, Chen X, Zhang J, Li M. Involvement of chromosome region maintenance 1 (CRM1) in the formation and progression of esophageal squamous cell carcinoma. Med Oncol 2014;31:155.
93. van der Watt PJ, Zemanay W, Govender D, Hendricks DT, Parker MI, Leaner VD. Elevated expression of the nuclear export protein, Crm1 (exportin 1), associates with human oesophageal squamous cell carcinoma. Oncol Rep 2014;32:730-8.
94. Huang WY, Yue L, Qiu WS, Wang LW, Zhou XH, Sun YJ. Prognostic value of CRM1 in pancreas cancer. Clin Invest Med 2009;32:E315.
95. Inoue H, Kauffman M, Shacham S, Landesman Y, Yang J, Evans CP, Weiss RH. CRM1 blockade by selective inhibitors of nuclear export attenuates kidney cancer growth. J Urol 2013;189:2317-26.
96. Yue L, Sun ZN, Yao YS, Shen Z, Wang HB, Liu XP, Zhou F, Xiang JY, Yao RY, Niu HT. CRM1, a novel independent prognostic factor overexpressed in invasive breast carcinoma of poor prognosis. Oncol Lett 2018;15:7515-22.
97. Sun H, Lin DC, Cao Q, Guo X, Marijon H, Zhao Z, Gery S, Xu L, Yang H, Pang B, Lee VK, Lim HJ, Doan N, Said JW, Chu P, Mayakonda A, Thomas T, Forscher C, Baloglu E, Shacham S, Rajalingam R, Koeffler HP. CRM1 Inhibition promotes cytotoxicity in ewing sarcoma cells by repressing EWS-FLI1-dependent IGF-1 signaling. Cancer Res 2016;76:2687-97.
98. Yao Y, Dong Y, Lin F, Zhao H, Shen Z, Chen P, Sun YJ, Tang LN, Zheng SE. The expression of CRM1 is associated with prognosis in human osteosarcoma. Oncol Rep 2009;21:229-35.

99. Pathria G, Wagner C, Wagner SN. Inhibition of CRM1-mediated nucleocytoplasmic transport: triggering human melanoma cell apoptosis by perturbing multiple cellular pathways. J Invest Dermatol 2012;132:2780-90.
100. Jardin F, Pujals A, Pelletier L, Bohers E, Camus V, Mareschal S, Dubois S, Sola B, Ochmann M, Lemonnier F, Viailly PJ, Bertrand P, Maingonnat C, Traverse-Glehen A, Gaulard P, Damotte D, Delarue R, Haioun C, Argueta C, Landesman Y, Salles G, Jais JP, Figeac M, Copie-Bergman C, Molina TJ, Picquenot JM, Cornic M, Fest T, Milpied N, Lemasle E, Stamatoullas A, Moeller P, Dyer MJ, Sundstrom C, Bastard C, Tilly H, Leroy K. Recurrent mutations of the exportin 1 gene (XPO1) and their impact on selective inhibitor of nuclear export compounds sensitivity in primary mediastinal B-cell lymphoma. Am J Hematol 2016;91:923-30.
101. Cosson A, Chapiro E, Bougacha N, Lambert J, Herbi L, Cung HA, Algrin C, Keren B, Damm F, Gabillaud C, Brunelle-Navas MN, Davi F Merle-Béral H, Le Garff-Tavernier M, Roos-Weil D, Choquet S, Uzunov M, Morel V, Leblond V, Maloum K, Lepretre S, Feugier P, Lesty C, Lejeune J, Sutton L, Landesman Y, Susin SA, Nguyen-Khac F. Gain in the short arm of chromosome 2 (2p+) induces gene overexpression and drug resistance in chronic lymphocytic leukemia: analysis of the central role of XPO1. Leukemia 2017;31:1625-29.
102. Golomb L, Bublik DR, Wilder S, Nevo R, Kiss V, Grabusic K, Volarevic S, Oren M. Importin 7 and exportin 1 link c-Myc and p53 to regulation of ribosomal biogenesis. Mol Cell 2012;45:222-32.
103. van der Watt PJ, Leaner VD. The nuclear exporter, Crm1, is regulated by NFY and Sp1 in cancer cells and repressed by p53 in response to DNA damage. Biochim Biophys Acta 2011;1809:316-26.
104. Camus V, Stamatoullas A, Mareschal S, Viailly PJ, Sarafan-Vasseur N, Bohers E, Dubois S, Picquenot JM, Ruminy P, Maingonnat C, Bertrand P, Cornic M, Tallon-Simon V, Becker S, Veresezan L, Frebourg T, Vera P, Bastard C, Tilly H, Jardin F. Detection and prognostic value of recurrent exportin 1 mutations in tumor and cell-free circulating DNA of patients with classical Hodgkin lymphoma. Haematologica 2016;101:1094-101.
105. Puente XS, Pinyol M, Quesada V, Conde L, Ordóñez GR, Villamor N, Escaramis G, Jares P, Beà S, González-Díaz M, Bassaganyas L, Baumann T, Juan M, López-Guerra M, Colomer D, Tubío JM, López C, Navarro A, Tornador C, Aymerich M, Rozman M, Hernández JM, Puente DA, Freije JM, Velasco G, Gutiérrez-Fernández A, Costa D, Carrió A, Guijarro S, Enjuanes A, Hernández L, Yagüe J, Nicolás P, Romeo-Casabona CM, Himmelbauer H, Castillo E, Dohm JC, de Sanjosé S, Piris MA, de Alava E, San Miguel J, Royo R, Gelpí JL, Torrents D, Orozco M, Pisano DG, Valencia A, Guigó R, Bayés M, Heath S, Gut M, Klatt P, Marshall J, Raine K, Stebbings LA, Futreal PA, Stratton MR, Campbell PJ, Gut I, López-Guillermo A, Estivill X, Montserrat E, López-Otín C, Campo E. Whole-genome sequencing identifies recurrent mutations in chronic lymphocytic leukaemia. Nature 2011;475:101-5.
106. Quesada V, Conde L, Villamor N, Ordóñez GR, Jares P, Bassaganyas L, Ramsay AJ, Beà S, Pinyol M, Martínez-Trillos A, López-Guerra M, Colomer D, Navarro A, Baumann T, Aymerich M, Rozman M, Delgado J, Giné E, Hernández JM, González-Díaz M, Puente DA, Velasco G, Freije JM, Tubío JM, Royo R, Gelpí JL, Orozco M, Pisano DG, Zamora J, Vázquez M, Valencia A, Himmelbauer H, Bayés M, Heath S, Gut M, Gut I, Estivill X, López-Guillermo A, Puente XS, Campo E, López-Otín C. Exome sequencing identifies recurrent mutations of the splicing factor SF3B1 gene in chronic lymphocytic leukemia. Nat Genet 2011;44:47-52.
107. Balatti V, Bottoni A, Palamarchuk A, Alder H, Rassenti LZ, Kipps TJ, Pekarsky Y, Croce CM. NOTCH1 mutations in CLL associated with trisomy 12. Blood 2012;119:329-31.
108. Landau DA, Carter SL, Stojanov P, McKenna A, Stevenson K, Lawrence MS, Sougnez C, Stewart C, Sivachenko A, Wang L, Wan Y, Zhang W, Shukla SA, Vartanov A, Fernandes SM, Saksena G, Cibulskis K, Tesar B, Gabriel S, Hacohen N, Meyerson M, Lander ES, Neuberg D, Brown JR, Getz G, Wu CJ. Evolution and impact of subclonal mutations in chronic lymphocytic leukemia. Cell 2013;152:714-26.
109. Jeromin S, Weissmann S, Haferlach C, Dicker F, Bayer K, Grossmann V, Alpermann T, Roller A, Kohlmann A, Haferlach T, Kern W, Schnittger S. SF3B1 mutations correlated to cytogenetics and mutations in NOTCH1, FBXW7, MYD88, XPO1 and TP53 in 1160 untreated CLL patients. Leukemia 2014;28:108-17.
110. Messina M, Del Giudice I, Khiabanian H, Rossi D, Chiaretti S, Rasi S, Spina V, Holmes AB, Marinelli M, Fabbri G, Piciocchi A, Mauro FR, Guarini A, Gaidano G, Dalla-Favera R, Pasqualucci L, Rabadan R, Foà R. Genetic lesions associated with chronic lymphocytic leukemia chemo-refractoriness. Blood 2014;123:2378-88.
111. Damm F, Mylonas E, Cosson A, Yoshida K, Della Valle V, Mouly E, Diop M, Scourzic L, Shiraishi Y, Chiba K, Tanaka H, Miyano S, Kikushige Y, Davi F, Lambert J, Gautheret D, Merle-Béral H, Sutton L, Dessen P, Solary E, Akashi K, Vainchenker W, Mercher T, Droin N, Ogawa S, Nguyen-Khac F, Bernard OA. Acquired initiating mutations in early hematopoietic cells of CLL patients. Cancer Discov 2014;4:1088-101.
112. Lawrence MS, Stojanov P, Mermel CH, Robinson JT, Garraway LA, Golub TR, Meyerson M, Gabriel SB, Lander ES, Getz G. Discovery and saturation analysis of cancer genes across 21 tumour types. Nature 2014;505:495-501.
113. Ojha J, Ayres J, Secreto C, Tschumper R, Rabe K, Van Dyke D, Slager S, Shanafelt T, Fonseca R, Kay NE, Braggio E. Deep sequencing identifies genetic heterogeneity and recurrent convergent evolution in chronic lymphocytic leukemia. Blood 2015;125:492-8.
114. Vollbrecht C, Mairinger FD, Koitzsch U, Peifer M, Koenig K, Heukamp LC, Crispatzu G, Wilden L, Kreuzer KA, Hallek M, Odenthal M, Herling CD, Buettner R. Comprehensive analysis of disease-related genes in chronic lymphocytic leukemia by multiplex PCR-based next generation sequencing. PLoS One 2015;10:e0129544.
115. Landau DA, Tausch E, Taylor-Weiner AN, Stewart C, Reiter JG, Bahlo J, Kluth S, Bozic I, Lawrence M, Böttcher S, Carter SL, Cibulskis K, Mertens D, Sougnez CL, Rosenberg M, Hess JM, Edelmann J, Kless S, Kneba M, Ritgen M, Fink A, Fischer K, Gabriel S, Lander ES, Nowak MA, Döhner H, Hallek M, Neuberg D, Getz G, Stilgenbauer S, Wu CJ. Mutations driving CLL and their evolution in progression and relapse. Nature 2015;526:525-30.
116. Guièze R, Robbe P, Clifford R, de Guibert S, Pereira B, Timbs A, Dilhuydy MS, Cabes M, Ysebaert L, Burns A, Nguyen-Khac F, Davi F, Véronèse L, Combes P, Le Garff-Tavernier M, Leblond V, Merle-Béral H, Alsolami R, Hamblin A, Mason J, Pettitt A, Hillmen P, Taylor

J, Knight SJ, Tournilhac O, Schuh A. Presence of multiple recurrent mutations confers poor trial outcome of relapsed/refractory CLL. Blood 2015;126:2110-7.

117. Hernández JÁ, Hernández-Sánchez M, Rodríguez-Vicente AE, Grossmann V, Collado R, Heras C, Puiggros A, Martín AÁ, Puig N, Benito R, Robledo C, Delgado J, González T, Queizán JA, Galende J, de la Fuente I, Martín-Núñez G, Alonso JM, Abrisqueta P, Luño E, Marugán I, González-Gascón I, Bosch F, Kohlmann A, González M, Espinet B, Hernández-Rivas JM; Grupo Cooperativo Español de Citogenética Hematológica (GCECGH) and Grupo Español de Leucemia Linfática Crónica (GELLC). A low frequency of losses in 11q chromosome is associated with better outcome and lower rate of genomic mutations in patients with chronic lymphocytic leukemia. PLoS One 2015;10:e0143073.
118. Sutton LA, Ljungström V, Mansouri L, Young E, Cortese D, Navrkalova V, Malcikova J, Muggen AF, Trbusek M, Panagiotidis P, Davi F, Belessi C, Langerak AW, Ghia P, Pospisilova S, Stamatopoulos K, Rosenquist R. Targeted next-generation sequencing in chronic lymphocytic leukemia: a high-throughput yet tailored approach will facilitate implementation in a clinical setting. Haematologica 2015;100:370-6.
119. Amin NA, Seymour E, Saiya-Cork K, Parkin B, Shedden K, Malek SN. A quantitative analysis of subclonal and clonal gene mutations before and after therapy in chronic lymphocytic leukemia. Clin Cancer Res 2016;22:4525-35.
120. Jain P, Kanagal-Shamanna R, Wierda W, Keating M, Sarwari N, Rozovski U, Thompson P, Burger J, Kantarjian H, Patel KP, Medeiros LJ, Luthra R, Estrov Z. Clinical and molecular characteristics of XPO1 mutations in patients with chronic lymphocytic leukemia. Am J Hematol 2016;91:E478-9.
121. Quijada-Álamo M, Hernández-Sánchez M, Robledo C, Hernández-Sánchez JM, Benito R, Montaño A, Rodríguez-Vicente AE, Quwaider D, Martín AÁ, García-Álvarez M, Vidal-Manceñido MJ, Ferrer-Garrido G, Delgado-Beltrán MP, Galende J, Rodríguez JN, Martín-Núñez G, Alonso JM, García de Coca A, Queizán JA, Sierra M, Aguilar C, Kohlmann A, Hernández JÁ, González M, Hernández-Rivas JM. Next-generation sequencing and FISH studies reveal the appearance of gene mutations and chromosomal abnormalities in hematopoietic progenitors in chronic lymphocytic leukemia. J Hematol Oncol 2017;10:83.
122. Takahashi K, Hu B, Wang F, Yan Y, Kim E, Vitale C, Patel KP, Strati P, Gumbs C, Little L, Tippen S, Song X, Zhang J, Jain N, Thompson P, Garcia-Manero G, Kantarjian H, Estrov Z, Do KA, Keating M, Burger JA, Wierda WG, Futreal PA, Ferrajoli A. Clinical implications of cancer gene mutations in patients with chronic lymphocytic leukemia treated with lenalidomide. Blood 2018;131:1820-32.
123. Dubois S, Viailly PJ, Mareschal S, Bohers E, Bertrand P, Ruminy P, Maingonnat C, Jais JP, Peyrouze P, Figeac M, Molina TJ, Desmots F, Fest T, Haioun C, Lamy T, Copie-Bergman C, Brière J, Petrella T, Canioni D, Fabiani B, Coiffier B, Delarue R, Peyrade F, Bosly A, André M, Ketterer N, Salles G, Tilly H, Leroy K, Jardin F. Next-generation sequencing in diffuse large B-cell lymphoma highlights molecular divergence and therapeutic opportunities: a LYSA study. Clin Cancer Res 2016;22:2919-28.
124. Tiacci E, Ladewig E, Schiavoni G, Penson A, Fortini E, Pettirossi V, Wang Y, Rosseto A, Venanzi A, Vlasevska S, Pacini R, Piattoni S, Tabarrini A, Pucciarini A, Bigerna B, Santi A, Gianni AM, Viviani S, Cabras A, Ascani S, Crescenzi B, Mecucci C, Pasqualucci L, Rabadan R, Falini B. Pervasive mutations of JAK-STAT pathway genes in classical Hodgkin lymphoma. Blood 2018;131:2454-65.
125. Camus V, Miloudi H, Taly A, Sola B, Jardin F. XPO1 in B cell hematological malignancies: from recurrent somatic mutations to targeted therapy. J Hematol Oncol. 2017;10:47.
126. Lin DC, Hao JJ, Nagata Y, Xu L, Shang L, Meng X, Sato Y, Okuno Y, Varela AM, Ding LW, Garg M, Liu LZ, Yang H, Yin D, Shi ZZ, Jiang YY, Gu WY, Gong T, Zhang Y, Xu X, Kalid O, Shacham S, Ogawa S, Wang MR, Koeffler HP. Genomic and molecular characterization of esophageal squamous cell carcinoma. Nat Genet 2014;46:467-73.
127. Pitt SC, Hernandez RA, Nehs MA, Gawande AA, Moore FD Jr, Ruan DT, Cho NL. Identification of novel oncogenic mutations in thyroid cancer. J Am Coll Surg 2016;222:1036-43.
128. Newlands ES, Rustin GJ, Brampton MH. Phase I trial of elactocin. Br J Cancer 1996;74:648-9.
129. Druker BJ, Tamura S, Buchdunger E, Ohno S, Segal GM, Fanning S, Zimmermann J, Lydon NB. Effects of a selective inhibitor of the Abl tyrosine kinase on the growth of Bcr-Abl positive cells. Nat Med 1996;2:561-6.
130. le Coutre P, Mologni L, Cleris L, Marchesi E, Buchdunger E, Giardini R, Formelli F, Gambacorti-Passerini C. In vivo eradication of human BCR/ABL-positive leukemia cells with an ABL kinase inhibitor. J Natl Cancer Inst 1999;91:163-8.
131. Vigneri P, Wang JY. Induction of apoptosis in chronic myelogenous leukemia cells through nuclear entrapment of BCR-ABL tyrosine kinase. Nat Med 2001;7:228-34.
132. Kancha RK, von Bubnoff N, Miething C, Peschel C, Götze KS, Duyster J. Imatinib and leptomycin B are effective in overcoming imatinib-resistance due to Bcr-Abl amplification and clonal evolution but not due to Bcr-Abl kinase domain mutation. Haematologica. 2008;93:1718-22.
133. Senapedis WT, Baloglu E, Landesman Y. Clinical translation of nuclear export inhibitors in cancer. Semin Cancer Biol 2014;27:74-86.
134. Sakakibara K, Saito N, Sato T, Suzuki A, Hasegawa Y, Friedman JM, Kufe DW, Vonhoff DD, Iwami T, Kawabe T. CBS9106 is a novel reversible oral CRM1 inhibitor with CRM1 degrading activity. Blood 2011;118:3922-31.
135. Turner JG, Marchion DC, Dawson JL, Emmons MF, Hazlehurst LA, Washausen P, Sullivan DM. Human multiple myeloma cells are sensitized to topoisomerase II inhibitors by CRM1 inhibition. Cancer Res 2009;69:6899-905.
136. Kalid O, Toledo Warshaviak D, Shechter S, Sherman W, Shacham S. Consensus Induced Fit Docking (cIFD): methodology, validation, and application to the discovery of novel Crm1 inhibitors. J Comput Aided Mol Des 2012;26:1217-28.
137. Lapalombella R, Sun Q, Williams K, Tangeman L, Jha S, Zhong Y, Goettl V, Mahoney E, Berglund C, Gupta S, Farmer A, Mani R, Johnson AJ, Lucas D, Mo X, Daelemans D, Sandanayaka V, Shechter S, McCauley D, Shacham S, Kauffman M, Chook YM, Byrd JC. Selective inhibitors of nuclear export show that CRM1/XPO1 is a target in chronic lymphocytic leukemia. Blood 2012;120:4621-34.
138. Turner JG, Dawson J, Emmons MF, Cubitt CL, Kauffman M, Shacham S, Hazlehurst LA, Sullivan DM. CRM1 inhibition sensitizes

drug resistant human myeloma cells to topoisomerase II and proteasome inhibitors both in vitro and ex vivo. J Cancer 2013;4:614-25.
139. Rosebeck S, Alonge MM, Kandarpa M, Mayampurath A, Volchenboum SL, Jasielec J, Dytfeld D, Maxwell SP, Kraftson SJ, McCauley D, Shacham S, Kauffman M, Jakubowiak AJ. Synergistic myeloma cell death via novel intracellular activation of caspase-10-dependent apoptosis by carfilzomib and selinexor. Mol Cancer Ther 2016;15:60-71.
140. Turner JG, Dawson JL, Grant S, Shain KH, Dalton WS, Dai Y, Meads M, Baz R, Kauffman M, Shacham S, Sullivan DM. Treatment of acquired drug resistance in multiple myeloma by combination therapy with XPO1 and topoisomerase II inhibitors. J Hematol Oncol 2016;9:73.
141. Turner JG, Kashyap T, Dawson JL, Gomez J, Bauer AA, Grant S, Dai Y, Shain KH, Meads M, Landesman Y, Sullivan DM. XPO1 inhibitor combination therapy with bortezomib or carfilzomib induces nuclear localization of IκBα and overcomes acquired proteasome inhibitor resistance in human multiple myeloma. Oncotarget 2016;7:78896-909.
142. Muz B, Azab F, de la Puente P, Landesman Y, Azab AK. Selinexor overcomes hypoxia-induced drug resistance in multiple myeloma. Transl Oncol 2017;10:632-40.
143. Argueta C, Kashyap T, Klebanov B, Unger TJ, Guo C, Harrington S, Baloglu E, Lee M, Senapedis W, Shacham S, Landesman Y. Selinexor synergizes with dexamethasone to repress mTORC1 signaling and induce multiple myeloma cell death. Oncotarget 2018;9:25529-44.
144. Ranganathan P, Yu X, Na C, Santhanam R, Shacham S, Kauffman M, Walker A, Klisovic R, Blum W, Caligiuri M, Croce CM, Marcucci G, Garzon R. Preclinical activity of a novel CRM1 inhibitor in acute myeloid leukemia. Blood 2012;120:1765-73.
145. Etchin J, Sun Q, Kentsis A, Farmer A, Zhang ZC, Sanda T, Mansour MR, Barcelo C, McCauley D, Kauffman M, Shacham S, Christie AL, Kung AL, Rodig SJ, Chook YM, Look AT. Antileukemic activity of nuclear export inhibitors that spare normal hematopoietic cells. Leukemia 2013;27:66-74.
146. Ranganathan P, Yu X, Santhanam R, Hofstetter J, Walker A, Walsh K, Bhatnagar B, Klisovic R, Vasu S, Phelps MA, Devine S, Shacham S, Kauffman M, Marcucci G, Blum W, Garzon R. Decitabine priming enhances the antileukemic effects of exportin 1 (XPO1) selective inhibitor selinexor in acute myeloid leukemia. Blood 2015;125:2689-92.
147. Zhang W, Ly C, Ishizawa J, Mu H, Ruvolo V, Shacham S, Daver N, Andreeff M. Combinatorial targeting of XPO1 and FLT3 exerts synergistic anti-leukemia effects through induction of differentiation and apoptosis in FLT3-mutated acute myeloid leukemias: from concept to clinical trial. Haematologica 2018; doi: 10.3324/haematol.2017.185082.
148. Etchin J, Sanda T, Mansour MR, Kentsis A, Montero J, Le BT, Christie AL, McCauley D, Rodig SJ, Kauffman M, Shacham S, Stone R, Letai A, Kung AL, Thomas Look A. KPT-330 inhibitor of CRM1 (XPO1)-mediated nuclear export has selective anti-leukaemic activity in preclinical models of T-cell acute lymphoblastic leukaemia and acute myeloid leukaemia. Br J Haematol 2013;161:117-27.
149. Zhong Y, El-Gamal D, Dubovsky JA, Beckwith KA, Harrington BK, Williams KE, Goettl VM, Jha S, Mo X, Jones JA, Flynn JM, Maddocks KJ, Andritsos LA, McCauley D, Shacham S, Kauffman M, Byrd JC, Lapalombella R. Selinexor suppresses downstream effectors of B-cell activation, proliferation and migration in chronic lymphocytic leukemia cells. Leukemia 2014;28:1158-63.
150. Hing ZA, Mantel R, Beckwith KA, Guinn D, Williams E, Smith LL, Williams K, Johnson AJ, Lehman AM, Byrd JC, Woyach JA, Lapalombella R. Selinexor is effective in acquired resistance to ibrutinib and synergizes with ibrutinib in chronic lymphocytic leukemia. Blood 2015;125:3128-32.
151. Walker CJ, Oaks JJ, Santhanam R, Neviani P, Harb JG, Ferenchak G, Ellis JJ, Landesman Y, Eisfeld AK, Gabrail NY, Smith CL, Caligiuri MA, Hokland P, Roy DC, Reid A, Milojkovic D, Goldman JM, Apperley J, Garzon R, Marcucci G, Shacham S, Kauffman MG, Perrotti D. Preclinical and clinical efficacy of XPO1/CRM1 inhibition by the karyopherin inhibitor KPT-330 in Ph+ leukemias. Blood 2013;122:3034-44.
152. Nie D, Huang K, Yin S, Li Y, Xie S, Ma L, Wang X, Wu Y, Xiao J, Wang J, Yang W, Liu H. KPT-330 inhibition of chromosome region maintenance 1 is cytotoxic and sensitizes chronic myeloid leukemia to Imatinib. Cell Death Discov 2018;4:48.
153. Zhang K, Wang M, Tamayo AT, Shacham S, Kauffman M, Lee J, Zhang L, Ou Z, Li C, Sun L, Ford RJ, Pham LV. Novel selective inhibitors of nuclear export CRM1 antagonists for therapy in mantle cell lymphoma. Exp Hematol 2013;41:67-78.e4.
154. Sekihara K, Saitoh K, Han L, Ciurea S, Yamamoto S, Kikkawa M, Kazuno S, Taka H, Kaga N, Arai H, Miida T, Andreeff M, Konopleva M, Tabe Y. Targeting mantle cell lymphoma metabolism and survival through simultaneous blockade of mTOR and nuclear transporter exportin-1. Oncotarget 2017;8:34552-64.
155. Azmi AS, Al-Katib A, Aboukameel A, McCauley D, Kauffman M, Shacham S, Mohammad RM. Selective inhibitors of nuclear export for the treatment of non-Hodgkin's lymphomas. Haematologica 2013;98:1098-106.
156. Han X, Wang J, Shen Y, Zhang N, Wang S, Yao J, Shi Y. CRM1 as a new therapeutic target for non-Hodgkin lymphoma. Leuk Res 2015;39:38-46.
157. Muqbil I, Aboukameel A, Elloul S, Carlson R, Senapedis W, Baloglu E, Kauffman M, Shacham S, Bhutani D, Zonder J, Azmi AS, Mohammad RM. Anti-tumor activity of selective inhibitor of nuclear export (SINE) compounds, is enhanced in non-Hodgkin lymphoma through combination with mTOR inhibitor and dexamethasone. Cancer Lett 2016;383:309-17.
158. Wettersten HI, Landesman Y, Friedlander S, Shacham S, Kauffman M, Weiss RH. Specific inhibition of the nuclear exporter exportin-1 attenuates kidney cancer growth. PLoS One 2014;9:e113867.
159. Mendonca J, Sharma A, Kim HS, Hammers H, Meeker A, De Marzo A, Carducci M, Kauffman M, Shacham S, Kachhap S. Selective inhibitors of nuclear export (SINE) as novel therapeutics for prostate cancer. Oncotarget 2014;5:6102-12.
160. Gravina GL, Tortoreto M, Mancini A, Addis A, Di Cesare E, Lenzi A, Landesman Y, McCauley D, Kauffman M, Shacham S, Zaffaroni N, Festuccia C. XPO1/CRM1-selective inhibitors of nuclear export (SINE) reduce tumor spreading and improve overall survival in preclinical models of prostate cancer (PCa). J Hematol Oncol 2014;7:46.

161. Gravina GL, Mancini A, Colapietro A, Marampon F, Sferra R, Pompili S, Biordi LA, Iorio R, Flati V, Argueta C, Landesman Y, Kauffman M, Shacham S, Festuccia C. Pharmacological treatment with inhibitors of nuclear export enhances the antitumor activity of docetaxel in human prostate cancer. Oncotarget 2017;8:111225-45.
162. Cheng Y, Holloway MP, Nguyen K, McCauley D, Landesman Y, Kauffman MG, Shacham S, Altura RA. XPO1 (CRM1) inhibition represses STAT3 activation to drive a survivin-dependent oncogenic switch in triple-negative breast cancer. Mol Cancer Ther 2014;13:675-86.
163. Wrobel K, Zhao YC, Kulkoyluoglu E, Chen KL, Hieronymi K, Holloway J, Li S, Ray T, Ray PS, Landesman Y, Lipka AE, Smith RL, Madak-Erdogan Z. ERα-XPO1 cross talk controls tamoxifen sensitivity in tumors by altering ERK5 cellular localization. Mol Endocrinol 2016;30:1029-45.
164. Arango NP, Yuca E, Zhao M, Evans KW, Scott S, Kim C, Gonzalez-Angulo AM, Janku F, Ueno NT, Tripathy D, Akcakanat A, Naing A, Meric-Bernstam F. Selinexor (KPT-330) demonstrates anti-tumor efficacy in preclinical models of triple-negative breast cancer. Breast Cancer Res 2017;19:93.
165. Miyake T, Pradeep S, Wu SY, Rupaimoole R, Zand B, Wen Y, Gharpure KM, Nagaraja AS, Hu W, Cho MS, Dalton HJ, Previs RA, Taylor ML, Hisamatsu T, Kang Y, Liu T, Shacham S, McCauley D, Hawke DH, Wiktorowicz JE, Coleman RL, Sood AK. XPO1/CRM1 inhibition causes antitumor effects by mitochondrial accumulation of eIF5A. Clin Cancer Res 2015;21:3286-97.
166. Chen Y, Camacho SC, Silvers TR, Razak AR, Gabrail NY, Gerecitano JF, Kalir E, Pereira E, Evans BR, Ramus SJ, Huang F, Priedigkeit N, Rodriguez E, Donovan M, Khan F, Kalir T, Sebra R, Uzilov A, Chen R, Sinha R, Halpert R, Billaud JN, Shacham S, McCauley D, Landesman Y, Rashal T, Kauffman M, Mirza MR, Mau-Sørensen M, Dottino P, Martignetti JA. Inhibition of the nuclear export receptor XPO1 as a therapeutic target for platinum-resistant ovarian cancer. Clin Cancer Res 2017;23:1552-63.
167. Corno C, Stucchi S, De Cesare M, Carenini N, Stamatakos S, Ciusani E, Minoli L, Scanziani E, Argueta C, Landesman Y, Zaffaroni N, Gatti L, Perego P. FoxO-1 contributes to the efficacy of the combination of the XPO1 inhibitor selinexor and cisplatin in ovarian carcinoma preclinical models. Biochem Pharmacol 2018;147:93-103.
168. Ferreiro-Neira I, Torres NE, Liesenfeld LF, Chan CH, Penson T, Landesman Y, Senapedis W, Shacham S, Hong TS, Cusack JC. XPO1 inhibition enhances radiation response in preclinical models of rectal cancer. Clin Cancer Res 2016;22:1663-73.
169. Zheng Y, Gery S, Sun H, Shacham S, Kauffman M, Koeffler HP. KPT-330 inhibitor of XPO1-mediated nuclear export has anti-proliferative activity in hepatocellular carcinoma. Cancer Chemother Pharmacol 2014;74:487-95.
170. Azmi AS, Aboukameel A, Bao B, Sarkar FH, Philip PA, Kauffman M, Shacham S, Mohammad RM. Selective inhibitors of nuclear export block pancreatic cancer cell proliferation and reduce tumor growth in mice. Gastroenterology 2013;144:447-56.
171. Gao J, Azmi AS, Aboukameel A, Kauffman M, Shacham S, Abou-Samra AB, Mohammad RM. Nuclear retention of Fbw7 by specific inhibitors of nuclear export leads to Notch1 degradation in pancreatic cancer. Oncotarget 2014;5:3444-54.
172. Kazim S, Malafa MP, Coppola D, Husain K, Zibadi S, Kashyap T, Crochiere M, Landesman Y, Rashal T, Sullivan DM, Mahipal A. Selective nuclear export inhibitor KPT-330 enhances the antitumor activity of gemcitabine in human pancreatic cancer. Mol Cancer Ther 2015;14:1570-81.
173. Azmi AS, Li Y, Muqbil I, Aboukameel A, Senapedis W, Baloglu E, Landesman Y, Shacham S, Kauffman MG, Philip PA, Mohammad RM. Exportin 1 (XPO1) inhibition leads to restoration of tumor suppressor miR-145 and consequent suppression of pancreatic cancer cell proliferation and migration. Oncotarget 2017;8:82144-55.
174. Sun H, Hattori N, Chien W, Sun Q, Sudo M, E-Ling GL, Ding L, Lim SL, Shacham S, Kauffman M, Nakamaki T, Koeffler HP. KPT-330 has antitumour activity against non-small cell lung cancer. Br J Cancer 2014;111:281-91.
175. Wang S, Han X, Wang J, Yao J, Shi Y. Antitumor effects of a novel chromosome region maintenance 1 (CRM1) inhibitor on non-small cell lung cancer cells in vitro and in mouse tumor xenografts. PLoS One 2014;9:e89848.
176. Kim J, McMillan E, Kim HS, Venkateswaran N, Makkar G, Rodriguez-Canales J, Villalobos P, Neggers JE, Mendiratta S, Wei S, Landesman Y, Senapedis W, Baloglu E, Chow CB, Frink RE, Gao B, Roth M, Minna JD, Daelemans D, Wistuba II, Posner BA, Scaglioni PP, White MA. XPO1-dependent nuclear export is a druggable vulnerability in KRAS-mutant lung cancer. Nature 2016;538:114-7.
177. Garg M, Kanojia D, Mayakonda A, Ganesan TS, Sadhanandhan B, Suresh S, Sneha S, Nagare RP, Said JW, Doan NB, Ding LW, Baloglu E, Shacham S, Kauffman M, Koeffler HP. Selinexor (KPT-330) has antitumor activity against anaplastic thyroid carcinoma in vitro and in vivo and enhances sensitivity to doxorubicin. Sci Rep 2017;7:9749.
178. Garg M, Kanojia D, Mayakonda A, Said JW, Doan NB, Chien W, Ganesan TS, Chuang LS, Venkatachalam N, Baloglu E, Shacham S, Kauffman M, Koeffler HP. Molecular mechanism and therapeutic implications of selinexor (KPT-330) in liposarcoma. Oncotarget 2017;8:7521-32.
179. Kashyap T, Argueta C, Aboukameel A, Unger TJ, Klebanov B, Mohammad RM, Muqbil I, Azmi AS, Drolen C, Senapedis W, Lee M, Kauffman M, Shacham S, Landesman Y. Selinexor, a selective inhibitor of nuclear export (SINE) compound, acts through NF-κB deactivation and combines with proteasome inhibitors to synergistically induce tumor cell death. Oncotarget 2016;7:78883-95.
180. Nakayama R, Zhang YX, Czaplinski JT, Anatone AJ, Sicinska ET, Fletcher JA, Demetri GD, Wagner AJ. Preclinical activity of selinexor, an inhibitor of XPO1, in sarcoma. Oncotarget 2016;7:16581-92.
181. Nair JS, Musi E, Schwartz GK. Selinexor (KPT-330) induces tumor suppression through nuclear sequestration of IκB and downregulation of Survivin. Clin Cancer Res 2017;23:4301-11.
182. De Cesare M, Cominetti D, Doldi V, Lopergolo A, Deraco M, Gandellini P, Friedlander S, Landesman Y, Kauffman MG, Shacham S, Pennati M, Zaffaroni N. Anti-tumor activity of selective inhibitors of XPO1/CRM1-mediated nuclear export in diffuse malignant peritoneal mesothelioma: the role of survivin. Oncotarget 2015;6:13119-32.

183. Green AL, Ramkissoon SH, McCauley D, Jones K, Perry JA, Hsu JH, Ramkissoon LA, Maire CL, Hubbell-Engler B, Knoff DS, Shacham S, Ligon KL, Kung AL. Preclinical antitumor efficacy of selective exportin 1 inhibitors in glioblastoma. Neuro Oncol 2015;17:697-707.
184. Wahba A, Rath BH, O'Neill JW, Camphausen K, Tofilon PJ. The XPO1 inhibitor selinexor inhibits translation and enhances the radiosensitivity of glioblastoma cells grown in vitro and in vivo. Mol Cancer Ther 2018;17:1717-26.
185. Salas-Fragomeni RA, Chung HW, Landesman Y, Senapedis W, Saint-Martin JR, Tsao H, Flaherty KT, Shacham S, Kauffman M, Cusack JC. CRM1 and BRAF inhibition synergize and induce tumor regression in BRAF-mutant melanoma. Mol Cancer Ther 2013;12:1171-9.
186. Yang J, Bill MA, Young GS, La Perle K, Landesman Y, Shacham S, Kauffman M, Senapedis W, Kashyap T, Saint-Martin JR, Kendra K, Lesinski GB. Novel small molecule XPO1/CRM1 inhibitors induce nuclear accumulation of TP53, phosphorylated MAPK and apoptosis in human melanoma cells. PLoS One 2014;9:e102983.
187. Burke RT, Marcus JM, Orth JD. Inhibition of exportin-1 function results in rapid cell cycle-associated DNA damage in cancer cells. Oncotarget 2017;8:39460-75.
188. Attiyeh EF, Maris JM, Lock R, Reynolds CP, Kang MH, Carol H, Gorlick R, Kolb EA, Keir ST, Wu J, Landesman Y, Shacham S, Lyalin D, Kurmasheva RT, Houghton PJ, Smith MA. Pharmacodynamic and genomic markers associated with response to the XPO1/CRM1 inhibitor selinexor (KPT-330): a report from the pediatric preclinical testing program. Pediatr Blood Cancer 2016;63:276-86.
189. Gandhi UH, Senapedis W, Baloglu E, Unger TJ, Chari A, Vogl D, Cornell RF. Clinical implications of targeting XPO1-mediated nuclear export in multiple myeloma. Clin Lymphoma Myeloma Leuk 2018;18:335-45.
190. Haines JD, Herbin O, de la Hera B, Vidaurre OG, Moy GA, Sun Q, Fung HY, Albrecht S, Alexandropoulos K, McCauley D, Chook YM, Kuhlmann T, Kidd GJ, Shacham S, Casaccia P. Nuclear export inhibitors avert progression in preclinical models of inflammatory demyelination. Nat Neurosci 2015;18:511-20.
191. Pickens JA, Tripp RA. Verdinexor targeting of CRM1 is a promising therapeutic approach against RSV and influenza viruses. Viruses 2018;10: pii: E48.
192. Mahipal A, Malafa M. Importins and exportins as therapeutic targets in cancer. Pharmacol Ther 2016;164:135-43.
193. Abdul Razak AR, Mau-Soerensen M, Gabrail NY, Gerecitano JF, Shields AF, Unger TJ, Saint-Martin JR, Carlson R, Landesman Y, McCauley D, Rashal T, Lassen U, Kim R, Stayner LA, Mirza MR, Kauffman M, Shacham S, Mahipal A. First-in-class, first-in-human phase I study of selinexor, a selective inhibitor of nuclear export, in patients with advanced solid tumors. J Clin Oncol 2016;34:4142-50.
194. Gounder MM, Zer A, Tap WD, Salah S, Dickson MA, Gupta AA, Keohan ML, Loong HH, D'Angelo SP, Baker S, Condy M, Nyquist-Schultz K, Tanner L, Erinjeri JP, Jasmine FH, Friedlander S, Carlson R, Unger TJ, Saint-Martin JR, Rashal T, Ellis J, Kauffman M, Shacham S, Schwartz GK, Abdul Razak AR. Phase IB study of selinexor, a first-in-class inhibitor of nuclear export, in patients with advanced refractory bone or soft tissue sarcoma. J Clin Oncol 2016;34:3166-74.
195. Alexander TB, Lacayo NJ, Choi JK, Ribeiro RC, Pui CH, Rubnitz JE. Phase I study of selinexor, a selective inhibitor of nuclear export, in combination with fludarabine and cytarabine, in pediatric relapsed or refractory acute leukemia. J Clin Oncol 2016;34:4094-101.
196. Kuruvilla J, Savona M, Baz R, Mau-Sorensen PM, Gabrail N, Garzon R, Stone R, Wang M, Savoie L, Martin P, Flinn I, Jacoby M, Unger TJ, Saint-Martin JR, Rashal T, Friedlander S, Carlson R, Kauffman M, Shacham S, Gutierrez M. Selective inhibition of nuclear export with selinexor in patients with non-Hodgkin lymphoma. Blood 2017;129:3175-83.
197. Garzon R, Savona M, Baz R, Andreeff M, Gabrail N, Gutierrez M, Savoie L, Mau-Sorensen PM, Wagner-Johnston N, Yee K, Unger TJ, Saint-Martin JR, Carlson R, Rashal T, Kashyap T, Klebanov B, Shacham S, Kauffman M, Stone R. A phase 1 clinical trial of single-agent selinexor in acute myeloid leukemia. Blood 2017;129:3165-74.
198. Wang AY, Weiner H, Green M, Chang H, Fulton N, Larson RA, Odenike O, Artz AS, Bishop MR, Godley LA, Thirman MJ, Kosuri S, Churpek JE, Curran E, Pettit K, Stock W, Liu H. A phase I study of selinexor in combination with high-dose cytarabine and mitoxantrone for remission induction in patients with acute myeloid leukemia. J Hematol Oncol 2018;11:4.
199. Chen C, Siegel D, Gutierrez M, Jacoby M, Hofmeister CC, Gabrail N, Baz R, Mau-Sorensen M, Berdeja JG, Savona M, Savoie L, Trudel S, Areethamsirikul N, Unger TJ, Rashal T, Hanke T, Kauffman M, Shacham S, Reece D. Safety and efficacy of selinexor in relapsed or refractory multiple myeloma and Waldenstrom macroglobulinemia. Blood 2018;131:855-63.
200. Vogl DT, Dingli D, Cornell RF, Huff CA, Jagannath S, Bhutani D, Zonder J, Baz R, Nooka A, Richter J, Cole C, Vij R, Jakubowiak A, Abonour R, Schiller G, Parker TL, Costa LJ, Kaminetzky D, Hoffman JE, Yee AJ, Chari A, Siegel D, Fonseca R, Van Wier S, Ahmann G, Lopez I, Kauffman M, Shacham S, Saint-Martin JR, Picklesimer CD, Choe-Juliak C, Stewart AK. Selective inhibition of nuclear export with oral selinexor for treatment of relapsed or refractory multiple myeloma. J Clin Oncol 2018;36:859-66.
201. Wei XX, Siegel AP, Aggarwal R, Lin AM, Friedlander TW, Fong L, Kim W, Louttit M, Chang E, Zhang L, Ryan CJ. A phase II trial of selinexor, an oral selective inhibitor of nuclear export compound, in abiraterone- and/or enzalutamide-refractory metastatic castration-resistant prostate cancer. Oncologist 2018;23:656.
202. Machlus KR, Wu SK, Vijey P, Soussou TS, Liu ZJ, Shacham E, Unger TJ, Kashyap T, Klebanov B, Sola-Visner M, Crochiere M, Italiano JE Jr, Landesman Y. Selinexor-induced thrombocytopenia results from inhibition of thrombopoietin signaling in early megakaryopoiesis. Blood 2017;130:1132-43.
203. Hing ZA, Fung HY, Ranganathan P, Mitchell S, El-Gamal D, Woyach JA, Williams K, Goettl VM, Smith J, Yu X, Meng X, Sun Q, Cagatay T, Lehman AM, Lucas DM, Baloglu E, Shacham S, Kauffman MG, Byrd JC, Chook YM, Garzon R, Lapalombella R. Next-generation XPO1 inhibitor shows improved efficacy and in vivo tolerability in hematological malignancies. Leukemia 2016;30:2364-72.
204. Etchin J, Berezovskaya A, Conway AS, Galinsky IA, Stone RM, Baloglu E, Senapedis W, Landesman Y, Kauffman M, Shacham S, Wang JC, Look AT. KPT-8602, a second-generation inhibitor of XPO1-mediated nuclear export, is well tolerated and highly active

against AML blasts and leukemia-initiating cells. Leukemia 2017;31:143-50.
205. Vercruysse T, De Bie J, Neggers JE, Jacquemyn M, Vanstreels E, Schmid-Burgk JL, Hornung V, Baloglu E, Landesman Y, Senapedis W, Shacham S, Dagklis A, Cools J, Daelemans D. The second-generation exportin-1 inhibitor KPT-8602 demonstrates potent activity against acute lymphoblastic leukemia. Clin Cancer Res 2017;23:2528-41.
206. Pettersen EF, Goddard TD, Huang CC, Couch GS, Greenblatt DM, Meng EC, Ferrin TE. UCSF Chimera-a visualization system for exploratory research and analysis. J Comput Chem 2004;25:1605-12.
207. Dong X, Biswas A, Chook YM. Structural basis for assembly and disassembly of the CRM1 nuclear export complex. Nat Struct Mol Biol 2009;16:558-560.
208. Bardou P, Mariette J, Escudié F, Djemiel C, Klopp C. jvenn: an interactive Venn diagram viewer. BMC Bioinformatics 2014;15:293.

European Journal of Cell Biology 98 (2019) 12–26

Contents lists available at ScienceDirect

European Journal of Cell Biology

journal homepage: www.elsevier.com/locate/ejcb

Research paper

WDR20 regulates shuttling of the USP12 deubiquitinase complex between the plasma membrane, cytoplasm and nucleus

Anne Olazabal-Herrero[a], Maria Sendino[a], Ignacio Arganda-Carreras[b,c,d], Jose Antonio Rodríguez[a,*]

[a] Department of Genetics, Physical Anthropology and Animal Physiology, University of the Basque Country (UPV/EHU), Leioa 48940, Spain
[b] Computer Science and Artificial Intelligence Department, University of the Basque Country (UPV/EHU), San Sebastian 20018, Spain
[c] Ikerbasque, Basque Foundation for Science, Maria Diaz de Haro 3, 48013 Bilbao, Spain
[d] Donostia International Physics Center (DIPC), P. Manuel Lardizabal 4, 20018 San Sebastian, Spain

ARTICLE INFO

Keywords:
Deubiquitinase
USP12
USP46
WDR20
UAF1
CRM1

ABSTRACT

The human deubiquitinases USP12 and USP46 are very closely related paralogs with critical functions as tumor suppressors. The catalytic activity of these enzymes is regulated by two cofactors: UAF1 and WDR20. USP12 and USP46 show nearly 90% amino acid sequence identity and share some cellular activities, but have also evolved non-overlapping functions. We hypothesized that, correlating with their functional divergence, the subcellular localization of USP12 and USP46 might be differentially regulated by their cofactors. We used confocal and live microscopy analyses of epitope-tagged proteins to determine the effect of UAF1 and WDR20 on the localization of USP12 and USP46. We found that WDR20 differently modulated the localization of the DUBs, promoting recruitment of USP12, but not USP46, to the plasma membrane. Using site-directed mutagenesis, we generated a large set of USP12 and WDR20 mutants to characterize in detail the mechanisms and sequence determinants that modulate the subcellular localization of the USP12/UAF1/WDR20 complex. Our data suggest that the USP12/UAF1/WDR20 complex dynamically shuttles between the plasma membrane, cytoplasm and nucleus. This shuttling involved active nuclear export mediated by the CRM1 pathway, and required a short N-terminal motif (^{1}MEIL^{4}) in USP12, as well as a novel nuclear export sequence (^{450}MDGAIASGVSKFATLSLHD^{468}) in WDR20. In conclusion, USP12 and USP46 have evolved divergently in terms of cofactor binding-regulated subcellular localization. WDR20 plays a crucial role in as a "targeting subunit" that modulates CRM1-dependent shuttling of the USP12/UAF1/WDR20 complex between the plasma membrane, cytoplasm and nucleus.

1. Introduction

Ubiquitination is a reversible posttranslational modification that modulates stability, function and/or localization of most cellular proteins. Deubiquitinases (DUBs) are the enzymes that catalyze the removal of ubiquitin moieties from substrate proteins and thus, play a crucial role in many physiological processes (Komander et al., 2009). Functional alterations of several DUBs have been causally linked to tumor development, and some of these enzymes are increasingly regarded as promising targets in cancer therapy (Wei et al., 2015).

There are around 100 human DUBs, which can be classified in 7 families (Fraile et al., 2012; Haahr et al., 2018; Kwasna et al., 2018). The largest DUB family includes 54 enzymes termed ubiquitin-specific proteases (USPs), which share a structurally conserved catalytic domain (Ye et al., 2009). USP12 and USP46 are two members of the USP family that have critical functions as tumor suppressors (Gangula and Maddika, 2013; Li et al., 2013). Human USP12 and USP46 are very similar paralogs that show nearly 90% of amino acid sequence identity, and evolved from a single ancestor gene by a duplication event (Vlasschaert et al., 2017). Lower eukaryotes, such as the fission yeast *Schizosaccharomyces pombe* and invertebrates, such as a *Caenorhabditis elegans*, express a single DUB that is homologous to both USP12 and USP46.

Given their importance for the maintenance of cellular homeostasis,

Abbreviations: ActD, actinomycin D; CHX, cycloheximide; co-IP, co-immunoprecipitation; DUB, deubiquitinase; FRAP, fluorescence recovery after photobleaching; LMB, leptomycin B; NES, nuclear export sequence; NLS, nuclear localization signal; PHLPP, pleckstrin homology domain leucine rich repeat protein phosphatase; PM, plasma membrane; USP, ubiquitin-specific protease; WDR, WD40-repeat; YFP, yellow fluorescent protein

* Corresponding author.
E-mail address: josean.rodriguez@ehu.eus (J.A. Rodríguez).

https://doi.org/10.1016/j.ejcb.2018.10.003
Received 18 April 2018; Received in revised form 1 October 2018; Accepted 25 October 2018

the function of DUBs needs to be tightly regulated, and several mechanisms that modulate the activity of these enzymes have been described (reviewed in Mevissen and Komander, 2017). In the case of USP12 and USP46, the most critical regulatory event is their binding to the WD40-repeat (WDR) containing proteins UAF1 (also called WDR48) (Cohn et al., 2007; Cohn et al., 2009) and WDR20 (Kee et al., 2010; Dahlberg and Juo, 2014). These WDR proteins act synergistically as cofactors that dramatically increase the enzymatic activity of both USP12 and USP46 through a series of allosteric rearrangements in the DUB structure (Cohn et al., 2007, 2009; Kee et al., 2010; Dahlberg and Juo, 2014; Yin et al., 2015; Dharadhar et al., 2016; Li et al., 2016). This regulatory mechanism shows a remarkable evolutionary conservation, being already present in the fission yeast. Thus, the enzymatic activity of *S. pombe* Ubp9 (USP12 and USP46 homologue) is regulated by binding to Bun107 and Bun62, the yeast homologues of UAF1 and WDR20, respectively (Kouranti et al., 2010).

Despite their strikingly similar amino acid sequence, USP12 and USP46 exhibit a certain degree of functional divergence. Thus, although both DUBs participate in common cellular processes, such as the regulation of Akt signalling (Gangula and Maddika, 2013; Li et al., 2013), USP12 and USP46 have also non-overlapping functions. On one hand, USP12 regulates the stability of the androgen receptor, the T-cell receptor complex and the Notch receptor, thus modulating signalling through these pathways (Moretti et al., 2012; Burska et al., 2013; McClurg et al., 2014, 2015; Jahan et al., 2016). On the other hand, USP46 regulates the turnover of neuronal AMPA receptors, thus modulating synaptic transmission in the brain (Huo et al., 2015).

It is presently unclear what biological features of USP12 and USP46 may have evolved differentially, correlating with their functional divergence. A crucial aspect in the biology of many enzymes is their targeting to specific subcellular compartments, which may in turn modulate access to their substrates. In this regard, the subcellular localization of human USP12 and USP46 has been a matter of controversy, with different studies describing them as either predominantly cytoplasmic (Sowa et al., 2009; Urbé et al., 2012; Burska et al., 2013; Lehoux et al., 2014; Olazabal-Herrero et al., 2015) or predominantly nuclear proteins (Joo et al., 2011; Jahan et al., 2016). These contrasting observations may reflect a dynamic localization of USP12 and USP46 to different cellular compartments. Supporting this view, both yeast Ubp9 and human USP12 have been shown to undergo nucleocytoplasmic shuttling mediated by the CRM1 nuclear export receptor (Kouranti et al., 2010; Jahan et al., 2016), although the sequence determinants that mediate CRM1-mediated export (i.e. nuclear export sequences or NESs) remain to be confidently identified. Interestingly, the subcellular localization of *S. pombe* Ubp9 was shown to be further regulated by its cofactors Bun107 and Bun62 (Kouranti et al., 2010). These findings raised the possibility that, like their yeast counterparts, human UAF1 and WDR20 might modulate subcellular localization of USP12 and USP46 and, furthermore, that cofactor binding might differentially affect the localization of each DUB.

In the present work, we use siRNA and co-expression approaches, as well as confocal and live microscopy analysis of epitope-tagged proteins to assess the effect of UAF1 and WDR20 on the localization of USP12 and USP46. Our study reveals that USP12 and USP46 have evolved divergently in terms of cofactor binding-regulated subcellular localization. Thus, the steady-state localization of the USP46/UAF1/WDR20 complex was cytoplasmic, while the USP12/UAF1/WDR20 complex localized mainly to the plasma membrane (PM). We further demonstrate that USP12/UAF1/WDR20 shuttles between the PM, cytoplasm and nucleus in a CRM1-dependent manner. From a mechanistic point of view, we show that localization to the PM required direct USP12/WDR20 interaction, as well as the presence of a short amino terminal motif (^{1}MEIL^{4}) in USP12, that is absent in USP46. Furthermore, our data suggest that a previously reported NES in USP12 (Sanyal, 2016) does not act as a relevant nuclear export determinant, and we identify a novel functional NES in WDR20 that mediates CRM1-dependent export of the USP12/UAF1/WDR20 complex. Altogether, our data provide novel insight into how the subcellular localization of these important deubiquitinase complexes is regulated.

2. Material and methods

2.1. Plasmids, cloning procedures and site-directed mutagenesis

Plasmid encoding GFP-USP1 and Xpress-UAF1 were generously provided by Dr. Rene Bernards (Netherlands Cancer Institute, Amsterdam, The Netherlands) and Dr. Jae U. Jung (University of Southern California, Los Angeles, USA), respectively. UAF1-mRFP has been described previously (Olazabal-Herrero et al., 2015). To generate plasmids encoding YFP-USP12, YFP-USP12$^{V279D/F287A}$, YFP-USP12$^{ST/AA}$ and YFP-WDR20, the corresponding cDNA sequences were purchased as gBlocks (IDT), and cloned into pEYFP-C1 (Clontech) using BamHI/HindIII restriction sites. To generate YFP-USP12$^{[+NLSs]}$, USP12 cDNA was cloned into a modified version of pEYFP-C1 containing two copies of the SV40 large T antigen NLS. Myc-WDR20, Myc-USP12, Myc-USP12^{delMEIL} and Myc-USP46 were generated by cloning WDR20, USP12, USP12^{delMEIL} and USP46 cDNAs into pMyc-MCS, a modified version of pEYFP-C1 where the Myc epitope replaces YFP. YFP-USP46 plasmid was obtained by subcloning USP46 cDNA from a previously described plasmid (Olazabal-Herrero et al., 2015) into pEYFP-C1 using BamHI/HindIII restriction sites. To generate YFP-USP12^{delMEIL}, YFP-USP46^{+MEIL} and YFP-WDR20 deletion mutants, the corresponding DNA sequences were amplified by PCR and cloned into pEYFP-C1 using BamHI/HindIII. Finally, Myc-WDR20$^{F262A/W306A}$, Myc-WDR20^{NESm}, YFP-WDR20^{NESm} and YFP-USP12$^{"NES"m}$ mutants were created using the Quick-Change Lightning Site-Directed Mutagenesis Kit (Stratagene).

All the new constructs were subjected to DNA sequencing (STABVIDA). The sequences of the gBlocks and oligonucleotides used in cloning and site-directed mutagenesis are available upon request.

2.2. Cell culture, plasmid and siRNA transfections, and leptomycin B treatment

Human embryonic kidney 293 T cells and HeLa cells were grown in Dulbecco´s modified Eagle´s medium, supplemented with 10% fetal bovine serum, 100 U/ml penicillin and 100 μg/ml streptomycin (all from Invitrogen). Twenty four hours before transfection cells were seeded in 12-well or 10 cm petri dishes. Plasmid transfections were carried out with X-tremeGENE 9 transfection reagent (Roche Diagnostics) following manufacturer's protocol. For knockdown experiments, cells were transfected with a pool of three siRNAs included in the TriFECTa RNAi Kits (IDT) targeting WDR20 (hs.Ri.WDR20.13) or UAF1 (hs.Ri.WDR48.13). Scramble silencer select siRNA #1 (Ambion, Life Technologies) was used as a negative control. siRNA transfections were carried out using Lipofectamine RNAiMAX (Invitrogen) following manufacturer's protocol.

Leptomycin B (LMB; Apollo Scientific) was added to the culture medium to a final concentration of 6 ng/ml for the indicated period of time.

2.3. Immunofluorescence, microscopy and image analysis

Cells were fixed with 3.7% formaldehyde in PBS for 30 min, permeabilized with 0.2% Triton X-100 in PBS for 10 min, blocked for 1 h in blocking solution (3% BSA in PBS) and incubated with primary antibodies diluted in blocking solution for 1 h at room temperature. Anti-Myc (Cell Signaling Technology; 1:300) and anti-pSer473-Akt (Cell Signaling Technology; 1:100) were used as primary antibodies. Cells were then washed and incubated with secondary antibodies (Alexa Fluor 594-conjugated anti-mouse/rabbit IgG and Alexa Fluor 633-conjugated anti-mouse IgG; Invitrogen; 1:400) for 1 h at room temperature. Coverslips were washed and mounted onto microscope slides using

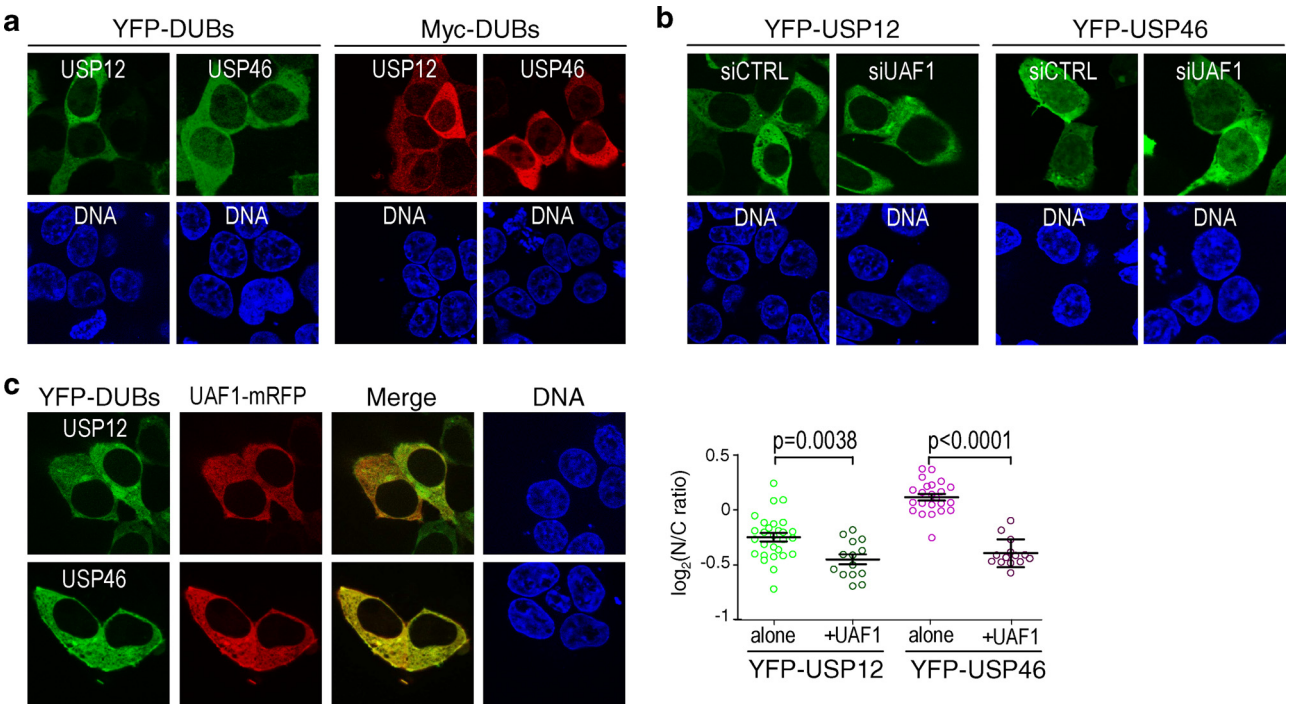

Fig. 1. Co-expression with UAF1 increases the cytoplasmic localization of USP12 and USP46.
a Confocal microscopy images show representative examples of 293 T cells expressing YFP- or Myc-tagged USP12 and USP46. DAPI was used to visualize the nuclei (DNA panels). **b** Representative examples of YFP-USP12 and YFP-USP46 localization in 293 T cells transfected with a scramble siRNA control (siCTRL) or with a pool of three siRNAs targeting UAF1 (siUAF1). **c** Confocal images of 293 T cells co-expressing YFP-USP12 or YFP-USP46 with UAF1-mRFP. Using image analyses, the intensity of the YFP signal in the nucleus and cytoplasm was quantified to calculate the nuclear to cytoplasmic (N/C) ratio. Each circle in the graph represents a single cell, and the mean (+/- SD) is also indicated. The data correspond to a single experiment, where 15–30 individual cells per condition were analysed. Comparable results were obtained in several independent experiments. The p values (Mann-Whitney U test) are indicated.

Vectashield mounting medium containing DAPI (Vector Laboratories). Single-slice images were acquired using a Zeiss ApoTome.2 microscope.

For live cell imaging, cells were grown in 35 mm IbiTreat μ-dish slides (Ibidi), and examined using a LEICA LCS SP2 AOBS microscope fitted with a temperature-controlled chamber.

Image analysis was carried out using Fiji (Schindelin et al., 2012). The "Linescan" tool and the "Coloc2" plug-in were used to assess co-localization of proteins. An ad-hoc script was developed to automatically quantify fluorescence intensity in nuclear and cytoplasmic regions using the MorphoLibJ library (Legland et al., 2016). Data were analysed using the Mann-Whitney U test and $p < 0.005$ were considered statistically significant.

2.4. Fluorescence recovery after photobleaching (FRAP) analysis

HeLa cells were grown in 35 mm ibiTreat μ-dish slides (Ibidi). Twenty four hours after transfection, FRAP analysis was carried out using a LEICA LCS SP2 AOBS microscope. The excitation (acquisition) laser was set at 10% power and the region of interest was bleached by 100% laser power. Five pre-bleach and thirty five post-bleach images were collected for each cell, with a 1.6 s time interval. Images were processed using Fiji (Schindelin et al., 2012), and data were analysed using GraphPad Prism. Halftime of recovery ($t_{1/2}$) and mobile fraction (F_m) were calculated as described in (http://www.embl.de/eamnet/frap/html/overview.html).

2.5. Sequence alignment and prediction of candidate nuclear export sequences (NESs)

Multiple sequence alignment was carried out with Clustal Omega (https://www.ebi.ac.uk/Tools/msa/clustalo/).

To identify candidate NESs, the amino acid sequence of WDR20 was analysed using the NES prediction tool WREGEX (http://ehubio.ehu.eus/wregex) (Prieto et al., 2014).

2.6. Rev(1.4)-GFP based nuclear export assay

In order to test the activity of candidate NESs, the pRev(1.4)–GFP-based nuclear export assay was carried out as reported previously (Henderson and Eleftheriou, 2000). Rev(1.4)–GFP is a chimaeric protein resulting from the fusion of an export-deficient (NES mutated) version of the HIV Rev protein to GFP. The Rev(1.4) protein bears an intact nuclear localization signal (NLS), and Rev(1.4)–GFP localizes to nucleoli. Candidate NESs are cloned between the Rev(1.4) and the GFP moieties, and active nuclear export signals are identified based on their ability to induce Rev(1.4)–GFP relocation to the cytoplasm. ActD, which disrupts nucleoli and blocks nuclear import mediated by Rev (1.4) NLS, is added to reveal the activity of weaker NESs. Double-stranded DNA fragments encoding USP12 sequence ^{75}RKKESLLTCLADLFHSIAT^{93} and WDR20 sequence ^{450}MDGAIASGVSKFATLSLHD^{468} were cloned into the Rev(1.4)-GFP reporter vector (a gift from Dr. Beric Henderson, University of Sydney, Australia) using BamHI/PinAI restriction sites. These plasmids, termed Rev(1.4)-[NES^{USP12}]-GFP and Rev(1.4)-[cNES^{WDR20}]-GFP, respectively, were transfected into HeLa cells. The empty Rev(1.4)-GFP reporter was included as negative control. Each plasmid was transfected in two wells. At 24 h post-transfection, one of the wells per sample was treated with 10 μg/ml cycloheximide (CHX; Sigma) and the other was treated with10 μg/ml CHX (Sigma) plus 5 μg/ml actinomycin D (ActD; Sigma). CHX is added to arrest protein translation and thus ensure that cytoplasmic GFP signal arises from nuclear export and not from newly synthesized proteins. Three hours after treatment, cells were fixed and mounted for microscopy analysis. Using a Zeiss Axioskop fluorescence microscope, the subcellular localization of the GFP-tagged proteins was determined in at

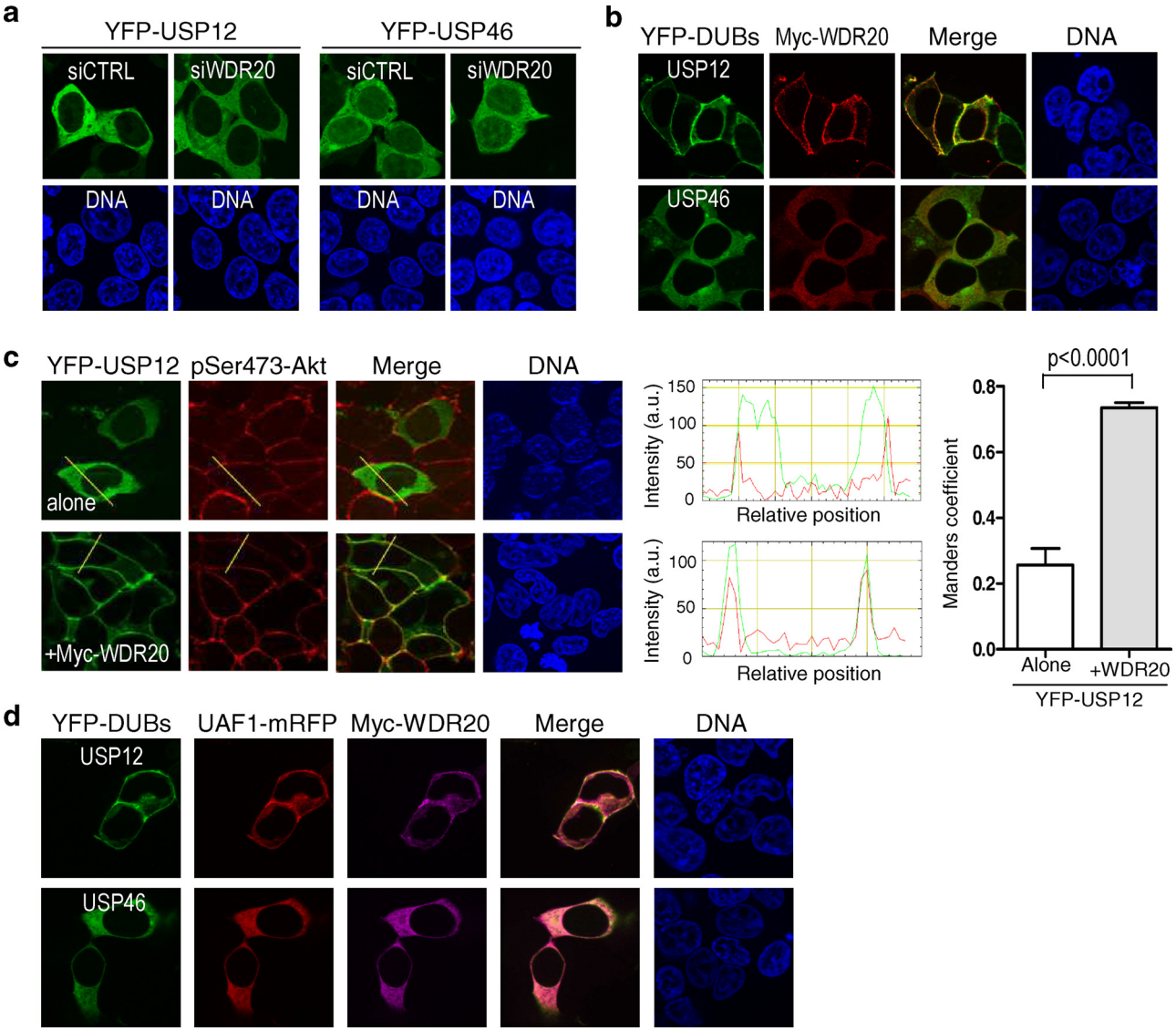

Fig. 2. Co-expression with WDR20 induces translocation of USP12, but not USP46 to the plasma membrane.
a Confocal microscopy images show representative examples of YFP-USP12 and YFP-USP46 localization in 293 T cells transfected with a scramble siRNA control (siCTRL) or with a pool of three siRNAs targeting WDR20 (siWDR20). **b** Representative examples of 293 T cells co-expressing YFP-USP12 or YFP-USP46 with Myc-WDR20. YFP-USP12 co-localizes with Myc-WDR20 at the cell periphery, whereas YFP-USP46 and Myc-WDR20 diffusely co-localize throughout the cytoplasm. **c** *Left.* Confocal images of 293 T cells transfected with YFP-USP12 alone or co-transfected with YFP-USP12 and Myc-WDR20. Cells were stained with an antibody to detect endogenous pSer473-Akt, a protein that transiently associates with the plasma membrane (PM). *Middle.* The Fiji "Linescan" tool was used to determine the intensity of the fluorescent signal along the yellow lines indicated in the images. The overlap between the green (YFP-USP12) and the red (pSer473-Akt) increases when the DUB is co-expressed with Myc-WDR20. *Right.* Graph shows the Manders correlation coefficient indicating the extent of YFP-USP12/pSer473-Akt co-localization in multiple ($n > 100$) cells transfected with either YFP-USP12 alone or co-transfected with YFP-USP12 and Myc-WDR20. The analysis was carried out using the "Coloc2" plugin from Fiji. Data represent the mean, and error bars indicate standard deviation (+/- SD). The p value (Student´s t-test) is indicated. **d** Confocal images of 293 T cells co-expressing YFP-USP12 or YFP-USP46 with UAF1-mRFP and Myc-WDR20. YFP-USP12 and its cofactors co-localized mostly at the cell periphery, suggesting recruitment of the complex to the PM. In contrast, YFP-USP46 and its cofactors co-localized diffusely in the cytoplasm.

least 200 cells per sample. Based on the proportion of cells showing nuclear, nuclear and cytoplasmic or cytoplasmic GFP signal, the level of export activity of the candidate NES was rated between 0 (non-functional) and 9+ using the assay scoring system (Henderson and Eleftheriou, 2000).

2.7. Co-immunoprecipitation analysis

Cells were lysed using IP Lysis buffer (Pierce), and lysates were subjected to anti-GFP immunoprecipitation using the GFP-Trap_MA reagent (Chromotek), following manufacturer´s directions. Immunoprecipitated proteins were analysed by immunoblot. To this end, protein samples were loaded into 10% SDS-PAGE gel, resolved by electrophoresis, and transferred to a nitrocellulose membrane. Membranes were blocked with 5% non-fat dry milk diluted in TTBS for 1 h and incubated with the primary antibodies: anti-Myc (Cell Signaling Technology, 1:2000), anti-GFP (Chromotek, 1:1000) or anti-Xpress (Invitrogen, 1:5000). Subsequently, membranes were incubated with the corresponding horseradish peroxidase-conjugated secondary antibody (Santa-Cruz, 1:3000), washed and developed using ECL (Thermo Scientific).

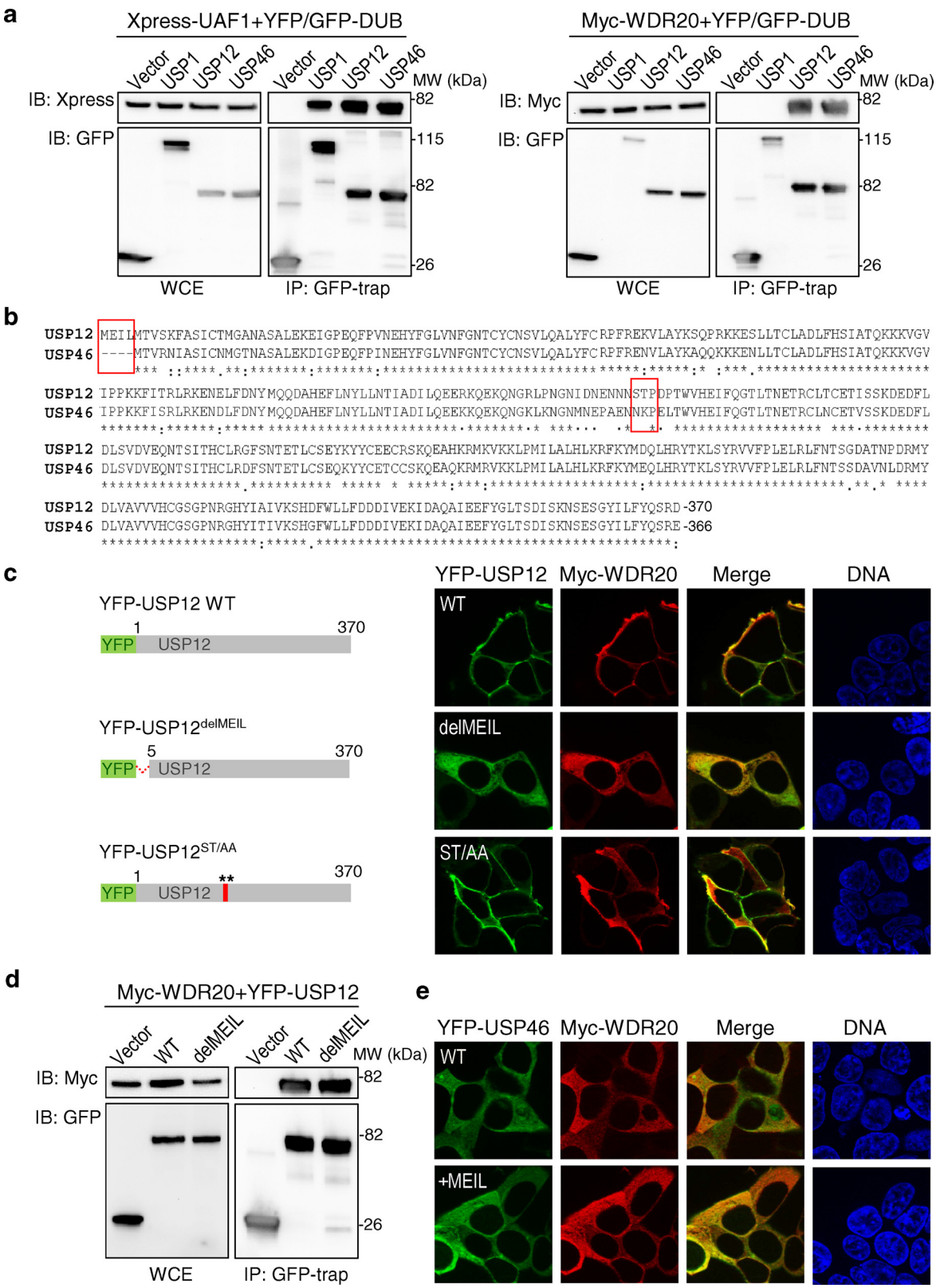

(caption on next page)

Fig. 3. A short motif in USP12, absent in USP46, contributes to plasma membrane localization of USP12/WDR20.
a. Co-immunoprecipitation (Co-IP) analyses of 293 T cells co-transfected with YFP-vector (negative control), GFP-USP1 (which is known to interact with UAF1 but not with WDR20), YFP-USP12 or YFP-USP46 and either Xpress-UAF1 (*left*) or Myc-WDR20 (*right*). Whole cell extracts (WCE) and proteins immunoprecipitated using the GFP-trap reagent were analyzed by immunoblot (IB) using anti-GFP, anti-Xpress or anti-Myc antibodies, as indicated. As expected, Xpress-UAF1 was efficiently co-immunoprecipitated by the three DUBs (*left panels*). Importantly, Myc-WDR20 was co-immunoprecipitated to a similar extent by YFP-USP12 and YFP-USP46, but not by GFP-USP1 (*right panels*). These results strongly suggest that the different effect of WDR20 on the localization of USP12 and USP46 is not due to differential binding of WDR20 to each DUB in our experimental setting. **b** Alignment of USP12 and USP46 amino acid sequences using Clustal Omega. Red squares highlight a short N-terminal motif (^{1}MEIL^{4}) and a potential minimal MAPK phosphorylation motif (^{165}STP^{167}) that are present in USP12 but not in USP46. **c** *Left*. Schematic representation of wild type YFP-USP12, and the mutants lacking the ^{1}MEIL^{4} motif (YFP-USP12^{delMEIL}) or the potential phosphorylation site (YFP-USP12$^{ST/AA}$). *Right*. Confocal images of 293 T cells co-expressing either wild type YFP-USP12, YFP-USP12^{delMEIL} or YFP-USP12$^{ST/AA}$ and Myc-WDR20. YFP-USP12^{delMEIL} mutant is not translocated to the PM when co-expressed with Myc-WDR20. **d** Blots show the results of co-immunoprecipitation (co-IP) analyses in 293 T cells showing that deletion of the ^{1}MEIL^{4} motif does not disrupt USP12/WDR20 interaction. Whole cell extracts (WCE) and proteins immunoprecipitated using the GFP-trap reagent were analyzed by immunoblot (IB) using the indicated antibodies. **e** Confocal images of 293 T cells co-expressing Myc-WDR20 with either wild type YFP-USP46 or YFP-USP46^{+MEIL}. Addition of the MEIL motif to the amino-terminal end of USP46 is not sufficient to confer WDR20-induced PM recruitment.

3. Results

3.1. Co-expression with UAF1 increases cytoplasmic localization of USP12 and USP46

We began our analysis by comparing the subcellular localization of human USP12 and USP46. The amino acid sequence of USP12 and USP46 is nearly 90% identical. To prevent confounding effects due to potential cross-reactivity of antibodies against these DUBs (Joo et al., 2011), we generated tagged versions of USP12 and USP46 fused to YFP or Myc epitopes. The subcellular localization of these proteins was assessed in transfected 293 T cells by confocal microscopy. Both DUBs, fused to either YFP or Myc (Fig. 1a), were predominantly located in the cytoplasm. A faint fluorescent signal was noticeable in the nucleus of some cells expressing USP12 and, more prominently, USP46. We also generated epitope-tagged versions of the two cofactors (UAF1-mRFP and Myc-WDR20), which were located to the cytoplasm (Additional File 1a).

In order to asses a potential effect of UAF1 on the localization of YFP-USP12 and YFP-USP46, cellular levels of UAF1 were either reduced using small interfering RNA (siRNA)-mediated knockdown or increased using UAF1-mRFP transfection. UAF1 knockdown was carried out with a pool of three siRNA oligonucleotides that consistently reduces UAF1 expression (Additional File 1b,c). As shown in Fig. 1b, UAF1 knockdown had no obvious effect on the localization of YFP-USP12 or YFP-USP46. On the other hand, YFP-USP12 and YFP-USP46 co-localized with UAF1-mRFP throughout the cytoplasm in co-transfection experiments (Fig. 1c) and, as shown by image analysis, co-expression with UAF1 markedly reduced the nuclear-to-cytoplasmic (N/C) ratio of both DUBs.

3.2. Co-expression with WDR20 induces translocation of USP12, but not USP46, to the plasma membrane

We used a similar knockdown/overexpression approach to asses a potential effect of WDR20 on the localization of YFP-USP12 and YFP-USP46. Similar to UAF1 knockdown, WDR20 siRNA had no obvious effect on the localization of YFP-USP12 or YFP-USP46 (Fig. 2a). However, we found that WDR20 co-expression had a strikingly different effect on the localization of each DUB. Whereas YFP-USP46 and Myc-WDR20 co-localized diffusely throughout the cytoplasm, YFP-USP12 and Myc-WDR20 co-localized at the cell periphery (Fig. 2b). Although less pronounced, a similar localization to the cell periphery was observed with Myc-tagged USP12, when co-expressed with YFP-WDR20 (Additional File 2a).

The localization of co-expressed USP12 and WDR20 suggested recruitment to the plasma membrane (PM). To further confirm this possibility, we carried out immunostaining with an antibody that recognizes endogenous Akt1 phosphorylated at Ser473 (hereafter termed pSer473-Akt). This phosphorylation event occurs at the PM, where pSer473-Akt remains transiently located (Manning and Toker, 2017). As expected, the co-localization of YFP-USP12 with PM-located pSer473-Akt significantly increased upon co-transfection with Myc-WDR20 (Fig. 2c).

Finally, we used triple co-transfection experiments to evaluate the localization of the ternary USP12/UAF1/WDR20 and USP46/UAF1/WDR20 complexes. Co-expressed YFP-USP12/UAF1-mRFP/Myc-WDR20 co-localized to the PM (Fig. 2d), whereas YFP-USP46/UAF1-mRFP/Myc-WDR20 diffusely co-localized in the cytoplasm.

Altogether, these results suggest that WDR20 binding promotes translocation of USP12/WDR20 to the plasma membrane, facilitating the recruitment of the USP12/UAF1/WDR20 complex to this subcellular compartment. In contrast, the steady-state localization of the USP46/UAF1/WDR20 complex is predominantly cytoplasmic.

Our finding that WDR20 differently modulates the localization of USP12 and USP46 led us to investigate the factors that may underlie this difference, as well as to further characterize the mechanisms that modulate the subcellular localization of the USP12 deubiquitinase complex.

3.3. A short amino acid motif in USP12, not present in USP46, contributes to plasma membrane localization of the USP12/WDR20 complex

We first used co-immunoprecipitation (co-IP) to rule out the possibility that the different effect of WDR20 on the localization of USP12 and USP46 was related to a different ability of the cofactor to bind these DUBs in our experimental system (Fig. 3a). Next, we considered the possibility that the different localization of USP12 and USP46 when co-expressed with WDR20 might be related to small differences in their amino acid sequence. We noticed that USP12 bears a four amino-acid motif at its extreme N-terminal end (^{1}MEIL^{4}) and a potential minimal MAPK phosphorylation motif (^{165}STP^{167}) (Bardwell, 2006), which are absent in USP46 (Fig. 3b). We generated USP12 mutant versions lacking these motifs (USP12^{delMEIL} and USP12$^{ST/AA}$). As shown in Fig. 3c, the ability of YFP-USP12^{delMEIL} mutant to relocate to the PM when co-expressed with Myc-WDR20 was virtually abrogated. A similar result was obtained using Myc-tagged USP12 and YFP-tagged WDR20 (Additional File 2b). In contrast, the YFP-USP12$^{ST/AA}$ mutant still co-localized with Myc-WDR20 to the PM. Importantly, co-IP analysis (Fig. 3d) showed that YFP-USP12^{delMEIL} interacts with Myc-WDR20 as efficiently as wild type YFP-USP12. We next added the MEIL motif to the N-terminal end of USP46. However, YFP-USP46^{+MEIL} remained in the cytoplasm when co-expressed with Myc-WDR20 (Fig. 3e).

Together, these results indicate that the amino-terminal ^{1}MEIL^{4} motif is necessary for the efficient recruitment of USP12/WDR20 to the PM, but is not sufficient to confer PM localization to a USP46/WDR20 complex.

3.4. Plasma membrane recruitment of YFP-USP12 requires direct binding to WDR20

The co-expression experiments described above are carried out in a

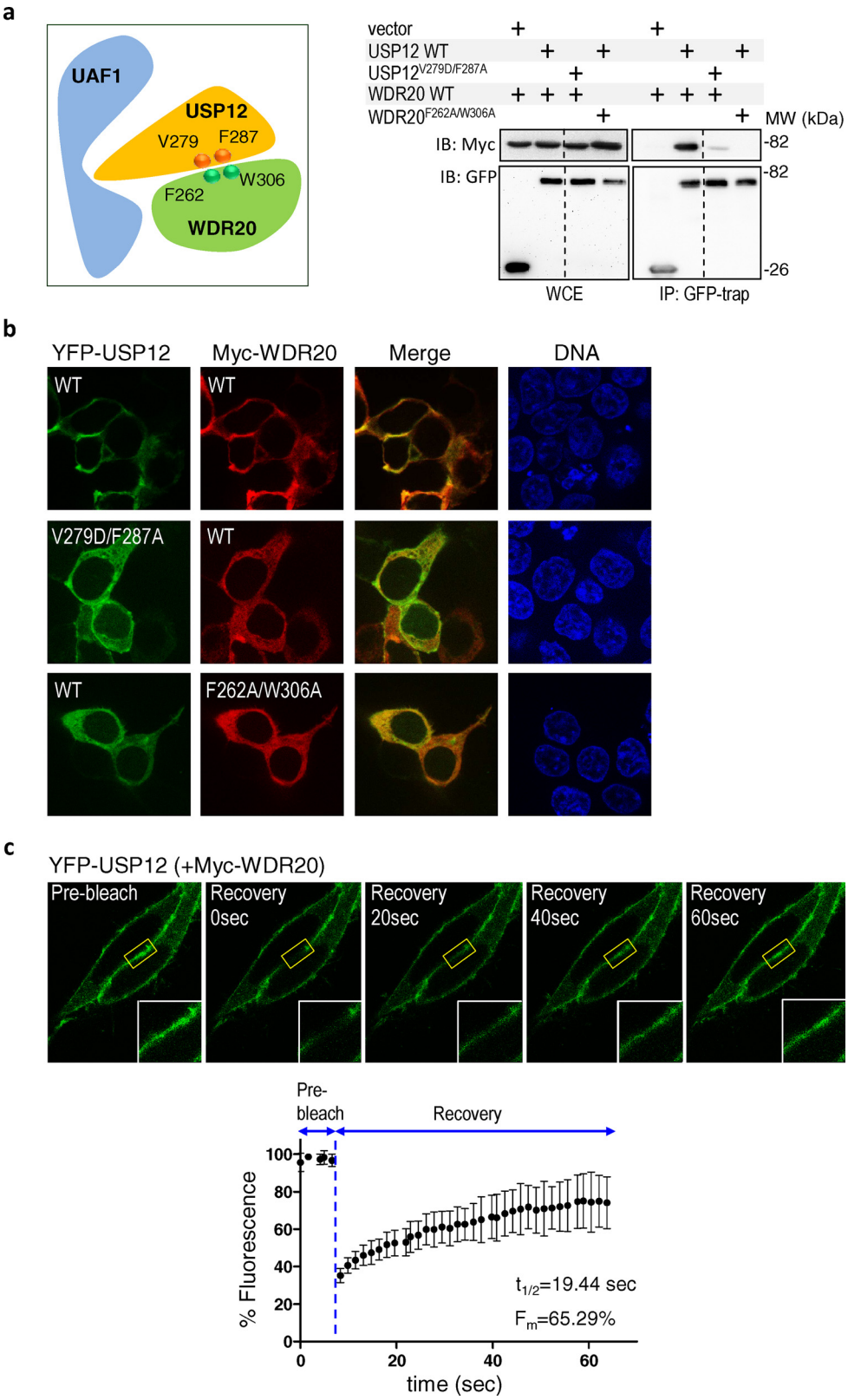

Fig. 4. Plasma membrane recruitment of USP12 requires binding to WDR20 and is highly dynamic.

a *Left.* Schematic representation of the USP12/UAF1/WDR20 complex, based on the reported three-dimensional structure (Li et al., 2016), showing the amino acids whose mutation has been shown to disrupt USP12/WDR20 interaction. *Rigth.* Blots showing the results of co-IP analysis of 293 T cells co-transfected with the indicated plasmids. The ability of YFP-USP12$^{V279D/F287A}$ to bind Myc-WDR20 is severely reduced, and Myc-WDR20$^{F262A/W306A}$ is unable to bind YFP-USP12. **b** Confocal images of 293 T cells showing that mutations that disrupt USP12/WDR20 binding abolish the translocation of co-expressed YFP-USP12 and Myc-WDR20 to the PM. **c** Representative example of fluorescence recovery after photobleaching (FRAP) analysis in live HeLa cells co-transfected with YFP-USP12 and Myc-WDR20. YFP-USP12 signal was bleached in a region of the PM (yellow rectangle), and the fluorescence recovery was followed during 65 s. Insets show a magnified image of the bleached region. Below, the recovery curve represents the average of 5 individual cells. Error bars indicate the SD. Halftime of recovery ($t_{1/2}$) and mobile fraction (F_m) values are indicated inside the graph.

complex cellular setting. It might be argued that co-expression of WDR20 might indirectly promote PM recruitment without requiring the formation of a USP12/WDR20 complex. To address this possibility, we made use of the information provided by a recent study (Li et al., 2016), where the three-dimensional structure of a ternary USP12/UAF1/WDR20 complex was reported, identifying critical residues in USP12 (V279 and F287) and WDR20 (F262 and W306) (Fig. 4a) whose mutation disrupts USP12/WDR20 interaction (Li et al., 2016). We generated YFP-USP12$^{V279D/F287A}$ and Myc-WDR20$^{F262A/W306A}$ mutants and confirmed that these mutations largely or completely abrogate WDR20 binding to USP12 in 293 T cells (Fig. 4a). As shown in Fig. 4b, YFP-USP12$^{V279D/F287A}$ did not relocate to the PM when co-expressed with

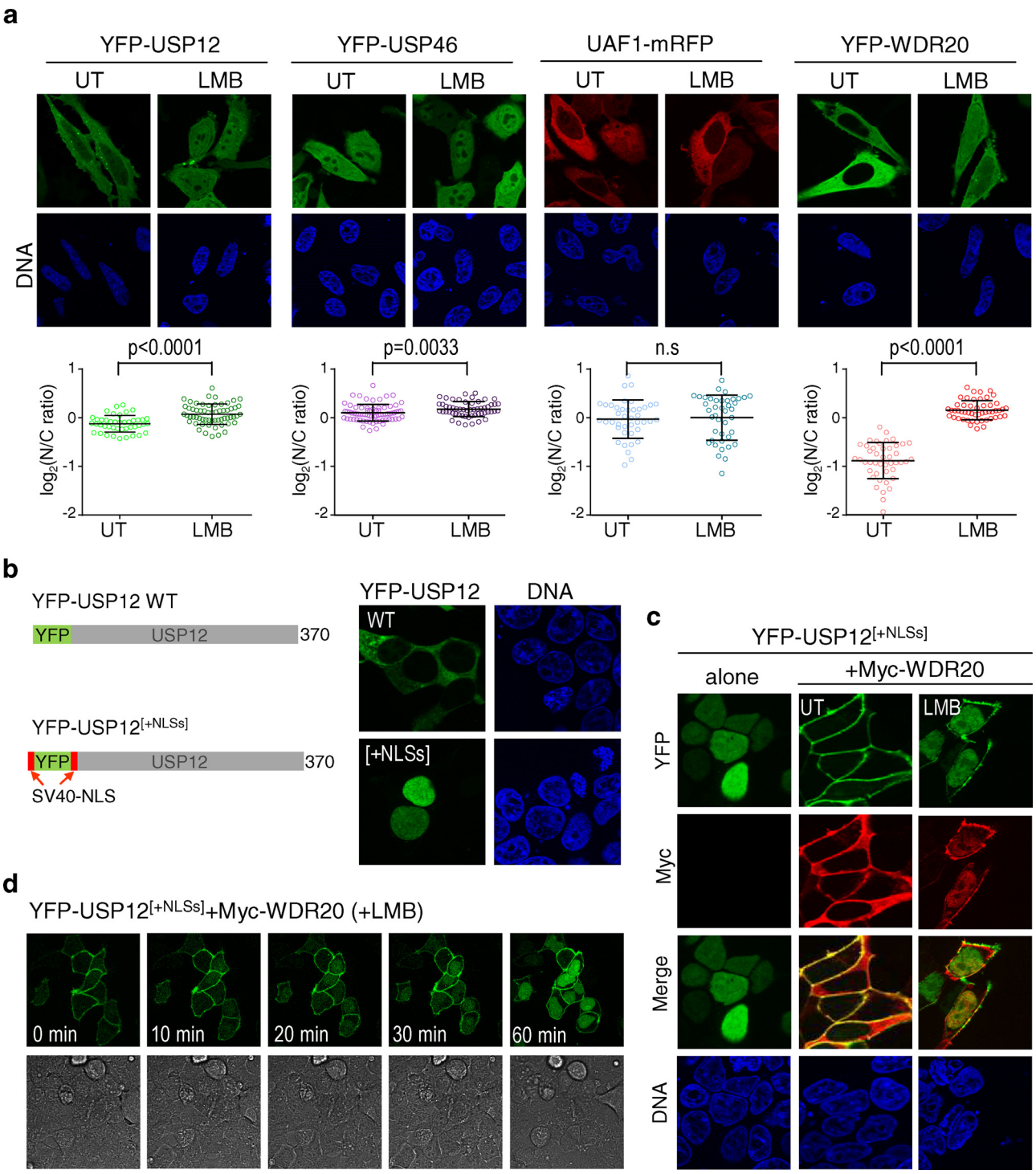

Fig. 5. CRM1-mediated nuclear export facilitates shuttling of USP12/WDR20 between the plasma membrane, cytoplasm and nucleus.
a Representative examples of the nucleocytoplasmic localization of YFP-USP12, YFP-USP46, UAF1-mRFP and YFP-WDR20 in HeLa cells untreated (UT) or treated with the CRM1 inhibitor leptomycin B (LMB) (6 ng/ml for 3 h). The N/C ratio of each protein in untreated or LMB-treated cells was determined using image analysis and is shown in the graphs below. Each circle in the graph represents a single cell, and the mean (+/- SD) is also indicated. The data correspond to a single experiment where at least 40 transfected cells per condition were analysed. Comparable results were obtained in at least two independent experiments. p values (Mann-Whitney U test) are indicated (n.s: non-significant). **b** *Left.* Schematic representation of wild type YFP-USP12 and YFP-USP12$^{[+NLSs]}$, a variant tagged with two copies of the SV40 large T antigen nuclear localization signal (SV40-NLS; in red). *Right.* Confocal images of 293 T cells showing nuclear accumulation of YFP-USP12$^{[+NLSs]}$. **c** Confocal images of 293 T cells expressing YFP-USP12$^{[+NLSs]}$ alone or co-expressing YFP-USP12$^{[+NLSs]}$ and Myc-WDR20. YFP-USP12$^{[+NLSs]}$ and Myc-WDR20 co-localize to the PM in untreated cells (UT), but partially relocalize to the nucleus after LMB treatment (6 ng/ml LMB for 3 h). **d** Confocal images of a time-lapse experiment in live 293 T cells co-expressing YFP-USP12$^{[+NLSs]}$ and Myc-WDR20. After treating the cells with LMB (6 ng/ml), the localization of YFP-USP12$^{[+NLSs]}$ was examined and recorded every 2 min for 1 h. Brightfield images at each time point are shown below. YFP-USP12$^{[+NLSs]}$ was detectable in the nucleus 10 min after LMB addition.

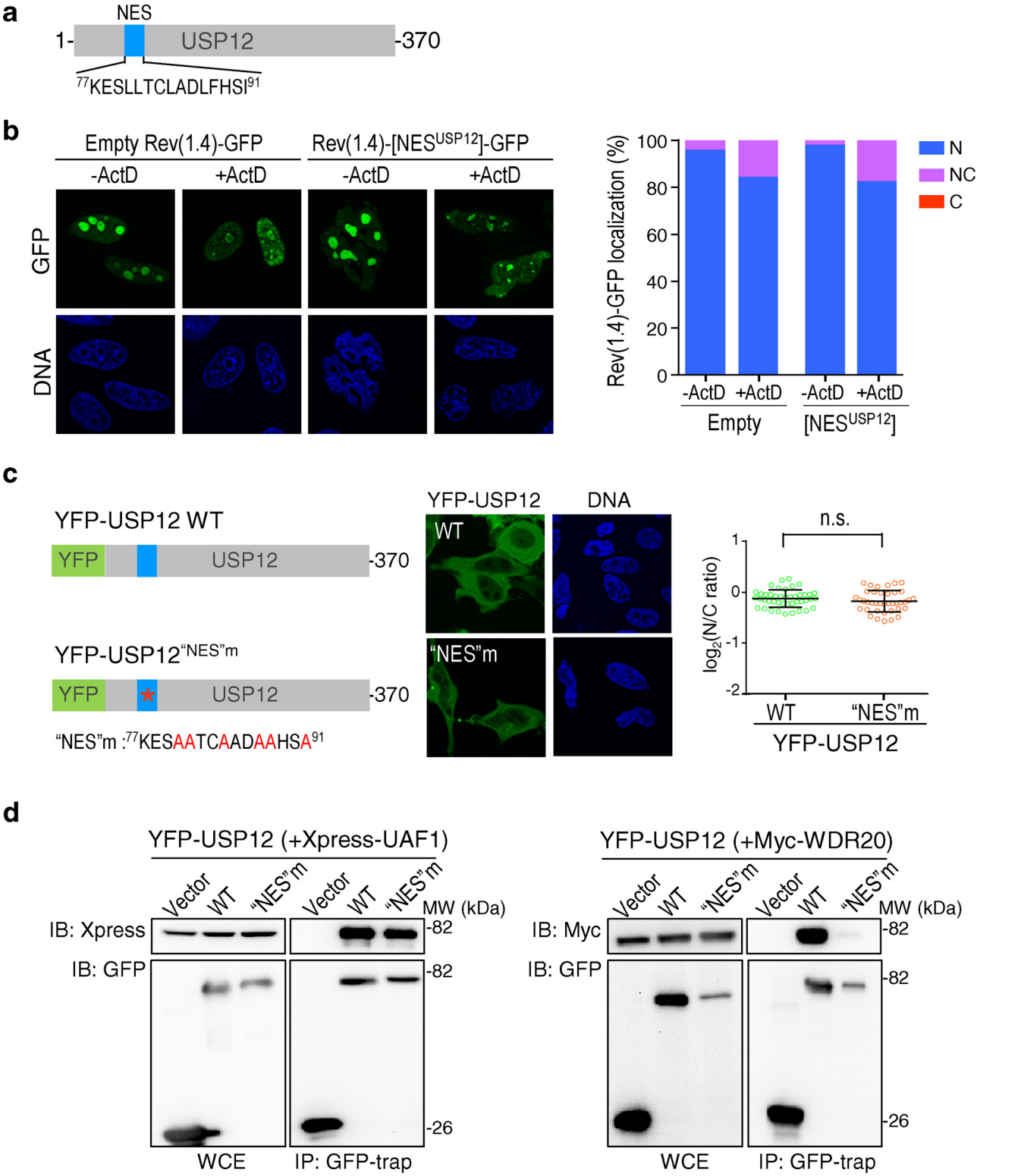

(caption on next page)

wild type Myc-WDR20, and conversely, co-expression with Myc-WDR20$^{F262A/W306A}$ did not result in PM localization of wild type YFP-USP12.

Although it cannot be formally ruled out that the introduced mutations may affect folding of the proteins and thus indirectly affect localization, this is unlikely in our view, considering that only two point mutations (and not large deletions or multiple aminoacid changes) are introduced in each protein. Thus, we believe that these findings indicate that direct binding to WDR20 is required for PM localization of USP12.

Fig. 6. A previously described NES in USP12 is not a direct nuclear export determinant.
a Schematic representation of USP12 showing the position and amino-acid sequence of a previously described NES motif (Jahan et al., 2016; Sanyal, 2016). **b** Results of a nuclear export assay to test the activity of this motif. The assay is based on the ability of functional NESs to promote export of the nuclear reporter protein Rev (1.4)-GFP to the cytoplasm (Henderson and Eleftheriou, 2000). As described in detail in the Methods section, actinomycin D (ActD) allows detection of weak NESs. *Left*. Confocal images showing representative examples of HeLa cells transfected with the empty Rev(1.4)-GFP reporter plasmid or with the plasmid Rev(1.4)-[NES^{USP12}]-GFP, containing the reported USP12 NES. *Right.* Graph showing the percentage of cells with mostly nuclear (N), nuclear and cytoplasmic (NC) or mostly cytoplasmic (C) localization of the reporter. At least 200 transfected cells were scored per condition. Even in the presence of ActD, the described USP12 NES motif was unable to promote nuclear export of Rev(1.4)-GFP. **c** *Left*. Schematic representation of wild type YFP-USP12 and a previously used "NES" mutant (YFP-USP12$^{"NES"m}$) bearing six amino-acid substitutions indicated in red (Jahan et al., 2016; Sanyal, 2016). *Center*. Confocal images of HeLa cells expressing YFP-USP12 and YFP-USP12$^{"NES"m}$. *Right*. Graph showing the N/C ratio of both proteins determined using image analysis of at least 30 transfected cells per sample. Each circle in the graph represents a single cell, and the mean (+/- SD) is shown. n.s: non-significant (Mann-Whitney U test). **d**. Results of co-IP analyses in 293 T cells co-transfected with YFP vector, wild type YFP-USP12 or YFP-USP12$^{"NES"m}$ and either Xpress-UAF1 (left) or Myc-WDR20 (right). The six mutations introduced into the "NES" motif of USP12 do not interfere with UAF1 interaction, but completely abrogate WDR20 binding.

3.5. WDR20-induced localization of YFP-USP12 to the plasma membrane is highly dynamic

To further characterize the PM localization of USP12, we carried out fluorescence recovery after photobleaching (FRAP) experiments. As in 293 T cells, YFP-USP12 also localized to the PM in live HeLa cells when co-expressed with Myc-WDR20 (Fig. 4c). The YFP-USP12 fluorescent signal was rapidly recovered in an area of the PM where it had been bleached. The calculated halftime of recovery ($t_{1/2}$) and mobile fraction (F_m) values were 19.44 s and 65.29%, respectively, indicating that the PM localization of YFP-USP12 is highly dynamic.

3.6. CRM1-mediated nuclear export facilitates shuttling of USP12/WDR20 between the plasma membrane, cytoplasm and nucleus

Together with the recent finding that USP12 can be exported from the nucleus to the cytoplasm by CRM1 (Jahan et al., 2016), our results raised the possibility that the USP12/WDR20 complex may undergo dynamic shuttling between the PM, cytoplasm and nucleus.

We tested the effect of the specific CRM1 inhibitor leptomycin B (LMB) on the nucleocytoplasmic distribution of epitope-tagged USP12, USP46, UAF1 and WDR20 in HeLa cells. As shown in Fig. 5a, a three hour LMB treatment did not alter the distribution of UAF1-mRFP. A statistically significant, but very limited, increase in the N/C ratio of YFP-USP46 was noted. The clearest and most statistically significant effect of LMB was on YFP-USP12 and, particularly, on YFP-WDR20, indicating that both proteins are actively exported from the nucleus by the CRM1-mediated nuclear export pathway.

Of note, YFP-USP12 and YFP-WDR20 were evenly distributed between nucleus and cytoplasm in LMB-treated cells, but they did not accumulate to a high level inside the nucleus. This observation suggests that the nuclear entry of these proteins is not a highly efficient process, which could be due to cytoplasmic retention or to the lack of strong nuclear localization signals (NLSs). To gauge these possibilities, we generated a version of YFP-USP12 bearing two copies of the strong SV40 large T antigen NLS (YFP-USP12$^{[+NLSs]}$) (Fig. 5b). YFP-USP12$^{[+NLSs]}$ readily accumulated into the nucleus, suggesting that YFP-USP12 inefficient import into the nucleus is most likely due to the lack of strong NLSs. Of note, a faint fluorescent signal at the PM was also noticeable in some cells expressing YFP-USP12$^{[+NLSs]}$ alone, probably due to the presence of endogenous WDR20.

The efficient nuclear import of YFP-USP12$^{[+NLSs]}$ provided a convenient experimental tool to test our hypothesis that USP12/WDR20 may shuttle between the PM, cytoplasm and nucleus. Despite the presence of the strong SV40 NLSs, YFP-USP12$^{[+NLSs]}$ localized to the PM when co-expressed with Myc-WDR20 (Fig. 5c) in 293 T cells. A similar result was obtained using Myc-tagged USP12$^{[+NLSs]}$ and YFP-tagged WDR20 (Additional File 2c). Importantly, YFP-USP12$^{[+NLSs]}$ and Myc-WDR20 partially relocated to the nucleus when CRM1-mediated export was inhibited by LMB treatment. In fact, live microscopy experiments revealed that YFP-USP12$^{[+NLSs]}$ was detectable in the nucleus only a few minutes after LMB addition (Fig. 5d).

These observations indicate that the USP12/WDR20 complex is able to dynamically shuttle between PM, cytoplasm and nucleus.

3.7. A previously described NES in USP12 is not a direct nuclear export determinant

The USP12 motif ^{77}KESLLTCLADLFHSI^{91} (Fig. 6a) has been recently proposed to be a CRM1-dependent NES, although its putative export function has not been characterized (Jahan et al., 2016; Sanyal, 2016). We tested a USP12 fragment containing this motif and flanking residues (^{75}RKKESLLTCLADLFHSIAT^{93}) using a nuclear export assay (Henderson and Eleftheriou, 2000) based on the ability of functional NESs to confer cytoplasmic localization to an otherwise nuclear reporter termed Rev (1.4)-GFP. As shown in Fig. 6b, the proposed USP12 NES was unable to increase the cytoplasmic localization of the Rev(1.4)-GFP reporter, even in the presence of actinomycin D (ActD), a drug used in this assay to identify very weak NESs (Henderson and Eleftheriou, 2000). The USP12 motif ^{77}KESLLTCLADLFHSI^{91} was therefore classified as a non-functional NES-like motif, and hereafter we refer to this motif as USP12 "NES".

Mutation of six residues within this "NES" has been previously reported to interfere with USP12 nuclear export in Jurkat cells (Jahan et al., 2016). We introduced these mutations into YFP-USP12 to generate YFP-USP12$^{"NES"m}$. The nucleocytoplasmic distribution of YFP-USP12$^{"NES"m}$ was identical to that of YFP-USP12 in HeLa cells (Fig. 6c), further supporting our view that the motif ^{77}KESLLTCLADLFHSI^{91} is not a direct determinant of USP12 nuclear export.

Importantly, it has been previously stated, as data not shown, that "NES" mutations prevent USP12 binding to UAF1 and WDR20 (Sanyal, 2016). Using co-IP analyses, we found that YFP-USP12$^{"NES"m}$ retained its ability to interact with Xpress-UAF1 (Fig. 6d, left). However "NES" mutations did efficiently disrupt the interaction of USP12 with Myc-WDR20 (Fig. 6d, right). The "NES" is located far away from the reported USP12/WDR20 interaction site (Li et al., 2016). It is likely that introducing six amino acid substitutions may result in non-specific changes in USP12 conformation that indirectly interfere with WDR20 binding. Importantly, by disrupting the interaction with WDR20, "NES" mutations abrogate WDR20-induced relocation of USP12 to the PM (Additional File 3), and would also prevent its full catalytic activation.

3.8. WDR20 bears a functional NES that mediates its CRM1-dependent nuclear export

The pronounced shift on the nucleocytoplasmic distribution of WDR20 caused by LMB prompted us to search for potential CRM1-dependent NESs in this protein. NESs usually adopt a characteristic secondary structure comprising an N-terminal alpha helix followed by a C-terminal loop (Dong et al., 2009). WDR20 does not present any alpha helical region according to the reported structure of the USP12/UAF1/WDR20 complex (Li et al., 2016). However, we noted that a WDR20 region comprising residues 394–509 was not solved in this structure. Thus, we decided to carry out a deletion analysis using three WDR20

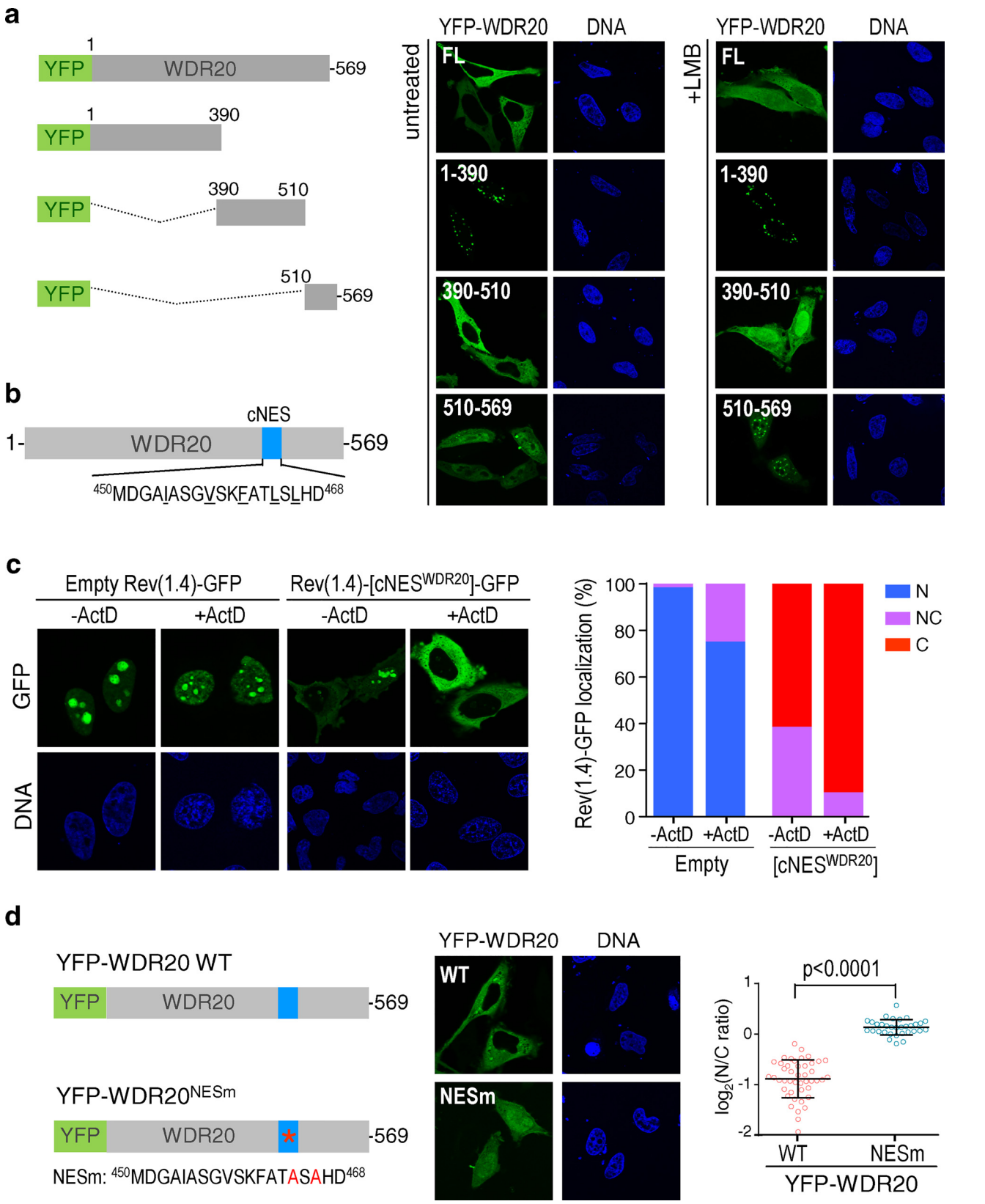

(caption on next page)

fragments: 1–390, 390–510 and 510-569. YFP-tagged versions of these fragments were expressed in HeLa cells, and their localization examined in the presence or absence of LMB (Fig. 7a). Like full-length YFP-WDR20, YFP-WDR20(390–510) clearly relocated from the cytoplasm to the nucleus in LMB-treated cells, suggesting that a CRM1-dependent NES may be located within this fragment. Using the NES prediction tool Wregex (Prieto et al., 2014), we found a candidate NES (cNES) motif (^{450}MDGAIASGVSKFATLSLHD^{468}) in this region (Fig. 7b), and tested it

Fig. 7. WDR20 bears a functional NES that mediates its CRM1-dependent nuclear export.
a. *Left*. Schematic representation of YFP-tagged WDR20 deletion mutants. *Right*. Confocal images of HeLa cells transfected with the different YFP-WDR20 deletion mutants and left untreated or treated with LMB (6 ng/ml for 3 h). LMB treatment induced relocation of full-length YFP-WDR20 and YFP-WDR20 (390–510) from the cytoplasm to the nucleus. **b**. Schematic representation of WDR20 protein showing the position and amino acid sequence of a candidate NES (cNES) predicted using the prediction webtool Wregex (Prieto et al., 2014). The hydrophobic residues that conform to the NES consensus are underlined. **c**. Results of a nuclear export assay to test the activity of the candidate WDR20 NES motif. *Left*. Confocal images showing representative examples of HeLa cells transfected with the empty Rev(1.4)-GFP plasmid or with the plasmid Rev(1.4)-[cNES^{WDR20}]-GFP, containing WDR20 candidate NES. *Right*. Graph showing the percentage of cells with mostly nuclear (N), nuclear and cytoplasmic (NC) or mostly cytoplasmic (C) localization of the reporter. At least 200 transfected cells were scored per condition. The WDR20 candidate NES motif readily promoted nuclear export of the Rev(1.4)-GFP reporter. **d**. *Left*. Schematic representation of wild type YFP-WDR20 and YFP-WDR20^{NESm}, a mutant bearing alanine substitutions of two NES residues (L464 and L466) (highlighted in red). *Center*. Representative examples of HeLa cells expressing YFP-WDR20 and YFP-WDR20^{NESm}. *Right*. Graph showing the N/C ratio of both proteins determined using image analysis of at least 30 transfected cells per sample. Each circle in the graph represents a single cell, and the mean (+/- SD) is shown. p value (Mann-Whitney U test) is indicated.

using the Rev(1.4)-GFP nuclear export assay. In contrast to USP12 "NES", WDR20 cNES efficiently promoted the export of the Rev(1.4)-GFP reporter to the cytoplasm (Fig. 7c), indicating that this motif constitutes a functional NES. Using the assay scoring system (Henderson and Eleftheriou, 2000), a score of 6+ was assigned to the WDR20 NES. Finally, we generated an NES-mutant version of YFP-WDR20 (YFP-WDR20^{NESm}) bearing mutations in two leucine residues (L464 A/L466 A). As shown in Fig. 7d, these mutations fully mimicked the effect of LMB treatment, confirming that the ^{450}MDGAIASGVSKF-ATLSLHD^{468} motif is a novel NES that mediates CRM1-dependent nuclear export of WDR20.

3.9. The CRM1 pathway and WDR20 NES mediate nucleocytoplasmic shuttling of the USP12/UAF1/WDR20 complex

In order to test the possibility that WDR20 NES regulates the localization of USP12 deubiquitinase complexes, 293 T cells were co-transfected with YFP-USP12$^{[+NLSs]}$ and either wild type or NES-mutant Myc-WDR20. As shown in Fig. 8a, YFP-USP12$^{[+NLSs]}$ located almost exclusively to the PM when co-expressed with wild type Myc-WDR20. In striking contrast, YFP-USP12$^{[+NLSs]}$ located to both the nucleus and the PM when co-expressed with Myc-WDR20^{NESm}, a distribution that was similar to that of YFP-USP12$^{[+NLSs]}$ co-expressed with wild type Myc-WDR20 after LMB treatment (see Fig. 5c). Of note, when a similar experiment was carried out using YFP-USP12 (without the added SV40 NLSs), both wild type and NES mutant Myc-WDR20 similarly co-localized with the DUB in the PM (Additional File 4a). This observation suggests that, in the absence of a strong NLS in USP12, recruitment to the PM largely prevails over slow diffusion into the nucleus upon formation of a USP12/WDR20 complex.

On the other hand, since YFP-USP46 was not recruited to the PM, but accumulated in the cytoplasm when co-expressed with Myc-WDR20 (see Fig. 2b), we tested the role of WDR20 NES on the localization of the USP46/WDR20 complex. Image analysis showed that the nuclear to cytoplasmic ratio of YFP-USP46 was significantly higher when expressed with Myc-WDR20^{NESm} than with wild type Myc-WDR20 (Additional File 4b), suggesting that the NES of WDR20 contributes to the cytoplasmic localization of the USP46/WDR20 complex.

Finally, triple co-transfection experiments were carried out to assess the role of the CRM1 pathway and WDR20 NES in the localization of the ternary USP12/UAF1/WDR20 complex. On one hand, 293 T cells were co-transfected with YFP-USP12$^{[+NLSs]}$, UAF1-mRFP, and wild type Myc-WDR20 and either left untreated or treated with LMB. On the other hand, cells were co-transfected with YFP-USP12$^{[+NLSs]}$, UAF1-mRFP and NES-mutant Myc-WDR20. As shown in Fig. 8b, LMB treatment or mutation of WDR20 NES resulted in a prominent relocation of the three co-expressed proteins to the nucleus. These findings strongly suggest the WDR20 NES described here mediates CRM1-dependent nuclear export of the USP12/UAF1/WDR20 complex.

4. Discussion

The mechanisms that regulate the subcellular localization of human deubiquitinating enzymes USP12 and USP46 have not been investigated in detail. Specifically, no attempts have been yet made to investigate potential differences between these very closely related DUBs in terms of their distribution inside the cell. The WDR proteins UAF1 and WDR20 have been well characterized as necessary cofactors that increase the catalytic activity of USP12 and USP46 (Cohn et al., 2009: Kee et al., 2010; Burska et al., 2013; Dahlberg and Juo, 2014; Li et al., 2016). UAF1, but not WDR20, is also a cofactor for the related DUB USP1 (Cohn et al., 2007). In this case, UAF1 plays a dual regulatory role, contributing not only to increase activity, but also to substrate recruitment (Lee et al., 2010; Yang et al., 2011). Here we show that WDR20 similarly plays a dual role in the regulation of USP12 and USP46. Besides increasing the activity of these enzymes, WDR20 contributes to modulate two aspects of their subcellular localization. On one hand, binding to WDR20 promotes relocation of USP12, but not USP46, to the plasma membrane (PM). On the other hand, WDR20 bears a nuclear export sequence (NES) that mediates CRM1-dependent nuclear export of WDR20-containing DUB complexes.

Contradictory findings regarding the subcellular localization of USP12 and USP46 have been previously reported in different cell types and using different experimental approaches (Joo et al., 2011; Urbé et al., 2012; Lehoux et al., 2014; Jahan et al., 2016). Here we have compared the distribution of USP12 and USP46 in 293 T and HeLa cells using epitope-tagged proteins. While we recognize that this approach may have limitations, our goal was to unequivocally assess the localization of each DUB. In this regard, it has been previously noted that the high similarity between USP12 and USP46 complicates the development of specific reagents to study the endogenous proteins (Joo et al., 2011).

In line with previous studies (Urbé et al., 2012; Lehoux et al., 2014), we found that YFP-USP12 and YFP-USP46 were located predominantly in the cytoplasm of 293 T and HeLa cells when expressed alone. In these conditions, ectopically expressed USP12 and USP46 would presumably be in excess over endogenous UAF1 and WDR20. Thus, we used double and triple co-transfections in an attempt to balance the expression levels of the complex subunits, and test a potential effect of the cofactors on the localization of the DUBs. The most striking finding was the relocation of YFP-USP12, but not YFP-USP46 to the PM when co-expressed with Myc-WDR20.

USP12 and USP46 are paralogs, evolved by duplication of a common ancestor gene (Vlasschaert et al., 2017), and the differential effect of WDR20 binding on their localization described here represents an example of evolutionary divergence, which correlates with the partial functional divergence exhibited by these enzymes. The yeast *S. pombe* encodes a single homologue of both human USP12 and USP46 (Ubp9), whose activity and localization is regulated by the yeast homologues of human UAF1 and WDR20 (Bun107 and Bun62) (Kouranti et al., 2010). Remarkably, while WDR protein-mediated catalytic activation of USP12 and USP46 has been conserved, these DUBs have evolved a striking difference in their ability to be recruited to the PM upon WDR20 binding. We have partially mapped this difference to a four amino-acid sequence (^{1}MEIL^{4}) present in USP12, but absent in USP46. We speculate that this motif could mediate transient

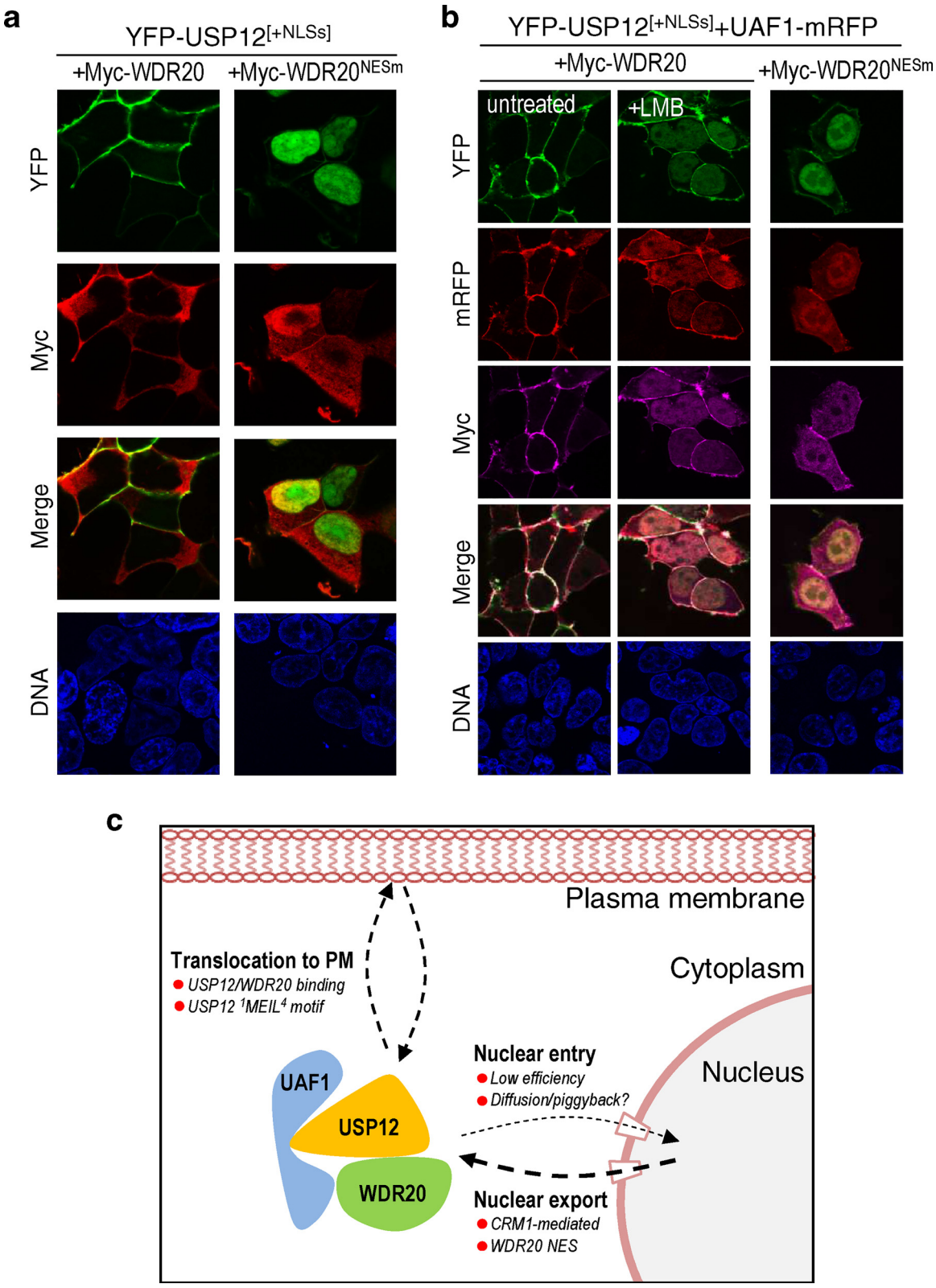

Fig. 8. The CRM1 pathway and WDR20 NES mediate nucleocytoplasmic shuttling of the USP12/UAF1/WDR20 complex.
a. Confocal images of 293 T cells co-expressing YFP-USP12$^{[+NLSs]}$ with either wild type Myc-WDR20 or Myc-WDR20^{NESm}. WDR20 NES mutation leads to accumulation of co-expressed YFP-USP12$^{[+NLSs]}$ and Myc-WDR20^{NESm} in the nucleus. **b**.Representative examples of the results of a triple co-transfection experiment in 293 T cells. On one hand, cells were co-transfected with YFP-USP12$^{[+NLSs]}$, UAF1-mRFP and wild type Myc-WDR20 and either left untreated or treated with LMB (6 ng/ml for 3 h). On the other hand, cells were co-transfected with YFP-USP12$^{[NLSs]}$, UAF1-mRFP and Myc-WDR20^{NESm}. In untreated cells, the ternary complex containing wild type WDR20 localizes almost exclusively to the PM. In contrast, the complex significantly accumulates in the nucleus when the CRM1 pathway is inhibited, or when it contains WDR20^{NESm}. **c**. A proposed model summarizing our results.

interactions of USP12 with still unidentified PM proteins or lipids. Since WDR20 binding induces a variety of rearrangements in USP12 structure (Li et al., 2016), it might promote PM recruitment by increasing the exposure of the ^{1}MEIL^{4} motif. Unfortunately, the currently available structure of the USP12/UAF1/WDR20 complex does not provide information on the extreme amino-terminal end of USP12. Further experiments should dissect the mechanisms by which WDR20 binding and the ^{1}MEIL^{4} motif contribute to the PM localization of USP12.

Besides uncovering the WDR20-promoted recruitment of USP12 to the PM, our data provide novel mechanistic insight into another closely related aspect of the subcellular localization of this DUB: its nucleocytoplasmic transport. We confirm that USP12 undergoes CRM1-dependent nuclear export in human cells, as described before (Jahan et al., 2016). In fact, our experiments indicate that both USP12 and WDR20 relocate from the cytoplasm to the nucleus when CRM1 is inhibited with LMB.

Importantly, neither USP12 nor WDR20 accumulate to high levels in the nucleus of LMB-treated cells, suggesting that they are not efficiently imported into the nucleus, probably due to the lack of active NLSs. In support of this view, we show that fusing two copies of the SV40 large T antigen NLS to YFP-USP12 readily induces its nuclear accumulation. We suggest that endogenous USP12 complexes may enter the nucleus by diffusion or by using a piggyback mechanism. In fact, an example of piggyback nuclear import of USP12 and USP46 mediated by the human papillomavirus E1 protein has been already described (Lehoux et al., 2014). Remarkably, we found that the variant of USP12 carrying strong heterologous NLSs (YFP-USP12$^{[+NLSs]}$) was exclusively located to the PM when co-expressed with Myc-WDR20, but partially relocated to the nucleus upon LMB treatment, suggesting that the YFP-USP12$^{[+NLSs]}$/Myc-WDR20 complex is in fact continuously shuttling between the PM, cytoplasm and nucleus in a CRM1-dependent manner.

Studies on yeast and human cells (Kouranti et al., 2010; Jahan et al., 2016) demonstrate that CRM1-dependent shuttling is an evolutionarily conserved, and thus probably important, feature of USP12 complexes, whose details remain poorly characterized. We provide novel mechanistic insight into the nucleocytoplasmic transport of USP12 complexes.

First, our data suggest that a previously reported USP12 "NES" (^{77}KESLLTCLADLFHSI^{91}) (Jahan et al., 2016; Sanyal, 2016) is not a direct determinant of CRM1-dependent export. This motif was nonfunctional in a nuclear export assay (Henderson and Eleftheriou, 2000), and mutations of this "NES" (unlike LMB treatment) did not decrease the cytoplasmic localization of YFP-USP12 in HeLa cells. In the previous report (Jahan et al., 2016), the localization of USP12 was determined in Jurkat cells using a fractionation protocol based on permeabilization of the PM to separate soluble (cytosolic) and pellet (nuclear) fractions. "NES" mutations were reported to prevent USP12 translocation to the cytosol, and to abrogate USP12-mediated stabilization of the T-cell receptor complex (Jahan et al., 2016). Importantly, it was pointed out (as data not shown) that "NES" mutations abrogate USP12 interaction with UAF1 and WDR20 (Sanyal, 2016). We confirmed that "NES" mutations disrupt USP12/WDR20 interaction. In the light of the novel evidence presented here, we believe that several conclusions from the previous report (Jahan et al., 2016) should be reconsidered. On one hand, it should be taken into account that their pellet fractions might contain PM-located as well as nuclear USP12. More importantly, since "NES" mutations disrupt WDR20 binding, the reported functional abrogation of "NES"-mutant USP12 (Jahan et al., 2016) might be related to incomplete catalytic activation of the enzyme rather than to altered nuclear export.

Second, we have identified a *bona fide* novel NES in WDR20. The WDR20 motif ^{450}MDGAIASGVSKFATLSLHD^{468} was clearly functional in the nuclear export assay, and mutation of this sequence caused a partial relocation of epitope-tagged WDR20 from the cytoplasm to the nucleus, mimicking the effect of LMB.

Finally, we show that mutation of WDR20 NES interferes with the nuclear export of USP12/WDR20 and USP12/UAF1/WDR20 complexes. Of note, we used the YFP-USP12$^{[+NLSs]}$ variant in these experiments as a tool to more clearly visualize the effect of WDR20 NES mutations. Although the WDR20 region containing the NES is not solved in the currently available structure of the USP12/UAF1/WDR20 complex, these results suggest that the WDR20 NES is accessible for CRM1 interaction in the context of the ternary complex.

The dynamic shuttling of USP12 complexes described here may facilitate access of this DUB to nuclear substrates such as histones (Joo et al., 2011), as well as to substrates that are located in the cytoplasm and the PM, such as PHLPP (Gangula and Maddika, 2013; Li et al., 2013). Our results are based on co-overexpression experiments to achieve balanced levels of the different subunits, and formation of different subcomplexes of USP12, UAF1 and WDR20. Although it is presently unclear if these different subcomplexes exist physiologically in the cell, we speculate that at endogenous (lower) levels of all subunits, those USP12 subcomplexes that contain WDR20 would be predominantly located to the PM. Thus, our data suggest that USP12 subcomplexes with different stoichiometry might not only have different level of catalytic activity, as it would be expected from previous results (Cohn et al., 2009; Kee et al., 2010; Kouranti et al., 2010; Burska et al., 2013; Dahlberg and Juo, 2014; Li et al., 2016) but they might also localize to different subcellular compartments. Mechanisms that may modulate WDR20 localization, such as post-translational modification, might in turn modulate the localization of DUB complexes containing this subunit.

5. Conclusions

Our results support a model (Fig. 8c) whereby the USP12/UAF1/WDR20 complex has the ability to dynamically shuttle between the PM cytoplasm and nucleus. WDR20 plays a crucial role in this shuttling as a "targeting subunit" of the complex. On one hand, its direct binding to USP12 would promote transient recruitment to the PM and, on the other hand, its NES would mediate CRM1-dependent nuclear export.

Authors´ contributions

AO-H designed and carried out experiments, and contributed to writing the manuscript. MS designed and carried out experiments. IA-C developed experimental tools. JAR conceived the study, designed experiments and contributed to writing the manuscript. All authors read and approved the final manuscript.

Funding

This work was supported by grants from the Spanish Government MINECO-FEDER (SAF2014-57743-R), the Basque Country Government (IT634-13) and the University of the Basque Country (UFI11/20), as well as fellowships from the Basque Country Government (to MS) and the University of the Basque Country (to AO-H). Our group is a member of the PROTEOSTASIS BM1307 COST Action, supported by European Cooperation in Science and Technology.

Competing interests

The authors declare that they have no competing interests.

Acknowledgements

We appreciate the generous gift of plasmids from Dr. René Bernards, Dr. Jae Jung and Dr. Beric Henderson. We appreciate the technical support by the staff from the High Resolution Microscopy Facility (SGIKER-UPV/EHU).

Appendix A. Supplementary data

Supplementary material related to this article can be found, in the online version, at doi:https://doi.org/10.1016/j.ejcb.2018.10.003.

References

Bardwell, L., 2006. Mechanisms of MAPK signalling specificity. Biochem. Soc. Trans. 34 (5), 837–841.

Burska, U.L., Harle, V.J., Coffey, K., Darby, S., Ramsey, H., O´Neill, D., et al., 2013. Deubiquitinating enzyme Usp12 is a novel co-activator of the androgen receptor. J. Biol. Chem. 288, 32641–32650.

Cohn, M.A., Kowal, P., Yang, K., Haas, W., Huang, T.T., Gygi, S.P., et al., 2007. A UAF1-containing multisubunit protein complex regulates the Fanconi anemia pathway. Mol. Cell 28, 786–797.

Cohn, M.A., Kee, Y., Haas, W., Gygi, S.P., D´Andrea, A.D., 2009. UAF1 is a subunit of multiple deubiquitinating enzyme complexes. J. Biol. Chem. 284, 5343–5351.

Dahlberg, C.L., Juo, P., 2014. The WD40-repeat proteins WDR-20 and WDR-48 bind and activate the deubiquitinating enzyme USP-46 to promote the abundance of the glutamate receptor GLR-1 in the ventral nerve cord of Caenorhabditis elegans. J. Biol. Chem. 289, 3444–3456.

Dharadhar, S., Clerici, M., van Dijk, W.J., Fish, A., Sixma, T.K., 2016. A conserved two-step binding for the UAF1 regulator to the USP12 deubiquitinating enzyme. J. Struct. Biol. 196, 437–447.

Dong, X., Biswas, A., Süel, K.E., Jackson, L.K., Martinez, R., Gu, H., et al., 2009. Structural basis for leucine-rich nuclear export signal recognition by CRM1. Nature 458 (7242), 1136–1141.

Fraile, J.M., Quesada, V., Rodríguez, D., Freije, J.M.P., López-Otín, C., 2012. Deubiquitinases in cancer: new functions and therapeutic options. Oncogene 31, 2373–2388.

Gangula, N.R., Maddika, S., 2013. WD repeat protein WDR48 in complex with deubiquitinase USP12 suppresses Akt-dependent cell survival signalling by stabilizing PH domain leucine-rich repeat protein phosphatise 1 (PHLPP1). J. Biol. Chem. 288, 34545–34554.

Haahr, P., Borgermann, N., Guo, X., Typas, D., Achuthankutty, D., Hoffmann, S., et al., 2018. ZUFSP deubiquitylates K63-linked polyubiquitin chains to promote genome stability. Mol. Cell 70 (1), 165–174.

Huo, Y., Khatri, N., Hou, Q., Gilbert, J., Wang, G., Man, H.Y., 2015. The deubiquiting enzyme USP46 regulates AMPA receptor ubiquitination and trafficking. J. Neurochem. 134 (6), 1067–1080.

Jahan, A.S., Lestra, M., Swee, L.K., Fan, Y., Lamers, M.M., Tafesse, F.G., et al., 2016. Usp12 stabilizes the T-cell receptor complex at the cell surface during signalling. Proc. Natl. Acad. Sci. U. S. A. 113 (6), E705–714.

Joo, H.Y., Jones, A., Yang, C., Zhai, L., Smith, A.D., Zhang, Z., et al., 2011. Regulation of histone H2A and H2B deubiquitination and Xenopus development by USP12 and USP46. J. Biol. Chem. 286, 7190–7201.

Kee, Y., Yang, K., Cohn, M.A., Haas, W., Gygi, S.P., D´Andrea, A.D., 2010. WDR20 regulates activity of the USP12-UAF1 deubiquitinating enzyme complex. J. Biol. Chem. 285, 11252–11257.

Komander, D., Clague, M.J., Urbé, S., 2009. Breaking the chains: structure and function of the deubiquitinases. Nat. Rev. Mol. Cell Biol. 10 (8), 550–563.

Kouranti, I., McLean, J.R., Feoktistova, A., Liang, P., Johnson, A.E., Roberts-Galbraith, R.H., et al., 2010. A global census of fission yeast deubiquitinating enzyme localization and interaction networks reveals distinct compartmentalization profiles and overlapping functions in endocytosis and polarity. PLoS Biol. https://doi.org/10.1371/journal.pbio.1000471.

Kwasna, D., Rehman, Abdul, SA, Natarajan, J., Matthews, S., Madden, R., De Ce sare, V., et al., 2018. Discovery and Characterization of ZUFSP/ZUP1, a distinct deubiquitinase class important for genome stability. Mol. Cell 70 (1), 150–164.

Lee, K.Y., Yang, K., Cohn, M.A., Sikdar, N., D´Andrea, A.D., Myung, K., 2010. Human ELG1 regulates the level of ubiquitinated proliferating cell nuclear antigen (PCNA) through its interactions with PCNA and USP1. J. Biol. Chem. 285 (14), 10362–10369.

Legland, D., Arganda-Carreras, I., Andrey, P., 2016. MorphoLibJ: integrated library and plugins for mathematical morphology with ImageJ. Bioinformatics 32 (22), 3532–3534.

Lehoux, M., Gagnon, D., Archambault, J., 2014. E1-mediated recruitment of a UAF1-USP deubiquitinase complex facilitates human papillomavirus DNA replication. J. Virol. 88 (15), 8545–8555.

Li, X., Stevens, P.D., Yang, H., Gulhati, P., Wang, W., Evers, B.M., et al., 2013. The deubiquitination enzyme USP46 functions as a tumor suppressor by controlling PHLPP-dependent attenuation of Akt signalling in colon cancer. Oncogene 32, 471–478.

Li, H., Lim, K.S., Kim, H., Hinds, T.R., Jo, U., Mao, H., et al., 2016. Allosteric activation of ubiquitin-specific proteases by β-propeller proteins UAF1 and WDR20. Mol. Cell 6, 249–260.

Manning, B.D., Toker, A., 2017. AKT/PKB signalling: navigating the network. Cell 169 (3), 381–405.

McClurg, U.L., Summerscales, E.E., Harle, V.J., Gaughan, L., Robson, C.N., 2014. Deubiquitinating enzyme Usp12 regulates the interaction between the androgen receptor and the Akt pathway. Oncotarget 5, 7081–7092.

McClurg, U.L., Harle, V.J., Nabbi, A., Batalha-Pereira, A., Walker, S., Coffey, K., et al., 2015. Ubiquitin-specific protease 12 interacting parterns Uaf-1 and WDR20 are potential therapeutic targets in prostate cancer. Oncotarget 6 (35), 37724–37736.

Mevissen, T.E.T., Komander, D., 2017. Mechanisms of deubiquitinase specificity and regulation. Annu. Rev. Biochem. 86, 159–192.

Moretti, J., Chastagner, P., Liang, C.C., Cohn, M.A., Israël, A., Brou, C., 2012. The ubiquitin-specific protease 12 (USP12) is a negative regulator of notch signaling acting on notch receptor trafficking toward degradation. J. Biol. Chem. 287, 2006–2016.

Olazabal-Herrero, A., García-Santisteban, I., Rodriguez, J.A., 2015. Structure-function analisis of USP1: insights into the role of Ser313 phosphorylation site and the effect of cancer-associated mutations on autocleavage. Mol. Cancer. https://doi.org/10.1186/s12943-015-0311-7.

Prieto, G., Fullaondo, A., Rodriguez, J.A., 2014. Prediction of nuclear export signals using weighted regular expressions (Wregex). Bioinformatics 30 (9), 1220–1227.

Sanyal, S., 2016. Reply to Rodriguez: mechanism of nuclear-cytosol chuttling of Usp12. Proc. Natl. Acad. Sci. U. S. A. 113 (24), E3317–3318.

Schindelin, J., Arganda-Carreras, I., Frise, E., Kaynig, V., Longair, M., Pietzsch, T., 2012. Fiji: an open-source platform for biological-image analysis. Nat. Methods 9 (7), 676–682.

Sowa, M.E., Bennett, E.J., Gygi, S.P., Harper, J.W., 2009. Defining the human deubiquitinating enzyme interaction landscape. Cell 138, 389–403.

Urbé, S., Liu, H., Hayes, S.D., Heride, C., Rigden, D.J., Clague, M.J., 2012. Systematic survey of deubiquitinase localization identifies USP21 as a regulator of centrosome- and microtubule-associated functions. Mol. Biol. Cell 23, 1095–1103.

Vlasschaert, C., Cook, D., Xia, X., Gray, D.A., 2017. The evolution and functional diversification of the deubiquitinating enzyme superfamily. Genome Biol. Evol. 9 (3), 558–573.

Wei, R., Liu, X., Yu, W., Yang, T., Cai, W., Liu, J., et al., 2015. Deubiquitinases in cancer. Oncotarget 6 (15), 12872–12889.

Yang, K., Moldovan, G.L., Vinciguerra, P., Murai, J., Takeda, S., D´Andrea, A.D., 2011. Regulation of the Fanconi anemia pathway by a SUMO-like delivery network. Genes Dev. 25, 1847–1858.

Ye, Y., Scheel, H., Hofmann, K., Komander, D., 2009. Dissection of USP catalytic domains reveals five common insertion points. Mol. Biosyst. 5 1979-1808.

Yin, J., Schoeffler, A.J., Wickliffe, K., Newton, K., Starovasnik, M.A., Dueber, E.C., et al., 2015. Structural insights into WD-repeat 48 activation of ubiquitin-specific protease 46. Structure 23 (11), 2043–2054.

Additional File 1

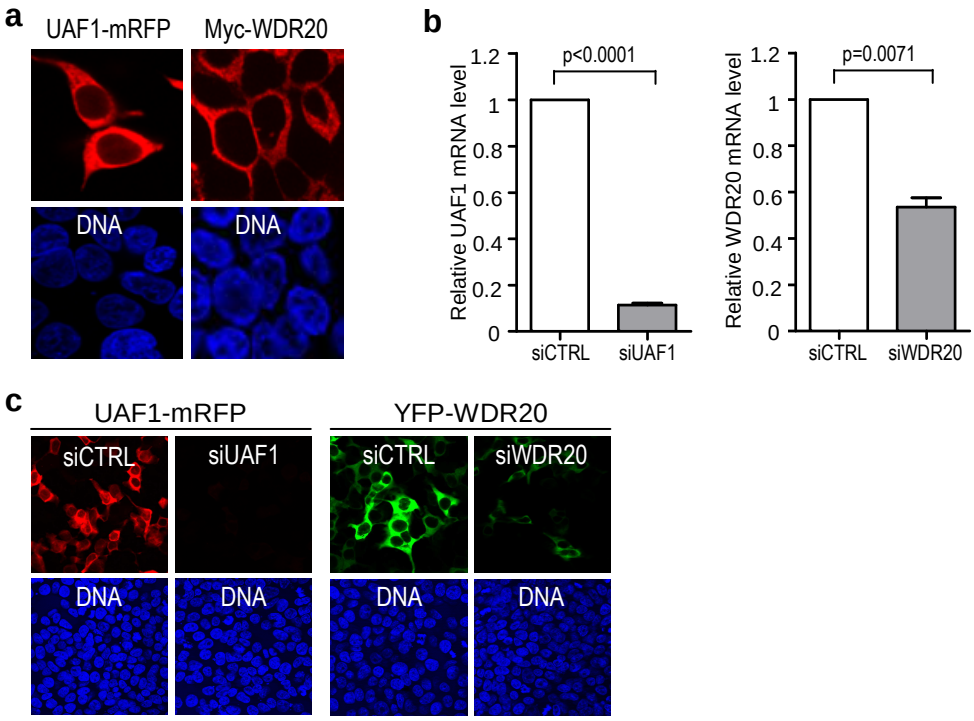

Additional File 1. Localization of epitope-tagged UAF1 and WDR20, and evaluation of siRNA-mediated knockdown efficiency.

a. Confocal microscopy images of 293T cells showing cytoplasmic localization of ectopically expressed UAF1-mRFP or Myc-WDR20. DAPI was used to visualize the nuclei (DNA panels). **b.** Graphs represent the relative expression level of UAF1 mRNA (*left*) and WDR20 mRNA (*right*) in 293T cells transfected with a scramble siRNA control (siCTRL) or with a pool of 3 siRNAs targeting UAF1 (siUAF1) and WDR20 (siWDR20). 48 h after siRNA transfection, RNA was isolated using TRIzol (Ambion), and cDNA was synthesized using the High Capacity cDNA Reverse Transcription Kit (Applied Biosystems). Quantitative real-time PCR (qRT-PCR) was performed using Premix Ex Taq (TaKaRa). Gene expression primers and probes (IDT) were used to specifically amplify UAF1 (#76415374) or WDR20 (#76415370) as well as human GAPDH (#65146232) as an endogenous control. Data were normalized to GAPDH and relative gene expression was calculated by using the ΔΔCt method. Bars represent the mean of three independent experiments, with error bars indicating standard deviation (S.D). The p values (Student´s t-test) are indicated. **c.** Representative images of 293T cells illustrating efficient siRNA-mediated knockdown of ectopically expressed UAF1-mRFP or YFP-WDR20 proteins. Cells were transfected with UAF1, WDR20 or scramble (control) siRNAs. 24 h later the same cells were transfected with the indicated expression plasmids. 24 h after plasmid transfection, cells were fixed, processed, and examined using confocal microscopy.

Additional File 2

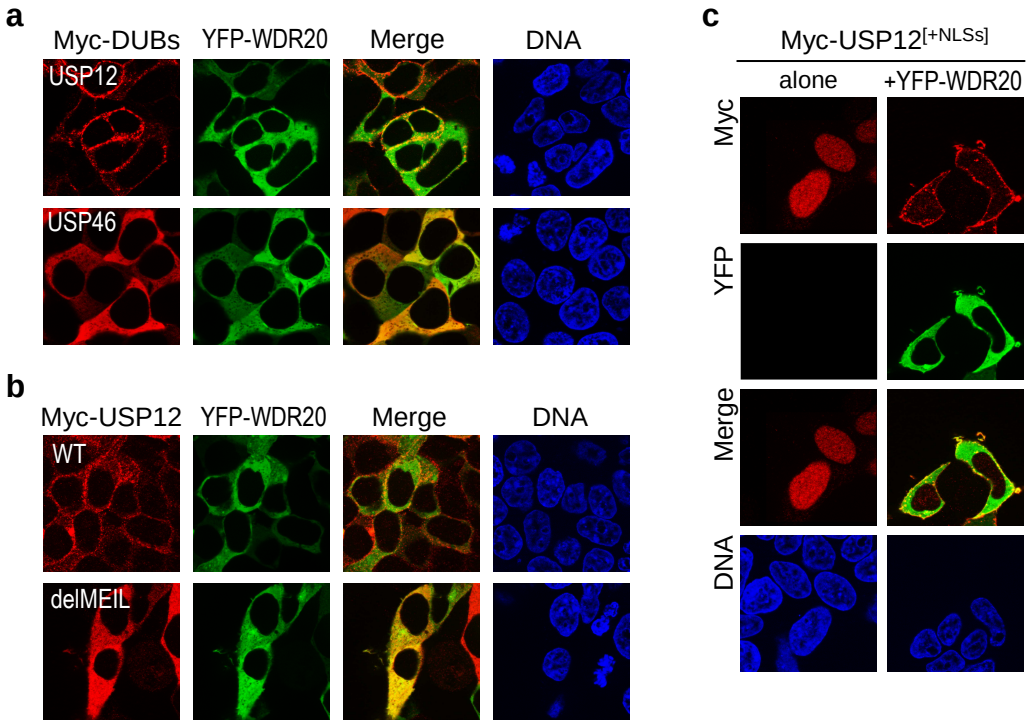

Additional file 2. Effect of YFP-WDR20 co-expression on the localization of Myc-tagged USP12.

a. Representative images of 293T cells co-expressing Myc-USP12 or Myc-USP46 with YFP-WDR20. Co-expression with WDR20 induced relocation of Myc-USP12, but not Myc-USP46, to the cell periphery. **b** Representative images of 293T cells co-expressing YFP-WDR20 with either wild type Myc-USP12 or Myc-USP12^{delMEIL}. Deletion of the MEIL motif abrogates WDR20-induced relocation of Myc-tagged USP12 to the cell periphery. **c**. Representative images of 293T cells expressing Myc-USP12$^{[+NLSs]}$ alone or co-expressing Myc-USP12$^{[+NLSs]}$ with YFP-WDR20. The localization of Myc-USP12$^{[+NLSs]}$ is exclusively nuclear due to the presence of two copies of the strong SV40 large T antigen NLS. However, co-expression with YFP-WDR20 strikingly changes its localization, leading to its relocation to the plasma membrane. Collectively, these observations recapitulate our observations made with YFP-tagged DUBs.

Additional File 3

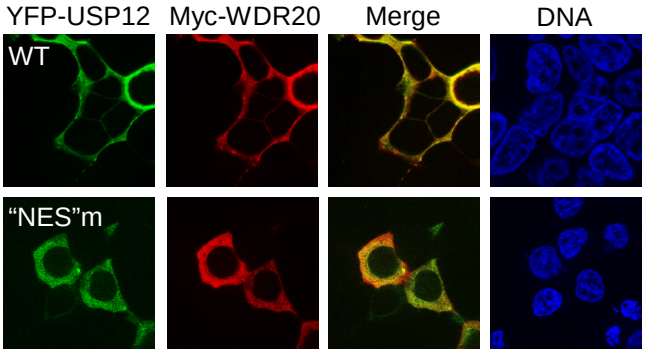

Additional file 3. Mutations in USP12 “NES” abrogate WDR20-induced relocation of USP12 to the plasma membrane.

Confocal microscopy images of 293T cells co-expressing either wild type YFP-USP12 or YFP-USP12$^{\text{"NES"m}}$ with Myc-WDR20. Mutations in USP12 “NES”, which disrupt WDR20 binding, abolished WDR20-induced relocation of USP12 to the plasma membrane.

Additional File 4

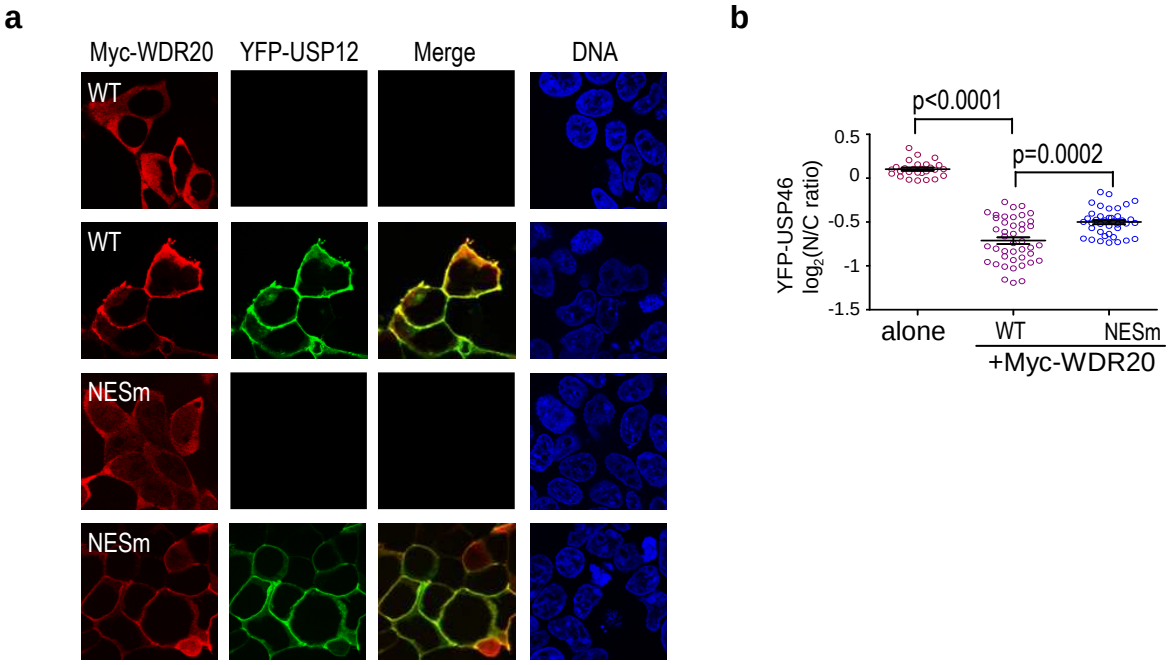

Additional file 4. Effect of WDR20 NES mutation in co-transfection experiments with YFP-USP12 and YFP-USP46.

a. Confocal microscopy images of 293T cells expressing Myc-WDR20 (wild type or NES-mutant) alone or with YFP-USP12. YFP-USP12 was similarly localized in the PM, with no detectable signal in the nucleus, when co-expressed with either version of Myc-WDR20. Of note, although Myc-WDR20^{NESm} is clearly more nuclear than the wild type when expressed alone, both versions of Myc-WDR20 similarly co-localized with YFP-USP12 in the PM. These observations suggest that, in the absence of a strong NLS in USP12, recruitment to the PM largely prevails over slow diffusion into the nucleus upon formation of a USP12/WDR20 complex, even if nuclear export is disrupted by mutation of WDR20 NES. **b.** Graph representing the nucleocytoplasmic distribution of YFP-USP46 in transfected 293T cells when expressed alone or when co-expressed with either wild type or NES-mutant Myc-WDR20. The intensity of the YFP signal in the nucleus and cytoplasm was quantified using image analysis and the nuclear to cytoplasmic (N/C) ratio was calculated. The N/C ratio of YFP-USP46 was significantly higher when expressed with Myc-WDR20^{NESm} than with wild type Myc-WDR20, suggesting that the NES of WDR20 contributes to the cytoplasmic localization of the USP46/WDR20 complex. Each circle in the graph represents a single cell, and the mean (+/-SD) is also indicated. The data correspond to a single experiment where at least 20 transfected cells per condition were analysed. The p value (Mann-Whitney U test) is indicated.

Published OnlineFirst July 8, 2019; DOI: 10.1158/2159-8290.CD-19-0298

RESEARCH ARTICLE

Altered Nuclear Export Signal Recognition as a Driver of Oncogenesis

Justin Taylor[1,2], Maria Sendino[3], Alexander N. Gorelick[1,4], Alessandro Pastore[1], Matthew T. Chang[1,4], Alexander V. Penson[1,4], Elena I. Gavrila[1,4], Connor Stewart[1], Ella M. Melnik[1], Florisela Herrejon Chavez[5], Lillian Bitner[1], Akihide Yoshimi[1], Stanley Chun-Wei Lee[1], Daichi Inoue[1], Bo Liu[1], Xiao J. Zhang[1], Anthony R. Mato[2], Ahmet Dogan[6], Michael G. Kharas[5], Yuhong Chen[7], Demin Wang[7], Rajesh K. Soni[8], Ronald C. Hendrickson[8], Gorka Prieto[9], Jose A. Rodriguez[3], Barry S. Taylor[1,4,10], and Omar Abdel-Wahab[1,2]

ABSTRACT Altered expression of XPO1, the main nuclear export receptor in eukaryotic cells, has been observed in cancer, and XPO1 has been a focus of anticancer drug development. However, mechanistic evidence for cancer-specific alterations in XPO1 function is lacking. Here, genomic analysis of 42,793 cancers identified recurrent and previously unrecognized mutational hotspots in *XPO1*. XPO1 mutations exhibited striking lineage specificity, with enrichment in a variety of B-cell malignancies, and introduction of single amino acid substitutions in XPO1 initiated clonal, B-cell malignancy *in vivo*. Proteomic characterization identified that mutant XPO1 altered the nucleocytoplasmic distribution of hundreds of proteins in a sequence-specific manner that promoted oncogenesis. XPO1 mutations preferentially sensitized cells to inhibitors of nuclear export, providing a biomarker of response to this family of drugs. These data reveal a new class of oncogenic alteration based on change-of-function mutations in nuclear export signal recognition and identify therapeutic targets based on altered nucleocytoplasmic trafficking.

SIGNIFICANCE: Here, we identify that heterozygous mutations in the main nuclear exporter in eukaryotic cells, XPO1, are positively selected in cancer and promote the initiation of clonal B-cell malignancies. XPO1 mutations alter nuclear export signal recognition in a sequence-specific manner and sensitize cells to compounds in clinical development inhibiting XPO1 function.

[1]Human Oncology and Pathogenesis Program, Memorial Sloan Kettering Cancer Center, New York, New York. [2]Leukemia Service, Department of Medicine, Memorial Sloan Kettering Cancer Center, New York, New York. [3]Department of Genetics, Physical Anthropology and Animal Physiology, University of the Basque Country, Barrio Sarriena s/n, Leioa, Spain. [4]Department of Epidemiology and Biostatistics, Memorial Sloan Kettering Cancer Center, New York, New York. [5]Molecular Pharmacology Program, Memorial Sloan Kettering Cancer Center, New York, New York. [6]Department of Pathology, Memorial Sloan Kettering Cancer Center, New York, New York. [7]Blood Research Institute, Blood Center of Wisconsin, Milwaukee, Wisconsin. [8]Microchemistry and Proteomics Core Facility, Memorial Sloan Kettering Cancer Center, New York, New York. [9]Department of Communications Engineering, University of the Basque Country (UPV/EHU), Bilbao, Spain. [10]Marie-Josée and Henry R. Kravis Center for Molecular Oncology, Memorial Sloan Kettering Cancer Center, New York, New York.

Note: Supplementary data for this article are available at Cancer Discovery Online (http://cancerdiscovery.aacrjournals.org/).

Current address for M.T. Chang: Genentech Inc., South San Francisco, CA; and current address for R.K. Soni: Proteomics Core, Herbert Irving Comprehensive Cancer Center, Columbia University Medical Center, New York, NY.

Corresponding Author: Omar Abdel-Wahab, Memorial Sloan Kettering Cancer Center, Zuckerman Research Building, 415 E 68th Street, New York, NY 10065. Phone: 347-821-1769; Fax: 646-422-0856; E-mail: abdelwao@mskcc.org

Cancer Discov 2019;9:1452–67

doi: 10.1158/2159-8290.CD-19-0298

Published OnlineFirst July 8, 2019; DOI: 10.1158/2159-8290.CD-19-0298

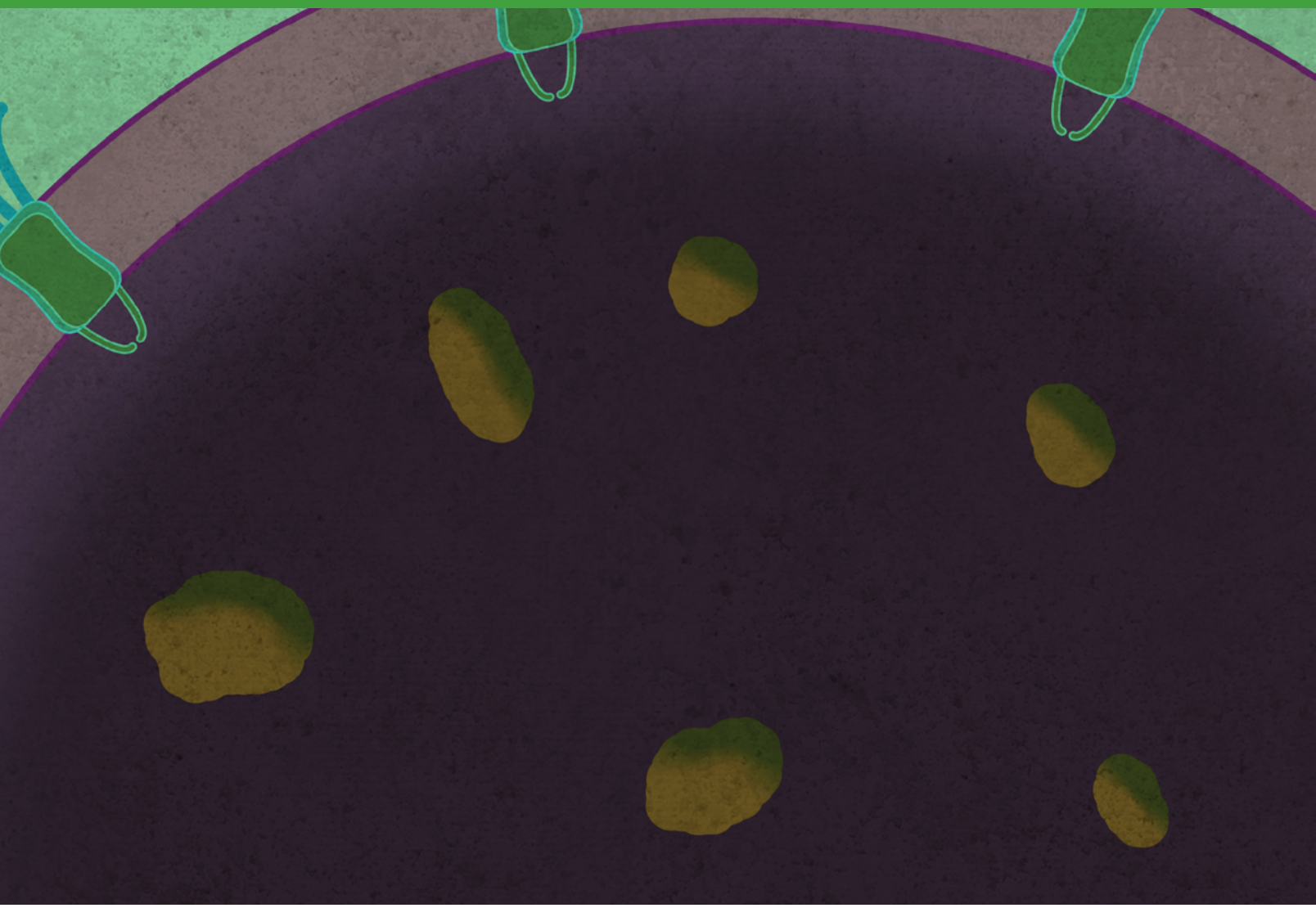

INTRODUCTION

Proper nucleocytoplasmic partitioning of macromolecules is essential to cellular homeostasis and is regulated by the nuclear pore complex and transport proteins that mediate trafficking of molecules across the nuclear envelope. Exportin-1 (XPO1; previously known as CRM1) is the major nuclear export receptor for proteins larger than approximately 40 kDa. To perform its exporting function, XPO1 identifies signals known as nuclear export signals (NES) embedded in the amino-acid sequence of cargo proteins. Protein cargoes bind XPO1 in the nucleus cooperatively with the small GTPase Ran, and the formation of ternary XPO1–RanGTP–cargo complexes begins the export process (1–3).

Numerous cellular pathways are regulated by controlling the subcellular localization of intermediate signaling proteins. Mutations that alter this nucleocytoplasmic localization in *cis* have been shown to drive transformation in a number of cancers (4–8). For example, mutations in nucleophosmin 1 (NPM1) that generate an NES and result in aberrant NPM1 cytoplasmic localization are among the most common genetic alterations in acute myeloid leukemia (9, 10). Similarly, mutations generating or eliminating an NES in *BRCA1* (11), *VHL* (12), and other recurrently mutated genes in cancer have been described. In addition, alterations in the machinery regulating nuclear export globally have been observed in cancer. Notably, increased expression of XPO1 has been described in numerous cancers (13–16), and many clinical trials have studied the efficacy of drugs inhibiting XPO1 in patients with cancer (16–21).

Despite interest in XPO1 as a therapeutic target in cancer, mechanistic evidence for cancer-specific derangements in XPO1 function has not been demonstrated. Mutations in *XPO1* occur in a variety of cancers (22–25), but the functional contributions of these mutations to tumorigenesis are also unknown. Further, there are no biomarkers of response to XPO1 inhibitors in advanced-phase clinical trials. Given that XPO1 is an essential protein in eukaryotic cells, defining biomarkers of response may define patients most likely to respond to these agents and potentially limit toxicity. Here,

Published OnlineFirst July 8, 2019; DOI: 10.1158/2159-8290.CD-19-0298

we find that *XPO1* mutations are positively selected for in a variety of cancers and sensitize cells to XPO1 inhibitors. Specific mutant residues in XPO1 directly promote malignant transformation by altering the ability of XPO1 to engage protein cargo for nuclear export. These data identify a novel model of oncogenesis: tumorigenesis driven by mutations that change the global distribution of proteins across the nuclear membrane. In addition, these data implicate mutant XPO1, as well as its consequently mistrafficked protein cargo, as targets for anticancer therapy.

RESULTS

XPO1 Mutations Are Recurrent across Cancers and Exhibit Lineage Specificity

Recent genomic analyses have identified recurrent heterozygous *XPO1*^{E571} mutations in a variety of cancer types, including chronic lymphocytic leukemia (CLL; refs. 22, 23), Hodgkin lymphoma (24), and esophageal carcinoma (25), among others. To systematically quantify the frequency and significance of *XPO1* mutational hotspots, we performed a large-scale analysis of whole-exome and genome sequencing data from 42,793 patients with cancer spanning 322 cancer types, using an extensively validated computational framework (26, 27). We identified highly recurrent and statistically significant hotspots in *XPO1* at E571 ($n = 99$ patients; q value = 10^{-204}), D624 ($n = 6$ patients; q value = 10^{-11}), and R749 ($n = 21$ patients; q value = 10^{-22}) residues (Fig. 1A), the latter two hotspots being previously unidentified. In addition, we found remarkable lineage specificity of *XPO1* hotspot mutations. E571K, the most common *XPO1* mutation, was enriched in B-cell lymphomas, including primary mediastinal B-cell lymphoma (PMBL; 33%), classic Hodgkin lymphoma (14%), and diffuse large B-cell lymphoma (DLBCL; 2%), and in CLL (3%; Fig. 1B and C; Supplementary Fig. S1A). In contrast, *XPO1* D624 mutations were found only in CLL, whereas those at R749 were found mostly in nonlymphoid solid-tumor malignancies (Supplementary Table S1). Strikingly, *XPO1* mutations were found only in the heterozygous state and never occurred as homozygous or hemizygous (i.e., LOH) mutations. We confirmed this in a separate cohort of 2,877 patients with hematologic malignancies in which we analyzed both mutations and copy-number state of *XPO1*. We found only a single patient who had both mutation and copy-number alteration in *XPO1* (a gain of mutant *XPO1*). Even in this case, the wild-type (WT) *XPO1* allele was retained (Supplementary Fig. S1B). These findings altogether suggest a novel change of function in *XPO1* caused by mutation.

XPO1^{E571K} Mutation Promotes Growth of Established Malignant B Cells

The recurrence, more often than expected in the absence of selection, of mutations at specific amino-acid residues in XPO1 suggests that *XPO1* hotspot mutations functionally promote B-cell malignancies and other cancers. To evaluate the functional effects of *XPO1* mutations, we used genome editing to generate isogenic B-cell leukemia cells (NALM-6 cells; ref. 28) with physiologic expression of the *XPO1*^{E571K} mutation from the endogenous *XPO1* locus (Supplementary Fig. S1C). There was an equal ratio of *XPO1*^{E571K} mutant allele to *XPO1*^{WT} allele at the level of genomic DNA and mRNA (50% variant allele frequency). Expression of the heterozygous *XPO1*$^{E571K/WT}$ mutation in NALM-6 cells resulted in increased proliferation *in vitro* in both noncompetitive and competitive growth assays relative to *XPO1*^{WT} counterparts (Supplementary Fig. S1D–S1F). Enhanced growth of *XPO1*$^{E571K/WT}$ mutant cells was also seen *in vivo* through xenotransplantation of equal numbers of luciferase-labeled *XPO1*$^{E571K/WT}$ mutant or *XPO1*$^{WT/WT}$ cells (Fig. 1D and E; Supplementary Fig. S1G). The effects of *XPO1* mutation were distinct from *XPO1* genetic depletion, which completely suppressed cell growth (Supplementary Fig. S1D), a finding consistent with the known essentiality of XPO1 for cell survival (29, 30).

Xpo1^{E571K} Mutations Promote B-cell Proliferation and Transformation *In Vivo*

Given the high conservation of XPO1 across mammals (Supplementary Fig. S2A), we next generated a conditional knock-in mouse model to express the *Xpo1*^{E571K} mutation from the endogenous *Xpo1* locus to determine its *in vivo* effects (Supplementary Fig. S2B and S2C). Heterozygous expression of *Xpo1*^{E571K} in the B-cell compartment using *CD19*-Cre *Xpo1*$^{E571K/WT}$ mice resulted in selective expression of the *Xpo1*^{E571K} mutation in B cells at approximately 50% allelic ratio and had no effect on XPO1 protein expression in B cells relative to Cre-negative *Xpo1*$^{E571K/WT}$ controls (Supplementary Fig. S2D–S2F).

CD19-Cre *Xpo1*$^{E571K/WT}$ mice were born at expected Mendelian ratios (Supplementary Fig. S3A) but were smaller in body weight relative to littermate controls (Supplementary Fig. S3B). Despite the smaller body size, *CD19*-Cre *Xpo1*$^{E571K/WT}$ mice had significantly larger spleens at 12 weeks of age (Fig. 1F). Colony-forming assays in IL7 using bone marrow (BM) from mice with tamoxifen-inducible pan-hematopoietic *Xpo1*$^{E571K/WT}$ expression (*CAG*-CreERT *Xpo1*$^{E571K/WT}$ mice) revealed increased numbers of B-cell colonies with enhanced clonogenicity upon replating (Fig. 1G), a finding restricted to the B-cell compartment (Supplementary Fig. S3C) and lost in the absence of IL7 supplementation (Supplementary Fig. S3D). *CD19*-Cre *Xpo1*$^{E571K/WT}$ mice died more rapidly than littermate controls and had increased B-cell proliferation, B-cell lymphocytosis, anemia, and thrombocytopenia (Fig. 2A; Supplementary Fig. S3E–S3H), and had increased numbers of mature (CD19$^+$ IgM$^+$ IgD$^+$) B cells in the BM and transitional T1 and T2 B cells (CD19$^+$ CD21^{lo} IgM^{hi} CD93$^+$ CD23$^-$ and CD19$^+$ CD21^{lo} IgM^{hi} CD93$^+$ CD23$^+$, respectively) in the spleen as well as splenomegaly (Fig. 2B–D). *CD19*-Cre *Xpo1*$^{E571K/WT}$ mice developed greater splenomegaly (Fig. 2E) as a result of increased generation of germinal centers and germinal center (B220$^+$ FAS$^+$ GL7$^+$) B cells upon alloimmunization with sheep red blood cells (SRBC), an effect that was evident 7 days after a single SRBC injection (Fig. 2F; Supplementary Fig. S3I and S3J).

A portion of *CD19*-Cre *Xpo1*$^{E571K/WT}$ mice developed a lethal B-cell disease infiltrating lymph nodes, spleen, lungs, and BM, with coexpression of CD5 and CD23, characteristic features of human CLL, a cancer type frequently carrying *XPO1*^{E571} mutations (Fig. 2G; Supplementary Fig. S4A–S4E). Next-generation sequencing of VDJ sequences from splenic mononuclear cells of these mice at the time of death

Published OnlineFirst July 8, 2019; DOI: 10.1158/2159-8290.CD-19-0298

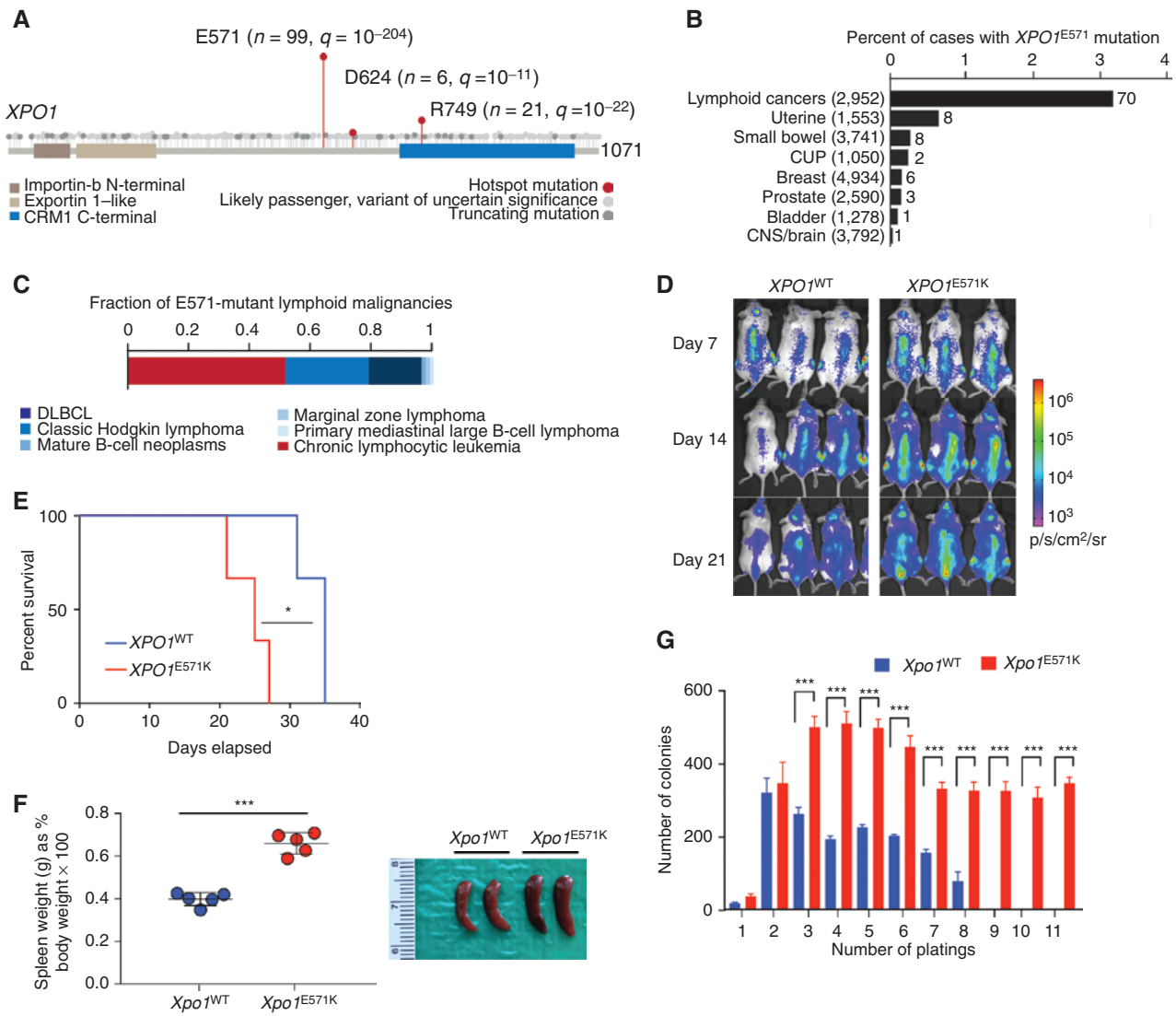

Figure 1. *XPO1* hotspot mutations promote proliferation *in vivo*. **A,** Lollipop plot of the distribution and frequency of *XPO1* mutations across patients with cancer and identification of statistically significant *XPO1* mutational hotspots (FDR < 1%). **B,** Frequency of *XPO1*^{E571} mutations by cancer type in 42,793 sequenced tumors (CNS, central nervous system; CUP, cancer of unknown primary). The number of individual patients with *XPO1*^{E571} mutations within each disease category is also shown. **C,** Fraction of *XPO1*^{E571} mutations by subtype of lymphoid malignancy. **D,** Imaging of luciferase-labeled *XPO1*^{WT} and *XPO1*^{E571K} mutant NALM-6 cells *in vivo* after xenografting into NSG mice. Four NSG mice were engrafted in each group. **E,** Kaplan–Meier survival curves of the mice from **D**. Survival was computed using the Kaplan–Meier estimator (*, $P = 0.02$). **F,** Spleen weights and representative photos from *CD19*-Cre *Xpo1*$^{WT/WT}$ and *CD19*-Cre *Xpo1*$^{E571K/WT}$ mice ($n = 5$ mice/group; ruler represents centimeters). **G,** Number of colonies of BM cells from *Xpo1*^{WT} and *Xpo1*$^{E571K/WT}$ mice in methylcellulose media containing IL7 ($n = 3$ mice/group). Equal numbers of cells were replated. Differences were calculated using a two-sided Student *t* test. *, $P < 0.05$; **, $P < 0.01$; ***, $P < 0.001$.

identified productive clonal sequences occupying >98% of the total reads, indicating the presence of a highly clonal B-cell malignancy (Supplementary Fig. S4F).

Xpo1^{E571K} Mutations Promote Lymphomagenesis Driven by c-MYC and BCL2

The above data reveal that expression of cancer-associated *XPO1* mutations can initiate lymphomagenesis when the correct microenvironmental stimulus is present (alloantigen from SRBC immunization). However, more aggressive lymphomas featuring *XPO1*^{E571K} mutations may require additional cooperating mutations to fully manifest the disease phenotype. To evaluate this hypothesis, we crossed *Xpo1*$^{E571K/WT}$ mice to mice with overexpression of either c-MYC (using the *Eμ*-Myc mouse model; ref. 31) or BCL2 (using *Vav*-BCL2 transgenic mice; ref. 32) to model the aggressive lymphomas marked by overexpression of either of these oncogenic proteins in addition to *XPO1* mutations.

First, we crossed *Eμ*-Myc mice (which express human c-MYC transgenically from the immunoglobulin locus) to *CAG*-CreERT *Xpo1*$^{E571K/WT}$ mice, allowing induction of mutant *XPO1* only after exposure to tamoxifen (Fig. 3A; Supplementary Fig. S5A). Mice transplanted with *Eμ*-Myc–driven lymphomas conditionally expressing *Xpo1*$^{E571K/WT}$ in hematopoietic cells

Published OnlineFirst July 8, 2019; DOI: 10.1158/2159-8290.CD-19-0298

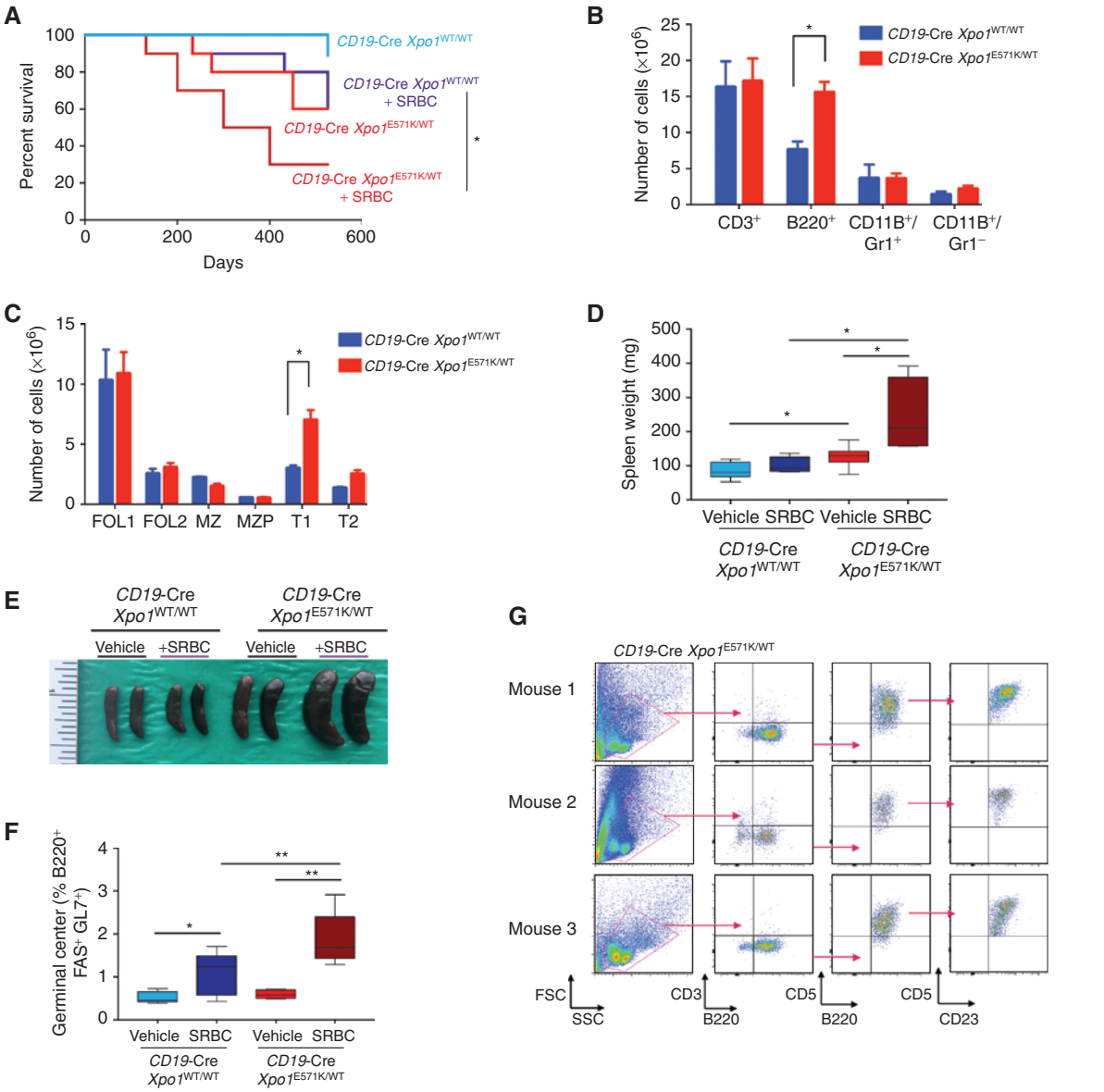

Figure 2. Endogenous expression of *Xpo1*^{E571K} mutant in mice enhances proliferation and promotes B-cell transformation. **A,** Kaplan–Meier survival curve of *CD19*-Cre *Xpo1*$^{WT/WT}$ and *CD19*-Cre *Xpo1*$^{E571K/WT}$ mice treated monthly with vehicle or alloimmunization with SRBCs ($n = 10$ mice/group). **B,** Number of mature myeloid and lymphoid cells in the BM and (**C**) B-cell subsets in spleens of 12-week-old *CD19*-Cre *Xpo1*$^{WT/WT}$ ($n = 5$ mice) and *CD19*-Cre *Xpo1*$^{E571K/WT}$ mice [$n = 5$ mice; MZ, marginal zone (CD19$^+$ CD21^{hi} IgM^{hi} B220$^+$ CD23$^-$); MZP, marginal zone precursor (CD19$^+$ CD21^{hi} IgM^{hi} B220$^+$ CD23$^-$); FOL, follicular (CD19$^+$ CD21$^+$ IgM$^+$ IgD$^+$); T, transitional (CD19$^+$ CD21^{lo} IgM^{hi} CD93$^+$)]. **D,** Spleen weights and (**E**) representative images of spleens at time of death from mice in **A** (ruler represents inches). **F,** Frequency of germinal center (B220$^+$ FAS$^+$ GL7$^+$) B cells in spleens from *CD19*-Cre *Xpo1*$^{E571K/WT}$ or *CD19*-Cre *Xpo1*$^{WT/WT}$ mice 1 week after SRBC or vehicle treatment ($n = 7$ mice/group). **G,** Flow cytometry of tumors from 3 independent *CD19*-Cre *Xpo1*$^{E571K/WT}$ mice showing B220/CD5/CD23 triple-positive cells in peripheral blood. Differences were calculated using a two-sided Student *t* test. *, $P < 0.05$; **, $P < 0.01$.

following engraftment (*CAG*-CreERT *Xpo1*$^{E571K/WT}$ *Eμ*-Myc mice exposed to tamoxifen) succumbed to lethal disease more rapidly than controls (*CAG*-CreERT *Xpo1*$^{E571K/WT}$ *Eμ*-Myc mice exposed to vehicle; Fig. 3B and C). Expression of *Xpo1*$^{E571K/WT}$ further increased B-cell lymphocytosis driven by *Eμ*-Myc throughout the blood, spleen, and BM, resulting in more rapidly lethal spleen and BM infiltration (Fig. 3D–F). Here again, sequencing of VDJ sequences from splenic mononuclear cells confirmed that death was due to infiltration of B cells which were >90% clonal (Supplementary Fig. S5B). Notably, a subset of the B cells gained aberrant CD5 expression (Supplementary Fig. S5C), and *Eμ*-Myc *CAG*-CreERT *Xpo1*$^{E571K/WT}$ mutant cells were larger as measured by flow cytometry as well as cytologic analysis with Wright–Giemsa stain compared with controls (Supplementary Fig. S5D and S5E). Whole transcriptomic analysis by mRNA sequencing (RNA-seq) of tumors from *CAG*-CreERT *Xpo1*$^{E571K/WT}$ *Eμ*-Myc and *CAG*-CreERT *Eμ*-Myc controls revealed that *Xpo1*^{E571K} expression in the context of

Published OnlineFirst July 8, 2019; DOI: 10.1158/2159-8290.CD-19-0298

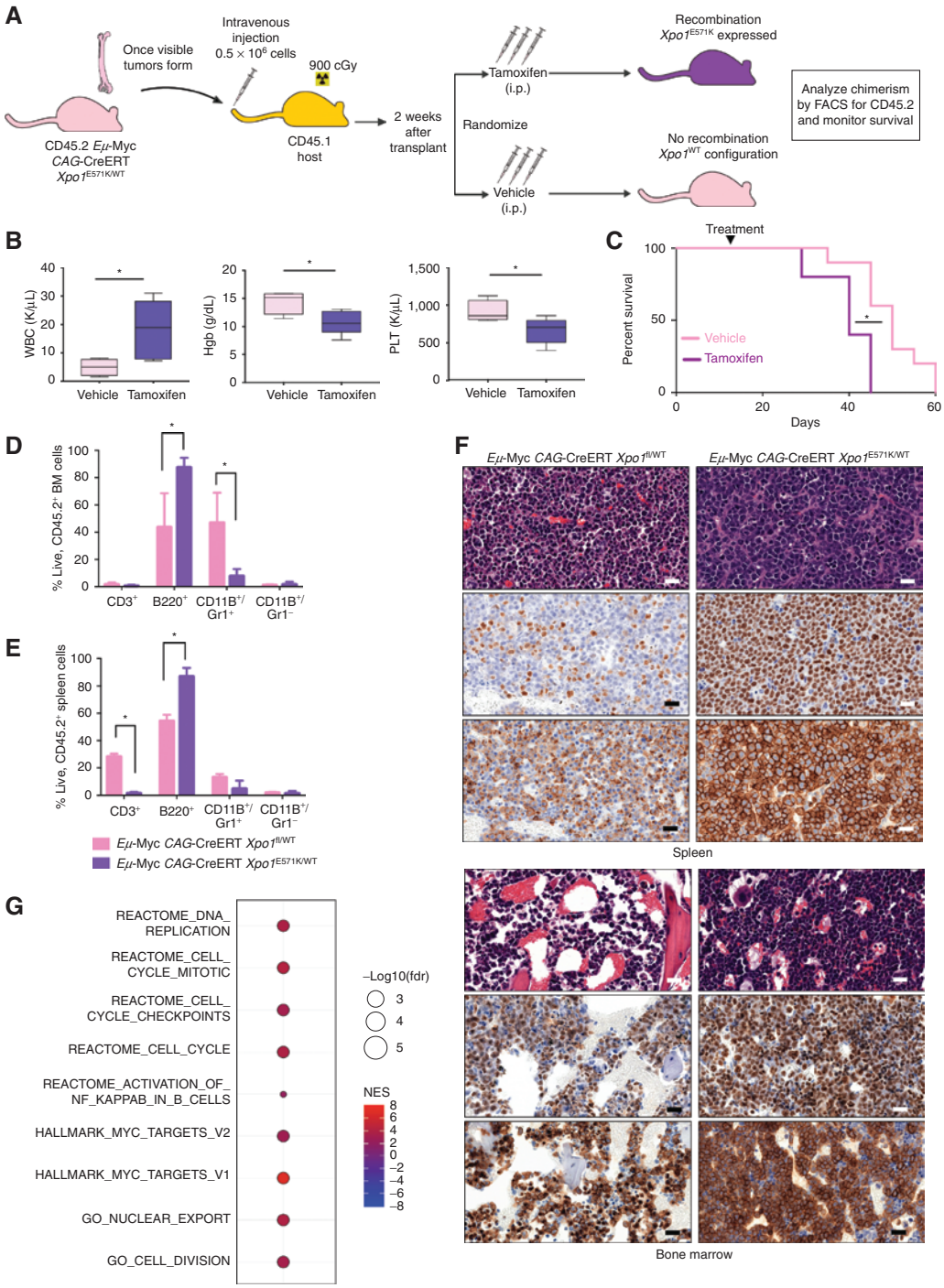

Figure 3. *Xpo1* mutations cooperate with MYC overexpression to drive lymphomagenesis. **A,** Schema of the method to analyze the effect of the *Xpo1*^{E571K} mutation on MYC-driven B-cell lymphomagenesis *in vivo*. *CAG*-CreERT *Xpo1*$^{E571K/WT}$ *Eμ*-Myc mice were generated on a CD45.2 C57BL/6J mice background and then 1×10^6 BM mononuclear cells were transplanted into lethally irradiated CD45.1 C57BL/6J recipient mice. Following 2 weeks of engraftment, tamoxifen was administered intraperitoneally (i.p.) to half of the recipients to result in expression of the mutant allele, and vehicle was administered to the other half of the recipients. **B,** Complete blood counts (Hgb, hemoglobin; PLT, platelets; WBC, white blood cells) from *CAG*-CreERT *Xpo1*$^{E571K/WT}$ *Eμ*-Myc mice with (tamoxifen) or without (vehicle) induction of the *Xpo1*$^{E571K/WT}$ at end-stage disease ($n = 5$ recipient mice/group). **C,** Kaplan–Meier survival curves of recipients of BM from *CAG*-CreERT *Xpo1*$^{E571K/WT}$ *Eμ*-Myc following tamoxifen or vehicle treatment resulting in expression of *Xpo1* mutant allele or *Xpo1*^{WT} configuration, respectively ($n = 5$ mice/group). Number of mature myeloid and lymphoid cells in the (**D**) BM and (**E**) spleen of recipients of mice from **C** at end-stage disease ($n = 5$ recipient mice/group). **F,** Hematoxyiln and eosin stain (top), anti-Ki67 IHC stain (middle), and anti-B220 IHC stain (bottom) in spleen (first three rows) and BM (bottom three rows) from *CAG*-CreERT *Xpo1*$^{WT/WT}$ *Eμ*-Myc and *CAG*-CreERT *Xpo1*$^{E571K/WT}$ *Eμ*-Myc mice. Scale bars, 100 μm (left) and 20 μm (right). **G,** Gene ontology analysis for biological processes significantly enriched in differentially expressed genes from mRNA sequencing of *CAG*-CreERT *Xpo1*$^{E571K/WT}$ *Eμ*-Myc versus *CAG*-CreERT *Xpo1*$^{WT/WT}$ *Eμ*-Myc tumors (NES, normalized enrichment score). Survival was computed using the Kaplan–Meier estimator. Differences were calculated using a two-sided Student *t* test. *, $P < 0.05$.

Published OnlineFirst July 8, 2019; DOI: 10.1158/2159-8290.CD-19-0298

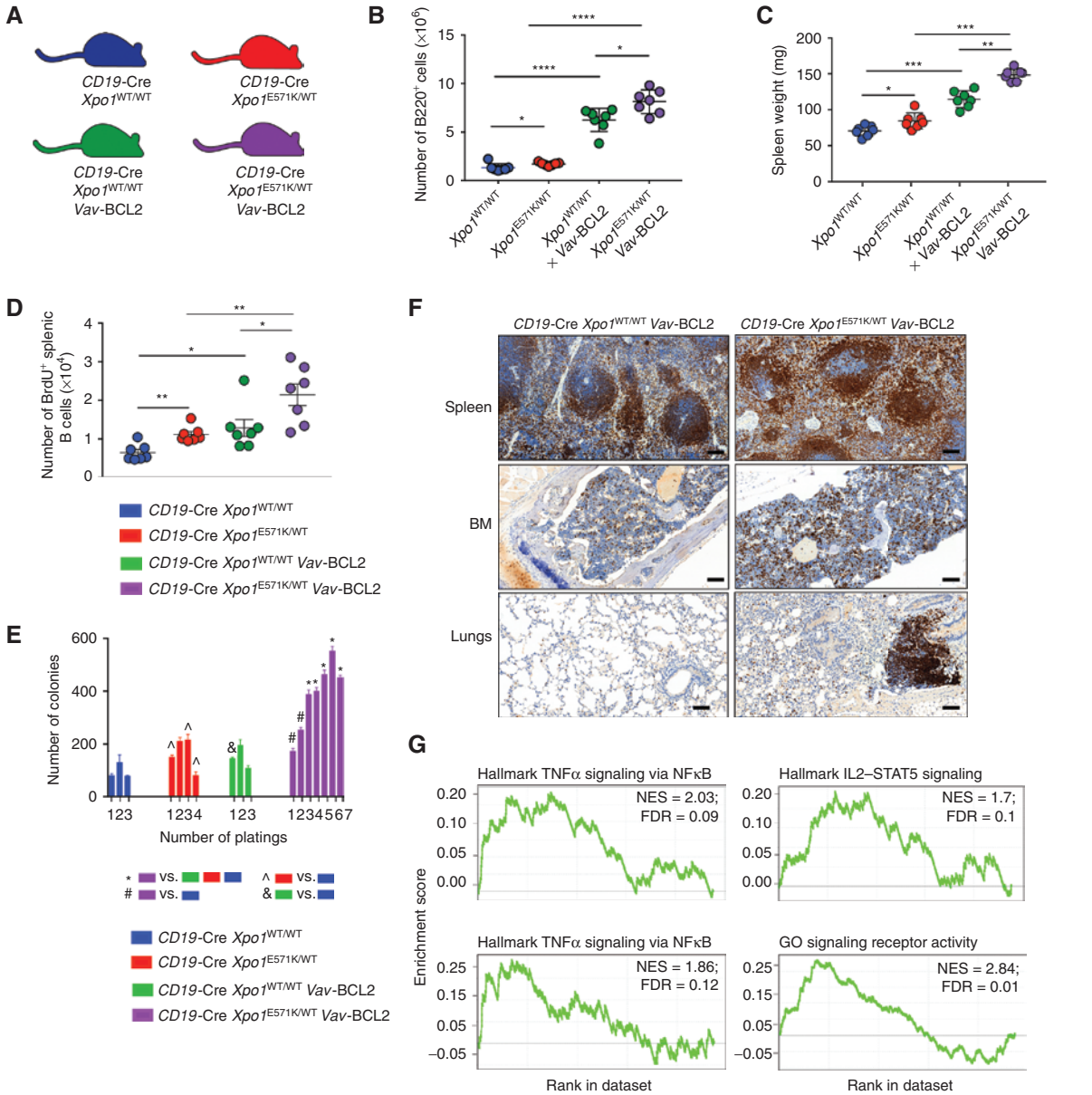

Figure 4. *Xpo1* mutations cooperate with BCL2 overexpression to drive lymphomagenesis. **A,** Schematic showing the four genotypes of mice created by crossing *CD19*-Cre *Xpo1*$^{E571K/WT}$ and *Vav*-BCL2 mice. **B,** Absolute number of B cells in the peripheral blood and (**C**) spleen weight of 12-week-old *CD19*-Cre *Xpo1*$^{WT/WT}$, *CD19*-Cre *Xpo1*$^{E571K/WT}$, *CD19*-Cre *Xpo1*$^{WT/WT}$ *Vav*-BCL2, and *CD19*-Cre *Xpo1*$^{E571K/WT}$ *Vav*-BCL2 mice ($n = 7$ mice/group). **D,** Number of BrdU$^+$ splenic B220$^+$ B cells from 12-week-old mice (BrdU was administered *in vivo* and animals were sacrificed 48 hours later for analysis). **E,** Number of colonies grown from BM cells from respective genotypes in IL7-containing methylcellulose. **F,** Anti-B220 IHC in *CD19*-Cre *Xpo1*$^{WT/WT}$ *Vav*-BCL2 and *CD19*-Cre *Xpo1*$^{E571K/WT}$ *Vav*-BCL2 mice. Scale bars, 200 μm. **G,** Gene set enrichment analysis of key pathways dysregulated from mRNA sequencing of *CD19*-Cre *Xpo1*$^{E571K/WT}$ *Vav*-BCL2 versus *CD19*-Cre *Xpo1*$^{WT/WT}$ *Vav*-BCL2 mice (NES, normalized enrichment score). Differences were calculated using a two-sided Student *t* test. *, $P < 0.05$; **, $P < 0.01$; ***, $P < 0.001$; ****, $P < 0.0001$.

Eμ-Myc tumors increased expression of established MYC targets as well as gene expression programs related to cell cycle, nuclear export, and NFκB activation (Fig. 3G).

Next, we crossed *Vav*-BCL2 transgenic mice (which overexpress human BCL2 throughout the hematopoietic system) to *CD19*-Cre *Xpo1*$^{E571K/WT}$ mice (Fig. 4A). *CD19*-Cre *Xpo1*$^{E571K/WT}$ *Vav*-BCL2 mice had increased peripheral blood leukocytosis, splenomegaly, and a greater absolute number of B cells in the blood, BM, and spleen compared with *CD19*-Cre *Vav*-BCL2 controls (Fig. 4B; Supplementary Fig. S6A and S6B). *In vivo* bromodeoxyuridine (BrdU) uptake assays also confirmed that mice with combined *Xpo1* mutation and BCL2 overexpression had greater splenomegaly and higher numbers and proliferation of BM and splenic B cells relative to controls (Fig. 4C and D; Supplementary Fig. S6C). *In vitro* proliferation and self-renewal (measured by colony-forming assays in IL7) was also greater in *CD19*-Cre *Xpo1*$^{E571K/WT}$ *Vav*-BCL2 than in *CD19*-Cre *Xpo1*$^{WT/WT}$ *Vav*-BCL2 mice (Fig. 4E). Overall, *CD19*-Cre *Xpo1*$^{E571K/WT}$ *Vav*-BCL2 mice had increased B-cell invasion in the spleen, BM, and lungs (Fig. 4F) and succumbed to lethal B-cell malignancy

Published OnlineFirst July 8, 2019; DOI: 10.1158/2159-8290.CD-19-0298

sooner than controls (Supplementary Fig. S6D). Gene set enrichment analysis of genes differentially expressed between *CD19*-Cre *Xpo1*$^{E571K/WT}$ *Vav*-BCL2 and *CD19*-Cre *Xpo1*$^{WT/WT}$ *Vav*-BCL2 mice was significant for cytokine receptor signaling via NFκB, a pattern that was seen in the *CD19*-Cre *Xpo1*$^{E571K/WT}$ versus WT mice in the absence of BCL2 (Fig. 4G).

Altered Nuclear/Cytoplasmic Compartmentalization of Proteins in *XPO1*^{E571K} Mutant Cells

To evaluate how mutations in *XPO1* might drive lymphoid malignancy development, we next sought to identify patterns of mutational co-occurrence or exclusivity in patients bearing *XPO1*^{E571K} mutations. In an additional cohort of 2,877 patients with hematologic malignancies who were uniformly sequenced by the MSK HemePACT assay (33), we identified 29 *XPO1*-mutant patients from patients with CLL ($n = 288$), Hodgkin lymphoma ($n = 16$), PMBL ($n = 9$), B-cell acute lymphoblastic leukemia ($n = 142$), or DLBCL ($n = 284$). Although we identified numerous genetic alterations coexisting with *XPO1* mutations in each of these histologic subtypes of B-cell malignancies (Supplementary Fig. S7A–S7D), there were no statistically different mutational co-occurrences between *XPO1*-mutant versus WT cases in each of these disease categories. We also similarly sequenced a cohort of splenocytes at time of death from 3 *CD19*-Cre *Xpo1*$^{E571K/WT}$ mice and 3 *CD19*-Cre *Xpo1*$^{WT/WT}$ mice of similar age (using a sequencing panel targeting the entire coding region of the mouse orthologs of 578 genes recurrently mutated in solid tumors, lymphomas, and leukemias; Supplementary Table S2). This revealed several somatic mutations in 1 of the 3 *CD19*-Cre *Xpo1*$^{E571K/WT}$ mice including compound p53 mutations (*Trp53*^{Y120S}, *Trp53*^{M157V}), an *Msh2* splice-site mutation (*Msh2* c.793-8A>T), and a missense mutation in *Tcf7l2* (*Tcf7l2*^{S512L}), a transcription factor through which β-catenin functions.

Given the known role of XPO1 in nuclear export, we next took an unbiased proteomics approach to detect pathways and individual XPO1 cargoes affected by the E571K mutation. We quantified the partitioning of proteins between the cytoplasm and nucleus of human B-cell malignant cells (NALM-6 cells) with or without knock-in of *XPO1*$^{E571K/WT}$. We performed stable isotope labeling with amino acids in cell culture (SILAC)–based mass spectrometry on fractionated nuclear and cytoplasmic lysates from *XPO1*$^{E571K/WT}$ and *XPO1*$^{WT/WT}$ NALM-6 cells (Fig. 5A). Several proteins were identified as significantly differentially exported in *XPO1*$^{E571K/WT}$ versus *XPO1*$^{WT/WT}$ cells [fold change ratios $>|2|$ and $-\log_{10}$ (P value) ≥ 1.30; Fig. 5B; Supplementary Tables S3–S5], including numerous members of the K63-ubiquitination, TLR4, and NFκB pathways, among others (Fig. 5C).

Phenotypically, *XPO1*$^{E571K/WT}$ cells demonstrated higher baseline and postactivation NFκB and NFAT transcriptional responses to stimulation with TNFα or PMA/ionomycin, respectively, than *XPO1*$^{WT/WT}$ cells (Fig. 5D and E). Differential gene-expression analysis of mRNA sequencing of pro-B (CD19$^+$ CD43$^+$ CD24$^+$ BP-1$^-$), pre-B (CD19$^+$ CD43$^-$ IgM$^-$ IgD$^-$), immature (CD19$^+$ CD43$^-$ IgM$^+$ IgD$^-$), and mature B cells (CD19$^+$ CD43$^-$ IgM$^+$ IgD$^+$) from *CD19*-Cre *Xpo1*$^{E571K/WT}$ and littermate *CD19*-Cre *Xpo1*$^{WT/WT}$ control mice identified prominent upregulation of pathways associated with cytokine signaling and immune responses in *Xpo1*$^{E571K/WT}$ mutant mature B cells relative to controls (Fig. 5F; Supplementary Fig. S8A and S8B). Consistent with this finding, serum from 12-week-old *CD19*-Cre *Xpo1*$^{WT/WT}$ and *CD19*-Cre *Xpo1*$^{E571K/WT}$ mice contained increased IgM autoantibodies to histone H1, a finding associated with dysregulated immune signaling (Supplementary Fig. S8C). Moreover, we identified a similar transcriptional signature of increased cytokine immune response and inflammation in patients with human CLL with *XPO1* mutations compared with patients with CLL without *XPO1* mutations (Fig. 5G; Supplementary Table S6). Differential export of NFκB and NFAT signaling proteins was confirmed by Western blot, which revealed enhanced nuclear phosphorylated p65 and NFAT2 in *XPO1* mutants relative to WT (Fig. 5H and I). Other proteins whose subcellular localization was altered by *XPO1*$^{E571K/WT}$ in our SILAC experiment were confirmed by Western blot, including TRAF2 (increased in nuclear export in the setting of mutant XPO1^{E571K}) and p120 catenin (which was decreased in nuclear export in the setting of mutant XPO1^{E571K}; Supplementary Fig. S8D). Finally, the increased NFκB and NFAT signaling and differential export of their member proteins by *XPO1*$^{E571K/WT}$ were validated in a CLL cell line (MEC1) engineered to express WT or E571K-mutant *XPO1* as well as a series of mature B-cell lymphoma cell lines naturally carrying endogenous *XPO1*^{E571K} mutations (Supplementary Fig. S8D–S8H).

XPO1^{E571K} Mutations Are Predicted to Alter the Function of XPO1 Nuclear Export

XPO1 binds to its cargo by recognizing 8- to 15-residue amino-acid motifs known as leucine-rich NESs (1–3, 34), which show a characteristic spacing of hydrophobic residues separated by other amino acids (described as $\Phi^1\text{-}X_{(2,3)} - \Phi^2\text{-}X_{(2,3)} - \Phi^3\text{-}X\text{-}\Phi^4$, where "Φ" represents leucine, isoleucine, valine, phenylalanine, or methionine). Atomic-level characterization of the XPO1/NES interaction has revealed that XPO1 binds NES of cargo proteins in a hydrophobic cleft on the outer convex surface of XPO1 (35–38). We therefore modeled the position of *XPO1* hotspot mutations on the three-dimensional structure of XPO1 to understand the mechanism by which these mutations alter nuclear export of the proteins we identified. Interestingly, the two hotspot mutations in *XPO1* arising in CLL and B-cell lymphomas (D624 and E571), although separated in two-dimensional amino-acid sequence, were both adjacent in the cognate folded protein structure of the NES binding cleft of XPO1 (Fig. 6A). Further structural modeling predicted that the change of a negatively charged glutamic acid at XPO1^{E571} to a positively charged lysine would promote XPO1 interaction with protein cargo bearing negatively charged amino-acid residues C-terminal to the NES (Fig. 6B). Simultaneously, XPO1^{E571K} mutation would be predicted to repel interactions with proteins bearing positively charged amino-acid residues C-terminal to the NES.

XPO1^{E571K} Mutations Alter NES Recognition in a Sequence-Specific Manner

As described above, analysis of our SILAC-based mass spectrometry data identified a number of NES-bearing proteins as depleted in the nucleus and/or enriched in the cytoplasm of *XPO1*$^{E571K/WT}$ mutant versus *XPO1*$^{WT/WT}$ cells beyond NFκB

Published OnlineFirst July 8, 2019; DOI: 10.1158/2159-8290.CD-19-0298

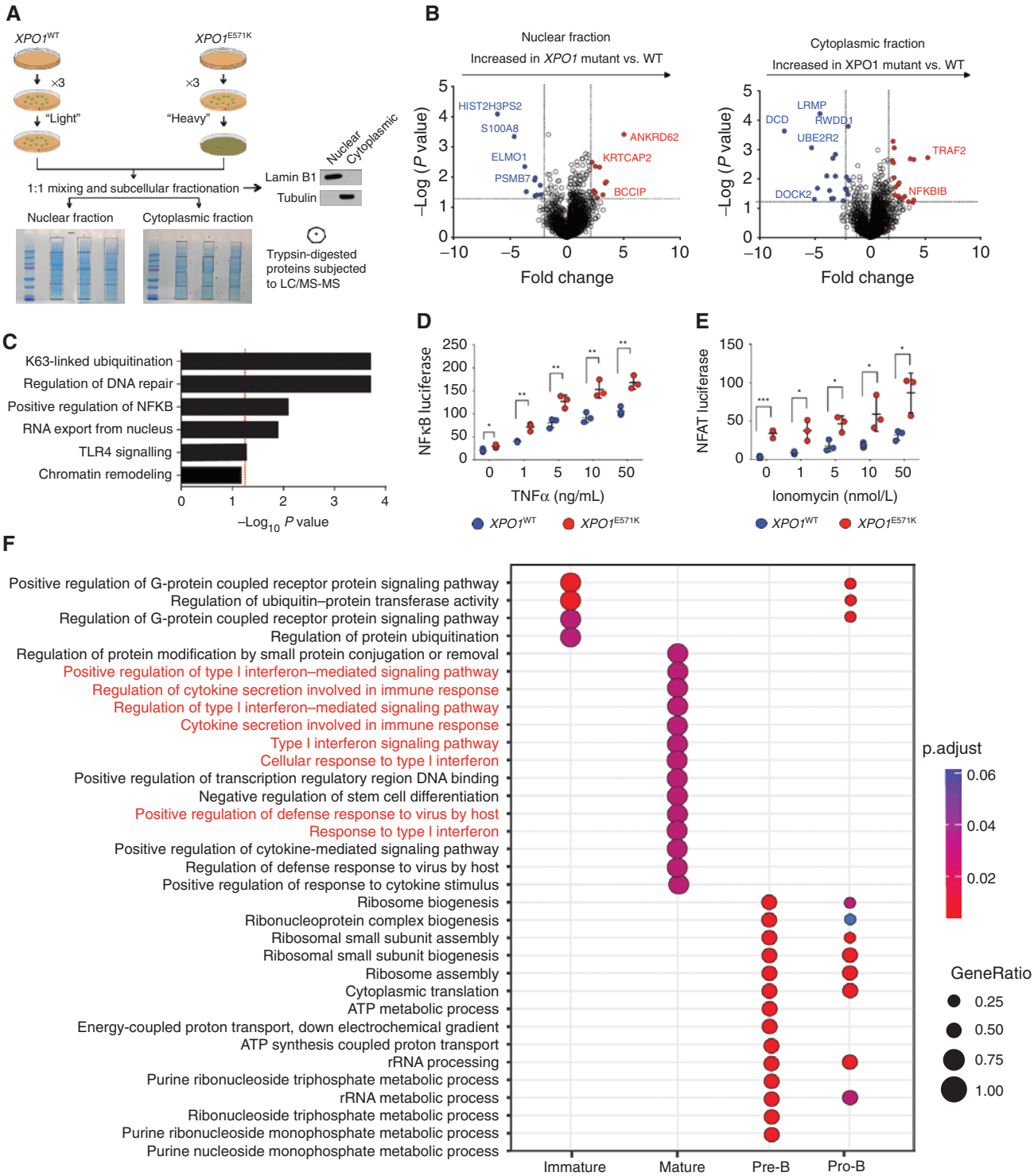

Figure 5. Aberrant nuclear/cytoplasmic compartmentalization of proteins and enhanced immune signaling in *XPO1* mutant cells. **A,** Schema of SILAC-based mass spectrometry analysis of nuclear and cytoplasmic proteins from isogenic NALM-6 *XPO1*$^{E571K/WT}$ and *XPO1*$^{WT/WT}$ cells. SILAC experiments were performed in biological triplicate. **B,** Volcano plots of differential protein abundance in *XPO1*$^{E571K/WT}$ compared with *XPO1*$^{WT/WT}$ cells in nucleus (left) and cytoplasm (right) from experiment in **A**. The *x* axis represents fold change with dotted lines indicating fold change ratios = |2|, and the *y* axis represents significance with dotted lines at $-\log_{10}$ (*P* value) of 1.30. **C,** Enrichment analysis of proteins mislocalized in *XPO1* mutant relative to WT cells from **B** [red line indicates pathways with significant enrichment at $-\log_{10}$ (*P* value) of 1.30]. **D,** Quantification of NFκB luciferase reporter activity after stimulation of cells with TNFα. **E,** NFAT luciferase reporter activity after stimulation with PMA/ionomycin. Differences were calculated using a two-sided Student *t* test. *, $P < 0.05$; **, $P < 0.01$; ***, $P < 0.001$. **F,** Gene ontology analysis for biological processes significantly enriched in *CD19*-Cre *Xpo1*$^{E571K/WT}$ versus *CD19*-Cre *Xpo1*$^{WT/WT}$ mice across several subpopulations of B cells. (*continued on following page*)

Published OnlineFirst July 8, 2019; DOI: 10.1158/2159-8290.CD-19-0298

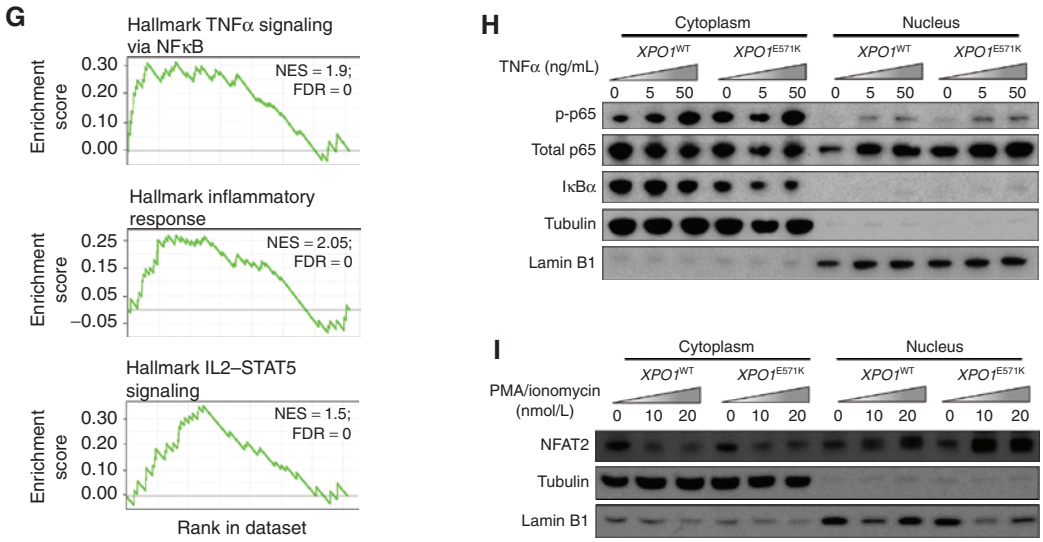

Figure 5. ***(Continued)*** **G,** Gene set enrichment analysis of key pathways dysregulated from RNA-seq of patients with CLL with or without *XPO1*^{E571K} mutations (NES, normalized enrichment score). **H,** Western blot of nuclear and cytoplasmic p-p65 and IκBα after stimulation of XPO1 mutant or WT cells with two doses of TNFα. **I,** Western blot of nuclear NFAT2 after stimulation of *XPO1* mutant or WT cells with PMA and two doses of ionomycin.

and NFAT proteins. Analysis of the amino-acid sequence of these proteins with an NES prediction tool (39) identified several putative NESs in these proteins in addition to the known NESs. In proteins showing enhanced export by mutant XPO1, the proportions of predicted NESs with a negative net charge in their C-terminal end were more frequent (Fig. 6C and D). Conversely, proteins showing reduced export by mutant XPO1 more frequently had NESs with a net positive charge in their C-terminal end.

We utilized a cellular reporter containing one of the NESs to evaluate the sequence-specific effects of XPO1 hotspot mutations on nuclear export, which were suggested by the structural and proteomic analyses above. We used a modified version of a previously described nuclear-export reporter (40) where the first 100 amino acids of the XPO1 substrate survivin (bearing its NES) are fused to a 3× FLAG epitope and two nuclear localization signals (Supplementary Fig. S9A). We generated three versions of this reporter: (1) the native NES, (2) a mutant NES where amino-acid residues C-terminal to the last hydrophobic residue were enriched in positive charges, and (3) a mutant version where amino-acid residues C-terminal to the last hydrophobic residue were enriched in negative charges. Cotransfection of each of these 3 NES reporters with either WT or E571K-mutant XPO1 revealed that the XPO1^{E571K} mutant significantly enhanced export of the negatively charged NES construct, while reducing export of the positively charged NES construct (Fig. 6E–G; Supplementary Fig. S9B and S9C). We validated these findings with a second reporter based on the HIV Rev protein NES [the Rev(1.4)-GFP reporter (41) with insertion of the IκBα NES] with an additional step of adding cycloheximide to inhibit new protein translation in the cytoplasm (Supplementary Fig. S9D). This experiment once again revealed that the XPO1^{E571K} mutant greatly enhanced nuclear export of negatively charged NES. Overall, these experiments confirmed that XPO1^{E571K} alters nuclear export on the basis of the charge properties of amino-acid residues surrounding the NES of XPO1 cargo proteins (Supplementary Fig. S9E and S9F). Interestingly, the XPO1^{D624G} hotspot mutation was predicted to disrupt hydrogen bonding between XPO1 and cargo protein at a site farther removed from the NES (Supplementary Fig. S10A). Consistent with this prediction, the XPO1^{D624G} mutant decreased export compared with XPO1^{WT}, a finding which was not altered by changing the C-terminal sequence of the NES (Supplementary Fig. S10B and S10C).

XPO1-Mutant Cells Are Preferentially Sensitive to XPO1 Inhibition

Inhibitors of nuclear export that bind to the C528 of XPO1 and occupy the NES-binding pocket of XPO1, thereby blocking XPO1 function, have recently been tested in phase II and III clinical trials. The XPO1 inhibitor selinexor recently received Orphan Drug and Fast Track FDA designation for relapsed multiple myeloma. However, biomarkers of response to XPO1 inhibition are not known, and it is not known if cancer-associated mutations in XPO1 modify response to XPO1 inhibitors. Interestingly, leukemia or lymphoma cells with naturally occurring *XPO1*^{E571K} mutations were among the most sensitive to the XPO1 inhibitor KPT-185 across 75 cell lines in publicly available cell line dependency data (depmap.org; Supplementary Fig. S11A). This finding was also seen in *XPO1*^{E571K} mutant B-cell lymphoma cell lines exposed to selinexor compared with those WT for *XPO1* (Supplementary Fig. S11B), where *XPO1*^{E571K} mutant cell lines were all more sensitive to selinexor compared with WT cells. The enhanced sensitivity of XPO1^{E571K} mutant cells to selinexor was further seen in isogenic human B cells (NALM-6 cells), B cells from *CD19*-Cre *Xpo1*$^{E571K/WT}$ knock-in mice, and mice with combined *Xpo1*^{E571K} mutation and BCL2 overexpression relative to *XPO1*^{WT} counterparts *in vitro* (Fig. 7A–C). Similar enhanced sensitivity of XPO1 mutant cells to selinexor was seen *in vivo*: Selinexor extended the

Published OnlineFirst July 8, 2019; DOI: 10.1158/2159-8290.CD-19-0298

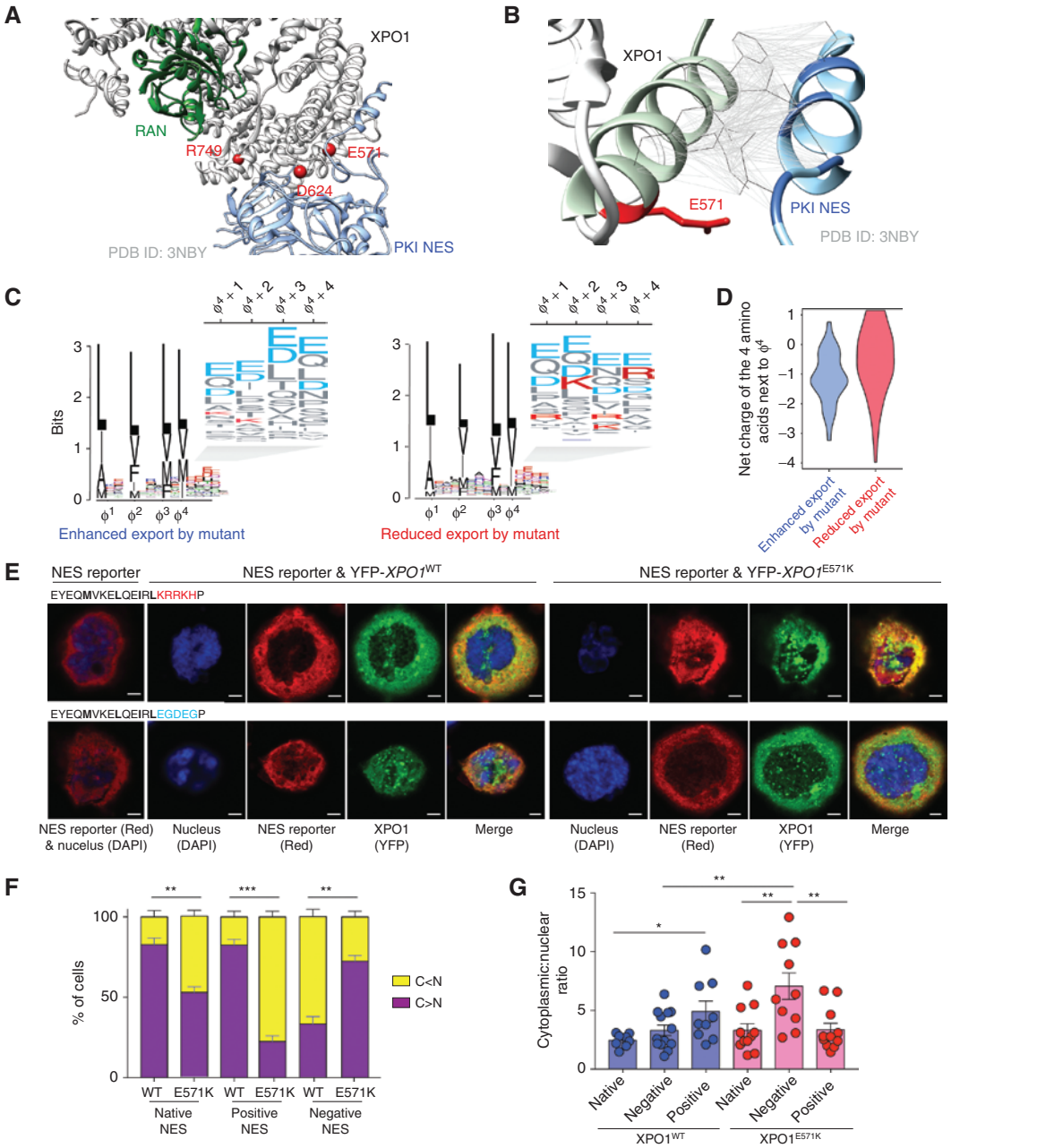

Figure 6. *XPO1* mutations alter nuclear export of cargo proteins based on the charge of amino-acid residues C-terminal to their NES. **A,** Structure of XPO1 (gray) in complex with a protein cargo [protein kinase inhibitor (PKI); in blue] having a classic NES (structure as previously published; ref. 37). In green is the GTP-binding nuclear protein RAN, whereas the positions of the two tumor-specific XPO1 hotspot mutations (E571 and D624) are labeled in red. **B,** In light green is the helix of XPO1 (gray) from which mutant E571 (red) directly interacts with the classic NES sequence (LALKLAGLDI) of the protein cargo (PKI; light blue). Critical hydrophobic positions on the cargo required for interactions with XPO1 are colored dark blue and shown as wire-frames along with those interacting XPO1 residues. Gray lines show the hydrophobic interactions between XPO1 and PKI. **C,** Sequence logos illustrating the amino-acid residue content of putative NESs predicted in proteins differentially exported in *XPO1* mutant relative to WT cells from the experiment in Fig. 4A. Φ^{1-4} indicate the four hydrophobic amino-acid positions (consisting of leucine, isoleucine, valine, phenylalanine, or methionine) in the consensus NES of XPO1 cargo proteins. Insets show the four amino-acid residues C-terminal to the last hydrophobic amino-acid residue within the NES (negatively charged residues shown in blue; positively charged residues shown in red). **D,** Violin plots quantifying the net charge of the four amino-acid residues following Φ^4 in proteins with enhanced versus reduced export in cells expressing the XPO1^{E571K} mutant. **E,** Confocal microscopy images of cells expressing YFP-*XPO1*^{WT} (left three plots) or YFP-*XPO1*$^{E571K/WT}$ (right three plots) constructs with a nuclear export reporter plasmid bearing IκBα NES mutagenized to possess either a positively (top) or negatively (bottom) charged C-terminal end (reporters alone on far left panels). Of note, the function of transfected XPO1^{E571K} or XPO1^{WT} was evaluated in isolation from endogenous XPO1 in these experiments as cells were exposed to the XPO1 inhibitor leptomycin B and both XPO1^{WT} and XPO1^{E571K} cDNAs also contained the C528S mutation (a mutation conferring resistance to leptomycin B; ref. 50; see Supplementary Fig. S6D). Scale bars, 5 μm. **F,** Ratio of enhanced (purple) or reduced (yellow) nuclear export of IκBα NES reporter in each condition from **B** (where "C" represents cytoplasmic localization of the reporter and "N" nuclear localization of the reporter). Bars represent an average of measurements of 10 to 12 cells by two independent assessments with error bars representing the SD between assessments. **G,** Mean cytoplasmic to nuclear ratio of intensity of IκBα NES reporter signal in each condition from **B** as measured by image analysis software. Individual points represent cytoplasmic to nuclear ratio, and error bars represent SD. *, $P < 0.05$; **, $P < 0.01$. Quantification of differences was calculated using a two-sided Student *t* test.

Published OnlineFirst July 8, 2019; DOI: 10.1158/2159-8290.CD-19-0298

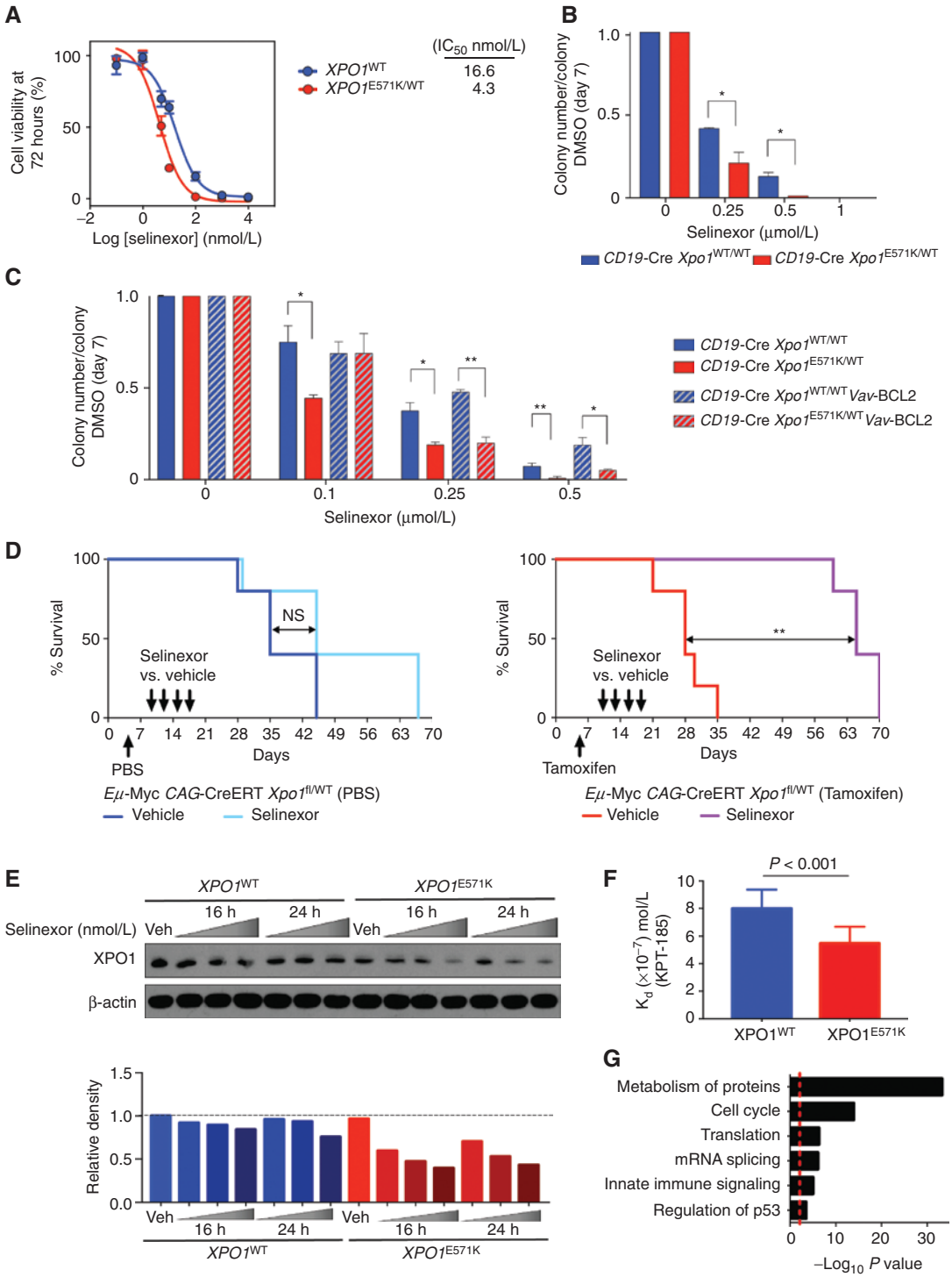

Figure 7. Enhanced sensitivity of XPO1 mutant cells to XPO1 inhibition *in vitro* and *in vivo*. **A,** Dose-response curve and IC_{50} values of isogeneic NALM-6 *XPO1*^{WT} or *XPO1*$^{E571K/WT}$ cell lines treated with selinexor. **B,** Number of colonies from bone marrow mononuclear cells (BM MNC) from *CD19*-Cre Xpo1$^{WT/WT}$ and *Xpo1*$^{E571K/WT}$ mice grown in IL7-containing methylcellulose with either vehicle (DMSO) or increasing doses of KPT-330. Bar graphs represent the number of colonies with each treatment relative to vehicle controls. **C,** Number of colonies from BM MNCs from *Vav*-BCL2 *CD19*-Cre *Xpo1*$^{WT/WT}$ or *Vav*-BCL2 *CD19*-Cre *Xpo1*$^{E571K/WT}$ knock-in mice treated with either vehicle (DMSO) or selinexor. **D,** Kaplan–Meier curves of *CAG*-CreERT *Xpo1*$^{E571K/WT}$ *Eμ*-Myc mice without induction of the *Xpo1*$^{E571K/WT}$ mutation (left) or with induction of the mutation (tamoxifen; right) treated with selinexor or vehicle. **E,** XPO1 protein levels by Western blot (top; quantification below) in NALM-6 *XPO1*^{WT} or *XPO1*$^{E571K/WT}$ cell lines treated with selinexor for 16 or 24 hours (5, 10, and 50 nmol/L doses). **F,** Bar plots of cell-free, *in vitro* binding affinity (K_d) values of the binding of KPT-185 to purified XPO1^{WT} or XPO1^{E571K} protein. **G,** Gene ontology analysis of proteins retained in the nucleus in *XPO1*$^{E571K/WT}$ cells relative to WT after XPO1 inhibition [red line indicates pathways with significant enrichment at $-\log_{10}$ (*P* value) of 1.30]. Differences were calculated using a two-sided Student *t* test. *, $P < 0.05$; **, $P < 0.01$.

Published OnlineFirst July 8, 2019; DOI: 10.1158/2159-8290.CD-19-0298

survival of mice bearing *Eμ*-Myc *Xpo1*^{E571K} mutant lymphomas compared with vehicle to a far greater extent than mice bearing *Eμ*-Myc *Xpo1*^{WT} lymphomas (Fig. 7D; Supplementary Fig. S11C). Selinexor also decreased the spleen size and percentage of CD5^{+} B cells in the spleens of secondary recipients engrafted with CLL cells from *CD19*-Cre *Xpo1*$^{E571K/WT}$ mice (Supplementary Fig. S11D–S11F).

To evaluate the basis for preferential effects of XPO1 inhibition on cells bearing cancer-associated *XPO1* hotspot mutations, we next assessed XPO1 protein abundance and nuclear/cytoplasmic protein compartmentalization by *XPO1* mutant genotype in the context of XPO1 inhibition. Interestingly, selinexor treatment resulted in enhanced dose-dependent degradation of XPO1 in *XPO1* mutants relative to WT cells (Fig. 7E). The close proximity of the XPO1^{E571} residue to the known binding residue of selinexor on XPO1 at C528 (Supplementary Fig. 11G) suggested that the XPO1^{E571K} mutation might influence the binding affinity of XPO1 inhibitors to the mutant XPO1 protein. Consistent with this prediction, microscale thermophoresis assays with the XPO1 inhibitor KPT-185 identified that the XPO1^{E571K} mutant protein bound KPT-185 with greater affinity than XPO1^{WT} protein (Fig. 7F; Supplementary Fig. S11H). Within cells, XPO1 inhibition resulted in preferential degradation of the XPO1^{E571K} protein as identified in MEC1 cells expressing XPO1^{WT} or XPO1^{E571K} FLAG-tagged protein treated with selinexor (Supplementary Fig. S12A). Finally, proteomic analysis by tandem mass tag mass spectrometry of cells treated with XPO1 inhibitor compared with vehicle also revealed mutant-selective changes in the localization of many proteins after XPO1 inhibition (Supplementary Fig. S12B and S12C). Certain proteins, including p53, although retained in the nucleus upon XPO1 inhibition in both WT and mutant cells, were retained at higher levels in *XPO1*^{E571K} mutant cells (Supplementary Fig. S12D). However, other proteins had increased nuclear retention upon XPO1 inhibition only in *XPO1*^{E571K} cells, suggesting potential synthetic lethal interactions. These proteins included members of critical cell pathways such as cell cycle, translation, mRNA splicing, and innate immune signaling (Fig. 7G).

DISCUSSION

Our data present a novel model of tumorigenesis: change-of-function mutations in nucleocytoplasmic trafficking machinery driving transformation. Systematic quantification of *XPO1* mutations across large-scale sequencing data from numerous cancer types enabled the identification of specific hotspot mutations in *XPO1* as among the most common mutations in patients with CLL, Hodgkin lymphoma, or PMBL, showing lineage specificity and occurring as heterozygous point mutations. Prior work suggests that XPO1 mutations in CLL are clonal at diagnosis and likely to be present at relapse as well, suggesting an early founder mutation (23). Consistent with this notion, XPO1^{E571} mutations have been tracked in plasma cell-free DNA in patients with Hodgkin lymphoma (24), where their presence correlates with tumor regression or progression, and the frequency of XPO1 mutations in CLL does not appear to be significantly different between the treatment-naïve or relapsed/refractory state (42).

Although the discovery of hotspot mutations in *XPO1* suggests an oncogenic driver function, XPO1 is expressed in every eukaryotic cell and is essential for cell survival. The essential housekeeping function of XPO1 has presented a barrier to manipulating endogenous XPO1 *in vivo*. Consequently, there has never been an animal model of any alteration in XPO1 previously. Here, we overcame this technical challenge and identified that a single amino acid–residue substitution in XPO1 *in vivo* increased B-cell proliferation and resulted in the development of clonal B-cell malignancies resembling human CLL. These models thereby provide one of the few genetically accurate murine models of CLL and establish the causality of XPO1 mutations in cancer development. Moreover, expression of the XPO1^{E571K} mutant *in vivo* also promoted development of other types of B-cell malignancies in concert with oncogenes such as MYC and BCL2.

The biochemical, structural, proteomic, and molecular studies here indicate that XPO1 mutations alter NES recognition in a sequence-specific manner, favoring the export of cargoes with negatively charged C-terminal NES sequences as a result of changes in charge near the NES binding cleft of XPO1. The generation of genetic models of mutant XPO1 enabled us to characterize the malignant mutant XPO1 exportome. Hundreds of proteins in various pathways were affected by altered NES recognition by mutant XPO1, including changes in the nucleocytoplasmic distribution of proteins involved in inflammatory signaling, DNA repair, RNA export, and chromatin remodeling pathways. Although it might be expected that the abundance of individual proteins detected in nuclear and cytoplasmic fractions would yield symmetrical results, with proteins enriched in nuclear analysis showing up as depleted in the cytoplasmic fraction and vice versa, this was not seen here or in prior analyses (43–45). In contrast, the vast majority of shuttling proteins assayed by mass spectrometric analysis of nuclear and cytoplasmic fractions show changes in only one cellular compartment without the expected reciprocal change in the other compartment. Potential explanations for this lack of overlap include the fact that many proteins are exported from the nucleus as part of their regulation and are degraded after nuclear export. In addition, the balance between nuclear export and import is important, and changing nuclear localization could result in changes in protein stability.

Drugs that inhibit XPO1 binding to cargo proteins have been demonstrated to have therapeutic efficacy for a number of cancer types (18–21, 46). As a result, altered function of XPO1 has been suggested to be common in cancer, but there has been no demonstration of XPO1 driving tumor development previously. The genomic data from patients as well as these functional data show that *XPO1* mutations are selected for in cancer cells and promote malignant transformation by altering activation of pathways such as NFκB and NFAT signaling. This discovery that mutant XPO1 can functionally drive tumorigenesis may be particularly useful for the development of targeted therapies for malignancies bearing XPO1 hotspot mutations; indeed, *XPO1*^{E571K} was associated with increased sensitivity to XPO1 inhibitors currently in clinical trials. Thus, these data establish oncogenic mutations

Published OnlineFirst July 8, 2019; DOI: 10.1158/2159-8290.CD-19-0298

in nuclear export machinery and identify these mutations as novel drivers of tumorigenesis and potential targets of anticancer therapy.

METHODS

See also Supplementary Materials for additional details.

Animals

All animals were housed at Memorial Sloan Kettering Cancer Center (MSKCC). All animal procedures were completed in accordance with the Guidelines for the Care and Use of Laboratory Animals and were approved by the Institutional Animal Care and Use Committees at MSKCC. Generation and genotyping of the *Xpo1*$^{E571K/WT}$ are described below.

Xpo1$^{E571K/WT}$ mice on a pure C57BL/6 background were crossed to CD19-Cre mice (47), tamoxifen-inducible *CAG*-CreERT mice (48), *Eμ*-Myc transgenic mice (31), and/or *Vav*-BCL2 transgenic mice (32), each of which was also maintained on a pure C57BL/6 background.

Eight-week-old female CD45.1 C57BL/6J mice (The Jackson Laboratory) were used as recipients for BM transplantation assays, and 8-week-old female NSG mice (The Jackson Laboratory) were used for cell-line xenografting. Blood was collected by submandibular bleeding using heparinized microhematocrit capillary tubes (Thermo Fisher Scientific). For assessment of germinal center formation, age- and sex-matched C57BL/6J mice were immunized intraperitoneally at 8 to 12 weeks old with 0.5 mL of a 2% SRBC suspension in PBS (Cocalico Biologicals) or PBS as control. Automated peripheral blood counts were obtained using a ProCyte Dx Hematology Analyzer (IDEXX).

Generation of Xpo1$^{E571K/WT}$ Conditional Knock-in Mice

An 8.4 kb genomic DNA used to construct the targeting vector was first subcloned from a positively identified B6 BAC clone (RP23: 123E19). The region was designed such that the long homology arm (LA) extends approximately 5.73 kb 5′ to the engineered *LoxP* site, and the short homology arm (SA) extends 2.15 kb 3′ to the insertion of the inverted mutant exon 26. The mutant exon 16 (GAA→AAA) plus the flanking genomic sequences for correct splicing (saEx26*sd) was inserted in the reverse direction in intron 17–18 and is 153 bp downstream of exon 16, which is immediately followed by a *Lox66* site. A *Lox71* site was placed 5′ to the inverted saEx16*sd sequence. The *FRT*-flanked neo cassette was inserted immediately upstream of the *Lox71/Lox66*–flanked inversion sequence. The targeting vector was confirmed by restriction analysis and sequencing after each modification. The boundaries of the 2 homology arms were confirmed by sequencing with P6 and T73 primers that read through both sides of the backbone vector into the genomic sequence. The *FRT*-neo cassette was confirmed by sequencing with LAN1 and iNeoN2 primers that read from the 5′- and 3′-ends of the neo cassette, respectively, into the inverted saEx16*sd (LAN1) and the genomic sequence (iNeoN2). saEx16*sd and its junction with the genomic sequence were sequencing confirmed with primer LAN1. LOX1 sequencing result confirmed the engineered single *LoxP* site upstream of exon 16.

The targeting vector was confirmed by restriction analysis and sequencing after each modification step. The boundaries of the 2 homology arms were confirmed by sequencing with P6 and T73 primers that read through both sides of the backbone vector into the genomic sequences. LAN1 and N2 primers read from the selection cassette into the inversion cassette (LAN1) and the 3′ end of the middle arm (N2). The 5′ *LoxP* site and the 5′ junction of genomic sequence/eGFP was confirmed by sequencing with *Lox1* primer. Primer GFP3 sequencing confirmed the remaining eGFP-T2A sequence and its 3′ junction with the genomic sequence. Primers LAN1, mCherrySQ1, and IMBPSQ1 confirmed the entire inversion cassette sequence and its junctions.

Primers used for sequencing:

Primer P6:	5′-GAG TGC ACC ATA TGG ACA TAT TGT C-3′
Primer T73:	5′-TAA TGC AGG TTA ACC TGG CTT ATC G-3′
Primer LAN1:	5′-CCA GAG GCC ACT TGT GTA GC-3′
Primer N2:	5′-TTC CTC GTG CTT TAC GGT ATC G-3′
Primer EXPO LOX1:	5′-CCC CTA ACC GCT TCC TCA TCT TAA GG-3′
Primer EXPO SQ1:	5′-GAC CAC ATG AAG CAG CAC GAC TTC-3′

The targeting construct was linearized using AscI prior to electroporation into embryonic stem (ES) cells. After selection with G418 antibiotic, surviving clones were expanded for PCR analysis to identify recombinant ES clones. Secondary confirmation of positive clones identified by PCR was performed by Southern blotting analysis. DNA was digested with XbaI (external long arm) or EcoRV (internal short arm), and electrophoretically separated on a 0.8% agarose gel. After transfer to a nylon membrane, the digested DNA was hybridized with a probe targeted against the 5′ external region. DNA from a normal C57BL/6 (B6) mouse was used as WT control. Positive C57BL/6 FLP ES cells were expanded and microinjected into BALB/c blastocysts. Resulting chimeras with a high percentage black coat color were mated to C57BL/6J mice (The Jackson Laboratory) to remove the FLP transgene, and subsequently to *CD19*-Cre or *CAG*-CreERT transgenic mice. Mice were backcrossed for six generations to C57BL/6 mice, and tamoxifen was administered to 6-week-old mice at 12 μg/g intraperitoneally every other day for 3 doses (as previously described; ref. 49). The XPO1^{E571K} mice are available at The Jackson Laboratory as Stock No. 033957.

Genotyping of Xpo1$^{E571K/WT}$ Conditional Knock-in Mice

Tail DNA samples from positive mice were amplified by PCR using the LOX1 and SDL2 primers. This reaction amplifies a WT product 409 bp in size. The presence of a second PCR product 62 bp greater than the WT product indicates a positive *LoxP* PCR. After a 2-minute hot start at 94°C, the samples were run using the following conditions for 30 cycles: 94°C for 30 seconds, followed by 55°C for 30 seconds, and 72°C for 1 minute. The PCR product was run on a 2% gel with a 100 bp ladder as reference.

Primers for PCR screening:

Forward oligo:

LOX1: 5′-TGG CTA AAC CAG AGG AGG TAC TG-3′

Reverse oligo:

SDL2: 5′-ATG GAG CCT ATT GCC CAA CAC AAC-3′

Cell Lines

NALM-6 cells engineered to express *XPO1*$^{E571K/WT}$ from the endogenous locus were generated by Horizon Discovery using recombinant adeno-associated virus-mediated homologous recombination and cultured in RPMI medium with 10% FCS. MEC1 cells were purchased from DSMZ. SUDHL-5, SUDHL-6, SUDHL-16, L428, and SUP-HD1 cells were a generous gift from Dr. Laura Pasqualucci. All cell lines were tested for *Mycoplasma* with the MycoAlert Mycoplasma Detection Kit (Lonsa) at time of receipt and before preparing stock aliquots for storage in liquid nitrogen. Cells were thawed and passaged no more than 10 times for all experiments performed. Validation of the *XPO1*^{E571K} mutation was performed by next-generation targeted capture sequencing, and serial routine testing was performed by PCR and Sanger sequencing.

Primary Patient Samples

Studies were approved by the Institutional Review Board of MSK and conducted in accordance to the Declaration of Helsinki protocol. We obtained written informed consent from patients before primary

Published OnlineFirst July 8, 2019; DOI: 10.1158/2159-8290.CD-19-0298

human deidentified CLL samples derived from whole peripheral blood or BM mononuclear cells were utilized.

Statistical Analysis

All data are presented as mean ± SD, unless otherwise stated. The replicate for each experiment is stated in the figure legend or indicated in the figure. Statistical significance was determined by a two-sided Student *t* test, and a *P* value of <0.05 was considered statistically significant. For non–normally distributed data, a nonparametric test (Kruskal–Wallis) was used, followed by multiple group comparisons using FDR. For the Kaplan–Meier survival analysis, a Mantel–Cox log-ranked test was used to determine statistical significance. For offspring frequency analysis, a χ^2 test was performed to test the difference between observed and expected frequencies from different genotypes. No blinding or randomization was used. Unless otherwise noted, all immunoblot quantitation and immunofluorescence image quantitation were representative of at least three biological replicates from independent experiments. Data were plotted using GraphPad Prism 7 software.

Disclosure of Potential Conflicts of Interest

A.R. Mato reports receiving commercial research grants from Celgene, Janssen, AstraZeneca, and AbbVie, and is a consultant/advisory board member for TG Therapeutics, Pharmacyclics, AstraZeneca, Loxo, Sunesis, Prime Oncolgy, Pfizer, and AbbVie. A. Dogan is a consultant/advisory board member for Roche, Novartis, Seattle Genetics, Celgene, PER, and Corvus. D. Wang is a member of the Adjunct Faculty at the Medical College of Wisconsin and Fujian Normal University. R.C. Hendrickson has ownership interest (including stock, patents, etc.) in Merck. O. Abdel-Wahab reports receiving commercial research support from H3 Biomedicine Inc., has received honoraria from the speakers bureau of Foundation Medicine Inc., and is a consultant/advisory board member for Foundation Medicine Inc., H3 Biomedicine Inc., Janssen, and Merck. No potential conflicts of interest were disclosed by the other authors.

Authors' Contributions

Conception and design: J. Taylor, D. Wang, B.S. Taylor, O. Abdel-Wahab
Development of methodology: J. Taylor, M. Sendino, C. Stewart, R.C. Hendrickson, G. Prieto, J.A. Rodriguez
Acquisition of data (provided animals, acquired and managed patients, provided facilities, etc.): J. Taylor, M.T. Chang, C. Stewart, E.M. Melnik, F. Herrejon Chavez, L. Bitner, A. Yoshimi, S.C.-W. Lee, D. Inoue, B. Liu, X.J. Zhang, A.R. Mato, Y. Chen, R.K. Soni, R.C. Hendrickson, B.S. Taylor
Analysis and interpretation of data (e.g., statistical analysis, biostatistics, computational analysis): J. Taylor, A.N. Gorelick, A. Pastore, M.T. Chang, A.V. Penson, E.I. Gavrila, C. Stewart, A. Yoshimi, X.J. Zhang, A. Dogan, R.K. Soni, G. Prieto, B.S. Taylor, O. Abdel-Wahab
Writing, review, and/or revision of the manuscript: J. Taylor, E.I. Gavrila, A. Yoshimi, S.C.-W. Lee, A.R. Mato, A. Dogan, D. Wang, R.K. Soni, G. Prieto, B.S. Taylor, O. Abdel-Wahab
Administrative, technical, or material support (i.e., reporting or organizing data, constructing databases): X.J. Zhang, O. Abdel-Wahab
Study supervision: M.G. Kharas, O. Abdel-Wahab

Acknowledgments

J. Taylor is supported by the Conquer Cancer Foundation of the American Society of Clinical Oncology, the American Association for Cancer Research, the American Society of Hematology (ASH), the Robert Wood Johnson Foundation, and the NIH/NCI (1K08CA230319-01). C. Stewart is supported by an ASH HONORS award. A. Yoshimi is supported by grants from the Aplastic Anemia and MDS International Foundation and the Lauri Strauss Leukemia Foundation. A. Yoshimi, S.C.-W. Lee, D. Inoue, and O. Abdel-Wahab are supported by the Leukemia and Lymphoma Society. S.C.-W. Lee is supported by the NIH/NCI (K99 CA218896), the ASH Scholar Award, and the EvansMDS Young Investigator Award. B.S. Taylor is supported by grants from NIH/NCI (R01 CA207244, R01 CA204749, U54 OD020355), the American Cancer Society (RSG-15-067-01-TBG), the Anna Fuller Fund, and the Robertson Foundation. D. Wang is supported by grants from the NIH/NIAID (AI079087) and NIH/NHLBI (R01 HL130724). M. Sendino and J.A. Rodriguez are supported by grants from the Spanish Government MINECO-FEDER (SAF2014-57743-R), the Basque Country Government (IT634-13 grant and a predoctoral fellowship) and the University of the Basque Country (UFI11/20). O. Abdel-Wahab is supported by grants from NIH/NHLBI (R01 HL128239) and NIH/NCI (1 R01 CA201247-01A1), an MSKCC Steven Greenberg Lymphoma Research Award, the Geoffrey Beene Research Center of MSKCC, and the Pershing Square Sohn Cancer Research Alliance. This work was also supported by P30 CA008748. Research supported AACR-Conquer Cancer Foundation of ASCO Young Investigator Award for Translational Cancer Research. Editorial support in the preparation of this manuscript was provided by Hannah Rice, ELS.

Received March 11, 2019; revised June 20, 2019; accepted July 1, 2019; published first July 8, 2019.

REFERENCES

1. Stade K, Ford CS, Guthrie C, Weis K. Exportin 1 (Crm1p) is an essential nuclear export factor. Cell 1997;90:1041–50.
2. Fukuda M, Asano S, Nakamura T, Adachi M, Yoshida M, Yanagida M, et al. CRM1 is responsible for intracellular transport mediated by the nuclear export signal. Nature 1997;390:308–11.
3. Ossareh-Nazari B, Bachelerie F, Dargemont C. Evidence for a role of CRM1 in signal-mediated nuclear protein export. Science 1997;278:141–4.
4. Jeyasekharan AD, Liu Y, Hattori H, Pisupati V, Jonsdottir AB, Rajendra E, et al. A cancer-associated BRCA2 mutation reveals masked nuclear export signals controlling localization. Nat Struct Mol Biol 2013;20:1191–8.
5. Pauty J, Couturier AM, Rodrigue A, Caron MC, Coulombe Y, Dellaire G, et al. Cancer-causing mutations in the tumor suppressor PALB2 reveal a novel cancer mechanism using a hidden nuclear export signal in the WD40 repeat motif. Nucleic Acids Res 2017;45:2644–57.
6. Nakagawa M, Kameoka Y, Suzuki R. Nucleophosmin in acute myelogenous leukemia. N Engl J Med 2005;352:1819–20.
7. Mariano AR, Colombo E, Luzi L, Martinelli P, Volorio S, Bernard L, et al. Cytoplasmic localization of NPM in myeloid leukemias is dictated by gain-of-function mutations that create a functional nuclear export signal. Oncogene 2006;25:4376–80.
8. Stommel JM, Marchenko ND, Jimenez GS, Moll UM, Hope TJ, Wahl GM. A leucine-rich nuclear export signal in the p53 tetramerization domain: regulation of subcellular localization and p53 activity by NES masking. EMBO J 1999;18:1660–72.
9. Falini B, Mecucci C, Tiacci E, Alcalay M, Rosati R, Pasqualucci L, et al. Cytoplasmic nucleophosmin in acute myelogenous leukemia with a normal karyotype. N Engl J Med 2005;352:254–66.
10. Brunetti L, Gundry MC, Sorcini D, Guzman AG, Huang YH, Ramabadran R, et al. Mutant NPM1 maintains the leukemic state through HOX expression. Cancer Cell 2018;34:499–512e9.
11. Rodriguez JA, Henderson BR. Identification of a functional nuclear export sequence in BRCA1. J Biol Chem 2000;275:38589–96.
12. Lee S, Neumann M, Stearman R, Stauber R, Pause A, Pavlakis GN, et al. Transcription-dependent nuclear-cytoplasmic trafficking is required for the function of the von Hippel-Lindau tumor suppressor protein. Mol Cell Biol 1999;19:1486–97.
13. Kojima K, Kornblau SM, Ruvolo V, Dilip A, Duvvuri S, Davis RE, et al. Prognostic impact and targeting of CRM1 in acute myeloid leukemia. Blood 2013;121:4166–74.

Published OnlineFirst July 8, 2019; DOI: 10.1158/2159-8290.CD-19-0298

14. Schmidt J, Braggio E, Kortuem KM, Egan JB, Zhu YX, Xin CS, et al. Genome-wide studies in multiple myeloma identify XPO1/CRM1 as a critical target validated using the selective nuclear export inhibitor KPT-276. Leukemia 2013;27:2357–65.
15. Akagi I, Okayama H, Schetter AJ, Robles AI, Kohno T, Bowman ED, et al. Combination of protein coding and noncoding gene expression as a robust prognostic classifier in stage I lung adenocarcinoma. Cancer Res 2013;73:3821–32.
16. Walker CJ, Oaks JJ, Santhanam R, Neviani P, Harb JG, Ferenchak G, et al. Preclinical and clinical efficacy of XPO1/CRM1 inhibition by the karyopherin inhibitor KPT-330 in Ph+ leukemias. Blood 2013;122:3034–44.
17. Abdul Razak AR, Mau-Soerensen M, Gabrail NY, Gerecitano JF, Shields AF, Unger TJ, et al. First-in-class, first-in-human phase I study of selinexor, a selective inhibitor of nuclear export, in patients with advanced solid tumors. J Clin Oncol 2016;34:4142–50.
18. Gounder MM, Zer A, Tap WD, Salah S, Dickson MA, Gupta AA, et al. Phase IB study of selinexor, a first-in-class inhibitor of nuclear export, in patients with advanced refractory bone or soft tissue sarcoma. J Clin Oncol 2016;34:3166–74.
19. Alexander TB, Lacayo NJ, Choi JK, Ribeiro RC, Pui CH, Rubnitz JE. Phase I study of selinexor, a selective inhibitor of nuclear export, in combination with fludarabine and cytarabine, in pediatric relapsed or refractory acute leukemia. J Clin Oncol 2016;34:4094–101.
20. Garzon R, Savona M, Baz R, Andreeff M, Gabrail N, Gutierrez M, et al. A phase 1 clinical trial of single-agent selinexor in acute myeloid leukemia. Blood 2017;129:3165–74.
21. Kuruvilla J, Savona M, Baz R, Mau-Sorensen PM, Gabrail N, Garzon R, et al. Selective inhibition of nuclear export with selinexor in patients with non-Hodgkin lymphoma. Blood 2017;129: 3175–83.
22. Puente XS, Pinyol M, Quesada V, Conde L, Ordonez GR, Villamor N, et al. Whole-genome sequencing identifies recurrent mutations in chronic lymphocytic leukaemia. Nature 2011;475:101–5.
23. Landau DA, Carter SL, Stojanov P, McKenna A, Stevenson K, Lawrence MS, et al. Evolution and impact of subclonal mutations in chronic lymphocytic leukemia. Cell 2013;152:714–26.
24. Camus V, Stamatoullas A, Mareschal S, Viailly PJ, Sarafan-Vasseur N, Bohers E, et al. Detection and prognostic value of recurrent exportin 1 mutations in tumor and cell-free circulating DNA of patients with classical Hodgkin lymphoma. Haematologica 2016;101: 1094–101.
25. Lin DC, Hao JJ, Nagata Y, Xu L, Shang L, Meng X, et al. Genomic and molecular characterization of esophageal squamous cell carcinoma. Nat Genet 2014;46:467–73.
26. Chang MT, Asthana S, Gao SP, Lee BH, Chapman JS, Kandoth C, et al. Identifying recurrent mutations in cancer reveals widespread lineage diversity and mutational specificity. Nat Biotechnol 2016;34: 155–63.
27. Chang MT, Bhattarai TS, Schram AM, Bielski CM, Donoghue MTA, Jonsson P, et al. Accelerating discovery of functional mutant alleles in cancer. Cancer Discov 2018;8:174–83.
28. Hurwitz R, Hozier J, LeBien T, Minowada J, Gajl-Peczalska K, Kubonishi I, et al. Characterization of a leukemic cell line of the pre-B phenotype. Int J Cancer 1979;23:174–80.
29. Wang T, Birsoy K, Hughes NW, Krupczak KM, Post Y, Wei JJ, et al. Identification and characterization of essential genes in the human genome. Science 2015;350:1096–101.
30. Blomen VA, Majek P, Jae LT, Bigenzahn JW, Nieuwenhuis J, Staring J, et al. Gene essentiality and synthetic lethality in haploid human cells. Science 2015;350:1092–6.
31. Adams JM, Harris AW, Pinkert CA, Corcoran LM, Alexander WS, Cory S, et al. The c-myc oncogene driven by immunoglobulin enhancers induces lymphoid malignancy in transgenic mice. Nature 1985;318:533–8.
32. Ogilvy S, Metcalf D, Print CG, Bath ML, Harris AW, Adams JM. Constitutive Bcl-2 expression throughout the hematopoietic compartment affects multiple lineages and enhances progenitor cell survival. Proc Natl Acad Sci U S A 1999;96:14943–8.
33. Durham BH, Getta B, Dietrich S, Taylor J, Won H, Bogenberger JM, et al. Genomic analysis of hairy cell leukemia identifies novel recurrent genetic alterations. Blood 2017;130:1644–8.
34. Fornerod M, Ohno M, Yoshida M, Mattaj IW. CRM1 is an export receptor for leucine-rich nuclear export signals. Cell 1997;90:1051–60.
35. Monecke T, Guttler T, Neumann P, Dickmanns A, Gorlich D, Ficner R. Crystal structure of the nuclear export receptor CRM1 in complex with Snurportin1 and RanGTP. Science 2009;324:1087–91.
36. Dong X, Biswas A, Suel KE, Jackson LK, Martinez R, Gu H, et al. Structural basis for leucine-rich nuclear export signal recognition by CRM1. Nature 2009;458:1136–41.
37. Guttler T, Madl T, Neumann P, Deichsel D, Corsini L, Monecke T, et al. NES consensus redefined by structures of PKI-type and Rev-type nuclear export signals bound to CRM1. Nat Struct Mol Biol 2010;17:1367–76.
38. Fung HY, Fu SC, Chook YM. Nuclear export receptor CRM1 recognizes diverse conformations in nuclear export signals. Elife 2017;6.
39. Prieto G, Fullaondo A, Rodriguez JA. Prediction of nuclear export signals using weighted regular expressions (Wregex). Bioinformatics 2014;30:1220–7.
40. Garcia-Santisteban I, Arregi I, Alonso-Marino M, Urbaneja MA, Garcia-Vallejo JJ, Banuelos S, et al. A cellular reporter to evaluate CRM1 nuclear export activity: functional analysis of the cancer-related mutant E571K. Cell Mol Life Sci 2016;73:4685–99.
41. Henderson BR, Eleftheriou A. A comparison of the activity, sequence specificity, and CRM1-dependence of different nuclear export signals. Exp Cell Res 2000;256:213–24.
42. Hu B, Patel KP, Chen HC, Wang X, Wang F, Luthra R, et al. Routine sequencing in CLL has prognostic implications and provides new insight into pathogenesis and targeted treatments. Br J Haematol 2019; 185:852–64.
43. Thakar K, Karaca S, Port SA, Urlaub H, Kehlenbach RH. Identification of CRM1-dependent nuclear export cargos using quantitative mass spectrometry. Mol Cell Proteomics: MCP 2013;12:664–78.
44. Kirli K, Karaca S, Dehne HJ, Samwer M, Pan KT, Lenz C, et al. A deep proteomics perspective on CRM1-mediated nuclear export and nucleocytoplasmic partitioning. Elife 2015;4.
45. Wuhr M, Guttler T, Peshkin L, McAlister GC, Sonnett M, Ishihara K, et al. The nuclear proteome of a vertebrate. Curr Biol 2015;25:2663–71.
46. Bahlis NJ, Sutherland H, White D, Sebag M, Lentzsch S, Kotb R, et al. Selinexor plus low-dose bortezomib and dexamethasone for patients with relapsed or refractory multiple myeloma. Blood 2018;132:2546–54.
47. Kuhn R, Schwenk F, Aguet M, Rajewsky K. Inducible gene targeting in mice. Science 1995;269:1427–9.
48. Hayashi S, McMahon AP. Efficient recombination in diverse tissues by a tamoxifen-inducible form of Cre: a tool for temporally regulated gene activation/inactivation in the mouse. Dev Biol 2002;244:305–18.
49. Moran-Crusio K, Reavie L, Shih A, Abdel-Wahab O, Ndiaye-Lobry D, Lobry C, et al. Tet2 loss leads to increased hematopoietic stem cell self-renewal and myeloid transformation. Cancer Cell 2011;20:11–24.
50. Kudo N, Matsumori N, Taoka H, Fujiwara D, Schreiner EP, Wolff B, et al. Leptomycin B inactivates CRM1/exportin 1 by covalent modification at a cysteine residue in the central conserved region. Proc Natl Acad Sci U S A 1999;96:9112–7.

Ekaia, 2020, 37, 221-239
https://doi.org/10.1387/ekaia.20861

ekaia
ZIENTZIA eta TEKNOLOGIA ALDIZKARIA

ISSN 0214-9001 – eISSN 2444-3255

XPO1en bidezko garraio nukleozitoplasmikoa: oinarrizko mekanismoak eta hurbilketa esperimentalak

(XPO1-mediated nucleocytoplasmic transport: basic mechanisms and experimental approaches)

Maria Sendino[1], *Anne Olazabal-Herrero*[1,2], *Jose Antonio Rodriguez*[1], *Miren Josu Omaetxebarria*[3]*

[1] Genetika, Antropologia Fisikoa eta Animalien Fisiologia Saila (UPV/EHU)
[2] Department of Pediatrics-Hematology/Oncology. Yale University School of Medicine
[3] Biokimika eta Biologia Molekularra Saila (UPV/EHU)

LABURPENA: Zelula eukariotoen nukleoa inguratzen duen mintzak zelularen bi konpartimentu nagusien (nukleoaren eta zitoplasmaren) arteko banaketa fisikoa ezartzen du. Bi konpartimentu horien arteko komunikazioa, etengabea izateaz gain, ezinbestekoa da zelularen homeostasia mantentzeko. Komunikazio hori, nukleoaren mintzean zehar noranzko bietan izaten den molekula-mugikortasunak egikaritzen du. Komunikazio horretan funtsezkoa den proteina bat dugu mintzagai honako artikuluan: XPO1 izeneko proteina, alegia. Nukleotik zitoplasmarako garraioan jarduten duen esportazio-hartzaile nagusia da XPO1, eta ehunka proteina eta zenbait RNA molekula esportatzen ditu. Artikulu honetan, garraio nukleozitoplasmikoaren mekanismo molekularrak deskribatzeaz gain, XPO1 esportazio-hartzailean zentratu gara, eta haren funtzioa aztertzeko erabili ohi diren hurbilketa esperimentalak jaso ditugu. Azken horien adibide gisa, berriki deskribatutako USP12/WDR20 konplexuaren kasua [1] aztertu dugu.

HITZ GAKOAK: garraio nukleozitoplasmikoa, XPO1, NES, WDR20, USP12.

ABSTRACT: *The nuclear envelope, a double membrane that encloses the nucleus of eukaryotic cells, establishes a physical separation between the two main cellular compartments: the nucleus and the cytoplasm. Continuous communication between these compartments is crucial for the maintenance of cellular homeostasis. This communication relies on the bidirectional transport of macromolecules across the nuclear envelope. We focus here on a protein, called XPO1, which plays a key role in nucleocytoplasmic transport. XPO1 is the main receptor that mediates the export of hundreds of proteins and several RNA molecules from the nucleus to the cytoplasm. In this article we first review the molecular mechanisms that underlie nucleocytoplasmic transport. Next, we focus on XPO1 to describe some of the experimental approaches that are frequently applied to investigate its function. Finally, we illustrate the use of these approaches using the recently described case of the USP12/WDR20 complex [1] as an example.*

KEYWORDS: nucleocytoplasmic transport, XPO1, NES, WDR20, USP12.

**** Harremanetan jartzeko / Corresponding author:*** Miren Josu Omaetxebarria, Biokimika eta Biologia Molekularra Saila, Zientzia eta Teknologia Fakultatea, Euskal Herriko Unibertsitatea (UPV/EHU), Sarriena auzoa zg, 48940, Leioa, Bizkaia, Euskal Herria. – mirenjosu.omaetxebarria@ehu.eus – https://orcid.org/0000- .

Nola aipatu / How to cite: Sendino, Maria; Olazabal-Herrero, Anne; Rodriguez, Jose Antonio; Omaetxebarria, Miren Josu (2020). «XPO1en bidezko garraio nukleozitoplasmikoa: oinarrizko mekanismoak eta hurbilketa esperimentalak»; *Ekaia*, 37, 2020, 221-239. (https://doi.org/10.1387/ekaia.20861).

Jasoa: 25 maiatza, 2019; Onartua: 27 abuztua, 2019.

ISSN 0214-9001 - eISSN 2444-3255 / © 2020 UPV/EHU

1. SARRERA

1.1. Molekulen nukleoaren eta zitoplasmaren arteko garraioa

Zelula eukariotoen nukleoan zeharreko molekula-garraioa nukleoaren mintzean mihiztatuta dauden kanal batzuetan zehar gertatzen da: nukleoko poro-konplexu deritze kanal horiei (*nuclear pore complexes, NPC*). Tamaina txikiko molekulek, horien artean <30 kDa-eko proteinek ere, NPCetan zehar difusioz zeharkatu ohi dute mintza; alabaina, proteina gehientsuenak (baita oso handiak diren proteina-konplexuak ere) garraio-hartzaileei lotzen zaizkie garraia ditzaten [2, 3]. Energiaren mendeko prozesu aktiboa da proteina gehienak nukleoaren mintzean zehar garraiatzea, eta lan horretan garraio-makineria espezializatuak dihardu. Makineria horrek hiru pieza nagusi ditu: (1) NPCak, (2) garraio-hartzaile disolbagarriak, zeintzuek garraiatuko dituzten kargo-proteinen seinale espezifikoak ezagutuko baitituzte, eta (3) mintz nuklearraren alde bien arteko Ran GTPasa txikiaren gradientea, zeinak garraioaren noranzkoa zehaztuko duen [4-6] (1. irudia).

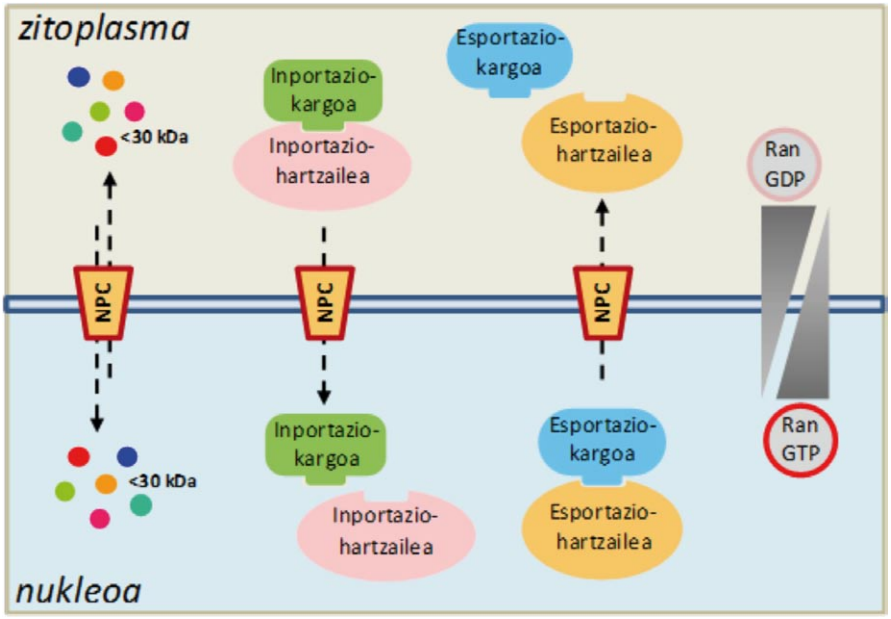

1. irudia. Nukleoko poro-konplexuetan (NPC) zeharreko proteina-garraio nukleozitoplasmikoa. Proteina txikiak (<30 kDa) nukleoaren eta zitoplasmaren artean difusioz mugi daitezke NPCetan zehar. Proteina handiagoek, berriz, garraio- (inportazio- edo esportazio-) hartzaileen beharra dute konpartimentu batetik bestera mugitu ahal izateko. RanGTP/RanGDP gradienteak (RanGTP-kontzentrazio handia nukleoan, eta RanGDP-kontzentrazio handia zitoplasman) garraioaren noranzkoa finkatzen du.

NPCak 30 proteina biltzen dituen nukleoporina familiako zenbait kidez osaturiko konplexuak dira. Konplexu horien ezaugarri fisiko-kimikoei esker, tamaina jakin batetik gorako proteinak ezin dira era askean mugitu nukleotik zitoplasmara edo zitoplasmatik nukleora [2, 4]. Proteina handi horiek garraio-hartzaileei lotuko zaizkie, eta nukleoporinekiko interakzio bidez, NPCa zeharkatuko dute [7].

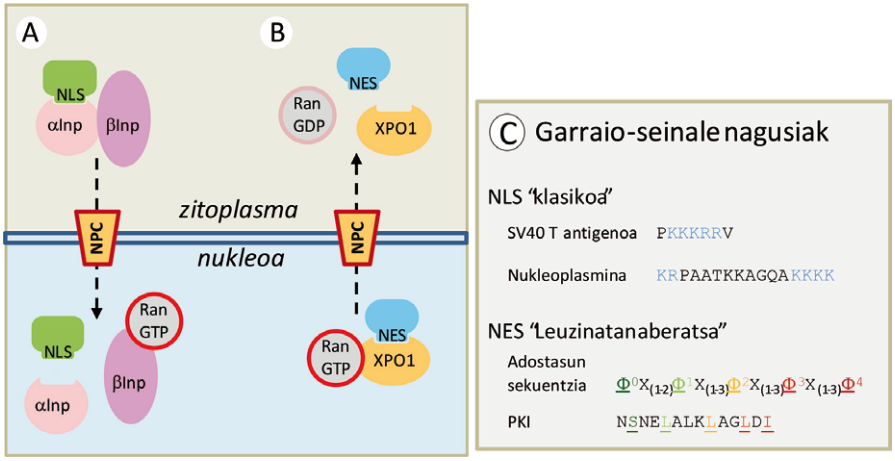

2. irudia. Garraio nukleozitoplasmikoaren mekanismo eta seinale nagusiak. A) Inportinen bidezko inportazioa: α-inportina/β-inportina (αInp/βInp) heterodimeroak NLS motako seinalea duten kargo-proteinak zitoplasman ezagutu eta nukleoko poroetan zehar nukleora garraiatzen ditu. Inportina/NLS-kargo konplexuak, behin nukleoan dagoenean, RanGTP-arekiko interakzioan jarduten du, eta eta inportazio-koplexua desmuntatzen da. B) XPO1en bidezko esportazio-kargoen garraioa: XPO1 hartzaileak NESa duten esportazio-kargoak ezagutzen ditu eta RanGTP-arekiko elkarrekintzaz esportatuko den konplexua eratzen da. Konplexu hori, zitoplasmara heltzean, GTParen hidrolisia dela medio desmuntatu, eta XPO1 hartzailea zein esportazio-kargoa askatuko dira. C) Garraio nukleozitoplasmikorako seinale nagusiak: NLS (*Nuclear Localization Signal*) seinale klasikoak bi motatakoak izan daitezke; aminoazido basikozko (urdinez markaturik) errenkada bakarraz osatuak, SV40 T antigeno luzea kasu, edo aminoazido basikozko (urdinez markaturik) errenkada biz osatuak, nukleoplasminarena kasu. Bestetik, XPO1 hartzaileak ezagutu eta lotzen dituen NES (*Nuclear Export Signals*) seinaleak adostasun-sekuentzia batekin bat datoz, zeinean aminoazido hidrofobikoek (ϕ bezala adierazita) posizio jakina betetzen duten errenkadan. Adibide moduan, PKI proteinaren NES seinalea erakusten da.

20 garraio-hartzaile inguru kodetzen ditu giza genomak [8]; horietako zenbaitzuek kargoak mintz nuklearrean zehar noranzko bietan garraia baditzakete ere, gehientsuenak nukleoranzko hartzaile gisa (inportinak) ala nukleotiko hartzaile gisa (esportinak) aritzen dira esklusiboki (2A eta 2B irudiak). Hartzaileok garraiorako seinaleak diren kargo-proteinen pepti-

do-sekuentzia espezifikoak ezagutu eta lotzen dituzte. Seinale horiek bitarikoak izan daitezke: nukleora lokalizatzeko seinaleak, inportinek ezagutzen dituztenak, NLSak (*nuclear localization signal*), eta nukleotik esportatzeko seinaleak, esportinek ezagutzen dituztenak, NESak (*nuclear export signal*). Inportaziorako ondoen karakterizatutako hartzailea α-inportina/β-inportina heterodimeroa da, zeinak NLS «klasikoa» (aminoazido basikozko errenkada batez edo biz osatutako peptido-sekuentzia) duten kargoak nukleorantz garraiatzea bideratzen baitu [9]. Esportinen artean, aldiz, XPO1 da karakterizatu zen lehena, eta baita gaur egun gehien ikertzen dena ere. XPO1ek arreta handia jaso du azken urteetan hainbat gaixotasunen garapenarekin lotura duelakoan. Argitalpen ugaritan adierazi da XPO1en jarduera desegokiak eragile gisara joka dezakeela zenbait minbiziren eta neuroendekapenezko gaixotasunen garapenean [10, 11]. XPO1ek «leuzinatan aberatsak» diren NESdun proteinen esportazioa bideratzen du. Leuzinatan aberatsak diren NES horietan aminoazido hidrofobikoek (leuzina da maiztasun handienean agertu ohi den aminoazidoa, baina isoleuzina, balina, fenilalanina zein metionina ere ager daitezke) «adostasun-sekuentzia» bat osatzen duen kokapen espezifikoa dute [12] (2C irudia). Aminoazidoen adostasun-sekuentzia horretaz gain, NESek konformazio jakina ere izan ohi dute: N muturrean, α helizearen egitura hartu ohi dute, eta C muturrean, berriz, begizta-erakoa [13]. Aipatzekoa da zenbait proteinek bi seinale motak (bai NLSa, bai NESa) dituztela eta, beraz, nukleotik zitoplasmara eta zitoplasmatik nukleora garraiatzen direla [14]. α/β-inportinak eta XPO1ek ehunka proteina desberdin garraiatuko dituzte; zitoplasmatik nukleora, lehenengoak, eta nukleotik zitoplasmara, bigarrenek.

Aipatutako garraio-makineria espezializatu horren azken pieza RanGTPasa txikia da. RanGTPasa GDPri (RanGDP) edo GTPri (RanGTP) lot dakioke garraio-hartzaile eta kargoen arteko elkarrekintza erregulatzeko [4, 5, 15]. RanGDP-aren kontzentrazioa zitoplasman da altua, eta RanGTP-aren kontzentrazioa, berriz, nukleoan da altua (1. irudia). Egoera fisiologikoetan, RanGDP/RanGTP gradiente hori mantentzen da nukleoaren eta zitoplasmaren artean. Gradiente hori Ran-en bi kofaktorek mantenaraziko dute: RanGAP1 (GTPasa aktibatzailea den proteina zitoplasmikoa) eta RCC1 (kromatinari lotutako nukleotidoak trukatzeko faktorea). Nukleoko RanGTPak, inportazio- zein esportazio- konplexuekin elkarreragiten du; batetik inportina/kargo konplexuen desmuntaketa bultzatzen du, horrela inportazio-kargoa nukleoan askatuz, eta bestetik XPO1 esportazio-hartzailearekin eta haren kargoekin bat eginez RanGTP/XPO1/kargo konplexu trimerikoa osatzen du, XPO1 eta haren kargoen arteko interakzioa egonkortzeko. Konplexu hori, zitoplasmara heldutakoan, RanGAP1ek GTPa hidrolizatzearekin batera desmuntatzen da, eta esportazio-kargoa zitoplasman askatzen. Beraz, RanGTP/RanGDP gradienteak, hartzaile/kargo interakzioei eraginez, nukleoaren mintzean zeharreko garraioaren noranzkoa zehaztuko du (2A eta 2B irudiak).

1.2. **XPO1en kargoen peskizan: hurbilketa esperimentalak**

XPO1 esportazio-hartzailearen balizko kargoak zer proteina izan daitezkeen mugatzeko eta kargoak diren horien NESak zehazteko, askotariko prozedurez baliatu gara (3. irudia).

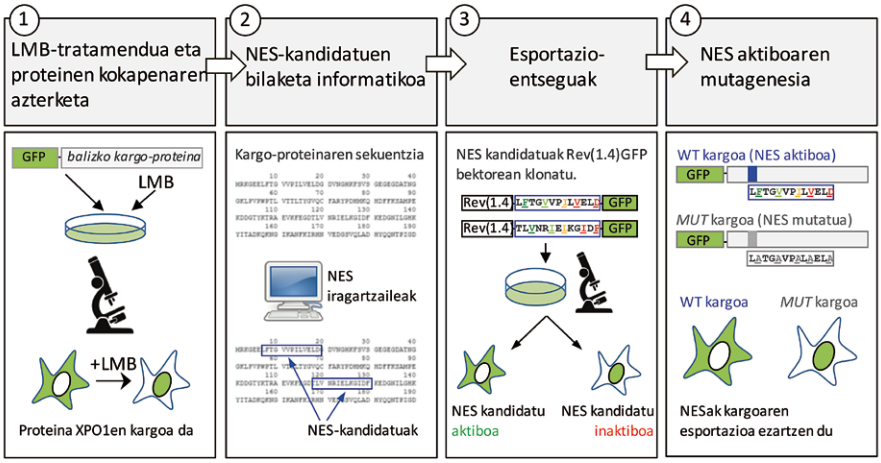

3. irudia. NES seinaleen karakterizaziorako pausoen hurrenkera. 1. Ikergai den proteina (balizko kargoa) gainadierazi eta zelulak leptomizina B-z (LMB) tratatzen dira XPO1ek proteina hori esportatzen duenetz aztertzeko. Behin XPO1ek esportatzen duela ebatzita, proteina horren delezio-mutanteak sortu, eta horiek zelulan hartzen duten kokapena azter daiteke, eta, honela, NES seinalea egon daitekeen zonaldea mugatu. 2. Paraleloan, proteinaren sekuentzia Wregex edo LocNES bezalako NES-iragarleak erabiliz mapatzen da. Iragarle horiek erakusten dute NES seinalea non koka daitekeen proteinaren sekuentzian zehar. 3. Lehen bi pausoen ostean, NES-kandidatuak hautatzen dira, eta horiek Rev(1.4)-GFP bektorean klonatzen dira esportazio-entseguak egiteko [27]. 4. Behin esportazio-entseguan NES aktiboa dela ebatzita, NESa mutatu egiten da proteina osoaren testuinguruan. Identifikatutako NESak kargoaren esportazioa ezartzen badu, NESaren mutazioak kargoaren kokapena aldatzea espero dugu. Horrela, NESaren funtzionaltasun biologikoa berrets daiteke. [WT kargoa: *wild type* kargoa (mutatugabeko NESdun kargoa); MUT kargoa: mutatutako NESdun kargoa].

1.2.1. *Leptomizina B-k (LMB) eragindako XPO1en bidezko esportazioaren inhibizioa*

CRM1 (*chromosome region maintenance factor 1*) proteinak beste proteina batzuk nukleotik esportatzeko hartzaile-lanetan ere jarduten zuela ikusi zuten 1997an, eta, orduz geroztik, exportin 1 (XPO1) izena ere hartu du [16-19]. Garai hartan argitaratutako lanek XPO1 nukleotiko esporta-

zioa inhibitzen duen LMBren itua dela frogatu zuten. *Streptomyces* bakterioak ekoizten duen metabolitoa da LMB; izan ere, aurkitu zutenean, antifungiko eraginkorra zela ikusi zuten [20]. Urte batzuk geroago, baina, ikusi zen LMBk XPO1ek bideratutako nukleotiko-esportazioa oztopatzen zuela [21]. 2009an ezagutarazi zen kargoen NESek XPO1i lotzerakoan okupatzen zuten eskualdearen egitura; hori horrela, NESak XPO1en poltsiko hidrofobiko jakin batera lotzen zirela ondorioztatu zen [13]. Aurkikuntza horrekin batera, ezagutu zen, halaber, LMB ere poltsiko hidrofobiko berberera lotzen dela, eta, honela, LMBk, poltsikoa okupatuz gero, kargoen NESak lotzea eragozten du. Aurkikuntza horrek XPO1en kargoak identifikatzeko lanak asko erraztu ditu; izan ere, LMB erabilitakoan XPO1en zitoplasmako kargoak maiz nukleora birlokalizatzen direla ikusi da zeluletan egindako esperimentuetan. Prozedura horrek badu bestelako abantaila bat; izan ere, LMB, kargo endogenoen portaera aztertzeko baliagarria izateaz gain, ektopikoki gainadierazitako kargoen esportazioa ikertzeko ere aproposa da. Honela, kargo-errepertorio zabala aztertzeko aukera emateaz gain, kargoen sekuentzietan delezio iturratuak eginez, horien NESak mapatzeko ere balia dezakegu LMB tratamendua. Hurbilketa hori, baina, ezin da konstitutiboki nukleora lokalizatzen diren proteinen XPO1 bidezko esportazioa frogatzeko erabili. Kasu horietan, hartzailea ektopikoki gainadieraz daiteke NESdun nukleoko kargoak zitoplasmara esportatzea eraginez [22].

Alabaina, kargo-kandidatuak XPO1en benetako kargoak direla frogatzeko eta, era berean, kargoak diren horien NESak identifikatu eta zehazteko, LMBren erabileran oinarritutako esperimentuez gain, bestelako hurbilketa batzuk beharrezkoak dira. Azken urteetan ikerketa esperimentalarekin batera ezinbesteko bihurtu den bioinformatikaren ekarpena ere aipatzekoa da lan honetan.

1.2.2. *Analisi bioinformatikoa: NES-iragarleak*

Adierazi bezala, leuzinatan aberatsak diren esportazio-seinaleak, NESak, aminoazido-motibo laburrak dira, zeinek kargo-proteinak XPO1 esportazio-hartzaileari lotzea ahalbidetzen duten. NES seinaleak, baina, askotarikoak dira, eta, horiek aurresateko, erreminta informatiko eraginkorrak eskura izatea garrantzitsua da oso. Badira gaur egun eskuragai zenbait NES-iragarle: esaterako, ELM [23], NetNES [24], NESsential [25] edota gure taldeak garatutako Wregex izenekoa [26]. Azken honek kargo-kandidatuen fidagarritasunaren hurrenkera zehazten du, eta modu horretan, lehentasunak markatzen dira esperimentalki ikergai izango diren kargoen artean. Benetako kargoak izateko aukera handienak dituzten aurresandako kandidatuak esperimentalki aztertuko ditugu.

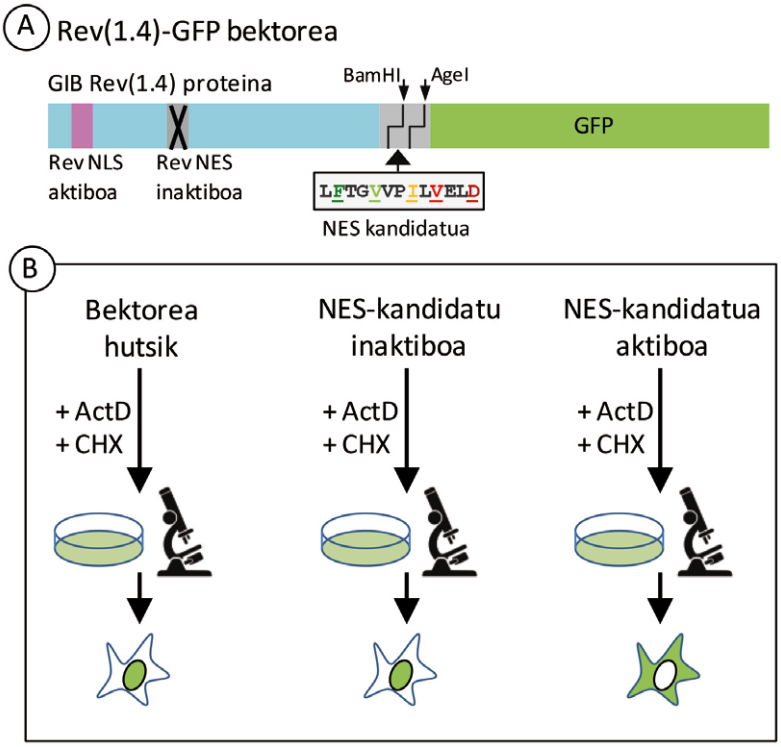

4. irudia. Esportazio-entseguaren nondik norakoak. A) Rev(1.4)-GFP plasmidoak kodetzen duen fusio-proteinaren irudi eskematikoa. Urdinez, Rev(1.4) proteina, non NES inaktiboa (grisez, gurutzea) eta NLS aktiboa (arrosaz) ageri diren. Berdez, GFP proteina. Plasmidoan, Rev(1.4) eta GFP kodetzen dituzten sekuentzien artean, BamHI eta AgeI murrizketa-lekuak daude, zeinak NES-kandidatua klonatzeko erabiliko diren. B) Esportazio-entseguan esperotako emaitzak: bektorea hutsik baldin badago kokapen nuklearra agertzen du; gauza bera gertatzen da klonatutako NES-kandidatua inaktiboa baldin bada. Aldiz, NES-kandidatua aktiboa bada, seinalea zitoplasman agertzen da [27]. ActD eta CHX erabilpenaren zehaztasunak *Material eta Metodoak* atalean daude deskribatuta.

1.2.3. *NES-kandidatuen gaineko esportazio-entseguak*

Henderson eta Eleftheriouk 2000. urtean garatu eta argitaratutako esportazio-entsegua da gure lan-fluxuan erabilitako prozedura baliagarrienetako bat [27]. Entsegu horretako pieza gakoa Rev(1.4)-GFP fusio-proteina da (4A irudia). Fusio-proteina horrek hiru zati ditu: (1) NESa mutatuta duen, hau da, esportatzen ez den GIB birusaren Rev proteina, Rev(1.4)

deritzona, (2) BamHI/AgeI murrizketa-lekuak, non ikergai diren NESak klona daitezkeen, eta (3) GFPa (*green fluorescent protein*). Rev(1.4)-GFP proteina, berez, hau da, hutsik, nukleoan kokatzen da; izan ere, Rev proteinak berezko NLS funtzional bat ere badu, zeinak proteina osoa nukleora inportatzea eragiten duen. Baina BamHI/AgeI arteko leku horretan NES-kandidatu aktibo bat sartuko bagenu, sortutako fusio-proteina berri hori zitoplasmara esportatuko litzateke, baldin eta Rev(1.4)-GFPk berezkoa duen NLSaren «indarra» gaindituko balu. Entseguaren emaitzaren arabera, beraz, NES-kandidatuak baieztatu edo baztertzen ditugu, eta NES aktiboen «indarra» ezagutzen dugu (4B irudia).

1.2.4. *NES aktiboen mutagenesi ituratua: funtzionaltasun biologikoaren berrespena*

Esportazio-entseguaren emaitzaren arabera aktibotzat ebatzi dugun NESa mutatu egingo dugu, honek XPO1en bidezko kargoaren garraioan izan dezakeen funtzionaltasuna berraztertu eta behar den kasuetan berresteko. Jatorrizko NES basatidun (*wild type*, WT) kargoa esportatu egingo litzateke, eta mutatutako NESdun kargoak, berriz, eragindako mutazioak direla eta, ezingo luke XPO1ekin elkarreragin eta, beraz, ezin izango litzateke nukleotik zitoplasmara esportatu. Modu honetan, lan-fluxu osoan zehar aktibotzat jo dugun NES-kandidatu jakin baten funtzionaltasuna berretsiko dugu, hala dagokionean.

LMBren erabilera aitzindaritik hasi eta osteko esportazio-entsegu eta eskala handiko proteomikako lanetaraino, hurbilketa guztien uztarketa ezinbestekoa da XPO1en kargoen errepertorioa (XPO1en «esportoma») osatuz joateko. Azken 15 urteetan, XPO1ek esportatutako 200 kargo inguru identifikatu dira modu fidagarrian [12] eta, berriki, masa espektrometriaren erabilerak XPO1en balizko kargoen bilduma 1.000 proteina baino gehiagotara zabaldu du [28].

1.3. **XPO1en kargoen peskizan: USP12/WDR20 konplexuaren kasua adibide**

Atarian adierazi legez, XPO1ek milaka proteinaren garraio nukleozitoplasmikoa bideratzen du eta, beraz, zelulan gertatzen diren prozesu ugariren erregulazioan gako da. Prozesu ugari horien artean, ubikuitinazio-bidezidorrak ditugu. Ubikuitinazioa itzulgarria den itzulpen osteko eraldaketa da, eta zeluletako proteina gehientsuenen egonkortasuna, funtzioa edota kokapena zuzentzen ditu. Deubikuitinasak (DUBak) ubikuitina-unitateak proteinetatik kentzen dituzten entzimak dira, eta funtsezko eginkizuna dute prozesu fisiologiko ugaritan [29]. Gure taldeak garraio nukleozitoplasmikoaren eta ubikuitinazioaren arteko lotura [30] ikertzen du. Esate baterako, 2012. urtean, DUB familiako zenbait kide-

ren NESak zehazteari ekin genion, eta horien funtzionaltasuna aztertu genuen [31].

100 giza DUB inguru daude 7 familiatan sailkatuta; familiarik handiena USP (*ubiquitin-specific proteases*) izenekoa da. Entzima-familia horretako kide batek, USP12 izenekoak, tumore ezabatzaile gisa jarduten duela ikusi da [32, 33]. Baina USP12k, berez, ez du aktibitate deubikuitinatzailerik, ez bada WDR20 eta UAF1 kofaktoreekin lotzen. Bi proteina horiek sinergistikoki jarduten dute, eta USP12ren aktibitate entzimatikoa handiagotzen. USP12k zelulen fisiologian duen garrantzia ezaguna bada ere, oraindik ez dago argi non, zein konpartimentutan kokatzen den zelulan, ezta aipaturiko bi kofaktoreek zer-nolako eragina izan dezaketen lokalizazio horretan, eraginik izatekotan. Kontu horrek eztabaidagai dirau gaur egun ere: ikerketa-lan batzuek USP12 gehienbat zitoplasmikoa dela diote [34-38], eta beste batzuek, aldiz, batez ere nuklearra dela [39, 40]. Argi dagoena da USP12 atzera eta aurrera mugitzen dela nukleoaren eta zitoplasmaren artean, eta mugimendu hori XPO1ek bideratzen duela [41, 40]. USP12aren NES bat deskribatu dute oraintsu Sanyal eta lankideek [40, 42]. Aurreko atalean azaldutako lan-fluxua erabilita, gure taldeak lortutako emaitzek iradokitzen dute deskribatutako NES hori ez dela modu argi eta nabarmenean esportaziorako seinale gisa aritzen. Bestalde, Kirli eta lankideek 2015. urtean zerrendatutako XPO1en HeLa zelulen mila kargo baino gehiagoren artean, WDR20 ageri da, USP12ren kofaktorea dena [28]. Hori guztia kontuan hartuta, guk honako hipotesia planteatzen dugu: USP12/WDR20 konplexuaren XPO1en bidezko esportazioa USP12k ez baizik WDR20k gidatu dezakeela. Gainera, hipotesi horrekin bat eginez, XPO1en menpekoa den USP12/WDR20 konplexuaren esportazioa bideratzen duen WDR20ren NES funtzional berri bat identifikatu dugu.

2. MATERIAL ETA METODOAK

2.1. Prozedura orokorrak: zelulen hazkuntza, transfekzioa eta mikroskopioan behatzeko laginen prestaketa

HeLa zelulak % 10 idi-umeki serodun (ingelesez *fetal bovine serum, FBS)* eta % 1 penizilina/estreptomizinadun DMEM (*Dulbecco's modified Eagle's medium*) medioan hazi ditugu (dena Invitrogen-ekoa) 37 °C-an, % 5eko CO_2-dun atmosferan. 24 ordu transfekzioa egin aurretik, zelulak 12 putzuko plaketan erein ditugu. Transfekzioak X-tremeGENE 9 transfekzio-agentea (Roche Diagnostics) erabiliz egin ditugu, fabrikatzailearen argibideei jarraituz.

Dagokien tratamendua jaso ostean, zelulak % 3,7 formaldehido PBStan fixatu ditugu 30 minutuz, eta DAPI-dun Vectashield muntaketa-medioa erabilita (Vector Laboratories), portetan muntatu ditugu.

1. pausoa. *Plasmidoen prestaketa, LMB tratamendua eta proteinen kokapenaren azterketa*

Gure intereseko proteinak diren USP12 eta WDR20 proteinen aurkako komertzialki eskuragarri dauden antigorputzak inespezifikoak izan ohi dira. Horrek arazo larria dakar, intereseko proteinez gain bestelako ituak ezagutu ditzaketelako antigorputzok. Hori horrela izanik, intereseko proteinak gainadierazteko helburuz, proteinok sustatzaile beraren pean klonatu ditugu YFP (*yellow fluorescent protein*) izeneko proteina fluoreszentearekin batera, pEYFP-C1 (Clontech) izeneko plasmidoan. Klonatutako intereseko proteina YFPrekin batera adierazten denez fusio-proteina gisara, adierazitako fluoreszentziaren behaketak intereseko proteinaren jarraipena egitea ahalbidetzen digu; hau da, zelulan non kokatzen den ikustea ahalbidetuko digu. Kasu honetan, USP12 eta WDR20 proteina basatien cDNA sekuentzien gBlock-ak (IDT) pEYFP-C1 plasmidoaren BamHI eta HindIII murrizketa-lekuen artean klonatu ditugu; ostean, HeLa zeluletan gainadierazi eta, fluoreszentzia-mikroskopioan aztertu dugu bi proteina horien kokapena. Prozedura berberari jarraitu diogu PCR bidez ekoitzitako WDR20ren delezio-mutanteak pEYFP-C1 plasmidoan klonatu eta gainadierazteko.

USP12, WDR20 eta azken honen delezio-mutanteen kokapena aztertzeko, transfekzioa egin eta 24 ordura HeLa zelulak 6 ng/ml LMB (Apollo Scientific) esportazio-inhibitzailez tratatu ditugu hiru orduz.

2. pausoa. *NES sekuentziaren iragarleen bidezko bilaketa*

WDR20 proteinaren NES seinalea aurresateko, Wregex (http://ehubio.ehu.eus/wregex) [26] erreminta bioinformatikoa erabili dugu.

3. pausoa. *Esportazio-entseguak eta entseguetan erabilitako plasmidoak*

pRev(1.4)-GFP bektorea (4A irudia) Beric Hendersonen (Westmead Institute for Cancer Research, University of Sydney, Australia) eskutik lortu dugu. USP12ren zein WDR20ren NESen cDNA-sekuentziak pRev(1.4)-GFP plasmidoaren BamHI eta AgeI murrizketa-lekuen artean klonatu ditugu. Klonatutako USP12 eta WDR20ren NES sekuentziak honakoak dira: ^{75}RKKESLLTCLADLFHSIAT^{93}, Rev(1.4)-NES^{USP12}-GFPren kasuan eta ^{450}MDGAIASGVSKFATLSLHD^{468}, Rev(1.4)-NES^{WDR20}-GFPren kasuan. Bai bi plasmido horiek eta bai kontrol negatibotzat hartuko dugun Rev(1.4)-GFP hutsa, HeLa zeluletan transfektatu ditugu. Hiru plasmidoetako bakoitza plakako bi putzu transfektatzeko erabili dugu. Zelulen transfekzioa egin eta 24 ordura, bi putzuetako bat 10 μg/ml zikloheximidaz (CHX; Sigma) tratatu dugu 3 orduz; besteari, berriz, 10 μg/ml CHX gehi 5 μg/ml aktimomizina D (ActD, Sigma) gehitu dizkiogu. Zikloheximida proteinen sintesia geldiarazten duen farmakoa da eta, beraz, horrekin tratatutako zeluletan, zitoplasman behatzen den seinale fluoreszentea

nukleotik zitoplasmara esportatu den GFP fusio-proteinaren seinalea da, eta ez zitoplasman sintetizatu berri den proteinarena. Bestetik, ActD farmakoak Rev(1.4) proteinaren NLSak gidatutako nukleoranzko inportazioa oztopatzen du eta, beraz, klonatutako NES ahulagoen aktibitatea ere sumatzea ahalbidetuko digu. Ikergai diren NESen aktibitatea zehazteko, bai kontrol negatiboarekin (Rev(1.4)-GFP hutsa) bai gure intereseko konstruktoekin (Rev(1.4)-NES^{USP12}-GFP ala Rev(1.4)-NES^{WDR20}-GFP) transfektatutako laginetako gutxienez 200 zelula zenbatu ditugu; 200 zelulen artean seinale zitoplasmikoa, seinale nuklearra ala seinale nukleozitoplasmikoa zein proportziotan behatu dugun kalkulatu dugu. Proportzio horien arabera, 0 eta 9ra arteko eskalan sailkatuko dugu aztertzen ari garen NESen aktibitatea edo indarra [27].

4. pausoa. *NESen mutagenesi ituratua*

Azkenik, NESek proteina osoaren testuinguruan duten eragina aztertzeko, proteina basatien (USP12 WT eta WDR20 WT) eta mutatutako NESak dituzten proteinen (USP12 NESmut eta WDR20 NESmut) portaera alderatu dugu. Mutatutako NESak dituzten proteinak ekoizteko, jatorrizko proteinak moldetzat hartu, eta mutagenesi ituratua egin dugu QuikChange Lighting Site-Directed Mutagenesis Kit-a (Stratagene) erabiliz. 1. pausoan USP12 eta WDR20 proteina basatietarako azaldutako prozedura berbera erabilita, YFP-USP12 NESmut eta YFP-WDR20 NESmut proteinek HeLa zeluletan duten kokapena aztertu dugu. Emaitzok proteina basatiekin lortutako emaitzekin alderatu ditugu.

3. EMAITZAK

3.1. USP12k eta WDR20k XPO1 hartzailearen mendeko garraioa jasaten dute

Lehenik eta behin, gainadierazitako USP12 deubikuitinasak eta haren kofaktorea den WDR20 proteinak zeluletan duten berezko kokapena aztertu dugu, eta bi proteinek kokapen zitoplasmikoa dutela ikusi dugu LMBrik gabeko (–LMB) laginetan. Alabaina, YFP-WDR20ren seinalea zitoplasmikoa da nabarmen, eta nukleoetan berriz, ezin beha daiteke seinalerik (6B irudia); YFP-USP12ren kasuan, aldiz, ahula bada ere, nukleoetan beha daiteke nolabaiteko seinalea (5A irudia). LMBren tratamenduaren mendeko (+LMB) XPO1en inhibizioak bi proteinen kokapenean eraginik duenetz ere aztertu dugu, eta bai YFP-WDR20ren kokapena bai YFP-USP12ren kokapena zitoplasmikoa izatetik nukleozitoplasmikoa izatera pasatu dela ikusi dugu; kasu bietan, nukleoetan behatzen den seinalea nabarmenagoa da –LMB laginetakoa baino (5A eta 6B irudiak). Hortaz, USP12 eta WDR20 proteinek XPO1 hartzailearen mendeko garraioa jasaten dute.

3.2. **Aurretiaz proposaturiko USP12ren NESa inaktiboa da**

USP12 proteinaren ^{77}KESLLTCLADLFHSI^{91} aminoazido-errenkada XPO1en mendeko garraiorako NES gisa proposatu da oraintsu [40, 42]. Proposatutako NES hori ez dator guztiz bat leuzinatan aberatsak diren NESen adostasun-sekuentziarekin (2C irudia); horretaz gain, ustezko NESa berresteko esportazio-entsegurik ez dute burutu egileek. Gauzak horrela, Rev(1.4)-NES^{USP12}-GFP fusio-proteinak zelulan duen kokapena aztertu dugu esportazio-entseguetan [27].

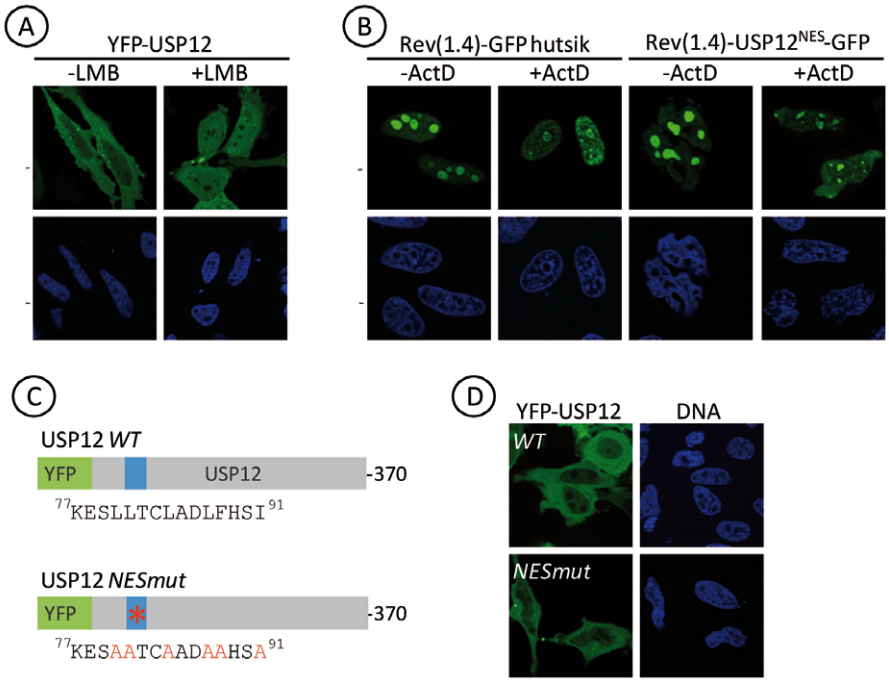

5. irudia. USP12 proteinaren ustezko NES sekuentziaren analisia. A) YFP-USP12 proteina, HeLa zeluletan gainadierazia, LMBz tratatua (+LMB) eta tratatu gabea (–LMB). Tratatu gabeko laginean, batez ere kokapen zitoplasmikoa du YFP-USP12 proteinak; tratatuta, aldiz, kokapen nuklearra eta zitoplasmikoa hartzen du. B) HeLa zeluletan eginiko esportazio-entseguaren irudiak: antzeko kokapena agertzen dute Rev(1.4)-GFP kontrol negatiboak eta USP12 proteinan deskribatutako NESa kodetzen duen plasmidoak (Rev(1.4)-NES^{USP12}-GFP). Hau da, ustezko NES sekuentzia hori ez da NES funtzional bat. Saiook ActD gehituz (+ActD) ala gehitu gabe (–ActD) egin ziren. C) USP12 fusio-proteina basatiaren (WT) eta NES mutatua duen (NESmut) fusio-proteinaren adierazpen eskematikoa. Mutatutako NESaren sekuentzian, aldatutako aminoazidoak gorriz erakusten dira. D) YFP-USP12 WT eta YFP-USP12 NESmut gainadierazten dituzten HeLa zelulen irudi konfokalak: proteina basatiak zein mutanteak kokapen zitoplasmikoa agertzen dute. Prestakinetako zelula-nukleoak DAPI tindaketaren bidez behatu dira. (1. erreferentziatik hartutako eta moldatutako irudia, Elsevierren baimenarekin).

Esportazio-entseguan erabilitako Rev(1.4)-NES^{USP12}-GFP fusio-proteinak ez du Rev(1.4)-GFP kontrol negatiboak baino kokapen zitoplasmikoagoa agertzen, ezta ActD-ren presentzian ere (5B irudia). Beraz, esportazio-entsegu horren emaitzek iradokitzen dute 2016an proposaturiko ustezko NES sekuentzia hori ez dela NES funtzional bat.

Proposaturiko NESak aktibitaterik erakutsi ez arren, proteina osoaren testuinguruan izan dezakeen funtzionaltasun biologikoa aztertzeko, mutagenesi-esperimentua egin dugu. Horretarako, YFP-USP12 basatiaren (USP12 *WT*) ^{77}KESLLTCLADLFHSI^{91} sekuentziatik aldatu ditugu leuzinatan aberatsak diren NESetan agertzen diren ohiko aminoazidoak; hortaz, NES mutatuaren (NESmut) sekuentzia honakoa da: ^{77}KES<u>AA</u>TC<u>A</u>AD<u>AA</u>HS<u>A</u>^{91} (5C irudia). Gainadierazitako YFP-USP12 WT eta YFP-USP12 NESmut proteinek zelulan zer kokapen duten aztertutakoan, ikusi dugu proteina biek kokapen zitoplasmikoa agertzen dutela (5D irudia). Beraz, USP12ren ^{77}KESLLTCLADLFHSI^{91} sekuentziak ez du proteinaren esportazioa gidatzen.

3.3. WDR20 proteinak haren kokapen nukleozitoplasmikoa gidatzen duen NES aktiboa du

Behin WDR20k XPO1en mendeko esportazioa jasaten duela egiaztatuta (6B irudia), haren NES seinalea zein den ikertu dugu. Ezaguna da NES seinale aktibo ohikoenek α helizearen erako egitura sekundarioa hartzen dutela amino-muturrean [13]. WDR20-USP12-UAF1 konplexua X izpien difrakzioa erabiliz aztertu bada ere [43], ez da α helizerik zehaztu WDR20 proteinaren kasuan. Alabaina, WDR20ren 394 eta 509 aminoazidoen arteko egitura zehaztea oraindik lortu ez denez [43], pentsatu genuen alde horretan α helizeren bat egon zitekeela eta, ondorioz, NESa izan zitekeen sekuentzia. Hortaz, YFP-WDR20ren hiru delezio-mutante egin ditugu; 1-390, 390-510 eta 510-569 aminoazidoen arteko zatiak direnak, hain zuzen ere (6A irudia). WDR20 proteina osoarekin egin bezala, zati horien kokapen zelularra ere zelulak LMBz tratatuz eta tratatu gabe aztertu dugu. YFP-WDR20(1-390) eta YFP-WDR20(510-569) zatiek kokapen nukleozitoplasmikoa hartzen dute, bai LMBz tratatutako laginetan bai tratatu gabeko laginetan. YFP-WDR20(390-510) zatiak, aldiz, proteina osoak zitoplasmatik nukleora jotzeko duen jokaera bera mantentzen du. Hau da, LMB tratamendurik gabe guztiz zitoplasmikoa da; LMBren presentzian, aldiz, kokapen nukleozitoplasmikoa hartzen du (6B irudia). Emaitza horrek WDR20 proteinaren NES seinalea 390 eta 510 aminoazidoen artean kokatuta dagoela ematen du aditzera.

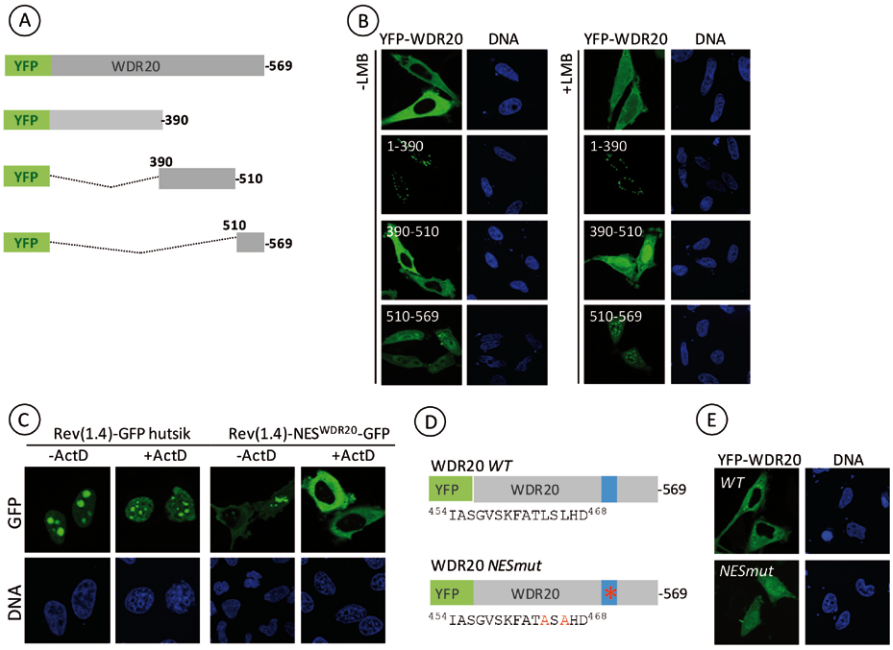

6. irudia. WDR20 proteinaren NESaren identifikazioa. A) YFP-WDR20 proteinaren delezio-mutanteen irudi eskematikoa. B) YFP-WDR20 osoa zein zatiak, HeLa zeluletan gainadierazita, LMBz tratatuta (+LMB) zein tratatu gabe (–LMB). WDR20 proteina osoak kokapen zitoplasmikoa du tratatu gabeko laginetan; LMBz tratatzean, aldiz, kokapen nukleozitoplasmikoa hartzen du. Zatiei erreparatuta, aldiz, LMB tratamenduak ez du YFP-WDR20(1-390) ez YFP-WDR20(510-569) zatien kokapena aldatzen. YFP-WDR20(390-510) zatiaren kokapena, aldiz, proteina osoarekin gertatzen den modu berean, zitoplasmikoa izatetik nukleozitoplasmikoa izatera pasatzen da LMB tratamenduaren ondorioz. C) WDR20 proteinaren cNESa aztertzeko asmoz HeLa zeluletan ActD-z tratatuta (+ActD) eta tratatu gabe (–ActD) Rev(1.4)-[NES^{WDR20}]-GFP eta Rev(1.4)-GFP bektore hutsek esportazio-entseguan erakutsitako kokapenaren irudi konfokalak. Rev(1.4)-[NES^{WDR20}]-GFP-ak kontrol negatiboak baino kokapen askoz ere zitoplasmikoagoa du. Horrek adierazten du WDR20 proteinaren proposatutako NESak haren esportazioa bultzatzen duela, hau da, NESa aktiboa dela. D) WDR20 basatidun (*WT*) eta WDR20 NES mutantedun (*NESmut*) fusio-proteinen adierazpen eskematikoa. Jatorrizko 464 eta 466 leuzinak alaninaz ordezkatu dira mutantean (gorriz adierazita). E) YFP-WDR20 basatia eta YFP-WDR20 mutantea, HeLa zeluletan gainadieraziak. NES mutantedun YFP-WDR20 proteinak zelulan duen kokapena YFP-WDR20 basatiak LMBz tratatutakoan duen kokapenaren oso antzekoa da. Prestakinetako zelula-nukleoak DAPI tindaketaren bidez behatu dira (1. erreferentziatik hartutako eta moldatutako irudia, Elsevierren baimenarekin).

WDR20 proteinaren NES seinalea zein den zehazteko, Wregex [26] erreminta bioinformatikoa erabili dugu. Wregex-ek WDR20 proteinean iragarritako balizko 9 NES-kandidatuetatik bakarra kokatzen da 390-510 aminoazidoen artean. NES-kandidatu horren sekuentzia honakoa da: ^{450}MDGAIASGVSKFATLSLHD^{468}. *Material eta Metodoak* ataleko 3. pausoan azaldutako prozedura berari jarraituz esportazio-entsegua egin dugu NES horren aktibitatea aztertzeko, eta, behatutakoaren arabera, NESaren indarra 6+ koa da; hau da, NESa aktiboa da (6C irudia). WDR20ren NESa aktiboa dela ikusita, proteina osoaren testuinguruan duen funtzionaltasuna aztertu dugu. Horretarako, NESaren sekuentziako L464 eta L466 aminoazidoak mutatu dira, leuzinak alaninaz ordezkatuta (6D irudia). Mutatutako NESdun WDR20k berezko kokapen nukleozitoplasmikoa agertzen duela ikusi dugu, eta kokapen hori WDR20 basatiak LMBz tratatutakoan duen kokapen bera da (6E irudia). Hortaz, baiezta dezakegu WDR20ren ^{450}MDGAIASGVSKFATLSLHD^{468} aminoazido-sekuentzia dela nukleotiko haren esportazioaren eragilea.

4. EZTABAIDA ETA ONDORIOAK

USP12/WDR20 konplexuaren adibideak erakusten du deskribatutako hurbilketa esperimentala XPO1en esportazio-kargoak karakterizatzeko hurbilketa egokia dela. Gure lanean lortutako emaitzek aditzera ematen dute USP12 proteinarako proposatutako NESak [40, 42] ez duela USP12ren esportazioa eragiten. Bestetik, USP12ren kofaktorea den eta masa espektrometriaren bidez XPO1en balizko kargotzat identifikatutako WDR20ren [28] NES aktiboa zehazki karakterizatu dugu. *Saccharomyces pombe* legamian, USP12/WDR20 konplexuaren homologoa den Ubp9/Bun62 konplexuaren garraioa Bun62 (WDR20 homologoa) kofaktorearen mendekoa da [41]. Homologia hori aintzakotzat hartuta, eta gure emaitzak ikusita, USP12/WDR20 konplexuaren garraioaren arduraduna WDR20 dela pentsatzen dugu.

5. ESKER ONAK

Lan honetako mikroskopio-analisiak UPV/EHUko mikroskopia-zerbitzuan (SGIker) egin dira. Lan hau Espainiako Gobernuaren MINECO-FEDER (SAF2014-57743-R), Eusko Jaurlaritzaren (IT1257-19) eta Euskal Herriko Unibertsitatearen (UPV/EHU) (UF111/20) finantziazioei esker egin da. Baita Eusko Jaurlaritzak (MS-ri) eta Euskal Herriko Unibertsitateak (UPV/EHU) (AO-Hri) emandako dirulaguntzei esker ere. Gure taldea PROTEOSTASIS BM1307 COST Action-eko kide da, European Cooperation in Science and Technology-k lagunduta.

6. **BIBLIOGRAFIA**

[1] OLAZABAL-HERRERO, A., SENDINO, M., ARGANDA-CARRERAS, I. eta RODRIGUEZ, J.A. 2019. «WDR20 regulates shuttling of the USP12 deubiquitinase complex between the plasma membrane, cytoplasm and nucleus». *European Journal ofCell Biology*, **98**, 12-26.

[2] KNOCKENHAUER, K.E. eta SCHWARTZ, T.U. 2016. «The Nuclear Pore Complex as a flexible and dynamic gate». *Cell,* **164**, 1162-1171.

[3] SCHMIDT, H.B eta GÖRLICH, D. 2016. «Transport selectivity of nuclear pores, phase separation, and membraneless organelles». *Trends in Biochemical Sciences,* **41,** 46-61.

[4] PEMBERTON, L.F. eta PASCHAL, B.M. 2005. «Mechanisms of receptor-mediated nuclear import and nuclear export». *Traffic,* **6**, 187-198.

[5] TRAN, E.J., KING, M.C. eta CORBETT, A.H. 2014. «Macromolecular transport between the nucleus and the cytoplasm: advances in mechanism and emerging links to disease». *Biochimica et Biophysica Acta,* **1843**, 2784-2795.

[6] CAUTAIN, B., HILL, R., DE PEDRO, N. eta LINK, W. 2015. «Components and regulation of nuclear transport processes». *The FEBS Journal,* **282**, 445-462.

[7] BECK, M. eta HURT, E. 2017. «The nuclear pore complex: understanding its function through structural insight». *Nature Reviews Molecular Cell Biology*, **18**, 73-89.

[8] ÇAĞATAY, T. eta CHOOK, Y.M. 2018. «Karyopherins in cancer». *Current Opinion in Cell Biology,* **52**, 30-42.

[9] SONIAT, M. eta CHOOK, Y.M. 2015. «Nuclear localization signals for four distinct karyopherin-β nuclear import systems». *Biochemical Journal,* **468**, 353-362.

[10] SENDINO, M., OMAETXEBARRIA, M.J eta RODRIGUEZ, J.A. 2018. «Hitting a moving target: inhibition of the nuclear export receptor XPO1/CRM1 as a therapeutic approach in cancer». *Cancer Drug Resistance,* **1**, 139-163.

[11] KIM, H.J. eta TAYLOR, J.P. 2017. «Lost in transportation: Nucleocytoplasmic transport defects in ALS and other neurodegenerative diseases». *Neuron*, **96**, 285-297.

[12] XU, D., FARMER, A., COLLETT, G., GRISHIN, N.V. eta CHOOK. Y.M. 2012. «Sequence and structural analyses of nuclear export signals in the NESdb database». *Molecular Biology of the Cell*, **23**, 3677-3693.

[13] DONG, X., BISWAS, A. eta CHOOK, Y.M. 2009. «Structural basis for assembly and disassembly of the CRM1 nuclear export complex». *Nature Structural & Molecular Biology,* **16**, 558-560.

[14] GAMA-CARVALHO, M. eta CARMO-FONSECA, M. 2001. «The rules and roles of nucleocytoplasmic shuttling proteins». *FEBS Letters*, **498**, 157-163.

[15] CAUTAIN, B., HILL, R., DE PEDRO, N. eta LINK, W. 2015. «Components and regulation of nuclear transport processes». *FEBS J*, **282**, 445-462.

[16] FUKUDA, M., ASANO, S., NAKAMURA, T., ADACHI, M., YOSHIDA, M., YANAGIDA, M. eta NISHIDA, E. 1997. «CRM1 is responsible for intracellular transport mediated by the nuclear export signal». *Nature*, **390**, 308-311.

[17] FORNEROD, M., OHNO, M., YOSHIDA, M. eta MATTAJ, I.W. 1997. «CRM1 is an export receptor for leucine-rich nuclear export signals». *Cell*, **90**, 1051-1060.

[18] STADE, K., FORD, C.S., GUTHRIE, C. eta WEIS, K. «Exportin 1 (Crm1p) is an essential nuclear export factor». *Cell,* **90**, 1041-1050.

[19] OSSAREH-NAZARI, B., BACHELERIE, F. eta DARGEMONT, C. 1997. «Evidence for a role of CRM1 in signal-mediated nuclear protein export». *Science,* **278**, 141-144.

[20] HAMAMOTO, T., UOZUMI, T. eta BEPPU, T. 1985. «Leptomycines A and B, new antifungal antibiotics III. mode of action of Leptomycin B on *Schizosaccharomyces pombe*». *The Journal of Antibiotics*, **38**, 1573-1580.

[21] KUDO, N., WOLFF, B., SEKIMOTO, T., SCHREINER, E.P., YONEDA, Y., TANAGIDA, M., HORINOUCHI, S. eta YOSHIDA, M. 1998. «Leptomycin B inhibition of signal-mediated nuclear export by direct binding to CRM1». *Experimental Cell Research*, **242**, 540-547.

[22] GARCÍA-SANTISTEBAN, I., ARREGI, I., ALONSO-MARIÑO, M., URBANEJA, M.A., GARCIA-VALLEJO, J.J., BAÑUELOS, S. eta RODRÍGUEZ, J.A. 2016. «A cellular reporter to evaluate CRM1 nuclear export activity: functional analysis of the cancer-related mutant E571K». *Cellular and Molecular Life Sciences,* **73**, 4685-4699.

[23] GOULD, C.M., DIELLA, F., VIA, A., PUNTERVOLL, P., GEMÜND, C., CHABANIS-DAVIDSON, S., MICHAEL, S., SAYADI, A., BRYNE, J.C., CHICA, C., SEILER, M., DAVEY, N.E., HASLAM, N., WEATHERITT, R.J., BUDD, A., HUGHES, T., PAS, J., RYCHLEWSKI, L., TRAVÉ, G., AASLAND, R., HELMER-CITTERICH, M., LINDING, R. eta GIBSON, T.J. 2010. «ELM: the status of the 2010 eukaryotic linear motif resource». *Nucleic Acids Research*, **38**, 167-180.

[24] LA COUR, T., KIEMER, L., MØLGAARD, A., GUPTA, R., SKRIVER, K. eta BRUNAK, S. 2004. «Analysis and prediction of leucine-rich nuclear export signals». *Protein Engineering, Design & Selection*, **17**, 527-536.

[25] FU, S.C., IMAI, K. eta HORTON, P. 2011. «Prediction of leucine-rich nuclear export signal containing proteins with NESsential». *Nucleic Acids Research*, **39**, e111.

[26] PRIETO, G., FULLAONDO, A. eta RODRIGUEZ J.A. 2014. «Prediction of nuclear export signals using weighted regular expressions (Wregex)». *Bioinformatics*, **30**, 1220-1227.

[27] HENDERSON, B.R. eta ELEFTHERIOU, A. 2000. «A comparison of the activity, sequence specificity, and CRM1-dependence of different nuclear export signals». *Experimental Cell Research,* **256**, 213-224.

[28] KIRLI, K., KARACA, S., DEHNE, H.J., SAMWER, M., PAN, K.T., LENZ, C., URLAUB, H. eta GÖRLICH, D. 2015. «A deep proteomics perspective on CRM1-mediated nuclear export and nucleocytoplasmic partitioning». *Elife*, **4**, e11466.

[29] KOMANDER, D., CLAGUE, M.J. ETA URBÉ, S. 2009. «Breaking the chains: structure and function of the deubiquitinases». *Nature Reviews Molecular Cell Biology*, **10**, 550-563.

[30] RODRIGUEZ, J.A. 2014. «Interplay between nuclear transport and ubiquitin/SUMO modifications in the regulation of cancer-related proteins». *Seminars in Cancer Biology*, **27**, 11-19.

[31] GARCIA-SANTISTEBAN, I., BAÑUELOS, S. eta RODRIGUEZ, J.A. 2012. «A global survey of CRM1-dependent nuclear export sequences in the human deubiquitinase family». *Biochemical Journal,* **441**, 209-217.

[32] GANGULA, N.R. eta MADDIKA, S. 2013. «WD repeat protein WDR48 in complex with deubiquitinase USP12 suppresses Akt-dependent cell survival signalling by stabilizing PH domain leucine-rich repeat protein phosphatise 1 (PHLPP1)». *The Journal of Biological Chemistry,* **288**, 34545-34554.

[33] LI, X., STEVENS, P.D., YANG, H., GULHATI, P., WANG, W., EVERS, B.M. eta GAO, T. 2013. «The deubiquitination enzyme USP46 functions as a tumor suppressor by controlling PHLPP-dependent attenuation of Akt signalling in colon cancer». *Oncogene,* **32**, 471-478.

[34] SOWA, M.E., BENNETT, E.J., GYGI, S.P. eta HARPER, J.W. 2009. «Defining the human deubiquitinating enzyme interaction landscape». *Cell*, **138**, 389-403.

[35] URBÉ, S., LIU, H., HAYES, S.D., HERIDE, C., RIGDEN, D.J. eta CLAGUE, M.J. 2012. «Systematic survey of deubiquitinase localization identifies USP21 as a regulator of centrosome and microtubule-associated functions». *Molecular Biology of the Cell*, **23**, 1095-1103.

[36] BURSKA, U.L, HARLE, V.J., COFFEY, K., DARBY, S., RAMSEY, H., O'NEILL, D., LOGAN, I.R., GAUGHAN, L. eta ROBSON, C.N. 2013. «Deubiquitinating enzyme Usp12 is a novel co-activator of the androgen receptor». *The Journal of Biological Chemistry,* **288**, 32641-32650.

[37] LEHOUX, M., GAGNON, D. eta ARCHAMBAULT, J. 2014. «E1-mediated recruitment of a UAF1-USP deubiquitinase complex facilitates human papillomavirus DNA replication». *Journal of Virology*, **88**, 8545-8555.

[38] OLAZABAL-HERRERO, A., GARCÍA-SANTISTEBAN, I. eta RODRIGUEZ, J.A. 2015. «Structure-function analysis of USP1: insights into the role of Ser313 phosphorylation site and the effect of cancer-associated mutations on autocleavage». *Molecular Cancer*, **14**.

[39] JOO, H.Y., JONES, A., YANG, C., ZHAI, L., SMITH, IV A.D., ZHANG, Z., CHANDRASEKHARAN, M.B., SUN, Z.W., RENFROW, M.B., WANG, Y., CHANG, C. eta WANG, H. 2011. «Regulation of histone H2A and H2B deubiquitination and *Xenopus* development by USP12 and USP46». *The Journal of Biological Chemistry,* **286**, 7190-7201.

[40] JAHAN, A.S., LESTRA, M., SWEE, L.K., FAN, Y., LAMERS, M.M. TAFESSE, F.G., THEILE, C.S., SPOONER, E., BRUZZONE, R., PLOEGH, H. L. eta SANYAL, S. 2016. «Usp12 stabilizes the T-cell receptor complex at the cell surface during signaling». *Proceedings of the National Academy of Sciences of the United States of America*, **113**, E705-714.

[41] KOURANTI, I., MCLEAN, J.R., FEOKTISTIVA, A., LIANG, P., JOHNSON, A.E., ROBERTS-GALBRAITH, R.H. eta GOULD, K.L. 2010. «A global census of fission yeast deubiquitinating enzyme localization and interaction networks reveals distinct compartmentalization profiles and overlapping functions in endocytosis and polarity». *PLOS Biology*, **8**, e1000471.

[42] SANYAL, S., 2016. «Reply to Rodriguez: mechanism of nuclear-cytosol shuttling of Usp12». *Proceedings of the National Academy of Sciences of the United States of America,* **113**, E3317-3318.

[43] LI, H., LIM, K.S., HINDS, T.R., JO, U., MAO, H., WELLER, C.E., SUN, J., CHATTERJEE, C., D'ANDREA, A.D. eta ZHENG, N. 2016. «Allosteric activation of ubiquitin-specific proteases by β-propeller proteins UAF1 and WDR20». *Molecular Cell*, **63**, 249-260.

International Journal of
Molecular Sciences

MDPI

Article

Using a Simple Cellular Assay to Map NES Motifs in Cancer-Related Proteins, Gain Insight into CRM1-Mediated NES Export, and Search for NES-Harboring Micropeptides

Maria Sendino [1], Miren Josu Omaetxebarria [2], Gorka Prieto [3] and Jose Antonio Rodriguez [1,*]

1 Department of Genetics, Physical Anthropology and Animal Physiology, University of the Basque Country (UPV/EHU), 48940 Leioa, Spain; maria.sendino@ehu.eus
2 Department of Biochemistry and Molecular Biology, University of the Basque Country (UPV/EHU), 48940 Leioa, Spain; mirenjosu.omaetxebarria@ehu.eus
3 Department of Communications Engineering, University of the Basque Country (UPV/EHU), 48013 Bilbao, Spain; gorka.prieto@ehu.eus
* Correspondence: josean.rodriguez@ehu.es

Received: 10 August 2020; Accepted: 26 August 2020; Published: 1 September 2020

Abstract: The nuclear export receptor CRM1 (XPO1) recognizes and binds specific sequence motifs termed nuclear export signals (NESs) in cargo proteins. About 200 NES motifs have been identified, but over a thousand human proteins are potential CRM1 cargos, and most of their NESs remain to be identified. On the other hand, the interaction of NES peptides with the "NES-binding groove" of CRM1 was studied in detail using structural and biochemical analyses, but a better understanding of CRM1 function requires further investigation of how the results from these in vitro studies translate into actual NES export in a cellular context. Here we show that a simple cellular assay, based on a recently described reporter ($SRV_{B/A}$), can be applied to identify novel potential NESs motifs, and to obtain relevant information on different aspects of CRM1-mediated NES export. Using cellular assays, we first map 19 new sequence motifs with nuclear export activity in 14 cancer-related proteins that are potential CRM1 cargos. Next, we investigate the effect of mutations in individual NES-binding groove residues, providing further insight into CRM1-mediated NES export. Finally, we extend the search for CRM1-dependent NESs to a recently uncovered, but potentially vast, set of small proteins called micropeptides. By doing so, we report the first NES-harboring human micropeptides.

Keywords: CRM1; XPO1; NES; micropeptide; cellular assay; nuclear export; nuclear export signal

1. Introduction

Cellular homeostasis requires a continuous trafficking of proteins between the nucleus and the cytoplasm. For most proteins, nucleocytoplasmic transport is an active process, carried out by a family of soluble receptors termed karyopherins [1–3]. Transport receptors recognize and bind specific amino acid sequence motifs in the cargo proteins that dictate import into the nucleus (nuclear localization signals or NLSs) or export to the cytoplasm (nuclear export signals or NESs). NLSs are recognized by nuclear import receptors, such as the Importin α/β heterodimer [4], whereas NESs are recognized by nuclear export receptors, such as CRM1 (also called XPO1) [5].

According to the number of cargos, CRM1 is the main receptor for protein nuclear export. In addition to several dozens of well-validated cargos, a global proteomics analysis in HeLa cells identified more than 1000 proteins that are probably exported by CRM1, constituting what was termed the "CRM1-dependent nuclear exportome" [6]. Binding to CRM1 is usually mediated by short amino

acid motifs in the cargo protein, often referred to as "classical" or "leucine-rich" NESs, which show a pattern of 4 or 5 characteristically spaced hydrophobic residues. Hundreds of different NES motifs that differ widely in their amino acid sequence and their affinity for CRM1 [7–9] were identified. According to the spacing between their hydrophobic residues and the conformation they adopt when bound to CRM1, NESs have been classified into four main groups (class 1, 2, 3 and 4) [10,11]. In addition, certain class 1 NESs (so called "minus" motifs) have been reported to bind CRM1 in a reverse orientation, and are thus classified as class 1-R [12].

CRM1 is often altered in human tumors. The most common cancer-related CRM1 alteration is protein overexpression, which was detected in most types of solid and hematological malignancies (reviewed in [13]). In addition, a recurrent hotspot mutation in CRM1 residue E571 is highly prevalent in specific types of leukemia and lymphoma (see below). CRM1 is increasingly regarded as an important target for cancer therapy. Therapeutic inhibition of CRM1, mainly using a family of drugs termed selective inhibitors of nuclear export (SINEs) was extensively validated in preclinical studies, and is being evaluated in multiple clinical trials [13]. The most clinically advanced SINE compound, KPT-330 or selinexor (marketed as XPOVIO^{TM}) was recently (July 2019) approved by the FDA for the treatment of relapsed or refractory multiple myeloma in combination with dexamethasone [14]. The antitumor activity of CRM1 inhibitors is thought to be mediated, at least in part, by their ability to restore the normal localization and activity of cancer-related CRM1 cargos that are mislocalized in tumors due to altered CRM1 expression or function. To better understand the biological effects of CRM1 inhibitors in cancer patients, it is thus essential to extend our current knowledge of cancer-related CRM1 cargos. In this regard, by combining the "CRM1-dependent nuclear exportome" protein set [6] with the subset of "Cancer-related gene" entries of the Human Protein Atlas (https://www.proteinatlas.org/), we recently proposed the term "XPO1/CRM1-cancer exportome" [13] to refer to a group of 136 cancer-related proteins that are known or potential CRM1 cargos (Supplementary Table S1. Importantly, the NES motifs that could mediate CRM1-dependent export of these proteins remain unknown in most cases. Identifying sequence motifs with nuclear export activity in these proteins would further validate them as CRM1 cargos, and pave the way for subsequent functional analyses.

NES peptides bind to a hydrophobic groove in the surface of CRM1. This NES-binding groove is wider at one end (where the N-terminus of most known NESs binds), and then displays a constriction, becoming narrower at the other end. A series of landmark studies a decade ago showed that NES peptides dock into five hydrophobic pockets of the CRM1 groove, and identified several key amino acids, including I521, L525, F561 and F572 (residue numbering of human CRM1 is used throughout the text) that establish hydrophobic interactions with NES residues [10–17]. Subsequent analyses have shown that different NES peptides can adopt different backbone conformations when bound to CRM1 [11]. These studies have also identified K568 as a key residue in CRM1 groove, [11]. This residue not only contributes to NES binding by hydrogen bonding with the NES backbone, but also appears to function as a "specificity filter" that physically blocks binding of those NES-like peptides whose structural features are not optimal for docking into the groove [11]. Importantly, K568 establishes electrostatic interactions with E571, the CRM1 residue recurrently mutated in certain hematological malignancies [18] (reviewed in [13]). We have previously shown that the cancer-related mutation E571K subtly alters binding of certain NESs [19], and acts as an oncogenic driver [20].

Structural and biochemical data have significantly advanced our understanding of NES binding and export by CRM1, but several questions remain to be explored. For example, combined mutations of multiple hydrophobic residues in CRM1 groove were shown to disrupt binding [16] and export [19] of a few NESs, but the contribution of individual hydrophobic groove residues to the export of different NES classes has not been investigated. On the other hand, while the effect of K568 and E571 mutations was separately analyzed, a direct comparison of how mutation of these residues affects NES export has not been yet carried out.

In the present study, we apply a recently described nuclear export reporter termed $SRV_{B/A}$ (Figure 1A–C) [20] to map new sequence motifs with nuclear export activity in "XPO1/CRM1-cancer

exportome" proteins, and to gain further insight into CRM1-mediated NES export. In addition, we use this reporter to describe, for the first time, the presence of CRM1-dependent NESs in a recently uncovered and largely uncharacterized set of small proteins termed micropeptides [21]. Altogether, our work illustrates how simple transfection-based cellular assays can be applied to obtain relevant information on different aspects of CRM1-mediated nuclear export.

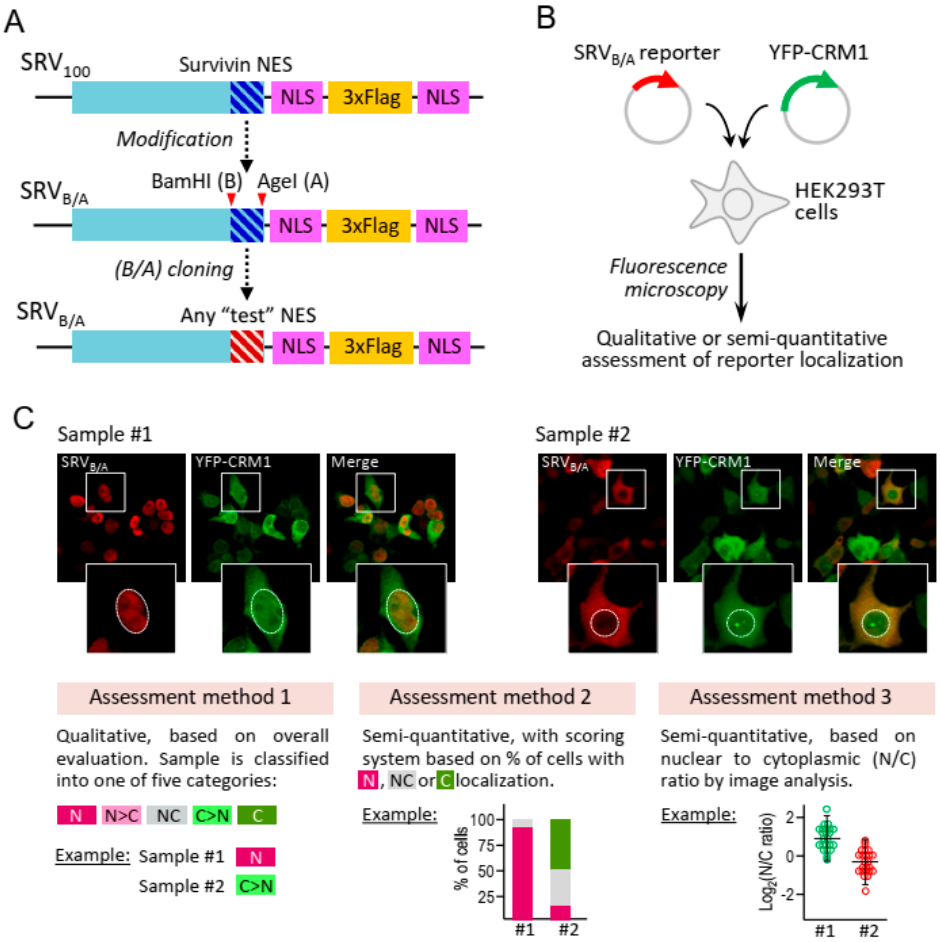

Figure 1. Description and use of the $SRV_{B/A}$ reporter with different assessment methods. (**A**) Schematic illustration showing the development and configuration of $SRV_{B/A}$. This reporter is derived from the previously described SRV100 reporter containing the NES of survivin [19]. As originally described in a recent report [20], the plasmid encoding SRV100 was modified to introduce two novel restriction sites (BamHI/AgeI), which allows replacing survivin NES by any other NES motif. Besides a survivin amino-terminal fragment and the cloned NES motif, the $SRV_{B/A}$ reporter includes two copies of the SV40 NLS (PKKKRKV) separated by three tandem copies of the Flag epitope. (**B**) To carry out $SRV_{B/A}$-based assays, HEK293T cells are co-transfected with plasmids encoding the reporter and the desired YFP-CRM1 variant. After anti-Flag immunostaining the localization of the reporter is determined using fluorescence microscopy. (**C**) Microscopy images show examples of the results of the assay with two reporters that contain different NES motifs. Insets show the magnified image of a single cell of each sample, with the nucleus delimited by a dotted line. Under the images, the three different methods used to manually assess the localization of the reporters in this study are described. Method 1 is a qualitative assessment, where the sample is ascribed, according to overall reporter localization, to one of five categories: exclusively nuclear (N), mainly nuclear (N > C), nuclear and cytoplasmic (NC), mainly cytoplasmic (C > N) or exclusively cytoplasmic (C). In the example, sample#1 is classified as N, and sample#2 as C > N. Method 2 is a more detailed, semiquantitative assessment that we have previously used with the SRV100 reporter [19]. The localization of the reporter in at least 200 individual

cells per sample is evaluated, and classified as exclusively/mainly nuclear (N), nuclear and cytoplasmic (NC), or exclusively/mainly cytoplasmic (C). Based on the percentage of cells showing N, NC or C localization of the reporter, a nuclear export score (termed "SRV export score") between 0 (no export) and 100 (complete export) is calculated as described in Methods. Graphs show the results for sample#1 and sample#2, corresponding to "SRV export scores" of 4 and 70, respectively. Method 3, the most detailed and laborious assessment method used here, is based on image analysis to determine the nuclear to cytoplasmic (N/C) ratio of the Alexa Fluor 594 fluorescent signal corresponding to the $SRV_{B/A}$ reporter in an average of 50 cells per sample. Graphs illustrating the results for sample#1 and sample#2 are shown.

2. Results

2.1. Using the $SRV_{B/A}$ Assay to Identify Novel NES Motifs in Cancer-Related CRM1 Cargos

Cellular assays based on the localization of reporter proteins are a common approach to evaluate nuclear export activity of putative NES motifs. A prominent example is the Rev(1.4)-GFP nuclear export assay [22]. In this widely used assay (cited 330 times, according to the Scopus citation database accessed in May 2020), export activity of candidate NESs is determined by their ability to induce cytoplasmic relocation of the otherwise nuclear Rev(1.4)-GFP reporter. We have previously shown that another cellular assay, based on a reporter termed SRV100, can be used to compare the export activity of different CRM1 variants [19]. The original SRV100 reporter contained the NES of survivin but, as recently described [20], we have subsequently modified the plasmid encoding SRV100 to introduce two novel restriction sites (BamHI/AgeI) that allow replacing survivin NES by any other NES (Figure 1A). Importantly, this modified reporter, called $SRV_{B/A}$, was designed in such a manner that candidate NES motifs can be easily shuttled to and from the Rev(1.4)-GFP reporter (Figure 2A).

The $SRV_{B/A}$ assay has not yet been applied to identify novel NES motifs. To determine how this assay compares to the well-established Rev(1.4)-GFP assay in this task, we decided to use both systems in an effort to map novel NESs in proteins that conform the "XPO1/CRM1-cancer exportome" (Figure 2B). As a first step, we carried out an in silico prediction of putative NES motifs in 112 of these proteins (those classified as "CRM1 cargo A" or CRM1 cargo B" in [6]). Their amino acid sequence was analyzed with two different programs: Wregex [23] and NESmapper [24]. To predict potential reverse ("minus") NES motifs, the amino acid sequence of each protein was inverted prior to being used as input for the analysis. A ranking approach, based on the score assigned by the programs to each predicted NES, was applied to select a reasonable number of candidate motifs to be experimentally tested. Thus, predicted NES motifs with scores within the first quartile for both programs were designed as Rank 1 candidates. Predicted motifs within the first quartile for one of the programs and within the second quartile for the other were designed as Rank 2. This in silico analysis identified 7 Rank 1 "plus" and 10 Rank 1 "minus" candidates.

The Rev(1.4)-GFP assay was used first to evaluate export activity of all Rank 1 motifs. In addition, all predicted Rank 2 "plus" candidates (19 motifs) were also included in the analysis. All in all, 35 candidates were tested and assigned an export score (hereafter referred to as "1.4 score") in a range between 0 and 9 [22]. As summarized in Supplementary Table S2, 25 of the 36 candidate sequences tested positive in the Rev(1.4)-GFP assay. Representative examples are shown in Supplementary Figure S1A. 19 of these sequences represent novel NES motifs (Supplementary Figure S1B), while six had been previously reported [25–30]. Among "plus" candidates, 19 out of 25 motifs tested positive, although 3 of them showed borderline activity (1.4 score = 1). On the other hand, 6 out of 10 "minus" candidates tested positive, 4 of them with borderline activity. The mean 1.4 score was 3.84 for "plus" motifs and 1.5 for "minus" motifs (Supplementary Figure S1C).

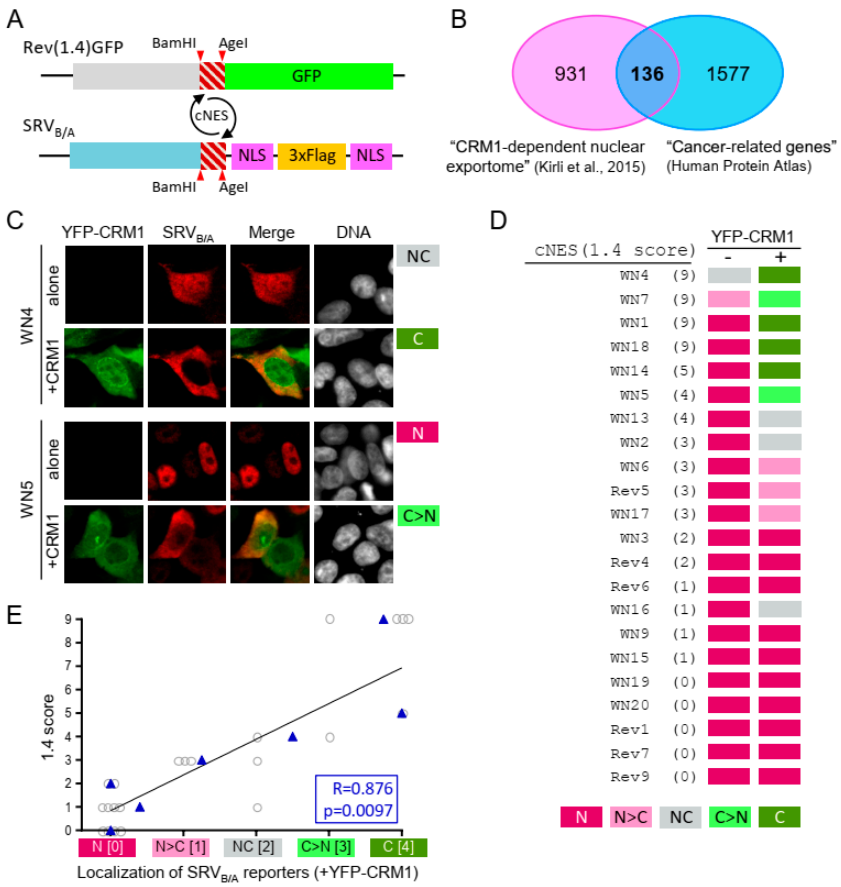

Figure 2. Using the SRV$_{B/A}$ assay to identify novel NES motifs in cancer-related CRM1 cargos. (**A**) Schematic representation of Rev(1.4)-GFP and SRV$_{B/A}$ reporters, illustrating how candidate NES motifs (cNES) can be easily shuttled between both reporters by BamHI/AgeI subcloning. (**B**) Venn diagram (modified from [13]) showing the overlap between the list of potential CRM1 cargos reported in [6] and the group of "Cancer-related gene" defined in the Human Protein Atlas. The 136 common proteins represent what we refer to as the "XPO1/CRM1-cancer exportome". (**C**) Fluorescence microscopy images showing representative examples of the localization of SRV$_{B/A}$ reporters containing two different cNES motifs (WN4 and WN5, see Supplementary Table S2), when transfected alone or co-transfected with YFP-CRM1 wild-type (+CRM1) into HEK293T cells. The DNA-staining dye DAPI was used to visualize the nuclei. As indicated to the right of the images, using assessment method 1 the localization of SRV-WN4 was classified as NC (alone) and C (+CRM1), while the localization of SRV-WN5 reporter was classified as N (alone) and C > N (+CRM1). (**D**). Summary of the localization of 22 SRV$_{B/A}$ reporters containing cNES motifs predicted in cancer-related proteins. The cNES ID (Supplementary Table S2) and the 1.4 score for each motif are indicated to the left. The localization of each reporter expressed alone (−) or co-expressed with YFP-CRM1 wild-type (+) was assessed using method 1. Ten motifs showed exclusively nuclear (N) localization when co-expressed with YFP-CRM1, and were thus considered inactive in this assay. (**E**). Graph showing the correlation between the results obtained with the Rev(1.4)-GFP and the SRV$_{B/A}$ assays for 22 cNES motifs that were tested using both systems. For each motif, the score assigned using the Rev(1.4)-GFP assay (1.4 score, between 0 and 9) was plotted against the localization (N, N > C, NC, C > N, or C) of the corresponding SRV$_{B/A}$ reporter when co-expressed with YFP-CRM1. To calculate the correlation coefficient between both sets of data, qualitative descriptions of SRV$_{B/A}$ localizations were assigned a numerical value (N = 0; N > C = 1; NC = 2; C > N = 3; C = 4). The mean of these values for cNES motifs with a given 1.4 score is represented as a blue triangle. Pearson correlation coefficient and *p* value are indicated.

Next, a subset of 22 motifs with different 1.4 scores were subcloned into the SRV$_{B/A}$ plasmid. These reporters were transfected into HEK293T cells either alone or with YFP-CRM1 and, after anti-Flag

immunostaining, their localization was globally assessed by fluorescence microscopy and classified as exclusively nuclear (N), mainly nuclear (N > C), nuclear and cytoplasmic (NC), mainly cytoplasmic (C > N) or exclusively cytoplasmic (C) (assessment method 1, detailed in Figure 1). Representative examples of the localization of two reporters are shown in Figure 2C, and the results obtained with the 22 reporters are summarized in Figure 2D. When transfected alone, all but two reporters (those containing cNES motifs WN4 and WN7, both with a 1.4 score of 9) showed exclusively nuclear localization. On the other hand, when co-transfected with YFP-CRM1, all reporters containing cNES motifs with 1.4 score above 2 showed partial or complete relocation to the cytoplasm. In contrast, all reporters containing cNES motifs with a 1.4 score equal or lower than 2, except SRV-WN16, were classified as exclusively nuclear, even when co-expressed with CRM1. In an attempt to evaluate the correlation between the results obtained with the two assays, 1.4 scores were plotted against the localization of the $SRV_{B/A}$ reporters (when co-transfected with YFP-CRM1). To calculate the correlation coefficient, the different $SRV_{B/A}$ localizations were assigned numerical values (N = 0; N > C = 1; NC = 2; C > N = 3; C = 4). As shown in Figure 2E, the results obtained with the Rev(1.4)-GFP and the $SRV_{B/A}$ assays were significantly correlated (R = 0.876; p = 0.0097). We noted that some sequence motifs with the lowest nuclear export activity (1.4 score equal or lower than 2) may be missed in the $SRV_{B/A}$ assay, when the localization of reporters is qualitatively analyzed. Conversely, the $SRV_{B/A}$ assay allowed to detect differences in activity between strong NES motifs. Thus, WN1, WN4, WN7 and WN18 were all assigned a 1.4 score of 9 (the highest possible in this assay), but only SRV-WN4 and SRV-WN7 reporters showed partial cytoplasmic localization when transfected alone, suggesting that WN4 and WN7 motifs are stronger NESs than WN1 and WN18.

In summary, we have experimentally validated 25 sequence motifs with nuclear export activity in "XPO1/CRM1-cancer exportome" proteins, 19 of which represent novel "plus" or "minus" potential NESs not previously described. Furthermore, these results validate the use of the $SRV_{B/A}$ reporter as a tool to search for novel NESs.

2.2. Using the $SRV_{B/A}$ Assay to Gain Further Insight into CRM1-Mediated NES Export. (i) Effect of Single-Residue NES-Binding Groove Mutations

The structural analyses that revealed how NES peptides dock into the NES-binding groove of CRM1 were supported by in vitro pull-down assays to evaluate how groove mutations affected NES interaction. Thus, it was shown that replacing groove residue A541 with a bulkier lysine (A451K) severely disrupted CRM1/NES interaction [17]. A similar disruption was observed when four groove residues that establish hydrophobic interactions with the NES (I521, L525, F561 and F572) were simultaneously mutated to alanine (I521A/L525A/F561A/F572A, hereafter referred to as 4X) [16]. Subsequent structural and biochemical studies have identified a key residue in the NES-binding groove, K568, which contributes to NES binding, and may also block docking of non-functional NES-like peptides [11]. Using the SRV100 reporter-based cellular assay, we have previously confirmed that the A541K and 4X mutations prevent nuclear export of survivin NES [19].

Here we sought to investigate, using the $SRV_{B/A}$ reporter, to what extent individual groove residues contribute to the export of different NES motifs in a cellular context. To this end, we generated a panel of YFP-CRM1 variants bearing single-residue mutations in five groove amino acids (I521A, L525A, F561A, F572A and K568A) whose position is illustrated in Figure 3A. The export activity of these mutants was interrogated using a panel of 14 extensively characterized NES motifs (PKI, superPKI, PAX, HDAC5, FMRP, FMRP-1b, SNUPN, Rev, SMAD4, mDia2, CDC7, X11L2, CPEB4 and hRio2). The binding of these NES peptides to CRM1 was previously studied using structural and biochemical analyses [11], and their export activity was analyzed using a cellular assay [31]. These well-studied NESs provide a unique resource to evaluate the export activity of the different CRM1 mutants against a variety of motifs that belong to different NES classes (1, 2, 3, 4 and 1-R), and dock into CRM1 groove using different backbone conformations [11].

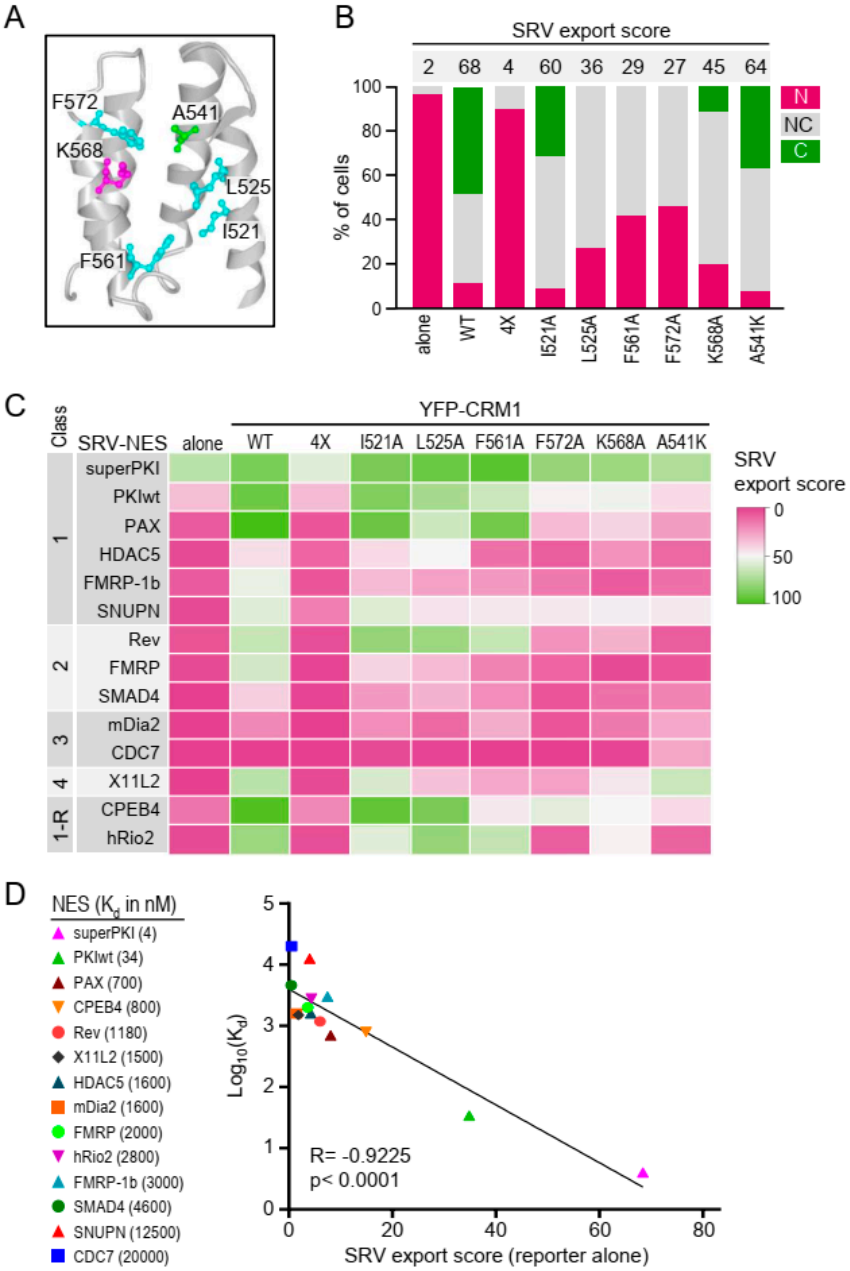

Figure 3. Using the $SRV_{B/A}$ assay to test the effect of single-residue mutations in CRM1 NES-binding groove. (**A**) View of CRM1 NES-binding groove generated with NCBI iCn3D viewer from PDB structure 3GJX [15]. The residues individually mutated in this study are highlighted using ball and stick representation, while the remaining residues are represented using ribbon style. (**B**) Graph shows an example of the results of $SRV_{B/A}$ assays testing export activity of the different YFP-CRM1 mutants against a reporter containing one of the previously characterized NES motifs (in this case SRV-X11L2). The localization of the reporter was determined in at least 200 cells per sample. Bar colors represent the percentage of cells showing the indicated reporter localization (N, NC or C). The number above each bar indicates the corresponding "SRV export score", derived as described in Methods section. (**C**) Heat map summarizing the results obtained with the 14 reporters (graphs for each reporter are provided in Supplementary Figure S2). The color indicates the SRV export score for each NES/variant combination, ranging from 0 (no export) to 100 (full export). (**D**) Graph showing the correlation between the previously reported CRM1 binding affinity (expressed as $Log_{10}(K_d)$) of each NES peptide [31] and the SRV export score of the corresponding reporter, when expressed alone. Pearson correlation coefficient and *p* value are indicated.

$SRV_{B/A}$ reporters containing each of these 14 NES motifs were either transfected alone or co-transfected with YFP-CRM1-encoding plasmids into HEK293T cells. Besides the five mutants indicated above, wild-type YFP-CRM1 and the previously studied A541K and 4X mutants were included in the analysis. All in all, 112 different combinations of SRV-NES reporter/CRM1 mutant (plus each reporter alone) were tested in these experiments. The percentage of cells where the reporter was located exclusively/mainly in the nucleus (N), the cytoplasm (C), or was similarly distributed between nucleus and cytoplasm (NC) was determined by counting at least 200 cells per sample (assessment method 2, detailed in Figure 1). As a representative example, the results obtained with the $SRV_{B/A}$ reporter containing X11L2 NES are shown in Figure 3B, and the graphs for all the NES reporters are presented in Supplementary Figure S2. From these semi-quantitative data, a nuclear export score (hereafter referred to "SRV export score"), ranging between 0 (no export) and 100 (complete export) was derived, as detailed in the Methods section. The SRV scores for the full set of experiments are represented as a heat map in Figure 3C.

When expressed alone, the SRV export score was lower than 10 (corresponding to mainly nuclear localization) for all the reporters except those containing PKI, superPKI and CPEB4 NES motifs. Co-expression with wild-type YFP-CRM1 readily induced nuclear export of all the reporters, with the exception of SRV-CDC7. Simultaneous mutations in the four hydrophobic residues (4X) fully abrogated YFP-CRM1-induced export of all NESs, while individual mutations of these amino acids had less dramatic consequences, as expected. Interestingly, the different single-residue mutations decreased export to a different extent, with I521A and L525A with the mildest effect, and F572A being consistently the most detrimental. These findings suggest that the degree of contribution of these residues to NES export could be expressed as I521 = L525 < F561A < F572A, irrespective of NES class. Of note, the effect of the K568A mutation was remarkably similar to the effect of F572A, even if these CRM1 residues engage in different types of chemical interaction with the NES. Finally, the A541K mutation severely reduced export of most reporters, but had a minor effect on SRV-X11L2, the only reporter containing a class 4 motif.

A recent analysis, which included the set of NES motifs tested here, showed that the affinity of NESs for CRM1 linearly correlates with their nuclear export activity, for those NESs with a dissociation constant (K_d) ranging between tens of nanomolar and tens of micromolar [31]. To further investigate the relationship between CRM1 binding affinity and export activity, we plotted the previously determined K_d values [31] against the SRV export score of the different reporters expressed alone (Figure 3D). In line with the previous report, a clear correlation ($R = -0.9225$; $p < 0.0001$) was found between both parameters. Of note, we found that the reporter containing the high affinity superPKI NES motif (K_d = 4 nM) exhibits higher export activity than the reporters containing NES motifs with lower affinity. This observation is in marked contrast with the reduced nuclear export activity of the superPKI NES previously reported [31]. This discrepancy is most likely due to the different experimental settings used to evaluate export activity in both studies.

2.3. Using the $SRV_{B/A}$ Assay to Gain Further Insight into CRM1-Mediated NES Export. (ii) Comparing the Effect of E571 and K568 Mutations

A particularly intriguing and clinically relevant aspect of CRM1-mediated NES export is the role of two adjacent, electrostatically interacting residues, namely E571 and K568 (Figure 4A). E571 mutations subtly alter nuclear export of certain NESs [19], and confer oncogenic potential to CRM1 [20]. K568 mutations (K568A or K568M), on the other hand, were shown to allow in vitro binding of some "inactive NES" motifs to CRM1 by disrupting a "selectivity filter" imposed by this residue that prevents docking of structurally inadequate NES-resembling peptides [11]. The relevance of this "selectivity filter" for nuclear export in a cellular setting, and the possibility that it is abrogated by cancer-related mutations in E571 remained to be investigated. Thus, we used the $SRV_{B/A}$ assay to directly compare how the E571K and K568A mutations affect nuclear export of: (i) three "inactive NES"

motifs previously characterized (COMMD1, Hxk2 and DEAF1) [11] and (ii) a subset of NES motifs from the "XPO1/CRM1-cancer exportome" proteins described above.

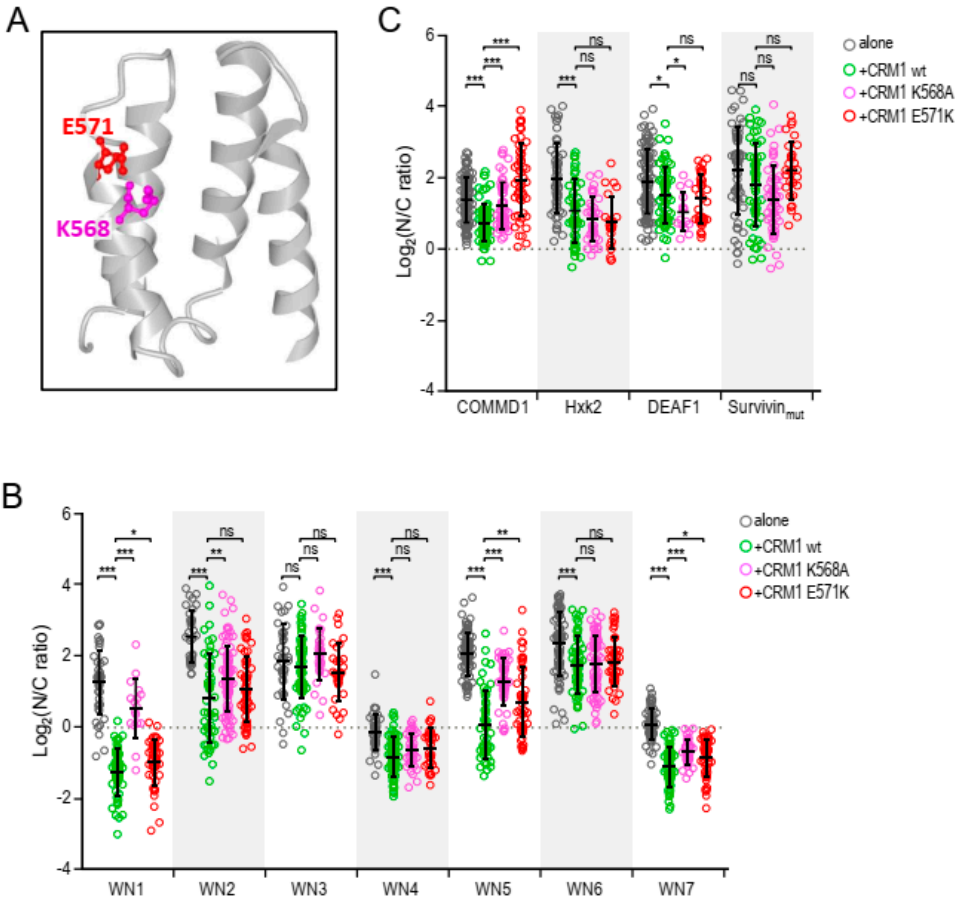

Figure 4. Using the $SRV_{B/A}$ assay to compare the effect of E571 and K568 mutations (**A**) View of CRM1 NES-binding groove generated with NCBI iCn3D viewer using PDB structure 3GJX [15]. The E571 and K568 residues are highlighted using ball and stick representation, while the remaining residues are represented using ribbon style. (**B**) Graph representing the nucleocytoplasmic localization of three $SRV_{B/A}$ reporters containing "inactive" NES motifs (COMMD1, Hxk2 and DEAF1) [11], plus an export defective mutant of survivin NES ($Survivin_{mut}$), when expressed alone or when co-expressed with YFP-CRM1 (wild-type, K568A or E571K). (**C**) Graph representing the nucleocytoplasmic localization of seven $SRV_{B/A}$ reporters containing NES motifs identified in cancer-related proteins (WN1-7) when expressed alone or when co-expressed with YFP-CRM1 (wild-type, K568A or E571K). In the graphs shown in panels (**B**) and (**C**), each circle represents a single cell where the nuclear to cytoplasmic (N/C) ratio of the fluorescent signal corresponding to the reporter was determined by image analysis using Fiji. The mean (+/− SD) is also shown. The level of statistical significance of the differences between the compared samples (Mann-Whitney U test) is indicated by the asterisks as follows: (*) $p < 0.05$; (**) $p < 0.01$; (***) $p > 0.001$; ns, non-significant.

On one hand, SRV reporters containing COMMD1, Hxk2 and DEAF1 motifs were either expressed alone or co-expressed with YFP-CRM1 (wild-type, K568A or E571K) in HEK293T cells. A fourth reporter, containing an export-deficient version of survivin NES mutated in two critical hydrophobic residues [19] was also included for comparison in these assays. After anti-Flag immunofluorescence, we used image analysis to quantify the intensity of the fluorescent signal of the reporters in the nucleus and the cytoplasm, and then calculated the nuclear to cytoplasmic (N/C) ratio (assessment method 3, detailed in Figure 1). As shown in Figure 4B, the localization of the four reporters was mainly nuclear (log_2(N/C ratio)> 0) under all conditions. A minor, but statistically significant reduction in NC ratio

was noted for SRV-COMMD1, SRV-Hxk2 and SRV-DEAF1 upon co-expression with wild-type CRM1, suggesting that these motifs may be NESs with extremely low activity. In comparison to the wild-type receptor, co-expression with the K568A mutant reduced export of the SRV-COMMD1 reporter, but slightly increased nuclear export of SRV-Hxk2 and SRV-DEAF1, although only the results with the later reporter reached statistical significance. These results are generally consistent with those of previous in vitro analyses that found increased binding of Hxk2 and DEAF1, but not COMMD1 motifs, to K568A mutant CRM1 [11]. In the case of the E571K mutant, the only statistically significant effect was a reduction in the nuclear export of the SRV-COMMD1 reporter.

On the other hand, we carried out a similar analysis with a set of SRV reporters containing seven different NES motifs (WN1-WN7) identified in cancer-related proteins (Figure 4C). Consistent with the data presented in Figure 2D, the localization of all the reporters, except SRV-WN3, was significantly more cytoplasmic when co-expressed with wild-type YFP-CRM1 than when expressed alone. In comparison to the wild-type receptor, co-expression with the K568A or E571K mutants significantly reduced the export of three reporters (SRV-WN1, SRV-WN5 and SRV-WN7). As detailed in Supplementary Table S2, WN1, WN5 and WN7 motifs are three previously validated NESs in MAP kinase kinase 2 (MP2K2) [25], cancer susceptibility candidate gene 3 protein (CASC3) [27] and period circadian protein homolog 1 (PER1) [28], respectively. Further studies should investigate whether these proteins are aberrantly exported in E571K-mutant cells. Importantly, E571K mutation consistently led to a considerably less pronounced reduction in the nuclear export of these three reporters than K568A. Furthermore, K568A decreased nuclear export of a fourth reporter (SRV-WN2), which was efficiently exported by E571K. In summary, these results clearly indicate that the E571K mutation has a subtler effect on the nuclear export activity of CRM1 than K568A.

2.4. Using the $SRV_{B/A}$ Assay to Search for NES-Harboring Micropeptides

With the progressive improvements in proteogenomics analyses, it has become apparent that the size and complexity of the cellular proteome may have been previously underestimated. Thus, there is growing evidence that a subset of RNA molecules initially annotated as non-coding may, in fact, contain short open reading frames that are translated into micropeptides, small proteins shorter than 100 amino acids in length [32]. Thousands of different micropeptides may be expressed in a cell, but there is still very little information on their biological function [21]. An important aspect of micropeptide biology that remains to be investigated is their nucleocytoplasmic localization. Given their small size, it is possible that many micropeptides can enter and exit the nucleus by passively diffusing through the nuclear pore. However, it is also possible that some micropeptides undergo active transport between the nucleus and the cytoplasm, and possess NLSs and/or NESs to interact with the nucleocytoplasmic transport machinery. To begin addressing this possibility, we decided to use the $SRV_{B/A}$ assay to carry out a search for functional NESs in human micropeptides.

Human micropeptides were retrieved from the SmProt database, a manually curated repository of small proteins detected or predicted in eight different species [33]. In silico prediction of putative NES motifs in the amino acid sequences of micropeptides was carried out with Wregex and NESmapper, as described above (no attempt to predict "minus" NES motifs was made in this case). Ten of the highest-ranking candidates (Supplementary Table S3) were selected and seven were successfully cloned into the $SRV_{B/A}$ reporter for experimental testing (two representative examples are shown in Figure 5A). When expressed alone into HEK293T cells, the localization of all the reporters (determined using assessment method 1) was exclusively nuclear (N), except for SRV-MICROP-2 that showed also a faint cytoplasmic signal (N > C localization) (Figure 5B). When co-expressed with YFP-CRM1, SRV-MICROP-5 and SRV-MICROP-7 reporters fully relocated to the cytoplasm (C localization), SRV-MICROP-1 and SRV-MICROP-10 showed a minor relocation to the cytoplasm (N > C localization) and SRV-MICROP-6 and SRV-MICROP-9 remained in the nucleus. Unexpectedly, the partial cytoplasmic localization of SRV-MICROP-2 was not increased by co-expression with YFP-CRM1, suggesting that this motif may mediate CRM1-independent export or retention in the cytoplasm, rather than

CRM1-mediated nuclear export. These findings identify at least two clearly active NES motifs (MICROP-5 and MICROP-7) in human micropeptides. To further confirm that these motifs are exported via CRM1, HEK293T cells co-expressing SRV-MICROP-5 or SRV-MICROP-7 with YFP-CRM1 were treated with the CRM1 inhibitor Leptomycin B (LMB). Blockade of CRM1-mediated export readily prevented cytoplasmic relocation of SRV-MICROP-7 (Figure 5C) and SRV-MICROP-5 (Supplementary Figure S3) reporters. To our knowledge, these sequences (Figure 5D) represent the first two functional CRM1-dependent NESs identified in human micropeptides.

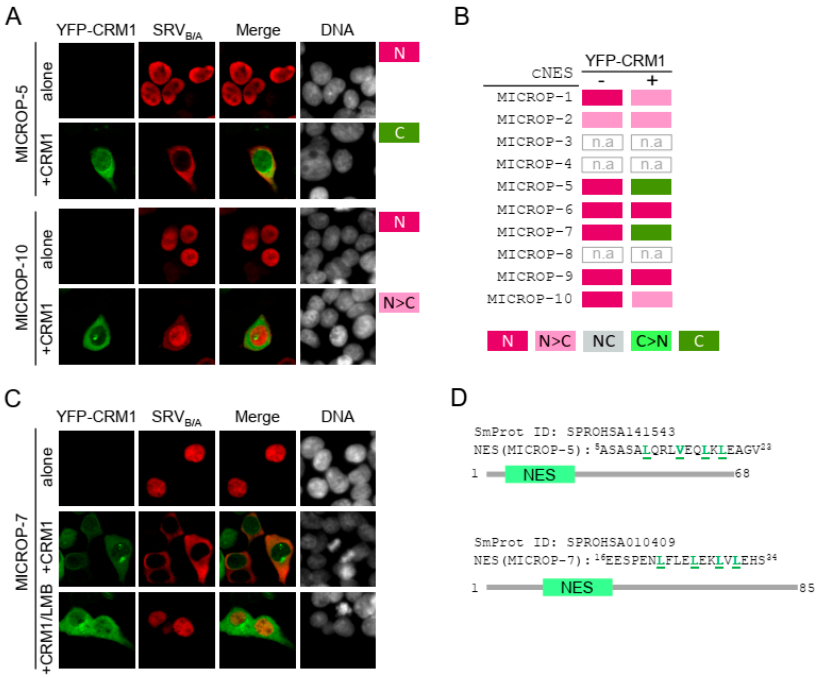

Figure 5. Using the SRV$_{B/A}$ assay to search for NES-harboring micropeptides. (**A**) Fluorescence microscopy images showing representative examples of the localization of SRV$_{B/A}$ reporters containing two different cNES motifs (MICROP-5 and MICROP-10, see Supplementary Table S3), when transfected alone or co-transfected with YFP-CRM1 wild-type (+CRM1) into HEK293T cells. The DNA-staining dye DAPI was used to visualize the nuclei. As indicated to the right of the images, using assessment method 1 the localization of SRV-MICROP-5 was classified as N (alone) and C (+CRM1), while the localization of SRV-MICROP-10 reporter was classified as N (alone) and N > C (+CRM1). (**B**) Summary of the localization of SRV$_{B/A}$ reporters containing candidate NES motifs. The cNES ID (Supplementary Table S3) for each motif are indicated to the left. The localization of each reporter expressed alone (−) or co-expressed with YFP-CRM1 wild-type (+) was assessed using method 1. Except SRV-MICROP-2, which showed a faint cytoplasmic signal (N > C localization), all reporters showed exclusively nuclear (N) localization when expressed alone. When co-expressed with YFP-CRM1, the localization of SRV-MICROP-2, SRV-MICROP-6 and SRV-MICROP-9 reporters remained invariable, SRV-MICROP-1 and SRV-MICROP-10 partially relocated to the cytoplasm and SRV-MICROP-5 and SRV-MICROP-7 fully relocated to the cytoplasm. n.a.: not assayed. (**C**) Fluorescence microscopy images showing that LMB treatment blocks the cytoplasmic relocation of SRV-MICROP-7 induced by co-expression with YFP-CRM1. (**D**). Schematic representation of human micropeptides SPROHSA141543 and SPROHSA010409 (SmProt IDs), showing the position of the novel NESs identified. The amino acid sequence of the NES motifs is indicated, with the hydrophobic residues that conform to the NES consensus highlighted in green.

3. Discussion

Our understanding of CRM1-mediated NES export derives largely from evidence obtained using structural and in vitro biochemical analyses with purified proteins [11,15–17,34–38]. These two

approaches are often combined, for example when using biochemical assays to validate predictions made from structural data [11,16,34,35]. On the other hand, cellular assays, based on the localization of reporter proteins, have been widely used to identify novel NESs or transport factors, and to test the effect of potential CRM1 inhibitors [22,39,40], but they are not routinely used to test assumptions made from structural and in vitro data. In fact, a possible correlation between the affinity of NESs for CRM1 and their export activity has only recently been evaluated [31]. To obtain a more integrative view it is important to determine how the structural and biochemical information on CRM1/NES interaction translates into NES export in the more physiological, albeit complex, cellular context.

We have recently described the $SRV_{B/A}$, reporter [20], a modification of the original SRV100 reporter [19] that allows evaluating how a variety of NES motifs are exported by different CRM1 variants. Here, we show how cellular assays with the $SRV_{B/A}$ reporter can be used not only to identify novel NES motifs, but also to provide relevant information on several aspects of CRM1-mediated NES export.

All in all, we have tested 60 different (validated or candidate) NES motifs and 9 different CRM1 variants in this study. Although not every NES motif was tested for export by every CRM1 variant, our study represents, to our knowledge, the largest set of NES/CRM1 variant combinations evaluated so far. In such an extensive study, the assessment of reporter localization in a large number of samples represents a major bottleneck, unless an automated analysis platform is used. However, these sophisticated and expensive systems are not readily available to many research groups, including ours. To facilitate manual sample analysis, we decided to use three assessment methods (Figure 1C) that are increasingly time-consuming, but provide a correspondingly more detailed description of reporter localization. Thus, we reasoned that a rapid qualitative assessment of general reporter localization could be sufficient to identify functional NES motifs, but more laborious semi-quantitative methods would be required to compare the activity of the different CRM1 variants.

By combining in silico prediction with nuclear export assays, we report the identification of 19 novel sequence motifs with nuclear export activity in 14 proteins (SPN90, TFE3, SHIP2, PER1, SEPT6, SIR2, UBR5, FR1OP, AP2B1, IF2B, mTOR, CRTC1, CDC27 and ZO2, see Supplementary Figure S1) that belong to a putative "XPO1/CRM1-cancer exportome". Of note, this is the first attempt to specifically search not only for "classical" ("plus") NES motifs, but also for "reverse" ("minus") motifs. The percentage of in silico predicted motifs that could be experimentally confirmed was similar for both types of NES, but "plus" motifs displayed, on average, higher export activity than "minus" motifs (Supplementary Figure S1C). Thus, although the number of "minus" NESs tested so far is limited, our data suggest that these motifs are, in general, weaker than "plus" motifs.

The role of each of the identified motifs as *bona-fide* NESs needs to be validated, as some of these sequences might not be accessible for CRM1 binding in the context of their cognate full-length proteins. Nevertheless, our findings further support previous results suggesting that these proteins are CRM1 cargos [6], and provide leads for further analyses of the nucleocytoplasmic localization of these important cancer-related proteins. A particularly noteworthy case is the SHIP2 protein, where two overlapping putative NES motifs were predicted, one as "plus" (WN6: 256- TGEQELESLVLKLSVLKDF-274) and the other as "minus" (REV5: 261-LESLVLKLSVLKDFLSGIQ-279). Both motifs displayed similar export activity in our assays. It would be interesting to apply structural analysis to establish in which orientation the SHIP2 peptide 256-279 may dock into CRM1 groove.

Testing candidate NESs in cancer-related proteins allowed us to compare the $SRV_{B/A}$ reporter with the widely used Rev(1.4)-GFP reporter [22]. We found that when using a rapid qualitative method to assess the localization of $SRV_{B/A}$ reporters, the results obtained with both assays are well correlated. These results validate the use of the $SRV_{B/A}$ reporter as a tool to identify novel NESs. However, it must be taken into account that while the $SRV_{B/A}$ assay allowed to better pinpoint differences in activity between some of the strongest NES motifs, it may miss some of the weakest NES motifs detected by the Rev(1.4)-GFP assay.

Unlike other commonly used cellular reporters, $SRV_{B/A}$, was applied to evaluate how different variants of CRM1 mediate export of a given NES [20]. Here, we have used $SRV_{B/A}$-based cellular assays to test different NESs and different CRM1 variants in multiple NES/variant combinations, in an attempt to extend and complement previous observations from structural and biochemical studies.

We investigated, on one hand, how mutations in individual CRM1 groove residues affect export of a panel of well-characterized NESs motifs that belong to different classes. These NESs have variable patterns of hydrophobic residues, and structural studies have shown that they dock into the groove with different backbone conformations, varying from all helix to an almost fully extended conformation [11,12,15–17]. We did not observe a consistent relationship between NES class and how export of these motifs is affected by the different groove mutations. However, we noted that irrespective of NES class, mutation of CRM1 residues located in the narrower part of the groove (A541, K568 and F572) consistently had a more detrimental effect on export than mutation of residues located in the wider part (I521, L525 and F561). Remarkably, mutations in K568 and F572, two residues that engage in chemically different types of interactions with the NES (main chain hydrogen bonding in the case of K568, and side chain hydrophobic interactions in the case of F572) [11,34] reduced NES export to a similar extent. These observations suggest that interaction of the NES motif with the narrower part of CRM1 groove may be particularly relevant for efficient NES export.

Our data also allowed us to confirm the recent report that affinity for CRM1 binding (measured in vitro) and export activity (evaluated using a cellular assay) are linearly correlated for NES motifs across a wide range of K_d values [31]. In fact, our observations extend these previous findings, and suggest that such a correlation is maintained even for motifs with a K_d below 10 nM. There was, nevertheless, a remarkable discrepancy between some of our findings and those in the previous report. We found that the SRV-superPKI reporter, containing an artificial NES motif with extremely high affinity for CRM1, was located in the cytoplasm when expressed alone in HEK293T cells. In contrast, the superPKI NES motif failed to promote efficient nuclear export of the reporter used in [31] (a chimeric protein with two tandem copies of YFP and one single copy of the SV40 NLS) in HeLa cells. The different configuration of the reporters, and potential differences in the endogenous nucleocytoplasmic transport machinery of the cell lines used probably contribute to these conflicting observations, which highlights the importance of considering the influence of the experimental setting when using cellular assays to evaluate NES export activity.

On the other hand, we investigated the effect of mutations in two particularly relevant CRM1 residues, one of them (E571) recurrently mutated in human cancer, and the other (K568) reported to play a crucial role preventing docking of "inactive NES" motifs into the CRM1 groove. These residues are located in close proximity, and establish an electrostatic interaction with each other that could be abrogated by cancer-related mutations in E571. Given the close relationship between E571 and K568, we decided to directly compare the effect of mutations affecting these two residues.

We first tested CRM1 mutants K568A and E571K against three $SRV_{B/A}$ reporters containing NES motifs previously characterized, and classified as inactive. In line with previous in vitro evidence showing that K568 functions as a "selectivity filter" for non-NES peptides [11], we found that two reporters containing "inactive NESs" (SRV-Hxk2 and SRV-DEAF1) were slightly better exported by a CRM1 variant carrying a K568A mutation than by the wild-type receptor. The cancer-related E571K mutation, on the other hand, does not appear to abrogate this filtering effect, as it did not lead to augmented export of any of the reporters. Importantly, the minor increment in nuclear export of the SRV-Hxk2 and SRV-DEAF1 reporters afforded by the K568A mutation in our cellular assays does not reflect the markedly increased in vitro binding of this mutant to the Hxk2 and DEAF1 peptides reported previously [11]. In this regard, it must be noted that besides abrogating the "selectivity filter", the K568A mutation reduces binding of CRM1 to "true" NES peptides [11], and negatively impacts nuclear export activity (see our results above). These somewhat opposing effects represent a confounding factor that needs to be considered when interpreting the results of experiments with this particular CRM1 variant. Thus, while our findings are consistent with the previously described role

of K568 as a "selectivity filter", we believe that further studies are needed to better establish to what extent this residue contributes to select for "true" NES motifs.

We also compared the effect of E571K and K568A mutations against a set of $SRV_{B/A}$ reporters containing functional NES motifs identified in cancer-related proteins. While both mutations significantly reduced the export of several of these reporters, our results clearly show that the detrimental effect of the E571K mutation is consistently less pronounced than the effect of K568A. This subtler effect on nuclear export, and our finding that E571K does not abrogate the "selectivity filter" imposed by K568, indicates that the biological consequences of E571 and K568 mutations are different. This is consistent with the fact that while E571 mutations are highly prevalent in certain types of hematological malignancy (reviewed in [13]), naturally occurring K568 mutations have never been detected in human samples. We speculate that the subtle nature of the effects of E571K may be crucial for it oncogenic role, as mutations that more grossly disrupt CRM1-mediated export would probably be incompatible with cell survival.

Finally, after validating the use of the $SRV_{B/A}$ assay for NES identification on the "XPO1/CRM1-cancer exportome" protein group, we used it to search for functional NES motifs within the recently uncovered "micropeptidome", a potentially vast and still largely unexplored group of small proteins shorter than 100 amino acids in length [21,32]. Although very few micropeptides have been characterized thus far, some of them have been shown to play a role in nuclear processes, such as DNA repair [41] and splicing [42], suggesting that the nucleocytoplasmic distribution of some small proteins may need to be actively regulated. Thus, our aim was to test the hypothesis that some micropeptides could represent novel CRM1 cargos. Indeed, we report here the identification of two human micropeptides (SmProt database ID SPROHSA141543 and SPROHSA010409) bearing CRM1-dependent NESs. Unlike longer proteins, where these motifs could be buried into their hydrophobic cores [8], short micropeptides (in this case, 68 and 85 amino acid long, respectively) provide a context where the identified NESs are more likely to be accessible for CRM1 binding, and thus physiologically relevant. The potential role, if any, of SPROHSA141543 and SPROHSA010409 is a mystery, as it is for the vast majority of micropeptides. It must be noted that the mere presence of these small proteins does not necessarily imply that all of them have a specific functional role. Nevertheless, our results provide the first proof-of-concept evidence, to our knowledge, that the micropeptidome can be a yet-to-be explored source of novel CRM1 cargos. Intriguingly, CRM1-binding NES motifs could also be present in some of the smallest micropeptides (15–25 amino acids in length), which raises the possibility that these micropeptides might act as "decoy NESs", contributing to regulate CRM1-mediated nuclear export. Experiments to test this possibility are currently underway.

4. Materials and Methods

4.1. In Silico NES Prediction

We described a putative "XPO1/CRM1-cancer exportome" [13] as a set of 136 cancer-related proteins (Supplementary Table S1) that are potentially exported by CRM1, according to a global proteomics analysis [6]. In their report [6], Kirli et al., classified potential CRM1 cargos as "cargo A", "cargo B" or "low abundant cargo". Here, we focused our analysis on those potential cargos (112 proteins) that were classified as either CRM1 cargo A or cargo B in [6]. The amino acid sequence of these proteins was analyzed using two different bioinformatics tools: Wregex [23] with the recommended configuration and NESmapper [24] with a minscore of 0 and trained profile. It was reported that some NES motifs (so called "minus" motifs) can bind CRM1 in an opposite orientation to that of most previously described motifs (hereafter referred to as "plus" motifs) [12]. To predict potential "minus" motifs, the amino acid sequence of each protein was reversed before being entered as input for the analysis. In silico predicted NES motifs were ranked according to the score provided by Wregex and NESmapper. Rank 1 motifs were defined as those included in the first quartile of both programs. Rank 2 motifs were defined as those included in the first quartile of one of the programs and the second

quartile of the other. This ranking was the criterion used to select those predicted candidate NES (cNES) motifs to be experimentally tested. Micropeptide sequences, on the other hand, were obtained from the high confidence set of the SmProt small protein database [33] and analyzed using Wregex and NESmapper. A set of 10 candidates in the first quartile of both programs was selected for experimental testing. The analysis was limited to the prediction of "plus" motifs.

4.2. Plasmids, Cloning Procedures, and Site-Directed Mutagenesis

The plasmid encoding the Rev(1.4)-GFP reporter [22] was a gift from Dr. Beric Henderson (University of Sydney, Australia). The plasmid encoding the $SRV_{B/A}$ reporter was recently described [20]. This plasmid, derived from SRV100 [19], allows cloning of desired cNES motifs as BamHI/AgeI fragments. These cloning sites and the reading frame in $SRV_{B/A}$ allow easily shuttling cNES-coding DNA sequences to and from the Rev(1.4)-GFP plasmid. DNA sequences encoding cNES motifs were purchased as gBlocks (IDT, Coralville, IA, USA), digested with BamHI and AgeI and cloned into Rev(1.4)-GFP and $SRV_{B/A}$ plasmids.

The plasmids encoding YFP-CRM1 wild-type, and several mutants used in this study (4X, F572A, E571K and A541K) were previously described [19,43]. The remaining CRM1 mutants (I521A, L525A, F561A and K568A) were generated by site-directed mutagenesis using the Quick-Change Lightning Site-Directed Mutagenesis Kit (Agilent Technologies, Santa Clara, CA, USA) according to the manufacturer's instructions.

All the new constructs were subjected to DNA sequencing (StabVida, Caparica, Portugal) and the absence of any unwanted mutation was confirmed.

4.3. Cell Culture, Plasmid Transfection and LMB Treatment

HeLa and human embryonic kidney 293T (HEK293T) cells (both cell lines were obtained from ECACC, Salisbury, UK) were grown in Dulbecco's modified Eagle's medium (DMEM) supplemented with 10% fetal bovine serum (FBS), 100 U/mL penicillin and 100 µg/mL streptomycin (all from Gibco (ThermoFisher Scientific), Waltham, MA, USA) at 37 °C in a humidified atmosphere containing 5% CO_2. 24 h before transfection, cells were seeded in 12-well plates with glass coverslips. Plasmid transfections were carried out using X-tremeGENE 9 DNA transfection reagent (Roche Diagnostics, Basel, Switzerland) following manufacturer's instructions. The CRM1 inhibitor Leptomycin B (Apollo Scientific, Bredbury, Stockport, UK) was used at a final concentration of 30 ng/mL for 3 h.

4.4. Rev(1.4)-GFP and $SRV_{B/A}$ Nuclear Export Assays

The Rev(1.4)-GFP nuclear export assay was carried out as previously described [22]. Briefly, Rev(1.4)-GFP plasmids with the different cNES motifs were transfected into HeLa cells. The empty Rev(1.4)-GFP plasmid was used as negative control. Each plasmid was transfected in two wells. 24 h after transfection, 10 µg/mL cycloheximide and 5 µg/mL actinomycin D (both drugs from Sigma-Aldrich, Saint Louis, Missouri, USA) were added to one of the wells. Only cycloheximide was added to the second well. As detailed in the original report [22], cycloheximide is added to ensure that the fluorescent signal in the cytoplasm corresponds to exported and not to newly synthesized GFP-tagged proteins, while actinomycin D facilitates detection of weaker NESs. After 3 h of treatment, cells were fixed with 3.7% formaldehyde (Sigma-Aldrich) in phosphate-buffered saline (PBS) for 30 min, washed with PBS, and directly mounted onto microscope slides using Vectashield mounting medium containing DAPI (Vector Laboratories, Burlingame, CA, USA). Samples were analyzed using a Zeiss Axioskop fluorescence microscope. To ensure unbiased assessment, the identity of the samples was masked before the analysis. At least 200 transfected cells per sample were examined to establish the proportion of cells where the reporter shows nuclear (N), nuclear and cytoplasmic (NC) or cytoplasmic (C) localization. Based on this proportion, each of the tested motifs was assigned a nuclear export activity score between 0 (no export activity, inactive motif) and 9 (maximal export activity) using the assay scoring system [22].

The $SRV_{B/A}$ assay was carried out in HEK293T cells. Plasmids encoding $SRV_{B/A}$ reporters with the different cNES motifs were transfected alone or co-transfected with the indicated YFP-CRM1 plasmids. 24 h after transfection, cells were fixed with 3.7% formaldehyde (Sigma-Aldrich) in phosphate-buffered saline (PBS) for 30 min, permeabilized with 0.2% Triton X-100 (Sigma-Aldrich) in PBS for 10 min, and blocked in 3% bovine serum albumin (BSA; Millipore, Burlington, MA, USA) in PBS for 1 h. Cells were incubated with anti-Flag M2 mouse monoclonal antibody (Sigma-Aldrich) diluted 1:400 in blocking solution for 1 h to detect $SRV_{B/A}$ reporters. After washing with PBS, cells were incubated with Alexa Fluor 594-conjugated anti-mouse secondary antibody (Invitrogen (ThermoFisher Scientific)) diluted 1:400 for 1 h. Finally, samples were washed and mounted onto microscope slides using Vectashield mounting medium containing DAPI (Vector Laboratories).

Samples were examined using either Zeiss Axioskop or Zeiss Apotome2 fluorescence microscopes, and the results of the assays were assessed using three different methods, illustrated in Figure 1C. Irrespective of the assessment method used, samples were coded before the analysis to avoid potential bias and, although we did not carry out a detailed quantification of YFP fluorescence, we confirmed that the level of expression of YFP-CRM1 plasmids was comparable among the different samples.

In method 1, samples were observed using a Zeiss Axioskop microscope and the overall localization of the reporter was classified as exclusively nuclear (N), mainly nuclear (N > C), equally nuclear and cytoplasmic (NC), mainly cytoplasmic (C > N) or exclusively cytoplasmic (C). A subset of the samples was independently analyzed by two of the authors (M.S and J.A.R), and the classification by the two observers was found to be highly concordant. In method 2, previously used with SRV100 [19], the localization of the reporter was determined in at least 200 individual transfected cells per sample using a Zeiss Axioskop microscope. Based on the percentage of cells with nuclear (N), nuclear and cytoplasmic (NC) or cytoplasmic (C) localization of the reporter, a nuclear export score (termed "SRV export score" and ranging between 0 and 100) was derived using the formula 0(%N) + 0.5(%NC) + 1(%C). The score values for the different reporter/CRM1 combinations tested were represented as a heatmap using the resources available at the Heatmapper web server (www.heatmapper.ca). In method 3, image analysis was used to quantify the intensity of the Alexa Fluor 594 fluorescent signal (corresponding to $SRV_{B/A}$ reporters) in the nucleus and the cytoplasm on an average of 50 individual cells per sample. To this end, optical sectioning images (channels with $SRV_{B/A}$ reporters and YFP-CRM1) or conventional fluorescence images (DAPI-stained nuclei) of 10–15 different areas in each sample were taken using a Zeiss Apotome2 microscope and Zen2.6 Blue edition software. Composite images were created using Fiji software [44], and analyzed using an ad-hoc script developed previously [45] to automatically quantify the fluorescence intensity in nuclear and cytoplasmic regions. Finally, the nuclear to cytoplasmic (N/C) ratios were calculated, plotted in logarithmic base 2, and samples were compared using the Mann-Whitney U test (GraphPad Prism software version 7, San Diego, CA, USA). Differences were considered statistically significant when $p < 0.05$.

4.5. Correlation Analyses

To statistically test their correlation with the results of Rev(1.4)-GFP assays, the qualitative localization data (N, N > C, NC, C > N or C) obtained using method 1 to assess $SRV_{B/A}$ assays were assigned numerical values. These values (N = 0, N > C = 1, NC = 2, C > N = 3 and C = 4) were plotted against the Rev(1.4)-GFP assay scores (values between 0 and 9), and the correlation between both sets of data was calculated using the Pearson correlation coefficient. The statistical analysis was performed using GraphPad Prism7 software.

For a subset of well-characterized NES motifs, we tested the correlation between their nuclear export activity in $SRV_{B/A}$ assays and their affinity for CRM1 in vitro. To this end, the SRV score value of each NES motif expressed alone (obtained using assessment method 2) was plotted against the previously reported K_d value of each CRM1/NES interaction [31] and the correlation between both sets of data was calculated as above.

Supplementary Materials: The following are available online at http://www.mdpi.com/1422-0067/21/17/6341/s1. Figure S1. Analysis of candidate NES (cNES) motifs in "XPO1-cancer exportome" proteins using the Rev(1.4)-GFP nuclear export assay. Figure S2. Raw data used to generate the heat map shown in Figure 3C. Figure S3. Nuclear export of MICROP-5 NES motif is blocked by LMB. Table S1. XPO1/CRM1-cancer exportome proteins classified according to "CRM1 cargo category" as reported by Kirli et al., 2015. Table S2. Selected candidate NES motifs in "XPO1/CRM1-cancer exportome" proteins predicted in silico and experimentally tested using the SRVB/A assay and/or the Rev(1.4)-GFP assay. Table S3. Selected in silico predicted candidate NES motifs in human micropeptides

Author Contributions: The authors have contributed to this work as follows: Conceptualization, J.A.R.; Methodology, all the authors contributed; Software, G.P.; Validation, J.A.R., M.J.O. and M.S.; Formal Analysis, M.S.; Investigation, J.A.R., M.J.O. and M.S.; Resources, J.A.R.; Data Curation, G.P. and M.S.; Writing—Original Draft Preparation, J.A.R and M.S.; Writing—Review & Editing, all the authors contributed; Visualization, J.A.R. and M.S.; Supervision, J.A.R.; Project Administration, J.A.R.; Funding Acquisition, J.A.R. All authors have read and agreed to the published version of the manuscript.

Funding: This work was supported by grants from the Spanish Government MINECO-FEDER (SAF2014-57743-R), the Basque Country Government (IT1257-19) and the University of the Basque Country (UFI11/20), as well as a fellowship from the Basque Country Government (to M.S.).

Acknowledgments: We are grateful to Beric Henderson for the generous gift of the Rev(1.4)-GFP plasmid. We appreciate the technical support by the staff from the High Resolution Microscopy Facility (SGIKER-UPV/EHU).

Conflicts of Interest: The authors declare no conflict of interests.

References

1. Pemberton, L.F.; Paschal, B.M. Mechanisms of receptor-mediated nuclear import and nuclear export. *Traffic* **2005**, *6*, 187–198. [CrossRef] [PubMed]
2. Tran, E.J.; King, M.C.; Corbett, A.H. Macromolecular transport between the nucleus and the cytoplasm: Advances in mechanism and emerging links to disease. *Biochim. Biophys. Acta (BBA)-Mol. Cell Res.* **2014**, *1843*, 2784–2795. [CrossRef] [PubMed]
3. Cautain, B.; Hill, R.; de Pedro, N.; Link, W. Components and regulation of nuclear transport processes. *FEBS J.* **2015**, *282*, 445–462. [CrossRef] [PubMed]
4. Soniat, M.; Chook, Y.M. Nuclear localization signals for four distinct karyopherin-β nuclear import systems. *Biochem. J.* **2015**, *468*, 353–362. [CrossRef] [PubMed]
5. Hutten, S.; Kehlenbach, R.H. CRM1-mediated nuclear export: To the pore and beyond. *Trends Cell Biol.* **2007**, *17*, 193–201. [CrossRef]
6. Kirli, K.; Karaca, S.; Dehne, H.J.; Samwer, M.; Pan, K.T.; Lenz, C.; Urlaub, H.; Görlich, D. A deep proteomics perspective on CRM1-mediated nuclear export and nucleocytoplasmic partitioning. *eLife* **2015**, *4*, e11466. [CrossRef]
7. Kutay, U.; Guttinger, S. Leucine-rich nuclear-export signals: Born to be weak. *Trends Cell Biol.* **2005**, *15*, 121–124. [CrossRef]
8. Xu, D.; Farmer, A.; Collett, G.; Grishin, N.V.; Chook, Y.M. Sequence and structural analyses of nuclear export signals in the NESdb database. *Mol. Biol. Cell* **2012**, *23*, 3677–3693. [CrossRef]
9. Fu, S.C.; Huang, H.C.; Horton, P.; Juan, H.F. ValidNESs: A database of validated leucine-rich nuclear export signals. *Nucleic Acids Res.* **2013**, *41*, D338–D343. [CrossRef]
10. Kosugi, S.; Hasebe, M.; Tomita, M.; Yanagawa, H. Nuclear export signal consensus sequences defined using a localization-based yeast selection system. *Traffic* **2008**, *9*, 2053–2062. [CrossRef]
11. Fung, H.Y.J.; Fu, S.C.; Chook, Y.M. Nuclear export receptor CRM1 recognizes diverse conformations in nuclear export signals. *eLife* **2017**, *6*, e23961. [CrossRef] [PubMed]
12. Fung, H.Y.J.; Fu, S.C.; Brautigam, C.A.; Chook, Y.M. Structural determinant of nuclear export signal orientation in binding to exportin CRM1. *eLife* **2015**, *4*, e10034. [CrossRef] [PubMed]
13. Sendino, M.; Omaetxebarria, M.J.; Rodríguez, J.A. Hitting a moving target: Inhibition of the nuclear export receptor XPO1/CRM1 as a therapeutic approach in cancer. *Cancer Drug Resist.* **2018**, *1*, 139–163. [CrossRef]
14. Syed, Y.Y. Selinexor: First global approval. *Drugs* **2019**, *79*, 1485–1494. [CrossRef] [PubMed]
15. Monecke, T.; Güttler, T.; Neumann, P.; Dickmanns, A.; Görlich, D.; Ficner, R. Crystal structure of the nuclear export receptor CRM1 in complex with snurportin1 and RanGTP. *Science* **2009**, *324*, 1087–1091. [CrossRef] [PubMed]

16. Dong, X.; Biswas, A.; Süel, K.E.; Jackson, L.K.; Martinez, R.; Gu, H.; Chook, Y.M. Structural basis for leucine-rich nuclear recognition by CRM1. *Nature* **2009**, *458*, 1136–1141. [CrossRef]
17. Güttler, T.; Madl, T.; Neumann, P.; Deichsel, D.; Corsini, L.; Monecke, T.; Ficner, R.; Sattler, M.; Görlich, D. NES consensus redefined by structures of PKI-type and Rev-type nuclear export signals bound to CRM1. *Nat. Struct. Mol. Biol.* **2010**, *17*, 1367–1377. [CrossRef]
18. Puente, X.S.; Pinyol, M.; Quesada, V.; Conde, L.; Ordóñez, G.R.; Villamor, N.; Escaramis, G.; Jares, P.; Beà, S.; González-Díaz, M.; et al. Whole-genome sequencing identifies recurrent mutations in chronic lymphocytic leukaemia. *Nature* **2011**, *475*, 101–105. [CrossRef]
19. García-Santisteban, I.; Arregi, I.; Alonso-Mariño, M.; Urbaneja, M.A.; García-Vallejo, J.J.; Bañuelos, S.; Rodríguez, J.A. A cellular reporter to evaluate CRM1 nuclear export activity: Functional analysis of the cancer-related mutant E571K. *Cell. Mol. Life Sci.* **2016**, *73*, 4685–4699. [CrossRef]
20. Taylor, J.; Sendino, M.; Gorelick, A.N.; Pastore, A.; Chang, M.T.; Penson, A.V.; Gavrila, E.I.; Stewart, C.; Melnik, E.M.; Herrejon Chavez, F.; et al. Altered nuclear export signal recognition as a driver of oncogenesis. *Cancer Discov.* **2019**, *9*, 1452–1467. [CrossRef]
21. Hartford, C.C.R.; Lal, A. When long noncoding becomes protein coding. *Mol. Cell Biol.* **2020**, *40*, e00528-19. [CrossRef] [PubMed]
22. Henderson, B.R.; Eleftheriou, A. A comparison of the activity, sequence specificity, and CRM1-dependence of difference nuclear export signals. *Exp. Cell Res.* **2000**, *256*, 213–224. [CrossRef] [PubMed]
23. Prieto, G.; Fullaondo, A.; Rodriguez, J.A. Prediction of nuclear export signals using weighted regular expressions (Wregex). *Bioinformatics* **2014**, *30*, 1220–1227. [CrossRef] [PubMed]
24. Kosugi, S.; Yanagawa, H.; Terauchi, R.; Tabata, S. NESmapper: Accurate prediction of leucine-rich nuclear export signals using activity-based profiles. *PLoS Comput. Biol.* **2014**, *10*, e1003841. [CrossRef]
25. Fukuda, M.; Gotoh, I.; Gotoh, Y.; Nishida, E. Cytoplasmic localization of MAP kinase kinase directed by its N-terminal, leucine-rich short amino acid sequence, which acts as a nuclear export signal. *J. Biol. Chem.* **1996**, *271*, 20024–20028. [CrossRef]
26. Toyoshima, F.; Moriguchi, T.; Wada, A.; Fukuda, M.; Nishida, E. Nuclear export of cyclin B1 and its possible role in the DNA damage-induced G2 checkpoint. *EMBO J.* **1998**, *17*, 2728–2735. [CrossRef]
27. Macchi, P.; Kroening, S.; Palacios, I.M.; Baldassa, S.; Grunewald, B.; Ambrosino, C.; Goetze, B.; Lupas, A.; St. Johnston, D.; Kiebler, M. Barentsz, a new component of the Staufen-containing ribonucleoprotein particles in mammalian cells, interacts with staufen in an RNA-dependent manner. *J. Neurosci.* **2003**, *23*, 5778–5788. [CrossRef]
28. Vielhaber, E.L.; Duricka, D.; Ullman, K.S.; Virshup, D.M. Nuclear export of mammalian PERIOD proteins. *J. Biol. Chem.* **2001**, *276*, 45921–45927. [CrossRef]
29. Bachmann, R.A.; Kim, J.H.; Wu, A.L.; Park, I.H.; Chen, J. A nuclear transport signal in mammalian target of rapamycin is critical for its cytoplasmic signalling to S6 kinase 1. *J. Biol. Chem.* **2006**, *281*, 7357–7363. [CrossRef]
30. North, B.J.; Verdin, E. Interphase nucleo-cytoplasmic shuttling and localization of SIRT2 during mitosis. *PLoS ONE* **2007**, *2*, e784. [CrossRef]
31. Fu, S.C.; Fung, H.Y.J.; Cağatay, T.; Baumhardt, J.; Chook, Y.M. Correlation of CRM1-NES affinity with nuclear export activity. *Mol. Biol. Cell* **2018**, *29*, 2037–2044. [CrossRef] [PubMed]
32. Yeasmin, F.; Yada, T.; Akimitsu, N. Micropeptides encoded in transcripts previously identified as long noncoding RNAs: A new chapter in transcriptomics and proteomics. *Front. Genet.* **2018**, *9*, 144. [CrossRef] [PubMed]
33. Hao, Y.; Zhang, L.; Niu, Y.; Cai, T.; Luo, J.; He, S.; Zhang, B.; Zhang, D.; Qin, Y.; Yang, F.; et al. SmProt: A Database of Small Proteins Encoded by Annotated Coding and Non-Coding RNA Loci. *Brief. Bioinform.* **2018**, *19*, 636–643. [CrossRef] [PubMed]
34. Dong, X.; Biswas, A.; Chook, Y.M. Structural basis for assembly and disassembly of the CRM1 nuclear export complex. *Nat. Struct. Mol. Biol.* **2009**, *16*, 558–560. [CrossRef]
35. Fox, A.M.; Ciziene, D.; McLaughlin, S.H.; Stewart, M. Electrostatic interactions involving the extreme C terminus of nuclear export factor CRM1 modulate its affinity for cargo. *J. Biol. Chem.* **2011**, *286*, 29325–29335. [CrossRef]

36. Dian, C.; Bernaudat, F.; Langer, K.; Oliva, M.F.; Fornerod, M.; Schoehn, G.; Müller, C.W.; Petosa, C. Structure of a truncation mutant of the nuclear export factor CRM1 provides insights into the auto-inhibitory role of its C-terminal helix. *Structure* **2013**, *21*, 1338–1348. [CrossRef]
37. Monecke, T.; Haselbach, D.; Vo, B.; Russek, A.; Neumann, P.; Thomson, E.; Hurt, E.; Zachariae, U.; Stark, H.; Grubmüller, H.; et al. Structural basis for cooperativity of CRM1 export complex formation. *Proc. Natl. Acad. Sci. USA* **2013**, *110*, 960–965. [CrossRef]
38. Saito, N.; Matsuura, Y. A 2.1-Å-resolution crystal structure of unliganded CRM1 reveals the mechanism of autoinhibition. *J. Mol. Biol.* **2013**, *425*, 350–364. [CrossRef]
39. Fetz, V.; Knauer, S.K.; Bier, C.; von Kries, J.P.; Stauber, R.H. Translocation biosensors—Cellular system integrators to dissect CRM1-dependent nuclear export by chemicogenomics. *Sensors* **2009**, *9*, 5423–5445. [CrossRef]
40. Kehlenbach, R.H.; Port, S.A. Analysis of CRM1-dependent nuclear export in permeabilized cells. *Methods Mol. Biol.* **2016**, *1411*, 489–501. [CrossRef]
41. Slavoff, S.A.; Heo, J.; Budnik, B.A.; Hanakahi, L.A.; Saghatelian, A. A human short open reading frame (sORF)-encoded polypeptide that stimulatesDNA end joining. *J. Biol. Chem.* **2014**, *289*, 10950–10957. [CrossRef] [PubMed]
42. Huang, J.-Z.; Chen, M.; Chen, D.; Gao, X.-C.; Zhu, S.; Huang, H.; Hu, M.; Zhu, H.; Yan, G.-R. A peptide encoded by a putative lncRNA HOXB-AS3 suppresses colon cancer growth. *Mol. Cell* **2017**, *68*, 171–184. [CrossRef] [PubMed]
43. Rodríguez, J.A.; Henderson, B.R. Identification of a functional nuclear export sequence in BRCA1. *J. Biol. Chem.* **2000**, *275*, 38589–38596. [CrossRef] [PubMed]
44. Schindelin, J.; Arganda-Carreras, I.; Frise, E.; Kaynig, V.; Longair, M.; Pietzsch, T.; Preibisch, S.; Rueden, C.; Saalfeld, S.; Schmid, B.; et al. Fiji: An open-source platform for biological-image analysis. *Nat. Methods* **2012**, *9*, 676–682. [CrossRef]
45. Olazabal-Herrero, A.; Sendino, M.; Arganda-Carreras, I.; Rodríguez, J.A. WDR20 regulates shuttling of the USP12 deubiquitinase complex between the plasma membrane, cytoplasm and nucleus. *Eur. J. Cell Biol.* **2019**, *98*, 12–26. [CrossRef]

Supplementary Figure 1

A

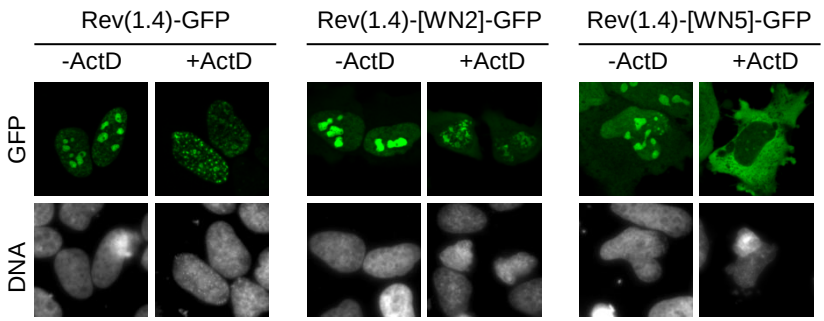

B

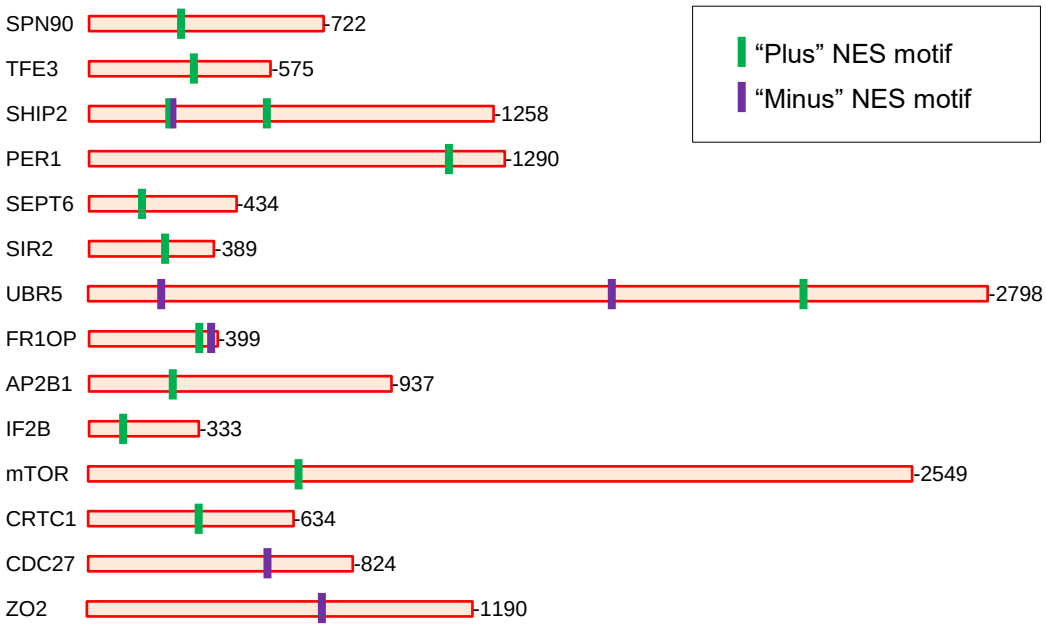

C

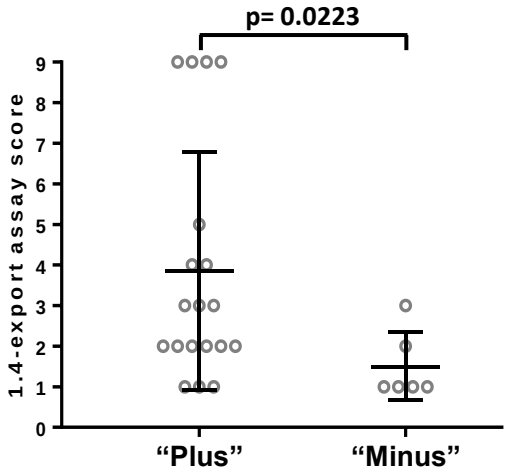

Supplementary Figure 1. Analysis of candidate NES (cNES) motifs in "XPO1-cancer exportome" proteins using the Rev(1.4)-GFP nuclear export assay.

A. Fluorescence microscopy images showing representative examples of the results of Rev(1.4)-GFP nuclear export assays in HeLa cells. The localization of the empty Rev(1.4)-GFP reporter (negative control) and reporters containing two different cNES motifs (WN2 and WN5) is shown. Cells were either treated (+ActD) or not (-ActD) with Actinomycin D. The DNA-staining dye DAPI was used to visualize the nuclei. The localization of the reporter in the nucleus (N), nucleus and cytoplasm (NC) or cytoplasm (C) was determined in at least 200 cells per sample. According to the percentage of cells showing each localization, the different cNESs were assigned a nuclear export score (1.4 score), as indicated in Supplementary Table 1. *B.* Schematic representation of 14 cancer-related proteins that are potential CRM1 cargos, showing the position of the 19 novel NES motifs. *C*. Graph comparing the nuclear export activity (1.4 score) of the active "plus" (n=19) and "minus" (n=6) NES motifs identified in this study. Each circle represents a single NES. The mean +/-SD is shown. The mean 1.4-score was 3.84 for "plus" motifs and 1.5 for "minus" motifs. The p value (Mann-Whitney U test) is indicated.

Supplementary Figure 2

Supplementary Figure 2. Raw data used to generate the heat map shown in Figure 3C.

Graphs show the results of 126 $SRV_{B/A}$ assays testing the export activity of the indicated YFP-CRM1 variants against a panel of 14 $SRV_{B/A}$ reporters, containing previously-characterized NES motifs. For each SRV-NES/CRM1 variant combination, the localization of the reporter to the nucleus (N), nucleus and cytoplasm (NC) or cytoplasm (C) was determined in at least 200 cells. Bar colours represent the percentage of cells showing the indicated reporter localization (N, NC or C). From this percentage, a “SRV export score” was derived, as described in Methods section, and represented in the heat map shown in Figure 3C. The NES motifs tested are shown grouped according to their class.

Supplementary Figure 3

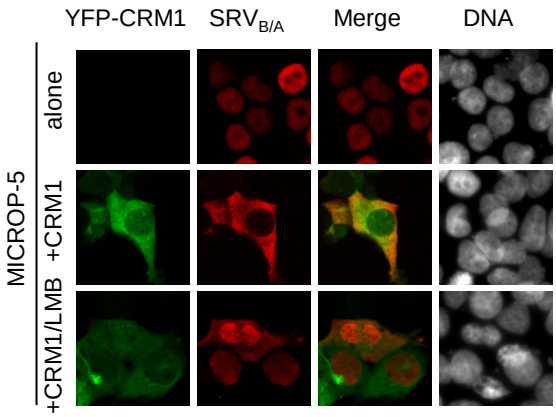

Supplementary Figure 3. Nuclear export of MICROP-5 NES motif is blocked by LMB.

Fluorescence microscopy images of HEK293T cells showing the localization of SRV-MICROP-5 reporter when transfected alone or co-transfected with YFP-CRM1 and left untreated (+CRM1) or treated with LMB (+CRM1/+LMB). LMB treatment largely prevents the cytoplasmic relocation of SRV-MICROP-5 induced by co-expression with YFP-CRM1. The DNA-staining dye DAPI was used to visualize the nuclei.

Supplementary Table 1: XPO1/CRM1-cancer exportome proteins classified according to "CRM1 cargo category" as reported by Kirli et al., 2015.

Uniprot ID	Cargo category (Kirli et al., 2015)
>sp|Q96IF1|AJUBA_HUMAN	Cargo A
>sp|P63010|AP2B1_HUMAN	Cargo A
>sp|O14965|AURKA_HUMAN	Cargo A
>sp|O95999|BCL10_HUMAN	Cargo A
>sp|P11274|BCR_HUMAN	Cargo A
>sp|O60566|BUB1B_HUMAN	Cargo A
>sp|P22681|CBL_HUMAN	Cargo A
>sp|Q16204|CCDC6_HUMAN	Cargo A
>sp|P14635|CCNB1_HUMAN	Cargo A
>sp|Q12834|CDC20_HUMAN	Cargo A
>sp|P30260|CDC27_HUMAN	Cargo A
>sp|Q6P1J9|CDC73_HUMAN	Cargo A
>sp|O75175|CNOT3_HUMAN	Cargo A
>sp|Q6UUV9|CRTC1_HUMAN	Cargo A
>sp|Q6UUV7|CRTC3_HUMAN	Cargo A
>sp|O75534|CSDE1_HUMAN	Cargo A
>sp|P49674|KC1E_HUMAN	Cargo A
>sp|P67870|CSK2B_HUMAN	Cargo A
>sp|O60716|CTND1_HUMAN	Cargo A
>sp|P17844|DDX5_HUMAN	Cargo A
>sp|P26196|DDX6_HUMAN	Cargo A
>sp|Q9NSV4|DIAP3_HUMAN	Cargo A
>sp|P11532|DMD_HUMAN	Cargo A
>sp|Q92997|DVL3_HUMAN	Cargo A
>sp|P20042|IF2B_HUMAN	Cargo A
>sp|P60228|EIF3E_HUMAN	Cargo A
>sp|O15372|EIF3H_HUMAN	Cargo A
>sp|P42566|EPS15_HUMAN	Cargo A
>sp|O95684|FR1OP_HUMAN / >sp|O95684|CEP43_HUMAN	Cargo A
>sp|P62873|GBB1_HUMAN	Cargo A
>sp|Q13322|GRB10_HUMAN	Cargo A
>sp|Q9Y4H2|IRS2_HUMAN	Cargo A
>sp|Q14145|KEAP1_HUMAN	Cargo A
>sp|Q9UNF1|MAGD2_HUMAN	Cargo A
>sp|Q9UDY8|MALT1_HUMAN	Cargo A
>sp|Q13164|MK07_HUMAN	Cargo A
>sp|P42345|MTOR_HUMAN	Cargo A
>sp|P01106|MYC_HUMAN	Cargo A
>sp|Q9NZQ3|SPN90_HUMAN	Cargo A
>sp|Q96PU5|NED4L_HUMAN	Cargo A
>sp|P25963|IKBA_HUMAN	Cargo A
>sp|O00221|IKBE_HUMAN	Cargo A

>sp|P49757|NUMB_HUMAN	Cargo A
>sp|Q13442|HAP28_HUMAN	Cargo A
>sp|Q9BRP1|PDD2L_HUMAN	Cargo A
>sp|Q13492|PICAL_HUMAN	Cargo A
>sp|O00743|PPP6_HUMAN	Cargo A
>sp|Q13162|PRDX4_HUMAN	Cargo A
>sp|P10644|KAP0_HUMAN	Cargo A
>sp|P04049|RAF1_HUMAN	Cargo A
>sp|Q01201|RELB_HUMAN	Cargo A
>sp|P15880|RS2_HUMAN	Cargo A
>sp|P23396|RS3_HUMAN	Cargo A
>sp|Q15019|SEPT2_HUMAN	Cargo A
>sp|Q14141|SEPT6_HUMAN	Cargo A
>sp|Q9UHD8|SEPT9_HUMAN	Cargo A
>sp|Q15047|SETB1_HUMAN	Cargo A
>sp|Q8IXJ6|SIR2_HUMAN	Cargo A
>sp|Q13485|SMAD4_HUMAN	Cargo A
>sp|Q01130|SRSF2_HUMAN	Cargo A
>sp|Q9BZK7|TBL1R_HUMAN	Cargo A
>sp|Q99081|HTF4_HUMAN	Cargo A
>sp|P15923|TFE2_HUMAN	Cargo A
>sp|P19532|TFE3_HUMAN	Cargo A
>sp|P19484|TFEB_HUMAN	Cargo A
>sp|Q9Y2W1|TR150_HUMAN	Cargo A
>sp|Q9UDY2|ZO2_HUMAN	Cargo A
>sp|O60784|TOM1_HUMAN	Cargo A
>sp|Q99816|TS101_HUMAN	Cargo A
>sp|O95071|UBR5_HUMAN	Cargo A
>sp|Q9H6R7|CB044_HUMAN / >sp|Q9H6R7|WDCP_HUMAN	Cargo A
>sp|P30291|WEE1_HUMAN	Cargo A
>sp|P23025|XPA_HUMAN	Cargo A
>sp|P67809|YBOX1_HUMAN	Cargo A
>sp|Q07352|TISB_HUMAN	Cargo A
>sp|P47974|TISD_HUMAN	Cargo A
>sp|P35869|AHR_HUMAN	Cargo B
>sp|P05090|APOD_HUMAN	Cargo B
>sp|Q9NYF8|BCLF1_HUMAN	Cargo B
>sp|O15234|CASC3_HUMAN	Cargo B
>sp|O95067|CCNB2_HUMAN	Cargo B
>sp|P19784|CSK22_HUMAN	Cargo B
>sp|O00571|DDX3X_HUMAN	Cargo B
>sp|P35659|DEK_HUMAN	Cargo B
>sp|P18074|ERCC2_HUMAN	Cargo B
>sp|Q12778|FOXO1_HUMAN	Cargo B
>sp|O43524|FOXO3_HUMAN	Cargo B
>sp|P63092|GNAS2_HUMAN	Cargo B
>sp|O15357|SHIP2_HUMAN	Cargo B
>sp|Q13887|KLF5_HUMAN	Cargo B
>sp|P31025|LCN1_HUMAN	Cargo B

>sp|Q93052|LPP_HUMAN	Cargo B
>sp|P36507|MP2K2_HUMAN	Cargo B
>sp|P49137|MAPK2_HUMAN	Cargo B
>sp|P61244|MAX_HUMAN	Cargo B
>sp|Q02078|MEF2A_HUMAN	Cargo B
>sp|O75030|MITF_HUMAN	Cargo B
>sp|Q969V6|MKL1_HUMAN MKL / >sp|Q969V6|MRTFA_HUMAN	Cargo B
>sp|Q9Y6Q9|NCOA3_HUMAN	Cargo B
>sp|P19838|NFKB1_HUMAN	Cargo B
>sp|Q00653|NFKB2_HUMAN	Cargo B
>sp|P11940|PABP1_HUMAN	Cargo B
>sp|O15534|PER1_HUMAN	Cargo B
>sp|P41743|KPCI_HUMAN	Cargo B
>sp|O95997|PTTG1_HUMAN	Cargo B
>sp|Q04864|REL_HUMAN	Cargo B
>sp|Q04206|TF65_HUMAN	Cargo B
>sp|P46777|RL5_HUMAN	Cargo B
>sp|P31151|S10A7_HUMAN	Cargo B
>sp|Q9Y3F4|STRAP_HUMAN	Cargo B
>sp|Q9UPN9|TRI33_HUMAN	Cargo B
>sp|Q6NZY4|ZCHC8_HUMAN	Cargo B
>sp|Q5JTC6|AMER1_HUMAN	Low abundant cargo
>sp|Q96GD4|AURKB_HUMAN	Low abundant cargo
>sp|O15169|AXIN1_HUMAN	Low abundant cargo
>sp|P30305|MPIP2_HUMAN	Low abundant cargo
>sp|P35222|CTNB1_HUMAN	Low abundant cargo
>sp|Q9NQC7|CYLD_HUMAN	Low abundant cargo
>sp|Q9NRR4|RNC_HUMAN	Low abundant cargo
>sp|O15287|FANCG_HUMAN	Low abundant cargo
>sp|Q6UN15|FIP1_HUMAN	Low abundant cargo
>sp|Q9UQL6|HDAC5_HUMAN	Low abundant cargo
>sp|Q13233|M3K1_HUMAN	Low abundant cargo
>sp|Q99759|M3K3_HUMAN	Low abundant cargo
>sp|Q93074|MED12_HUMAN	Low abundant cargo
>sp|P42568|AF9_HUMAN	Low abundant cargo
>sp|Q13772|NCOA4_HUMAN	Low abundant cargo
>sp|Q15233|NONO_HUMAN	Low abundant cargo
>sp|P60201|MYPR_HUMAN	Low abundant cargo
>sp|Q92733|PRCC_HUMAN	Low abundant cargo
>sp|Q9BYW2|SETD2_HUMAN	Low abundant cargo
>sp|Q15797|SMAD1_HUMAN	Low abundant cargo
>sp|Q969G3|SMCE1_HUMAN	Low abundant cargo
>sp|O60347|TBC12_HUMAN	Low abundant cargo
>sp|Q15650|TRIP4_HUMAN	Low abundant cargo
>sp|O43542|XRCC3_HUMAN	Low abundant cargo

Supplementary Table 2. Selected candidate NES motifs in "XPO1-cancer exportome" proteins predicted *in silico* and experimentally tested using the SRVB/A assay and/or the Rev(1.4)-GFP assay

	cNES ID	Entry [CRM1 cargo category (Kirli et al., 2015)]	cNES Position	cNES Sequence	Wregex score (quartile)	NESmapper score (quartile)	Rank	1.4 score	Previoulsy assayed? (REF)
Plus cNES	WN1	sp|P36507|MP2K2_HUMAN [cargo B]	33-51	---------NLVD-L-QKK-L-EE-L-E-L-DEQQK-	100 (Q1)	32,4 (Q1)	1	9	YES (Fukuda et al. 1996)
	WN2	sp|Q9NZQ3|SPN90_HUMAN [cargo A]	282-300	---------SASDD-L-EA-L-GT-L-S-L-GTTEE-	100 (Q1)	13,5 (Q1)	1	3	NO
	WN3	sp|P19532|TFE3_HUMAN [cargo A]	418-436	--------QANRS-L-QLR-I-QE-L-E-L-QAQI--	84,8 (Q1)	27 (Q1)	1	2	NO
	WN4	sp|Q8IXJ6|SIR2_HUMAN [cargo A]	37-55	--------DMDF-L-RNL-F-SQT-L-S-L-GSQK--	74,9 (Q1)	11,2 (Q1)	1	9	YES (North and Verdin, 2007)
	WN5	sp|O15234|CASC3_HUMAN [cargo B]	457-475	--------SSTSG-L-EQD-V-AQ-L-N-I-AEQN--	73,5 (Q1)	11,2 (Q1)	1	4	YES (Macchi et al., 2003)
	WN6	sp|O15357|SHIP2_HUMAN [cargo B]	256-274	--------TGEQE-L-ESL-V-LK-L-S-V-LKDF--	73,5 (Q1)	8,8 (Q1)	1	3	NO
	WN7	sp|O15534|PER1_HUMAN [cargo B]	483-501	-------DTDIQE-L-SEQ-I-HR-L-L-L-QPV---	70,1 (Q1)	18 (Q1)	1	9	YES (Vielhaber et al., 2001)
	WN8	sp|O15357|SHIP2_HUMAN [cargo B]	625-643	--------RKEFEP-L-LR-V-DQ-L-N-L-EREK--	84,8 (Q1)	4,5 (Q2)	2	2	NO
	WN9	sp|O15534|PER1_HUMAN [cargo B]	1215-1233	---------PDDP-L-FSE-L-DG-L-G-L-EPMEE-	74,9 (Q1)	6,3 (Q2)	2	1	NO
	WN10	sp|Q14141-2|SEPT6_HUMAN [cargo A]	155-174	-------IAPTGHS-L-KS-L-DL-V-T-M-KKLD--	71,9 (Q1)	4,0 (Q2)	2	2	NO
	WN11	sp|Q8IXJ6|SIR2_HUMAN [cargo A]	244-267	FSCMQSDFLKVDL-L-LV-M-GTS-L-Q-V-Q-----	70,1 (Q1)	4,3 (Q2)	2	2	NO
	WN12	sp|O95071-2|UBR5_HUMAN [cargo A]	2206-2224	--------AEPGSI-L-TE-L-GG-F-E-V-KESK--	70,1 (Q1)	3,1 (Q2)	2	2	NO
	WN13	sp|P42345|MTOR_HUMAN [cargo A]	1274-1292	-------RVSKDDW-L-EW-L-RR-L-S-L-ELL---	68,1 (Q1)	5,4 (Q2)	2	4	YES (Bachmann et al., 2006)
	WN14	sp|P14635|CCNB1_HUMAN [cargo A]	138-156	---------AEED-L-CQA-F-SD-V-I-L-AVNDV-	64,9 (Q2)	18,9 (Q1)	2	5	YES (Toyoshima et al., 1998)
	WN15	sp|O95684|FR1OP_HUMAN [cargo A]	352-370	---------EIS-I-GEE-I-EED-L-S-V-EIDDI-	64,9 (Q2)	15,7 (Q1)	2	1	NO
	WN16	sp|P63010|AP2B1_HUMAN [cargo A]	256-274	---------VLS-A-VKV-L-MKF-L-E-L-LPKDS-	64,9 (Q2)	10,8 (Q1)	2	1	NO
	WN17	sp|P20042|IF2B_HUMAN [cargo A]	89-107	--------FDIDE-A-EEG-V-KD-L-K-I-ESDV--	63,1 (Q2)	25,2 (Q1)	2	3	NO
	WN18	sp|P42345|MTOR_HUMAN [cargo A]	649-668	-------VQVVADV-L-SK-L-LV-V-G-I-TDPD--	63,1 (Q2)	9,1 (Q1)	2	9	NO
	WN19	sp|P11274|BCR_HUMAN [cargo A]	1091-1111	------VSGVATD-I-QA-L-KAA-F-D-V-NNKD--	63,1 (Q2)	3,7 (Q2)	2	0	NO
	WN20	sp|Q14145|KEAP1_HUMAN [cargo A]	272-290	---------RCHS-L-TPN-F-LQ-M-Q-L-QKCEI-	63,1 (Q2)	3,1 (Q2)	2	0	NO
	WN21	sp|Q6UUV9-3|CRTC1_HUMAN [cargo A]	329-347	----------LSP-L-SP-I-TQA-V-A-M-DALSLE	58,7 (Q2)	21,6 (Q1)	2	2	NO
	WN22	sp|P15923|TFE2_HUMAN [cargo A]	566-584	--------NEAFKE-L-GR-M-CQ-L-H-L-NSEK--	58,7 (Q2)	18 (Q1)	2	0	NO
	WN23	sp|Q99081|HTF4_HUMAN [cargo A]	594-612	--------NEAFKE-L-GR-M-CQ-L-H-L-KSEK--	58,7 (Q2)	18 (Q1)	2	0	NO
	WN24	sp|Q12778|FOXO1_HUMAN [cargo B]	62-80	--------SAAAVS-A-DF-M-SN-L-S-L-LEES--	58,7 (Q2)	11,2 (Q1)	2	0	NO
	WN25	sp|Q13492-2|PICAL_HUMAN [cargo A]	212-230	---------NEG-I-INL-L-EKY-F-D-M-KKNQC-	58,1 (Q2)	4,5 (Q2)	2	0	NO
	WN26	sp|P35869|AHR_HUMAN [cargo B]	114-132	--------EGEF-L-LQA-L-NGF-V-L-V-VTTD--	58,1 (Q2)	4,5 (Q2)	2	0	NO
	cNES ID	**Entry [CRM1 cargo category (Kirli et al., 2015)]**	**cNES Position**	**cNES Sequence**	**Wregex score (quartile)**	**NESmapper score (quartile)**	**Rank**	**1.4 score**	**Previoulsy assayed? (REF)**
Minus (reverse) cNES	REV1	sp|P25963|IKBA_HUMAN [cargo A]	267-285	-----QQLGQ-L-T-L-EN-L-QM-L-PESED-----	85,7 (Q1)	18 (Q1)	1	0	NO
	REV2	sp|Q16204|CCDC6_HUMAN [cargo A]	297-315	-----MREEN-L-R-L-QRK-L-QRE-M-ERR-----	85,7 (Q1)	16,2 (Q1)	1	0	NO
	REV3	sp|P19484|TFEB_HUMAN [cargo A]	431-449	-----KDLDL-M-L-L-DDS-L-LPL-A-SDP-----	76,2 (Q1)	36 (Q1)	1	0	NO
	REV4	sp|O95071-2|UBR5_HUMAN [cargo A]	209-227	-----LQRTN-L-D-V-NLA-V-NN-L-LSRD-----	74,9 (Q1)	9 (Q1)	1	2	NO
	REV5	sp|O15357|SHIP2_HUMAN [cargo B]	261-279	-----LESLV-L-K-L-SV-L-KDF-L-SGIQ-----	73,5 (Q1)	49,5 (Q1)	1	3	NO
	REV6	sp|P30260|CDC27_HUMAN [cargo A]	545-563	-----HLQKD-V-A-L-SV-L-SKD-L-TDMD-----	73,5 (Q1)	16,2 (Q1)	1	1	NO
	REV7	sp|O95071-2|UBR5_HUMAN [cargo A]	1607-1625	-----EDGSD-M-E-L-DL-L-AA-A-ETESD-----	71,9 (Q1)	13,5 (Q1)	1	1	NO
	REV8	sp|Q9UDY2-3|ZO2_HUMAN [cargo A]	715-733	------PIAD-I-A-M-EK-L-ANE-L-PDWFQ----	70,1 (Q1)	17,6 (Q1)	1	1	NO
	REV9	sp|Q92997-2|DVL3_HUMAN [cargo A]	24-42	------PAER-V-T-L-AD-F-KGV-L-QRPSY----	70,1 (Q1)	12,6 (Q1)	1	0	NO
	REV10	sp|O95684|FR1OP_HUMAN [cargo A]	379-397	------LTQD-L-T-V-SQ-L-SDV-A-DYLED----	70,1 (Q1)	10 (Q1)	1	1	NO

REFERENCES

Kirli K., et al. *Elife* **4**:e11466 (2015)
Fukuda M., et al. *The Journal of Biological Chemistry* **271:**20024–20028 (1996).
North BJ and Verdin E. *PLoS ONE* **2**(8):e784. (2007)
Macchi P., et al. *The Journal of Neuroscience* **23**(13):5778-5788. (2003)
Vielhaber EL., et al. *The Journal of Biological Chemistry* **276**:45921–45927 (2001)
Bachmann RA., et al. *The Journal of Biological Chemistry* **281**:7357-7363 (2006)
Toyoshima F., et al. *The EMBO Journal* **17**:2728-2735 (1998)

Supplementary Table 3. Selected in silico predicted candidate NES motifs in human micropeptides

cNES ID	SmProt peptide ID and size (aa)	cNES Position	Sequence	Wregex score (quartile)	NESmapper score (quartile)	Rank
MICROP-1	SPROHSA011142 (96)	13-31	----KKEE-L-LKQ-L-DD-L-K-V-ELSQL	86,5 (Q1)	22,6 (Q1)	1
	SPROHSA011145 (47)	13-31				
MICROP-2	SPROHSA018908 (84)	57-75	----IRDR-L-PVN-V-RE-L-S-L-DDPEV	86,5 (Q1)	11,7 (Q1)	1
MICROP-3	SPROHSA012652 (70)	29-47	----GLDD-L-DVA-L-SN-L-E-V-KLEGS	85,7 (Q1)	34,2 (Q1)	1
MICROP-4	SPROHSA141226 (78)	40-58	---DGTSD-L-PLK-L-EA-L-S-V-KEDA-	85,7 (Q1)	20,2 (Q1)	1
	SPROHSA141826 (85)	47-65				
MICROP-5	SPROHSA141543 (68)	5-23	---ASASA-L-QRL-V-EQ-L-K-L-EAGV-	83,7 (Q1)	30,6 (Q1)	1
MICROP-6	SPROHSA011811 (57)	30-48	--SHYHET-L-GEA-L-QG-V-E-L-EFS--	83,7 (Q1)	17,6 (Q1)	1
MICROP-7	SPROHSA010409 (85)	16-34	--EESPEN-L-FLE-L-EK-L-V-L-EHS--	83,7 (Q1)	13,8 (Q1)	1
MICROP-8	SPROHSA009911 (99)	78-96	--RMSKEE-L-RAK-L-SE-F-K-L-ETR--	83,7 (Q1)	12,6 (Q1)	1
MICROP-9	SPROHSA020870 (100)	46-64	--LSKCGEE-L-GR-L-KL-V-L-L-ELN--	82,5 (Q1)	16,3 (Q1)	1
MICROP-10	SPROHSA180177 (93)	49-67	AKIKLLTKE-L-SV-L-KD-L-F-L-E----	81,1 (Q1)	11,2 (Q1)	1
	SPROHSA180747 (93)	49-67				
	SPROHSA181614 (93)	49-67				

The strength of a NES motif in the nucleocapsid protein of human coronaviruses is related to genus, but not to pathogenic capacity

Maria Sendino[a], Miren Josu Omaetxebarria[b], Jose Antonio Rodriguez[a]

[a]Department of Genetics, Physical Anthropology and Animal Physiology, University of the Basque Country (UPV/EHU), Leioa 48940, Spain.

[b]Department of Biochemistry and Molecular Biology, University of the Basque Country (UPV/EHU), Leioa 48940, Spain.

KEYWORDS: coronavirus pathogenicity, nucleocapsid protein, nuclear export signal, NES, CRM1

ABSTRACT

Seven members of the *Coronaviridae* family infect humans, but only three (SARS-CoV, SARS-CoV-2 and MERS-CoV) cause severe disease with a high case fatality rate. Using *in silico* analyses (machine learning techniques and comparative genomics), several features associated to coronavirus pathogenicity have been recently proposed, including a potential increase in the strength of a predicted novel nuclear export signal (NES) motif in the nucleocapsid protein.

Here, we have used a well-established nuclear export assay to experimentally establish whether the recently proposed nucleocapsid NESs are capable of mediating nuclear export, and to evaluate if their activity correlates with coronavirus pathogenicity.

The six NES motifs tested were functional in our assay, but displayed wide differences in export activity. Importantly, these differences in NES strength were not related to strain pathogenicity. Rather, we found that the NESs of the strains belonging to the genus *Alphacoronavirus* were markedly stronger than the NESs of the strains belonging to the genus *Betacoronavirus.*

We conclude that, while some of the genomic features recently identified *in silico* could be crucial contributors to coronavirus pathogenicity, this does not appear to be the case of nucleocapsid NES activity, as it is more closely related to coronavirus genus than to pathogenic capacity.

INTRODUCTION

Seven members of the *Coronaviridae* family (SARS-CoV, SARS-CoV-2, MERS-CoV, HCoV-NL63, HCoV-229E, HCoV-HKU1 and HCoV-OC43) are known to infect humans, but only the first three cause severe disease. Identifying molecular determinants of coronavirus pathogenicity is an important issue. In this regard, several genomic features that could differentiate highly pathogenic coronaviruses from less pathogenic strains have been recently identified *in silico*, using machine learning techniques and comparative genomics (1).

Eleven genomic regions corresponding to four different viral proteins, including the nucleocapsid (N) protein, were found to predict a high pathogenic capacity, but the underlying biological mechanisms remain to be elucidated. Interestingly, pathogenicity-associated deletions, insertions and substitutions within the N protein mapped to four potential nucleocytoplasmic transport motifs: three nuclear localization signals (NLSs) and one nuclear export signal (NES). In highly pathogenic strains, these four motifs showed an increased content of positively charged amino acids and were proposed to have an enhanced transport activity (1). However, while a direct correlation between NLS activity and positive charge has indeed been reported (2), such a correlation cannot be extrapolated to the NES motif. The activity of NES motifs, (i.e. their ability to bind to the nuclear export receptor CRM1) crucially relies on the presence of several hydrophobic (Φ) residues with a characteristic spacing (Φ_0-$X_{(2)}$-Φ_1-$X_{(2-3)}$-Φ_2-$X_{(2-3)}$-Φ_3-X-Φ_4, where X represents any amino acid) (reviewed in 3). Importantly, this NES “consensus” pattern is remarkably loose (4), and thus, predicting NES activity solely from amino acid sequence is a notoriously challenging task (5).

A different, more carboxy-terminally located sequence in the N protein of SARS-CoV was previously reported as a functional NES (6), but the more recently predicted motif (figure 1A) has not been yet experimentally evaluated. Two necessary steps towards elucidating the mechanism behind a potential relationship between the recently proposed nucleocapsid NESs and coronavirus pathogenicity are (i) to establish if these sequence motifs are functional (i.e, capable of mediating CRM1-dependent nuclear export) and, in that case, (ii) to determine if their activity level (their strength) correlates with the pathogenic capacity of the corresponding viral strain. To address these issues, we experimentally tested the NES motifs predicted in the N protein of SARS-CoV-2, MERS-CoV, HCoV-NL63, HCoV-229E, HCoV-HKU1 and HCoV-OC43

strains (Figure 1B) using a well-established nuclear export assay (7). Our results validate these sequences as functional NES motifs with different levels of nuclear export activity, and show that differences in NES strength are related to genus (*Alpha*- or *Betacoronavirus*), but not to pathogenicity of human coronavirus strains.

MATERIALS AND METHODS

Cloning procedures

The Rev(1.4)-GFP plasmid (7) was a gift from Dr. Beric Henderson (University of Sydney, Australia). DNA sequences encoding coronavirus nucleocapsid NES motifs were purchased as gBlocks (IDT), digested with BamHI and AgeI and cloned into Rev(1.4)-GFP. Constructs were confirmed using DNA sequencing (StabVida).

Cell culture and transfection

HeLa cells were grown in Dulbecco's modified Eagle's medium (DMEM) supplemented with 10% fetal bovine serum (FBS), 100 U/ml penicillin and 100 µg/ml streptomycin (all from Gibco; ThermoFisher Scientific) at 37°C in a humidified atmosphere containing 5% CO_2. 24 hours before transfection, cells were seeded in 12-well plates with glass coverslips. Transfections were carried out using X-tremeGENE 9 DNA transfection reagent (Roche Diagnostics) following manufacturer's instructions.

Rev(1.4)-GFP nuclear export assay

Rev(1.4)-GFP plasmids with the different NES motifs (as well as the Rev(1.4)-GFP plasmid, as negative control) were transfected into duplicated wells of HeLa cells. 24 hours after transfection, 10 µg/ml cycloheximide (CHX) was added to all the wells to arrest protein translation and thus ensure that any fluorescent signal present in the cytoplasm corresponds to exported and not to newly synthesized GFP-tagged proteins. For each transfection, the cells in one of the wells were additionally treated with 5 µg/ml actinomycin D (AD) to block nuclear import mediated by Rev NLS and thus facilitate detection of weaker NESs (7). Both drugs were purchased from Sigma-Aldrich. After 3 hours of incubation with the drugs, cells were fixed with 3.7% formaldehyde (Sigma-Aldrich) in phosphate-buffered saline (PBS) for 30 min, washed with

PBS, and mounted onto microscope slides using DAPI-containing Vectashield (Vector Laboratories). Slides were analysed using a Zeiss Axioskop fluorescence microscope. To ensure unbiased assessment, the identity of the samples was masked before the analysis. At least 200 transfected cells per sample were examined to establish the proportion of cells where the reporter shows nuclear (N), nuclear and cytoplasmic (NC) or cytoplasmic (C) localization. Based on this proportion, each of the tested motifs was assigned a nuclear export activity score using the assay scoring system (7). Representative images were taken using a Zeiss Apotome2 microscope and Zen2.6 Blue edition software.

RESULTS AND DISCUSSION

The Rev(1.4)-GFP assay (7) is a well-established method that has been used in numerous studies to experimentally establish the functionality of potential NES motifs and to compare the strength of different NESs. With this assay, functional NES motifs can be ascribed a score ranging between 1+ (weakest) and 9+ (strongest). As shown in Figure 2, the novel predicted NES motifs in the N protein of different human coronavirus strains tested here were all functional in the export assay. Of note, the N protein of SARS-CoV has been reported before to have a more carboxy-terminally located NES (6). The contribution of these sequences to the localization of human coronavirus N proteins needs to be further investigated. On the other hand, functional NES motifs have been also previously identified in the accessory proteins 3b and 9b of SARS-CoV (8-10). The presence of functional NESs in viral proteins is a common finding, and in fact, several viruses crucially rely on CRM1-mediated nuclear export of viral components (either RNA or proteins) during various stages of their life cycle (reviewed in 11). Together with previous findings (6, 8-10), our data support the possibility that nucleocytoplasmic shuttling may play an important role, still to be determined, in the life cycle of human coronaviruses.

Importantly, the six NES motifs tested here displayed a wide range of nuclear export activity (scores between 1+ and 8+). However, in contrast to what has been proposed based on *in silico* analyses (1), the differences in NES activity were not obviously related to pathogenicity (Figure 3). Rather, we found that the NESs of strains belonging to the genus *Alphacoronavirus* (HCoV-NL63 and HCoV-229E) were stronger (mean activity score= 6) than the NESs of the strains

belonging to the genus *Betacoronavirus* (SARS-CoV-2, MERS-CoV, HCoV-HKU1 and HCoV-OC43; mean activity score= 2).

CONCLUSION

We conclude that, while some of the features recently identified *in silico* (1) could be crucial contributors to coronavirus pathogenicity, this is not the case of the activity of the nucleocapsid NES motifs tested here, as it seems more closely related to coronavirus genus than to pathogenic capacity.

ACKNOWLEDGMENTS

We are grateful to Beric Henderson for the generous gift of the Rev(1.4)-GFP plasmid. This work was supported by grants from the Spanish Government MINECO-FEDER (SAF2014-57743-R), the Basque Country Government (IT1257-19) and the University of the Basque Country (UFI11/20), as well as a fellowship from the Basque Country Government (to M.S.).

REFERENCES

1. Gussow AB, Auslandera N, Faureb G, Wolfa YI, Zhang F, Koonin EV. 2020. Genomic determinants of pathogenicity in SARS-CoV-2 and other human coronaviruses. Proc. Natl. Acad. Sci. U.S.A. 117:15193–9.

2. Cokol M, Nair R, Rost B. 2000. Finding nuclear localization signals. EMBO Rep. 1:411–5.

3. Sendino M, Omaetxebarria MJ, Rodríguez JA. 2018. Hitting a moving target: inhibition of the nuclear export receptor XPO1/CRM1 as a therapeutic approach in cancer. Cancer Drug Resistance. 1:139-163.

4. Kosugi S, Hasebe M, Tomita M, Yanagawa H. 2008. Nuclear export signal consensus sequences defined using a localization-based yeast selection system. Traffic 9:2053-62.

5. Prieto G, Fullaondo A, Rodriguez JA. 2014. Prediction of nuclear export signals using weighted regular expressions (Wregex). Bioinformatics 30:1220-27.

6. You JH, Reed ML, Hiscox JA. 2007. Trafficking motifs in the SARS-coronavirus nucleocapsid protein. Biochem Biophys Res Commun. 358:1015-20.

7. Henderson BR, Eleftheriou A. 2000. A comparison of the activity, sequence specificity, and CRM1-dependence of different nuclear export signals. Exp. Cell Res. 256:213-24.

8. Freundt EC, Yu L, Park E, Lenardo MJ, Xu XN. 2009. Molecular determinants for subcellular localization of the severe acute respiratory syndrome coronavirus open reading frame 3b protein. J Virol. 83:6631-40.

9. Moshynskyy I, Viswanathan S, Vasilenko N, Lobanov V, Petric M, Babiuk LA, Zakhartchouk AN. 2007. Intracellular localization of the SARS coronavirus protein 9b: evidence of active export from the nucleus. Virus Res.127:116-21.

10. Sharma K, Åkerström S, Sharma AK, Chow VTK, Teow S, Abrenica B, Booth SA, Booth TF, Mirazimi A, Lal SK. 2011. SARS-CoV 9b protein diffuses into nucleus, undergoes active Crm1 mediated nucleocytoplasmic export and triggers apoptosis when retained in the nucleus. PLoS One 6(5):e19436.

11. Mathew C, Ghildyal R. 2017. CRM1 Inhibitors for Antiviral Therapy. Front Microbiol. 8:1171.

LEGEND TO FIGURES

Figure 1. Location and amino acid sequence of predicted NES motif in the nucleocapsid (N) protein of human coronaviruses.

A. Schematic representation (not at scale) of the nucleocapsid (N) protein of human coronaviruses indicating the location of the novel predicted NES motifs (green) whose activity has been proposed to correlate with strain pathogenicity (1). The location of a previously reported NES motif in SARS-CoV N protein (6) is shown in purple. Proteins corresponding to strains of the *Betacoronavirus* genus are represented in orange, and those corresponding to strains of the *Alphacoronavirus* genus are represented in blue. **B**. Amino acid sequence of a segment of the N protein from different coronavirus strains encompassing the proposed NES described in (1) (highlighted in green). These 19 amino acid-long sequences were tested using the Rev(1.4)-GFP nuclear export assay (7). Given the high similarity between SARS-CoV and SARS-CoV-2 motifs, only the last one was tested.

Figure 2. Experimental analysis of predicted NES motifs in human coronavirus N protein.

A. Images show representative examples of the results of the nuclear export assay in HeLa cells. The empty Rev(1.4)-GFP vector was used as a negative control. Results for MERS-CoV

NES and HCoV-NL63 NESs are shown. Where indicated (+AD), Actinomycin D was added to block nuclear import mediated by Rev NLS, and thus detect the activity of weaker NESs (7). Cell nuclei are visualized using DAPI. **B**. Graphs represent the percentage of HeLa cells showing nuclear (N), nuclear and cytoplasmic (NC) or cytoplasmic (C) localization of the reporter containing the indicated NES motif. At least 200 cells per sample were scored. From these percentages, each NES was assigned an export assay score as described in (7), which is indicated in the graph by the numbers above the bars.

Figure 3. Relationship between nucleocapsid NES strength and pathogenic capability or genus of human coronaviruses.

Graphs represent the strength (nuclear export assay score) of the nucleocapsid NESs in relation to the pathogenicity (left) or the genus (right) of the corresponding viral strain. Horizontal bars represent the mean activity of each group.

Figure 1

A

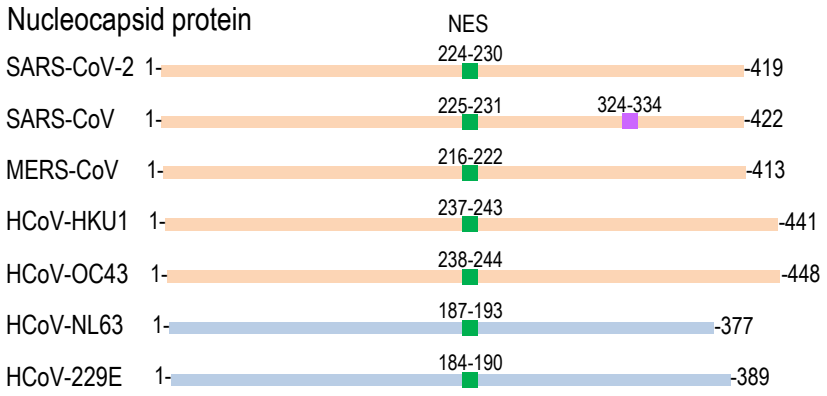

B

Strain	Predicted NES motif
SARS-CoV-2	ALALLLLDRLNQLESKMSG
SARS-CoV	ALALLLLDRLNQLESKVSG
MERS-CoV	GGDLLYLDLLNRLQALESG
HCoV-HKU1	MADEIANLVLAKLGKDSKP
HCoV-OC43	MADQIASLVLAKLGKDATK
HCoV-NL63	SSSDLVAAVTLALKNLGFD
HCoV-229E	SQDDIMKAVAAALKSLGFD

Figure 2

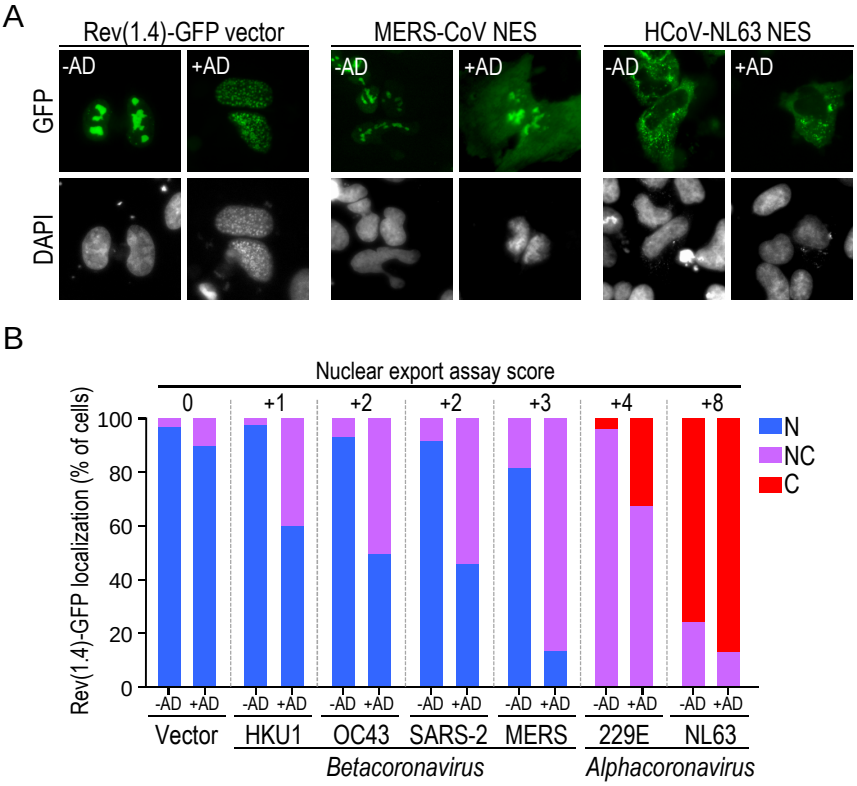

Figure 3

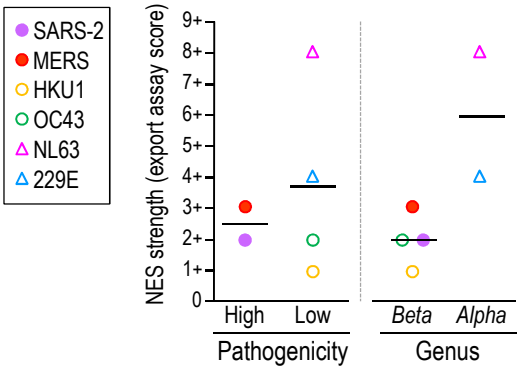

The FEBS Journal

FEBS PRESS
science publishing by scientists

The dystrophia myotonica WD repeat-containing protein DMWD and WDR20 differentially regulate USP12 deubiquitinase

Anne Olazabal-Herrero[1,2], Martin Bilbao-Arribas[1], Onintza Carlevaris[3], Maria Sendino[1], Endika Varela-Martinez[1], Begoña M. Jugo[1], Edurne Berra[3,4] and Jose Antonio Rodriguez[1]

1 Department of Genetics, Physical Anthropology and Animal Physiology, University of the Basque Country (UPV/EHU), Leioa, Spain
2 Department of Pediatrics, Yale School of Medicine, New Haven, CT, USA
3 Cell Signaling and Metabolism Lab, Center for Cooperative Research in Biosciences (CIC bioGUNE), Basque Research and Technology Alliance (BRTA), Bizkaia, Spain
4 CIBERONC, Madrid, Spain

Keywords
cofactor; deubiquitinase; DMWD; USP12; WDR20

Correspondence
J. A. Rodriguez, Department of Genetics, Physical Anthropology and Animal Physiology, University of the Basque Country (UPV/EHU), 48940, Leioa, Bizkaia, Spain
E-mail: josean.rodriguez@ehu.eus

(Received 13 November 2020, revised 5 March 2021, accepted 9 April 2021)

doi:10.1111/febs.15875

Despite its potential clinical relevance, the product of the *DMWD* (dystrophia myotonica, WD repeat containing) gene is a largely uncharacterized protein. The DMWD amino acid sequence is similar to that of WDR20, a known regulator of the USP12 and USP46 deubiquitinases (DUBs). Here, we apply a combination of *in silico* and experimental methods to investigate several aspects of DMWD biology. Molecular evolution and phylogenetic analyses reveal that WDR20 and DMWD, similar to USP12 and USP46, arose by duplication of a common ancestor during the whole genome duplication event in the vertebrate ancestor lineage. The analysis of public human gene expression datasets suggests that *DMWD* expression is positively correlated with *USP12* expression in normal tissues and negatively correlated with WDR20 expression in tumors. Strikingly, a survey of the annotated interactome for DMWD and WDR20 reveals a largely nonoverlapping set of interactors for these proteins. Experimentally, we first confirmed that DMWD binds both USP12 and USP46 through direct coimmunoprecipitation of epitope-tagged proteins. We found that DMWD and WDR20 share the same binding interface in USP12, suggesting that their interaction with the DUB may be mutually exclusive. Finally, we show that both DMWD and WDR20 promote USP12 enzymatic activity, but they differentially modulate the subcellular localization of the DUB. Altogether, our findings suggest a model whereby mutually exclusive binding of DMWD and WDR20 to USP12 may lead to formation of deubiquitinase complexes with distinct subcellular localization, potentially targeting different substrate repertoires.

Abbreviations
ActD, actinomycin D; BCa, breast cancer; Co-IP, coimmunoprecipitation; CRC, colorectal cancer; C-tail, carboxy-terminal tail; DAPI, 4′,6-diamidino-2-phenylindole; DM1, myotonic dystrophy 1; DUB, deubiquitinase; FBS, fetal bovine serum; HA-Ub-VS, HA-tagged ubiquitin vinyl sulfone; LCR, low complexity region; LMB, leptomycin B; NES, nuclear export signal; NLS, nuclear localization signal; PCa, prostate cancer; PM, plasma membrane; PTM, post-translational modification; TPM, transcripts per million; USP, ubiquitin-specific protease; WDR, WD40-repeat; WGD, whole genome duplication; YFP, yellow fluorescent protein.

Introduction

Ubiquitination, the covalent conjugation of ubiquitin, is a crucial post-translational modification (PTM) that regulates the levels and function of many proteins to modulate various cellular processes [1]. Many different types of ubiquitination have been described, including the conjugation of a single ubiquitin moiety (monoubiquitination) or the generation of polyubiquitin chains with different length and linkage topology. The fate of ubiquitinated proteins can be differently affected, depending on the type of ubiquitin modification imposed on them [1]. A vast repertoire of ubiquitin tags stems from the carefully orchestrated activity of a set of enzymes that either attach ubiquitin moieties to substrate proteins (and to ubiquitin itself) or remove ubiquitin tags. The enzymes that catalyze ubiquitin removal are termed deubiquitinases (DUBs).

Deubiquitinases are a group of proteolytic enzymes composed, in humans, by around 100 members [2]. Based on the structure of their catalytic domains, human DUBs can be classified into seven families [3]. The largest group of DUBs is the ubiquitin-specific protease (USP) family, which includes 57 members [4]. USPs share a common structure of their catalytic domain, which resembles an open hand with three characteristic subdomains named 'Palm', 'Fingers', and 'Thumb' [5].

Deubiquitinases need to be carefully regulated in order to prevent their aberrant activation and to ensure a proper ubiquitination state of their substrates. The catalytic activity of DUBs is regulated through several intertwined mechanisms, including PTMs, substrate-induced activation, and, prominently, interaction with nonsubstrate proteins [4,6]. A first global view of the wide array of DUB-interacting proteins was obtained in a large proteomics analysis of the interactome of 75 human DUBs [7]. Among several other features, a detailed analysis of the 774 high-confidence interactions identified in this landmark study revealed that the DUB interactome was significantly enriched in partners bearing the so-called WD40 repeat (WDR) domain [7]. In particular, more than 20 members of the USP family are reported to interact with WDR-containing proteins [7,8]. Although the biological significance of most of these interactions remains to be elucidated, the regulation of two DUBs belonging to the USP family (USP12 and USP46) by two WDR-containing proteins (WDR48, also called UAF1, and WDR20) has been characterized in detail [9–14].

USP12 and USP46 function in a variety of cellular signaling pathways, including those mediated by Akt, the androgen receptor, the T-cell receptor, the Notch receptor, and AMPA brain receptors [15–22]. The basal catalytic activity of USP12 and USP46 is extremely low when they are not bound to their WDR-containing cofactors. USP12 and USP46 are partially activated by WDR48, but require concomitant binding of WDR20 to reach their peak activity in the context of a ternary DUB/WDR48/WDR20 complex [9,10].

A series of structural and biochemical analyses [11–14] have provided significant insight into the molecular mechanisms that mediate activation of USP12 and USP46 by their cofactors WDR48 and WDR20. As illustrated in the schematic representation of the ternary USP12/WDR48/WDR20 complex shown in Fig. 1A, USP12 interacts with WDR48 through the tip of its 'Fingers' domain, while WDR20 binds to the bottom of the 'Palm' domain. Both binding sites are distant from the catalytic center of the enzyme, and the binding of WDR proteins has been shown to induce USP12 activation through an allosteric mechanism [12].

Importantly, the regulatory effect of WDR proteins on USP12 and USP46 extends beyond increasing their enzymatic activity. Thus, we have recently shown that WDR20 mediates XPO1-dependent nuclear export of USP12 and promotes its relocation to the plasma membrane (PM) [23].

The mechanism of DUB regulation by WDR proteins described above is evolutionarily conserved [24]. Such a regulatory mechanism is already present in the fission yeast *Schizosaccharomyces pombe*, where the homologs of WDR48 (Bun107) and WDR20 (Bun62) regulate the enzymatic activity and subcellular localization of Ubp9, the yeast homolog of USP12 and USP46 [25]. In this context, it must be noted that the *S. pombe* genome encodes only 20 DUBs [25], about one fifth of the number of DUB genes present in the human genome, clearly illustrating that the number of DUB-coding genes has notably expanded during the course of evolution. According to a detailed analysis of DUB evolution [26], a significant increase in the number of DUB genes took place during two whole genome duplication (WGD) events that occurred early in vertebrate evolution. In fact, USP12 and USP46, which show nearly 90% amino acid identity, are a prominent example of paralog DUBs that evolved by duplication of a common ancestor during these events [26]. Conceivably, the WGD events that expanded the DUB repertoire may have also led to the coemergence of DUB regulators. In this regard, we noted that a third WDR protein, called DMWD, was reported to bind USP12 and USP46 in the global DUB interactome study [7], but its role in the context of these DUB complexes has not yet been investigated.

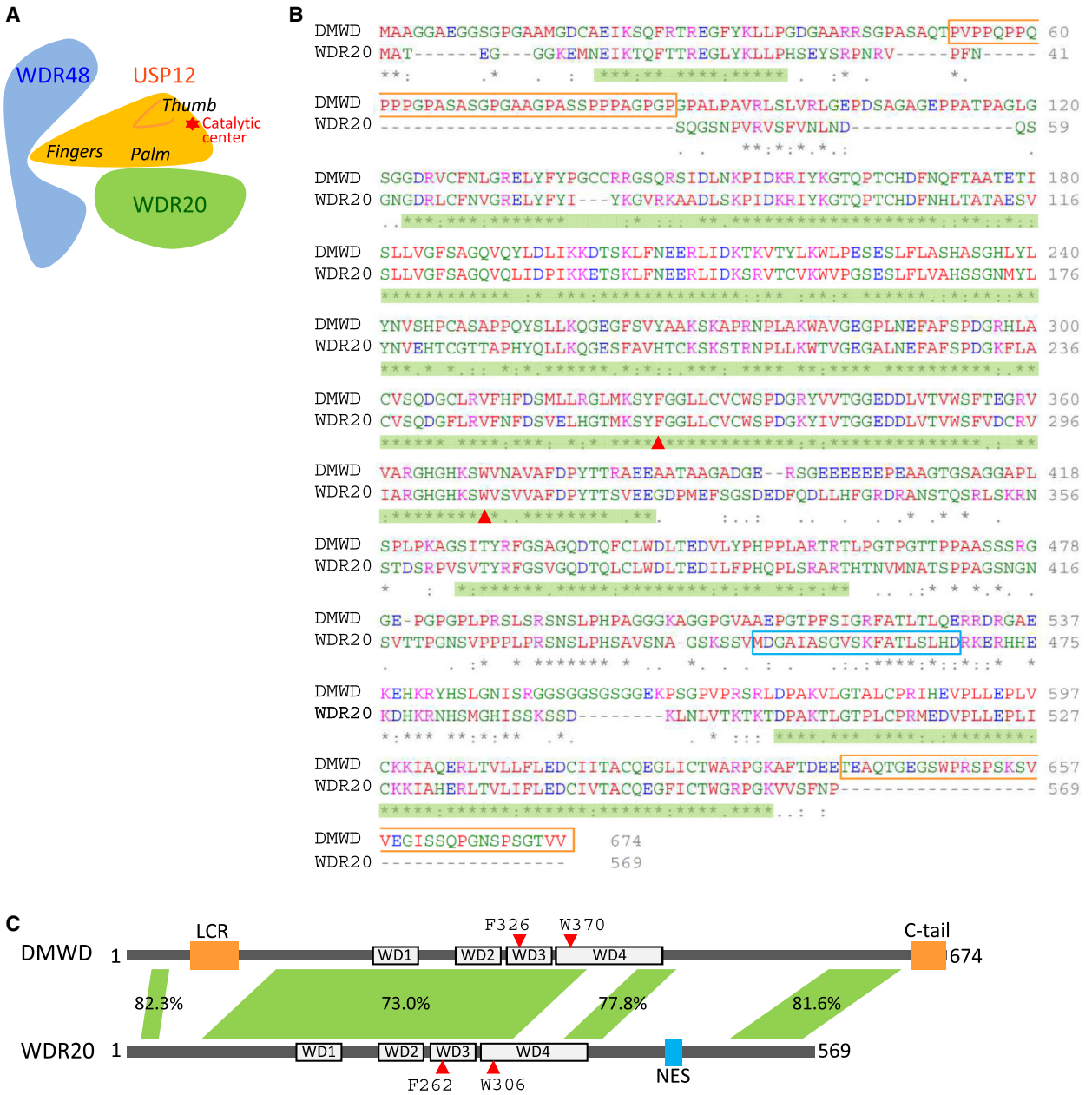

Fig. 1. Schematic representation of the USP12/WDR48/WDR20 ternary complex and comparison of human DMWD and WDR20 amino acid sequences. (A) The 'Palm', 'Fingers', and 'Thumb' subdomains of USP12 are shown. WDR48 binds to the tip of the 'Fingers', whereas WDR20 binds to the bottom of the 'Palm'. Both WDR-binding sites are distant from the catalytic center of the DUB. (B) Clustal Omega-based alignment of DMWD (Q09019) and WDR20 (Q8BTZ3) amino acid sequences. The symbols (*/:/.) under the aligned sequences reflect the degree of conservation of each position, with an asterisk indicating identical residues. Four highly conserved regions with more than 70% amino acid identity are shaded in green. A proline-rich, LCR, and a short C-tail present in DMWD, but absent in WDR20, are boxed in orange. Red arrowheads indicate the WDR20 residues (F262 and W306) that mediate binding to USP12. Both residues are conserved in DMWD (corresponding to F326 and W370, respectively). A NES that mediates XPO1-dependent shuttling of WDR20 is boxed in blue. The sequence of this motif is partially conserved in DMWD. (C) Schematic representation of DMWD and WDR20 proteins illustrating the position of the elements highlighted in the alignment above. The position of four WD40 domains (WD1–4) in WDR20 (140–178; 209–248; 251–290 and 293–382) and DMWD (206–242; 276–312; 315–354 and 357–444) is also shown. These domains were defined according to the 'Pfam/Smart domain' feature of the ELM resource (accessed on March 2020). The shaded areas between the proteins represent highly conserved segments, with the percentage of amino acid identity indicated.

DMWD is a poorly characterized protein with a high degree of sequence similarity to WDR20. The human *DMWD* [myotonic dystrophy 1 (DM1) locus, WD repeat containing] gene is located on chromosome 19q13.3, within the DM1 genomic region. DM1 is an autosomal dominant genetic disease caused by abnormal expansion of a CTG repeat in the 3′UTR of the dystrophia myotonica protein kinase (*DMPK*) gene, located downstream of *DMWD* [27]. DM1 patients present a complex array of multisystemic symptoms. These symptoms have been mainly ascribed to a toxic gain-of-function effect of expansion-bearing *DMPK* mRNA [27,28], but additional pathogenic mechanisms are likely to play a role. In this regard, a recently developed mouse model of DM1 shows that a reduced dosage of DMWD significantly contributes to the severity of the disease [29]. This novel genetic evidence supports the involvement of DMWD in DM1 pathogenesis, but does not provide information on the biological function of this protein, which is still completely unknown. In particular, despite its reported binding to USP12 and USP46, the potential role of human DMWD as a DUB regulator remains to be established.

Here, we present phylogenetic evidence that DMWD and WDR20 arose by duplication of a common ancestor concomitantly with their cognate DUBs, USP12, and USP46. We show that DMWD interacts with USP12 and promotes its enzymatic activity. Importantly, our results indicate that DMWD and WDR20 share the same binding interface in USP12, suggesting that the DUB cannot bind to both cofactors simultaneously. While both WDR proteins can activate USP12, they differently regulate the localization of this DUB. We propose a model whereby competition between these closely related cofactors for binding to USP12 may lead to the formation of mutually exclusive USP12/DMWD and USP12/WDR20 complexes with different subcellular localization, which could potentially target a different substrate repertoire.

Results

Comparison of human DMWD and WDR20 amino acid sequence

DMWD and WDR20 are closely related proteins. A BLAST search of the human proteome using DMWD amino acid sequence as a query identified WDR20 as the human protein with the highest homology to DMWD. BLAST analysis and Clustal Omega-based alignment [30] revealed that the overall amino acid identity between both proteins was 54.49%, being higher than 70% in four particularly well-conserved segments, separated by regions with lower or no conservation (Fig. 1B,C). Two particularly prominent features of DMWD sequence, not present in WDR20, were an N-terminal low complexity region (LCR), rich in proline, glycine, alanine, and serine residues, and a short carboxy-terminal tail (C-tail).

We examined to what extent functionally relevant sequence elements previously identified in WDR20 are conserved in DMWD. These elements include, on one hand, the crucial residues that mediate binding to USP12. Structural and mutagenesis analyses [12] have shown that the USP12/WDR20 interaction critically requires residues V279 and F287 in USP12, and residues F262 and W306 in WDR20. As shown in Fig. 1B, WDR20 residues F262 and W306 are conserved in DMWD, corresponding to positions F326 and W370, respectively. On the other hand, the WDR20 450-MDGAIASGVSKFATLSLHD-468 motif has been shown to function as a nuclear export signal (NES) that mediates XPO1-dependent export of WDR20 to the cytoplasm [23]. Our alignment revealed a partial conservation of this motif in DMWD, with sequence similarity limited to the C-terminal half of the NES.

Molecular evolution of DMWD and WDR20

The high similarity between WDR20 and DMWD amino acid sequences suggests that they may share a common ancestral protein, and it seems reasonable to assume that the WGD events that expanded the DUB repertoire [26] may have also led to the expansion of DUB regulators. Therefore, we hypothesize that WDR20 and DMWD arose by duplication of a common ancestor protein, concomitantly with the emergence of USP12 and USP46.

To test this hypothesis, we carried out phylogenetic and molecular evolutionary analysis using the coding sequences of *WDR20* and *DMWD* orthologous genes (see Tables S1 and S2, and details of the analysis in the Methods section). In the species before the emergence of vertebrates, there is only one copy of the orthologous gene, while in vertebrates, including cartilaginous fishes (the oldest extant jawed vertebrate group), there are at least two copies. As shown in Fig. 2, a phylogenetic tree constructed with *WDR20* and *DMWD* sequences is divided into three main clusters: (a) vertebrate *WDR20* sequences, (b) vertebrate *DMWD* sequences, and (c) ancestral sequences in invertebrates. This phylogeny places the emergence of the second copy just after the WGD events. Of note, it

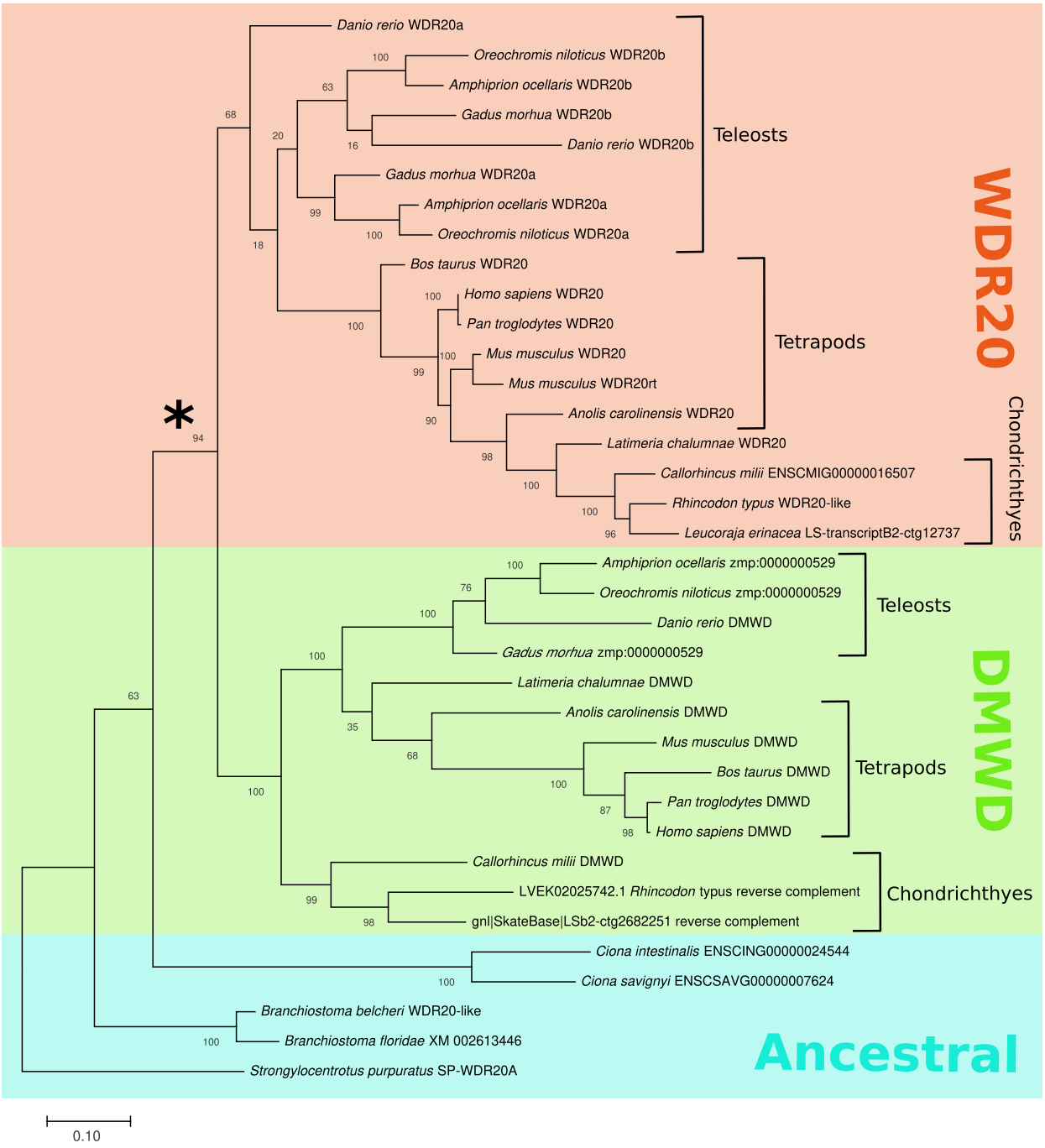

Fig. 2. Phylogenetic tree of *DMWD* and *WDR20*. The phylogenetic tree shown was constructed with *WDR20* and *DMWD* coding sequences using MEGA version X [56]. The maximum-likelihood method, using the Tamura–Nei model, was applied. The tree is divided into three main clusters: vertebrate *WDR20* sequences (orange), vertebrate *DMWD* sequences (green), and ancestral invertebrate sequences (blue). Duplication is indicated by an asterisk. The numbers at the branching points indicate bootstrap values, and the scale represents number of substitutions per site.

is known that other WGD events took place in teleosts [31], which would explain the presence of two copies of *WDR20* (*WDR20a* and *WDR20b*) in this clade.

The results of this analysis suggest that, like *USP12* and *USP46*, *WDR20* and *DMWD* arose by duplication of an ancestor gene during the vertebrate WGD

events, thus revealing an evolutionary coincidence in the emergence of two copies of these DUBs and their cofactors. The fact that both WDR20 and DMWD are maintained in the vertebrate lineage suggests that these proteins underwent some degree of sub- or neo-functionalization. Thus, we sought to compare the expression and function of human WDR20 and DMWD.

Comparison of *DMWD* and *WDR20* gene expression in DM1 samples, normal human tissues, and cancer

The expression of DMWD has been previously analyzed in human and mouse brain and muscle tissue samples, mainly in the context of DM1-related studies [32–36]. We made use of a recently published RNA-seq-based gene expression dataset [37], available through the Myotonic Dystrophy Deep Sequencing Data Repository (http://www.dmseq.org/), to compare the expression level of DMWD and WDR20 in tibialis anterior muscle samples derived from DM1 patients and controls using *limma* software [38]. According to these data (Fig. 3A), *DMWD* expression was slightly higher in DM1 patient samples compared to controls, whereas no significant differences in *WDR20* expression were observed. In this context, it must be noted that there have been conflicting reports regarding altered expression of *DMWD* in DM1 patient samples [32–35], a controversy that may be, at least in part, related to allele-specific expression [33].

On the other hand, to have a more comprehensive view of how the expression of *DMWD* and *WDR20* genes compares across different normal human tissues, we used mRNA expression data from the Genotype-Tissue Expression (GTEx) project [39]. In nearly every tissue analyzed, such as in adipose tissue and brain, shown as examples in Fig. 3B, *DMWD* was consistently expressed at a higher level than *WDR20*. Data for *USP12* and *USP46* were also obtained, and both hierarchical clustering and correlation analyses were carried out to evaluate the possible relationship between the expression levels of these four genes. Unsupervised clustering revealed that the expression of *DMWD* is most closely related to the expression of *USP12* (Fig. 3C). Furthermore, when the six possible pairwise correlations of these four genes were evaluated in the pooled set of GTEx samples (n = 17 382), the highest correlation coefficient (Spearman's r = 0.65) corresponded to the *DMWD*/*USP12* gene pair (Fig. 3D). These observations suggest that it might be particularly relevant to investigate the functional relationship of DMWD with this DUB.

Finally, we examined the expression of *DMWD*, *WDR20*, *USP12*, and *USP46* in 18 publicly available gene expression datasets of breast cancer (BCa, five datasets), colorectal cancer (CRC, seven datasets), and prostate cancer (PCa, six datasets) including a total of 5827 samples. These data, obtained from GEO, cBioPortal, and TCGA repositories, were analyzed using the CANCERTOOL analysis suite [40]. Eight datasets (one BCa, two CRC, and five PCa datasets) provided data on gene expression in the corresponding normal tissue for some of their patients. Significant differences in the expression level of *DMWD*, *WDR20*, *USP12*, and *USP46* between normal and cancer samples were noted in several studies. In particular, as shown in Fig. 4A, a consistent upregulation of *DMWD* and downregulation of *WDR20* and *USP12* were observed in the two available CRC datasets. We examined how the expression of *DMWD* and *WDR20* correlates with each other and with the expression of their cognate DUBs in human tumors. As shown in Fig. 4B, an inverse correlation between the expression of *DMWD* and *WDR20* was consistently observed in all BCa and CRC and also in most PCa studies. Remarkably, while no consistent correlation with the expression of *USP12* was noted, a striking correlation was found between the expression of both WDR genes and the expression of *USP46*. Thus, in virtually every tumor series analyzed, *USP46* expression was directly correlated with the expression of *WDR20*, but inversely correlated with the expression of *DMWD*.

Altogether, the findings above prompted us to focus our functional comparison between DMWD and WDR20 within the context of USP12 regulation.

Like WDR20, DMWD promotes USP12 catalytic activity

Using tandem mass spectrometry (MS/MS) analysis, Sowa *et al.* [7] identified endogenous DMWD as one of the proteins coimmunoprecipitated with Flag-HA-USP12 and Flag-HA-USP46 in HEK293T cells. Conversely, they identified endogenous USP12 and USP46 by MS/MS analysis of Flag-HA-DMWD immunoprecipitates [7]. We first aimed to further validate these interactions by direct coimmunoprecipitation (co-IP) of epitope-tagged proteins. To this end, expression plasmids encoding yellow fluorescent protein (YFP)-tagged DUBs (or the empty pEYFP-C1 plasmid as a negative control) were cotransfected with Myc-tagged DMWD into HEK293T cells, and GFP-trap pull-down assays were carried out. As a positive control, similar experiments were carried out in parallel with Myc-WDR20. Neither Myc-WDR20 nor Myc-DMWD

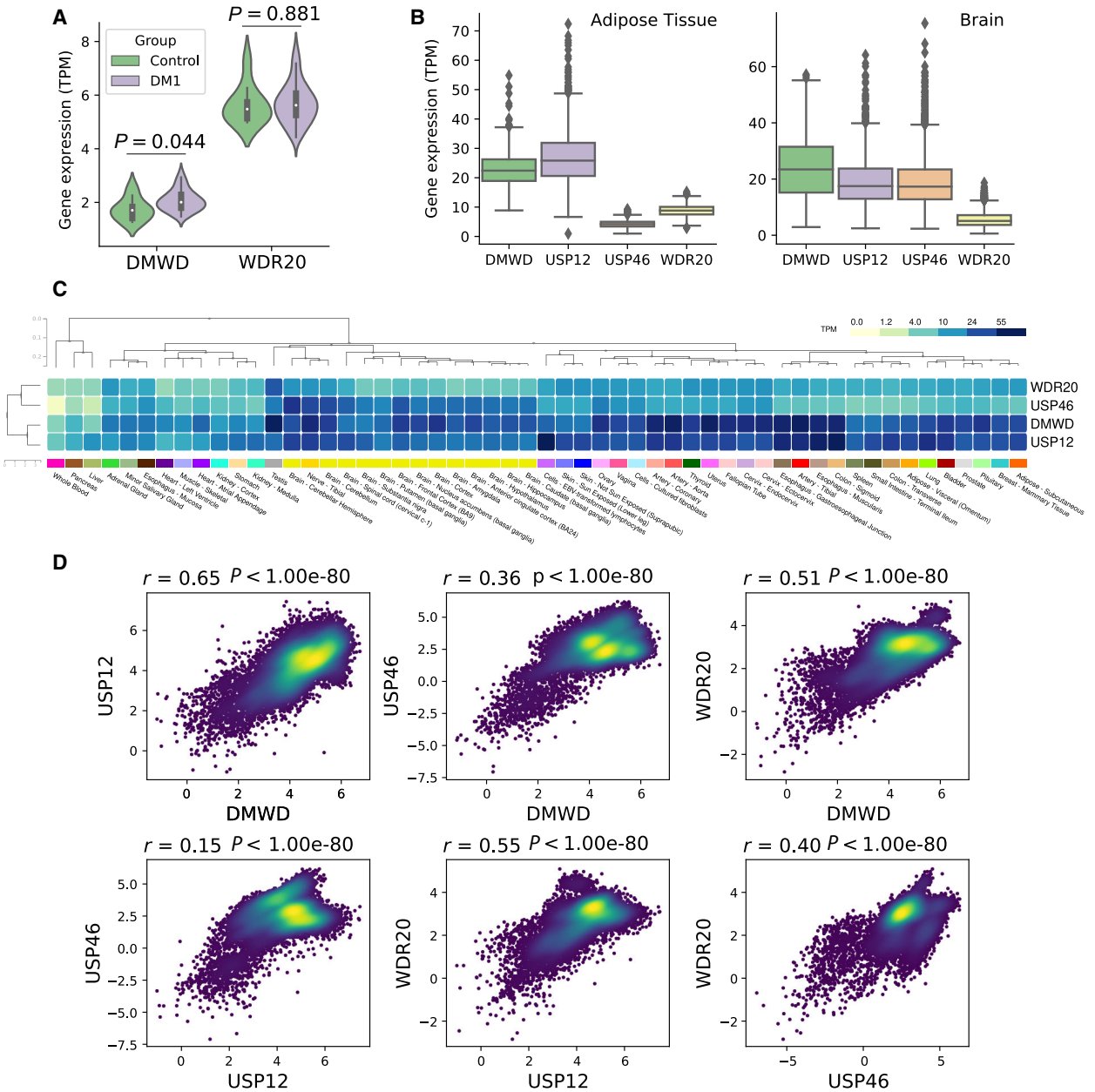

Fig. 3. Expression of *DMWD* and *WDR20* mRNA in DM1 patient samples and normal human tissues. (A) Violin plots showing the expression level of *DMWD* and *WDR20* mRNA in tibialis anterior muscle samples from controls and DM1 patients. Data were retrieved from the Myotonic Dystrophy Deep Sequencing Data Repository (http://www.dmseq.org/) and correspond to a recently published RNAseq-based gene expression dataset [37]. We downloaded gene expression data from the repository and performed a differential gene expression analysis between controls (n = 10) and DM1 samples (n = 40). We fitted a linear model and computed empirical Bayes statistics with *limma* [38] and calculated the adjusted P value (FDR) with Bonferroni–Hochberg correction. (B) Box plots showing the mRNA expression level (TPM) of endogenous *DMWD*, *USP12*, *USP46*, and *WDR20* in normal human adipose tissue and brain tissue samples. The boxes show the interquartile range (IQR), extending from the first (Q1) to the third (Q3) quartiles, with the median indicated by the line inside the box. The whiskers extend to indicate the maximum (Q3 plus 1.5 times the IQR) and minimum (Q1 minus 1.5 times the IQR), while values above or below these limits (outliers) are shown as diamonds. (C) Heatmap showing the mRNA expression level (TPM) of *DMWD*, *WDR20*, *USP12*, and *USP46* across 53 different human tissue types, indicated below. Color indicates the level of expression as indicated by the scale on the upper right corner. The expression level of *DMWD* is consistently higher than the expression level of *WDR20*, and clusters with the expression of *USP12*. (D) Graphs show density scatter plots of $\log_2$ expression values for the indicated pairs of genes. Spearman's rank correlation was used for the tests. All the correlations are highly statistically significant, with P values below $1.00e^{-80}$. The data shown in panels B, C, and D were obtained from the GTEx Portal [39] on September 2020.

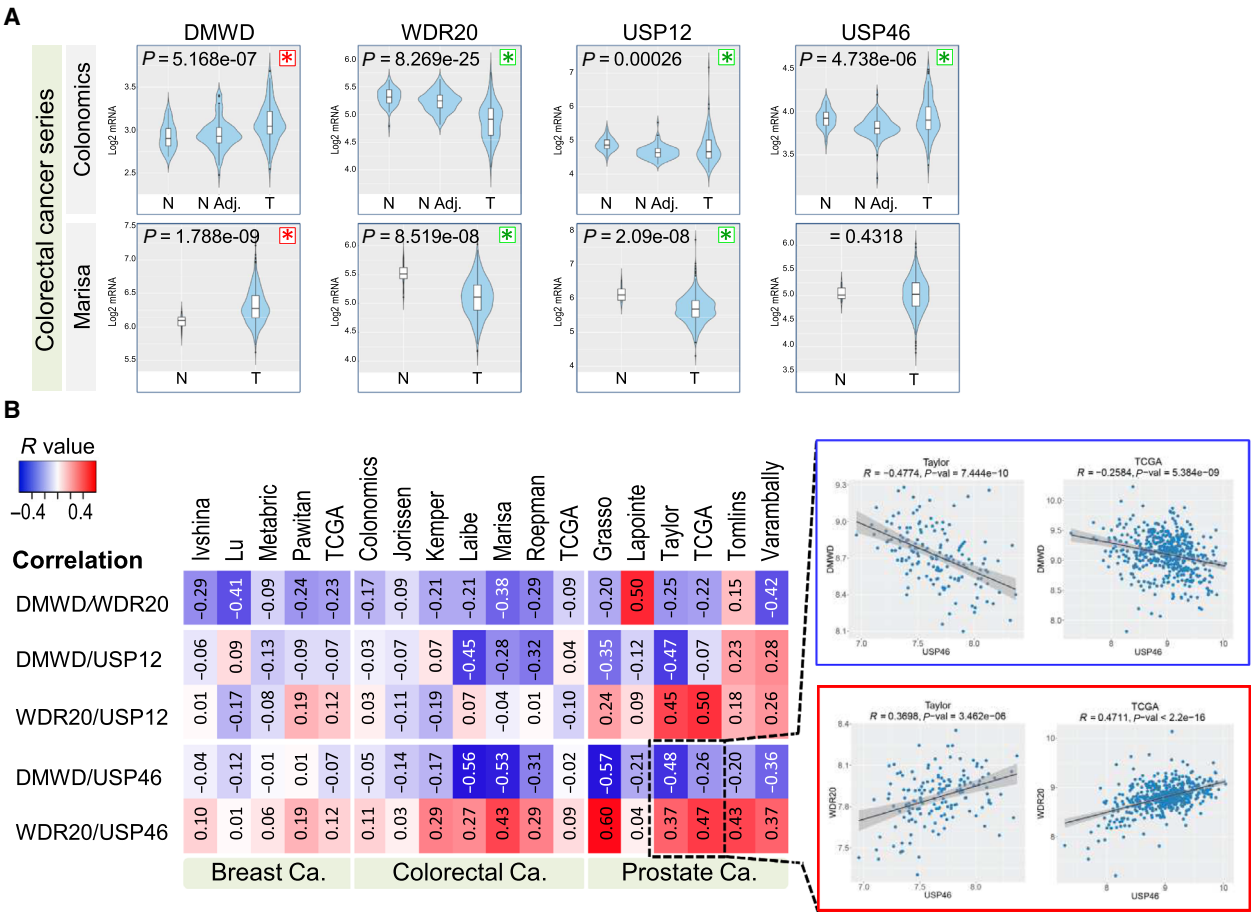

Fig. 4. Expression of *DMWD* and *WDR20* mRNA in cancer. (A) Violin plots showing mRNA expression levels of *DMWD*, *WDR20*, *USP12*, and *USP46* genes in normal tissue (N), normal tissue adjacent to tumor (NAdj.), and tumor (T) tissue samples in two colorectal patient datasets (details available at http://web.bioinformatics.cicbiogune.es/CANCERTOOL/index.html). Red asterisks indicate statistically significant overexpression of the gene in tumor samples. Green asterisks indicate statistically significant underexpression of the gene in tumor samples. The *P* values (Student *t*-test) are indicated within each graph. The analyses were carried out using the CANCERTOOL analysis suite [40]. (B) Heatmap showing how the expression of the indicated gene pairs correlates in human tumor samples. Eighteen gene expression datasets (details available at http://web.bioinformatics.cicbiogune.es/CANCERTOOL/index.html) of breast, colorectal, and PCa, including a total of 5827 samples, were analyzed using the CANCERTOOL analysis suite [40]. Blue color indicates inverse correlation, and red color indicates direct correlation, with color intensity representing the Pearson's correlation value (R), as indicated by the scale on the upper left corner. The *R* value is indicated inside each heatmap cell. The scatter plots on the right show detailed examples of the inverse correlation between *DMWD* and *USP46* expression (blue) and the direct correlation between *WDR20* and USP46 expression (red). The examples selected correspond to the two largest datasets of PCa analyzed here. Each dot in the graphs represents a tumor sample.

was detected in YFP coimmunoprecipitates, but both WDR proteins readily coprecipitated with YFP-USP12 and YFP-USP46 (Fig. 5A,B).

Next, we sought to evaluate the enzymatic activity of USP12 ternary complexes containing WDR48 and either WDR20 or DMWD. To this end, we used a HA-tagged ubiquitin vinyl sulfone (HA-Ub-VS) probe that irreversibly labels active DUBs by covalently binding to their catalytic-site cysteine [41]. Immunoblot analysis showed that coexpression of YFP-USP12 with Xpress-WDR48 and either Myc-WDR20 or Myc-DMWD resulted in effective labeling of the DUB (Fig. 5C,D). This observation indicates that the USP12/WDR48/DMWD ternary complex is catalytically active. Therefore, these data reveal for the first time that DMWD, like WDR20, functions as a cofactor that promotes USP12 enzymatic activity.

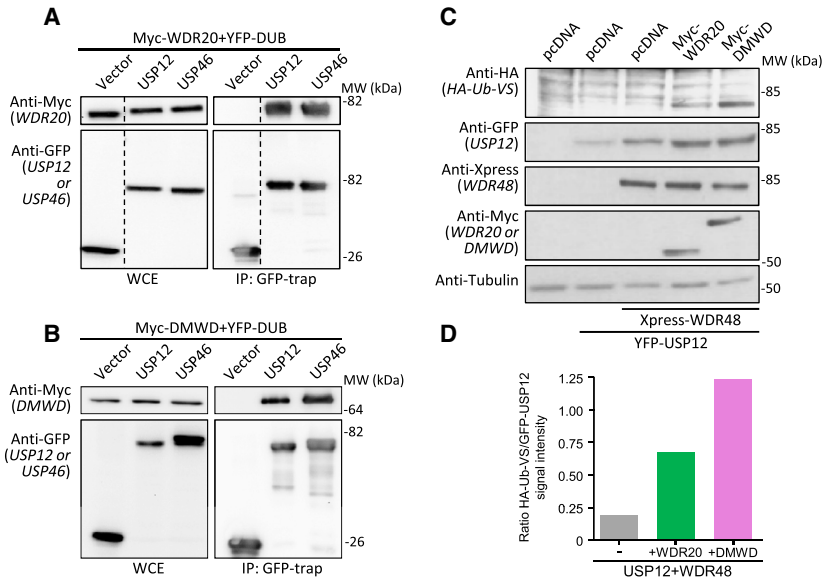

Fig. 5. DMWD interacts with USP12 and USP46 and promotes USP12 catalytic activity. (A, B) Blots showing the results of co-IP analyses of HEK293T cells cotransfected with YFP-vector (negative control), YFP-USP12, or YFP-USP46 and either Myc-WDR20 (panel A) or Myc-DMWD (panel B). Whole cell extracts (WCE) and proteins IP using the GFP-trap reagent were analyzed by immunoblot using anti-GFP, or anti-Myc antibodies, as indicated. Both Myc-WDR20 and DMWD were coimmunoprecipitated by YFP-USP12 and YFP-USP46, but not by YFP. The vertical dotted line indicates that an additional lane between the 'vector' and 'USP12' lanes, originally present in the gel, has been spliced out in the image for clarity. Results shown are representative of 4 (panel A) or 2 (panel B) independent experiments where similar results were obtained. (C) Blots showing the results of an HA-Ub-VS-based DUB activity assay to evaluate the ability of DMWD to promote USP12 enzymatic activity. HEK293T cells were transfected with YFP-USP12, Xpress-WDR48, Myc-WDR20, and Myc-DMWD expression plasmids in the indicated combinations. The empty pCDNA vector was used to equalize the total amount of DNA used in each experimental condition. Transfected cells were incubated with an HA-Ub-VS probe that irreversibly labels active DUBs [41]. Labeling was detected using an anti-HA antibody (upper blot), the expression of YFP-USP12 and the cofactors was examined using the indicated antibodies, and the amount of loaded protein was determined using anti-tubulin (lower blot). The assay was independently replicated four times with similar results, and a representative experiment is shown. (D) Graph showing the ratio between the HA-Ub-VS and GFP-USP12 signals in the indicated three samples. The intensity of the bands in the HA-Ub-VS and GFP-USP12 blots was quantified using IMAGEJ (NIH, Bethesda, MD, USA).

DMWD and WDR20 share a common binding interface in USP12

Since WDR20 activates USP12 through an allosteric mechanism [12], our finding that DMWD also promotes USP12 enzymatic activity led us to hypothesize that both cofactors could bind the DUB in a similar fashion.

To test this hypothesis, we took advantage of the fact that the interaction between USP12 and WDR20 has been previously characterized in detail and has been shown to critically require V279/F287 residues in USP12 and F262/W306 residues in WDR20 [12]. Using site-directed mutagenesis and GFP-trap pull-down assays, we found that the USP12 mutations (V279D/F287A) that prevent binding to wild-type (WT) WDR20 also disrupt binding to WT DMWD (Fig. 6A,B). Conversely, alanine substitutions of DMWD residues F326 and W370 (homologous to the WDR20 residues F262 and W306) disrupt binding to WT USP12 (Fig. 6B). As schematically illustrated in Fig. 6C, our results indicate that DMWD and WDR20 share a common binding site in the 'Palm' domain of USP12, and thus, they would be unable to bind simultaneously to the DUB.

DMWD and WDR20 have largely nonoverlapping interactomes

To further explore potential differences between DMWD and WDR20, we used the BioGRID repository [42] to retrieve available interactome data for both proteins. As of November 2019, 65 DMWD-interacting proteins and 47 WDR20-interacting proteins were included in this repository (Table S3). Remarkably, DMWD and WDR20 have a largely nonoverlapping set of interacting partners. In fact, only seven of the retrieved proteins are reported to interact with

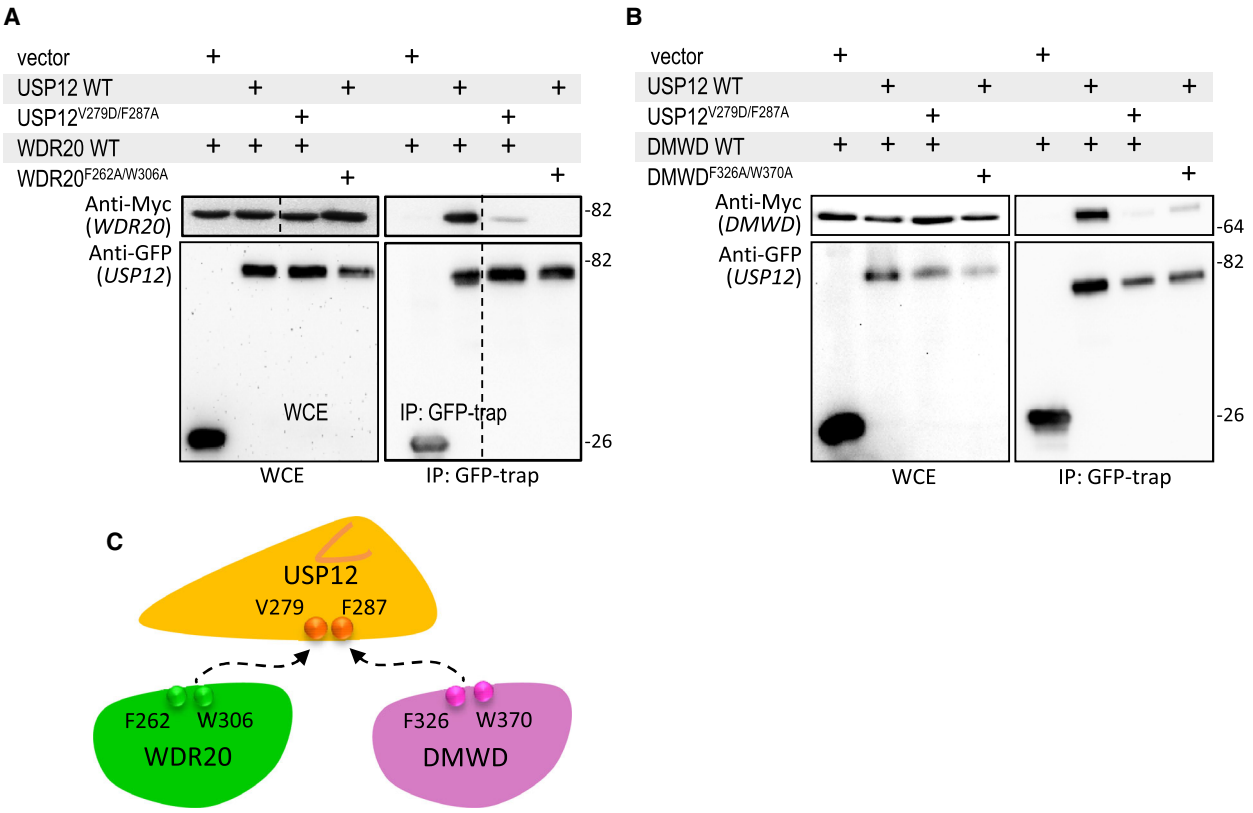

Fig. 6. DMWD and WDR20 share a common binding interface in USP12. (A, B) Blots showing the results of Co-IP (GFP-trap) analysis of HEK293T cells cotransfected with the indicated combination of plasmids. Whole cell extracts (WCE) and proteins IP using the GFP-trap reagent were analyzed by immunoblot using anti-GFP, or anti-Myc antibodies, as indicated. The molecular weight (kDa) is indicated on the right side of the blot. In panel A, plasmids encoding YFP (vector), YFP-USP12 WT, or YFP-USP12$^{V279D/F287A}$ were cotransfected with plasmids encoding either Myc-WDR20 WT or Myc-WDR20$^{F262A/W306A}$. The vertical dotted line indicates that the image is a composite of two images from a single gel. A lane showing the results of a USP12 mutant that is not relevant for the present study has been spliced out in the final image for clarity. In panel B, the same YFP plasmids were cotransfected with plasmids encoding either Myc-DMWD WT or Myc-DMWD$^{F326A/W370A}$, a variant where the residues homologous to WDR20 F262 and W306 have been mutated to alanine. Results shown are representative of two independent experiments where similar results were obtained. (C) Schematic representation of USP12, WDR20, and DMWD, indicating the residues that participate in their interactions. As represented by the dotted arrows, our findings suggest that WDR20 and DMWD share a common binding interface at the bottom of the Palm domain of USP12.

both DMWD and WDR20 (Fig. 7A). Besides the DUB complex partners (USP12, USP46, and WDR48), shared interactors included the phosphatases PHLPP1 and PHLPP2, the adapter protein YWHAH, and the nuclear export receptor XPO1. Of note, we have previously reported that XPO1 mediates the active export of WDR20 to the cytoplasm [23] through a NES motif that is partially conserved in DMWD (Fig. 1B).

Using data from UniProt [43], we next explored the subcellular localization of the proteins reported to interact with either DMWD ('DMWD-only' interactors) or WDR20 ('WDR20-only' interactors). As illustrated in Fig. 7B, and detailed in Table S3, both 'DMWD-only' and 'WDR20-only' interactors are most commonly annotated to localize to the nucleus, the cytoplasm, or the PM. This is consistent, in the case of WDR20, with its ability to shuttle between these three compartments [23]. Interestingly, while a similar proportion of 'DMWD-only' and 'WDR20-only' interactors are reported as cytoplasmic proteins, the proportion of interactors reported to localize to the nucleus or the PM was lower in the case of DMWD (Fig. 7C). These data suggest the possibility that DMWD may have a more limited access to the nucleus and the PM than WDR20 and prompted us to directly compare the subcellular localization of both proteins.

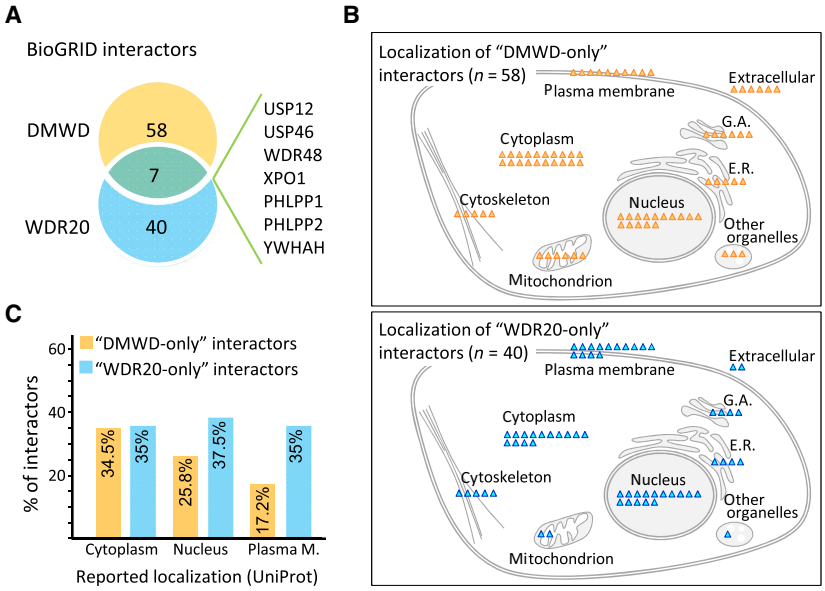

Fig. 7. *In silico* analysis of reported WDR20 and DMWD interactomes. (A) Venn diagram showing that the reported interactomes of WDR20 and DMWD (retrieved from the BioGRID repository) are largely nonoverlapping. The number of reported interactors is indicated inside each circle. Only seven proteins (listed on the right) are reported to interact with both WDR20 and DMWD. (B) Schematic representation of a cell showing the different subcellular compartments where nonoverlapping interactors of DMWD and WDR20 are reported to localize, according to the information available in Uniprot. Orange triangles represent 'DMWD-only' interactors (i.e., proteins reported to interact with DMWD but not with WDR20). Blue triangles represent 'WDR20-only' interactors. Several interactors are reported to localize to more than one compartment, and thus, the number of symbols exceeds the number of interactors. G.A: golgi apparatus. E.R: endoplasmic reticulum. (C) Graph showing the percentage of nonoverlapping interactors of DMWD and WDR20 reported to localize to the cytoplasm, nucleus, and PM.

Both WDR20 and DMWD are nucleocytoplasmic shuttling proteins, but DMWD enters the nucleus less efficiently than WDR20

Using immunofluorescence analysis, we evaluated the localization of Myc-WDR20 and Myc-DMWD in HeLa and HEK293T cells in the presence or absence of leptomycin B (LMB), a specific inhibitor of XPO1 [44]. As shown in Fig. 8A, both WDR proteins localized mainly to the cytoplasm of untreated cells. As previously reported [23], a clear relocation of Myc-WDR20 to the nucleus was observed upon LMB treatment. In the case of Myc-DMWD, a less pronounced, but noticeable LMB-induced nuclear relocation was also observed in HeLa cells. Strikingly, Myc-DMWD remained in the cytoplasm of LMB-treated HEK293T cells. Similar results (Fig. 8B) were obtained in an experiment with the clinically relevant XPO1 inhibitor Selinexor. These findings are consistent with the reported interaction of DMWD with XPO1 mentioned above and show that DMWD, like WDR20, is a XPO1-dependent nucleocytoplasmic shuttling protein. However, our results indicate that DMWD enters the nucleus less efficiently than WDR20 when XPO1-mediated export is blocked. Several mechanisms, including reduced nuclear import and/or increased retention in the cytoplasm, might account for the limited access of DMWD to the nucleus, which is more evident in HEK293T cells.

The only sequence motif related to nucleocytoplasmic transport that has been mapped to date in these two WDR proteins is a NES in WDR20 [23]. Since the corresponding homologous sequence in DMWD is very similar (Fig. 8C), and these motifs are conserved in DMWD and WDR20 proteins across different species (Fig. 8D), we aimed to directly compare the activity of both motifs. To this end, we used a nuclear export assay that allows to establish a NES activity score, ranging from 1+ (lowest export activity) to 9+ (highest export activity) [45]. As shown in Fig. 8E, WDR20 NESs was scored as 6+, while DMWD NES was scored as 3+. Thus, the NES motif of DMWD is markedly weaker than the corresponding homologous sequence in WDR20.

Finally, in an attempt to map sequence determinants that may contribute to its reduced nuclear entry, we generated DMWD deletion mutants lacking two amino acid segments that are conspicuously absent in

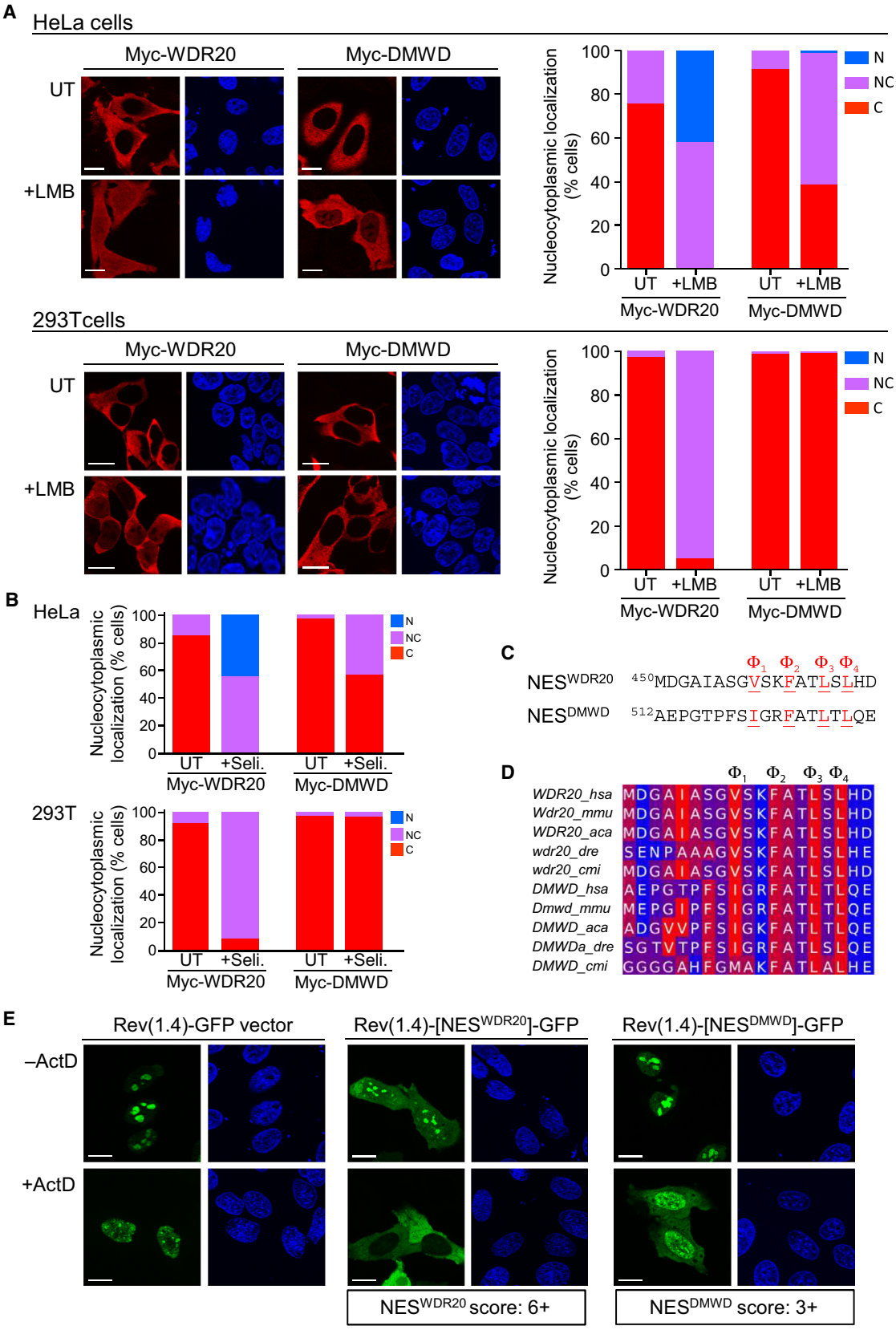
A
HeLa cells
Myc-WDR20
Myc-DMWD
UT
+LMB
Nucleocytoplasmic localization (% cells)
N
NC
C
293Tcells
B
HeLa
293T
+Seli.
C
NESWDR20 450MDGAIASGVSKFATLSLHD
NESDMWD 512AEPGTPFSIGRFATLTLQE
D
WDR20_hsa
Wdr20_mmu
WDR20_aca
wdr20_dre
wdr20_cmi
DMWD_hsa
Dmwd_mmu
DMWD_aca
DMWDa_dre
DMWD_cmi
E
Rev(1.4)-GFP vector
Rev(1.4)-[NESWDR20]-GFP
Rev(1.4)-[NESDMWD]-GFP
–ActD
+ActD
NESWDR20 score: 6+
NESDMWD score: 3+

Fig. 8. XPO1-dependent nucleocytoplasmic shuttling of WDR20 and DMWD. (A) Effect of the XPO1 inhibitor LMB on the nucleocytoplasmic localization of Myc-WDR20 and Myc-DMWD in HeLa and HEK293T cells. Left. Fluorescence microscopy images showing representative examples of the localization of Myc-tagged WDR20 and DMWD in untreated (UT) cells or in cells treated (6 ng·mL^{-1} for 3 h) with the nuclear export inhibitor (+LMB). Cell nuclei were visualized by staining the DNA with DAPI. Right. Graphs representing the percentage of transfected cells where the Myc-tagged WDR protein is located mainly/exclusively in the nucleus (N), mainly/exclusively in the cytoplasm (C), or is similarly distributed between both compartments (NC). At least 200 transfected cells were analyzed per sample. Results shown are representative of two (HeLa cells) or three (HEK293T cells) independent experiments where similar results were obtained. (B) Effect of the clinically relevant XPO1 inhibitor Selinexor (Seli.; 1 μM for 3 h) on the nucleocytoplasmic localization of Myc-WDR20 and Myc-DMWD in HeLa and HEK293T cells. (C) Amino acid sequence of the WDR20 NES motif and the corresponding homologous sequence in DMWD. The hydrophobic (Φ) residues that conform to the consensus NES pattern indicated above (type="InGreek_and_Coptic">Φ_1-$X_{(2)}$-type="InGreek_and_Coptic">Φ_2-$X_{(2)}$-type="InGreek_and_Coptic">Φ_3-X-Φ_4) are highlighted in red. (D) Alignment of NES amino acid sequences in WDR20 and DMWD proteins from *Homo sapiens* (hsa), *Mus musculus* (mmu), *Anolis carolinensis* (aca), *Danio rerio* (dre), and *Callorhincus milii* (cmi), showing conservation of the Φ_2, Φ_3, and Φ_4 hydrophobic residues across different organisms. The alignment was carried out using Clustal Omega and was visualized with Jalview. Residues are colored according to hydrophobicity. (E) Fluorescence microscopy images of HeLa cells illustrating the results of the nuclear export assay carried out to compare the activity of WDR20 and DMWD NES motifs. The empty Rev(1.4)-GFP reporter (Rev(1.4)-GFP vector) was used as negative control. ActD was added to block nuclear import mediated by Rev NLS (see Materials and methods for details). The nucleocytoplasmic localization of the reporter was determined in at least 200 cells per sample and used to derive a NES activity score (indicated under the images). Two independent replicas of the nuclear export assay were carried out, and similar results were obtained. Scale bars = 10 μm.

WDR20: the N-terminal LCR and the short C-tail. However, none of the DMWD mutants tested entered the nucleus in LMB-treated HEK293T cells (Fig. 9), indicating that these motifs are not responsible for the limited access of DMWD to the nucleus.

DMWD promotes relocation of USP12 to the plasma membrane less efficiently than WDR20

Since we have previously shown that coexpression of YFP-USP12 with Myc-WDR20 leads to a dramatic relocation of the DUB from the cytoplasm to the PM [23], we compared the ability of DMWD and WDR20 to regulate the subcellular localization of this DUB. To this end, confocal microscopy analyses were carried out in HEK293T expressing YFP-USP12 alone or coexpressing YFP-USP12 with either Myc-WDR20 or Myc-DMWD. As shown in Fig. 10A, coexpression with Myc-DMWD did not induce the striking relocation of YFP-USP12 to the PM induced by coexpression of Myc-WDR20. In fact, although a faint YFP fluorescent signal was noted in the PM of some cells, most YFP-USP12 remained in the cytoplasm of cells coexpressing Myc-DMWD. In order to more clearly visualize the different effect of both WDR proteins, we carried out similar experiments using a version of YFP-USP12, tagged with two copies of the SV40 large T antigen nuclear localization signal (YFP-NLS-USP12). As shown in Fig. 10B, YFP-NLS-USP12 localizes exclusively to the nucleus when expressed alone, but undergoes full relocation to the PM when coexpressed with Myc-WDR20. In contrast, only a fraction of YFP-NLS-USP12 relocates to the PM when coexpressed with Myc-DMWD, while a significant fraction remains in the nucleus.

Finally, we tested whether the reduced ability of DMWD to promote USP12 relocation to the PM could be mapped to the amino-terminal LCR or the carboxy-terminal C-tail motifs. However, DMWD mutants lacking either one or both motifs remained unable to promote full relocation of YFP-USP12 and YFP-NLS-USP12 to the PM (Fig. 10C).

Altogether, these results show that WDR20 and DMWD differently modulate USP12 localization. Specifically, DMWD promotes relocation of USP12 to the PM less efficiently than WDR20.

Discussion

Taking into account the potential clinical relevance of *DMWD* gene as a contributor to myotonic dystrophy (DM1) pathogenesis, it is remarkable that its protein product remains virtually uncharacterized. In particular, in spite of its similarity to WDR20, the potential role of DMWD as a regulator of the DUBs USP12 and USP46 has been completely overlooked. This may have been due, in part, to the fact that the first report of WDR20 as a USP12 regulator [10] was based on pull-down experiments carried out in HeLa cells. The amount of endogenous DMWD protein in this cell line is nearly 6 times lower that the amount of WDR20 [46], and Kee *et al.* [10] failed to identify DMWD as a USP12 interactor. Shortly afterward, another study in the same cells did identify DMWD, together with WDR48, WDR20, WDR26, and WDR77, as interacting partner of Flag-USP12 [47], but all subsequent

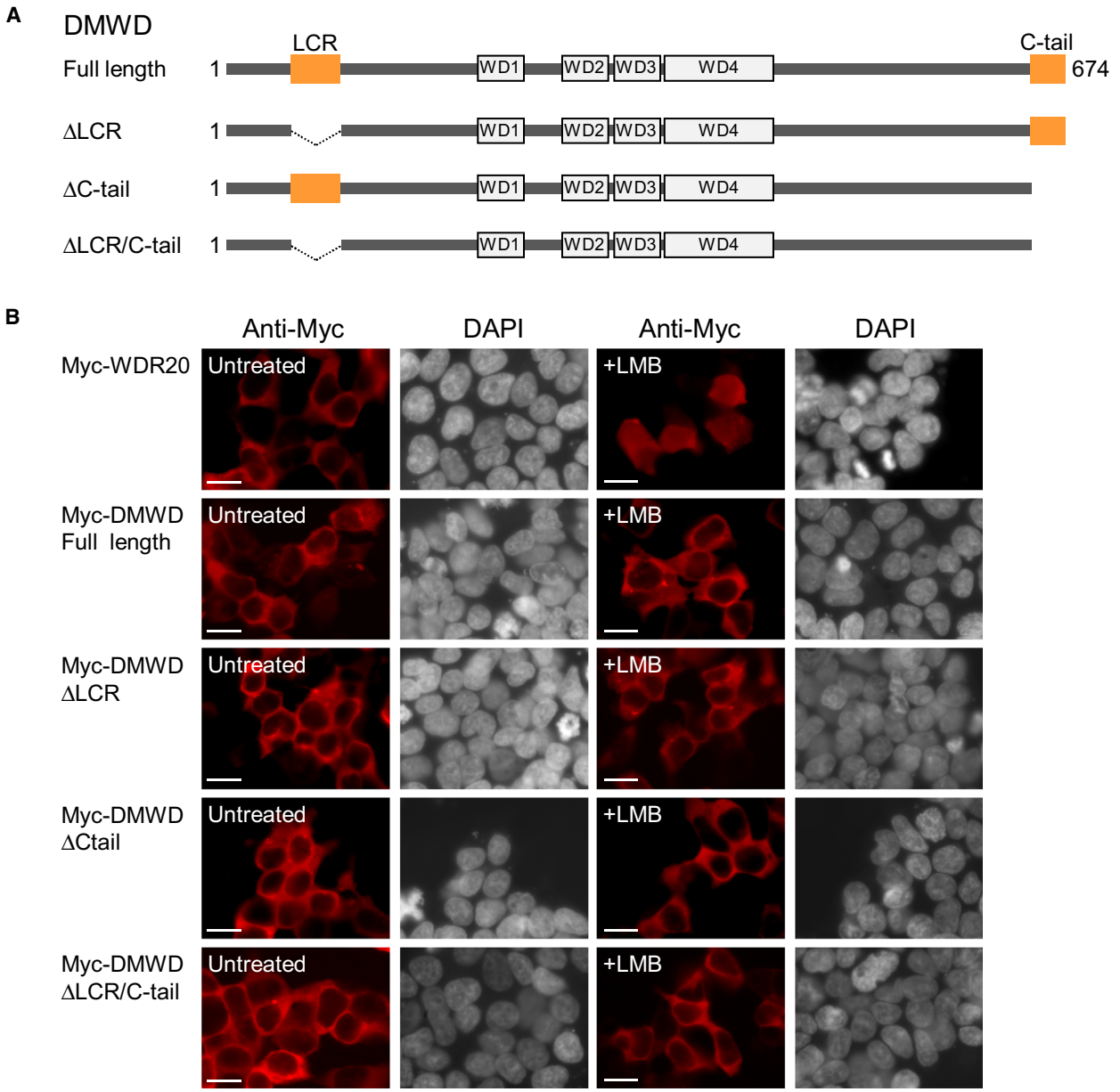

Fig. 9. Deletion of LCR and C-terminal tail motifs does not lead to increased DMWD nuclear entry. (A) Schematic representation of full-length DMWD and three deletion mutants lacking the N-terminal LCR (ΔLCR), the C-terminal tail (ΔC-tail), or both domains (ΔLCR/C-tail). (B) Fluorescence microscopy images of HEK293T cells showing the localization of the indicated protein in the absence (Untreated) or presence (+LMB) of the XPO1 inhibitor LMB. Cell nuclei were visualized using DAPI. The images shown correspond to one out of two independent experiments carried out. Similar results were obtained in both experiments. Scale bars = 10 μm.

studies on the regulation of USP12 and USP46 have been limited to WDR48 and/or WDR20. Here, we have used a combination of *in silico* and experimental approaches to shed some light on several aspects of DMWD biology.

Our molecular evolution and phylogenetic analyses reveal an interesting coincidence in the evolutionary history of two DUBs (USP12 and USP46) and their cofactors (WDR20 and DMWD). Our findings suggest that *WDR20* and *DMWD*, like *USP12* and *USP46*, arose by duplication of an ancestor gene during the vertebrate WGD events. WDR20 is more similar to the single ancestral copy present in invertebrates than DMWD, which has acquired several novel amino acid

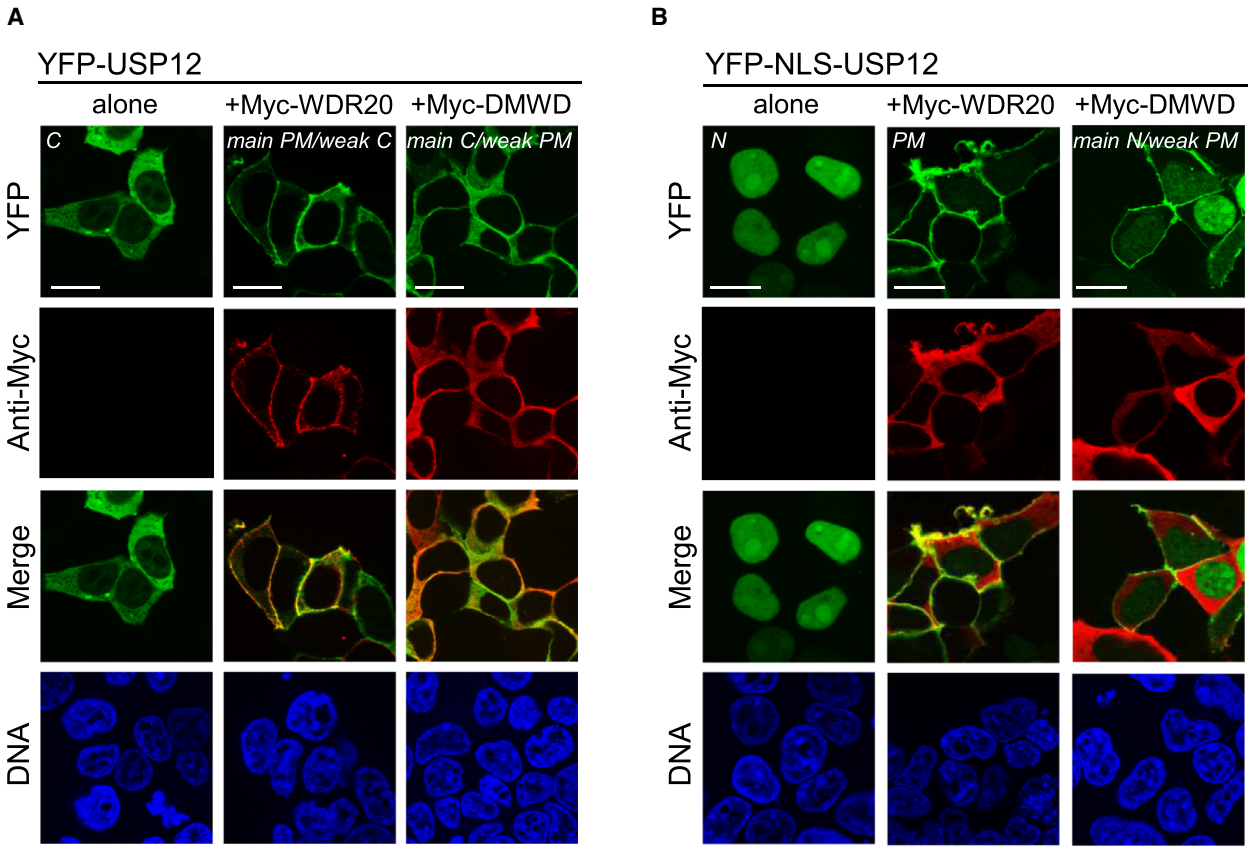

C

	Subcellular localization of YFP-tagged USP12 in HEK293T cells					
	Alone	+Myc-WDR20	+Myc-DMWD	+Myc-DMWD ΔLCR	+Myc-DMWD ΔC-tail	+Myc-DMWD ΔLCR/C-tail
YFP-USP12	C	Main PM weak C	Main C weak PM	Main C weak PM	Main C weak PM	Main C weak PM
YFP-NLS-USP12	N	PM	Main N weak PM	Main N weak PM	Main N weak PM	Main N weak PM

Fig. 10. Myc-DMWD promotes relocation of YFP-tagged USP12 to the PM less efficiently than Myc-WDR20. (A, B) Confocal microscopy images of HEK293T cells showing the localization of YFP-USP12 (panel A) or YFP-NLS-USP12 (panel B) when expressed alone and when coexpressed with Myc-WDR20 or Myc-DMWD. Cell nuclei were visualized using DAPI. The images shown correspond to a representative experiment out of 3 (panel A) or 2 (panel B) independent replicas. Similar results were consistently obtained in the different replicas. Based on an overall qualitative assessment of the sample, carried out in a blinded fashion, the localization of YFP-tagged USP12 proteins was categorized as indicated within each image (C: cytoplasm; N: nucleus). Coexpression with Myc-WDR20 led to a dramatic relocation of both YFP-USP12 and YFP-NLS-USP12 to the PM. In comparison, coexpression with Myc-DMWD had a much more limited effect. (C) Table summarizing the subcellular localization of YFP-tagged USP12 (either YFP-USP12 or YFP-NLS-USP12) in HEK293T cells when expressed alone or coexpressed with the indicated Myc-tagged proteins. Samples were qualitatively assessed in a blinded fashion, and the overall localization of YFP-tagged USP12 proteins was categorized as in panels A and B. When coexpressed with Myc-DMWD(ΔLCR), Myc-DMWD(ΔC-tail), or Myc-DMWD(ΔLCR/C-tail), the localization of YFP-tagged USP12 proteins is essentially nondistinguishable from their localization when coexpressed with full-length Myc-DMWD. Two independent experiments with Myc-DMWD deletion mutants were performed, with similar results. Scale bars = 10 μm.

sequence features that include a LCR proximal to its N terminus, and a C-tail. Since completely redundant copies of duplicated genes would be eliminated by selective pressure, the fact that both *WDR20* and *DMWD* are maintained in the vertebrate lineage suggests that these proteins have undergone some degree of functional diversification. This view is further supported by the recent finding that heterozygous deletion of DMWD in a mouse model of DM1 has clear phenotypic consequences [29], showing that WDR20 does not functionally substitute for DMWD. Thus, we sought to directly compare several crucial aspects of DMWD and WDR20 biology, including their expression level in human tissues, their interactome, and their ability to regulate the enzymatic activity and localization of USP12.

By analyzing publically available mRNA expression datasets, we found that the gene expression of *DMWD* in normal human tissues is more closely correlated to the expression of *USP12* than to the expression of *USP46*. Furthermore, the mRNA levels of *DMWD* and *USP46* were found to be negatively correlated in tumor samples. Therefore, although we confirmed that DMWD can bind to both USP12 and USP46, we decided to focus our subsequent functional comparison between DMWD and WDR20 on their role as regulators of USP12. We found that, like WDR20, DMWD enhances the catalytic activity of USP12. This finding expands the potential repertoire of active USP12 complexes, with different combinations of the cofactors (WDR48, WDR20, and DMWD) bound to the DUB. *In vitro* experiments with purified proteins will be needed to address the level of enzymatic activity of the different complexes. Importantly, we provide evidence that DMWD and WDR20 share the same binding interface in the 'Palm' domain of USP12. It is not uncommon for USP family members to interact with more than one WDR protein [reviewed in [8]]. However, this is, to the best of our knowledge, the first description of a DUB that binds two different (albeit closely related) WDR proteins using the same molecular interface. Our observations raise the interesting possibility that DMWD and WDR20 may compete for USP12 binding. This competition would need to be further characterized using *in vitro* experiments to establish the relative binding affinity of WDR20 and DMWD to USP12. Nonetheless, the results of our mutagenesis analyses strongly suggest that DMWD and WDR20 interact with USP12 in a mutually exclusive manner.

Beyond catalytic activation, WDR cofactors may contribute to DUB regulation by mediating the recruitment of substrates or other interacting proteins to DUB/WDR complexes. The first mechanism is exemplified by WDR48-mediated targeting of the USP1/WDR48 complex to its substrates ubiquitinated FANCD2 and ubiquitinated PCNA [48]. An example of the second mechanism is XPO1-dependent nuclear export of USP12, which is mediated by a NES motif in WDR20 [23]. Since the interactome of DMWD and WDR20 may contribute to define the set of cellular interactions of USP12 complexes, we compared the reported interactome of both cofactors using the BioGRID repository [42]. Although many of these interactions are derived from high-throughput proteomics analyses and remain to be further validated, some of the reported interactors, such as the PHLPP phosphatases, are *bona fide* USP12 substrates [15,19]. Remarkably, we found that DMWD and WDR20 are reported to interact with a largely different set of proteins. If, as suggested by our results, binding of DMWD and WDR20 to USP12 is mutually exclusive, their different interactomes could translate into differences in the set of proteins recruited to USP12 complexes containing one or the other cofactor. This would significantly expand the repertoire of cellular interactors and/or potential substrates of USP12 complexes.

A more detailed inspection of DMWD- and WDR20-specific interactors revealed differences in their subcellular localization, as annotated in Uniprot. Thus, a smaller fraction of 'DMWD-only' interactors was reported to localize to the nucleus or the PM, suggesting that DMWD may have a more limited access to these subcellular locations than WDR20. Indeed, we experimentally confirmed that, although both DMWD and WDR20 are nucleocytoplasmic shuttling proteins predominantly located in the cytoplasm, they exhibit different dynamics of transport between the nucleus and the cytoplasm. We have previously shown that WDR20 is not efficiently imported and proposed that it may enter the nucleus by passive diffusion [23]. Here, we show that DMWD enters the nucleus even less efficiently than WDR20. We speculate that, besides inefficient nuclear import, the localization of DMWD is largely determined by retention in the cytoplasm, while WDR20 relies on active nuclear export to attain its cytoplasmic localization. Our finding that the NES motif is only partially conserved and has weaker export activity in DMWD is consistent with this view: if DMWD is more efficiently retained in the cytoplasm, the selective pressure to maintain a highly active NES would be reduced. Similar to other cellular proteins [49], DMWD may bear sequence determinants that contribute to its increased cytoplasmic retention. Somewhat surprisingly, neither the LCR nor the C-tail

motifs (two obvious candidates, as they are absent in WDR20) were involved, according to our deletion analysis.

In addition to being less efficiently imported into the nucleus, DMWD also exhibits a more limited ability to promote relocation of USP12 to the PM than WDR20. Thus, although binding of either cofactor would increase the enzymatic activity of the USP12, the resulting DUB complexes may display different subcellular localization. This finding, combined with the strikingly different interactome of these two WDR proteins, leads us to propose a model whereby binding to DMWD or WDR20 may target USP12 DUB complexes to a different set of substrates in different subcellular compartments. Further studies will be needed to identify these substrates and define the potentially different biological function of DMWD- or WDR20-containing USP12 complexes.

Materials and methods

Phylogenetic and molecular evolutionary analyses

The coding sequences of WDR20 and DMWD orthologous genes, defined by Ensembl Compara, were downloaded. To test the hypothesis that WDR20 and DMWD arose by duplication of a common ancestor during the WGD events in early vertebrate evolution, more sequences of clades just after the appearance of vertebrates were needed. The earliest extant vertebrates are the cyclostomes (hagfishes and lampreys), but due to their early divergence from the gnathostomates after the WGD events, the paralogous genes in their genomes were most likely lost independently [50,51]. On the other hand, it is still unclear whether the second WGD event took place before or after the split between cyclostomes and gnathostomates [52]. Therefore, we used the oldest extant jawed vertebrates, chondrichthyans (cartilaginous fishes), as a reference. The only annotated chondrichthyan genome in Ensembl (accessed in November 2019) was the elephant shark (*Callorhincus milii*) genome. Thus, we performed reciprocal best BLAST (RBB) searches against other unannotated genomes from Skatebase [53] and NCBI genome databases (see Tables S1 and S2).

Sequences were aligned with MUSCLE [54]. Before tree construction, the resulting alignment was cleaned with Gblocks [55] to eliminate positions with poor alignment, enabling the options for a less stringent selection. Phylogenetic and molecular evolutionary analyses were conducted using MEGA version X [56]. The phylogenetic trees were constructed by the maximum-likelihood method using the Tamura–Nei model and testing with 500 bootstrap replications. Trees were rooted on *Strongylocentrotus purpuratus*.

In silico gene expression analyses and survey of DMWD and WDR20 annotated interactomes

Gene expression data from 17 382 healthy tissue samples were downloaded from the GTEx Portal [39] in the form of gene transcripts per millions (TPMs). The expression of *DMWD*, *WDR20*, *USP12*, and USP46 was displayed as either heatmap including all tissues or single-tissue box plots. Pairwise correlations were calculated with the non-parametric Spearman's rank correlation coefficient and data were displayed as density scatter plots of log2 TPM expression values.

On the other hand, the analysis of gene expression in tumor samples was carried out using the CANCERTOOL webpage (http://genomics.cicbiogune.es/CANCERTOOL/) [40], accessed in November 2018. Detailed information on the datasets is available through the CANCERTOOL webpage.

To compare the reported interactome of DMWD and WDR20, the BioGRID repository was accessed on November 2019, and the interactors for both proteins were retrieved. The annotated subcellular localizations of nonoverlapping interactors (i.e., proteins reported to interact only with DMWD or with WDR20) were retrieved from Uniprot. Only manual annotations were considered.

Cell culture, transfection, and drug treatment

HEK293T and HeLa cells were grown in Dulbecco's modified Eagle's medium supplemented with 10% FBS, 100 U·mL^{-1} penicillin, and 100 μg·mL^{-1} streptomycin (all from Thermo Fisher Scientific, Waltham, MA, USA). Cells were kept at 37 °C in a humidified atmosphere containing 5% CO_2. Twenty-four hours before transfection, cells were seeded as follows: 6.5×10^6 HEK293T cells per dish in 10 cm Petri dishes for co-IP analyses, 3×10^5 HEK293T cells per well in six-well plates for DUB activity assays, and 1.5×10^5 HEK293T or 1×10^5 HeLa cells per well in 12-well plates (with glass coverslips) for fluorescence microscopy analyses.

Transfections were carried out using X-tremeGENE 9 DNA transfection reagent (Roche Diagnostics, Indianapolis, IN, USA) or Lipofectamine 2000 (Thermo Fisher Scientific) following manufacturer's instructions. The total amount of DNA used for transfection was as follows: 600 ng per well in 12-well plates, 2500 ng per well in six-well plates, and 7200 ng per dish in 10 cm Petri dishes.

LMB (Apollo Scientific, Bredbury, Stockport, UK) and Selinexor (Selleckchem, Munich, Germany) were used as indicated.

Plasmids, cloning procedures, and site-directed mutagenesis

The plasmids encoding YFP-USP12 (wt and mutant V279D/F287A), YFP-NLS-USP12, YFP-USP46, and Myc-

WDR20 (wt and mutant F262A/F287A) have been previously described [23]. The plasmid encoding Xpress-WDR48 (UAF1) was generously provided by J. U. Jung (University of Southern California, Los Angeles, USA). The plasmid encoding Myc-DMWD was created using Gibson cloning methodology in two steps. First, two overlapping double-strand DNA fragments (gBlocks, IDT, Coralville, IA, USA) encoding full-length DMWD were assembled into the pEYFP-C1 vector (Invitrogen, Carlsbad, CA, USA) using Gibson Assembly® Cloning Kit (New England Biolabs, Ipswich, MA, USA) to create YFP-DMWD. Then, the DMWD cDNA was excised from YFP-DMWD as a HindIII/BamHI fragment and subcloned into pMyc-MCS, a modified version of pEYFP-C1 where the Myc epitope replaces YFP. A similar Gibson-based method was used to generate Myc-DMWD(ΔLCR), while Myc-DMWD(ΔC-tail) and Myc-DMWD(ΔLCR/C-tail) were created using a PCR-based approach. The mutant Myc-DMWD$^{F326A/W370A}$ was generated using the Quick-Change Lightning Site-Directed Mutagenesis Kit (Stratagene, La Jolla, CA, USA).

For the nuclear export assay, a double-stranded DNA fragment (geneBlocks, IDT) encoding DMWD NES sequence (512-AEPGTPFSIGRFATLTLQE-530) was cloned as a BamHI/PinAI fragment into the Rev(1.4)-GFP vector (a gift from B. Henderson, University of Sydney, Australia) to generate the reporter Rev(1.4)-[NES^{DMWD}]-GFP. The reporter Rev(1.4)-[NES^{WDR20}]-GFP, containing WDR20 NES, has been previously described [23].

All the new constructs were subjected to DNA sequencing (STABVIDA, Caparica, Portugal). The sequences of the gBlocks and oligonucleotides used are available upon request.

Coimmunoprecipitation and immunoblot

Twenty-four hours after transfection, all cells from each 10 cm Petri dish were collected in 1 mL of IP lysis buffer (Pierce) and lysed for 30 min on ice. Lysates were cleared by centrifugation (15781 ***g*** for 10 min at 4 °C), and 50 μL of cleared lysate was stored to be used as whole cell extract (WCE). The remaining 950 μL of lysate was subjected to anti-GFP immunoprecipitation using the GFP-Trap_MA reagent (Chromotek, Planegg-Martinsried, Germany), following manufacturer's protocol. Immunoprecipitated (IP) proteins were eluted by boiling the beads (95 °C, 5 min) in 80 μL of 2× SDS sample buffer. For immunoblot analysis, the 50 μL of WCE and the 80 μL of eluted, IP proteins were loaded onto 10% SDS/PAGE gels, resolved by electrophoresis, and transferred to a nitrocellulose membrane. Membranes were blocked with 5% nonfat dry milk diluted in TTBS for 1 h and incubated with the primary antibodies: anti-GFP (Chromotek, 1 : 1000) or anti-Myc (Cell Signaling Technology, Danvers, MA, USA, 1 : 2000). Subsequently, membranes were incubated with the corresponding horseradish peroxidase-conjugated secondary antibody (Santa Cruz, Dallas, TX, USA, 1 : 3000), washed, and developed using ECL (Thermo Fisher Scientific).

DUB activity assay

HEK293T cells growing in six-well trays were transfected with the different constructs. Per well, the amount of DNA used for each construct was as follows: 400 ng of YFP-USP12, 400 ng of Xpress-WDR48, and 200 ng of either Myc-WDR20 or Myc-DMWD. Empty pCDNA plasmid DNA was added to equalize the total amount of DNA transfected per well to 2500 ng. After 48 h, cells were lysed with HR buffer (50 mM Tris pH 7.5, 5 mM $MgCl_2$, 250 mM sucrose, 1 mM DTT, 2 mM ATP, 1 mM AEBSF, 25 mM β-Glycerophosphate, 1 mM O-Vanadate and 50 mM NaF) under mechanical disruption with a 27G syringe. HA-ubiquitin vinyl sulfone probe was incubated with protein extracts for 2 h at 25 °C shaking at 1250 r.p.m. Finally, the extracts were migrated in SDS/PAGE gels, and membranes were probed with the corresponding antibodies.

Immunofluorescence and fluorescence microscopy

Twenty-four hours after transfection, cells were fixed with 3.7% formaldehyde in PBS for 30 min, permeabilized with 0.2% Triton X-100 in PBS for 10 min, blocked for 1 h in blocking solution (3% BSA in PBS), and incubated with anti-Myc primary antibody (Cell Signaling Technology; 1 : 300) diluted in blocking solution for 1 h at room temperature. Cells were then washed with PBS and incubated with an Alexa Fluor 594-conjugated secondary antibody (Invitrogen; 1 : 400) for 1 h at room temperature. Coverslips were washed with PBS and mounted onto microscope slides using Vectashield mounting medium containing 4′,6-diamidino-2-phenylindole (DAPI; Vector Laboratories, Burlingame, CA, USA). Images were acquired using either a Zeiss Axioskop with NIS Elements software or a Zeiss ApoTome.2 microscope with Zen2.6 Blue edition software (Carl Zeiss Microscopy, Oberkochen, Germany). Immunofluorescence samples were analyzed in a qualitative or semiquantitative manner. For qualitative analysis (e.g., subcellular localization of YFP-USP12 when coexpressed with different Myc-DMWD deletion mutants), the overall localization of the protein of interest in each sample was assessed. For semiquantitative analysis (e.g., percentage of cells showing nuclear, cytoplasmic, or nuclear/cytoplasmic localization of the protein of interest in cells treated or not with LMB), at least 200 individual cells were assessed per sample. In both cases, the analysis was carried out in a blinded fashion to ensure unbiased results. To this end, the identity of the samples was coded before microscopy analysis.

Nuclear export assay

A nuclear export assay [45] was carried out as detailed previously [23] to compare the NESs motifs of WDR20 and DMWD.

Briefly, the reporter plasmids Rev(1.4)-[NES^{WDR20}]-GFP and Rev(1.4)-[NES^{DMWD}]-GFP (see above) were transfected into HeLa cells. The empty Rev(1.4)-GFP plasmid was included as negative control. Each plasmid was transfected in two wells of a 12-well tray. At 24 h post-transfection, 10 $\mu g \cdot mL^{-1}$ cycloheximide (Sigma, St. Louis, MO, USA) was added to all the wells to arrest protein translation and thus ensure that any fluorescent signal present in the cytoplasm corresponds to exported proteins and not to newly synthesized GFP-tagged proteins. For each reporter, the cells in one of the wells were additionally treated with 5 $\mu g \cdot mL^{-1}$ actinomycin D (ActD; Sigma) to block nuclear import mediated by Rev NLS. Three hours after drug treatment cells were fixed, washed, and mounted for microscopy analysis. This analysis was carried out in a blinded fashion. The subcellular localization of the GFP-tagged proteins was examined in at least 200 cells per sample using a Zeiss Axioskop fluorescence microscope, and the proportion of cells where the reporter shows nuclear, nuclear, and cytoplasmic or cytoplasmic localization was determined. Based on this proportion, WDR20 and DMWD NESs were assigned a nuclear export activity score as described in the original paper [45].

Acknowledgements

We are grateful to Jae U. Jung and Beric Henderson for sharing plasmids. We appreciate the technical support by the staff from the High Resolution Microscopy Facility (SGIKER-UPV/EHU). JAR is supported by grants from the Spanish Government MINECO-FEDER (SAF2014-57743-R), the Basque Country Government (IT1257-19), the University of the Basque Country UPV/EHU (UFI11/20) and the PROTEOSTASIS BM1307 COST (Cooperation in Science and Technology) Action, financed by the European Union. The work of EB is supported by the Basque Department of Industry, Tourism and Trade (Elkartek) and the MINECO (BFU2016-76872-R (FEDER/EU), PID2019-108112RB-I00, Severo Ochoa Excellence Accreditation SEV-2016-0644, and Excellence Networks SAF2017-90794-REDT). BJ is supported by the University of the Basque Country UPV/EHU (UFI11/20; GIU14/20 and PPGA20/17). AO-H, MB-A and EV-M received fellowships from the University of the Basque Country UPV/EHU. MS is the recipient of a fellowship from the Basque Country Government.

Conflict of interest

The funding sources had no involvement in study design; in the collection, analysis, and interpretation of data; in the writing of the report; or in the decision to submit the article for publication. The authors do not have competing interests to declare.

Author contributions

AO-H planned and performed experiments and analyzed data. MB-A analyzed data. OC performed experiments. MS performed experiments. EV-M analyzed data. BMJ analyzed data. EB planned experiments and analyzed data. JAR conceived the study, planned experiments, analyzed data, and wrote the paper.

Peer Review

The peer review history for this article is available at https://publons.com/publon/10.1111/febs.15875.

References

1 Komander D & Rape M (2012) The ubiquitin code. *Annu Rev Biochem* **81**, 203–229.
2 Reyes-Turcu FE, Ventii KH & Wilkinson KD (2009) Regulation and cellular roles of ubiquitin-specific deubiquitinating enzymes. *Annu Rev Biochem* **78**, 363–397.
3 Clague MJ, Urbé S & Komander D (2019) Breaking the chains: deubiquitylating enzyme specificity begets function. *Nat Rev Mol Cell Biol* **20**, 338–352.
4 Leznicki P & Kulathu Y (2017) Mechanisms of regulation and diversification of deubiquitylating enzyme function. *J Cell Sci* **130**, 1997–2006.
5 Komander D, Clague MJ & Urbé S (2009) Breaking the chains: structure and function of the deubiquitinases. *Nat Rev Mol Cell Biol* **10**, 550–563.
6 Sahtoe DD & Sixma TK (2015) Layers of DUB regulation. *Trends Biochem Sci* **40**, 456–467.
7 Sowa ME, Bennett EJ, Gygi SP & Harper JW (2009) Defining the human deubiquitinating enzyme interaction landscape. *Cell* **138**, 389–403.
8 Villamil MA, Liang Q & Zhuang Z (2013) The WD40-repeat protein-containing deubiquitinase complex: catalysis, regulation, and potential for therapeutic intervention. *Cell Biochem Biophys* **67**, 111–126.
9 Cohn MA, Kee Y, Haas W, Gygi SP & D'Andrea AD (2009) UAF1 is a subunit of multiple deubiquitinating enzyme complexes. *J Biol Chem* **284**, 5343–5351.
10 Kee Y, Yang K, Cohn MA, Haas W, Gygi SP & D'Andrea AD (2010) WDR20 regulates activity of the

USP12 x UAF1 deubiquitinating enzyme complex. *J Biol Chem* **285**, 11252–11257.
11 Yin J, Schoeffler AJ, Wickliffe K, Newton K, Starovasnik MA, Dueber EC & Harris SF (2015) Structural insights into WD-repeat 48 activation of ubiquitin-specific protease 46. *Structure* **23**, 2043–2054.
12 Li H, Lim KS, Kim H, Hinds TR, Jo U, Mao H, Weller CE, Sun J, Chatterjee C, D'Andrea AD *et al.* (2016) Allosteric activation of ubiquitin-specific proteases by β-propeller proteins UAF1 and WDR20. *Mol Cell* **63**, 249–260.
13 Dharadhar S, Clerici M, van Dijk WJ, Fish A & Sixma TK (2016) A conserved two-step binding for the UAF1 regulator to the USP12 deubiquitinating enzyme. *J Struct Biol* **196**, 437–447.
14 Zhu H, Zhang T, Wang F, Yang J & Ding J (2019) Structural insights into the activation of USP46 by WDR48 and WDR20. *Cell Discov* **5**, 34.
15 Gangula NR & Maddika S (2013) WD repeat protein WDR48 in complex with deubiquitinase USP12 suppresses Akt-dependent cell survival signaling by stabilizing PH domain leucine-rich repeat protein phosphatase 1 (PHLPP1). *J Biol Chem* **288**, 34545–34554.
16 Li X, Stevens PD, Yang H, Gulhati P, Wang W, Evers BM & Gao T (2013) The deubiquitination enzyme USP46 functions as a tumor suppressor by controlling PHLPP-dependent attenuation of Akt signaling in colon cancer. *Oncogene* **32**, 471–478.
17 Moretti J, Chastagner P, Liang CC, Cohn MA, Israël A & Brou C (2012) The ubiquitin-specific protease 12 (USP12) is a negative regulator of notch signaling acting on notch receptor trafficking toward degradation. *J Biol Chem* **287**, 29429–29441.
18 Burska UL, Harle VJ, Coffey K, Darby S, Ramsey H, O'Neill D, Logan IR, Gaughan L & Robson CN (2013) Deubiquitinating enzyme Usp12 is a novel co-activator of the androgen receptor. *J Biol Chem* **288**, 32641–32650.
19 McClurg UL, Summerscales EE, Harle VJ, Gaughan L & Robson CN (2014) Deubiquitinating enzyme Usp12 regulates the interaction between the androgen receptor and the Akt pathway. *Oncotarget* **5**, 7081–7092.
20 McClurg UL, Harle VJ, Nabbi A, Batalha-Pereira A, Walker S, Coffey K, Gaughan L, McCracken SR & Robson CN (2015) Ubiquitin-specific protease 12 interacting partners Uaf-1 and WDR20 are potential therapeutic targets in prostate cancer. *Oncotarget* **6**, 37724–37736.
21 Jahan AS, Lestra M, Swee LK, Fan Y, Lamers MM, Tafesse FG, Theile CS, Spooner E, Bruzzone R, Ploegh HL *et al.* (2016) Usp12 stabilizes the T-cell receptor complex at the cell surface during signaling. *Proc Natl Acad Sci USA* **113**, E705–E714.
22 Huo Y, Khatri N, Hou Q, Gilbert J, Wang G & Man HY (2015) The deubiquitinating enzyme USP46 regulates AMPA receptor ubiquitination and trafficking. *J Neurochem* **134**, 1067–1080.
23 Olazabal-Herrero A, Sendino M, Arganda-Carreras I & Rodríguez JA (2019) WDR20 regulates shuttling of the USP12 deubiquitinase complex between the plasma membrane, cytoplasm and nucleus. *Eur J Cell Biol* **98**, 12–26.
24 Hodul M, Dahlberg CL & Juo P (2017) Function of the deubiquitinating enzyme USP46 in the nervous system and its regulation by WD40-repeat proteins. *Front Synaptic Neurosci* **9**, 16.
25 Kouranti I, McLean JR, Feoktistova A, Liang P, Johnson AE, Roberts-Galbraith RH & Gould KL (2010) A global census of fission yeast deubiquitinating enzyme localization and interaction networks reveals distinct compartmentalization profiles and overlapping functions in endocytosis and polarity. *PLoS Biol* **8**, e1000471.
26 Vlasschaert C, Cook D, Xia X & Gray DA (2017) The evolution and functional diversification of the deubiquitinating enzyme superfamily. *Genome Biol Evol* **9**, 558–573.
27 LoRusso S, Weiner B & Arnold WD (2018) Myotonic dystrophies: targeting therapies for multisystem disease. *Neurotherapeutics* **15**, 872–884.
28 Lanni S & Pearson CE (2019) Molecular genetics of congenital myotonic dystrophy. *Neurobiol Dis* **132**, 104533.
29 Yin Q, Wang H, Li N, Ding Y, Xie Z, Jin L, Li Y, Wang Q, Liu X, Xu L *et al.* (2020) Dosage effect of multiple genes accounts for multisystem disorder of myotonic dystrophy type 1. *Cell Res* **30**, 133–145.
30 Sievers F, Wilm A, Dineen D, Gibson TJ, Karplus K, Li W, Lopez R, McWilliam H, Remmert M, Söding J *et al.* (2011) Fast, scalable generation of high-quality protein multiple sequence alignments using Clustal Omega. *Mol Syst Biol* **7**, 539.
31 Glasauer SMK & Neuhauss SC (2014) Whole-genome duplication in teleost fishes and its evolutionary consequences. *Mol Genet Genomics* **289**, 1045–1060.
32 Hamshere MG, Newman EE, Alwazzan M, Athwal BS & Brook JD (1997) Transcriptional abnormality in myotonic dystrophy affects DMPK but not neighboring genes. *Proc Natl Acad Sci USA* **94**, 7394–7399.
33 Alwazzan M, Newman E, Hamshere MG & Brook JD (1999) Myotonic dystrophy is associated with a reduced level of RNA from the DMWD allele adjacent to the expanded repeat. *Hum Mol Genet* **8**, 1491–1497.
34 Eriksson M, Hedberg B, Carey N & Ansved T (2001) Decreased DMPK transcript levels in myotonic dystrophy 1 type IIA muscle fibers. *Biochem Biophys Res Commun* **286**, 1177–1182.

35 Frisch R, Singleton KR, Moses PA, Gonzalez IL, Carango P, Marks HG & Funanage VL (2001) Effect of triplet repeat expansion on chromatin structure and expression of DMPK and neighboring genes, SIX5 and DMWD, in myotonic dystrophy. *Mol Genet Metab* **74**, 281–291.
36 Westerlaken JH, Van der Zee CE, Peters W & Wieringa B (2003) The DMWD protein from the myotonic dystrophy (DM1) gene region is developmentally regulated and is present most prominently in synapse-dense brain areas. *Brain Res* **971**, 116–127.
37 Wang ET, Treacy D, Eichinger K, Struck A, Estabrook J, Olafson H, Wang TT, Bhatt K, Westbrook T, Sedehizadeh S *et al.* (2019) Transcriptome alterations in myotonic dystrophy skeletal muscle and heart. *Hum Mol Genet* **28**, 1312–1321.
38 Ritchie ME, Phipson B, Wu D, Hu Y, Law CW, Shi W & Smyth GK (2015) limma powers differential expression analyses for RNA-sequencing and microarray studies. *Nucleic Acids Res* **43**, e47.
39 The GTEx Consortium (2020) The GTEx Consortium atlas of genetic regulatory effects across human tissues. *Science* **369**, 1318–1330.
40 Cortazar AR, Torrano V, Martín-Martín N, Caro-Maldonado A, Camacho L, Hermanova I, Guruceaga E, Lorenzo-Martín LF, Caloto R, Gomis RR *et al.* (2018) CANCERTOOL: a visualization and representation interface to exploit cancer datasets. *Cancer Res* **78**, 6320–6328.
41 Borodovsky A, Ovaa H, Kolli N, Gan-Erdene T, Wilkinson KD, Ploegh HL & Kessler BM (2002) Chemistry-based functional proteomics reveals novel members of the deubiquitinating enzyme family. *Chem Biol* **9**, 1149–1159.
42 Stark C, Breitkreutz B-J, Reguly T, Boucher L, Breitkreutz A & Tyers M (2006) BioGRID: a general repository for interaction datasets. *Nucleic Acids Res* **34** (Database issue), D535–D539.
43 The UniProt Consortium (2019) UniProt: a worldwide hub of protein knowledge. *Nucleic Acids Res* **47**, D506–D515.
44 Kudo N, Wolff B, Sekimoto T, Schreiner EP, Yoneda Y, Yanagida M, Horinouchi S & Yoshida M (1998) Leptomycin B inhibition of signal-mediated nuclear export by direct binding to CRM1. *Exp Cell Res* **242**, 540–547.
45 Henderson BR & Eleftheriou A (2000) A comparison of the activity, sequence specificity, and CRM1-dependence of different nuclear export signals. *Exp Cell Res* **256**, 213–224.
46 Kulak NA, Pichler G, Paron I, Nagaraj N & Mann M (2014) Minimal, encapsulated proteomic-sample processing applied to copy-number estimation in eukaryotic cells. *Nat Methods* **11**, 319–324.
47 Joo HY, Jones A, Yang C, Zhai L, Smith AD 4th, Zhang Z, Chandrasekharan MB, Sun ZW, Renfrow MB, Wang Y *et al.* (2011) Regulation of histone H2A and H2B deubiquitination and Xenopus development by USP12 and USP46. *J Biol Chem* **286**, 7190–7201.
48 Yang K, Moldovan GL, Vinciguerra P, Murai J, Takeda S & D'Andrea AD (2011) Regulation of the Fanconi anemia pathway by a SUMO-like delivery network. *Genes Dev* **25**, 1847–1858.
49 Patenaude AM, Orthwein A, Hu Y, Campo VA, Kavli B, Buschiazzo A & Di Noia JM (2009) Active nuclear import and cytoplasmic retention of activation-induced deaminase. *Nat Struct Mol Biol* **16**, 517–527.
50 Smith JJ, Kuraku S, Holt C, Sauka-Spengler T, Jiang N, Campbell MS, Yandell MD, Manousaki T, Meyer A, Bloom OE *et al.* (2013) Sequencing of the sea lamprey (Petromyzon marinus) genome provides insights into vertebrate evolution. *Nat Genet* **45**, 415–421.
51 Sacerdot C, Louis A, Bon C, Berthelot C & Roest Crollius H (2018) Chromosome evolution at the origin of the ancestral vertebrate genome. *Genome Biol* **19**, 166.
52 Holland LZ & Ocampo Daza D (2018) A new look at an old question: when did the second whole genome duplication occur in vertebrate evolution? *Genome Biol* **19**, 209.
53 Wyffels J, King BL, Vincent J, Chen C, Wu CH & Polson SW (2014) SkateBase, an elasmobranch genome project and collection of molecular resources for chondrichthyan fishes. *F1000Res* **3**, 191.
54 Edgar RC (2004) MUSCLE: multiple sequence alignment with high accuracy and high throughput. *Nucleic Acids Res* **32**, 1792–1797.
55 Castresana J (2000) Selection of conserved blocks from multiple alignments for their use in phylogenetic analysis. *Mol Biol Evol* **17**, 540–552.
56 Kumar S, Stecher G, Li M, Knyaz C & Tamura K (2018) MEGA X: molecular evolutionary genetics analysis across computing platforms. *Mol Biol Evol* **35**, 1547–1549.

Supporting information

Additional Supporting Information may be found online in the Supporting Information section at the end of the article.

Table S1. Sequences used for the phylogenetic analysis of WDR20.

Table S2. Sequences used for the phylogenetic analysis of DMWD.

Table S3. DMWD and WDR20 interactors reported in the BioGRID repository as of November 2019.

Ekaia, 2021, 41, 151-169
https://doi.org/10.1387/ekaia.22591

ekaia
ZIENTZIA eta TEKNOLOGIA ALDIZKARIA

ISSN 0214-9001 – eISSN 2444-3255

Konpartimentu espezifikoko gertuko biotinilazioa: XPO1en esportazio-kargoak identifikatzeko hurbilketa berria

(Compartment-specific proximity biotinylation: a new approach to identify nuclear export cargos of XPO1)

Maria Sendino[1], *Juanma Ramírez*[2], *Ugo Mayor*[2,3], *Gorka Prieto*[4], *Miren Josu Omaetxebarria*[2], *Jose Antonio Rodríguez**[1]

[1] Genetika, Antropologia Fisikoa eta Animalien Fisiologia Saila, Zientzia eta Teknologia Fakultatea, Leioa (UPV/EHU)
[2] Biokimika eta Biologia Molekularra Saila, Zientzia eta Teknologia Fakultatea, Leioa (UPV/EHU)
[3] Ikerbasque Ikerkuntzarako Euskal Fundazioa, Bilbo
[4] Komunikazioen Ingeniaritza Saila, Bilboko Ingeniaritza Eskola (UPV/EHU)

LABURPENA: Nukleo eta zitoplasmaren arteko banaketa da zelula eukariotoen ezaugarririk bereizgarriena. Konpartimentuok fisikoki banaturik egon arren, elkarren arteko komunikazioa etengabea da, eta horretarako estuki erregulaturiko garraio-sistema dago, zeina zelularen homeostasia mantendu eta minbizia eta gisako gaixotasunak ekideiteko ezinbestekoa den. Garraio-sistema horretako pieza gakoa XPO1 esportina da, zeinak kargo deritzen proteina askoren nukleotik zitoplasmaranzko esportazioa egikaritzen duen. Esportina horren eta minbiziaren arteko lotura maiz aipatu izan da, eta badira XPO1 inhibitzen duten agente terapeutikoak. XPO1en inhibizioak bere kargoen banaketa azpizelularrean aldaketak eragingo dituela espero daiteke. Alabaina, XPO1en kargo asko ezagunak badira ere, haren kargo bilduma osoa ez da zehaztu oraindik, eta horrek XPO1 ikerketa proteomikoetarako kandidatu oso interesgarri bilakatzen du. Hori horrela, estrategia proteomiko berri bat diseinatu dugu, zeinean APEX2 peroxidasa erabiliz konpartimentu espezifikoko gertuko biotinilazioa burutu dugun XPO1en kargo berriak bilatzeko. Horretarako, APEX2 zitoplasma eta nukleora iturutu dugu eta, biotinilatutako proteinak afinitate-purifikazioz isolatu ostean, masa-espektrometriaz identifikatu ditugu. Lan honetan azaldutako kontzeptu-froga esperimentuaren emaitzek erakusten dute estrategia hori, XPO1en inhibizio espezifikoarekin konbinatuz, kargo berriak identifikatzeko baliagarria izan daitekeela. Hurbilketa berri honek beraz, kargo gehiagoren identifikazioa erraztearekin batera, XPO1en mendeko garraioan sakondu eta terapeutikoki erabiltzen diren XPO1en inhibitzaileek zelula mailan duten eragina argitzeko ere balio dezake.

HITZ GAKOAK: XPO1, CRM1, garraio nukleozitoplasmatikoa, gertuko biotinilazioa, MS/MS, kargoa.

ABSTRACT: *A major feature of eukaryotic cells is the separation between nucleus and cytoplasm. Although physically separated, these two compartments are in permanent communication through a transport system that must be precisely regulated to maintain cell homeostasis and avoid serious diseases, such as cancer. A crucial element in this transport system is the exportin XPO1, which exports many proteins (so-called cargoes) from the nucleus to cytoplasm. XPO1 alteration has been frequently associated with cancer and XPO1 is an important therapeutic target. The cellular effect of XPO1 inhibition is expected to be mediated by changes in the subcellular distribution of its cargoes. However, while many of XPO1 cargoes have been already identified, the complete set remains uncharacterized, making XPO1 a very interesting candidate for proteomic studies. Thus, we have designed a novel proteomics strategy, based on compartment-specific proximity biotinylation using the APEX2 peroxidase, to search for XPO1 cargos. To this end, we have targeted APEX2 to cytoplasm and nucleus, isolated the biotinylated proteins by affinity purification, and identified them by mass spectrometry. The results of a proof-of concept experiment reported here show that this strategy, combined with specific XPO1 inhibition, can lead to the identification of XPO1 cargoes. This novel approach, therefore, may advance our understanding of XPO1-dependent nuclear export by facilitating the identification of novel cargoes, and may also contribute to better characterize the cellular effect of therapeutically used XPO1 inhibitors.*

KEYWORDS: XPO1, CRM1, nucleocytoplasmic transport, proximity biotinylation, MS/MS, cargo.

**** Harremanetan jartzeko / Corresponding author:*** Jose Antonio Rodríguez. Genetika, Antropologia Fisikoa eta Animalien Fisiologia Saila, Zientzia eta Teknologia Fakultatea, Leioa (UPV/EHU), Sarriena auzoa, zg (48940 Leioa). . – josean.rodriguez@ehu.es – https://orcid.org/0000-0002-2823-3733

Nola aipatu / How to cite: Sendino, Maria; Ramírez, Juanma; Mayor, Ugo; Prieto, Gorka; Omaetxebarria, Miren Josu; Rodríguez, Jose Antonio (2021). «Konpartimentu espezifikoko gertuko biotinilazioa: XPO1en esportazio-kargoak identifikatzeko hurbilketa berria». *Ekaia*, 41, 2021, 151-169. (https://doi.org/10.1387/ekaia.22591).

Jasotze-data: 2021, martxoak 11; Onartze-data: 2021, maiatzak 18.

ISSN 0214-9753 - eISSN 2444-3581 / © 2021 UPV/EHU

1. SARRERA

1.1. Proteinen garraio nukleozitoplasmatikoa: prozesua bera eta minbiziaren garapenarekin duen lotura

Zelula eukariotoek unean uneko beharrizanen arabera nukleo eta zitoplasmaren artean proteinak lekualdatzeko gai den garraio-sistema garatu dute. Proteinen nukleo eta zitoplasmaren arteko garraiorako bi hartzaile mota dira ezinbesteko: inportinak, kargo proteinak zitoplasmatik nukleora garraiatzen dituztenak, eta esportinak, kargoak nukleotik zitoplasmara garraiatzen dituztenak. Hartzaileok garraiatuko dituzten kargoen aminoazido segida laburrak diren seinale espezifikoak ezagutu eta lotuko dituzte: inportinek nukleora lokalizatzeko seinaleak (NLS), esportinek aldiz, nukleotik esportatzeko seinaleak (NES) [1].

Nukleo eta zitoplasmaren arteko garraio-sistema estuki erregulatuta egotea ezinbestekoa da zelulen homeostasia mantentzeko. Asaldurarik gertatuz gero, minbizia eta gisako gaixotasun larriak sor daitezke. Ikergai dugun XPO1 proteina (CRM1 izenaz ere ezaguna) nukleotik zitoplasmaranzko proteinen garraioan aritzen den esportina da [2-5]. Ikerketa proteomikoen bidez aurreikusi da XPO1ek mila proteina ingururen esportazioa eragiten duela, hau da, mila kargo inguru dituela [6]. XPO1en kargo ugari jada ezagunak badira ere, ez dugu oraindik XPO1en esportazio-kargo bilduma osoa, XPO1en esportoma, ezagutzen. XPO1ek minbiziarekin zerikusi estua ere badu: XPO1en gainadierazpena gaixoen prognosi okerrarekin erlazionatu da maiz [1-en berrikusia], eta XPO1en mutazio onkogenikoak ere aurkitu izan dira [7]. Horrek, XPO1 minbiziaren aurkako itu terapeutiko garrantzitsu bilakatu du [8], eta berriki, XPO1en inhibitzailea den selinexor farmakoak mieloma anizkoitza tratatzeko oniritzia jaso du [9]. Selinexor farmakoak XPO1 kargoen NESetara lotzea eragozten du. Hortaz, XPO1en inhibizioak zelula mailan duen eragin zehatza ezagutu ez arren, kargo askoren banaketa aldatuko duela aurreikus daiteke. Kargo horiek zein diren jakiteak minbiziaren aurkako terapien garapenean garrantzi handia izan dezake. Horregatik guztiagatik, XPO1 proteomikarako aztergai interesgarria da.

1.2. Proteomikaren bidezko XPO1en kargoen identifikazioa

Proteomikak sistema biologikoetako proteinak identifikatzea, kuantifikatzea eta proteinen arteko elkarrekintzak ezagutzea ahalbidetzen du [10]. Proteomikan oinarritutako XPO1en esportomaren karakterizaziorako ikerketak ere badira [6, 11]. Ikerketa horietan, XPO1en kargoak identifikatzeko proteomikan oso ohikoak diren bi prozedura erabili dira: zelulen frakzionamendua [11] eta afinitate-purifikazioa [6].

Aipatutako bi prozedurok emaitza onak ematen dituzten arren, mugak ere badituzte. Zelulen frakzionamenduan, esaterako, purutasun handiko

frakzioak lortzea zaila da. Afinitate-purifikazioari dagokionez, ohikoa da amua den proteinari estuki lotzen ez zaizkion proteinak prozeduran zehar galtzea [12]. Azken horrek badu zuzeneko eragina XPO1en esportoma aztertzerakoan, XPO1 eta bere kargoen arteko lotura oso ahula izan ohi baita [13]. Muga horiek buruan, hurbilketa berriak garatu dira azkenaldian proteomika arloan, hala nola proteinen gertuko biotinilazioa (PGB) [14]. PGB XPO1en esportomaren karakterizaziorako prozedura baliagarria denetz aztertzeko artikulu honetan deskribatutako kontzeptu-froga ikerketa osatu dugu.

1.3. **Proteinen gertuko biotinilazioa (PGB)**

PGB prozedura entzima markatzaileen erabileran oinarritzen da. Entzima horiek zelula barneko intereseko organulu edo konpartimentura ituratuko dira, eta substratu egokiaren presentzian, gertuko proteinei biotina gehituko die. PGB bidez biotinilatutako proteinak bestelako proteinetatik bereizteko, laginetako zelulak jaso, proteinak erauzi eta biotina marka duten proteinak abidinan oinarritutako afinitate-purifikazioaren bidez isolatuko dira. Biotinaz markatutako proteinetan aberastutako frakzioa tandem masa-espektrometriaz (MS/MS) analizatuko da bertako proteinak identifikatzeko (1. irudia). Egun, biotina-ligasak (BirA* esaterako) [14, 15] eta peroxidasak (APEX2, esaterako) [16-18] dira entzima markatzaile erabilienak [12 eta 19-n berrikusia]. BirA* entzimak mediora gehitutako biotina substratutzat hartu, eta gertuko proteinak biotinilatzen ditu 15-24 orduko epean [20]. APEX2 peroxidasaren kasuan, zelulek 30 minutuz mediora gehitutako biotin-fenola barneratuko dute, jarraian APEX2a H_2O_2-arekin aktibatu eta minutu bakar batean gertuko proteinen biotinilazio eraginkorra ematen da.

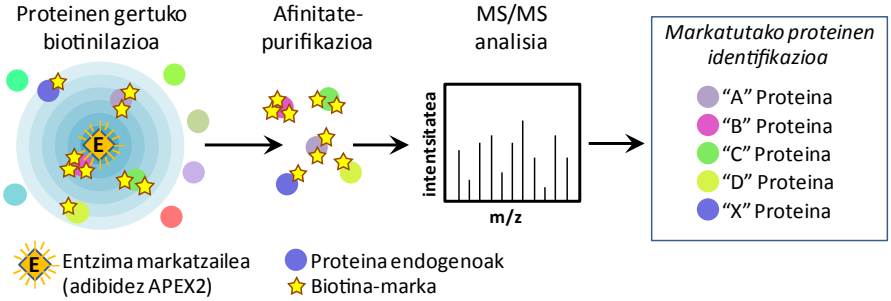

1. irudia. PGB bidezko proteinen identifikazioa. Entzima markatzailea beharrezko substratuaren presentzian inguruko proteinetan biotina-marka kobalenteak ezarriko ditu. Biotina-markei esker, entzimatik gertu dauden proteinak zelulako bestelako proteinetatik banatu ahal izango dira afinitate-purifikazioaren bidez. Azkenik, purifikatutako proteinak MS/MS bidez identifikatuko dira.

PGB prozedura ikergaiaren arabera egokitu daiteke, hots, ikergaia proteina baten interaktoma bada, entzima markatzailea proteina jakin horrekin fusionatuko da [21-24]. Ikergaia, ordea, konpartimentu bateko proteoma bada, entzima markatzailea intereseko kokapen horretara ituratuko da [14, 17, 25-27]. Guk dakigula, gure ikergaia den XPO1en esportoma ez da PGB bidez aztertu, eta beraz, ekarpen interesgarria egin dezakeelakoan, PGB testuinguru honetara egokitu dugu.

1.4. XPO1en kargo prototipikoak identifikatzeko konpartimentu espezifikoko PGB estrategia

XPO1en kargo prototipikoak bilatzeko orduan bi kontu aintzat hartu behar dira. Bata, proteinen nukleo eta zitoplasmaren arteko garraioa etengabekoa dela, eta, beraz, PGB azkar gertatzea beharrezkoa dela. Bestea, XPO1 inhibitzeak kargo askoren banaketa azpizelularra aldatuko duela. Lekualdaketa hori, partziala izan badaiteke ere, kargo prototipikoen kasuan erabatekoa izango da, hau da, egoera basalean kokapen zitoplasmatikoa baino ez dute izango, eta, XPO1 inhibitzean, ordea, nuklearra.

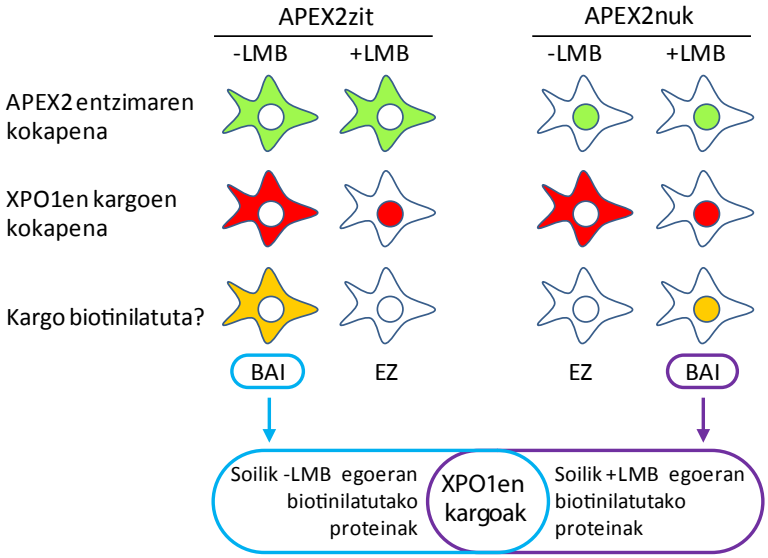

2. irudia. XPO1en kargo prototipikoak konpartimentu espezifikoko PGBaren bidez identifikatzeko estrategia. APEX2a zitoplasma edo nukleoan gainadieraztea XPO1en inhibizioarekin konbinatuko da hurrengo lau egoerak sortuz: (i) APEX2zit gainadierazita eta XPO1 aktibo, (ii) APEX2zit gainadierazita eta XPO1 inhibituta, (iii) APEX2nuk gainadierazita eta XPO1 aktibo eta (iv) APEX2nuk gainadierazita eta XPO1 inhibituta. XPO1en kargo prototipiko izateko baldintzak betetzen dituzten proteinak bai (i) eta bai (iv) egoeretan biotinilatzen direnak izango dira.

Lan honetan, PGB XPO1en kargo prototipikoak identifikatzeko baliagarria dela erakusten duen kontzeptu-froga deskribatzen dugu. Horretarako, APEX2 entzimaren bidezko konpartimentu espezifikoko PGB eta XPO1en inhibizioa uztartzen dituen estrategia garatu dugu (2. irudia). Zehazki, APEX2zit eta APEX2nuk markatzaileak sortu ditugu APEX2 entzima zitoplasmara eta nukleora ituratzeko, hurrenez hurren; bi markatzaile horien adierazpena XPO1en inhibitzaile espezifikoa den leptomizina B (LMB) tratamenduarekin konbinatu dugu.

2. MATERIAL ETA METODOAK

Plasmidoen prestaketa

APEX2zit eta APEX2nuk entzima markatzaileak kodetzen dituzten plasmidoak diseinatu eta sortu ditugu pEYFP-C1 (Clontech) plasmidoa erabilita. APEX2zit eratzeko aukeratutako seinalea XPO1ekiko independenteki esportatzen den RIP3 proteinaren NESa [28] izan da, eta proteina fluoreszentea, berriz, sinGFP4a [29]. Proteina horien sekuentzia kodetzaileak HindIII/EcoRI eta NheI/BglII murriztegunеak erabilita klonatu dira, hurrenez hurren. APEX2nuk eratzeko aukeraturiko seinaleak SV40 T antigeno luzearen 4 NLS izan dira; horietako bat NheI eta AgeI murriztegunеen artean klonatu da eta beste hirurak, berriz, BglII eta EcoRI guneen artean. Proteina fluoreszenteari dagokionez, plasmidoaren jatorrizko YFP mantendu da. APEX2 sekuentzia kodetzailea KpnI eta BamHI murriztegunеak erabilita klonatu da APEX2zit zein APEX2nuk plasmidoetan.

Bestalde, Myc-SBSN eta Myc-CK2α' proteinak gainadierazi ahal izateko, SBSN eta CK2α' kodetzen dituzten cDNA sekuentziak pMyc-MSC plasmidoan [30] klonatu ditugu BamHI eta HindIII murriztegunеen artean.

Zelulen hazkuntza, transfekzioa eta LMB tratamendua

HEK293T zelulak % 10 idi-umeki seruma, 100 U/ml penizilina eta 100 μg/ml estreptomizinadun DMEM medioan hazi ditugu (dena Gibco-koa) 37 °C-tan, % 5eko CO_2-dun atmosfera hezean. Transfekzioa egin baino 24 ordu lehenago, HEK293T zelulak estalkidun 12 putzutako edo 10 cm-ko Petri plakatan erein ditugu. Transfekziorako X-tremeGENE 9 transfekzio-agentea (Roche Diagnostics) erabili dugu, fabrikatzailearen argibideei jarraituz. Transfekziotik 24 ordura LMB (Apollo Scientific) 6 ng/ml-ko kontzentrazioan gehitu dugu mediora eta zelulak 3 orduz inkubatu ditugu.

Mikroskopiarako laginen prestaketa eta proteinen kokapen azpizelularra aztertzeko irudi analisia

Zelulak % 3,7 formaldehido PBStan fixatu ditugu 30 minutuz. Myc etiketadun proteinak adierazten dituzten zelulak % 0,2 Triton X-100 PBStan iragazkortu ditugu 10 minutuz, eta ordubetez blokeatu ditugu % 3 BSA PBStan. Jarraian, saguaren anti-Myc antigorputzarekin (Cell Signaling Technology; 1:300) inkubatu ditugu laginok ordu bete; ondoren, PBStan garbitu eta saguaren antigorputzen kontrako AF594 antigorputzarekin (Invitrogen; 1:400) inkubatu ditugu beste ordubetez. Laginak DAPIdun Vectashield muntaketa-medioa erabilita (Vector Laboratories) mikroskopiarako portetan muntatu ditugu. sinGFP4a edo YFP fusio-proteinak adierazten dituzten zelulak fixatu eta garbitu ostean, zuzenean muntatu ditugu. Irudiak Zeiss Apotome2.0 fluoreszentzia-mikroskopioa eta Zen2.6 Blue Edition softwarea erabilita hartu ditugu UPV/EHUko SGIker mikroskopiazerbitzuan.

Irudi-analisia Fiji softwarerako [31] gure taldeak ad hoc sortutako script bat [30] erabiliz egin dugu lagin bakoitzeko gutxienez 50 zelulatan.

APEX2 peroxidasaren bidezko PGB

PGB aurretik deskribatutako protokoloa [32] oinarritzat hartuta egin dugu. Petri plaka bakoitza 500 μM biotin-fenol (BP; Iris Biotech) DMEM-tan inkubatu dugu 30 minutuz eta 37°C-tan. Ostean, plakei, markaketa-kontrolerako laginei salbu, H_2O_2-a (Riedel-deHaën) gehitu diegu 10 mM-eko amaierako kontzentrazioan. Minutu bakar bateko inkubaziodenbora igarotakoan, H_2O_2-aren efektua bertan behera geratzeko, plaka guztiak quencher-soluziotan [32] garbitu ditugu hiru aldiz. Azkenik, zelulak PBStan garbitu, plakatik desitsasteko tripsinarekin tratatu, eta 10 ml PBStan jaso ditugu; 1 ml western plapaketan erabili da, beste 9 ml-ak afinititate purifikazioan.

Western plapaketa

Zelulak bromofenol urdin gabeko 200 μl Laemmli lisi-tanpoitan (125 mM Tris-HCl pH 6,8, % 20 glizerol, % 4 SDS) 10 minutuz eta 95°C-tan inkubatuta lisatu ditugu. Laginetako proteina kantitatea Lowry metodoaren bidez kuantifikatu eta lagin bakoitzetik 20 μg proteina zamatu dugu % 12ko SDS-PAGE geletan. Proteinak elektroforesiz banatu eta nitrozelulosazko mintzetara transferitu ditugu. Mintzak blokeo-soluziotan (% 5 esne gaingabetua TTBStan) ordubetez inkubatu ostean, anti-Biotin-HRP antigorputzetan (Cell Signaling Technology; 1:1.000) inkubatu ditugu beste ordubetez. Amaitzeko, mintzak TTBStan garbitu eta Pierce ECL Plus detekzio-agentea (ThermoFisher Scientific) erabiliz errebelatu ditugu.

Biotinilatutako proteinen afinitate-purifikazioa

Afinitate-purifikaziorako laginak zentrifugatu, jalkinak proteasa inhibitzailedun (PI; Roche) 2,9 ml lisi-tanpoitan (8 M urea, % 1 SDS, 50 mM N-etimaleimida (NEM) PBStan) berreseki, 30 minutuz 4ºC-tan inkubatu eta zentrifugazioz jasotako gainjalkinak lotze-tanpoitan (3 M urea, 1 M NaCl, % 0,25 SDS, 50 mM NEM) orekatutako PD10 zutabeetan (Healthcare) zehar pasarazi ditugu. Eluzioa, 25X PIdun 250 µl lotze-tanpoitan egin dugu.

Afinitate-purifikazioa aurretik deskribatutako moduan [33] egin dugu. Laburbilduz, lotze-tanpoitan ditugun laginak 150 µl Pierce High Capacity NeutrAvidin agarosa bihitxoekin (ThermoFisher Scientific) inkubatu ditugu 3 orduz. Ondoren, bihitxoak sei garbiketa tanpoi (GT) desberdinetan [33] garbitu ditugu. Azken garbiketaren ostean, eta biotinilatutako proteinen eta bihitxoen arteko interakzioak hausteko, bihitxoak 80 µl 100 mM DTTdun 4X Laemmli eluzio-tanpoitan inkubatu ditugu 5 minutuz eta 95°C-tan. Azkenik, bihitxoak biotinilatutako proteinetatik banantzeko, laginak Vivaclear Mini 0.8 µm PES filtrodun zutabeetan (Sartorious) zehar pasarazi ditugu. Jarraian lagineko proteinak SDS-PAGEz banatu eta gela GelCode Blue Stain tindaketa medioan (Thermo-Fisher Scientific) tindatu dugu. Hemendik aurrerako laginen prozesamendua UPV/EHUko SGIker proteomika-zerbitzuan egin da.

Masa-espektrometria analisia

Geletik APEX2 exogenoari, abidinari eta fronteari dagozkien bandak baztertu dira. Gainontzeko intereseko gel zatietan geleango proteinen digestio tripsina entzima erabiliz egin da [34]. Digestioan lortutako peptido triptikoen soluzioa gatzgabetzeko C18 (3M Empore C18) mikrozutabeetan zehar pasarazi dugu.

Peptidoak Acclaim PepMap RSLC (75 µm × 25 cm, Thermo Scientific) zutabe analitiko batera konektatutako Acclaim PepMap100 (75 µm × 2 cm, Thermo Scientific) aurre-zutabe batean zamatu dira. Peptidoak % 2,4-% 80 azetonitrilo-gradientean banatu dira. Masa-espektrometria analisiak nanospray flex ioi-iturri baten bidez konektatuta dauden EASY-nLC 1.200 likido-kromatografiako sistema eta Q Exactive HF-X masa-espektrometroan (Thermo Scientific) egin dira. Masa-espektrometroa ioi positibo funtzioan erabili da, eta 375-1.800 m/z tarteko MS *scan* osoak jaso dira 200 m/z-tan 60 000ko bereizmenarekin. Seinalerik handieneko 10 ioiak fragmentatu eta MS/MS espektroak 200 m/z-tan 15 000ko bereizmenean jaso dira. Datuak Xcalibur softwarea (Thermo Scientific) erabilita jaso dira.

Datuak MaxQuant (v.1.6.0.16) [35] erabilita prozesatu dira UniProtKB SwissProt Human (v 2017-11) datu basea erabilita, non APEX2dun proteinen sekuentziak gehitu diren. Bilaketetarako hurrengo parametroak era-

bili dira: prekurtsoreen eta fragmentuen tolerantziak 8 eta 20 ppm-koak hurrenez hurren, tripsinak gehien jota bi mozketa egin gabe uztea, oxidazioa eta azetilazioa modifikazio aldakor kontsideratzea, eta karbamidometilazioa modifikazioa, finko. Peptido eta proteinen FDRa (*false discovery rate)* % 1ean ezarri da.

Identifikatutako proteina-zerrenden kudeaketa eta analisia

Identifikatutako proteinen sei zerrenda ditugu, horietako bi kontrol laginei ($-H_2O_2$) dagozkie, beste laurak 2. irudian azaldutako egoerei. Egoera horiei dagozkien laginetan zein proteina identifikatu den aztertzeko lehen urratsa zeluletan berez biotinilatzen diren proteinak zerrendetatik kentzea da. Horretarako kontrol laginean identifikatutako proteinak beste zerrendetatik ezabatu ditugu.

Identifikatutako proteinekin bi analisi mota egin dira. Batetik, laginen arteko konparaketak egin dira Venn diagramak erabiliz [36]. Bestetik, UniProtKB datu-baseko [37] (2020-10-22ko bertsioa) *Subcellular location* sailkapenaren arabera egoera basalean identifikatu ditugun proteinak aurretiaz zein konpartimentutan deskribatu diren aztertu dugu.

3. EMAITZAK

3.1. APEX2zit eta APEX2nuk plasmidoen diseinua, eta APEX2 entzimaren kokapen nukleozitoplasmatikoa

Lehenik eta behin, zitoplasmara eta nukleora ituratuko diren APEX2zit eta APEX2nuk proteina-markatzaileen plasmidoak diseinatu ditugu. Proteina kimeriko horiek hiru osagai dituzte; APEX2 peroxidasa, APEX2 intereseko konpartimentura ituratzeko seinalea (NES edo NLSak) eta kokapenaren jarraipena ahalbidetuko duen proteina fluoreszente bat (3A irudia). 2. irudiko estrategia eraginkorra izateko, ezinbestekoa da APEX2zit proteina zitoplasman baino ez adieraztea egoera guztietan. Horretarako, APEX2 zitoplasmara ituratzeko XPO1en menpekoa ez den RIP3 proteinaren NESa [28] aukeratu dugu. Helburu berarekin, sinGFP4a erabili dugu proteina fluoreszente bezala, GFP bertsio hori YFP baino astiroago translokatzen baita nukleora [29]. APEX2nuk proteinaren diseinurako, ordea, SV40 T antigeno luzearen NLSaren lau kopia eta ohikoa den YFP proteina fluoreszentea erabili ditugu.

APEX2zit eta APEX2nuk proteinak kodetzen dituzten plasmidoak HEK293T zeluletan transfektatutakoan, gainadierazitako proteinen kokapena fluoreszentzia-mikroskopiaren bidez aztertu dugu. APEX2zit proteinak kokapen zitoplasmatikoa du egoera basalean zein XPO1 inhibituriko egoeran, eta APEX2nuk proteinak, aldiz, nuklearra (3B irudia).

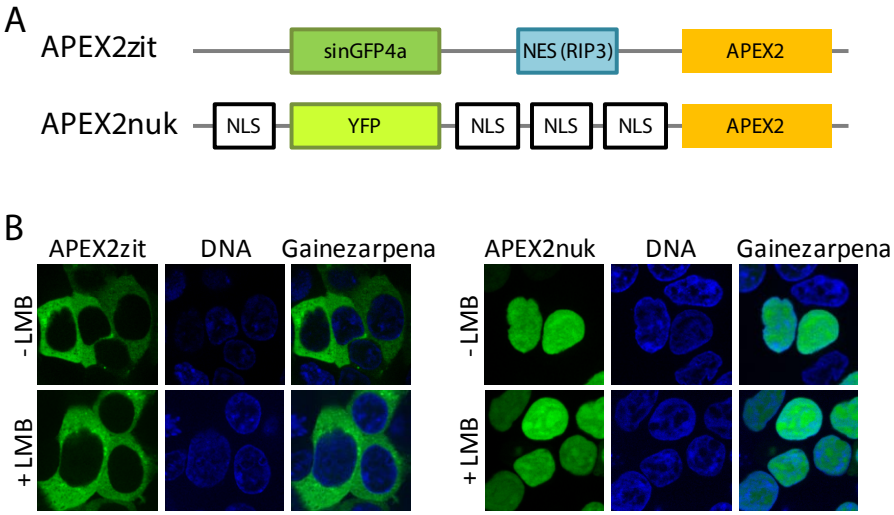

3. irudia. APEX2dun plasmidoen eraketa eta proteinaren kokapenaren balioespena. A) APEX2dun plasmidoen irudi eskematikoak. Goialdean, APEX2zit plasmidoan sinGFP4a, RIP3 proteinaren NESa eta APEX2 sekuentziek duten kokapenaren irudia. Behealdean, APEX2nuk plasmidoan YFP, lau NLS eta APEX2 sekuentziek dutena. B) APEX2zit eta APEX2nuk proteina-markatzaileak HEK293T zeluletan gainadierazitakoan hartzen duten kokapenaren fluoreszentzia-irudiak.

3.2. Markatzaileen aktibitate entzimatikoa eta MS/MSrako laginen prestaketa

Bi markatzeileen kokapen egokia berretsita, gertuko proteina endogenoen biotinilazioa eragiteko gai diren aztertu dugu. Horretarako, APEX2zit eta APEX2nuk gainadierazten dituzten zelulen proteina erauzkinak erabiliz biotinaren kontrako western plapaketa egin dugu (4. irudia); APEX2 peroxidasa aktibatu gabeko ($-H_2O_2$) kontrol laginei dagozkien kaleetan, APEX2zit edota APEX2nuk proteinen autobiotinilazioari [32] dagozkien bandak baino ez dira ageri. APEX2a aktibatutako ($+H_2O_2$) laginetan, ordea, proteina endogeno ugari biotinilatu direla adierazten duten banda ugarik osatzen duten arrastoak ageri dira. Hau da, APEX2zit eta APEX2nuk proteina endogenoak biotinilatzeko gai dira.

APEX2zit eta APEX2nuk proteinen kokapena (3B irudia) zein biotinilazio ahalmena (4. irudia) berretsita, MS/MSrako laginak prestatu, eta UPV/EHUko SGIker proteomika-zerbitzura bidali ditugu.

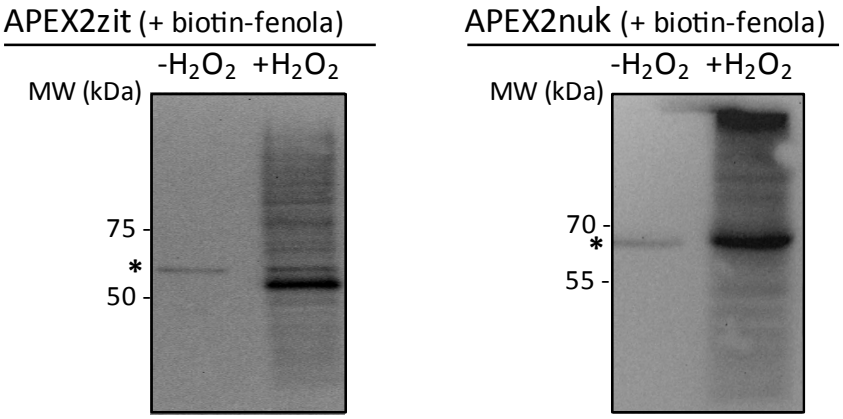

4. irudia. APEX2zit eta APEX2nuk bidezko PGB. APEX2zit eta APEX2nuk proteina erauzkinekin biotinaren kontrako western plapaketak: APEX2 aktibatutako laginetan (+H_2O_2) tamaina ezberdineko proteina bilduma zabalak biotinilatu direlako seinale diren banda ugarik osatzen duten arrastoak ageri dira. APEX2 peroxidasa aktibatu gabeko laginetan (–H_2O_2) gainadierazitako proteinaren autobiotinilazioari dagokion intentsitate baxuko banda baino ez da ageri (*).

3.3. **MS/MS analisien emaitzak: kontsiderazio orokorrak**

MS/MS analisian, guztira, 2053 proteina identifikatu ditugu gutxienez peptido batekin (1. taula). Markatzaile bakoitzeko erauzkinetan identifikatutako proteina kopurua antzekoa izan da; APEX2zit erauzkinean 1248 proteina, APEX2nuk erauzkinean, ordea, 1318. Era berean, egoera basalean zein XPO1 inhibitutako egoeran identifikatutako proteina kopurua ere antzekoa izan da APEX2zit zein APEX2nuk erauzkinetan; egoera basalean 1884 proteina, XPO1 inhibitutako egoeran, ordea, 1757. Emaitza hauek iradokitzen dute markatzaile bien aktibitate biotinilatzailea antzekoa dela, LMB tratamenduak ez duela aktibitate hori nabarmen eraldatzen eta lagin guztien prozesamendua antzekoa izan dela.

1. taula. MS/MS analisiaren emaitzen laburpena. APEX2zit eta APEX2nuk proteina-markatzaileak gainadierazitako zelulen erauzkinetan gutxienez peptido batekin identifikatutako proteina kopurua, egoera basalean (–LMB) eta XPO1 inhibiturik dagoela (+LMB). «Guztira» izeneko zutabea, egoera basalean edo XPO1 inhibiturik dagoen egoeran identifikatutako proteinen erredundantzia gabeko batura da. Era berean, «guztira» izeneko lerroa APEX2zit edo APEX2nuk markatzaileekin prestatutako erauzkinetan identifikatutako proteinen batura ez erredundantea da.

	APEX2zit	APEX2nuk	Guztira
–LMB	1157	1195	1884
+LMB	995	1156	1757
Guztira	1248	1318	2503

3.4. Konpartimentu espezifikoko proteinen identifikazioa egoera basalean

Identifikatutako proteina kopurua aztertu ostean, APEX2zit markatzaileak markatutako proteinak zitoplasmatikoak direnetz eta APEX2nuk markatzaileak markatutako proteinak nuklearrak direnetz aztertu dugu. Lehenik eta behin, egoera basalean APEX2zit erauzkinean identifikatutako 1 157 proteinak APEX2nuk erauzkinean identifikatutako 1195 proteinekin erkatu ditugu. APEX2zit erauzkinean esklusiboki identifikatu direnak 689 izan dira, APEX2nuk erauzkinekoak, 727; bestelako 468 proteinak, ordea, bi erauzkinetan identifikatu dira (5A irudia). Emaitza horiek markatzaile bakoitzarekin markatutako proteinak, neurri batean behintzat, ezberdinak direla erakusten dute. Jarraian, UniProtKB datu-basea erabiliz identifikatutako proteinak aurretik zein kokapenetan deskribatu diren aztertu dugu.

UniProtKBn identifikatutako proteina gehienen kokapenaren gaineko informazioa badago: APEX2zit erauzkineko proteinen % 63 zitoplasmatiko (edo zitoplasmatiko eta nuklear) gisa dago deskribatuta, APEX2nuk erauzkinean identifikatutako proteinen kasuan, % 69 da nuklear (edo nuklear eta zitoplasmatiko) gisa deskribatutakoa (5B irudia). Datu horiek agerian uzten dute APEX2zit eta APEX2nuk konpartimentu espezifikoko biotinilaziorako markatzaile baliagarriak direla.

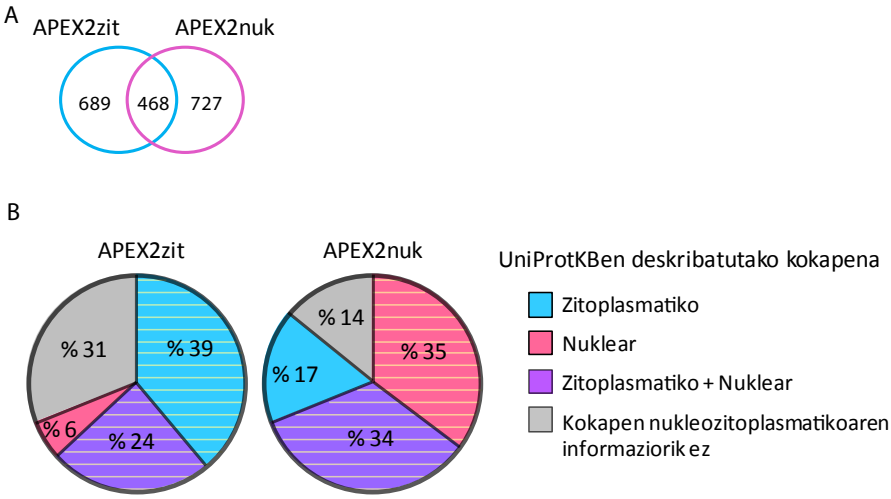

5. irudia. PGB-MS/MS bidez konpartimentu espezifikoko proteinen identifikazioa. A) Egoera basalean APEX2zit eta APEX2nuk erauzkinetan identifikatutako proteinen Venn diagrama. B) Ikerketa honetan identifikatutako proteinek UniProtKB datu-basearen arabera duten kokapena erakusten duten sektore-diagramak. Ehuneko handi batean, gure analisiaren araberako kokapena eta UniProtKBen araberakoak bat egiten dute (marra horizontalek adierazita).

3.5. **XPO1en balizko kargoen identifikazioa**

APEX2zit eta APEX2nuk bidezko markaketaren egokitasuna berretsita, XPO1en balizko kargoak bilatzeari ekin diogu. Horretarako, 2. irudiko estrategiari jarraikiz, APEX2zit gainadierazitako erauzkinetan eta egoera basalean identifikatutako proteinak APEX2nuk gainadierazitako erauzkinetan eta XPO1 inhibitutako egoeran identifikatutako proteinekin erkatu ditugu. Egoera basalean, 253 proteina identifikatu dira esklusiboki APEX2zit erauzkinean. XPO1 inhibitutako egoeran, 123 proteina identifikatu dira esklusiboki APEX2nuk erauzkinean. Proteina-zerrenda bi horiek erkatzean, lau proteina komun aurkitzen dira; LIMD1 (*LIM domain containing protein 1*), TUBAL3 (*tubulin alpha chain-like 3*), CK2α' (*casein kinase II subunit alpha'*) eta SBSN (*suprabasin*) proteinaren bigarren isoforma (6. irudia). LIMD1 eta TUBAL3 proteinak XPO1en kargo gisa deskribaturik daude jada [38,39], eta CK2α' balizko kargotzat proposatu zen aurreko analisi proteomiko batean [6], proteina honen XPO1en mendeko esportazioa oraindik konfirmatu ez bada ere. Emaitza horiek gure prozeduraren eta estrategiaren bermetzat har ditzakegu. Gauzak horrela, XPO1en kargotzat deskribatu gabe dauden CK2α' eta SBSN proteinen banaketa nukleozitoplasmatikoa aztertu nahi izan dugu.

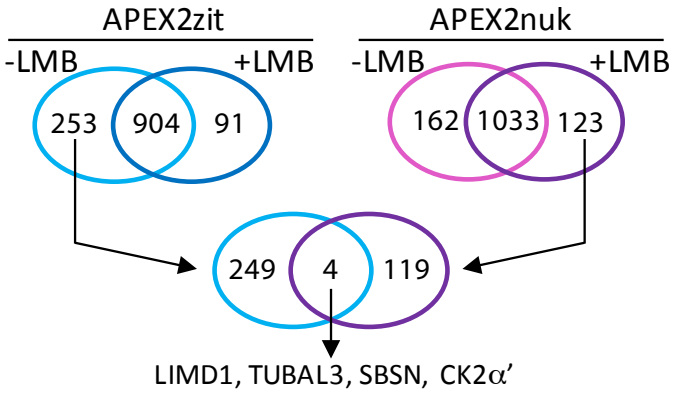

6. irudia. PGBaren bidezko XPO1en kargoen identifikazioa. Egoera basalean eta XPO1 inhibitutako egoeran APEX2zit eta APEX2nuk erauzkinetan identifikatutako proteinak konparatzen dituen Venn diagrama sorta. Soilik APEX2zit erauzkinean egoera basalean eta soilik APEX2nuk erauzkinean XPO1 inhibitutako egoeran identifikatutako proteinak erkatzean (beheko aldea) XPO1en lau balizko kargo aurkitzen dira; LIMD1, TUBAL3, SBSN eta CK2α'.

3.6. CK2α' eta SBSN proteinen banaketa nukleozitoplasmatikoaren azterketa

Myc-CK2α' eta Myc-SBSN proteinak HEK293T zeluletan gainadierazi ditugu. Myc-SBSN proteinaren kokapenak ez du XPO1en mendekotasunik erakusten; zitoplasman eta jariatze-besikulak izan daitezkeen egituretan metatzen da egoera basalean zein XPO1 inhibiturik dagoenean (7A irudia). Behatutako kokapen hori literaturan deskribatutakoarekin bat dator, SBSN jariatze-proteina legez deskribatuta baitago [40, 41]. Myc-CK2α'ren kokapenari dagokionez, egoera basalean zein XPO1 inhibiturik dagoenean nukleozitoplasmatikoa da. Alabaina, LMB tratamenduak nukleoranzko lekualdaketa txikia eragiten duela atzeman dugu. Kokapen-aldaketa hau irudi-analisi semikuantitatiboa eginez egiaztatu dugu (7B irudia). Gauzak horrela, CK2α' XPO1en kargo berria izan daitekeela proposatzen dugu.

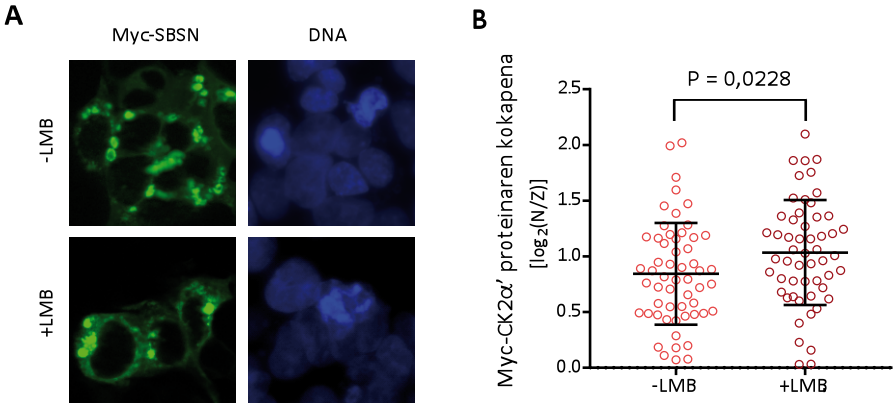

7. irudia. CK2α' eta SBSN proteinen banaketa nukleozitoplasmatikoaren azterketa. A. Myc-SBSN HEK293T zeluletan gainadieraztean hartzen duen kokapenaren irudi adierazgarriak**.** Myc-SBSN proteinak ez du XPO1en mendeko kokapenik agertzen, XPO1 aktibo zein inhibiturik egon, zitoplasman eta jariatze besikulak izan daitezkeen egituretan metatzen da. B. Myc-CK2α' proteinak HEK293T zeluletan erakusten duen kokapen nukleozitoplasmatikoa irudi-analisiaren bidez aztertu dugu, bai egoera basalean eta bai XPO1 inhibituriko egoeran. Zirkulu bakoitzak adierazten du zelula bakar baten nukleoan eta zitoplasman antzematen den fluoreszentziaren arrazoia 2 oinarriko logaritmoan [$\log_2$(N/Z)]. Lagin bakoitzaren $\log_2$(N/Z)-ren batezbestekoa eta desbiderapen estandarrak adierazten dira, baita Mann-Whitney U estatistikoa erabiltzean lortutako p balioa ere. Aztertutako bi egoeretan Myc-CK2α' proteinak kokapen gehienbat nuklearra erakusten badu ere, XPO1en inhibizioak CK2α' nukleoan egoera basalean baino gehiago metatzea eragiten du.

4. EZTABAIDA ETA ONDORIOAK

XPO1 esportinak mila inguru kargo-proteinen nukleotiko esportazioa bideratzen du [6]. XPO1 zelularen homeostasirako gako izateaz gain, minbiziaren tratamenduan izan dezakeen rola geroz eta ozenago aipatzen ari da azken urteetan [1-en berrikusia]. XPO1en mendeko garraioaren nondik norakoak ulertu eta minbizian duen garrantzia argitzeko, aurrerapauso handia izango litzateke XPO1en esportoma ondo karakterizatzea. Bide horretan, hurbilketa berri bat planteatu dugu zeinak konpartimentu espezifikoko PGB, XPO1en inhibizioa, afinitate-purifikazioa eta MS/MS analisiak uztartzen dituen.

Hurbilketa berri honen erronkarik handiena PGB eragingo duten markatzaileen diseinua izan da, zitoplasmako eta nukleoko proteinen bildumak era bereizian markatzea berebizikoa baita emaitza esanguratsuak lortuko

baditugu. Hori horrela, APEX2 peroxidasan oinarritutako bi proteina markatzaile kimeriko berri sortu ditugu: APEX2zit eta APEX2nuk. Gainadierazitako APEX2zit zitoplasman eta APEX2nuk nukleoan kokatzen direla berretsita, diseinatu dugun hurbilketa osoa proteomikako kontzeptu-froga erako esperimentu baten bidez balioetsi dugu.

Esperimentuaren diseinua sinplifikatze aldera, aztertutako egoeren erreplika bana eta ez ohikoak diren hiru erreplikak analizatu dugu. Jakitun gara horrek proteina-identifikazioen ziurgabetasuna emendatzen duela; halere, egoera basalean egindako esperimentuen emaitzek erakusten dute ziurgabetasun horrek ez duela hurbilketa bera baliogabetzen. Izan ere, APEX2zit eta APEX2nuk erauzkinetan identifikatutako proteina sortak neurri handi batean ezberdinak badira ere, badira komunak diren beste hainbat proteina ere (5A irudia). Emaitza horrek APEX2zit eta APEX2nuk-ek bideratutako PGB arrakastatsua izan dela ematen digu aditzera, batetik APEX2zit eta APEX2nuk-ekin proteina bilduma ezberdinak markatzea aurreikusi eta lortu dugulako, eta bestetik proteina ugari konpartimentu bietan agertzea aurreikus daitekeelako [42]. Are gehiago, APEX2zit eta APEX2nuk erauzkinetan identifikatutako proteinak UniProtKB datu-basean proteinok duten zelula-kokapenaren deskribapenarekin bat datoz neurri handi batean (5B irudia). Aipaturikoa kontuan hartuta, guk diseinatu eta esperimentalki testatutako proteina markatzaileek konpartimentu espezifikoko PGBrako egokiak direla deritzogu.

Identifikatutako proteina bildumei oniritzia emanda, XPO1en balizko kargoak bilatzen hasitakoan erreplika bakarrarekin lan egiteak dakarren beste muga topatu dugu: erreplika bakarreko datuekin ez dago analisi kuantitatiborik egiterik; ondorioz, kargo prototipikoak baino ezin izan ditugu bilatu. Bilaketa horren emaitza lau proteina izan dira: LIMD1, TUBAL3, CK2α' eta SBSNren bigarren isoforma, alegia. LIMD1 eta TUBAL3 aurretik ere XPO1en kargotzat deskribatuta egoteak [38,39] gure estrategiari nolabaiteko bermea ematen diola deritzogu. SBSN eta CK2α' balizko kargoen nukleo eta zitoplasmaren arteko garraioaren gaineko informaziorik, guk dakigula, eskuragarri ez dagoenez, proteinok HEK293T zeluletan gainadierazi eta XPO1 inhibitzean erakusten duten kokapen nukleozitoplasmatikoa aztertu dugu. SBSN proteinaren kasuan ez dugu XPO1en inhibizioaren menpeko kokapenaren aldaketarik behatu. CK2α' aztertzean, berriz, XPO1 inhibitzean CK2α' proteinaren nukleoranzko aldaketa partzial bat behatu dugu (7A eta B irudiak). Emaitzok ikusita, CK2α' XPO1en kargotzat proposatzen dugu eta planteatutako hurbilketa berria XPO1en kargoak identifikatzeko prozedura aproposa dela planteatzen dugu.

Deskribatutako hurbilketa, beraz, XPO1en esportomaren ezagutzan sakontzeko eta klinikan erabiltzen diren eta XPO1en inhibizioa helburu duten agente terapeutikoek, selinexor kasu [9], zelula mailan duten eragina ikertzeko erabilgarria izan daitekeela planteatzen dugu.

5. **ESKER ONAK**

Lan honetako mikroskopia- eta proteomika-analisiak UPV/EHUko mikroskopia- eta proteomika-zerbitzuetan (SGIker) egin dira, hurrenez hurren. Lan hau Espainiako Gobernuaren MINECO-FEDER (SAF2014-57743-R eta SAF2016-76898-P), Eusko Jaurlaritzaren (IT1257-19) eta Euskal Herriko Unibertsitatearen (UPV-EHU) (UF111/20) finantziazioei esker egin da. Baita Eusko Jaurlaritzak (MS-ri) emandako dirulaguntzari esker ere. Gure taldea PROTEOSTASIS BM1307 COST Action-eko kide da, European Cooperation in Science and Technology-k lagunduta.

BIBLIOGRAFIA

[1] SENDINO, M., OMAETXEBARRIA, M. J., RODRÍGUEZ, J. A. 2018. «Hitting a moving target: inhibition of the nuclear export receptor XPO1/CRM1 as a therapeutic approach in cancer». *Cancer Drug Resistance*, **1**, 138-163.

[2] STADE, K., FORD, C. S., GUTHRIE, C., WEIS, K. 1997. «Exportin 1 (Crm1p) is an essential nuclear export factor». *Cell*,**90**, 1041-1050.

[3] OSSAREH-NAZARI, B., BACHELEIRE, F., DARGEMONT, C. 1997. «Evidence for a Role of CRM1 in Signal-Mediated Nuclear Protein Export». *Science*, **278**, 141-144.

[4] FORNEROD, M., VAN DEURSEN, J., VAN BAAL, S., REYNOLDS, A., DAVIS, D., MURTI, K. G., FRANSEN, J., GROSVELD, G. 1997. «The human homologue of yeast CRM1 is in a dynamic subcomplex with CAN/Nup214 and a novel nuclear pore component Nup88». *EMBO Journal*, **16**, 807-816.

[5] FUKUDA, M., ASANO, S., NAKAMURA, T., ADACHI, M., YOSHIDA, M., YANAGIDA, M., NISHIDA, E. 1997. «CRM1 is responsible for intracellular transport mediated by the nuclear export signal». *Nature*, **390**, 308-311.

[6] KIRLI, K., KARACA, S., DEHNE, H. J., SAMWER, M., PAN, K. T., LENZ, C., URLAUB, H., GÖRLICH, D. 2015. «A deep proteomics perspective on CRM1-mediated nuclear export and nucleocytoplasmic partitioning». *eLife*, **4**, e11466.

[7] TAYLOR, J., SENDINO, M., GORELICK, A. N., PASTORE, A., CHANG, M. T., PENSON, A. V, GAVRILA, E. I., STEWART, C., MELNIK, E. M., HERREJON CHAVEZ, F., BITNER, L., YOSHIMI, A., LEE, S. C.-W., INOUE, D., LIU, B., ZHANG, X. J., MATO, A. R., DOGAN, A., KHARAS, M. G., CHEN, Y., WANG, D., SONI, R. K., HENDRICKSON, R. C., PRIETO, G., RODRIGUEZ, J. A., TAYLOR, B. S., ABDEL-WAHAB, O. 2019. «Altered nuclear export signal recognition as a driver of oncogenesis». *Cancer Discovery*, **9**, 1452-1467.

[8] MAHIPAL, A., MALAFA, M. 2016. «Importins and exportins as therapeutic targets in cancer». *Pharmacology and Therapeutics*, **164**, 135-143.

[9] SYED, Y. Y. 2019. «Selinexor: first global approval». *Drugs*, **79**, 1485-1494.

[10] AEBERSOLD, R., MANN, M. 2003. «Mass spectrometry-based proteomics». *Nature*, **422**, 198-207.

[11] THAKAR, K., KARACA, S., PORT, S. A., URLAUB, H., KEHLENBACH, R. H. 2013. «Identification of CRM1-dependent nuclear export cargos using quantitative mass spectrometry». *Molecular and Cellular Proteomics*, **12**, 664-678.

[12] BOSCH, J. A., CHEN, C. L., PERRIMON, N. 2021. «Proximity-dependent labeling methods for proteomic profiling in living cells: An update». *Wiley Interdisciplinary Reviews: Developmental Biology*, **10**, e392.

[13] KUTAY, U., GÜTTINGER, S. 2005. «Leucine-rich nuclear export signals: born to be weak». *Trends in Cell Biology*, **15**, 121-124.

[14] ROUX, K. J., KIM, D. I., RAIDA, M., BURKE, B. 2012. «A promiscuous biotin ligase fusion protein identifies proximal and interacting proteins in mammalian cells». *Journal of Cell Biology*, **196**, 801-810.

[15] CHOI-RHEE, E., SCHULMAN, H., CRONAN, J. E. 2004. «Promiscuous protein biotinylation by Escherichia coli biotin protein ligase». *Protein Science*, **13**, 3043-3050.

[16] MARTELL, J. D., DEERINCK, T. J., SANCAK, Y., POULOS, T. L., MOOTHA, V. K., SOSINSKY, G. E., ELLISMAN, M. H., TING, A. Y. 2012. «Engineered ascorbate peroxidase as a genetically-encoded reporter for electron microscopy». *Nature Biotechnology*, **30**, 1143-1148.

[17] RHEE, H.-W., ZOU, P., UDESHI, N. D., MARTELL, J. D., MOOTHA, V. K., CARR, S. A., TING, A. Y. 2013. «Proteomic mapping of mitochondria in living cells via spatially-restricted enzymatic tagging». *Science*, **339**, 1328-1331.

[18] LAM, S. S., MARTELL, J. D., KAMER, K. J., DEERINCK, T. J., ELLISMAN, M. H., MOOTHA, V. K., TING, A. Y. 2015. «Directed evolution of APEX2 for electron microscopy and proteomics». *Nature Methods*, **12**, 51-54.

[19] ZHOU, Y., ZOU, P. 2021. «The evolving capabilities of enzyme-mediated proximity labeling». *Current Opinion in Chemical Biology*, **60**, 30-38.

[20] KWON, K., BECKETT, D. 2000. «Function of a conserved sequence motif in biotin holoenzyme synthetases». *Protein Science*, **9**, 1530-1539.

[21] ZUZOW, N., GHOSH, A., LEONARD, M., LIAO, J., YANG, B., BENNETT, E. J. 2018. «Mapping the mammalian ribosome quality control complex interactome using proximity labeling approaches». *Molecular Biology of the Cell*, **29**, 1258-1269.

[22] HUANG, X., LEDUC, R. D., FORNELLI, L., SCHUNTER, A. J., BENNETT, R. L., KELLEHER, N. L., LICHT, J. D. 2019. «Defining the NSD2 interactome: PARP1 PARylation reduces NSD2 histone methyltransferase activity and impedes chromatin binding». *Journal of Biological Chemistry*, **294**, 12459-12471.

[23] LI, Y., MERKEL, C. D., XUEMEI, Z., HEIER, J. A., CANTRELL, PA. S., SUN, M., STOLZ, D. B., WATKINS, S. C., YATES, N. A., KWIATKOWSKI, A. V. 2019. «The N-cadherin interactome in primary cardiomyocytes as defined by quantitative proximity proteomics». *Journal of Cell Science*, **132**, jcs221606.

[24] AMER, Y. O., HEBERT-CHATELAIN, E. 2020. «Insight into the interactome of intramitochondrial PKA using biotinylation-proximity labeling». *International Journal of Molecular Sciences*, **21**, 8283-8295.

[25] Mick, D. U., Rodrigues, R. B., Leib, R. D., Adams, C. M., Chien, A. S., Gygi, S. P., Nachury, M. V. 2015. «Proteomics of primary cilia by proximity labeling». *Developmental Cell*, **35**, 497-512.

[26] Bersuker, K., Peterson, C. W. H., To, M., Sahl, S. J., Savikhin, V., Grossman, E. A., Nomura, D. K., Olzmann, J. A. 2018. «A proximity labeling strategy provides insights into the composition and dynamics of lipid droplet proteomes». *Developmental Cell*, **44**, 97-112.

[27] Youn, J. Y., Dunham, W. H., Hong, S. J., Knight, J. D. R., Bashkurov, M., Chen, G. I., Bagci, H., Rathod, B., MacLeod, G., Eng, S. W. M., Angers, S., Morris, Q., Fabian, M., Côté, J. F., Gingras, A. C. 2018. «High-density proximity mapping reveals the subcellular organization of mRNA-associated granules and bodies». *Molecular Cell*, **69**, 517-532.

[28] Yang, Y., Ma, J., Chen, Y., Wu, M. 2004. «Nucleocytoplasmic shuttling of receptor-interacting protein 3 (RIP3): Identification of novel nuclear export and import signals in RIP3». *Journal of Biological Chemistry*, **279**, 38820-38829.

[29] Frey, S., Rees, R., Schünemann, J., Ng, S. C., Fünfgeld, K., Huyton, T., Görlich, D. 2018. «Surface properties determining passage rates of proteins through nuclear pores». *Cell*, **174**, 202-217.

[30] Olazabal-herrero, A., Sendino, M., Arganda-carreras, I., Rodríguez, J. A. 2019. «WDR20 regulates shuttling of the USP12 deubiquitinase complex between the plasma membrane, cytoplasm and nucleus». *European Journal of Cell Biology*, **98**, 12-26.

[31] Schindelin, J., Arganda-Carreras, I., Frise, E., Kaynig, V., Longair, M., Pietzsch, T., Preibisch, S., Rueden, C., Saalfeld, S., Schmid, B., Tinevez, J.-Y., White, D. J., Hartenstein, V., Eliceiri, K., Tomancak, P., Cardona, A. 2012. «Fiji - an Open platform for biological image analysis». *Nature Methods*, **9**, 676-682.

[32] Hung, V., Udeshi, N. D., Lam, S. S., Loh, K. H., Cox, K. J., Pedram, K., Carr, S. A., Ting, A. Y. 2016. «Spatially resolved proteomic mapping in living cells with the engineered peroxidase APEX2». *Nature Protocols*, **11**, 456-475.

[33] Franco, M., Seyfried, N. T., Brand, A. H., Peng, J., Mayor, U. 2011. «A novel strategy to isolate ubiquitin conjugates reveals wide role for ubiquitination during neural development». *Molecular and Cellular Proteomics*, **10**, M110.002188.

[34] Shevchenko, A., Wilm, M., Vorm, O., Mann, M. 1996. «Mass spectrometric sequencing of proteins from silver-stained polyacrylamide gels». *Analytical Chemistry*, **68**, 850-858.

[35] Cox, J., Mann, M. 2008. «MaxQuant enables high peptide identification rates, individualized p.p.b.-range mass accuracies and proteome-wide protein quantification». *Nature Biotechnology*, **26**, 1367-1372.

[36] Bardou, P., Mariette, J., Escudié, F., Djemiel, C., Klopp, C. 2014. «jvenn: an interactive Venn diagram viewer». *BMC Bioinformatics*,**15**, 293-300.

[37] UNIPROT CONSORTIUM. 2019. «UniProt: A worldwide hub of protein knowledge». *Nucleic Acids Research*,**47**, D506-D515.

[38] SHARP, T. V., MUNOZ, F., BOURBOULIA, D., PRESNEAU, N., DARAI, E., WANG, H. W., CANNON, M., BUTCHER, D. N., NICHOLSON, A. G., KLEIN, G., IMREH, S., BOSHOFF, C. 2004. «LIM domains-containing protein 1 (LIMD1), a tumor suppressor encoded at chromosome 3p21.3, binds pRB and represses E2F-driven transcription». *Proceedings of the National Academy of Sciences of the United States of America*, **101**, 16531-16536.

[39] SCHWARZEROVÁ, K., BELLINVIA, E., MARTINEK, J., SIKOROVÁ, L., DOSTÁL, V., LIBUSOVÁ, L., BOKVAJ, P., FISCHER, L., SCHMIT, A. C., NICK, P. 2019. «Tubulin is actively exported from the nucleus through the Exportin1/CRM1 pathway». *Scientific Reports*, **9**, 5725-5738.

[40] MATSUI, T., HAYASHI-KISUMI, F., KINOSHITA, Y., KATAHIRA, S., MORITA, K., MIYACHI, Y., ONO, Y., IMAI, T., TANIGAWA, Y., KOMIYA, T., TSUKITA, S. 2004. «Identification of novel keratinocyte-secreted peptides dermokine-α/-β and a new stratified epithelium-secreted protein gene complex on human chromosome 19q13.1». *Genomics*, **84**, 384-397.

[41] MOFFATT, P., SALOIS, P., ST-AMANT, N., GAUMOND, M. H., LANCTÔT, C. 2004. «Identification of a conserved cluster of skin-specific genes encoding secreted proteins». *Gene*, **334**, 123-131.

[42] THUL, P. J., ÅKESSON, L., WIKING, M., MAHDESSIAN, D., GELADAKI, A., BLAL, H. A., ALM, T., ASPLUND, A., BJÖRK, L., BRECKELS, L. M., BÄCKSTRÖM, A., DANIELSSON, F., FAGERBERG, L., FALL, J., GATTO, L., GNANN, C., HOBER, S., HJELMARE, M., JOHANSSON, F., LEE, S., LINDSKOG, C., MULDER, J., MULVEY, C. M., NILSSON, P., OKSVOLD, P., ROCKBERG, J., SCHUTTEN, R., SCHWENK, J. M., SIVERTSSON, Å., SJÖSTEDT, E., SKOGS, M., STADLER, C., SULLIVAN, D. P., TEGEL, H., WINSNES, C., ZHANG, C., ZWAHLEN, M., MARDINOGLU, A., PONTÉN, F., VON FEILITZEN, K., LILLEY, K. S., UHLÉN, M., LUNDBERG, E. 2017. «A subcellular map of the human proteome». *Science* ,**356**, eaal3321.